THE JOURNAL
OF
CHEMICAL PHYSICS

VOLUME 35, NUMBER 6 DECEMBER, 1961

Absolute Infrared Intensities of the CS_2 Fundamentals in CCl_4 Solution and of the 768–797 cm^{-1} Fermi Doublet of CCl_4 in Cyclohexane Solution*

OTTO F. KALMAN† AND J. C. DECIUS‡
Department of Chemistry, Oregon State University, Corvallis, Oregon

(Received April 17, 1961)

The absolute infrared intensities of two nonpolar solute molecules were determined in nonpolar solvents by extrapolating the apparent intensities to zero concentration. For CS_2 the intensities were found to be 5.8×10^7 cm mole^{-1} in CCl_4 in 5.2×10^7 cm mole^{-1} in C_6Cl_6 for the ν_3 (1523 cm^{-1}) mode, and 9.5×10^6 cm mole^{-1} in CCl_4 for the ν_2 (395 cm^{-1}) mode. For CCl_4 the intensity of the 768–797 cm^{-1} Fermi doublet was found to be 5.4×10^7 cm mole^{-1} in cyclohexane. The results are discussed in relation to the Polo-Wilson, Person, and Buckingham expressions for the gas to solution intensity ratio. Modifications of the dielectric expressions were investigated.

INTRODUCTION

THE relation between the absolute intensity of infrared absorption bands in the gas phase and in solution has been investigated by several workers with conflicting results.[1–4] Interpretations of the data have been so far based mostly on the work of Polo and Wilson[5] for liquids and its modified form for solutions given by Person[6] which yields an expression for the ratio of solution and gas phase absolute intensities in terms of the refractive index of the solvent and solute. These treatments are based on Onsager's[7] theory of dielectric polarization. The expressions predict an increase of approximately 30% in the intensity in the condensed phase as compared to that in the gas phase. Experimental data are still sparce on simple molecules for which this prediction can be tested; to this end we have studied two relatively simple nonpolar molecules in nonpolar solvents.

The apparent solution intensities were obtained at several solute concentrations and the absolute intensities were determined by the use of the Wilson-Wells method as described by Ramsay.[8] According to this method the absolute intensity A is given by

$$A=\lim_{mL\to0}\left[mL^{-1}\int\ln(T_0/T)_\nu d\nu\right],$$

where the expression in the brackets is the apparent integrated absorption, m the solute concentration in moles/cm^3, L the cell length, and T/T_0 the apparent fractional transmission.

CS_2

Experimental

Stretching mode. The range of concentrations m for this mode in CCl_4 was from 1.1×10^{-2} to 5.5×10^{-2} moles per liter. The solutions were run "double beam" (on a Perkin-Elmer model 21 instrument) using a 0.112-mm liquid cell for the solution and a variable liquid cell (set at about 0.109 mm) for the solvent to compensate for solvent absorption. A spectral slit width of 9 cm^{-1} was used which gives approximately 0.6 for the ratio of spectral slit width to apparent half-intensity width. Ramsay's wing corrections were used for the area 40 cm^{-1} beyond the band center on either side. The wing correction amounted to about 9% of

* Presented in part at the Symposium on Molecular Structure and Spectroscopy, Ohio State University, Columbus, Ohio, June, 1960.
† DuPont Summer Fellow 1960.
‡ Alfred P. Sloan Research Fellow.
[1] H. D. Whiffen, Trans. Faraday Soc. **49,** 878 (1953).
[2] E. E. Ferguson and R. E. Kagarise, J. Chem. Phys. **31,** 236 (1959).
[3] T. Wentink and S. H. Bauer, J. Chem. Phys. **31,** 834 (1959).
[4] I. C. Hisatsune and E. S. Jayadevappa, J. Chem. Phys. **31,** 565 (1960). (1) and (2) found the solution intensities lower and (3) and (4) higher than the gas phase intensities.
[5] S. R. Polo and M. K. Wilson, J. Chem. Phys. **23,** 2376 (1955).
[6] W. B. Person, J. Chem. Phys. **28,** 319 (1958).
[7] L. Onsager, J. Am. Chem. Soc. **58,** 1486 (1936).
[8] D. A. Ramsay, J. Am. Chem. Soc. **74,** 72 (1952).

Copyright © 1961 by the American Institute of Physics

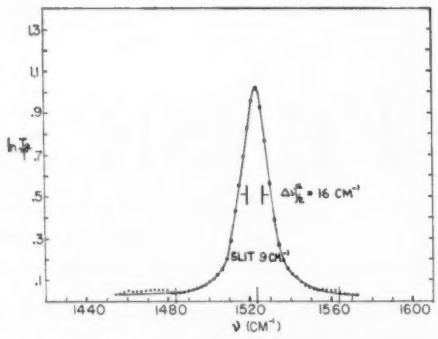

FIG. 1. Absorption band of CS_2 near 1523 cm^{-1} in CCl_4 solution.

the apparent area. The results are shown on Figs. 1 and 2. The value of $A_{3\text{soln}}$, together with the probable error obtained from treatment of the data by the method of least squares, is $5.8\pm0.16\times10^7$ cm^{-1} per mole per cm^2 at 25°C. This mode was also measured in C_2Cl_4 solvent according to the above procedure with spectral slit width of about 9 cm^{-1} and 30 cm^{-1}. The results are shown on Fig. 3. The value of $A_{3\text{soln}}$ is $5.2\pm.1\times10^7$ cm^{-1} per mole per cm^2 at 25°C.

Bending mode. For this mode the concentration range was $1.5-6.2\times10^{-1}$ moles per liter. The solutions were run on a single beam instrument (Perkin-Elmer model 112 with CsBr prism) using a 0.473 mm KBr fixed liquid cell for both solution and solvent and running them in succession. There was no noticeable solvent absorption. The spectral slit width was approximately 6 cm^{-1} which gives 0.92 for the ratio of spectral slit width to apparent half intensity width. Under these conditions the wing corrections by Ramsay's method amount to only a few percent, these have not been included in the measured apparent absorption areas plotted on Fig. 4. Since there was no noticeable solvent absorption near this band, the measurements were also carried out with variable cell thicknesses using a KBr variable liquid cell at 0.666–0.166-mm cell thicknesses and a solution of 2.35×10^{-1} moles per liter concentration. Solvent spectra were determined at the same cell lengths as the solution spectra. The slit-

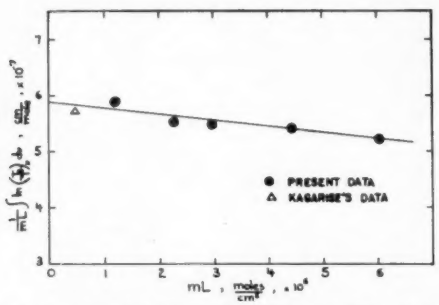

FIG. 2. Intensity of the ν_3 mode of CS_2 in the CCl_4 solution.

width was about the same as the one used for the constant cell thickness and variable concentration run. The results are shown on Fig. 4 and Fig. 5. The value of $A_{2\text{soln}}$ obtained from the two sets of results is $9.5\pm0.2\times10^5$ cm^{-1} mole per cm^2 at 25°C.

Comparison with Previous Data

Table I shows the previous data on the absolute intensities of the CS_2 modes. The solution data (at a single concentration) in CCl_4 and in C_2Cl_4 by Ferguson and Kagarise are in very good agreement with our data. Their sample cell thickness was[9] 5.9×10^{-4} cm giving 4.85×10^{-7} mole per cm^2 for mL. Using the gas-phase data the ratio $A_{3\text{soln}}/A_{3\text{gas}}$ is about 1.07.

For the bending mode so far we do not have absolute intensity values obtained from gas-phase data. Very approximate estimates of the gas-intensity value were

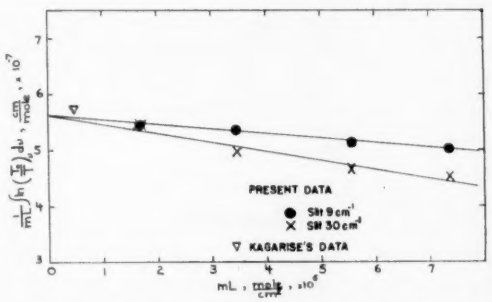

FIG. 3. Intensity of the ν_3 mode of CS_2 in C_2Cl_4 solution.

given by Schatz,[10] and Kagarise and Ferguson. These were obtained by subtracting the atomic polarization due to the ν_3 mode from the total atomic polarization, calculated from the static dielectric constants and indices of refraction, and then calculating the intensity corresponding to this atomic polarization of the ν_2 mode. Inherent in these results is the assumption that the $A_{\text{liquid}}/A_{\text{gas}}$ ratio is the same for the stretching and the bending modes. For the stretching mode the ratio used is approximately 1.4. Comparing these approximate gas intensity values with our solution results, the ratio $A_{2\text{soln}}/A_{2\text{gas}}$ turns out to be about 0.48.

Our bending mode intensity gives a bond moment of 0.78D. Compared to this, Schatz's estimate is 1.17 D and Kagarise's is 1.24 D.

DISCUSSION

Several workers have considered the calculation of $A_{\text{soln}}/A_{\text{gas}}$ ratios from dielectric polarization theory. Notably Polo-Wilson[5] and Person[6] gave expressions for $A_{\text{liquid}}/A_{\text{gas}}$ and $A_{\text{soln}}/A_{\text{gas}}$ ratios. These are based on the relation

$$A_{\text{soln}}/A_{\text{gas}}=F^2/E_0^2,$$

[9] Private communications with Dr. R. E. Kagarise.
[10] P. N. Schatz, J. Chem. Phys. **29**, 959 (1958).

where F is the "effective" field acting upon the unperturbed absorbing molecule in the solution (or liquid) phase while E_0 is the field acting on it in a vacuum. The dielectric theory is used to calculate F which is taken to be the internal field acting at the center of a small spherical cavity of radius a in the dielectric medium. The calculations are based on Onsager's treatment of the internal field as the sum of the cavity field **G** and the reaction field **R**, due to the polarization of the dielectric by the total (permanent and induced) dipole moment of the molecule.

A further assumption is the use of the Clausius-Mossotti[11] expression for the polarizability α of the molecule

$$\alpha=[(n_0^2-1)/(n_0^2+2)]a^3,$$

where n_0 is the refractive index of the solute. The Clausius-Mossotti expression is based on treatment of the molecules as isotropic spheres, where

$$\alpha=\tfrac{1}{3}(\alpha_1+\alpha_2+\alpha_3)=\alpha_1=\alpha_2=\alpha_3.$$

Such a situation may be encountered if we consider a triply degenerate mode of a spherical molecule where the polarizability associated with a particular mode would indeed be α. The result of Person's treatment is the expression

$$A_{\text{soln}}/A_{\text{gas}}=n^{-1}\{(n_0^2+2)/[(n_0/n)^2+2]\}^2, \quad \text{(I)}$$

where n refers to the solvent and n_0 to the solute.

More recently A. D. Buckingham[12] has discussed the solution-gas intensity ratios for diatomic molecules, by giving a more detailed treatment of the modification of the time dependent perturbation theory which for nonpolar molecules leads to

$$A_{\text{soln}}/A_{\text{gas}}=[9n^3/(2n^2+1)^2][(1-g\alpha)^{-1}]^2.$$

Actually Buckingham's result can be derived from the previous type treatment (i.e., Polo-Wilson or Person) if one does not substitute for the value of α the Clausius-Mossotti expression, but expresses the effective field in terms of α (see Appendix A).

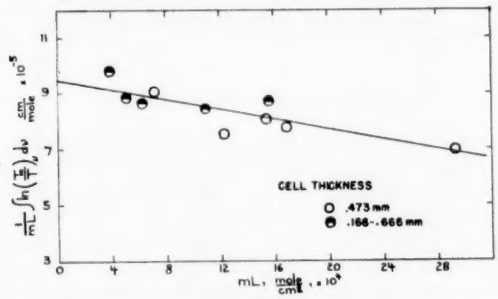

FIG. 4. Intensity of the ν_2 mode of CS_2 in CCl_4 solution.

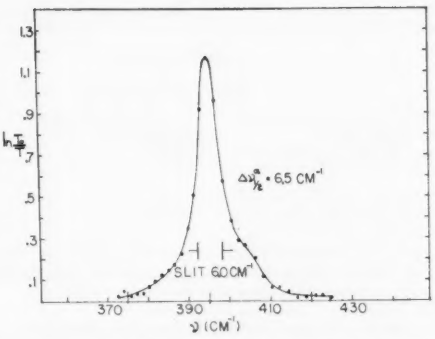

FIG. 5. Absorption band of CS_2 near 397 cm^{-1} in CCl_4 solution.

To extend the Polo-Wilson or Buckingham treatment to polyatomic molecules, instead of replacing α by the Clausius-Mossotti expression, one may consider the three principal components of the polarizability: α_x, α_y, and α_z. For the two infrared active modes of CS_2 one may consider two different polarizabilities. Taking as the molecular axis the x axis, for the stretching mode α_x may be considered as the polarizability determining the induced dipole moment oscillating with the frequency of the field. Thus the reaction field would also be determined by the polarizability associated with the particular mode. The intensity ratio would become for this mode (see Appendix A)

$$A_{3\text{soln}}/A_{3\text{gas}}=n^{-1}[3n^2/(2n^2+1)]^2[(1-g\alpha_x)^{-1}]^2, \quad \text{(II)}$$

and a similar expression would hold for the ν_2 mode of CS_2, with α_y instead of α_x.

Since the polarizabilities, α_x and α_y are quite different, the ratios would also be different to a sufficiently large extent to be measurable.

The $A_{\text{soln}}/A_{\text{gas}}$ ratios, calculated from the formulas given, are shown in Table II.

Our results from Table I give a ratio for the stretching mode that is much smaller than the predicted one. The difference between the experimental and predicted values is larger than the usual 5–10% uncertainty in the experimental results. For the bending mode the gas-phase estimates available for comparison are very approximate but there is some indication that the ratio is less than 1. The ratio of the soln/gas ratios of the two modes according to the modified treatment above should be about 0.79, while according to the Person equation, 1.0.

The fact remains however that the actually observed $A_{3\text{soln}}/A_{3\text{gas}}$ ratio is about 35% smaller than the one predicted by the dielectric theory. Several modifications of the dielectric treatment were considered. So far the absorbing molecule has been considered to be located at the center of a spherical cavity. It is possible

[11] C. J. F. Böttcher, *Theory of Electric Polarization* (Elsevier Publishing Company, Inc., New York, 1952), p. 199.
[12] A. D. Buckingham, Proc. Roy. Soc. **A248,** 169 (1958); **A255,** 32 (1960).

TABLE I. Absolute infrared intensities of the CS_2 fundamentals.

	Present results 25° (cm^{-1}/mole per cm^2)	Other solution data cm^{-1}/mole per cm^2(STP)	Gas phase data cm^{-1}/mole per cm^2(STP)	Liquid results cm^{-1}/mole per cm^2(STP)
ν_3 (1523 cm^{-1}) mode	5.8×10^7 [h] 5.2×10^7 [i]	5.47×10^7 [a] 5.58×10^7 [b]	5.67×10^7 [c] 5.58×10^7 [d] 5.76×10^7 [e]	7.35×10^7 [f] 7.50×10^7 [g]
ν_2 (395 cm^{-1}) mode	9.5×10^5			

[a] 5% (by volume) solution in CCl_4. E. E. Ferguson and R. E. Kagarise, J. Chem. Phys. **31**, 236 (1959).
[b] 5% (by volume) solution in C_2Cl_4 by Ferguson and Kagarise.
[c] D. Z. Robinson, J. Chem. Phys. **19**, 881 (1951).
[d] R. Kiyama and K. Ozawa, Rev. Phys. Chem. Japan **25**, 40 (1955).
[e] D. C. McKean, H. J. Callomon, and H. W. Thompson, J. Chem. Phys. **20**, 520 (1952).
[f] From liquid dispersion data by Kagarise and Ferguson.
[g] P. N. Schatz, J. Chem. Phys. **31**, 1146 (1959); **29**, 959 (1958).
[h] In CCl_4 solution.
[i] In C_2Cl_4 solution.

to modify the dielectric description[13] so that an ellipsoidal cavity is considered. To see the effect of the two factors, the cavity factor) $\times 1/n$, i.e., $(a_i)^2/n$, and the $[(1-g_i\alpha_i)^{-1}]^2$ term in $n^{-1}(a_i)^2[(1-g_i\alpha_i)^{-1}]^2=(A_{soln}/A_{gas})_i$, where i refers to a particular mode, are listed separately in Table AI.

The net effect is practically a reversal of the magnitudes of the predicted intensity ratios for the stretching and bending modes. For the stretching mode both the (cavity factor) $\times 1/n$ and the reaction field term decreased considerably by going from the spherical to ellipsoidal cavity while for the bending mode each increased somewhat. The effect is evidently much larger for the stretching mode.

The justification for using an ellipsoidal cavity for CS_2 in CCl_4, however, may be questionable because of the spherical symmetry and the relative size of CCl_4 as compared to CS_2. Presumably CS_2 would fit into a cavity created by the removal of a CCl_4 molecule in pure CCl_4 [also some investigators[14] find it more reasonable to use $(MW/\rho N_{Avog})_{solvent}=a^3 4\pi/3$ rather than the solute values]. The molecular dimensions (along the long axis of CS_2) calculated from bond distances and van der Waals radii are: $a=3.56$ A for CCl_4 and $a=3.39$ A for CS_2. From the assumption of closest packing of spheres and molecular weight and density data one estimates $a=3.05$ A for CCl_4 and $a=2.62$ A for CS_2. In any case, CS_2 appears to fit well into a CCl_4 cavity, without necessarily distorting much the arrangement of the other CCl_4 molecules in its neighborhood.

TABLE II. Calculated intensity ratios.

Mode	Solvent	Eq. (I)	Eq. (II)[b]
ν_3 (CS_2)	CCl_4	1.37[a]	1.46
ν_3	C_2Cl_4	1.37[c]	1.46
ν_2	CCl_4	1.37	1.15

[a] Using n_0 (at 6.57μ) = 1.434 for CCl_4 at 20°C; n (at 2μ) = 1.585 for CS_2.
[b] $A=3.38$ A obtained from $MW/N_{Av}=a^3 4\pi/3\,\alpha_z=151.4\times10^{-25}$ cm^3 $\alpha_y=55.4\times10^{-25}$ cm^3; C. P. Smyth, *Dielectric Behavior and Molecular Structure* (McGraw-Hill Company, Inc., New York, 1955), p. 415.
[c] n_0 (at 5.83μ) = 1.477 for C_2Cl_4 at 21°C.

The CS_2 stretching mode intensity in C_2Cl_4 solution is about 10% lower than the one in CCl_4 solution. One may consider a somewhat less spherical cavity for CS_2 in this solvent, but the actual intensity reduction is not nearly that which would be required for an ellipsoidal cavity of the shape of the CS_2 molecule.

The possibility of a noncentrally located dipole in a spherical cavity was also considered.[15] The results show that the intensity ratio A_{soln}/A_{gas} tends to increase as compared to that of the centrally located dipole. Calculation of this effect for an ellipsoidal cavity have not been considered here.

Repulsive forces may be producing an effect in the opposite direction to that of the internal field. Repulsive forces between CS_2 and neighboring CCl_4 molecules might change the polarizability α_x in such a way as to give an effective polarizability α_x and change the

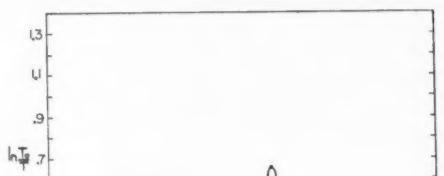

FIG. 6. Absorption band of CCl_4 near 780 cm^{-1} in cyclohexane solution.

[13] Reference 11, p. 74.
[14] A. D. E. Pullin, Spectrochim. Acta **13**, 125 (1958).
[15] Reference 11, p. 101.

ratio $(1-g\alpha_x)^{-1}$. For a spherical cavity, however, in the first approximation, the effect of a repulsive potential appears to be zero for the antisymmetric stretching and bending modes, presumably because the potential energy must be expressed in terms of the totally symmetric normal coordinates Q_1, and the derivatives of the potential energy with respect to the other normal coordinates, Q_3, Q_2 are zero.

Our treatment is limited to nonpolar solute and solvent molecules. Within this general limitation, however, different results are possible depending upon the cavity shape and the magnitudes of the polarizability values along the principal axes. One would need intensity data, both in the gas phase and in solution, for a number of selected molecules, for which different cavity shapes and polarizabilities may be assigned. Such data are still meager and thus it appears premature at this time to discuss further the extent to which our modifications might remedy major experimental discrepancies. We have also left open the question of the effect of short range forces. These may contribute significantly to the intensity changes from gas phase to solution, but the magnitude of these is not yet well understood.

768–797 cm^{-1} FERMI DOUBLET OF CCl_4 IN CYCLOHEXANE SOLUTION

Experimental

The range of concentrations of CCl_4 in cyclohexane was $1–10\times10^{-2}$ moles per liter. The solutions were run "double beam" (on a Perkin-Elmer model 21 instrument) using a 0.112-mm NaCl and a 0.473-mm KBr liquid cell for the solutions and a variable liquid cell set at about 0.109 and 0.468 mm, respectively, for the solvent to compensate for solvent absorption. Because of the shape of the band no wing corrections were applied. Integration was carried out 60 cm^{-1} toward the short wavelength side and 70 cm^{-1} toward the long wavelength side from the approximate center of the band. The area obtained is about 5.4×10^7 cm^{-1}/mole per cm^2 at 25°C. The results are shown on Fig. 6 and Fig. 7.

Comparison with Previous Data

Kagarise[16] determined the intensity of this band in a dilute (10% by volume) solution of CCl_4 in CS_2 at a cell thickness of 5.9×10^{-4} cm. He obtained a value of $A=4.51\times10^5$ cm^{-2}, which he compared with his pure liquid dispersion results of $A=4.77\times10^{-5}$ cm^{-2}. Dividing the A values by moles per cm^3 of CCl_4, one obtains for the CS_2 solution $A_{soln}=4.38\times10^7$ cm^{-1}/mole per cm^2 at 25°C, and from the pure liquid, $A_{soln}=4.63\times10^7$ cm^{-1}/mole per cm^2. Using the dielectric expressions for the solution gas intensity ratios one can calculate $A_{soln\ cyclohex}/A_{soln\ CS_2}$ and this turns out to be about 1. Conversion of the concentration from 10% by volume to moles of CCl_4 per cm^3 leads to $m=1.03\times10^{-3}$ moles per cm^3 and $mL=6.07\times10^{-4}$ moles cm per liter. Kagarise's point is shown on Fig. 7 and is in very good agreement with our more extensive solution measurements. Our A_{soln} value is about 20% higher than his converted solution intensity; this is expected from the slope of the extrapolation line in Fig. 7.

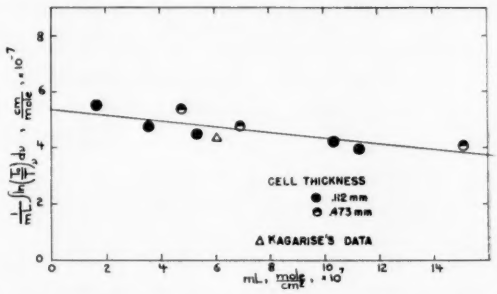

FIG. 7. Intensity of the 768–797 cm^{-1} Fermi doublet of CCl_4 in Cyclohexane solution.

Discussion

Gas phase absolute intensity data are not yet available for this band. Such data would allow determination of the A_{soln}/A_{gas} ratio and it would be of interest to determine whether this is in agreement with the ratio proposed by the dielectric theories of Polo-Wilson or Person, and Buckingham and our modification of these. Since for a triply degenerate mode $\alpha_1=\alpha_2=\alpha_3=\alpha$, in our modification, all of the proposed ratios would be approximately equal to 1.35. The cavity shape could also be considered strictly spherical here so that the conditions, aside from the relative sizes of the solute and solvent, are ideal for testing the dielectric theories.

APPENDIX A. EFFECTIVE FIELD CORRECTION FOR INFRARED INTENSITY OF NONSPHERICAL SOLUTE IN HOMOGENEOUS DIELECTRIC MEDIUM

According to Onsager, the effective field $\mathbf{E}_e$ is given by

$$\mathbf{E}_e=\frac{3\epsilon}{2\epsilon+1}\mathbf{E}+\frac{2(\epsilon-1)}{2\epsilon+1}(\mathbf{p}/r^3)=\mathbf{G}+\mathbf{R}.$$

This becomes identical, upon replacement of ϵ by n^2, with the equation used by Polo and Wilson. Taking for a nonpolar molecule, $\mathbf{p}=\boldsymbol{\alpha}\mathbf{E}_e$ and replacing

$$[2(\epsilon-1)/(2\epsilon+1)](r^3)^{-1}$$

by g, the reaction field factor, we obtain

$$\mathbf{E}_e=[3\epsilon/(2\epsilon+1)]\mathbf{E}+g\boldsymbol{\alpha}\mathbf{E}_e$$

and

$$E_e^2/E^2=[3\epsilon/(2\epsilon+1)]^2[(1-g\alpha)^{-1}]^2.$$

[16] R. E. Kagarise, J. Chem. Phys. **31**, 1258 (1959).

TABLE AI. Effect of cavity shape on predicted intensity ratio for the CS_2 fundamentals.

	Spherical cavity			Ellipsoida cavity		
	Cavity factor $\times 1/n$	Reaction field term $\left(\frac{1}{1-g\alpha_i}\right)^2$	$\frac{A_{soln}}{A_{gas}}$	Cavity factor $\times 1/n$	Reaction field term $\left(\frac{1}{1-g\alpha_i}\right)^2$	$\frac{A_{soln}}{A_{gas}}$
ν_3 mode	1.015	1.43	1.46	0.80	1.14	0.91
ν_2 mode	1.015	1.13	1.15	1.18	1.16	1.37

If we replace ϵ by n^2 and use the additional relations $E_0^2=nE^2$ and $Al/Ag=E_e^2/E_0^2$ used by Polo and Wilson, we obtain

$$Al/Ag=[9n^3/(2n^2+1)^2][(1-g\alpha)^{-1}]^2.$$

This is for a nonpolar liquid; n refers to the refractive index of the medium and α refers to the polarizability of a nonpolar molecule. For a very dilute solution of a nonpolar solute in a nonpolar solvent, n can be taken as the refractive index of the solvent and Al can be replaced by A_{soln}. The above equation becomes then identical with Buckingham's expression for a nonpolar solute in a nonpolar solvent, as mentioned in the discussion of our paper.

If we abbreviate the second equation above, we have

$$\mathbf{E}_e=a\mathbf{E}+g\boldsymbol{\alpha}\mathbf{E}_e.$$

The ir intensity is based fundamentally on electrostatic perturbation, and for a particular mode will be assumed to arise due to a vibrating molecular dipole oriented along molecular axis number 1; further, for axes 1, 2, 3, polarizability is diagonal, and of form

$$\boldsymbol{\alpha}=\begin{pmatrix}\alpha_1 & 0 & 0\\ 0 & \alpha_2 & 0\\ 0 & 0 & \alpha_3\end{pmatrix}.$$

The perturbation energy is

$$\mathbf{p}\cdot\mathbf{E}_e=a\mathbf{p}\cdot\mathbf{E}+g\mathbf{p}\boldsymbol{\alpha}\mathbf{E}_e.$$

We can now compute each of the scalar products in either laboratory, or molecular axes. Let us do so in molecular axes

$$\mathbf{p}\cdot\mathbf{E}_e=p_2(E_e)_2+p_3(E_e)_3+p_1(E_e)_1=p_1(E_e)_1,$$

because of the assumption about the vibrating dipole. Similarly

$$a\mathbf{p}\cdot\mathbf{E}=ap_1E_1 \text{ and } g\mathbf{p}\boldsymbol{\alpha}\mathbf{E}_e=gp_1\alpha_1(E_e)_1.$$

Hence, $$p_1(E_e)_1=ap_1E_1+gp_1\alpha_1(E_e)_1$$

or $$p_1(E_e)_1=[a/(1-g\alpha_1)]p_1E_1.$$

Now we have merely to calculate E_1 and $(E_e)_1$ in terms of components in laboratory axes; without loss of generality, assume $E_x=0$, $E_y=0$, $E_z=E$. Then[17]

$$E_1=\Phi_{1x}E_x+\Phi_{1y}E_y+\Phi_{1z}E_z.$$

Now $p_1(E_e)_1$ is the perturbation energy, and the transition probability is therefore governed by it:

Transition probability $\sim[a/(1-g\alpha_1)]^2p_1^2E^2$. Since $a\rightarrow 1$ and $b\rightarrow 0$ in vacuum, and since $E=E_0/(n)^1$:

Transition probability $\sim p_1^2E^2=p_1^2E_0^2$ in vacuum (dilute gas). Thus the correction factor is

$$A_{soln}/A_{gas}=n^{-1}[a/(1-g\alpha_1)]^2.$$

Spherical case. If

$$\alpha_1=\alpha_2=\alpha_3, \text{ then } \alpha=\tfrac{1}{3}(\alpha_1+\alpha_2+\alpha_3)=\alpha_1.$$

Under this condition upon substitution of the Clausius-Mossotti expression for the value of α one obtains Person's equation for solutions and Polo-Wilson's for liquids.

Nonspherical case. If $\alpha_1\neq\alpha_2=\alpha_3$ we have for

$$(A_{soln}/A_{gas})_1>(A_{soln}/A_{gas})_{Person}>(A_{soln}/A_{gas})_2.$$

APPENDIX B. EFFECTIVE FIELD IN ELLIPSOIDAL CAVITY

In Table AI we listed the result of calculations carried out for spherical and ellipsoidal cavities. For the ellipsoidal cavity we used the ideas of the previous appendix except that both a and b depend now also on the particular mode. For CS_2 the direction of the long axis of the molecule is taken to coincide with the direction of the major axis of the ellipsoid. Expressions for a and b are given by Böttcher. We used ellipsoids of the same volume as the sphere above.

[17] See E. B. Wilson, Jr., J. C. Decius and P. C. Cross, *Molecular Vibrations* (McGraw-Hill Book Company, Inc., New York, 1955), p. 164.

THE JOURNAL OF CHEMICAL PHYSICS VOLUME 35, NUMBER 6 DECEMBER, 1961

s-Tetrazine. I. High-Resolution Vapor-Phase Study of the Visible $n \rightarrow \pi^*$ Vibronic Absorption Band Systems†

GLENN H. SPENCER, JR.,‡ PAUL C. CROSS, AND KENNETH B. WIBERG
Department of Chemistry, University of Washington, Seattle 5, Washington

(Received October 31, 1960)

The low-resolution electronic spectrum of *s*-tetrazine vapor has been measured down to about 190 mμ, and the complex systems of vibronic bands that comprise the $n \rightarrow \pi^*$ visible absorption spectrum have been studied under higher resolution. These latter spectra were photoelectrically recorded in the third order of a 21-ft grating spectrograph, using path lengths from 0.05 to 48 m and temperatures from −70° to 70°C. In the absorption region, 4500 to 6100 A, the spectrum consists of over 500 sharp, vibronic band peaks. Their collected *Q*-branch maxima have been measured to the nearest cm^{-1}, but no discrete rovibronic structure was resolved.

The outstanding feature of the visible spectrum is a set of four intense progressions, each of which is propagated by the consecutive excitation of the same vibration (believed to be the totally symmetric mode 6*a*). In the ground state, the frequency of this vibration is 737 cm^{-1} for *s*-tetrazine-d_0 and 720 cm^{-1} for *s*-tetrazine-d_2; these frequencies drop to about 700 and 690 cm^{-1}, respectively, in the excited $n \rightarrow \pi^*$ state(s). From simple molecular orbital theory and the Herzberg-Sponer-Teller selection rules, a plausible, preliminary, singlet absorption model is developed and is qualitatively applied to the spectral data. Because there may be an "almost accidental degeneracy" of some of the $n \rightarrow \pi^*$ states of the azines (excluding pyridine), the need for a more elaborate model that will properly treat the electronic-vibrational interaction problem is emphasized. Although a complete vibronic analysis has not yet been obtained, the presence of three electronic transitions forbidden on the basis of D_{2h} excited state molecular symmetry, as well as the electronically allowed $n \rightarrow \pi^*$ transition, is suspected.

1. INTRODUCTION

THE symmetrical tetrazine molecule $C_2H_2N_4$ is one of an isoelectronic family (homologous with benzene) of eleven possible heterocyclic, nitrogen-containing, aromatic, six-membered ring compounds named the azines, of which six so far have yielded to the techniques of chemical synthesis. This is the first of a series of papers that will be concerned in general with the infrared, visible, and ultraviolet spectra of *s*-tetrazine, and in particular, with the understanding of the energetics of its four lone pairs of nitrogen, nonbonding electrons. In order to aid in the interpretation of the molecular spectra of *s*-tetrazine, certain correlations of its electronic and vibrational dynamics with those of benzene and the other azines have been examined. Involved primarily with experimental details, this first paper reports some of the electronic spectral data that we have obtained for *s*-tetrazine. However, because the finer aspects of a general $n \rightarrow \pi^*$ theory for the azines have not yet been well formulated, only certain general, qualitative arguments pertaining to the vibronic analysis of the visible spectrum can be presented at this time. Since our study of this spectrum may be of interest to persons investigating the nature of other $n \rightarrow \pi^*$ transitions or the problem of electronic-vibrational interaction, the experimental results from this study are herein reported.

A drawing of the *s*-tetrazine molecule is presented in Fig. 1 showing the approximate bond angles and distances that have been determined by the x-ray diffraction studies of Bertinotti, Giacomello, and Liquori.[1,2] The molecule is reported to be planar in the ground electronic state, has a molecular symmetry given by the point group $D_{2h}(V_h)$, and is an asymmetric rotor. What little is known about the chemistry of *s*-tetrazine has been well summarized recently in a monograph by Erickson, Wiley, and Wystrach.[3] However, the fundamental vibrational frequencies of *s*-tetrazine have not yet been generally discussed in the literature from either

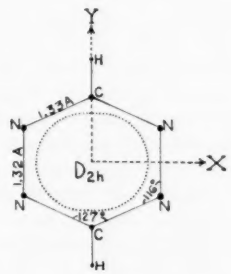

FIG. 1. The geometry of the *s*-tetrazine molecule.

† Work supported in part by the U.S. Air Force Office of Scientific Research, Air Research and Development Command. It represents part of the Ph.D. thesis research of GHS and was reported in part at the Ohio State Molecular Structure and Spectroscopy Symposium, June, 1959.

‡ National Science Foundation Postdoctoral Research Fellow (1958–59) at Harvard University. Present address: Department of Chemistry, Stanford University, Stanford, California.

[1] F. Bertinotti, G. Giacomello, and A. M. Liquori, Acta Cryst. **8**, 513 (1955); **9**, 510 (1956).

[2] In this and in future discussions of the symmetry properties of the azines, we shall adopt the convention that these molecules lie in an *XY* plane. A twofold axis passing through atoms will then be taken as the *Y* axis; for pyridazine, however, the *X* axis is taken as the twofold axis to emphasize that the symmetry axis bisects bonds.

[3] J. G. Erickson, P. F. Wiley, and V. P. Wystrach, *The Chemistry of Heterocyclic Compounds, Monograph Series, Tenth Volume. The 1,2,3- and 1,2,4-Triazines, Tetrazines, and Pentazines* (Interscience Publishers, Inc., New York, 1956).

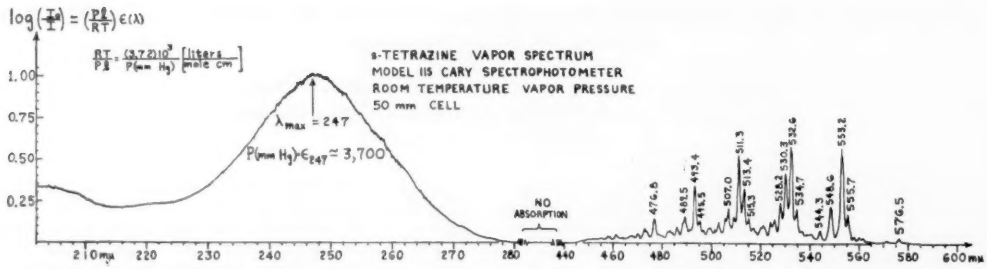

FIG. 2. The visible and near ultraviolet spectrum of *s*-tetrazine vapor under low resolution. Comparison with high-resolution spectra suggests a calibration correction of -1.5 mμ to the indicated wavelengths.

an experimental or theoretical point of view.[4] The molecule, which has not been found in nature, is a red solid and is metastable with respect to decomposition at room temperature, but may be sublimed at 99°C. Its room temperature decomposition rate is strongly increased upon exposure of the vapor to the intense illumination of the light sources usually used in spectroscopic studies. Although *s*-tetrazine crystals may be stored in the dark at -5°C for several months without appreciable decomposition, they decompose in a few days in a stoppered, air-containing glass vial at room temperature under normal lighting conditions. The kinetics of the decomposition has not yet been studied, but we know that at least one of the immediate decomposition products is a solid and that hydrogen cyanide is produced. No vapor pressure studies have yet been performed, but we estimate that at 25°C the pressure of *s*-tetrazine vapor is between 0.1 and 1.5 mm Hg. Because they are not well understood, some interesting thermochromic effects that are observed with *s*-tetrazine in a condensed phase deserve mentioning. A compact collection of crystals of *s*-tetrazine, which appears quite red at 298°K, turns continuously more orange as the temperature is reduced, and appears yellow-orange at 78°K. Yet solutions of *s*-tetrazine in various low-melting solvents show no yellowing of their room temperature red color as the temperature is reduced to 195°K.

The red color that visually characterizes a room temperature assembly of *s*-tetrazine molecules is now considered to be the collective, chromatic consequence of $n\rightarrow\pi^*$ absorption transitions. According to the prevalent model of $n\rightarrow\pi^*$ transitions in the azine molecules, one pictures the excitation of one of the nitrogen lone-pair electrons from its ground state, more or less localized, nonbonding molecular orbital n to one of the vacant, delocalized, more energetic, antibonding molecular orbitals π^* of the ring. A valuable review of work that has been reported on electronic transitions involving nonbonding electrons of polyatomic molecules has recently been given by Sidman[5] in which the definitive work of Kasha, Platt, and others is well discussed. Hirt[6] was perhaps the first to specifically point out the $n\rightarrow\pi^*$ character of the visible absorption spectral data of *s*-tetrazine that has been reported by other workers,[7–12] and satisfaction of the criteria proposed by Kasha[13] for distinguishing between $n\rightarrow\pi^*$ and $\pi^*\rightarrow\pi^*$ transitions is perhaps not more easily demonstrated in the solution spectra of any other molecule.[14] It is of historical interest to note that in 1913 Koenigsberger[8] had already expressed a healthy curiosity regarding the special nature, the characteristically sharp structure, of the visible spectrum.

2. VAPOR-PHASE ELECTRONIC SPECTRUM UNDER LOW-RESOLUTION

The electronic absorption spectrum of *s*-tetrazine vapor shown in Fig. 2 was taken with a Cary recording spectrophotometer, model 11S. The millimicron values labeling certain peaks of the spectrum are direct, uncalibrated spectral readings. From a comparison with the high-resolution results, Fig. 3, and from an analysis of all of the errors involved, it appears that the mean uncertainty inherent in the measurement of the wavenumber difference between two peaks of this spectrum is at least ± 11 cm^{-1}. Thus it would be extremely diffi-

[4] In the second paper of this series we shall present the results of our studies on the infrared absorption spectra of various mixtures of *s*-tetrazine-d_0, -d_1, and -d_2. Because descriptions of most of the somewhat ambiguous preparative chemical details are spread over a number of papers in the German literature before the turn of the nineteenth century, we shall also give there a brief discussion of a convenient synthesis and the deuteration of *s*-tetrazine.

[5] J. W. Sidman, Chem. Revs. **58,** 689 (1958).
[6] R. C. Hirt and R. G. Schmitt, J. Chem. Phys. **23,** 600 (1955).
[7] T. Curtius, A. Darapsky, and F. Muller, Ber. **40,** 84 (1907).
[8] J. Koenigsberger and K. Vogt, Physik. Z. **14,** 1269 (1913).
[9] E. Müller and L. Herrdegen, J. prakt. Chem. **102,** 113 (1921).
[10] C. Lin, E. Lieber, and J. Horwitz, J. Am. Chem. Soc. **76,** 472 (1954).
[11] A. M. Liquori and A. Vaciago, Ricerca sci. **26,** 181 (1956).
[12] S. F. Mason, J. Chem. Soc. **1959,** 1240, 1263, 1269.
[13] M. Kasha, Discussions Faraday Soc. **9,** 14 (1950). See Sidman's review article (reference 5) for references to more recent work by McConnell, Pimentel, Platt, and Brealey and Kasha.
[14] Low-resolution studies of the temperature dependence and red and blue shifts of the *s*-tetrazine absorption spectrum have been carried out (reference 20), and the spectra published by Mason (reference 12, p. 1265) are in excellent agreement with our low-resolution visible spectra taken under corresponding conditions. It is of interest to point out that our high-resolution visible spectrum of a pure, 80°K *s*-tetrazine film is almost identical with Mason's Cary spectrum of *s*-tetrazine in a 77°K 5:1 isopentane-methylcyclohexane glass; i.e., a liquid nitrogen cooled crystal is too warm for the resolution of much crystal vibronic structure.

cult to perform more than a very crude vibronic analysis of the *s*-tetrazine visible band systems from low-resolution absorption data alone even if all of the fundamental vibrational frequencies in the ground electronic state and a good electronic model for the visible absorption had been established.

The *s*-tetrazine vapor spectrum shows no appreciable absorption in the region between 290 and 430 mμ, $\log(I_0/I)$ certainly being less than 0.01 for a 50-mm path of *s*-tetrazine vapor at or near its room temperature vapor pressure. If it is assumed that this pressure is approximately 1 mm Hg, $\epsilon(247\ \text{m}\mu) \approx 3700$ and $\epsilon(532.6\ \text{m}\mu) \approx 2200$ liters/mole-cm. From rough intensity measurements,[14] the oscillator strength of the visible absorption spectrum of a room temperature, 0.001 *M* solution of *s*-tetrazine in cyclohexane is estimated to be about $(8\pm4)10^{-3}$, corresponding to a transition moment of about $(20\pm5)10^{-2}$ A.

We have also made an attempt to obtain the spectrum of *s*-tetrazine vapor in the region between 190 and 203 mμ with a Beckman DU spectrophotometer. Admittedly, the measurements were quite crude, but there does appear to be a pair of absorption maxima in this region at about 191 and 193 mμ, each of about 3000 in extinction coefficient.

Because it does not present enough quantitative information different from that contained in Fig. 2, our Cary spectrum of a gaseous sample of a deuterated *s*-tetrazine mixture (88% d_2, 11% d_1, 1% d_0) is not given here. Although there are real, but only roughly measurable blue and red shifts of the main peaks, of the order of 0.5 to 2.0 mμ, the general, over-all appearance of the low-resolution visible absorption spectrum of natural *s*-tetrazine vapor remains invariant to deuteration.[15]

3. HIGH-RESOLUTION n→π* SPECTRA

A more highly resolved absorption spectrum of the visible $n\rightarrow\pi^*$ transitions of *s*-tetrazine vapor is presented in Fig. 3. It was taken photoelectrically in the third diffraction order of a kinematically focused 21-ft concave-grating spectrometer, the 6-in. 1500-line/in. grating of which is Eagle mounted, as previously described,[16] on a chord of the Rowland circle. In order to confirm our belief that the absorption bands in the visible region represented vibronic transitions to the lowest singlet electronic states of *s*-tetrazine, we also explored the region beyond 610 mμ to the first-order, long wavelength limit of this spectrometer, about 1800 mμ, using a lead sulfide detector. No appreciable absorption was found for long paths of room temperature *s*-tetrazine vapor in this region.

3.1 Experimental Arrangement

In order to secure long light paths through *s*-tetrazine vapor, a cylindrical, multiple-reflection 2-m glass absorption cell[17] of the type previously employed in this laboratory was used for path lengths of 4 to 48 m.[18] Any particular cell vapor temperature between −72 and 75°C could be maintained within a degree or two by rapidly circulating an appropriately cooled or heated liquid through Tygon tubing wrapped tightly around the entire cell.

A 500-w tungsten-filament projection bulb, supplied by 115-v, regulated dc power, was used as a radiation source, and an RCA 1P21 (S4) photomultiplier tube (maximum sensitivity near 500 mμ) was used as a detector. The method of phase sensitive detection[18] was employed with a chopping frequency of 240 cps, the spectrum being displayed on a Leeds and Northrup dual pen recorder. The exit slitwidth of the spectrometer was fixed at 0.08 mm. For short cell vapor path lengths of the order of 4 m or less, an entrance slitwidth of 0.1 mm was used; for an equivalent signal-to-noise ratio using a 48-m path length, an entrance slitwidth of about 0.3 mm was necessary at 5000 A at the expense of resolution.

Emission lines from a hollow cathode, iron-neon discharge tube[19] and detected by an RCA 1P28 (S5) photomultiplier tube (maximum sensitivity near 340 mμ) were used for calibration by taking the mean wavelengths of emission lines obtained immediately before and after the recording of the absorption spectra.

The high-resolution spectrum was taken at a scanning speed such that the absorption between 16 000 and 23 000 cm^{-1} in the third order could be continuously recorded in about 3 hr on a 30 ft length of chart paper. A scanning speed such that this region could be covered in about 12 min was also used, mainly for relative intensity studies.

3.2 Accuracy of the Wavelength Calibration and Relative Intensity Measurements

The wavenumber (not corrected to vacuum) and percentage absorption, $\%A = 100 - I$, where I_0 is set equal to 100, of each of the 517 strongest absorption peaks in the high-resolution visible spectrum of *s*-tetrazine vapor are given in Table I. They are arranged so as to show clearly their tabular representation of the spectrum given in Fig. 3; the cm^{-1} and $\%A$ values correspond to the conditions of path length and temperature of saturated vapor marked on the eight sections of the spectrum.

[15] Mason (reference 12) reports that the *s*-tetrazine-d_2 peak that corresponds to the natural *s*-tetrazine 18 134 cm^{-1} peak is about 15 cm^{-1} lower in energy. Both our high- and low-resolution work indicate that this peak is at about 18 140 and 18 147 (±4 cm^{-1}) for *s*-tetrazine-d_1 and *s*-tetrazine-d_2, respectively. This disagreement with Mason has been substantiated by the experimental studies of Hexter and Kiefer (private communication). Our high-resolution studies do show, however, that certain of the other prominent vibronic bands do shift to the red upon deuteration; e.g., the 18 283 cm^{-1} band of *s*-tetrazine-d_0 shifts to about 18 273 (±4 cm^{-1}) in *s*-tetrazine-d_2.

[16] E. Bair, P. Cross, T. Dawson, E. Wilson, and J. Wise, J. Opt. Soc. Am. **43,** 681 (1953).

[17] J. U. White, J. Opt. Soc. Am. **32,** 285 (1942).

[18] E. Bair, J. Lund, and P. Cross, J. Chem. Phys. **24,** 961 (1956).

[19] H. Crosswhite, G. Dieke, and C. Legagneur, J. Opt. Soc. Am. **45,** 270 (1955).

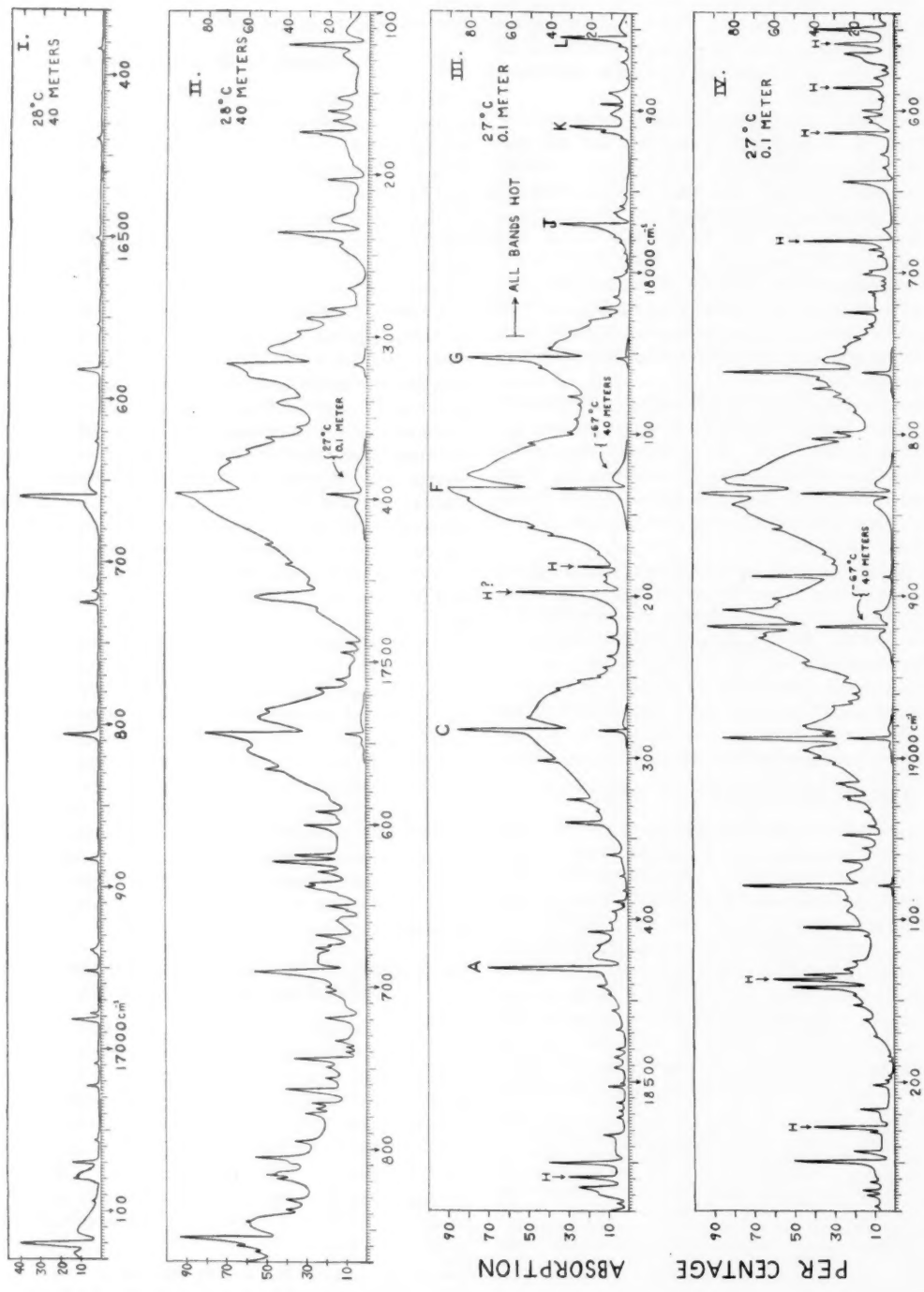
I.
28°C
40 METERS
II.
28°C
40 METERS
-27°C
0.1 METER
III.
27°C
0.1 METER
ALL BANDS HOT
-67°C
40 METERS
IV.
27°C
0.1 METER
-67°C
40 METERS
PER CENTAGE ABSORPTION
17000cm⁻¹
18500
17500
18000cm⁻¹
19000cm⁻¹

FIG. 3(a).

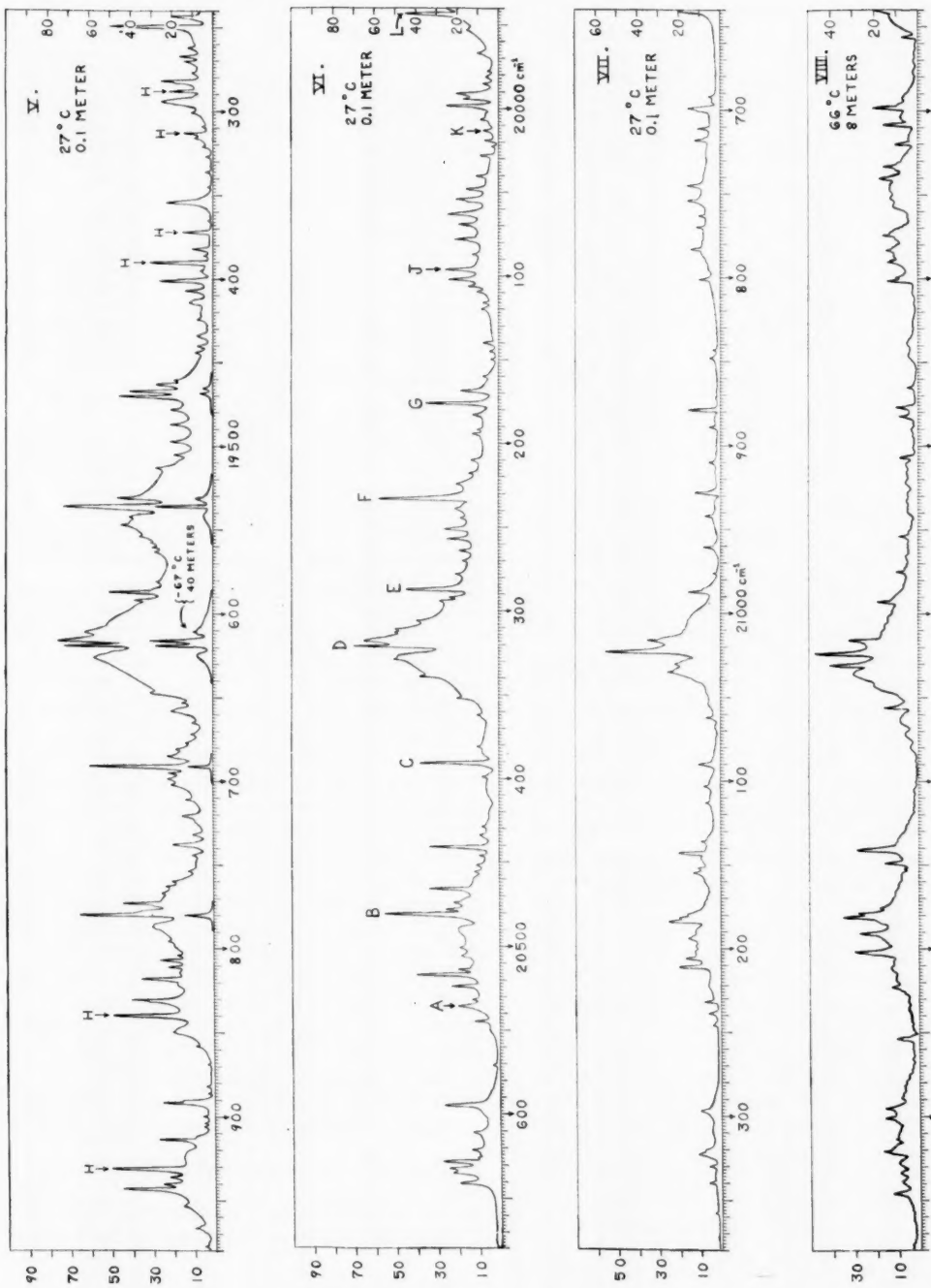

FIG. 3. A high-resolution spectrum of the visible $n \rightarrow \pi^*$ vibronic absorption band systems of *s*-tetrazine vapor (vacuum uncorrected reciprocal wavelength scale).

FIG. 3 (b).

TABLE I. The vacuum uncorrected reciprocal wavelength and percentage absorption for the 517 strongest peaks in the high-resolution $n \rightarrow \pi^*$ spectrum of *s*-tetrazine vapor. These values form a tabular representation of Fig. 3.

cm^{-1}	%A
Section I	
16 384.0	3
16 438.9	3
16 501.0	3
16 554.1	2
16 581.8	12
16 625.8	3
16 659.8	40
16 718.0	4
16 725.3	10
16 805.6	18
16 883.4	8
16 938.6	5
16 952.2	8
16 978.0	5
16 982.0	14
17 009.0	3
17 022.8	7
17 056.1	3
17 069.7	14
17 080.4	13
17 094.3	4
I & II	
17 119.6	40
Section II	
17 152.8	16
17 160.9	21
17 166.9	18
17 174.0	35
17 202.6	20
17 235.9	45
17 269.6	10
17 283.2	20
17 288.5	30
17 296.8	35
17 317.2	70
17 340.8	45
17 355.7	35
17 362.5	50
17 370.4	60
17 375.7	70
17 396.8	95
17 428.4	50
17 440.1	40
17 460.5	55
17 488.2	10
17 493.7	12
17 510.5	15
17 515.7	25
17 528.9	50
17 544.0	80
17 565.7	50
17 591.9	25
17 600.5	30
17 619.4	35
17 623.3	46
17 628.6	24
17 635.7	28
17 637.5	30
17 650.0	20
17 658.7	15
17 667.7	25
17 676.0	25
17 691.0	55
17 699.5	20
17 702.8	20
17 719.4	20
17 733.3	15
17 736.6	10
17 739.6	10
17 744.2	35
17 749.4	20
17 755.8	20
17 762.9	40
17 771.6	27
17 774.6	25
17 778.3	30
17 794.9	35
17 804.7	55
17 815.7	50
17 818.5	45
17 830.8	40
17 837.3	40
	II III
17 844.7	60 —
17 855.3	93 35
17 859.6	65 6
17 863.3	55 3
17 869.6	60 5
Section III	
17 879.8	2
17 889.0	11
17 896.4	15
17 901.6	10
17 910.1	30
17 913.2	15
17 917.0	5
17 951.9	3
17 958.5	5
17 963.0	8
17 970.3	35
17 977.5	8
17 980.7	5
17 988.0	3
17 992.5	2
17 998.5	2
18 003.3	8
18 015.1	8
18 021.5	15
18 025.6	10
18 030.4	20
18 037.2	30
18 046.5	40
18 052.9	80
18 059.3	45
18 076.7	30
18 081.6	25
18 090.6	27
18 099.4	30
18 105.5	50
18 126.7	80
18 133.9	90
18 141.1	80
18 157.8	50
18 163.0	40
18 173.8	15
18 181.7	25
18 186.6	12
18 190.6	12
18 198.2	55
18 213.7	10
18 225.0	10
18 237.3	10
18 243.9	12
18 248.9	15
18 252.3	25
18 257.0	35
18 275.7	50
18 283.0	85
18 301.5	45
18 325.8	30
18 332.9	15
18 339.7	30
18 359.7	10
18 372.6	4
18 382.2	2
18 389.4	7
18 391.4	3
18 395.2	8
18 401.7	9
18 407.8	20
17 416.1	15
18 430.5	70
18 440.9	15
18 446.0	10
18 456.0	8
18 468.2	6
18 479.6	6
18 485.2	7
18 490.7	7
18 501.2	4
18 503.3	10
18 512.7	6
18 518.0	5
18 521.8	6
18 532.0	12
III & IV	
18 549.9	40
18 559.4	30
18 565.0	25
18 574.6	6
18 579.9	10
Section IV	
18 586.2	30
18 592.6	7
18 599.7	15
18 603.6	15
18 607.5	12
18 614.2	35
18 627.1	6
18 635.3	5
18 643.5	25
18 672.5	5
18 681.2	45
18 686.2	12
18 689.5	8
18 699.2	12
18 701.0	15
18 705.4	6
18 708.2	6
18 711.9	12
18 713.7	10
18 724.6	25
18 731.8	12
18 735.4	14
18 739.8	20
18 745.6	25
18 754.0	35
18 761.7	85
18 765.7	38
18 771.9	40
18 776.7	30
18 780.3	25
18 786.5	20
18 799.4	30
18 803.1	40
18 828.5	85
18 837.0	95
18 844.4	80
18 858.9	60
18 874.1	35
18 879.7	30
18 888.3	70
18 902.1	60
18 908.8	85
18 918.6	92
18 923.5	65
18 926.1	67
18 940.8	45
18 952.5	25
18 960.4	20
18 964.9	22
18 968.3	30
18 979.7	45
18 985.4	35
18 988.1	85
18 995.3	45
18 999.8	40
19 004.4	30
19 016.2	28
19 023.9	25
19 025.8	22
19 032.7	14
19 041.9	12
19 048.0	25
19 055.7	15
19 063.7	25
19 078.8	75
19 088.4	25
19 094.6	23
19 105.4	45
19 110.1	14
19 126.0	20
19 130.7	25
19 134.6	45
19 137.3	60
19 142.0	50
19 147.1	20
19 152.5	20
19 162.3	15
19 171.7	10
19 183.9	3
19 186.6	2
19 195.7	3
19 198.8	4
19 202.4	10
19 216.9	17
19 228.0	40
19 231.2	12
IV & V	
19 243.1	20
19 249.4	50
19 262.1	12
19 267.3	16
19 270.1	14
19 277.3	10
Section V	
19 281.7	25
19 288.1	21
19 294.1	25
19 300.5	10
19 309.3	5
19 312.9	14
19 314.9	9
19 321.4	5
19 327.4	3
19 335.9	3
19 345.1	2
19 354.4	22
19 364.9	2
19 371.8	14
19 382.4	9
19 386.0	4
19 390.1	30
19 394.6	6
19 401.1	25
19 407.2	13
19 413.7	11
19 424.3	7
19 434.2	7
19 439.9	7
19 444.4	8
19 460.5	18
19 462.9	27
19 466.7	40
19 470.4	45
19 477.5	20
19 486.5	20
19 497.0	20
19 505.0	18
19 512.8	27
19 531.0	46
19 535.8	72
19 542.1	40
19 546.5	44
19 553.6	35
19 557.6	30
19 560.5	29
19 563.4	28
19 581.0	27
19 586.9	50
19 591.9	38
19 610.9	62
19 616.0	75
19 619.3	72
19 625.7	58
19 646.9	30
19 653.1	15
19 658.4	20
19 664.8	10
19 672.4	10
19 677.1	13
19 681.4	18
19 684.8	22
19 690.8	60
19 694.6	22
19 698.5	22
19 701.9	20
19 711.3	13
19 721.2	15
19 732.0	10
19 738.2	20
19 744.5	10
19 753.9	12
19 759.6	20
19 763.0	23
19 766.9	25
19 772.8	44
19 780.4	65
19 787.3	30
19 795.6	22
19 804.3	18
19 807.4	26
19 811.3	22
19 818.3	35
19 830.6	40
19 840.3	48
19 849.9	20
19 858.3	9
19 868.7	3
19 881.8	4
19 886.3	3
19 891.7	25
19 899.6	5
19 903.6	5
19 906.2	5
19 914.4	27
19 930.6	50
19 936.0	22
V & VI	
19 940.0	25
19 943.0	45
19 952.9	15
19 966.6	10
19 977.5	5
Section VI	
19 980.7	6
19 984.7	7
19 990.8	20
19 994.1	17
19 998.2	25
20 006.4	8
20 013.2	7
20 018.5	6
20 022.5	3
20 027.9	8
20 039.8	10
20 047.5	15
20 054.4	20
20 062.9	24
20 069.4	19
20 077.6	21
20 086.5	12
20 096.3	25
20 101.6	24
20 105.7	14
20 109.4	10
20 115.7	7
20 119.9	8
20 140.1	7
20 145.2	4
20 149.9	3
20 160.0	7
20 168.5	18
20 176.1	35
20 183.2	12
20 191.7	10
20 194.5	12
20 210.2	13
20 217.6	14
20 224.4	20
20 233.3	58
20 239.3	21
20 244.5	18
20 250.9	26
20 257.4	25
20 263.7	19
20 269.8	17
20 277.8	20

Table I (*continued*)

cm^{-1}	%A	cm^{-1}	%A	cm^{-1}	%A
20 286.7	44	20 473.7	22	Section VII	
20 291.5	23	20 478.0	26		
20 294.3	28	20 481.4	55	20 691.9	5
20 305.6	39	20 500.9	19	20 698.8	15
20 311.3	50	20 505.8	18	20 711.1	10
20 313.2	50	20 514.1	20	20 718.0	12
20 317.9	65	20 517.0	40	20 744.6	17
29 320.7	70	20 524.4	23	20 754.1	17
20 328.6	50	20 531.7	13	20 763.0	10
20 339.3	38	20 535.7	20	20 770.1	11
20 352.1	20	20 544.7	12	20 783.1	14
20 361.8	10	20 571.0	3	20 800.9	10
20 381.2	10	20 595.2	27	20 842.8	3
20 390.8	38	20 611.0	13	20 848.2	5
20 399.4	8	20 621.4	14	20 879.4	15
20 428.7	8	20 627.9	28	20 888.6	5
20 433.6	9	20 632.4	25	20 910.4	5
20 440.8	34	20 634.9	23	20 928.1	13
20 445.6	9			20 941.7	7
20 451.9	11	VI & VII		20 960.5	8
20 456.3	12			20 975.7	3
20 465.9	34	20 641.4	20	20 987.5	15

cm^{-1}	%A	cm^{-1}	%A	cm^{-1}	%A
21 016.2	35	VII VIII		21 693.2	18
21 022.6	55			21 715.5	31
21 030.5	22	21 339.8	6 20	21 723.7	47
21 034.7	25	21 357.5	3 7	21 731.3	40
21 062.3	6			21 756.1	15
21 090.0	10	Section VIII		21 841.0	28
21 102.8	8			21 849.3	15
21 112.5	7	21 398.2	20	21 881.1	34
21 135.6	9	21 408.2	15	21 891.4	27
21 142.5	20	21 419.5	10	21 901.5	29
21 152.2	11	21 433.0	15	21 923.3	12
21 155.5	13	21 440.3	17	21 954.8	10
21 185.0	25	21 473.6	15	21 995.0	15
21 194.4	15	21 483.2	14	22 000.5	15
21 205.8	17	21 489.5	13	22 021.3	15
21 211.0	20	21 500.8	13	22 045.9	12
21 231.7	8	21 564.7	5		
21 238.7	6	21 577.3	10	Not Plotted	
21 246.2	4	21 582.5	8		
21 297.2	10	21 607.3	8	22 431.6	5
21 322.9	11	21 653.6	8	22 533.9	4
21 330.3	6	21 674.6	9	22 578.3	3

In the calibration process,[20] vacuum uncorrected interferometric wavelengths were used for those hollow cathode iron-neon discharge emission lines for which they are known.[21] Parts of the absorption spectrum could be measured in the second and fourth orders, and calibration of spectra taken in these two orders provided a good check on the accuracy of the calibration of the third-order spectra. In general, from considerations of all errors throughout the entire calibration procedure, the reciprocal wavelengths given in Table I should be uncertain by no more than ± 1 cm^{-1}.

Relative intensity measurements were only qualitatively successful; the photodecomposition of the vapor over the rather long scanning times prevented the accurate estimation of vibrational frequencies in the ground electronic state from the temperature dependence of the Boltzmann factor. However, by scanning the spectrum both forwards and backwards with respect to wavelength, and by examining the temperature dependence of the relative intensities of a few bands in a small region of the spectrum, we have been able to assign rough values of the relative percentage absorption and to pick out a few bands that definitely represent transitions from a vibrationally excited ground electronic state (hot bands). A reasonably good estimate of the uncertainty in the %A value is $\pm(\%A)^{\frac{1}{2}}$.

3.3 General Features of the $n\rightarrow\pi^*$ Spectrum

The spectrum has been presented in eight sections to emphasize the many striking, obvious progressions that appear. The ten most prominent progressions are tabulated in Table II. They are of the general symbolic form $[n(700)+y\leftarrow x+m(737)]$, where m and n are integers that denote the degree of excitation of a totally symmetrical vibrational mode which has a frequency of 737 and 700 cm^{-1} in the ground and excited electronic state(s), respectively, and x and y denote the, as yet unknown, degree of further vibrational excitation in the ground and excited electronic state(s), respectively. It seems clear that x is zero for most of the progressions. Notice that progressions are not prominent when n and m are both simultaneously unequal to zero. There are a number of shorter, less intense progressions that also involve the 737 and 700 cm^{-1} spacings, but no clearly defined progressions involving any other frequencies have been located (see Appendix). All vibronic bands at energies below 18 040 cm^{-1} are believed to be hot. Some of the stronger vibronic bands above 18 040 cm^{-1} which are also believed to be hot are labeled in Fig. 3 with an **H**.

We believe that our data reflect the presence of anharmonicity in the excited state(s) 700 cm^{-1} mode (possibly vibrational interaction as well). The deviations of the successive frequency differences within any one progression can not all be interpreted in terms of uncertainties in the measurement of wavelength. While it is true that the center of a vibronic band may be displaced by one or two wave numbers from the frequency of the sharp absorption maximum,[22] nevertheless this error tends to cancel out in taking frequency differences within a progression. Thus the values of the differences

[20] The details of the calibration procedure are described in the Ph.D. thesis of GHS, University of Washington, Seattle (1958). L. C. Card No. Mic 59-1239.

[21] H. M. Crosswhite and G. H. Dieke, "Section 7g" in *American Institute of Physics Handbook* (McGraw-Hill Book Company, Inc., New York, 1957).

[22] If azine moments of inertia for the excited $n\rightarrow\pi^*$ states are as nearly identical to the ground state moments as is now believed (reference 12), the energy of the sharp band maximum may be a very good approximation to the $0_0\rightarrow 0_0$ transition energy (J_r notation). In regard to this matter, we would like to thank Professor K. K. Innes for showing us his rovibronic analysis results for certain $n\rightarrow\pi^*$ bands of pyridazine.

TABLE II. The ten most prominent vibronic band progressions in the high-resolution $n\rightarrow\pi^*$ absorption spectrum of *s*-tetrazine vapor (values in cm^{-1}, vacuum corrected). All of the frequencies in column labeled **H** and in spectrum sections **I** and **II** (see Fig. 3) represent bands that are suspected of being hot.

	Vibronic band progression symbol									
Sec. No.	*A*(**H**)	*B*(**H**)	*C*	*D*	*E*(**H**?)	*F*	*G*	*J*(**H**)	*K*(**H**)	*L*(**H**)
I	16 948 738		16 801 738		16 721 735	16 655 737	16 577 736	16 496 735	16 434 735	16 379 736
II	17 686 739		17 539 739		17 456 737	17 392 737	17 313 735	17 231 735	17 169 736	17 115 736
III	18 425 707	18 335? 739	18 278 705	18 177? 736	18 193? 690	18 129 703	18 048 709	17 966 710	17 905 704	17 851 694
IV	19 132 703	19 074 701	18 983 702	18 913 701	18 883 699	18 832 698	18 757 708	18 676 709	18 609 699	18 545 699
V	19 835 695	19 775 701	19 685 700	19 614 701	19 582 699	19 530 698	19 465 706	19 385 706	19 308 700	19 244 694
VI	20 530	20 476 703	20 385 699	20 315 702	20 281 701	20 228 694	20 171 703	20 091 704	20 008	19 938 698
VII		21 179 696	21 084	21 017 701	20 982 705	20 922	20 874	20 795		20 636
VIII		21 875		21 718	21 687					

given in Table II are probably in error by less than three wave numbers. The reasonable constancy of the common ground-state frequency of 737 cm^{-1} verifies this. In particular, progressions **G** and **J** show upper-state vibrational spacings of this α_9 mode that are measurably larger than those for the other progressions. This suggests that these two progressions might be associated with an excited electronic state different from those represented by the other progressions.

Our high-resolution spectrum of *s*-tetrazine-d_2 vapor (slightly contaminated with the $-d_1$ and $-d_0$ forms) shows that the characteristic progression frequencies for dideuterotetrazine, analogous to the 737 and 700 cm^{-1} spacings in the natural *s*-tetrazine vapor spectrum, are 720 and approximately 690 cm^{-1}, respectively.

4. DEVELOPMENT OF A SIMPLE ELECTRONIC MODEL

It is conceivable that a direct trial-and-error approach to the analysis of the $n\rightarrow\pi^*$ vibronic band systems could hit upon a successful, unambiguous interpretation of the *s*-tetrazine electronic spectral data so far collected. In view of the numerous papers written on the 2600 A band system of benzene, however, it seems unlikely that such an approach could produce a unique and satisfactory set of vibronic assignments for all of the major bands without further experimental data. Such an approach would suffer mainly because 10 of the 18 ground-state fundamental vibrational frequencies are as yet unknown, and seven of the remaining eight, obtained from our infrared studies,[4] are only tentative. Undoubtedly, the normal coordinates, frequencies, polarizations, and other data utilizable in developing an understanding of the molecular vibronics of *s*-tetrazine will eventually be obtained. For the present, however, it would be interesting to examine the major features of the existing electronic data in terms of a simple, preliminary, absorption transition model that might be constructed from existing theory. The main function of a practical model would be to predict the number of electronic states represented in the visible $n\rightarrow\pi^*$ band systems, their symmetries, and, at least in a qualitative manner, the degree of electronic-vibrational interaction that might be expected.

4.1 Singlet Electronic States

The most convenient model for the description of the electronic states of the azines seems to be that of the LCAO–MO approach,[23] and, independently, Mataga[24] and Paoloni[25] have treated theoretically the states resulting from the $\pi\rightarrow\pi^*$ transitions in *s*-tetrazine. Although a well-tested model for $n\rightarrow\pi^*$ transitions has not yet been developed, Orgel[26] has given a preliminary discussion of the $n\rightarrow\pi^*$ transitions in the azines; Goodman and Shull[27] have outlined a semiempirical treatment which has been extended by Goodman and Harrell[28] to a number of nitrogen heterocyclic molecules; and Anno and Sado[29] have formulated a semiempirical

[23] Early theoretical studies, such as Maccoll's valence bond calculation of the transition wavelengths and resonance energies of all the azine molecules, J. Chem. Soc. **1946,** 670, are only of minor interest because they are "pre-$n\rightarrow\pi^*$", so to speak; they attempt to explain as $\pi\rightarrow\pi^*$ transitions absorption bands which are now quite reasonably regarded as $n\rightarrow\pi^*$ transitions.

[24] N. Mataga, Bull. Chem. Soc. Japan **31,** 453 (1958); Z. physik. Chem. Neue Folge **13,** 140 (1957).

[25] L. Paoloni, Gazz. chim. ital. **87,** 313 (1957); J. Chem. Phys. **25,** 1277 (1956).

[26] L. E. Orgel, J. Chem. Soc. **1955,** 121.

[27] L. Goodman and H. Shull, J. Chem. Phys. **22,** 1138 (1954).

[28] L. Goodman and R. W. Harrell, J. Chem. Phys. **30,** 1131 (1959).

[29] T. Anno, J. Chem. Phys. **29,** 1161 (1958); T. Anno and A. Sadô, *ibid.* **29,** 1170 (1958).

theory applicable to pyrazine.[30] Although some degree of finality has been approached in the pyridine spectra through the work of Sponer *et al.*,[31] the actual vibronic details of other azine spectra are not yet well understood. We shall therefore pay close attention to the assumptions made in constructing a model for the observed vibronic absorption transitions of *s*-tetrazine.

Let us begin with the pi and nonbonding molecular orbitals that result from the naive LCAO–MO method as a reference on which to base our discussion. For convenience, their symmetries are listed in Fig. 4. The pi MO's are qualitatively drawn on an energy scale according to the calculations of Mataga,[24] and the energy lowering and splitting of the degenerate benzene pi MO's upon nitrogen substitutional perturbation is depicted. Nodal sign diagrams[32] for the MO's have been provided to aid the discussion of the model. According to the naive MO theory, the energies of separation of the four nonbonding lone pair MO's may be given as functions of six integrals[20]: A set of three overlap and a set of 3 one-electron resonance integrals that correspond with the ortho, meta, and para pairs of nitrogen lone pair AO's (only approximately sp^2 hybridized). The separation energies are given, neglecting overlap, in Fig. 4 in which o, m, and p denote the resonance integrals. It is assumed that these integrals, "coupling parameters" that might be evaluated from the vibronic

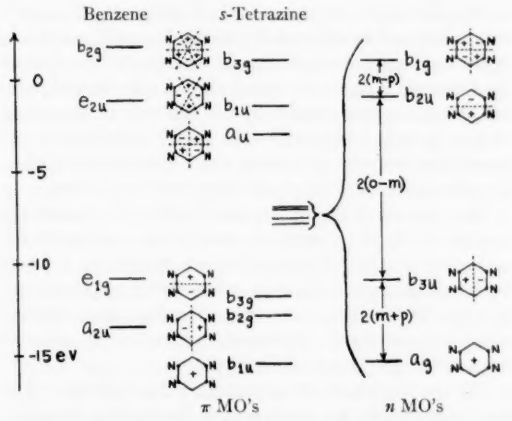

FIG. 4. The pi and nonbonding electron molecular orbital symmetries. The splittings of the n MO's are depicted in terms of one electron resonance integrals for the ortho, meta, and para nitrogen lone pair electron interactions.

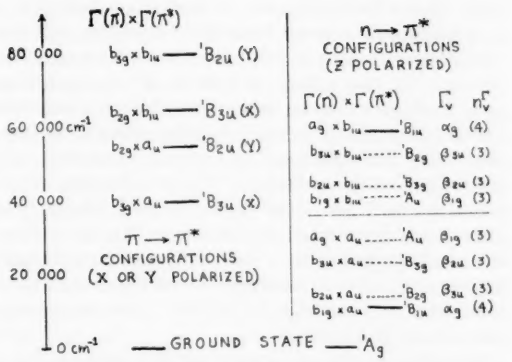
$\Gamma(n)\times\Gamma(\pi^*)$
80 000
60 000 cm^{-1}
40 000
20 000
0 cm^{-1}
$b_{3g}\times b_{1u}$ —— $^1B_{2u}$ (Y)
$b_{2g}\times b_{1u}$ —— $^1B_{3u}$ (X)
$b_{2g}\times a_u$ —— $^1B_{2u}$ (Y)
$b_{3g}\times a_u$ —— $^1B_{3u}$ (x)
$\pi\longrightarrow\pi^*$ CONFIGURATIONS (X OR Y POLARIZED)
GROUND STATE —— ^1A_g
$n\longrightarrow\pi^*$ CONFIGURATIONS (Z POLARIZED)
$\Gamma(n)\times\Gamma(\pi^*)$ Γ_v $n\Gamma_v$
$a_g\times b_{1u}$ —— $^1B_{1u}$ α_g (4)
$b_{3u}\times b_{1u}$ —— $^1B_{2g}$ β_{3u} (3)
$b_{2u}\times b_{1u}$ —— $^1B_{3g}$ β_{2u} (3)
$b_{1g}\times b_{1u}$ —— ^1A_u β_{1g} (3)
$a_g\times a_u$ —— ^1A_u β_{1g} (3)
$b_{3u}\times a_u$ —— $^1B_{3g}$ β_{2u} (3)
$b_{2u}\times a_u$ —— $^1B_{2g}$ β_{3u} (3)
$b_{1g}\times a_u$ —— $^1B_{1u}$ α_g (4)

FIG. 5. The symmetries of the lowest singlet electronic states of *s*-tetrazine. The symmetries of those vibrations which make allowed the electronically forbidden X- and Y-polarized $n\rightarrow\pi^*$ transitions have been omitted because of the rather minor role that these vibrations probably play in the visible absorption spectrum.

analysis of azine $n\rightarrow\pi^*$ spectra, are of the order of, possibly much less than, a few thousand wave numbers[33] and that $o\ll m<p<0$.

The resulting singlet electronic configurations of lowest energy are depicted in Fig. 5. Since Mataga's calculation[24] shows the antibonding pi MO of symmetry $\Gamma(\pi^*)=a_u$ to be about 1.3 ev lower than the $b_{1u}\pi^*$ MO, the eight lowest $n\rightarrow\pi^*$ single configurations should qualitatively lie, as depicted, in two separated groups, four configurations per group. This is consistent with a qualitative charge density picture based on Coulombic energy arguments; namely, that the group corresponding to n electron excitation to the $b_{1u}\pi^*$ MO should lie at higher energy because, relative to the four possible $n\rightarrow a_u\pi^*$ configurations, such excitation results in a net decrease in charge density on the nitrogen atoms. We have ordered the $n\rightarrow\pi^*$ configurations within each group so as to correspond in separation energy to the n orbital picture in Fig. 4. Rough estimation yields the difference in the mean energies of the two groups to be larger than the energy between the two most widely separated $n\rightarrow\pi^*$ configurations (^1A_u, $^1B_{1u}$) within either group. We assume from our spectral data that the four $n\rightarrow\pi^*$ configurations for which $\Gamma(\pi^*)=a_u$ have energies in the vicinity of 18 000 cm^{-1}, but the higher energy of the second group is not yet known.

Now because we wish to discuss absorption transitions to excited electronic *states*, we shall, at this point, neglect electronic configuration interaction for the sake of simplicity and replace the notion of electronic configuration in the preceeding discussion by that of electronic

[30] M. Ito, R. Shimada, T. Kuraishi, and W. Mizushima, J. Chem. Phys. **26,** 1508 (1957); L. Goodman and M. Kasha, J. Mol. Spectroscopy **2,** 58 (1958); R. C. Hirt, Spectrochim. Acta **12,** 114 (1958).

[31] J. H. Rush and H. Sponer, J. Chem. Phys. **20,** 1847 (1952), which see for earlier references to pyridine.

[32] As is often done, the nonessential, symmetry undetermined nodal planes that pass through the C—N bonds are drawn here as bisectors of these bonds; more precisely, however, they should be drawn in accordance with the LCAO coefficients which, in the case of benzene, require them to be at a 45° angle to the X and Y axes.

[33] The axis of a lone pair orbital is only uniquely determined in those azines which possess a symmetry axis that passes through a nitrogen atom. Thus the problem of the tilt of the lone pair orbital axis from the axis that bisects the CNN angle in *s*-tetrazine prevents a very good calculation of the lone pair overlap integrals. We therefore feel that the semiempirical estimation of lone pair molecular orbital energy differences must, at this stage of development, be regarded as only of very qualitative significance.

state. Figure 5 will then, out of necessity, be interpreted as a *zeroth-order representation of the low-lying electronic states*. We must bear in mind, however, that interaction between the two groups of four $n\rightarrow\pi^*$ configurations and, possibly even more important, vibronic interaction within either group (more generally, vibronic interaction among the eight lowest $n\rightarrow\pi^*$ configurations) may seriously alter the ordering of the $n\rightarrow\pi^*$ states as depicted in Fig. 5. The $\pi\rightarrow\pi^*$ states are much less likely to suffer from this complication however. We have therefore actually plotted the $\pi\rightarrow\pi^*$ configurations as though they were states on the energy scale of Fig. 5 so as to be consistent with the SCF LCAO–MO state energy calculations of Mataga.[24]

While interaction considerations may well lead to a reordering of our zeroth order $n\rightarrow\pi^*$ states, they will not prevent us from adopting, for descriptive purposes, a reference scheme in which an excited state is labeled by the same irreducible representation symbol that represents the symmetry of a single configuration. Furthermore, the D_{2h} symmetry species labeling the excited states of Fig. 5 may be used for semantic convenience even though it is quite likely that many of the electronic configurations, especially those of higher energy, may more nearly correspond in zeroth approximation to excited electronic states which have nuclear configuration symmetries lower than that of the ground electronic state. *Until it has been experimentally proven to be more meaningful to do otherwise, the symmetry species symbol for an electronic wave-function describing an excited electronic state of a molecule will be obtained as if the molecular symmetry of the excited state were the same as that of the ground electronic state.* Since the molecular symmetry of even the lowest excited states of most simple polyatomic molecules has not yet been established, nor indeed, of the ground state of tetrazine *vapor*, adoption of this convention seems necessary in order to provide a basis for defining the allowedness of a heretofore unanalyzed electronic transition.

4.2 Selection Rules

Adopting the preceding terminology, we can then derive from Herzberg-Sponer-Teller theory[34] the following selection rules for *s*-tetrazine. Electronic transitions allowed by molecular symmetry and arising from the ground electronic state may only take place to excited states of ungerade B symmetry. All other electronic transitions arising from the ground state will be electronically unallowed by molecular symmetry; i.e., the integrand of the electronic transition moment integral will not be totally symmetric at the equilibrium configuration. Note that under alteration of the molecular symmetry of a particular excited electronic state, an allowed transition remains allowed and an unallowed transition may or may not become electronically allowed.

It can thus be derived that the four lowest $\pi\rightarrow\pi^*$ singlet transitions of *s*-tetrazine will be allowed. Excluding from any future consideration the presumably high-energy $b_{2u}n\rightarrow b_{3g}\pi^*$ allowed transition, there should also be at least one (not more than two) low-lying Z-polarized electronically allowed $n\rightarrow\pi^*$ singlet transition(s). It is possible that the absorption band systems for these allowed $n\rightarrow\pi^*$ transitions would also contain unallowed X- and Y-polarized components due to appropriate nuclear-coordinate dependence and to the "$^1B_{2u}$ and $^1B_{3u}$ character" of the excited state. They would be expected to be only of minor importance in the visible spectrum of *s*-tetrazine, however, because there are no allowed X- or Y-polarized transitions sufficiently nearby for intensity borrowing to become highly significant; X- and Y-polarized $n\rightarrow\pi^*$ transitions are electronically forbidden. There should also be at least three (not more than six) low-lying Z-polarized electronically unallowed $n\rightarrow\pi^*$ singlet transitions that could appear in the visible absorption spectrum. They may achieve intensity not only by the usual mechanism—sufficient dependence of the excited-state electronic wavefunction on a vibrational coordinate of appropriate symmetry; their appearance *may also be considerably strengthened* by a mixing in of the very nearby $n\rightarrow\pi^*$ $^1B_{1u}$ state, at the expense of the intensity of the allowed $n\rightarrow\pi^*$ transition. Finally, any X and Y components of unallowed Z-polarized $n\rightarrow\pi^*$ transitions in the visible region would again be expected to be weak for the same reason mentioned above. (We should point out, however, that especially for the case of the group of four $n\rightarrow b_{1u}\pi^*$ transitions, X- and Y-polarized $n\rightarrow\pi^*$ transitions may be relatively quite strong should they lie sufficiently close to one of the $\pi\rightarrow\pi^*$ transitions.)

The column of Fig. 5 labeled Γ_v gives the symmetry species of those vibrations which may be observed, according to the vibronic selection rules,[34] as $0\leftarrow 1$ or $1\leftarrow 0$ transitions in a Z-polarized $n\rightarrow\pi^*$ absorption band system. The number of normal modes of *s*-tetrazine which possess these vibrational symmetries is given in the adjoining column labelled $\mathbf{n}_v$.

The framework of the preliminary model having thus been completed, we shall review the rather stringent assumptions on which it is based. In order to theoretically interpret the major vibronic bands in the visible absorption spectrum of *s*-tetrazine vapor, it is assumed that: (1) MO theory may be used profitably, as has been done by previous workers, to predict the symmetries and to roughly estimate the ordering of excited states; (2) magnetic dipole, electric quadrupole, and singlet-triplet transitions will be unimportant; (3) electronic-rotational interaction may be neglected; (4) vibrationally induced X- or Y-polarized transitions will only be of minor importance; (5) no unusual electronic-vibrational interaction stronger than that needed for the observation of Z-polarized $1_a\leftarrow 0$ vibronic bands

[34] G. Herzberg and E. Teller, Z. Physik. Chem. **B21**, 410 (1933); H. Sponer and E. Teller, Revs. Modern Phys. **13**, 75–170 (1941).

need be considered, where 1_a represents the excitation of an appropriate vibrational mode in the excited electronic states $^1B_{2g}$, $^1B_{3g}$, and ^1A_u; (6) the molecular symmetry of any excited states represented in the visible spectrum remains unchanged from that of the ground electronic state; (7) only the four states resulting from the $n\rightarrow a_u\pi^*$ transitions are present, the four $n\rightarrow b_{1u}\pi^*$ transitions lying at much higher energy; and finally, certainly the weakest assumption by far, (8) these four $n\rightarrow a_u\pi^*$ states will rank in energy in the order depicted in the lower-right portion of Fig. 5.

These assumptions may then be relaxed when experimental evidence dictates the necessity. Fairly sound theoretical arguments may be used to debate the validity of the first four assumptions, but present theory is not sufficiently powerful to soundly judge the last three. It would certainly not be surprising if these latter three assumptions all proved to be invalid. The analysis of assumption 5 poses difficult theoretical questions. We believe at present that the key to understanding the vibronic details of the $n\rightarrow\pi^*$ spectra of molecules which have two or more symmetrically equivalent lone electron pairs may lie in a much fuller understanding of these theoretical questions than has anywhere been attempted.

5. QUALITATIVE DISCUSSION OF THE SPECTRAL DATA IN TERMS OF THE SIMPLE ELECTRONIC MODEL

Probably the most obvious consequence of examining the high-resolution spectral data with the model is the following. If the $n\rightarrow\pi^*$ singlet state of lowest energy does have electronic symmetry $^1B_{1u}$, as in Fig. 5, then its allowed $0\leftarrow 0$ transition should appear at that wavelength such that all vibronic bands observed at longer wavelengths are hot. This reasoning thus demands that we assign the moderately intense band observed at 18 053 cm^{-1} as this $0\leftarrow 0$ transition. It then becomes difficult, however, to explain successfully the nearby, more intense bands at 18 134 and 18 283 cm^{-1} in terms of either allowed or unallowed transitions. Relaxation of either assumptions 6 or 8 removes this difficulty but does not result in a unique set of vibronic assignments. Without relaxing assumption 6, the bands that most likely represent an allowed $0\leftarrow 0$ transition seem to be the two intense bands at 18 134 and 18 919 cm^{-1}. (They might both represent allowed $0\leftarrow 0$ transitions if assumption 7 were completely relaxed; i.e., if the separation energies among the four states of both the $n\rightarrow a_u\pi^*$ and $n\rightarrow b_{1u}\pi^*$ groups were sufficiently small, all eight $n\rightarrow\pi^*$ transitions could conceivably appear in the visible spectrum. Without a detailed study of its many spectral implications, this line of pursuit looks at first quite attractive.)

Using many kinds of band-frequency difference tables and estimates for those ground-state vibrational frequencies not presently available, it has been possible to explore the logical consequences of these and many other initial starting points for vibronic analysis in terms of the model. In so doing, we have found that several partial but plausible sets of vibronic assignments can be made without relaxing the first five assumptions made above, each of them involving one or more unallowed transitions. It is because of these conflicting ambiguities, therefore, that no set of vibronic assignments warrants mentioning at this time. Although further discussion of assignments is thus relegated to an appendix, the following tentative but important result of our analytical work with vibronic term schemes should here be reported. *It does not appear that all of the major features of Fig. 3 are explainable in terms of only two or as many as eight excited electronic states.* If this strictly empirical result holds true in the final analysis, it will be in accord with our present semitheoretically derived belief that present $n\rightarrow\pi^*$ theory would need serious revision were electronically unallowed $n\rightarrow\pi^*$ transitions present only to a negligible degree in the $n\rightarrow\pi^*$ absorption spectra of those azines containing more than one nitrogen atom. Thus if assumption 7 is retained, there will therefore be four electronic transitions in the visible region. Their relative forbiddeness will depend on the validity of assumption 6 and/or assumption 5.

Our goal in the vibronic analysis, therefore, is not only to explain the observed absorption bands by vibronic assignment. It is to determine as well the degree to which each of the three unallowed $n\rightarrow\pi^*$ singlet transitions contributes to the major features of the spectrum. The location of the $0\leftarrow 0$ energy for each of these three unallowed transitions requires identification of both $0\leftarrow 1_a$ and $1_a\leftarrow 0$ bands as well as knowledge of the ground electronic state frequency of the corresponding nontotally symmetric vibration. (If assumption 6 is valid, then the $0\leftarrow 0$ bands of these three unallowed transitions may be unidentifiably weak; the above requirement is thus necessary for locating the $0\leftarrow 0$ position and identifying the symmetry of the excited state to which it corresponds. If the excited-state molecular symmetry is lower than D_{2h}, it cannot be higher, the $0\leftarrow 0$ band of an unallowed transition could conceivably be moderately strong; but the above requirement would still be necessary for the symmetry classification of the transition.) We believe that the most important consequence of determining the four $0\leftarrow 0$ positions will be the utilization of their separation energies in the semiempirical derivation of some useful ortho, meta, and para lone-pair electron coupling parameters. By comparing these parameters with the corresponding, similar parameters derivable from the vibronic analysis of other azine $n\rightarrow\pi^*$ spectra, it may be possible through a consideration of the slightly different azine geometries to develop an $n\rightarrow\pi^*$ theory of power similar to that which we now enjoy for $\pi\rightarrow\pi^*$ transitions.[35]

Let us now turn to discussion of vibronic band progression length. The following questions thus arise. Is

[35] For example, R. Pariser and R. G. Parr, J. Chem. Phys. **21**, 466 (1953); **21**, 767 (1953), and references therein.

a progression such as **F** of Fig. 3 to be regarded as a relatively long one, and, if so, is it clear that it necessarily indicates more than a very small change in the molecular geometry of the excited state? A negative answer is inferred by accepting the conclusions of some preliminary rovibronic analysis studies[36]—that there is a surprisingly small change in the moments of inertia upon passing from the ground to the excited $n\rightarrow\pi^*$ state. This experimental conclusion receives at least some support by the fact that the main vibronic progression (band difference) frequency drops by only 5% in passing from the ground to the excited $n\rightarrow\pi^*$ state(s). This ground state frequency of 737 cm^{-1} is thought to represent[12,20] the totally symmetric vibrational mode in which the nitrogen atoms move away from the center of the ring as the carbon and hydrogen atoms move, in phase, towards the ring center. This mode corresponds to the ϵ_{2g} mode 6*a* of benzene,[37] the principal mode responsible for the observation of the electronically forbidden $^1B_{2u}$ transition near 2600 A. In benzene,this mode drops from 606 cm^{-1} in the ground state to 520 cm^{-1} in the excited state, a decrease of 14%. For *s*-tetrazine, it appears that this mode drops by only about 30 to 40 cm^{-1} for all of the $n\rightarrow\pi^*$ states represented in the visible spectrum. This may be taken as an indication that the vibrational force constants of the excited state(s), at least for mode 6*a*, are not radically different from those of the ground state.

Further support of this is indicated by the fact that the most intense members of the nonhot part of each major progression are the first or second bands of lowest energy. However, the fact that the band intensities do not drop off sharply within a progression indicates that a certain degree of expansion takes place in the mode 6*a* normal coordinate upon $n\rightarrow\pi^*$ excitation. There is internal consistency, therefore, among the above excited state geometry arguments if we assume that the rovibronic analysis studies were not sufficiently sensitive to detect the small changes in molecular geometry that appear to occur. Now if electronic and vibrational motion are separable,[38] the concepts of progression length and relative band intensity are related to the degree of overlap between the upper- and lower-state vibrational eigenfunctions that characterize the individual bands of a progression. The Franck-Condon principle, which is well understood at least for the very simple polyatomic molecules, may then be used in the customary way to draw conclusions about excited-state molecular geometry. We have done this in the preceeding discussion. *But just how separable* are the electronic and vibrational motions of *s*-tetrazine in the quantized excited state(s) represented in its visible absorption spectrum? It is certainly reasonable that a refined configuration interaction calculation might yield several $n\rightarrow\pi^*$ singlet states with energy differences not greater than the energy of an azine ring vibration. Because of the resulting possibility of strong vibronic mixing of excited electronic states, it might then be difficult to give a successful interpretation of azine $n\rightarrow\pi^*$ spectra (excluding pyridine) in terms of the usual independent excited electronic states treatment. Although useful for reference, much of our preliminary model would then be invalid (recall assumption 5) as an aid to successful vibronic analysis. Further, if strong vibronic mixing is present, it is not yet clear that the above progression band intensity arguments would be soundly based. It is possible, therefore, that even the major vibronic structure of Fig. 3 may not be explainable without a more elaborate model; studies aimed at the development of such a model, ones that may serve to aid the vibronic analysis of the high-resolution spectra of the other azines as well, have been initiated by one of us (GHS) in collaboration with Dr. Martin Gouterman of Harvard University.

Before concluding our present discussion, the present status of our understanding of the *s*-tetrazine $\pi\rightarrow\pi^*$ transitions should be mentioned. The semiempirical calculations of Mataga[24] and Paoloni[25] predict that the lowest singlet $\pi\rightarrow\pi^*$ transition, $^1B_{3u}\leftarrow{}^1A_g$ (or $^1L_b\leftarrow{}^1A$ in Platt notation[39]), is *X* polarized and in the vicinity of 4.9 ev. Although the polarization has not yet been checked, it is very likely that at least a major portion of the absorption (see Fig. 2) around 247 mμ corresponds to this transition. There are several interesting implications if the absorption between 230 and 280 mμ is almost completely due to a single excited electronic state.

First of all, the rather symmetrical absorption contour may indicate that the lowest $\pi\rightarrow\pi^*$ excited-state molecular geometry differs markedly from that of the ground state, especially if the 0$\leftarrow$0 transition occurs at a longer wavelength than say 265 mμ. Secondly, while the density of observable vibronic transitions per wavenumber may be considerably greater in the 230 to 270 mμ region than that of benzene, the almost complete lack of any vibronic band structure in the gas-phase Cary spectrum may indicate that the more intense vibronic transitions lead to dissociation. This implication is not inconsistent

[36] Although the symmetric rotor analyses of Mason and Innes (references 12 and 22) indicate that the *A* and *B* moments suffer little change in passing to an azine excited $n\rightarrow\pi^*$ state, there is still the possibility that the bond distances and angles may coincidentally change more than might at first be indicated by the rather surprisingly small changes in $A+B$. The exact degree and absolute direction of the *A* and *B* moment changes must come from further data analysed by asymmetric rotor theory.

[37] E. B. Wilson, Phys. Rev. **45,** 706 (1934).

[38] M. Born and K. Huang, *Dynamical Theory of Crystal Lattices* (Oxford University Press, New York, 1954), pp. 166, 402, and 406.

[39] The Platt notation, J. R. Platt, J. Opt. Soc. Am. **43,** 252 (1953), is most useful in discussing $n\rightarrow\pi^*$ transitions in general; however, since the *s*-tetrazine $n\rightarrow\pi^*$ transitions are all $^1W\leftarrow{}^1A$, allowed at least by local symmetry (because of the partial 2*s* character of the *n* orbital) if not by molecular symmetry, we shall use only the more informative group theoretical designation of the $n\rightarrow\pi^*$ states even though in most cases the molecular symmetry of the excited state has not been experimentally confirmed. Of course for those azines in which a symmetry axis passes through a nitrogen atom, the locally unallowed $n\rightarrow\pi^*$ transitions, $^1U\leftarrow{}^1A$, are also possible.

with the observed photounstability of *s*-tetrazine. The photodecomposition rate is not rapid under ordinary lighting where there is little ultraviolet radiation present. Finally, if the dissociation interpretation of this absorption region is correct, it implies that the theoretical calculations[24,25] for the lowest $\pi\rightarrow\pi^*$ transition yield an energy that may be too high by 0.4 ev or more.

Mataga and Paoloni predict that the second-lowest $\pi\rightarrow\pi^*$ singlet transition should be *Y* polarized, $^1B_{2u}\leftarrow{}^1A_g$ ($^1L_a\leftarrow{}^1A$), and occur at about 6.8 and 5.9 ev (183 and 210 mμ), respectively. Our low-resolution data thus lend some support to Paoloni's calculation. Until more is known about the location of all of the $n\rightarrow\pi^*$ transitions, however, this support as well as our dissociation interpretation can only be tentative; the $n\rightarrow b_{1u}\pi^*$ group might well lie in the 210 or 260 mμ regions.

6. CONCLUSION

The new spectral data presented here have been discussed in terms of a preliminary model for the absorption. The difficulties encountered in attempting to achieve a unique vibronic analysis of the existing visible absorption data are more likely a reflection of the lack of auxiliary empirical data than an over-all inability of the preliminary model to serve as a guide. However, it has been pointed out that several aspects of the model may be unsound. Aside from those which have long been obvious in the theoretical treatment of the excited states of aromatic molecules, the most interesting (and so far neglected) of these aspects may be the degree of vibronic mixing of adjacent $n\rightarrow\pi^*$ states. Positive evidence of the importance of molecular symmetry-forbidden $n\rightarrow\pi^*$ transitions will probably only come from a rather complete vibronic analysis. There is real need at the theoretical level, however, of a deeper examination of the Born-Oppenheimer approximation and Franck-Condon principle for the case of almost accidentally degenerate electronic states.

In concluding the present discussion we wish to express our hope that the data and arguments given here will stimulate the interest of other investigators in the detailed nature of $n\rightarrow\pi^*$ transitions and in the important role that the lone-pair electrons play in the chemistry of the azines. Looking back over the historical development of electronic spectroscopy, it seems likely that a satisfactory understanding of the energetics of these and the pi electrons will be reached only after contributions have been made in many laboratories.

ACKNOWLEDGMENTS

The authors wish to express their appreciation to Dr. C. E. Coffey, Dr. W. B. Olson, Mr. R. L. Reddington, and Mr. R. E. Wilde for their valuable assistance in the measurement and calibration of the high resolution spectra. Illuminating theoretical discussions with Dr. M. Gouterman, Dr. R. Hexter, Dr. R. Hirt, Dr. H. Shull, and Dr. W. Simpson are gratefully acknowledged. The help of Professor K. K. Innes of Vanderbilt University in the preparation of the manuscript has been especially appreciated.

APPENDIX

For the benefit of future investigators, we wish to record a particularly interesting and simple example of certain types of problems encountered in the logic of vibronic analysis. Ambiguity in a vibronic analysis is profitably illustrated by considering the following arguments for and against one of the most attractive and simplest possible analyses proposable; namely, the vibronic term scheme represented by

$$\sigma^{\text{air}}(\text{cm}^{-1}) = 18134 + 700v_a' + 149v_b' - 737v_a'' - 232v_b'',$$

where v_a and v_b are vibrational quantum numbers for the two different normal modes *a* and *b*. The single and double primes refer, respectively, to the excited and ground states of an allowed electronic transition. This empirically determined scheme rather successfully accounts for many of the major spectral features of the *s*-tetrazine visible absorption spectrum; namely the progressions **A**, **C**, **E**, **F**, **G**, and **J** of Fig. 3 and Table II. It can explain these progressions in terms of a single, electronically-allowed $^1B_{1u}$ $n\rightarrow\pi^*$ transition, having a $0\leftarrow0$ band at 18 134 cm^{-1}. Further, some of the other major spectral features (i.e., progressions **B**, **D**, **K**, and **L**) may be rationalized, with varying degrees of plausibility, within this framework without invoking the presence of electronically unallowed transitions. (It would, however, not be necessary to explain these other spectral features in terms of the allowed transition; the validity of the proposed term scheme is independent of them.)

Successful as this basis for analysis may appear, however, we can not yet accept it with confidence because of the following three arguments against it, none of which can easily be dismissed at the present stage of experimental and theoretical work on azine $n\rightarrow\pi^*$ spectra.

(i) The proposed analysis assigns all of the members of progression **G** as being hot bands; in particular, the moderately intense band at 18 053 cm^{-1} is assigned as the $1_b'\leftarrow1_b''$ transition. Because, near room temperature, this transition arises from a moderately well-populated ground state (232 cm^{-1}), the percentage change in absorption intensity with temperature would not be as pronounced as that of a band arising from a ground electronic state that is vibrationally excited by 737 cm^{-1}. Although our relative intensity studies were not well designed for resolving small changes in absorption intensity with temperature, we believe, nevertheless, that they were at least on the threshold of being able to tell whether or not there was a positive or negative variation of the 18 053 cm^{-1} band intensity with temperature. To the best of our present experimental knowledge, the intensity of this band varies with temperature in the same way as do the bands at 18 134 and 18 283 cm^{-1}. Thus it does not appear that the 18 053

cm^{-1} band is hot. If this experimental conclusion is correct, then, independent of the nature of the excited state molecular symmetry, it automatically negates the proposed analysis. Settlement of this point awaits a more careful study of temperature dependence.

(ii) The proposed analysis implies the existence of a 232 cm^{-1} ground state vibration that drops by 36% to 149 cm^{-1} in the excited state. From examination of the normal frequencies of benzene and the other azines, it seems this 232 cm^{-1} mode would correspond to an out-of-plane vibration of symmetry β_{1u}, α_u, or possibly β_{3g}. However, only α_g vibrations may appear as 0←1 or 1←0 transitions in an electronically-allowed band system. Furthermore, it is highly unreasonable to expect a 149 cm^{-1} totally symmetric vibration to occur in an excited $n\rightarrow\pi^*$ state unless the excited state molecular symmetry were much lower than D_{2h}. In order to explain progressions **C** and **E** by the proposed analysis without relaxing the assumption of D_{2h} excited-state symmetry, it would be necessary that they be assigned as Y-polarized transitions involving only the lowest vibration of β_{3g} symmetry (the symmetry of the integrand of the electronic part of the transition moment integral); they cannot be assigned as X-polarized transitions because there are no β_{2g} vibrations in s-tetrazine. From our vibrational studies, however, it appears that, of the three out-of-plane vibration symmetries mentioned above, a β_{3g} vibration is the most unlikely prospect for the 232 cm^{-1} mode. Further, a Y-polarization assignment seems unlikely because of the relatively large intensity of progressions **C** and **E**. Under such an assignment, these progressions would be forbidden at equilibrium configuration. They could only appear in the absorption spectrum through considerable β_{3g} vibrational coordinate dependence of the electronic state wavefunctions and through B_{2u} character of the electronic excited state. Since the nearest B_{2u} electronic state ($\pi\rightarrow\pi^*$ transition) probably lies at least 29 000 cm^{-1} higher[24,25] than the lowest $n\rightarrow\pi^*$ transition (at say 18 000 cm^{-1}), it does not seem likely that progressions **C** and **E** could achieve much intensity by borrowing from allowed Y-polarized transitions.

(iii) The third argument against the proposed analysis arises from our search for other interpretations that may be given to the many 232±3, 149±3, 83±3 cm^{-1} vibronic band difference frequencies present in the visible spectrum. The 81-cm^{-1} separation of the first members of the nonhot part of progressions **F** and **G** is, according to the model, the difference between the ground and excited state frequency of some normal vibration. The 18 053 and 17 970 bands are to be interpreted, respectively, as the electronically allowed transitions $1_b'\leftarrow 1_b''$ (progression **G**) and $2_b'\leftarrow 2_b''$ (progression **J**). However, the progression difference frequencies within each of the **G** and **K** progressions are almost identical and uniformly 6 to 10 wavenumber greater than the corresponding progression difference frequencies within progression **F**. Thus while the excited state mode 6*a* seems to have about the same anharmonicity for all three progressions, explanation of why its overtone spacing is different in **F** from that of **G** and **K** would require rather penetrating theoretical argument. This cause for doubting the proposed analysis may not, however, be as strong as the following reason. Notice that the first major appearance of the intense progression **D** occurs at 18 919 cm^{-1}, 82 cm^{-1} higher than the second member of the nonhot part of progression **F**. It does not seem likely that these two bands, representing the two most intense progressions in the spectrum, are only coincidentally related by a wavenumber number difference that figures so prominently throughout the entire spectrum. Yet interpretation of this 82 cm^{-1} difference within the framework of the proposed analysis has not yet been found.

It seems improbable that all three of the above arguments (the first based on experiment, the second on theory, and the third on plausibility) can be invalid. At this stage it is therefore wise to turn to other possible explanations for the 149 and 83 cm^{-1} spacings. At present, we believe they may represent a manifestation of the eigenvalue differences that arise from an "electronically mixed vibronic-state problem." This is another story, however.

THE JOURNAL OF CHEMICAL PHYSICS VOLUME 35, NUMBER 6 DECEMBER, 1961

s-Tetrazine. II. Infrared Spectra*

GLENN H. SPENCER, JR.† PAUL C. CROSS, AND KENNETH B. WIBERG
Department of Chemistry, University of Washington, Seattle 5, Washington

(Received October 31, 1960)

To aid in the vibronic analysis of the $n\rightarrow\pi^*$ visible absorption band systems of *s*-tetrazine vapor, infrared spectra of vapor, solution, and cold, solid film phases of natural and deuterated mixtures of *s*-tetrazine have been obtained. By use of the product rule and by correlation of the fundamental modes of *s*-tetrazine with those of benzene and the other azines, it is possible to make tentative vibrational assignments for all seven of the fundamental bands that would be expected to be infrared active in the wavelength region from 2 to 15 μ. However, the low-frequency modes 16a and 16b, A_u and B_{1u}, respectively, have not yet been observed, and the lack of knowledge of the frequencies of eight of the nine gerade modes (Raman active only) has prevented any definite assignment of combination bands. The observation of an interesting and peculiar phenomenon—what is believed to be the totally symmetrical mode 6*a* near 730 cm^{-1} in the solid film spectra of the various deuterated mixtures—is also reported.

1. INTRODUCTION

THIS paper is the second of a series that is concerned both experimentally and theoretically with the molecular and electron dynamics of *s*-tetrazine. Electronic absorption spectra of *s*-tetrazine vapor and a general introduction to the nature of the problems of interest were given in the previous paper,[1] hereafter denoted as I. The experimental investigations reported in the present paper II were motivated by the desirability of knowing as many of the ground electronic state, fundamental vibrational frequencies of *s*-tetrazine as possible, before attempting to perform a complete vibronic analysis of its $n\rightarrow\pi^*$ visible absorption band systems.

Bertinotti, Giacomello, and Liquori[2] have reported that there are two centrosymmetric molecules per unit cell in the *s*-tetrazine crystal and that the space group is $P2_1/c$ (International Standard No. 14). From the tables given by Halford,[3] one finds that this space group (Schoenflies symbol C_{2h}^5) contains four distinct sets of sites having point symmetry C_i with two equivalent sites per set: $4C_i(2)$. Thus the vibrational selection rules for the *s*-tetrazine crystal are the same as for the benzene crystal; the unit cell of the latter,[4,5] which is similar to that of *s*-tetrazine, is described by V_h^{15}: $2C_i(4)$. Mutual exclusion will be operative: all of the ungerade modes (including translations and binary combination bands but no first overtones) will be infrared active for the case of a pure *s*-tetrazine-d_0 or a pure *s*-tetrazine-d_2 crystal, but no gerade fundamentals will be infrared active.

The selection rules for the absorption of infrared radiation by either of these molecules in the vapor phase (assuming a molecular symmetry of D_{2h}), allow only the eight normal vibrations that are of ungerade B symmetry to be active as fundamental bands, and again there will be mutual exclusion. The D_{2h} symmetry species of the 18 normal vibrations of *s*-tetrazine are given in Fig. 1. The symmetry displacement coordinate diagrams given in this figure are labelled with the notation that is used for the benzene molecule,[6–8] from which the diazine vibration notation has been derived.[9] It must be remembered that, in general, these diagrams do not represent actual normal vibrational motion; they have been drawn merely to aid the understanding of possible vibrational frequency assignments of the infrared spectral data.

As was mentioned in I, the frequency of only one gerade vibration has so far been reported; experimentally determined from the *s*-tetrazine $n\rightarrow\pi^*$ spectra, this frequency, 737 and 720 cm^{-1} for *s*-tetrazine-d_0 and *s*-tetrazine-d_2, respectively, is thought to belong to the totally symmetrical mode 6*a* of the ground electronic state. However it is possible that the infrared spectra of *s*-tetrazine-d_1 (molecular symmetry C_{2v}) could provide valuable information regarding the gerade modes of the two D_{2h} molecules. Theoretically, only the single out-of-plane A_2 vibrational mode in *s*-tetrazine-d_1 vapor is infrared inactive, and all 18 modes would probably be active in the pure solid phase. Unfortunately, however, we would not expect those infrared active modes of *s*-tetrazine-d_1 which correlate with the gerade modes of the two D_{2h} molecules to absorb very

* This work was supported in part by the Air Force Office of Scientific Research, Air Research and Development Command. It represents part of the Ph.D. thesis research of GHS and was reported in part at the Ohio State Molecular Structure and Spectroscopy Symposium, June, 1959.

† National Science Foundation Postdoctoral Research Fellow (1958–59) at Harvard University. Present address: Department of Chemistry, Stanford University, Stanford, California.

[1] G. H. Spencer, Jr., P. C. Cross, and K. B. Wiberg, J. Chem. Phys. **35,** 1925 (1961).

[2] Reference 1 of Part I (see for an illustration of the unit cell).

[3] R. S. Halford, J. Chem. Phys. **14,** 8 (1946).

[4] R. S. Halford and O. A. Schaeffer, J. Chem. Phys. **14,** 141 (1946).

[5] R. D. Mair and D. F. Hornig, J. Chem. Phys. **17,** 1236 (1949).

[6] E. B. Wilson, Phys. Rev. **45,** 706 (1934).

[7] C. K. Ingold *et al.*, J. Chem. Soc. (London) **1936,** 912; **1946,** 222.

[8] F. A. Miller, J. Chem. Phys. **24,** 996 (1956).

[9] R. C. Lord, A. L. Marston, and F. A. Miller, Spectrochim. Acta **9,** 113 (1957).

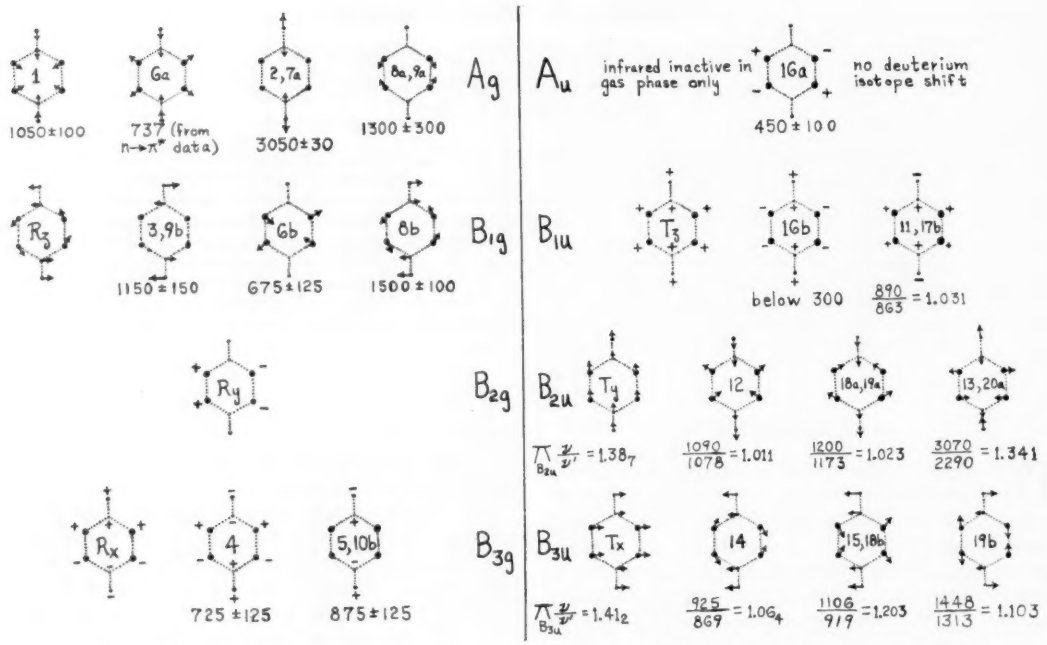

All gerade vibrations are Raman active.

Theoretical: $\Gamma_{\pi k}(\nu_k/\nu_k') = 1.397$ for $\Gamma = B_{1u}$, B_{2u}, and B_{3u}.

FIG. 1. Symmetry displacement coordinate diagrams and fundamental frequency estimates for the vibrational modes of *s*-tetrazine.

strongly. Further, we have not been able to produce even approximately pure *s*-tetrazine-d_1. Nevertheless, we have been able to extract some useful data from the cold film spectra of various mixtures of *s*-tetrazine-d_0, -d_1, and -d_2.

II. EXPERIMENTAL

Infrared absorption spectra of *s*-tetrazine were taken between 2 and 15 μ on a Perkin-Elmer model 21 spectrophotometer with a sodium chloride prism. Some of these spectra are shown in Figs. 2(a) and 2(b), and although no attempt was made to do more than a merely qualitative study of the relative intensity of the absorption bands, the absorption frequencies were measured with care. Frequencies of the known rotational structure peaks of water, carbon dioxide, and ammonia, and those of the polystyrene film spectrum were used for calibration. Absorption peaks lying at less than 1600 cm^{-1} in all of the *s*-tetrazine spectra taken, could be measured quite reproducibly to within two wavenumbers, and a table of the uncertainties in the measurement of absolute frequencies of absorption peaks for various wavenumber regions is given at the right in spectrum **A** of Fig. 2(a). The eight spectra presented here are direct tracings from the laboratory data, and they are all drawn on the same linear transmission scale; no attempt has been made to subtract out baseline effects due to noise of general unbalancing of the two light beams. The slight presence of water and carbon dioxide can be detected in some of the spectra, but for our purposes this has not caused any difficulty. All external windows used in our work were made of potassium bromide. For a particular deuterated mixture, the relative percentages *s*-tetrazine-d_0, -d_1, and -d_2 were determined mass spectrometrically.

The infrared spectrum of natural *s*-tetrazine vapor, **B**, of Fig. 2(a), is one of the intermediate spectra taken in a study of the time dependence of the band intensities. Crystals of *s*-tetrazine were placed in an ordinary 10-cm gas absorption cell that had been wrapped with insulating tape and nichrome ribbon, and the vapor spectrum rerun continuously as the cell temperature was electrically increased. We attribute the 712 cm^{-1} band that increases with time to be due to the very strong bending mode of hydrogen cyanide. The two other bands whose intensity increased with time, at 1758 and 2930 cm^{-1}, must also be due to absorption by decomposition products, but their nature has not yet been identified. The spectra **C** and **D** of Fig. 2(a) are of an approximately saturated solution of natural *s*-tetrazine and of a mixture of the deuterated *s*-tetrazines, respectively, in carbon tetrachloride (about 0.1 g/ml of solvent). Attempts, using conventional pellet production techniques, to produce alkali halide-*s*-tetrazine pellets suitable for taking infrared spectra were unsuccessful; upon grinding, the red crystals of *s*-tetrazine increase in waxiness.

The infrared spectra of cold, solid films of natural

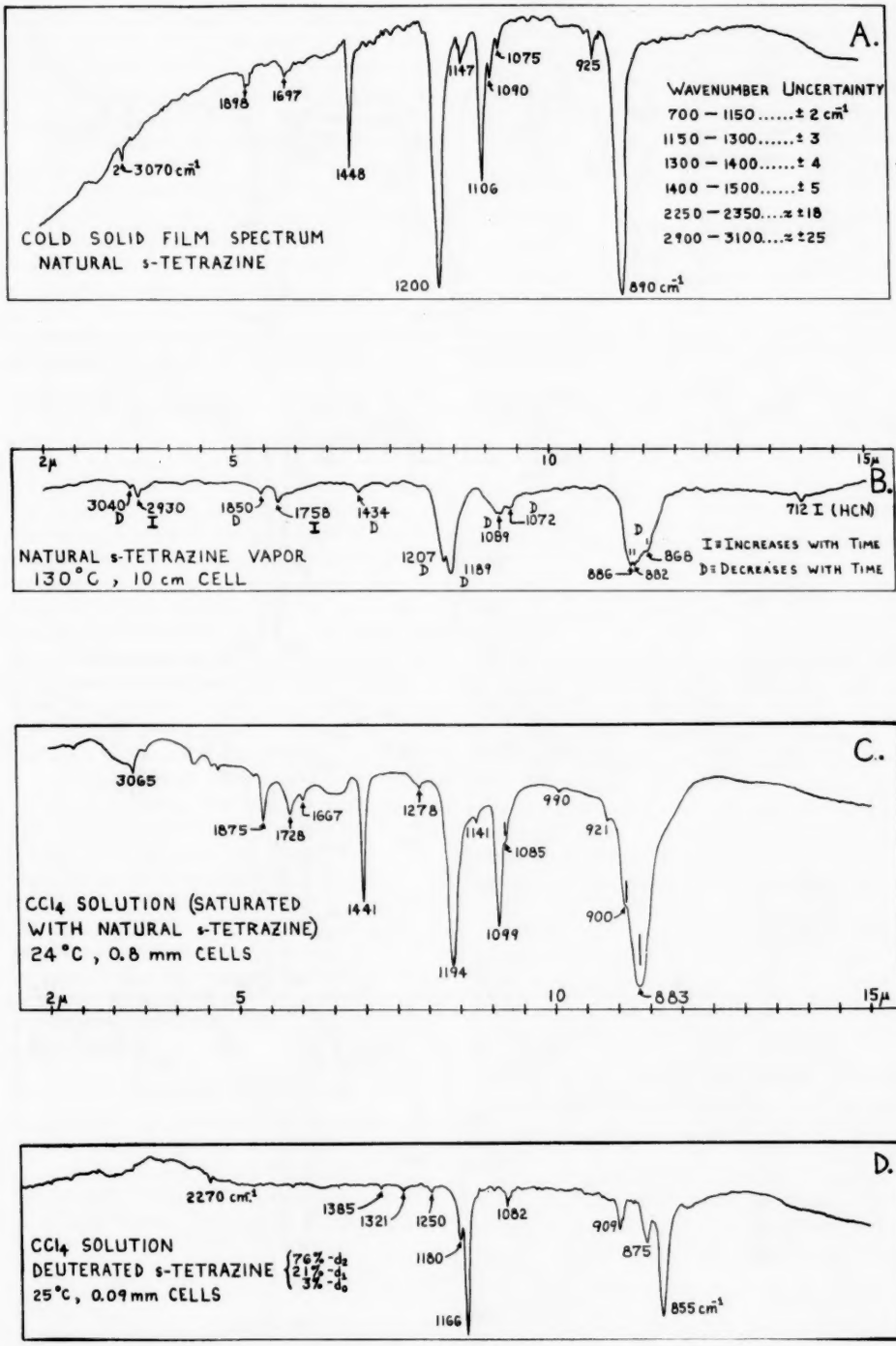

FIG. 2(a)

FIG. 2(a). Infrared spectra for three different phases of *s*-tetrazine; (b) cold, solid film infrared spectra of four different mixtures of deuterated *s*-tetrazine.

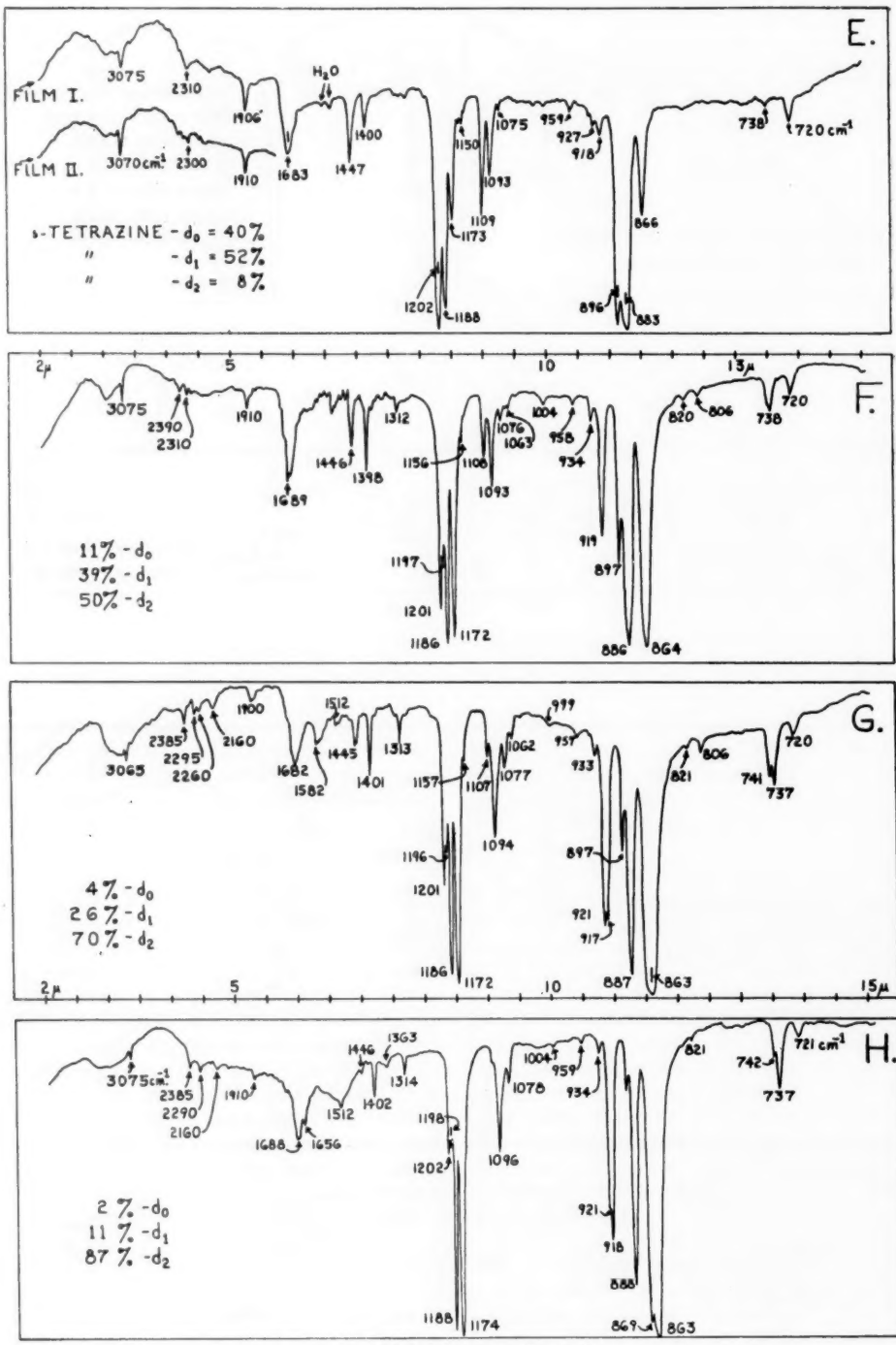

FIG. 2(b) [caption under Fig. 2(a)]

and of various deuterated mixtures of *s*-tetrazine are shown in A of Fig. 2(a) and in Fig. 2(b), respectively. The cold cell design used in obtaining these spectra was based on that of Wagner,[10] and for each of these five spectra the refrigerant used to cool the brass sample block was liquid nitrogen. The rapid deposition technique for forming the solid film was used: *s*-tetrazine was deposited at its room temperature vapor pressure (roughly 0.5 mm of Hg) on the cold sodium chloride window of the sample block. After a 10-min deposition time, a solid film of natural *s*-tetrazine was of a thickness such that its optical transmission at 890 cm^{-1} was about 10%. A vacuum of better than 10^{-4} mm of Hg was maintained in the cold cell throughout the recording of the solid film spectra. Although an internal thermocouple was not used, we estimate that the film temperature may not have been much less than −130°C. This estimate is based on a comparison of a solid benzene spectrum obtained with our cold cell with the benzene crystal spectra of Mair and Hornig.[5,11] When a dry ice-acetone mixture is used as a refrigerant, the absorption bands of the cold film spectrum of *s*-tetrazine are slightly broader, and their peaks are displaced by one to three wavenumbers towards lower energy.

An attempt to find the frequency of the out-of-plane B_{1u} ring bending mode 16*b* of *s*-tetrazine was unsuccessful. Using a single-beam spectrometer (Perkin-Elmer Universal Monochromator model 83), a cesium bromide prism, and a 10-cm gas absorption hot cell with potassium iodide windows, we measured the spectrum of hot *s*-tetrazine vapor between 700 and 300 cm^{-1}. No absorption due to *s*-tetrazine was observed in this region.[12] Unless the intensity of the low-lying B_{1u} fundamental is far weaker than it would be expected to be, we conclude that this band lies below 300 cm^{-1}.

In collaboration with Professor E. L. Wagner, one of us (GHS) tried to obtain the Raman spectrum of moderately concentrated solutions of *s*-tetrazine in water and in carbon tetrachloride, using the 4047 A mercury emission line for excitation. None of the *s*-tetrazine gerade frequencies were obtained, the usual difficulties in obtaining the Raman spectra of colored compounds prevailing.

III. DISCUSSION

In attempting to provide vibrational assignments for the absorption peaks of the *s*-tetrazine infrared spectra, we have taken into consideration the existing assignments, frequencies, and relative intensities of the infrared peaks and Raman lines that have been reported for benzene,[4–8] pyridine,[13,14] the diazines,[9,15] *s*-trizaine,[16] and some of their deuterated derivatives. In particular, examination of the spectral data for pyrazine (which has the same symmetry as *s*-tetrazine-d_0 and -d_2), pyridazine (the only other available azine, besides *s*-tetrazine, that has ortho lone pair interaction), and *p*-benzene-d_2 and benzene-d_1 has been quite valuable. The tentative vibrational assignments that we propose for *s*-tetrazine are given in Fig. 1. The gerade frequencies that are given there are estimates based on considerations of the above mentioned data. Since the frequency of the single A_u mode is not likely to be above 670 cm^{-1}, we can exclude it in considering which bands of the 2 to 15 μ solid film spectra are due to ungerade fundamentals; we estimate that it should give only a mildly intense band at about 450 cm^{-1}, and it should show no deuterium isotope shift. The B_{1u} mode 16*b* should give a very strong band, probably lie below 300 cm^{-1} as mentioned earlier, and show a large deuterium isotope shift. The other B_{1u} mode and the B_{2u} and B_{3u} modes of *s*-tetrazine have been related to absorption peak frequencies, partially by considering the spectral data for benzene and the other azines, but mainly by use of the Teller-Redlich product rule. These assignments deserve further discussion.

We shall assume that the frequencies of solid film peaks given in Table I are placed correctly according to the molecule that they properly represent. (This

TABLE I. Assignment of some of the peak frequencies (in cm^{-1}) of the cold film spectra to *s*-tetrazine-d_0, -d_1, and -d_2.

s-Tetrazine-d_0 D_{2h}	*s*-Tetrazine-d_1 C_{2v}	*s*-Tetrazine-d_2 D_{2h}
737 A_g	741 ? A_1	720 A_g
	806 ?	
890 B_{1u}	888 B_2	863 B_{1u}
925 B_{3u}	921 B_1	869 B_{3u}
1075 ?	958 ?	934 ?
1090 B_{2u}	1076 ? A_1	1078 B_{2u}
1106 B_{3u}	1095 B_1	919 B_{3u}
1147 too broad to be a fundamental ?	1063 ?	1004 ?
	1150 ?	
	1156 ?	
1200 B_{2u}	1187 A_1	1173 B_{2u}
1448 B_{3u}	1400 B_1	1313 B_{3u}
	1682 ?	
	2300 ?	2290 B_{2u}
3070 B_{2u}	3070 ?	

[10] E. L. Wagner, Ph.D. thesis, Brown University, Providence, Rhode Island (1948); E. L. Wagner and D. F. Hornig, J. Chem. Phys. **18,** 296 (1950).

[11] Their accurate work on the infrared spectrum of a carefully prepared crystal of benzene well shows certain band intensity and narrowing effects which are temperature dependent.

[12] An experiment to determine the frequencies of the two low-energy modes, 16a and 16b, from solid film studies is now in progress.

[13] L. Corrsin, B. J. Fax, and R. C. Lord, J. Chem. Phys. **21,** 1170 (1953).

[14] F. A. Andersen, B. Bak, S. Brodersen, and J. Rastrup-Andersen, J. Chem. Phys. **23,** 1047 (1955).

[15] M. Ito, R. Shimada, T. Kuraishi, and W. Mizushima, J. Chem. Phys. **25,** 597 (1956).

[16] J. E. Lancaster and N. B. Colthup, J. Chem. Phys. **22,** 1149 (1954); R. F. Stamm and J. E. Lancaster, *ibid.* **22,** 1280 (1954).

may not prove to be such a good assumption for some of the values listed in the *s*-tetrazine-d_1 column, but it is quite reasonable for the frequencies of the two D_{2h} molecules.) The *s*-tetrazine-d_0 frequencies showing the largest shift upon passing to *s*-tetrazine-d_2 are then at about 3070, 1448, and 1106 cm^{-1}. We can immediately assign the 3070 cm^{-1} peak to the out-of-phase carbon-hydrogen stretching vibration (very little nitrogen atom motion) of symmetry species B_{2u}. Now the product rule for the ungerade B modes simply states that

$$^{\Gamma}\prod_{k}(\nu_k/\nu_k') = [\mu_H M(d_0)/\mu_D M(d_2)]^{\frac{1}{2}},$$

where μ_H and μ_D are the reciprocal masses of hydrogen and deuterium, $M(d_0)$ and $M(d_2)$ are the molecular weights of *s*-tetrazine-d_0 and -d_2, and ν_k and ν_k' are the frequencies of *s*-tetrazine-d_0 and -d_2, respectively, for normal mode k that is symmetry classified in the irreducible representation Γ of D_{2h}. This product has a theoretical value of 1.397. We would predict that the high-frequency B_{1u} mode would be seen as the fundamental band of lowest frequency in our spectra. We thus assign the 890 cm^{-1} peak to this out-of-plane, out-of-phase carbon-hydrogen motion; but since this implies that the B_{1u} mode 16*b* frequency should show an extremely large deuterium isotope shift, we are a bit skeptical of this assignment. However, the remaining assignments easily follow from the product rule; because the agreement is at least as good as could be expected, we do not believe that a better set of assignments can be made on the basis of the available spectral data.

Because there are 81 possible ungerade binary combination bands (not including rotational and translational modes) that can theoretically appear in the solid film spectrum of the natural *s*-tetrazine perfect crystal, it is difficult to attempt to gain information about the gerade frequencies from them. No binary combinations involving mode 6*a* can be found, and undoubtedly most of the unexplained structure in spectra **E** through **H** is due in some way to the monodeuterotetrazine. It is interesting to note that there do not seem to be any intensely absorbing vibrations of this C_{2v} molecule that correlate with the gerade frequencies of the two D_{2h} molecules.

The peculiar absorptions at 737 and 720 cm^{-1} of spectra **E** through **H** signify that an especially interesting phenomenon is being observed. Since these are the frequencies of the totally symmetric, gerade 6*a* vibrations of *s*-tetrazine-d_0 and -d_2, respectively, we are most likely observing a breakdown of the strict, perfect crystal selection rules. Whether or not the shoulder at 741 cm^{-1} is due to *s*-tetrazine-d_1 is unclear, but the change in the relative intensity of the other two peaks with the composition of the deuterated mixture strongly suggests the following. In the solid film, a ground state *s*-tetrazine-d_0 molecule may pass into the mode 6*a* vibrational state upon photon absorption if it is surrounded by molecules that have only slightly different perturbational interaction properties from those of another identical *s*-tetrazine d_0 molecule. It is quite clear that the rapid deposition technique does not produce a relatively large number of perfect crystals on the surface of the salt plate. The exact local symmetry of many of the *s*-tetrazine-d_0 molecules in the film that gave spectrum **A** is not necessarily that of the perfect unit cell. Thus the absence of the 737 cm^{-1} band from spectrum **A** indicates that this interesting phenomenon can not be entirely due to the deviations of the film structure from the perfect crystal model: the selection rules seem to be closely obeyed for the film spectra of pure substances. The really puzzling feature, however, is that we observed only this one gerade frequency, the frequency that is so intimately related to the visible $n\rightarrow\pi^*$ spectrum of *s*-tetrazine. It is difficult to associate any of the other peaks in the cold film spectra with a similar phenomenon; moreover, it seems impossible that the 737 and 720 cm^{-1} bands could both be due to the monodeuterotetrazine. Further investigations of deuterated mixtures are imperative, and, if extended to other systems, may yield useful information regarding the nature of the solid state of the film.

ACKNOWLEDGMENTS

We are extremely grateful to Professor E. L. Wagner of Washington State University both for his advice on the techniques of taking cold film spectra and for his valuable assistance during certain of the experiments. We should also like to acknowledge the kind assistance of Professor D. Eggers, Professor F. Schubert, Mr. D. Hamilton, and Mr. D. Yarian in various stages of the research.

APPENDIX

The following procedure for preparing pure *s*-tetrazine has been used successfully by us many times.[17] Because of their marked unstability towards decomposition and rearrangement, the intermediate compounds have not been unambigously characterized.

Sodium dihydrotetrazine-3,6-dicarboxylate.[18] To a solution of 180 g. of sodium hydroxide in 265 ml of water, 114 g (1 mole) of ethyl diazoacetate was added with stirring, over a period of 1 hr. The temperature was maintained at 90°C during the addition. After cooling, the product was poured into 1 liter of 95% ethanol and the mixture was stirred. The alcohol was decanted, and the washing procedure was repeated five times. The precipitate was filtered, washed with absolute alcohol and dry ether, and air dried, giving 125–145 g of the sodium salt.

s-Tetrazine-3,6-dicarboxylic acid. With stirring, 870

[17] More detailed directions and further discussion is given in the Ph.D. thesis of GHS, University of Washington, Seattle (1958). L. C. Card No. Mic 59–1239. See also reference 3 of I.

[18] The numbering convention for the ring atoms of the azines is that the nitrogens be labeled with the smallest integers possible.

g of cold 4.3*m* sulfuric acid was slowly added to 135 g of the above sodium salt. The mixture was allowed to stand for 9 hr and was then filtered. The precipitate was washed four times with 15-ml portions of water and dried on a clay plate giving 40 g of the yellow dihydrotetrazine-3,6-dicarboxylic acid. The acid was dissolved in a solution of 41 g of anhydrous sodium acetate in 300 ml of water and cooled to 10°C. To this solution was added a cold solution of 45 g of sodium nitrite in 100 ml of water over a period of 45 min. The mixture was stirred for 1 hr, and 40 ml of 10% acetic acid was added. After 1 hr, the solution was added to 2 l of 95% ethanol. The precipitate thus formed was filtered, washed with dilute ethanol, and air dried giving 52 g of sodium tetrazine-3,6-dicarboxylate.

To a solution of 50 g of the sodium salt in 700 ml of water at 10°C, 120 ml of cold 6*N* hydrochloric acid was rapidly added with stirring. The solution was filtered immediately, and the precipitate was washed with three 10 ml portions of ice water. After drying over phosphorus pentoxide, there was obtained 32 g of the reddish-pink *s*-tetrazine dicarboxylic acid.

s-Tetrazine. A finely ground mixture of one part of *dry* tetrazine dicarboxylic acid and five parts of dry, clean sand was placed in a sublimer and covered with a 5 mm layer of sand. The sublimer was rapidly heated in an oil bath to 150°C, at which temperature the decarboxylation occurred. The tetrazine which was collected on the cold finger was resublimed, giving 0.3 g of *s*-tetrazine per gram of diacid used. Tetrazine must be stored at low temperature (preferably in an evacuated tube) and in the absence of light.

Preparation of the deuterated mixtures. Various mixtures of *s*-tetrazine-d_0, *s*-tetrazine-d_1, and *s*-tetrazine-d_2 can be prepared by the pyrolytic decarboxylation of 3,6-*s*-tetrazine dicarboxylic acid that has received some degree of proton exchange with D_2O. This exchange reaction is inefficient not only because of its heterogeneous nature, but also because of the instability of wet diacid towards spontaneous decarboxylation, rearrangement, and/or decomposition. Our best yield of *s*-tetrazine-d_1 by this procedure was 52% (40%-d_0 and 8%-d_2). Attempts to prepare pure *s*-tetrazine-d_1 by first making the pure monocarboxylic acid were unsuccessful. The synthesis remains a challenge to the organic chemist.

THE JOURNAL OF CHEMICAL PHYSICS VOLUME 35, NUMBER 6 DECEMBER, 1961

Effects of Anharmonicity of Molecular Vibrations on the Diffraction of Electrons. II. Interpretation of Experimental Structural Parameters*

KOZO KUCHITSU† AND L. S. BARTELL

Department of Chemistry, Iowa State University, Ames, Iowa

(Received February 20, 1961)

The effects of anharmonic vibrations on the molecular intensity function $M(s)$ of electron diffraction and on the radial distribution function $f(r)$ considered in paper I, are treated more rigorously to meet current needs. More definitive general relations for interpreting experimental diffraction data in terms of molecular structure parameters of known absolute significance are presented.

IT was pointed out some time ago that the interpretation of experimental internuclear parameters of free molecules derived by electron diffraction is complicated by vibrational anharmonicity.[1] The effects of vibration on the molecular intensity function $M(s)$ and the radial distribution function $f(r)$ were studied in a preliminary way, particularly for diatomic molecules, assuming a Morse potential function.

The improvement of experimental techniques since that time permits the observation of vibrational effects with appreciably greater precision. Our recent study[2] of methane and deuteromethane by electron diffraction has demonstrated isotopic differences in the C–H and C–D mean distances and mean amplitudes which are satisfactorily explained by the difference in mass of the atoms vibrating in an anharmonic potential field. A phase shift of the molecular intensity from that expected for a harmonic oscillator has also been observed and shown to have a reasonable magnitude.

In addition, considerable interest has recently been expressed in the possibility of using amplitudes of vibration measured by electron diffraction to augment spectroscopic data in the characterization of the force fields of polyatomic molecules.[3,4] Because the number of

* This work was supported by the National Science Foundation.

† Present address: Department of Chemistry, Faculty of Science, University of Tokyo, Tokyo, Japan.

[1] L. S. Bartell, J. Chem. Phys. **23,** 1219 (1955), paper I.

[2] L. S. Bartell, K. Kuchitsu, and R. J. deNeui, J. Chem. Phys. **35,** 1211 (1961); see also J. Chem. Phys. **33,** 1254 (1960).

[3] Y. Morino, Y. Nakamura, and T. Iijima, J. Chem. Phys. **32,** 643 (1960).

[4] K. Hedberg, Proceedings of American Chemical Society Symposium on Status of Problems in Molecular Structure, Seattle, Washington, June 29, 1960; M. Iwasaki and K. Hedberg, Acta Cryst. **13,** 1108 (1960); see also G. W. Chantry and L. A. Woodward, Trans. Faraday Soc. **56,** 1110 (1960).

constants associated with a general force field usually exceeds the number of observed fundamental frequencies, it would be extremely useful to have the additional independent vibrational data provided by electron diffraction. It has been found,[3,4] however, that the accuracy demanded of the diffraction parameters for this purpose is very great. Amplitudes must be known to the order of 0.001 A or better if useful additional information is to be derived. It will be shown below that the arbitrariness in the diffraction parameters may be appreciably greater than this unless careful distinctions are made.

The purpose of this study is to extend the discussion given in paper I and to calculate the effects of zero-point vibrations on the determination of the mean amplitude l and the anharmonicity parameter a. The formulas of paper I, being concerned primarily with internuclear distances, neglect small terms in the distribution functions and consequently leave the interpretation of amplitudes somewhat ambiguous. The following discussion deals principally with the diatomic case since the potential energy functions of polyatomic molecules are complicated and uncertain. In many cases, however, the result will be transferable to polyatomic molecules, especially to the parameters of bonded distances.

PROBABILITY DISTRIBUTION FUNCTION

The internuclear probability distribution function assumed for the present calculations is

$$P(x)=A(\alpha/\pi)^{\frac{1}{2}}(1+\sum_{n=1}^{\infty}c_n x^n)\exp(-\alpha x^2), \qquad (1)$$

where

$$\alpha=4\pi^2\mu\nu_e/h=1/2l_\alpha^2, \qquad (2)$$

and $x=r-r_e$, with μ representing the reduced mass, ν_e the normal frequency of vibration, and A a normalization constant close to unity given by

$$A=\{1+\sum_{m=1}[c_{2m}(2\alpha)^{-m}(2m-1)!/2^{m-1}(m-1)!]\}^{-1}.$$

The form of $P(x)$ in Eq. (1) is the form naturally encountered in perturbation treatments of anharmonic oscillators[5] and is also a convenient form for handling the distribution function of the Morse anharmonic oscillator for which exact analytic expressions of the wave functions have been given.[6] Results of calculations will be given both for arbitrary coefficients c_n and for the ground vibrational state of the Morse oscillator. Although the use of the Morse distribution function is not completely justified,[7] it is considered to provide a reasonable model for the characterization of diffraction data.

For the ground vibrational state, the Morse oscillator distribution function is given by[6]

$$P_0(x)=K\exp\{-[(2\alpha/a^2)\exp(-ax)]+[a-(2\alpha/a)]x\}, \qquad (3)$$

in which the parameter a serves as a useful index of the anharmonicity, for a given value of α, such that the oscillator becomes harmonic as a tends to zero. The associated c_n are

$$c_1=a, \quad c_2=a^2/2, \quad c_3=a\alpha/3+a^3/6,$$
$$c_4=a^2\alpha/4+a^4/24, \quad c_5=a^3\alpha/10+a^5/120,$$
$$c_6=a^2\alpha^2/18+a^4\alpha/36+a^6/720, \quad \text{etc.} \qquad (4)$$

It is useful to note that $\alpha\gg a^2$, in general. By way of comparison, it is helpful in assessing the generality of the Morse form to observe that the coefficients resulting from a first-order perturbation treatment of the ground state of the anharmonic oscillator for which $V(x)=(k/2)(x^2-ax^3)$, are

$$c_1=a, \quad c_2=a^2/4, \quad c_3=a\alpha/3,$$
$$c_4=a^2\alpha/6, \quad c_6=a^2\alpha^2/36, \qquad (5)$$

and $c_n=0$ for all other n.

The way of characterizing the anharmonicity is not unique. However, it seems profitable at the present stage to represent the anharmonicity by a parameter a and to define it in relation to the potential function as c_1.

The relationship between $P(r)$ and the scattering of electrons by an assembly of gaseous diatomic molecules has been shown by Debye[8] to be

$$M(s)=c\int_0^\infty P(r)\frac{\sin sr}{sr}dr, \qquad (6)$$

where $M(s)$ is the reduced intensity function $(I_{\text{tot}}-I_{\text{at}})/I_{\text{at}}$, and c is a constant related to the scattering power of atoms.

MEAN DISTANCES

The important distance parameters, in terms of the notation of paper I, are $r_g(1)$ and $r_g(0)$. The former is the center of gravity of the radial distribution function $f(r)$ [Eq. (8) of paper I], and is therefore the parameter most naturally associated with electron diffraction experiments. The latter is the center of gravity of the probability distribution function. By using Eq. (1) the following simple expressions are obtained for $r_g(1)$ and $r_g(0)$:

$$r_g(1)=r_e+\epsilon_1 l_\alpha^2/\epsilon_0, \qquad (7)$$

and

$$r_g(0)=r_e+[(\epsilon_0+\epsilon_1 r_e+2\epsilon_2 l_\alpha^2)/(\epsilon_0 r_e+\epsilon_1 l_\alpha^2)]l_\alpha^2, \qquad (8)$$

[5] A. Reitan, Kgl. Norske Videnskabers Selskabs Skrifter, NR2 (1958).
[6] P. M. Morse, Phys. Rev. **34,** 57 (1929).
[7] Y. P. Varshni, Revs. Modern Phys. **29,** 664 (1957).
[8] P. Debye, J. Chem. Phys. **9,** 55 (1941). The simplified form of Eq. (6) strictly applies only if corrections have been made for the scattering by planetary electrons and for the failure of the Born approximation.

where the constants ϵ_n are given by

$$\epsilon_n=\sum_{m=0}[(n+2m)!/2^m n!m!]d_{n+2m}g^m,$$

$$(n, m=0, 1, 2, \cdots) \quad (9)$$

with

$$g=1/2\alpha=l_\alpha^2, \qquad d_0=1, \quad (10)$$

and

$$d_n=c_n-(d_{n-1}/r_e). \quad (11)$$

The summation of ϵ_n [Eq. (9)] converges fairly rapidly when n is a small number, so that the addition of the first few terms is sufficient to evaluate ϵ_n. The constant ϵ_0 is very nearly unity.

For the zero-point Morse oscillator the expressions reduce to

$$r_g(0)=r_e+(\tfrac{3}{2})al_\alpha^2+(1\tfrac{3}{4})a^3l_\alpha^4+\cdots, \quad (12)$$

and

$$r_g(1)=r_g(0)-l_\alpha^2/r_e-(3a^2/2r_e-5a/2r_e^2+2/r_e^3)l_\alpha^4+\cdots. \quad (13)$$

The terms with l_α^4 are generally less than 10^{-3} A.

MEAN AMPLITUDES

The mean amplitudes reckoned from the equilibrium position r_e and from the mean position $r_g(0)$ are denoted by l_e and l_g, respectively.[3,9] It can be shown that[5]

$$l_g^2=l_e^2-[r_g(0)-r_e]^2, \quad (14)$$

where

$$l_e^2=\int_{-\infty}^{\infty}x^2P(x)dx. \quad (15)$$

It follows from Eqs. (1) through (14) that

$$l_e^2=l_\alpha^2+2l_\alpha^4[(\epsilon_1+\epsilon_2r_e+3\epsilon_3l_\alpha^2)/(\epsilon_0r_e+\epsilon_1l_\alpha^2)], \quad (16)$$

and

$$l_g^2=l_\alpha^2+l_\alpha^4[6\epsilon_3(\epsilon_0r_e+\epsilon_1l_\alpha^2)l_\alpha^2+(r_e^2-2l_\alpha^2)(2\epsilon_0\epsilon_2-\epsilon_1^2)-\epsilon_0^2-2r_e\epsilon_1\epsilon_2l_\alpha^2-4\epsilon_2^2l_\alpha^4]/(\epsilon_0r_e+\epsilon_1l_\alpha^2)^2. \quad (17)$$

The Morse results are[10]

$$l_e^2=l_\alpha^2+(1\tfrac{5}{4})a^2l_\alpha^4+(4\tfrac{5}{2})a^4l_\alpha^6+\cdots, \quad (18)$$

and

$$l_g^2=l_\alpha^2+(\tfrac{3}{2})a^2l_\alpha^4-(5\tfrac{9}{2})a^4l_\alpha^6+\cdots. \quad (19)$$

Accordingly, l_e and l_g are readily calculated if l_α and a (or the more general coefficients c_n) are determined from the experiment. In the case of diatomic molecules, l_α is directly defined in relation to μ and ν_e as indicated in Eq. (2). For polyatomic molecules, l_e and l_g would seem the more significant parameters, with l_α simply representing a convenient parameter for expressing $P(r)$. In that case, l_α can be uniquely determined only if the coefficient c_2 is defined. It seems most convenient to define c_2 to be $a^2/2$ as in the case of the diatomic Morse oscillator.

The difference between l_e and l_α is particularly important in the case of hydrides. For hydrogen fluoride, for example, the spectroscopic data,[11] $\nu_e=4138.52$ cm^{-1} and $\nu_ex_e=90.069$ cm^{-1}, lead to the following results: $a=2.36_1$ A^{-1}, $l_\alpha=0.0652$ A, $l_g=0.0663$ A, and $l_e=0.0679$ A.

For the nitrogen molecule, however, the difference is much smaller. It is calculated that $a=2.417$ A^{-1}, $l_\alpha=0.0320$ A, $l_g=0.0321$ A, and $l_e=0.0323$ A, from Stoicheff's spectroscopic values,[12] $\nu_e=2357.84$ cm^{-1} and $\nu_ex_e=14.062$ cm^{-1}.

RADIAL DISTRIBUTION FUNCTION

The radial distribution function[13] $f(r)$, the Fourier sine transform of the modified molecular intensity curve, $sM(s)\exp(-bs^2)$, where $\exp(-bs^2)$ is a convergence factor, is related to $P(r)$ by

$$f(r)=c(\pi/16b)^{\frac{1}{2}}\int_{-\infty}^{\infty}P(x)(r_e+x)^{-1}\times\exp[-(r-r_e-x)^2/4b]dx, \quad (20)$$

where c is the constant of Eq. (6). The substitution of Eq. (1) into Eq. (20) leads to a function which is analogous to Eq. (9) of paper I but includes higher powers of x,

$$f(r)=A(c/2r_e)(\alpha\pi/\gamma)^{\frac{1}{2}}E(x)\exp(-\alpha x^2/\gamma), \quad (21)$$

where

$$E(x)=\sum_n\epsilon_n'\gamma^{-n}x^n \quad (22)$$

and $\gamma=4b\alpha+1$. The function $f(r)$ has a form similar to $P(r)$ given in Eq. (1), and the coefficients ϵ_n' of the polynomial $E(x)$ are related to the coefficients c_n of $P(x)$ by Eq. (9) if the quantity g is identified with $2b/\gamma$ rather than $1/2\alpha$ given in Eq. (10). The magnitude of g is commonly the order of 2×10^{-3} A^2.

EXPERIMENTAL MEAN AMPLITUDE

A method for obtaining the experimental amplitude from electron diffraction data has been described elsewhere,[14] but the relation between the experimental mean amplitude and the rational parameter l_g has not been discussed. The radial distribution curve computed from the experimental $M(s)$, given in Eq. (3) of reference 14, is comparable to $f(r)$ of Eq. (21) of the present paper when proper corrections have been made to $f(r)$ for

[9] K. Kuchitsu, Bull. Chem. Soc. Japan **32,** 748 (1959).

[10] Equations for r_g and l similar to (12), (13), (18), and (19) can be derived from the cubic oscillator model, Eq. (5). They agree with the corresponding Morse expressions through the terms proportional to l_α^3, as naturally expected.

[11] G. Herzberg, *Molecular Spectra and Molecular Structure, I* (D. Van Nostrand Company, Inc., New York, 1950), p. 536.

[12] B. P. Stoicheff, Can. J. Phys. **32,** 630 (1954).

[13] Although, strictly, it is $P(r)$ that is the radial distribution function, it is common usage to refer to $f(r)$ as the radial distribution function.

[14] R. A. Bonham and L. S. Bartell, J. Chem. Phys. **31,** 702 (1959).

TABLE I. Mean amplitudes of methane (in A units).

	l_c[a]	l_α[b]	l_g	l_e
C—H(CH_4)	0.074_5	0.073_2	0.075_1	0.078_1
C—D(CD_4)	0.066_0	0.065_0	0.066_2	0.068_4

[a] Corrected for the failure of Born approximation (reference 2).
[b] Calculated assuming $a=2.60\text{A}^{-1}$ and $r_e=1.085\text{A}$.

the effect of the finite upper limit of the Fourier integral, for the failure of the Born approximation, and for the finite specimen size. The corrected $f(r)$ is denoted by $f_0(r)$. The parameter l_α can be derived from $f_0(r)$ on the assumption that $f_0(r)$ has the form given by Eq. (21), with known c_n.

Since $E(x)$ has a suitable form for digital computations, a least-squares analysis may be made to fit $f_0(r)$ to Eq. (21) numerically with the adjustable parameters α, r_e, and a. The parameters α and r_e should be made self-consistent, but, unless the diffraction data are unusually precise, it is probably better to fix a at a plausible value than to vary it arbitrarily. Then l_α can be obtained from α by Eq. (2), and l_g and l_e are derived from l_α and a by Eqs. (16) through (19). This straightforward procedure is perhaps the best method for simple molecules if a reasonably fast digital computer is available.

An alternative procedure with the virtue of simplicity is to relate l_α to the l_c derived by a conventional analysis. As suggested in reference 14, the principal skewness of $f_0(r)$ can be eliminated by converting $f_0(r)$ to

$$f_c(r)=f_0(r)-(\pi^{\frac{1}{2}}ca_0\alpha_0^{\frac{1}{2}}/6r_0\gamma_0^{7/2})(r-r_0)^3 \times \exp[-\alpha_0(r-r_0)^2/\gamma_0], \quad (23)$$

where a_0, α_0, r_0, and γ_0 are the approximate values of the parameters a, α, r_e, and γ, respectively, used for the correction. The second term of Eq. (23) corresponds to the leading term of the cubic contribution to $E(x)$ in Eq. (21).[15] Since $f_c(x)$ is very nearly a Gaussian function it is readily fitted by

$$f_G(r)=(Rc/2r_c)[\pi/(4b+2l_c^2)]^{\frac{1}{2}} \times \exp[-(r-r_c)^2/(4b+2l_c^2)]. \quad (24)$$

If a least-squares criterion[16] is used to determine the optimum values of the parameters R, r_c, and l_c, the desired parameters $r_g(1)$ and l_α may be derived with the aid of the relations

$$r_c\simeq r_g(1)-a_0/4\alpha_0\gamma_0, \quad (25)$$

and

$$l_c^2\simeq l_\alpha^2+l_\alpha^4(-\epsilon_1'^2+2\epsilon_2'+6\epsilon_4'l_\alpha^2/\gamma+30\epsilon_6'l_\alpha^4/\gamma^2). \quad (26)$$

[15] For vibrational states higher than the ground state, terms higher than the cubic term begin to influence the center of gravity appreciably, however.
[16] With respect to the minimization of $\Sigma_i[f_c(r_i)-f_G(r_i)]^2$. For a convenient method suitable for the simultaneous fitting of many peaks in $f(r)$, see reference 14.

This procedure should be recycled to self-consistency if the input parameters r_e and α_0 are found to be in error by several fold more than (r_c-r_e) and $(l_c-l_\alpha)/l_\alpha^3$, respectively.

An example of the differentiation between the various amplitude parameters encountered in a diffraction investigation[2] of CH_4 and CD_4 is given in Table I. According to a perturbed normal coordinate analysis of methane using a modified anharmonic Urey-Bradley force field,[17] the distributions for C—H and C—D bonds are well characterized by the parameters r_e, a, and α.

FREQUENCY MODULATION OF MOLECULAR INTENSITY

As shown in reference 2, the phase shift of the molecular intensity curve from a sine curve, which takes place at large s and increases uniformly with s, is a sensitive measure of the vibrational anharmonicity. If the molecular intensity $M(s)$ as given by Eq. (6) is used with $P(r)$ as given by Eq. (1), it is found[18]

$$M(s)=Ac(\sigma_1^2+\sigma_2^2)^{\frac{1}{2}}\exp(-s^2/4\alpha)\{\sin s[r_e+\varphi(s)]\}/sr_e, \quad (27)$$

where

$$\sigma_1=\sum_{n=0}(-1)^n\epsilon_{2n+1}(l_\alpha^2s)2^{n+1} \quad (28)$$

and

$$\sigma_2=\sum_{n=0}(-1)^n\epsilon_{2n}(l_\alpha^2s)^{2n}. \quad (29)$$

Coefficients ϵ are given in Eqs. (9) through (11). The effective mean amplitude l_m^2, which is approximated by

$$l_m^2=l_\alpha^2+(2\epsilon_2/\epsilon_0-\epsilon_1^2/\epsilon_0^2)l_\alpha^4+\cdots, \quad (30)$$

is very nearly l_g^2. The phase shift $\varphi(s)$ is given by

$$\varphi(s)=(1/s)\tan^{-1}(\sigma_1/\sigma_2). \quad (31)$$

TABLE II. Calculation of phase shift[a] for methane (in 10^{-2} A).

	CH_4			CD_4		
s	I[b]	II[c]	III[d]	I	II	III
20	−0.564	−0.566	−0.528	−0.330	−0.332	−0.313
25	−0.871	−0.873	−0.825	−0.512	−0.514	−0.489
30	−1.234	−1.236	−1.188	−0.731	−0.733	−0.704
35	−1.643	−1.648	−1.617	−0.984	−0.986	−0.958
40	−2.087	−2.100	−2.112	−1.268	−1.270	−1.251

[a] Parameter a is assumed to be 2.60A^{-1}.
[b] Phase shift $\phi(s)$ calculated by Eqs. (31) and (32).
[c] $\phi(s)$ approximated by Eq. (35).
[d] $\phi(s)$ approximated by Eq. (38).

[17] K. Kuchitsu and L. S. Bartell (to be published).
[18] The necessary integrals are listed in: Bateman Manuscript Project, California Institute of Technology, *Table of Integral Transforms* (McGraw-Hill Book Company, Inc., New York, 1954), Vol. 1, pp. 15, 74, and 369.

If $\varphi(s)$ is expanded as a power series of s, it takes the form,

$$\varphi(s)=l_a^2\epsilon_1/\epsilon_0+\phi(s). \quad (32)$$

By the use of Eq. (7), Eq. (27) can be rewritten as

$$M(s)=Ac\exp(-l_m^2s^2/2)\{\sin s[r_g(1)+\phi(s)]\}/sr_e, \quad (33)$$

and accordingly, the phase shift $\phi(s)$ is defined with respect to $r_g(1)$. The function $\phi(s)$ is given by

$$\phi=\sum_{n=1}\phi_n(l_\alpha s)^{2n}. \quad (34)$$

In general, ϕ is approximated with considerable accuracy by the first two terms of Eq. (34). Namely,

$$\phi\sim\phi_1l_\alpha^2s^2+\phi_2l_\alpha^4s^4, \quad (35)$$

where, in the Morse case,

$$\phi_1=-al_\alpha^2/6-(a^2+1/r_e^2)(a/2-1/3r_e)l_\alpha^4-\cdots, \quad (36)$$

and

$$\phi_2=a^2l_\alpha^4/20+\cdots. \quad (37)$$

It should be noted that simply the first term of Eq. (36) can give a fairly good representation of the phase shift, which, in that approximation, is

$$\phi\sim-al_\alpha^4s^2/6. \quad (38)$$

This corresponds to the term $a\eta/4\alpha$ in Eq. (7) of paper I. To calculate ϕ with more accuracy than that given in Eq. (35), it is better to use Eqs. (31) and (32) with a digital computer.

A numerical calculation of $\phi(s)$ is made for CH_4 and CD_4, and the result is given in Table II.

CONCLUSION

If a sufficiently accurate radial distribution curve $f_0(r)$ is obtained by the Fourier sine transform of an experimental molecular intensity curve $M(s)$ followed by a series of appropriate corrections, it is then possible to derive the following structural parameters from $f_0(r)$: The internuclear distances, $r_g(1)$, $r_g(0)$, and r_e, the root mean square amplitudes of vibration, l_α, l_g, and l_e, and the anharmonicity parameter, a. The necessary analytical expressions are given in terms of the ϵ_n (or ϵ_n') of Eq. (9) which are readily computed from the coefficients c_n of Eq. (3).

In practical cases, it is convenient to use the following procedures based on the assumption that the probability distribution function is Morse-like. This assumption seems to be a reasonable approximation at the present stage of experimental accuracy.

1. $f_0(r)$ is converted to $f_c(r)$ using Eq. (23) by eliminating the principal skewness of $f_0(r)$.

2. By a least-squares analysis discussed in reference 14, r_c and l_c are obtained from $f_c(r)$ by Eq. (24).

3. $r_g(1)$ and l_α are obtained from r_c and l_c by Eqs. (25) and (26), respectively.

4. The phase shift $\phi(s)$ of Eq. (33) is calculated from the experimental $M(s)$ using $r_g(1)$ and l_α.

5. The parameter a is estimated from $\phi(s)$ and l_α by Eq. (35) or by Eq. (38).

6. The above procedures are recycled if necessary to make the parameter a assumed in the procedures 1 and 3 consistent with the result of the procedure 5.

7. l_e and l_g are obtained from l_α and a by Eqs. (18) and (19), respectively.

8. $r_g(0)$ and r_e are obtained from $r_g(1)$, l_α, and a by Eqs. (13) and (12), respectively.

Neutron Diffraction Studies of CaC_2, YC_2, LaC_2, CeC_2, TbC_2, YbC_2, LuC_2, and UC_2†

MASAO ATOJI

Chemistry Division, Argonne National Laboratory, Argonne, Illinois and
Institute for Atomic Research and Department of Chemistry, Iowa State University, Ames, Iowa

(Received April 13, 1961)

The complete-matrix least-squares analysis on the neutron diffraction intensities of CaC_2, YC_2, LaC_2, CeC_2, TbC_2, YbC_2, LuC_2, and UC_2 yielded the C—C distances in the C_2 groups, 1.191±0.009, 1.275±0.002, 1.303±0.012, 1.283±0.004, 1.293±0.009, 1.287±0.010, 1.276±0.012, and 1.340±0.007 A, respectively. The statistical averages of the neutron scattering amplitudes obtained from the dicarbide data and those reported previously are 0.488±0.007, 0.796±0.009, 0.832±0.014, 0.482±0.006, 0.756±0.020, 1.262±0.012, 0.73±0.02, and 0.851±0.022, all in 10^{-12} cm with positive sign, for Ca, Y, La, Ce, Tb, Yb, Lu, and U, respectively.

The paramagnetic scattering analyses revealed that all metal atoms in these dicarbides are in their trivalent Hund ground state, except Ca (divalent), Yb (possible valency of 2.8), and U (possible tetravalent). The scattering data also deduced the screening constants for the 4*f* electrons in Ce, Tb, and Yb as 39, 43, and 43, respectively, which are compared with those obtained by other methods. The bond numbers for the rare-earth dicarbides are briefly discussed.

INTRODUCTION

A NUMBER of metal dicarbides MC_2 possess the CaC_2-type structure but the divalent metals form nonmetallic dicarbides, whereas the metals of potential trivalent or higher valency form metallic dicarbides.[1–4] Our previous neutron analyses[5,6] have shown that the C–C distances in the C_2 groups in CaC_2, LaC_2, and UC_2 are 1.20±0.01, 1.28±0.02, and 1.34±0.01 A, respectively. The C–C distance increases as the potential metallic valency increases. These reported data of CaC_2, LaC_2, and UC_2 have been re-examined using the least-squares method. The refined parameters confirm previous results but are defined within narrower limits as described below. The experimental details for CaC_2, LaC_2, and UC_2 have been reported in our previous papers.[5,6]

The program has been extended to a series of rare-earth dicarbides, because, in general, their structural parameters are not only governed by the lanthanide contraction, but also are characterized by the individual electronic energy-level configuration. In particular, the abnormal lattice constants of YbC_2 may be interpreted as a possible indication of the divalent state of Yb, but YbC_2 is also a typical metallic compound.[2,3] The dicarbides of Pm and Eu have not been successfully prepared, although EuC_2 would provide an interesting problem similar to the case of YbC_2. Since some of the rare-earth elements possess prohibitively large capture cross sections, the dicarbides with low cross sections, CeC_2, TbC_2, YbC_2, and LuC_2 have been chosen as the respresentative compounds. The neutron-diffraction study of YC_2 has also been carried out, since most of the chemical and physical properties of yttrium characterize it as being a typical heavy lanthanide. In the present paper, the terminology "rare earths" implies also the yttrium atom, unless otherwise specified. The paramagnetic diffuse scattering of these rare-earth dicarbides was investigated in relation to the valency states of the metal atoms and to the screening constants for the 4*f* electrons. The measure of precision for all results reported in this paper is expressed in terms of the standard deviation.

EXPERIMENTAL

YC_2, CeC_2, TbC_2, YbC_2, and LuC_2 were prepared from the high-temperature direct combination of the respective metal (99.9 weight % pure, except Lu with an impurity of 2.0±0.2% Ta) and the powdered spectroscopic graphite-electrode.[2] In most of the dicarbide preparations, the formations of eutectic conglomerates are unavoidable as seen, for example, from the La–C phase diagram.[7] Hence, all samples were subjected to emission-spectrographic, chemical, and x-ray diffraction analyses for the determination of impurities. The results, within the maximum detectable limits of 0.05% and 0.1%, respectively, for metallic and nonmetallic impurities, are as follows: No impurities were detectable in YC_2 and TbC_2; 4.6±0.2% Ce_2C_3 in CeC_2; 4.04±0.03% graphite in YbC_2; and 2.2±0.1% graphite and 2.0±0.1% TaC in LuC_2. Special efforts were made for detecting the impurities with high capture and/or large paramagnetic cross sections, but none of them were found in our samples, except in CeC_2, where an impurity of 0.052±0.003 atomic % Gd in Ce was noted.

† Based on work performed under the auspices of the U. S. Atomic Energy Commission.

[1] M. von Stackelberg, Z. physik. Chem. (Leipzig) **9B**, 437 (1930); Z. Elektrochem. **37**, 542 (1931).

[2] F. H. Spedding, K. Gschneidner, Jr., and A. H. Daane, J. Am. Chem. Soc. **80**, 4499 (1958).

[3] R. C. Vickery, R. Sedlacek, and A. Ruben, J. Chem. Soc. **1959**, 498.

[4] R. E. Rundle, N. C. Baenziger, A. S. Wilson, and R. A. McDonald, J. Am. Chem. Soc. **70**, 99 (1948).

[5] M. Atoji, K. Gschneidner, A. H. Daane, R. E. Rundle, and F. H. Spedding, J. Am. Chem. Soc. **80**, 1804 (1958).

[6] M. Atoji and R. C. Medrud, J. Chem. Phys. **31**, 332 (1959).

[7] F. H. Spedding, K. Gschneidner, Jr., and A. H. Daane, Trans. Am. Inst. Mining Met. Petrol. Engrs. **215**, 192 (1959).

The hydrolyses of the rare-earth dicarbides take place in moist air,[2,8] although their reaction rates are generally slower than that for CaC_2. Consequently, finely powdered samples were sealed into the Ti–Zr alloy or aluminum cylindrical holders under dry nitrogen or argon atmosphere. Neutron-diffraction data at 293± 3°K were obtained with the neutron wavelength, $\lambda = 1.055 \pm 0.002$ A (0.0735 ev), using the Oak Ridge neutron spectrometer. The continuous scanning technique was employed but step-scanning data were also used for calibration purposes. Optimum experimental conditions were so chosen that the peak profiles obtained by the continuous scanning method should be identical to the step-scanning rocking curves and that the latter curves can be approximated by the Gaussian normal distribution function.[9] Accordingly, the total neutron intensity at the given angle θ is given by

$$P(\theta) = C(\theta) + \sum_{hkl} P_{hkl} \frac{h(\theta)}{\pi^{\frac{1}{2}}} \exp\{-h(\theta)(\theta - \theta_{hkl})\}^2, \quad (1)$$

where $C(\theta)$ is the background intensity and P_{hkl} is the integrated power of the coherently diffracted neutrons for the (hkl) peak with the Bragg angle of θ_{hkl}. The function $h(\theta)$ can be readily obtained from the relation $h(\theta) = 2(\ln 2)^{\frac{1}{2}}/A_{\frac{1}{2}}$, where $A_{\frac{1}{2}}$ is the full-width at half-height of the peak. The $A_{\frac{1}{2}}$ value[9] is a function of the horizontal angular divergence $\alpha_i (i = 1, 2, 3)$ of the ith collimator, the incident peak profile, the full width at half-maximum of the Gaussian mosaic distribution of the monochromating crystal β and $k = \tan\theta/\tan\theta_B$, where θ_B is the monochromating Bragg angle and is equal to 14.67° for the Cu(111) reflection used in the present study. In addition to the available geometrical data on the collimating system, analyses on the single-crystal diffraction patterns using a modified Willis'[10] formula (to be published elsewhere) yielded $\alpha_1 = \alpha_2 = 0.37°$, $\alpha_3 = 0.62°$, and $\beta = 0.27°$. The formula for $A_{\frac{1}{2}}$ in the powder case with the Gaussian incident peak profile is then expressed by

$$A_{\frac{1}{2}} = 0.523(k^2 - k + 1.783)^{\frac{1}{2}}. \quad (2)$$

The calculated $A_{\frac{1}{2}}$ values are compared with the observed ones in Fig. 1, where the values obtained from the carbides, nickel, graphite, and rare-earth metals are summarized. At higher angles, the observed peak widths suffer from larger statistical errors and the calculated peak widths are more sensitive to the parameters employed, particularly to the shape of the incident beam cross section. Nevertheless, the $h(\theta)$ values can be expressed either numerically or analytically and hence $P(\theta)$ is a function of $C(\theta)$ and P_{hkl} only. These two unknowns in the overlapped peaks at low angles were evaluated using the least-squares method with the $P(\theta)$ values at 0.1° intervals in θ. The $h(\theta)$ values at higher angles are less reliable as discussed above and therefore Wilson's statistical method[11] was supplemented to the least-squares method for determining the $C(\theta)$ values of the group reflections. The impurity peaks were subtracted from the main reflections with the help of the methods described above.

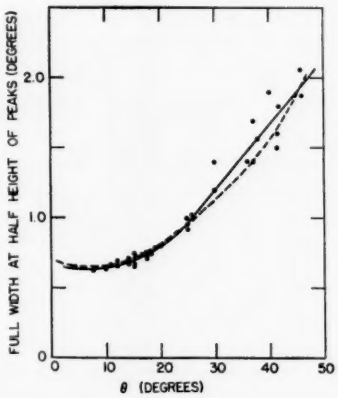

FIG. 1. Comparison between the observed and calculated full widths at half-height of the peaks. The observed values are shown by dots and the solid line, the calculated values by the dashed line.

The neutron power of the coherent reflection for the continuous scanning method is given by

$$P_{hkl} = (K/\Omega) N_c^2 \frac{\rho' j \mid F \mid^2 A}{\rho \sin\theta \sin 2\theta} \exp\left[-2B\left(\frac{\sin\theta}{\lambda}\right)^2\right], \quad (3)$$

where K represents the instrumental constants,[12] Ω the angular velocity of the counter, N_c the number of unit cells per cm³, ρ' and ρ, respectively, the apparent powder density and crystal density, j the multiplicity factor for the reflection (hkl), F the crystal structure factor, A the absorption factor, and B the temperature factor coefficient. The P_{hkl} values were obtained by measuring the coherent peak areas with a polar planimeter and the scaler recordings were also extensively utilized in the intensity determination.[13] The absorption factors were obtained from the transmission cross sections with three-place accuracy and the absorption corrections were made with quadratically interpolated values based on Bond's table.[14] The coherent scattering from the sample holders were corrected for absorption[15] and were subtracted from the total coherent scattering.

The total differential cross section for the diffuse scattering, $d\sigma/d\omega$ per molecule, is obtained from the relation

$$C(\theta) = (8\pi K/\lambda^3) N_c n_c (\rho'/\rho)(d\sigma/d\omega) A, \quad (4)$$

where n_c is the number of molecules or chemical units per unit cell of crystal. The instrumental and sample

[8] G. L. Putnam and K. A. Kobe, Chem. Revs. **20,** 131 (1937).
[9] G. Caglioti, A. Paoletti, and F. P. Ricci, Nuclear Instr. **3,** 223 (1958).
[10] B. T. M. Willis, Acta Cryst. **13,** 763 (1960).
[11] A. J. C. Wilson, Nature **150,** 152 (1942).
[12] W. O. Milligan, L. W. Vernon, H. A. Levy, and S. W. Peterson, J. Phys. Chem. **57,** 535 (1953).
[13] S. W. Peterson and H. A. Levy, J. Chem. Phys. **20,** 704 (1952).
[14] W. L. Bond, Acta Cryst. **12,** 375 (1959).
[15] H. A. Levy and P. C. Sharrah, Oak Ridge National Laboratory Rept. ORNL-1832.

TABLE I. Coherent scattering amplitudes of metal atoms, b_M in 10^{-12} cm,[a] carbon parameters, z, temperature factor coefficients, B in A^2, percentage standard deviations for scale factors, $\sigma k/k$ in %, and agreement factors in % obtained from (a) three-variable and (b) four-variable refinements. The weighted averages are given in (c).

		CaC_2	YC_2	LaC_2	CeC_2	TbC_2	YbC_2	LuC_2	UC_2[e]
b_M	(a)	0.489 ±0.008[16]	0.80 ±0.01[b]	0.832 ±0.014[16]	0.464 ±0.017[16]	0.75 ±0.03[c]	1.262 ±0.013[d]	0.73 ±0.02[d]	0.846 ±0.024[16]
	(b)	0.484 ±0.013	0.786 ±0.017	0.826 ±0.057	0.484 ±0.006	0.762 ±0.030	1.263 ±0.036	...	0.878 ±0.056
	(c)	0.488 ±0.007	0.796 ±0.009	0.832 ±0.014	0.482 ±0.006	0.756 ±0.020	1.262 ±0.012	0.73 ±0.02	0.851 ±0.022
z	(a)	0.4068±0.0009	0.3968±0.0003	0.4009±0.0012	0.4005±0.0006	...	0.3947±0.0008	0.393 ±0.001	0.3881±0.0008
	(b)	0.4066±0.0010	0.3966±0.0004	0.4009±0.0013	0.4013±0.0004	0.3960±0.0007	0.3946±0.0012	...	0.3880±0.0009
	(c)	0.4067±0.0007	0.3967±0.0002	0.4009±0.0009	0.4011±0.0003	0.3960±0.0007	0.3947±0.0007	0.393 ±0.001	0.3881±0.0006
B	(a)	0.90 ±0.09	0.36 ±0.02	0.18 ±0.16	0.58 ±0.07	...	0.75 ±0.08	0.75 ±0.10	0.15 ±0.07
	(b)	0.90 ±0.10	0.36 ±0.02	0.18 ±0.17	0.56 ±0.04	0.74 ±0.05	0.77 ±0.10	...	0.15 ±0.07
$\frac{\sigma k}{k}$	(a)	2.0	0.8	5.2	1.4	...	1.4	1.8	2.2
	(b)	2.3	1.8	7.8	0.9	3.4	3.4	...	6.0
R	(a)	2.3	2.4	4.0	4.2	...	2.2	0.76	2.3
	(b)	2.4	2.5	4.2	2.2	4.0	2.5	...	2.4
R_3	(a)	3.3	1.3	7.3	2.3	...	1.6	2.0	3.4
	(b)	3.3	1.3	7.3	1.1	2.5	1.6	...	3.3

[a] All b_M's have positive sign.
[b] E. Prince, Acta Cryst. **10,** 787 (1957).
[c] W. C. Koehler (private communication, 1960).
[d] M. Atoji, Phys. Rev. **121,** 610 (1961).
[e] The three-variable refinement on A. E. Austin's data on UC_2 [Acta Cryst. **12,** 159 (1959)] yielded z=0.389±0.003, B=0.30±0.27, $\sigma k/k$=10, R=2.5 and R_3=12.

holder scattering corrected for absorption[15] and epicadmium neutrons were properly subtracted from the observed background. The factor K was determined from the coherent scattering of pure nickel powder for which the coherent scattering cross section, 13.2±0.2 b, was used.[16] The Debye temperature of Ni was found to be 413±5°K from the neutron data, while the calorimetric Debye temperature is 413°K.[17] More precise values of K were obtained from the least-squares method described in the following section. The secondary extinction and preferred orientation effects were found to be negligible. No coherent magnetic scattering was observed from CaC_2, YC_2, LaC_2, CeC_2, TbC_2, YbC_2, LuC_2, and UC_2 at 293±3°K.

LEAST-SQUARES REFINEMENTS

The method of least squares with the full-matrix treatment for minimizing a function $\sum_u w(\sum_\sigma I_{\text{obs}} - \sum_\sigma I_{\text{calc}})^2$ was used in the structure refinement. Here $\sum_\sigma$ represents the sum over a group of reflections which are not accurately resolvable into the individual reflections, and $\sum_u$ represents a sum over the independent groups. The weighting factor w is set to be equal to $(\sigma I_{\text{obs}})^{-2}$, where σI_{obs} is the standard deviation of the observed intensity. With the aid of the IBM 650 digital computer the least-squares procedure was repeated until the parameters no longer changed, and the matrix of the normal equations was then inverted to determine the standard deviations of the final parameters. Using the reported coherent scattering amplitudes of Ca, Y, La, Ce, Yb, Lu, U [see (a) in Table I] and C, the three variables, the positional parameter for carbon atoms at (000, $\frac{1}{2}\frac{1}{2}\frac{1}{2}$)±(00$z$), the isotropic temperature factor coefficient B, and the scale factor K, were refined for CaC_2, LaC_2, YC_2, CeC_2, YbC_2, LuC_2, and UC_2. Since the scattering amplitude of carbon is accurately known (b_c=0.662±0.0024 in 10^{-12} cm),[16] the four-variable refinement, taking the scattering amplitude of the metal atom as an additional parameter, was carried out for CaC_2, LaC_2, YC_2, CeC_2, YbC_2, UC_2, as well as for TbC_2, where b_{Tb} was unknown. The LuC_2 data suffered from many impurity peaks and were not used for the latter refinement. The anisotropic temperature factors were introduced into the refinements but the results failed to meet the physical significance, partly because of the small number of independent reflections relative to the number of the variables. On the other hand, it is rather doubtful to expect large anisotropic thermal motions in these metallic compounds. The anisotropic temperature factors for CaC_2 have been discussed in our previous paper.[6]

The final results obtained from two independent refinements and their weighted averages are listed in Table I. The agreement factors listed in Table I are defined by

$$R=[\sum_u w(I_{\text{obs}}-I_{\text{calc}})^2/n-m]^{\frac{1}{2}}, \quad (5)$$

$$R_3=[\sum_u w(I_{\text{obs}}-I_{\text{calc}})^2/\sum_u wI_{\text{obs}}{}^2]^{\frac{1}{2}}, \quad (6)$$

where R and R_3 are the standard deviation of an observation of unit weight and the root-mean-square discrepancy factor with weighting factors, respectively. In the above expressions, the symbol $\sum_\sigma$ has been omitted and n and m are the number of observations and variables, respectively. The expectation value of R is unity if the errors in I_{obs} follow the Gaussian law and σI_{obs}'s are properly assigned. The R values in Table I imply underestimated σI_{obs}, except for the case of LuC_2, where σI_{obs}'s are overestimated. The standard deviations in the scattering amplitudes, the temperature-factor coefficients and the scale factors are much larger than those for the carbon parameters. Inversely, the precision positional parameters can generally be obtained with less precise scattering amplitudes, and deduction of the veracious thermal parameters would be by far a difficult task in structure determination. The scattering amplitudes obtained from the dicarbide data are not significantly different from the reference values, except in the case of Ce. The change in the scattering amplitude of Ce from the literature value of 0.46×10^{-12} cm to the present one of 0.484×10^{-12} cm shows considerable improvement in the over-all agreements. The most probable values of the coherent scattering cross sections of Ca, Y, La, Ce, Tb, Yb, Lu, and U are deduced from the values in Table I are, respectively, 2.99±0.09, 7.96±0.18, 8.7±0.3, 2.92±0.07, 7.18±0.38, 20.0±0.4, 6.7±0.4, and 9.1±0.5, all in barns. In Table II(a) to (h), the observed intensities with their standard deviations are listed with the calculated values obtained from the four-variable refinements, except for LuC_2, where the results obtained from the three-variable refinements are shown. The neutron wave lengths employed are also indicated in Table II(a) to (h). All I_{calc} values in Table II are equal to

$$\frac{jF^2\exp[-2B(\sin\theta/\lambda)^2]}{\sin\theta\sin2\theta} \quad \text{in } 10^{-24}\text{ cm}^2.$$

PARAMAGNETIC SCATTERING

The observed total diffuse scattering was interpreted using the methods developed by Trammell,[18] and Koehler and Wollan.[19] Assuming the rare-earth ions have the Russell-Saunders LS coupling and are in the Hund ground state,[20] and using the hydrogenlike radial wave function, Trammell[18] has obtained the expression for

[15] D. J. Hughes and R. B. Schwartz, *Neutron Cross Sections* (U. S. Government Printing Office, Washington, D. C., 1958).
[16] W. H. Keesom and C. W. Clark, Physica **2**, 513 (1935).
[18] G. T. Trammell, Phys. Rev. **92**, 1387 (1953).
[19] W. C. Koehler and E. O. Wollan, Phys. Rev. **92**, 1380 (1953).
[20] J. H. Van Vleck, *The Theory of Electric and Magnetic Susceptibilities* (Clarendon Press, Oxford, England, 1932), p. 241.

TABLE II. Observed and calculated neutron diffraction intensities.

Indices	I_{calc}		I_{obs}	Indices	I_{calc}		I_{obs}
	(a) CaC_2 (λ=1.090 A)						
101	216.7	348	350±4	312		110	146±20
002	130.8			303	27.2	344	358±7
110		629	637±5	006	6.4		
112		213	212±4	321	34.7		
200	300.9	392	371±8	224	8.5		
103	91.2			215	267.3		
211	101.2			116	21.3	133	177±22
202	130.0	237	212±6	314	14.3		
004	5.8			400	59.4		
114	16.7			323	38.2		
220	138.5	242	234±6	206	18.2	224	199±18
213	87.2			411	24.9		
301	26.7			402	32.2		
222	69.0			330	51.0		
204	12.8	522	523±8	305	97.3		
310	212.7						
105	200.6						
	(b) YC_2 (λ=1.055 A)						
101	40.1	217	220±2	314	11.5		
002	177.1			400	105.8		
110		851	842±4	323	152.9		
112		292	291±3	206	1.4		
200	423.7	720	718±3	411	6.2	662	645±6
103	296.4			402	57.2		
211	20.1			305	189.6		
202	183.2	207	206±2	330	94.6		
004	4.0			107	42.4		
114	11.8			332	51.7		
220	210.6	523	529±3	420	171.5		
213	301.0			413	124.3		
301	5.7			226	1.2		
222	104.9			422	94.6		
204	9.3	797	812±4	404	4.3	857	859±7
105	340.5			325	315.1		
310	336.7			217	70.8		
312	173.0			008	17.0		
303	101.0	274	277±3	316	2.1		
006	0.5			334	4.0		

Indices	I_{calc}		I_{obs}	Indices	I_{calc}		I_{obs}
	(b) YC_2 (λ=1.055 A)						
321	8.0						
224	6.6	501	490±4				
215	484.8						
116	1.6						
	(c) LaC_2 (λ=1.277 A)						
101	27.3	193	200±3	312		180	202±5
002	166.1			303		80	79±4
110		706	947±30	006		1	<7
112		281	279±4	321	6.1		
200	357.2	574	557±8	224	2.5	457	421±16
103	216.6			215	448.1		
211	14.2			116		3	<7
202	179.6	195	175±3	314	4.5		
004	1.4			400	100.4	232	197±20
114	4.2			323	127.0		
220	184.0	417	418±6				
213	229.2						
301	4.2						
222	106.8						
204	3.4	715	751±2				
105	300.7						
310	299.6						
	(d) CeC_2 (λ=1.055 A)						
101	219.2	344	347±2	312	114.7	162	172±4
002	124.4			303	47.4		
110		691	589±2	006	5.8		
112		204	206±2	321	40.5		
200	399.2	485	474±6	224	17.5	445	439±4
103	146.1			215	360.8		
211	107.2			116	20.0		
202	126.5	245	241±2	314	30.2		
004	11.2			400	77.7		
114	32.5			323	69.6		
220	164.0	342	349±3	206	17.4		
213	145.0			411	30.4	505	496±7
301	29.7			402	36.3		
222	70.5			305	137.0		
204	25.4	644	652±5	330	68.3		
105	260.1			107	38.0		
310	258.5						

Table II (*continued*)

Indices	I_{calc}		I_{obs}	Indices	I_{calc}		I_{obs}
(e) TbC_2 (λ=1.055 A)							
101	46.3	212	213±3	314	11.3		
002	166.2			400	83.5	217	218±4
110		821	836±4	323	121.4		
112		266	265±3	206	1.2		
200	397.0	676	669±3	411	5.7		
103	279.4			402	42.7		
211	21.9			305	145.6	296	299±8
202	162.3	189	175±2	330	72.6		
004	4.5			107	29.4		
114	12.9			332	37.5		
220	196.5	467	459±4	420	127.9		
213	268.0			413	93.1		
301	5.9			226	0.9		
222	87.8			422	66.6		
204	9.9	687	701±3	404	3.8	619	637±8
105	293.3			325	228.3		
310	289.7			217	46.4		
312	140.7			008	12.7		
303	84.9	226	219±3	316	1.6		
006	0.4						
321	7.8						
224	6.6						
215	394.2	410	391±4				
116	1.4						
(f) YbC_2 (λ=1.055 A)							
101	27.9	369	381±5	114	1.1		
002	340.9			220	339.8	983	974±12
110		1289	1289±6	213	642.5		
112		575	570±7	301	4.3		
200	655.1	1260	1257±16	222	220.6		
103	605.2			204	0.9	1334	1372±17
211	14.6			105	553.6		
202	369.1	384	370±5	310	554.7		
004	0.4						
(g) LuC_2 (λ=1.055 A)							
101	48.8	180	176±7	211	23.0		
002	130.8			202	128.3	157	162±7
110		739	754±20	004	6.0		
112		210	203±8	114	17.1		
200	356.7	628	620±25	220	166.7	444	445±20
103	271.5			213	260.3		
(h) UC_2 (λ=1.090 A)							
101	8.3	153	146±4	312	152.3		
002	144.9			303	146.5	300	329±11
110		815	818±7	006	1.0		
112		240	237±5	321	1.8		
200	412.0	815	891±27	224	7.6	497	426±30
103	403.3			215	484.0		
211	4.3			116	3.4		
202	152.9	162	152±5	314	13.6		
004	4.3			400	115.6	363	333±13
114	12.9			323	230.8		
220	212.5	647	631±8	206	3.1		
213	421.4			411	1.5		
301	1.3			402	53.6		
222	90.6			305	196.9	373	375±13
204	10.4	777	795±8	107	15.7		
105	328.7			330	105.7		
310	346.2						

the paramagnetic differential cross section,

$$d\sigma/d\omega=\tfrac{2}{3}(e^2\gamma/2mc^2)^2[L_JF_0^L(k)+2S_JF_0^S(k)-\tfrac{1}{2}L_JF_2^L(k)], \quad (7)$$

where γ is the magnetic moment of the neutron in nuclear Bohr magnetons, $L_J=\mathbf{L}\cdot\mathbf{J}/|\mathbf{J}|$, $S_J=\mathbf{S}\cdot\mathbf{J}/|\mathbf{J}|$, and the parameter k is equal to $8\pi a_0\sin\theta/[\lambda(Z-S)]$, where a_0 is the Bohr radius and S is the screening constant. The formulas for $F_0^L(k)$, $F_0^S(k)$, and $F_2^L(k)$ have been given by Trammell but their numerical values in his Table V are too coarse in k for practical use and are in error in some instances. Hence, they are calculated for the finer intervals of ka and are given in Table III. The (L_J, S_J) values are (3.38, −0.423), (3.24, 3.24), and (3.40, 0.567) for $Ce^{+3}(4f\ ^2F_{5/2})$, $Tb^{+3}(4f^8\ ^7F_6)$, and $Yb^{+3}(4f^{13}\ ^2F_{7/2})$, respectively. No paramagnetic scattering is expected from the ground states of Ca^{+2}, Y^{+3}, La^{+3}, and Lu^{+3}. The paramagnetic scattering from UC_2 is not discussed in this paper. The paramagnetic differential cross sections of the free tri-

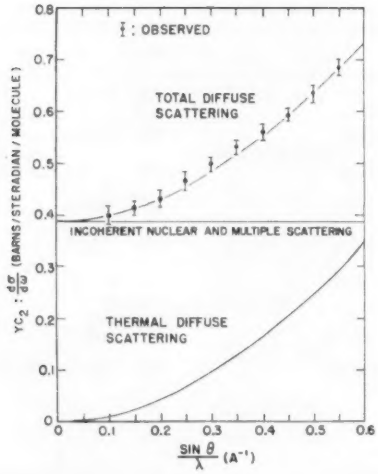

FIG. 2. Diffuse scattering by YC_2. Good agreement between observed diffuse scattering represented by dots and expected total diffuse scattering (a sum of the thermal diffuse scattering and the incoherent nuclear and multiple scattering) indicate no paramagnetic scattering from this compound.

valent ions at $k=0$ are 0.311, 4.58, and 0.994 b/ion for Ce^{+3}, Tb^{+3}, and Yb^{+3}, respectively. The thermal incoherent differential cross sections were computed from the Debye approximation,

$$\sum b^2\{1-\exp[-2B(\sin\theta/\lambda)^2]\}.$$

The nuclear and multiple incoherent scattering were assumed to be isotropic[21] and their contributions were evaluated from the total diffuse background at high scattering angles, where the paramagnetic contribution is small enough to be neglected. However, it should be noted that the paramagnetic scattering for the high effective nuclear charge $(Z-S)$ may still contribute considerably to the background even at our instrumental maximum angle $(2\theta=130°)$. Although the possible errors due to this uncertainty have been included in the observed values, more conclusive results could have been obtained, if wider instrumental limitations were available.

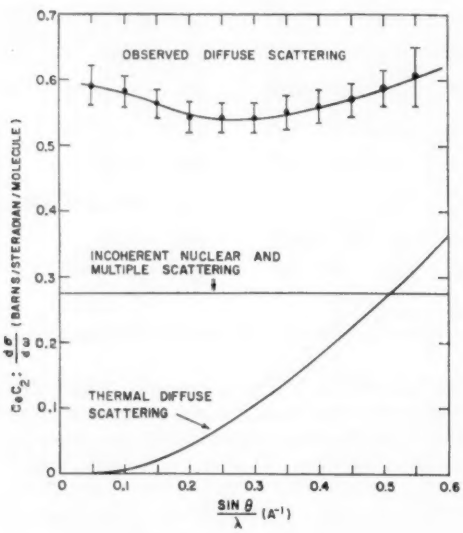

FIG. 3. Diffuse scattering by CeC_2. The paramagnetic scattering is obtained by subtracting both the incoherent nuclear and multiple scattering and the thermal diffuse scattering from the observed diffuse scattering.

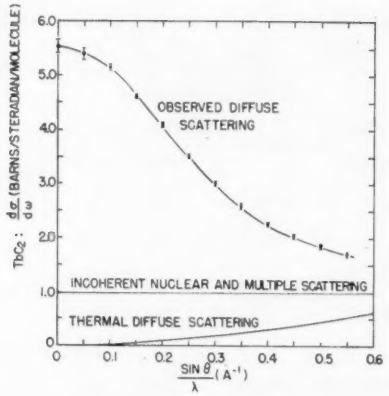

FIG. 4. Diffuse scattering by TbC_2.

The observed total incoherent differential cross section per molecule is compared with the thermal, nuclear, and multiple scattering cross sections in Figs. 2–5 for YC_2, CeC_2, TbC_2, and YbC_2, respectively. Even though the contribution of the impurity diffuse scattering to the total background is very small, the incoherent scatterings from graphite (Fig. 6) and Ce_2C_3 were analyzed independently and their proportions

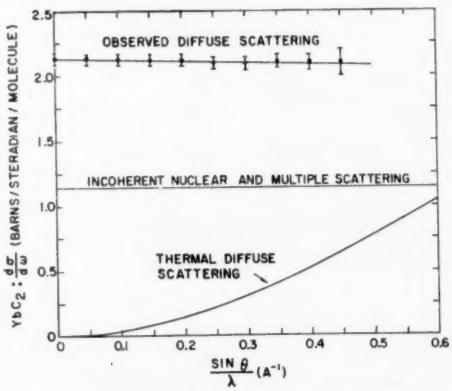

FIG. 5. Diffuse scattering by YbC_2.

[21] G. H. Vineyard, Phys. Rev. **96**, 93 (1954).

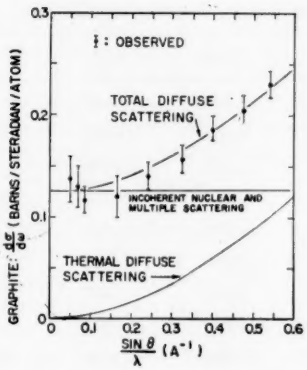

FIG. 6. Diffuse scattering by graphite. Paramagnetic component is too small to be detected.

were subtracted from the total values. The resultant maximum errors in the observed values are schematically shown in Figs. 2–6.

No paramagnetic scattering was observed for YC_2 (Fig. 2). Hence, both yttrium and the C_2 group in YC_2 must be nonparamagnetic or very weakly paramagnetic, in accordance with the expectations from the $^1S_0$ state of Y^{3+} and the ground state of the acetylene ion C_2^{-2}.[6] Similarly, although less precisely, CaC_2, LaC_2, and LuC_2 were found to be essentially nonparamagnetic. The observed paramagnetic cross sections as obtained by subtracting the thermal, nuclear, and multiple components from the total incoherent cross sections, are shown in Figs. 7–9, respectively, for CeC_2, TbC_2, and YbC_2. The effective nuclear charges for the $4f$ electrons as determined by comparison between the observed and calculated values are 19 for Ce^{3+}, 22 for Tb^{3+}, and 27 for Yb^{3+}. The maximum and minimum possible values of $(Z-S)$ are also shown in Figs. 7–9. The relative accuracy in the paramagnetic analysis is proportional to the magnitude of the paramagnetic scattering. Hence, the TbC_2 data provide good accuracy in its interpretation, that is, the observed values are in accordance with those for the free ion but failed to reveal the crystalline-field effects on the $4f$ energy levels.[18]

TABLE III. Numerical values for the Trammell paramagnetic scattering functions.

k	F_0^L	F_2^L	F_0^S
0	1.000	0	1.000
0.02	0.996	0.001	0.994
0.04	0.988	0.005	0.977
0.06	0.973	0.011	0.947
0.08	0.953	0.018	0.908
0.10	0.929	0.028	0.860
0.12	0.899	0.040	0.803
0.14	0.865	0.052	0.741
0.16	0.828	0.065	0.674
0.18	0.788	0.080	0.605
0.20	0.747	0.094	0.534
0.22	0.704	0.108	0.464
0.24	0.660	0.122	0.396
0.26	0.616	0.135	0.331
0.28	0.572	0.147	0.270
0.30	0.530	0.158	0.214
0.32	0.488	0.168	0.163
0.34	0.448	0.176	0.118
0.36	0.411	0.184	0.079
0.38	0.375	0.189	0.047
0.40	0.341	0.193	−0.017
0.42	0.310	0.196	−0.006
0.44	0.281	0.197	−0.024
0.46	0.254	0.198	−0.038
0.48	0.230	0.197	−0.048
0.50	0.208	0.195	−0.055
0.55	0.162	0.187	−0.061
0.60	0.126	0.175	−0.056
0.65	0.100	0.161	−0.047
0.70	0.081	0.146	−0.036

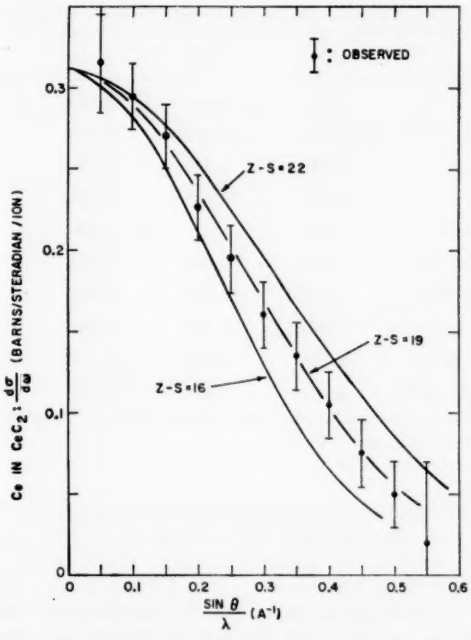

FIG. 7. Paramagnetic scattering cross section of Ce in CeC_2. The solid curves are calculated for screened hydrogen radial wave function with $Z-S=19$ (most probable value), $Z-S=16$ (possible minimum value) and $Z-S=22$ (possible maximum value).

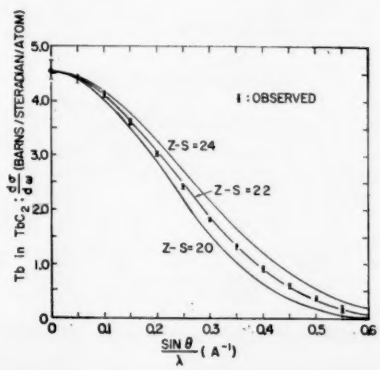

FIG. 8. Paramagnetic scattering cross section of Tb in TbC_2.

TABLE IV. Tetragonal lattice constants, a and c, interatomic distances and their standard deviations σ in A.

	CaC_2	YC_2	LaC_2	CeC_2	TbC_2	YbC_2	LuC_2	UC_2
a	3.89	3.664	3.934	3.878	3.690	3.637	3.563	3.517
σa	0.01	0.0015	0.003	0.0015	0.003	0.006	0.0015	0.002
c	6.38	6.169	6.572	6.488	6.217	6.109	5.964	5.987
σc	0.01	0.006	0.0015	0.003	0.0074	0.015	0.009	0.002
C—C	1.191	1.275	1.303	1.283	1.293	1.287	1.276	1.340
σ(C—C)	0.009	0.002	0.012	0.004	0.009	0.010	0.012	0.007
C—M[a]	2.595	2.447	2.635	2.602	2.462	2.411	2.344	2.324
σ(C—M)	0.005	0.003	0.006	0.002	0.005	0.007	0.007	0.004
C—4M′[b]	2.814	2.668	2.857	2.816	2.688	2.651	2.599	2.575
σ(C—4M′)	0.001	0.001	0.007	0.001	0.002	0.004	0.002	0.002

[a] Metal atom at (000).
[b] Metal atom at $(\frac{1}{2}\frac{1}{2}\frac{1}{2})$.

The effective Bohr magneton numbers (μ_{eff}) of the free ions are 2.54, 9.72, and 4.54 for Ce^{3+}, Tb^{3+}, and Yb^{3+}, respectively. Recently, Vickery *et al.*[22] obtained 2.19 for CeC_2, 9.57 for TbC_2, and 3.69 for YbC_2, from the magnetic measurement. All of their values are considerably smaller than the free-ion values and they interpreted the discrepancy as due to the partial quenching of the orbital angular momentum. The neutron values are 2.54 ± 0.07 for CeC_2, 9.7 ± 0.2 for TbC_2, and 4.5 ± 0.2 for YbC_2 and are not completely in agreement with those reported by Vickery, *et al.*[22] Since the statistical error in the neutron-paramagnetic determination for YbC_2 is considerably large, P. E. Roughan and A. H. Daane of the A.E.C. Ames laboratory have recently carried out the magnetic measurement on YbC_2 and obtained $\mu_{eff}=4.14$, $C=2.12$ emu/mol, and $\Delta=-532°$K in the Curie-Weiss formula, $\chi_M=C/(T-\Delta)$, with the molecular susceptibility $\chi_M=2.54\times10^{-3}$ emu/mol at 304°K. The value, $\mu_{eff}=4.14$, may be interpreted as 83% Yb^{+3} and 17% Yb^{+2} for Yb in YbC_2. Since the graphite impurity is rather common in all metallic dicarbides and since graphite is strongly diagmagnetic,[23,24] the values reported by Vickery *et al.* must be in error, unless the impurity susceptibility was properly subtracted from the total value. It should be noted that the temperature dependency of the susceptibility of graphite can be closely approximated by a Curie-Weiss-like formula for the temperature range which Vickery *et al.* studied. Hence, the apparent susceptibility of the dicarbide with the graphite impurity can also be approximated by the Curie-Weiss law. In summary, it is concluded that the rare-earth atoms in their dicarbides are in the trivalent Hund ground state, except Yb in YbC_2, and possibly Eu in EuC_2.

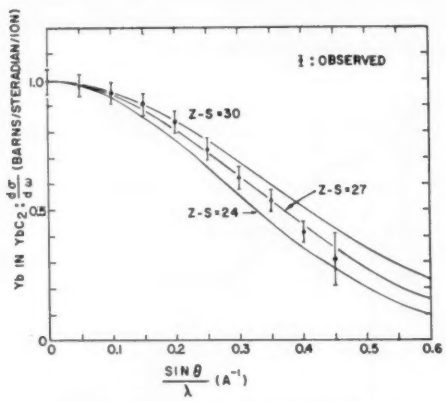

FIG. 9. Paramagnetic scattering cross section of Yb in YbC_2.

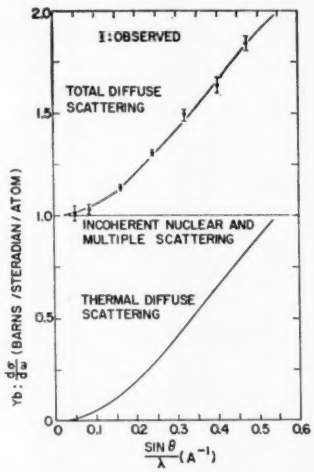

FIG. 10. Diffuse scattering by Yb metal, showing no paramagnetic scattering.

[22] R. C. Vickery, R. Sedlacek, and A. Ruben, J. Chem. Soc. **1959,** 503.

[23] H. T. Pinnick and P. Kiive, Phys. Rev. **102,** 58 (1956).
[24] K. S. Drishnan and N. Ganguli, Z. Krist. **A100,** 530 (1939).

DISCUSSION

The interatomic distances and their standard deviations listed in Table IV were computed from the weighted averages of the carbon parameters in Table I and the reported lattice constants.[2,4,6] The uncertainties in the lattice constants have been included in the standard deviations for the calculated distances.

The C–C distances in the C_2 groups in the rare-earth dicarbides are insignificantly different from their weighted average value of 1.278 A. In particular, the C–C distance in YbC_2 revealed no substantial effect due to a possible anomalous valence of Yb in this compound. No significant changes were observed in the refined C–C distances in CaC_2 and UC_2 from those reported previously.[5]

However, other interatomic distances in the rare-earth dicarbides show unusual features. Pauling's bond numbers[25] for the carbon-metal and metal-metal bonds in these dicarbides increase roughly with the atomic number of the metal atom: 0.5 (C–La) to 0.9(C–Lu) for the closest carbon-metal distances (C–M); 0.2 to 0.3_5 for the next closest carbon-metal distances (C–4M′); 0.1 to 0.2 for the closest metal-metal distances which are equal to the a lattice constants; 3 to 5 and 3.5 to 4.5, respectively, for the total bond numbers of the carbon and metal atoms. The bond numbers for YC_2 fall between Ho and Lu, indicating that Y in YC_2 behaves as a heavy lanthanide. The bond numbers for UC_2 have been discussed in our previous paper.[6]

If the divalent single-bond radius, $R(1)=1.706$ A,[26] is assigned for Yb in YbC_2, unusually large total bond numbers 5.5 and 8.3 are obtained for C and Yb, respectively. On the other hand, the trivalent Yb radius, $R(1)=1.558$ A,[26] and $R(1)=1.588$ A[26] for Yb with valency 2.8, deduce the total bond numbers for (C, Yb), respectively, (4.1, 4.3) and (4.3, 4.9), both of which are conformable to the values obtained for other rare-earth dicarbides. It may also be noted that the closest metal-metal distances in the rare-earth dicarbides are 2 to 6% longer than the closest interatomic distances in the metals, except for the case of YbC_2, where the closest Yb–Yb distance is 6.7% shorter than the closest distance in the Yb metal. The metal atoms in the rare-earth metals under consideration are trivalent, except for Yb in the Yb metal which is divalent (cf. Fig. 10).[27] These results support, although indirectly, the magnetic and neutron data that Yb in YbC_2 is approximately in the trivalent state. Further discussions on the valency and metallic bonds in the metal carbides will be presented soon.[26]

The effective nuclear charges for the $4f$ electrons of the rare-earth elements obtained from the various methods are summarized in Fig. 11. Pauling's values were calculated using his size screening constants.[28] Slater's values[29] are equal to $(Z-S)n/n^*$, where the Slater rule was used for obtaining the screening constant S, n is the principal quantum number and n^* is Slater's empirical value 3.7. Klinkenberg's values[30] were deduced from various experimental constants for the spectroscopic multiplet structures. Van Vleck[20] has obtained $S=34$ from the experimental magnetic susceptibilities. The neutron data include those reported by Koehler *et al.*[19,31]

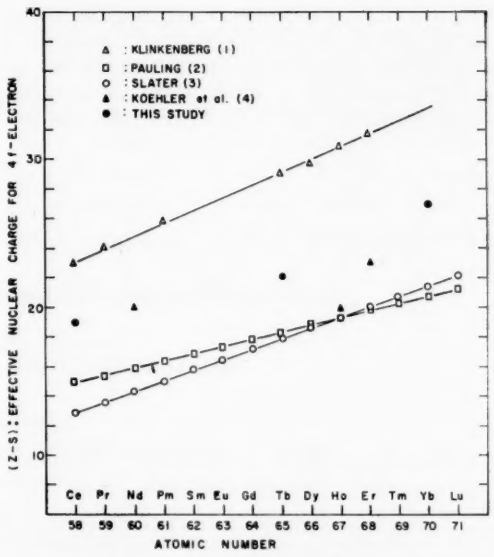
Δ : KLINKENBERG (1)
□ : PAULING (2)
○ : SLATER (3)
▲ : KOEHLER et al. (4)
● : THIS STUDY
(Z-S): EFFECTIVE NUCLEAR CHARGE FOR 4f-ELECTRON
40
30
20
10
Ce Pr Nd Pm Sm Eu Gd Tb Dy Ho Er Tm Yb Lu
58 59 60 61 62 63 64 65 66 67 68 69 70 71
ATOMIC NUMBER

FIG. 11. The effective nuclear charge for the $4f$ electrons in rare earth elements. See reference 30 for (1), reference 28 for (2), reference 29 for (3) and references 19 and 31 for (4).

As Hartree[32] has pointed out, the screening constants may vary considerably with the property chosen to define it, especially those for outer electrons. However, a large spread of the $(Z-S)$ values are shown in Fig. 11 is rather unexpected for the $4f$ electrons. Further studies on this subject will be published shortly.[26]

ACKNOWLEDGMENT

The author is greatly indebted to Dr. H. A. Levy of the Oak Ridge National Laboratory for making it possible to use the ORNL neutron spectrometer and for his kind hospitality at the ORNL, during the period in which a portion of this work was performed. The

[25] L. Pauling, *The Nature of the Chemical Bond* (Cornell University Press, Ithaca, New York, 1960), 3rd ed.
[26] M. Atoji (to be published).
[27] J. M. Lock, Proc. Phys. Soc. (London) **B70,** 476 (1957).
[28] L. Pauling and J. Sherman, Z. Krist. **81,** 1 (1932).
[29] J. C. Slater, Phys. Rev. **36,** 57 (1930).
[30] P. F. A. Klinkenberg, Physica **13,** 1 (1947).
[31] W. C. Koehler, E. O. Wollan, and M. K. Wilkinson, Phys. Rev. **110,** 37 (1958).
[32] D. R. Hartree, Revs. Modern Phys. **30,** 63 (1958).

author is very grateful to Dr. F. H. Spedding, Dr. R. E. Rundle, Dr. A. H. Daane, Dr. F. A. Smidt and Dr. J. E. Powell for providing the samples, to Dr. D. E. Williams and Dr. H. A. Smith for their help in some of the computations and to Dr. V. A. Fassel and Dr. C. V. Banks for the spectroscopic and chemical analyses of the samples. The author would like to express his thanks to Dr. W. H. Koehler, Dr. S. W. Peterson, and Dr. H. G. Smith for stimulating discussions on the experimental techniques.

THE JOURNAL OF CHEMICAL PHYSICS VOLUME 35, NUMBER 6 DECEMBER, 1961

Neutron-Diffraction Studies of La_2C_3, Ce_2C_3, Pr_2C_3, and Tb_2C_3†

MASAO ATOJI

Chemistry Division, Argonne National Laboratory, Argonne, Illinois

AND

DONALD E. WILLIAMS

Institute for Atomic Research and Department of Chemistry, Iowa State University, Ames, Iowa

(Received April 13, 1961)

The neutron diffraction data of the rare-earth sesquicarbides with the Pu_2C_3-type structure ($D5_c$ type), La_2C_3, Ce_2C_3, Pr_2C_3, and Tb_2C_3, were analyzed using the complete-matrix least-squares method. These sesquicarbides contain the C_2 groups with the C—C distances, 1.236±0.009, 1.276±0.005, 1.239±0.003, and 1.240±0.005 A, respectively, for La_2C_3, Ce_2C_3, Pr_2C_3, and Tb_2C_3. These values are, except for Ce_2C_3, significantly longer than the C—C distance in CaC_2, 1.191 A, but are shorter than the average C—C distance in the rare-earth dicarbides, 1.278 A.

The paramagnetic scattering analyses show that all metal atoms in these sesquicarbides are in their trivalent Hund ground state, except Ce in Ce_2C_3, whose possible valency is about 3.4. The screening constants for the 4*f* hydrogenic radial wave functions of Pr and Tb as determined from the diffuse scattering analyses of their sesquicarbides are 40 and 43, respectively. The valency and metallic bonds in these sesquicarbides are briefly discussed.

INTRODUCTION

THE rare-earth sesquicarbide M_2C_3 with the cubic body-centered Pu_2C_3-type structure ($D5_c$ type) has been found to exist in all of the rare earths, from M = La to Ho, except for M = Eu and Pm.[1] The previous x-ray and neutron-diffraction studies of La_2C_3 have shown that La_2C_3 contains the C_2 groups with the C–C distance of 1.32±0.03 A.[2] The neutron data of La_2C_3 have been re-examined and refined by the least-squares method. The present results require some amendments to our previous discussion on the structure of La_2C_3.[2]

In addition to La_2C_3, the rare-earth sesquicarbides with relatively small neutron total cross sections, Ce_2C_3, Pr_2C_3, and Tb_2C_3, were chosen for the neutron structure analyses as a part of our metal carbides program. In particular, the lattice constant of Ce_2C_3 has been found to be smaller than expected for the pure trivalent Ce atom.[1] The results of the least-squares refinement on the neutron data of U_2C_3 reported by Austin[3] are also given. The paramagnetic scattering analyses were carried out for Ce_2C_3, Pr_2C_3, and Tb_2C_3. The statistical errors in this paper are expressed in terms of the standard deviation.

EXPERIMENTAL

The rare-earth sesquicarbides selected for the present study were prepared by arc melting the stoichiometric mixtures of rare-earth metals, 99.9% pure, and spectroscopic graphite electrode under an inert atmosphere.[1] The powder neutron-diffraction data were obtained at 293±3°K with the neutron wave length, λ = 1.055± 0.002 A, using the diffractometer at the Oak Ridge National Laboratory. Other details of the diffraction techniques have been fully described in the preceding paper.[4] The La_2C_3 data were taken at the Argonne National Laboratory with the wavelength of λ = 1.277± 0.002 A.

In all of our sesquicarbide samples, a considerable amount of dicarbide impurity was noted. Since the preparation of pure sesquicarbides is prohibitively laborious, impure samples were used for this study and careful chemical, emission-spectroscopic, x-ray, and neutron analyses were carried out to determine the impurity contents with at least two-place accuracy. The results in weight % are: 6.6% CeC_2 and 0.55%

† Based on work performed under the auspices of the U. S. Atomic Energy Commission.

[1] F. H. Spedding, K. Gschneider, Jr., and A. H. Daane, J. Am. Chem. Soc. **80,** 4499 (1958).

[2] M. Atoji, K. Gschneider, Jr., A. H. Daane, R. E. Rundle, and F. H. Spedding, J. Am. Chem. Soc. **80,** 1804 (1958).

[3] A. E. Austin, Acta Cryst. **12,** 159 (1959).

[4] M. Atoji, J. Chem. Phys. **35,** 1950 (1961) (preceding article).

graphite in Ce_2C_3; 12.4% PrC_2 in Pr_2C_3; 12.5% TbC_2 in Tb_2C_3. No other impurities were found within the maximum detectable limits of 0.05% and 0.1% for metallic and nonmetallic impurities, respectively. As an example of the peak profile analysis on the neutron diffraction pattern,[4] the least-squares separation of the Ce_2C_3 peaks, (400) and (321), and the CeC_2 impurity peak, (112), is illustrated in Fig. 1. The best values for the impurity contents were obtained in this manner. In some regions of the diffraction patterns, several different schemes for separating overlapped peaks were applied. Using additional Soller collimators, diffraction patterns with higher resolution were also obtained. They showed larger counting statistical errors but supplied supplementary information to the intensity analyses. The resultant variances in the least-squares peak analysis are very sensitive to small errors in the assigned Bragg angles and increase almost exponentially with the degree of peak overlapping. Hence, the least-squares peak separation was not very successful at large scattering angles, where uncertainties in the peak widths were also large. As in the cases of the dicarbides, the Wilson method[5] was extensively utilized for determining the incoherent background at high angles. The intensities were standardized against the nickel-powder diffraction data but the scale factors were refined by the least-squares method as described in the following section. No coherent magnetic scattering was observed from La_2C_3, Ce_2C_3, Pr_2C_3, or Tb_2C_3 at room temperature.

LEAST-SQUARES REFINEMENTS

The rare-earth sesquicarbides studied here belong to space group $T_d^6-I\bar{4}3d$ with eight chemical formulas per unit cell. The metal and carbon atoms occupy the 16(c) (xxx) and 24(d) (y, 0, $\frac{1}{4}$) positions, respectively.[6]

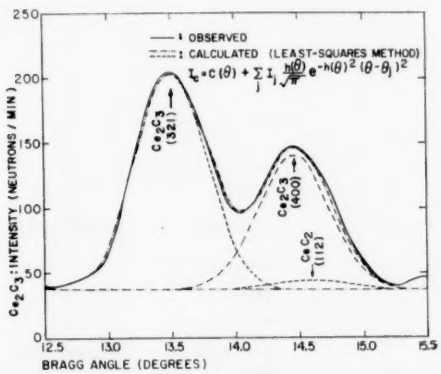

FIG. 1. Example of separation of the overlapped and impurity peaks by the least-squared method. The CeC_2 impurity reflection overlapped with the Ce_2C_3 reflections is shown. For details, see reference 4.

[5] A. J. C. Wilson, Nature **150**, 152 (1942).
[6] *International Tables for X-ray Crystallography* (The Kynoch Press, Birmingham, England, 1952), Vol. 1.

TABLE I. Metal parameters, x; carbon parameters, y; temperature factor coefficients, B in A^2; percentage standard deviations for scale factors, $\sigma k/k$ in %; and agreement factors, R and R_3 in %.

	La_2C_3	Ce_2C_3	Pr_2C_3	Tb_2C_3
x	0.0504	0.0505	0.0515	0.0516
σx	0.0007	0.0007	0.0004	0.0004
y	0.3049	0.2995	0.3029	0.2999
σy	0.0005	0.0003	0.0002	0.0003
B	0.90	0.47	1.63	1.45
σB	0.20	0.08	0.20	0.21
$\sigma k/k$	4.0	3.3	2.8	3.0
R	1.7	1.9	1.7	1.4
R_3	3.8	2.7	2.5	2.0

Four variables, the scale factor K, the positional parameters x and y, and the temperature factor coefficient B in $\exp[-2B(\sin\theta/\lambda)^2]$ were refined using the IBM 650 complete-matrix least-squares programs similar to the one employed for the dicarbide structures.[4] For reasons described in the preceding section, the diffraction intensities at low scattering angles were used for the least-squares analyses. The scattering amplitudes employed are 0.832,[4] 0.482,[4] 0.437,[7] 0.756,[4] and 0.662,[7] all in 10^{-12} cm, for La, Ce, Pr, Tb, and C, respectively. Because of the experimental conditions employed and because of the uncertainty involved in the impurity contents during the earlier stages of the refinements, accurate correlations among the scale factors obtained by comparing with the nickel pattern were not obtainable. Therefore, the refinements were carried out using at least four sets of intensity data for each compound rather than using a single set composed of average intensities. The statistical averages of the final parameters are listed in Table I, except for the percentage standard deviation for the scale factor $\sigma k/k$ in % for which the arithmetical means are given. The adjusted observed intensities obtained using the individual final scale factors were compared with the values calculated from the average final parameters in Table II. The agreement factors in Table I, R and R_3 as defined in the preceding paper,[4] are based on the data in Table II, (a) to (d). The calculated values in Table II are equal to

$$\frac{jF^2\exp[-2B(\sin\theta/\lambda)^2]}{\sin\theta\sin 2\theta} \quad \text{in } 10^{-24}\text{ cm}^2.$$

The least-squares refinement on the U_2C_3 data (Austin's Table 2)[3] yielded $K=1.2\pm0.3$, $B=1.4\pm1.9$ A^2, $x=0.0519\pm0.0037$, $y=0.292\pm0.011$, $R_3=0.21$, and the C–C distance, 1.34 ± 0.17 A. Austin's values are $x=0.050\pm0.003$, $y=0.295\pm0.0025$, and the C–C dis-

[7] D. J. Hughes and R. B. Schwartz, *Neutron Cross Sections* (U. S. Government Printing Office, Washington, D. C., 1958).

TABLE II. Observed and calculated neutron diffraction intensities.

Indices	I_{calc}		I_{obs}	Indices	I_{calc}		I_{obs}
			(a) La_2C_3 (λ=1.277 A)				
211	5254	6800	7200±300	611	3542		
220	1546			532	509	11557	11750±300
310	25300		25400±600	620	3894		
321	20170		21200±500	541	3612		
400	8219		8720±200	631	6290		
420	1997			444	2023		
332	5928	9916	10700±300	710	4769	16295	15700±400
422	1991			543	2506		
510	2178	14468	14600±300	640	707		
431	12290						
521	55		60±20				
440	2326	5266	5300±200				
530	2940						
			(b) Ce_2C_3 (λ=1.055 A)				
211	13410		13550±200	611	4917		
220	18		<50	532	477	11087	11500±300
310	17450		17500±300	620	3940		
321	17730		17500±200	541	1753		
400	10020		10600±200	631	7155		
420	1940	6135	6390±200	444	1482		
332	4195			710	4933	16563	16000±400
422	842			543	2271		
510	1051	10441	10500±300	640	722		
431	8548						
521	2053						
440	4067	8681	8200±300				
530	2561						
			(c) Pr_2C_3 (λ=1.055 A)				
211	14840		14000±300	521	1889		
220	131		<200	440	2581	6204	6240±300
310	16450		16500±300	530	1734		
321	15510		15500±200	611	3835		
400	8135		8090±200	532	478	8370	8090±300
420	2167	5538	5550±200	620	2970		
332	3371			541	1087		
422	637						
510	549	8205	8510±300				
431	7019						

Table II (*continued*)

Indices	I_{calc}		I_{obs}	Indices	I_{calc}		I_{obs}
			(c) Pr_2C_3 (λ=1.055 A)				
631	4534						
444	776						
710	3257	10552	10500±400				
543	1357						
640	628						
			(d) Tb_2C_4 (λ=1.055 A)				
211	6975		6917±200	611	3758		
220	993		905±100	532	175	11197	11000±300
310	25580		25500±300	620	4106		
321	22440		22900±300	541	3158		
400	9655		10053±200	631	6356		
420	1660			444	1945		
332	5905			710	4006	14799	15000±400
422	1808	22938	23500±400	543	2002		
510	2385			640	490		
431	11180						
521	352						
440	3140	6129	6200±200				
530	2637						

tance, 1.30±0.04 A. These values possess too large variances to bear detailed structural discussion.

The standard deviations for the positional parameters are satisfactorily small, but those for the B values are rather large. Nevertheless, it can be said that the B values for the sesquicarbides excluding Ce_2C_3 are in general significantly larger than those for the dicarbides. The B value for Ce_2C_3 is small relative to the others. This seems reasonable, since the Ce_2C_3 crystal possesses a higher density (ρ=6.97 g/cm³) than the value (6.36 g/cm³) interpolated from the densities of the other rare-earth sesquicarbides, which can be expressed by ρ=

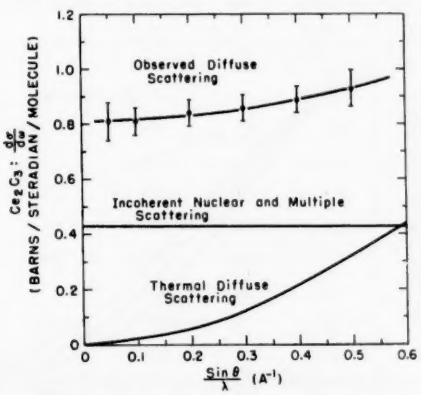
Observed Diffuse Scattering
Incoherent Nuclear and Multiple Scattering
Thermal Diffuse Scattering
Ce_2C_3 : $\frac{d\sigma}{d\Omega}$ (BARNS / STERADIAN / MOLECULE)
$\frac{\sin\theta}{\lambda}$ (A⁻¹)

FIG. 2. Diffuse scattering by Ce_2C_3. The paramagnetic scattering is obtained by substracting the incoherent nuclear and multiple scattering and the thermal diffuse scattering from the observed total diffuse scattering. The maximum errors in the observed values are schematically shown.

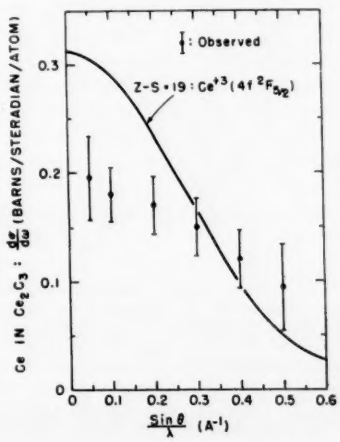

FIG. 3. Paramagnetic differential scattering cross section of Ce in Ce_2C_3. The cross section of $Ce^{+3}(4f\ ^2F_{5/2})$ with $Z-S=19$ is also shown for comparison.

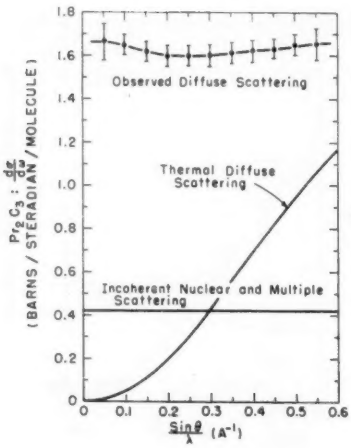
Observed Diffuse Scattering
Thermal Diffuse Scattering
Incoherent Nuclear and Multiple Scattering
Pr_2C_3 : $\frac{d\sigma}{d\omega}$ (BARNS / STERADIAN / MOLECULE)
$\frac{\sin\theta}{\lambda}$ (A^{-1})

FIG. 4. Diffuse scattering by Pr_2C_3.

$0.2813Z-9.955$ (Z=atomic number of metal atom) with the maximum error of about 0.4%.

PARAMAGNETIC SCATTERING

The diffuse scattering of rare-earth sesquicarbides was interpreted using the techniques employed previously.[4,8,9] The multiple incoherent scattering is largely dependent on the sizes of the coherent scattering domains. However, no significant differences among the peak widths of the sesquicarbides, dicarbides, and graphite in their main and impurity states were found. Therefore, the subtraction of the impurity scattering was carried out assuming the additivity of the main and impurity incoherent scatterings.

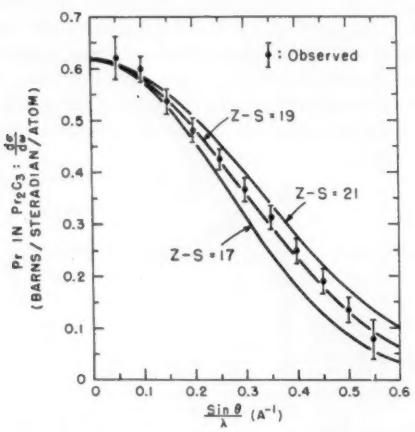

FIG. 5. Paramagnetic scattering cross section of Pr in Pr_2C_3. The solid curves are calculated for the screened $4f$ hydrogen radial wave function with $Z-S=19$ (most probable value), $Z-S=16$ (possible minimum value) and $Z-S=22$ (possible maximum value).

[8] G. T. Trammell, Phys. Rev. **92,** 1387 (1953).
[9] W. C. Koehler and E. O. Wollan, Phys. Rev. **92,** 1380 (1953).

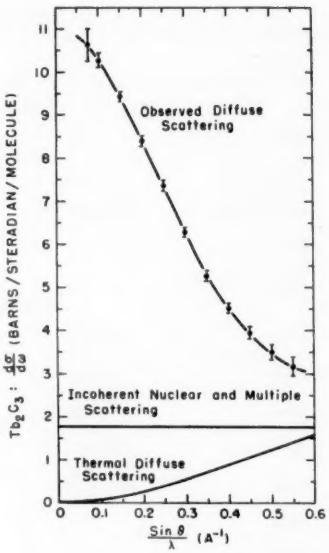
Observed Diffuse Scattering
Incoherent Nuclear and Multiple Scattering
Thermal Diffuse Scattering
Tb_2C_3 : $\frac{d\sigma}{d\omega}$ (BARNS / STERADIAN / MOLECULE)
$\frac{\sin\theta}{\lambda}$ (A^{-1})

FIG. 6. Diffuse scattering by Tb_2C_3.

No paramagnetic scattering was detected from La_2C_3. Accordingly, it can reasonably be concluded that the La_2C_3 crystal is composed of the diamagnetic ions, La^{+3} ($^1S_0$) and $C_2^{=}$ in its ground state.[10] The expected paramagnetism associated with the conduction electrons in La_2C_3 is, of course, too small to be detected. The observed diffuse scattering of Ce_2C_3 is shown in Fig. 2. The resultant paramagnetic differential cross section per Ce atom and the theoretical values for Ce^{3+} ($4f^2F_{5/2}$) with the effective nuclear charge for the $4f$ electrons, $(Z-S)=19$,[4] are shown in Fig. 3. The paramagnetic differential cross section at $(\sin\theta/\lambda)=0$ is given by[8,9]

$$d\sigma/d\omega=\tfrac{2}{3}(e^2\gamma/2mC^2)(\mu_{\text{eff}})^2=0.04829(\mu_{\text{eff}})^2 \text{ b/sr.}$$

The experimental $d\sigma/d\omega$ value at the zero scattering

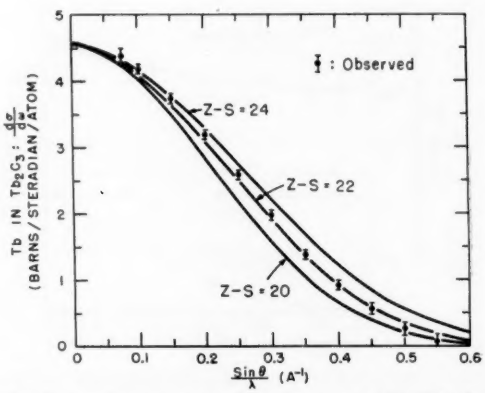

FIG. 7. Paramagnetic scattering cross section of Tb in Tb_2C_3.

[10] M. Atoji and R. C. Medrud, J. Chem. Phys. **31,** 332 (1959).

angle, 0.20±0.03 b/sr/Ce atom, corresponds to the effective Bohr magnetcon numbers, $\mu_{eff}=2.04\pm0.15$ for Ce in Ce_2C_3, while $\mu_{eff}=2.54$ for $Ce^{+3}(4f\,^2F_{5/2})$. The observed μ_{eff} value may be interpreted as 64±10% Ce^{+3} and 36±6% Ce^{+4} ($^1S_0$) for Ce_2C_3. Although the experimental standard deviations are large, it can be concluded that Ce in Ce_2C_3 is definitely not in the pure trivalent Hund ground state. The interpretation given to the paramagnetic diffuse scattering of Pr_2C_3 and Tb_2C_3 is shown in Figs. 4 and 5 and Figs. 6 and 7, respectively. The observed differential cross sections at $(\sin\theta/\lambda)=0$ are in good agreement with the calculated values for $Pr^{+3}(4f^2\,^3H_4)$ and $Tb^{+3}(4f^8\,^7F_6)$. The effective nuclear charges $(Z-S)$ for the $4f$ hydrogenic radial wave function as deduced from the Pr_2C_3 and Tb_2C_3 data are 19 and 22 for Pr and Tb, respectively, the latter of which is identical to the value deduced from the TbC_2 data.[4]

DISCUSSION

In Table III, the lattice constants, the interatomic distances and their standard deviations σ of La_2C_3, Ce_2C_3, Pr_2C_3, and Tb_2C_3 are given (see also Fig. 8). The standard deviations for the lattice constants have been included in the σ's for the interatomic distances. The difference between the refined and previously reported C—C bond distances in La_2C_3, respectively, 1.236±0.009 and 1.32±0.03 A, is probably significant. Differences among the C—C bond distances in La_2C_3, Pr_2C_3, and Tb_2C_3 are not significant. The generalization of this result, that all Pu_2C_3-type rare-earth sesquicarbides, except Ce_2C_3, possess the C—C distance of 1.238 A (the average of presently determined values), is quite plausible. The value, 1.238 A is significantly longer than the C–C distance in CaC_2, 1.191±0.009 A[4] and shorter than the average C–C distance in the rare-earth dicarbides, 1.278 A. The C–C distance in Ce_2C_3, 1.276±0.005 A is significantly different from the C–C distances in other rare-earth sesquicarbides, but is insignificantly different from those in the rare-earth dicarbides.[4] All C–C distances in the sesquicarbides and dicarbides are significantly different from the C–C distance in UC_2, 1.340±0.007 A.[4] The C–C distances between the C_2 groups in Table III, $C_0\cdots4C_1$, are slightly longer than those in the dicarbides, 3.416, 3.371, and 3.179 A, respectively, for LaC_2, CeC_2, and TbC_2. Both $C_0\cdots4C_1$ and $C_0\cdots4C_2$ distances are too long to expect any appreciable chemical bonding.

The closest carbon-metal distances C–2M in the sesquicarbides are approximately equal to C–M in the dicarbides and, C–2M′ and C–2M″ in the sesquicarbides to C–4M′ in the dicarbides.[4] The shortest M–M distances in the sesquicarbides, M_0-3M_1 are

TABLE III. Cubic lattice constants a interatomic distances less than 4.2 A and their standard deviations σ in A (cf. Fig. 8).

	La_2C_3	Ce_2C_3	Pr_2C_3	Tb_2C_3
a[a]	8.8170	8.4476	8.5902	8.2526
σ[b]	0.0045	0.0004	0.0057	0.0031
C—C	1.236	1.276	1.239	1.240
σ	0.009	0.005	0.003	0.005
$C_0\cdots4C_1$	3.510	3.322	3.404	3.248
σ	0.004	0.002	0.003	0.003
$C_0\cdots4C_2$	3.879	3.705	3.775	3.621
σ	0.002	0.001	0.003	0.001
C—2M	2.686	2.574	2.628	2.525
σ	0.006	0.006	0.004	0.004
C—2M′	2.886	2.729	2.787	2.657
σ	0.007	0.006	0.004	0.004
C—2M″	2.973	2.879	2.910	2.807
σ	0.007	0.006	0.004	0.004
M_0—$3M_1$	3.630	3.477	3.523	3.383
σ	0.009	0.009	0.005	0.005
M_0—$2M_2$	3.818	3.6579	3.720	3.573
σ	0.002	0.0002	0.002	0.001
M_0—$6M_3$	4.019	3.852	3.924	3.771
σ	0.005	0.005	0.004	0.003

[a] The lattice constants of Pr_2C_3 and Tb_2C_3 are the average values of their carbon-rich and metal-rich lattice constants.[1] The lattice constants of La_2C_3 and Ce_2C_3 are those for the ideal composition.[1,2].

[b] These values include uncertainty in the lattice constants due to possible deviations from the ideal composition.

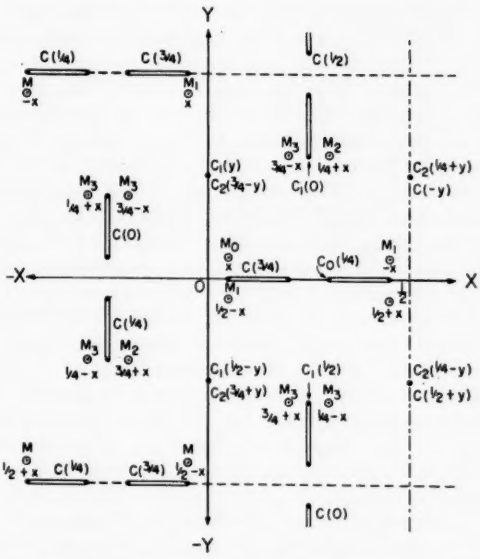

FIG. 8. The projection of the M_2C_3 structure along the Z axis. The double circles represent the metal atoms and the filled circles represent the C_2 groups. The z parameters for the carbon atoms are shown in brackets. For the perspective figures, see reference 2.

nearly 10% shorter than the shortest M–M distances in the dicarbides, which are equal to their a lattice constants. The M_0-2M_2 and M_0-6M_3 distances do not differ greatly from the shortest M–M distances in the dicarbides. The next shortest M–M distances in the dicarbides are 4.306, 4.217, and 4.058 A, respectively for M=La, Pr, and Tb. In conclusion, these surveys of the M–M distances show clearly the stronger metal-metal interactions in the sesquicarbides than in the dicarbides. The interatomic distances in Ce_2C_3, particularly the Ce–Ce distances are markedly smaller than the expected values for Ce_2C_3 with the pure trivalent Ce atoms. This is in accordance with the result obtained from the paramagnetic scattering analysis.

Although Pauling's semiempirical formula[11] for the resonating valency bonds in metals is in general not satisfactorily applicable to the metal-nonmetal alloys,[4,12,13] for comparative purpose the Pauling bond numbers for the sesquicarbides are discussed here with those for the dicarbides. As in the cases of the dicarbides, the total bond numbers of both metal and carbon atoms in the sesquicarbides increase, roughly, in proportion to the atomic number of the metal atom. The total bond numbers for the metal atoms are: 4.4 for La in La_2C_3; 3.3 for La in LaC_2; 5.8 for Tb in Tb_2C_3; 4.3 for Tb in TbC_2. These figures support the previous conclusion that the metal-metal bonds in the sesquicarbides are considerably stronger than those in the dicarbides. The bond numbers for the carbon atoms and other detailed discussions on these structures will be reported separately.[13]

In the metal sesquicarbides with the trivalent metal atoms, the number of delocalizing electrons are two per chemical formula or $\frac{4}{3}$ per C_2 group, while the metal dicarbides with the trivalent metal atom possess one delocalizing electron per C_2 group. If the C_2 antibonding orbital $(\pi_g 2p)$[10] is equally participating in forming the lowest conduction bands of the sesquicarbides and the dicarbides, the C—C bond distances in the sesquicarbides should be longer than those in the dicarbides, in contradiction to the experimental results. Hence, the $C_2-\pi_g 2p$ contribution to the conduction bands must be smaller in the sesquicarbides than in the dicarbides. In other words, the conduction electrons in the sesquicarbides are associated with the metal orbitals with a higher order than those in the dicarbides. The interatomic distances support this aspect. In Ce_2C_3, more electrons occupy the C_2 antibonding orbitals than in other sesquicarbides. The observed C–C distance in Ce_2C_3 seems in agreement with this interpretation.

ACKNOWLEDGMENT

The neutron experiments were carried out at the Oak Ridge National Laboratory through the kind invitation of Dr. H. A. Levy. One of the authors (M.A.) is deeply indebted to Dr. H. A. Levy and his colleagues at the ORNL for their hospitality and for many stimulating discussions. The authors would like to express their thanks to Dr. F. H. Spedding, Dr. W. M. Manning, and Dr. R. E. Rundle for their continued encouragement, to Dr. H. G. Smith for his generous help in the neutron experiment and to Dr. A. H. Daane and Dr. F. A. Smidt for providing the samples.

[11] L. Pauling, *The Nature of the Chemical Bond* (Cornell University Press, Ithaca, New York, 1960), 3rd ed.
[12] R. Kiessling, Acta Chem. Scand. **4**, 209 (1950).
[13] M. Atoji (to be published).

Studies in Molecular Structure. VI. Potential Curve for the Interaction of Two Hydrogen Atoms in the LCAO MO SCF Approximation*

SERAFIN FRAGA AND BERNARD J. RANSIL

Laboratory of Molecular Structure and Spectra, Department of Physics, The University of Chicago, Chicago 37, Illinois

(Received April 13, 1961)

The LCAO MO SCF method, both in the single-configuration and a limited configuration interaction approximation, has been utilized to evaluate the potential curve of the ground state of H_2; wave functions and total molecular energies are presented for a wide range of the internuclear distance (1.0 a.u. $\leq R \leq 18.0$ a.u.). These solutions were then used to construct potential curves for the ground states of the molecular ions H_2^+ and H_2^- and for the lower-lying excited states of the neutral molecule. Results of vibration-rotation analyses for the stable states are presented. The results for a population analysis of the single-configuration ground-state function over the whole range of R are given, and compared to similar results for He_2.

INTRODUCTION

IN the spirit of the earlier papers in this series,[1] attention was given to the usefulness of the LCAO MO SCF approximation[2] in calculating interaction curves for H_2 and He_2 over the full range of atomic interaction. Simple two- and four-electron closed-shell systems have been chosen because of their simplicity and because of the availability of extensive experimental and theoretical data for checking purposes. Results of calculations on H_2 are reported and discussed in this paper. Work on He_2 has been reported elsewhere.[3]

GENERAL THEORY

Molecular orbitals (MO's) and single-determinant functions were constructed in the usual manner, using $1s$, $2s$, and $2p\sigma$ Slater-type atomic orbitals (STO's). A limited ζ variation was employed, i.e., all ζ's were kept equal and the single parameter $\zeta = \zeta_{1s} = \zeta_{2s} = \zeta_{2p\sigma}$ varied in a separate calculation [this restriction was lifted in a separate calculation at the equilibrium internuclear (R_e) distance in order to get an idea of the importance of the free ζ variation]. The equal-ζ restriction was imposed for reasons of economy; consequently these results are to be regarded as a good first approximation to what should be possible given high-speed programs and sufficient computing time.

Once ground-state LCAO MO's and their corresponding orbital energies (ϵ's) have been obtained, it is possible to approximate excited states of the neutral molecule by filling the virtual MO's in the proper manner to obtain the correct term designation. Also the ground states of singly charged (positive or negative) molecular ions can be approximated by subtraction or addition of appropriate orbital energies. Such an approximation for the ionized states is possible only with single-determinant functions where the orbital energy is clearly defined. Configuration interaction scrambles the MO's in a complicated manner and consequently the term "orbital energy" (as defined in the single configuration scheme) loses its heretofore precise meaning when taken in the context of configuration interaction. Although the single-determinant function does not give the asymptotic tapering off at large values of the internuclear distance R which is expected in the ground-state potential curve for H_2, the curves for H_2^+ and H_2^- derived from it do.

Limited configuration interaction (CI) was introduced in the manner described elsewhere[4] to obtain the correct asymptotic behavior for the ground state.

DETAILS OF THE CALCULATIONS

A single-determinant LCAO MO SCF function was computed for 16 values of the internuclear distance (over the range 1.0 a.u. $\leq R \leq 18.0$ a.u.) varying ζ as described for each point. At the equilibrium distance, a separate calculation was done permitting independent variation of the three orbital exponents. A limited CI was then performed using as interacting configurations all those which can be obtained from the ground-state configuration by excitation of one or two electrons to virtual excited MO's, and from which electronic states with the correct symmetry ($^1\Sigma_g^+$) can be derived. The electron distributions for these configurations are given in Table I.[5]

Potential curves were calculated for the singly ionized molecules H_2^+ and H_2^- and for all those excited states which lie lower energetically than the singly charged positive ion (or which lie very closely above it), in order to obtain an idea of how well the crude ground-

* This work was assisted by the National Science Foundation and by the Office of Ordnance Research and the University of Chicago.

[1] See B. J. Ransil, Revs. Modern Phys. **32**, 239, 245 (1960), parts I and II of this series, for definitions, conventions and notation.

[2] C. C. J. Roothaan, Revs. Modern Phys. **23**, 69 (1951).

[3] The results for He_2 have already been presented by B. J. Ransil, J. Chem. Phys. **34**, 2109 (1961); results for He_2^{+} will appear later.

[4] S. Fraga and B. J. Ransil, J. Chem. Phys. (to be published).

[5] The derivation of the formulas for the evaluation of the energy matrix elements is a straightforward exercise and therefore the formulas not presented here.

TABLE I. Electronic distribution of configurations for states with $^1\Sigma_g^+$ symmetry.

MO Configuration	Electron distribution $1\sigma_g$	$1\sigma_u$	$2\sigma_g$	$2\sigma_u$	$3\sigma_g$	$3\sigma_u$
I	2					
II		2				
III			2			
IV				2		
V					2	
V						2
VII		1		1		
VIII		1				1
IX			1		1	
X				1		1
XI	1		1			
XII	1				1	

state virtual orbitals approximate those of lower-lying excited states.

For all those states for which the potential curve exhibited a minimum, vibration-rotation analyses were made. The curves were fitted about the minima by a third-degree polynomial in R, and spectroscopic constants were calculated by methods discussed in a previous publication.[6]

Electron population analyses were made of the single-determinant ground-state wave function using Mulliken's scheme.[7]

The calculations were carried out on a Univac Scientific 1103 computer. Two separate programs were used, one for the single determinant calculations,[8] and other for the CI calculations; the latter utilized as input data the results (atomic integrals, molecular orbital coefficients and energies, and total molecular energy) of the single-determinant LCAO MO SCF calculations.

RESULTS AND DISCUSSION

In discussing these results, care must be taken to avoid hasty generalizations to large systems because the H_2 molecule is a special case. Unlike molecular species with a large complement of electrons, (1) theoretical and experimental values for the energy of the dissociation products (two H atoms) coincide; (2) although *only 96%* of the total molecular energy E_m of H_2 is obtained by the simple single-configuration calculation (as compared to usually 99% or better for larger systems), roughly 75% of the dissociation energy D_e is readily obtained because the binding energy is three to four times greater than the calculational error. For all other molecules the binding energy is less than the error inherent in the calculation. Another way of looking at it is that the binding energy for H_2 is relatively insensitive (compared to all other molecules) to the form of approximation: The crudest approximation often gives remarkably good results from the standpoint of energy criteria.

The MO coefficients, orbital energies, total molecular energies, and ζ values for the single-determinant ground-state calculations are given in Table II. The CI coefficients and the total molecular energies obtained in the CI treatment of the ground state are listed in Table III.

The best results obtained in the present calculations at the equilibrium distance are compared in Table IV with recent calculations by Kolos and Roothaan,[8] and by Weiss, Yoshimine, and McLean.[9] It is significant that the single-configuration LCAO MO SCF calculation, using $1s$, $2s$, and $2p\sigma$ STO's with full ζ variation, yields a total energy differing from the Kolos-Roothaan accurate analytical Hartree-Fock value by only 0.004 ev. From the standpoint of energy at least it would therefore appear that this relatively simple function is a very good representation of the much more complex Kolos-Roothaan function, and of greater value to the chemist for purposes of application, calculation and interpretation.

The introduction of CI provides appreciable energy improvement, but the result remains poorer by comparison than that obtained by the best direct CI calculation of Weiss, Yoshimine, and McLean[9] (WYM function). The difference is due to the fact that in the latter calculation $2p\pi$ STO's have been included. On the other hand, a direct CI function with four configurations, involving only σ-type orbitals,[9] yields poorer results (dissociation

TABLE IIa. Single- and many-configuration wave functions for the ground state $^1\Sigma_g^+$ of H_2 at the experimental equilibrium distance (R=1.402 a.u.).

ζ_{1s}=1.378 ζ_{2s}=1.176 $\zeta_{2p\sigma}$=1.820

		c_{ip}	ϵ_i (a.u.)	Configurations	C_I
$1\sigma_g$	$c_{11}=c_{14}$	0.43262	−0.59443	I	0.99269
	$c_{12}=c_{15}$	0.12384			
	$c_{13}=c_{16}$	0.02827		II	−0.07956
$1\sigma_u$	$c_{21}=-c_{24}$	−0.47957	0.26557	III	−0.05569
	$c_{22}=-c_{25}$	−1.59631			
	$c_{23}=-c_{26}$	−0.09903		IV	−0.03236
$2\sigma_g$	$c_{31}=c_{34}$	−0.80612	0.70721	V	−0.01273
	$c_{32}=c_{35}$	0.87316			
	$c_{33}=c_{36}$	−0.12801		VI	−0.00639
$2\sigma_u$	$c_{41}=-c_{44}$	−0.60580	1.41793	VII	−0.05846
	$c_{42}=-c_{45}$	2.57077			
	$c_{43}=-c_{46}$	0.67831		VIII	−0.00907
$3\sigma_g$	$c_{51}=c_{54}$	−0.69580	2.10479	IX	0.01294
	$c_{52}=c_{55}$	0.43595			
	$c_{53}=c_{56}$	0.80431		X	−0.01088
$3\sigma_u$	$c_{61}=-c_{64}$	−2.34355	4.30680	XI	−0.00523
	$c_{62}=-c_{65}$	−1.51176			
	$c_{63}=-c_{66}$	−1.93429		XII	−0.00854
E_M (a.u.)		−1.13349		−1.15919	

[6] S. Fraga and B. J. Ransil, J. Chem. Phys. **35,** 669 (1961).
[7] R. S. Mulliken, J. Chem. Phys. **23,** 1833, 1841, 2338, 2345 (1955).
[8] W. Kolos and C. C. J. Roothaan, Revs. Modern Phys. **32,** 219 (1960).
[9] A. D. McLean, A. Weiss, and M. Yoshimine, Revs. Modern Phys. **32,** 211 (1960).

TABLE IIb. Single configuration wave functions for H_2.

	c_{ip}	ϵ_i (a.u.)	c_{ip}	ϵ_i (a.u.)	c_{ip}	ϵ_i (a.u.)	c_{ip}	ϵ_i (a.u.)
R (a.u.)	1.0		1.1		1.2		1.3	
ζ_{1s}	1.3288		1.3024		1.2773		1.2538	
ζ_{2s}	1.3288		1.3024		1.2773		1.2538	
$\zeta_{2p\sigma}$	1.3288		1.3024		1.2773		1.2538	
$c_{11} = c_{14}$	0.51796		0.52103		0.52421		0.52749	
$1\sigma_g$ $c_{12} = c_{15}$	0.01293	−0.66567	0.01463	−0.64530	0.01603	−0.62626	0.01729	−0.60847
$c_{13} = c_{16}$	0.03933		0.03996		0.04039		0.04066	
$c_{21} = -c_{24}$	1.17175		1.12358		1.08418		1.05137	
$1\sigma_u$ $c_{22} = -c_{25}$	0.49989	0.42328	0.46790	0.38676	0.43969	0.35314	0.41436	0.32226
$c_{23} = -c_{26}$	−0.23960		−0.23322		−0.22683		−0.22041	
$c_{31} = c_{34}$	−0.06308		−0.06923		−0.07518		−0.08088	
$2\sigma_g$ $c_{32} = c_{35}$	−0.47350	0.81041	−0.46931	0.77361	−0.46503	0.73933	−0.46063	0.70792
$c_{33} = c_{36}$	0.41789		0.43542		0.45082		0.46462	
$c_{41} = -c_{44}$	4.14382		3.43040		2.89746		2.48686	
$2\sigma_u$ $c_{42} = -c_{45}$	0.50600	2.68772	0.30510	2.40662	0.15825	2.16828	0.04763	1.96546
$c_{43} = -c_{46}$	1.28000		1.16709		1.07830		1.00708	
$c_{51} = c_{54}$	0.45944		0.45470		0.44967		0.44440	
$3\sigma_g$ $c_{52} = c_{55}$	−0.37746	1.77179	−0.38780	1.67852	−0.39763	1.59086	−0.40704	1.50945
$c_{53} = c_{56}$	−1.37822		−1.26339		−1.16620		−1.08221	
$c_{61} = -c_{64}$	31.18976		24.79541		20.16837		16.70329	
$3\sigma_u$ $c_{62} = -c_{65}$	12.58052	4.64851	10.25255	4.30674	8.55566	4.00085	7.27542	3.72780
$c_{63} = -c_{66}$	8.72453		7.54017		6.61833		5.88086	
E_M (a.u.)	−1.0827 38471		−1.1083 33685		−1.1231 39556		−1.1303 36615	
R (a.u.)	1.4		1.5		1.6		1.8	
ζ_{1s}	1.2313		1.2098		1.1894		1.1502	
ζ_{2s}	1.2313		1.2098		1.1894		1.1502	
$\zeta_{2p\sigma}$	1.2313		1.2098		1.1894		1.1502	
$c_{11} = c_{14}$	0.53086		0.53429		0.53779		0.54490	
$1\sigma_g$ $c_{12} = c_{15}$	0.01823	−0.59184	0.01891	−0.57627	0.01939	−0.56169	0.01928	−0.53521
$c_{13} = c_{16}$	0.04082		0.04089		0.04088		0.04078	
$c_{21} = -c_{24}$	1.02370		1.00002		0.97950		0.94572	
$1\sigma_u$ $c_{22} = -c_{25}$	0.39127	0.29365	0.36995	0.26712	0.35006	0.24252	0.31353	0.19805
$c_{23} = -c_{26}$	−0.21403		−0.20770		−0.20142		−0.18926	
$c_{31} = c_{34}$	−0.08635		−0.09159		−0.09657		−0.10583	
$2\sigma_g$ $c_{32} = c_{35}$	−0.45616	0.67839	−0.45169	0.65067	−0.44718	0.62487	−0.43853	0.57653
$c_{33} = c_{36}$	0.47679		0.48759		0.49730		0.51321	
$c_{41} = -c_{44}$	2.16291		1.90180		1.68742		1.35763	
$2\sigma_u$ $c_{42} = -c_{45}$	−0.03807	1.79035	−0.10598	1.63825	−0.16076	1.50566	−0.24392	1.28416
$c_{43} = -c_{46}$	0.94874		0.90022		0.85943		0.79425	
$c_{51} = c_{54}$	0.43890		0.43321		0.42734		0.41517	
$3\sigma_g$ $c_{52} = c_{55}$	−0.41592	1.43270	−0.42430	1.36050	−0.43226	1.29295	−0.44653	1.16771
$c_{53} = c_{56}$	−1.00925		−0.94513		−0.88807		−0.79240	
$c_{61} = -c_{64}$	14.06059		11.99974		10.35838		7.97160	
$3\sigma_u$ $c_{62} = -c_{65}$	6.29149	3.48109	5.51817	3.25774	4.89739	3.05554	2.98382	2.69986
$c_{63} = -c_{66}$	5.28350		4.79124		4.36868		3.73732	
E_M (a.u.)	−1.1321 11030		−1.1299 98169		−1.1250 95657		−1.1098 95404	

Table IIb (*continued*)

		c_{ip}	ϵ_i (a.u.)	c_{ip}	ϵ_i (a.u.)	c_{ip}	ϵ_i (a.u.)	c_{ip}	ϵ_i (a.u.)
R (a.u.)		2.0		2.5		3.0		4.0	
ζ_{1s}		1.1150		1.0383		0.9804		0.9079	
ζ_{2s}		1.1150		1.0383		0.9804		0.9079	
$\zeta_{2p\sigma}$		1.1150		1.0383		0.9804		0.9079	
	$c_{11} = c_{14}$	0.55215		0.57040		0.58839		0.64160	
$1\sigma_g$	$c_{12} = c_{15}$	0.01866	−0.51182	0.01398	−0.46415	0.00867	−0.42792	0.01270	−0.37738
	$c_{13} = c_{16}$	0.04048		0.03942		0.03799		0.03499	
	$c_{21} = -c_{24}$	0.91866		0.86861		0.83191		0.78033	
$1\sigma_u$	$c_{22} = -c_{25}$	0.28039	0.15948	0.20763	0.08217	0.14761	0.02519	0.06526	−0.05138
	$c_{23} = -c_{26}$	−0.17735		−0.14979		−0.12505		−0.08537	
	$c_{31} = c_{34}$	−0.11413		−0.13117		−0.14450		−0.16560	
$2\sigma_g$	$c_{32} = c_{35}$	−0.42975	0.53477	−0.40854	0.44925	−0.38383	0.38968	−0.30572	0.31845
	$c_{33} = c_{36}$	0.52651		0.55048		0.57030		0.60943	
	$c_{41} = -c_{44}$	1.11632		0.72630		0.49674		0.25434	
$2\sigma_u$	$c_{42} = -c_{45}$	−0.30272	1.11118	−0.39396	0.81099	−0.43986	0.63189	−0.46745	0.44994
	$c_{43} = -c_{46}$	0.74553		0.66451		0.61867		0.57895	
	$c_{51} = c_{54}$	0.40246		0.36899		0.33315		0.25355	
$3\sigma_g$	$c_{52} = c_{55}$	−0.45954	1.05854	−0.48662	0.83664	−0.51159	0.67916	−0.56753	0.48853
	$c_{53} = c_{56}$	−0.71321		−0.56617		−0.45569		−0.26834	
	$c_{61} = -c_{64}$	6.31889		3.91016		2.61701		1.30150	
$3\sigma_u$	$c_{62} = -c_{65}$	3.34084	2.40459	2.37708	1.84625	1.83729	1.47219	1.25675	1.02525
	$c_{63} = -c_{66}$	3.25498		2.46709		1.97624		1.37882	
E_M (a.u.)		−1.0906 85746		−1.0379 93067		−0.98848 08822		−0.91033 48970	
R (a.u.)		5.0		6.0		12.0			
ζ_{1s}		0.8691		0.8485		0.8412			
ζ_{2s}		0.8691		0.8485		0.8412			
$\zeta_{2p\sigma}$		0.8691		0.8485		0.8412			
	$c_{11} = c_{14}$	0.64966		0.67092		0.70633			
$1\sigma_g$	$c_{12} = c_{15}$	−0.00270	−0.34450	−0.00450	−0.32170	−0.00096	−0.26642		
	$c_{13} = c_{16}$	0.03232		0.02943		0.00836			
	$c_{21} = -c_{24}$	0.74913		0.73099		0.70766			
$1\sigma_u$	$c_{22} = -c_{25}$	0.02190	−0.09809	0.00146	−0.12746	−0.00221	−0.18236		
	$c_{23} = -c_{26}$	−0.05806		−0.03963		−0.00615			
	$c_{31} = c_{34}$	−0.17565		−0.15998		−0.01543			
$2\sigma_g$	$c_{32} = c_{35}$	−0.17453	0.27613	−0.02764	0.24653	0.07241	0.25797		
	$c_{33} = c_{36}$	0.63603		0.63186		0.68979			
	$c_{41} = -c_{44}$	0.14283		0.08701		0.01141			
$2\sigma_u$	$c_{42} = -c_{45}$	−0.46013	0.36944	−0.43854	0.33031	−0.09920	0.28183		
	$c_{43} = -c_{46}$	0.57132		0.57986		0.70900			
	$c_{51} = c_{54}$	0.16621		0.09132		0.00350			
$3\sigma_g$	$c_{52} = c_{55}$	−0.62406	0.39150	−0.65146	0.34620	−0.69343	0.34274		
	$c_{53} = c_{56}$	−0.08199		0.08020		0.09291			
	$c_{61} = -c_{64}$	0.69654		0.38732		0.01054			
$3\sigma_u$	$c_{62} = -c_{65}$	0.97008	0.77560	0.81763	0.62138	0.71132	0.36704		
	$c_{63} = -c_{66}$	1.03121		0.80609		0.12207			
E_M (a.u.)		−0.85727 69471		−0.82199 36576		−0.75419 57931			

TABLE III. H_2 CI wave functions (configuration coefficients and molecular energies).

R (a.u.)	1.0	1.1	1.2	1.3	1.4	1.5	1.6	1.8
ζ: 1s	1.3288	1.3024	1.2773	1.2538	1.2313	1.2098	1.1894	1.1502
Conf. 2s	1.3288	1.3024	1.2773	1.2538	1.2313	1.2098	1.1894	1.1502
Coeff. 2σ	1.3288	1.3024	1.2773	1.2538	1.2313	1.2098	1.1894	1.1502
I	0.99543	0.99492	0.99432	0.99279	0.99275	0.99175	0.99058	0.98764
II	−0.06155	−0.06688	−0.07278	−0.08025	−0.08644	−0.09423	−0.10272	−0.12177
III	−0.05620	−0.05524	−0.05425	−0.07037	−0.05222	−0.05120	−0.05017	−0.04812
IV	−0.02379	−0.02559	−0.02732	0.01310	−0.03052	−0.03198	−0.03334	−0.03580
V	−0.01057	−0.01108	−0.01158	−0.01327	−0.01252	−0.01295	−0.01334	−0.01399
VI	−0.00167	−0.00237	−0.00286	−0.00325	−0.00329	−0.00344	−0.00357	−0.00383
VII	0.03726	−0.04125	−0.04544	0.04898	−0.05432	0.05902	0.06386	−0.07401
VIII	−0.00197	−0.00211	0.00226	−0.00258	−0.00267	−0.00291	0.00316	0.00370
IX	0.00588	−0.00613	−0.00627	0.00934	0.00629	−0.00617	0.00599	0.00541
X	0.00164	−0.00159	0.00159	0.00191	−0.00167	0.00172	−0.00177	0.00186
XI	−0.00196	−0.00173	−0.00148	−0.00858	−0.00096	−0.00069	−0.00041	0.00019
XII	−0.00738	0.00846	0.00967	−0.00737	−0.01252	0.01419	−0.01602	−0.02029
E_{CI} (a.u.)	−1.10374	−1.13004	−1.14567	−1.15035	−1.15661	−1.15567	−1.15207	−1.13988

R (a.u.)	2.0	2.5	3.0	4.0	5.0	6.0	12.0
ζ: 1s	1.1150	1.0383	0.9804	0.9079	0.8691	0.8485	0.8412
Conf. 2s	1.1150	1.0383	0.9804	0.9079	0.8691	0.8485	0.8412
Coeff. 2σ	1.1150	1.0383	0.9804	0.9079	0.8691	0.8485	0.8412
I	0.98371	0.96795	0.94086	0.85633	0.77550	0.72715	0.68961
II	−0.14393	−0.21292	−0.29898	−0.47597	−0.59160	−0.64770	−0.69029
III	−0.04604	−0.04062	−0.03479	−0.02350	−0.01456	−0.00661	−0.00016
IV	−0.03773	−0.04024	−0.03890	−0.02894	−0.01930	−0.01341	0.00001
V	−0.01440	−0.01407	−0.01130	0.00059	0.01195	0.01606	0.01704
VI	−0.00406	−0.00443	−0.00440	−0.00333	−0.00238	−0.00270	−0.01570
VII	0.08450	−0.11127	0.13464	−0.15689	0.15170	0.13792	−0.03326
VIII	0.00433	0.00635	−0.00941	0.02022	0.03712	−0.05748	−0.14746
IX	−0.00462	−0.00201	−0.00073	−0.00252	0.00347	0.01112	0.00517
X	−0.00197	0.00232	0.00292	0.00499	−0.00751	0.00972	−0.00520
XI	−0.00081	0.00243	−0.00311	0.00616	0.03510	−0.06742	−0.03190
XII	−0.02541	0.04251	0.06552	0.11687	0.14892	−0.15541	−0.15321
E_{CI} (a.u.)	−1.12426	−1.08333	−1.04988	−1.01363	−1.00278	−1.00015	−0.99936

energy of 4.2652 ev) compared to our CI treatment (4.3315 ev), but it would be expected that the inclusion of more configurations, involving only σ-type orbitals, would bring the necessary energy improvements. Such comparison effectively demonstrates the importance of configurations involving MO's of higher angular momentum than those occupied in the ground state.

To evaluate the individual merits of the different improvements introduced in our best wave function (extended basis set, full ζ variation and CI), the results

TABLE IV. Evaluated total molecular and dissociation energies of H_2 at the equilibrium separation.

Authors and references	R (a.u.)	E_M (a.u.)	D (ev)	Methods and remarks
S. Fraga and B. J. Ransil This paper	1.402	−1.133494	3.6324	LCAO MO SCF; STO-ζ procedure using 1s, 2s, 2$p\sigma$ STO's. Single configuration. All ζ's varied independently.
W. Kolos and C. C. J. Roothaan[8]	1.400	−1.133630	3.6360	Nine-term analytical SCF function; closed shell.
S. Fraga and B. J. Ransil This paper	1.402	−1.159187	4.3315	Same as first case, but using 12 configurations.
A. D. McLean, A. Weiss and M. Yoshimine[9]	1.400	−1.167236	4.5505	Five-configuration direct CI utilizing 1s, 2s, 2$p\sigma$, 2$p\pi$ STO's.
W. Kolos and C. C. J. Roothaan[9]	1.4009	−1.174448	4.7467	50-term James-Coolidge type function
Experimental	1.4006[a]	−1.174443	4.7466±0.0007[10]	

[a] G. Herzberg and L. L. Howe, Can. J. Phys. **37**, 636 (1959).

of separate calculations making use of these improvements are collected in Table V. Inspection of these results confirm earlier observations[4]: (1) ζ variation alone, once an adequate basis set is used, does not lead to appreciable energy improvement (i.e., to improvement commensurate with the computational effort involved); (2) CI, coupled with expansion of the basis set and full ζ variation, appears to be the most promising procedure if energy is taken as the criterion for judgment of accuracy.

A similar comparison to the one given in Table IV has been made over the whole range of the internuclear distance, and the results are presented in Fig. 1 and Table VI together with all the other related potential curves calculated in this series.

TABLE V. Evaluated total molecular energies for H_2 in the LCAO MO SCF approximation.

Method and remarks	Total molecular energy (a.u.)	Percentage of observed energy
1s STO only		
1. Single configuration R=1.4 a.u.; ζ_{1s}=1.0	−1.09092	92.89
1s STO only (ζ varied)		
2. Single configuration R=1.4 a.u.; ζ_{1s}=1.2	−1.12804[a]	96.05
1s, 2s, 2$p\sigma$ STO's (common ζ varied)		
3. Single configuration R=1.4 a.u.; ζ=1.2313	−1.13211	96.40
1s, 2s, 2$p\sigma$ STO's (all ζ's varied independently)		
4. Single configuration R=1.402 a.u.; ζ_{1s}=1.378, ζ_{2s}=1.176, $\zeta_{2p\sigma}$=1.820	−1.13349	96.51
Same as case 3		
5. 12 configurations	−1.15661	98.48
Same as case 4		
6. 12 configurations	−1.15919	98.70

[a] Not completely minimized.

The behavior of the single-configuration LCAO MO SCF functions can be qualitatively followed through the changes in the coefficients of the ground-state MO. At large R(18 a.u.) the $1\sigma_g$ MO coefficients are 0.70704, 0.00006, and 0.00322, respectively, for 1s, 2s, and 2$p\sigma$ STO's. The single determinant energy for the configuration $(1\sigma_g)^2$ corresponds to an excited state for the dissociated products involving 1s with a slight admixture of 2s and 2$p\sigma$ STO's. As R decreases, and the united atom (He) approached, the 2s and 2$p\sigma$ coefficients become the same order of magnitude and decrease slowly, whereas the 1s coefficient increases. The common ζ value appears to climb smoothly towards a limiting

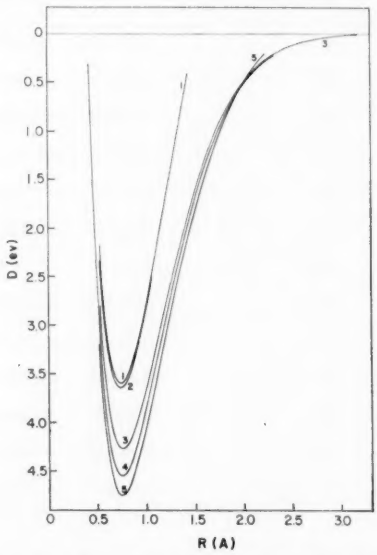

FIG. 1. Potential curves for the ground state $X\ ^1\Sigma_g^+$ of H_2 in different approximations: (1) Single configuration best limited LCAO MO SCF (present calculation); (2) Accurate analytical SCF[8]; (3) Best limited LCAO MO SCF with CI (present calculation); (4) Direct CI[9]; (5) Accurate calculation with James-Coolidge type functions.[8]

TABLE VI. Potential curves[a] for the ground-state and lowest-lying excited states of H_2, and the ground states of the molecular ions H_2^+ and H_2^-.

Molecule	H_2								H_2^+	H_2^-
State Excitation[b]	$X\ ^1\Sigma_g^+$ [c]	$^3\Sigma_u^+$ $1\sigma_g \rightarrow 1\sigma_u$	$^1\Sigma_g^+$ [c] $(1\sigma_g)^2 \rightarrow (1\sigma_u)^2$	$^1\Sigma_u^+$ $1\sigma_g \rightarrow 1\sigma_u$	$^3\Sigma_g^+$ $1\sigma_g \rightarrow 2\sigma_g$	$^1\Sigma_g^+$ [c] $1\sigma_g \rightarrow 2\sigma_g$	$^3\Sigma_g^+$ $1\sigma_g \rightarrow 3\sigma_g$	$^1\Sigma_g^+$ [c] $1\sigma_g \rightarrow 3\sigma_g$	$X\ ^2\Sigma_g^+$	$X\ ^2\Sigma_u^-$
1.0	−1.082738 (−1.103738)	−0.512528	0.425024 (0.372853)	−0.331511	−0.189235	0.062683 (0.036428)	0.772223	0.877049 (0.868609)	−0.417073	−0.659454
1.1	−1.108334 −1.130043	−0.583871	0.298082 (0.245875)	−0.401173	−0.251773	−0.012938 (−0.041329)	0.644954	0.750825 (0.741534)	−0.463036	−0.721570
1.2	−1.123140 (−1.145665)	−0.641178	0.189408 (0.137420)	−0.456365	−0.300952	−0.074241 (−0.104982)	0.534928	0.641771 (0.631535)	−0.496875	−0.770003
1.4	−1.132111 (−1.156613)	−0.726464	0.012798 (−0.037139)	−0.536208	−0.371185	−0.165941 (−0.202457)	0.354721	0.463344 (0.450805)	−0.540275	−0.838463
1.5	−1.129998 (−1.155671)	−0.758713	−0.060091 (−0.107806)	−0.565317	−0.396873	−0.201176 (−0.241467)	0.279186	0.388552 (0.374671)	−0.553727	−0.862879
1.6	−1.125096 (−1.152070)	−0.785916	−0.124923 (−0.169011)	−0.589116	−0.417898	−0.231002 (−0.276172)	0.211658	0.321703 (0.306349)	−0.563403	−0.882576
1.8	−1.109895 (−1.139876)	−0.828905	−0.235182 (−0.265655)	−0.624946	−0.450917	−0.279838 (−0.340421)	0.093851	0.204856 (0.186394)	−0.574688	−0.911850
2.0	−1.090686 (−1.124256)	−0.860862	−0.324896 (−0.328577)	−0.648993	−0.473638	−0.316013 (−0.403748)	−0.002283	0.109530 (0.087660)	−0.578865	−0.931209
2.5	−1.037993 (−1.083334)	−0.911661	−0.487044 (−0.411297)	−0.678766	−0.506858	−0.375421 (−0.538592)	−0.180769	−0.067940 (−0.098062)	−0.573844	−0.955828
3.0	−0.988481 −1.049884)	−0.939540	−0.590614 (−0.453440)	−0.684597	−0.519034	−0.405644 (−0.620154)	−0.293596	−0.179954 (−0.218119)	−0.560566	−0.963294
4.0	−0.910335 (−1.013633)	−0.964335	−0.700337 (−0.495812)	−0.668385	−0.521301	−0.429213 (−0.681491)	−0.407800	−0.293287 (−0.350463)	−0.532953	−0.961720
5.0	−0.857277 (−1.002781)	−0.971529	−0.744775 (−0.519270)	−0.641798	−0.524180	−0.441909 (−0.681742)	−0.444398	−0.332816 (−0.419146)	−0.512775	−0.955369
6.0	−0.821994 (−1.000152)	−0.973232	−0.761395 (−0.534630)	−0.615833	−0.530464	−0.452266 (−0.664639)	−0.445514	−0.340091 (−0.461351)	−0.500294	−0.949452
12.0	−0.754196 (−0.999363)	−0.975298	−0.752899 (−0.563383)	−0.531862	−0.456161	−0.393655 (−0.573187)	−0.394025	−0.290568 (−0.502908)	−0.487772	−0.936553
18.0	−0.739715 (−0.999403)	−0.975564	−0.739653 (−0.542675)	−0.503812	−0.428628	−0.366671 (−0.565305)	−0.370950	−0.265541 (−0.500978)	−0.487810	−0.936020

[a] All energies and internuclear distances (first column) in atomic units.

[b] The electronic configuration of the ground state of H_2 is taken as the basis in deriving the excited and ionized species. The excitation given refers only to the single-configuration calculations.

[c] The values in brackets correspond to the CI calculation (using 12 configura ions). All other values were obtained in the single-configuration approximation, the excited states functions having been approximated using virtual orbitals determined in the ground-state single-configuration calculation.

TABLE VII. Correlation correction.[a]

R (a.u.)	Correlation correction a.u.	Correlation correction Percentage of total correlation energy
1.0	0.018600	47.23
1.2	0.020636	51.72
1.4	0.022983	56.32
1.6	0.025718	60.96
1.8	0.028909	65.69
2.0	0.032608	70.35

[a] The correlation correction has been evaluated as the difference between the results of the present calculation (with CI; see Table VI) and the values obtained by Kolos and Roothaan,[8] with an accurate analytical SCF function. The percentage is referred to the total correlation energy as given by those authors.

value of 1.6875, which would indicate that the single-determinant function is going smoothly over to an excited state of the He atom involving $1s$, $2s$, or $1s$, $2p\sigma$ STO's. The exact energy level and functional form would have to be determined by a molecular calculation in the united atom region although plausible extrapolation of the coefficients might be made.

The curves of Fig. 1 demonstrate that qualitatively good behavior is obtained over the whole range of R of the curve when CI is superimposed, leading to a correct energy for the dissociation products. Nevertheless, the approximation used (equal ζ, with the common value varied for each point in the single-configuration calculation, and CI performed afterwards) does not give the best value for each point; for best results one would vary ζ after introducing CI. In any case, it can be seen that the CI function is more realistic at large distances than the 40-term Kolos-Roothaan function, as would be expected.

The difference between the best CI values given here and the best analytical SCF values of Kolos and Roothaan (interpreted as electron correlation energy) are tabulated in Table VII. The increase in the correlation correction as R increases is not to be interpreted as an increase in actual electron correlation; rather it is a theoretical measure of the inadequacy of the single-configuration functions at large distances.

The potential curves for the different excited and ionized states are given in tabular form to provide a point-for-point comparison against existing theoretical data. The corresponding curves are given in Fig. 2 together with those of Kolos and Roothaan, using both 34- and 40-term analytical wave functions.

The results derived for the molecular ions H_2^+ and H_2^- from the ground-state H_2 solution, are of special interest from a predictive standpoint. The energies of these charge species were evaluated from the calculated ground-state total energies, electron affinities and ionization potentials (IP), using the formulas

$$E(H_2^+, X\ ^2\Sigma_g^+) = E(H_2, X\ ^1\Sigma_g^+) - \epsilon_{1\sigma_g},$$

$$E(H_2^-, X\ ^2\Sigma_u^+) = E(H_2, X\ ^1\Sigma_g^+) + \epsilon_{1\sigma_u}.$$

The above approximation utilizing the appropriate H_2 data provides a good account of H_2^+. But this success does not necessarily mean that $\epsilon_{1\sigma_g}$ should correctly approximate the observed H_2 ionization potential which is calculated to be 16.10 ev at $R=1.4$ a.u. compared to an experimental value of 15.422 ev. A more accurate computation of the IP for H_2 would involve the determination of the thermal distribution for the different vibrational (and rotational) levels of both states (to cover the possibilities of both absorption and emission spectra), and the consequent (graphical) determination of the vibrational (and rotational) levels which will give the long-wavelength limit.[10] In the present case, leaving apart the rotational levels, the theoretical value for the IP should be considered to lie within the range 14.90 ev (ν_{00}) and 15.13 (ν_{01}). Of course, these results would have to be modified by: (a) correction of the ionized state energy to an accuracy equivalent to the one of the ground state (close-to-accurate SCF); (b) correlation correction for the ground state (in a general case a correlation correction would also have to be introduced for the ion). In this consideration, it would be necessary to assume that these corrections would leave the rotational and vibrational levels unchanged.

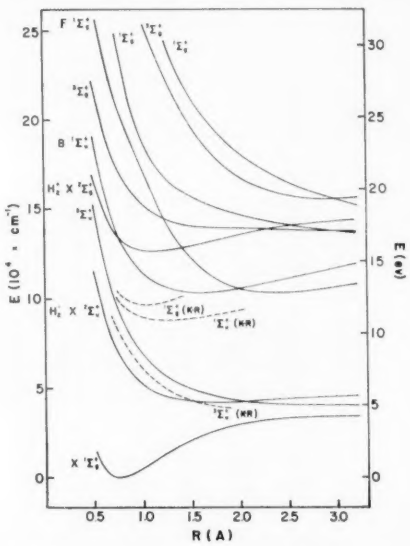

FIG. 2. Potential curves for the ground and lowest-lying excited states of H_2 and for the ground states of H_2^- and H_2^+. The full line curves have been plotted taking the values obtained in the present calculations: for the $^1\Sigma_g^+$ states, results from CI calculations; for all others, results from simple-configuration calculations. The dashed curves are from accurate calculations by W. Kolos and C. C. J. Roothaan.[8] The lowest $^1\Sigma_g^+$ excited state of Kolos-Roothaan can be identified as the $E\ ^1\Sigma_g^+$ state, while the lowest $^1\Sigma_g^+$ excited state obtained in the present calculations has been identified as the $F\ ^1\Sigma_g^+$ state (see reference 10 and Table VIII).

[10] See G. Herzberg, *Spectra of Diatomic Molecules* (D. Van Nostrand Company, Inc., Princeton, New Jersey, 1950), pp. 387, 414, 459.

TABLE VIII. Vibration-rotation constants[a] for the ground-state and lowest-lying excited states of H_2 and the ground states of the molecular ions H_2^+ and H_2^-.

State	Excitation[b]	T_e[c] (cm^{-1})	ω_e (cm^{-1})	$\omega_e x_e$ (cm^{-1})	B_e (cm^{-1})	α_e (cm^{-1})	R_e (A)	E_M (a.u.)	$10^{-5}k_e$[d] (dyne/cm)
H_2									
$B\ ^1\Sigma_u^+$	$1\sigma_g \rightarrow 1\sigma_u$	98203	1612	17.42	12.80	−0.09037	1.617	−0.68467	0.7711
		[91689]	[1357]	[19.93]	[20.02]	[1.193]	[1.293]		[0.5468]
$F\ ^1\Sigma_g^+$	$(1\sigma_g)^2 \rightarrow (^1\sigma_u)^2$	(103192)	(1465)	(28.40)	(6.001)	(0.08676)	(2.361)	(−0.68655)	(0.6373)
		[103480]	[1000]		[6.24]		[2.32]		
$X\ ^1\Sigma_g^+$		0	4631	216.7	61.61	1.816	0.7367	−1.13212	6.369
		(0)	(4359)	(181.8)	(58.78)	(1.350)	(0.7542)	(−1.15673)	(5.643)
		[0]	[4401]	[121.0]	[60.86]	[3.017]	[0.7412]	[−1.17444]	[5.751]
H_2^+[e]									
$X\ ^2\Sigma_g^+$		121375	2275	226.6	28.00	2.227	1.093	−0.57909	1.536
		[124429]	[2297]	[62]	[29.8]	[1.4]	[1.06]	[−0.6026]	[1.566]
H_2^-									
$X\ ^2\Sigma_u^+$		36771	975.4	32.32	10.62	0.1898	1.775	−0.96458	0.2825

[a] The values given without brackets have been obtained from curves evaluated in the single-configuration LCAO MO SCF approximation, while the values in parentheses correspond to curves obtained introducing CI. The observed values, where available, are given in square brackets and have been taken from: reference 10, B. P. Stoicheff Can. J. Phys. **35,** 730 (1957); and G. Herzberg and L. L. Howe, Can. J. Phys. **37,** 636 (1959).

[b] The electronic configuration of the ground state of H_2 is taken as the basis in deriving the excited and ionized species.

[c] These values are referred to the ground state of the neutral molecule H_2.

[d] The experimental value for k_e has been evaluated utilizing the same formula as for the theoretical values but making use of the observed value of ω_e.

[e] Theoretical values are given by O. W. Richardson, Nuovo cimento **15,** 232 (1938).

Poorer results are to be expected for negatively charged H_2^-, for which the total error in the energy should probably be larger because the correlation correction is larger in this case than for the neutral molecule or the positive ion. It is therefore interesting to compare the present results for H_2^- with those of Fischer-Hjalmars.[11] Very nearly equivalent results are obtained for the equal-ζ case although both calculations give unsatisfactory results both from the standpoint of energy and shape of curve. Plausible theoretical values for the electron affinity of H_2 are subsequently obtained

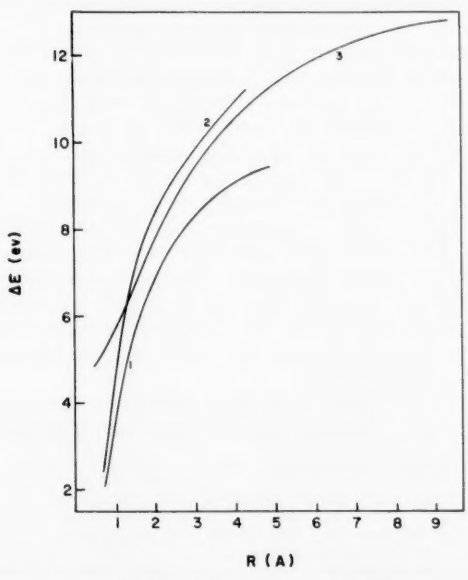

FIG. 3. Curves for the splitting $^1\Sigma_u^+ - {}^3\Sigma_u^+$ in different approximations: (1) Accurate calculation with James-Coolidge type function[8,12]; (2) MO−ξ approximation[14]; (3) Single-configuration LCAO MO SCF approximation, using virtual MO's (present calculation).

TABLE IX. Atomic populations as function of internuclear distance (single configuration).[a]

R (a.u.)	n $(1\sigma_g; 1s)$	n $(1\sigma_g; 2s)$	n $(1\sigma_g; 2p\sigma)$
1.0	1.949592	0.006309	0.044099
1.1	1.945038	0.007922	0.047040
1.2	1.941001	0.009464	0.049535
1.3	1.937411	0.010983	0.051606
1.4	1.934366	0.012316	0.053318
1.5	1.931845	0.013448	0.054711
1.6	1.929782	0.014410	0.055808
1.8	1.927358	0.015282	0.057360
2.0	1.926455	0.015494	0.058051
2.5	1.930434	0.012211	0.057355
3.0	1.938282	0.007600	0.054118
4.0	1.954887	0.001027	0.044086
5.0	1.968801	−0.001817	0.033016
6.0	1.979648	−0.002290	0.022642
12.0	1.999510	−0.000021	0.000511
18.0	1.999915	0.000000	0.000042

[a] Significance, if any, probably should not be given to these figures beyond three significant figures. Data are reported to six decimal places for those interested in computer-program checks.

[11] I. Fischer-Hjalmars, Arkiv Fysik **16,** 33 (1959).

TABLE X. Overlap populations as function of internuclear distance (single configuration).[a]

R (a.u.)	$n(1s_A, 1s_B)$	$n(1s_A, 2s_B) + n(2s_A, 1s_B)$	$n(1s_A, 2p\sigma_B) + n(2p\sigma_A, 1s_B)$	$n(2s_A, 2s_B)$	$n(2s_A, 2p\sigma_B) + n(2p\sigma_A, 2s_B)$	$n(2p\sigma_A, 2p\sigma_B)$	Total overlap
1.0	0.829007	0.011226	0.083656	0.000404	−0.000752	−0.003542	0.919999
1.1	0.807794	0.013984	0.088750	0.000487	−0.000824	−0.003308	0.906883
1.2	0.787040	0.016624	0.092948	0.000551	−0.000856	−0.003036	0.893271
1.3	0.766659	0.019220	0.096320	0.000607	−0.000856	−0.002738	0.879212
1.4	0.746877	0.021514	0.098996	0.000641	−0.000822	−0.002433	0.864773
1.5	0.727695	0.023484	0.101062	0.000656	−0.000760	−0.002128	0.850009
1.6	0.709039	0.025172	0.102580	0.000659	−0.000678	−0.001829	0.834943
1.8	0.674036	0.026854	0.104436	0.000602	−0.000470	−0.001275	0.804183
2.0	0.640900	0.027398	0.104788	0.000527	−0.000252	−0.000774	0.772587
2.5	0.567067	0.022184	0.101740	0.000262	0.000152	0.000193	0.691598
3.0	0.499030	0.014142	0.094770	0.000094	0.000268	0.000826	0.609130
4.0	0.369617	0.001966	0.075530	0.000002	0.000072	0.001389	0.448576
5.0	0.254778	−0.003536	0.055078	0.000008	−0.000174	0.001386	0.307540
6.0	0.163163	−0.004518	0.036438	0.000020	−0.000262	0.001089	0.195930
12.0	0.003714	−0.000048	0.000444	0.000000	−0.000002	0.000009	0.004117
18.0	0.000004	0.000000	0.000000	0.000000	0.000000	0.000000	0.000004

[a] Significance, if any, probably should not be given to these figures beyond three significant figures. Data are reported to six decimal places for those interested in computer-program checks.

by Fischer-Hjalmars when free ζ variation is permitted and a certain amount of CI is admitted.

Correct asymptotic behavior is obtained for both H_2^+ and H_2^-. The total energy for H_2^+ asymptotically approaches a limit of 0.5 a.u., which is the correct value for a dissociation into $H(^2S)$ and H^+. Similarly, H_2^- tends to a limit of about 0.93 a.u. which is very close to the Hartree-Fock value of 0.98793 a.u. corresponding to a dissociation into $H(^2S)$ and $H^-(^1S)$.

The results for the two lowest-lying $^1\Sigma_g^+$ excited states show an interesting feature. The potential curves obtained in the single-configuration approximation violate the noncrossing rule. When CI is introduced, the curves no longer cross over. The interaction is rather strong in the region of the crossing point and both curves separate from each other. But their curvature clearly indicates that there had been crossing in the simpler approximation.

In Fig. 3 the singlet-triplet splitting for the excited states $^1\Sigma_u^+$–$^3\Sigma_u^+$ has been plotted. The results from accurate calculations[12] plotted in the same figure, can be taken as a basis for comparison. Only in the region 1.0–2.0 A (where the minimum of the potential curve of $^1\Sigma_u^+$ lies) is rather good agreement obtained, on both sides of this region serious discrepancies arise. This behavior is mainly determined by the $^1\Sigma_u^+$ state. While the $^3\Sigma_u^+$ state is adequately approximated (see Fig. 2) over the full range of R, this is not true for the $^1\Sigma_u^+$ state outside the small region around its equilibrium position. In particular a very poor energy is obtained in the dissociation region.[13] Improved MO's[14] (i.e., with an extended basis set and ζ variation) cannot overcome this shortcoming in the single determinantal approximation; CI would correct this situation (as it has done for the ground state). It is well known, that the single-configuration LCAO MO SCF method, both in direct calculations and in the virtual MO's approximation, leads in general to excessively steep curves on both sides of the minimum, which in turn leads to computed values of the force constants k_e which are larger than the observed ones (see Table VIII).

At this point it is pertinent to mention the results obtained by Ehrenson and Phillipson[15] for the oscillator

[12] The accurate values for the $^1\Sigma_u^+$–$^3\Sigma_u^+$ splitting have been partly evaluated from the results given by Kolos and Roothaan,[8] and complemented by values taken from Phillipson and Mulliken,[14] who determined them from results of accurate calculations on $^3\Sigma_u^+$ by James and Coolidge, J. Chem. Phys. **6,** 730 (1938), and from the values obtained for $^1\Sigma_u^+$ based on a Morse potential curve constructed from spectroscopic data.

[13] The $B\ ^1\Sigma_u^+$ state dissociates into H $(1\ ^2S)$+H $(2\ ^2S)$ [or H $(1\ ^2S)$+H $(2\ ^2P)$] (see reference 10, p. 380), with a total energy of −0.625 a.u., while the theoretical value (at R=18.0 a.u.) is −0.501112 a.u. This difference (3.37 ev), partly canceled by the error in the theoretical value of the total energy of $^3\Sigma_u^+$, determines the discrepancy (2.65 ev) for the $^1\Sigma_u^+$–$^3\Sigma_u^+$ splitting between the theoretical and the accurate value (12.84 ev vs 10.20 ev) at large distances.

[14] P. E. Phillipson and R. S. Mulliken, J. Chem. Phys. **28,** 1248 (1958).

[15] S. Ehrenson and P. E. Phillipson, J. Chem. Phys. **34,** 1224 (1961).

strength of the transition $B\,^1\Sigma_u^+$(V state)–$X\,^1\Sigma_g^+$(N state) using our single-configuration wave functions at $R=1.4$ a.u. The f values evaluated using the dipole-length, -velocity, and -acceleration operators are 0.762, 0.538, and 0.607, respectively, which compare poorly with the best estimated value of 0.27. Such results are mainly due to the inadequate description (at the distance) of the V state by virtual orbitals. In a separate calculation, using our ground state function and Phillipson-Mulliken's[14] for the V state, they obtained 0.273, 0.225, and 0.354, respectively, which provides more evidence for the semiquantitative accuracy of the single-configuration function which extended basis set and Phillipson-Mulliken's V state function, at least at R_e.

Comparison of the calculated spectroscopic constants with experiment (Table VIII) for those cases where values are available shows rather good agreement. In the case of the ground state it can be seen that the introduction of CI betters the agreement with the observed values.[16]

Interesting qualitative, though tentative, conclusions can be drawn from inspection of the results of the single-configuration population analysis. The atomic populations (Table IX) indicate that in the extreme cases ($R=0$, $R=\infty$) the atomic population will practically be concentrated on the $1s$ STO (united or separated atom), which agrees with the picture obtained by direct inspection of the $1\sigma_g$ MO coefficients. The $1s$ atomic population reaches a minimum around 2.0 a.u., while the $2s$ and $2p\sigma$ populations reach a maximum (larger for $2p\sigma$ than for $2s$) around that point. These results agree qualitatively with what has already been reported[3] for He_2. On the basis of those results, it would be expected that the $2s$ contribution, though small, is not negligible. Analogously it would be expected to find the $2p\sigma$, and perhaps the $2s$ contribution larger around the equilibrium position, leading to a maximum overlap. That this is not so is probably attributable to the inherent deficiencies in approximating an open-shell system by the single configuration approximation.

The computed total overlap population (Table X) decreases as distance increases. There is no maximum in the binding region as would be expected on the basis of previous experience with He_2 where a maximum overlap population coincides with the region of the Van der Waal's minimum.[3] This again may be due to the inherent defficiencies of the SCF function at $R \neq R_e$ or possibly to a misinterpretation of the meaning of the overlap population.

[16] The good agreement obtained in the single-configuration calculations was expected.[6] The results reported there for Li_2, LiH, and HF, using many-configuration functions, did not offer a clear improvement over the single-configuration values. Those calculations were handicapped by using the same set of ζ's, determined variationally in the single-configuration calculation at the equilibrium distance, for all other internuclear separations.

ACKNOWLEDGMENT

The authors are greatly indebted to Professor R. S. Mulliken, Dr. Peter Fontana and Dr. Stanton Ehrenson for reading and criticizing the manuscript during various stages of its preparation.

Nickel-Activated Calcium and Strontium Sulfide Phosphors

M. AVINOR, A. CARMI, AND Z. WEINBERGER
Scientific Department, Ministry of Defense, Israel

(Received April 6, 1961)

Calcium sulfide activated by nickel and copper or nickel and silver gives an emission band at 680 and 625 mμ, respectively. In strontium sulfide the emission bands appear at 775 and 710 mμ, respectively. The presence of both activators is necessary for the production of these emissions.

IN the classical work of Lenard and his school[1] it was found that activation by nickel produced red luminescence in calcium sulfide and near infrared in strontium sulfide. Nickel is well known as a killer of the luminescence in zinc and cadmium sulfide phosphors[2] and is not known to function as an activator in any other host lattice. Therefore there is some theoretical interest in cases where it produces luminescence. It was shown recently[3] that the red emission ascribed to nickel in calcium sulfide is due to double activation by nickel and copper. In this paper we present the results of further investigations on nickel-activated phosphors.

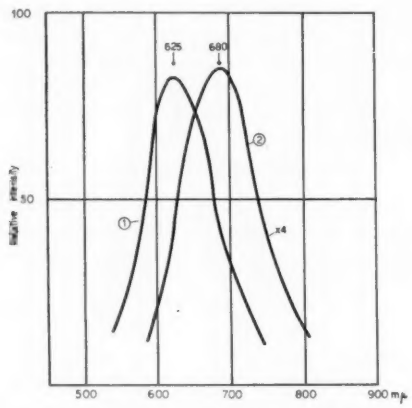

FIG. 1. Emission spectra of calcium sulfide activated by: curve 1 2×10^{-4} Ni, 2×10^{-4} Ag; curve 2 2×10^{-4} Ni, 2×10^{-4} Cu. Note the scale factor in curve 2.

EXPERIMENTAL

A new method has been developed for the preparation of luminescent pure alkaline earth sulfates by homogeneous precipitation from a single solution. A solution of the alkaline earth sulfamate is prepared by dissolving the carbonate in sulfamic acid solution. The solution is first purified by precipitation with hydrogen sulfide in the conventional manner.[4] It is then rendered slightly alkaline by ammonia and the last traces of heavy metals are extracted by a solution of dithizone in carbon tetrachloride. The purified solution is introduced into a Pyrex flask loosely covered with a Pyrex beaker and hydrolyzed by heating it in an autoclave to 200°C. The precipitated alkaline earth sulfate is washed several times with pure water and dried at 200°C. The yield is quantitative. Because of the high solubility of the alkaline earth sulfamates a large crop is obtained from a relatively small volume of solution. The phosphors were prepared by adding the activators as a solution of the sulfate or nitrate to the alkaline earth sulfate and drying at 150°C. The sulfate was reduced to the sulfide by heating to 1000°C in a stream of hydrogen sulfide. The sulfide was then mixed with 2 to 4% by weight lithium fluoride flux and fired at 1500°C in oxygen-free nitrogen.

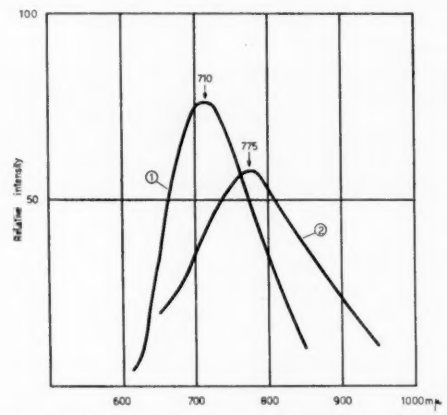

FIG. 2. Emission spectra of strontium sulfide activated by: curve 1 2×10^{-4} Ni, 2×10^{-4} Ag; curve 2 2×10^{-4} Ni, 2×10^{-4} Cu.

Luminescence was excited by the filtered radiation from a high-pressure mercury lamp (mainly 365 mμ) and measured on a Beckman DU quartz monochromator. An infrared photomultiplier (DuMont 6911) served as a detector. Corrections have been applied for obtaining equal energy spectra.

[1] P. Lenard, F. Schmidt, and R. Tomaschek, *Handbuch der Experimental physik* (Verlag Julius Springer, Berlin, 1928), pp. 331, 363.
[2] H. W. Leverenz, *An Introduction to Luminescence of Solids* (John Wiley & Sons, Inc., New York, 1950), pp. 333–337.
[3] M. Avinor, J. Chem. Phys. **32**, 621 (1960).
[4] G. R. Fonda and F. Seitz, editors, *Preparation and Characteristics of Solid Luminescent Materials* (John Wiley & Sons, Inc., New York, 1948), p. 29.

RESULTS

We have found that activation of calcium and strontium sulfides by nickel alone gave only very weak luminescence effects, which were probably due to some residual impurities. Activation by nickel and copper or nickel and silver produced a well-defined emission band in the red and near-infrared region of the spectrum. The emission band produced by nickel and silver appears at shorter wavelengths than the emission of nickel and copper in both calcium and strontium sulfides (Figs. 1 and 2). In calcium sulfide the nickel-copper band appears at 680 mμ and the nickel-silver band at 625 mμ (Fig. 1). Visually, the nickel-silver emission seems much

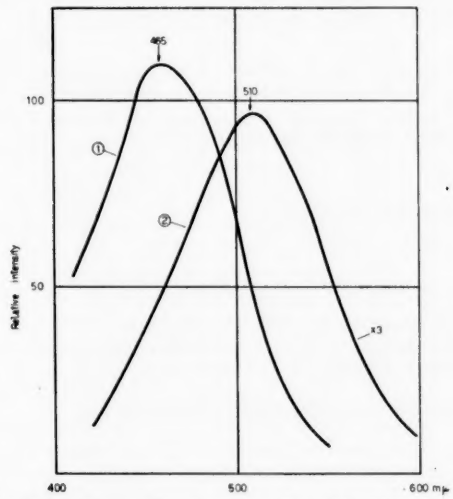

FIG. 3. Emission spectra of copper-activated phosphors: curve 1 CaS: 2×10^{-4} Cu; curve 2 SrS: 2×10^{-4} Cu. Note the scale factor in curve 2.

stronger than the nickel-copper emission, not only because it is actually about four times more intense but also because it is better detected by the eye. Indeed the nickel-silver case is rather striking because neither element alone produces any significant visible emission in either calcium sulfide or strontium sulfide. The very weak and nonhomogeneous visible luminescence effects which we find in silver-activated calcium and strontium sulfides are probably due to the presence of impurities.

In strontium sulfide the nickel-silver band appears at 710 mμ, but is otherwise similar to the corresponding band in calcium sulfide (Fig. 2) Nickel-copper activated strontium sulfide gives a near-infrared emission band centered at 775 mμ which extends weakly into the visible region. In addition it shows a relatively strong orange phosphorescence.

Copper alone as an activator in calcium and strontium sulfides gives the well-known blue and green emissions at 465 and 510 mμ respectively (Fig. 3). The energy difference in the peak positions is 0.23 ev. The same difference is found between the peak emissions of nickel-

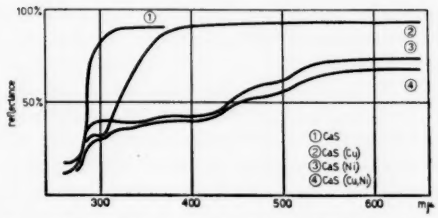

FIG. 4. Reflection spectra of calcium sulfide phosphors.

copper activated calcium sulfide and strontium sulfide (Fig. 1, curve 1 and Fig. 2, curve 1), as well as between nickel-silver activated calcium sulfide and strontium sulfide (Fig. 1, curve 2 and Fig. 2, curve 2).

In view of the clear evidence of activator interaction in these cases we tried to determine the molecular ratio of nickel to silver for maximum interaction effect in calcium sulfide. To this end we used the method of continuous variation. Keeping the total molecular concentration of the activators nickel and silver constant at 4×10^{-4} atom/mole and varying the ratio of nickel to silver, we measured the intensity of emission at 625 mμ under identical conditions. No definite conclusion could be drawn from these experiments because of scatter in the results, but in general we find that higher intensities are obtained when the silver-to-nickel ratio is larger than one. Phosphorescence effects are then also stronger.

Reflection spectra of the phosphors (Figs. 4 and 5) show that nickel activation introduces a very wide absorption region extending from the absorption edge of the base material in the ultraviolet down into the visible region. It seems to be composed of several ill-defined absorption bands. Copper activation of the base material introduces some additional absorption beyond the edge and in the case of CaS(Cu) we find a clear indication of a single absorption band due to copper at 300 mμ (Fig. 4). Silver activation produces little additional absorption. In phosphors activated by silver and nickel or copper and nickel, the absorption seems to be due to simple superposition of the absorption bands of each activator alone.

DISCUSSION

The foregoing experimental facts show that definite emission bands are produced by interaction between

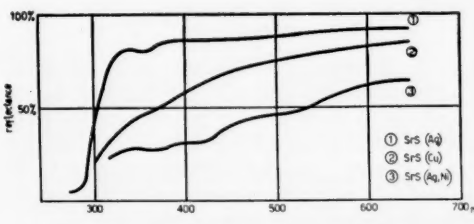

FIG. 5. Reflection spectra of strontium sulfide phosphors.

two activators, nickel and silver, or nickel and copper, in calcium and strontium sulfides. The presence of both activators is necessary for the occurrence of the emission and therefore this case is different from the interaction found in the case of sensitization. It is similar to the activator-coactivator interaction found in zinc sulfide[5] but in this case it is difficult to decide which atom is the main activator and which is the coactivator. It seems plausible to assume that nickel is the main activator because its presence suppresses the characteristic blue band of copper,[3] and that copper and silver act as coactivators in producing the red emission. A somewhat similar case of coactivation by copper and silver was found in vanadium-activated phosphors.[6] However, in the present case the influence of the silver and copper on the position of the emission band (a difference of 0.15 ev) is considerably larger than the influence of the various coactivators on the position of the green copper band in zinc sulfide. It is possible that the red band is due to trivalent nickel centers and that the monovalent silver and copper facilitate the introduction of nickel in the trivalent state. Paramagnetic resonance experiments could settle this point perhaps.

[5] F. A. Kröger and J. Dikhoff, Physica **16**, 297 (1950).

[6] M. Avinor and G. Meijer, J. Phys. Chem. Solids **12**, 211 (1960).

THE JOURNAL OF CHEMICAL PHYSICS VOLUME 35, NUMBER 6 DECEMBER, 1961

Structural Requirements of Organic Liquid Scintillators

ADAM HELLER
Israel Atomic Energy Commission Laboratories, Rehovoth, Israel

(Received May 8, 1961)

A theory is proposed to explain the relationship between the structure and the scintillation efficiency of organic liquid scintillators.

The requirements for good scintillation properties in given solvent-solute systems are found to be: (a) the existence of pairs of energy levels in the solute which are identical with those involved in the excitation of the solvent and (b) a nonrigid structure in the solute, capable of undergoing conformational changes in the excited state.

It was found that the behavior of liquid scintillators satisfied these requirements. Good scintillation properties were predicted for some hitherto unknown scintillators.

INTRODUCTION

In recent years many hundreds of compounds have been screened in the search for improved liquid scintillators. However, no quantitative or semiquantitative theory has been proposed that could explain the relationship between the structures and the efficiencies of these scintillators.

The aim of the present paper is (a) to state the requirements for good scintillation properties of a scintillator dissolved in a solvent, (b) to calculate some of these properties for several groups of aromatic hydrocarbons, (c) to compare the theoretical and experimental efficiencies, and (d) to suggest some new efficient scintillators.

THEORY

Since the radiation is absorbed mainly by the solvent and commercial photomultipliers are sensitive only to light emitted by the solute, the two main requirements for efficient scintillation properties are (1) efficient and irreversible energy transfer from the solvent to the solute and (2) negligible absorption of the emitted radiation by the solute and the solvent.

The first requirement implies that the transfer of energy from the solvent to the solute should be sufficiently fast to be completed in a time much shorter than the lifetime of the excited solvent molecule, which is of the order of 10^{-9} sec. Irreversibility is required to avoid equipartition of the energy between solvent and solute molecules. This would cause the greater part of the energy to be emitted at wavelengths characteristic of the solvent, which is present in great excess. Since the emission and the absorption spectra of the usual solvents are similar, a continuous reabsorption by the solvent of the emitted photons would be contrary to the second requirement.

The second requirement is a result of the finite, though small, probability of nonradiative energy losses in excited molecules. Even in dilute solutions with medium absorption coefficients, in flasks only a few centimeters in diameter, the emitted photons would be reabsorbed many times, and the probability of losses due to nonadiabatic transitions would be strongly increased.

If a molecule, surrounded by a group of similar molecules, is excited, one may assume that because of well-known quantum-mechanical principles, exchange forces that tend to form aggregates of molecules will appear.

In these aggregates the molecules are stabilized by sharing both the gap which is left in one of the populated orbitals of the excited molecule and the electron in the orbital which is not populated in the ground state. Within the aggregate the excess energy is delocalized and thus the necessary and sufficient condition for high efficiency in the transfer is the existence of pairs of electron levels of equal energy in the solvent and in the solute. These pairs enable strong exchange interaction between the excited and nonexcited molecules. Since the transition moments in the solvent molecules are high only for the transitions to the lower singlet states, and since energy transfer occurs mainly between the lower singlet states of the solvent and the solute,[1] only correlations with the lower electron levels of the solvent need be considered.

If the number of pairs of electron levels in the solute that have energy differences equal to those involved in the excitation of the solvent is n, there are n^2 possible combinations between the levels by which the energy of the excited solvent molecule can be transferred or shared. Therefore, the probability of inclusion of a molecule of the solute in an excited aggregate of solvent molecules should be proportional to the number of possible combinations per unit volume (n^2/V).

Since the density of the aromatic hydrocarbons is fairly constant, their molar volumes are roughly proportional to their molecular weights. As a consequence, the rate of energy transfer should be closely proportional to n^2/M, M being the molecular weight of the solute. Since the efficiency of the energy transfer is expected to depend on its rate (due to the short duration of the process), a close relationship should exist between the efficiency and n^2/M.

Convenient semiempirical quantum-mechanical methods for the computation of the energy levels of aromatic hydrocarbons are known[2] and the results of a considerable number of such computations have been published.[3] The approximations made by such calculations would introduce serious errors if absolute energy values were sought. Since only a comparison of the levels in solvents and solutes is made, the application of the results of the method of linear combination of atomic orbitals (LCAO) is justified.

Fulfillment of the requirement for effective energy transfer is necessary but not sufficient for good scintillation properties. As was already mentioned, irreversibility of the transfer and low excitation coefficients of both solvent and solute in the regions of the emission bands of the scintillator are essential.

Although the superposition of vibrational transitions on the purely electron ones causes considerable differences in the limits of the regions of absorption and emission in large conjugated molecules, the overlap of the absorption and emission spectra is still considerable and leads to losses in scintillation yields. Effective separation of the absorption and emission bands is possible only if the absorbing molecules differ in some way from the emitters. Such a separation does, indeed, exist in the scintillators and may be illustrated by the following examples. (1) On excitation of either *trans*- or *cis*-stilbene, a mixture of the isomers is produced. Hence the excited state does not correspond in its configuration to either of the ground-state configurations. It has an independent structure and therefore independent spectral transitions. (2) Conformational change in the excited state also occurs in the linear polyphenyls (biphenyl, *p*-terphenyl). In these compounds the rings are not coplanar because of steric hindrance at the *ortho*-positions. In the excited states the angles of distortion are changed and new conformations are produced.

A conformational change in the excited state also provides the required irreversibility of the energy transfer from the solvent to the solute. Since only a limited number of vibrations is required to bring the excited molecule to its new configuration, the duration of the conformational change process is estimated to be of the order of 10^{-12} sec. This is much shorter than the lifetime of the excited molecules (10^{-9} sec). The new excited state formed does not have the former correlation between the electron levels and the solvent. Because of the vibrational dissipation of energy in the new species, the gap between the levels involved in the excitation is smaller than before. Thus, energy flow from the solute back to the solvent is blocked.

One of the self-evident requirements, which will not be dealt with, is the solubility of the solute in the solvents. It should be pointed out that the solubilities can be modified by introducing various aliphatic groups into the aromatic compounds, without changing the electron levels or the transfer properties significantly.[4]

EVALUATION OF THE SCINTILLATION PROPERTIES OF SOME AROMATIC HYDROCARBONS

Table I gives the theoretical relative energy transfer efficiencies from a benzenelike solvent to a number of aromatic hydrocarbons and predicts their classification. (A benzenelike solvent molecule is defined as one having a benzene ring not conjugated to other π-electron systems).

The following comments may be made on the values in Table I. The compounds included in class D do not have appreciable scintillation properties, as was, in many cases, found by experiment.

The compounds in class C (coronene and perylene), although possessing high-energy transfer indices, have rigid structures and therefore are not suitable scintillators.

Class B compounds have intermediate values of the

[1] J. B. Birks, IRE Trans. on Nuclear Sci. NS-7, 2 (1960).
[2] B. Pullman and A. Pullman, *Les Theories Electroniques de la Chimie Organique* (Mason, Paris, 1952).
[3] C. A. Coulson and R. Dandel, *Dictionary of Values of Molecular Constants* (calculated theoretically by wave-mechanical methods)

[4] V. Nay, H. J. Eichhoff, G. Herrmann, and H. O. Wirth, Z. Electrochem. **64**, 1098 (1960).

transfer index. Some, such as stilbene, phenylhexatriene and diphenylhexatriene, are mediocre scintillators in solution.

The compounds in class A with high transfer indices and nonrigid structures are expected to be good scintillators. Some of them however, for example *p*-terphenyl, need wavelength shifters. *p*-Terphenyl, quaterphenyl and diphenylbutadiene have been found experimentally to fulfill this expectation of good performance.

9-Vinylanthracene and 9,10-divinyl-anthracene, which have not, as yet, been used as liquid scintillators, have excellent transfer properties. Both meet the other

TABLE I. Classification of aromatic hydrocarbons with regard to their predicted scintillation properties.[a]

Compound	n^2	Mol. wt. (M)	$n^2/M \times 10^2$	Class
Naphthalene	1	128	0.8	D
Anthracene	4	178	2.2	B
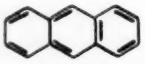				
Naphthacene	1	228	0.4	D
Pentacene	4	278	1.4	D
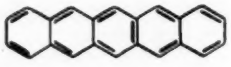				
Phenanthrene	0	178	0	D
3,4 - Benzophenanthrene	1	228	0.4	D
Chrysene	0	228	0	D
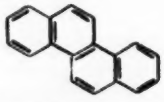				
1,2 - Benzanthracene	1	228	0.4	D
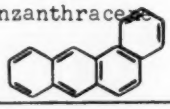				

[a] *Notes*: n denotes the number of pairs of energy levels in the compounds corresponding to those in benzene (or similar compounds).

The classification of the compounds is indicated according to the following criteria: Class A includes those compounds where conformational change is possible and which have an index $n^2/M > 0.030$; class B includes those where conformational change is possible but $0.015 < n^2/M < 0.030$; class C includes those where $n^2/M > 0.03$ but which do not undergo conformational change; class D includes all compounds with $n^2/M < 0.015$.

The calculated relative transfer efficiency from benzene-like solvents to the compound is given in Col. 4.

Table I (*continued*)

Pyrene 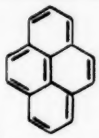	1	202	0.5	D
Triphenylene 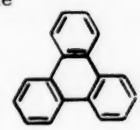	0	228	0	D
Pentaphene 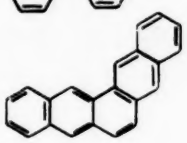	4	278	1.4	D
Picene 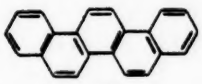	1	278	0.4	D
Perylene 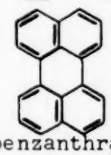	16	272	5.9	C
1,2-3,4-Dibenzanthracene 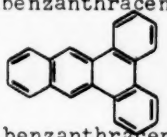	0	278	0	D
1,2-5,6-Dibenzanthracene 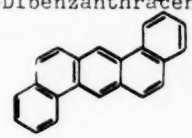	0	278	0	D
3,4-5,6-Dibenzophenanthrene 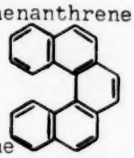	0	278	0	D
1,12-Benzoperylene	4	276	1.4	D
Coronene 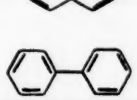	9	300	3.0	C
Biphenyl	4	154	2.6	B

Table I (*continued*)

p-Terphenyl	16	230	7.0	A
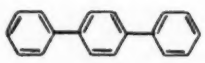				
m-Terphenyl	4	230	1.7	B
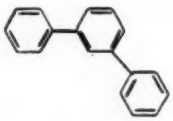				
o-Terphenyl	4	230	1.7	B
Quaterphenyl	16	306	5.2	A
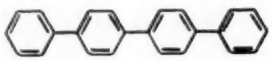				
1,3,5-Triphenylbenzene	4	306	1.3	D
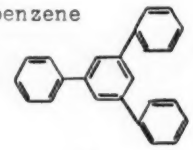				
Styrene	1	104	1.0	D
p-Divinylbenzene	4	130	3.0	A
m-Divinylbenzene	0	130	0	D
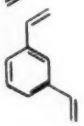				
o-Divinylbenzene	0	130	0	D
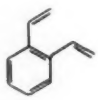				
trans-Stilbene	4	180	2.2	B
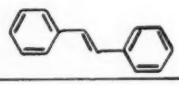				

Table I (*continued*)

1,4-Diphenylbutadiene 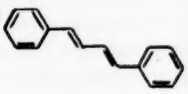	9	206	4.4	A
1,6-Diphenylhexatriene	4	232	1.7	B
1,8-Diphenyloctatetraene	4	258	1.6	B
1,10-Diphenyldecapentaene	9	284	3.2	A
1-Phenylbutadiene 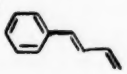	1	130	0.8	D
1-Phenylhexatriene 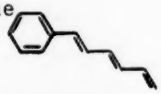	4	156	2.6	B
1-Vinylnaphthalene	4	154	2.6	B
2-Vinylnaphthalene 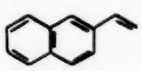	0	154	0	D
9-Vinylanthracene 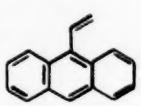	9	204	4.4	A
9,10-Divinylanthracene 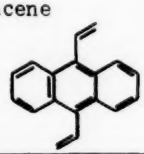	16	230	7.0	A

requirements stated. The scintillation properties of 9-vinylanthracene were examined. The compound was found to exhibit properties approaching those of *p*-terphenyl and to be capable of replacing the expensive 1,4-bis-2-(5-phenyloxazolyl)-benzene (POPOP) in toluene or xylene solutions of *p*-terphenyl and related compounds.[5]

Since only the correlation with levels of benzenelike solvents was sought, efficient scintillators in these solvents might be very poor ones in other solvents. One noteworthy example is that of the polystyrenes. The repeating units of these polymers contain benzene-like structures with six conjugated π electrons, but their monomers contain a system of eight conjugated π electrons. Thus, although the conventional solutes produce good scintillators when dissolved in the polymers, the solutions in the monomers are poor scintillators.[6]

ACKNOWLEDGMENTS

The author is grateful to Professor E. D. Bergmann, Dr. Y. Marcus, and Dr. M. Givon for reading the manuscript.

[5] A. Heller and D. Katz, J. Chem. Phys. **35,** 1987 (1961), following paper.

[6] A. Weinreb and P. Avivi, *Liquid Scintillation Counting* (Pergamon Press, London, 1958), p. 270.

Scintillation Properties of 9-Vinylanthracene

ADAM HELLER
Israel Atomic Energy Commission Laboratories, Rehovoth, Israel
AND
DOV KATZ
Scientific Department, Israel Ministry of Defense Tel-Aviv, Israel
(Received May 8, 1961)

9-Vinylanthracene, for which good scintillation properties were predicted, was found to be a high-grade primary and secondary scintillator, capable of replacing the widely used 1,4-bis-(2-(5-phenyl)-oxazolyl)-benzene (POPOP).

INTRODUCTION

A THEORETICAL study[1] has shown that the solutions of 9-vinyl-anthracene[2] in benzene, toluene, xylene, and other alkylbenzenes should exhibit good scintillation properties, comparable to those of *p*-terphenyl or diphenylbutadiene. The theory indicated that in addition to having properties of a primary scintillator, 9-vinylanthracene (9-VA) should exhibit also properties characteristic of secondary scintillators ("wavelength shifters"). The fluorescence maximum of the solutions is near the maximum sensitivity region of the most widely used phototubes. The compound is

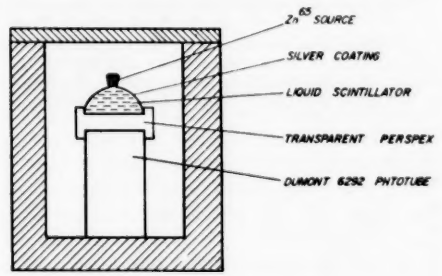

FIG. 1. Measuring arrangement.

easily prepared in a simple three step process from anthracene and acetylchloride.[2]

Since the scintillation behaviour of 9-vinylanthracene has not yet been reported, an experimental study seemed indicated.

EXPERIMENTAL

Materials and Method

Anhydrous sulfur free solvents were used. 9-VA was purified by chromatography on activated alumina and two recrystallizations from methanol. The yellow crystals of the compound melted at 68°C. Terphenyl and 1,4-bis-(2-(5-phenyl)-oxazolyl)-benzene (POPOP) were commercial products of "scintillation grade."

The measuring arrangement is shown in Fig. 1. The optical connection between the 26 ml vessel containing

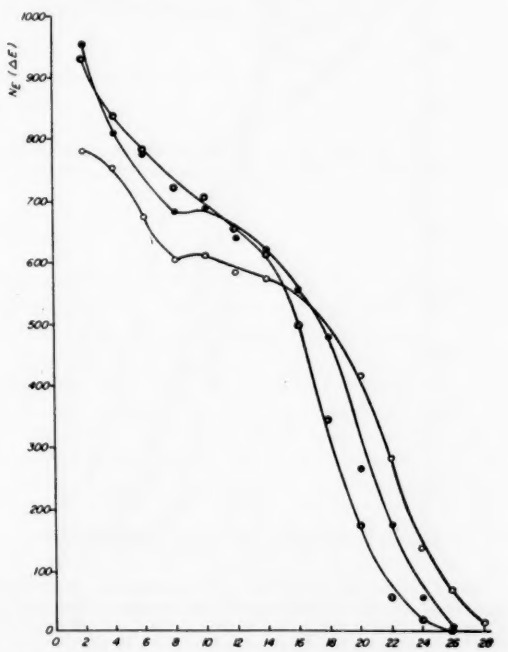

FIG. 2. Variation of the scintillation efficiency of 9-vinylanthracene solutions in xylene with concentration. The abscissa is the pulse height (arbitrary units). ○=0.9 g/l, ●=0.45 g/l, ⊙=1.8 g/l.

the scintillator and the 6292 DuMont phototube consisted, in order, of a layer of analytical grade paraffin oil, a Perspex light pipe, and a thin layer of Dow-Corning silicone grease. A 0.05-μC Zn^{65} source was used; all the measurements were carried out at 24°C after argon had been bubbled through the scintillator solutions for 20 min.

[1] Adam Heller, J. Chem. Phys. **35**, 1980 (1961), preceding paper.
[2] D. Katz and E. D. Bergmann, J. Chem. Soc. **1958**, 3216; also unpublished results.

Results

Figures 2–5 describe the distribution of the pulses as a function of their energies or relative pulse heights. The scale of the energies is the same in all measurements. Data on a solution containing 4 g/l *p*-terphenyl in xylene and a solution of 4 g/l of *p*-terphenyl and 0.1 g/l of POPOP in xylene are included for comparison. The ordinates, denoted by $N_e(\Delta E)$, indicate the number of pulses per unit time per unit interval of energy.

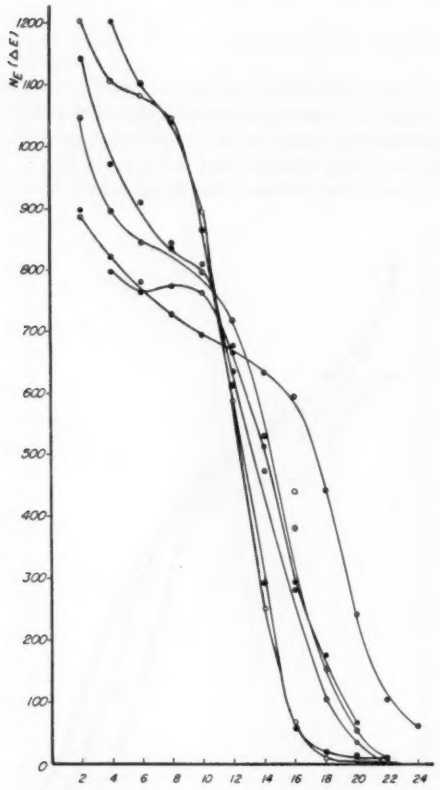

FIG. 3. Variation of the scintillation efficiency of 9-vinylanthracene solution in toluene with concentration. The abscissa is the pulse height (arbitrary units). ○=2.2 g/l, ●=1.3 g/l, ⊕=1.08 g/l, ◐=0.88 g/l, ⊙=0.78 g/l, ⊖=0.44 g/l.

Figures 2 and 3 give the distribution of the number of pulses as a function of their energy in solutions of 9-VA in xylene and toluene. The optimum concentration was found to be 0.9 g/l for both solvents and also for benzene. A comparison of the efficiency of 9-VA in benzene, toluene, and xylene, and of *p*-terphenyl in xylene at their optimal concentrations (Fig. 4) shows that the scintillation efficiency of 9-VA approaches that of *p*-terphenyl, although the concentration of 9-VA is smaller by a factor of 4 or 5. The scintillation efficiency of solutions of 9-VA increases with the substitution in the ring in the sequence, benzene<toluene<xylene.

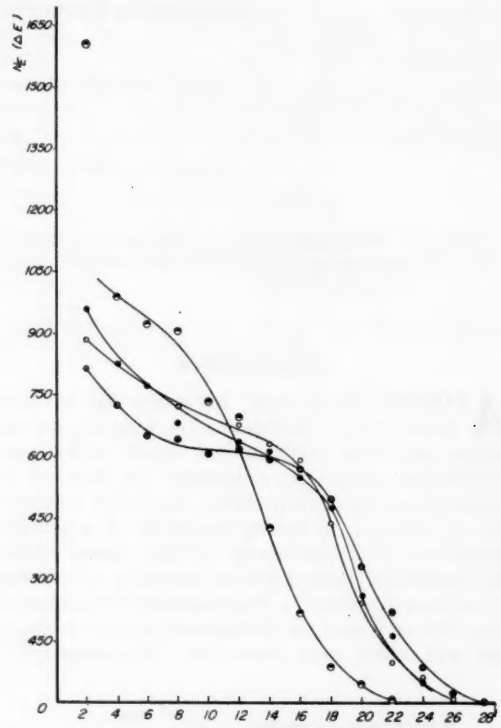

FIG. 4. Influence of the solvent on the scintillation efficiency of 9-vinylanthracene (at a concentration of 0.90±0.02 g/l. The abscissa is the pulse height (arbitrary units). ⊙=4 g/l *p*-terphenyl in xylene, ●=xylene, ○=toluene, ◓=benzene.

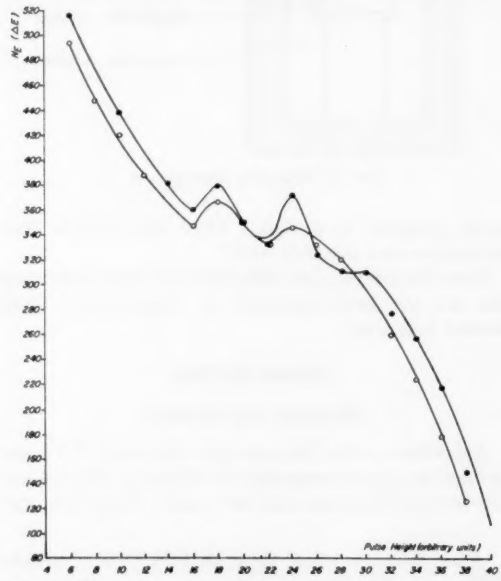

FIG. 5. Comparison of the efficiencies of 9-vinylanthracene and 1,4-bis-2-(phenyloxazolyl)-benzene (POPOP) as secondary scintillators in xylene solutions of *p*-terphenyl. ●=50 mg 9-vinylanthracene+4 g *p*-terphenyl/l, ○=100 mg POPOP+4 g *p*-terphenyl/l.

Experiments have also been carried out with 9-VA as secondary scintillator. Already 20 mg/l of 9-VA increases substantially the scintillation efficiency of a xylene solution of 4 g/l *p*-terphenyl. The optimum concentration is 50 mg/l of 9-VA as compared with 100 mg/l POPOP in similar solutions. The light output of the xylene solution of 4 g/l *p*-terphenyl with 50 mg/l 9-VA is similar to that of a solution of 4 g/l *p*-terphenyl and 100 mg/l POPOP in xylene. Both solutions have an efficiency of about 70% of an anthracene crystal of similar dimensions.

DISCUSSION

In good agreement with predictions made on purely theoretical grounds,[1] 9-VA has been proved to be an efficient primary and secondary scintillator in solutions in alkylbenzenes. Because of the simplicity of its preparation from cheap starting materials[2] it is expected that the compound will replace the expensive POPOP.

The low melting point and the yellow color of 9-VA seem to indicate that, in contrast to a widely accepted hypothesis,[3] scintillators may be efficient even if they have low mp and are colored.

ACKNOWLEDGMENTS

The authors wish to express their thanks to Professor E. D. Bergmann and to Dr. Y. Marcus for reading the manuscript and to Mr. Leon Gefen for technical help.

[3] R. C. Sangster and S. W. Irwine, J. Chem. Phys. **24,** 670 (1956).

THE JOURNAL OF CHEMICAL PHYSICS VOLUME 35, NUMBER 6 DECEMBER, 1961

NMR Chemical Shift of Hydroxyl and Hydronium Ions*

J. I. MUSHER

Lyman Laboratory, Harvard University, Cambridge, Massachusetts

(Received May 8, 1961)

The NMR absorption of protons in hydroxyl and hydronium ions is displaced about 10 ppm to low field from the proton-resonance absorption in water. This shift is roughly explained by a model locating all the ionic charge on the oxygen atom for both ions.

SEVERAL years ago a series of experiments[1,2] were performed on the nuclear magnetic resonance (NMR) of protons in solutions of aqueous electrolytes. These studies were concerned with the equilibria involved in the hydrolysis of mono- and dibasic acids and bases. Important parameters for this work are the NMR chemical shifts of the proton in the hydrolyzed form, i.e., H_3O^+ and OH^-, relative to the proton in water. This was determined for monobasic acids as the ratio of change of chemical shift to change of electrolyte concentration in the limit of zero concentration and is therefore the relative chemical shift of the ion at infinite ionic dilution. Thus, although solvent (H_2O) association might be a contributing factor to the observed shift, interactions with other solute ions will only give a negligible, and in the true limit, a zero contribution. It was found that both the hydroxide ion and the hydronium ion have their resonances shifted about 10 ppm to low field from the resonance in water. The exact values obtained are: -11.8, -11.4, -9.2, -13.1, ~-10, ~-10 ppm for nitric acid, hydrochloric acid, perchloric acid (in which there are other factors contributing to the shift[2]), sulfuric acid[3] (dibasic), sodium hydroxide, and potassium hydroxide.

Two possible explanations for this very large low-field shift have been given. The first[1] explains only H_3O^+ and compares its shift to the calculated shift for a bare proton. It is suggested that one-third ionic character be associated with the OH bond locating the positive charge on the hydrogens. The major objection to this is that it would predict a shift of opposite sign for the OH^- ion. The second discussion[4] considers the shift as due to the "molecular environment" of the ions and principally to "strong hydration" as in hydrogen bonding. This explanation is not entirely satisfactory, (a) because such molecular associations (in infinite ionic dilution) should not be greatly different for an ion in water than for a water molecule in water; (b) the "hydrogen bond shift"—defined as the chemical shift between molecules in the liquid[5] and in the gaseous state[6]—is not necessarily all attributable

* This investigation was supported in part by a fellowship from the National Cancer Institute, Public Health Service, and by the joint program of the Office of Naval Research and the U. S. Atomic Energy Commission.

[1] H. S. Gutowsky and A. Saika, J. Chem. Phys. **21,** 1688 (1953).

[2] G. C. Hood, O. Redlich, and C. A. Reilly, J. Chem. Phys. **22,** 2067 (1954).

[3] G. C. Hood and C. A. Reilly, J. Chem. Phys. **27,** 1126 (1957).

[4] J. A. Pople, W. G. Schneider, and H. J. Bernstein, *High-Resolution Nuclear Magnetic Resonance* (McGraw-Hill Book Company, Inc., New York, 1959).

[5] After correcting for bulk magnetic susceptibility.

[6] Reference 4, p. 403. See also S. Gordon and B. P. Dailey, J. Chem. Phys. **34,** 1084 (1961) for a discussion of the negligible association shifts in liquids.

to association, but perhaps in part to changes in molecular shape. Molecular parameters such as bond lengths can change with change of state and correlation of intramolecular electronic distributions between gas and liquid phases should not be expected to be rigorous; and (c) the magnitude of the hydrogen bond shift is too small although it is of the correct sign.[6] For water it is -4.6 ppm and except for HF it is less than -2.5 ppm for the other molecules studied. It must be remembered that these values refer to concentrated (concentrated in the solvent—zero solute) solutions of like molecules and not infinitely dilute solutions as with the ions studied.

We wish to propose a simple model which accounts for the gross feature of this phenomenon. We assume that the OH bond for both ions is basically the same (ionic character, etc.) as for the water molecule. For this to hold, therefore, the imbalance of charge or electron density (excess or lack) should be principally located on the oxygen atom for both ions. Thus we assume that we can treat OH^- as a complex of a hydrogen atom with an O^- ion, H_3O^+ as a complex of three H atoms with an O^+ ion, and water as a complex of two H atoms with an O^0 atom.[7] Based on this model it is possible to explain the low-field chemical shifts of the protons in these ions as arising from the interaction of their 1*s* electrons with the electric field of the "point charge" on the oxygen atoms.

The isotropic chemical shift for a proton in a hydrogen atom in a uniform electric field E has been shown to be[8] $\Delta\sigma = -(881/216)\times a_0^3E^2/mc^2 = -7.38\times10^{-19}E^2$, where a_0 and m are the Bohr radius and the mass of the electron, respectively. This is the isotropic chemical shift since it is the average over all directions of **E** relative to the external magnetic field $\mathbf{H}_0$. This is the expression which we use for $\Delta\sigma$ of a proton attached to a molecule containing a localized charge and rapidly tumbling in an external magnetic field. The shift $\Delta\sigma$ is caused by the perturbation of the proton's electron distribution, and is exact for an isolated H atom in a uniform electric field (and can be considered as giving a reasonable approximation for a covalently bound H atom in a molecule in the radial field of a point charge).

In our model, the protons (and their 1*s* electrons) in the H_3O^+ ion and the OH^- ion will "see," respectively, an electric field of magnitude $\pm e/r_{OH}^2$, where r_{OH} is the oxygen-hydrogen internuclear distance. E^2 is identical for both ions and we therefore expect the protons in both to be equally unshielded with $\Delta\sigma = -7.38\times10^{-19}e^2/r_{OH}^4$. If this is the sole contributing term to $\Delta\sigma$ it is possible to calculate r_{OH} from the experiment. Using $\Delta\sigma = -12\times10^{-6}$ as the average of the most reliable values (HCl, HNO_3, H_2SO_4) we calculate $r_{OH} = 1.09$ A. This is a fair approximation to the true value.[9] r_{OH} in water vapor is actually 0.96 A; r_{OH} in crystalline $C(CH_2OH)_4$ is 0.94 A; r_{OD} in heavy ice (which should be less than r_{OH}) is 1.01 A; and in formic acid dimer $r_{OH} = 1.075$ A. There have been no estimates of OH distances in ions. We could turn the problem around, and taking $r_{OH} = 0.96$ A, the gas value, estimate $\Delta\sigma = -20\times10^{-6}$. Thus it appears that we have a reasonable explanation for the low-field chemical shift of hydroxyl and hydronium ions.

We have neglected the contributions to the shift due to the polarization of the surrounding medium. This would give at any instant of time an electric field at the proton located in the ion. The total shift would be proportional to $\langle(E^{ion}+E_{||}^{pol})^2\rangle_{Av}$, where $E_{||}^{pol}$ is the component of the net polarization field at the proton parallel to the field due to the ionic charge E^{ion} and $\langle\ \rangle_{Av}$ is the average over molecular motions during $\sim$1 sec. Were the ion spherically symmetrical so that E^{pol} had no preferred direction relative to the ion, or were the polarization of the surrounding medium not to change significantly as the molecule tumbles then $\langle E_{||}^{pol}\rangle = 0$. However, because of ionic shape (requiring H_3O^+ to be pyramidal rather than planar) there might be favored direction of the polarization field. This would contribute a field parallel to E^{ion} but probably of opposite sign and therefore $\Delta\sigma \propto -E^{ion2} + 2\,|\,E^{ion}\,||\,\langle E_{||}^{pol}\rangle\,|$ plus terms of higher order. Thus such contributions will reduce the calculated $\Delta\sigma$. Our model has no dipole moment and therefore the Onsager reaction field is neglected.[10]

In order to confirm this explanation for the ionic shifts we had hoped to study aqueous solutions of various concentrations of CH_3ONa. However, $\Delta\sigma$ will be only ~-0.7 ppm since the protons are much further from the charge on the oxygen and we were unable to get a sufficiently concentrated solution to give a detectable change in resonance frequency. Either the sodium salt of *t*-butanol or *o*-cresol might be suitable although in the latter one would be worried about the interaction of the ionic electron with the benzene ring. Perhaps a model such as this will be useful in studying nucleoprotein structures via magnetic resonance.

ACKNOWLEDGMENT

The author would like to thank Dr. A. D. Buckingham for his comments on the manuscript.

[7] This is analogous to considering covalently bound halides as having essentially an unfilled *p* shell or being effectively atomic as is demonstrated by the large electric field gradients observed at the halide nuclei in nuclear quadrupole experiments.

[8] T. W. Marshall and J. A. Pople, Mol. Phys. **1,** 199 (1958). See also P. J. Frank and H. S. Gutowsky, Arch. sci. (Geneva) **11,** 216 (1958) who obtain too low a value for such chemical shifts by considering only the lowest terms in a perturbation expansion. The error introduced in this manner is discussed by L. C. Snyder and R. G. Parr, J. Chem. Phys. **34,** 837 (1961).

[9] L. Pauling, *The Nature of the Chemical Bond* (Cornell University Press, Ithaca, New York, 1960), 3rd ed., p. 464 ff.

[10] For x-ray studies of OH^- ions in solution see G. W. Brady, J. Chem. Phys. **28,** 464 (1958).

Energy Distribution and Fragmentation Processes Resulting from Electron Impact on Propane and *n*-Butane*

WILLIAM A. CHUPKA AND MANFRED KAMINSKY
Argonne National Laboratory, Argonne, Illinois

(Received May 4, 1960)

The internal energy distribution has been determined for propane and *n*-butane ions produced by electron impact. The method involves the use of differential ionization efficiency curves and depends on the validity of the linear threshold law for simple ionization. The experimental distributions are in fair agreement with theoretical calculations of Lennard-Jones and Hall and indicate that the major fraction of the parent ions are formed by simple removal of a valence electron. Only a minor fraction of the parent ions are apparently formed by removal of one valence electron together with excitation of one or more remaining electrons. Breakdown curves for propane and *n*-butane have been determined experimentally and, except for the energy scales, are in fair qualitative agreement with the predictions of the statistical theory of mass spectra. The discrepancy between theoretical and experimental energy scales is ascribed at least in part to inadequacy of the theoretical rate equations used in the statistical theory. There is no evidence for gross failure of the assumptions of the theory regarding energy randomization although the number of crossings of potential surfaces of the molecular ion is shown to be very much smaller than originally assumed by Rosenstock *et al.*

INTRODUCTION

WAHRHAFTIG, Eyring and their associates[1,2] have developed a statistical theory to explain the mass spectra of polyatomic molecules in terms of competing and successive reactions of excited molecular ions. This theory employs a number of doubtful assumptions and approximations. Friedman, Long, and Wolfsberg[3] and King and Long[4] have indicated the inadequacy of simplified applications of the theory to the calculation of mass spectra of certain molecules. Some attempts (see references 5 and 6, for example) have been made to investigate some assumptions and consequences of the theory more directly. These studies indicate that the assumption of energy randomization is not always valid and that the calculated rate constants are often badly in error.

The statistical theory of mass spectra (STMS) is usually employed in the following manner. It is assumed that the mass spectrum represents the charged reaction products of unimolecular decompositions of excited parent molecular ions at a time approximately 10^{-5} sec after the initial act of ionization. Rate constants for these decompositions are calculated by a variation of the theory of absolute reaction rates and a breakdown graph is constructed. This breakdown graph gives the fractional yield, after 10^{-5} sec of reaction, of each ion as a function of the total internal energy of the original parent ion. An internal energy distribution of the parent ions is then assumed and used with the breakdown graph to calculate a mass spectrum. Earlier work[5] based on the technique of Morrison[7] has shown that both the breakdown graph and the internal energy distribution may be determined experimentally to a fair approximation. The energy distribution is given by the appropriate derivative of the total ionization as a function of the energy of the ionizing agent. The breakdown graph is made up of the normalized derivatives of the intensities of the different ions as a function of the energy of the ionizing agent. The first derivative is appropriate to ionization by photons while the second derivative is appropriate to ionization by electron impact. This difference is a result of the different threshold laws for ionization. The accuracy of the results is determined by the accuracy to which the assumed threshold laws hold over the energy region of interest. The purpose of this experiment was to determine both the breakdown graphs and internal energy distributions for propane and *n*-butane and to compare the results with the calculations and assumptions of previous workers.

EXPERIMENTAL DETAILS

The mass spectrometer used in this work is a single-focusing, 60° instrument with a 12-in. radius of curvature. The source and analyzer sections are pumped separately so that the pressure may differ by as much as a factor of thirty. The electron-emitting element was a dc heated iridium ribbon coated with thorium oxide to provide adequate emission at a relatively low temperature. The electron beam current was electronically regulated at about 1.0 μa and the electron voltage was

* Work performed under the auspices of the U. S. Atomic Energy Commission. Presented at the Washington meeting of the American Physical Society, May 1, 1959.

[1] M. B. Wallenstein, A. L. Wahrhaftig, H. M. Rosenstock, and H. Eyring, "Chemical reactions in the gas phase connected with ionization," in *Symposium on Radiobiology* (John Wiley & Sons, New York, 1952).

[2] H. M. Rosenstock, M. B. Wallenstein, A. L. Wahrhaftig, and H. Eyring, Proc. Natl. Acad. Sci. U. S. **38,** 667 (1952).

[3] L. Friedman, F. A. Long, and M. Wolfsberg, J. Chem. Phys. **27,** 613 (1957); **30,** 1605 (1959).

[4] A. B. King and F. A. Long, J. Chem. Phys. **29,** 374 (1958).

[5] W. A. Chupka, J. Chem. Phys. **30,** 191 (1959).

[6] W A. Chupka and J. Berkowitz, J. Chem. Phys. **32,** 1546 (1960).

[7] J. D. Morrison, Revs. Pure Appl. Chem. **5,** 22 (1955).

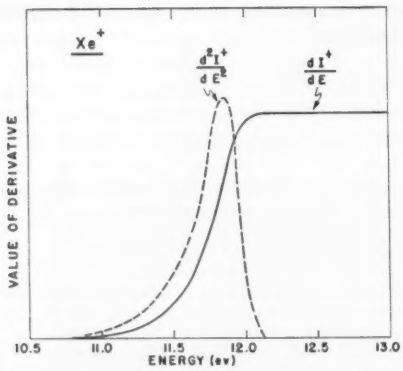

FIG. 1. Typical differential ionization efficiency curves for Xe^+ taken during runs on propane. The solid line gives the first derivative and the dashed line the second derivative of the ion current with respect to electron energy. The energy scale has been corrected.

continuously variable from 0 to 150 v by means of a 10-turn helipot. The helipot could be turned at several speeds by means of a synchronous motor and a system of gears.

The detector system of the mass spectrometer employs an electron multiplier to provide high sensitivity. The output of the multiplier is fed into a vibrating reed electrometer and then displayed on a strip chart recorder. Alternatively the output of the electrometer can be fed into an analogue computer which then determines the first derivative of the ion current with respect to time and displays it on the strip chart recorder.

The propane and *n*-butane gases were Research Grade obtained from Phillips Petroleum Company. The gas being studied, together with a small amount of xenon gas used for calibration, was leaked into the source region of the mass spectrometer at such a rate as to maintain a pressure of about 10^{-6} mm in that region.

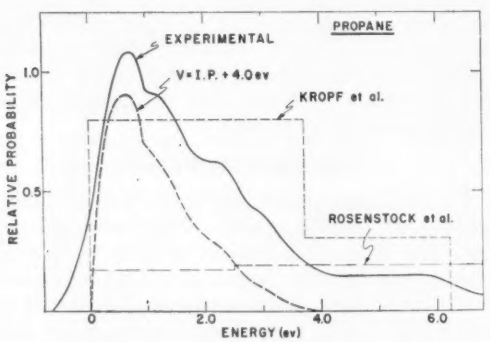

FIG. 2. Total second differential ionization efficiency curve for propane (solid line). The light dashed line gives the energy distribution produced by electrons of energy 4.0 ev above the ionization potential of propane. Also shown are the energy distributions assumed by Rosenstock *et al.* and Kropf *et al.* The area under each of the latter curves is approximately equal to that under the experimental curve.

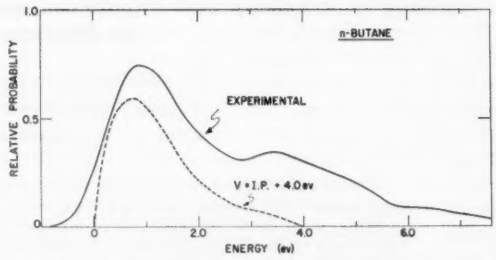

FIG. 3. Total second differential ionization efficiency curve for *n*-butane (solid line). The dashed line gives the energy distribution produced by electrons of energy 4.0 ev above the ionization potential of *n*-butane.

The mass spectrum was scanned by sweeping the magnetic field. Mass peaks which were greater than about 5% of the most intense peak were then studied in the following manner. A mass peak was focused on the collector of the mass spectrometer and the electron voltage reduced until the ion intensity was below the limit of detection. The electron voltage was then swept upward at an appropriate selected speed and the first derivative of the ion current with respect to time (and hence electron voltage) was recorded at an appropriate sensitivity. The sweep speed was kept constant for all peaks. At intervals, the xenon peak of mass 132 was swept in the same manner to provide a voltage calibration and a check on the effective electron energy distribution. Second derivatives were computed from a smooth line drawn through the recorder trace of the first derivative.

The effective electron energy distribution was appreciably wider than the Maxwellian distribution at the temperature of the filament. This excess spread was attributed in part to the voltage drop across the filament due to the heating current and in part to variations in the potential drop across the oxide layer. The spread appeared to increase very slowly over a period of weeks, possibly due to changes in the oxide layer. Typical data for the mass 132 peak of xenon taken along with the data on propane are shown in Fig. 1. The half-width of the second derivative was found to vary by less than

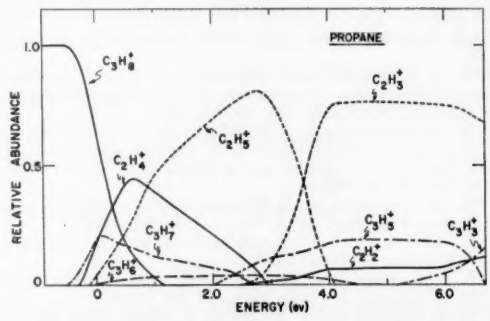

FIG. 4. Normalized second differential ionization efficiency curves for propane.

±0.2 ev throughout this experiment. The ionization potential of xenon was also used to calibrate the energy scale. In this calibration, the voltage at which the second derivative of the xenon ionization efficiency curve dropped to zero (i.e., about 12.1 ev in Fig. 1) was taken as the ionization potential of xenon in the manner described by Morrison.[7] During the experiments on *n*-butane, the effective electron energy distribution was found to be about 50% wider than during the experiments on propane.

RESULTS

The computed second-derivative ionization efficiency curves of the major ionic species from each compound were added together and the resulting curves are given in Fig. 2 and 3 for propane and *n*-butane respectively. The second-derivative curve for each ionic species was then normalized by dividing it by the second-derivative curve of total ionization given in either Fig. 2 or 3. The resulting normalized derivative curves are given in Fig. 4 and 5 for propane and *n*-butane respectively. The position of the zero was chosen as the ionization potential determined by Watanabe.[8] Thus, the energy scale represents only the internal energy given to the molecular ion by electron impact. The extension of the curves of Figs. 2 and 3 to negative energies represents mostly the effect of the electron energy distribution and possibly a small effect of internal thermal energy (hot bands). The amount of the latter effect is difficult to estimate, since in this case it is also a function of the Franck-Condon integrals. The probable error in the position of the zero of energy is estimated to be about ±0.2 ev. Low-energy tails also appear on the normalized derivative curves of all fragment ions. These tails are a result of the same two factors except that in these cases the internal thermal energy is expected to contribute fully as was found to be the case for the *n*-alkylamines.[5]

It is difficult to estimate the probable error in the curves of Figs. 2–5, since this error varies along any curve for the following reasons. The curves of Figs. 2 and 3 result from the addition of curves which often rise and fall steeply over a short energy region. In such a region slight errors in energy will produce fictitious structure and rather large errors in the ordinate of the final summed curve. The error in the energy scale of the nonnormalized derivative curve for each fragment has a probable error of about 0.2 ev. The probable error of the ordinate of each such curve is about ±10% except at the high-energy side where the curve begins to fall to zero. In this region, the probable error is usually about ±10% of the maximum value of the curve. For the curves of Figs. 2 and 3, the probable error of the ordinate is roughly 20% or the change in ordinate given by a shift of 0.3 ev along the energy scale, whichever is the greater. The high-energy region of the curves of Figs. 2 and 3 must be discussed further. The curves in this region are mostly the sums of individual curves which are near their maxima in this region and thus an error of about 20% is expected. However additional error is possible as a result of the fact that curves which are already supposed to have dropped to zero at lower energies may actually have values of ±10% of their maximum values. Actually all derivative curves for individual ions became slightly negative at sufficiently high energies. These negative values were neglected as being due to departure from the assumed behavior of ionization cross section with energy. The errors discussed above exclude the effect of the electron energy distribution in smearing out fine structure which undoubtedly occurs.

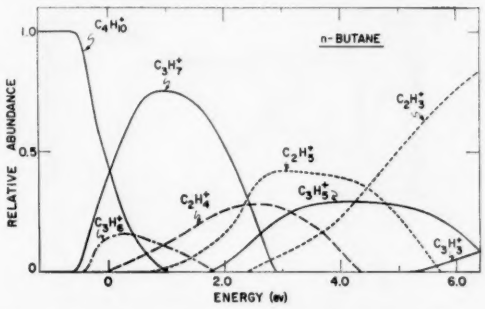

FIG. 5. Normalized second differential ionization efficiency curves for *n*-butane.

The occurence of autoionization can also introduce some error. Since the cross section for such a process is probably approximately a step-function of energy, this process, to a first approximation, will not contribute to the total area under the second-derivative curve, but can change the shape of the curve to some extent. Autoionization very likely contributes only a rather minor amount to the total ionization produced by electrons of moderate and high energies (~20 ev and above) because of the approximate constancy of the cross section with energy. However, at voltages near the ionization potential, the contribution of autoionization may not be negligible in some instances. The same remarks apply to the production of ions by dissociation of neutral excited molecules into positive and negative ions. With sufficiently monoenergetic electrons or photons, such processes can be identified and accounted for. However, the present data are not capable of such resolution and the effects of these processes will be negligible compared to the errors discussed above.

DISCUSSION

A. Internal Energy Distribution—General

As shown by Morrison[8] (and used by others[5,9] in photoionization studies) experimental derivative curves of the type shown in Figs. 2 and 3 represent band envelopes of the relative transition probabilities for forma-

[8] K. Watanabe, J. Chem. Phys. **26,** 542 (1957).

[9] H. Hurzeler, M. G. Inghram, and J. D. Morrison, J. Chem. Phys. **28,** 76 (1958).

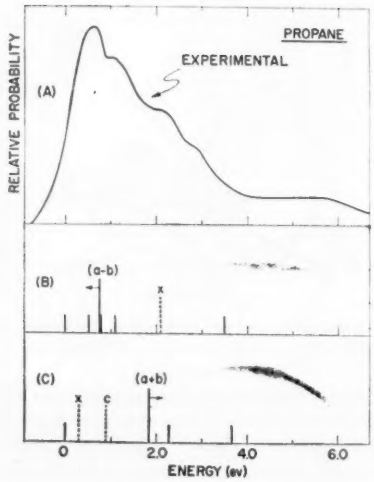

FIG. 6. Experimental energy distribution compared with calculated electronic energy levels of propane. (A) experimental curve, (B) energy levels calculated according to assumption (1), (C) energy levels calculated according to assumption (2) as explained in text. The height of a line is proportional to the degeneracy of the energy level.

tion of the parent ion in states with total internal energy given by the abscissa. It is assumed in deriving the above relation that this transition probability is also directly proportional to $(V-E)$, where V is the electron energy and E is the total energy of the states in question. Therefore, in order to get the energy distribution produced by electrons of energy V, the transition probability curves of Figs. 2 and 3 should be multiplied by the function $(V-E)$. It is seen that the transition probabilities are appreciable for only a short range of a few volts above the ionization potential ($I.P.$). For values of $V \gg I.P.$ the function $(V-E)$ is practically constant, and thus the transition probability curve can be taken as the energy distribution to a fair approximation. This approximation will be good, even though the assumed linear threshold law is no longer valid, as long as the transition probability curves for individual electronic states have nearly the same shape. The latter situation is certainly not precisely true but it is the best assumption that can be made at present. In the low-energy region where the linear threshold law is at all valid, multiplication by $(V-E)$ has an appreciable effect and energy distributions for $V=I.P.+4.0$ ev are also shown in Figs. 2 and 3. (It was found in this research that the linear threshold law for ionization of argon and xenon was obeyed within experimental error for at least 4 ev above the ionization potential. Thus it would appear reasonable to apply the correction for electron energies lower than about 10–15 ev above the ionization potential. At higher voltages the correction becomes comparable to experimental error and could be omitted.)

The experimental curves should be compared with the energy distribution originally assumed by Rosenstock *et al.*[2] and shown in Fig. 2. The disagreement is far beyond any experimental error. The distribution used by these authors was chosen to give best agreement between calculated and experimental mass spectra. As will be discussed later, the energy range of this distribution was exaggerated in order to compensate for a similar flaw in the calculated breakdown curves. A modified distribution, chosen by Knopf *et al.*[10] according to Chupka's[5] suggestion, is also shown in Fig. 2 and is seen to be in much better agreement with the experimental curve.

The experimental curves may also be compared with some results obtained by Stevenson.[11] Stevenson considered the appearance potential obtained by linear extrapolation to be a measure of the average energy required for the formation of a particular ion. These energies, suitably weighted by the ion abundances, were summed to give the average energy acquired by a molecule in ionization by electrons of energy well above the ionization potential. Such a procedure depends upon precisely the same assumptions made here and indeed it can be shown that averages so obtained should be practically identical with those obtained from experimental curves such as those of Figs. 2 and 3, if they were extended to sufficiently high energies. The average energy $\bar{E}$ is defined by the equation

$$\bar{E}=\int P(E)EdE \Big/ \int P(E)dE, \qquad (1)$$

where $P(E)$ is the probability of formation of ions of internal energy E and is given by the experimental curves of Figs. 2 and 3. Since these curves were not extended to sufficiently high energies to allow an accurate determination of $\bar{E}$, a lower limit was obtained by graphical integration over the energy range shown in the figures. These lower limits are 2.1 and 2.4 ev for propane and *n*-butane, respectively, and may be compared with the values 3.1 and 2.8 ev obtained by Stevenson for these compounds. Reasonable extrapolation of the experimental curves could easily lead to the values determined by Stevenson. Thus the present results are not in disagreement with those of Stevenson. The quantity $\bar{E}$ is of less interest than the function $P(E)$ which is given here over an energy range which accounts for by far the major fraction of ionization produced by electrons of moderate energies.

B. Internal Energy Distribution—Comparison of Theory with Experiment

It is of interest to consider the general form of $P(E)$ expected for saturated hydrocarbons. In general, three kinds of electronic states may be expected. These are formed by. (1) simple removal of a valence electron,

[10] A. Kropf, E. M. Eyring, A. L. Wahrhaftig, and H. Eyring, J. Chem. Phys. **32,** 149 (1960).
[11] D. P. Stevenson, Radiation Research **10,** 610 (1959).

(2) removal of a valence electron together with simultaneous excitation or removal of one or more remaining electrons, and (3) removal of nonvalence, inner-shell electrons. Process (3) will occur only at much higher energies (i.e., roughly 280 ev for carbon atoms) than those considered here and will not be discussed further.

1. *Simple electron removal.* An analysis of the molecular orbitals of long chain saturated normal hydrocarbons has been made by Hall[12,13] and Lennard-Jones and Hall.[14] By treating such molecules mathematically as an infinite sequence of CH_2 groups but imposing such boundary conditions as to give the molecule the correct length, these authors were able to obtain simple expressions for the energies of the molecular orbitals. The general distribution of these energies is such that there is a band spread about the value $(a-b)$ and two interacting bands around c and $(a+b)$, where a, b, and c are certain energy parameters which are evaluated by comparison of calculated and experimental ionization potentials. Unfortunately it has not been possible to decide whether the first ionization potential corresponds to the lowest member of the band spread about the value $(a-b)$ or the lowest member of the two interacting bands at c and $(a+b)$. The present data also do not lead to an unequivocal decision. Figures 6 and 7 show the experimental energy distributions together with the electronic energy levels calculated using the two different assumptions for propane and *n*-butane. Parts (*B*) of the figures show the electronic energy levels calculated according to Lennard-Jones and Hall[14] using the assumption (1) that the observed ionization potential corresponds to removal of an electron from a symmetrical molecular orbital localized mainly over the C—C bonds of the molecule, i.e., the lowest member of the interacting bands at c and $(a+b)$. The constants used in the calculation are the same as those determined by Lennard-Jones and Hall. Parts (C) of the figures show the electronic levels calculated according to Hall[13] using the assumption (2) that the observed ionization potential corresponds to removal of an electron from an antisymmetrical molecular orbital localized over the C—H bonds, i.e., the lowest member of the group spread about $(a-b)$. In the calculations using assumption (1) the values of $(a-b)$ and the appropriate interaction parameters are undetermined and hence the states spread about this value are shown in parts (B) of the figures as one level (of degeneracy equal to the number of carbon atoms in the molecule) located at some energy less than -12.0 ev which is the value of $(a+b)$. Similarly, in the calculations using assumption (2) the value of $(a+b)$, c and the appropriate interaction parameters are undetermined. The states of unperturbed energy $(a+b)$ are shown as one level (of degeneracy equal to the number of carbon atoms) located at some energy greater than -13.04 ev which is the value of $(a-b)$ determined according to assumption (2). The value of c is completely undetermined in this case and the states corresponding to this energy are shown by dotted lines located arbitrarily at -12.1 ev to give best agreement with the experimental curves. Both calculations neglect two states corresponding to the two extra C—H bonds on the end carbon atoms. These two states, labeled X in the figures, are placed arbitrarily at -13.3 ev in parts (B) of the figures and at -11.5 ev in parts (C) of the figures to give best agreement with the experimental curves. If one now makes the additional assumption that the cross sections for removal of valence electrons are all approximately equal, it is seen that assumption (1) is in fair agreement with experiment. It is difficult to compare assumption (2) with experiment since the energies of most states are undetermined. It may be possible to find a set of reasonable parameters which will give results in agreement with the experimental curves. A quick attempt to find such a set was unsuccessful and the search was abandoned in view of the uncertainties and highly arbitrary nature of the process. Thus the evidence is far from conclusive although it may be considered to provide some support for assumption (1) as used by Lennard-Jones and Hall.

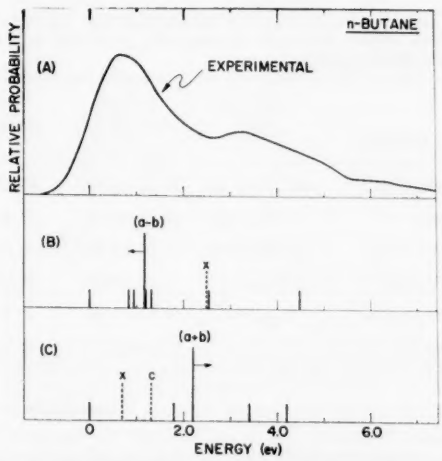

FIG. 7. Experimental energy distribution compared with calculated electronic energy levels of *n*-butane. (A) experimental curve, (B) energy levels calculated according to assumption (1), (C) energy levels calculated according to assumption (2) as explained in text. The height of a line is proportional to the degeneracy of the energy level.

Further complications should be mentioned. The parameters determined by these authors may not be nearly invariant for all molecules and in fact this must be true if their calculations using assumption (1) are valid. The latter calculations lead to the value of $(a+b)=-12.0$ ev while Hall[12] has shown that for methane $(a-b)=-13.04$ ev and $(a+b)\cong-16.5$ ev.

Since the determination of the values of the parameters is based on the assumption that ionization poten-

[12] G. G. Hall, Proc. Roy. Soc. (London) **A205,** 541 (1951).
[13] G. G. Hall, Trans. Faraday Soc. **50,** 319 (1954).
[14] J. Lennard-Jones and G. G. Hall, Trans. Faraday Soc. **48,** 581 (1952).

TABLE I. Comparison of ionization potentials determined by electron impact with vertical ionization potentials determined by photoionization.

Molecule	Vertical I. P.[9] (ev)	Electron impact I. P.[15] (ev)	Band median (ev)
acetaldehyde	10.25±0.03	10.28±0.04	10.30
acetone	9.75±0.03	9.92±0.04	9.85
me-et-ketone	9.55±0.03	9.76±0.04	9.65
ethylamine	9.5±0.1	9.32±0.04	9.33
n-propylamine	9.4±0.1	9.17±0.04	9.23
n-propanol	10.5±0.1	10.46±0.04	10.43

tials measured by electron impact correspond to the vertical transition, it is of interest to examine this assumption. The small amount of experimental evidence on this point strongly suggests that this assumption is incorrect. The only quantitative test of this assumption would appear to be a comparison of electron impact values of Morrison and Nicholson[15] with vertical ionization potentials determined by Hurzeler *et al.*[9] as shown in Table I. In all but two cases the two values differ by much more than the limits of error or reproducibility claimed by the authors and the mean of the absolute values of the deviations is 0.14 ev. Watanabe[7] has noted that in the case of the halogenated benzenes, this deviation is probably about 0.4 ev. There seems to be little reason to expect that vertical ionization potentials are precisely determined by the usual electron-impact methods. The electron-impact ionization efficiency curve for the parent ion is determined by the sum of the regions of the band envelopes for all transitions which result in a stable parent ion (lifetime$\gtrsim 10^{-5}$ sec). This composite curve is determined not only by the band envelope for the transition to the ground state of the ion but also by those for transitions to nearby excited states below the lowest dissociation limit. This curve is further affected by the occurrence of "hot bands," by the possible occurrence of autoionization, by the lowest dissociation energy of the molecular ion which determines the position of the high-energy cutoff, and by the original thermal internal energy of the molecule which determines, at least in part, the shape of the cutoff. To a first approximation, in cases for which the resulting transition probability curve for the parent ion is relatively narrow, conventional electron-impact experiments might be expected to determine the median energy of this curve. Such values were determined from the photoionization data of Hurzeler *et al.* and are given in the last column of Table I. The mean deviation of these values from the electron-impact ionization potentials is 0.05 ev. The complete analysis of the meaning of the ionization potentials of large molecules as determined by conventional electron-impact methods is certainly more complicated than this but will not be pursued here.

The above considerations lead to the conclusion that the electron-impact ionization potentials of Honig,[16] whose technique was duplicated by Morrison and Nicholson, and whose values were used by Lennard-Jones and Hall, are not as accurate as supposed. The quoted error of ±0.02 ev almost certainly represents only the reproducibility of the measurements and a more reasonable probable error would be in the range 0.1–0.2 ev. Even more serious is the possibility that much of this error is systematic and varies monotonically with molecular size, since several of the factors affecting the form of the ionization efficiency curve will vary in this fashion. The resulting errors in the parameters calculated by Lennard-Jones and Hall could produce not just shifts of all energy levels by one or two tenths of a volt but even larger shifts in their relative positions. More accurate parameters could be obtained from the analysis of the appropriate derivatives of total ionization efficiency curves obtained with monochromatic electrons or photons.

In view of the above uncertainties and within the rather large experimental error, the theory of Lennard-Jones and Hall, employing assumption (1) appears to be adequate in explaining the internal energy distribution of propane and *n*-butane ions produced by electron impact. The theory then provides a method for calculating such distributions for the higher paraffin molecular ions. Until better parameters are available, those of Lennard-Jones and Hall may be used together with the value $(a-b)\cong -11.8$ ev for locating the antisymmetric states. The interactions which spread these states may either be neglected or considered to be of the order of a few tenths of a volt (e.g., the value of $(g-f)$ of reference 12 may be of the order of 0.4 ev). The two undetermined states, corresponding to the 2 neglected C—H bonds on the end carbon atoms, may either be omitted or else located at about 13.3 ev as in parts (B) of Figs. 6 and 7. The latter procedure is certainly arbitrary and unsatisfactory and its only justification is the apparently improved agreement with experiment. Typical band envelopes may be constructed for each state and then summed to give the desired distribution. As an example, such a distribution was constructed for the propane ion and is shown in Fig. 8. The states at $(a-b)$ were taken to be degenerate and the two undetermined states placed at 13.3 ev. The form of the band envelope used for each state was suggested by those of Hurzeler *et al.*[9] and is shown as a dotted line for the ground state. The ordinates of each band envelope were made proportional to the degeneracy of the level. (This is equivalent to the previous assumption that the cross sections for removal of valence electrons are all equal. This assumption is certainly not precisely true, but is the most reasonable

[15] J. D. Morrison and A. J. C. Nicholson, J. Chem. Phys. **20,** 1021 (1952).

[16] R. E. Honig, J. Chem. Phys. **16,** 105 (1948).

assumption that can be made in the absence of further information). The difference between the vertical and adiabatic ionization potentials shown by the band envelope is 0.3 ev which is suggested by Watanabe's[7] qualitative description of the photoionization cross section as a function of energy. There is a slight inconsistency in this procedure, since if this difference is correct, the parameters used in the calculation of energies should be changed somewhat. However, sufficient data are not available to allow any such refinement.

In order to obtain the distribution curve for total internal energy (including the original internal thermal energy of the molecule), the product of the curve of Fig. 8 and the internal thermal energy distribution should be integrated over the entire energy range. The major result of this operation would be a smoother curve. This curve would be the appropriate one for use in the calculation of mass spectra by the statistical theory and would be more satisfactory than the completely arbitrary distributions heretofore assumed.

2. *Electron removal plus excitation.* Process (2), in which a valence electron is removed and one or more remaining electrons are simultaneously excited, will produce states with energies ranging up to that of the incident electron. The density (number per unit energy interval) of these states will be greater than that of the states produced by process (1) and will increase rapidly with energy. However, this process involves the simultaneous excitation of two or more electrons and, in analogy with the case of optical spectra,[17] the cross section for such a process is expected to be much smaller than that for a process involving the excitation of only one electron. This expectation is further supported by the very low probability of double ionization[18] which is a special case of this process. Doubly charged ions generally account for less than 1% of the total ionization for large organic molecules. It may be expected that a large fraction of such doubly-charged ions dissociate to singly-charged ions. However, due to coulombic repulsion, the resulting ions would possess appreciable kinetic energies. Only very small amounts of ions with appreciable kinetic energies are observed in the mass spectra of large organic molecules and much of the observed amounts are probably of other origin. Even allowing for lower transmission of ions with high kinetic energy it is unlikely that multiple ionization is responsible for more than about 5 to 10 percent of the ionization produced by electrons of moderate energy (~100 ev).

Upon examination of the curves of Figs. 2 and 3, it is very reasonable to associate the high-energy tail with process (2). The states produced by process (2) may overlap those produced by process (1) to some extent. The major contribution of process (2) is very likely made by ionization plus simultaneous excitation of only one electron, for reasons similar to those given above. A crude prediction of the density of such states near the second ionization potential might be given by a set of Rydberg levels, each originating in one of the states produced by process (1) and terminating at the second ionization potential (~30 ev). Higher excited states would mostly autoionize in a time of the order of 10^{-15} sec[19] to produce doubly-charged ions. Thus autoionization would probably occur more readily than dissociation which would require at least 10^{-14} sec, although some autoionizations of appreciably longer half-lives are known. Since double ionization contributes only a negligible amount to total ionization, the contribution of process (2) may be considered to be negligible above about 30 ev. By considering the abundance of ions which are produced predominantly at energies in the range of process (2), it may be concluded that the total contribution of process (2) is very roughly 20% of the total ionization for propane and *n*-butane. A detailed knowledge of the contribution of process (2) to the internal distribution must await further experiments. In the theoretical construction of internal energy distribution curves for paraffins, a high-energy tail comparable to those shown in Figs. 2 and 3 might be added.

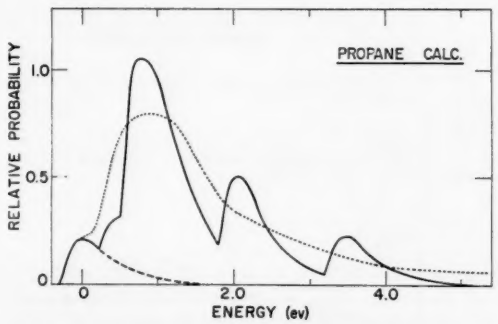

FIG. 8. Calculated energy distribution curve for propane. The smoothed dotted curve with high-energy tail is an example of the type of curve appropriate for use in a statistical calculation of a mass spectrum.

C. Internal Energy Distribution and Randomization

It is of interest to examine one of the major postulates of Rosenstock *et al.*[2] in the light of the above interpretation of the experimental energy distribution. Rosenstock *et al.* postulate that the rapid energy transfer necessary for the applicability of a statistical theory occurs by radiationless transitions among the many potential surfaces of the molecular ion. They calculate that the average spacing between electronic states for the propane ion is about one millivolt, while the thermal vibrational energy is several hundred times larger. They therefore conclude that the necessary number of crossings exist. However, the present interpretation leads to the conclusion that the major fraction (~80%) of the

[17] G. Herzberg, *Atomic Spectra and Atomic Structure* (Dover Publications, New York, 1944), 2nd ed., p. 153.

[18] F. H. Field and J. L. Franklin, *Electron Impact Phenomena* (Academic Press Inc., New York, 1957), p. 184.

[19] G. Wentzel, Z. Physik **43**, 524 (1927).

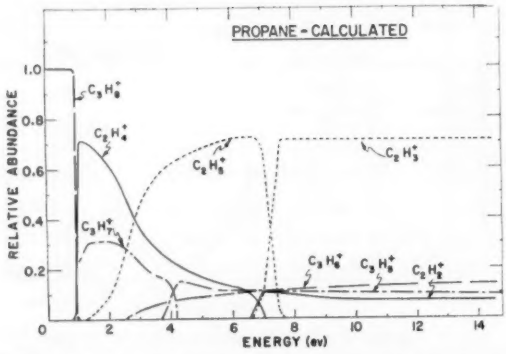

FIG. 9. Breakdown curve for propane according to Rosenstock *et al.*

ions are produced in electronic states with an average spacing of about 0.35 ev for propane and *n*-butane while the average thermal vibrational energy is about 0.10 and 0.18 ev respectively at 400°K.[5] (The situation improves rapidly with molecular size since both the density of states and the internal thermal energy increase approximately linearly with hydrocarbon chain length.) Thus the number of crossings of potential surfaces is drastically reduced from the estimate of Rosenstock *et al.* and their postulate of rapid energy transfer by this mechanism is placed in serious doubt. There is some evidence[5] that energy transfer among vibrational modes purely as a result of anharmonicity is sufficiently rapid in at least some instances. However, the interconversion of electronic and vibrational energy is also required by the present form of the theory. Such transfer is certainly not excluded by the present interpretation. The energy gap between two electronic states must be larger than the total atomization energy of the lower state in order to exclude, on this basis alone, the possibility of crossing of potential surfaces. Since the atomization energy of the propane ion is of the order of 40 ev this is obviously not the case here. However, if the energy gap between the ground state and the first excited electronic state of the ion is greater than its thermal (plus Franck-Condon) vibrational energy, then transfer of energy among normal vibrational modes of the ion in the ground electronic state obviously cannot occur by the mechanism of radiationless electronic transitions. Such is the case for the lower *n*-alkyl amines[5] and is very possibly the case for the lower *n*-alkanes if the present interpretation is correct. The question as to whether the two processes of energy transfer usually provide the necessary energy randomization required by a statistical theory is far from answered. The data of this experiment give no evidence of any gross absence of energy randomization. In particular, the ionization efficiency curves for the parent ions show no upward breaks at energies above the onset of fragmentation. In an earlier paper[5] it was stated that when "a (normalized derivative) curve for any ion drops to zero or even begins to decrease with increasing energy, it should never thereafter show any sharp increase at higher energies if energy randomization is attained before dissociation or radiation occurs." Exceptions to this statement can occur for fragment ions produced by two or more different reaction paths requiring quite different energies. However the statement remains valid for parent ions and those fragment ions which can be produced by only one reaction path. The general structure of the experimental breakdown curves may be considered as evidence in favor of efficient energy randomization. This evidence is appreciably weakened by the rather large errors and poor energy resolution of the data which would obscure all but some of the grossest effects of nonrandomization.

D. Breakdown Curves

As was pointed out in an earlier paper,[5] normalized derivative curves such as those of Figs. 4 and 5 correspond to the breakdown curves calculated by the method of Rosenstock *et al.*[2] These authors have calculated such a set of curves for propane and the result is shown in Fig. 9. A comparison of Figs. 4 and 9 shows a qualitative similarity between the calculated and experimental curves. However, as previously observed for the case of *n*-propanol,[5] there is a gross discrepancy in the energy scales. This discrepancy is in such a direction as to indicate that the calculated rates of decomposition vary much too slowly with energy. This quantitative defect of the theory is compensated for by the arbitrary choice of an energy distribution which is much wider than the experimental one as shown in Figs. 2 and 3. This conclusion was also reached in an earlier study[5] and the subsequent modified calculations of Kropf *et al.*[10] are in agreement with it.

The qualitative agreement between calculated and experimental breakdown curves for propane provides some support for the basic assumptions of the statistical theory of mass spectra. Due to the rather large errors and low energy resolution of the data, the evidence is certainly not conclusive. However, it may be concluded that well over half of the ions produced from electron bombardment of propane appear in a manner consistent with the qualitative predictions of the statistical theory.

While no breakdown curves were calculated for *n*-butane, the experimental curves of Fig. 5 are for the most part consistent with the breakdown scheme proposed by Rosenstock.[20] There are indications of the increasing complexity that is to be expected with larger molecules. This is a result of the increasing number of reaction paths which can produce a given ion. Thus, while the $C_2H_3^+$ ion may be produced at the lowest energies by decomposition of $C_3H_7^+$ as proposed by Rosenstock, the curves of Fig. 5 indicate that at higher energies it may also be produced by decomposition of $C_2H_5^+$ and $C_2H_4^+$ ions.

[20] H. M. Rosenstock, Ph.D. thesis, University of Utah, 1952.

Diffusion of Kr and He in Liquid Hydrogen

G. CINI CASTAGNOLI*
Istituto di Fisica dell'Università di Roma, Istituto Nazionale di Fisica Nucleare, Sezione di Roma, Italy
(Received March 9, 1961)

Experimental results about diffusion of He and Kr in liquid H_2 are given. Quantum deviations are analyzed with the principle of corresponding states.

INTRODUCTION

WITH regard to transport phenomena, many experimental data are available concerning the viscosity of quantum liquids. However little is available regarding diffusion in the same substances.

In a previous paper[1] we reported the diffusion coefficient as a function of temperature of Ne, HT, and D_2 in liquid hydrogen between 15 and 20°K. We have found large deviations, consisting essentially in a value for the total diffusivity much higher than one could expect from classical liquids.

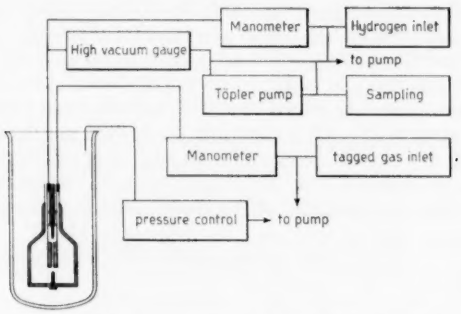

FIG. 1. Schematic diagram of diffusion apparatus.

We give here the results obtained on the diffusion of other tracers, namely Kr and He in liquid hydrogen, in order to investigate the behavior of quantum deviations as a function of the quantum parameters of the diffusing substances.

APPARATUS AND EXPERIMENTAL PROCEDURE

A schematic diagram of the apparatus with the details of the diffusion chamber is shown in Fig. 1.

The technique is essentially the same as the one previously used for the diffusion coefficient measurements of tracers in liquid argon[2] and nitrogen. The diffusion of a mixture (Kr^{85}–H_2 or He^4–H_2), condensed in a 10 cc copper chamber, is allowed to proceed for a certain time t into a slab filled with pure liquid hydrogen. The capillaries, of diameter 0.04 cm and length $\phi \sim 2$ cm, are drawn in brass and sealed in a copper block. The sealing of the ends of the capillary is performed with needle valves which are adjusted from the top of the apparatus at room temperature. The temperature of the chamber is maintained by putting it in a liquid H_2 bath which is boiling under constant pressure (controlled within less than 5 mm Hg by means of an oil-differential manometer). The pressure on the diffusing mixture is kept constant at about 1.5 atm.

Making good seals at the needle valves and avoiding thermal inputs from the outside of the chamber (which produce turbulent diffusions), were the main difficulties in working at liquid H_2 temperatures. For these reasons the connection lines of the present diffusion cell to the filling system have a lower heat conduction than those used for the liquid argon experiments, and the needles are sharper (giving a somewhat lower precision of the capillary length measurements).[2]

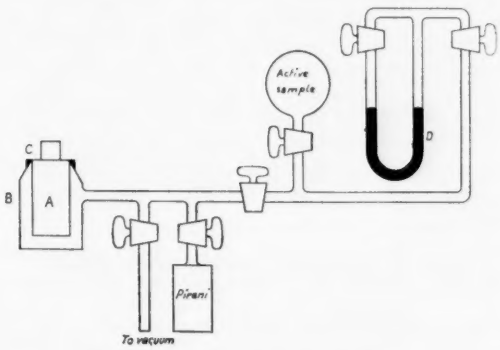

FIG. 2. Counting apparatus.

As is well known,[3] the diffusion coefficient D can be evaluated from the average concentration c_d in the capillary after diffusion (the initial concentration is zero in our cases), the concentration c_a of the tracer in the bath, the length L of the capillary and the time t of the diffusion. We make sure that there are no variations

* Present address: c/o Consiglio Nazionale delle Ricerche, Istituto Nazionale di Metrologia, Sezione Termometrica, Torino, Italy.

[1] G. Cini Castagnoli, A. Giardini Guidoni, and F. P. Ricci, Phys. Rev. **123**, 404 (1961).

[2] G. Cini Castagnoli and F. P. Ricci, J. Chem. Phys. **32**, 19 (1960).

[3] W. Jost, *Diffusion* (Academic Press Inc., New York, 1952), p. 37.

TABLE I. Experimental results for Kr—H_2 diffusion.

Run No.	Length of the capillary (cm)	Time (sec)	Temperature (°K)	D (cm²/sec×10⁵)
1	2.45±0.05	7200	19.70±0.03	16.7±4.0
2	2.45±0.05	14 400	19.40±0.03	13.7±2.8
			$\bar{T}$=19.6°K	$\bar{D}$=14.7±2.3

in the concentration of the bath mixture during diffusion by removing a sample from the chamber before and after each diffusion. The gas removing system is very close to the lines coming out of the Dewar in order to avoid losses and fractioning during the sampling. Moreover, a high-vacuum gauge on this line allows us to check the vacuum (10^{-4} mm Hg) in the diffusion apparatus before and after each run. The samples are removed from the capillary 7 times with the Töpler pump in order to reach this reading on the vacuum gauge.

In this paper we report the diffusion coefficient measurements made on a 10^{-9}-% mixture of Kr^{85} in H_2 (the solubility is extremely low), at a temperature of 19.6°K, and on a mixture of about 1‰ He^4 in H_2 at temperatures between 15 and 20°K. In the first case, c_s and c_d were measured by counting the activity of the Kr–H_2 samples. The counting apparatus is shown in Fig. 2. A thin glass-wall GM tube (Mullard $MX133$) designated by A in the diagram (Fig. 2), was sealed into a glass envelope, B, 10 cm long and 3.5 cm in diameter, by means of red-sealing wax C. This section was surrounded by 5 cm of lead shielding to reduce the background. A manometer, D, indicates the pressure in the counting system, the readings being performed with a cathetometer.

TABLE II. Experimental results for He—H_2 diffusion.

Run No.	Length of the capillary (cm)	Time (sec)	Temperature (°K)	D (cm²/sec×10⁵)
1	2.23±0.05	9120	20.25±0.05	7.90±0.20
2	2.23±0.05	4200	20.25±0.05	7.40±0.60
3	2.23±0.05	8760	14.90±0.03	4.75±0.30
7	2.19±0.05	10 800	17.38±0.03	6.70±0.20
8	2.19±0.05	8700	17.38±0.03	6.50±0.20
10	2.68±0.05	16 260	17.25±0.03	5.74±0.30
12	2.61±0.05	7800	19.50±0.03	7.62±0.50
13	2.61±0.05	14 400	15.40±0.03	5.55±0.20
14	2.61±0.05	10 800	18.30±0.03	6.69±0.40
16	2.45±0.05	11 700	15.74±0.03	5.27±0.50

[4] c_{s1} was always equal to c_{s2} for Kr diffusions. This supports the view that Kr was really dissolved in H_2 and not in microscopic crystallites randomly distributed.

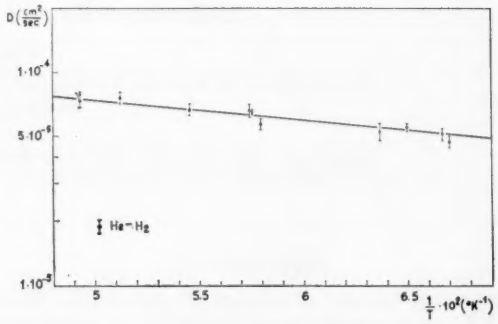

FIG. 3. Diffusion coefficient of He in liquid H_2 as a function of temperature, at constant pressure.

The active sample transferred from the diffusion capillary, gives rise to a pressure in section D of about 5 cm Hg, which was measured with a precision of 1%. The counts from a sample were found to be proportional to the pressure. Two-hour counts were taken on each diffusion specimen, and one-hour counts on each standard specimen, in order to reduce statistical counting errors. The concentrations c_s and c_d were given within an error of 3%. After counting, the system was flushed with dry air, and pumped for 10 min, after which time the background count returned to normal. The concentration measurements of the He–H_2 samples were performed instead with an "Italelettronica SPZIF, $\pi/3$ sector analyzer mass spectrometer" with a precision of 1%.

EXPERIMENTAL RESULTS AND DISCUSSION

The diffusion coefficient D is obtained by solving the well-known differential equation for the one-dimensional diffusion with our boundary conditions.[2]

The experimental results are listed in Tables I and II. Runs Nos. 4, 5, 9, 11, 15, and 17 for the He–H_2 diffusion at ~20°K were discarded because $c_{s1} \neq c_{s2}$, indicating that turbulence occurred during the time of diffusion.[4] The errors in D are determined, taking into account those due to the concentration measurements and those due to the length of the capillary.

The weighted mean of the values obtained for

TABLE III. Diffusion coefficients of binary mixture in liquid H_2 at 20°K and predicted values.

Tracer in H_2	D_{exp} at 20°K cm²/sec×10⁵	D_{calc} cm²/sec×10⁵	$\frac{D_{exptl}}{D_{calc}}$
Kr	15±2	0.995	15±2
Ne	6.10±0.1	0.81	7.55±0.1
D_2	5.10±0.1	0.92	5.55±0.1
He	7.60±0.2	0.72	10.6±0.3

$D(\mathrm{Kr}\text{–}\mathrm{H_2})$ at 19.6°K is

$$D(\mathrm{Kr}\text{–}\mathrm{H_2}) = (14.7 \pm 2.3) \times 10^{-5}\ \mathrm{cm^2/sec}.$$

The best fit of the experimental values of $D(\mathrm{He}\text{–}\mathrm{H_2})$ between 20 and 15°K is

$$D(\mathrm{He}\text{–}\mathrm{H_2}) = 20 \exp[-20/T] \times 10^{-5}\ \mathrm{cm^2/sec},$$

which is shown in Fig. 3.

First we shall consider here the available data on the diffusion coefficients of binary mixture in liquid H_2 at 20°K. In Table III these values are reported together with the values predicted by the principle of corresponding states.[5] We have previously verified that this principle applies very well to binary diffusion coefficients in liquid argon and nitrogen. We can see in column 4 of Table III that the deviations from the principle of corresponding states due to quantum effects, become very important for liquid H_2. We may therefore expect the quantum deviations from the classical principle to depend upon the magnitude of a parameter which expresses the importance of diffraction effects due to the wave nature of molecules. This parameter is

$$\Lambda_{ii}^* = h/\sigma_{ii}(m_{ii}\epsilon_{ii})^{\frac{1}{2}},$$

which is the reduced De Broglie wavelength of a system of two particles[6] with mass m_i, m_1,

$$(m_{ii} = 2m_i m_1/[m_i + m_1])$$

and intermolecular radius and energy $\sigma_{ii} = \frac{1}{2}(\sigma_i + \sigma_1)$, $\epsilon_{ii} = (\epsilon_1 \cdot \epsilon_1)^{\frac{1}{2}}$. The subscripts i and 1 refer to the tracer and to the liquid hydrogen, respectively. In Fig. 4 we have plotted $D_{\mathrm{exp}}/D_{\mathrm{calc}}$ as a function of Λ_{ii}^*. The curve is merely indicative and traced by eye. It seems that in liquid hydrogen at 20°K, a minimum in the quantum-deviations occurs in a range of Λ^* values around Λ_{11}^*, i.e., for self diffusion.

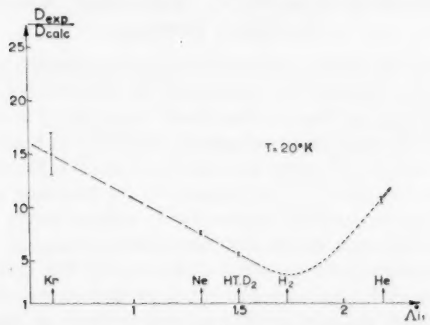

FIG. 4. $D_{\mathrm{expti}}/D_{\mathrm{calc}}$ in liquid H_2 at 20°K for different tracers against quantum parameter $\Lambda_{ii}^* = [h/\sigma_{ii}(m_{ii}\epsilon_{ii})^{\frac{1}{2}}]$.

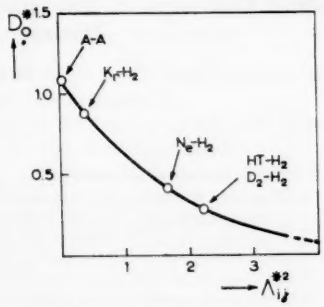

FIG. 5. $D_0^* = D_0(\sigma_{ij}/\sigma_{jj}^2)(m_{ij}/\epsilon_{ij})^{\frac{1}{2}}$ as a function of Λ_{ij}^{*2}.

Owing to the very low solubility of Kr in H_2, it is not easy to measure with accuracy the $D(\mathrm{Kr}\text{–}\mathrm{H_2})$ value at temperatures lower than 20°K. However the data on He, D_2, and Ne, seem to maintain a behavior similar to Fig. 4, even at lower temperatures.

Looking at the experimental results for $D(\mathrm{He}\text{–}\mathrm{H_2})$ given in Fig. 3, we can see that it is still possible to fit the data with an Arrhenius law. The activation energy in this case, however, is significantly different from that of $D(\mathrm{Ne}\text{–}\mathrm{H_2})$ or $D(\mathrm{D_2}\text{–}\mathrm{H_2})$. On the contrary, in classical liquids the activation energy always has been found[5] to be independent of the nature of the tracer. In the case of He in H_2 however, ΔH has the same value as the energy kT, and the meaning of the activated process under these conditions is not clear.

In order to give a possible phenomenological explanation to the large value obtained for the diffusion coefficient $D(\mathrm{Kr}\text{–}\mathrm{H_2})$, one can assume that an Arrhenius law still holds for diffusion in quantum liquids[1] and that the activation energy is independent of the nature of the tracer (excluding helium). This was found[1] for the diffusion of D_2, HT and Ne in liquid H_2. By then applying the principle of corresponding states to the pre-exponential factor D_0[5], we can see (Fig. 5) that the reduced values of D_0 as a function of the parameter Λ_{ij}^{*2} for binary diffusions of Kr, Ne, D_2, and HT in H_2, lie well on a smooth curve with the value of D_0 found for argon self-diffusion.[5]

ACKNOWLEDGMENTS

We wish to thank the Cryogenic Group of the National Laboratories of Frascati for technical help. Thanks also are due Dr. A. Giardini and Mr. M. Bartolini for their valuable help during the experiments.

[5] G. Cini Castagnoli and F. P. Ricci, Nuovo cimento **15**, 795 (1960).

[6] The values of m, ϵ, and σ for the substances listed in Table III are taken from J. De Boer, Physica **14**, 139 (1948).

Billiard-Ball Collisions in the Reactions of Hot Hydrogen Atoms. Isotope Effect on the Hydrogen Displacement in Methane

R. J. Cross, Jr.,† and R. Wolfgang

Sterling Chemistry Laboratory, Yale University, New Haven, Connecticut

(Received April 26, 1961)

The nature of collisions leading to reactions of hydrogen atoms of high kinetic energy (in the form of recoil tritium) is investigated. Two extreme models, both originally due to Libby, are examined. One assumes very weak coupling by valence bonds in the molecule attacked, so that the reaction can be represented by a quasi-elastic atom-atom collision (billiard-ball model) and the other assumes strong valence bond coupling (epithermal model). Calculations on the billiard-ball (hard sphere) model of the reaction $T^*+CH_4 \rightarrow H+CH_3T$ leads to an estimate of its relative cross section as a function of energy. An isotope effect for reaction with CH_4 and with CD_4 is calculated and measured experimentally. Consideration of both the calculations and the experimental results indicate that the billiard-ball model is unimportant in the reactions of gas phase hot hydrogen (as recoil tritium), and that reactions occur nearly exclusively at less than 10–20 ev of kinetic energy, by mechanisms involving strong bond coupling. The possible importance of the billiard-ball model in the reactions of other hot atoms is briefly discussed.

INTRODUCTION

SEVERAL recent studies of the properties of recoil hydrogen have shown that hot hydrogen atoms can efficiently displace hydrogen atoms and other atoms and groups.[1,2] This class of reactions appears to occur in a single step of the type

$$RH+T^* \rightarrow RT+H,$$

and there is evidence that its course is governed primarily by steric considerations, i.e., the direction and point of impact.[1,2] Such reactions do not occur with thermal hydrogen but have a threshold of about 2 to 3 ev. In this paper we inquire into the nature of the collision which can lead to such hot displacement reactions.

There are two possible models for momentum and energy transfer in hot hydrogen reactions. Both were first enunciated for hot atom reactions in general by Libby.[3,4]

1. Billiard-Ball Model[3]

At high kinetic energies of the incoming atom (>10–20 ev) bond energies appear relatively small, and the time scale of the collision is short compared to vibrational relaxation. The molecule thus appears to the hot atom as a weakly coupled collection of atoms. The impact is not well transmitted by the bonds, and the event approximates a quasi-elastic collision with a single atom in the molecule. The energy lost by the hot atom tends to appear as kinetic energy of the atom struck rather than as internal energy of the molecule. The displacement reaction will occur in such a collision if two conditions are satisfied: (a) the struck atom must have received enough energy in the collision to break the bond holding it to the molecule; (b) the incoming atom must be left with a low enough energy to form a bond with the remaining radical.

A mechanical model of such a billiard-ball displacement in methane would show a methyl radical as providing a potential well in which a hydrogen atom may rest. Displacement occurs if the incident hot atom transfers enough kinetic energy to this hydrogen atom to eject it from the well, and loses enough energy in the process so that it itself becomes trapped in the same potential well.

2. Strong Coupling Model ("Epithermal" Reactions[4] in Libby's Notation)

As a hot atom is slowed to energies approaching that of valence bonds, the time scale of its collisions becomes comparable to that of vibrational relaxation. The weak coupling condition progressively breaks down until at a sufficiently low energy the reaction loses all billiard-ball character. The molecule appears to the incoming atom as a system strongly coupled by its valence bonds. Not only the atom struck but neighboring atoms as well will absorb the momentum of the impact. The collision is essentially inelastic and much of the energy of the hot atom appears as internal rather than as kinetic energy of the products.

In a billiard-ball displacement process energy is transferred in an elastic atom-atom collision to the ejected atom. The probability that an incoming hot atom of given energy will eject the atom struck and be itself left with little enough energy to be bound may therefore be calculated by simple application of momentum and energy conservation conditions. The isotope effect in the billiard-ball displacement of

† Studies undertaken in partial fulfillment of the requirements of the B.S. degree at Yale University, New Haven, Connecticut.

[1] M. Henchman, D. Urch, R. Wolfgang, Can. J. Chem. **38,** 1722 (1960). This article gives references to relevant earlier papers.

[2] D. Urch, R. Wolfgang, J. Am. Chem. Soc. **83,** 2982 (1961).

[3] W. Libby, J. Am. Chem. Soc. **69,** 2523 (1947).

[4] M. S. Fox, W. Libby, J. Chem. Phys. **20,** 487 (1952).

hydrogen from CH_4 and CD_4 thus computed (see below) is very large since the ratio of masses of the struck H and D atoms is directly determining. On the other hand, the inelastic or strong coupling mechanism is much less sensitive to the mass of the hydrogen struck, since the neighboring carbon atom provides the major momentum sink and since the excess kinetic energy is dissipated as internal modes of motion. Although the exact isotope effect expected for this mechanism is difficult to calculate precisely, it will be much smaller (at least an order of magnitude) than that for billiard-ball collisions. A measurement of the hydrogen-deuterium isotope effect can thus provide an indication of the relative importance of mechanisms I and II in the displacement reactions of recoil tritium.

This paper presents such a measurement of the relative probabilities of the displacement reactions,

$$T^*+CH_4 \rightarrow CH_3T+H$$

$$T^*+CD_4 \rightarrow CD_3T+D,$$

as initiated by hot hydrogen in the form of tritium recoiling from nuclear reactions. The experimentally determined isotope effect is compared with that calculated for a pure billiard-ball displacement.[5] Such a comparison provides the basis for an evaluation of the importance of billiard-ball collisions in the reactions of recoil tritium in the gas phase.

CALCULATION OF THE ISOTOPE EFFECT

The experimental procedure described subsequently utilizes recoil tritium produced by the $He^3(n, p)T$ reaction, as the source of hot hydrogen. The hydrogen atoms thus have a continuous, though well defined, range of energy.[6] Making use of the collision theory previously developed[6] it is possible to measure the isotope effect as the ratio of two integrated cross-sections for the displacement reaction in CH_4 and CD_4

$$I_{CH_4}=\int_{E_1}^{E_2}\frac{p(E_h)_{CH_4}}{E_h}dE_h \quad \text{and} \quad I_{CD_4}=\int_{E_1}^{E_2}\frac{p(E_h)_{CD_4}}{E_h}dE_h. \tag{1}$$

Here E_h is the energy of the incident tritium atom and $p(E_h)$ is the probability that a collision at energy E_h results in a displacement reaction. E_2 and E_1 are the upper and lower limits, respectively, of the energy range where the reaction is possible.

In this section I_{CH_4} and I_{CD_4} are calculated theoretically on the basis of the billiard-ball model. This involves the following assumptions:

(1) Only collisions with hydrogen atoms can lead to reaction.

(2) Such collisions are elastic; no energy is transferred to the rest of the molecule.

(3) The displacement reaction occurs if the struck atom receives kinetic energy exceeding its binding energy and if the incident hot atom is left with less kinetic energy than its bonding energy to the carbon atom.

(4) To facilitate the calculation the hydrogen atoms are assumed to be spherical and integrations are carried out over all possible impact parameters. This procedure ignores: (a) the shielding by the methyl groups which precludes certain angles of approach; (b) the fact that certain collisions, specifically those in a cone around the C—H bond axis,[1,2] lead to abstraction rather than displacement.[7] These factors indicate that the I's computed will only be upper limits for the billiard-ball displacement. However, since the geometry of CH_4 and CD_4 do not differ significantly, the ratio I_{CD_4}/I_{CH_4} should not be greatly affected by these approximations.

A further assumption involves the use of classical mechanics in the computation. This is justified since at an energy of 10 ev the de Broglie wavelength is 5.25×10^{-2}A, well below the atomic radius.

Consider the collision of a hot atom (subscript h) with a struck atom (subscript s) at an angle θ with respect to their line of centers. It can readily be shown (see Appendix I for derivation and Fig. 5) that the ratio $G(\theta)$ of the energies of the atoms after collision, respectively, E_s' and E_h', is given by

$$G(\theta)=\frac{E_s'}{E_h'}=\frac{4k\cos^2\theta}{(1+k)^2-4k\cos^2\theta}, \tag{2}$$

where k is the ratio of the masses, $k=m_s/m_h$. If the initial energy of the hot atom is E_h and that of the struck atom, $E_s=0$, then

$$E_h=E_h'+E_s'$$

$$E_h=E_h'[1+G(\theta)]=E_s'[1+1/G(\theta)]. \tag{3}$$

The reaction occurs if $E_s'\geq E_b$ and $E_h'\leq E_b$ where E_b is the bond energy (assumed to be the same for both atoms). The energy of the hot atom must then be within the limits

$$E_h=E_b[1+G(\theta)], \tag{4a}$$

$$E_h=E_b[1+1/G(\theta)]. \tag{4b}$$

These limiting loci are shown in Fig. 1 giving θ as a function of E_h/E_b for collisions with CH_4.

[5] The isotope effects calculated here relate to those resulting from the application of momentum conservation laws. The influence of mass in slightly affecting bond energies, which forms the basis of most isotope effects in thermal reactions, is negligible for hot reactions in which excess energy is available. (In any case, the calculations in this paper do take account of the differences between strengths of the C—H and C—D bonds.)

[6] P. Estrup, R. Wolfgang, J. Am. Chem. Soc. **82**, 2665 (1960).

[7] Experimental results obtained in this study indicate that the ratio of abstraction to displacement is the same in CH_4 and CD_4 (see Fig. 4).

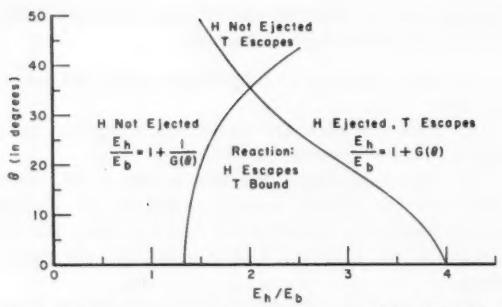

FIG. 1. Maximum possible angle θ for which billiard-ball collision can lead to displacement reaction, $CH_4+T^*\rightarrow CH_3T+H$ vs. E_h/E_b for CH_4.

At energies lower than E_1 the reaction is not possible. Just above E_1 only a head-on collision ($\theta\approx 0$) can eject the struck atom, but at higher energies collisions over an increasing range of θ provide sufficient energy for the ejection. As the energy increases further, reaction at larger θ again becomes impossible because the incident particle retains too much energy to be bound. Finally, at E_2, only a head-on collision will cause a reaction. The maximum θ will be at $E_h=2E_b$ and $G(\theta)=1$.

We shall now compute the probability, $p(E_h)$, that a collision at energy E will satisfy conditions (4a) and (4b). It can readily be shown (see Appendix II) that the geometrical probability of a collision between angles 0 and θ is

$$q=1-\cos^2\theta. \tag{5}$$

Two cases are then considered:

Case I, $E_h\leq 2E_b$.
The maximum possible angle for reaction is then given by (4b),

$$E_h=E_b[1+1/G(\theta)]. \tag{6}$$

Combining (6) and (2),

$$\cos^2\theta=(E_b/E_h)[(1+k)^2/4k]. \tag{7}$$

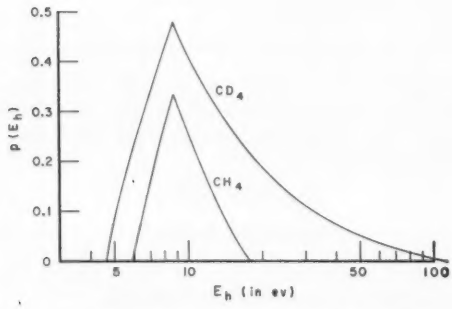

FIG. 2. Probability of displacement reaction on billiard-ball collision of tritium with methane, as a function of the kinetic energy.

Substituting (7) into (4),

$$p(E_h)=1-[(1+k)^2/4k](E_b/E_h). \tag{8}$$

Case II, $E_h\geq 2E_b$.
The maximum possible angle for reaction is then given by (4a),

$$E_h=E_b[1+G(\theta)]. \tag{9}$$

Combining (9) and (2) and substituting into (5),

$$p(E_h)=1-[(1+k)^2/4k](1-E_b/E_h). \tag{10}$$

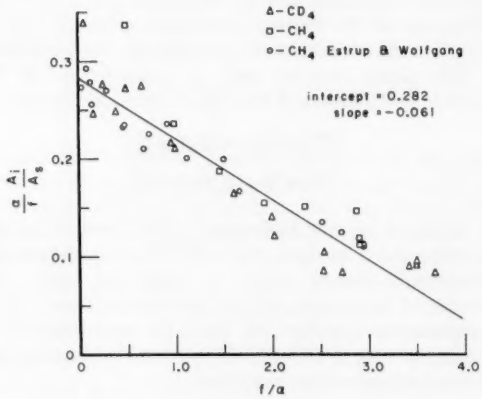

FIG. 3. Analysis of experimental results on displacement reactions. The value of

$$I=\int_{E_1}^{E_2}\frac{p(E_h)}{E_h}dE_h$$

is given by the intercept at $f/\alpha=0$.

These probabilities for the billiard-ball reaction on collision are plotted vs log E_h in Fig. 2 for both CH_4 and CD_4. Now,

$$I=\int_{E_1}^{E_2}\frac{p(E_h)}{E_h}dE_h.$$

$$I=\int_{E_1}^{2E_b}\frac{1}{E_h}\left[1-\frac{(1+k)^2}{4k}\frac{E_b}{E_h}\right]dE_h + \int_{2E_b}^{E_2}\frac{1}{E_h}\left[1-\frac{(1+k)^2}{4k}\left(1-\frac{E_b}{E_h}\right)\right]dE_h. \tag{11}$$

Then, by manipulations shown in Appendix III,

$$I=\ln\frac{4k}{(1-k)^2}-\frac{(1+k)^2}{4k}\ln\frac{(1+k)^2}{2(1-k)^2}. \tag{12}$$

Substituting for T^*+CD_4, $k=2/3$, and for T^*+CH_4, $k=1/3$,

$$I_{CD_4}/I_{CH_4}=3.06.$$

DETERMINATION OF THE ISOTOPE EFFECT

The experimental determination of I_{CH_4} and I_{CD_4} was carried out using the method described previously.[6] Mixtures of He^3, CH_4, and He^4; and mixtures of He^3, CD_4, and He^4 were irradiated in the Brookhaven reactor. The fate of the recoil tritium produced was determined using gas chromatography with a proportional counter detector. The data are plotted in the manner prescribed by Estrup and Wolfgang[6] in Figs. 3 and 4. Here A_i/A_s is the fraction of tritium reacting to give product i, f is the mole fraction of CH_4 weighted for the relative collision cross section with T, and α is the average logarithmic energy loss per collision of the tritium atom.

Within the limits of error, the data fall on a common straight line. The cross-section integrals are given by the intercept at $f/\alpha=0$:

$$I_{CD_4}=I_{CH_4}=0.29\pm0.04.$$

The data for the abstraction reaction are not directly relevant here but are included in Fig. 4 for reference. They also show no isotope effect greater than 20%. This may be compared to the findings of Lee *et al.*[8] that there is a small tendency in favor of H abstraction from CH_2D_2. The fact that a straight line is not obtained for abstraction has been discussed previously.[6]

DISCUSSION

Failure of the Billiard-Ball Model for Recoil Tritium

Evidently, the isotope effect is so small as to be within the limit of error. Since on the basis of a pure billiard-ball model an isotope effect $I_{CD_4}/I_{CH_4}=3.06$ would be expected, it is clear that this mechanism is an unimportant factor in the displacement reaction of recoil tritium. A collision leading to such a reaction will generally be of an inelastic nature with strong valence bond coupling of the atoms in the molecule struck. This conclusion, that mechanism II (strong-coupling model) is dominant, was expected on the basis

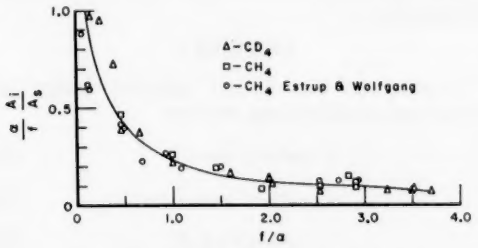

FIG. 4. Analysis of experimental results on the abstraction reaction of tritium in methane.

[8] J. K. Lee, B. Musgrave, F. S. Rowland, J. Phys. Chem. **64**, 1950 (1960).

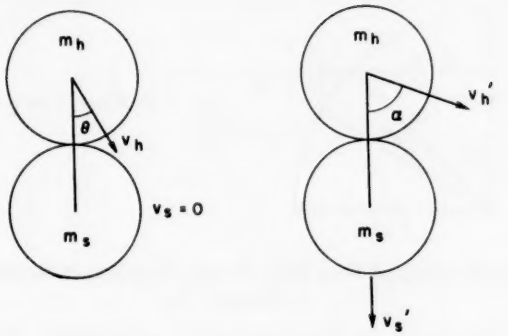

FIG. 5. Geometry of the collision.

of previous observations that alkyl groups and halogen atoms could be replaced by recoil tritium. These entities are too massive for replacement in a pure billiard-ball event.

The complete absence of any evidence for billiard-ball character in the displacement reactions may at first sight be somewhat surprising. However, a closer examination of the quantitative aspects of this model shows this to be reasonable. Figure 2 shows that the collision cross section in which the billiard-ball momentum requirements are satisfied is highest at lower energies (<10–20 ev). This, however, is precisely the energy region in which the weak-coupling assumption breaks down and where displacements would not have billiard-ball character. At higher energies this assumption should be progressively better satisfied. There is still a considerable energy range above 20 ev in which, as shown in Fig. 2, the displacement reaction could occur in CD_4. Since there is no such range in CH_4, an appreciable isotope effect would still be expected if there were a relatively significant number of displacement reactions having billiard-ball character at these high energies. However, two factors greatly diminish the probability of such reactions. One is the E_h in the denominator in the expression for I. The other is the small range of impact angle θ and the resultant small cross section $p(E_h)$ (Fig. 2) over which the momentum requirements for billiard-ball replacement are met. The value of the cross-section integral I above 20 ev,

$$\int_{20\text{ ev}}^{E_2}\frac{p(E_h)}{E_h}dE_h,$$

for CD_4 as calculated on the basis of the billiard-ball model is only 22% of its total value over the entire energy range. Thus, when the obvious limitation of the billiard-ball model at lower energies is taken into account, only a small isotope effect would be expected. The fact that none whatever is observed is not surprising. It indicates that even at 20 ev a pure billiard-ball event is unlikely.

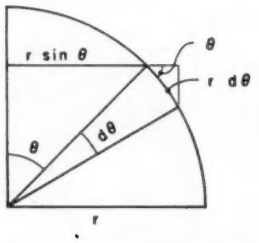

FIG. 6. Geometry of the collision.

Probability of Very High Energy Reaction of Recoil Tritium

At this point it is appropriate to summarize the situation regarding the probability of hot hydrogen reactions at high energies (>20 ev). The results just discussed show that the billiard-ball mechanism is probably not important in gas phase reactions of hot hydrogen. The alternative mechanism II, the strong coupling or inelastic collision model (epithermal mechanism in Libby's original notation), can also be expected to be ineffective at high energies. There are two reasons for this: (1) As the energy increases, valence bond coupling necessarily becomes relatively less important, and collisions tend to become atomic or billiard-ball; (2) At higher energies it becomes difficult to satisfy the requirement of the strong-coupling mechanism that the excess energy of the hot atom appear as internal modes of energy. Because of the small size of the hot hydrogen atom and its high velocity (even below 10 ev) the collision it makes is localized and its duration is only of the order of a bond vibration. Its energy can therefore be deposited only in the one, two, or possibly three bonds directly struck.[9] Thus, if the hydrogen atom's energy exceeds 10 ev the energy sinks available to it will not be adequate to slow it sufficiently so that it may be captured by the molecule struck. The products observed from the reaction of recoil tritium with hydrocarbons have provided confirmation for this view of inelastic hot atom collisions. These products are not those that would be expected if the hot reaction had deposited more than a few electron volts of exitation energy in the molecule struck. Actually, 90% of the yield can be accounted for by the rupture of only a single bond in the reacting hydrocarbons.[1,2] Highly degraded products (such as allene from butane) which would be formed by the de-exitation with bond rupture of highly excited intermediates are formed in less than 1% of all the reactions.

Thus, there appears to be no satisfactory mechanism by which a hot hydrogen may react to become bound at energies greater than 10–20 ev. The probability of displacement reaction upon collision $p(E_h)$ appears to rise from zero at a threshold of about 2 ev to perhaps $\frac{1}{2}$ and then drops again to near zero when the energy exceeds 10 ev. A more exact evaluation of this excitation function will probably have to await the development of appropriate atomic beam techniques.

[9] M. Henchman and R. Wolfgang, J. Am. Chem. Soc. **83**, 2991 (1961).

Billiard-Ball Mechanism for Other Gas Phase Hot Atoms

The most favorable condition for billiard-ball displacement is between atoms of very similar mass. Thus, this mechanism might be expected to be much more significant for hot halogen reactions than for those of recoil tritium. By the methods developed here we have evaluated the cross section $p(E_h)$ for which billiard-ball momentum requirements are satisfied for the reaction

$$Br^{82*}+CBr_4^{81}\rightarrow CBr_3^{81}Br^{82}+Br^{81}.$$

On integrating this we find that, despite the much higher energy limit, the value of the cross-section integral I from 20 ev to 78 200 ev is still only 21% of its total value over the total energy range. This suggests that even for displacements of atoms of similar mass the billiard-ball mechanism is quantitatively unimportant compared to the low energy inelastic processes.

Billiard-Ball Mechanism in Liquids and Solids

It should be noted that the above considerations apply in their simple form only to gas phase reactions. As pointed out by Libby,[3,4] the cage effect in the condensed phase makes it more difficult for the projectile atom to escape following billiard-ball displacement. Thus even though it may not become bound in the initial collision, it may be held in the same solvent cage with the radical just created and can eventually combine with it. This secondary process could significantly increase the probability molecular incorporation as a result of billiard-ball collisions.

ACKNOWLEDGMENTS

One of the authors (R. J. C.) wishes to acknowledge support by an N.S.F. undergraduate summer fellowship.

This work was sponsored by the U. S. Atomic Energy Commission.

APPENDIX I

Referring to Fig. 5 and applying energy and momentum considerations, we have

$$v_h \sin\theta = v_h' \sin\alpha, \tag{I1}$$

$$v_h \cos\theta = v_h' \cos\alpha + k v_s', \tag{I2}$$

$$v_h^2 = v_h'^2 + k v_s'^2, \tag{I3}$$

where $k=m_s/m_h$.

Then, from (I1),

$$\cos\alpha = [(v_h'^2 - v_h^2 \sin^2\theta)^{\frac{1}{2}}/v_h']^{\frac{1}{2}}. \tag{I4}$$

From (I2) and (I4),

$$v_h \cos\theta = (v_h'^2 - v_h^2 \sin^2\theta)^{\frac{1}{2}} + kv_s'. \quad \text{(I5)}$$

From (I3) and (I5),

$$(v_h'^2 + kv_s'^2)^{\frac{1}{2}} \cos\theta = (v_h'^2 - v_h'^2 \sin^2\theta - kv_s'^2 \sin^2\theta)^{\frac{1}{2}} + kv_s'. \quad \text{(I6)}$$

Squaring and simplifying,

$$\tfrac{1}{2}v_s'(1-k) = (v_h'^2 \cos^2\theta - kv_s'^2 \sin^2\theta)^{\frac{1}{2}}. \quad \text{(I7)}$$

Squaring and simplifying,

$$\tfrac{1}{4}v_s'^2(1+k)^2 - kv_s'^2 \cos^2\theta = v_h'^2 \cos^2\theta, \quad \text{(I8)}$$

$$v_s'^2/v_h'^2 = (4\cos^2\theta)/[(1+k)^2 - 4k\cos^2\theta], \quad \text{(I9)}$$

$$E_s'/E_h' = (4k\cos^2\theta)/[(1+k)^2 - 4k\cos^2\theta] = G(\theta). \quad \text{(I10)}$$

APPENDIX II

The collision of two spheres is represented as the collision of a point with a sphere of combined collision radius (see Fig. 6). The probability that a collision will occur between θ and $\theta+d\theta$ is the probability that the collision will occur on a circular strip around the sphere cut off by θ and $\theta+d\theta$. The area of this strip is $2\pi r \sin\theta r d\theta$. The probability, dq, that a collision will occur between θ and $\theta+d\theta$ is the projection of this area on a plane perpendicular to the path of the colliding atom divided by the projection of the whole sphere,

$$dq = (2\pi r \sin\theta r d\theta \cos\theta)/\pi r^2 = \sin 2\theta d\theta.$$

The probability that a collision will occur between 0 and θ is

$$q = \int_0^\theta \sin 2\theta d\theta = \tfrac{1}{2} - \tfrac{1}{2}\cos 2\theta = 1 - \cos^2\theta.$$

APPENDIX III

$$I = \int_{E_1}^{2E_b} \frac{1}{E_h}\left[1 - \frac{(1+k)^2}{4k}\frac{E_b}{E_h}\right]dE_h + \int_{2E_b}^{E_2} \frac{1}{E_h}\left[1 - \frac{(1+k)^2}{4k}\left(1 - \frac{E_b}{E_h}\right)\right]dE_h \quad \text{(III1)}$$

$$I = \ln E_h + \frac{(1+k)^2}{4k}\frac{E_b}{E_h}\Big|_{E_1}^{2E_b} + \ln E_h - \frac{(1+k)^2}{4k}\left(\ln E_h + \frac{E_b}{E_h}\right)\Big|_{2E_b}^{E_2} \quad \text{(III2)}$$

$$I = \ln\frac{E_2}{E_1} - \frac{(1+k)^2}{4k}\left(\ln\frac{E_2}{2E_b} + \frac{E_b}{E_1} + \frac{E_b}{E_2} - 1\right). \quad \text{(III3)}$$

At E_1 and E_2, $\theta = 0$ (see Fig. 1), $G(\theta) = 4k/(1-k)^2$.

$$E_1 = E_b[1 + 1/G(\theta)] = [(1+k)^2/4k]E_b \quad [\text{see (6) in main text}] \quad \text{(III4)}$$

$$E_2 = E_b[1 + G(\theta)] = [(1+k)^2/(1-k)^2]E_b \quad [\text{see (9) in main text}] \quad \text{(III5)}$$

$$I = \ln\frac{4k}{(1-k)^2} - \frac{(1+k)^2}{4k}\ln\frac{(1+k)^2}{2(1-k)^2}.$$

Oscillator Models in Unimolecular Reactions*

M. L. VESTAL

Wm. H. Johnston Laboratories, Inc., Baltimore, Maryland

AND

H. M. ROSENSTOCK†

Wm. H. Johnston Laboratories, Inc., and National Bureau of Standards, Washington, D. C.

(Received April 27, 1961)

The absolute reaction-rate theory for the unimolecular decomposition of isolated excited molecules is applied to two models. The first considers the molecule as a set of harmonic oscillators in which only a finite amount of energy may be stored in a particular degree of freedom. In the second model the spacing between adjacent levels is assumed to decrease exponentially. The first leads to a decrease in the lifetime above that calculated for the conventional harmonic oscillator model for short-lived molecules. The second produces an increase depending directly on the rate of change of the level spacing.

INTRODUCTION

CURRENT theories of the unimolecular decomposition of molecules and ions are based on one of two approaches. In the first type of theory, due principally to Slater,[1,2] an energized molecule decomposes when the various excited normal modes are properly phased so as to produce an extension of a chemical bond beyond a critical length. It is assumed that energy transfer among normal modes does not occur. The second type of theory, due principally to Rice and Ramsperger[3] and to Kassel,[4,5] focuses attention on the energy content of the internal degrees of freedom. It is assumed that the internal energy is continually being redistributed and that when a sufficient amount of energy has accumulated in a particular degree of freedom, the molecule will decompose. In recent years, this approach has been reformulated in terms of absolute reaction-rate theory by Marcus,[6] Eyring,[7,8] and co-workers.

In spite of the great conceptual differences between the two models, they lead to very similar equations for the unimolecular decomposition rate of an energized molecule

$$k(E)=\nu(1-\epsilon_0/E)^n, \qquad (1)$$

where E is the excitation energy of the molecule, and ϵ_0 is the activation energy for decomposition. The parameter n is, in the Slater model, related to the number of normal modes n_s contributing to the critical extension of the bond and, in the Kassel model, the number of oscillators or degrees of freedom n_K whose internal energy can contribute to the decomposition. The two models lead to nearly the same numerical result if $n_s-1=2(n_K-1)$. The frequency factor ν is, in the Slater model, a weighted average of the normal frequencies; in the Kassel model it is the frequency of redistribution of the internal energy. In the Marcus and Eyring formulation it is, in the simplest case, the frequency of that degree of freedom of the reactant which has been transformed into a translation along the reaction coordinate.

The comparison of these theories with experiment is based, for the most part, on the pressure dependence of the unimolecular rate constant. This test, which contains implicitly some simplifying assumptions concerning the energization of molecules by collision,[9] reveals that sometimes one model fits the data and sometimes the other.[10] Very frequently it is necessary, in order to fit the data, to assume a Kassel model in which the effective number of oscillators is reduced below the total number of vibrational degrees of freedom. Plausible reasons have been advanced for this type of assumption.[10,11] However, these considerations do not as yet lead to generalizations useful for *a priori* calculations.

In recent times another test of unimolecular reaction rate theory has been provided by the statistical theory of mass spectra.[7] In this theory, the processes leading to the formation of a mass spectrum are considered to be a series of consecutive and competing unimolecular decomposition reactions of excited molecule-ions. Application of unimolecular reaction-rate theory leads to the consequence that, for a given configuration of the

* The major portion of this work was supported by the Office of Isotopes Development, U. S. Atomic Energy Commission and Wm. H. Johnston Laboratories, Inc.

† Present address: Physical Chemistry Division, National Bureau of Standards, Washington 25, D. C.

[1] N. B. Slater, *Theory of Unimolecular Reactions* (Cornell University Press, Ithaca, New York, 1959).

[2] N. B. Slater, Proc. Cambridge Phil. Soc. **35,** 56 (1939).

[3] O. K. Rice and H. C. Ramsperger, J. Am. Chem. Soc. **49,** 1617 (1927).

[4] L. S. Kassel, J. Phys. Chem. **32,** 225 (1928).

[5] L. S. Kassel, *Kinetics of Homogeneous Reactions* (Chemical Catalog Company, Inc., New York, 1932).

[6] R. A. Marcus and O. K. Rice, J. Phys. Chem. **55,** 894 (1951).

[7] H. M. Rosenstock, M. B. Wallenstein, A. L. Wahrhaftig, and H. Eyring, Proc. Natl. Acad. Sci. U. S. **38,** 667 (1952).

[8] J. Calvin Giddings and H. Eyring, J. Chem. Phys. **22,** 538 (1954).

[9] F. P. Buff and D. J. Wilson, J. Chem. Phys. **32,** 677 (1960).

[10] E. K. Gill and K. J. Laidler, Proc. Roy. Soc. (London) **A250,** 121 (1959).

[11] R. A. Marcus, J. Chem. Phys. **20,** 359 (1952).

activated complex and for a given (assumed known) activation energy, molecule-ions can decompose with any one of a range of lifetimes, depending on the amount of excitation energy imparted to them in the ionization excitation act.[7,12] Of particular importance in the present connection is the fact that in a mass spectrometer one can observe decomposition processes occurring at a rate of 10^5–10^6 sec. These give rise to the so-called metastable ions. With the development of photoionization techniques,[13] it was found possible to study the dependence of the rate constant in this range as a function of the excitation energy imparted by photionization. It is of considerable interest, therefore, that this fundamentally different avenue of experimental verification leads to the current conclusion that mass spectral data can be fitted by a Kassel-type model only if the effective number of oscillators is much reduced.[14–16] Wahrhaftig and co-workers have carried out calculations on propane mass spectra and find that the data can be fitted with either the full number of oscillators or a reduced number.[17,18] However, the conclusions based on the theory of mass spectra must be treated with caution because of the sensitive dependence of the results on the activation energies assumed for the processes.

In any event, the situation regarding agreement between theory and experiment is such as to call for further examination of the theoretical models. In this paper some new results are presented resulting from two modifications of the oscillator model of unimolecular reactions. One modification is a physically more realistic enumeration of the number of configurations, incorporating the assumption that only a limited amount of energy can be stored in any one degree of freedom. This problem has been discussed briefly by Slater.[19] A second modification is to incorporate the effects of anharmonicity into the oscillator model. This problem has been discussed by Slater[19] in his formulation of unimolecular reaction rates.

MICROCANONICAL RATE CONSTANT

If one considers only molecules having excitation energy between E and $E+\delta E$, a microcanonical formulation of absolute reaction rate theory is appropriate. In brief, one assumes an equilibrium between reactant molecules of energy E and activated complexes of the same energy in which an amount ϵ_0 is localized as potential energy and an amount between ϵ_t and $\epsilon_t+\delta\epsilon_t$ is localized as kinetic energy, both in the reaction coordinate. The expression for the density of translational states per length of the reaction coordinate is

$$\rho_t(\epsilon_t)=(2l/h)(2\mu/\epsilon_t)^{\frac{1}{2}}, \tag{2}$$

where μ is the reduced mass of translation. The rate of passage r in the forward direction along the reaction coordinate is

$$r=v/l=(2\epsilon_t/\mu)^{\frac{1}{2}}/2l \tag{3}$$

and the rate constant is

$$K(E)=\int_0^{E-\epsilon_0}\frac{\rho^{\ddagger}(E,\epsilon_0,\epsilon_t)}{\rho(E)}h^{-1}d\epsilon_t, \tag{4}$$

where one has averaged over all possible values of the translational kinetic energy ϵ_t.

For the case of N harmonic oscillators one obtains

$$K(E)=\frac{\prod_{i=1}^{N}\nu_i}{\prod_{j=1}^{N-1}\nu_j^{\ddagger}}\left(\frac{E-\epsilon_0}{E}\right)^{N-1}, \tag{5}$$

and assuming all frequencies unchanged in going from the energized to the activated state

$$K(E)=\nu(1-\epsilon_0/E)^{N-1}. \tag{6}$$

An integration of Eq. (4) over a Boltzmann distribution of energy readily recovers the standard form obtained with the use of partition functions.[20]

Recalling that the energy levels of a harmonic oscillator are uniformly spaced, the number of states of a set of N such oscillators having an energy equal to or less than E is obtained by computing the hypervolume in an N-dimensional quantum number space bounded by a hyperplane defined by

$$\sum_{i=1}^{N}\epsilon_i=E. \tag{7}$$

The volume is taken only of that hyperoctant in which all energies, or quantum numbers, are positive. This problem has been discussed by Tolman.[21] The result is for the total number of states $W(E)$

$$W(E)=(1/h^N)\prod_{i=1}^{N}(1/\nu_i)[E^N/\Gamma(N+1)], \tag{8}$$

where Γ is the gamma function. The density of states in the interval E to $E+\delta E$ follows directly by differentiation. This method of enumerating is an approximation in which quantum effects are ignored.

Another significant approximation in the above development, the constraint (7), is unrealistic. If the

[12] H. M. Rosenstock, A. L. Wahrhaftig and H. Eyring, J. Chem. Phys. **23,** 2200 (1955).
[13] F. P. Lossing and I. Tanaka, J. Chem. Phys. **25,** 1031 (1956).
[14] W. A. Chupka, J. Chem. Phys. **30,** 191 (1959).
[15] W. A. Chupka and J. Berkowitz, J. Chem. Phys. **32,** 1546 (1960).
[16] B. Steiner, C. F. Giese, and M. G. Inghram, J. Chem. Phys. **34,** 189 (1961).
[17] Edward M. Eyring, Ph.D. thesis, University of Utah, 1960.
[18] A. Kropf, E. M. Eyring, A. L. Wahrhaftig, and H. Eyring, J. Chem. Phys. **32,** 149 (1960).
[19] N. B. Slater, Proc. Leeds Phil. Soc. Sci. Sec. **6,** 268 (1955).
[20] J. L. Magee, Proc. Natl. Acad. Sci. U. S. **38,** 764 (1952).
[21] R. C. Tolman, *Principles of Statistical Mechanics* (Oxford University Press, London, 1938).

total excitation energy exceeds that required to rupture a bond other than the one in question, some distributions of energy are still considered as contributing to the number of reactant states, even though sufficient energy has accumulated in another bond to rupture that one. It appears physically more appropriate to confine the enumeration of reactant states to those in which none of the bonds is excited to the point of dissociation. The constraints must then be

$$\sum_{i=1}^{N}\epsilon_i \leq E \tag{9}$$

and

$$\epsilon_i \leq \epsilon_{0i}, \tag{10}$$

where ϵ_{0i} is the activation energy for rupturing the ith bond. The rate expression for this can be developed for the special case where all oscillators are identical in respect to activation energy for bond rupture.

DENSITY OF STATES FOR BOUNDED OSCILLATOR

The more complete set of constraints has the following geometric interpretation. The sum of energies being less than E defines a hyperpyramid bounded by the plane $\sum_i \epsilon_i = E$ and the N planes determined by setting each of the ϵ_i in turn equal to zero. The constraint on each of the ϵ_i not exceeding ϵ_{i0} defines a hyperparallelepiped with edge lengths ϵ_{i0}, or in the special case of identical oscillators, a hypercube of edge ϵ_0. The volume consistent with both sets of constraints is thus the volume common to the hyperpyramid and the hypercube.

The procedure for computing this volume will be illustrated in three dimensions. A rigorous mathematical proof will be published elsewhere. Consider the cube of edge ϵ_0 and the plane $x+y+z=E$. When E is less than ϵ_0, no value of the coordinates is greater than ϵ_0 and the volume of the octant determined by the plane is entirely within the cube. It is a regular pyramid of slant height E and volume $\frac{1}{6}E^3$. As E increases to a value between ϵ_0 and $2\epsilon_0$, the pyramid volume extends out beyond the cube faces at each axis, forming three pyramids of slant height $E-\epsilon_0$. The common volume is now

$$(E^3/3!)-[3(E-\epsilon_0)^3/3!]. \tag{11}$$

But now when E exceeds $2\epsilon_0$, the projecting pyramids overlap, generating regular overlap pyramids of slant height $E-2\epsilon_0$. This must be subtracted, so that in the range $2\epsilon_0 < E < 3\epsilon_0$ the volume is

$$\frac{E^3}{3!}-\frac{3(E-\epsilon_0)^3}{3!}+\frac{3(E-2\epsilon_0)^3}{3!}. \tag{12}$$

Alternately, in this last range the volume may be computed starting with the cube. Its volume is ϵ_0^3, but the common volume is decreased by the regular pyramid with its apex at coordinates $(\epsilon_0, \epsilon_0, \epsilon_0)$. The slant height of this pyramid is $(3\epsilon_0-E)$, and its volume is $(3\epsilon_0-E)^3/3!$, so that the common volume is

$$\epsilon_0^3-[(3\epsilon_0-E)^3/3!], \tag{13}$$

which is identically equal to the volume computed by the previous method.

In the general N-dimensional case the reasoning is analogous, using the fact that the volume of an N-dimensional regular pyramid of slant height l is $l^N/N!$ and the volume of an N-dimensional cube of edge l is l^N.

With this process of repeated correction of overlapping pyramids in successive ranges of value of E, the result is readily generalized to the expression

$$V_K{}^N=\sum_{m=0}^{K-1}\frac{(-1)^m[E-m\epsilon_0]^N}{(N-m)\,!m!} \qquad (K-1)\epsilon_0 \leq E \leq K\epsilon_0 \tag{14}$$

for the common volume V_K. It can also be verified for the four-dimensional cube in the case $3\epsilon_0 \leq E \leq 4\epsilon_0$ by comparing the result using the above equation to the expression

$$V_4{}^4=\epsilon_0{}^4-[(4\epsilon_0-E)^4/4!] \tag{15}$$

obtained by computing the common volume considering a four-dimensional cube whose corner $(\epsilon_0, \epsilon_0, \epsilon_0, \epsilon_0)$ is truncated by the four-dimensional plane $x_1+x_2+x_3+x_4=E$ with $3\epsilon_0 \leq E \leq 4\epsilon_0$.

Since the density of states of a single harmonic oscillator is uniform and equal to $1/h\nu$ one obtains for the density of states of N loosely coupled bounded harmonic oscillators of equal frequency ν and equal dissociation energy ν_0.

$$\rho(\nu, E, \epsilon_0, N)=\frac{N}{(h\nu)^N}\sum_{m=0}^{K-1}\frac{(-1)^m[E-m\epsilon_0]^{N-1}}{(N-m)\,!m!}, \tag{16}$$

where K is defined by the relation

$$(K-1)\epsilon_0 \leq E \leq K\epsilon_0. \tag{17}$$

This is a polynomial with a number of terms depending both on the number of oscillators and on the amount of excitation energy E, expressed in terms of multiples of the dissociation energy ϵ_0.

MICROCANONICAL RATE CONSTANT

The microcanonical rate constant is now obtained as before, using Eq. (4). One must be careful, however, in the integration of $\rho^\ddagger$ over the translational kinetic energy ϵ_t. It is convenient to introduce the term nonlocalized energy[7] E' referring to that amount of energy out of the total E which is available for random distribution among the oscillators. In the case of the activated complex, the nonlocalized energy is equal to $E'=E-\epsilon_0-\epsilon_t$. It is apparent from the density of states function [Eq. (16)], and from the fact that one integrates over all possible values of ϵ_t, from zero to $E-\epsilon_0$, that the amount of nonlocalized energy varies from $E-\epsilon_0$ to zero. Accordingly, the integration over ϵ_t must be broken into a succession

of regions with a density function appropriate to each range of values of the nonlocalized energy.

When $\epsilon_0 \leq E \leq 2\epsilon_0$, the integration over ϵ_t occurs entirely in the interval where the nonlocalized energy lies between zero and ϵ_0. Accordingly, the integral is

$$\int_0^{E-\epsilon_0} \rho^{\ddagger}(E, \epsilon_0, \epsilon_t, N-1)\,d\epsilon_t = \frac{N-1}{(h\nu)^{N-1}} \int_0^{E-\epsilon_0} \frac{[E-\epsilon_0-\epsilon_t]^{N-2}}{(N-1)!}\,de_t = \frac{1}{(h\nu)^{N-1}} \frac{[E-\epsilon_0]^{N-1}}{(N-1)!}. \tag{18}$$

When $2\epsilon_0 \leq E \leq 3\epsilon_0$, the integration must be broken into two parts

$$\int_0^{E-\epsilon_0} \rho^{\ddagger}(\epsilon_1, \epsilon_0, \epsilon_t, N-1)\,d\epsilon_t = \frac{N-1}{(h\nu)^{N-1}} \int_{E-2\epsilon_0}^{E-\epsilon_0} \frac{[E-\epsilon_0-\epsilon_t]^{N-2}}{(N-1)!}\,d\epsilon_t + \frac{N-1}{(h\nu)^{N-1}} \int_0^{E-2\epsilon_0} \left\{ \frac{[E-\epsilon_0-\epsilon_t]^{N-2}}{(N-1)!} - \frac{[E-2\epsilon_0-\epsilon_t]^{N-2}}{(N-2)!} \right\} d\epsilon_t = \frac{1}{(h\nu)^{N-1}} \left\{ \frac{[E-\epsilon_0]^{N-1}}{(N-1)!} - \frac{[E-2\epsilon_0]^{N-1}}{(N-2)!} \right\}. \tag{19}$$

Inserting the appropriate density function for the reactant molecules, which have N degrees of freedom and all energy nonlocalized, we obtain for the respective rate constants

$$k_2 = \nu \frac{[1-(\epsilon_0/E)]^{N-1}}{1-N[1-(\epsilon_0/E)]^{N-1}}, \qquad \text{when } \epsilon_0 \leq E \leq 2\epsilon_0 \tag{20}$$

$$k_3 = \nu \frac{[1-(\epsilon_0/E)]^{N-1} - (N-1)[1-(2\epsilon_0/E)]^{N-1}}{1-N[1-(\epsilon_0/E)]^{N-1} - \frac{N(N-1)}{2}[1-(2\epsilon_0/E)]^{N-1}}, \tag{21}$$

when $2\epsilon_0 \leq E \leq 3\epsilon_0$.

This is readily generalized to

$$k_n = \frac{\nu \sum_{m=1}^{n-1} \frac{(-1)^{m-1}[1-(m\epsilon_0/E)]^{N-1}}{(N-m)!(m-1)!}}{N \sum_{m=0}^{n-1} \frac{(-1)^m[1-(m\epsilon_0/E)]^{N-1}}{(N-m)!m!}}, \tag{22}$$

where $(n-1)\epsilon_0 \leq E \leq n\epsilon_0$.

LIMITING HIGH-ENERGY FORM OF CANONICAL RATE CONSTANT

The form of rate constant derived above for the bounded harmonic oscillator increases more rapidly with E than does the rate constant for the unbounded harmonic oscillator. For the latter case it is readily seen from the expression $k(E) = \nu[1-(\epsilon_0/E)]^{N-1}$ that the limiting rate is ν, the bracketed expression tending to unity as E increases. The rate constant for the bounded case, however, does not reach such a finite value.

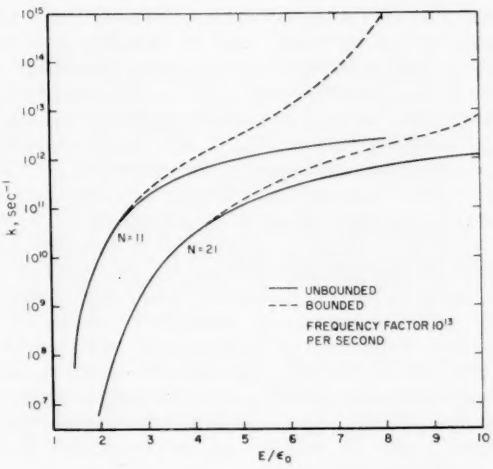

FIG. 1. Effect of boundedness on the unimolecular rate constant.

Consider the number of states for the reactant molecules in the energy range $(N-1)\epsilon_0 \leq E \leq N\epsilon_0$. It is convenient to write this in the form of a hypercube volume minus the one hyperpyramid projecting beyond the hyperplane

$$V = \epsilon_0{}^N - [(N\epsilon_0 - E)^N/N!],$$

so

$$\rho(E) = \partial V/\partial E = N(N\epsilon_0 - E)^{N-1}/N!, \tag{23}$$

which vanishes as E approaches N_0. Since this is in the denominator of the rate expression, the rate constant goes to infinity as the energy of the molecule approaches N_0.

This behavior of the rate constant, although at first glance disconcerting, is in fact physically more correct than is true of the unbounded harmonic oscillator. The essence of the absolute rate-theory method for calculating a rate constant is to postulate an equilibrium between reactants and activated complexes, compute the equilibrium concentration by statistical mechanical methods and independently formulate a rate constant for the decomposition of the activated complexes. In the bounded harmonic oscillator case, the reason for the infinite rate constant is that there are many more states available for the activated complexes, than for the reactants as the excitation energy increases. In the limit $E = N\epsilon_0$, there are no more reactant states, subject to the bound that $\epsilon_i \leq \epsilon_0$, and the ratio is infinite. This suggests a definite limitation on the absolute rate-theory method for this model. The finite limit on the

rate constant for the unbounded harmonic case is the result of the increasing error in including into the reactant states "virtual" states in which the energy in one or more particular degrees of freedom exceeds the dissociation energy. The variation of the rate constant with energy is shown in Fig. 1, both for the bounded and the unbounded cases for two values of N. The values of N have been chosen solely for computational convenience, and correspond approximately to a six-atom and a nine-atom molecule. It is seen that for molecules with low excitation energy, the correction is negligible. In particular, assuming a frequency of about 10^{13} sec^{-1}, the correction is negligible for species with lifetimes of the order of a microsecond, such as metastable ions in the mass spectrometer. However, the rapidly increasing deviation at higher energies suggests that the pressure dependence of the unimolecular rate constant may be changed by this constraint. This should be studied further.

CANONICAL RATE CONSTANT

If the microcanonical rate constant is averaged over a Maxwell-Boltzmann distribution, one obtains for the unbounded oscillator model the well-known Arrhenius expression

$$\frac{\int_0^\infty k(E)\rho(E)\exp(-E/RT)dE}{\int_0^\infty \rho(E)\exp(-E/RT)dE}=\nu\exp(-E/RT). \quad (24)$$

The corresponding averaging process for the bounded oscillator model is somewhat more complex. The upper limit of integration extends only to $N\epsilon_0$. Further, the integrands contain polynomials with the number of terms depending on the value of the energy. Hence, the integral is broken into a set of integrations over an interval ϵ_0, and becomes

$$I=\int_{\epsilon_0}^{N\epsilon_0}k(E)\rho(E)\exp(-E/RT)dE$$

$$=\frac{\nu}{(h\nu)^N}\sum_{n=2}^{N}\sum_{m=1}^{n-1}\frac{(-1)^{m-1}\exp(-m\epsilon_0/RT)}{(N-m)\,!\,(m-1)\,!}\times\int_{(n-m-1)\epsilon_0}^{(n-m)\epsilon_0}x^{N-1}\exp(-x/RT)dx.$$

Integrating by parts and rearranging, one obtains

$$I=\nu(N-1)\,!\,(RT/h\nu)^N\sum_{n=2}^{N}\sum_{m=1}^{n-1}\frac{(-1)^{m-1}\exp(-n\epsilon_0/RT)}{(N-m)\,!\,(m-1)\,!}\cdot\sum_{j=1}^{N-1}\frac{[(n-m-1)(\epsilon_0/RT)]^j\exp(\epsilon_0/RT)-[(n-m)(\epsilon_0/RT)]^j}{j\,!}.$$

In summing over n and m, many of the terms in brackets cancel pairwise because the first term for given n and m equals the second term for a corresponding $n-1$ and m. Thus one obtains

$$I=\nu(N-1)\,!\,(RT/h\nu)^N\exp(\epsilon_0/RT)\left\{\sum_{n=2}^{N}\frac{(-1)^n\exp(-n\epsilon_0/RT)}{(N+1-n)\,!\,(n-2)\,!}\sum_{j=0}^{N-1}\frac{(\epsilon_0/RT)^j}{j\,!}+\sum_{m=1}^{N-1}\frac{(-1)^{m-1}\exp[-(N+1)\epsilon_0/RT]}{(N-m)\,!\,(m-1)\,!}\sum_{j=0}^{N-1}\frac{[(N-m)(\epsilon_0/RT)]^j}{j\,!}\right\}. \quad (25)$$

The partition function is obtained in an analogous manner from the integral

$$\text{P.F.}=\frac{N}{(h\nu)^N}\sum_{n=1}^{N}\int_{(n-1)\epsilon_0}^{n\epsilon_0}\left[\sum_{m=0}^{n-1}\frac{(-1)^m[E-m\epsilon_0]^{N-1}}{(N-m)\,!\,m!}\right]\exp(-E/RT)dE \quad (26)$$

by successive integration by parts. One obtains finally for the canonical rate constant the rather lengthy expression

$$k(T)=(\nu/N)\times\frac{\sum_{r=0}^{N-2}\frac{(-1)^r\exp[-(r+2)\epsilon_0/RT]}{(N-r-1)\,!\,r!}\sum_{j=0}^{N-1}\frac{(\epsilon_0/RT)^j}{j\,!}-\sum_{r=0}^{N-2}\frac{(-1)^r\exp[-(N+1)\epsilon_0/RT]}{(N-r-1)\,!\,r!}\sum_{j=0}^{N-1}\frac{[(N-r-1)(\epsilon_0/RT)]^j}{j\,!}}{\sum_{r=0}^{N-1}\frac{(-1)^r\exp[-(r+1)\epsilon_0/RT]}{(N-r)\,!\,r!}\sum_{j=0}^{N-1}\frac{(\epsilon_0/RT)^j}{j\,!}-\sum_{r=0}^{N-1}\frac{(-1)^r\exp[-(N+1)\epsilon_0/RT]}{(N-r)\,!\,r!}\sum_{j=0}^{N-1}\frac{[(N-r)(\epsilon_0/RT)]^j}{j\,!}}. \quad (27)$$

Now for most reactions of interest $\epsilon_0/RT \gg 1$. In this case the second terms in the numerator and denominator are small compared to the first because of the factor $\exp[-(N+1)\epsilon_0/RT]$. Neglecting these, the expression simplifies to

$$k(T)=\nu \exp(-\epsilon_0/RT) \times \frac{\sum_{r=0}^{N-2} \frac{(-1)^r \exp(-r\epsilon_0/RT)}{(N-r)\,!r!}(N-r)}{\sum_{r=0}^{N-1} \frac{(-1)^r \exp(-r\epsilon_0/RT)}{(N-r)\,!r!}N},$$

which can be rewritten in the form of exponentials as

$$k(T)=\nu \exp(-\epsilon_0/RT) \times \frac{(1-\exp(-\epsilon_0/RT)]^N-\exp[-(N-1)\epsilon_0/RT]}{[1-\exp(-\epsilon_0/RT)^N-\exp(-N\epsilon_0/RT)}. \quad (28)$$

Numerically this result is negligibly different from the Arrhenius expression, in agreement with the earlier, more approximate treatment of Slater.[19] The reason for this negligible difference is that the bounded oscillator correction to the microcanonical rate constant occurs significantly only at such high excitation energies that the properly weighted contribution to the canonical rate constant is negligible.

ANHARMONIC OSCILLATOR

In the oscillator model, considerations of anharmonicity center on the problem of the proper enumeration of states. The potential function of the oscillator appears only implicitly in determining the density of states as a function of energy. In contrast to Slater's treatment, anharmonicity effects in all oscillators will be considered; the degree of freedom transforming into the reaction coordinate is not singled out for special attention.

In this modification of the harmonic oscillator model, two facts are immediately apparent. First, anharmonicity always produces a gradually decreasing spacing of levels with increasing energy, i.e., the density of states increases with energy. Second, at a finite value of the vibrational energy corresponding to the dissociation energy, the density of states becomes infinite. This second fact makes use of the bounded oscillator treatment mandatory. However, some insight into the general effect of anharmonicity can be deduced readily without this restriction, and will be confirmed later by more exact considerations.

If there is no restriction on the amount of energy that may be retained in any reactant degree of freedom, the total number of vibrational states of an assembly of N oscillators having a total energy of E or less is given by the integral

$$W=\int\cdots\int \rho_1(\epsilon_1)\rho_2(\epsilon_2)\cdots\rho_N(\epsilon_N)d\epsilon_1 d\epsilon_2\cdots d\epsilon_N \quad (29)$$

subject to the restriction

$$\sum_{i=1}^{N}\epsilon_i \leq E,$$

where ϵ_i is the energy of the ith oscillator and $\rho_i(\epsilon_i)$ is the density of states of the ith oscillator. This is closely related to the Dirichlet integral[22] which can be written in the form

$$\int\cdots\int x_1^{i_1-1}x_2^{i_2-1}\cdots x_N^{i_N-1}dx_1dx_2\cdots dx_N \quad (30)$$

subject to the restriction $\sum x_i \leq F$. The value of the integral is

$$\frac{\Gamma(i_1)\,\Gamma(i_2)\cdots\Gamma(i_N)}{\Gamma(i_1+i_2+\cdots+i_N+1)}F^{i_1+i_2+\cdots+i_N}.$$

In the case of harmonic oscillators, which have a constant density of levels equal to $1/h\nu$, one obtains the total number of levels

$$W=(E^N/N!)[1/(h\nu)^N],$$

from which the unbounded oscillator rate equations follow readily. This is the semiclassical approximation for enumerating states. If, however, the density of levels increases with energy and $\rho(E)$ can be represented by an ascending power series in E, the number of levels W will also contain terms of a higher power than E^N, and the rate equation will change correspondingly. For example, a linear dependence of level density on energy will lead to

$$W=[E^{2N}/(2N)\,!][1/(h\nu)^{2N}]$$

and the system will behave as if the number of effective oscillators were twice the number of molecular oscillators, i.e., the rate will decrease. These considerations suggest that a more realistic density of states function may significantly affect the pressure dependence of the rate constant and, consequently, the conclusions concerning the effective number of oscillators.

For the anharmonic oscillator defined by the equation

$$\epsilon=h\nu(v+\tfrac{1}{2})-(h^2\nu^2/4\epsilon_0)(v+\tfrac{1}{2})^2 \quad (31)$$

the density of vibrational levels is

$$\rho(\epsilon)=1/h\nu[1-(\epsilon/\epsilon_0)]^{-1},$$

where v is the vibrational quantum number and ϵ_0 is the dissociation energy referred to the potential minimum. The expression for the anharmonicity constant in terms of h, ν and ϵ_0 follows from the Morse

[22] Reference 21, p. 656.

treatment of the anharmonic oscillator.[23] With this density of states, the total number of states for an assembly of N such oscillators with an energy equal to or less than E may be expressed formally by the N-fold integral

$$W=(h^N\prod_{i=1}^{N}\nu_i)^{-1}\int\cdots\int\prod_{i=1}^{N}[1-(\epsilon_i/\epsilon_{0i})]^{\frac{1}{2}}d\epsilon_i \qquad (32)$$

with the restrictions

$$\sum_{i=1}^{N}\epsilon_i\leq E, \qquad 0\leq\epsilon_i\leq\epsilon_{0i}.$$

In the present case, the additional restriction on the maximum amount of energy in a given oscillator is essential since the density function tends to infinity as ϵ approaches ϵ_0, and becomes imaginary for $\epsilon>\epsilon_0$. This type of restriction is not inherent in the Dirichlet integral.

Although we have not been able to carry through the development for this case, it is of interest to see how this problem can be transformed to a common-volume problem in hyperspace, analogous to the bounded oscillator case.

We assume all oscillators identical and use the transformation $u=2[1-(\epsilon/\epsilon_0)]^{\frac{1}{2}}$. With this transformation, the integral becomes

$$W=(\epsilon_0/h\nu)^N\int\cdots\int du_1\cdots du_N, \qquad (33)$$

which is just a volume integral. The constraints transform as follows

$$0\leq\epsilon_i\leq\epsilon_{0i}\rightarrow 0\leq u_i\leq 2,$$

$$\sum_{i=1}^{N}\epsilon_i\leq E\rightarrow\sum_{i=1}^{N}u_i^2\geq 4[N-(E/\epsilon_0)]. \qquad (34)$$

In the u space these constraints are satisfied for that volume, in the positive hyperoctant, which lies inside a hypercube of edge 2 and lies outside a hypersphere of radius $R=2[N-(\epsilon/\epsilon_0)]^{\frac{1}{2}}$. We have been unable to compute this volume for any case of interest.

EXPONENTIAL OSCILLATOR

In view of the intractability of the anharmonic oscillator problem it appeared worthwhile to carry out the analysis for a solvable case which retains the essence of the above, namely, one retaining the bound on the maximum energy in an oscillator and characterized by a level density which increases with energy. This is so for the so-called exponential oscillator, in which there is an exponential increase in level density with energy, i.e.,

$$\rho(\epsilon)=\exp(a\epsilon)/h\nu, \qquad (35)$$

where a is an arbitrary parameter. For a set of N identical coupled bounded oscillators one can write immediately for the density of states

$$\rho_N(E)=\frac{\exp(aE)}{(h\nu)^N}\sum_{j=0}^{K-1}\frac{(-1)^j N[E-j\epsilon_0]^{N-1}}{(N-j)!\,j!}, \qquad (36)$$

where $(K-1)\epsilon_0\leq E\leq K\epsilon_0$.

For the activated complex with energy ϵ_0 and ϵ_t localized in the reaction coordinate one can write a similar expression, using the definition $x=E-\epsilon_0-\epsilon_t$,

$$\rho_{N-1}^{\ddagger}(E_1\epsilon_0,\ \epsilon_t)=\frac{N-1}{(h\nu)^{N-1}}\sum_{j=0}^{K-1}\frac{(-1)^j\exp(ax)[x-j\epsilon_0]^{N-2}}{(N-j-1)!\,j!}, \qquad (37)$$

where $(K-1)\epsilon_0\leq x\leq K\epsilon_0$.

Averaging over all possible values of the translational energy ϵ_t we have again a double summation. Now in integrating over ϵ_t, the range of x is from $E-\epsilon_0$ to 0. From 0 to ϵ_0 there is only one term in the polynomial. From ϵ_0 to $2\epsilon_0$ there are two, and so on. So the $j=0$ term appears throughout the whole range of integration, the $j=1$ term only from ϵ_0 to $E-\epsilon_0$, the $j=2$ from $2\epsilon_0$ to $E-\epsilon_0$ and so on. Hence the integral can be written in the form

$$\rho_{N-1}^{\ddagger}=\frac{(N-1)}{(h\nu)^{N-1}}\sum_{j=0}^{K-2}\frac{(-1)^j}{(N-j-1)!\,j!}\int_{j\epsilon_0}^{E-E_0}e^{ax}[x-j\epsilon_0]^{N-2}dx,$$

where $j\epsilon_0\leq x\leq(j+1)\epsilon_0$. Changing the summation limit to $K-2$ identifies this k with the reactant k. Letting $y=a(x-j\epsilon_0)$,

$$\rho^{\ddagger}=\frac{(N-1)}{(ah\nu)^{N-1}}\sum_{j=0}^{K-2}\frac{(-1)^j\exp(aj\epsilon_0)}{(N-j-1)!\,j!}\int_0^{a[E-(j+1)\epsilon_0]}y^{N-2}e^y dy.$$

The integration is again carried out by successive integration by parts, yielding for the activated complex density of states

$$\rho^{\ddagger}=\frac{(N-1)}{(ah\nu)^{N-1}}\sum_{j=0}^{K-2}\frac{(-1)^{j+N-2}}{(N-j-1)!\,j!}\left[\exp[a(E-\epsilon_0)]\sum_{m=0}^{N-2}\frac{(-1)^m a^m}{m!}[E-(j+1)\epsilon_0]^m-\exp(aj\epsilon_0)\right]. \qquad (38)$$

The rate constant is then

$$k(E)=\frac{\nu(N-1)!}{a^{N-1}N}\exp(-a\epsilon_0)\frac{\sum_{j=0}^{K-2}\frac{(-1)^{j+N-2}}{(N-j-1)!\,j!}\left[\sum_{m=0}^{N-2}\frac{(-1)^m a^m}{m!}[E-(j+1)\epsilon_0]^m-\exp\{-a[E-(j+1)\epsilon_0]\}\right]}{\sum_{j=0}^{K-1}\frac{(-1)^j}{(N-j)!\,j!}[E-j\epsilon_0]^{N-1}}. \qquad (39)$$

[23] G. Herzberg, *Spectra of Diatomic Molecules* (D. Van Nostrand Company, Inc., Princeton, New Jersey, 1950), p. 101.

An instructive approximate form for the rate constant is obtained by noting that the expression in square brackets is just the remainder of approximating $-\exp\{-a[E-(j+1)\epsilon_0]\}$ by the first $N-1$ terms of a series expansion. An upper bound on this remainder is obtained from Taylor's theorem[24]

$$\text{rem} \leq a^{N-1}[E-(j+1)\epsilon_0]^{N-1}/(N-1)!. \quad (40)$$

Using this upper bound, the rate constant reduces to the rate constant for the bounded oscillator case, multiplied by a correction factor $\exp(-a\epsilon_0)$. It follows from this that the rate is reduced by at least the factor $\exp(-a\epsilon_0)$ and the reduction is greater as the rate of change of spacing between energy levels increases. Also, in this approximation, a corresponding decrease will occur in the canonical rate constant.

For quantitative comparisons it is now necessary to evaluate the parameter a. A not too unreasonable procedure is to choose the parameter so that the total number of vibrational levels below the dissociation limit is equal to that for the anharmonic oscillator. In this case, a simple calculation using the density of states expressions for the two models shows that $a\epsilon_0=1.26$. Consequently the rate constant is reduced by at least a factor of 0.28. In Fig. 2 a graph of the rate constant as a function of energy is shown, calculated from the exact expression. It is seen that the reduction in the rate constant becomes larger at higher energies.

A comparison of the density of states functions for the anharmonic and the exponential oscillator shows that the former varies less rapidly with energy at low energies and more rapidly at high energies than does the exponential function (see Fig. 3). This, together with the behavior of the rate constant strongly suggests that an analysis with a better approximation to the anharmonic density of states might lead to a rate equation which has an energy dependence very similar to that of the original Rice-Ramsperger-Kassel model.

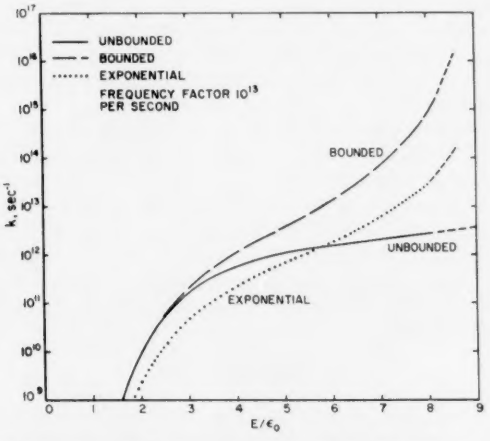

FIG. 2. Comparison of unimolecular rates for the unbounded, bounded and exponential oscillator.

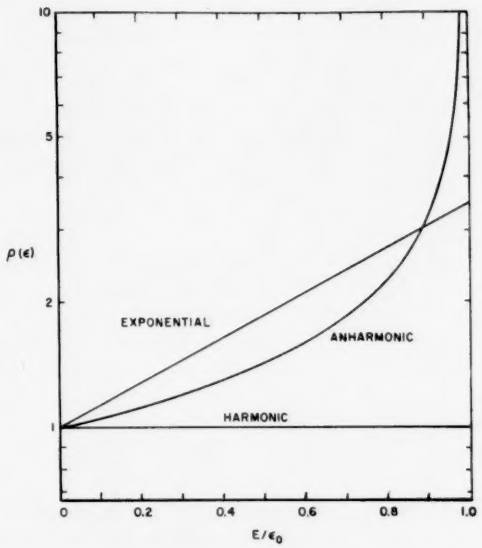

FIG. 3. Energy dependence of the density of states for the harmonic, anharmonic, and exponential oscillator.

SUMMARY

The modification of the semiclassical oscillator model by the introduction of boundedness and anharmonicity does not have an appreciable effect on the calculated lifetime of molecules with lifetimes longer than about 10^{-10} sec.

For more highly excited molecules the calculated magnitude of the rate constant may differ significantly from the Rice-Ramsperger-Kassel model. In addition, the energy dependence of the rate constant may have a functional form differing from that of the Rice-Ramsperger-Kassel model. This change in functional form is related to the energy dependence of the vibrational density of states. The results suggest anharmonicity may account for some of the disagreement between the number of oscillators of a molecule and the value of the parameter N in unimolecular reaction theory required to explain the pressure dependence of the rate constant.

In the case of molecules with comparatively long lifetimes, i.e., 10^{-5} sec, the modifications of rate theory developed here can offer no explanation for the greatly reduced effective number of degrees of freedom which are required to fit the data obtained for such cases by mass spectrometry. In particular, the energy dependence of the rate constant is essentially unchanged. Marcus[11] has pointed out that the enumeration of vibrational states by means of the semiclassical Dirichlet

[24] I. S. Sokolnikoff, *Advanced Calculus* (McGraw-Hill Book Company, Inc., New York, 1939).

integral is an approximation which becomes poorer as the amount of excitation energy decreases. He has pointed out that the approximation is particularly poor for the activated complexes, which have a large part of the energy fixed in the reaction coordinate. It is possible that a large part of the problem in explaining the mass spectrometric results is due to the poorness of the integral approximation.

Another aspect of the problem is the question of the validity of the equilibrium assumption fundamental to the absolute rate theory approach to chemical kinetics. This assumption has been questioned recently by several authors in connection with the theory of mass spectra. At the present time this assumption remains unproven. It is entirely possible that the mass spectral results cannot be explained by an equilibrium chemical kinetics treatment. In this connection it is to be noted that, in contrast to conventional chemical kinetics, the reactants in the mass spectrometer consist of excited molecule-ions which have been formed in a certain (unknown) region of phase space by a Franck-Condon transition and, subsequent to this event, they remain isolated until they are collected prior to or subsequent to unimolecular decomposition. A proof that such a situation can indeed be approximated by an equilibrium treatment is a formidable task, and further work, both theoretical and experimental, is needed.

THE JOURNAL OF CHEMICAL PHYSICS VOLUME 35, NUMBER 6 DECEMBER, 1961

Organic Semiconductors. V. Comparison of Measurements on Single-Crystal and Compressed Microcrystalline Molecular Complexes*

PAUL L. KRONICK AND MORTIMER M. LABES
The Franklin Institute, Laboratories for Research and Development, Philadelphia 3, Pennsylvania

(Received April 28, 1961)

Utilizing specialized micromanipulative techniques, measurements of conductivity, activation energy of conduction, and Seebeck coefficient have been performed on charge-transfer complex single crystals. The results are compared with previous measurements on compressed microcrystalline materials.

I. INTRODUCTION

IN several earlier papers,[1] it has been established that the resistivities of charge-transfer complexes are generally lower than those of conventional organic solids, and that one can cover the range of poor insulator to nearly metallic behavior by suitable chemical and structural modifications of these complexes. It has been suggested[1b] that crystal structure is an extremely important factor in determining the electronic behavior and that in many cases a chainlike crystal structure with alternate stacking of donor and acceptor molecules exists in the more highly conductive complexes.

The need for single-crystal measurements on materials of this sort has been obvious to all workers. Measurements which indicated both rough agreement[2] and wide disagreement[1c] in room-temperature resistivity have been reported but there was question as to the validity of some of these meaurements.[1c] The first report of activation energy of conduction and Seebeck coefficient measurements on a charge-transfer complex single crystal was made only recently.[1a] Complete single-crystal measurements on the somewhat related anion-radical salt complexes involving tetracyanoquinodimethane have also appeared.[3]

Although techniques of crystal growth are poorly understood for these materials, we have succeeded in growing some very small single crystals—nevertheless large enough to be handled by specialized micromanipulative methods, which are described in the next section. In this paper, measurements on single crystals of three diamine-quinone complexes are reported and discussed in relationship to measurements on the compressed materials.

II. EXPERIMENTAL

Using slow cooling or evaporative techniques, the molecular complexes were prepared from the solvents

* These results were presented at the Inter-Industry Conference on Organic Semiconductors, Chicago, Illinois, April 18–19, 1961.

[1] (a) M. M. Labes, R. Sehr, and M. Bose (Part IV), Proc. International Conference on Semiconductor Physics, Prague, Czechoslovakia, August 29–September 2, 1960, p. 850; (b) R. Sehr, M. M. Labes, M. Bose, F. Wilhelm, and H. Ur (Part III), *Proceedings Conference on Electronic Conductivity in Organic Solids, Duke University, April, 1960* (Interscience Publishers, Inc., New York, to be published); (c) M. M. Labes, R. Sehr, and M. Bose, J. Chem. Phys. **33,** 868 (1960); (d) **32,** 1570 (1960).

[2] J. Kommandeur and F. R. Hall, J. Chem. Phys. **34,** 129 (1961).

[3] R. G. Kepler, P. E. Bierstedt and R. E. Merrifield, Phys. Rev. Letters **5,** 503 (1960).

TABLE I. Microanalytical data on molecular complex single crystals.

Compound	Solvent in preparation	% C		% H		% N	
		Calc	Found	Calc	Found	Calc	Found
1,5-Diaminonaphthalene-chloranil	C_6H_6	47.5	47.9	2.5	2.4	6.9	7.1
Diaminodurene-chloranil	$CHCl_3$	46.8	46.8	3.9	4.2	6.8	6.8
1,6-Diaminopyrene-chloranil	$CHCl_3$	55.3	55.5	2.5	2.7	5.9	5.4

indicated in Table I in the form of long flat needles or plates; microanalyses gave values in good agreement with the theoretical values for the 1:1 complexes.

Crystallographic work is not yet completed on these complexes; we have identified the directions parallel to the three sets of faces of the crystal in terms of the arbitrary axes X, Y, and Z (Fig. 1).

Two methods were used to study conductance in the X direction. Crystals of diaminodurene-chloranil and 1,6-diaminopyrene-chloranil[4] were imbedded in a resin with their ends protruding, the ends were coated with Aquadag or silver paint, and the resulting molded samples were ground to the same shape as the pressed pellets previously studied.[1]

In addition another method[5] of mounting has been used, sketched in Fig. 2. A crystal is braced against a glass slide by a probe held in a micromanipulator while silver cement electrodes are painted onto the Y–Z faces by means of a very fine copper wire. It is important that these electrodes adhere to nothing except the crystal so that they cannot be pulled away from the crystal faces. The crystal is raised from the slide before the paint is dry. The final operation is to apply the small copper probes against the silver electrodes by holding the probes in two micromanipulators with the crystal between them. The probes are advanced toward each other until they grip the crystal under a small amount of spring tension (resulting from the U bends in the probes), and then the cement is poured between the probes and the glass slide. The cement applied is either an Epon resin or Sauereisen No. 1.

For measurements in one of the short directions in the crystal a different system was found to be effective (Fig. 3). A thin film of Aquadag is drawn down over the surface of a copper plate. The thickness of the film is chosen to be small compared to the thickness of the crystal. Before the film is quite dry the crystal is pressed into it while being held at the waxed end of a flexible wire (the wax is used as an adhesive between wire and crystal). The crystal should be held in the drying film by the spring tension of the bent wire. When dry, the crystal is secured mechanically by a thin strand of Epon resin. When the resin is hard, silver cement is painted on the top face of the crystal with a very fine copper wire and allowed to harden. The copper plate is then cemented to a glass slide and a copper probe shaped as in Fig. 3 is pressed down against the silver face. In this operation the copper probe is held in a micromanipulator while the slide rests on the microscope stage. After making the U bend in the copper probe it is necessary to anneal it, or relaxation occurs separating the probe from the crystal. Cement is applied around the probe, held under its flexural tension. When the cement dries the probe is disengaged from the micromanipulator, another wire is attached to the copper plate, and the specimen is ready for measurement. The sample dimensions can be measured with a calibrated microscope eyepiece before application of the top electrode.

The specimen is placed into an evacuable Pyrex cell with current leads sealed in. The probe wires of the specimen are attached to the lead-in wires of the cell by mercury contact. The cell can be mounted either in a shielded Dewar flask holding refrigerant or in a shielding tube immersed in a constant-temperature bath. The cell as a whole was guarded, utilizing the three electrode input system of the Keithley 610 electrometer.

Temperature runs made on the Z direction of 1,5-diaminonaphthalene-chloranil crystal at both constant current (10^{-10} amp) and constant voltage showed very little difference between the two curves. This was true even at voltages as high as 2 to 5 kv/cm.

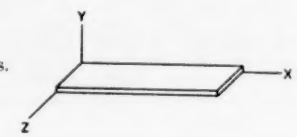

FIG. 1. Crystal directions.

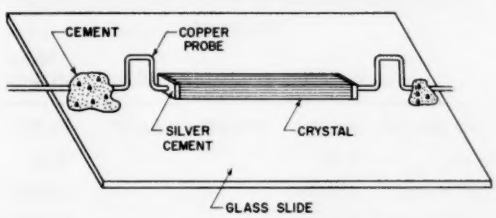

FIG. 2. Sample mount—long direction.

[4] This compound was previously referred to as 3,8-diaminopyrene-chloranil; "1,6" is the correct Chemical Abstract nomenclature.

[5] W. C. Shaw, D. E. Hudson, and G. C. Danielson, Rev. Sci. Instr. **26**, 237 (1955).

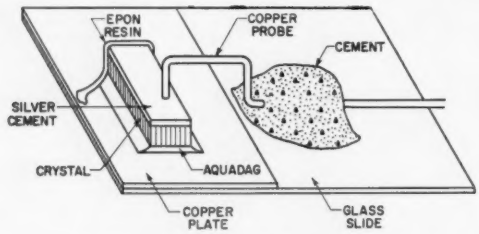

FIG. 3. Sample mount—short direction.

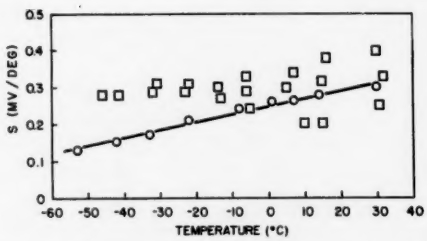

FIG. 4. Seebeck coefficient of diaminodurene-chloranil as a function of temperature. ○, compressed sample; □, single crystals. Each point represents an average of 6–10 measurements at different ΔT around the ambient T.

III. RESULTS

Using the above methods we measured the resistivity in three directions through a small crystal of diaminodurene-chloranil. Table II compares these results with that for a polycrystalline sample, showing that the resistivities are all about the same within a factor of 10. The activation energy E_a measured in the X direction is essentially the same as that in the polycrystalline sample. In this material, then, resistivities measured parallel and perpendicular to the most prominent cleavage planes are about the same. Agreement of these values with the polycrystalline data suggests that one would measure a value of about 10^4 ohm cm no matter what direction was studied.

It is apparent that the resistivity data on the compressed powder did provide useful information about electronic conduction in diaminodurene-chloranil. Besides providing reliable values of resistivities and activation energy, a Seebeck coefficient of 3×10^{-4} v deg^{-1} could be observed in both the pressed powders and in the X direction of the small crystal imbedded in resin at room temperature.

Deviation from a temperature-independent Seebeck coefficient for the single-crystal measurements in the range $-50°$ to $+30°$C was within experimental scatter, the mean value being $3.0\times10^{-4}\pm15\%$ v deg^{-1}, whereas measurements on the pressed powder showed a small increase in S in this temperature range (Fig. 4).

Table III reports data for conduction in 1,5-diaminonaphthalene-chloranil. This material had a high resistivity measured on a polycrystalline pellet and a correspondingly high activation energy. Poor conduction was noted in all three directions of the single crystals, but the resistivity in the X direction was nearly three orders of magnitude lower than the other values.[6] The resistivity-temperature data are plotted in Fig. 5. The lowest curve is drawn through two series of points taken on successive temperature cycles with extremely good reproducibility. The resistivities in the other directions returned to the room temperature value after temperature cycling. It is interesting to observe how close the resistivities of the microcrystalline pellet lie to that of the high resistivity directions in the crystal. The value at room temperature was reproduced on three polycrystalline specimens. Apparently in the polycrystalline material the current is limited by the directions of high resistance, the Y and Z directions of the single grains. This result is predicted if one averages the conductivities over all directions in a single crystal.

An attempt was made to measure thermopower in a polycrystalline sample. Because of a large persistent internal polarization, a Seebeck coefficient could not be measured accurately but was less than 50 μv deg^{-1}.

Table IV lists data on 1,6-diaminopyrene-chloranil. In the form of a polycrystalline pellet it had a resistivity of 4000 to 10 000 ohm cm, depending upon conditions of preparation and electrode systems. We present these data as an example of caution to be taken in studying "single crystals." Of all the crystals that we have studied, using all of the methods described earlier, the lowest values of resistivity in the three directions are shown in Table IV. It is seen that none

TABLE II. Conduction in diaminodurene-chloranil.

	Single crystal			
	X	Y	Z	Microcrystalline
$\rho(25°)$ ohm cm	7×10^4	6.9×10^4	8.4×10^4	3×10^4
E_a, ev	0.26			0.29
$S(30°)$ v deg^{-1}	3.0×10^{-4}			3.0×10^{-4}
$S(-50°)$ v deg^{-1}	3.0×10^{-4}			1.3×10^{-4}

TABLE III. Conduction in 1,5-diaminonaphthalene-chloranil.

	Single crystal			
	X	Y	Z	Microcrystalline
$\rho(25°)$ ohm cm	1.3×10^9	6.3×10^{11}	2.0×10^{11}	7.2×10^{11}
E_a, ev	0.60	0.74	0.74	0.65

[6] *Note added in proof.* We have recently performed measurements on some single crystals of 1,5-diaminonaphthalene-chloranil which have a higher resistivity (8.7×10^{10} ohm cm at 25°) and activation energy (E_a=0.79 ev in the X direction than those reported herein. In the absence of criteria for crystal perfection and the further elucidation of crystal structure, the reasons for these differences cannot be properly ascertained.

of these agrees even within an order of magnitude of the pressed pellet resistivity but are, surprisingly, very much higher. A rough estimate of the activation energy in the Y direction, derived from a run in which there was considerable scatter in the data, is about the same as that characterizing the polycrystalline pellet. It is possible that the resistivities are changed by the process of making the pellet, which involves grinding the powder twice and pressing it twice, and that surface conductance plays an important role. It is also possible that the crystals studied may have had cracks or voids in them which greatly increased their resistance. It is not likely that electrode effects would account for this difference, because the same electrode materials were used on the microcrystalline pellets. Further work with this system on single crystals grown under different conditions is in progress.

IV. DISCUSSION

Detailed interpretation of these data must await crystallographic analyses, since not only do we not know what kind of molecular stacking occurs in the X, Y, and Z directions of the crystals, but it is also possible that none of these directions are true crystallographic axes. However, because of the amount of data being accumulated on pressed powders, these results are of interest in that they point out the dangers and pitfalls of powder measurements, which must only be used as a rather crude indication of the electrical properties of a molecular crystal. The activation energy, being essentially isotropic, is the most reliable information to be obtained from the powder measurements.

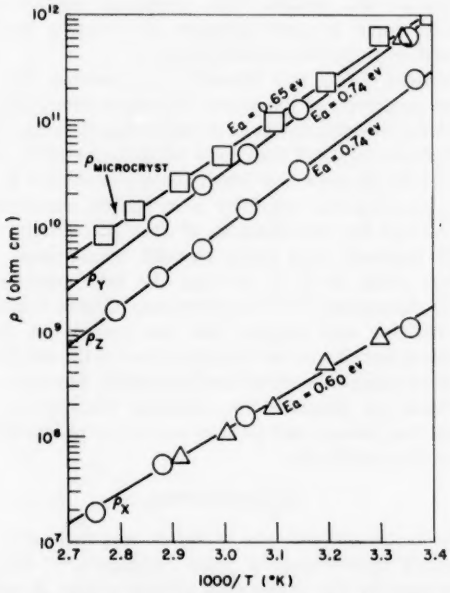

FIG. 5. Conduction anisotropy in 1,5-diaminonaphthalene-chloranil. ○, □, first temperature cycle; Δ, second temperature cycle.

TABLE IV. Conduction in 1,6-diaminopyrene-chloranil.

	Single crystal			
	X	Y	Z	Micro-crystalline
$\rho(25°)$ ohm cm	(10^5)	(10^6)	(10^9)	4×10^3
E_a, ev		(0.19)		0.15

In the present work a large anisotropy of the conductivity was observed for 1,5-diaminonaphthalene-chloranil. Kepler, Bierstedt, and Merrifield[3] have observed anisotropy of the conductivity and Seebeck coefficient for the tetracyanoquinodimethane salts and an isotropic activation energy. While the detailed explanation of the lack of anisotropy of the diamino-durene-chloranil complex must await crystallographic analysis, it is interesting to note infrared spectral evidence[7] for the strong interaction between the amine and quinone components. For example, the normal —C═O stretching frequency of chloranil is not observable in the spectrum of this complex. These spectral changes may be due to both molecule-molecule interaction in the alternate donor-acceptor stack proposed for the structure,[1e] and to interactions between an amine molecule in one stack and a quinone molecule in the neighboring stack. This would lead to an analog of a three-dimensional network, which might be responsible for the isotropic properties of this complex.

The observation of a conductivity anisotropy of almost three orders of magnitude in the poorly conducting 1,5-diaminonaphthalene-chloranil complex is in accord with the hypothesis based on chemical and structural arguments,[1e] which has been substantiated in the work of Kepler, Bierstedt, and Merrifield.[3] It is important to realize the enhancement of conductivity possible by structural or chemical features in a single direction of a crystal.

The assistance of Mr. P. J. Hackett and Mrs. H. Ur is gratefully acknowledged.

[7] M. M. Labes and H. Ur (unpublished results).

Nuclear Relaxation in Gases: Mixtures of Methane and Oxygen*

C. S. JOHNSON, JR,† AND J. S. WAUGH‡

Department of Chemistry, Laboratory of Chemical and Solid State Physics, and Research Laboratory of Electronics, Massachusetts Institute of Technology, Cambridge 39, Massachusetts

Three previously proposed mechanisms of nuclear relaxation in fluids are qualitatively discussed: (1) modulation of intramolecular fields by collisions, (2) transient, and (3) diffusively modulated dipolar interactions with paramagnetic impurities. It is shown that the dependence of T_1 for the protons in methane-oxygen mixtures on composition, density, and temperature is adequately described by a superposition of these contributions to $1/T_1$, and that the magnitudes involved are consistent with *a priori* estimates. It is suggested that the spin-rotation interaction provides an important relaxation mechanism in both gaseous and liquid methane.

INTRODUCTION

ONE usually thinks of the nuclear relaxation in a dense fluid as having its origin in the fluctuating dipolar fields which arise from the rotational and translational diffusion of the molecules—that is, by the mechanism discussed at length by Bloembergen, Purcell, and Pound (BPP)[1] with special reference to water. Evidence is now accumulating[2,3] that in some, and, very likely, in many cases the BPP mechanism needs to be supplemented. In particular, the persistence of something like free rotation of simple, quasi-spherical molecules in the liquid state may permit important contributions from the collision-modulated interaction between spins and rotational magnetic moments. This mechanism is known to be important in many dilute polyatomic gases.[4–6] In addition, a third view of the relaxation process (first proposed by Bloembergen[7]) may be useful under special circumstances. This is the *transient* dipolar interaction between magnetic moments belonging to different molecules which occurs when they collide. It is undoubtedly the dominant mechanism in diamagnetic monatomic gases when large amounts of paramagnetic impurities are present, and accounts for the success of Anderson's observation of the He^3 resonance in helium-oxygen mixtures.[8] (The main relaxation process in *pure* inert gases is different but also transient in its time dependence.)[9,10]

Our aim in this paper is to demonstrate the utility of all three descriptions mentioned above in a single system. In order to separate their effects it is helpful to make use of the fact that they have different dependences on density. Thus, unless elaborate high-pressure apparatus is available, it is desirable to study gases rather than liquids. Gases offer the further advantage that they can be studied at densities low enough to permit at least qualitative reliance to be placed on the simplest ideas of kinetic theory in interpreting the results. This statement applies with special force to any attempts at relating nuclear relaxation to intermolecular forces.

Sandhu, Lees, and Bloom[11] have pointed out the great sensitivity of the proton relaxation time in liquid methane to small amounts of paramagnetic impurities. It is to be expected that some of the same effect may persist in the region of lower density accessible to us. The paramagnetic impurity is in general expected to accentuate the contributions of the Bloembergen and BPP processes (the latter through translational diffusion alone) to T_1 in the gas. We have accordingly made measurements on appropriately chosen mixtures of methane and oxygen. For the present we have confined out theoretical interpretation of the results to order-of-magnitude considerations which, however, are sufficient to illustrate the essential features of the relaxation process and its relation to the properties of molecules and fluids.

EXPERIMENTAL

T_1 in the various gas mixtures was measured by standard radio-frequency pulse techniques,[12,13] for the most part by the observation of spin echoes. A set of Tektronix waveform and pulse generators triggered a 40-Mc oscillator and power amplifier whose final tank coil contained the sample. The latter was mounted in a brass pressure probe equipped with Kovar seals for electrical connections and mostly filled with a nylon

* This work was supported in part by the U. S. Army Signal Corps, the Air Force Office of Scientific Research, and the Office of Naval Research, and in part by the National Science Foundation.

† National Science Foundation Predoctoral Fellow.

‡ Alfred P. Sloan Fellow.

[1] N. Bloembergen, E. M. Purcell, and R. V. Pound, Phys. Rev. **73**, 679 (1948).

[2] H. S. Gutowsky, I. J. Lawrenson, and K. Shimomura, Phys. Rev. Letters **6**, 349 (1961).

[3] M. R. Baker, H. M. Nelson, J. A. Leavitt, and N. F. Ramsey, Phys. Rev. **121**, 807 (1961).

[4] I. Oppenheim and M. Bloom, Can. J. Phys. **39**, 845 (1961).

[5] M. Bloom and M. Lipsicas, Can. J. Phys. **39**, 870 (1961).

[6] C. S. Johnson, Jr., J. Pinkerton, and J. S. Waugh, J. Chem. Phys. **35**, 1128 (1961).

[7] N. Bloembergen, thesis, Leiden University (1948).

[8] H. L. Anderson, Phys. Rev. **76**, 1460 (1949).

[9] R. L. Streever and H. Y. Carr, Phys. Rev. **121**, 20 (1961).

[10] H. C. Torrey (to be published).

[11] H. S. Sandhu, J. Lees, and M. Bloom, Can. J. Chem. **38**, 493 (1960).

[12] E. L. Hahn, Phys. Rev. **80**, 580 (1950).

[13] H. Y. Carr and E. M. Purcell, Phys. Rev. **94**, 630 (1954).

plug so as to confine the sample to a region of more or less uniform H_1. The response signal was tapped from the final tank capacitor at a point of suitable impedance and fed directly to a Varian V4310A receiver which had been modified to speed up its recovery from overloads.

The rf pulses were applied in a 180°–90°–180° sequence, and the echo following the last pulse was recorded. In this experiment[13] the intensity of the (detected) echo decreases, passes through a null, and asymptotically approaches an equilibrium value as the time t_{12} between the first and second pulses is increased from a small initial value. Some of our initial experiments made use of the fact that $t_{12} = 0.693T_1$ when a null echo is obtained. This method is unfortunately somewhat sensitive to changes in the width of the initial pulse, and in our experience consistently gave values of T_1 which were 5–10% too small. Accordingly, our later measurements were made by plotting the logarithm of the difference between the echo amplitude and its equilibrium value against t_{12} and obtaining the slope of the resulting straight line.

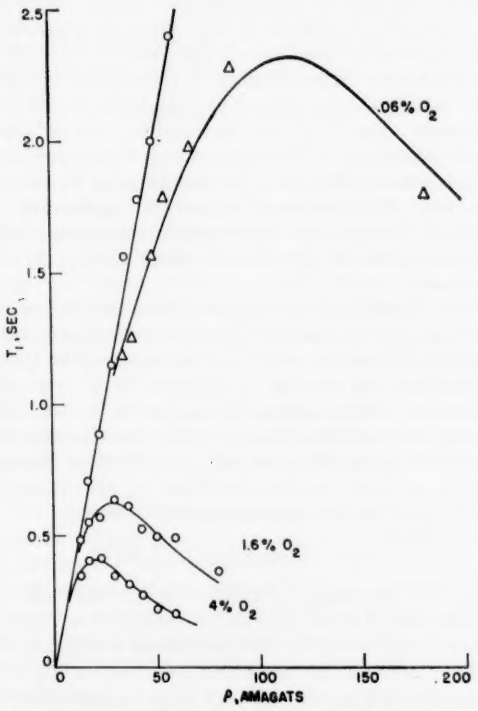

FIG. 1. Proton relaxation times (T_1) in three mixtures of methane and oxygen at 194°K. The solid curve for 4.0% O_2 was obtained by fitting the constants in Eq. (5) to the experimental points. The other solid curves were calculated from the same constants. The circles represent our measurements and the triangles are taken from the results of Bloom, Lipsicas, and Muller (reference 14). The experimental points from that reference fit the solid curve satisfactorily to considerably higher densities than those shown.

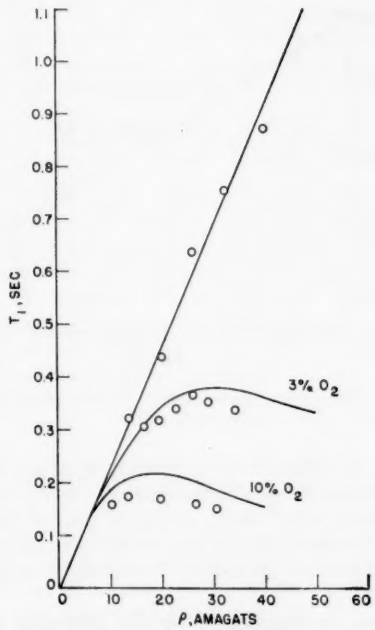

FIG. 2. Proton relaxation times in methane-oxygen mixtures at 293°K. The solid curves were calculated directly from the results of Fig. 1 at 194°K, as described in the text. The experimental points for 10% O_2 are probably too low. (See text).

The probe assembly was mounted in a glass Dewar vessel in the 2½-in. gap of a 12-in. Harvey-Wells electromagnet. The temperature was controlled with a variety of baths ranging from dry ice-methanol to boiling water and was monitored with a copper-constantan thermocouple embedded in the probe.

The methane (Matheson Company cp) and oxygen were mixed at room temperature in a small steel tank and the mixture then allowed to flow into the probe. Compositions of the mixtures were calculated from the total pressures of the mixtures before and after addition of the second component, these pressures being measured with Bourdon gauges calibrated against the vapor pressure of CO_2.

RESULTS AND DISCUSSION[14]

Low Densities

Figures 1 and 2 show that as the gas density is increased from a small value there is an initial linear increase of T_1 with number density. (Throughout we use a unit of number density which is equal to 2.6336×10^{19} molecules cm^{-3}. We loosely call this unit an amagat, although that name would be strictly appropriate only if all gases studied were ideal at STP.) This behavior

[14] M. Bloom, M. Lipsicas, and B. H. Muller, Can. J. Phys. (to be published), have also measured T_1 for CH_4 containing up to 1% O_2. Their point of view and conclusions differ from ours in several respects.

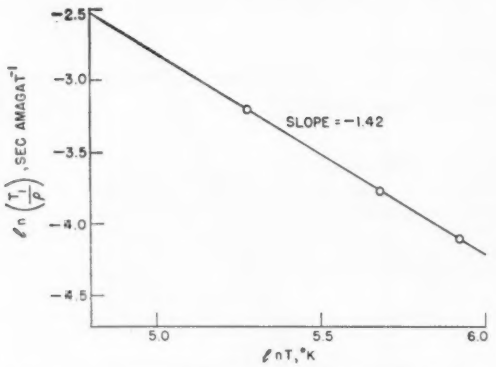

FIG. 3. Temperature dependence of T_1/ρ for methane at low densities.

is what is expected if the relaxation arises from a modulation of the spin Hamiltonian of the free molecule by collisions which occur at a rate greater than the Larmor frequency. It was first described quantitatively by Schwinger and applied by Bloembergen to the case of H_2.[1]

Methane is complicated by the fact that it is a spherical top and moreover has three nuclear spin isomers, namely meta ($I=2$), ortho ($I=1$), and para ($I=0$). To be strictly correct we should allow for more than one relaxation time even for a single species since the motions of the protons in a methane molecule are correlated. Hubbard has treated the case of four spin $\frac{1}{2}$ nuclei situated at the corners of a tetrahedron whose motion is governed by rotational diffusion.[15] His expression for the departure from equilibrium of the z component of magnetization (M_z-M_{eq}) did, in fact, contain two terms with different relaxation times. However, the coefficient of one of the terms was 50 times larger than the coefficient of the other, and the relaxation time associated with the larger term was within 2% of the value for T_1 that would be calculated for a proton with three uncorrelated pairwise interactions. This result, coupled with the fact that experimentally we have been able to detect only one relaxation time, is taken as justification for our discussion of a single T_1. It is worth pointing out that while Hubbard's treatment should predict the order of magnitude of the dipolar contribution to T_1 in gaseous methane it is in principle not applicable since transitions to states of different J are infrequent.[16,17]

Both the meta and ortho species contribute strongly to the nuclear resonance signal, and hence the T_1's that we measure are not clearly associated with either variety. If we make the assumption that there is no important distinction between the ortho and meta species when J is large and that the rate of molecular reorientation τ_c^{-1} is insensitive to the rotational quantum number J, we can apply an approximate formula of the Schwinger variety as follows:

$$T_1^{-1}\approx\gamma_n^2\langle H'^2\rangle\langle J(J+1)\rangle+\langle H''^2\rangle\tau_c, \qquad (1)$$

where H' is the field at a proton arising from rotation of the molecule and H'' is the corresponding dipolar field at one proton arising from the others. We have implicitly assumed that transitions from one value of J to another do not affect the relaxation, a question which will be discussed in detail in another paper.[18]

The average value of the spin-rotational interaction [i.e., $\frac{1}{3}(H_{\|}'+2H_{\perp}')$] has been found from molecular beam experiments to be about 2.4 gauss,[19] a value considerably smaller than the 27 gauss appropriate to H_2.[20] However, in the neighborhood of room temperature $\langle J(J+1)\rangle$ is around 57 for CH_4 compared to about 3 for H_2. The contribution of the spin-rotation interaction to proton relaxation is thus reduced from that in hydrogen only by something like a factor of 6. The dipolar interaction H'' can be estimated from the structure of the CH_4 molecule to be approximately 5 gauss (lumping the ortho and meta species together), as compared to 34 gauss for H_2. Since in the temperature region of interest the dipolar contribution to T_1 is approximately independent of J, it becomes clear that this contribution is reduced by a factor of 30–40 from hydrogen. Since the two contributions are of about equal importance in H_2 at room temperature, we may expect that modulation of the spin-rotation interaction provides the dominant relaxation mechanism in methane. The fact that both contributions are relatively small accounts in part for the relatively long T_1's in methane.

The dominance of spin-rotational relaxation in methane may be further supported through the temperature dependence of T_1 in the region of its linear dependence on density. It appears likely that the anisotropic forces leading to changes of m_J are sufficiently weak and of sufficiently short duration that the transition probabilities per unit time for these changes can be at least roughly described by the quantum mechanical transient approximation.[21] That is,

$$W\sim(t_0^2|\langle m_J|V_1|m_J'\rangle|^2Z)/\hbar^2, \qquad (2)$$

where Z is the number of collisions per second made by a molecule, d is a molecular diameter, v a relative velocity, and $t_0\sim d/v$ is the duration of a collision. V_1 is the anisotropic intermolecular potential leading to a transition. In general, we expect V_1 to be characteristic of the colliding molecules and, therefore, different for

[15] P. S. Hubbard, Phys. Rev. **109**, 1153 (1958).
[16] A. Abragam, *The Principles of Nuclear Magnetism* (Oxford University Press, London, 1961), p. 321.
[17] B. T. Kelley, J. Acoust. Soc. Am. **29**, 1005 (1957).
[18] C. S. Johnson, Jr., and J. S. Waugh (to be published).
[19] C. Anderson (private communication).
[20] J. M. B. Kellogg, I. I. Rabi, N. F. Ramsey, Jr., and J. R. Zacharias, Phys. Rev. **56**, 728 (1939).
[21] L. I. Schiff, *Quantum Mechanics* (McGraw-Hill Book Company, Inc., New York, 1949), p. 219.

CH_4—CH_4 and CH_4—O_2 encounters. The experiments described below are limited to a maximum of 10% oxygen and the results may be well enough described by a single V_1. For larger concentrations of oxygen the low-density T_1 equation would necessarily contain two terms.[18] The average temperature dependence of these quantities in the framework of a hard sphere model is such that $W/\rho \propto T^{-0.5}$. Theoretical estimates of this dependence by other methods have predicted T^0 to $T^{-0.5}$ for fairly long range interactions,[22–24] and experimental results from the nonresonant absorption of microwaves by molecules with dipole moments have been interpreted to give temperature dependences of $T^{-0.27}$ to $T^{-0.60}$.[25,26] We have found these results to be consistent with the temperature dependence of T_1/ρ for hydrogen extrapolated to infinite dilution in CO_2.[18] (The collisions in pure H_2 represent a special case which requires a more sophisticated treatment.[5,18])

T_1/ρ in pure methane in a given rotational state might therefore be expected to vary as $T^{-\frac{1}{2}}$. Since $\langle J(J+1)\rangle$ is approximately proportional to T in the region of room temperature, however, we should expect an additional factor of T^{-1} if the spin-rotation interaction dominates, but not if the spin-spin interaction leads to the chief relaxation mechanism. The experimental dependence of T_1 on temperature shown in Fig. 3 supports the former conclusion.

Intermediate Densities

At low densities it is apparent that the presence or absence of paramagnetic impurities such as oxygen is of little consequence. At sufficiently high densities we expect a deviation from the linear increase of T_1 with ρ even in pure methane, since intermolecular dipolar couplings during collisions should become important as the collision frequency increases. However, the dipole couplings are very weak and it is not clear that other transient relaxation mechanisms such as those suggested by Streever and Carr can be neglected.[9,10] The range of densities experimentally available to us is restricted to the extent that we found it convenient to produce the deviation by the deliberate addition of oxygen.

The first deviations from constancy of T_1/ρ in methane-oxygen mixtures are expected to result from the transient magnetic interaction proposed by Bloembergen and mentioned above.[7] We again resort to the transient approximation (this time with excellent justification), and estimate the matrix element of the magnetic interaction during a collision to be of the order of $\gamma_n\gamma_p\hbar^2 d^{-3}$, where the gyromagnetic ratios refer to the nucleus and to the colliding paramagnetic species. The relaxation arising in this manner may then be approximately expressed as

$$\frac{1}{T^1}\simeq 2\gamma_n^2\gamma_p^2\hbar^2\left(\frac{l_0^2}{d^6}\right)Z\simeq\frac{2\gamma_n^2\gamma_p^2\hbar^2}{v_r^2 d^4}Z, \qquad (3)$$

where v_r is the relative velocity of the colliding molecules and d is the distance of closest approach. In the context of an ideal gas, hard sphere point of view the quantity on the right of (3) should be proportional to density (at constant composition) and to $T^{-\frac{1}{2}}$. This effect is sufficiently mixed up experimentally with the situation at still higher densities that we shall briefly defer a comparison with experiment.

High Densities

As the density increases further, collisions can no longer be considered to be distinct events separated by intervals of zero interaction. We must in fact take into account the possibility that magnetic moments may remain in the vicinity of the nucleus of interest for times which are long compared to the mean free time. This is just the situation investigated first in great detail by Bloembergen *et al.*[1], and the result which they derived for solutions of paramagnetic ions is directly applicable to the methane-oxygen system

$$1/T_1\simeq(2\gamma_n^2/Dd)N_p\langle\mu^2\rangle. \qquad (4)$$

Here N_p is the number of oxygen molecules per cm^3, D is a diffusion coefficient (strictly a mutual diffusion coefficient), and $\langle\mu^2\rangle$ is the mean-square magnetic moment of the oxygen molecule.

It is important to note that D depends on density, and is in fact proportional to ρ^{-1} for dilute gases.[27] In a hard-sphere gas D should in addition be proportional to $T^{\frac{1}{2}}$. Experimentally the dependence even for rather dilute gases tends to be slightly steeper than this,[28] but the precision of the present experiments and, particularly, of their theoretical interpretation, is insufficient to justify making any deliberate departure from the ideal gas value for the purposes of discussion. We shall assume that $1/T_1$ for methane-oxygen mixtures depends on ρ^2 and $T^{-\frac{1}{2}}$ insofar as it is determined by the BPP mechanism.

Combined Relaxation Mechanisms

We shall now make the assumption that all three of the above mechanisms make independent contributions to the relaxation process, so that it is possible to write

$$1/T_1=(A/\rho)+(Bx_0)\rho+(Cx_0)\rho^2, \qquad (5)$$

[22] P. W. Anderson, Phys. Rev. **76,** 647 (1949).
[23] G. Birnbaum and A. A. Maryott, J. Chem. Phys. **29,** 1422 (1958).
[24] C. H. Townes and A. L. Schawlow, *Microwave Spectroscopy* (McGraw-Hill Book Company, Inc., New York, 1955), Chap. 13.
[25] A. A. Maryott, A. Estin, and G. Birnbaum, J. Chem. Phys. **32,** 1501 (1960).
[26] J. E. Boggs, A. P. Dean, and J. M. King, J. Chem. Phys. **33,** 1852 (1960).
[27] J. O. Hirschfelder, C. F. Curtiss, and R. B. Bird, *Molecular Theory of Gases and Liquids* (John Wiley & Sons, Inc., New York, 1954), p. 539.
[28] J. Jeans, *An Introduction to the Kinetic Theory of Gases* (Cambridge University Press, New York, 1948), pp. 171–4, 202.

where x_0 is the mole fraction of O_2 and A, B, and C functions of temperature. To be sure, such a superposition is not justified in principle in the case of the last two mechanisms discussed; both involve the same interaction Hamiltonian and simply represent different limiting approximations to the correlation function of this operator. A complete theory[4] would consider the dependence of the correlation function on density in detail, but our purpose is simply to point out that a satisfactory and consistent physical description of the experimental results can be obtained much more simply.

The sensitivity of T_1 to the details of the correlation function is not great enough to make any discrepancies evident in the region of density where one limiting approximation is giving way to the other.

We have adjusted B and C to fit the experimental points for 4% O_2 in Fig. 1 and have set A equal to the inverse of the slope of the pure methane curve. This choice for A amounts to considering a single value of V_1 in Eq. (2) as discussed above. Using the facts, stated earlier, that B and C should be proportional to $T^{-\frac{1}{2}}$ and that $A \propto T^{+1.42}$, we have calculated the other solid curves in Figs. 1 and 2. The temperature dependences of B and C, being based on a hard sphere model, are only approximate. The lower experimental points in Fig. 2 were measured by a null method and, as previously indicated, are perhaps 5 to 10% too low.

The values of the parameters at 194°K are $A=25$ amagat sec^{-1}; $B=1.25$ amagat^{-1} sec^{-1}; $C=0.011$ amagat^{-2} sec^{-1}. In order to be sure that the success of this procedure is not simply one of the well-known miracles which can be wrought with three adjustable parameters, it is important to verify that the values of A, B, and C needed to fit the experimental points agree, at least in order of magnitude, with *a priori* estimates. The estimation of A poses certain difficulties which we shall discuss elsewhere,[18] although we may mention that there is nothing about the experimental value of A which is disturbing. B and C have been calculated from Eqs. (3) and (4) at 194°K using $d=3.6\times10^{-8}$ cm, $D=0.15\ \rho$ cm^2 sec^{-1} amagat, and $\langle\mu^2\rangle\cong7\times10^{-40}$ erg^2 gauss^{-2} with the result $B=1.3$ amagat^{-1} sec^{-1}; $C=0.006$ amagat^{-2} sec^{-1}. The agreement with the experimental values is to be regarded as somewhat fortuitous.

Some experimental points obtained by Lipsicas[14] are shown in Fig. 1. The calculated curve also passes through his points at 200 and 300 amagat, which are not shown in our figure. Since the low-density slope reported by Bloom and Lipsicas at 193°K was somewhat less than our slope at 194°K we were forced to use $A=30$ amagat sec^{-1} to fit their points. On the basis of our experimental values of B and C we would estimate that their mixture contained 0.06% O_2. They have stated the O_2 content to be 0.1%.

In conclusion, it appears that the relaxation of the protons in methane-oxygen mixtures, and presumably in many other systems as well, can be adequately described over a considerable range of density, composition, and temperature by a very simple superposition of the three relaxation mechanisms described above. The constants appearing in the final expression for T_1 are consistent with *a priori* estimates. Of the three contributions, that of Bloembergen is probably the least important except in the presence of large amounts of paramagnetic impurities. From the point of view of this paper, it is only the strong dependence of the BPP mechanism on density that frequently permits it to dominate in the liquid state. Even in liquids it appears[2,3] that when intermolecular forces are relatively weak and molecular motion is rapid a significant contribution of spin-rotational interaction to the relaxation process may persist. This is very likely true of methane, as suggested by the following argument: We have already seen that the first term of Eq. (5) is dominated by the spin-rotational interaction. Evaluating it under the conditions appropriate to liquid methane at its boiling point, we find $T_1^{-1}=0.02$ sec^{-1}, to be compared with a total T_1^{-1} of only 0.07.[11]

Both the Bloembergen transient mechanism and the one which dominates at low densities, particularly the latter, offer interesting possibilities for the study of anisotropic intermolecular forces.[4,5,29] We intend to discuss this matter at greater length elsewhere,[18] with special reference to experimental studies on hydrogen and mixtures of hydrogen with other gases.

ACKNOWLEDGMENT

We are very grateful to Professor M. Bloom, Professor I. Oppenheim, and Professor M. Lipsicas for communication of their results before publication, particularly in the case of reference 14.

[29] J. S. Waugh and C. S. Johnson, Jr., Bull. Am. Phys. Soc. **6**, 363 (1961).

Ultraviolet Spectrum of Dibenzene Chromium Vapor*†

R. STEPHEN BERRY

Sterling Chemical Laboratory, Yale University, New Haven, Connecticut

(Received May 22, 1961)

The ultraviolet spectrum of dibenzene chromium vapor has been observed under medium resolution conditions. At least three separate band systems are found, at least two of which display progressions of the totally symmetric vibration frequencies. Possible assignments are considered and compared with alternative level structures. It is concluded that the $3de_{2u}$ level probably lies below the metal a_{1g} orbital, and that term splitting may play a considerable role in determining the order of the excited states.

INTRODUCTION

THE absorption spectrum of dibenzene chromium vapor has been investigated in the region 2100–6000 A. This study was undertaken because of recent interest in the electronic energy levels and structure of dibenzene chromium[1–6] and more specifically, because the reported ultraviolet absorption spectrum of dibenzene chromium itself in cyclohexane[5] shows none of the banded character found in the spectra of a number of other chromium-arene molecules.[7,8] Proposed level schemes for these molecules imply that all their spectra should display several reasonably strong band systems in the visible and near-uv region. Only dibenzene chromium itself failed to show such a spectrum; the absorption spectrum reported by Feltham[5] showed a very broad peak having a maximum at about 3200 A and a shoulder in the 4000 A region, and a second, much weaker maximum at about 6500 A. Other spectra of solutions and crystals of compounds of this kind characteristically show several absorption bands: six for the one Cr(0) compound reported, and seven for the Cr(I) systems.[7,8] The vapor spectrum of dibenzene chromium was examined in hopes that it would display more structure than the solution spectrum, enough perhaps to display separate electronic transitions.

EXPERIMENTAL

The sample of dibenzene chromium was supplied by Dr. R. L. Pruett of the Union Carbide Chemicals Company. The material was transferred into the sample cell in an atmosphere of nitrogen; the cell was evacuated to remove volatile contaminants; argon was admitted to give a pressure of approximately 30 cm Hg at 25°C. The sample cell itself was a fused silica tube, 25 mm in diameter and about 24 in. long, with clear fused silica end windows attached with Apiezon W wax. The middle third of the tube was wrapped with asbestos, wound with Nichrome heating wire and wrapped with a second layer of asbestos. A copper-constantan thermocouple measured the temperature of the tube.

Solution spectra and preliminary gas-phase spectra were taken on a Cary model 11 spectrometer. The final gas-phase investigation was carried out with a Bausch & Lomb medium-quartz spectrograph. A variety of photographic plates were used to investigate various regions of the spectrum: Eastman 103–0 plates for general use, Ilford Q–3 and HPS for the far ultraviolet, and Ilford HPS and R–50 plates for the visible region. The light source for the photographic work was a fused-silica capillary flash lamp, through which approximately 90 joules were discharged in about 30 μsec.

The first spectra showed the presence of a small amount of benzene; after the cell and sample had been warmed and re-evacuated, no traces of benzene would be seen in the spectrum. When the cell was reopened after a number of spectra had been taken, crystals of the sublimed dibenzene chromium were removed from the cell and dissolved in cyclohexane. The spectrum of this material was essentially indistinguishable from that reported by Feltham.[5]

The absorption spectrum of dibenzene chromium vapor is dramatically different from that of the solution. Instead of a broad, featureless single peak, the spectrum shows at least three distinct band systems, which in turn have well-defined vibrational structure. Table I lists the prominent maxima. These are rather diffuse, and permitted measurement to only about ±3 A in the middle of the spectrum. Representative spectra are shown in Fig. 1.

The absorptions described here are classified into three systems; system I, whose strongest band lies at 3748 A; system II, a diffuse system with a maximum near 3050, and with definite bands only at the short-wavelength end; and system III, which actually includes bands of three groups, a long progression in the 2820–2670 region with the strongest maximum at

* Contribution No. 1665 from Sterling Chemistry Laboratory.
† This work was supported by the Directorate of Chemical Sciences, Air Force Office of Scientific Research.

[1] E. M. Shustorovich and M. E. Dyatkina, Doklady Akad. Nauk S.S.S.R. **128,** 1234 (1959); for recent work on similar systems see *ibid.* **131,** 113 (1960); **133,** 141 (1960).
[2] R. E. Robertson and H. M. McConnell, J. Phys. Chem. **64,** 70 (1960).
[3] F. Jellinek, Nature **187,** 871 (1960).
[4] D. A. Levy and L. E. Orgel, Mol. Phys. **4,** 93 (1961).
[5] R. D. Feltham, J. Inorg. & Nuc. Chem. **16,** 197 (1961).
[6] R. S. Berry, J. Chem. Phys. **35,** 29 (1961).
[7] S. Yamada, H. Nakamura, and R. Tsuchida, Bull. Chem. Soc. Japan **30,** 647 (1957).
[8] S. Yamada, H. Yamazaki, H. Nishikawa, and R. Tsuchida, Bull. Chem. Soc. Japan **33,** 481 (1960).

TABLE I. Absorption maxima of dibenzene chromium.[a]

Long wave bands λ(A)	System I	System II	System III
4370	3907 ?	3010	(a) 2823
4315	3833	2970±10	2800 vs
4156	3781	2946	2781 s
	3748 vs	(plus diffuse	2760 b
	3711 s	absorption at	2730 ms
	3674	longer wave-	2711
	3640 s	lengths)	2694
	3606		2669
	3571		
	3533		(b) 2604
	3480 ?		2570 s
	3365		2552 ms
			2465 s
			2450 ms
			2408 s
			2395
			2373
			2343
			2332

[a] vs, very strong; s, strong: b, broad; ms, moderately strong.

2800, at least three more bands at about 2570, and another long, diffuse series between 2465 and 2332 A. Of these, the middle group extends into a region of silicon absorption lines of the lamp which prohibits investigation of the 2500 A region. The classification of systems was chosen to correspond to that used by Yamada *et al.*[7,8] in their investigation of the solution and crystal spectra of chromium arene compounds. Our photographic study did not extend to long enough wavelengths to search for the very weak band at about 6500 A reported by Feltham; we did find such a band in the solution spectrum. This band is presumably the spin-forbidden band of references 7 and 8.

The gas-phase spectrum failed to show any strong absorption in the 2100 A region. Presumably the strong $\pi \rightarrow \pi^*$ transition denoted as IV in reference 7 lies at a wavelength too short to be detected with our system; that is, it must fall beyond 2100 A.

System II has only three well-defined bands, all far from the center of the absorbtion, so one may be hesitant to try to associate the frequency differences with any of the observed vibration frequencies of dibenzene chromium.[9,10] Systems I and III, on the other hand, have very clearly defined progressions which can probably be associated with known vibrations. In both systems, the most obvious frequency is the ν_{21} totally symmetric vibration of the rings against the central chromium. This has been estimated as 280 cm^{-1}.[9] The estimate we make from systems I and III is 260–270 cm^{-1}.

System I also shows the ν_{11g} totally symmetric CH bending frequency, previously found to be 790 cm^{-1} in dibenzene chromium iodide[9,10] and estimated at about 787 cm^{-1} from the present work. One narrow band at 3365 A looks similar to the bands of system I and lies 3037 cm^{-1} to the violet of the strongest band of this system. It may be associated with the ν_{2g} symmetrical CH stretching mode; the corresponding frequency in $(C_6H_6)_2CrI$ is 3095 cm^{-1}. The band at 3781 A is probably a "hot" band from the first excited vibrational state of the ν_{21} symmetrical valence mode, according to the analysis below.

The absorption at wavelengths greater than 3781 A might be due to more excited vibrations in system I. We prefer, however, to assign this as a separate electronic transition. This point is discussed further in the next section.

Differences taken from system III show not only ν_{21} but also a 911 cm^{-1} frequency which may be the ν_{1g} symmetric ring-breathing frequency of the upper state. Frequency measurements of the shorter wavelength bands attributed to this system are complicated by emission lines of the light source. Nonetheless the ν_{21} frequency seems to appear throughout the system. The band at 2823 A seems to be a hot band of this vibration.

The extended 260 cm^{-1} progressions have their strongest band near but not at the long wavelength end of the progressions. Moreover, the intensity in the bands on the red side of the most intense bands seems to be more sensitive to temperature than the intensity on the violet side. These observations indicate that the short-wavelength parts of the progressions are due to upper-state levels, and the long-wave side, to hot bands. This, in turn, indicates that in series I and III, at least, the electronic excitation produces no drastic changes in the ring-metal bonds. Since the frequency differences of the bands in these series seem to be those of totally symmetric vibrations, we believe these to be allowed transitions involving nonbonding orbitals.

DISCUSSION

In a previous note, an attempt was made to assign the spectra of several compounds of chromium and benzene.[6] The assignments were made in terms of a strong-field formalism, and were carried out for the threefold-symmetric symmetry reported for dibenzene chromium in the crystal and for the sixfold symmetry which the molecules are supposed to exhibit in fluid phases. Only the orbital levels were considered; term-splitting was not considered except as it affected the intensities of various bands. The most probable assignments, it was felt, were as follows. Referring to the bands in the notation of Yamada *et al.*,[7,8] and using D_{6h} symmetry for the molecule, we have

band I: $3de_{2g}(^1A_{1g}) \rightarrow 4pe_{1u}'(^1B_{1u}, {}^1B_{2u}, {}^1E_{1u})$;

band II: $3da_{1g}(^1A_{1g}) \rightarrow 4pe_{1u}'(^1E_{1u})$,
$e_{1u}(^1A_{1g}) \rightarrow 3de_{1g}'(^1A_{1u}, {}^1A_{2u}, {}^1E_{2u})$,
$3de_{2g}(^1A_{1g}) \rightarrow 4pa_{1u}'(^1E_{2u})$;

band III: $3da_{1g}(^1A_{1g}) \rightarrow 4pa_{1u}'(^1A_{1u})$.

[9] H. P. Fritz, W. Lüttke, H. Stammreich, and R. Forneris, Ber. deut. chem. Ges. **92,** 3246 (1959).
[10] R. G. Snyder, Spectrochim. Acta **15,** 807 (1959).

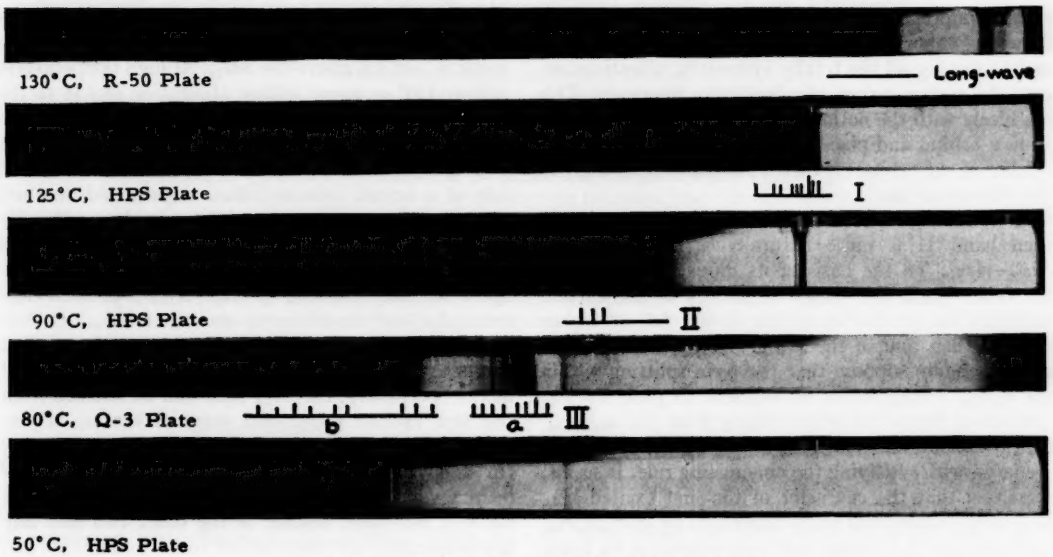

FIG. 1. Representative spectra of dibenzene chromium vapor.

The transitions listed include all those below the $\pi e_u \rightarrow 3da_{1g}'$ and $\pi \rightarrow \pi^*$ transitions, having components allowed in D_{3d} symmetry. In D_{6h} symmetry, only the $^1A_{1g} \rightarrow {}^1A_{1u}$ and $^1A_{1g} \rightarrow {}^1E_{1u}$ transitions are allowed; they are polarized parallel and perpendicular to the sixfold axis, respectively. According to this assignment, in D_{3d} symmetry, band I has a z component as well as one with x, y polarization. An alternative assignment was given, based on placement of the filled $a_{1g}(3d+4s)$ orbital above the $3de_{2g}$. This alternative, harder to reconcile with the solution spectra, better explains the observed g value of the paramagnetic $(C_6H_6)_2$ CrI molecule. The only major change in the assignments of the spectral bands is the interchange of the $e_{2g} \rightarrow e_{1u}'$ and $\pi e_{1u} \rightarrow e_{1g}'$ bands. This in turn changes the polarization expected for band I in D_{6h} symmetry. In the former assignment, the transition moment of band I is polarized parallel to the planes of the rings and band II contains both parallel and perpendicularly polarized components. In the latter assignment, band I has its moment perpendicular to the rings, and band II is due entirely to a parallel transition. Let us also consider the possibility that dibenzene chromium in solution is threefold symmetric, as it is in the crystal. Then both bands would have parallel and perpendicular components in either scheme.

If band I of the solution spectra is indeed due to the same transition as system I of the vapor spectrum of dibenzene chromium itself, and if system I appears as a distinct uv-fluorescent system when dibenzene chromium is dissolved in a rigid glass, then a measurement of the fluorescence depolarization of system I would demonstrate whether the dibenzene chromium molecule has D_{6h} or D_{3d} symmetry (in the glass, at least), and, if its symmetry is sixfold, whether the $^1E_{1u}$ or $^1A_{1u}$ excited state lies lower.

The amount of information in the vapor spectrum of dibenzene chromium prompts us to re-examine our level scheme, and to try to correlate the observed spectrum with the binding in this and perhaps other sandwich compounds. One recent limited molecular orbital calculation, for example, suggests that the major contribution to the metal-ring bond in $(C_6H_6)_2Cr$ is the mixing of the $3de_{2g}$ orbitals of the chromium atom with the empty ring orbitals of the same symmetry.[1] The same effect has been inferred by Levy and Orgel[4] from their discussion of the energetic order of the a_{1g} and e_{2g} orbitals of ferricinium ion and dibenzene chromium iodide. This would imply that the e_{2g} orbital is strongly bonding, and that removal of an electron from this orbital would weaken the bond between the rings and the chromium atom.

If the e_{2g} orbital is indeed a strongly bonding orbital, then it is difficult to reconcile the assignment of system I as an $e_{2g} \rightarrow e_{1u}'$ transition. It now seems more probable, in view of the appearance of the bands system and of the ν_{21} vibration in particular, that it arises from the $\pi e_{1u} \rightarrow 3de_{1g}'$ transition, and that the a_{1g} orbital does indeed lie above the e_{2g}. Shustovorich and Dyatkina[1] compute the a_{1g} energy slightly lower than the e_{2g}, but point out that the two levels are so close that their calculation cannot be trusted to give the exact order. Levy and Orgel,[4] on the other hand, conclude that the a_{1g} orbital must be at least 2.9 ev above the e_{2g} if the ground state of dibenzene chromium iodide is $^2A_{1g}$. Previously, the $e_{2g} \rightarrow e_{1u}'$ assignment was preferred because the alternative was essentially to say that band I was due to a charge-transfer process, which

seemed improbable according to the solution spectra. Now, the vapor spectrum shows system I to be strong, and to display all the totally symmetric vibrations except the carbon-carbon ring-breathing frequency. This fits nicely with the notions that an electron is removed from a orbital and placed in a metal orbital, and that neither of the orbitals involved contributes strongly to the ring-metal bond.

If we reassign band I to the $\pi e_{1u} \rightarrow 3de_{1g}'$ transition, then band II is quite naturally attributed to the $3de_{2g} \rightarrow 4pe_{1u}'$ on the basis of its diffuse structure. On the other hand, the center of gravity of the excited configuration of this transition should fall at higher energies than that of the $3da_{1g} \rightarrow 4pe_{1u}'$ excitation. We must therefore suppose that the term splitting within the $e_{2g}^3 e_{1u}'$ configuration is sufficient to push its $^1E_{1u}$ component below the state coming from the $a_{1g} \rightarrow e_{1u}'$ excitation. But this state is also a $^1E_{1u}$ state; now we are faced with satisfying the noncrossing rule. It seems, therefore, that the character of the first excited $^1E_{1u}$ state may change from being dominated by an $e^4{}_{2g} a_{1g} e_{1u}'$ configuration in a strong-field approximation to being predominantly $e_{2g}^3 a_{1g}^2 e_{1u}'$ when term-splitting and configuration mixing is included.

This change might be observable as a change in the appearance of systems II and III if the benzene rings of dibenzene chromium were replaced by rings completely substituted, say, with fluorines.

It is not possible to say at present whether system III is actually composed of one, two, or three electronic transitions. From the appearance of the band structure, it seems improbable that three transitions contribute. This argues for the regular-hexagon structure of the benzene rings, since if the symmetry were D_{3d}, we would have three and not just two low-energy allowed electronic transitions to assign. If there are two allowed transitions, then the lower-energy one, around 2800 A, is presumably the $^1A_{1g} \rightarrow {}^1E_{1u}$ transition due primarily to the $a_{1g} \rightarrow e_{1u}'$ transition and the bands at shorter wavelengths are due to the $a_{1g} \rightarrow a_{1u}'$ excitation. These transitions are polarized parallel to the ring plane and perpendicular to it, respectively, so that again, they might be distinguished experimentally.

Finally we can add one more factor which lends more support to the identification of system I as a $\pi e_u \rightarrow 3de_{1g}'$ transition, and thereby, to the placement of the metal a_{1g} orbital above the $3de_{2g}$. At high temperatures (about 120° or more) diffuse absorption sets in to the red of system I. This absorption is probably too widespread to be part of the same system, although it does overlap system I. There are two maxima on the red side of a broad, intense diffuse region, and another, somewhat stronger, on the violet side. If we identify system I as due to the $\pi e_{1u} \rightarrow 3de_{1g}'$ transition, we find that of the three terms derived from the excited configuration, the transition to one ($^1A_{1u}$) is allowed electronically, and transition to one other ($^1A_{2u}$) is electronically forbidden but becomes vibrationally allowed through the action of a low-frequency vibrational mode. Specifically, the $^1A_{2u}$ state can be reached from the first excited vibrational state of the a_{2u} asymmetrical ring-metal stretching mode, which lies 459 cm^{-1} above the ground state.[9] The alternative assignment gives three excited states of which one is again allowed, but here, neither of the other two find any low-frequency vibrations which could make them become allowed.

We summarize our results by presenting the spectral assignment which, according to this analysis seems most probable. Unobserved states are placed in brackets, and the vibrationally allowed, electronically forbidden state in braces.

System I:

$$e_{1u}(^1A_{1g}) \rightarrow 3de_{1g}'(^1A_{1u})\{^1A_{2u}\}[^1E_{2u}];$$

system II:

$$3de_{2g}(^1A_{1g}) \rightarrow 4pe_{1u}'(^1E_{1u})[^1B_{1u}, {}^1B_{2u}];$$

system III: (long-wave bands)

$$3da_{1g}(^1A_{1g}) \rightarrow 4pe_{1u}'(^1E_{1u})$$

system III: (short-wave bands)

$$3da_{1g}(^1A_{1g}) \rightarrow 4pa_{1u}'(^1A_{1u}).$$

Further work, particularly utilizing fluorescence from a glass if this is possible, would be necessary to test this assignment.

THE JOURNAL OF CHEMICAL PHYSICS VOLUME 35, NUMBER 6 DECEMBER, 1961

Molecular Friction in Dilute Gases. II. Thermal Relaxation of Translational and Rotational Degrees of Freedom*

NORMAN F. SATHER† AND JOHN S. DAHLER
Department of Chemical Engineering, University of Minnesota, Minneapolis 14, Minnesota

(Received May 18, 1961)

Expressions for the rates of equilibration of the translational energies in multicomponent gas mixtures of structureless molecules are derived in terms of characteristic relaxation times. The approach to equilibrium is found to be completely dominated by an exponential decay factor for molecules interacting with inverse power potentials; the decay should be essentially exponential for more realistic potential functions. The calculations of rotational relaxation times are presented for several rigid molecular models: rough and partially rough spheres, spherocylinders, and loaded spheres. The relaxation times obtained are in good agreement with those observed experimentally and with those predicted by previous theories. It is found that, in general, on the order of 10 collisions are required to reduce an initial temperature difference by a factor of $1/e$ for translational-rotational equilibration.

I. INTRODUCTION

THE collisional degradation of molecular momentum and kinetic energy in dilute gases has recently been examined by O'Toole and Dahler.[1] Here we shall be concerned with the extension of their results to thermal relaxation phenomena. In particular, we wish to determine the mean rates of change of the average kinetic energies associated with the different molecular species present in a gas mixture and of the energies associated with the internal rotational motions of polyatomic species. Subject to certain simplifying but very reasonable assumptions, the rates at which these equilibration processes take place can be expressed in terms of characteristic relaxation times.

Although most of the calculations presented here seem to be novel, our results will be compared whenever possible with those of previous investigators. In Sec. II we determine the relaxation times associated with equilibration of the translational energies of the various components in a mixture of structureless molecules. The remaining sections are devoted to the calculation of rotational relaxation times for several molecular models: rough and partially rough spheres, spherocylinders, and loaded spheres. Except for the case of perfectly rough spheres, previous estimates of rotational relaxation times have invariably been dependent upon approximate rather than exact treatments of the collisional dynamics. We have attempted to avoid such approximations by limiting our attention to molecular models so simple that exact mathematical analyses of the collisional dynamics are possible. The advantages of this approach are, of course, somewhat offset by the artificiality of the molecular models themselves. However, the *dynamical* approximations attendant to the use of more realistic but nevertheless empirical choices for the molecular interactions are also of a somewhat artificial nature.

Since it appears that rotational relaxation times are relatively insensitive to the detailed nature of molecular interactions, the very simplicity of the models considered here constitutes a strong argument in their favor. On the other hand, calculations of vibrational relaxation times depend much more critically upon an accurate knowledge of the interactions and upon intricasies of the collisional events such as chattering. Because of the more sophisticated and careful analysis required for calculations of this sort we defer the subject of vibrational relaxation to a separate communication.

II. EQUILIBRATION OF TRANSLATIONAL ENERGIES IN A GAS MIXTURE

Our purpose here is to examine the relaxation rates of the mean translational energies associated with the separate molecular species in a multicomponent gas mixture. The molecular mass and number density of the α component will be denoted by m_α and n_α, respectively. The temperature or mean translational energy of this species is defined in the conventional manner by the formula

$$\tfrac{3}{2}kT_\alpha = n_\alpha^{-1}\int f_\alpha \tfrac{1}{2}m_\alpha C_\alpha^2 d\mathbf{c}_\alpha,$$

where $\mathbf{c}_\alpha$ is the velocity and f_α the singlet distribution function.

Let us now imagine that at a particular moment the state of the system is characterized by a set of Boltzmann distributions

$$f_\alpha = n_\alpha(m_\alpha/2\pi kT_\alpha)^{\frac{3}{2}}\exp(-m_\alpha C_\alpha^2/2kT_\alpha),$$

with separate and distinct temperatures T_α. The experimental preparation of initial states of this sort is very nearly realizable in several instances, e.g., the homogeneous production by a chemical reaction of molecular species with energy distributions significantly

* This research was supported in part by a grant from the National Science Foundation.

† National Science Foundation predoctoral fellow in Chemical Engineering.

[1] J. T. O'Toole and J. S. Dahler, J. Chem. Phys. **33**, 1496 (1960).

different from those of the reactants, the mixing of hot and cold molecules at a shock or detonation front, and the slow thermalization of massive molecules by a much lighter diluent. The last of these, the Lorentz gas, is of particular interest because of its direct applicability to the description of ions and electrons in a plasma.

In reference 1 it was established that the rate of change of kinetic energy of an α-species molecule may be expressed by the equation

$$(d/dt)(\tfrac{1}{2}m_\alpha c_\alpha^2)=\sum_\beta {}^\alpha\langle(P_{\alpha\beta})_\tau\rangle + [\mathbf{F}_\alpha\cdot\mathbf{c}_\alpha-\sum_\beta {}^\alpha\langle(P_{\alpha\beta})_\tau\rangle], \quad (1)$$

where $\mathbf{F}_\alpha$ is the instantaneous force acting upon the molecule. ${}^\alpha\langle(P_{\alpha\beta})_\tau\rangle$, the ensemble average power transfer from β-species members of the system, is related to the frictional force ${}^\alpha\langle(\mathbf{F}_{\alpha\beta})_\tau\rangle=-\zeta_{\alpha\beta}(c_\alpha)\mathbf{c}_\alpha$ in the manner

$${}^\alpha\langle(P_{\alpha\beta})_\tau\rangle=(\mu_{\alpha\beta}/m_\beta)\,{}^\alpha\langle(\mathbf{F}_{\alpha\beta})_\tau\rangle\cdot\mathbf{c}_\alpha - [kT_\beta/(m_\alpha+m_\beta)]\nabla_{\mathbf{c}_\alpha}\cdot{}^\alpha\langle(\mathbf{F}_{\alpha\beta})_\tau\rangle, \quad (2)$$

where $\mu_{\alpha\beta}=m_\alpha m_\beta/(m_\alpha+m_\beta)$.

The ensemble expectation value for the temporal average of the power fluctuation, $\mathbf{F}_\alpha\cdot\mathbf{c}_\alpha-\sum_\beta{}^\alpha\langle(P_{\alpha\beta})_\tau\rangle$, is of course identically zero. Consequently, the equation of change for T_α may be written in the form

$$(dT_\alpha/dt)=(\tfrac{3}{2}n_\alpha k)^{-1}\sum_\beta\int f_\alpha\,{}^\alpha\langle(P_{\alpha\beta})_\tau\rangle d\mathbf{c}_\alpha = -\sum_\beta[(T_\alpha-T_\beta)/\tau_{\alpha\beta}], \quad (3)$$

where the relaxation times are given by the formula

$$\tau_{\alpha\beta}=\tfrac{3}{4}n_\alpha kT_\alpha(m_\alpha+m_\beta)\Big/\int f_\alpha\zeta_{\alpha\beta}(c_\alpha)\tfrac{1}{2}m_\alpha c_\alpha^2 d\mathbf{c}_\alpha \quad (4)$$

and the friction coefficients by[1]

$$\zeta_{\alpha\beta}(c_\alpha)=n_\beta\mu_{\alpha\beta}(kT_\beta/2\pi m_\beta)^{\frac{1}{2}}c_\alpha^{-3}\exp(-m_\beta c_\alpha^2/2kT_\beta) \times\int_0^\infty dg\,g^5Q_{\alpha\beta}^{(1)}(g)\exp(-m_\beta g^2/2kT_\beta) [(m_\beta c_\alpha g/kT_\beta+1)\exp(-m_\beta c_\alpha g/kT_\beta) +(m_\beta c_\alpha g/kT_\beta-1)\exp(m_\beta c_\alpha g/kT_\beta)]. \quad (5)$$

Here

$$Q_{\alpha\beta}^{(l)}(g)=2\pi\int_0^\infty(1-\cos\chi)\,bdb$$

is a cross section[2] defined in terms of the scattering angle $\chi=\chi(b,g)$ and the impact parameter or "miss-distance" b. From (4) and (5) it may then be verified that

$$\tau_{\alpha\beta}=3(m_\alpha+m_\beta)/32n_\beta\mu_{\alpha\beta}\Omega_{\alpha\beta}^{(1,1)}(T_{\alpha\beta}), \quad (6)$$

with

$$\Omega_{\alpha\beta}^{(1,1)}(T)=(kT/2\pi\mu_{\alpha\beta})^{\frac{1}{2}}\int_0^\infty e^{-\gamma^2}\gamma^5Q_{\alpha\beta}^{(1)}[(2kT/\mu_{\alpha\beta})^{\frac{1}{2}}\gamma]d\gamma. \quad (7)$$

$T_{\alpha\beta}=M_\alpha T_\beta+M_\beta T_\alpha$, and $M_\alpha=m_\alpha/(m_\alpha+m_\beta)$. According to the theory of Chapman and Enskog[3] the omega integral $\Omega_{\alpha\beta}^{(1,1)}$ is inversely proportional to the diffusion coefficient for a binary mixture of α- and β-species molecules. Therefore, numerical estimates of the relaxation times can be obtained very easily from the extensive tables of omega integrals which have been constructed for a wide variety of pair potential functions.[4,5]

From (6) we see that for a given value of $T_{\alpha\beta}$ the relaxation time $\tau_{\alpha\beta}$ is proportional to the symmetrical function of the molecular masses, $(m_\alpha+m_\beta)^2/m_\alpha m_\beta$. Since this factor assumes its minimum value when $m_\alpha=m_\beta$, formula (6) correctly predicts the well-known result that thermalization of a particular molecular species is most efficiently accomplished by another of equal mass. The fact that $\tau_{\alpha\beta}$ depends upon $T_{\alpha\beta}$ and not upon some other function of the two temperatures T_α and T_β is of considerable interest for it implies that if there is a sizeable difference in the molecular masses of the species, the temperature of the lighter will be the more significant in determining the relaxation time. From this we may conclude that in a plasma it is the electron temperature which governs the rate of thermal equilibration between ions and electrons.

To estimate the ion(α)-electron(β) relaxation time the interactions of the charged particles may be represented approximately by the shielded-Coulomb potential $\phi(r)=(Z_\alpha e^2/r)\exp(-K_{\alpha\beta}r)$. Here e denotes the magnitude of the electronic charge and $Z_\alpha e$ the charge on an ion. Although the parameter $K_{\alpha\beta}$ is essentially empirical, its reciprocal should very nearly equal the Debye length $l_D=(kT_\beta/4\pi n_\beta e^2)^{\frac{1}{2}}$. According to Liboff[5] the omega integral for this potential is given by

$$\Omega_{\alpha\beta}^{(1,1)}(T_{\alpha\beta})=\tfrac{1}{2}(\pi kT_{\alpha\beta}/2m_\beta)^{\frac{1}{2}}(Z_\alpha e^2/kT_{\alpha\beta})^2 [\log_e(2kT_{\alpha\beta}/Z_\alpha e^2K_{\alpha\beta})-0.961]. \quad (8)$$

From (6) and (8) it then follows that

$$\tau_{\alpha\beta}^{-1}=\frac{16n_\beta(m_\beta/m_\alpha)}{3(1+m_\beta/m_\alpha)^2}(\pi kT_{\alpha\beta}/2m_\beta)^{\frac{1}{2}}(Z_\alpha e^2/kT_{\alpha\beta})^2 [\log_e(2kT_{\alpha\beta}/Z_\alpha e^2K_{\alpha\beta})-0.961]. \quad (9)$$

[2] J. O. Hirschfelder, C. F. Curtiss, and R. B. Bird, *The Molecular Theory of Gases and Liquids* (John Wiley & Sons, Inc., New York, 1954), p. 525.

[3] Reference 2, p. 539.

[4] Reference 2, Appendixes.

[5] R. L. Liboff, Phys. Fluids **2,** 40 (1959). A similar calculation has also been performed by T. Kihara, J. Phys. Soc. Japan **14,** 402 (1959).

If the plasma contains only a single ionic species conservation of energy requires that $\tau_{\alpha\beta}/n_\alpha=\tau_{\beta\alpha}/n_\beta$ and so $d(T_\alpha-T_\beta)/dt=-(T_\alpha-T_\beta)/\tau$, where

$$\tau^{-1}=\tau_{\alpha\beta}^{-1}[(n_\alpha+n_\beta)/n_\beta]\simeq\tfrac{8}{3}(n_\alpha+n_\beta)(m_\beta/m_\alpha)(2\pi kT_\beta/m_\beta)^{\frac{1}{2}}(Z_\alpha e^2/kT_\beta)^2[\log_e(2kT_\beta/Z_\alpha e^2K_{\alpha\beta})-0.961]. \quad (10)$$

Kihara[6] has obtained this same result by a different method of calculation.

Because of the manner in which it has been derived the relaxation equation, (3), is strictly applicable only to states of the system for which our assumption of local Boltzmann distributions is valid. Even if such a state were to be established at one instant of time (or at one point of the flow in the case of a shock transition) the subsequent evolution of the distribution functions would most certainly not proceed through a sequence of Boltzmann functions which differ only in the values of their temperature variables. However, the calculation of temperature-time profiles involves only second moments of the distribution functions and so should be relatively insensitive to minor distortions of these functions. This leads one to expect that the integration of (3) will not lead to results which are grossly unrealistic. Proceeding on this note of optimism we obtain [from (3) and (6)] for a binary mixture

$$\int_{T_{\alpha\beta}(0)}^{T_{\alpha\beta}(t)}\frac{dR}{(T-R)\Omega_{\alpha\beta}^{(1,1)}(R)}=\frac{32n\mu_{\alpha\beta}}{3(m_\alpha+m_\beta)}t. \quad (11)$$

Here $T=(n_\alpha/n)T_\alpha+(n_\beta/n)T_\beta$, the mole average temperature, is a constant and $n=n_\alpha+n_\beta$. In terms of the dimensionless time, $\Theta=16n\sigma_{\alpha\beta}^2(2\pi\mu_{\alpha\beta}\epsilon_{\alpha\beta})^{\frac{1}{2}}t/3(m_\alpha+m_\beta)$, this equation may be written as

$$\Theta=\int_{T_{\alpha\beta}^*(0)}^{T_{\alpha\beta}^*(t)}\frac{dS}{(T^*-S)S^4\Omega_{\alpha\beta}^{(1,1)*}(S)}, \quad (12)$$

where $T_{\alpha\beta}^*=kT_{\alpha\beta}/\epsilon_{\alpha\beta}$, $T^*=kT/\epsilon_{\alpha\beta}$, and

$$\Omega_{\alpha\beta}^{(1,1)*}(T_{\alpha\beta}^*)=(\pi\sigma_{\alpha\beta}^2)^{-1}(2\pi\mu_{\alpha\beta}/kT_{\alpha\beta})^{\frac{1}{2}}\Omega_{\alpha\beta}^{(1,1)}(T_{\alpha\beta})$$

is the reduced omega integral.

Finally, (12) can be transformed into an implicit equation for $\Delta T=T_\alpha-T_\beta$ by invoking the relationship $T_{\alpha\beta}=T+m\Delta T$ with $m=(n_\beta M_\beta-n_\alpha M_\alpha)/n$. For the inverse power potential, $\phi_{\alpha\beta}(r)=\epsilon_{\alpha\beta}(\sigma_{\alpha\beta}/r)^\delta$, the omega integrals are easily evaluated[7] and the temperature-time profile obtained in closed form. In the case of Maxwell molecules ($\delta=4$) the approach to equilibrium is given by the exponential,

$$\Delta T(t)/\Delta T(0)=\exp(-t/\tau),$$

with a characteristic time

$$\tau=(m_\alpha+m_\beta)/16\pi\sigma_{\alpha\beta}^2nA^{(1)}(4)(\tfrac{1}{2}\mu_{\alpha\beta}\epsilon_{\alpha\beta})^{\frac{1}{2}}.$$

[6] T. Kihara and Y. Midzuno, University of Wisconsin, Theoretical Chem. Lab. Rept. WIS-AEC-24 (1960).
[7] Reference 2, p. 547.

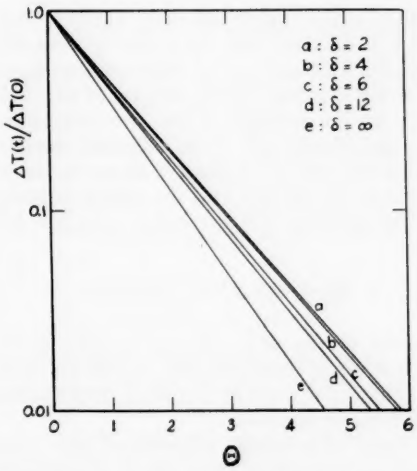

FIG. 1. Dependence of the temperature difference upon reduced time for molecules interacting with inverse power potentials. The curves are calculated for equimolar gas mixtures for which $m_\beta=1.5\,m_\alpha$ and $\Delta T(0)=T=\epsilon_{\alpha\beta}/k$.

For other values of δ the decay, although not precisely exponential, is very nearly so. Calculations based upon an equimolar mixture with $m_\beta=1.5m_\alpha$ are illustrated in Fig. 1. For the sake of convenience we have chosen $T=\Delta T(0)=\epsilon_{\alpha\beta}/k$, which for simple molecules is usually on the order of several hundred degrees Kelvin.

III. ROTATIONAL RELAXATION OF ROUGH SPHERES

The simplest molecular model which incorporates a collisional mechanism for the transfer and interchange of rotational and translational energies is the rough sphere model of Bryan and Pidduck.[8] A rough sphere may be described as a radially symmetrical distribution of mass characterized by its moment of inertia I, total mass m, and radius σ. The linear and rotational velocities (relative to a space-fixed frame of reference) of such a molecule will be denoted by the symbols $\mathbf{c}$ and $\mathbf{w}$, respectively.

The collisional dynamics of these molecules can be determined from an examination of the equations of impact,

$$\mathbf{c}_2'-\mathbf{c}_2=-(\mathbf{c}_1'-\mathbf{c}_1)=\mathbf{J}, \quad (13)$$

$$I(\mathbf{w}_2'-\mathbf{w}_2)=I(\mathbf{w}_1'-\mathbf{w}_1)=-\sigma\mathbf{k}\times m\mathbf{J}, \quad (14)$$

and

$$\Delta E=\tfrac{1}{2}m\mathbf{J}\cdot(\mathbf{g}_{21}'+\mathbf{g}_{21})=0, \quad (15)$$

which are, in order of their presentation, statements of the conservation laws for the linear momentum, angular momentum, and energy of the two colliding molecules.[8] The primed and unprimed variables refer to the

[8] This model is considered in great detail by S. Chapman and T. G. Cowling, *The Mathematical Theory of Non-Uniform Gases* (Cambridge University Press, London, 1953), 2nd ed., Chap. 11.

dynamical states before and after collision. The unit vector $\mathbf{k}$ is directed from the center of molecule 1 to that of 2 at the moment of their contact; $\mathbf{g}_{21}=\mathbf{c}_{21}+\sigma\mathbf{k}\times(\mathbf{w}_1+\mathbf{w}_2)$ is the relative velocity of the points of contact on the surfaces of the two molecules, and $\mathbf{c}_{21}=\mathbf{c}_2-\mathbf{c}_1$. Finally, $m\mathbf{J}$ is the collisional impulse imparted to molecule 2 as a result of its encounter with 1. With the aid of (13) and (14) the primed variables can be eliminated from (15) to yield an equation for this impulse

$$\kappa\mathbf{g}_{21}\cdot\mathbf{J}-\mathbf{k}\mathbf{k}:\mathbf{J}\mathbf{J}+(1+\kappa)J^2=0. \tag{16}$$

The value of the dimensionless moment of inertia $\kappa=4I/m\sigma^2$ varies from zero when the mass is localized at the center of the sphere to $\frac{2}{3}$ when all of the mass is concentrated on its surface.

Our choice of a radially symmetrical mass distribution can be expected to apply better to spherical top molecules such as CH_4, CCl_4, $C(CH_3)_4$, and SF_6 than to species with more eccentric mass distributions. Although the theory for more complicated situations can easily be constructed, it is not presented here because of the notational complexity which it would introduce.

Previous studies have been limited to the two solutions of Eq. (16),

$$\mathbf{J}=-\mathbf{k}\mathbf{k}\cdot\mathbf{c}_{21} \tag{17a}$$

for perfectly smooth spheres, and

$$\mathbf{J}=-\kappa/(\kappa+1)[\mathbf{g}_{21}+(1/\kappa)\mathbf{k}\mathbf{k}\cdot\mathbf{c}_{21}] \tag{17b}$$

for perfectly rough spheres. Other solutions define molecular models which one reasonably enough may describe as "partially rough." As an example let us consider the function

$$\mathbf{J}=A\mathbf{k}\mathbf{k}\cdot\mathbf{g}_{21}-B\mathbf{g}_{21}+C\mathbf{k}\times\mathbf{g}_{21}, \tag{18}$$

where the coefficients A, B, and C are assumed to depend only upon the collisional invariants. This particular choice for $\mathbf{J}$ satisfies the physically appealing condition that the angular velocities of the two colliding molecules are unaltered when $\mathbf{g}_{21}$ lies parallel to $\mathbf{k}$. From (16) and (18) we obtain the relationship

$$[\kappa(A-B)(A-B+1)](\mathbf{k}\cdot\mathbf{g}_{21})^2 +[-\kappa B+(\kappa+1)(B^2+C^2)]G_{21}^2=0, \tag{19}$$

where $\mathbf{G}_{21}$ is the component of $\mathbf{g}_{21}$ normal to $\mathbf{k}$.

Although more elaborate models are certainly possible, we prefer one which involves a single parameter ρ the value of which varies from zero for smooth spheres to unity in the case of perfectly rough spheres. Therefore, we shall assume that A, B, and C depend only upon ρ and so satisfy the conditions [cf. Eqs. (17a) and (17b)]

ρ	A	B	C
0	-1	0	0 (20)
1	$-(1+\kappa)^{-1}$	$\kappa(1+\kappa)^{-1}$	0.

Inasmuch as $\mathbf{k}\cdot\mathbf{g}_{21}$ and G_{21} are independent of one another (19) implies that the coefficients must obey the relationships

$$(A-B)(A-B+1)=0 \tag{21a}$$

$$\kappa B-(1+\kappa)(B^2+C^2)=0. \tag{21b}$$

The solution $A-B=0$ is incompatible with the conditions (20) and so the only acceptable solution of (21a) is $A=B-1$.

Now the equations of change for the rotational and translational temperatures, $T_{\rm rot}$ and $T_{\rm tr}$, may be written as

$$dT_{\rm rot}/dt=-dT_{\rm tr}/dt=(\tfrac{3}{2}nk)^{-1}\sigma^2\int\cdots\int_{\mathbf{k}\cdot\mathbf{c}_{21}<0}\mathbf{k}\cdot\mathbf{c}_{21}\tfrac{1}{2}m \times(c_1'^2-c_1^2)f_1f_2d\mathbf{k}d\mathbf{c}_1d\mathbf{c}_2d\mathbf{w}_1d\mathbf{w}_2. \tag{22}$$

Here $-\sigma^2\mathbf{k}\cdot\mathbf{c}_{21}d\mathbf{k}dt$ is the element of volume in which molecule 2 must lie if it is to collide with 1 during the interval $(t, t+dt)$. The condition $\mathbf{k}\cdot\mathbf{c}_{21}<0$ ensures that the two actually are proceeding toward one another at the instant immediately prior to collision.[9]

If we next assume that the distribution functions are of the form,

$$f_i=n(m/2\pi kT_{\rm tr})^{\frac{3}{2}}(I/2\pi kT_{\rm rot})^{\frac{1}{2}} \exp[-(mc_i^2/2kT_{\rm tr}+Iw_i^2/2kT_{\rm rot})]. \tag{23}$$

the integration of (22) can easily be performed with the result that

$$\frac{dT_{\rm rot}}{dt}=-\frac{mn\sigma^2}{3k(\kappa+1)}B\left(\frac{m}{4\pi kT_{\rm tr}}\right)^{\frac{3}{2}}\left(\frac{I}{2\pi kT_{\rm rot}}\right)^{\frac{1}{2}} \times\iiiint_{\mathbf{k}\cdot\mathbf{c}_{21}<0}(\mathbf{k}\cdot\mathbf{c}_{21})(\mathbf{U}-\mathbf{k}\mathbf{k}):[\mathbf{c}_{21}\mathbf{c}_{21}-\tfrac{1}{4}\kappa\sigma^2(\mathbf{w}_1\mathbf{w}_1+\mathbf{w}_2\mathbf{w}_2)] \times\exp\{-[(m/4kT_{\rm tr})c_{21}^2+(I/2kT_{\rm rot})(w_1^2+w_2^2)]\} \times d\mathbf{c}_{21}d\mathbf{w}_1d\mathbf{w}_2d\mathbf{k}, \tag{24}$$

or

$$dT_{\rm rot}/dt=-dT_{\rm tr}/dt=-(T_{\rm rot}-T_{\rm tr})/\tau, \tag{25}$$

[9] Equation (23) can, of course, be derived from arguments precisely like those used in Sec. II. A detailed discussion of the volume element $-\sigma^2\,\mathbf{k}\cdot\mathbf{c}_{21}\,d\mathbf{k}\,dt$ and of the "precollisional" condition $\mathbf{k}\cdot\mathbf{c}_{21}<0$ can be found in the papers by O'Toole and Dahler, J. Chem. Phys. **32**, 1097 (1960); **33**, 1487, 1496 (1960).

where the relaxation time τ is given by

$$\tau^{-1}=\{[16n\sigma^2/3(\kappa+1)](\pi kT_{\rm tr}/m)^{\frac{1}{2}}\}B(\rho). \quad (26)$$

There are, of course, an infinite set of functions $B(\rho)$ which satisfy the conditions (20), e.g.,

$$B(\rho)=\rho\kappa/(1+\kappa), \quad B(\rho)=\rho\kappa/(1+\rho\kappa),$$

etc. The first of these two choices is somewhat unique in that it implies collisional invariance of g_{21}, i.e., that

$$g_{21}'=g_{21}.$$

The rate at which an individual molecule collides with others is given by the ensemble average collision frequency $Z=4\pi\sigma^2 n(kT_{\rm tr}/\pi m)^{\frac{1}{2}}$. Therefore,

$$N=Z\tau=\tfrac{3}{4}(\kappa+1)/B(\rho) \quad (27)$$

provides a rough measure of the number of collisions necessary to accomplish thermal equilibration of the rotational and translational degrees of freedom. In the case of $\rho=1$ Eq. (27) reduces to the collision number for perfectly rough spheres calculated by Widom.[10] As ρ approaches zero N becomes arbitrarily large and so reflects the poor communication which exists between the rotational and translational degrees of freedom of almost smooth spheres.

The calculation can easily be extended to a mixture of ν species, each with different translational and rotational temperatures. A molecule of the α species has mass m_α, radius σ_α, number density n_α, and a reduced moment of inertia $\kappa_\alpha=4I_\alpha/m_\alpha\sigma_\alpha^2$. The rate of equilibration of the translational temperature of the α component is then given by

$$\frac{dT_{{\rm tr},\alpha}}{dt}=-\sum_\beta\frac{T_{{\rm tr},\alpha}-T_{{\rm tr},\beta}}{\tau_{\alpha\beta 1}}-\sum_\beta\frac{T_{{\rm tr},\alpha}-T_{{\rm rot},\alpha}}{\tau_{\alpha\beta 2}}-\sum_\beta\frac{T_{{\rm tr},\alpha}-T_{{\rm rot},\beta}}{\tau_{\alpha\beta 3}}. \quad (28)$$

The relaxation times, expressed in terms of the α-β collision frequency $Z_{\alpha\beta}=2\sigma_{\alpha\beta}^2 n_\beta(2\pi kT_{{\rm tr},\alpha\beta}/\mu_{\alpha\beta})^{\frac{1}{2}}$ are

$$\tau_{\alpha\beta 1}^{-1}=8\mu_{\alpha\beta}^2 Z_{\alpha\beta}(\kappa_{\alpha\beta}+1+\kappa_{\alpha\beta}B_{\alpha\beta})/3m_\alpha m_\beta(\kappa_{\alpha\beta}+1), \quad (29a)$$

$$\tau_{\alpha\beta 2}^{-1}=8\mu_{\alpha\beta}^2 Z_{\alpha\beta}\kappa_{\alpha\beta}B_{\alpha\beta}/3m_\alpha^2\kappa_\alpha(\kappa_{\alpha\beta}+1), \quad (29b)$$

and

$$\tau_{\alpha\beta 3}^{-1}=8\mu_{\alpha\beta}^2 Z_{\alpha\beta}\kappa_{\alpha\beta}B_{\alpha\beta}/3m_\alpha m_\beta\kappa_\beta(\kappa_{\alpha\beta}+1). \quad (29c)$$

In these formulas $\sigma_{\alpha\beta}=\sigma_\alpha+\sigma_\beta$, $\mu_{\alpha\beta}=m_\alpha m_\beta/(m_\alpha+m_\beta)$,

$$T_{{\rm tr},\alpha\beta}=M_\alpha T_{{\rm tr},\beta}+M_\beta T_{{\rm tr},\alpha},$$

and

$$\kappa_{\alpha\beta}=\kappa_\alpha\kappa_\beta/(M_\alpha\kappa_\alpha+M_\beta\kappa_\beta).$$

The roughness factors, $B_{\alpha\beta}=B_{\alpha\beta}(\rho)$, must satisfy conditions similar to (20),

$$B_{\alpha\beta}=0: \quad \text{perfectly smooth} \quad (30a)$$

$$B_{\alpha\beta}=\kappa_{\alpha\beta}/(\kappa_{\alpha\beta}+1): \quad \text{perfectly rough.} \quad (30b)$$

[10] B. Widom, J. Chem. Phys. **32**, 913 (1960).

The rate of change of the rotational temperature is

$$\frac{dT_{{\rm rot},\alpha}}{dt}=-\sum_\beta\frac{T_{{\rm rot},\alpha}-T_{{\rm rot},\beta}}{\tau_{\alpha\beta 1}'}-\sum_\beta\frac{T_{{\rm rot},\alpha}-T_{{\rm tr},\alpha}}{\tau_{\alpha\beta 2}'}-\sum_\beta\frac{T_{{\rm rot},\alpha}-T_{{\rm tr},\beta}}{\tau_{\alpha\beta 3}'}, \quad (31)$$

where

$$\tau_{\alpha\beta 1}'=(m_\beta\kappa_\beta/m_\alpha)\tau_{\alpha\beta 2}, \quad (32a)$$

$$\tau_{\alpha\beta 2}'=\tau_{\alpha\beta 2}, \quad (32b)$$

and

$$\tau_{\alpha\beta 3}'=(m_\beta/m_\alpha)\tau_{\alpha\beta 2}. \quad (32c)$$

Let us now attempt to relate the mathematical model of rough spheres to realistic collisional processes. With all due regard for the inherent limitations of any rigid molecular model, no one should be too seriously offended by the statement that spherical top molecules such as those mentioned above are knobby, the protrusions of peripheral groups providing the hooks and handles necessary for collisional transmission of angular momentum and energy. Therefore, a possible rationale for the rough sphere model is obtained by identifying roughness with knobbiness. Perfect roughness then implies a degree of knobbiness so extreme that slipping of the molecules over one another is utterly impossible. Such a drastic situation is very unlikely to exist. Instead, we are inclined to expect that a rather large fraction of the collisions will involve almost no surface friction, while in others roughness will be very much in evidence. Ideally one would examine these collisions of knobby molecules in full detail and then determine the rotational relaxation times by performing a statistical averaging over dynamical states. The rough sphere model replaces the first of these steps by an implicit but unspecified averaging procedure which serves to define a sort of "average collisional event." The before-the-fact nature of this averaging process would seem to preclude the possibility of determining a precise correlation between roughness and knobbiness. Nevertheless, an examination of the MO electron clouds for spherical tops or even of the familiar Hirschfelder classroom demonstration models does allow one to develop an intuitive feeling for the degree of roughness to be expected for a particular molecular species. While this does not provide a means for quantitatively estimating "absolute roughness factors," it could prove quite adequate for correlating and interpolating experimental data on rotational relaxation times of spherical top molecules. In fact, it seems likely that a close correlation will exist between the roughness parameter ρ and the ratio of the mean radius of curvature of peripheral groups to that of the entire molecule.

At the present time there appears to be no experimental data from which one can extract values for the effective roughness function $B(\rho)$. However, it is certainly reasonable to expect that most complex molecular species will behave more nearly as partially rough

than as perfectly rough spheres. Calculations based upon the assumption of perfect roughness may therefore grossly underestimate rotational relaxation times. This conclusion has an important bearing upon our use of the distribution function (23). Although it is generally agreed that the relaxation in momentum space to a Boltzmann distribution proceeds very rapidly, it is quite another thing to assume the establishment of separate Boltzmann distributions with different temperatures for rotational and translational degrees of freedom. Indeed this will be a reasonable assumption only if the collisional mechanism provides for much more efficient translational-translational and rotational-rotational exchanges of energy than it does for the rotational-translational interchange. Thus, it is precisely the case for which the roughness function is small compared to unity, i.e., when the rough sphere equivalent to the knobby molecule is very nearly smooth, where the use of a two-temperature distribution function will be justified. We assume this type of poor communication between translational and rotational degrees of freedom to exist here in the case of rough spheres and in the following sections where spherocylinders and loaded spheres are considered.

As a final step let us examine the rotational relaxation of rough spheres α in the presence of an "atomic species" β. The physical model here is that of point masses colliding with a rough molecule of radius $\sigma_{\alpha\beta}=\sigma_\alpha+\sigma_\beta$. This case can be obtained directly from our previous results by setting $\kappa_\beta=0$. Thus,

$$\frac{dT_{\mathrm{rot},\alpha}}{dt}=-\left[\frac{16}{3}\frac{\mu_{\alpha\beta}n_\beta\sigma_{\alpha\beta}^2}{m_\beta}\frac{B_{\alpha\beta}}{\kappa_{\alpha\beta}+1}\left(\frac{2\pi kT_{\mathrm{tr},\alpha\beta}}{\mu_{\alpha\beta}}\right)^{\frac{1}{2}}\right]$$

$$\times(T_{\mathrm{rot},\alpha}-T_{\mathrm{tr},\beta})-\frac{16}{3}\left[\frac{\mu_{\alpha\beta}n_\beta\sigma_{\alpha\beta}^2}{m_\alpha}\frac{B_{\alpha\beta}}{\kappa_{\alpha\beta}+1}\left(\frac{2\pi kT_{\mathrm{tr},\alpha\beta}}{\mu_{\alpha\beta}}\right)^{\frac{1}{2}}\right.$$

$$\left.+\frac{n_\alpha B_{\alpha\alpha}\sigma_{\alpha\alpha}^2}{\kappa_{\alpha\alpha}+1}\left(\frac{4\pi kT_{\mathrm{tr},\alpha}}{m_\alpha}\right)^{\frac{1}{2}}\right](T_{\mathrm{rot},\alpha}-T_{\mathrm{tr},\alpha}),\qquad(33)$$

where $\kappa_{\alpha\alpha}=2\kappa_{\alpha\beta}\mu_{\alpha\beta}(\sigma_{\alpha\beta}/\sigma_{\alpha\alpha})^2/m_\alpha$ and $\kappa_{\alpha\beta}=I_\alpha/\mu_{\alpha\beta}\sigma_{\alpha\beta}^2$.

The reciprocal of the coefficient of $T_{\mathrm{rot},\alpha}-T_{\mathrm{tr},\beta}$ in (33) should correspond to the atom–rough sphere relaxation time calculated by Widom. A direct comparison of his results with ours is obtained by considering the product of this relaxation time [Eq. (33)] with the collision frequency $Z_{\alpha\beta}$. This derived quantity, which represents the number of collisions required to effect thermal equilibrium between the atomic translational temperature and the molecular rotational temperature, is found to be

$$N_{\mathrm{rot},\alpha}{}^{\mathrm{tr},\beta}=\tfrac{3}{8}[(m_\alpha+m_\beta)/m_\alpha][(\kappa_{\alpha\beta}+1)/B_{\alpha\beta}].\qquad(34)$$

For the case of perfect roughness ($\rho=1$) our formula (34) contains a factor of $(m_\alpha+m_\beta)/m_\alpha$ which does not appear in Widom's result.[11] The reason for this difference lies in the fact that Widom took the rough spheres to be at rest translationally and so effectively endowed them with infinite inertial masses. From (34) we see that light atoms are more efficient than heavy ones in robbing rough spheres of their rotational energy.

[11] Our $\sigma_{\alpha\beta}=\sigma_\alpha+\sigma_\beta$ is to be identified with Widom's molecular radius a.

IV. ROTATIONAL RELAXATION OF SPHEROCYLINDERS

The remainder of this paper is devoted to the calculation of rotational relaxation times for molecules which interact with impulsive, noncentral forces and whose internal mass distributions are nonspherical. The surfaces of the molecules with which we shall be concerned are rigid, smooth, convex and symmetrical about a principal axis of the internal mass distribution. As a first step it will be established that for such molecules the component of internal angular momentum about the symmetry axis is collisionally invariant.

We denote by $\boldsymbol{\delta}_1$ and $\boldsymbol{\delta}_2$ the vectors from the centers of mass of two such molecules to the point of their mutual contact at the instant of collision, and by $\mathbf{k}$ the unit vector directed toward molecule 2 and normal to the common tangent plane at the point of contact. All three of these vectors lie in the plane determined by $\mathbf{e}_1$ and $\mathbf{e}_2$, the unit vectors directed along the molecular symmetry axes. The rotation matrix associated with the transformation from the space-fixed frame of reference to that fixed in the ith molecule will be indicated by the symbol $\mathbf{R}_i$. The orientation of this body-fixed frame (with orthonormal unit vectors $\mathbf{x}_i$, $\mathbf{y}_i$, and $\mathbf{z}_i$) is such that $\mathbf{z}_i$ lies in the direction of $\mathbf{R}_i\cdot\mathbf{e}_i$, i.e., $\mathbf{z}_i=\mathbf{R}_i\cdot\mathbf{e}_i$.

The equations of impact for molecules of this sort are [in analogy with (14) and (15)]

$$m_2(\mathbf{c}_2'-\mathbf{c}_2)=-m_1(\mathbf{c}_1'-\mathbf{c}_1)=\mathbf{k}(\mu J/2).\qquad(35)$$

$$\mathbf{I}_1\cdot(\mathbf{w}_1'-\mathbf{w}_1)=-(\boldsymbol{\delta}_1\times\mathbf{k})(\mu J/2),\qquad(36a)$$

$$\mathbf{I}_2\cdot(\mathbf{w}_2'-\mathbf{w}_2)=(\boldsymbol{\delta}_2\times\mathbf{k})(\mu J/2),\qquad(36b)$$

where $\mathbf{c}_i$ and $\mathbf{w}_i$ are the linear and rotational velocities, respectively, and $\mathbf{I}_i$, the inertial tensor of the ith molecule (referred to the space-fixed frame). The quantity $\mu J/2$ is the magnitude of the collisional impulse.

By employing the rotation matrices $\mathbf{R}_1$ and $\mathbf{R}_2$ we obtain from (36a) and (36b) the equations of impact for the axial components of the angular momenta of the two molecules

$$\mathbf{z}_1{}^T\cdot(\mathbf{R}_1\cdot\mathbf{I}_1\cdot\mathbf{R}_1{}^T)\cdot\mathbf{R}_1\cdot(\mathbf{w}_1'-\mathbf{w}_1)$$

$$=-\mathbf{z}_1{}^T\cdot\mathbf{R}_1\cdot(\boldsymbol{\delta}_1\times\mathbf{k})(\mu J/2)$$

$$=-\mathbf{e}_1{}^T\cdot(\boldsymbol{\delta}_1\times\mathbf{k})(\mu J/2)=0,\qquad(37a)$$

$$\mathbf{z}_2{}^T\cdot(\mathbf{R}_2\cdot\mathbf{I}_2\cdot\mathbf{R}_2{}^T)\cdot\mathbf{R}_2\cdot(\mathbf{w}_2'-\mathbf{w}_2)$$

$$=\mathbf{z}_2{}^T\cdot\mathbf{R}_2\cdot(\boldsymbol{\delta}_2\times\mathbf{k})(\mu J/2)$$

$$=\mathbf{e}_2{}^T\cdot(\boldsymbol{\delta}_2\times\mathbf{k})(\mu J/2)=0.\qquad(37b)$$

Here the superscript T indicates the transpose of a tensor. In proving this collisional invariance of the axial components of the angular momenta explicit use has been made of the coplanarity of the vectors $\mathbf{\delta}_i$, $\mathbf{e}_i$, and $\mathbf{k}$.

Due to the symmetry of the inertial tensor the collisional change of the rotational energy of the ith molecule may be expressed in the form

$$\Delta E_{\mathrm{rot},i}=\Delta(\tfrac{1}{2}\mathbf{w}_i^T\cdot\mathbf{I}_i\cdot\mathbf{w}_i)=\tfrac{1}{2}(\mathbf{w}_i'+\mathbf{w}_i)\cdot\mathbf{I}_i\cdot(\mathbf{w}_i'-\mathbf{w}_i). \tag{38}$$

To eliminate the post-collisional variables appearing in this formula we must employ the impact equations, (35) and (36). Since $\mathbf{\delta}_i$, $\mathbf{e}_i$, and $\mathbf{k}$ are coplanar, we may write $\mathbf{\delta}_i$ in the form $\mathbf{\delta}_i=\chi_i\mathbf{e}_i+\Psi_i\mathbf{k}$ and so deduce that $\mathbf{\delta}_i\times\mathbf{k}=\chi_i\mathbf{e}_i\times\mathbf{k}$. If $\mathbf{I}$ is nonsingular its inverse, $\mathbf{I}^{-1}$ will exist and so the impact equations can immediately be solved for the collisional increments of the angular velocities. By performing these operations and substituting the results into (38) one finds that

$$\Delta E_{\mathrm{rot},i}=\tfrac{1}{2}\mu J\left[\mathbf{k}^T\cdot(\mathbf{w}_i\times\mathbf{\delta}_i)\pm\tfrac{1}{4}\mu J\chi_i^2\sum_{s=1}^{3}\Gamma_{is}^{-1}(\mathbf{a}_{is}^T\cdot\mathbf{z}_i\times\mathbf{k})^2\right]. \tag{39}$$

In (39) $\mathbf{\Gamma}_i=\mathbf{R}_i\cdot\mathbf{I}_i\cdot\mathbf{R}_i^T$ is the (diagonal) inertial tensor referred to the coordinate frame fixed in the ith molecule. The plus sign appearing in (39) is to be used when $i=2$ and the negative when $i=1$. The vectors $\mathbf{a}_{is}$ are defined to be: $\mathbf{a}_{i1}=\mathbf{x}_i$, $\mathbf{a}_{i2}=\mathbf{y}_i$, and $\mathbf{a}_{i3}=\mathbf{z}_i$.

In the event that the inertial tensors are singular, i.e., if $\mathbf{z}_i^T\cdot\mathbf{\Gamma}_i\cdot\mathbf{z}_i=\Gamma_{i3}=0$, the inverse is not defined and so to solve the impact equations one must deal directly with the components of the rotational velocities. These manipulations are easily accomplished and the results, when substituted into (38), lead to the expression

$$\Delta E_{\mathrm{rot},i}=\tfrac{1}{2}\mu J\left[\mathbf{k}^T\cdot(\mathbf{w}_i\times\mathbf{\delta}_i)\pm\tfrac{1}{4}\mu J\chi_i^2\sum_{s=1}^{2}\Gamma_{is}^{-1}(\mathbf{a}_{is}^T\cdot\mathbf{z}_i\times\mathbf{k})^2\right]. \tag{40}$$

Because the term in (39) involving $s=3$ is identically zero, the two formulas (39) and (40) are precisely the same. Thus we see that the collisional change of the rotational energy for molecules with singular inertial tensors is in no way different from that for molecules with nonsingular mass distributions.

Because of its collisional invariance, the rotational degree of freedom associated with the symmetry axis of the convex molecule is "thermally inactive." This means that the equipartition theorem can not be applied to this degree of freedom even though the mass distribution be nonsingular. This unusual situation is an artifact arising from our definition of the molecular model, for even the very slightest amount of coupling would suffice to establish the thermal communication necessary for this degree of freedom to participate fully in determining the *equilibrium* properties of the fluid. However, kinetic theory calculations based upon molecular models of this sort must rely solely upon collision processes which are allowed *by the model* to effect transfers of energy and momentum. The rotational temperature should therefore be related to the mean rotational energy in the manner

$$nkT_{\mathrm{rot}}=\iiint f(\mathbf{c},\mathbf{w},\boldsymbol{\alpha})\tfrac{1}{2}\mathbf{w}^T\cdot\mathbf{I}\cdot\mathbf{w}d\mathbf{w}d\mathbf{c}d\boldsymbol{\alpha}, \tag{41}$$

since the inclusion of a factor of $\frac{3}{2}$ on the left-hand side of this formula would be inconsistent with the assumed collisional dynamics. The nature of the molecular interactions will also have a significant effect upon the attenuation of sonic disturbances by the gas for ϕ, the volume viscosity arising from the interchange of rotational and translational energy, is related to the corresponding relaxation time in the fashion

$$\phi=2\nu p\tau/3(\nu+3),$$

where p is the pressure and ν, the number of thermally active rotational degrees of freedom per molecule.[12] For rough spheres ν will be equal to 3 but $\nu=2$ for the class of convex molecules described above.

The spherocylindrical model is a special limiting case of the type of molecule just discussed. The virial coefficients for this model have been examined by Kihara[13] and the gas-transport coefficients investigated by Curtiss and Muckenfuss.[14] A spherocylinder is a rigid smooth cylinder of length L and radius a with rigid smooth hemispherical caps, also of radii a, attached at each end. By neglecting chattering—repetitive collisional contacts occurring in the course of an isolated binary encounter—an analysis of collisions between spherocylinders is easily accomplished. However, the error introduced by the omission of chattering will be negligible only if the eccentricities of the molecules are very small, i.e., if $L\ll a$. It should be noted that this same condition is necessary in justifying the use of the two-temperature distribution functions

$$f(\mathbf{c},\mathbf{w},\boldsymbol{\alpha})=n^*(\boldsymbol{\alpha})(m/2\pi kT_{\mathrm{tr}})^{\frac{3}{2}}[(\Gamma_1\Gamma_2\Gamma_3)^{\frac{1}{2}}/(2\pi kT_{\mathrm{rot}})^{\frac{3}{2}}]\times\exp[-mc^2/2kT_{\mathrm{tr}}-\mathbf{w}^T\cdot\mathbf{I}\cdot\mathbf{w}/2kT_{\mathrm{rot}}]. \tag{42}$$

Here, $n^*(\boldsymbol{\alpha})$ is the number density of molecules with a specific orientation, $\boldsymbol{\alpha}=(\alpha,\beta,\gamma)$ is the set of Eulerian

[12] M. Kohler, Z. Phys. **124,** 757 (1947); **125,** 715 (1949), and Sidney Chapman and T. G. Cowling, *The Mathematical Theory of Non-Uniform Gases* (Cambridge University Press, London, 1953), 2nd ed. p. 396. For a description of this attenuation in terms of the heat capacities associated with internal degrees of freedom, see K. F. Herzfeld, *Thermodynamics and Physics of Matter* (Princeton Press, Princeton, New Jersey, 1955).

[13] T. Kihara, J. Phys. Soc. Japan **6,** 289 (1951); Revs. Modern Phys. **25,** 831 (1953).

[14] C. F. Curtiss and C. Muckenfuss, J. Chem. Phys. **26,** 1619 (1957).

angles characterizing the orientation of the body-fixed reference frame, and $\Gamma_1\Gamma_2\Gamma_3$ the determinant of the inertial tensor.[15]

The relaxation equation can then be written in the form

$$dT_{tr}/dt = -(2/3nk)\int\cdots\int S(\mathbf{k})\mathbf{k}\cdot\mathbf{g}_{21}f(\mathbf{c}_1,\mathbf{w}_1,\boldsymbol{\alpha}_1)$$
$$\mathbf{k}\cdot\mathbf{g}_{21}<0$$
$$\times f(\mathbf{c}_2,\mathbf{w}_2,\boldsymbol{\alpha}_2)[E^2(\mathbf{k}\cdot\mathbf{g}_{21})^2+2E\mathbf{k}\cdot\mathbf{c}_1\mathbf{k}\cdot\mathbf{g}_{21}]$$
$$\times d\mathbf{c}_1 d\mathbf{w}_1 d\boldsymbol{\alpha}_1 d\mathbf{c}_2 d\mathbf{w}_2 d\boldsymbol{\alpha}_2 d\mathbf{k}, \quad (43)$$

where $S(\mathbf{k})d\mathbf{k}$ is the differential surface element of the excluded volume.[16] The function E is defined in the manner

$$E^{-1}=1+\mu[(\boldsymbol{\vartheta}_1\times\mathbf{k})\cdot\mathbf{I}_1^{-1}\cdot(\boldsymbol{\vartheta}_1\times\mathbf{k})$$
$$+(\boldsymbol{\vartheta}_2\times\mathbf{k})\cdot\mathbf{I}_2^{-1}\cdot(\boldsymbol{\vartheta}_2\times\mathbf{k})]. \quad (44)$$

Equation (43) can be integrated by the procedures developed by Curtiss and Muckenfuss. The result for a simple gas is

$$dT_{tr}/dt = -(T_{tr}-T_{rot})/\tau, \quad (45)$$

where

$$\tau^{-1}=(16n/3)(\pi kT_{tr}/m)^{\frac{1}{2}}[\Theta_{11}+2\Theta_{12}+\Theta_{22}], \quad (46)$$

and

$$\Theta_{11}=(2a)^2\int_0^1\int_0^1\frac{\alpha(2-x^2-y^2)[1+\alpha\epsilon(2-x^2-y^2)]^{\frac{1}{2}}}{[1+\alpha(2-x^2-y^2)]^2}dxdy, \quad (47a)$$

$$\Theta_{12}=La\int_0^1\int_0^1\frac{\alpha(1+x^2-y^2)[1+\alpha\epsilon(1+x^2-y^2)]^{\frac{1}{2}}}{[1+\alpha(1+x^2-y^2)]^2}dxdy, \quad (47b)$$

$$\Theta_{22}=\tfrac{1}{8}L^2\int_0^1\int_0^1\frac{\alpha(x^2+y^2)[1+\alpha\epsilon(x^2+y^2)]^{\frac{1}{2}}}{[1+\alpha(x^2+y^2)]^2}dxdy. \quad (47c)$$

The parameter α appearing in (47) is equal to

$$mL^2/8(\Gamma_1\Gamma_2\Gamma_3)^{\frac{1}{3}}$$

when $\mathbf{I}$ is nonsingular and $mL^2/8I$ when $\mathbf{I}$ is singular. When $\epsilon=T_{rot}/T_{tr}$ is equal to unity the Θ functions are related to the $U_{ij}^{(1)}$ integrals of Curtiss and Muckenfuss[14] in the manner $\Theta_{ij}=-(\alpha/2\pi)dU_{ij}^{(1)}/d\alpha$. In all other cases the Θ's must be evaluated by numerical methods.

The collision frequency can be expressed in the form

$$Z=4n(\pi kT_{tr}/m)^{\frac{1}{2}}(\Phi_{11}+2\Phi_{12}+\Phi_{22}) \quad (48)$$

and so the number of collisions required to achieve thermal equilibrium between the rotational and translational degrees of freedom is

$$N=\tfrac{3}{4}(\Phi_{11}+2\Phi_{12}+\Phi_{22})/(\Theta_{11}+2\Theta_{12}+\Theta_{22}). \quad (49)$$

The Φ integrals,

$$\Phi_{11}=(2a)^2\int_0^1\int_0^1[1+\alpha\epsilon(2-x^2-y^2)]^{\frac{1}{2}}dxdy, \quad (50a)$$

$$\Phi_{12}=La\int_0^1\int_0^1[1+\alpha\epsilon(1+x^2-y^2)]^{\frac{1}{2}}dxdy, \quad (50b)$$

and

$$\Phi_{22}=\tfrac{1}{8}L^2\int_0^1\int_0^1[1+\alpha\epsilon(x^2+y^2)]^{\frac{1}{2}}dxdy, \quad (50c)$$

can be integrated to give

$$\Phi_{11}=(4a^2/3)\left\{\left[\frac{3}{(\alpha\epsilon)^{\frac{1}{2}}}+5(\alpha\epsilon)^{\frac{1}{2}}\right]\sin^{-1}\left(\frac{\alpha\epsilon}{1+\alpha\epsilon}\right)^{\frac{1}{2}}\right.$$
$$\left.+1-\frac{(1+2\alpha\epsilon)^{\frac{1}{2}}}{\alpha\epsilon}\sin^{-1}\left(\frac{\alpha\epsilon}{1+\alpha\epsilon}\right)\right\}, \quad (51a)$$

$$\Phi_{12}=(La/3)\left\{\frac{1}{2}\left[\frac{3}{(\alpha\epsilon)^{\frac{1}{2}}}+4(\alpha\epsilon)^{\frac{1}{2}}\right]\sin^{-1}\left(\frac{\alpha\epsilon}{1+2\alpha\epsilon}\right)^{\frac{1}{2}}\right.$$
$$+\frac{1}{2}\left[\frac{3}{(\alpha\epsilon)^{\frac{1}{2}}}+2(\alpha\epsilon)^{\frac{1}{2}}\right]\sinh^{-1}(\alpha\epsilon)^{\frac{1}{2}}$$
$$\left.+(1+\alpha\epsilon)^{\frac{1}{2}}-\frac{(1+\alpha\epsilon)^{\frac{1}{2}}}{\alpha\epsilon}\sinh^{-1}\frac{\alpha\epsilon}{(1+2\alpha\epsilon)^{\frac{1}{2}}}\right\}, \quad (51b)$$

$$\Phi_{22}=(L^2/24)\left\{\left[\frac{3}{(\alpha\epsilon)^{\frac{1}{2}}}+4(\alpha\epsilon)^{\frac{1}{2}}\right]\sinh^{-1}\left(\frac{\alpha\epsilon}{1+\alpha\epsilon}\right)^{\frac{1}{2}}\right.$$
$$\left.+(1+2\alpha\epsilon)^{\frac{1}{2}}-(\alpha\epsilon)^{-1}\sin^{-1}\left(\frac{\alpha\epsilon}{1+\alpha\epsilon}\right)\right\}. \quad (51c)$$

The dependence of N upon α, ϵ, and $\beta=L/2a$ is shown in Fig. 2. From this figure we see that the number of collisions required to reduce the initial temperature difference by a factor of $1/e$ is quite insensitive to the values of the two temperatures. In fact, use of the value of N for $\epsilon=1$ over the entire range $0\leq\epsilon\leq2$ results in errors of less than 1%. For many simple molecules such as N_2, O_2, Cl_2, and CO_2, α lies in the range from 0.1 to 0.3 and so N varies from 4 to 8. Experimental measurements[17] for these gases yield values of N in this same range. Parker[18] has calculated rotational relaxation times based upon soft (nonimpulsive) pair interactions. For the molecular species mentioned above he found N to be about equal to 4 and to gradually increase with rising translational temperature. In the limit of rigid interactions his results, like ours, become virtually independent of temperature.

Equations (43) and (46) can be generalized in a straightforward manner to include an arbitrary number

[15] In the event that this tensor is singular $\Gamma_1\Gamma_2\Gamma_3$ must be replaced with I^3 where $I=\Gamma_1=\Gamma_2$.

[16] See reference (14) or J. S. Dahler, J. Chem. Phys. **30**, 1447 (1959) for details concerning the excluded volume.

[17] The sources of experimental data are listed in the article by Parker; cf. reference (18).

[18] J. G. Parker, Phys. Fluids **2**, 449 (1959).

of components. Since the results are quite lengthy, we present here only one special application of the general multicomponent formulas. In shock-tube experiments the polyatomic species is often present only in trace quantities and so the relaxation of the rotational temperature occurs principally as the result of atom-molecule collisions. By allowing one of the spherocylindrical species to degenerate into a sphere ($L_1=0$) we obtain from the binary rate expression the atom-molecule rotational relaxation time

$$\tau^{-1}=(8n_1/3)(2\pi kT_{\rm tr}/\mu)^{\frac{1}{2}}(\Theta_{11}^{(1)}+\Theta_{-1}^{(1)}). \tag{52}$$

In arriving at this result we have consistently neglected terms proportional to n_2, the number density of molecules, and have set the translational temperatures of both species equal to $T_{\rm tr}$. The atom-molecule collision frequency is found to be

$$Z=2n_1(2\pi kT_{\rm tr}/\mu)^{\frac{1}{2}}(\Phi_{11}^{(1)}+\Phi_{21}^{(1)})$$

and so the rotational collision number may be written as

$$N=\tfrac{3}{4}(\Phi_{11}^{(1)}+\Phi_{21}^{(1)})/(\Theta_{11}^{(1)}+\Theta_{21}^{(1)}). \tag{53}$$

Here

$$\Theta_{11}^{(1)}=2(a_1+a_2)^2\left\{-\frac{1}{2(1+\alpha)}+(\epsilon/\alpha)^{\frac{1}{2}}\sin^{-1}\left(\frac{\alpha\epsilon}{1+\alpha\epsilon}\right)^{\frac{1}{2}}\right.$$
$$\left.+\frac{1-2\epsilon+\alpha(2-3\epsilon)}{2[\alpha(\epsilon-1)]^{\frac{1}{2}}(1+\alpha)^{\frac{1}{2}}}\sin^{-1}\left[\frac{\alpha(\epsilon-1)}{1+\alpha\epsilon}\right]^{\frac{1}{2}}\right\}, \tag{54a}$$

$$\Theta_{21}^{(1)}=2L_2(a_1+a_2)\left\{-\frac{(1+\alpha\epsilon)^{\frac{1}{2}}}{2(1+\alpha)}+\sinh^{-1}(\alpha\epsilon)^{\frac{1}{2}}\right.$$
$$\left.+\frac{(1-2\epsilon)}{2[\alpha(\epsilon-1)]^{\frac{1}{2}}}\sinh^{-1}\left[\frac{\alpha(\epsilon-1)}{1+\alpha}\right]^{\frac{1}{2}}\right\}, \tag{54b}$$

$$\Phi_{11}^{(1)}=\tfrac{1}{2}(a_1+a_2)^2\left\{1+[1/(\alpha\epsilon)^{\frac{1}{2}}+(\alpha\epsilon)^{\frac{1}{2}}]\sin^{-1}\left(\frac{\alpha\epsilon}{1+\alpha\epsilon}\right)^{\frac{1}{2}}\right\}, \tag{54c}$$

$$\Phi_{21}^{(1)}=\tfrac{1}{4}L_2(a_1+a_2)\{(1+\alpha\epsilon)^{\frac{1}{2}}+[1/(\alpha\epsilon)^{\frac{1}{2}}]\sinh^{-1}(\alpha\epsilon)^{\frac{1}{2}}\}, \tag{54d}$$

and $\alpha=\mu L_2^2/4\Gamma_2$ and $\epsilon=T_{\rm rot,2}/T_{\rm tr}$.

V. ROTATIONAL RELAXATION OF LOADED SPHERES

A second example of the general model discussed at the beginning of Sec. IV is the loaded sphere. This model, which was previously considered by Jeans,[19] is a rigid sphere of radius a with its center of mass displaced from the geometrical center by a distance ξ. In this case $\mathbf{\sigma}_i\times\mathbf{k}$ is also equal to $-\boldsymbol{\xi}_i\times\mathbf{k}$, where $\boldsymbol{\xi}_i$ is the vector of length ξ directed from the center of mass to the center of geometrical symmetry of the ith molecule. The magnitude of the collisional impulse is given by $\frac{1}{2}\mu J=-2E\mu\mathbf{k}\cdot\mathbf{g}_{21}$, where

$$E^{-1}=1+\mu[(\boldsymbol{\xi}_1\times\mathbf{k})\cdot\mathbf{I}_1^{-1}\cdot(\boldsymbol{\xi}_1\times\mathbf{k})$$
$$+(\boldsymbol{\xi}_2\times\mathbf{k})\cdot\mathbf{I}_2^{-1}\cdot(\boldsymbol{\xi}_2\times\mathbf{k})]. \tag{55}$$

The mathematical procedure for this model is precisely analogous to that previously described for spherocylinders. Thus, by neglecting chattering (a reasonable approximation if $\xi\ll a$) one first constructs formulas for the collisional changes of the rotational and translational energies, then introduces two-temperature distribution functions, and finally evaluates the mean collisional rate of change of the molecular energies. For a simple gas the resulting equation of change is

$$dT_{\rm tr}/dt=-\tfrac{2}{3}dT_{\rm rot}/dt=-(T_{\rm tr}-T_{\rm rot})/\tau, \tag{56}$$

where the relaxation time is given by

$$\tau^{-1}=(16/3)n(\pi kT_{\rm tr}/m)^{\frac{1}{2}}\Theta_{11} \tag{57}$$

and the collision number by

$$N=\tfrac{3}{4}\Phi_{11}/\Theta_{11}. \tag{58}$$

The Θ and Φ integrals appearing in these formulas are the same as those given by (47a) and (50a); here α is to be identified with $m\xi^2/2(\Gamma_1\Gamma_2\Gamma_3)^{\frac{1}{2}}$ if the mass distribution is nonsingular or with $m\xi^2/2I$ if it is singular. When α is extremely small (compared with unity), Θ_{11} reduces to $\frac{4}{3}\alpha(2a)^2$ and the relaxation time given by (57) becomes identical to that reported by Jeans. The functional dependence of N on ϵ and α is given in Fig. 2 as the lines corresponding to $\beta=0$.

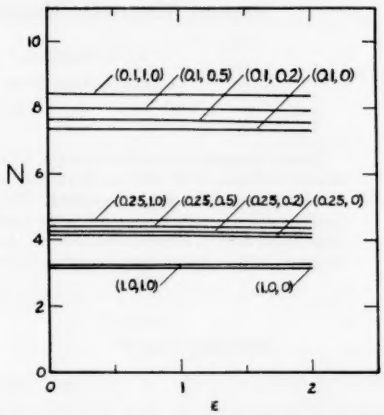

FIG. 2. Variation of the collision number for spherocylindrical molecules with the parameters ϵ, α, and β. Each curve is labeled with the two indices (α, β). The curves for which $\beta=0$ also apply to the collision numbers for the loaded sphere model described in Sec. V.

[19] J. H. Jeans, *The Dynamical Theory of Gases* (Cambridge University Press, London, 1916), p. 121. A recent study of this same model [J. S. Dahler, University of Wisconsin Naval Research Laboratory Rept. WIS-ONR-23 (1956)] will, in a revised and amended version, soon be submitted for publication.

Proton Magnetic Resonance Spectra of Vinylmethylsilanes

R. T. HOBGOOD,* J. H. GOLDSTEIN, AND G. S. REDDY
Chemistry Department, Emory University, Atlanta 22, Georgia
(Received May 10, 1961)

Proton magnetic resonance spectra of vinyltrimethylsilane and divinyldimethylsilane in dilute cyclohexane solution, at 40 Mc/sec, have been analyzed and the parameters compared with those obtained for alkylethylenes under similar conditions. The results indicate the presence of $d_\pi - p_\pi$ structures in these silanes. Additional anisotropy effects due to the presence of Si may also be involved but are believed not to be solely responsible for the effects observed. All the vinyl coupling constants are considerably greater than those observed in the alkenes, but are comparable to values obtained for molecules containing vinyl-metal bonds.

INTRODUCTION

A CONSIDERABLE body of evidence has been offered in support of the idea that silicon is able to withdraw π electrons from an unsaturated system to which it is bonded, despite the fact that it is less electronegative than carbon. Presumably this involves transfer of charge into the vacant d-orbitals of Si, an effect which is superposed on the usual inductive transfer in the opposite direction. Evidence for such $d_\pi - p_\pi$ bonding has been reported, for example, from studies of dipole moments,[1] molecular structure,[2] and Hammett σ constants.[3] This mechanism has also been invoked to account for certain aspects of the NMR spectra of compounds containing C—Si bonds.[4,5]

This communication reports the results of a detailed study and analysis of the NMR spectra of vinyltrimethylsilane ($ViMe_3Si$) and divinyldimethylsilane (Vi_2Me_2Si). The data so obtained have been examined for implications concerning the bonding situation in these compounds.

EXPERIMENTAL

The spectra were observed and measured at 21°C on the Varian model 4300B high-resolution spectrometer operating at 40 Mc/sec. Spectrograde cyclohexane was used as solvent and internal reference. The samples were the commercially available materials whose purity had been checked independently by gas chromatography. A TMS (tetramethylsilane) reference in cyclohexane was obtained by measurements at 20, 50, and 80%, with no perceptible concentration shift outside the mean deviation of the calibrations. The spectra of the silanes were observed at 10 and 50% concentration in cyclohexane with no measurable effect on selected strong peaks of the vinylic protons. Finally, the vinylic pattern of divinyldimethylsilane was observed in TMS and found to be identical with that in cyclohexane. Accordingly, the vinyl region was measured at ~10% and the methyl peak at ~50% in cyclohexane. Each spectrum was measured four times, and the mean deviation for each peak was 0.1 cps, or less.

Figure 1 shows the vinylic region of $ViMe_3Si$ which is that of a collapsed ABC pattern. The two small peaks designated 2 and 4 are real. They were repeatedly observed and were accounted for in the analysis. The methyl peak (not shown) is a single sharp peak, indicating the absence of any observable coupling with the vinyl protons. All of the observed peaks and their intensities are given in Tables I and II, except for the methyl peak which is simply listed as ω_d at the top of each table.

RESULTS AND DISCUSSION

The values of the chemical shifts and coupling constants, shown in Tables I and II, were obtained by numerically fitting the observed spectra. The maximum discrepancy between observed and calculated shifts, 0.2 cps, occurs for only two peaks, and the over-all agreement is within the mean deviation of the measurements. The calculated intensities also agree quite well, especially in view of the fact that partial overlapping of some of the stronger lines in the central region of the spectra increases the uncertainty in the observed intensities.

Initially, attempts were made to fit the spectra using trial values of the coupling constants typical of most vinylic systems. As these values failed to provide a satisfactory solution, the range was extended considerably. The final values obtained are much larger than the usual ones (J_{cis}~10 cps, J_{trans}~16 cps), but are quite comparable to the coupling constants recently reported for tetravinyltin, trivinylaluminum etherate, and divinylmercury.[6] It is interesting to observe that for all of these compounds and the silanes the sum of the coupling constants is ~40 cps. Commonly, this sum in vinyl derivatives will be ~20 cps or ~30 cps, the former being associated with substituents capable of donating lone-pair electrons and the latter with substituents that do not possess this

* National Science Foundation Cooperative Graduate Fellow, 1960–61.
[1] H. Soffer and T. DeVries, J. Am. Chem. Soc. **73,** 5817 (1951).
[2] K. Hedberg, J. Am. Chem. Soc. **77,** 77 (1955).
[3] R. A. Benkeser and H. R. Krysiak, J. Am. Chem. Soc. **75,** 2421 (1953).
[4] D. E. Webster, J. Chem. Soc. **1960,** 5132.
[5] E. Schnell and E. G. Rochow, J. Inorg. & Nuclear Chem. **6,** 303 (1958).
[6] D. W. Moore and J. A. Happe, J. Phys. Chem. **65,** 224 (1961).

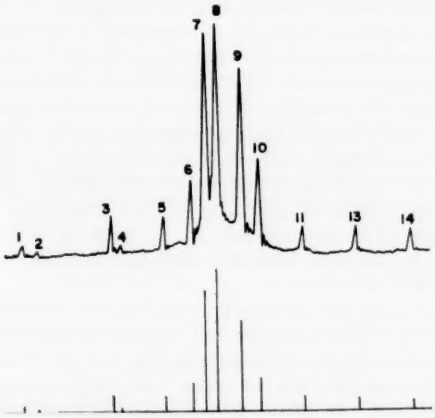

FIG. 1. Proton magnetic resonance spectrum of vinyltrimethylsilane in dilute cyclohexane solution (~10%) at 40 Mc/sec.

capacity.[7] The sum of 40 cps is also associated with relatively large values of J_{gem}, implying a decrease in the HCH angle.[8] For tetravinylsilane two other sets of

TABLE I. NMR Spectrum and parameters for vinyltrimethylsilane.[a]

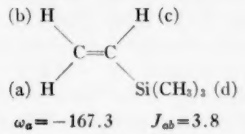

$\omega_a = -167.3$ $J_{ab} = 3.8$

$\omega_b = -177.0$ $J_{ac} = 20.4$

$\omega_c = -186.5$ $J_{bc} = 14.6$

$\omega_d = 55.4$

Peak No.	Frequency Obs	Frequency Calc	Intensity Obs	Intensity Calc
1	−209.4	−209.4	0.06	0.04
2	(−207.0)	−207.1	(0.01)	0.01
3	−195.1	−195.1	0.16	0.12
4	(−193.5)	−193.5	(0.02)	0.02
5	−186.1	−186.1	0.13	0.11
6	−181.5	−181.4	0.25	0.21
7	−179.1	−179.2	0.88	0.88
8	−177.5	−177.5	1.00	1.09
9	−174.0	−174.1	0.78	0.80
10	−171.7	−171.8	0.34	0.26
11	−165.5	−165.5	0.11	0.10
12	...	−163.2	...	...
13	−158.2	−158.2	0.12	0.09
14	−149.6	−149.6	0.09	0.07
15	...	−142.2	...	0.01

[a] Values are in cps at 40 Mc/sec relative to cyclohexane as solvent and internal reference. Values in parentheses were measured by interpolation between peaks calibrated from sideband markers, and are probably accurate to within 0.3 cps.

[7] G. S. Reddy and J. H. Goldstein, J. Chem. Phys. **35,** 380 (1961).

[8] H. S. Gutowsky, M. Karplus, and D. M. Grant, J. Chem. Phys. **31,** 1278 (1959).

TABLE II. NMR Spectrum and parameters for divinyldimethylsilane.[a]

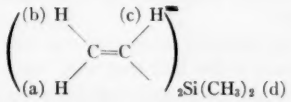

$\omega_a = -168.7$ $J_{ab} = 3.7$

$\omega_b = -179.3$ $J_{ac} = 20.2$

$\omega_c = -186.3$ $J_{bc} = 14.6$

$\omega_d = 52.9$

Peak No.	Frequency Obs	Frequency Calc	Intensity Obs	Intensity Calc
1	−209.4	−209.4	0.03	0.03
2	...	−208.2	...	0.01
3	−195.4	−195.4	0.12	0.11
4	...	−194.0	...	0.01
5	−188.1	−188.1	0.12	0.11
6	−181.4	−181.2	0.33	0.21
7	−180.0	−180.0	0.98	0.81
8	−179.0	−179.0	1.00	1.00
9	−175.5	−175.3	0.78	0.73
10	−174.1	−174.1	0.37	0.24
11	−166.2	−166.2	0.09	0.09
12	...	−165.0	...	0.00
13	−159.9	−160.0	0.09	0.08
14	−150.8	−150.8	0.06	0.06
15	...	−144.9	...	0.01

[a] Values are in cps at 40 Mc/sec relative to cyclohexane as solvent and internal reference.

coupling constants have recently been reported: $J_{gem} = 1.0$, $J_{cis} = -10.7$, $J_{trans} = 15.3$ and $J_{gem} = 0.2$, $J_{cis} = -11.6$ and $J_{trans} = 14.4$.[9] However, difficulties in identification due to overlapping of some spectral lines were reported and in any case these parameters will not fit our spectra.

In order to discuss the chemical shifts of the two silanes they have been converted to a TMS reference and are compared with the vinyl proton shifts for hexene-1[10] in Table III. The hexene values differ by no

TABLE III. Comparison of chemical shifts in vinylsilanes and hexene-1.[a]

	Hexene-1	Vi_2Me_2Si	$ViMe_3Si$
ω_a (*cis*)	−197.6	−226.6	−225.2
ω_b (*trans*)	−195.1	−237.2	−234.9
ω_c (α)	−228.7	−244.2	−244.4
ω_{Me}	−80.0[b]	−5.0	−2.5

[a] All values in cps at 40 Mc/sec relative to TMS, using −57.9 cps as the shift of cyclohexane relative to TMS. The values for hexene-1 are those of reference 10, converted to 40 Mc/sec.

[b] Terminal methyl group in butene 1. Data from reference 10 converted to 40 Mc/sec.

[9] W. Brugel, Th. Ankel, and F. Kruckeberg, Z. Elektrochem. **64,** 1121 (1960).

[10] A. A. Bothner-By and C. Naar-Colin, J. Am. Chem. Soc. **83,** 231 (1961).

more than a cycle from those for propylene, and were obtained under conditions quite similar to those employed here.

The most unusual feature of the vinyl proton shifts in the silanes is the fact that they are all considerably lower than the corresponding shifts in hexene-1. The greatest difference occurs for the *trans* proton which in the silanes is about 40 cps lower than that in hexene-1 or propylene. Since the shift for ethylene in dilute TMS solution is -211 cps it is evident that alkyl substitution, as in propylene or hexene-1, displaces each β proton upfield by 13–16 cps. In view of the fact that carbon is appreciably more electronegative than silicon ($x_C=2.5$ and $x_{Si}=1.8$),[11] an even greater upfield displacement would be expected on the basis of naive inductive considerations alone. However, $d_\pi-p_\pi$ bonding between carbon and silicon would oppose this effect and could conceivably reverse it.

Additional evidence of an indirect nature bearing on the possibility of $d_\pi-p_\pi$ bonding in the vinylsilanes is provided by the NMR spectrum of vinyltrichlorosilane, $ViSiCl_3$. As observed here, the spectrum of this compound in TMS ($\sim$10% solution) consists of a single slightly broadened peak, with a suggestion of structure, at -248 cps from TMS. The spectrum appears to be that of a strongly collapsed ABC system, with all three vinylic shifts lying near -248 cps. Examination of the spectrum in 5% TMS solution also revealed no significant concentration effect. Comparison with the vinylic shifts in $ViMe_3Si$ indicates that replacement of the three methyl groups by chlorines has affected the α proton only moderately, $\sim$4 cps, but has displaced the β protons downfield by 10–20 cps. This could be accounted for by an increase in $d_\pi-p_\pi$ bonding resulting from the electron-withdrawing effect of the chlorine atoms on the silicon atom, which would act to release silicon orbitals for use in double bonding. Such an explanation, for example, has been proposed to account for the dependence of the Si-Cl bond length upon the nature of the other groups attached to the Si atom.[12]

To a lesser extent, progressive replacement of methyl by the more electronegative vinyl group might also increase double-bonding, thus accounting for the downfield trends in Vi_2Me_2Si as compared with $ViMe_3Si$. The α-proton shifts are essentially identical in these two compounds but all other shifts are unmistakably, though not greatly, lower in the divinyl compound. The methyl shifts decrease regularly in the sequence TMS, $ViMe_3Si$, and Vi_2Me_2Si, indicating also the possible occurrence of such structures as $Me^+=Si^-=$. Hyperconjugated structures of this type have been suggested to account for the decrease in C-Si bond length in the sequence $MeSiH_3$, $MeSiH_2F$, and $MeSiHF_2$.[13,14]

It has at times been suggested that the anomalously low value of the α-proton shift in propylene might result from diamagnetic anisotropy of the $=C-C$ bond, but this explanation does not appear completely satisfactory at present.[10] In all the vinyl silanes discussed here the α-proton shifts (-244 to -248 cps) lie 15–20 cps lower than in propylene, and approach the α-shift value in vinyl chloride (-247 cps). A possible explanation for this situation could be formulated in terms of the anisotropy of the $=C-Si$ bond, which could reasonably be expected to exceed that in $=C-C$. Although this possibility should be left open, pending further investigation, the dependence of the β shifts upon the substituents on the Si atom indicates that $d_\pi-p_\pi$ bonding is at least partially, and possibly largely, responsible for the low values observed. Thus, for example, replacement of $-SiMe_3$ by $-SiCl_3$ depresses the β shifts by about the same amount as does replacement of an alkyl group by $SiMe_3$. This appears to be too great a change to ascribe solely to the difference in anisotropy of $C-SiMe_3$ and $C-SiCl_3$.

ACKNOWLEDGMENTS

The authors are indebted to the National Institutes of Health for a grant in partial support of this investigation, and to the National Science Foundation for a grant which provided the LGP-30 digital computer used in this study. They also wish to thank Miss Virginia H. Brinson for preparing the programs used in computing the spectral intensities.

[11] L. Pauling, *The Nature of the Chemical Bond* (Cornell University Press, Ithaca, New York, 1960), 3rd ed., p. 90.
[12] Reference 11, pp. 311–2.
[13] L. Pierce and D. H. Petersen, J. Chem. Phys. **33**, 907 (1960).
[14] J. M. O'Reilly and Louis Pierce, J. Chem. Phys. **34**, 1176 (1961).

THE JOURNAL OF CHEMICAL PHYSICS VOLUME 35, NUMBER 6 DECEMBER, 1961

Optical Absorption Study of Co-Doped Oxide Systems.* II

R. PAPPALARDO,† D. L. WOOD, AND R. C. LINARES, JR.
Bell Telephone Laboratories, Inc., Murray Hill, New Jersey

(Received May 22, 1961)

The optical absorption spectra of several Co-doped oxide systems (MgO, ZnO, aluminum spinel, yttrium gallium garnet, and germanium garnets) have been studied at room temperature, 78°, and 4.2°K, and analyzed using the formalism of the crystal-field theory. Oscillator strengths and cubic-field parameters have been derived. The observed data for tetrahedrally coordinated Co^{2+} are found to agree satisfactorily with the theoretical predictions. The effect of the spin-orbit coupling on the cubic-field terms has been calculated and the predicted splitting compared with the structure of the absorption bands of MgO:Co and ZnO:Co. The optical absorption properties of MgO:Co and ZnO:Co are used to infer the site symmetry of Co^{2+} in systems (spinels and garnets) in which the cations occupy sites of different symmetry.

I. INTRODUCTION

THE optical absorption properties of oxide systems doped with Ni have been discussed in the previous article,[1] using the formalism of the crystal-field theory with considerable success, even in the case of ZnO, whose properties are usually treated using the approximation of the band model.

A similar approach will be presently used in considering the optical properties of the oxide systems previously investigated, and doped now with Co. Also with the Co-doped systems in question, the experimental study was begun with the aim of verifying some predictions of the crystal-field theory for tetrahedrally coordinated ions and in order to have some direct evidence as to the ionic site preference in spinel and garnet systems, where the iron-group ions have available different valence states and different symmetry sites.

Another general purpose of the present study was to look for narrow absorptions, using properly dilute samples and low temperatures, since, whenever experimentally narrow absorptions are found, more detailed information can be obtained on the nature of the electronic energy levels of unfilled *d*-shell systems and, by inference, on the effect of the rest of the lattice at the site of the paramagnetic electron. So the following oxide systems have been studied: Co-doped single crystals of MgO; ZnO; $MgAl_2O_4$, yttrium gallium garnet, and two germanium garnet powders. The origin and preparation of the samples will be discussed in the sections describing the details of the absorption spectra. Details of the experimental procedure are given in references 1 and 2.

II. MgO:Co

A. Observed Spectrum

The absorption spectrum of a Co-doped magnesium oxide crystal has been reported by Low.[3] The spectra we report here show considerably more detail and have furthermore been taken at much lower temperatures. Co ions in MgO are octahedrally coordinated to the oxygen anions. Therefore the spectra of MgO:Co together with the corresponding ones for ZnO:Co, in which Co is tetrahedrally coordinated, form reference spectra from which conclusions may be drawn by analogy about the site preference of the Co impurity in systems where different kinds of sites are available.

Also, in a system possessing cubic symmetry and a center of inversion, such as MgO, effects due to lattice vibrations should be very important in making possible electric-dipole transitions within the 3*d* shell. The presence of considerable structure in the observed absorption should be of great help in performing an analysis of the lattice vibrations associated with the electronic transitions. The importance of these spectra, in connection with the analogous spectrum of ZnO:Co (where the site symmetry is tetrahedral) is that it allows one to draw conclusions from the absorption spectra, as to the site preference of Co in various systems (spinel, garnets, etc.) where different kinds of sites are available to the Co impurity ions.

The pink MgO crystal used (3.7 mm thick) was supplied by Semielements Inc., Saxonbourg, Pennsylvania and has a spectrum consisting of two groups of absorptions, one near 8500 cm^{-1} and one near 20 000 cm^{-1}. The absorption spectra at 78° and 4.2°K are shown in Figs. 1 and 2 and relevant data are listed in Tables I and II. The effects of cooling from 78° to 4.2°K on the first absorption band at 8500 cm^{-1} are not very pronounced, with the exception of the remarkable sharpening of the first triplet A_0 at 8150 cm^{-1}. The energy separations of the components of the triplet are quite small (16 and 40 cm^{-1}, respectively) and the half-widths of the lines are only 6 and 11 cm^{-1}, at 4.2°K, with a scanning speed of 25 A/sec and slit-width 0.15 mm. The same triplet structure seems to be present, though less distinct, in the narrow absorptions we labeled A_1 and A_2 (Fig. 1).

The absorption band at 20 000 cm^{-1} has a threefold structure at 78°K, with the main peaks separated by some 1000 cm^{-1} and it shows some finer structure at 4.2°K (Fig. 2, Table II).

* Paper presented at the Thanksgiving meeting of the American Physical Society, Chicago, November, 1960.
† Visiting Scholar, 1959–60.
[1] R. Pappalardo, D. L. Wood, and R. C. Linares, Jr., J. Chem. Phys. **35**, 1460 (1961).
[2] R. Pappalardo and D. L. Wood, J. Chem. Phys. **33**, 1734 (1960).
[3] W. Low, Phys. Rev. **109**, 256 (1958).

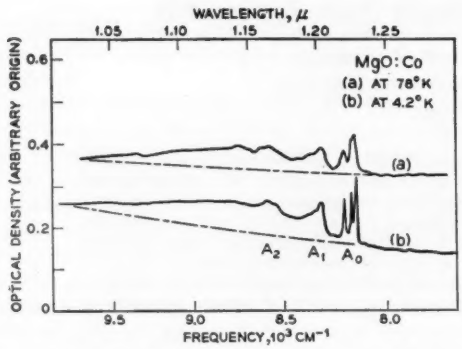

FIG. 1. Absorption in the 8500 cm^{-1} region of a single crystal of MgO:Co. Sample thickness, 0.37 cm. Amount of Co, 0.20% of total weight. (a) At 78°K. (b) At 4.2°K. The ordinates are given in optical density $[\log_{10}(I_0/I)]$.

B. Identification of Bands and Determination of Crystal-Field Parameters

There is little doubt that the absorption is due[3–5] to Co^{2+}. Since there is only a small amount of Co present in the crystal, one expects to detect only the crystal-field transitions which have higher probability, namely, the transitions within quartet cubic-field terms.[6] The energy separation of these levels, in a treatment which neglects the effects due to the spin-orbit interaction,[7] is expressed in terms of two parameters Dq and B as shown in Table III, together with the corresponding absorption bands.

With typical values for the parameters found for divalent ions[5,7] in octahedral coordination of oxygens (and water molecules), namely $Dq/B \sim 1$, a doublet term $_a{}^2E$ is predicted to have energy close to that of $^4F_2$. This might in principle affect the position of $^4F_2$ when spin-orbit coupling is taken into account. At any rate, we assume this effect to be small (this will be discussed later) and that the position of $^4F_2$ coincides with the observed triplet A_0 (that is, within the uncertainty of a lattice vibrational energy and of the spin-orbit stabilization both of $^4F_2$ and $_a{}^4F_1$, to be discussed later).

As far as the band B at $\sim 20\,000$ cm^{-1} is concerned, one expects the quartet $_b{}^4F_1$ and $^4A_2$ to fall close in energy to the doublets $_a{}^2F_1$, $_a{}^2F_2$; so we tentatively assign the position of the baricenter of the $_b{}^4F_1$ multiplet as the center peak of band C. These assignments allow the determination of the values of the crystal parameters as

$$B = 845 \text{ cm}^{-1}; \quad |Dq| = 927 \text{ cm}^{-1}; \quad Dq/B = 1.097. \quad (1)$$

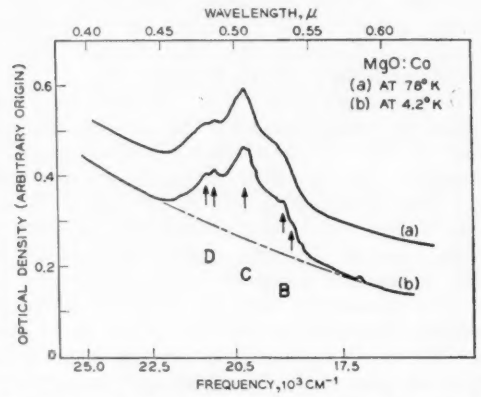

FIG. 2. Same as Fig. 1, but in the 20 000 cm^{-1} region. (a) At 78°K. (b) At 4.2°K. Arrows indicate minor structure present at 4.2°K.

TABLE I. MgO:CO (0.20% of total weight). Sample 0.37 cm thick. Temperature: 78°K.

Absorption peaks	Wavelength (Å)	Wave number (cm^{-1})	Extinction coefficient α_{max} (cm^{-1})	Half-width at $\alpha=\frac{1}{2}\alpha_{max}$ (cm^{-1})	Oscillator strength
A_0	12 270	8150	0.24	30	2.7×10^{-7}
	12 245	8166	0.13		
A_1	12 025	8316	0.16	20	1.2×10^{-7}
A_2	11 650	8583	0.15		1.7×10^{-6} [a]
	11 420	8756	0.13		
	7100 (?)	14 084 (?)			
B	5300 [b]	18 868	0.3		1.6×10^{-5}
C	5065	19 745	0.6		
D	4850	20 618	0.32		

[a] Inclusive of long tail towards high energies (Fig. 1).
[b] Shoulder.

TABLE II. MgO:Co (0.20%); Sample 0.37 cm thick. Temperature 4.2°K.

Absorption peaks	Wavelength (Å)	Wave number (cm^{-1})	Extinction coefficient α_{max} (cm^{-1})	Half-width at $\alpha=\frac{1}{2}\alpha_{max}$ (cm^{-1})	Oscillator strength
A_0	12 275	8146.6	0.43	6	1.0×10^{-7}
	12 250	8163.2	0.38	11	1.6×10^{-7}
	12 190	8203	0.32	11	1.3×10^{-7}
A_1	12 020	8319.4	0.24		4.0×10^{-7}
	11 975	8350.7	0.18		
	11 900	8403.3	0.17		
A_2	11 700	8547	0.17		2.3×10^{-6} [a]
	11 630	8598.4	0.21		
	11 583	8633.3	0.17		
B	5388	18 559			
	5320	18 797	0.32		
C	5070	19 723	0.6		1.6×10^{-5}
D	4865	20 555	0.6		
	4800	20 833			

[a] Inclusive of long tail to high energies (Fig. 1).

[4] A. Abragam and M. H. L. Pryce, Proc. Roy. Soc. (London) **A205,** 135 (1951); **A206,** 173 (1951).
[5] C. K. Jørgensen, Report to the Tenth Solvay Council, 1956.
[6] The considerations of the present article will only be related to cubic-field terms (identified by a given ST, e.g., $^4F_2$) so that no confusion should arise with the free-ion multiplet components $^{2S+1}L_J$.
[7] Y. Tanabe and S. Sugano, J. Phys. Soc. Japan **9,** 753 (1954).

TABLE III. MgO:Co. Quartet terms (see text).

Cubic-field term		Energy	Observed absorption
$a\,{}^4F_1$	(mainly $de^3d\gamma^3$)	ground term.	
${}^4F_2$	($de^4d\gamma^3$)	$\frac{1}{2}[10Dq-15B+(225B^2+180BDq+100Dq^2)^{\frac{1}{2}}]$	8150 cm^{-1} (group A_0)
$b\,{}^4F_1$	(mainly $de^4d\gamma^3$)	$[225B^2+180BDq+100Dq^2]^{\frac{1}{2}}$	19 700 cm^{-1} (central peak of band)
${}^4A_2$	($de^3d\gamma^4$)	$\frac{1}{2}[30Dq-15B+(225B^2+180BDq+100Dq^2)^{\frac{1}{2}}]$	

The position of the doublet terms will also depend on the value of the parameter C of electrostatic interaction. When this is known, the eigenvalues of the orbital and Coulombic energy are obtained by solving secular equations of the fifth order for ${}_i{}^2F_1$ and ${}_i{}^2F_2$, and of fourth order for ${}_i{}^2E$.

The energy-levels scheme of Fig. 3 has been drawn assuming the value $C=4.5\ B$. Wavefunctions for the various doublet terms in the cubic-symmetry basis are tabulated in Appendix I.

C. Spin-Orbit Coupling Effects for Co^{2+}

Since the absorption shows considerable structure, it will be worth while to see if this structure can be correlated to spin-orbit effects. Both in tetrahedral and octahedral coordination the ground state of Co^{2+} is a quartet; this implies that the more intense transitions within the $3d$ shell will connect the quartet levels.

When the spin-orbit coupling interaction is taken into account, some of the degeneracy of the cubic-field terms (characterized by a given couple of $S\Gamma$ quantum numbers) is lifted and accordingly the cubic-field terms will split. We are, in particular, interested in considering these effects on the quartet levels.

A prediction of the maximum number of levels to be expected from the spin-orbit splitting of the cubic-symmetry terms can be obtained by considering the transformation properties of the spin and angular momentum product space. Since the cubic-group representation corresponding[8] to $S=\frac{1}{2}$ is Γ_6 and that corresponding to $S=\frac{3}{2}$ is Γ_8 one will have to consider the products:

for
$$
\begin{aligned}
{}^4F_1&:\ \Gamma_8\times\Gamma_4=\Gamma_6+\Gamma_7+2\Gamma_8,\\
{}^4F_2&:\ \Gamma_8\times\Gamma_5=\Gamma_6+\Gamma_7+2\Gamma_8,\\
{}^4A_2&:\ \Gamma_8\times\Gamma_2=\Gamma_8,
\end{aligned}
\qquad (2)
$$

while for the doublet terms the corresponding products are

$$
\begin{aligned}
{}^2E&:\ \Gamma_6\times\Gamma_3=\Gamma_8,\\
{}^2F_1&:\ \Gamma_6\times\Gamma_4=\Gamma_8+\Gamma_6,\\
{}^2F_2&:\ \Gamma_6\times\Gamma_5=\Gamma_8+\Gamma_7.
\end{aligned}
\qquad (3)
$$

The effect of the spin-orbit coupling will also cause a mixing of the various cubic-field terms. The matrices of the spin-orbit coupling in such case are expressed as

$$\langle\alpha S\Gamma M_s\gamma\,|\,V_{q\gamma}(1F_1)\,|\,\alpha' S'\Gamma' M_s'\gamma'\rangle$$

and can be evaluated by using the formalism of Tanabe and Sugano[7] (TS) and the tables of Tanabe and Kamimura[9] (TK).

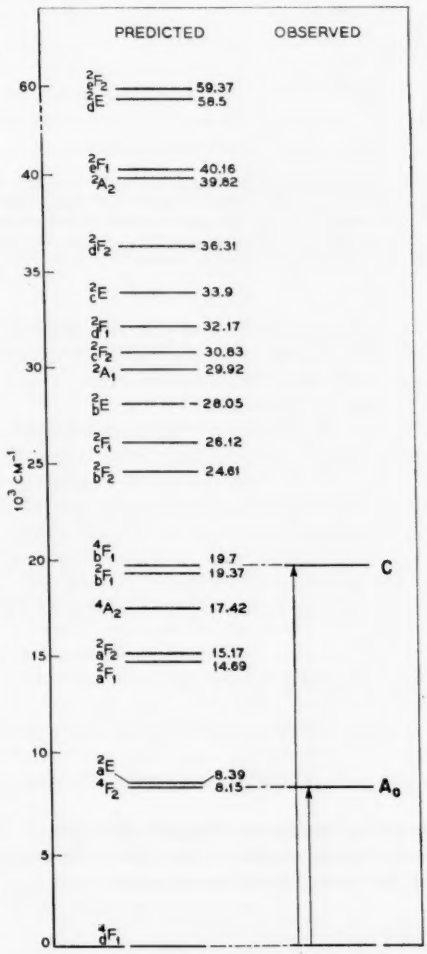

FIG. 3. Left: Energy-level scheme for Co^{2+} in MgO, assuming $|Dq|=927$ cm^{-1}; $B=845$ cm^{-1}; $C=4.5B$. Transitions to quartet terms are expected to have higher probability. Right: Position of experimental absorptions used in the calculations.

[8] H. Bethe, Ann. phys **3**, 181 (1929).

[9] Y. Tanabe and H. Kamimura, J. Phys. Soc. Japan **13**, 394 (1958).

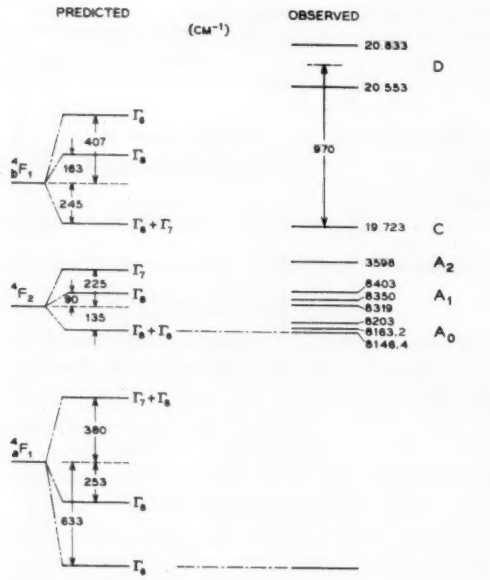

FIG. 4. Left: Spin-orbit splitting of quartet terms (first order); $c_b=1.81$; $c_a=-2.82$. The energy separation of cubic-field terms is only schematic. Right: Observed energy differences in the absorption of MgO:Co. The assignment is made that the first peak of the band in the visible is connected to ${}_b{}^4F_2$ (Fig. 3 and text).

For the sake of simplicity we shall first limit our considerations to matrix elements which are diagonal in the cubic-field terms, with some remarks about nondiagonal matrix elements.

In TS and TK formalism[7,9] the matrix elements are evaluated using systematically the Wigner-Eckart theorem[10] in order to split the matrix element into one part which depends on the symmetry properties of the system (implicitly expressed by Clebsch-Gordon coefficients) and another part, a double-barred matrix, which will be constant for given $S\Gamma$ and $S'\Gamma'$ pairs and all the allowed values of the pairs $M_s\gamma$ and $M_s'\gamma'$. In detail,

$$\langle \alpha S\Gamma M_s\gamma \mid V_{q\gamma}(1F_1) \mid \alpha' S'\Gamma' M_s'\gamma' \rangle = \langle \alpha S\Gamma \parallel V(1F_1) \parallel \alpha' S'\Gamma' \rangle [(2S+1)(\Gamma)]^{-\frac{1}{2}} \times (SM_s \mid S'M_s'q)(\Gamma\gamma \mid \Gamma'\gamma' F_1\tilde{\gamma}). \quad (4)$$

The following results are obtained: For the ${}^4F_2$ term, one finds the eignevalues of the spin-orbit energy by solving the following secular equation:

$$\parallel \langle {}^4F_2 M_s\gamma \mid V_{q\gamma}(1F_1) \mid {}^4F_2 M_s'\gamma' \rangle - W_s\delta(M_sM_s')\delta(\gamma\gamma') \parallel = 0. \quad (5)$$

[10] M. E. Rose, *Elementary Theory of Angular Momentum* (John Wiley & Sons, Inc., New York, 1957).

The spin-orbit splitting in first-order is given by

$$W_1=-\tfrac{1}{4}\zeta_d$$

[sixfold degeneracy; representations $\Gamma_8+\Gamma_7$ (or Γ_6)]

$$W_2=\tfrac{1}{6}\zeta_d$$

(fourfold degeneracy; representations Γ_8)

$$W_3=\tfrac{5}{12}\zeta_d$$

[twofold degeneracy; representations Γ_6 (or Γ_7)]. (6)

Note, incidentally, that the prediction of the group-theory on the degeneracy of the resulting levels are verified in the results of the calculations. There exists, though, an accidental degeneracy of Γ_8 and one of the twofold-degenerate multiplet components. The relation between the two spin-orbit coupling constants in the JLSM scheme ($H_{so}=\lambda\mathbf{L}\cdot\mathbf{S}$) and in the zero-order scheme

$$(H_{so}=\sum_i \zeta_d \mathbf{l}_i\cdot\mathbf{s}_i),$$

both using cubic-symmetry $3d$ wave functions as basis, is given by $\zeta_d=-3\lambda$, and can also be derived using TK formalism.

It must be pointed out that the calculated first-order effect of spin-orbit coupling does not depend on the type of coordination present (octahedral, tetrahedral, or dodecahedral) but simply on the value of the spin-orbit constants. With $\lambda=-180$ cm^{-1}, which is the value deduced from free-ion emission spectra,[5] one has the energy splitting shown in Fig. 4.

The situation is less simple for ${}^4F_1$ symmetry species. There are in fact two such cubic-field terms ${}_a{}^4F_1$ and ${}_b{}^4F_1$, which are a linear combination of states with well-defined subshell configuration,

$$\mid {}_a{}^4F_1\rangle = \cos\theta \mid d\epsilon^4({}^3F_1)d\gamma^3\rangle - \sin\theta \mid d\epsilon^5 d\gamma^2({}^3A_2)\rangle, \quad (7)$$

and analogously for ${}_b{}^4F_1$. This implies that the value of the spin-orbit interaction matrices will depend on the values of the mixing coefficients $\cos\theta$ and $\sin\theta$. Since the mixing of states with well-defined subshell configuration is caused by the Coulombic interaction and depends on the crystal-field separation of the two terms $\mid {}^4F_1[d\epsilon^4({}^3F_1)d\gamma^3]\rangle$ and $\mid {}^4F_1[d\epsilon^5 d\gamma^2({}^3A_2)]\rangle$, one obtains $\cos\theta$ and $\sin\theta$ from the consideration of the secular determinant[7]

$$\begin{array}{c|cc} {}^4F_1 & d\epsilon^4({}^3F_1)d\gamma^3 & d\epsilon^5 d\gamma^2({}^3A_2) \\ \hline d\epsilon^4({}^3F_1)d\gamma^3 & 2Dq-3B-W & 6B \\ d\epsilon^5 d\gamma^2({}^3A_2) & 6B & -8Dq-12B-W \end{array} = 0 \quad (8)$$

with eigenvalues[11]

$$W_a=\tfrac{1}{2}[-15B+6Dq-(225B^2+180DqB+100Dq^2)^{\frac{1}{2}}],$$
$$W_b=\tfrac{1}{2}[-15B+6Dq+(225B^2+180DqB+100Dq^2)^{\frac{1}{2}}]. \quad (9)$$

A similar treatment for the spin-orbit splitting of $^4F_1$ has been given by Koide.[12] The nondiagonal matrix element in Eq. (8) is given by Koide with a different sign from Tanabe and Sugano.[7] Using the value $6B$ for the matrix element in question, we evaluated the spin-orbit splitting using TK formalism.[9]

First, the $^4F_1$ cubic-field terms are expressed as follows:

$$|\,{}_b{}^4F_1\rangle=\cos\theta\,|\,d\epsilon^4d\gamma^3\rangle-\sin\theta\,|\,d\epsilon^5d\gamma^2\rangle,$$
$$|\,{}_a{}^4F_1\rangle=\cos\theta'\,|\,d\epsilon^4d\gamma^3\rangle-\sin\theta'\,|\,d\epsilon^5d\gamma^2\rangle, \quad (7b)$$

and the mixing coefficients are obtained via the relations

$$\tan2\theta=-12B/(10Dq+9B);\quad \theta'=\theta-90°;$$
$$\sin2\theta=-12B(225B^2+180DqB+100Dq^2)^{-\frac{1}{2}}. \quad (8)$$

The spin-orbit splittings are

${}_n{}^4F_1$:

$$W_1=-\tfrac{1}{45}\zeta c_n, \quad \text{(sixfold: } \Gamma_8+\Gamma_7\text{)}$$
$$W_2=+\tfrac{1}{60}\zeta c_n, \quad \text{(fourfold: } \Gamma_8\text{)}$$
$$W_3=\tfrac{5}{12}\zeta c_n, \quad \text{(twofold: } \Gamma_6\text{)} \quad (9)$$

with $n=a,\ b$

$$c_b=\cos^2\theta-2\sin^2\theta-2\sin2\theta, \quad (10)$$

and similarly for c_a.

The value of c_n will be altered by a change of the coordination from octahedral to tetrahedral or cubic (body-centered). Once the values of B and Dq are known in a given coordination, $\tan2\theta$ and c_n can be easily evaluated.

In the particular case of MgO:Co^{2+} one finds, for $B=845$ cm^{-1}; $|Dq|=927$ cm^{-1}, the following expressions:

$$c_b=1.81, \qquad c_a=-2.81,[13] \quad (11a)$$
$$|\,{}_b{}^4F_1\rangle=0.9636\,|\,d\epsilon^4d\gamma^3\rangle+0.2672\,|\,d\epsilon^5d\gamma^2\rangle,$$
$$|\,{}^4F_1\rangle=-0.2672\,|\,d\epsilon^4d\gamma^3\rangle+0.9636\,|\,d\epsilon^5d\gamma^2\rangle. \quad (12)$$

As a check on the correctness of the form of the two wave functions, the energy separation of the two $^4F_1$ terms has been calculated directly using the wave functions and the values of the crystal-field parameters derived in Eq. (1). The energy separation obtained coincided with the numerical value given in Table III.

[11] We use for the sake of notational simplicity Dq^2 instead of the more correct $(Dq)^2$.
[12] S. Koide, Phil. Mag. 4, 243 (1959).
[13] In close agreement with Koide's values.[12]

As it will be shown treating the case of ZnO:Co, the corresponding spin-orbit splitting factors for $^4F_1$ terms are

$$c_b=1.835, \qquad c_a=-2.834, \quad (11b)$$

so that the difference from tetrahedral to octahedral coordination is not large. The numerical value of the splitting is given in Fig. 4.

The spin-orbit stabilization of the ground level is 633 cm^{-1}, and on account of the experimental uncertainty as to the position of the baricenter of ${}_b{}^4F_1$, no attempt will be made to improve the sets of values for B and Dq [Eq. (1)], by considering the small effect of the spin-orbit stabilization of the ground level.

D. Second-Order Treatment of Spin-Orbit Effects

So far we have only considered the effect of the spin-orbit coupling on the individual cubic-field terms. In a more complete treatment the mixing of different cubic-field terms should be taken into account, because it might considerably affect the energy of terms lying close to each other. Unfortunately, the complications of the secular equations to be solved are considerably increased in a second-order treatment. The first-order treatment of $^4F_1$, for example, involves a 12×12 secular determinant; in second order even limiting the mixing to one $^2F_1$ term, the secular equation has dimensions 18×18. We wish now simply to point out that spin-orbit mixing may *a priori* be important for $^4F_2$ and the nearby ${}_a{}^2E$ and for ${}_b{}^4F_1$ and ${}_b{}^2F_1$ (Fig. 3).

In order to have the eigenvalues and eigenvectors of the doublet terms it is necessary to know the parameter C of electrostatic interaction. When this is known, it is possible to express the doublets ${}_i{}^2F_1$ and ${}_i{}^2F_2$ as a linear combination of *five* states with definite subshell configuration and symmetry properties; similarly ${}_i{}^2E$ as a linear combination of *four* such states. However, in the limit in which the nondiagonal matrix elements of the Coulomb interaction are neglected, the lowest ^2E level will be (Appendix I) essentially $^2E(d\epsilon^5d\gamma)$ and as such it will not be coupled to $^4F_2(d\epsilon^4d\gamma^3)$ by spin-orbit interaction, as one can immediately see.

Second-order treatment of the spin-orbit mixing of $^4F_2$ and ${}_a{}^4F_1$ (also ${}_b{}^4F_1$) with other terms (doublets for simplicity) can be used to determine the symmetry properties of the multiplet components of $^4F_2$ and $^4F_1$ which are accidentally degenerate in first-order treatment.

This can be exemplified, for instance, by the mixing of $^4F_1$ and $^2F_1$. In the total angular momentum space the double-valued representations pertaining to $^4F_1$ and $^2F_1$ in cubic symmetry are

$$^4F_1\rightarrow\Gamma_6+\Gamma_7+2\Gamma_8, \quad (2b)$$
$$^2F_1\rightarrow\Gamma_6+\Gamma_8. \quad (3b)$$

When the angular part of the secular equation (18×18) for the mixing of $^4F_1$ and $^2F_1$ is considered, two roots

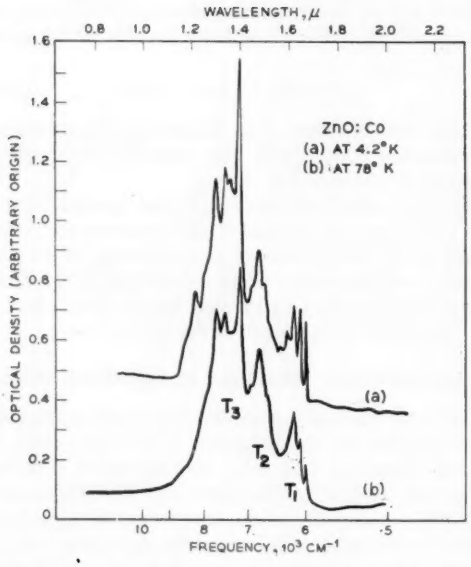

FIG. 5. ZnO:Co (0.17%; sample thickness, 0.2 mm). Absorption in the 7000 cm^{-1} region. (a) At 4.2°K. (b) At 78°K.

factor out of the secular equation. Their energy is $-\frac{1}{4}\zeta c_n$, so they belong to the sixfold-degenerate (first-order) multiplet components. This immediately shows that the transformation properties for the Kramers doublets contained therein is Γ_7. The results are shown in Eq. (9).

A similar reasoning applied to $^4F_2$ shows that the symmetry properties for the sixfold (first-order) multiplet component are Γ_8 and Γ_6.

E. Comments on the Structure of the Absorption

When the observed distance $A_0 \rightarrow A_1$ in the absorption at ~8000 cm^{-1} is compared with the predicted separation due to first-order spin-orbit effects, the agreement found is good (Fig. 4). As for the fine structure of triplet A_0, it could, for example, be due to higher-order effects of the spin-orbit interaction, or to very weak departure from cubic symmetry.

On the other hand, the observed agreement could be fortuitous; in fact, there is a close similarity in the structure of A_0, A_1, and A_2 to support the contention that A_1 and A_2 may be vibrational replicas of A_0. Also we would like to point out the close similarity in the separation of groups $A_0 \rightarrow A_1$; $A_1 \rightarrow A_2$ in MgO:Co and the separations of lines $A_1 \rightarrow A_2$; $A_2 \rightarrow A_3$ in MgO:Ni in the corresponding frequency region.[1] As far as the $_b{}^4F$ term is concerned, if the first peak of the group at 20 000 cm^{-1} is assigned, according to the energy-level scheme of Fig. 3, to $_b{}^2F_1$, then the central peak (19 720 cm^{-1}) and the third peak of the band at ~20 000 cm^{-1} correspond to the multiplet components of $_b{}^4F_1$. However, it is found that the width of the group is in poor agreement with the predicted multiplet width (Fig. 4).

On the other hand, an alteration of the value of the parameter C (we assumed $C=4.5B$) would increase the number of cubic-field terms with energy in the vicinity of the absorption band at ~20 000 cm^{-1}. Additional work on more heavily doped samples should be performed in order to find the position of some of the predicted doublet levels, so as to have a sounder experimental basis on which to try to interpret the absorption in the 20 000 cm^{-1} region.

III. ZnO:Co

A. Preparation of Samples

Thin plates of Co-doped single crystals of ZnO (hexagonal, zincite structure) were prepared using the flux technique,[14] in which the ZnO-PbF_2 melt contained in a platinum crucible was slowly cooled from 1150° to 800°C at the rate of cooling of 5°C/hr. Single crystals containing a nominal doping of 5% Co, are almost opaque in thickness ~0.010 in.: A more convenient amount of Co impurities was found with a nominal doping of 0.5%, the plates having a bluish-green color. The quantitative determination of Co-doping in the samples used was performed by Miss S. Vincent of these Laboratories using the x-ray fluorescence technique, and for a nominal doping of 0.5% Co, it was

TABLE IV. ZnO:Co 0.17% (0.02 cm thick) at 78°K.

Absorption peaks	λ (A)	$\bar{\nu}$ (cm^{-1})	Extinction coefficient α_{max} (cm^{-1})	Half-width at $\alpha=\frac{1}{2}\alpha_{max}$ (cm^{-1})	Oscillator strength
S_1[a]	24 160	4140	3.3		
S_2[a]	23 060	4336	3.3		
	16 640	6009	7	30	0.6×10^{-5}
T_1	16 400	6097.5	11.5		
	16 140	6195.8	15.5		
	15 040[b]	6649	19		
T_2	14 710	6798	27		0.6×10^{-3}
	14 400	6944	21		
	13 910	7189	40		
T_3	13 300	7518.8	32		
	12 990	7698	33		
	6490	15 408	120		
D	6390[b]	15 650			
	6265[b]	15 961			
	6140	16 268	100	~2000	0.6×10^{-2}
E	6000	16 666			
F	5665	17 652	32		
G	4940	20 243	4.5		

[a] In a sample 0.33 cm thick, and containing a nominal 5% Co.
[b] Shoulder.

[14] J. W. Nielsen and E. F. Dearborn, J. Phys. Chem. **64**, 1762 (1960).

found that the crystals actually contained 0.17% Co (of total weight). The ratio of Co ions to Zn ions is $Co/Zn \sim 2.1 \times 10^{-3}$. In the hexagonal ZnO structure, the coordination number for Zn is *four*, but the site symmetry is not perfectly cubic, due to an axial distortion.[1]

B. Observed Spectrum

The optical absorption was studied in samples containing 0.17% Co and some weaker absorptions also with a sample containing 5% Co (nominal). Two main absorptions were found, one in the infrared region at ~ 7000 cm^{-1} and another at 16 000 cm^{-1}.

At 78°K considerable structure is present in the band at ~ 7000 cm^{-1}: The absorption consists apparently of three triplets T_1, T_2, T_3 of progressively increasing intensity (Fig. 5, Table IV). The band in the visible region of the spectrum is very intense and rather narrow, showing a complex structure in which two peaks are dominant. On the high-energy side of this band a characteristic narrow absorption (F) is present and at $\sim 20\,000$ cm^{-1} a narrow absorption (G) which is very weak, appears (Fig. 6). Considerable sharpening in the fine structure components of the first intense band is found cooling the samples to 4.2°K (Fig. 5). At this temperature the only change that takes place for the band in the visible region, is the increase in the number of fine structure components. Pertinent data are listed in Tables IV and V.

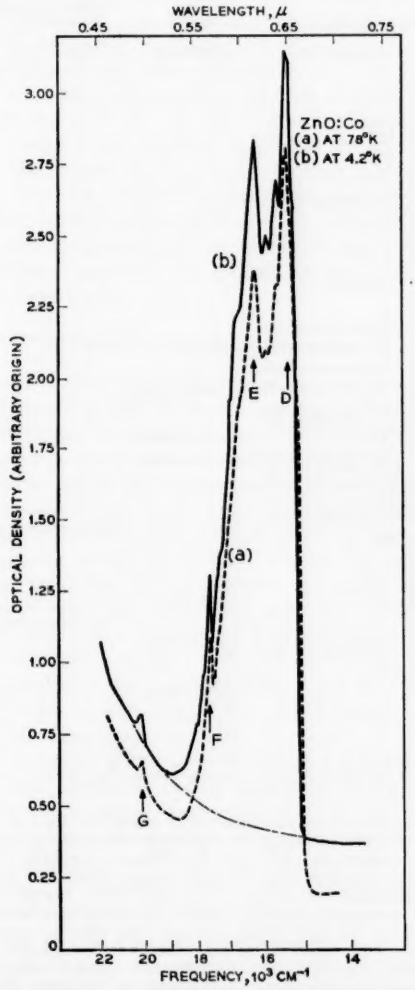

FIG. 6. Same as Fig. 5. Intense absorption band in the $\sim 16\,000$ cm^{-1} region. (a) At 78°K. (b) At 4.2°K.

TABLE V. ZnO:Co. 0.17% (0.02 cm thick) at 4.2°K.

Absorption peaks	λ (A)	$\bar{\nu}$ (cm^{-1})	Extinction coefficient α_{max} (cm^{-1})	Half-width at $\alpha = \frac{1}{2}\alpha_{max}$ (cm^{-1})	Oscillator strength
	16 540	6045.9	11	12.6	0.6×10^{-5}
T_1	16 390	6101.3	17.5	34	1.7×10^{-5}
	16 160	6188.1	18.5	47	2.5×10^{-5}
	15 900	6289.3	12.5		
	15 300	6535.9	9		
T_2	15 000	6666.6	17		
	14 730	6788.8	24		
	14 400	6944.4			
	13 950	7168.4	60		0.53×10^{-3}
	13 665	7317.9			
	13 510	7401.9	31.5		
T_3	13 335	7499	34		
	13 000	7692.3	32.5		
	12 500	8000	15.5		
	12 200	8196	10		
	6500	15 384	138		
D	6380	15 674	115		
	6270	15 949	107		0.68×10^{-3}
E	6150	16 260	120		
F	5665	17 652	40		
G	4950	20 202	4		

A more heavily doped sample (nominally 5% Co) was also studied at 78°K in the 4000 cm^{-1} region. There a band was detected (Fig. 7). The sensitivity of the instrumentation is not high in this region.

C. Interpretation of the Spectrum

The assumption is made that Co is present as Co^{2+} in sites possessing tetrahedral symmetry.[15] The ground state for Co^{2+} is then $^4A_2$ (as in the corresponding system Cr^{3+} in octahedral coordination). No appreciable stabilization of the ground state, due to spin-orbit coupling effects, is then expected in the present system.

[15] For Co^{3+} in tetrahedral sites one expects a single intense intrasystem band in the 10 000 cm^{-1} region. Besides, from consideration of electroneutrality of the crystal, only a very limited amount of Co^{3+} could be present.

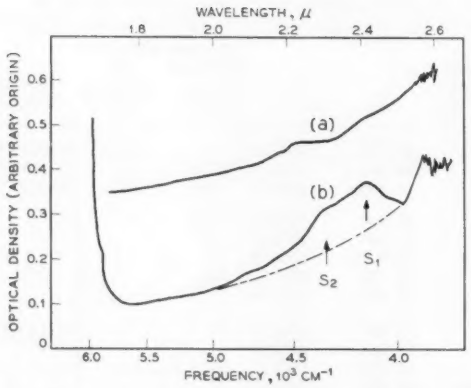

FIG. 7. Absorption in the 4000 cm^{-1} region. (a) ZnO undoped (0.5 mm thick) at 78°K. (b) ZnO:Co (5% nominal; 0.33 mm thick) at 78°K.

A reasonable assignment of the observed intense bands to intrasystem transitions is the following:

$$^4A_2 \rightarrow {}_a{}^4F_1 \quad \text{energy } 6750 \text{ cm}^{-1} \text{ (center of first band)},$$

$$^4A_2 \rightarrow {}_b{}^4F_1 \quad \text{energy } 15\,500 \text{ cm}^{-1}$$

$$\text{(first intense peak of visible band)}. \quad (13)$$

From this assignment it follows that

$$Dq(\text{ZnO:Co}) = 390 \text{ cm}^{-1}; \quad B = 700 \text{ cm}^{-1}, \quad (14)$$

where a marked decrease in the value of B is observed, when compared to the value $B = 845$ cm^{-1} for MgO:Co.

The predicted[16] and experimental ratios for Dq in tetrahedral and octahedral coordination of oxygens are in very good agreement

$$|\, Dq(\text{ZnO:Co})/Dq(\text{MgO:Co}) \,| = 0.42;$$

$$|\, Dq_{\text{tet}}/Dq_{\text{oct}} \,|_{\text{pred}} = \tfrac{4}{9} = 0.44. \quad (15)$$

In order to estimate the effect of the spin-orbit coupling on the quartet terms, the form of the wave functions of the $^4F_1$ terms was derived

$$|\, {}_a{}^4F_1 \rangle = 0.6022 \,|\, d\epsilon^4 d\gamma^3 \rangle - 0.7983 \,|\, d\epsilon^5 d\gamma^2 \rangle,$$

$$|\, {}_b{}^4F_1 \rangle = 0.7983 \,|\, d\epsilon^4 d\gamma^3 \rangle + 0.6022 \,|\, d\epsilon^5 d\gamma^2 \rangle \quad (16)$$

(checked to give the correct energy).

The corresponding spin-orbit splitting constants [Eq. (10)] are

$$c_a = -2.834, \qquad c_b = 1.835. \quad (17)$$

These values are quite close to the corresponding values for MgO:Co.

For a second-order treatment of the spin-orbit coupling effects, it is important to know the position of the various doublet levels of the d^7 configuration. This requires, though, the knowledge of Racah's parameter C. Assuming $C/B = 4.5$ and solving numerically the corresponding secular equations,[7] we can then derive the complete energy-level scheme for Co^{2+} in ZnO. This is given in Fig. 8. The form of the wavefunctions for the cubic-symmetry terms is given in Appendix II as a linear combination of states characterized by given subshell configuration and symmetry properties.

Figure 8 shows the predicted energy-level scheme for the quartet terms of Co^{2+} in the body-centered cube approximation for dodecahedral symmetry using the relation [1,17]

$$Dq_{\text{bcc}} = 2Dq_{\text{tet}}, \quad (18)$$

we assumed $|\, Dq \,| = 800$ cm^{-1} and $B = 800$ cm^{-1}. For a more complete energy level scheme see Appendix III.

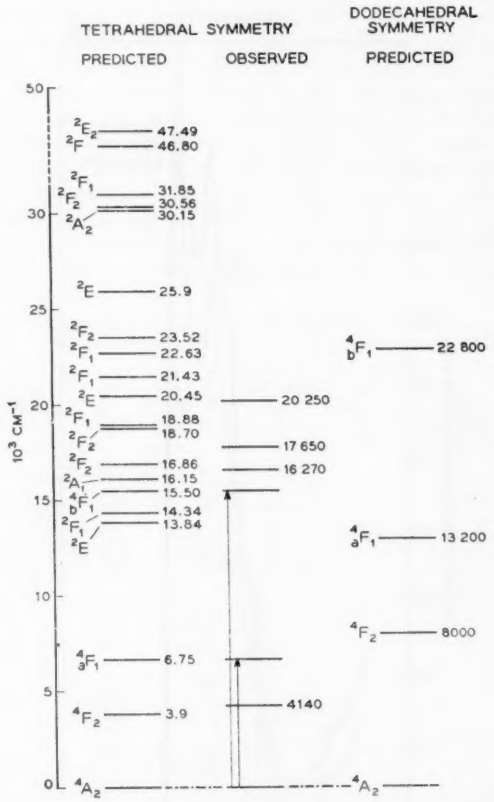

FIG. 8. Left: Predicted energy-level scheme for Co^{2+} in tetrahedral coordination, using the following values for the crystal-field parameters: $Dq = 390$ cm^{-1}; $B = 700$ cm^{-1}; $C = 4.5B$. Center: Observed absorption. The observed energy separations used in the calculations are indicated by the arrows. Transitions to quartet terms have higher probability. Right: Schematic energy-level scheme for Co^{2+} in the eightfold body-centered coordination (this is the approximate coordination of dodecahedral sites in garnets). $Dq = 800$ cm^{-1}; $B = 800$ cm^{-1}. Quartet terms only. For a more complete energy level scheme see Appendix III.

[16] C. J. Ballhausen, Kgl. Danske Videnskab. Selskab., Mat.-fys. Medd. **29** (4), (1954).

[17] R. Pappalardo, J. Mol. Spectroscopy **6**, 554 (1961).

D. Fine Structure in the Absorption Bands

The first-order treatment of spin-orbit effects on the ${}_a{}^4F_1$ term (which is fairly isolated, being located 2900 cm^{-1} away from the nearest term ${}^4F_2$) should be sufficient to describe the main effects due to spin-orbit coupling. The results of such calculations are then shown in Fig. 9 (left) and compared with the observed energy separations of the leading lines of each group at ~ 6000 cm^{-1}.

The over-all separation of the leading lines of the two extreme groups is in very good agreement with the predicted multiplet width. It is also interesting that the pattern of the intensity increases with the increase in the predicted degeneracy of the multiplet components. But the agreement ceases at this point: The internal splitting of the multiplet is reproduced in the observed absorption with the opposite sign. Besides, while the first absorption, connected to a Γ_6 level, according to the scheme in Fig. 9, can only produce a single line, in effect at least four lines are detected at 4.2°K (Fig. 5).

The predicted first-order splitting of ${}_b{}^4F_1$ is also shown in Fig. 9. The agreement with the experiment is poor which is not surprising in view of the fact that at least three cubic-field terms are clustered in this region (Fig. 8). This requires a higher-order treatment of the spin-orbit effects and conversely will make more difficult the assignment of the observed absorptions to transitions between the ground state and definite cubic-field terms.

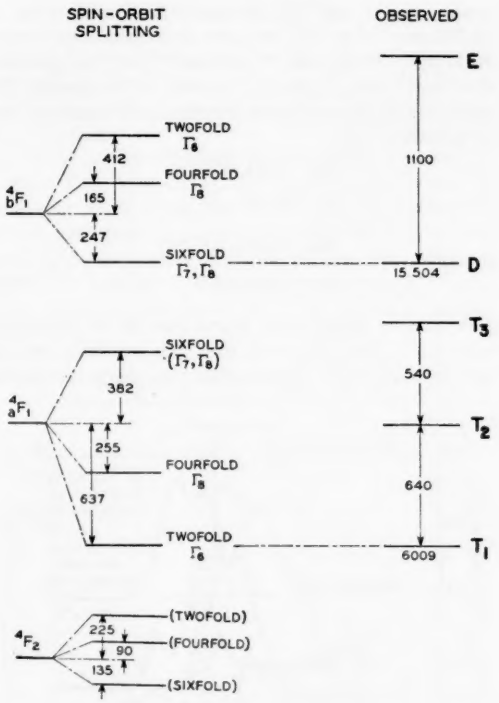

FIG. 9. ZnO:Co. Left: First-order treatment of spin-orbit effects for ${}^4F$ terms assuming for the spin-orbit coupling constant $\zeta_d = 540$ cm^{-1} and for the spin-orbit splitting constants $c_a = -2.834$ and $c_b = 1.835$. Right: Observed energy separations: for ${}_a{}^4F_1$ the energy separation for the leading lines of the three V triplets is given; for ${}_b{}^4F_1$ the separation of the two intense peaks D and E is indicated.

E. The Oscillator Strength

The f number of the observed absorptions was calculated assuming that all the Co ions are located in sites of tetrahedral symmetry and in the divalent state. If these assumptions are not fully verified, then the f values we report would represent a lower limit of the actual oscillator strength. Using the result of the x-ray spectrochemical analysis, which gives the amount of Co present as 0.17% of total weight, the oscillator strengths of the absorptions were calculated and are given in Tables IV and V. The values are found to be very high, $\sim 10^{-2}$ for the band in the visible region, and $\sim 10^{-3}$ for the band at ~ 7000 cm^{-1}. This is to be compared with the f values of 10^{-5} and 10^{-6} for the absorptions of MgO:Co in the corresponding regions. A simple calculation shows that in crystals of ZnO:Co one can detect of the order of one part in a million of Co^{2+} ions, simply by optical absorption measurements in the visible region, preferably at 78°K. We believe that the high f number, together with the position of the absorption bands and the different shape of the band in the 7000–8000 cm^{-1} region can be used as a powerful criterion to discriminate between Co^{2+} in tetrahedral and octahedral coordination.

In conclusion, the predictions of the crystal-field theory for Co^{2+} in tetrahedral coordination have been satisfactorily checked [Eq. (15)] even in a system, such as ZnO, which is commonly treated using the collective-band model, in order to describe its electronic properties.

In ZnO:Co considerable structure and narrow absorption lines were found, from which accurate information concerning the crystal-field can be derived. An attempt has been made, with a fair measure of success, to describe the observed main structure in the band at ~ 7000 cm^{-1} by means of the spin-orbit splitting of the ${}^4F_2$ cubic-field term.

Very high values of the f number for the absorptions have also been reported for the absorption band in the visible region for the $CoCl_4^{2-}$ complex ion.[18]

IV. $MgAl_2O_4$:Co

A blue-colored spinel of commercial origin, 3.15 mm thick, was studied at room temperature and 78°K. The absorptions of this sample are located in the near infrared and in the visible. In the infrared there is a strong band, with peaks at 6455, 7290, and 8085 cm^{-1} (Fig. 10). The intense band in the visible region has a double

[18] C. J. Ballhausen and C. K. Jørgensen, Acta. Chem. Scand. **9**, 397 (1955).

peak (16 010 and 17 240 cm^{-1}) and a shoulder at 18 280 cm^{-1} (Fig. 11). Weaker absorptions are located at 14 925, 20 965, and 25 160 cm^{-1}; they are probably due to the other impurities present in the sample. The results of a spectrochemical qualitative analysis were as follows:

Ti, 0.01–0.3%;
V, 0.01–0.3%;
Co, 0.005–0.03%;
Fe, 0.005%. (14)

The intense absorptions found are to be associated with Co^{2+}. Two kinds of sites are available for the Co^{2+} impurity ions, namely sites possessing tetrahedral

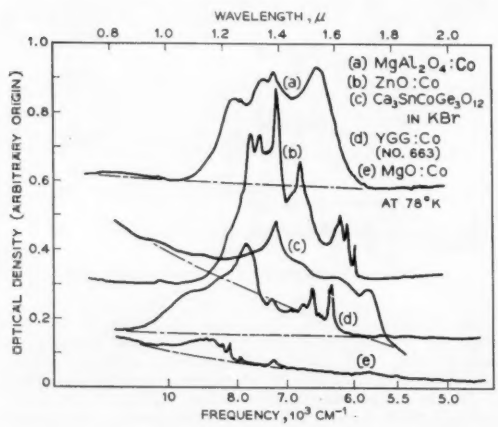

FIG. 10. Comparison of the absorption spectra, at 78°K and in the 7000 cm^{-1} region of several oxide systems doped with Co. All single crystals except the germanium garnet. (a) $MgAl_2O_4$:Co; 3.15 mm thick. (b) ZnO:Co 0.17%; 0.2 mm. (c) $Ca_3SnCoGe_3O_{12}$ powder in KBr pellet (4% dilution). (d) Co-doped yttrium gallium garnet (YGG:Co). Sample 663. (e) MgO:Co 0.20%; 3.7 mm.

and sites possessing octahedral symmetry. By comparison with the spectra both of MgO:Co and ZnO:Co one can infer that the intense absorptions found are to be correlated to Co^{2+} present in tetrahedral sites.

The lower limit for the value of the f number has been calculated, on the assumption that all the Co is present in tetrahedral sites as Co^{2+} and that the concentration is 0.03%. The value found (Table VI) for the f number is very high, of the order of 10^{-2}. It agrees quite well with the corresponding oscillator strength of Co^{2+} in ZnO, but it differs by three orders of magnitude from that of MgO:Co (Table I).

V. Co-DOPED YTTRIUM GALLIUM GARNETS

A. Preparation of Samples

Several single crystals of yttrium gallium garnets doped with Co were grown by Nielsen using the flux

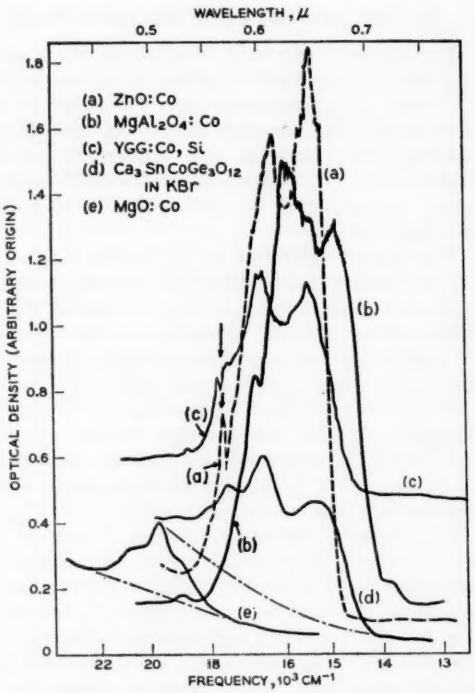

FIG. 11. Absorption band in the visible region for Co-doped oxide systems. Temperature, 78°K. All single crystals except the germanium garnet. (a) ZnO:Co (0.17%); 0.2 mm. (b) $MgAl_2O_4$: Co; 3.15 mm. (c) YGG:Co, Si. (d) $Ca_3SnCoGe_3O_{12}$ powder in KBr, 1.08 mm. (e) MgO:Co (0.20%) 3.7 mm.

technique.[19] The crystals were obtained by slowly cooling the melt contained in a platinum crucible from 1275° to 1000°C at the rate of cooling of 1°C/hr. The flux was a PbO-PbF_2 mixture. Crystals were grown

TABLE VI. $MgAl_2O_4$:Co (3.15 mm) at 78°K.

Absorption peaks	λ (A)	$\bar{\nu}$ (cm^{-1})	Extinction coefficient α_{max} (cm^{-1})	Half-width at $\alpha=\frac{1}{2}\alpha_{max}$ (cm^{-1})	Oscillator strength
	15 340	6518.9	1.1		
T	13 670	7315.3	1.0		1.2×10^{-2} [a]
	12 450	8032.1	0.8		
D	6700	14 925	0.2		
E	6200	16 129	3.55		
	5960	16 778	3.74		0.68×10^{-2} [a]
F	5800	17 241	4.28		
	5465	18 298	2.22		
G	4700	20 964	0.08		
	3975	25 157	0.05		

[a] Assuming 0.03% Co (see text).

[19] J. W. Nielsen, J. Appl. Phys. **31**, 515S (1960); **5**, 202 (1958).

TABLE VII. Spectrochemical quantitative YGG.

Element \ Sample No.	Percent found (of total weight) 645	662	663	664	665
Ti	...	0.10	...	0.61	0.49
Co	0.24[a]	0.16	0.024	0.21	0.14
Al	0.028	0.017	0.014	0.02	0.023
Spectrochemical qualitative YGG					
Al	3	3	3	3	3
Ca	3	3	3	3	3
Co	5	5	4	5	5
Cu	2	2	2	2	2
Fe	3	3	3	3	3
Ga	7	7	7	7	7
Mg	2	2	2	2	2
Mn	2	2	2	2	2
Pb	2	2	2	2	2
Si	3	3	3	3	3
Ti	0	5	0	5	5
Y	7	7	7	7	7

Estimated ranges: 7>10%, 6>1, 5 0.1–3.0, 4 0.01–0.3, 3<0.03, 2<0.005.

[a] The presence of 0.24% Co gives an ionic dilution $Co/Ga = 0.9 \times 10^{-2}$.

using the following dopings: Co; Co and Ti; Co and Si; Co and Sn. In cases of interest spectrochemical analyses were performed on the crystals obtained, in order to find the impurity content. The results of such analyses for samples No. 662, 663, 664, 665, and 645 are given in Table VII.

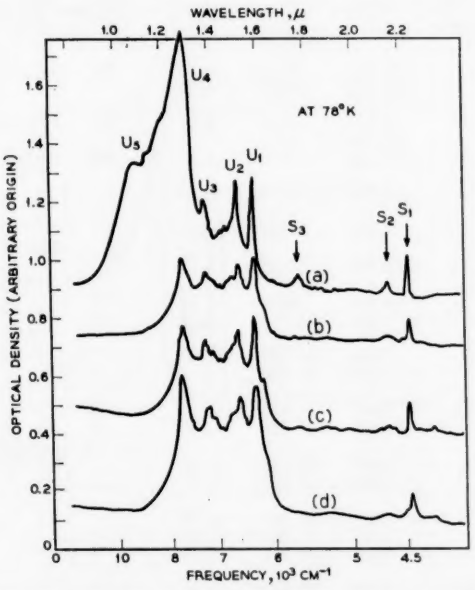

FIG. 12. Absorption from 4500 to 10 000 cm^{-1}. Temperature, 78°K. (a) YGG:Co (No. 645) 0.63 mm; Co 0.24%. (b) YGG:Co, Ti (No. 665) 0.68 mm; Co 0.14%; Ti 0.49%. (c) YGG:Co (No. 663) 1.64 mm; Co 0.024%. (d) YGG:Co, Ti (No. 664) 0.63 mm; Co 0.21%; Ti 0.61%.

B. Absorption Spectra

We shall now briefly describe the appearance of the spectra of YGG:Co samples. Let us see in detail first a typical case, that of sample No. 663. Beginning from the low-energy region (2.6μ) two weak absorption lines are located at 4500 cm^{-1} [temp. 78°K; Fig. 12(c); compare Fig. 7 for ZnO]. The doublet is followed by some very weak absorptions and then by a complex intense absorption, centered at 7880 cm^{-1}. Then no absorptions are found, until one reaches the energy of 13 500 cm^{-1} where a weak flat absorption is found; then a more intense band at 14 200 cm^{-1}; a double-peaked intense absorption centered at 16 000 cm^{-1} and showing on its high-energy tail a peculiar sharp absorption at 17 800 cm^{-1} [Fig. 13(d)]. Finally, superposed on the edge absorption in the violet region of the spectrum, a very intense absorption band is found, with peak at 26 300 cm^{-1} (Fig. 14). It is to be noted that in the sample we are discussing the intensity of the band at ~7800 cm^{-1} and that of the band at ~16 000 cm^{-1} are roughly equal (Figs. 12 and 13). No remarkable changes in the absorption spectrum are observed at 4.2°K, except for a considerable sharpening of the line absorptions (Figs. 14–16). All details pertinent to the spectra of sample No. 663, and of the other samples, are given in Tables VIII to XIV.

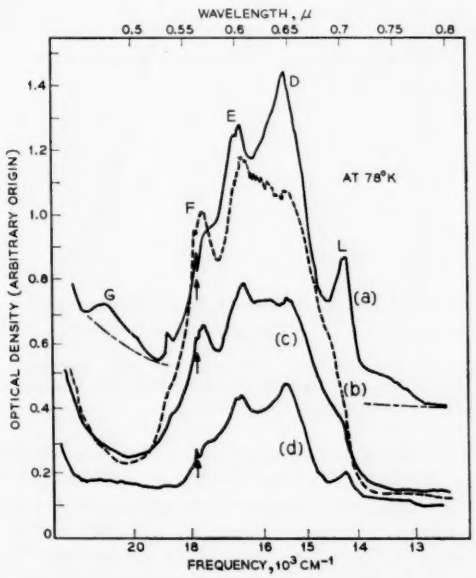

FIG. 13. Absorption in the 16 000 cm^{-1} region. Temperature 78°K. (a) YGG:Co (No. 645); 0.63 mm; Co 0.24%. (b) YGG:Co, Ti (No. 664); 0.63 mm; Co 0.21%; Ti 0.61%. (c) YGG:Co, Ti (No. 665); 0.68 mm; Co 0.14%; Ti 0.49%. (d) YGG:Co (No. 663); 1.64 mm; Co 0.024%. Note sharp line (marked by arrow) at ~17 800 cm^{-1}; compare line *F* in Fig. 6.

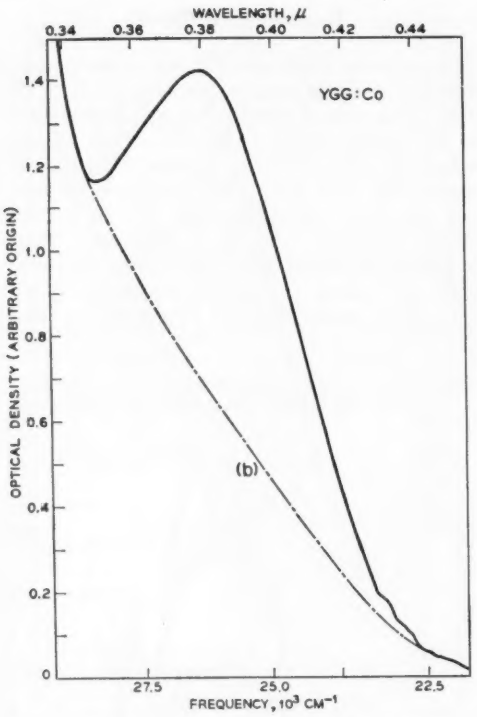

FIG. 14. Intense band superposed on edge absorption in YGG:Co (No. 663). Sample thickness, 0.63 mm. Temperature 4.2°K. (b) Extrapolated background.

The spectrum of sample No. 645 (Fig. 17) resembles that of sample No. 663. Both the infrared and the visible band have comparable intensity, and the peak at 7800 cm^{-1} is very pronounced (Fig. 12). The spectrum at 4.2°K shows remarkably intense and sharp lines in the 4500 cm^{-1} and 6000 cm^{-1} region (Fig. 17, Table XI).

The position of the main absorption bands in the other garnets doped with Co are similar to those of the two samples previously discussed, except for a

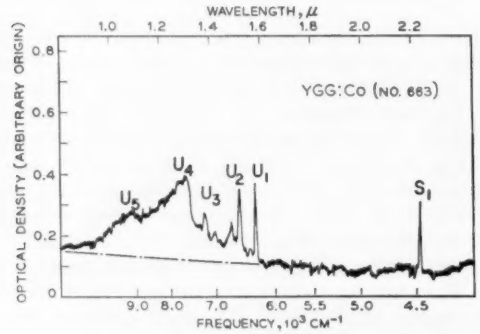

FIG. 15. YGG:Co (No. 663). Detail of absorption in the infrared region. Temperature, 4.2°K; sample thickness, 1.64 mm.

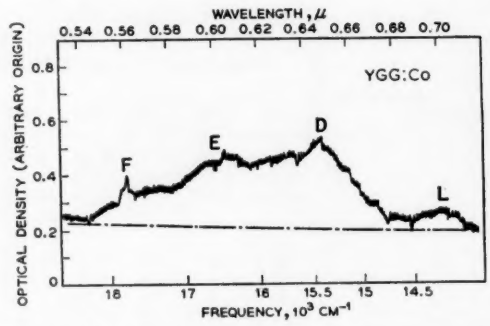

FIG. 16. YGG:Co (No. 663); 0.63 mm. Temperature 4.2°K. Detail of the absorption in the 16 000 cm^{-1} region. The absorption peaks are comparable in intensity with the main peaks in Fig. 15.

different structure in the absorption. For sample No. 664, e.g., at 78°K, there are four weak peaks in the 4500 cm^{-1} region and a flat weak absorption at ~5300 cm^{-1}. The band at 7000 cm^{-1} shows a pattern of *four* main peaks of similar intensity [Fig. 12(d)]. The band in the visible region of the spectrum has twice as much intensity as the infrared band, and has a threefold structure [Fig. 13(b)]. The spectra of samples No.

TABLE VIII. YGG:Co (sample 663) 0.024% Co. Thickness, 1.64 mm; temperature 78°K.

Absorption peaks	λ (A)	$\bar{\nu}$ (cm^{-1})	Extinction coefficient α_{max} (cm^{-1})	Half-width at $\alpha=\frac{1}{2}\alpha_{max}$ (cm^{-1})	Oscillator strength
S_1	22 350	4474	0.42	20	2×10^{-6}
S_2	21 500	4651	0.18		
U_1	15 840	6313	0.91	80	1.7×10^{-5}
	15 760	6345			
U_2	15 120	6616	0.87	100	2×10^{-5}
	14 800	6756	0.55		
U_3	13 720	7289	0.61		2.9×10^{-4}
U_4	12 800	7812	1.6		
U_5	10 800	9259	0.73		
	7400	13 514	0.18		
L	7040	14 205	0.36		
	6640	15 060			
D	6480	15 432	1.1		
	6360	15 723			
E	6050	16 529	1.52		0.3×10^{-3}
	6000	16 667	1.5		
F	5720	17 483	0.79		
	5616[a]	17 806[a]	0.82		
	5340	18 727	0.09		
G	4800[b]	20 833[b]	0.12		
H	3800	26 316	3.96		1.25×10^{-3}

[a] Sharp.
[b] Very flat absorption.

TABLE IX. YGG:Co (Sample 663), 0.024% Co. Thickness, 1.64 mm. Temperature, 4.2°K.

Absorption peaks	λ (A)	$\bar{\nu}$ (cm^{-1})	Extinction coefficient α_{max} (cm^{-1})	Half-width at $\alpha=\frac{1}{2}\alpha_{max}$ (cm^{-1})	Oscillator strength
S_1	22 300	4484	1.46	7	2.5×10^{-6}
U_1	15 720	6363.2	1.64	20	0.8×10^{-5}
U_2	15 100	6622.5	1.46	50	1.75×10^{-5}
	14 800	6706.8	0.85	120	2.5×10^{-5}
	14 100	7092.2	0.62		
U_3	13 700	7299.3	1.03		0.42×10^{-3}
U_4	13 000	7692.3	1.58		
U_5	10 800	9203.3	0.85		
L	7030	14 225	0.42		
D	6470	15 406	1.95		
	6320	15 823	1.64		
E	6060	16 502	1.62		0.64×10^{-3}
	6000	16 667	1.4		
F	5616[a]	17 806[a]	1.1		
	5360	18 656			
H	3780	26 455	4.1		0.8×10^{-3}

[a] Broad line.

662 and 665 are very similar to the spectrum of No. 664 (Figs. 12 and 13).

Single crystals of YGG were also studied in which the impurity content was comparable to that of the samples discussed above and which contained as impurities Co and Si; Co and Sn. The corresponding spectra at 78°K are shown in Figs. 18 and 19 and are contrasted with the corresponding spectra of YGG:Co No. 663.

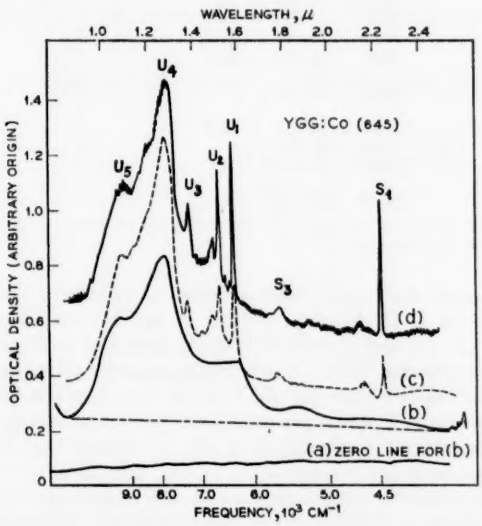

FIG. 17. Detail of the absorption in the infrared region of YGG:Co (No. 645); Co 0.24%, and no Ti; 0.63 mm thick. (a) Zero line (no sample) for curve (b), (b) At room temperature, (c) At 78°K, (d) At 4.2°K. Note very sharp lines at 4.2°K (Table XI).

C. Discussion of the Spectra

The main problem concerning the important garnet systems, from the point of view of chemical crystallography and magnetochemistry, is that of determining the ionicity and site preference of the impurity paramagnetic ions. Both these questions can be tackled in many cases by examining the optical absorption spectra.

In particular for the case of YGG, it is of interest to determine from the absorption spectrum whether the Co impurity ions are present as Co^{2+} or Co^{3+}, and in which of the three sites available (tetrahedral, octa-

TABLE X. YGG:Co (0.24% Co in weight). Sample No. 645 at 78°K.

Absorption peaks	λ (A)	$\bar{\nu}$ (cm^{-1})	Extinction coefficient α_{max} (cm^{-1})	Half-width at $\alpha=\frac{1}{2}\alpha_{max}$ (cm^{-1})	Oscillator strength
S_1	22 150	4514.6	2.2	20	1.0×10^{-6}
S_2	21 520	4646.8	0.63		
	21 360	4681	0.3		
S_3	17 830	5608.5		120	1.8×10^{-6}
	17 880	5592.8	0.63		
	16 700	5988			
	16 500	6060.6	0.16		
U_1	15 850	6309	5.87	90	1.27×10^{-5}
	15 770	6341			
	15 160	6596.3	5.7		
U_2	14 870	6725	4		
	14 400	6944	2.85		
U_3	13 730	5340	4.7		2.7×10^{-4}
U_4	12 800	7812	12.8		
	10 970	9115			
U_5	10 850	9216.6	6.6		
	7640[a]	13 090	0.95		
	7540[a]	13 262			
L	7030	14 225	5.2		
D	6480	15 410	13.8		
	6360	15 723			3.0×10^{-4}
E	6055	16 515	11.1		
	6010	16 639			
F	5740	17 421	5.7		
	5360	18 656	0.47	230	2.6×10^{-6}
G	5040[a]	19 841	0.8		2.4×10^{-5}
	4780	20 920	1.6		
	[4260][b]	[23 474][b]			

[a] Shoulder.
[b] $I_0/I=10$ (the optical density has value *one* at this frequency).

In particular for the case of YGG, it is of interest to determine from the absorption spectrum whether the Co impurity ions are present as Co^{2+} or Co^{3+}, and in which of the three sites available (tetrahedral, octa-

TABLE XI. YGG:Co (0.24% Co in weight). Sample No. 645 at 4.2°K.

Absorption peaks	λ (A)	$\bar{\nu}$ (cm^{-1})	Extinction coefficient α_{max} (cm^{-1})	Half-width at $\alpha=\frac{1}{2}\alpha_{max}$ (cm^{-1})	Oscillator strength
S_1	22 160	4512.6	7.9	5	1.0×10^{-6}
S_2	21 260	4703.6	0.63		
S_3	17 850	5602.2	1.4	100	3.4×10^{-6}
U_1	15 880	6297.2	9.2[a]	20[a]	0.4×10^{-5} [a]
	15 800	6229.1			
U_2	14 960	6684.5	6.82[a]	50[a]	0.82×10^{-5} [a]
	14 830	6743.1	2.54[a]		
U_3	13 860	7215	2.54[a]		1.85×10^{-4}
U_4	12 860	7776	13.65		
U_5	10 850	9216.6	7.4		
L	7030	14 225	5.55	450	0.6×10^{-4}
	6720[b]	14 880[b]			
	6600[b]	15 150[b]			
D	6500	15 455	14.3		
	6340	15 772	12		
	6050	16 528	10.8		2.9×10^{-4}
E	5980	16 722	9.8		
F	5720	17 482	5.7		
	5614	17 812	6.5		
	5340	18 726	0.8	350	0.7×10^{-5}
G	4780	20 920	2.22		0.35×10^{-4}

[a] Considering the peaks over the absorption continuum.
[b] Shoulder.

hedral, or dodecahedral[20]), they are located. On comparing the predicted energy levels of Co^{2+} in the three coordinations and the levels for Co^{3+} in oxides it can be concluded that the absorptions found in the garnets are due to tetrahedral Co^{2+}, on the basis of optical data alone.

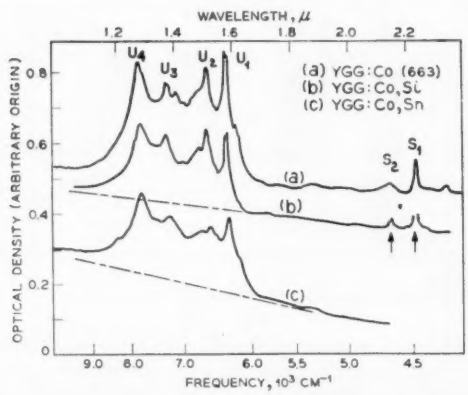

FIG. 18. Absorption bands of single crystals of Co-doped YGG at 78°K in the 7000 cm^{-1} region. (a) YGG:Co (sample 663). (b) YGG:Co, Si (1.92 mm). (c) YGG:Co, Sn (sample 762, thickness, 1.96 mm).

[20] In the body-centered cube approximation.

It has been observed, however, by Geller *et al.*[21] that in garnets where the dodecahedral sites are occupied by yttrium, a rare earth, or another large ion such as Ca^{2+} the Co^{2+} preferentially occupies octahedral sites. But the strong similarity in line position and relative intensity throughout the spectrum between ZnO:Co and YGG:Co can be considered very strong evidence in favor of the tetrahedral coordination. We believe that this discrepancy can be resolved in the following way. The tetrahedrally coordinated ion has much stronger absorption than that for the octahedral ion

TABLE XII. YGG:Co (sample 664) thickness 0.63 mm; Co, 0.21%; Ti, 0.61%. Temperature, 78°K.

Absorption peaks	λ (A)	$\bar{\nu}$ (cm^{-1})	Extinction coefficient α_{max} (cm^{-1})	Half-width at $\alpha=\frac{1}{2}\alpha_{max}$ (cm^{-1})	Oscillator strength
S_1	23 600	4237.2	0.3		
	22 370	4470.8	1.5	40	1.6×10^{-6}
	22 140	4516.7	0.7	35	0.67×10^{-6}
	21 510	4649	0.55		
	18 720	5342	0.24		
	16 180	6180.5	3.65		
U_1	15 800	6329	7.3		
	15 600	6410			
	15 170	6592	6.35		1.3×10^{-4}
	14 900	6711	5.4		
U_2	14 400	6944			
	14 070	7107	5.2		
U_3	13 880	7204.6	5.7		
U_4	12 720	7861.6	7.3		
	6960	14 367.8	4.9		
D	6480	15 432	13.5		
	6320	15 832	13.5		
	6080	16 447	15		
E	6000	16 667			0.5×10^{-3}
F	5700	17 544	11.9		
	5620	17 794			
	5360	18 657	4		
	[4160[a]	[24 038][a]			

[a] At this point $I_0/I=10$.

because the former lacks a center of symmetry (cf., Tables I, II, IV, V). Further it can be seen from Table IV and Tables VIII–XIV that the oscillator strengths for YGG:Co are almost an order of magnitude smaller than for ZnO:Co. If the observed absorption in YGG is from tetrahedral Co^{2+} as the energy-level diagram indicates, it is safe to assume that its true oscillator strengths are about the same as in ZnO, and therefore there must be only a small fraction of the total Co^{2+} present in this type of site. If the remainder were in octahedral sites it would not contribute

[21] S. Geller, C. E. Miller, and R. G. Treuting, Acta. Cryst. **13**, 179 (1960).

materially to the spectrum, since the oscillator strengths for the octahedral ion are much more than one order of magnitude smaller. Thus in YGG:Co^{2+} the spectrum may be accounted for on the basis of a small fraction of the total Co^{2+} content being present in tetrahedral coordination.

Geller *et al.*[21] have raised an additional question about the color of the garnets containing Co^{2+}. They call attention to the case of $CoWO_4$ which has an intense blue color and in which the Co^{2+} is in six-coordinated sites. From this they draw some support for the supposition that the octahedral Co^{2+} may show the same blue color in the garnets instead of the usual red color associated with octahedral Co^{2+}. We believe, however, that the color of $CoWO_4$ is anomalous for octahedral Co^{2+}, and that the blue color of the garnets is that usual for tetrahedral Co^{2+}. This is a point which should be further clarified by a thorough study of the spectrum of $CoWO_4$. Until this is done we feel justified in discussing the special features of the various garnet spectra on the assumption that the spectrum observed arises from Co^{2+} present in sites possessing predominantly tetrahedral symmetry, even though this may be but a minor constituent of the lattice.

One interesting point concerns the weak line absorption found at 4500 cm^{-1} in all of the various garnets investigated (as well as in the ZnO:Co system). The oscillator strength of this absorption is an order of magnitude less (compare also with ZnO:Co, Fig. 7) than that of the next absorption band which we identified in ZnO:Co as the transition $^4A_2 \rightarrow {}^4F_2$. Liehr and Ballhausen[22] have pointed out that the transition $^4A_2 \rightarrow {}^4F_2$ is symmetry forbidden while all the other transitions are symmetry allowed. The band is predicted by these authors to have an oscillator strength about $\frac{1}{10}$ that of the symmetry allowed bands in agreement with what we find here.

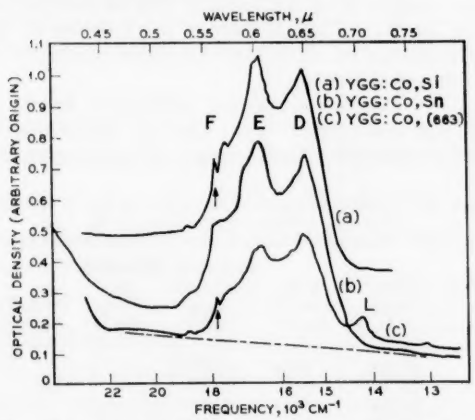

FIG. 19. Absorption bands in the visible region of Co-doped single crystals of YGG. Temperature 78°K. (a) YGG:Co, Si (1.92 mm). (b) YGG:Co, Sn; (No. 762; 1.96 mm). (c) YGG:Co (No. 663). Note sharp peak F (marked with arrow) at ~17 800 cm^{-1}, also in Fig. 6.

TABLE XIII. YGG:Co (sample 662) 0.16% Co; 0.10% Ti. Thickness, 0.63 mm at 78°K.

Absorption peaks	λ (A)	$\bar{\nu}$ (cm^{-1})	Extinction coefficient α_{max} (cm^{-1})	Half-width at $\alpha=\frac{1}{2}\alpha_{max}$ (cm^{-1})	Oscillator strength
	23 400	4273.5	0.47		
S_1	22 170	4510.6	1.6	20	1.1×10^{-6}
S_2	21 450	4662	0.4		
S_3	18 800	5319	0.32		
	16 100	6211.2	2.7		
U_1	15 860	6305	6.0		
	15 790	6333			
U_2	15 140	6605	5.2		2.4×10^{-4}
	14 800	6756			
U_3	14 090	7097	3.8		
	13 760	7267.4	4.3		
U_4	12 800	7812.5	5.2		
L	7040[a]	14 205[a]			
	6960[a]	14 368[a]			
D	6470	15 456	11.6		
	6315	15 835			
E	6050	16 529			0.6×10^{-3}
	5987	16 702			
F	5670	17 636	9		
	5603	17 847			
	5380	18 587			
	3320	30 120			

[a] Shoulder.

Another point to consider concerns the differences found in the fine structure of the absorptions, depending on the impurity content of the various crystals. Compare, for instance, the various spectra of YGG:Co. In particular, some of the crystals contain a large amount of Ti as shown in Table VII. If Ti is present as Ti^{3+} or Ti^{2+}, there should be absorption bands associated with such ions. However, a comparison of the theoretical expectations for such ions in fourfold, sixfold, and eightfold coordination with the observed spectra shows that these ions are not present in the samples studied. The experimental situation is as follows. First one can say, from comparison of the spectrum of sample No. 645, which contains 0.24% Co and no appreciable amount of Ti (Table VII) with the spectrum of sample No. 664 (which has 0.21% Co and 0.49% Ti) that there are no additional absorptions one can associate with Ti. This means that Ti is in the form Ti^{4+}, with closed-shell configuration, and as such can only absorb via high-energy transitions of a different kind than those we are now discussing.

[22] C. J. Ballhausen and A. D. Liehr, J. Mol. Spectroscopy **2**, 342 (1958); errata, *ibid.* **4**, 190 (1960).

TABLE XIV. YGG:Co (sample 665) Co, 0.14%; Ti, 0.49%. Temperature, 78°K.

Absorption peaks	λ (A)	$\bar{\nu}$ (cm^{-1})	Extinction coefficient α_{max} (cm^{-1})	Half-width at $\alpha=\frac{1}{2}\alpha_{max}$ (cm^{-1})	Oscillator strength
S_1	22 350	4474	1.2	25	1.2×10^{-6}
S_2	21 500	4651	0.3		
	16 100	6211	1.83		
U_1	15 800	6329	4		
U_2	15 100	6623	3.7		
	14 900	6711	3		1.0×10^{-4}
	14 000	7141			
U_3	13 800	7249	3.23		
U_4	12 800	7812	4		
L	7040	14 204	1.6		
	7000	14 286	2.6		
D	6500	15 432	8.1		
	6320	15 523	8.1		0.45×10^{-3}
E	6080	16 447	8.7		
	6000	16 667	8		
F	5700	17 544	6.5		
	5620	17 794	6.3		
	5320	18 652	2.0		
	[4080][a]	[24 510][a]			

[a] At this energy $I_0/I=10$.

There is, however, a rather large difference between the spectrum of YGG:Co^{2+} No. 645 and essentially all the other samples, especially in the region near 8000 cm^{-1}. This can be explained at least qualitatively in the following way. The Co^{2+} in YGG is substituting for a trivalent Ga^{3+} ion, and to preserve electrical neutrality something must compensate for the charge deficit. For the crystal No. 645 no other ion is present in sufficient concentration to compensate for the Co^{2+}, and presumably oxygen vacancies must play this role. In all the other crystals except No. 663 there have been intentionally introduced enough tetravalent ions (Si^{4+}, Ti^{4+}, Sn^{4+}) to compensate the charge. For crystal No. 663 no intentional doping is present, but since the Co^{2+} is very dilute (0.024%) there is enough residual Si^{4+} impurity (<0.03%) to perform this function. We may thus conclude that YGG:Co^{2+} No. 645 has a charge compensation mechanism different from the rest and this may account for the unique features of its spectrum. We have not pursued the question of charge compensation further, but it is clearly evident first that charge compensation may have a profound effect on the energy levels of an ion in a crystal, and second that optical spectra can be used to investigate the mechanism of charge compensation. A similar situation was found in the case of Cu^{2+} in YGG.[17]

VI. GERMANIUM GARNETS

New synthetic garnets have been prepared and studied in powder form by Geller and Miller.[21,23] The absorption spectra of some of these powder samples of $Ca_3MCoGe_3O_{12}$ (where M=Ti, Sn, and Zr) have been taken and they are all similar; we shall simply mention in detail the spectrum of $Ca_3SnCoGe_3O_{12}$. Amounts of the order of 15 mg of the garnet were mixed with about 400 mg of KBr and pellets made; the absorption spectra are shown in Fig. 10(c) and Fig. 11(d) and data collected in Table XV.

The absorption consists of two bands, one in the 6300 cm^{-1} region and one in the 16 000 cm^{-1} region, both of them showing considerable structure at 78°K. The spectra of these germanium garnets are similar to those of the gallium garnets mentioned above, and are very similar to the absorption spectrum of ZnO:Co. It is possible to conclude here also that the spectrum observed is due to Co^{2+} in tetrahedral coordination, though this may arise from a small fraction of the total number of Co impurity ions because the absorption intensity in this particular spectrum is so large.

VII. CONCLUSION

We shall now summarize the implications of the present study with the following concluding remarks:

(a) There is clearly evidence of vibrational structure in the absorption bands both of MgO:Co and ZnO:Co.

(b) Spin-orbit effects (in first or higher order) are not sufficient to account for all of the fine structure lines observed. Also the spin-orbit treatment is more successful in accounting for the *main* structure of the observed absorptions, when applied to the absorptions in the 7000 cm^{-1} region, where the cubic-field terms are fairly isolated from one another. But in order to explain smaller splittings, such as the splitting in the triplet absorption A_0 in MgO:Co, other effects are to be taken into account.

(c) A comparison of the absorption bands of MgO:Co and ZnO:Co shows that the ZnO:Co spectrum is markedly shifted towards lower energies and

TABLE XV. $Ca_3SnCoGe_3O_{12}$ in KBr pellet (4.2% in weight), thickness, 1.08 mm, temperature, 78°K.

Absorption peaks	Wavelength (A)	Wave number (cm^{-1})	Extinction coefficient α_{max} (cm^{-1})	Half-width at $\alpha=\frac{1}{2}\alpha_{max}$ (cm^{-1})	Oscillator strength
	17 200	5814	1.4		
	16 100	6192	1.3		
	14 700	6802	1.4		
	13 800	7246			
D	6500	15 384	3.4		
	5800	16 660	4.0		
F	5700	17 543	2.5		
	5300	18 760	0.5		

[23] S. Geller, J. Appl. Phys. **31**, 30S (1960).

that the shape of the bands in the infrared region is markedly different for the two systems. On the contrary, the shape of the bands in the visible region of the spectrum does not show the drastic difference found[1] for Ni^{2+} in MgO and ZnO. The oscillator strength in tetrahedral coordination (ZnO:Co) is greater by a factor $\sim 10^3$ than for MgO:Co. This is another spectral characteristic which can help in the assignment of the site symmetry in case of uncertainty.

(d) The predictions of the crystal-field theory for Co^{2+} in tetrahedral coordination are satisfactorily verified experimentally for the quartet terms; in the case of doublet terms the experimental situation is less amenable to a comparison with the theoretical predictions.

(e) As for the assignment of site symmetry of impurities in garnets and spinels, using optical absorption data, the reported spectra show that the method is quite feasible. The close similarity of the absorption spectra of Co-doped spinels and garnets, with the spectra of ZnO:Co suggests that Co^{2+} is present in such systems in sites possessing (predominant) tetrahedral coordination. This does not agree with previous assignments[21] for Co-containing garnets, according to which Co^{2+} in these particular garnets is preferentially located in octahedral sites unless it is assumed that the strong absorption of a minority of Co^{2+} ions in tetrahedral coordination swamp out the weaker spectrum of the majority of ions in other coordinations. The previous assignments[21] are based on consideration of electronic configuration, ionic radii, and relative size of tetrahedral and dodecahedral sites in garnets containing Co.

We have not studied experimentally oxide systems in which only dodecahedral sites are available for the metallic ions, so that we cannot really sharpen our assignments further; at this stage of our work we simply wish to point out the close similarity of the absorption spectra of ZnO:Co and that of Co-doped spinels and garnets, which suggest a coordination number *four* for Co^{2+}.

The closest approximation to an ideal oxide system in which only eight-coordinated sites are available for the metallic ion, is that of Li_2O and K_2O, which crystallize in the fluorite structure. These systems are subject to the following limitations: (1) One can expect some deformation of the cubic symmetry at the site of the metallic ion, due to the substitution of divalent ions to monovalent cations, (2) their hygroscopic nature makes their handling inconvenient. Yet we believe it will be worthwhile to attempt to work with these systems, both to obtain an experimental check on the predictions of the crystal-field theory for eightfold coordination and as a complement to the present optical absorption study.

ACKNOWLEDGMENTS

The authors wish to thank for their friendly help and advice the following members of the Bell Telephone Laboratories Staff: A. D. Liehr for useful discussions on the crystal-field theory and spin-orbit coupling and for valuable criticism of the manuscript; S. Sugano and J. E. Guesic for important discussions on spin-orbit calculations; J. W. Nielsen for making available the single crystals of yttrium gallium garnet; S. Geller for supplying the germanium garnet powders and for illuminating discussions on ionic-site preference in garnets; E. K. Jaycox and D. L. Nash for the spectrochemical determination of the impurity content of the samples; Miss D. M. Dodd for assistance in the spectrophotometric measurements. Particular thanks are due to Miss M. A. Lounsberry of the Computing Center for the numerical solutions of the secular equations for the doublet terms of Co^{2+}.

APPENDIX I

Wave functions for doublet terms of $MgO:Co^{2+}$. Values of crystal-field parameters:

$$|Dq| = 927 \text{ cm}^{-1}; \qquad B = 845 \text{ cm}^{-1}; \qquad C = 4.5B.$$

The wave functions are expressed as linear combinations of states with given subshell configuration and symmetry properties[7]:

e.g.,
$$|\,{}^2F_2\rangle = \sum_j \alpha_j \,|\, d\epsilon^n(S_1\Gamma_1)d\gamma^{7-n}(S_2\Gamma_2), {}^2F_2\rangle. \tag{A1}$$

Term	Energy (10^3 cm^{-1})	$d\epsilon^3(^2F_2)d\gamma^4$;	$d\epsilon^4(^3F_1)d\gamma^3$;	$d\epsilon^4(^1F_2)d\gamma^3$;	$d\epsilon^5d\gamma^2(^1A_1)$;	$d\epsilon^5d\gamma^2(^1E)$
a^2F_2	15.17	0.0953	−0.2307	−0.0859	−0.3944	0.8801
b^2F_2	24.61	−0.1362	0.8313	−0.2153	0.4938	−0.0028
c^2F_2	30.83	−0.5503	−0.4295	−0.5894	0.3157	0.2561
d^2F_2	36.31	−0.1619	−0.1601	0.7192	0.5407	0.3720
e^2F_2	59.37	0.8020	−0.2132	−0.2855	0.4565	0.1457

Term	Energy (10^3 cm^{-1})	$d\epsilon^3(^2F_1)d\gamma^4$;	$d\epsilon^4(^3F_1)d\gamma^3$;	$d\epsilon^4(^1F_2)d\gamma^3$;	$d\epsilon^5d\gamma^2(^3A_2)$;	$d\epsilon^5d\gamma^2(^1E)$
a^2F_1	14.69	−0.0797	0.00267	0.1364	0.8644	−0.4772
b^2F_1	19.37	0.0683	−0.3191	0.1697	0.4344	0.8221
c^2F_1	26.12	−0.1264	0.3596	0.9135	−0.1379	0.0343
d^2F_1	32.17	0.6400	0.7095	−0.1705	0.1748	0.1650
e^2F_1	40.16	0.7505	−0.5151	0.2983	−0.1200	−0.2604

Term	Energy (10^3 cm^{-1})	$d\epsilon^3(^2E)d\gamma^4$	$d\epsilon^4(^1A_1)d\gamma^3$	$d\epsilon^4(^1E)d\gamma^3$	$d\epsilon^5d\gamma$
a^2E	8.39	0.1355	0.1917	−0.0100	0.9720
b^2E	28.05	−0.0257	0.3326	0.9412	−0.0522
c^2E	33.91	0.9307	−0.3322	0.1393	−0.0627
d^2E	58.50	0.3386	0.8615	−0.3074	−0.2203

APPENDIX II

Wave functions for the doublet terms of ZnO:Co^{2+}. Values of the crystal-field parameters

$$Dq=390\ \text{cm}^{-1};\qquad B=700\ \text{cm}^{-1};\qquad C=4.5B.$$

The wave functions are expressed as linear combinations of states with given subshell configuration and symmetry properties[7]:

e.g.,
$$|\ ^2F_2\rangle=\sum\alpha_j\,|\,d\epsilon^n(S_1\Gamma_1)d\gamma^{7-n}(S_2\Gamma_2),\,^2F_2\rangle. \tag{A2}$$

Term	Energy (10^3 cm^{-1})	$d\epsilon^3(^2F_2)d\gamma^4$;	$d\epsilon^4(^3F_1)d\gamma^3$;	$d\epsilon^4(^1F_2)d\gamma^3$;	$d\epsilon^5d\gamma^2(^1A_1)$;	$d\epsilon^5d\gamma^2(^1E)$
a^2F^2	16.86	0.4436	0.8016	0.0367	−0.1689	0.3613
b^2F_2	18.7	0.6478	−0.3902	0.5708	−0.2939	−0.1251
c^2F_2	23.52	−0.0449	−0.3939	−0.2858	−0.4485	0.7484
d^2F_2	30.56	−0.4267	0.0566	0.7479	0.2500	0.4390
e^2F_2	47.49	0.4464	−0.2158	−0.1787	0.7883	0.3174

Term	Energy (10^3 cm^{-1})	$d\epsilon^3(^2F_1)d\gamma^4$;	$d\epsilon^4(^3F_1)d\gamma^3$;	$d\epsilon^4(^1F_2)d\gamma^3$;	$d\epsilon^5d\gamma^2(^3A_2)$;	$d\epsilon^5d\gamma^2(^1E)$
a^2F_1	14.34	0.9118	0.1004	−0.3456	−0.1396	0.1470
b^2F_1	18.88	0.3027	0.4210	0.8294	0.2039	−0.0383
c^2F_1	21.43	−0.1563	0.7279	−0.2304	−0.4205	−0.4644
d^2F_1	22.63	0.1038	0.0308	−0.2705	0.7778	−0.5568
e^2F_1	31.85	−0.2042	0.5308	−0.2613	0.3961	0.6717

Term	Energy (10^3 cm^{-1})	$d\epsilon^3(^2E)d\gamma^4$;	$d\epsilon^4(^1A_1)d\gamma^3$;	$d\epsilon^4(^1E)d\gamma^3$;	$d\epsilon^5d\gamma$
a^2E	13.84	0.9496	0.2203	0.1732	−0.1402
b^2E	20.45	−0.0516	−0.4105	0.9024	0.1202
c^2E	25.9	0.2447	−0.2987	−0.2405	0.8905
d^2E	46.8	−0.1889	0.8328	0.3126	0.4157

APPENDIX III

Wave functions for Co^{2+} doublet terms in body-centered cube coordination, with the following choice of crystal-field parameters:

$$|Dq| = \tfrac{5}{9} \times Dq(\mathrm{MgO{:}Co}) = 825\ \mathrm{cm}^{-1}; \qquad B = 845\ \mathrm{cm}^{-1}; \qquad C = 4.5B.$$

The wavefunctions are expressed as linear combinations of states with given subshell configuration and symmetry properties[7]:

e.g.,

$$|\ {}_i{}^2F_2\rangle = \sum_j \alpha_j\ |\ d\epsilon^n(S_1\Gamma_1)d\gamma^{7-n}(S_2\Gamma_2), {}^2F_2\rangle. \tag{A3}$$

Term	Energy (10^3 cm^{-1})	$d\epsilon^3({}^2F_2)d\gamma^4$;	$d\epsilon^4({}^3F_1)d\gamma^3$;	$d\epsilon^4({}^1F_2)d\gamma^3$;	$d\epsilon^5d\gamma^2({}^1A_1)$;	$d\epsilon^5d\gamma^2({}^1E)$
${}_a{}^2F_2$	22.90	0.7520	0.5276	0.2812	−0.2267	0.1595
${}_b{}^2F_2$	25.47	−0.3618	0.7585	−0.4571	0.1661	0.2391
${}_c{}^2F_2$	34.63	0.0723	−0.3201	−0.3846	−0.4755	0.7198
${}_d{}^2F_2$	40.75	−0.4014	0.0631	0.7370	0.1027	0.5301
${}_e{}^2F_2$	62.97	0.3702	−0.1995	−0.1437	0.8272	0.3436

Term	Energy (10^3 cm^{-1})	$d\epsilon^3({}^2F_1)d\gamma^4$;	$d\epsilon^4({}^3F_1)d\gamma^3$;	$d\epsilon^4({}^1F_2)d\gamma^3$;	$d\epsilon^5d\gamma^2({}^3A_2)$;	$d\epsilon^5d\gamma^2({}^1E)$
${}_a{}^2F_1$	17.80	0.9594	0.1073	−0.2298	−0.0654	0.1039
${}_b{}^2F_1$	26.24	0.1791	0.4068	0.8842	0.1402	−0.0299
${}_c{}^2F_1$	30.47	−0.1382	0.7923	−0.3001	−0.3156	−0.4042
${}_d{}^2F_1$	34.17	0.0726	0.0087	−0.1680	0.8282	−0.5294
${}_e{}^2F_1$	44.27	−0.1514	0.4417	−0.2168	0.4365	0.7378

Term	Energy (10^3 cm^{-1})	$d\epsilon^3({}^2E)d\gamma^4$;	$d\epsilon^4({}^1A_1)d\gamma^3$;	$d\epsilon^4({}^1E)d\gamma^3$;	$d\epsilon^6d\gamma$
${}_a{}^2E$	17.04	0.9674	0.1936	0.1427	−0.0783
${}_b{}^2E$	28.26	−0.0523	−0.3908	0.9170	0.0587
${}_c{}^2E$	40.01	0.1919	−0.4459	−0.2330	0.8425
${}_d{}^2E$	61.49	−0.1563	0.7815	0.2902	0.5295

The energy of the remaining levels, with the same choice of Dq, B, and C parameters is given by

$${}^4A_2 \quad \text{(ground levels)}$$

$${}^4F_2 \quad 8250\ \mathrm{cm}^{-1} \qquad {}^2A_1 = 23\,030\ \mathrm{cm}^{-1}$$

and

$${}_a{}^4F_1 \quad 13\,630\ \mathrm{cm}^{-1}$$

$${}^2A_2 = 39\,930\ \mathrm{cm}^{-1}.$$

$${}_b{}^4F_1 \quad 23\,780\ \mathrm{cm}^{-1}$$

Normal Vibrations and Urey-Bradley Force Constants of Methyl Amine

ELLEN L. WU, GIUSEPPE ZERBI,* SALVATORE CALIFANO,† AND BRYCE CRAWFORD, JR.
Molecular Spectroscopy Laboratory, School of Chemistry, University of Minnesota, Minneapolis 14, Minnesota
(Received May 9, 1961)

Using least-squares fitting to the experimental frequencies, the Urey-Bradley force constants and their uncertainties have been calculated for methyl amine and deuterated derivatives. From the calculation, new assignments of the NH_2 twisting vibrations are proposed: CH_3NH_2, 977 cm^{-1}; CH_3ND_2, 744 cm^{-1}; CD_3NH_2, 1078 cm^{-1}; and CD_3ND_2, 701 cm^{-1}. Potential-energy distributions of these four molecules are reported.

ALTHOUGH methyl amine is the simplest amino compound, a satisfactory normal-coordinate treatment has not previously been carried out in order to provide an estimate of the forces governing its vibrations. Many authors have been interested in the vibrational problem of methyl amine. The Raman spectrum has been studied by Kirby-Smith and Bonner,[1] the infrared spectrum by Cleaves and Plyler,[2] Bailey, Carson, and Daly,[3] Owens and Barker,[4] Bellanato, Sardina, and Barcelo Matutano.[5] More recently Gray and Lord[6] carried out a vibrational analysis of methyl amine and three deuterated derivatives. In this study they discussed the assignments of the previous authors and proposed a new one which seems quite reasonable. Nevertheless, some doubt still remains about the frequency of the NH_2 twisting vibration.

Approximate force constants of methyl amine have been calculated by Barcelo and Bellanato[7] and by Stewart[8] as a four-body problem assuming a point mass for the CH_3 group. More recently Yamaguchi[9] carried out a normal-coordinate calculation using a Urey-Bradley force field, transferring the force constants for the CH_3 group from ethane[10] and those for the NH_2 group from hydrazine.[11] However, the fit between observed and calculated frequencies is somewhat unsatisfactory. Consequently, we thought it worth while to undertake a new normal-coordinate calculation, again using the Urey-Bradley force field, with a least-squares adjustment of the force constants to fit the observed vibrational frequencies of all available isotopic molecules. Some information about the NH_2 twisting mode can be obtained also as a result of this calculation.

POTENTIAL FUNCTION

We used the Urey-Bradley force field which, at the present time, seems to be the most useful representation of the forces between atoms and which provides force constants transferable to other more complex molecules. According to general use, we designated bond-stretching force constants by K, angle-bending by H, and repulsions between nonbonded atoms by F. In terms of these constants and the coordinates indicated in Fig. 1, the Urey-Bradley potential function of

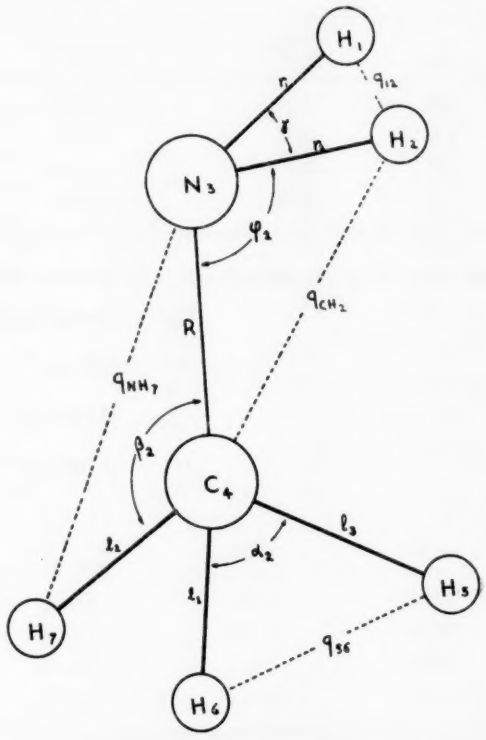

FIG. 1. Coordinates.

* Present address: Istituto di Chimica Industriale del Politecnico, Milano, Italy.
† Present address: Istituto Chimico, via Mezzocannone 4, Napoli, Italy.
[1] J. S. Kirby-Smith and L. G. Bonner, J. Chem. Phys. **7,** 880 (1939).
[2] A. P. Cleaves and E. K. Plyler, J. Chem. Phys. **7,** 563 (1939).
[3] C. R. Bailey, S. C. Carson, and E. F. Daly, Proc. Roy. Soc. (London) **A173,** 339 (1939).
[4] R. G. Owens and E. F. Barker, J. Chem. Phys. **8,** 229 (1940).
[5] J. Bellanato, M. T. Sardina, and J. R. Barcelo Matutano, Anales real soc. expañ. fís. y quim. (Madrid) **51B,** 271 (1955).
[6] A. P. Gray and R. C. Lord, J. Chem. Phys. **26,** 690 (1957).
[7] J. R. Barcelo and J. Bellanato, Spectrochim. Acta **8,** 27 (1956).
[8] J. E. Stewart, J. Chem. Phys. **30,** 1259 (1959).
[9] A. Yamaguchi, J. Chem. Soc. Japan **80,** 1105 (1959).
[10] I. Nagakawa, J. Chem. Soc. Japan **77,** 1030 (1956).
[11] A. Yamaguchi, J. Chem. Soc. Japan **80,** 1109 (1959).

TABLE I. Observed, calculated frequencies in cm^{-1} and deviations of methyl amine and deuterated derivatives.

	CH_3NH_2			CH_3ND_2			CD_3NH_2			CD_3ND_2		
	ν_{obs}	ν_{calc}	$\Delta\nu\%$	ν_{obs}	ν_{calc}	$\Delta\nu\%$	ν_{obs}	ν_{calc}	$\Delta\nu\%$	ν_{obs}	ν_{calc}	$\Delta\nu\%$
ν_1[a]	3361	3371	0.30	2479	2451	−1.13	3361	3370	0.27	2477	2452	−1.01
ν_2	2961	2980	0.64	2961	2980	0.64	2203	2211	0.36	2202	2210	0.36
ν_3	2820	2835	0.53	2817	2835	0.64	2077	2040	−1.78	2073	2039	−1.64
ν_4	1623	1621	−0.12	1234	1239	0.41	1624	1620	−0.25	1227	1242	1.22
ν_5	1473	1486	0.88	1468	1486	1.23	1065[b]	1060	−0.47	1065[b]	1058	−0.66
ν_6	1430	1442	0.84	1430	1442	0.84	1142	1139	−0.26	1123	1113	−0.89
ν_7	1130	1147	1.50	1117	1140	2.06	913	913	0	880	890	1.14
ν_8	1044	1044	0	997	977	−2.01	973	986	1.34	942	938	−0.42
ν_9	780	797	2.18	624	615	−1.44	740	759	2.57	601	595	−1.00
ν_{10}	3427	3437	0.29	2556	2536	−0.78	3427	3437	0.29	2556	2535	−0.82
ν_{11}	2985	2980	−0.17	2985	2980	−0.17	2236	2212	−1.07	2238	2212	−1.16
ν_{12}	1485[b]	1486	0.07	1485[b]	1485	0	1077	1050	−2.51	1077	1056	−1.95
ν_{13}	...	977	...	...	744	...	...	1078	...	...	701	...
ν_{14}	1195[b]	1178	−1.42	1187	1148	−3.29	910[b]	834	−8.35	910	938	3.08

[a] The numbering of the fundamental frequencies is according to Gray and Lord.
[b] Bands not directly observed.

methyl amine is expressed as

$$2V = K_{CN}(\Delta R)^2 + 2K_{CN}'(R\Delta R) + \sum^{3} K_{CH}(\Delta l_i)^2$$
$$+ 2\sum^{3} K_{CH}'(l_i \Delta l_i) + \sum^{2} K_{NH}(\Delta r_j)^2 + 2\sum^{2} K_{NH}'(r_j \Delta r_j)$$
$$+ H_\gamma r^2(\Delta\gamma)^2 + 2H_\gamma' r^2 \Delta\gamma + \sum^{2} H_\phi r^2(\Delta\phi_j)^2$$
$$+ 2\sum^{2} H_\phi' r^2(\Delta\phi_j) + \sum^{3} H_\beta l^2(\Delta\beta_i)^2 + 2\sum^{3} H_\beta' l^2(\Delta\beta_i)$$
$$+ \sum^{3} H_\alpha l^2(\Delta\alpha_i)^2 + 2\sum^{3} H_\alpha' l^2(\Delta\alpha_i) + F_{12}(\Delta q_{12})^2$$
$$+ 2F_{12}'(q_{12}\Delta q_{12}) + \sum^{3} F_{56}(\Delta q_{ik})^2 + 2\sum^{3} F_{56}'(q_{ik}\Delta q_{ik})$$
$$+ \sum^{3} F_{NH}(\Delta q_{NH_i})^2 + 2\sum^{3} F_{NH}'(q_{NH_i}\Delta q_{NH_i})$$
$$+ \sum^{2} F_{CH}(\Delta q_{CH_j})^2 + 2\sum^{2} F_{CH}'(q_{CH_j}\Delta q_{CH_j}),$$

where each of the q's may be expressed in terms of the internal coordinates in the usual way.[12] The r's, l's, and R are equilibrium bond lengths which are linearly independent; however, the six angles α_1, α_2, α_3, β_1, β_2, and β_3 around the carbon atom are not independent. Introduction of the redundancy relation among them[12] gives rise as usual to an additional force constant κ, the "intramolecular tension."

The linear constants K' and H' disappear when the q coordinates are eliminated; we adopted the customary convention of setting F' equal to $\mp 0.1F$.

[12] T. Shimanouchi, J. Chem. Phys. **17**, 245 (1949).

Tetrahedral angles were assumed; equilibrium bond distances were taken as $R=1.474$ A, $r=1.014$ A, and $l=1.093$ A.[13,14]

In the potential field described above, the interaction between an amino hydrogen and a methyl hydrogen atom is ignored. If we assume that the torsional principal force constant is equal to zero, no force is then opposing the torsional mode of the NH_2 group around

TABLE II. Urey-Bradley force constants and uncertainties in md/A for methyl amine.

	UBFC	Uncertainty
K_{NH}	6.399	0.064
K_{CH}	4.446	0.048
K_{CN}	3.347	0.223
H_{HNH}	0.610	0.034
H_{HNC}	0.522	0.077
H_{NCH}	0.427	0.086
H_{HCH}	0.477	0.024
$F_{H(N)H}$	−0.021	0.057
$F_{H(C)H}$	−0.076	0.026
F_{NH}	0.683	0.074
F_{CH}	0.042	0.110
κ	−0.116	0.069

[13] T. Nishikawa, T. Itoh, and K. Shimoda, J. Chem. Phys. **23**, 1735 (1955).
[14] D. R. Lide, Jr., J. Chem. Phys. **27**, 343 (1957).

the C—N bond and we are allowed to leave it out of the calculation. Furthermore, in methyl amine this mode is probably slightly coupled with the other vibrations because of its low frequency; Hadni[15] assigned a band at 269 cm^{-1} to this vibration.

SYMMETRY COORDINATES AND SECULAR EQUATION

Methyl amine belongs to the point group C_s and of its 15 vibrations, 9 belong to the A' and 6 to the A'' species; both are infrared and Raman active. With the neglect of the torsional mode, we are left with 14 symmetry coordinates which can be set up in terms of the internal coordinates as follows:

A' species:

$$S_1 = (2)^{-\frac{1}{2}}(\Delta r_1+\Delta r_2),$$

$$S_2 = \Delta R,$$

$$S_3 = (3)^{-\frac{1}{2}}(\Delta l_1+\Delta l_2+\Delta l_3),$$

$$S_4 = (6)^{-\frac{1}{2}}(\Delta l_1+\Delta l_2-2\Delta l_3),$$

$$S_5 = \Delta\gamma,$$

$$S_6 = (2)^{-\frac{1}{2}}(\Delta\phi_1+\Delta\phi_2),$$

$$S_7 = (6)^{-\frac{1}{2}}(\Delta\beta_1+\Delta\beta_2-2\Delta\beta_3),$$

$$S_8 = (6)^{-\frac{1}{2}}(\Delta\alpha_1+\Delta\alpha_2-2\Delta\alpha_3),$$

$$S_9 = (6)^{-\frac{1}{2}}(\Delta\beta_1+\Delta\beta_2+\Delta\beta_3-\Delta\alpha_1-\Delta\alpha_2-\Delta\alpha_3).$$

A'' species:

$$S_{10} = (2)^{-\frac{1}{2}}(\Delta r_1-\Delta r_2),$$

$$S_{11} = (2)^{-\frac{1}{2}}(\Delta l_1-\Delta l_2),$$

$$S_{12} = (2)^{-\frac{1}{2}}(\Delta\phi_1-\Delta\phi_2),$$

$$S_{13} = (2)^{-\frac{1}{2}}(\Delta\beta_1-\Delta\beta_2),$$

$$S_{14} = (2)^{-\frac{1}{2}}(\Delta\alpha_1-\Delta\alpha_2).$$

The standard Wilson FG-matrix method was used for the calculations of the normal coordinates. The elements of the symmetrized G matrix and of the transformation matrix Z, relating the Urey-Bradley constants to the symmetrized F matrix ($F=ZF_{UB}$), are on file in the Molecular Spectroscopy Laboratory in the University of Minnesota.

The numerical calculations were carried out with the aid of an electronic digital computer Univac 1103 at the University of Minnesota. In order to perform this calculation for the four isotopes of methyl amine, a program for the least-squares refinement of the Urey-Bradley force constants was written in which the NOCO and MAC routines coded by Dr. E. Curtis were used. A trial set of force constants taken from Mizushima and Shimanouchi[16] was used to solve the secular equation at the beginning.

The least-squares refinement of the force constants to fit all the frequencies of four isotopic species was carried out by means of the following relation:

$$Z'J'PJZ\Delta F_{UB}=Z'J'P\Delta\Lambda,$$

where Z is the transformation matrix, J is a Jacobian matrix with elements $J_{mn}=\partial\lambda_m/\partial F_n$, P is a weighting matrix, proportional to $1/\lambda$, ΔF_{UB} is the correction to be applied to the Urey-Bradley force constants, and $\Delta\Lambda=\Lambda_{obs}-\Lambda_{calc}$. Since we used all four isotopic species of methyl amine giving a total of 56 frequencies, the least-squares refinement of 12 Urey-Bradley force constants was feasible.

Furthermore, in order to have a complete analysis of the normal coordinates of these molecules, we calculated the potential-energy distributions and the moment matrix. The potential-energy distributions were calculated using the relation[17]: $\Lambda^{-1}JZ\Phi^*$, where Λ^{-1} is a diagonal matrix of the $1/\lambda_{i(calc)}$, Φ^* is a diagonal matrix of the Urey-Bradley force constants, and J and Z have the usual meaning.

The uncertainties in the force constants were obtained from the square root of the diagonal elements of the moment matrix defined in the case of the Urey-Bradley force field as[18]: $\sigma^2(Z'J'PJZ)^{-1}$, where $\sigma^2=\Delta\Lambda'P\Delta\Lambda/d$, and d is the statistical degree of freedom, i.e., the difference between the number of observed frequencies and the number of force constants. The dispersions of the Urey-Bradley force constants are given in the tables.

RESULTS AND DISCUSSION

In our first calculation we refined the force constants to fit the Gray-Lord assignments. The calculated frequencies corresponded reasonably to those observed, but the force constants thus obtained were extremely unreasonable.

The NH_2 twisting frequency ν_{13} of A'' species has been assigned to different bands by various authors. Very recently, Stewart assigned the band at 695 cm^{-1} to this mode for the undeuterated methyl amine, whereas 1455 cm^{-1} was given by Gray and Lord.

In view of this disagreement, we tried a new refinement in order to fit the Gray-Lord assignments with the Stewart correction, but the calculated frequencies deviated considerably from the observed ones. Therefore, in order to overcome this difficulty in the refining process, we gave zero weight to the NH_2 twisting frequencies for all isotopes and inspected the calculated frequencies.

Since we have only 12 force constants plus the product rule relations to fit 52 experimental frequencies,

[15] A. Hadni, J. phys. radium **15**, 375 (1954).

[16] S. Mizushima and T. Shimanouchi, *Infrared Absorption and Raman Spectroscopy* (Kyoritsu Publishing Company, Tokyo, 1958).

[17] J. Overend and J. R. Scherer, J. Chem. Phys. **32**, 1289 (1960).

[18] E. Curtis, dissertation, University of Minnesota, 1959.

TABLE III. Potential-energy distributions of some isotopic species of methyl amine (entries rounded to nearest %).[a]

			K_{NH}	K_{CH}	K_{CN}	H_γ	H_φ	H_β	H_α	$F_{H(N)H}$	$F_{H(C)H}$	F_{NH}	F_{CH}	κ
ν_1	NH_2	st.	99											
			99			1								
			99											
			99			1								
ν_2	CH_3	st.		93					1		−1	7		
				93					1		−1	7		
				93					1		−1	6		
				93					1		−1	6		
ν_3	CH_3	st.		94							−4	9		
				94							−4	9		
				93	1			1	1		−3	8		
				93	1			1	1		−3	8		
ν_4	NH_2	d.			2	77	20			−1		1	1	
			1	1	20	52	19			−1		7		
					2	77	20			−1		1	1	
			1		24	49	18	3	3	−1		4		−1
ν_5	CH_3	d.		2				14	77		−5	10		2
				2				14	78		−6	10		2
				2			1	17	71		−5	12		2
				2			1	16	74		−5	11		2
ν_6	CH_3	d.		4	3			41	46		−4	20		−10
				4	3			41	46		−4	20		−10
				2	36	2		29	33		−3	7	1	−7
				4	13	15	2	32	36		−4	10	1	−7
ν_7	CH_3	w.			1	2	4	39	32		−2	32		−8
						2	1	41	33		−2	33		−8
				1	16	1	10	27	25		−2	31	1	−6
				1	13	3	4	30	21		−2	34	1	−6
ν_8	C—N	st.		2	63	7	2	2	1			23	1	
				1	49	30	1	1				18	1	
				4	21	9	12	11	21		−2	28		−3
				2	21	20	2	13	20		−2	27		−4
ν_9	NH_2	w.			5	16	70	2	1			3	4	
					2	16	75	1				2	4	
					4	12	53	13	6			12	3	−2
					2	15	70	4	2			4	4	−1
ν_{10}	NH_2	st.	100											
			99											
			100											
			99											
ν_{11}	CH_3	st.		93					1		−1	7		
				93					1		−1	7		
				93					1		−1	6		
				93					1		−1	6		
ν_{12}	CH_3	d.		2				14	78		−6	10		2
				2				14	78		−6	10		2
				2			19	3	81		−6	1	1	−1
				2				15	76		−5	10		2
ν_{13}	NH_2	tw.					71	12	8			9	3	−2
							90	3	2			2	4	−1
							58	18	6			15	3	1
							70	12	7			10	3	−2
ν_{14}	CH_3	w.					25	31	26		−2	25	1	−6
							6	40	31		−2	32		−8
							19	36	23		−1	29	1	−7
							25	30	27		−2	25	1	−6

[a] For each normal mode, the distributions of the potential energy are listed in the following order: CH_3NH_2, CH_3ND_2, CD_3NH_2, CD_3ND_2.

we think that a good fit together with a reasonable set of force constants can be considered a good check of the assignments used and can confirm the consistency of the Urey-Bradley force field. For these reasons we suggest, with confidence, a modified assignment based only upon the normal-coordinate calculations. The calculated frequencies and the new assignments are reported in Table I with force constants and potential-energy distributions in Table II and III, respectively. As it can be seen from Table I, the agreement between calculated and experimental frequencies is rather satisfactory; the worst mean deviation being only 1.50%.

The NH_2 twisting frequencies were found to be 977 cm^{-1} for CH_3NH_2, 744 cm^{-1} for CH_3ND_2, 1078 cm^{-1} for CD_3NH_2, and 701 cm^{-1} for CD_3ND_2. From simple arguments, one would expect the value for CD_3NH_2 to be near or lower than that of CH_3NH_2. However, the obtained rise in frequency can be understood from consideration of perturbation effects due to a mixing of different normal modes occurring in a narrow range of frequencies, clearly revealed in the potential-energy distribution (Table III).

Although the calculated NH_2 twisting frequency at 977 cm^{-1} is 478 cm^{-1} lower than that given by Gray and Lord, it is not too unreasonable. Earlier Cleaves and Plyler proposed for this either a band at 620 cm^{-1} or at 1127 cm^{-1}.

Examining the vibrational assignments of other simple amino compounds in the literature, we found that Kohlrausch[19] observed a strong band at about 1100 cm^{-1} in the Raman spectrum of hydrazine and a weaker one in the same region in the spectra of 13 primary amines. On the basis of these observations he suggested that this band may be assigned to a deformation of the NH_2 group. Later Fresenius and Karweil,[20] as well as Goubeau,[21] assigned two bands occurring between 965 and 1108 cm^{-1} to the NH_2 rocking modes of hydrazine. More recently, Giguère and Liu[22] proposed new values of 1098 and 1275 cm^{-1}. Furthermore, Evans[23] in the study of the spectra of anilines assigned one of the two bands occurring at 1050 and 1118 cm^{-1} to the NH_2 twisting mode; and this suggestion agrees with that proposed at the same time by Tsuboi[24] from a careful study of the spectra of aniline and aniline-N^{15}.

Unfortunately in the spectra reported by Gray and Lord it is impossible to find any reasonable bands that can be assigned to these vibrations. Nevertheless, it is well known that these bands are usually very weak, and often they can be detected only when a sample is studied with a long absorption path. To our knowledge no spectra of high-pressure samples are reported in the literature for this region.

The assignments proposed in the present work for methyl amine and deuterated derivatives are confirmed by the distributions of the potential energy that clearly show how the various potential-energy constants are involved in the different normal modes. From the good fit of the calculated to the experimental frequencies together with the small uncertainties of the calculated Urey-Bradley force constants, we can deduce that the force field used is reasonably good.

Moreover, the calculated force constants K_{CH}, K_{NH}, H_{HCH}, and H_{NCH} are in very good agreement with those published in the literature. The other interaction force constants between nonbonded atoms need some words of comment. Surprisingly, the interaction between nonbonded hydrogen atoms in the CH_3 group, though very small, is negative. Overend and Scherer[25] reported an attractive force constant for CH_3F, and the interaction between gem-hydrogens obtained by Curtis[18] in a careful study of ethylenes is negative too. However, the full physical meaning of this number cannot be understood until a larger collection of Urey-Bradley force constants is available.

No meaning can be attributed either to the F_{CH} or the $F_{H(N)H}$, since the uncertainties are higher than the force constants themselves, so that we could either use different values or choose zero without affecting the calculation. Finally, the high value of F_{NH} can be easily explained in terms of a strong interaction between the hydrogen and the nitrogen atoms arising from the unshared pair of electrons on the latter.

ACKNOWLEDGMENTS

G. Zerbi wishes to thank the U. S. National Academy of Sciences for a research fellowship under the Visiting Research Scientists Program supported by the International Cooperation Administration. S. Califano expresses his thanks to the Fondazione Alberto Beneduce for a fellowship for the academic year 1958–59 and to the Consiglio Nazionale delle Ricerche (Italy) for a traveling grant. We also gratefully acknowledge financial support from the U.S. Army Research Office.

[19] K. W. F. Kohlrausch, Monatsh. Chem. **68,** 349 (1936).
[20] W. Fresenius and J. Karweil, Z. physik. Chem. **44B,** 1 (1939).
[21] J. Goubeau, Z. physik. Chem. **45B,** 237 (1940).
[22] P. A. Giguère and I. D. Liu, J. Chem. Phys. **20,** 136 (1952).
[23] J. C. Evans, Spectrochim. Acta **16,** 428 (1960).
[24] M. Tsuboi, Spectrochim. Acta **16,** 505 (1960).
[25] J. Overend and J. R. Scherer, J. Chem. Phys. **33,** 446 (1960).

Construction of Reliable Internuclear Potential Curves from Equilibrium Bond Lengths and Vibrational Frequencies

D. STEELE AND E. R. LIPPINCOTT
Department of Chemistry, University of Maryland, College Park, Maryland

(Received March 13, 1961)

A method is presented for the construction of reliable internuclear potential curves using a previously proposed function and observed values of equilibrium bond lengths and vibrational frequencies. The function has the form

$$V=D_e\{1-\exp[-(n\Delta r^2/2r)]\}\{1+af(r)\}.$$

An explicit form is presented for the observed periodicity of the parameter a when referring to the ground states of diatomic molecules. This periodicity is shown to lead to relationships from which D_e, α_e, and $x_e\omega_e$ can be calculated solely from ω_e and r_e. An empirical relationship between the values of the parameter a in the ground and the excited states is presented from which D_e, α_e, and $x_e\omega_e$ can be deduced for any nonionic excited state from ω_e and r_e of that state. This latter relationship demonstrates that $\omega_e r_e^2$ is not constant for all states of any molecule but is dependent in a predictable manner on the other spectroscopic constants. These relationships enable potential curves to be constructed solely from a knowledge of ω_e and r_e. Calculated curves for the $X^1\Sigma_g^+$ states of H_2 and I_2 and ground and excited states of N_2 agree extremely well with experimental curves, deviating by no more than 2% of the dissociation energy. The agreement is very good for large values of r for H_2 and I_2, which indicates that a general form exists for the interaction of bonding atoms at large distances.

THE construction of potential curves is of considerable value for the understanding of kinetics mechanisms, spectral phenomena, stellar structure, and many associated problems. In principle, such curves may be calculated *ab initio* from the Schrödinger equation. However, in practice, reliable curves cannot be obtained at present for anything more complicated than three-particle systems. They may be constructed for bound states of diatomic molecules from a knowledge of the experimental energy levels of the system by the method of Rydberg, Klein, and Rees as modified by Vanderslice and others[1,2] (hereafter referred to as the R.K.R.V. method). This method is a semiclassical one and consequently may give rise to errors for small changes in the bond lengths from the equilibrium values, that is, for small Δr. This has been checked[3] by comparison of the R.K.R.V. curve of H_2 in the region of r_e with a calculated curve based on the Dunham method which is known to be reliable in this range. The results agreed to considerably better than 0.1%. This indicates that the curves obtained in the former manner may be taken as correct.

Unfortunately the curves obtainable by this method may be deduced only over the energy range for which energy levels are given by the spectroscopic data. Complete potential curves (that is, for all values of the interaction energy less than D_e) are consequently known only for the ground states of H_2 and I_2. In the vast majority of cases the experimental curves are known only for small internuclear displacements. A further disadvantage of the R.K.R.V. method is that spectroscopic constants, such as anharmonicity $x_e\omega_e$, the vibrational-rotational coupling constant α_e, and higher terms cannot be deduced from limited experimental data and hence the technique is of little value in predicting data. These considerations make empirical approaches to these problems of considerable value. In this paper it will be shown how an empirical approach can be used to obtain reliable potential curves for ground and excited states of diatomic molecules using very limited data, in particular, from the vibrational frequency ω_e and the equilibrium bond length r_e. This implies that the anharmonic corrections can be deduced from the same limited data. Rules and equations are developed for doing the latter, which are then used to reduce the necessary amount of data required to plot curves using a previously proposed potential function.[4] Most empirical approaches require sufficient data to determine the first-order correction terms from the harmonic oscillator model, that is, the anharmonicity $x_e\omega_e$ and the vibrational rotational coupling constant α_e. Even when these are known the resulting curves are not usually of high accuracy.

The most successful approach to the potential problem is to assume a general analytical form for potential curves and to solve the Schrödinger equation using the general form for $V(r)$. Considerable simplification of this technique was effected by Dunham,[5] who solved the Schrödinger equation for a general power series expansion of $V(r)$ and related the coefficients of Δr^n to the molecular constants. These relations may lead to useful correlations between the molecular constants for any given assumed form of $V(r)$. The earliest successful potential function was that of Morse,[6] which leads to a relation between ω_e, $\omega_e x_e$, and D_e from which either $\omega_e x_e$ or D_e can be deduced from the other two constants with a reliability of about $\pm 20\%$. Many

[1] J. T. Vanderslice, E. A. Mason, and E. R. Lippincott, J. Chem. Phys. **30,** 129 (1959).
[2] J. T. Vanderslice, E. A. Mason, W. G. Maisch, and E. R. Lippincott, J. Chem. Phys. **33,** 614 (1960).
[3] J. T. Vanderslice, E. A. Mason, W. G. Maisch, and E. R. Lippincott, J. Mol. Spectroscopy **3,** 17 (1959).
[4] (a) E. R. Lippincott and R. Schroeder, J. Chem. Phys. **23,** 1131 (1955); J. Am. Chem. Soc. **78,** 5171 (1956); J. Phys. Chem. **61,** 921 (1957). (b) E. R. Lippincott and M. O. Dayhoff, Spectrochim. Acta **16,** 807 (1960); E. R. Lippincott, J. Chem. Phys. **26,** 1678 (1957).
[5] J. L. Dunham, Phys. Rev. **41,** 721 (1932).
[6] P. M. Morse, Phys. Rev. **34,** 57 (1929).

other general forms have been suggested, some involving only three parameters, others more. Those involving more than three parameters are generally of very limited value for the prediction of spectroscopic parameters since so many are necessary to define the function. One simple internuclear potential function which has been used very successfully in correlation and prediction studies[4,7] is

$$V(r)=D_e[1-\exp(-n\Delta r^2/2r)][1+af(r)]. \quad (1)$$

n is given by $n=k_e r_e/D_e$, where k_e is the force constant referred to zero displacement of the nuclei. In its simplest form a is taken as zero. This leads to reliable relationships between ω_e, $\omega_e x_e$, and D_e for ground and excited states of diatomic and polyatomic molecules. The relevant equations are

$$D_e(\text{ergs/molecule})=k_e/[64\pi^2 c\mu\omega_e x_e/3h-1/r_e^2], \quad (2a)$$

$$\omega_e x_e=3h(n/r_e+1/r_e^2)/64\pi^2 c\mu, \quad (3a)$$

and

$$\alpha_e=0. \quad (4a)$$

In terms of Varshni's notation[8] (2a) and (4a) may be written

$$G=3[2\Delta+1] \quad (2b)$$

and

$$F=0, \quad (4b)$$

where $F=\alpha_e\omega_e/6B_e^2$, $G=8x_e\omega_e/B_e$, $\Delta=k_e r_e^2/2D_e$.

However, Eq. (1) with $a=0$ (hereafter designated S.F. or simple function) suffers from the disadvantages that it predicts α_e equal to zero and that its limiting forms are unsatisfactory. On the other hand, it may be derived from a semiempirical delta-function model of chemical binding.[4b]

With $a\neq 0$ the internuclear potential function assumes a five-parameter form. To reproduce potential curves of bound molecular states the quantity $f(r)$ must be chosen such that $V(r)=\infty$ when $r=0$, and $V(r)=D_e$, when $r=\infty$. For large values of r, $f(r)$ was originally assumed to take the form of a Lennard-Jones (6–12) attractive potential[4] which is compatible with these conditions. The general form was

$$V(r)=D_e[1-\exp(-n\Delta r^2/2r)]\left\{1-a(r_e/r)^6\cdot\left[1-\exp\left(-\frac{b^2 n\Delta r^2 r^{11}}{2r_e^{12}}\right)^{\frac{1}{2}}\right]+a\left(\frac{r_e}{r}\right)^{12}\cdot\left[1-\exp\left(-\frac{b^2 n\Delta r^2 r^{11}}{2r_e^{12}}\right)\right]\right\}. \quad (5a)$$

This leads to the following relations:

$$D_e=\omega_e^2/2nr_e B_e, \quad (6)$$

$$\alpha_e=(6abB_e^2/\omega_e)(nr_e/2)^{\frac{1}{2}} \quad \text{or} \quad F=ab\Delta^{\frac{1}{2}}, \quad (7)$$

$$x_e\omega_e=\tfrac{3}{2}B_e[\tfrac{1}{4}+\tfrac{1}{4}nr_e+ab(\tfrac{1}{2}nr_e)^{\frac{1}{2}}+(\tfrac{5}{4}a^2b^2-ab^2)\tfrac{1}{2}nr_e], \quad (8)$$

or

$$\tfrac{1}{12}G=\tfrac{1}{4}+\tfrac{1}{2}\Delta+ab\Delta^{\frac{1}{2}}+(\tfrac{5}{4}a^2b^2-ab^2)\Delta.$$

Another proposed form for (1) which leads to the same relations between ω_e, r_e, α_e, $x_e\omega_e$, and D_e (see below) is

$$V(r)=D_e\{1-\exp[-(n\Delta r^2/2r)]\}\cdot\{1-a(b^2 n/2r)^{\frac{1}{2}}\Delta r\exp[-(b^2 n/2r_e)^{\frac{1}{2}}\Delta r]\}. \quad (5b)$$

This will be shown to be superior to (5a). Eliminating a from (7) and (8) and using the experimental values for the spectroscopic constants, b is found to have a constant value of 1.065 ± 0.03 for all states of all molecules with the exception of hydrogen, for which it is 1.16.[7] Equations (2) to (4) and (6) to (8) are based on the much used assumption that B_e^2/ω_e^2 is negligible in comparison with unity.[5] This is not strictly true for hydrogen and would appear to be a plausible reason for the value of b for this molecule being out of line with its value for other molecules. Combining Eqs. (6), (7), and (8) allows D_e to be calculated from experimental values of k_e, $x_e\omega_e$, α_e, r_e, and b. Where the data are reliable it has been shown that the dissociation energies calculated from the three- and five-parameter forms agree extremely well. This suggests an equivalence of the two forms. Comparing (2b) with (8) and eliminating Δ using (2b) leads to

$$\tfrac{1}{3}G=1+2[1+\tfrac{5}{4}F]^2/b^2. \quad (9)$$

Substituting $b=1.065$ in (9) results in a relationship between α_e, ω_e, $x_e\omega_e$, and B_e only, which is very similar to the Pekeris relation (10)[9] obtained from the Morse function.

$$\tfrac{1}{8}G=(1+F)^2 \quad (10)$$

Equation (9) is slightly superior to Eq. (10), particularly for hydrogen-containing molecules, and allows $x_e\omega_e$ to be calculated with an average error of approximately 5%. For the ground states of CS, O_2, O_2^+, CO, IO, and NO for which the data are accurate and well established, the error is less than 1%. Solving (2b), (7), and (9) for a in terms of F one obtains

$$a=F/(1+\tfrac{5}{4}F). \quad (11)$$

This allows the parameter a to be conveniently and rapidly evaluated from α_e, ω_e, and B_e only. The results of such calculations show that for the ground states of homonuclear diatomic molecules a is periodic within the periodic table, rising from 0.344 for H_2 to 0.636 for

[7] E. R. Lippincott and D. Steele, J. Chem. Phys. (to be published).

[8] Y. P. Varshni, Revs. Modern Phys. **29**, 664 (1957).

[9] C. L. Pekeris, Phys. Rev. **45**, 98 (1934).

TABLE I. Calculation of ground-state data from periodic a rule. (a) homonuclear diatomics.[a]

Mol.	a calc	ω_e (cm^{-1})	r_e (A)	α_e calc (cm^{-1})	α_e obs (cm^{-1})	$x_e\omega_e$ calc (cm^{-1})	$x_e\omega_e$ obs (cm^{-1})	D_e calc (ev)	D_e obs[b] (ev)
Li_2	0.475	351.43	2.6725	0.00903	0.00704	2.946	2.592	1.065	1.10±0.05
Na_2	0.495	159.23	3.0786	0.00117	0.00079	0.761	0.726	0.837	0.75±0.03
K_2	0.515	92.64	3.923	0.000296	0.000219	0.314	0.354	0.681	0.520
B_2	0.515	1051.3	1.589	0.0121	0.014	6.770	9.4	4.066	3.0±0.5
$C_2\ ^3\Pi$	0.535	1641.35	1.3117	0.0157	0.01683	10.454	11.67	6.365	~5.6
$C_2\ ^1\Sigma$	0.535	1855.63	1.2422	0.0173	0.01832	11.656	14.08	7.297	~5.6
Si_2	0.555	506.72[c]	2.252[c]	0.00121	0.00135[c]	1.762	1.97[c]	3.564	3.2[c]
N_2	0.555	2358.07[d]	1.0975[d]	0.0184	0.01709[d]	14.840	14.188[d]	9.175	9.902[d,e]
P_2	0.575	780.89[f]	1.8931[f]	0.00145	0.001477[f]	2.657	2.820[f]	5.584	5.08[f]
O_2	0.575	1580.36	1.2074	0.0162	0.01579	12.625	12.0730	4.804	5.213
S_2	0.595	725.68	1.889	0.00168	0.00160	3.094	2.852	4.114	4.4
Se_2	0.605	391.77	2.157	0.000313	0.00027	1.144	1.06	3.536	2.8±0.1
Te_2	0.615	251.	2.59	0.000099		0.502	0.55	3.008	2.3±0.2
F_2	0.595	891.9	1.435	0.01234		9.280		2.131	1.6
Cl_2	0.615	564.9	1.988	0.00168	0.0017	3.109	4.0	2.460	2.51
Br_2	0.635	323.2	2.2836	0.00037	0.000275	1.265	1.07	1.931	1.971
I_2	0.655	214.52	2.6666	0.000141	0.0001208	0.766	0.6127	1.423	1.556

[a] Unless additional references are listed the spectroscopic constants have been taken from G. Herzberg's *Spectra of Diatomic Molecules* (D. Van Nostrand Company, Inc., Princeton, New Jersey, 1950), pp. 502–581.

[b] Unless additional references are listed the observed dissociation energies are taken from a tabulation by A. G. Gaydon, *Dissociation Energies* (Chapman and Hall, Ltd., London, 1953), 2nd ed.

[c] A. E. Douglas, Can. J. Phys. **33,** 801 (1955).

[d] A. Lofthus, Can. J. Phys. **34,** 780 (1956).

[e] B. P. Stoicheff, Can. J. Phys. **35,** 730 (1957).

[f] A. E. Douglas and P. T. Rao, Can. J. Phys. **36,** 565 (1958).

I_2. For heteronuclear molecules the a values are given satisfactorily by the mean value of the a's of the constituent atoms with the sole exception of hydrides for which a(H) is best taken as 0.376. Since the a values for the second column of the periodic table are unknown and those for the first column do not appear to be too reliable, it is not possible to give an unequivocal empirical form for a in terms of the position of the element within the periodic table. The present data are satisfactorily represented by

$$a(x)=0.335+0.080\delta+0.02[n_c+n_r], \qquad (12)$$

where $a(x)$ is the a value for the ground state, δ is equal to unity for all molecules except hydrogen (hydrides) for which it is zero, and n_c and n_r are the column and row numbers of the element in the periodic table.

The above relationships allow D_e, $x_e\omega_e$, and α_e to be derived for the ground states of all diatomic molecules, apart from those involving transition atoms, solely from a knowledge of ω_e and r_e. The appropriate equation for D_e is

$$D_e=(\tfrac{1}{2}b^2)k_e r_e^2(1-\tfrac{5}{4}a)^2. \qquad (13)$$

The results of some such calculations are tabulated in Tables I–III, where they are compared with the experimental quantities. The average percent deviations are 10, 8, and 13% for α_e, $x_e\omega_e$, and D_e, respectively.

EXCITED STATES

The empirical equation (12) is valid only for the ground states of diatomic molecules. To extend these correlations to excited states it is necessary to find a relationship between ω_e, r_e, and a of the ground states and the corresponding parameters of the excited states. Birge[10] and Mecke[11] have shown that $\omega_e r_e^2$ is a constant for the different electronic states of one and the same molecule. This suggests relationships of the form

$$a^*=\frac{4}{5}\left\{1-\frac{\omega^{(*)x}r^{(*)y}}{\omega(x)^x r(x)^y}\left[1-\frac{5}{4}a(x)\right]\right\}, \qquad (14)$$

which were tried and found very successful with $x=1$ and $y=2$. The result that the variations in a can be correlated with variations in $\omega_e r_e^2$ indicates that, although the constancy of $\omega_e r_e^2$ is a good approximation,

[10] R. T. Birge, Phys. Rev. **25,** 240 (1925).

[11] R. Mecke, Z. Physik **31,** 709 (1925).

TABLE II. Calculation of ground state data from periodic a rule. (b) heteronuclear.[a]

Mol.	a calc	ω_e (cm^{-1})	r_e (Å)	α_e calc (cm^{-1})	α_e obs (cm^{-1})	$x_e\omega_e$ calc (cm^{-1})	$x_e\omega_e$ obs (cm^{-1})	D_e calc (ev)	D_e obs[b] (ev)
BO	0.545	1885.44	1.2049	0.0172	0.01648	12.351	11.769	7.132	7.6±0.4
BN	0.535	1514.6	1.281	0.0178	0.025	10.666	12.3	5.310	4.0±0.5
CO	0.555	2169.83[c]	1.1282[c]	0.0187	0.0175[c]	14.342	13.295[c]	8.038	11.245[c]
CP	0.555	1239.67	1.5621	0.00559	0.00597	5.924	6.86	6.345	6±1
CS	0.565	1285.1[d]	1.5344[d]	0.00604	0.00624[d]	6.593	6.5[d]	6.106	7.2±1.0[d]
ICl	0.635	384.293	2.3207	0.000626	0.000534	1.8155	1.501	1.943	2.178
IO	0.615	681.47[e]	1.8679[e]	0.00271	0.002696[e]	4.333	4.29[e]	2.567	1.9±0.2[e]
NO	0.565	1904.03[f]	1.1508[f]	0.0176	0.0178[f]	13.701	13.97[f]	6.452	6.609[f]
PbS	0.605	428.14	2.3948	0.000391	0.000873	1.222	1.201	3.610	3.25±0.3
PN	0.565	1337.24	1.4910	0.00533	0.00557	6.313	6.983	6.900	6.1±0.8
PO	0.575	1230.64	1.4457	0.00578	0.0055	6.654	6.52	5.509	5.4
SiN	0.555	1151.68	1.5718	0.00504	0.00567	5.421	6.560	5.983	4.5±0.4
SiO	0.565	1241.44	1.509	0.00492	0.00508	5.846	5.92	6.428	8.0±0.3
SrO	0.565	653.5	1.921	0.00202	0.0020	2.724	4.0	3.837	5.0 or 3.6
SO	0.585	1123.73	1.4933	0.00584	0.00562	6.754	6.116	4.523	5.22

[a] See reference a, Table I.
[b] See reference b, Table I.
[c] D. H. Rank, A. H. Guenther, G. D. Saksena, T. N. Shearer, and T. A. Wiggins, J. Opt. Soc. Am. **47**, 686 (1957).
[d] A. Lagerquist *et al.* Arkiv. Fysik **14**, 387 (1959).
[e] R. A. Durie, F. Legay, and D. A. Ramsey, Can. J. Phys. **38**, 444 (1960).
[f] W. H. Fletcher and G. M. Begun, J. Chem. Phys. **27**, 579 (1957).

small changes in this quantity can be simply related to changes in other molecular vibration-rotation parameters. The wide range of vibrational frequencies and bond lengths for hydrogen make it a very sensitive molecule for these correlations, and it was found that $\omega_e r_e^2$ is not nearly constant and using these powers of ω_e and r_e in (14) does not reproduce the a's of excited states. $\omega_e r_e^{7/4}$, however, yields good correlations. Apart from hydrogen, $\omega_e r_e^2$ can be used with little error. Equation (13) in conjunction with (14) does not always predict the molecular parameters with high accuracy, particularly D_e, but serves to indicate the approximate value of the dissociation energy, from which the dissociation products may be deduced and hence an

TABLE III. Calculation of ground state data from periodic a rule. (c) hydrides.[a]

Mol.	a calc	ω_e (cm^{-1})	r_e (Å)	α_e calc (cm^{-1})	α_e obs (cm^{-1})	$x_e\omega_e$ calc (cm^{-1})	$x_e\omega_e$ obs (cm^{-1})	D_e calc (ev)	D_e obs[b] (ev)
AlH	0.455	1682.57	1.64592	0.154	0.188	25.14	29.145	2.89	3.0
BaH	0.475	1172	2.2318	0.068	0.066	14.82	16	2.36	1.8±0.1
BeH	0.435	2058.6	1.3431	0.295	0.300	36.60	35.5	3.01	2.4±0.3
CH	0.455	2861.6	1.1198	0.462	0.534	56.83	64.3	3.70	3.66[a]
CsH	0.465	890.7	2.494	0.055	0.057	11.23	12.6	1.81	1.8±0.3
HCl	0.495	2989.74	1.2744	0.292	0.304	52.17	52.05	4.31	4.38[a]
HBr	0.505	2649.22[c]	1.41468[c]	0.222	0.232[c]	42.14	44.077[c]	3.97	3.93[c]
HF	0.485	4137.25	0.91717	0.784	0.789	97.19	88.726	4.46	6.114[a]
LiH	0.425	1405.65[d]	1.59535[d]	0.218	0.213[d]	25.43	23.20[d]	2.02	2.515[d]
OH	0.475	3735.21	0.9706	0.669	0.714	82.70	82.81	4.29	4.624[a]

[a] See reference a, Table I.
[b] See reference b, Table I.
[c] H. M. Mould, W. C. Price, G. R. Wilkinson, Spectrochim. Acta. **16**, 479 (1960).
[d] R. Velasco, Can. J. Phys. **35**, 1204 (1957).

TABLE IV. Calculation of excited state data from empirical a rules.[a]

Mol.	State	ω_e (cm^{-1})	r_e (A)	a calc	α calc (cm^{-1})	α obs (cm^{-1})	$x_e\omega_e$ calc (cm^{-1})	$x_e\omega_e$ obs (cm^{-1})	D_e calc (ev)	D_e obs[b] (ev)	Dissociation products
H_2	$c\ ^3\Pi_u$	2465.0	1.0376	0.316	1.189	1.425	66.42	61.4	2.97	3.03	$2\ ^2P+1\ ^2S$
	$a\ ^3\Sigma_g^+$	2664.8	0.9887	0.319	1.450	1.671	77.28	71.65	3.12	3.01	$2\ ^2S+1\ ^2S$
	$e\ ^3\Sigma_u^+$	2195.8	1.1069	0.317	0.791	1.515	50.84	65.80	2.67	3.42	$3\ ^2P+1\ ^2S$
	$h\ ^3\Sigma_g^+$	2395.2	1.045	0.324	1.238	1.26	67.22	64.2	2.76	2.83	$3\ ^2P+1\ ^2S$
	$c\ ^1\Pi_u$	2442.72	1.0331	0.324	1.501	1.626	77.25	67.03	2.80	2.49	$2\ ^2P+1\ ^2S$
	$d\ ^3\Pi_u$	2371.58	1.0496	0.325	1.218	1.545	66.24	66.27	2.71	2.81	$3\ ^2P+1\ ^2S$
CH	$A\ ^2\Delta$	2921.0	1.1026	0.459	0.781	0.670	102.65	68.849	3.65	2.05	$2\ ^1D+1\ ^2S$
	$C\ ^2\Sigma^+$	2824.1	1.1132	0.465	0.668	0.744	83.34	95.199	3.36	2.39	$2\ ^1S+1\ ^2S$
Li_2	$A\ ^1\Sigma_u^+$	255.46	3.108	0.458	0.00442	0.00541	1.439	1.574	0.84	1.2	$2\ ^2S+2\ ^2P$
	$B\ ^1\Pi_u$	269.69	2.936	0.487	0.0127	0.00804	4.24	2.744	0.70	0.4	$2\ ^2S+2\ ^2P$
C_2	$A\ ^3\Pi_g$	1788.2	1.2660	0.545	0.0264	0.01608	21.09	16.44	6.52	4.5	$2\ ^3P+2\ ^1D$
	$B\ ^3\Pi_g$	1106.6	1.5350	0.579	0.0417	0.0242	48.00	39.26	2.76	0.7	$2\ ^3P+2\ ^3P$
	$a\ ^1\Sigma_g^+$	1855.6	1.2422	0.544	0.0204	0.01832	14.40	14.08	6.67	5.6	$2\ ^3P+2\ ^3P$
	$b\ ^3\Pi_u$	1608.3	1.3180	0.554	0.0195	0.01720	13.66	12.14	5.32	4.6	$2\ ^3P+2\ ^3P$
	$c\ ^1\Pi_g$	1809.1	1.2730	0.539	0.049	0.0180	20.14	15.81	7.06	5.3	$2\ ^1D+2\ ^1S$
CO	$A\ ^1\Pi$	1515.6	1.2351	0.563	0.0248	0.02229	17.83	17.2505	4.40	3.16	$2\ ^3P+2\ ^3P$
	$a'\ ^3\Sigma^+$	1230.7	1.3518	0.574	0.0143	0.0187	8.67	11.013	3.16	4.30	$2\ ^3P+2\ ^3P$
	$a\ ^3\Pi^+$	1739.3	1.2093	0.537	0.0195	0.0193	14.20	14.47	6.84	5.18	$2\ ^3P+2\ ^3P$
CS	$A\ ^1\Pi$	1072.3	1.5732	0.577	0.00996	0.005922	11.46	6.46	4.02	2.4	$2\ ^3P+2\ ^3P$
N_2	$A\ ^3\Sigma_u^+$	1460.60	1.293	0.591	0.0187	0.01798	13.85	13.851	3.55	3.71	$2\ ^4S+2\ ^4S$
	$B\ ^3\Pi_g$	1734.42	1.212	0.578	0.0196	0.01794	14.94	15.198	4.97	4.90	$2\ ^4S+2\ ^2D$
	$^3\Delta_u$	1490	1.28	0.590	0.00959	...	6.116	...	3.66	4.74	$2\ ^4S+2\ ^2D$
	$a\ ^1\Pi_g$	1693.7[c]	1.2197[c]	0.581	0.0164	0.0183[c]	11.60	13.83[c]	4.67	6.07[c]	$2\ ^2D+2\ ^2D$
	$a\ ^1\Sigma_u^-$	1530[d]	1.270[d]	0.587	0.0139	0.0164[d]	9.497	12.0[d]	3.92	5.92[d]	$2\ ^2D+2\ ^2D$
	$y\ ^3\Sigma_u^-$	1522	1.276	0.587	0.0152	...	10.565	12.5	3.93	5.36	$2\ ^4S+2\ ^2P$
	$w\ ^1\Delta_u$	1548	1.263	0.587	0.0170	...	12.34	8±1	3.94	5.53	$2\ ^2D+2\ ^2D$
	$c\ ^3\Pi_u$	2047.09	1.148	0.563	0.0238	0.01868	20.26	28.446	4.09	4.92	$2\ ^2P+2\ ^2D$
	$E\ ^3\Sigma_g^+$	2184.5	1.12	0.556	0.0183	...	14.098	...	8.12	8.33	$2\ ^4S+3s\ ^4P$
	$[^1\Pi_u]$	2035.0	1.15	0.562	0.0161	...	11.879	...	7.08	8.64	$2\ ^4S+sp\ ^4P$
	$[^1\Sigma_g^+]$	2215.0	1.12	0.553	0.0188	...	14.880	...	8.57	8.02	$2\ ^4S+3s\ ^4P$
	$[^3\Pi_u]$	1950.0	1.18	0.562	0.0166	...	12.661	...	6.84	7.4	$2\ ^4S+3s\ ^4P$
	$p'^1\Sigma_u^+$	2217.0	1.12	0.553	0.0205	...	16.598	19	8.58	7.27	$2\ ^4S+3s\ ^4P$
	$o\ ^1\Pi_u$	2020.0	1.19	0.550	0.0168	...	13.948	32.3	8.19	7.09	$2\ ^4S+3s\ ^4P$
	$e\ ^1\Sigma_u^+$	2180.0	1.12	0.557	0.0171	...	12.880	...	8.04	8.40	$2\ ^4S+4s\ ^4P$
	$x\ ^1\Sigma_g^-$	1910.0[d]	1.168[d]	0.571	0.0160	0.0225[d]	11.888	20.7[d]	5.96	7.41[d]	$2\ ^4S+3p\ ^4P$
	$y\ ^1\Pi_g$	1708.0[e]	1.16[e]	0.597	0.0197	...	12.70	...	3.69	5.65	$2\ ^4S+3s\ ^4P$

Table IV (*continued*)

Mol.	State	ω_e (cm^{-1})	r_e (A)	a calc	α calc (cm^{-1})	α obs (cm^{-1})	$x_e\omega_e$ calc (cm^{-1})	$x_e\omega_e$ obs (cm^{-1})	D_e calc (ev)	D_e obs[b] (ev)	Dissociation products
NO	$A\ ^2\Sigma^+$	2374.8	1.0637	0.541	0.0211	0.01928	18.05	16.46	10.4	7.6	$2\ ^2D+2\ ^1S$
	$B\ ^2\Pi_i$	1036.96	1.448	0.606	0.0121	0.0116	7.990	7.603	2.1	3.3	$2\ ^2D+2\ ^3P$
	$E\ ^2\Sigma^+$	2373.6[e]	1.0661[e]	0.540	0.0199	0.0182[e]	16.77	15.85[e]	10.5	8.2[e]	$2\ ^4S+3\ ^5S$
	$D\ ^2\Sigma^+$	2323.90[f]	1.0620[f]	0.548	0.0256	...	23.38	23[f]	9.4	5.5[f]	$2\ ^2D+2\ ^1D$
					0.0166		12.84			or 10.3 or 3	$^5S+2\ ^4S$
	$B\ ^2\Delta$	1216.6	1.303	0.612	0.0196	0.019	13.26	15.88	2.2	2.7	$2\ ^2P+2\ ^3P$
O_2	$a\ ^1\Delta_g$	1509.3	1.2155	0.574	0.0171	0.0171	13.01	12.9	4.48	4.24	$2\ ^3P+2\ ^3P$
	$b\ ^1\Sigma_g^+$	1432.69	1.2267	0.582	0.0183	0.01817	13.84	13.9501	3.55	3.58	$2\ ^3P+2\ ^3P$
	$B\ ^3\Sigma_u^-$	700.36	1.604	0.629	0.0164	0.011	11.63	8.002	0.96	1.01	$2\ ^3P+2\ ^1D$
	$^1\Sigma_u^-$	650.49[g]	1.597[g]	0.643	0.0211	0.02055[g]	15.051	17.036[g]	0.69	0.67[g]	$2\ ^3P+2\ ^3P$
O_2^+	$a\ ^4\Pi_u$	1035.69	1.3813	0.610	0.0146	0.01575	9.812	10.39	1.93	2.64	$2\ ^3P+2\ ^4S$
	$A\ ^2\Pi_u$	900	1.4089	0.629	0.0173	0.01906	10.986	13.4	1.23	1.78	$2\ ^3P+2\ ^4S$
	$b\ ^4\Sigma_g^-$	1196.77	1.2795	0.608	0.0194	0.02206	13.574	17.09	2.25	2.54	$2\ ^1D+2\ ^4S$
IO	$A\ ^2\Pi_i$	514.57	2.0723	0.656	0.00306	0.00273	5.228	5.52	1.09	1.2	$5\ ^2P+2\ ^1D$
K_2	$B\ ^1\Pi_u$	75.00	4.235	0.571	0.000495	0.000219	0.6153	0.354	0.336	0.22	$4\ ^2P+4\ ^2S$
S_2	$B\ ^3\Sigma_u^-$	434.0	2.180	0.637	0.00181	0.0018	2.826	2.75	1.24	1.6	$3\ ^3P+3\ ^1D$
Si_2	$H\ ^3\Sigma_u^-$	271.32	2.663	0.633	0.00148	0.00135	1.772	1.99	0.67	1.0	$3\ ^3P+3\ ^1D$
I_2	$B\ ^3\Pi_0^+$	128.0	3.016	0.687	0.000157	0.00017	0.6886	0.834	0.39	0.56	$5\ ^3P_i+5\ ^2P_i$

[a] See reference a, Table I.
[b] See reference b, Table I.
[c] A. Lofthus, Can. J. Phys. **34**, 780 (1956).
[d] A. Lofthus, J. Chem. Phys. **25**, 494 (1956).
[e] E. Miescher, Can. J. Phys. **33**, 355 (1955).
[f] R. F. Barrows and E. Miescher, Proc. Phys. Soc. (London) **70A**, 219 (1957).
[g] G. Herzberg, Can. J. Phys. **31**, 57 (1953).

accurate value of D_e determined. The corrected D_e can then be used to determine an improved a, then α_e and $x_e\omega_e$. Calculated values of D_e, α_e, and $x_e\omega_e$ are listed along with the observed values in Table IV. When the dissociation products are ionic, (1) is not valid and consequently none of the derived formulas are applicable. Generally, however, the ionic states can be recognized by their very low vibrational frequencies or negative anharmonicities. No known potential function is applicable to such states.

ALTERNATIVE FORMS FOR THE FIVE-PARAMETER FUNCTION

Expansion of the $1+af(r)$ part of (5) as far as the second power of Δr leads to

$$1+af(r)=1-a\left\{\left(\frac{b^2nr_e}{2}\right)^{\frac{1}{2}}\frac{\Delta r}{r_e}-\left(\frac{b^2nr_e}{2}\right)\left(\frac{\Delta r}{r_e}\right)^2+\cdots\right\}. \quad (15)$$

Higher powers of $\Delta r/r_e$ do not affect the relations between D_e, B_e, ω_e, α_e, and $x_e\omega_e$. The function (5a), as has been previously pointed out,[7] is not the only function which will yield the above expansion and hence lead to Eqs. (6) to (8). Some of the alternative forms for $1+af(r)$ are listed below

$$1+af(r)=1-a(b^2n/2r)^{\frac{1}{2}}\Delta r\exp[-(b^2n/2r)]^{\frac{1}{2}}\Delta r \quad (16a)$$

$$=1-a(b^2n/2r)^{\frac{1}{2}}\Delta r\exp[-(b^2n/2r_e)]^{\frac{1}{2}}\Delta r \quad (16b)$$

$$=1-a(b^2n/2r)^{\frac{1}{2}}\Delta r(r_e/r)^x\exp[-(b^2n/2r)]^{\frac{1}{2}}\Delta r. \quad (16c)$$

Others such as

$$1+af(r)=1-a(b^2n/2r)^{\frac{1}{2}}\Delta r \times\{1-\log_e[1+(b^2n/2r)^{\frac{1}{2}}\Delta r]\}$$

do not go to the correct limits and need be considered no further. The test of the validity of the functions (16a) to (16c) is their ability to reproduce known

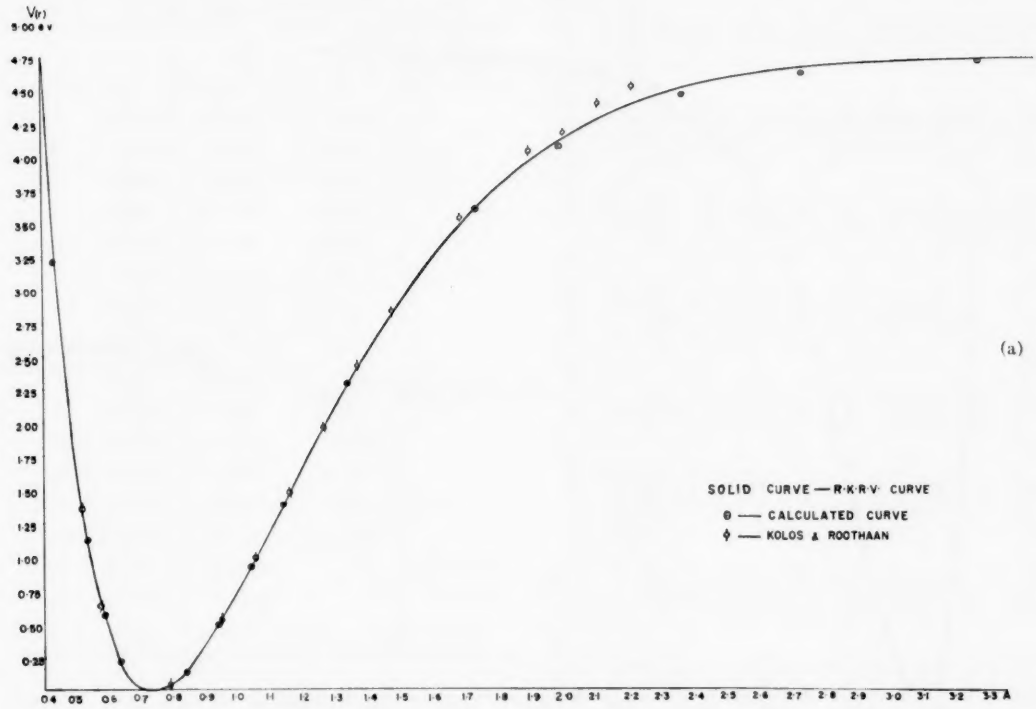

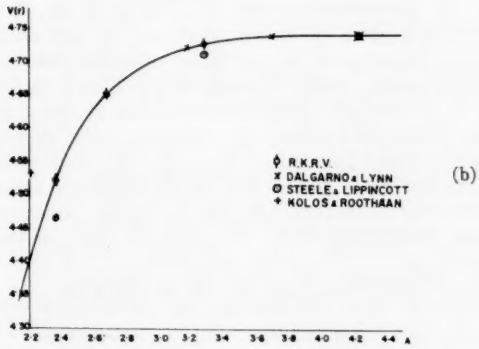

FIG. 1. (a) Potential energy curve of $X\,{}^1\Sigma_g^+$ state of hydrogen. (b) $V(r)$ curve for $X\,{}^1\Sigma_g^+$ state of H_2 at large Δr.

potential curves and to allow higher-order vibration-rotation energy terms to be predicted. The latter will be discussed in a future publication. In the present paper the capability of the proposed functions to reproduce experimental curves, as given by the R.K.R.V. method, will be examined, and then formulas given in the previous section will be applied to constructing curves from limited data.

CONSTRUCTION OF POTENTIAL CURVES

Experimental curves are known for a considerable range of bond lengths for the following: $X\,{}^3\Sigma_g^-$, ${}^3\Delta_u$, ${}^1\Sigma_u^-$, and $B\,{}^3\Sigma_u^-$ states of O_2[12,2]; $X\,{}^2\Pi_i$, $B\,{}^2\Pi$ of NO[13]; $X\,{}^1\Sigma^+$ of HF[14]; $X\,{}^1\Sigma_g^+$, $A\,{}^3\Sigma_u^+$, $B\,{}^3\Pi_g$, $a\,{}^1\Pi_g$ states of N_2[1]; $X\,{}^2\Pi_i$, and $A\,{}^2\Sigma^+$ states of OH[15]; $X\,{}^1\Sigma_g^+$ state of H_2[2] and $X\,{}^1\Sigma_g^+$ state of I_2.[16] The most complete curves are for the latter two molecules and consequently were

[12] J. T. Vanderslice, E. A. Mason, and W. G. Maisch, J. Chem. Phys. **32,** 515 (1960).
[13] J. T. Vanderslice, E. A. Mason, and W. G. Maisch, J. Chem. Phys. **31,** 738 (1959).
[14] R. J. Fallon, J. T. Vanderslice, and E. A. Mason, J. Chem. Phys. **32,** 698 (1960); **33,** 944 (1960).
[15] R. J. Fallon, I. Tobias, and J. T. Vanderslice, J. Chem. Phys. **34,** 167 (1961).
[16] R. D. Verma, J. Chem. Phys. **32,** 738 (1960).

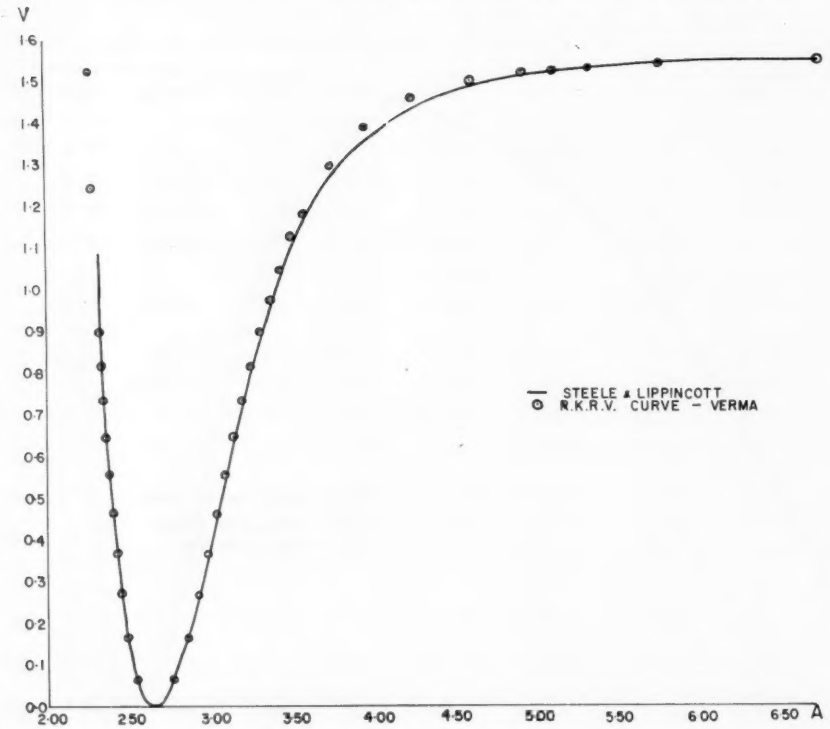

FIG. 2. Potential energy curve of $X\ ^1\Sigma_g^+$ state of I_2.

used first, along with that of the $X\ ^1\Sigma_g^+$ state of N_2, to test the proposed functions. $V(r)$ as given by (5a) consistently gives potentials which are far too small for negative values of Δr and values somewhat too high for intermediate positive values of Δr. This is shown for N_2 in Table V, where the potentials as given by (5a), (16a), and (16b) are compared with experimental values.[1] Equations (16a) and (16b) both yield potentials for the ground state of N_2 which are never in error by more than 2% over the range of known values. Proceeding to H_2 the potential curve of the ground state has already been evaluated using (5)[3] and the results were similar to those of N_2. Clearly this function need no longer be considered. For large values of Δr, (16b) is much superior to (16a) (see Table VI). A comparison of observed curves with that calculated using (16b) is shown in Figs. 1 and 2. Good agreement for large values of Δr is also obtained for the $X\ ^1\Sigma_g^+$ state of iodine using (16b), though the potential curve is 2 to 3% low for values of Δr, for which $V(r) \simeq \frac{1}{2}D_e$ (Table VII). It should be noted that Verma's curve for $v^{11} > 84$ is not completely reliable as it is based on an extrapolation procedure for estimating $r_{\min}$. This was necessary due to lack of data on B_v and α_v. Also Verma's Eqs. (17) and (18) are in error.[2] These results and the simplicity of (16b), as far as computing curves are concerned, have led the authors to adopt this form for the five-parameter function until more reasonably complete experimental potential curves are available on which to test the functions. A detailed comparison of the simple function, the complex function as defined by (16b) and functions proposed by other authors is now in progress.

TABLE V. Potential energy of $X\ ^1\Sigma_g^+$ state of N_2.

	$r_e = 1.0976$ A		$\omega_e = 2358.07$ cm^{-1}	
Δr	V(5a)	V(16a)	V(16b)	V[R.K.R.V.]
−0.3	5.912 ev	14.708 ev	13.557 ev	
−0.2	2.590	4.907	4.792	4.96 ev
−0.1	0.675	0.931	0.929	0.935
0.1	0.572	0.560	0.568	0.57
0.2	1.895	1.794	1.810	1.77
0.4	5.278	4.542	4.716	4.59
0.6		6.559	6.996	
1.0	9.589	8.219	9.073	
2.0		9.311	9.861	

CONSTRUCTION OF POTENTIAL CURVES FROM LIMITED DATA

As has already been shown, the parameter a can be estimated for any bound nonionic state of any diatomic molecule for which ω_e and r_e are known. From this, an approximate value for the dissociation energy can be

TABLE VI. Potential energy curve of $X\,^1\Sigma_g^+$ state of H_2.

Δr	V (16a)	V (16b)	V [R.K.R.V.]	V [Dunham and Lynn]
−0.3	3.4585 ev	3.2066 ev	3.50 ev	
−0.2	1.1437	1.1250	1.13	
−0.15	0.5654	0.5620	0.595	
−0.1	0.2232	0.2229	0.202	
0.1	0.1480	0.1481	0.147	
0.2	0.4895	0.4928	0.496	
0.3	0.9165	0.9271	0.905	
0.4	1.3679	1.3957	1.373	
0.6	2.2150	2.3022	2.260	
1.0	3.3854	3.6093	3.622	
1.2544	3.8093	4.0877	4.1309	
1.6331	4.1596	4.4665	4.5217	
2.0	4.3299	4.6267	4.670	
2.5418	4.4609	4.7136	4.7289	
3.49	4.5575	4.7430	...	4.744 ev
4.55	4.6193	4.47594	...	4.74595
D_e=4.7462 ev		ω_e=4400.39 cm^{-1}	r_e=0.74173 A	

obtained. Assuming that the dissociation energy of the ground state $D_e(x)$ and the electronic excitation energy T_e are known, the atomic excitation energy Δ' of the dissociation products of the excited state is then given by the relation.

$$T_e+D_e^*=D_e(x)+\Delta'. \tag{17}$$

This relation has been discussed in reference 7. Com-

TABLE VII. Potential energy curve of $X\,^1\Sigma_g^+$ state of I_2.

Δr	V (16b)	V obs
−0.3	0.7987 ev	0.759 ev
−0.2	0.3012	0.291
−0.1	0.0633	0.061
0.1	0.0460	0.044
0.2	0.1562	0.160
0.4	0.4653	0.484
0.6	0.7810	0.811
1.0	1.2128	1.242
2.0	1.4979	1.510
2.895	1.5438	1.5406
3.342	1.5512	1.5468
3.854	1.5546	1.5508
4.155	1.5556	1.5524
D_e=1.5570 ev	ω_e=214.518 cm^{-1}	r_e=2.668 A

TABLE VIII. Potential curves of states of N_2.

State	T_e (ev)	Dissociation products	D_e (ev)	a	$V(-0.3)$	$V(-0.2)$	$V(-0.1)$	$V(0.1)$	$V(0.2)$	$V(0.4)$	$V(0.6)$	$V(1.0)$	$V(2.0)$	$V(3.0)$
$X\,^1\Sigma_g^+$	0	$2\,^4S+2\,^4S$	9.92	0.545	13.5172	4.7735	0.9258	0.5680	1.8080	4.7130	6.9928	9.0603	9.8591	13.5172
$A\,^3\Sigma_u^+$	6.209	$2\,^4S+2\,^4S$	3.71	0.586	5.1276	1.8178	0.3540	0.2172	0.6907	1.7967	2.6487	3.3957	3.6863	3.7079
$B\,^3\Pi_g$	7.392	$2\,^4S+2\,^2D$	4.90	0.580	7.4045	2.6104	0.5037	0.3040	0.9584	2.4577	3.5801	4.5229	4.8739	4.8986
$(^3\Delta_u)$	[7.552]	$[2\,^4S+2\,^2D]$	4.74	0.561	5.0575	1.8120	0.3607	0.2302	0.7484	2.0237	3.1033	4.2110	4.6944	4.7354
$y\,^3\Sigma_u^-$	8.119	$2\,^4S+2\,^2P$	5.36	0.550	5.1613	1.8615	0.3722	0.2417	0.7926	2.1714	3.3819	4.6916	5.2994	5.3539
$a\,^1\Pi_g$	8.590	$2\,^2D+2\,^2D$	6.07	0.550	6.5534	2.3452	0.4660	0.2977	0.9639	2.5966	3.9805	5.4000	6.0150	6.0644
$a'\,^1\Sigma_u^-$	8.740	$2\,^2D+2\,^2D$	5.92	0.538	5.1927	1.8572	0.3745	0.2472	0.8135	2.2661	3.5849	5.0934	5.8403	5.9112
$W\,^1\Delta_u$	9.23	$2\,^2D+2\,^2D$	5.53	0.548	5.3235	1.9181	0.3837	0.2495	0.8163	2.2379	3.4858	4.8397	5.4566	5.5238
$C\,^3\Pi_u$	10.927	$2\,^2P+2\,^2D$	4.92	0.601	11.1996	3.9120	0.7236	0.3996	1.2249	2.9250	3.9652	4.6773	4.9087	4.9203
$E\,^3\Sigma_g^+$	11.88	$2\,^4S+3s\,^4P$	8.33	0.553	11.5852	4.0879	0.7930	0.4838	1.5391	3.999	5.9135	7.6315	8.2789	8.3258
$[^1\Pi_u]$	[12.16]	$2\,^4S+s^3p^4P$	8.64	0.537	9.3620	3.4146	0.6765	0.4271	1.3852	3.7264	5.6949	7.7059	8.5664	8.6322
$[^1\Sigma_g^+]$	[12.19]	$2\,^4S+s^3p3s\,^4P$	8.02	0.561	12.1352	4.2694	0.8223	0.4945	1.5612	4.0052	5.8416	7.4059	7.9797	8.0179
$[^3\Pi_u]$	12.8	$2\,^4S+3s\,^4P$	7.4	0.552	8.9327	3.1776	0.6257	0.3903	1.2560	3.3354	5.0312	6.6756	7.3433	7.3947
$j'\,^1\Sigma_u^+$	12.94	$2\,^4S+3s\,^4P$	7.27	0.573	12.3961	4.3763	0.7548	0.4874	1.5304	3.8432	5.4903	6.7890	7.2465	7.2680
$O\,^1\Pi_u$	13.12	$2\,^4S+3s\,^4P$	7.09	0.568	9.8650	3.4885	0.6783	0.4145	1.3173	3.4430	5.0530	6.4949	7.0458	7.0862
$e\,^1\Sigma_u^+$	14.33	$2\,^4S+s^2p4s\,^4P$	8.40	0.551	11.5035	4.0632	0.7827	0.4831	1.5375	4.0035	5.9354	7.6845	8.3489	8.3958
$x\,^1\Sigma_g^-$	14.35	$2\,^4S+s^2p3p\,^4P$	7.41	0.545	8.4787	3.0252	0.5974	0.3758	1.2149	3.2490	4.9432	6.6385	7.3488	7.4031
$y\,^1\Pi_g$	(14.56)	$2\,^4S+s^2p3s\,^4P$	5.65	0.549	6.8689	2.4430	0.4803	0.2997	0.9621	2.5509	3.8470	5.0985	5.6088	5.6459

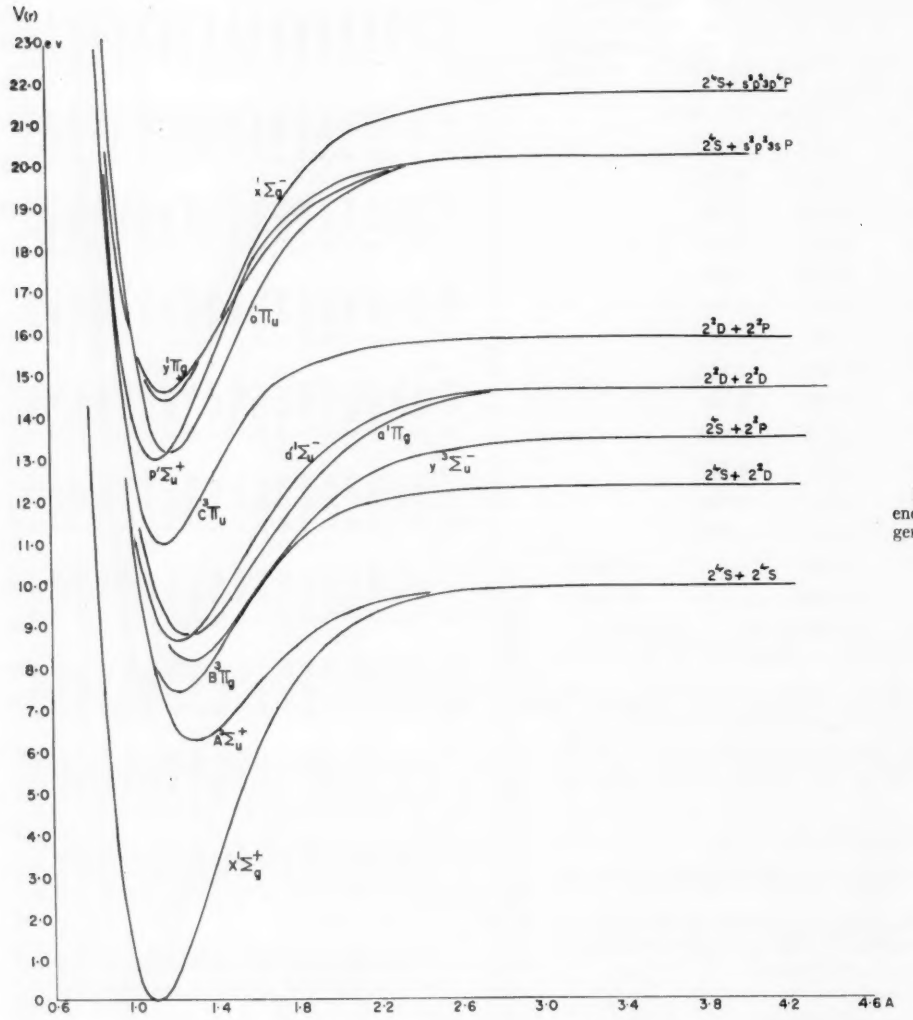

FIG. 3. Potential energy curves of nitrogen.

parison of the calculated Δ' with the possible atomic excitation energies of the dissociation products will usually allow the states of the dissociated atoms to be determined unambiguously. Using the corrected value of Δ', a more accurate value of the dissociation energy of the excited state can then be deduced. Since b is a known constant no further information is necessary to construct the potential curve using (5b). The parameter n is computed from $n=k_e r_e/D_e$.

The published data on N_2[17–19] have been analyzed in this manner and potential curves constructed for all known states which do not dissociate to ionic products (see Table VIII and Fig. 3). An inherent assumption in this approach is that the states concerned retain the same character over all range of bond lengths, that is, that they are not seriously disturbed by other states over any given range of bond lengths. Not in all cases could the dissociation products of N_2 be unambiguously determined on account of the large number of atomic excitation energies near to 12 ev. In the majority of such cases the products as assigned by Mulliken[17] were accepted as correct. Only two states deserve comment. The dissociation energy of the $\omega\,{}^1\Delta_u$ state as derived from the empirical a rules is 3.94 ev, whereas that derived from the simple potential function using the observed anharmonicity of $\sim$8 cm^{-1} is 7.5 ev. α_e is known to a much higher precision than $x_e\omega_e$ for this state. Calculating $x_e\omega_e$ from α_e by (9) leads to a value

[17] R. S. Mulliken, Laboratory of Molecular Structure and Spectra, University of Chicago, Tech. Rept., 1956, p. 189.
[18] G. H. Dieke and D. F. Heath, J. Chem. Phys. **33**, 432 (1960).
[19] G. H. Dieke and D. F. Heath, Johns Hopkins Spectroscopic Rept. No. 17, Baltimore, Maryland (1959).

of 11.92 cm^{-1} for $x_e\omega_e$ and 4.91 ev for D_e. This is in excellent agreement with the dissociation energy based on the dissociation products being 2^2D+2^2D.

The $^5\Sigma_g^+$ state arising from ground state atoms is suggested[20] to have a bond length of about 1.6 A and a vibrational frequency of $\sim$12 cm^{-1}. These values lead to an impossibly low dissociation energy. Equating (13) and (14) and using the known D_e and the above value for r_e leads to $\omega_e=469$ cm^{-1}. Clearly more reliable data are needed before an accurate curve can be constructed by this method.

The calculated potential curves agree well with the R.K.R.V. curves where these are available. For example, Eq. (16b) gives values of $V(r)$ which are rarely more than 2% in error for the ground states of I_2, H_2, and N_2. The discrepancy is somewhat larger for the $C\,^3\Pi_u$ state. This is of interest as this state is strongly disturbed by another $^3\Pi_u$ state, suggesting that the discrepancy is a consequence of this perturbation.

CONCLUSION

On the basis of the observed dependence of a on the position of the element in the periodic table for the function (1) in the form (5a) or (5b), the first-order anharmonic corrections to the potential $x_e\omega_e$ and α_e have been calculated from the vibrational frequencies and bond lengths. This allows the potential curves for the ground states to be evaluated. The potential function as defined by (5b), in conjunction with the simplification resulting from the above, lead to surprisingly accurate potential curves for ground states and excited states. Since in general the anharmonicity and/or the vibrational-rotational coupling constant are not well known—if known at all—this technique should be of considerable value when other information is not available and a knowledge of potential curves is desirable.

Such curves are not readily calculated from first principles. The difficulty of calculating potential curves is well illustrated by the recent work of Kolos and Roothaan.[21] Using 50-term wave functions and a S.C.F. procedure, the potential curve was calculated for values of r from 0.423 to 2.22 A. For small internuclear displacements from equilibrium the calculated curve agrees extremely well with the experimental. However, for $r>1.6$ A the calculated curve deviates seriously from the R.K.R.V. curve (see Fig. 1). This is because the wave functions are a power series in r and cannot behave properly for large values of r.

The excellent agreement between the calculated and experimental curves as defined by the R.K.R.V. method especially for hydrogen and iodine, even for large internuclear separations is indicative of the nature of the interatomic forces. The dissociation products for I_2 are $5^2P_{\frac{3}{2}}+5^2P_{\frac{1}{2}}$ while for H_2 they are 1^2S+1^2S. It is interesting that this agreement appears to hold for the states of separated atoms which have and do not have quadrupole moments since the long-range interaction potential is often believed to be different for the two cases. An improved R.K.R.V. curve for I_2 at large internuclear separations would be of considerable value in this connection.

ACKNOWLEDGMENT

This work was supported in part by a grant from the U. S. Army Research Office.

[20] C. M. Herzfeld and H. P. Broida, Phys. Rev. **101,** 606 (1956).

[21] W. Kolos and C. C. J. Roothaan, Revs. Modern Phys. **32,** 219 (1960).

THE JOURNAL OF CHEMICAL PHYSICS VOLUME 35, NUMBER 6 DECEMBER, 1961

Gaseous Diffusion in Porous Media at Uniform Pressure

R. B. EVANS, III, AND G. M. WATSON
Oak Ridge National Laboratory, Oak Ridge, Tennessee*
AND
E. A. MASON
Institute for Molecular Physics, University of Maryland, College Park, Maryland

(Received May 26, 1961)

A model is presented for the diffusion of gases in porous media in the absence of pressure gradients, in which the porous medium is visualized as a collection of uniformly distributed "dust" particles which are constrained to be stationary. By formally considering the dust particles as giant molecules, it is possible to derive all the desired results very simply from rigorous kinetic theory as special cases of multicomponent mixtures. By formally varying the mole fractions of the real gas molecules, the entire pressure range from the Knudsen region to the normal diffusion region can be covered. This model permits the first satisfactory theoretical derivation of the experimentally discovered fact that the flux ratio for binary mixtures is equal to $(m_2/m_1)^{\frac{1}{2}}$ at *all* pressures (not just in the Knudsen region). It also permits a rigorous theoretical treatment of the entire transition region for the first time, from which is obtained the usual Bosanquet interpolation formula and a differential equation for diffusion which covers the entire range (and appears to be new). The model gives no quantitative *a priori* characterization of the porous medium itself, but if one gas mixture is measured in a given medium, then the behavior of other gas mixtures in the same medium can be predicted.

INTRODUCTION

DIFFUSION in porous media can occur via three paths: through the pore volumes, along pore surfaces, and through the solid matrix material of the media. The relative importance of these paths depends on many factors, but a large fraction of the diffusion at ordinary and high temperatures will occur in the pore volumes unless the porosity and permeability of the medium are very low. The present discussion is limited to diffusion in the pore volumes.

Two limiting cases of such diffusion are usually distinguished: Knudsen diffusion (or free molecule flow) and normal diffusion. In Knudsen diffusion the limiting mechanism is the collision of the gas molecules with the solid walls of the medium, the collisions between gas molecules having negligible effect. In normal diffusion it is the gas-gas collisions which are limiting, and the gas-wall collisions are negligible. The usual rough criterion for Knudsen diffusion is that the mean free path of the gas molecules be much larger than some characteristic dimension of the apparatus (the pore diameter in the case of porous media), and for normal diffusion that the mean free path be smaller than the characteristic apparatus dimension. Most real cases of diffusion are probably intermediate between these two limiting cases.

The purpose of the present paper is to give a discussion of uniform-pressure diffusion in porous media from a single consistent point of view which embraces the entire range from the Knudsen region to the normal diffusion region. This is done by means of a model, in which the porous medium is visualized as a collection of spherical particles which are very large in size as compared to a gas molecule, and which are constrained to be fixed in space by the experimental conditions. In other words, the system is visualized as a "dusty" gas[1] in which the dust particles are held stationary. By formally treating the dust particles as giant "molecules," which are merely one more component of a multicomponent mixture, we are able to treat the system by means of the classical kinetic theory of multicomponent mixtures, and to derive many of the usual results for diffusion in porous media (as well as some new results) very simply as special cases of standard kinetic theory.

Although the results derived in this way are rather general, most of our discussions of specific cases will be limited to binary gas mixtures and steady-state diffusion, simply because most experimental results are of this type.

BASIC CONSIDERATIONS

Normal Diffusion in Tubes

For orientation and the definition of some of the terms, it is convenient to consider first the normal diffusion of gases through capillary tubes (one-dimensional diffusion). In the usual experiment, two large closed vessels containing different gases at the same temperature and pressure are connected together by a capillary tube through which diffusion occurs. There is an initial transient condition in which more of the fast-moving light molecules pass through the capillary in one direction than slow-moving heavy molecules pass

* Operated by Union Carbide Corporation for the U. S. Atomic Energy Commission.

[1] *Note added in proof.* It has recently come to our attention that a "dusty gas" model has been previously proposed by B. F. Derjaguin and S. P. Bakanov in connection with the problem of gas flow in a porous body near the Knudsen region [Soviet Physics-Doklady **2**, 326 (1957); Discussions Faraday Soc. **30**, 130 (1960)].

in the opposite direction. This net flux of molecules soon results in a small pressure difference between the vessels, which causes an over-all back flow of gas through the capillary. This pressure difference has been directly observed in the normal diffusion region by Kramers and Kistemaker,[1a] who used a sensitive diaphragm differential manometer, and by McCarty and Mason,[2] who used the pressure difference to move a small "marker" piston in a horizontal tube. It has also been observed in the Knudsen region by Bernstein.[3] If the volume of the vessels is much larger than the volume of the capillary tube, a quasi-steady state is soon set up in which there is no net flux of molecules between the vessels, the pressure difference assuming a steady value just sufficient to cause the net flux to be zero.

The conditions are drastically altered if the pressures at the two ends of the tube are maintained exactly equal. This can be done, for instance, by sweeping the ends with the pure component gases, and determining the fluxes by analysis of the gas diffused into the sweep streams (see Fig. 1). In this case there is a net flux J (molecules/cm^2-sec) through the tube in the same direction as the flux of light molecules. If the tube is large enough in diameter that molecule-wall collisions are negligible, it is easy to show, from the one-dimensional equations of motion and continuity of the gas, that the mass average velocity of the gas is zero.[2] The mass average velocity is defined as[4]

$$v=(1/\rho)\,(n_1m_1\bar{v}_1+n_2m_2\bar{v}_2), \tag{1}$$

where

$$\rho=n_1m_1+n_2m_2. \tag{2}$$

Here n_1 and n_2 are the concentrations of the two species 1 and 2 in molecules/cm^3 and m_1 and m_2 are their molecular masses, so that ρ is the total gas density in g/cm^3. The average molecular velocities[4] (not to be confused with average molecular speeds) are $\bar{v}_1$ and $\bar{v}_2$. Since the fluxes of the species are $J_1=n_1\bar{v}_1$ and $J_2=n_2\bar{v}_2$, Eq. (1) with $v=0$ leads directly to

$$J_1/J_2=-m_2/m_1. \tag{3}$$

The minus sign occurs because the fluxes are in the opposite direction in the present case. For example, if He and Ar are diffusing, 10 times more He atoms pass through the capillary than Ar atoms. For the usual closed vessel case, however,

$$J=J_1+J_2=0, \tag{4}$$

so that the ratio of the individual fluxes is unity. [The multicomponent generalization of Eq. (3) is $\sum m_iJ_i=0$.]

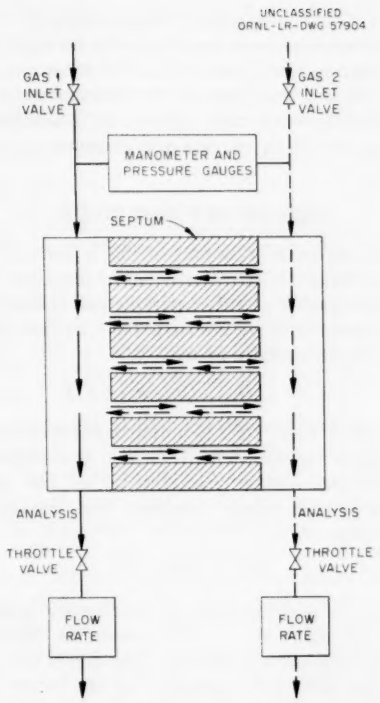

FIG. 1. Diagram of typical steady diffusion experiment.

It should be remarked that Eq. (3) probably represents an unattainable limiting case in practice, since it is derived on the assumption of negligible gas-wall interactions. The walls *do* have an important effect on gas flow even in large tubes, however, producing a parabolic velocity profile across the tube diameter (Poiseuille flow). In other words, the gas-wall interactions introduce viscous terms into the equation of motion, which had been dropped in the proof that $v=0$.

In any case, whether the net flux J is zero or not, the usual diffusion equations for the two species can be written as follows in the normal diffusion region[5,6]:

$$J_i=-D_{12}(\partial n_i/\partial z)+x_iJ_i \quad i=1 \text{ or } 2, \tag{5}$$

where $n=n_1+n_2$ is the total molecular concentration and $x_i=n_i/n$ is the mole fraction of species i. The distance coordinate is z. D_{12} is the normal diffusion coefficient, given in terms of molecular quantities by[7]

$$D_{12}^{-1}=(16n/3)\,(\mu/2\pi kT)^{\frac{1}{2}}(\pi\sigma_{12}^2)\Omega_{12}^{(1,1)*}, \tag{6}$$

where $\mu=m_1m_2/(m_1+m_2)$ is the reduced mass, k is Boltzmann's constant, σ_{12} is the collision diameter,

[1a] H. A. Kramers and J. Kistemaker, Physica **10,** 699 (1943).
[2] K. P. McCarty and E. A. Mason, Phys. Fluids **3,** 908 (1960).
[3] R. B. Bernstein, J. Chem. Phys. **17,** 209 (1949). See also B. V. Derjaguin and D. A. Batova, Doklady Akad. Nauk S.S.S.R. **128,** 323 (1959).
[4] J. O. Hirschfelder, C. F. Curtiss, and R. B. Bird, *Molecular Theory of Gases and Liquids* (John Wiley & Sons, Inc., New York, 1954), pp. 453–454.
[5] R. D. Present, *Kinetic Theory of Gases* (McGraw-Hill Book Company, Inc., New York, 1958), p. 49.
[6] R. B. Bird, W. E. Stewart, and E. N. Lightfoot, *Transport Phenomena* (John Wiley & Sons, Inc., New York, 1960), p. 502.
[7] Reference 4, p. 539.

and $\Omega_{12}^{(1,1)*}$ is the so-called collision integral for diffusion, defined so as to be equal to unity for rigid spheres of diameter σ_{12}. Deviations of $\Omega_{12}^{(1,1)*}$ from unity are a measure of the deviations of the intermolecular forces from forces between rigid spheres. It is assumed that the gases are ideal, so that the pressure is given by $p=nkT$.

Diffusion in Porous Media

Normal diffusion in porous media is formally analogous to diffusion in tubes, and can be described by the same equations if suitable parameters characterizing the porous medium are inserted. Thus, in close analogy to Eq. (5), one usually writes

$$J_i=-(D_{12})_{\text{eff}}(\partial n_i/\partial z)+x_iJ, \tag{7}$$

where J_i and J now refer to unit area of porous medium and $(D_{12})_{\text{eff}}$ is proportional to D_{12}, the constant of proportionality being characteristic of the internal geometry of the porous medium. For instance, one often writes

$$(D_{12})_{\text{eff}}=\epsilon D_{12}/q, \tag{8}$$

where ϵ is the porosity and q is a tortuosity factor.[8,9]

Knudsen diffusion in porous media is different in character from normal diffusion. The flux of one species is not affected by the presence of the other species since gas-gas collisions are negligible, and so the Knudsen diffusion coefficient D_{iK} becomes identical with the permeability coefficient K_i, which is defined by the expression

$$J_i=-\frac{K_i}{kT}\frac{\partial p_i}{\partial z}=-K_i\frac{\partial n_i}{\partial z}, \tag{9}$$

where p_i is the partial pressure of the ith species.[8] Thus in the Knudsen region in place of Eq. (7) we have

$$J_i=-D_{iK}(\partial n_i/\partial z), \tag{10}$$

an equation which has no contribution from a flow term like x_iJ in Eq. (7). The Knudsen diffusion coefficient is given by the expression[8,10]

$$D_{iK}=\tfrac{4}{3}(8kT/\pi m_i)^{\frac{1}{2}}K_0, \tag{11}$$

where K_0 is a constant (with the dimensions of a length) characteristic of the porous medium (just as ϵ/q is a characteristic constant of the porous medium in the normal diffusion range). One well-known result that follows immediately from Eqs. (10) and (11) when the total pressure is uniform (so that $\partial p_1/\partial z=-\partial p_2/\partial z$) is

$$J_1/J_2=-(m_2/m_1)^{\frac{1}{2}}, \tag{12}$$

which has been experimentally verified for porous media.[11]

The different pressure dependence of the diffusion coefficient in the normal and Knudsen regions should be noted. In the normal diffusion region D_{12} is inversely proportional to pressure, but in the Knudsen region D_{iK} is independent of pressure.

In the intermediate pressure region the effective diffusion coefficient is usually represented by the Bosanquet interpolation formula,[12]

$$(D_1)_{\text{eff}}^{-1}=(D_{12})_{\text{eff}}^{-1}+D_{1K}^{-1}. \tag{13}$$

This formula was originally obtained by an elementary mean free path argument, but it appears to be in agreement with more elaborate calculations,[10] and with the limited experimental data available.[13]

EXPERIMENTAL STUDIES

The arrangement of Fig. 1, with a septum composed of porous material rather than parallel tubes, is a representation of the experimental method developed by Wicke[14,15] to study the diffusion of CO_2 in various N_2-saturated media. Wicke's method was later used by others[16–19] to study diffusion in porous catalysts, although Hoogschagen[18,19] was apparently the first of these workers to consider the fact that the net flux $J=J_1+J_2$ was not zero in this experiment. Previous workers had assumed (erroneously) that $J_1+J_2=0$, presumably by analogy with the closed vessel case. Although Hoogschagen's measurements were far outside the Knudsen region, he found the ratio of the fluxes to be equal to $(m_2/m_1)^{\frac{1}{2}}$ within experimental error, just as given by Eq. (12) for pure Knudsen flow. This rather surprising result has since been confirmed more extensively.[13,20] It appears to hold throughout the entire range of pressures and pore sizes investigated.

The experiments of Evans with He and Ar diffusing through a large pore graphite (pore radius $\sim 3\ \mu$) may profitably be discussed in more detail. Two types of measurements were made. In the first type the pressure difference Δp across the septum was kept as nearly equal to zero as possible and the fluxes of He and Ar were measured. Since it was difficult to hold Δp exactly zero, a second type of experiment was performed in

[8] P. C. Carman, *Flow of Gases Through Porous Media* (Academic Press Inc., New York, 1956), pp. 78–79.

[9] J. M. Hutcheon, B. Longstaff, and R. K. Warner, *Industrial Carbon and Graphite* (Society of Chemical Industry, London, 1957), p. 259.

[10] W. G. Pollard and R. D. Present, Phys. Rev. **73,** 762 (1948).

[11] See, for example, R. M. Barrer, *Diffusion in and through Solids* (Cambridge University Press, New York, 1951), pp. 65–73.

[12] C. H. Bosanquet, British TA Rept. BR–507 (1944), referred to on p. 770 of reference 10.

[13] (a) R. B. Evans, III, J. Truitt, and G. M. Watson, J. Chem. Eng. Data, to be published (1961). (b) "Superposition of forced and diffusive flow in a large pore graphite," ORNL–3067 (1961).

[14] E. Wicke, Kolloid Z. **93,** 129 (1940).

[15] E. Wicke and R. Kallenbach, Kolloid Z. **97,** 135 (1941).

[16] A. Wheeler, "Reaction rates and selectivity in catalyst pores," *Advances in Catalysis* (Academic Press Inc., New York, 1951) Vol. III, pp. 260–275.

[17] P. B. Weisz and C. D. Prater, "Measurements in experimental catalysis," in *Advances in Catalysis,* (Academic Press Inc., New York, 1954), Vol. VI, pp. 185–195.

[18] J. Hoogschagen, J. Chem. Phys. **21,** 2096 (1953).

[19] J. Hoogschagen, Ind. Eng. Chem. **47,** 906 (1955).

[20] E. Wicke and P. Hugo, Z. physik Chem. **28,** 26 (1961).

which Δp was deliberately varied (but the mean pressure p_m was held constant at 2 atm) and the fluxes measured. The results are shown in Fig. 2, from which the fluxes at $\Delta p=0$ can be obtained by interpolation. [The curves for J_{He} and J_{Ar} were obtained by integrating Eq. (7), taking J to be an experimentally determined constant.] The results for both types of measurements are summarized in Table I, where it can be seen that Eq. (12) is followed within experimental error, although the measurements were made within the normal diffusion region.

Hoogschagen's data are summarized in Table II, and it is seen that Eq. (12) is again followed within experimental error, although the pore size of the septum (which was made by compressing carbonyl iron spheres) was about 0.8 μ, which was much larger

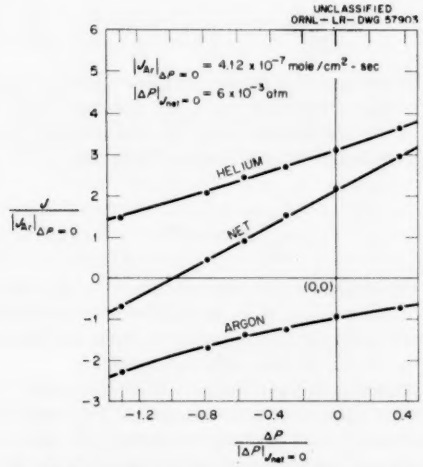

FIG. 2. Diffusive flow as a function of total pressure drop ($P_{He}-P_{Ar}$) across a large pore graphite at $P_m=2$ atm and 100°C.

than the mean free paths of the molecules at atmospheric pressure.[19]

Our attempts to explain the foregoing observations have led to the model described in the next section.

A PORE DIFFUSION MODEL

There are three main results which should be explained by a model which claims any generality:

1. The fact that the flux ratio is accurately given by $(m_2/m_1)^{\frac{1}{2}}$ in both the Knudsen and normal diffusion regions.
2. The Bosanquet interpolation formula, Eq. (13).
3. The flux equation is given by Eq. (7) in the normal region and by Eq. (10) in the Knudsen region.

In fact we may hope to find the general equation to be of the form

$$J_i=-(D_i)_{\text{eff}}(\partial n_i/\partial z)+x_iJ\cdot\delta_i(p), \quad i=1 \text{ or } 2, \quad (14)$$

TABLE I. Experimental and calculated flux ratios for He and Ar in a large pore graphite at uniform total pressure.

Source	$-J_{He}/J_{Ar}$
Exptl, $\Delta p=0$[a]	3.28
Exptl, interpolated from Fig. 2	3.10
Calc, $(m_{Ar}/m_{He})^{\frac{1}{2}}$	3.16

[a] Average of 18 experiments as reported in J. Chem. Eng. Data, (to be published) 1961,[19a] at various temperatures and pressures.

where both $(D_i)_{\text{eff}}$ and $\delta_i(p)$ are functions of pressure. At very low pressures $\delta_i(p)=0$ and $(D_i)_{\text{eff}}=D_{iK}$, so that Eq. (10) is recovered. At high pressures $\delta_i(p)=1$ and $(D_1)_{\text{eff}}=(D_2)_{\text{eff}}=(D_{12})_{\text{eff}}$, so that Eq. (7) is recovered.

The most obvious physical difference between diffusion through a large capillary tube and through a porous diaphragm is that in the latter case the gas molecules will make many collisions with the walls of the porous diaphragm before finding their way through. In this case we cannot use the equation of motion of the gas in free space to derive a boundary condition like that of Eq. (3), but must resort to another approach. One obvious procedure would be to introduce the viscous terms into the equation of motion to allow for the gas-wall interactions. This procedure was used by McCarty and Mason[2] for capillaries with diameters of several hundred microns, but it is mathematically complicated and appears hopeless for application to porous media. Another approach seems called for, and we imagine that the solid materials along the pore surfaces can be idealized as a collection of large spherical particles among which the small gas molecules must diffuse. The rest of the solid matrix of the porous diaphragm merely contributes to the porosity and tortuosity factors, as in Eq. (8). We now consider these large diaphragm particles as giant molecules, which form merely another component of a multicomponent gas mixture that we can treat by classical kinetic theory methods. *The model is thus that of a dusty gas in which the dust particles are fixed in space and uniformly distributed*, so that the following special conditions hold:

$$\bar{v}_d=0, \qquad \partial n_d/\partial z=0, \qquad (15)$$

where the subscript d refers to the dust or diaphragm

TABLE II. Hoogschagen's equal pressure diffusion data for three gas pairs in a large pore medium.

Gas pair (1–2)	$-J_1/J_2$ (Av. exptl)	Calc. $(m_2/m_1)^{\frac{1}{2}}$
He—O_2	2.74	2.83
N_2—O_2	1.08	1.07
CO_2—O_2	0.85	0.85

particles. Since the dust particles are considered formally as giant gas molecules, we can cover the entire pressure range from the Knudsen to the normal diffusion region by the trick of allowing the mole fractions of the real gas molecules to vary between 0 and 1. This model was suggested by Waldmann's recent work on the forces acting on small spheres suspended in an inhomogeneous gas.[21]

If we now write the diffusion equations for the multicomponent mixture and apply the conditions of Eq. (15), we can obtain all the desired results after a little algebra. For a mixture containing ν components, the diffusion equations can be written as the following set of $\nu-1$ independent equations (there is also a νth equation, but it is the sum of the other $\nu-1$ equations)[22]:

$$\sum_{i\neq j}^{\nu}{}_i(n_in_j/n^2D_{ij})\,(\bar{v}_i-\bar{v}_j)=n^{-1}(\partial n_j/\partial z), \qquad (16)$$

where the D_{ij} are binary diffusion coefficients given by Eq. (6). Two modifications of Eq. (16) need to be made for porous media. In free space $J_i=n_i\bar{v}_i$, but in a porous medium J_i is referred to unit area of medium, not of free space. A factor is thus needed for porosity and tortuosity. Furthermore, the total molecular density n in Eq. (16) formally includes the dust particles, whereas we prefer to keep the notation that n refers only to true gas molecules. We therefore write $n'=n+n_d$, and D_{ij}' in place of D_{ij} to emphasize that these diffusion coefficients formally refer to a total density of n'. Making these changes, we obtain in place of Eq. (16)

$$\sum_{i\neq j}^{\nu}{}_in'(D_{ij}')_{\text{eff}}^{-1}(n_jJ_i-n_iJ_j)=\partial n_j/\partial z, \qquad (17)$$

from which we can derive all our desired results.

We derive first the condition on the flux ratio. From the $\nu-1$ equations in Eq. (17) we pick out the one for which $j=d$ (the diaphragm particles), and apply the conditions of Eq. (15) to obtain

$$\sum_{i\neq d}^{\nu}{}_i[n_d/n'(D_{id}')_{\text{eff}}]J_i=0. \qquad (18)$$

For diaphragm particles which are much heavier and much larger than the gas molecules, the expression, for D_{id}, Eq. (6), is greatly simplified. We find $\mu=m_i$ and $\sigma_{12}=r$, the radius of the particles. The collision integral in Eq. (6) also simplifies. If the gas molecules are scattered specularly from the diaphragm particles, then $\Omega_{id}^{(1,1)*}=1$. If, however, a fraction f is scattered diffusely but elastically and a fraction $1-f$ is scattered specularly, then for this "elastic diffuse" scattering the collision integral is[23]

$$\Omega_{id}^{(1,1)*}=1+\tfrac{4}{9}f_i. \qquad (19)$$

If a fraction a is scattered diffusely and at the same time has its speeds "thermalized" so that the molecules are reflected from the particle with random speeds distributed according to a Maxwellian distribution, then for this "thermal diffuse" scattering the collision integral is [21,23]

$$\Omega_{id}^{(1,1)*}=1+\tfrac{1}{8}\pi a_i. \qquad (20)$$

This latter situation seems most likely on physical grounds, although there is little numerical difference between Eqs. (19) and (20). Inserting these results into Eq. (18) and canceling out all constant factors, we obtain the general result

$$\sum_{i\neq d}^{\nu}{}_im_i^{\frac{1}{2}}J_i(1+\tfrac{1}{8}\pi a_i)=0. \qquad (21)$$

Available evidence[24] indicates that $a_i=1$ for most gases. (This is also consistent with the diffusion data discussed in the previous section.) We can therefore cancel out the collision integral factor from Eq. (21) and obtain

$$\sum_{i\neq d}^{\nu}{}_im_i^{\frac{1}{2}}J_i=0, \qquad (22)$$

which for a binary gas mixture leads to the desired result, $J_1/J_2=-(m_2/m_1)^{\frac{1}{2}}$. It is to be emphasized that this result holds for all gas pressures from the Knudsen region up to the normal diffusion region.

The foregoing derivation has implicitly assumed that all the dust particles are the same size. This restriction is unnecessary, and is easily removed. If there is a distribution of sizes, we can write one equation of the form of Eq. (17) for each size, and then add all these equations up to obtain a single equation like Eq. (18), but with $\pi\sigma_{12}^2=\pi\langle r^2\rangle_{Av}$ in the diffusion coefficient. The rest of the derivation to obtain Eq. (22) then follows as before. For simplicity we will carry out derivations from here on as if the diaphragm particles were all the same size, with the understanding that this restriction can easily be removed.

Let us now specialize to a binary gas mixture and write down that one of the equations (17) which corresponds to $j=1$:

$$n'(D_{12}')_{\text{eff}}^{-1}(n_1J_2-n_2J_1)+n'(D_{1d}')_{\text{eff}}^{-1}(n_1J_d-n_dJ_1)=\partial n_1/\partial z. \qquad (23)$$

Substituting $J_d=0$, $J_2=J-J_1$, and $n'=n_1+n_2+n_d=n+n_d$, we obtain after rearrangement

$$\left[1+\frac{n_d}{n}\frac{(D_{12}')_{\text{eff}}}{(D_{1d}')_{\text{eff}}}\right]J_1=-\frac{n'}{n}(D_{12}')_{\text{eff}}\frac{\partial n_1}{\partial z}+\frac{n_1}{n}J. \qquad (24)$$

[21] L. Waldmann, Z. Naturforsch. **14a**, 589 (1959). Waldmann uses an impulse calculation rather than a Chapman-Enskog kinetic theory approach, but the methods are essentially equivalent for the present case.

[22] Reference 4, p. 517, Eq. (8.1-3).

[23] P. S. Epstein, Phys. Rev. **23**, 710 (1924).

[24] K. H. Schmitt, Z. Naturforsch. **14a**, 870 (1959).

We see that this is essentially the form of diffusion equation we sought, namely Eq. (14), with

$$\delta_1(p)^{-1}=1+\frac{n_d}{n}\frac{(D_{12}')_{\text{eff}}}{(D_{1d}')_{\text{eff}}}$$

$$=1+\frac{n_d kT}{p}\left(\frac{m_1+m_2}{m_2}\right)^{\frac{1}{2}}\frac{r^2}{\sigma_{12}^2\Omega_{12}^{(1,1)*}}(1+\tfrac{1}{8}\pi a_1), \quad (25)$$

where $p=nkT$ is the *gas* pressure. Furthermore, substituting from Eqs. (6) and (8), and remembering that the $(D_{ij}')_{\text{eff}}$ in Eq. (24) are to be calculated on the basis of a total density of n' rather than n, we find by comparing coefficients that

$$(D_1)_{\text{eff}}^{-1}=\tfrac{1}{3}(16n)(q/\epsilon)(\mu/2\pi kT)^{\frac{1}{2}}(\pi\sigma_{12}^2)\Omega_{12}^{(1,1)*}$$

$$+\tfrac{1}{3}(16n_d)(q/\epsilon)(m_1/2\pi kT)^{\frac{1}{2}}(\pi r^2)(1+\tfrac{1}{8}\pi a_1). \quad (26)$$

But this is just the Bosanquet interpolation formula, Eq. (13), provided we write

$$(D_{12})_{\text{eff}}^{-1}=\tfrac{1}{3}(16n)(q/\epsilon)(\mu/2\pi kT)^{\frac{1}{2}}(\pi\sigma_{12}^2)\Omega_{12}^{(1,1)*}, \quad (27)$$

$$D_{iK}^{-1}=\tfrac{16}{3}(n_d q/\epsilon)(m_1/2\pi kT)^{\frac{1}{2}}(\pi r^2)(1+\tfrac{1}{8}\pi a_1). \quad (28)$$

We see that Eq. (27) is identical with Eqs. (6) and (8), as it should be. Furthermore, we see that Eq. (28) is a satisfactory expression for D_{1K} in that it has the proper dependence on pressure, temperature, and molecular weight. Comparing Eq. (28) with the usual expression Eq. (11) for D_{1K}, we find the following expression for the constant K_0:

$$K_0^{-1}=\tfrac{128}{9}(n_d q/\epsilon)r^2(1+\tfrac{1}{8}\pi a_1). \quad (29)$$

According to Eq. (29) a slight dependence of K_0 on the gas is possible through the scattering factor a_1, although it is likely that no such dependence will be observed by virtue of all such factors being unity.

We have thus derived all three of the results mentioned at the beginning of this section. The expressions for $\delta_2(p)$ and $(D_2)_{\text{eff}}$ are obtained from Eqs. (25) and (26) for $\delta_1(p)$ and $(D_1)_{\text{eff}}$ by the interchange of the subscripts 1 and 2. It is important to note that $\delta_1\neq\delta_2$ and $(D_1)_{\text{eff}}\neq(D_2)_{\text{eff}}$. The only new property of the model (other than porosity and tortuosity) which appears in the final results is the group $[n_d r^2(1+\frac{1}{8}\pi a)]$ which occurs in the expressions for δ_i and D_{iK}. This group is probably best determined experimentally by measurement of D_{iK}; that is, we use measurements of D_{iK} to evaluate δ_i. The explicit relation for $\delta_i(p)$ in terms of experimentally determined quantities is formed from Eqs. (25), (27), and (28):

$$\delta_1(p)^{-1}=1+[(D_{12})_{\text{eff}}/D_{iK}]. \quad (30)$$

Since $D_{2K}=(m_1/m_2)^{\frac{1}{2}}D_{1K}$, we find from Eq. (30) that

$$\delta_2(p)^{-1}=1+(m_2/m_1)^{\frac{1}{2}}\{[\delta_1(p)]^{-1}-1\}. \quad (31)$$

In terms of the system illustrated in Fig. 2, it was found[13] that $D_{\text{He}K}=0.32$ cm²/sec and $D_{\text{Ar}K}=0.10$ cm²/sec at 100°C. The value of $(D_{12})_{\text{eff}}$ corresponding to 2 atm (the pressure of most of the runs) was 0.00484 cm²/sec. From Eq. (30) we thus find $\delta_{\text{He}}=0.985$ and $\delta_{\text{Ar}}=0.954$ at 2 atm, and from Eq. (13) we find $(D_{\text{He}})_{\text{eff}}=0.00477$ cm²/sec and $(D_{\text{Ar}})_{\text{eff}}=0.00462$ cm²/sec at 2 atm. The mechanism was clearly predominantly normal diffusion with respect to δ_i and $(D_i)_{\text{eff}}$, and yet the ratio J_1/J_2 was equal to $-(m_2/m_1)^{\frac{1}{2}}$ within experimental error, as was shown in Table I.

We may also note the pressure dependence of $\delta_i(p)$ and $(D_i)_{\text{eff}}$. A plot of $\delta_i(p)$ vs p rises linearly from the origin, bends gradually over, and reaches a constant value of unity at high values of p (similar to a Langmuir adsorption isotherm). A plot of $1/\delta_i$ vs $1/p$ is linear, as is clear from Eq. (25). Similarly, a plot of $(D_i)_{\text{eff}}$ vs $1/p$ rises linearly from the origin, bends over, and reaches a constant value of D_{iK} at high values of $1/p$. A plot of $1/(D_i)_{\text{eff}}$ vs p is linear, but does not pass through the origin, as Eq. (26) shows.

One final point of interest concerns the force exerted on the diaphragm particles by the diffusing gas mixture. In other words, if one of the particles came unstuck from the rest of the diaphragm, would it move, and if so in which direction? The force on such a single dust particle has been calculated by Waldmann.[21] In our notation, his expression can be written (leaving out the porosity and tortuosity factors and setting $a_1=a_2=0$ for simplicity) for the normal diffusion region as

$$F_d=(-8r^2/3)(2\pi kT)^{\frac{1}{2}}[(n_1m_1^{\frac{1}{2}}+n_2m_2^{\frac{1}{2}})(v_d-n^{-1}J)$$

$$+(m_1^{\frac{1}{2}}-m_2^{\frac{1}{2}})D_{12}(\partial n_1/\partial z)], \quad (32)$$

where F_d is the force on the dust particle and v_d is its velocity. Substituting $D_{12}(\partial n_1/\partial z)=-(J_1-x_1J)$ and $J_1/J_2=-(m_2/m_1)^{\frac{1}{2}}$, we find that most of the terms in brackets in Eq. (32) cancel out, leaving only a sort of Stokes' law result:

$$F_d=(-8r^2/3)(2\pi kT)^{\frac{1}{2}}(n_1m_1^{\frac{1}{2}}+n_2m_2^{\frac{1}{2}})v_d, \quad (33)$$

so that there is no force exerted on the particle unless it is given an initial velocity. We may thus conclude that the diffusing gas mixture exerts no force on the porous diaphragm, a result which is physically very plausible (although perhaps not intuitively obvious).

DISCUSSION

One of the most interesting features of the present model is its prediction that $J_1/J_2=-(m_2/m_1)^{\frac{1}{2}}$ even outside the Knudsen region. To the authors' knowledge, this is the first satisfactory theoretical explanation of the flux ratio in very porous materials at high pressures. Many investigators,[1,18–20] the authors included,[13] have attempted an explanation of this phenomenon by momentum transfer arguments. It is assumed that there is zero net momentum transfer (zero force) to the walls of the porous diaphragm if no pressure gradient exists in the gas. This happens to be correct, as shown in the preceding section, but does not seem *a priori* obvious. The previous calculations of the net momentum trans-

fer, however, were all incorrectly given as the product of the average flux and the average momentum, i.e.,

$$\text{momentum transfer} = (n_1\bar{v}_1)(m_1\bar{v}_1) + (n_2\bar{v}_2)(m_2\bar{v}_2). \quad (34)$$

On setting this equal to zero and noting that $\bar{v}_i$ varies as $m_i^{-\frac{1}{2}}$, one readily obtains the desired result. However, the momentum transfer is *not* given by Eq. (34), but is the average of the product (flux times momentum), i.e.,

$$\text{momentum transfer} = \langle (n_1 v_1)(m_1 v_1) \rangle_{Av} + \langle (n_2 v_2)(m_2 v_2) \rangle_{Av}$$
$$= n_1 m_1 \langle v_1^2 \rangle_{Av} + n_2 m_2 \langle v_2^2 \rangle_{Av}. \quad (35)$$

But this corrected calculation is merely the kinetic theory expression for the pressure of the gas, and gives no new information. In fact, Eq. (34) really involves a subtle confusion between average *speed* and average *velocity*. The correct calculation of the momentum transferred to the wall particles by collisions is fairly complicated and has been given by Waldmann,[21] who also allowed for the fact that the velocity distribution in a diffusing gas mixture is not Maxwellian. The present derivation from the kinetic theory diffusion equations is much simpler and also needs no assumption of zero force on the diaphragm.

Another interesting feature of the present model is its ability to cover the transition region between the Knudsen and normal regions. So far as we know, this is the first time it has been possible to give a rigorous theoretical treatment of the entire transition region.

One fundamental question remains unanswered however: Under what conditions of pore size and/or gas pressure does the present model start to fail? As the pore size becomes larger and larger with respect to the mean free path, the flux ratio should depart from the value $(m_2/m_1)^{\frac{1}{2}}$ and tend towards the value m_2/m_1, which was derived in Eq. (3) on the basis of negligible gas-wall interactions. Experiments with capillaries of diameters of a few tenths of a millimeter have given results corresponding to a flux ratio intermediate between these two values.[1,2] It is therefore clear that the model probably fails when the pore size or capillary diameter becomes very much larger than the mean free path, but we have at present no detailed information.

Finally, some mention should be made as to the method of analyzing experimental measurements to determine values of diffusion coefficients. For a given gas pair and porous medium, the two quantities $(D_{12})_{\text{eff}}$ and D_{1K} (or D_{2K}) completely characterize the system. If D_{12} is also known, then the porous medium alone is completely characterized in terms of the groups (ϵ/q) and $[n_d r^2(1+\frac{1}{8}\pi a)]$. One should then be able to predict, with confidence, the diffusion behavior of a number of different gas mixtures in the same medium on the basis of a set of experiments involving a single gas mixture.

The model itself gives no quantitative characterization of the porous medium, but treats the groups (ϵ/q) and $[n_d r^2(1+\frac{1}{8}\pi a)]$ as constants to be found by experiment. It is therefore important to discuss the determination of $(D_{12})_{\text{eff}}$ and D_{1K}. If one can be sure that the measurements refer either to the pure Knudsen or the pure normal diffusion region, then the integration of Eq. (14) for the steady state with $\delta(p)$ equal to either zero or one is straightforward, and yields an algebraic equation from which one of the diffusion coefficients can be calculated. It is presumed that the quantities J_1, $x_1(0)$ and $x_1(L)$ are measured as indicated in Fig. 1). Probably J_2 should also be measured as an experimental check, to see if Eq. (13) is followed. Unfortunately, it is not always easy to tell whether measurements are in the pure Knudsen or pure normal diffusion region, especially since the ratio J_1/J_2 is no indication. Many experiments are thus likely to be at least partly in the transition region, whether this is desired or not.

In such a case it is still possible to integrate Eq. (14) for the steady state. Let us pick as our two unknowns not $(D_{12})_{\text{eff}}$ and D_{1K}, but $(D_{12})_{\text{eff}}$ and their ratio,

$$\Delta_1 \equiv (D_{12})_{\text{eff}}/D_{1K}, \quad (36)$$

which varies as $1/p$. Integrating Eq. (14) for the steady state and using Eqs. (12), (13), and (30), we obtain

$$J_1 = \frac{n(D_{12})_{\text{eff}}}{\beta L} \ln\left[\frac{(1+\Delta_1)-\beta x_1(L)}{(1+\Delta_1)-\beta x_1(0)}\right], \quad (37)$$

where $n = p/kT$, L is the thickness of the porous diaphragm, and

$$\beta = 1-(m_1/m_2)^{\frac{1}{2}}. \quad (38)$$

If J_1 is measured as a function of pressure, then Eq. (37) shows that at sufficiently high pressures J_1 will be a constant (since $\Delta_1 \to 0$ as $p \to \infty$). If measurements can be made at sufficiently high pressures for J_1 to reach this asymptotic value, $(D_{12})_{\text{eff}}$ can be calculated directly; then Δ_1 and hence D_{1K} can be calculated from one measurement in the transition region. At very low pressures, on the other hand, J_1 is directly proportional to p (since $\Delta_1 \to \infty$ as $p \to 0$), and D_{1K} can be calculated from the proportionality constant; $(D_{12})_{\text{eff}}$ can then be calculated from one measurement in the transition region. If it is not possible to make measurements at either sufficiently high or sufficiently low pressures, and all measurements are made in the transition region, then Eq. (37) can be solved simultaneously for the two constants $p(D_{12})_{\text{eff}}$ and $p\Delta_1$ if measurements are made at two or more pressures. If measurements are made at a number of pressures in the transition region, the two constants can be found by a successive approximation

least-squares procedure[25] (the usual least-squares procedure does not work because Eq. (37) is not linear in the constants to be found). The mathematical analysis of measurements in the transition region is therefore a little more involved than in the Knudsen or normal regions, but is not difficult in principle.

[25] W. E. Deming, *Statistical Adjustment of Data* (John Wiley & Sons, Inc., New York, 1943).

ACKNOWLEDGMENTS

Two of the authors, R. B. Evans and G. M. Watson, wish to acknowledge the assistance of W. B. Cottrell and H. L. Weissberg during the initial stages of these studies. The helpful criticisms of M. Blander, the encouragement of P. H. Emmett, and the dependable assistance of J. Truitt were most stimulating and helpful.

THE JOURNAL OF CHEMICAL PHYSICS VOLUME 35, NUMBER 6 DECEMBER, 1961

A High-Resolution Study of CO_2 Absorption Spectra between 15 and 18 Microns*

ROBERT P. MADDEN

Laboratory of Astrophysics and Physical Meteorology, The Johns Hopkins University, Baltimore 18, Maryland†

(Received May 15, 1961)

A study has been made of the absorption due to individual lines and Q branches of CO_2 bands in the 15- to 18-μ spectral region. The strengths and widths of absorption lines on the low-frequency side of the ν_2 fundamental band and in the 02^00—01^10 band of $C^{12}O_2^{16}$ have been measured. In the latter band the variation of line strength and width with J has been determined as well as the Coriolis interaction parameter. The strengths of five other bands of $C^{12}O_2^{16}$ have been determined from measurements on their Q branches, and the strengths of the ν_2 fundamental bands of the isotopes $C^{13}O_2^{16}$ and $O^{18}C^{12}O^{16}$ have been estimated. The rotational structure of the ν_2 fundamental Q branch for $C^{12}O_2^{16}$ is partially resolved, and the band constants determined. The ν_2 fundamental band head of the $O^{18}C^{12}O^{16}$ isotope is reported.

The spectra were taken in 1956 after construction of the large infrared spectrometer at the Laboratory of Astrophysics and Physical Meteorology, The Johns Hopkins University. This $f/6$ spectrometer utilizes 3-in. long curved slits and a 14- by 12-in. grating in a Fastie-Ebert mounting. It is demonstrated that this instrument has available an optical slit width of 0.06 cm^{-1} at 17 μ.

I. INTRODUCTION

A STUDY of the CO_2 band strengths at elevated temperatures on the high-frequency side of the ν_2 fundamental at 667.4 cm^{-1} has been made by Kostkowski.[1,2]

Several investigators[3–8] have measured the total absorption of CO_2 in the 13- to 18-μ spectral region under various conditions. More recently the total strength of all the CO_2 bands in the 15-μ region was determined by Kaplan and Eggers[9] using the "curve of growth" method and by Overend *et al.*[10] using the "Wilson-Wells-Penner-Weber" method. The last two investigations agree on a value of 240 cm^{-2} atm^{-1} for the total strength of all the bands in this region. No study of the strength of individual absorption lines has previously been made in the 15- to 18-μ spectral region. In fact, none of the above investigations allow the determination of the strength of individual bands in this region.

The principal objective of this investigation has been the determination of line and band strengths and linewidths for CO_2 absorption in the 15- to 18-μ region. Rossmann *et al.*[11,12] have measured the wavelength positions of most of the lines in this region with good accuracy, and their wavelength values appear in the tables, with the exception of the position of the 01^10—000 band head of the $O^{18}C^{12}O^{16}$ isotope, and the positions of the Q branch lines for the 01^10—000 band of $C^{12}O_2^{16}$, which are reported here for the first time. The wavelength measurements of Rossmann *et al.* have been used as a calibration for these determinations.

The observed widths of the absorption lines in this spectral region, for the pressures used in these experi-

* This work has been supported by the Office of Naval Research.

† Present address, Physics Research Laboratory, U. S. Army Engineer Research and Development Laboratories, Fort Belvoir, Virginia.

[1] H. J. Kostkowski, dissertation, The Johns Hopkins University, 1955.

[2] H. J. Kostkowski and L. D. Kaplan, J. Chem. Phys. **26,** 1252 (1957).

[3] H. Rubens and E. Ladenburg, Verhandl. deut. physik. Ges. **7,** 179 (1905).

[4] A. M. Thorndike, J. Chem. Phys. **13,** 868 (1947).

[5] W. Peters, dissertation, The Johns Hopkins University, 1949.

[6] D. F. Eggers, Jr. and B. L. Crawford, Jr., J. Chem. Phys. **19,** 1554 (1951).

[7] W. H. Cloud, "The 15 micron band of CO_2," ONR Progr. Rept., The Johns Hopkins University, 1952.

[8] J. N. Howard, D. L. Burch, and D. Williams, "Near infrared transmission through synthetic atmospheres," Rept. No. 1, Ohio State University (1954).

[9] L. D. Kaplan and D. F. Eggers, Jr., J. Chem. Phys. **25,** 876 (1956).

[10] J. Overend, M. Youngquist, E. C. Curtis, and B. L. Crawford, J. Chem. Phys. **30,** 532 (1959).

[11] K. Rossmann, K. Narahari, K. N. Rao, and H. H. Nielsen, J. Chem. Phys. **24,** 103 (1956).

[12] K. Rossmann, W. L. France, K. N. Rao, and H. H. Nielsen, J. Chem. Phys. **24,** 1007 (1956).

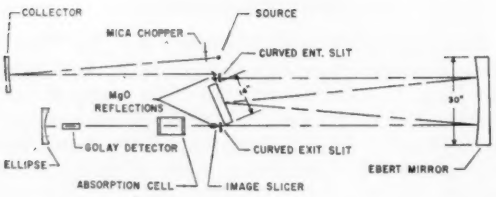

FIG. 1. Optical diagram showing a central ray traced through the large infrared spectrometer at the Laboratory of Astrophysics and Physical Meteorology, The Johns Hopkins University. This $f/6$ instrument utilizes 3-in. high slits and a 14-in. wide by 12-in. high grating in a Fastie-Ebert mounting.

ments, may be considered as caused only by collision broadening. Adel[13] has determined an upper limit of 0.12 cm^{-1} for the average self-broadened half-width of the CO_2 absorption lines in the ν_2 fundamental band. The average self-broadened half-width for the 2077 cm^{-1} band of CO_2 was determined by Benedict and Silverman[14] to be 0.075 cm^{-1}. Kostkowski[1] determined the average self-broadened half-width for the peak of the R branch of the 961 cm^{-1} band to be 0.084 cm^{-1}. The linewidths given in the results of this study were determined from actual measurements on individual lines. The most accurate determination of linewidths is in the $02^{\circ}0$–$01^{1}0$ band of $C^{12}O_2^{16}$ where no previous measurements have been made.

II. EXPERIMENTAL DISCUSSION

High resolution is necessary to make measurements of strength and width on individual absorption lines, and to reduce the uncertainty in band strength determinations caused by the overlap of different bands. The large infrared spectrometer of the Laboratory of Astrophysics and Physical Meteorology has available the highest resolution yet attained in the 15- to 25-μ spectral region.

An optical diagram of this instrument, the construction of which was completed in 1956, is shown in Fig. 1. The $f/6$ spectrometer utilizes a 30-in. Ebert mirror, 3 in. high slits curved on a 15 in. circle, and a high-quality grating with a ruled area 14 in. wide by 12 in. high. The 1000 lines/in. ruling was performed under the direction of Dr. Babcock of Mount Wilson and Palomar Observatories in a 13-μ thick silver film evaporated onto a glass blank.[15] The grating figure is estimated to be $\lambda/20$ at 20μ.

The spectrum is scanned by rotation of the grating using a sine drive technique to obtain a linear variation of wavelength with time at the exit slit. The 15- to 25-μ spectral region is isolated through the use of several reststrahlen reflections from MgO crystals. An image-slicing device is used at the exit slit to chop the 3-in. high slit into three 1-in. segments which are imaged on the $\frac{1}{8}$-in. diam entrance window of a Golay detector using an elliptical mirror. A similar image-slicing device is used at the entrance slit when it is desired to illuminate the entrance slit with a carbon arc source.

The resolution attainable from this high-flux spectrometer was tested by observing individual absorption lines of N_2O in the 17-μ band. R branch lines with

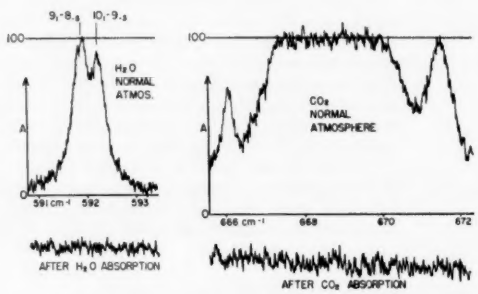

FIG. 3. Spectral scans showing the absorption due to H_2O and CO_2 in the 15-m optical path of the spectrometer before and after overnight circulation of the spectrometer atmosphere through a dessicant and KOH pellets. The ν_2 fundamental Q branch of CO_2 and the double water line at 592 cm^{-1} represent the strongest absorption of these gases encountered in this study.

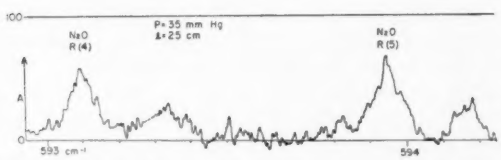

FIG. 2. A scan of the absorption due to the $J''=4$, 5 lines in the R branch of the 17-μ band of N_2O which demonstrates the ultimate single-pass resolution of the monochromator. The optical slitwidth deduced from this scan is 0.06 cm^{-1} which is only 12% greater than the value expected theoretically for slits equal to the diffraction pattern width.

$J''=4$, 5 are shown in Fig. 2. Hot band satellite lines can also be seen. For this test the slits were set equal to the width of the theoretical central diffraction maximum, and a carbon-arc source was used. The observed linewidths, as shown in Fig. 2 are 0.08 cm^{-1}. A correction for the actual linewidths leads to an effective optical slitwidth for the spectrometer of 0.06 cm^{-1}. This represents 70% of the theoretical limit of resolution for the grating at this angle, and compares favorably with the 80% expected theoretically (for slits equal to the diffraction width). Since the signal-to-noise ratio demonstrated in Fig. 2 is at the limit of usability, it would appear that this infrared spectrometer has the distinction of reaching the theoretical limit and the energy limit to resolution simultaneously.

In the present study a Globar source was used and an optical slitwidth of 0.1 cm^{-1}. The spectrometer is enclosed in a copper housing and the CO_2 and H_2O are removed from the 15-m optical path of the spectrometer by circulating the air through KOH pellets and a dessicant (Linde Air Products' Molecular Sieve).

[13] A. Adel, Phys. Rev. **52**, 53 (1953).
[14] W. S. Benedict and S. Silverman, Phys. Rev. **94**, 752 (A) (1954).
[15] R. P. Madden, J. Opt. Soc. Am. **45**, 408 (A) (1955).

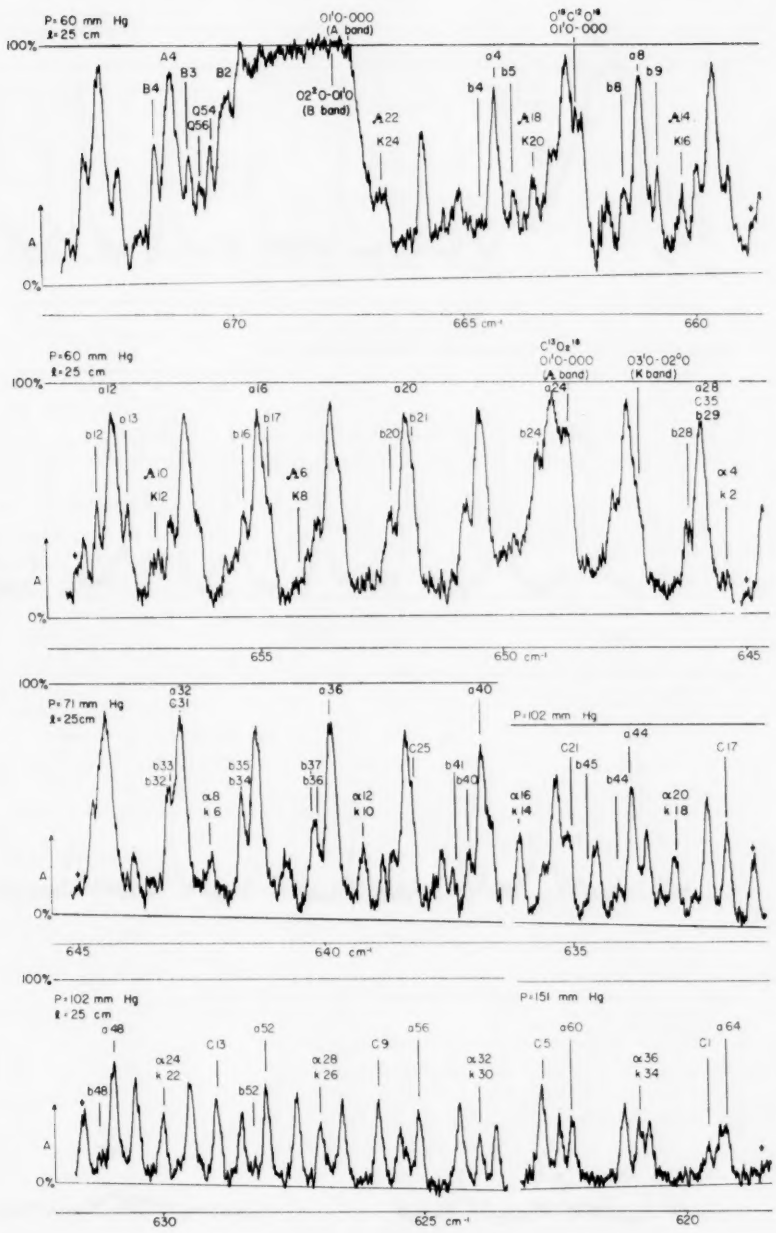

FIG. 4. CO_2 absorption spectra from 619 to 674 cm^{-1}. The spectra were obtained with an optical slit-width varying between 0.10 and 0.11 cm^{-1} in a 25-cm absorption cell at the pressures shown and a temperature of 300°K. The unmarked lines are easily identified by considering the identity of the marked lines.

Figure 3 demonstrates the effectiveness with which the H_2O and CO_2 are removed.

Four absorption cells of lengths 0.1994, 1.133, 5.08, and 25.17 cm were used in this study. The gas content of the absorption cell in use could be controlled from outside the spectrometer housing. The pressure was determined from two Hg manometers, and a thermocouple attached to the absorption cell gave a constant check on the gas temperature. The cells were filled to prescribed pressures with commercially pure CO_2—all measurements reported here pertain to self-broadened CO_2.

III. SPECTRA

It would be impractical to include here all the spectra from which measurements were taken. The tables include the results from all measurements, but only representative spectra are shown. Figures 4 and 5 con-

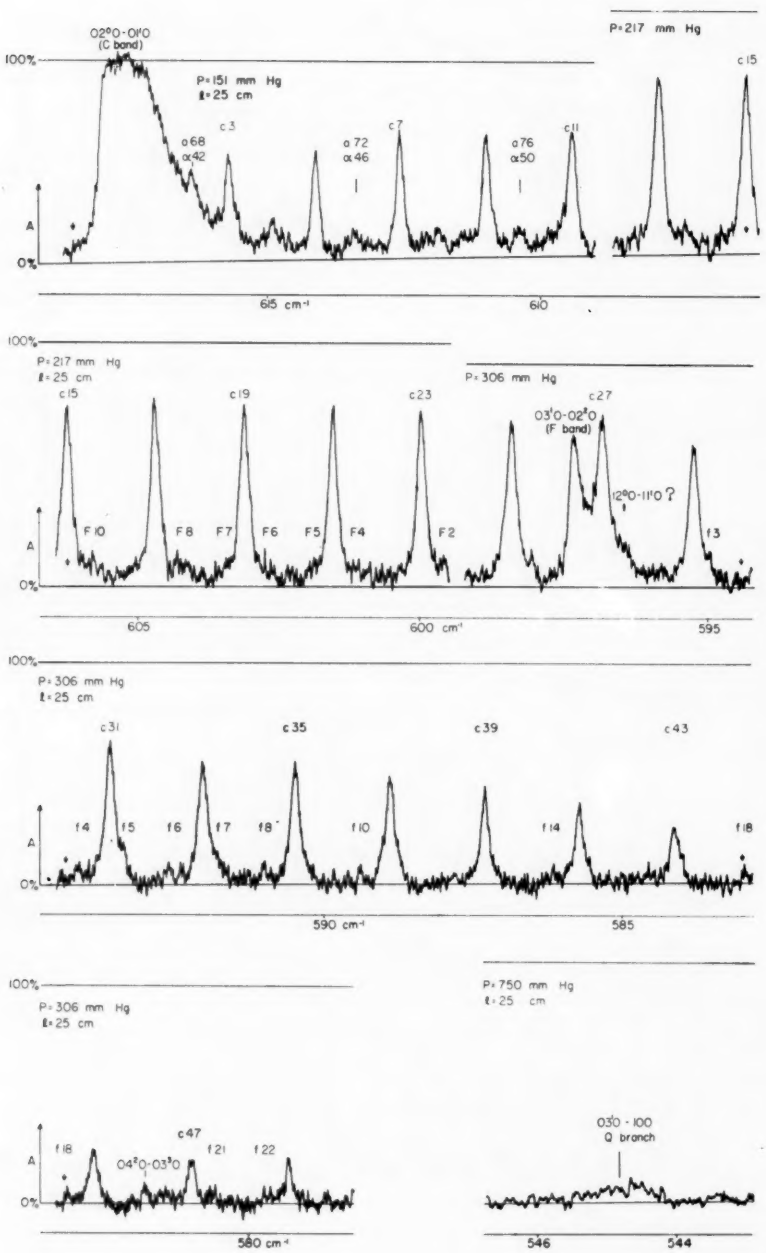

FIG. 5. CO_2 absorption spectra from 544 to 619 cm^{-1}. The spectra were obtained with an optical slit-width varying between 0.09 and 0.10 cm^{-1} in a 25-cm absorption cell at the pressures indicated and a temperature of 300°K. The unmarked lines are easily identified by considering the identity of the marked lines.

tain spectra of the entire range of study in these experiments, using the 25-cm absorption cell with the pressures indicated. Each vibrational transition is indicated at the band head, and the P and R branch lines are labeled according to the J quantum number of the lower state and the convention given in Table I.

The CO_2 spectra shown here were taken with a spectral slitwidth of $\sim$0.1 cm^{-1}, which is the highest resolution with which it has been measured in this region. Therefore, more lines are distinguishable and a better identification of satellites is possible than was previously possible.

Figure 6 is a scan of the 01^10—000 Q branch with higher dispersion. The Q branch line positions are

TABLE I. Letter notation used in this paper to refer to the bands studied.

			Upper state $(v_1, v_2^l, v_3)'$	Lower state $(v_1, v_2^l, v_3)''$
$C^{12}O_2^{16}$	A,a	: R,P branch	01^10	000
	B,b	: R,P branch	02^20	01^10
	C,c	: R,P branch	02^00	01^10
	K,k	: R,P branch	03^10	02^00
	F,f	: R,P branch	03^10	02^20
$C^{13}O_2^{16}$	α,α	: R,P branch	01^10	000

marked. The frequencies of the clearly observed Q branch lines together with the constant $(B''-B')$ they define, are given in Table II.

From a study of these spectra it is obvious that a considerable portion of the spectral range is crowded to the extent that measurements on individual lines would be difficult. Therefore measurements were not made on all lines. Three regions were selected for concentrated study: 660–667, 625–630, and 598–613 cm^{-1}. These regions were selected for the following reasons: (a) the principal lines in these regions involve less overlap; (b) lines of low, medium, and high J occur; and (c) the strengths of the lines occurring in these regions allow convenient-sized absorption cells to be used.

These three regions of greatest interest are shown in Figs. 7–9. In each case a scan for each of the absorption path lengths used is represented. The scans in Figs. 7 and 8 were taken with considerably greater dispersion

IV. ANALYSIS OF THE SPECTRA

A. Definitions

The quantities to be obtained from the spectra are line and band strengths, and line half-widths. These are defined below.

The *line strength per atmosphere*, S^0, at 300°K is defined as

$$S^0 = S/P,$$

where

$$S = \int_0^\infty k_\nu d\nu; \tag{1}$$

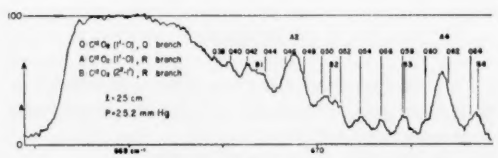

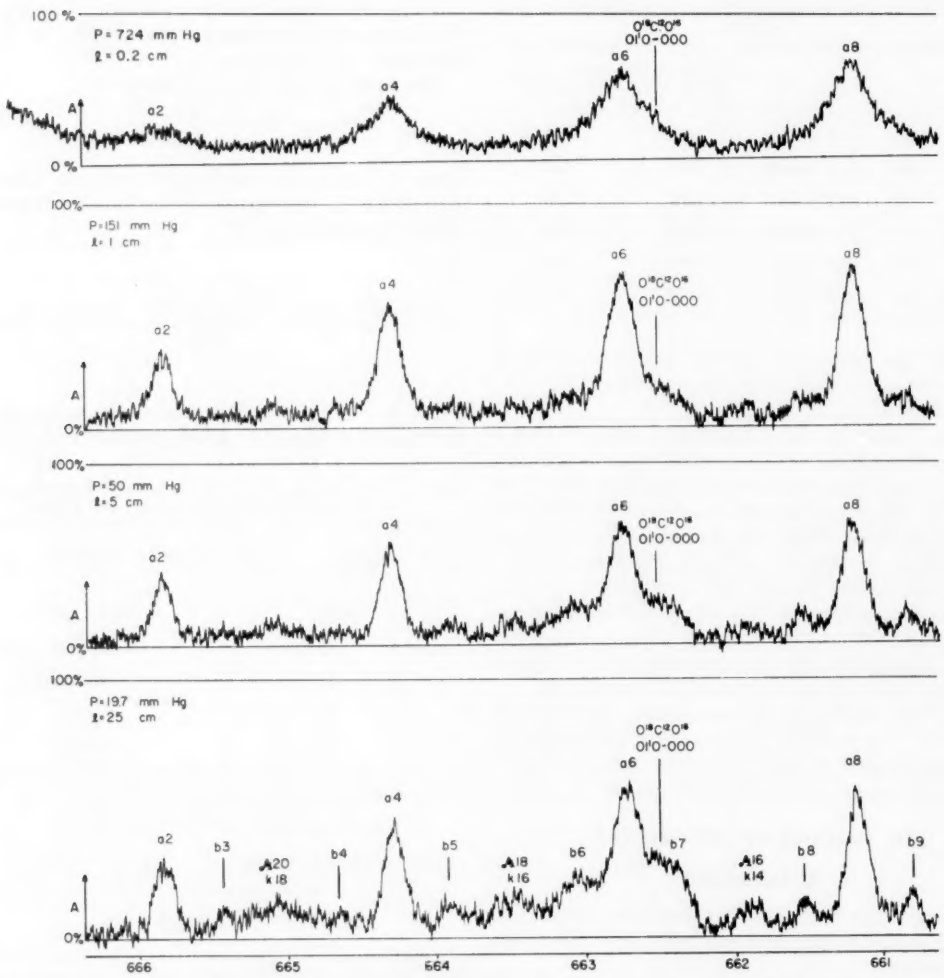

FIG. 7. CO_2 absorption spectra between 660 and 667 cm^{-1} showing an example of the spectrum obtained for each of the absorption path lengths used. The principal lines in this region are low J lines in the R branch of the ν_2 fundamental band. Note that the background lines become relatively more prominent as the absorption path length is increased.

Finally, the *equivalent width corrected to atmospheric pressure* at 300°K is defined as

$$W^0 = W/P, \tag{4}$$

where

$$W = \int A_\nu d\nu$$

and P is the pressure in atmospheres at 300°K. Here the integration must begin and end in regions of zero absorption if the definition is to be useful. When this condition is satisfied, the W observed is independent of the slitwidth of the spectrometer. (W^0 has the dimensions cm^{-1} atm^{-1}.) Ladenburg and Reiche[16] have demonstrated that if W^0 is obtained from the absorption due to a single Lorentz line, it is related to S^0 and γ^0 for that line by

$$W^0 = 2\pi\gamma^0 F(x), \tag{5}$$

where

$$x = S^0 l/2\pi\gamma^0$$

and $F(x)$ (called the Ladenburg-Reiche function) $= xe^{-x}[I_0(x)+I_1(x)]$, where I_0 and I_1 are Bessel functions of imaginary arguments.

The two limiting cases are of interest,

$$\lim_{x\to 0} F(x) = x \qquad \text{("linear" region)} \tag{6}$$

and for $x>>0$,

$$F(x) \approx (2x/\pi)^{\frac{1}{2}} \qquad \text{("square-root" region).} \tag{7}$$

[16] R. Ladenburg and F. Reiche, Ann. Physik **421**, 181 (1911).

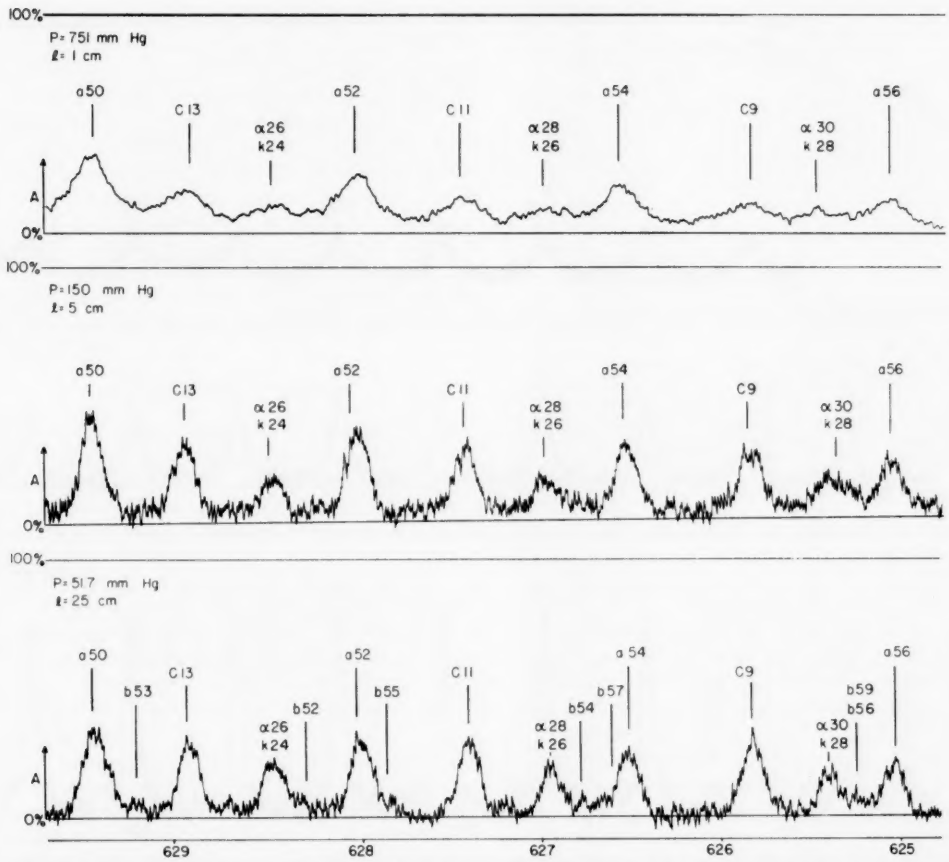

FIG. 8. CO_2 absorption spectra between 625 and 630 cm^{-1} showing an example of the spectrum obtained for each of the absorption path lengths used. The principal lines in this region are high J lines in the R branch of the ν_3 fundamental, and low J lines in the P branch of the $02^00—01^10(C)$ band. The upper scan was taken with a somewhat longer time constant than the others.

The curve of W^0 vs l is called the "curve of growth." A graphical technique has been developed[17] by which S^0 and γ^0 are determined from a comparison of a $\log W^0$ vs $\log l$ curve with a $\log F(x)$ vs $\log x$ curve (here called the $L—R$ curve). This will be referred to as the graphical "curve of growth" method.

The following is a discussion of the methods by which the data were reduced. A band-by-band treatment would be unduly repetitive and instead the discussion is organized according to the three principal spectral regions of interest. The results are summarized later in tabular form. In the following, the methods used to treat the P and R branch lines are considered for these three spectral regions in turn, followed by a discussion of the treatment of the various Q branches observed.

B. 660–667 cm^{-1} Region

The principal lines in the 660–667 cm^{-1} region are the lowest J lines belonging to the P branch of the fundamental ($01^10—000$) band. These are denoted $a2$, $a4$, $a6$, and $a8$. In addition, many weaker lines occur. In Fig. 7 a scan is shown of this region for each of the absorption path lengths used. This region is the only one for which the 0.2-cm cell was used. This short cell was required to obtain near-linear region absorption for these strong lines. The absorption due to the Q branch of the fundamental band for the $O^{18}C^{12}O^{16}$ molecule can be seen beneath the line $a6$. The experimentally determined band head frequency is 662.39 ± 0.05 cm^{-1}. Because of the interference of this isotope band, the absorption data on line $a6$ were not fully analyzed. The 1-, 5-, and 25-cm absorption-cell data on $a2$, $a6$, and $a8$ were obtained at low enough pressures so that the overlap corrections were not very large. However, pressures up to 1 atm were used in the 0.2-cm cell and the overlap problem was more serious. In particular, the overlap of the fundamental Q branch tail on the line $a2$ prevents a satisfactory analysis of the absorption due to $a2$ at 1 atm.

The strengths and widths of the lines $a2$, $a4$, and $a8$

[17] W. S. Benedict, R. Herman, G. E. Moore, and S. Silverman, Can. J. Phys. **34**, 840 (1956).

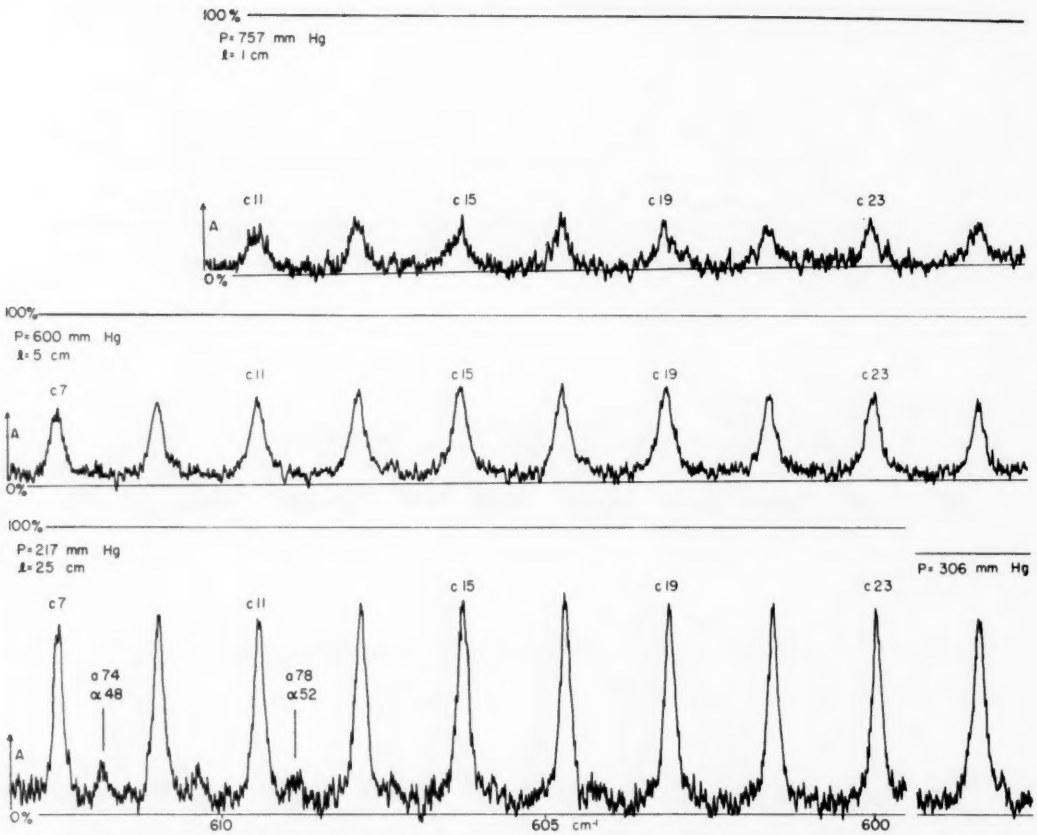

FIG. 9. CO_2 absorption spectra between 598 and 613 cm^{-1} showing an example of the spectrum obtained for each of the absorption path lengths used. The principal lines in this region, relatively free from overlap, are the medium J lines in the P branch of the 02^00—$01^10(C)$ band.

were derived from the spectra by the graphical "curve of growth" method, and by direct measurement on the high-pressure scans. The equivalent width of each of these lines was measured at each of the four absorption path lengths, with the exception of line $a2$ with the 0.2-cm path length. From these equivalent widths, the values of W^0 were calculated, corrected for overlap, and $\log W^0$ was plotted against $\log l$. The fit of the data to the L—R curve $[\log F(x)$ vs $\log x]$ is shown in Fig. 10 for line $a4$. The "linear" region asymptote and the "square-root" region asymptote, also indicated in Fig. 10, are useful in deducing S^0 and γ^0 by the graphical curve of growth method.[17] In particular, the value of W^0 read from the graph at the intersection of the "linear" region asymptote with the "square-root" region asymptote is equal to $4\gamma^0$, while the value of W^0 at the intersection of the "linear" region asymptote with the vertical line $l=1$ cm is equal to S^0. S^0 and γ^0 were obtained from such graphs for the lines $a4$ and $a8$.

The product $S^0\gamma^0$ was derivable from the values of equivalent width for the longer absorption path lengths. It has been shown,[17] that near the "square-root" region an approximate relation between S^0, γ^0, and W^0 is

$$W^0 \approx 2(S^0\gamma^0 l)^{\frac{1}{2}}(1-\tfrac{1}{8}x^{-1})$$

(error less than $\frac{1}{4}\%$ for $x>3.5$) (8)

Since the $S^0\gamma^0$ products determined in this way are not dependent on measurements of linear region absorption, these products were also determined for the lines $a4$ and $a8$ and combined with the direct measurements of S^0 and γ^0 to give increased reliability to those values.

In making direct measurements of line strength and width, only the spectra taken at 1-atm pressure were used. Therefore, corrections due to the smearing of the spectrum by the spectrometer are small since at 1-atm pressure the widths of the absorption coefficient curves are considerably larger than the optical slitwidth (approximately 0.11 cm^{-1} at this frequency). The logarithm of the transmission curve was calculated and $S_{obs}{}^0$ for each line obtained by integration. The $\gamma_{obs}{}^0$ was obtained by direct measurement. The appropriate

corrections for the "smearing" effect of the finite spectrometer slit have been calculated by Kostkowski and Bass.[18] The best averages of the various determinations of S^0 and γ^0 for $a4$ and $a8$ are given in Table III. The product $S^0\gamma^0$ for the line $a2$ is 0.051 cm^{-3} atm^{-2}.

The values of W^0 for the lines $b8$ and $b9$ were determined from the spectra taken with the 25-cm absorption cell. Equation (8) was used to determine $S^0\gamma^0$ for $b8$ and $b9$. If the assumption is made that γ^0 for $b8$ and $b9$ is equal to γ^0 for $a8$, the ratio of S^0 for $b8$ and $b9$ to S^0 for $a8$ may be determined. [In a similar manner, the strength of $b34+b35$ (see Fig. 4) was determined relative to the strength of $a34$.] These results are tabulated in Table III.[19]

C. 625–630 cm^{-1} Region

The second region studied, from 625 to 630 cm^{-1}, contains many closely spaced lines as shown in Fig. 8. P branch lines of the A, K, and α bands and R branch lines of the C band occur predominantly. Also P branch lines of the B band and R branch lines of the F band occur weakly.

The equivalent widths of $a50$, 52, 54, 56, and $C9$, 11, 13, were measured for pressures from 0.05 to 1 atm, and an average W^0 calculated for each line for each absorption path length. Small corrections were made on these values of W^0 for background. These corrections averaged only a few percent, and the largest was 8%.

Due to the weak absorption, overlap, and the corrections necessary, the values of W^0 for lines in this region obtained with the 1- and 5-cm path lengths have considerable uncertainty. To increase the accuracy obtained by the graphical "curve of growth" method, the data for $a50$, 52, 54, and 56 were plotted together for a single comparison to the L—R curve. Two assumptions are necessary for this step. The first is that the value of γ^0 is the same for all four lines. The second is that the ratios of the line strengths are known. Here the theoretical ratios were assumed for a Boltzmann distribution with a rigid-rotor model. For a few adjacent high J lines these assumptions are expected to be quite good. The data are plotted as $\log W^0$ vs $\log S^0 l$, where S^0 for each line is given in units of $S^0 50$. Thus 12 points instead of three determine the fit of the data to the L—R curve. γ^0 (assumed the same for all lines) is obtained from the curve and the value of S^0 for $a50$. S^0 for the other lines is determined by the theoretical ratios. This method was also used to plot data for the lines $C9$, 11, and 13 of the R branch of the (02°0—01′0) band. Here the assumptions regarding γ^0 and the ratio of the strengths seem valid if one considers the expected values estimated from measurements in this study of γ^0 and S^0 in the P branch of the C band.

The values of S^0 and γ^0 determined for the lines in this region are included in Table III.

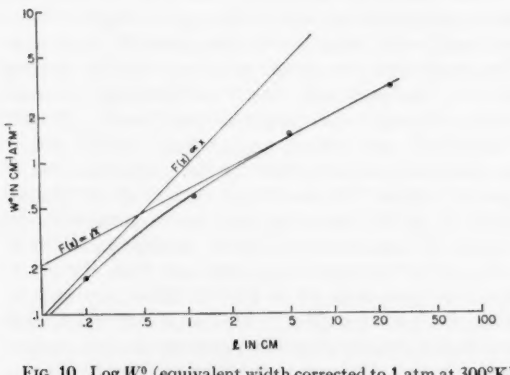

FIG. 10. Log W^0 (equivalent width corrected to 1 atm at 300°K) plotted against log$l$ (absorption path length) for the line $J''=4$ in the P branch of the ν_2 fundamental band. The data are plotted as circled points, while the solid curve shows the "fit" of the data to the Ladenburg-Reiche curve [$F(x)$ vs x, see Eq. (5)]. The straight lines define the "linear" and "square-root" asymptotes to the Ladenburg-Reiche curve.

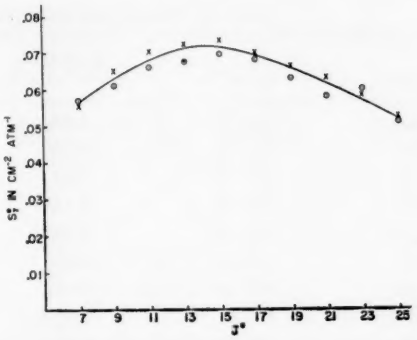

FIG. 11. Experimental values of line strength ($S°$) plotted as a function of J'' for the P branch of the 02°0–01¹0 (C) band. The data were obtained from direct measurements (integration over the absorption coefficient) as well as by the "curve of growth" technique. The solid line merely indicates the trend of the data. × Determined by "curve of growth" method; ⊙ corrected direct measurements.

D. 598–613 cm^{-1} Region

This region of the spectrum is shown in Fig. 9. The only strong lines present are the $c7$—$c25$ lines of the 02°0—01¹0 band P branch. (The F band lines occuring here are only 2 or 3% as strong as the C band lines and a correction for their effect is easily made.) Here, pressures up to 1 atm do not cause serious overlap, and S^0 and γ^0 were determined for these lines by direct measurement as well as by the curve of growth method. These are the most accurate S^0 and γ^0 values determined in this study.

Direct measurements were possible with only small corrections, since the width of the absorption coefficient curve at a pressure of 1 atm is over twice the optical slitwidth of the spectrometer. The logarithm of the

[18] H. J. Kostkowski and A. M. Bass, J. Opt. Soc. Am. **46**, 1060 (1956).

[19] In Table III, the strength of $b34+b35$ is divided into a contribution from each line assuming a Boltzmann distribution with a rigid-rotor model.

TABLE III. Strengths and half-widths of individual lines determined in this study.

Line	ν (cm^{-1})	$S°$ at 300°K (cm^{-2} atm^{-1})	Estimate of uncertainty	$\gamma°$ at 300°K (cm^{-1} atm^{-1})	Estimate of uncertainty
*a*4	664.29	1.00	6%	0.126	11%
*b*8	661.52	0.106	15%		
*a*8	661.18	2.24	6%	0.10	22%
*b*9	660.81	0.140	15%		
*b*34	641.65	0.105	20%		
*b*35	641.65	0.095	20%		
*a*50	629.46	0.143	7%	0.06	9%
C13	628.91	0.0750	7%	0.11	9%
*a*52	627.99	0.101	7%	0.06	9%
C11	627.38	0.0695	7%	0.11	9%
*a*54	626.51	0.0704	7%	0.06	9%
C9	625.83	0.0613	7%	0.11	9%
*a*56	625.05	0.0481	7%	0.06	9%
*c*7	612.56	0.0565	3%	0.111	15%
*c*9	611.00	0.0627	3%	0.108	15%
*c*11	609.42	0.0682	3%	0.105	12%
*c*13	607.84	0.0712	3%	0.104	10%
*c*15	606.27	0.0715	3%	0.103	10%
*c*17	604.70	0.0692	3%	0.103	10%
*c*19	603.13	0.0656	3%	0.103	10%
*c*21	601.56	0.0614	3%	0.102	10%
*c*23	599.98	0.0568	3%	0.101	12%
*c*25	598.40	0.0522	3%	0.099	15%

transmission curve was calculated for four runs with the 1- and 5-cm absorption cells where the pressure was between 0.8 and 1 atm. Then γ_{obs} was measured directly, and S_{obs} was obtained from the integral of the log$T$ curve for each line. The appropriate corrections for the "smearing" effect of the spectrometer slit were made. Corrected values of S^0 for each line obtained by direct measurement are plotted as circled points in Fig. 11 and the corrected values of γ^0 are plotted as circled points in Fig. 12.

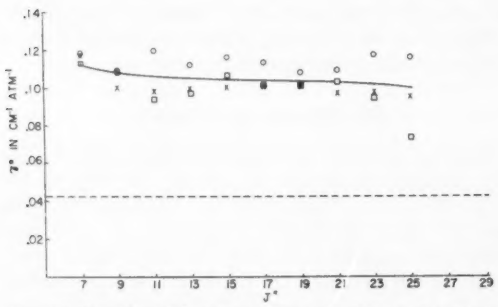

FIG. 12. Experimental values of line half-width ($\gamma°$) plotted as a function of J'' for the P branch of the 02°0–01¹0 (C) band. The data shown were obtained from directly measured widths by the "curve of growth" method and from strength-width products ($S°\gamma°$) determined from "square-root-region" measurements combined with the best determinations of line strength ($S°$). The solid curve represents the average trend of the data. ⊙ Average of corrected direct measurements; × determined by curve of growth method; ⊡ determined from $S°\gamma°$ for 25-cm cell; – – – kinetic theory value.

The equivalent width of each line $c7$—$c25$, was measured for the 1-, 5-, and 25-cm path lengths for several runs with pressures varying from 0.2 to 1 atm. The resulting values of W^0 were smoothed by plotting W^0 vs J for each path length and drawing a smooth curve through the experimental points. LogW^0 (smoothed) was plotted against log$l$, and S^0 and γ^0 for each line was determined by the graphical curve of growth method. The resulting values of S^0 are plotted as x's in Fig. 11, where they may be compared with the results of the corrected direct measurements. The values of γ^0 for these lines obtained from the L—R curve are plotted as x's in Fig. 12. Here they may be compared with the directly measured half-widths and also with values of γ^0 determined from the best experimental values of the line strengths and the $S^0\gamma^0$ products obtained from the data using the 25-cm absorption cell. Also appearing in Fig. 12 is the value of half-width determined from kinetic theory—which merely indicates the magnitude by which the optical collision diameter exceeds the collision diameter calculated from viscosity and conductivity measurements.[20]

[20] A handbook value of $d=3.3\times10^{-8}$ cm was assumed for the kinetic collision diameter.

TABLE IV. Measured values of Q branch strength.

Isotope	Transition	Letter notation	ν (cm^{-1})	S° of Q branch (cm^{-2} atm^{-1}) Weak absorption method	Wilson and Wells method	Elsasser band method	Estimate of uncertainty
$O^{18}C^{12}O^{16}$	01^10–000		662.39			0.50	35%
$C^{13}O_2^{16}$	01^10–000	$\mathfrak{a}$	648.52			1.07	25%
$C^{12}O_2^{16}$	03^10–02^00	K	647.02			0.52	30%
$C^{12}O_2^{16}$	02^00–01^10	C	618.03		1.86		7%
$C^{12}O_2^{16}$	03^10–02^20	F	597.29		0.0725		12%
$C^{12}O_2^{16}$	03^10–100	G	544.26	0.002			10%

E. Q Branch Measurements

The Q branch strengths of six bands were determined. In the discussion below, they will be grouped according to the method used to reduce the data.

The Q branch of the 03^10—100 band at 544.26 cm^{-1} is weak and is free from overlap with other bands. The "linear region" approximation [Eq. (6)] was used to determine the strength of this Q branch. The value obtained is given in Table IV.

The Q branch strengths of the 02^00—01^10 transition (C band) and the 03^10—02^20 transition (F band) were determined by the method of Wilson and Wells.[21] For each band,

$$\int(-\ln T)d\nu$$

was evaluated at several conditions of path length and pressure and S^0 determined by extrapolation to zero path length, as shown in Fig. 13 for the C band. Here the extrapolation yields the strength of the Q branch plus the strength of the line $c1$ and weak lines of several other bands that are well surrounded by the Q branch structure. The C band Q branch strength given in Table IV was determined from the extrapolated value by making small theoretical corrections for these overlapping lines.

The F band Q branch measurement was a much more approximate procedure. Before the method of Wilson and Wells could be applied, it was necessary to remove the effect of line $c27$ from the absorption due to the FQ branch. This was done by first reconstructing the $c27$ line as it would appear in the absence of the FQ branch. It was assumed that the absorption due to $c27$ was equal to the average value of absorption for the lines $c25$ and $c29$ which could be clearly observed. After constructing the $c27$ line, the difference between the constructed and observed absorption was assumed to be due to the FQ branch, and the method of Wilson and Wells was pursued. The resulting Q branch strength is included in Table IV.

The remaining three Q branches are nearly buried beneath P branch lines of the fundamental A band, and are also overlapped with lines of the B and C bands. An accurate determination of their strengths cannot be made by direct measurements; however, a rough value was obtained using the following technique. First an estimate was made of the absorption due to the Q branch as a function of ν. From the band constants, the spacing of the Q branch lines was calculated at different frequencies, at intervals greater than the spectrometer slit function width. At each frequency for which the line separation had been calculated it was assumed that the spectrometer saw an Elsasser band,[22] and S^0 for the average strength line being passed by the spectrometer was calculated by the Elsasser formula.[22] A γ^0 of 0.11 cm^{-1} was assumed for the calculation. For each of the line strengths thus determined, a Q-branch strength may be calculated if a distribution is assumed for the Q branch. Here a Boltzmann distribution with a rigid-rotor model was assumed. The Q-branch strengths for the K band and the isotopic $\mathfrak{a}$ band were determined in this manner, and the results are given in Table IV. The Q-branch strength of the $01'0$—000 transition of the $O^{18}C^{12}O^{16}$

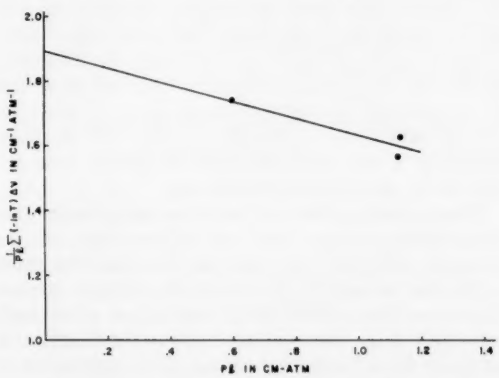

FIG. 13. Extrapolation of experimental data by the "Wilson and Wells" technique to determine the strength of the Q branch of the 02^00–01^10 (C) band. The ordinate value at $Pl=0$ is the strength in cm^{-2} atm^{-1}, but in this case a slight correction must be made for the presence of background lines to obtain the Q branch strength. The result is given in Table IV.

[21] E. B. Wilson, Jr. and A. J. Wells, J. Chem. Phys. **14**, 578 (1946).

[22] W. M. Elsasser, Phys. Rev. **54**, 126 (1938).

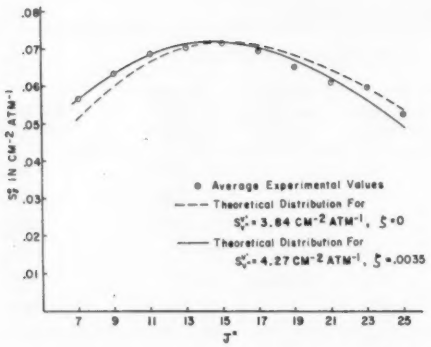

FIG. 14. Two choices of theoretical distribution of line strength with J'' fitted to the average experimental data for the P branch of the $02^{0}0$–$01^{1}0$ (C) band. Equation (9) multiplied by factor (10) was used for the calculation. This curve fitting determines the Coriolis interaction parameter ζ for the band.

isotope was also estimated by this method. In this molecule the oxygen atoms are not identical, and the fundamental Q branch has two series of lines as a result of l doubling. Since the even J series diverges more rapidly, it makes the major contribution to the absorption in the wing of the Q branch. The measurements were made in the wing of the Q branch, and an estimated correction of 30% for the contribution of the odd J series was made after the reduction. The resulting value of Q-branch strength is found in Table IV.

V. DISCUSSION OF RESULTS

A. Introductory Comments

The primary results of this study are the values of S^0 and γ^0 determined for the lines listed in Table III, and the Q-branch strengths listed in Table IV—also the results in Table II. The methods by which these parameters have been determined from the spectra have been discussed, and an estimate of the uncertainty in these results is listed for each value in the tables. Except for the overlap problem in the case of several of the Q-branch strength determinations the most important source of uncertainty was the lack of reproducibility of the quantities derived directly from the spectra due to the noise fluctuations.

These primary results can not be compared with other experimental values since no other study of the strengths and widths of individual lines has been made in this spectral region. It is, however, of great interest to compare the experimental distribution of strength and width of the lines within a band to the distribution predicted by a theoretical model. This comparison is best made for the $02^{0}0$—$01^{1}0$ transition (C band) since the most accurate and comprehensive data were obtained for this band.

B. J'' Dependence of Line Strength

In a first attempt to compare the experimental line strengths of the C band with theory, the rotational distribution was calculated assuming a Boltzmann distribution with a rigid-rotor model. It has been shown[6,23] that this distribution for CO_2 is given by

$$S_J^0=\frac{S_{v''v'}F(J'')}{Q_J}\,\frac{[1-\exp(-h\nu/kT)]}{[1-\exp(-h\nu_0/kT)]}\times\exp(-E_{J''}/kT); \quad (9)$$

where S_J^0, $S_{v''v'}$ have been defined, $F_{(J'')}$ is a function of J'' which differs for the P, Q, and R branches and depends on the vibrational transition.

For the P branch of the C band, $F_{(J'')}=\frac{1}{2}(J''+1)$, ν_0 is the frequency of the band origin,

$$[1-\exp(-h\nu/kT)]$$

is the induced emission term, and $\exp(-E_{J''}/kT)$ is the Boltzmann factor.

$$Q_J\equiv\sum_{J''}(2J''+1)\exp(-E_{J''}/kT)$$

is the rotational partition function.

The value of $S_{v''v'}$ was adjusted to give the most favorable fit of this distribution to the data, and the result can be seen in Fig. 14. Here the best average experimental values (taken from Fig. 11) are plotted as circled points, while the theoretical curve for $S_{v''v'}=3.84$ cm^{-2} atm^{-1} is shown as the dashed curve. The experimental points show a consistent deviation from the calculated distribution suggesting a refinement of the theoretical distribution. Benedict[24] has shown that a consideration of the Coriolis vibration-rotation interaction leads to a formula for the rotational-intensity distribution given by Eq. (9) multiplied by the following term:

$$(1+\zeta m)^2, \quad (10)$$

where m is the ordinal number of the line, and ζ is a parameter depending on the strength of the Coriolis interaction and the vibrational transition involved. No theoretical estimates have been made of the value of ζ for the C band.

Using Eq. (9) multiplied by term (10) and adjusting the parameters $S_{v''v'}$ and ζ, a more satisfactory fit to the experimental data is obtained. This is shown in Fig. 14 as the solid curve for $S_{v''v'}=4.27$ cm^{-2} atm^{-1} and $\zeta=+0.0035$.

The parameters were adjusted for agreement with experiment in the P branch. The effect of a positive ζ is to decrease the intensity of the P branch and increase the intensity of the R branch. For the R branch, the predicted value of S^0 for $C11$ is 0.0736 cm^{-2} atm^{-1} while the experimental value is 0.070 cm^{-2} atm^{-1}. This agreement is well within the estimate of reliability for the measurement of S^0 for $C11$.

In the case of the $01^{1}0$—000 fundamental band, values of S^0 have been obtained for $a4$, $a8$, and $a50$, which

[23] B. L. Crawford, Jr. and H. L. Dinsmore, J. Chem. Phys. **18**, 983 (1950).

[24] W. S. Benedict, "Theoretical studies of infrared spectra of atmospheric gases," AFCRC Final Rept., 1956.

TABLE V. Band strengths and vibrational transition moments.

Isotope	Transition	Letter notation	ν (cm^{-1})	$S_{v''v'}$ at 300°K (cm^{-2} atm^{-1})	Estimate of uncertainty	$\lvert R \rvert$ (debyes)
$C^{12}O_2^{16}$	01^10–000	*A*	667.40	194	5%	0.180
$C^{12}O_2^{16}$	02^20–01^10	*B*	667.76	30	15%	0.249
$C^{12}O_2^{16}$	02^00–01^10	*C*	618.03	4.27	3%	0.138
$C^{12}O_2^{16}$	03^10–02^20	*F*	597.29	0.14	12%	0.09
$C^{12}O_2^{16}$	03^10–02^00	*K*	647.02	1.0	30%	0.29
$C^{12}O_2^{16}$	03^10–100	*G*	544.26	0.0040	10%	0.026
$C^{13}O_2^{16}$	01^10–000	α	648.52	2.1	25%	0.18
$O^{18}C^{12}O^{16}$	01^10–000		662.39	1.0	35%	0.20

allows a theoretical curve fitting. $F_{(J'')}=\frac{1}{2}(J''-1)$ for the fundamental-band *P* branch. A calculation shows a theoretical fit to the S^0 values given in Table III for $S_{v''v'}=194$ and $\zeta=0$. It must be mentioned that Benedict has predicted[24] a value for the Coriolis parameter of the fundamental band of $\zeta=+0.0016$. This value of ζ would require that the value of S^0 for *a*50 be reduced with respect to the value of *a*4 and *a*8 by 15% from the experimental values given in Table III. In view of the experimental errors involved, and in consideration of the value of $\zeta=+0.0035$ experimentally indicated for the *C* band, the possibility of a positive ζ of this magnitude (+0.0016) for the fundamental band can not be definitely ruled out at present.

C. J'' Dependence of Linewidth

The variation of line half-width with J'' in the *P* branch of the 02^00—01^10 or *C* band may again be considered by referring to Fig. 12. It can here be seen that γ^0 has the essentially constant value of approximately 0.10 cm^{-1} from *c*9 to *c*23. There is a slight indication of higher values of γ^0 at lower J'' and lower values at higher J''. The γ^0 determined from *R* branch measurements on *C*9, 11, 13 has the value 0.11 cm^{-1} atm^{-1}, which is in reasonable agreement with the values obtained in the *P* branch at the same J''.

Further evidence to support this dependence of the half-width on J'' is obtained from the values of γ^0 determined in the fundamental band. γ^0 for *a*4 is 0.126 cm^{-1} atm^{-1}; for *a*8, $\gamma^0=0.10$; and for *a*50–*a*56, $\gamma^0=0.06$. These values would appear to fit quite compatibly with the γ^0 variation with J'' plotted in Fig. 12 for the 02^00—01^10 band.

The J'' dependence of the half-width demonstrated here has considerable theoretical support. It has been shown[25,26] that molecules with a strong dipole moment have a maximum value of γ^0 at a J'' value near the peak of the Boltzmann distribution, since a molecule making a transition at such a J'' finds a greater number of perturbing molecules with which it may resonate. However, this effect is very weak for molecules with a small dipole moment. Smith, Lackner, and Volkov[26] have measured γ^0 for OCS in the microwave region and measure only a 7% increase in γ^0 from $J''=1$ to $J''=5$. They have also calculated the expected widths using Anderson's theory[25] of collision broadening extended to include the effects of near-resonant interactions and conclude that the expected increase in γ^0 is only 4% from $J''=1$ to $J''=5$ for OCS.

CO is another molecule with a weak dipole which has been investigated. Measurements of γ^0 for the CO fundamental have been reported by Benedict,[24] and by Eaton and Thompson.[27] Their results show a variation with J consistent with the results of this study for CO_2. The observed increase in γ^0 at low J has been explained by Benedict[28] using the following argument: In the case of a very weak dipole-dipole interaction, or for a quadrupole-quadrupole interaction (which must be the principal cause of collision diameters greater than the kinetic theory diameter in a nonpolar molecule such as CO_2), the collisions in which exact resonance occur are relatively less important than those in which a moderate degree of near-resonance takes place. Since the low J levels are more closely spaced, a molecule radiating from a low J quantum state will have significant near-resonant collisions with a greater number of molecules, causing an increased linewidth.

D. Band Strength and Transition Moment Determinations

Values of $S_{v''v'}$ have been calculated for all of the bands represented by lines and *Q* branches observed in this study. These values of band strength are to be considered secondary results since an assumed band strength distribution must be used to make the calculation. Only in the case of the 02^00—01^10 band was there sufficient experimental data to attempt a choice of the Coriolis parameter. All other band strength determinations from line strength data were calculated from Eq. (9). In the case of the *Q*-branch measurements the band strengths were determined from the theoretical ratios of *Q* branch to total band strength calculated

[25] P. W. Anderson, Phys. Rev. **76,** 647 (1949).
[26] W. V. Smith, H. A. Lackner, and A. B. Volkov, J. Chem. Phys. **23,** 389 (1955).
[27] D. R. Eaton and H. W. Thompson, Proc. Roy. Soc. (London) **A251,** 486 (1959).
[28] W. S. Benedict (private communication).

for a rigid-rotor model. The resulting band strengths are given in Table V.

In the case of the $02^{0}0$—$01^{1}0$ band the value of $S_{v'',v'}$ given in Table V was taken from the fit of the theoretical strength distribution curve to the experimental line strength data as shown in Fig. 14. This band strength can also be calculated from the Q branch strength measurement. The value obtained is $S_{v'',v'} = 3.72$ cm^{-2} atm^{-1}, which is lower by 13%. The uncertainty in the value obtained from the Q-branch measurement is considerably greater than that for the determination from the P-branch measurements, however, due to the abundance of data in the latter case. It should also be mentioned that a consideration of the effects due to the Fermi resonance between the $02^{0}0$ state (upper state for the C band), and the 100 state leads one to conclude that the observed strength of the CQ branch should give too low a value of $S_{v'',v'}$ if the effects are neglected, as they were here. The magnitude of this effect, however, has been estimated by Benedict[28] as less than 5%.

The vibrational transition moment has been calculated from the experimentally determined band strengths for each band using Eq. (3). These moments are given in Table V.

E. Comparison of Results with Other Experimental Investigations

In Table II the band constant $B'-B''$ was determined for the $01^{1}0$—$00^{0}0$ band of $C_{12}O_2^{16}$ from an analysis of the Q-branch structure. Actually, there are two values of B' characterizing the rotational structure of the $01^{1}0$ level—due to l doubling. The Q-branch line spacing involves the larger of the two values, usually referred to as B^d, while the smaller value B^e can be determined from an analysis of the P and R branches. The difference $q=(B^d-B^e)$ is the l-doubling constant. Using the value of $(B^d{}_{01^{1}0}-B_{00^{0}0})$ found in this study, and the value of $(B^e{}_{01^{1}0}-B_{00^{0}0})$ determined by Rossmann *et al.*,[11] the l-doubling constant is $q_{01^{1}0}=(6.07\pm0.2)\times10^{-4}$ cm^{-1}. Courtoy[29] has determined the l-doubling constant for the $01^{1}0$ level somewhat less directly, arriving at the value $q_{01^{1}0}=6.3\times10^{-4}$ cm^{-1}.

The value of 194 cm^{-2} atm^{-1} determined at 300°K for the fundamental band strength deserves further attention. As was previously mentioned, Kaplan and Eggers[9] using the "curve-of-growth" method and Overend *et al.*[10] using the "Wilson-Wells-Penner-Weber" method have agreed on a value of 240 cm^{-2} atm^{-1} for the total strength of all the CO_2 bands in the 15-μ region. It is of considerable interest to see if this value is, in addition, compatible with strength determinations from individual line studies. Kaplan and Eggers indicate that a value of 240 cm^{-2} atm^{-1} for the total strength of all the bands implies a value of 213 cm^{-2} atm^{-1} for the fundamental band strength at 298°K. To determine this ratio they assumed a value of 15.0 cm^{-2} atm^{-1} for the strength of the first harmonic band $(02^{2}0$—$01^{1}0)$.[30]

Assuming that the value of 30 cm^{-2} atm^{-1} for the strength of the band determined in this study is correct, Kaplan and Eggers have overestimated the portion of the total strength of all the bands which is due to the fundamental. The use of 240 cm^{-2} atm^{-1} for the total strength, and the larger value for the strength of the first harmonic band would lead to a value of 198 cm^{-2} atm^{-1} for the fundamental band strength—in excellent agreement with the value obtained in this study. In reality, their determination of the total strength of all the bands depended on an assumed ratio of fundamental to other band strength, and the value of 240 cm^{-2} atm^{-1} would be somewhat affected by altering the B band strength.

A further comparison with the work of Kaplan and Eggers concerns the effective half-width determined. Their analysis yielded a value of 0.064 cm^{-1} for the effective half-width of the fundamental band for nitrogen-broadened CO_2 at 1 atm and 298°K. In the present study a value of 0.10 cm^{-1} would appear appropriate for self-broadened CO_2 at 1 atm and 300°K. This implies that the nitrogen-broadened half-width is 36% smaller than the self-broadened half-width. Kostkowski[1] estimated this difference to be 30% as a result of a low-resolution study of the hot bands on the high-frequency side of the fundamental—which is a good agreement. Kaplan[31] indicates that the value of half-width which was obtained in their work would be somewhat greater if the higher value of strength for the $(02^{2}0$—$01^{1}0)$ band had been used. A small change in this direction would result in an even closer agreement.

The value of the total strength of all the CO_2 bands in the 15 μ region obtained by Overend *et al.*, being in agreement with the result of Kaplan and Eggers is also completely compatible with the analysis of the individual line strengths in the present study. A further comparison with their work concerns the important question of line shape. Overend *et al.* make the point that their total strength result is in best agreement with that of Kaplan and Eggers if they neglect making a wing correction for absorption which would be present if the lines were Lorentzian in shape. Benedict *et al.*[17] have indicated that the Lorentzian description of line shape may begin to fail at distances of the order of 1 cm^{-1} from the line center. The present study offers an opportunity to further investigate this question by an analysis of the low-frequency wing absorption in the fundamental Q branch. This is best observed using a short absorption path and higher pressures, such as in

[29] C. P. Courtoy, Can. J. Phys. **35**, 608 (1957).

[30] A preliminary report on the present study was available in 1957 as an ONR Progress Report entitled "Study of CO_2 absorption spectra between 15 and 18 microns." In that report an error was made in the value given for the strength of the first harmonic band. The value given was 16.3 cm^{-2} atm^{-1}, while the value correctly derived from the data is 30 cm^{-2} atm^{-1}. Data obtained since the publishing of that report have modified many of the other derived quantities.

[31] L. D. Kaplan (private communication).

the top scan of Fig. 7. Here the Q-branch tail appears at the left as a background absorption increasing to higher frequencies. Using the Q-branch constants and band strength determined in this study, the absorption at 666.4 cm^{-1} due to the fundamental Q-branch lines was calculated, assuming a rigid-rotor model with Lorentzian lines of width $\gamma^0=0.10$ cm^{-1}. The observed absorption coefficient was approximately 25% less than the calculated value at this frequency which is displaced 1.0 cm^{-1} from the Q-branch head, and approximately 1.4 cm^{-1} from the strongest Q-branch lines. This result is definite evidence that the absorption in the wings of self-broadened CO_2 lines is less than that predicted by the Lorentzian shape.

ACKNOWLEDGMENTS

The author wishes to express his appreciation to Professor J. Strong for his collaboration in solving the many experimental problems involved in this work, and to Dr. W. S. Benedict for his extensive guidance in the analysis presented here, and for the use of unpublished tables. In addition the author wishes to thank Dr. L. D. Kaplan for many helpful discussions relating to this work.

THE JOURNAL OF CHEMICAL PHYSICS VOLUME 35, NUMBER 6 DECEMBER, 1961

Analysis of the Absorption Spectrum of $YbCl_3 \cdot 6H_2O$

J. C. EISENSTEIN

National Bureau of Standards, Washington 25, D. C.

(Received April 21, 1961)

The measurements of Dieke and Crosswhite on the absorption spectrum of $YbCl_3 \cdot 6H_2O$ are discussed. Their interpretation of the spectrum is extended by the identification of two of the weaker lines. The entire spectrum is considered on the basis of crystal-field theory, and the possibility of determining the parameters of the crystal-field potential is assessed. It is suggested that this compound may be ferroelectric (or antiferroelectric). The spin-orbit coupling constant is determined to be -2924 cm^{-1}.

TWO experimental studies of the $YbCl_3 \cdot 6H_2O$ absorption spectrum have been reported in recent years. The more complete of the two was made by Dieke and Crosswhite[1] and included observations of the Zeeman effect. Some of the absorption lines found by Dieke and Crosswhite were also observed by Pappalardo and Wood.[2]

The absorption lines in $YbCl_3 \cdot 6H_2O$ are due to transitions of the single hole in the otherwise closed $4f$ shell from the $^2F_{7/2}$ ground state to the excited $^2F_{5/2}$ state. The separation of these two states is approximately $7\zeta/2$, where ζ is the spin-orbit coupling constant. The ground state is split into four doublets and the excited state into three doublets by the internal electrostatic field. As a consequence several absorption lines occur whose separations are indicative of the strength of the internal crystal field.

According to Marezio, Plettinger, and Zachariasen[3] the local symmetry about the Yb^{3+} ion is C_2. The twofold symmetry axis is parallel to the b axis of the crystal. It is natural to take this symmetry axis as the z axis so that in the absence of the internal field the allowed values of J_z would be J, $J-1$, $\cdots$, $-J$. A consequence of this choice of the direction of quantization is that all the doublets should be split when a magnetic field is applied parallel to the symmetry axis. When the field is applied perpendicular to the symmetry axis only two of the seven doublets should exhibit a first-order Zeeman splitting. The experimental results are just the other way around; that is, the observed Zeeman splittings are small or zero when the magnetic field is parallel to the symmetry axis and have their maximum values when the field is in a plane perpendicular to the twofold axis.

The implication of these experimental results is that one must choose a pseudo-axis perpendicular to the b axis as the direction of quantization of the angular momentum. It is possible that $YbCl_3 \cdot 6H_2O$ is ferroelectric (or antiferroelectric) and that the internal field created by the ferroelectric alignment causes the axis of quantization to shift from the crystallographic axis to a plane perpendicular to this axis. It is not necessary for the following argument that $YbCl_3 \cdot 6H_2O$ be ferroelectric. Nevertheless, in view of the low symmetry and the extensive hydrogen bonding, it seems worthwhile to investigate this possibility experimentally.

Dieke and Crosswhite observed two sharp lines, much stronger than any of the others, at 10 297.13 and 10 282.32 cm^{-1} which they attributed to the transitions $(7/2, 5/2) \rightarrow (5/2, 5/2)$ and $(7/2, 5/2) \rightarrow (5/2, 3/2)$, respectively. Here the bracketed numbers stand for (J, m_J). Two weaker lines, observed only at 77°K, at 10 163.9 and 10 149.8 cm^{-1} were attributed by Dieke

[1] G. H. Dieke and H. M. Crosswhite, J. Opt. Soc. Am. **46**, 885 (1956).
[2] R. Pappalardo and D. L. Wood, J. Chem. Phys. **33**, 1734 (1960).
[3] M. Marezio, H. A. Plettinger, and W. H. Zachariasen, Acta Cryst. **14**, 234 (1961).

TABLE I. Calculated positions of the (7/2, 1/2) and (5/2, 1/2) energy levels as a function of the assumed identity of the absorption lines at 10 182.4 and 10 193.6 cm^{-1}.

Assumed identity of transition	Observed energy	Calculated position of (7/2, 1/2) level	Calculated position of (5/2, 1/2) level
(7/2, 1/2)→	10 193.6 cm^{-1}	377.36 cm^{-1}	10 570.96
(5/2, 1/2)	10 182.4	425.75	10 618.15
(7/2, 3/2)→	10 193.6	53.85	10 326.13
(5/2, 1/2)	10 182.4	38.16	10 314.93
(7/2, 1/2)→	10 193.6	88.72	10 351.24
(5/2, 3/2)	10 182.4	99.92	10 359.37

and Crosswhite to transitions from an excited state 132.8 cm^{-1} above the ground state. If one invokes the selection rule $\Delta m_J = \pm 1, 0$ it follows that this excited state is (7/2, 3/2) since this state is the only one other than the ground state from which transitions can take place to both the (5/2, 5/2) and (5/2, 3/2) states. The existence of nonaxial components of the crystal field spoils the rigor of this selection rule, but detailed calculations indicate that alternative identifications of this level do not lead to reasonable agreement between experimental and calculated energy levels.

It is interesting to consider how well one can determine the spin-orbit coupling constant and the parameters of the crystal field from the information given above; that is, from the positions and identifications of the levels at 0, 132.8, 10 282.32, and 10 297.13 cm^{-1}. We shall assume for the initial calculations that the crystalline potential, when referred to a pseudo-axis perpendicular to the b axis, has rotational symmetry about this pseudo-axis. It will be shown later that the nonaxially symmetric components of the crystal field can shift the energy levels by only a few cm^{-1}.

We can write, in the usual way,

$$V = 4A_2^0 r^2 \Theta_2^0/(10)^{\frac{1}{2}} + 16A_4^0 r^4 \Theta_4^0/3(2)^{\frac{1}{2}} + 32A_6^0 r^6 \Theta_6^0/(26)^{\frac{1}{2}}.$$

In view of the lack of symmetry with respect to the pseudo-axis the potential undoubtedly contains odd spherical harmonics also. However, since the matrix elements of the odd harmonics within the f^{13} configuration are all zero, they need not be considered here.

The following abbreviations will be used:

$$B_2^0 = \tfrac{2}{15} A_2^0 \langle r^2 \rangle;$$

$$B_4^0 = \tfrac{8}{33} A_4^0 \langle r^4 \rangle;$$

$$B_6^0 = \tfrac{80}{429} A_6^0 \langle r^6 \rangle.$$

One finds that the spin-orbit coupling constant is determined uniquely by the information given, and has the value -2924.42 cm^{-1}. It is rather difficult to set limits on the accuracy with which ζ is determined because no information is available about the perturbing effects of highly excited configurations. Apart from these effects it appears that the nonaxial components of the crystal field are sufficiently small so that the value of ζ can hardly differ from -2924.42 cm^{-1} by more than 0.1%.

One also finds that

$$7B_6^0 = 4B_2^0 - B_4^0 - 58.855,$$

$$11B_4^0 = 9B_2^0 + 27.248,$$

and that the position of the (7/2, 7/2) state is completely determined. This state lies 73.89 cm^{-1} above the ground state. By choosing properly the value of B_2^0 an "allowed" transition (that is, a transition for which $\Delta m_J = \pm 1, 0$) can be made to have the same energy as one of the, as yet, unassigned absorption lines at 10 182.4 and 10 193.6 cm^{-1}. These weak absorption lines may not be due to the kind of purely electronic transition we are discussing here. Nevertheless we need to examine the possibility that they are. The transitions which might be identified with the 10 182.4 and 10 193.6 cm^{-1} lines are (7/2, 1/2)→(5/2, 3/2), (7/2, 3/2)→(5/2, 1/2), and (7/2, 1/2)→(5/2, 1/2). The consequences of the six possible ways in which an allowed transition can be associated with one of the observed lines are shown in Table I.

If the transition is (7/2, 1/2)→(5/2, 1/2) it appears unlikely, in view of the small occupation of the initial state at 77°K, that the line would have been observed. If the transition is (7/2, 3/2)→(5/2, 1/2) it is difficult to understand why no transitions from the relatively low (7/2, 1/2) level have been observed at 77°K. It seems most likely that the (7/2, 1/2)→(5/2, 3/2) transition corresponds to the line at 10 193.6 or the one at 10 182.4 cm^{-1}; for definiteness in the remaining calculations it has been assumed to be 10 182.4 cm^{-1}. In this case, as in all the others, one observed absorption line is unaccounted for, and three allowed transitions are not observed.

With the assumptions finally made, one has $B_2^0 = 6.424$ cm^{-1}, $B_4^0 = 7.733$ cm^{-1} and $B_6^0 = -5.842$ cm^{-1}. The calculated energy levels are as follows:

(5/2, 1/2)	10 359.38 cm^{-1}
(5/2, 5/2)	10 297.15
(5/2, 3/2)	10 282.33
(7/2, 3/2)	132.54
(7/2, 1/2)	99.92
(7/2, 7/2)	73.89
(7/2, 5/2)	0.00.

The allowed but unobserved transitions are

$(7/2, 1/2) \rightarrow (5/2, 1/2)$ at 10 259.46 cm^{-1},

$(7/2, 3/2) \rightarrow (5/2, 1/2)$ at 10 226.84 cm^{-1},

$(7/2, 7/2) \rightarrow (5/2, 5/2)$ at 10 223.26 cm^{-1}.

It is not possible, by switching the identifications of the levels and adjusting the B_4^0 to make six calculated transitions coincide with the six observed transitions.

The calculated g values are rather insensitive to small changes in the axial components of the crystal field and therefore cannot be used to establish the correctness of the choice of these components. Table II gives the g values found[4] by Dieke and Crosswhite and two calculated sets of g values for cases where all the nonaxial components of the field are zero.

We must now consider the effect on the energy levels and the g values of nonaxially symmetric components of the crystalline potential. Again, the terms for which l is odd can be ignored but because of the lack of symmetry the number of free parameters is still so large they are not determined uniquely by the available data.

TABLE II. Observed and calculated g values for $YbCl_3 \cdot 6H_2O$. The calculated values in column two are obtained by assuming $B_2^0 = 6.424$ cm^{-1}, $B_4^0 = 7.733$ cm^{-1}, $B_6^0 = -5.842$ cm^{-1}, and $\zeta = -2924.42$ cm^{-1}. The calculated values in column 3 are obtained by assuming that $A_2^0 = A_4^0 = A_6^0 = 0$.

	Calc	Calc	Obs
$g(5/2, 5/2)$	4.2816	4.2857	4.05
$g(5/2, 3/2)$	2.5879	2.5714	2.70
$g(7/2, 5/2)$	5.7183	5.7143	5.65

For simplicity we shall take the nonaxially symmetric part of the crystalline potential to have twofold symmetry about the pseudo-axis.

$$V' = \{2A_2^2\langle r^2\rangle\Theta_2^2/(15)^{\frac{1}{2}} + 4A_4^2\langle r^4\rangle\Theta_4^2/3(5)^{\frac{1}{2}} + 32A_6^2\langle r^6\rangle\Theta_6^2/(2730)^{\frac{1}{2}}\}\{e^{i2\varphi}+e^{-i2\varphi}\} + \{8A_4^4\langle r^4\rangle\Theta_4^4/3(35)^{\frac{1}{2}} + 16A_6^4\langle r^6\rangle\Theta_6^4/3(91)^{\frac{1}{2}}\}\{e^{i4\varphi}+e^{-i4\varphi}\} + \{32A_6^6\langle r^6\rangle\Theta_6^6/(6006)^{\frac{1}{2}}\}\{e^{i6\varphi}+e^{-i6\varphi}\}.$$

The complete interaction matrix, from which the secular equation for the energy levels can immediately be derived is

	$\lvert 3+\rangle$	$\lvert 2-\rangle$	$\lvert 1+\rangle$	$\lvert 0-\rangle$	$\lvert -1+\rangle$	$\lvert -2-\rangle$	$\lvert -3+\rangle$
$\langle 3+\rvert$	$-5B_2^0+3B_4^0 -B_6^0+\frac{3}{2}\zeta$	0	$(15)^{\frac{1}{2}}(-B_2^2 +6B_4^2-B_6^2)$	0	$(15)^{\frac{1}{2}}(B_4^4 -B_6^4)$	0	$-B_6^6$
$\langle 2-\rvert$		$-7B_4^0+6B_6^0 -\zeta$	$\frac{1}{2}(10)^{\frac{1}{2}}\zeta$	$(30)^{\frac{1}{2}}(-B_2^2 -B_4^2+2B_6^2)$	0	$5B_4^4+6B_6^4$	0
$\langle 1+\rvert$			$3B_2^0+B_4^0 -15B_6^0+\frac{1}{2}\zeta$	0	$-(6B_2^2 +20B_4^2 +15B_6^2)$	0	$(15)^{\frac{1}{2}}(B_4^4 -B_6^4)$
$\langle 0-\rvert$				$4B_2^0+6B_4^0 +20B_6^0$	$\sqrt{3}\zeta$	$(30)^{\frac{1}{2}}(-B_2^2 -B_4^2+2B_6^2)$	0
$\langle -1+\rvert$					$3B_2^0+B_4^0 -15B_6^0-\frac{1}{2}\zeta$	0	$(15)^{\frac{1}{2}}(-B_2^2 +6B_4^2-B_6^2)$
$\langle -2-\rvert$						$-7B_4^0+6B_6^0 +\zeta$	$\frac{1}{2}(6)^{\frac{1}{2}}\zeta$
$\langle -3+\rvert$							$-5B_2^0+3B_4^0 -B_6^0-\frac{3}{2}\zeta$.

The following additional abbreviations were used:

$$B_2^2 = \tfrac{2}{4\,5} A_2^2\langle r^2\rangle$$
$$B_4^2 = \tfrac{2}{1\,6\,5} A_4^2\langle r^4\rangle$$
$$B_6^2 = \tfrac{3\,2}{1\,2\,8\,7} A_6^2\langle r^6\rangle$$
$$B_4^4 = \tfrac{8}{1\,6\,5} A_4^4\langle r^4\rangle$$
$$B_6^4 = \tfrac{8\,0}{1\,2\,8\,7} A_6^4\langle r^6\rangle$$
$$B_6^6 = \tfrac{1\,2\,0}{4\,2\,9} A_6^6\langle r^6\rangle$$

Most of these matrix elements are also given in the paper by Pappalardo and Wood.[2]

Although one cannot hope to determine uniquely the nonaxially symmetric components of the field one might expect that for some values of these components the calculated and observed transition energies would agree for all six observed absorption lines. This expectation seems incompatible with the observed Zeeman splitting factors when V' has twofold symmetry and probably for any V'.

Table III gives the calculated energy levels and the

[4] The calculated and observed values of s_1 for the $^2F_{5/2}$ state should be interchanged in Dieke and Crosswhite's Table II.

TABLE III. Calculated energy levels and g values for $YbCl_3 \cdot 6H_2O$ when the nonaxial components of the crystal field are different from zero. It is assumed that $B_2^0 = 6.424$ cm^{-1}, $B_4^0 = 7.733$ cm^{-1}, $B_6^0 = -5.842$ cm^{-1}, and $\zeta = -2924.42$ cm^{-1}. All energies are in cm^{-1}.

	$B_2^2=2$	$B_4^2=0.4$	$B_6^2=2$	$B_4^4=1$	$B_6^4=10$	$B_6^6=30$
$E(5/2, 1/2)$	10 362.83	10 360.22	10 361.31	10 359.48	10 362.13	10 361.05
$E(5/2, 5/2)$	10 297.15	10 296.59	10 299.00	10 298.05	10 300.02	10 298.90
$E(5/2, 3/2)$	10 281.66	10 282.07	10 284.22	10 281.64	10 285.27	10 284.01
$E(7/2, 3/2)$	137.54	134.36	136.60	132.75	137.42	134.22
$E(7/2, 1/2)$	98.47	99.16	101.95	100.27	117.86	101.60
$E(7/2, 7/2)$	74.05	72.86	74.99	73.76	61.22	77.17
$E(7/2, 5/2)$	0.00	0.00	0.00	0.00	0.0	0.00
$g(5/2, 5/2)$	4.1849	4.2459	4.2816	3.9490	4.2716	4.2815
$g(5/2, 3/2)$	2.4811	2.5716	2.5877	2.2553	2.5777	2.5879
$g(7/2, 5/2)$	5.6761	5.7181	5.6381	5.7111	5.5618	5.4194

g values for cases where the nonaxial components of the field are taken to be nonzero, one by one. If the nonaxial field components are appreciably larger than the ones used for these calculations the agreement between the calculated and measured g values will be rather poor. On the basis of these limited numerical results one cannot exclude the possibility that two or more of the nonaxial crystal-field components are appreciably larger than the ones used in Table II and, simultaneously, the g values remain close to their experimental values. However, such an occurrence seems unlikely. The effect on the energy levels of these small, nonaxial field components is clearly small. In particular, they will not alter by more than a few cm^{-1} the calculated positions of the various allowed transitions. Consequently the interpretation of the observed absorption peaks at 10 193.6 and 10 182.4 cm^{-1} remains obscure.

Electron spin-resonance and static-susceptibility measurements should be made on $YbCl_3 \cdot 6H_2O$. Although $g_\perp$ for the ground doublet is undoubtedly small it may be possible to measure $g_\parallel$ and confirm the spectroscopic value. The susceptibility measurements, if carried out over a wide temperature range, might provide information about the locations of the (7/2, 7/2) and (7/2, 1/2) levels which are here predicted to occur at 73.89 and 99.92 cm^{-1} but which have not been observed spectroscopically.

ACKNOWLEDGMENT

I am indebted to Dr. Ernest Ambler for an interesting discussion and the suggestion that $YbCl_3 \cdot 6H_2O$ might be ferroelectric.

THE JOURNAL OF CHEMICAL PHYSICS VOLUME 35, NUMBER 6 DECEMBER, 1961

Molecular Weight Distribution and Reaction Sequence in Polymerization Kinetics

F. C. GOODRICH
California Research Corporation, Richmond, California

(Received April 28, 1961)

A general technique is presented for the prediction of molecular weight distributions from an assumed reaction sequence in addition polymerizations. Several problems in Szwarc polymerizations are worked as examples.

1. INTRODUCTION

THE application of the conventional equations of chemical kinetics to polymerization reactions often presents the investigator with large sets of differential equations whose solution in the general case is plagued with impressive difficulties. In particular cases, such sets of differential equations have been integrated by special devices[1–6]; but the only general method so far applicable to wide classes of polymerization reactions appears to be that of Bamford and Tompa.[7] To this technique, which involves use of the Laplace transform, I should like in the following to add a second, involving use of the method of steepest descents. It appears to be fully as powerful as the Laplace transform method. Several problems in the kinetics of addition polymerization will be investigated with its use.

2. METHOD OF STEEPEST DESCENTS

The approximate evaluation of complicated integrals by the method of steepest descents is a well-known mathematical device which shall be employed here in only a restricted sense. In the applications to be considered, the contour of integration will always be the axis of reals, so that none of the complications of complex variable theory need be introduced. We shall, in fact, need only the following lemma, for whose proof the reader is referred to the appendix.

Lemma: If in the integral

$$J_n(x)=n!^{-1}\int_0^x g(\xi)[f(x)-f(\xi)]^n \times\exp\{-[f(x)-f(\xi)]\}d\xi \quad (1)$$

$f(x)$ is a monotonically increasing function of x, and both $f'(x)$ and $g(x)$ are slowly varying functions of x over the range of integration; then for n large, $J_n(x)$ is given to good approximation by

$$J_n(x)\rightarrow\tfrac{1}{2}g(\Theta)/f'(\Theta)[1+\operatorname{erf} f(\Theta)/(2n)^{\frac{1}{2}}], \quad (2)$$

in which Θ is a function of x and n defined to be the algebraic root of

$$f(\Theta)=f(x)-n,$$

and erf x is the error integral

$$\operatorname{erf} x=2/(\pi)^{\frac{1}{2}}\int_0^x \exp(-z^2)dz.$$

The range of validity of this approximation is the same as that for the familiar Stirling approximation to the factorial, which is included in the lemma as a special case.

3. STEREOREGULATED POLYMERIZATION WITH CHAIN TRANSFER

According to Natta,[8] a possible mechanism for a stereoregulated polymerization is the following:
Initiation and propagation:

$$\left.\begin{aligned} &M_1+M\rightarrow M_2,\\ &M_n+M\rightarrow M_{n+1}.\end{aligned}\right\}k_1$$

Chain transfer:

$$M_n+M\rightarrow M_1+A_n;\quad k_2.$$

An aluminum alkyl M_1 is attacked by monomer M and builds up long chains M_n with a chemical rate constant k_1. The growth of the chain is terminated either by the exhaustion of monomer or by chain transfer with monomer to produce a polymer A_n, a reaction which proceeds with chemical rate constant k_2. The A_n are assumed inert to further reaction with the exception of A_1, which is taken to be identical with M. Kinetic equations for this series of reactions are

$$\begin{aligned} &(d/dt)M_1=-k_1MM_1+k_2M\sum_2^\infty M_n;\\ &(d/dt)M_n=k_1MM_{n-1}-(k_1+k_2)MM_n;\quad n>1 \quad (3)\\ &(d/dt)A_n=k_2MM_n;\quad n>2\\ &(d/dt)M\ =-(k_1+k_2)M\sum_1^\infty M_n+k_2MM_1, \end{aligned}$$

[1] P. J. Flory, J. Am. Chem. Soc. **62,** 1561 (1940).
[2] H. Mark and R. Raff, *High Polymeric Reactions* (Interscience Publishers, Inc., New York, 1941), p. 166–8.
[3] E. F. G. Herington and A. Robertson, Trans. Faraday Soc. **38,** 490 (1942).
[4] R. Simha and R. Ginell, J. Am. Chem. Soc. **65,** 706, 715 (1943).
[5] L. Gold, J. Chem. Phys. **28,** 91 (1958).
[6] W. T. Kyner, J. R. M. Radok, and M. Wales, J. Chem. Phys. **30,** 363 (1959).
[7] C. H. Bamford, W. G. Barb, A. D. Jenkins, and P. F. Onyon, *The Kinetics of Vinyl Polymerization by Radical Mechanisms* (Academic Press, Inc., New York, 1958), p. 283–290.
[8] G. Natta, La Chimica e l'Industria (2) **38,** 124 (1956).

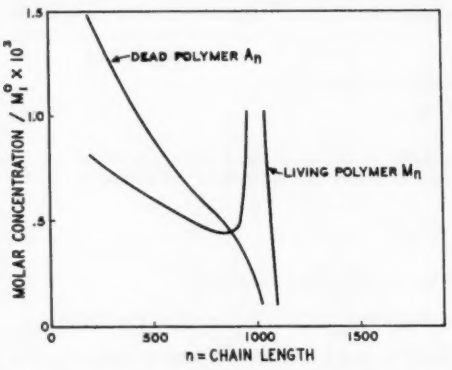

FIG. 1. Number density distributions for living and dead polymer for the mechanism of Sec. 3 in the case $K=k_2/k_1=10^{-3}$; $x=10^3$.

and we seek solutions to this set under the initial conditions $M_1=M_1^0$; $M=M^0$ at $t=0$. In the special case $k_2=0$, the number density distribution M_n is contained in the work of Flory[1]:

$$M_{n+1}/M_1^0=(1/n!)x^n e^{-x},$$
$$x\equiv(M^0/M_1^0)[1-\exp(-k_1M_1^0t)], \quad (4)$$

which is to say that for M^0/M_1^0 large, the resulting polymers are practically monodisperse and of chain-length x.

If $k_2\neq 0$, we employ Flory's device and linearize the equations by changing the independent variable to $du=Mdt$; $u=0$ at $t=0$. A recurrence relationship between the M_n may then be established,

$$M_{n+1}=k_1\int_0^u M_n(\eta)\exp[-(k_1+k_2)(u-\eta)]d\eta,$$

and by repeated integrations by parts this recurrence formula may be made to yield

$$M_{n+2}=k_1^{n+1}n!^{-1}\int_0^u M_1(\eta)(u-\eta)^n \times\exp[-(k_1+k_2)(u-\eta)]d\eta. \quad (5)$$

The sums appearing in the first and last of Eqs. (3) may now be evaluated, yielding in the first case an integro-differential equation for the explicit determination of M_1 and in the second a differential equation for the determination of M. The solutions to these equations are

$$M_1/M_1^0=(k_1+k_2)^{-1}\{k_2+k_1\exp[-(k_1+k_2)u]\},$$
$$M=M^0-(k_1+k_2)M_1^0u[1-k_2^2/(k_1+k_2)^2]$$
$$+k_1k_2/(k_1+k_2)^2M_1^0\{1-\exp[-(k_1+k_2)u]\},$$
$$\rightarrow M^0-(k_1+k_2)M_1^0u, \quad (6)$$

in which the approximation involved in the second of Eqs. (6) consists in letting $k_2\ll k_1$. From this approximation, u may be obtained as an explicit function of time:

$$t=\int_0^u du/M(u),$$
$$(k_1+k_2)u=(M^0/M_1^0)\{1-\exp[-(k_1+k_2)M_1^0t]\}. \quad (7)$$

To complete the problem, substitute (5) into the third of Eqs. (3) and carry out the indicated integration.

$$A_{n+2}=k_2k_1^{n+1}n!^{-1}\int_0^u M_1(\eta)(u-\eta)^{n+1} \times\exp[-(k_1+k_2)(u-\eta)]d\eta. \quad (8)$$

Although Eqs. (5) through (8) comprise a complete formal solution to the problem, they are not convenient for computing purposes, for n will in general be a large number; and any attempt to carry out the quadratures indicated in either (5) or (8) by conventional techniques will lead to awkward series whose convergence is exasperatingly slow. It is, however, for precisely such situations that the method of steepest descents is most powerful; and by comparison of (5) and (8) with (1), the reader will anticipate the possibility that the molecular weight distributions may be described simply in terms of known or easily calculable functions. Let us define $x=(k_1+k_2)u$; $\xi=(k_1+k_2)\eta$. After substitution of (6) into (5) and some elementary simplification, we have

$$M_{n+2}/M_1^0=[k_1/(k_1+k_2)]^{n+2}[x^{n+1}/(n+1)!]e^{-x}$$
$$+[k_2/(k_1+k_2)][k_1/(k_1+k_2)]^{n+1}n!^{-1}\int_0^x(x-\xi)^n \times\exp[-(x-\xi)]d\xi, \quad (9)$$

in which the second term on the right contains an integral (formally an incomplete gamma function) which for large n may be evaluated approximately by the lemma of Sec. 1. If $k_2=0$, we recover Eq. (4), but even for $k_2\neq 0$, chemical intuition as well as examination of (9) show that for the production of long chains the condition $k_2\ll k_1$ must obtain. By defining $K=k_2/k_1\ll 1$ and replacing the Poisson function first on the right in (9) by its Gaussian approximation, we have for convenient computation

$$M_n/M_1^0=\exp(-Kn)\cdot(2\pi n)^{-\frac{1}{2}}\exp[-(x-n)^2/2n]$$
$$+K\exp(-Kn)\cdot\tfrac{1}{2}[1+\operatorname{erf}(x-n)/(2n)^{\frac{1}{2}}]. \quad (10)$$

Identical considerations in the case of (8) lead to a distribution of dead polymers

$$A_n/M_1^0=K[1+K(x-n)] \times\exp(-Kn)(\tfrac{1}{2})[1+\operatorname{erf}(x-n)/(2n)^{\frac{1}{2}}]. \quad (11)$$

These distributions are plotted in Fig. 1 for the particular case $K=10^{-3}$, $x=10^3$ so that $Kx=1$. The outstanding feature of the curves is the exaggerated peak retained in the distribution of living polymers M_n followed by the abrupt cutoff excluding any poly-

mers of chainlength $n>x$. Despite the presence of the chain transfer reaction, much of the population of living polymers remains monodisperse so long as $Kx\leq O(1)$. Equations (10) and (11) are thus quantitative statements of the conclusions arrived at qualitatively by Szwarc[9] for polymerization reactions involving chain transfer. For $Kx>O(1)$, which may be achieved either by increasing the ratio of starting monomer to catalyst or by waiting for longer reaction times, the polymer becomes more inhomogeneous; the peak disappears, and the distributions become approximately exponential. By varying the ratio of starting monomer to catalyst and letting the reaction run to completion, the disappearance of the peak may be used for an approximate determination of the ratio of the rate constants: $k_2/k_1\simeq M_1^0/M^0$. In at least one case,[10] this peak has actually been observed.

The usual molecular weight averages may be calculated either from (10) and (11) or more conveniently from the exact distributions (8) and (9). The analysis involves no features of particular interest, and I shall merely quote the results. Let the moments of the distributions be defined by

$$\mu_r=\sum_n n^r M_n \text{ and } \lambda_r=\sum_n n^r A_n.$$

Then for $K=k_2/k_1\ll 1$ and $x=(k_1+k_2)u\rightarrow(M^0/M_1^0)\times[1-\exp(-k_1M_1^0t)]\gg 1$,

$$\mu_0/M_1^0=1,$$

$$\mu_1/M_1^0=K^{-1}(1-e^{-Kx}),$$

$$\mu_2/M_1^0=(2/K^2)[1-(1+Kx)e^{-Kx}],$$

$$\lambda_0/M_1^0=Kx,$$

$$\lambda_1/M_1^0=K^{-1}(Kx-1+e^{-Kx}),$$

$$\lambda_2/M_1^0=(2/K^2)[Kx(1+e^{-Kx})-2(1-e^{-Kx})]. \quad (12)$$

The number average P_N and weight average P_w molecular weights, are defined in the usual way by

$$P_N(\mu)=\mu_1/\mu_0; \quad P_w(\mu)=\mu_2/\mu_1,$$

and similarly for the population of dead polymer $P(\lambda)$ and for the combined populations $P(\mu+\lambda)$. In Fig. 2 are plotted the inhomogeneity ratios P_w/P_N-1 for each of the various populations as a function of $k_1M_1^0t$ in the special case $k_2M^0/k_1M_1^0=4$.

4. INITIATION SECOND ORDER IN MONOMER IN THE ABSENCE OF A TERMINATION REACTION

A mechanism considered by Simha[11] in connection with a problem in molecular biology is the following:

Initiation: $M+M\rightarrow M_2$; k_1,

Propagation: $M_n+M\rightarrow M_{n+1}$; k_2,

Termination: none.

[9] M. Szwarc and M. Litt, J. Phys. Chem. **62,** 568 (1958).
[10] W. L. Carrick, R. W. Kluiber, E. F. Bonner, L. H. Wartman, F. M. Rugg, and J. J. Smith, J. Am. Chem. Soc. **82,** 3883 (1960).
[11] R. Simha, J. Polymer Sci. **42,** 309 (1960).

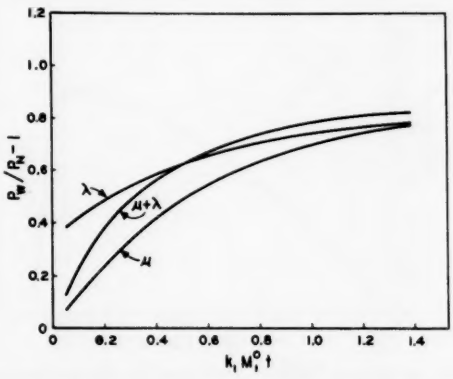

FIG. 2. Inhomogeneity P_W/P_N-1 of various polymer populations as a function of time for the mechanism of Sec. 3. In these calculations, $k_2M^0/k_1M_1^0=4$. μ=living polymer; λ=dead polymer; $\mu+\lambda$=combined populations.

Simha obtained a formally complete solution to the kinetic equations appropriate to this mechanism, but his expression for the resulting number density distribution M_n is in the form of an infinite series which is practically useless for computational purposes. For a discussion of the molecular weight averages and inhomogeneity of the polymer, the reader is referred to Simha's article. I shall here concern myself only with the derivation of a simple expression which to an excellent approximation represents the molar distribution of polymer molecules M_n.

We have to solve the set of differential equations[12]

$$(d/dt)M=-2k_1M^2-k_2M\sum_2^\infty M_n,$$

$$(d/dt)M_2=k_1M^2-k_2MM_2,$$

$$(d/dt)M_n=k_2MM_{n-1}-k_2MM_n; \quad n>2, \quad (13)$$

with the initial condition $M=M^0$; $M_n=0$ at $t=0$. As with the problem of Sec. 3, (13) can be linearized by a change in independent variable $du=Mdt$; $u=0$ at $t=0$. The third of Eqs. (13) may then be used to establish a recurrence relation

$$M_n=k_2\int_0^u M_{n-1}(\eta)\exp[-k_2(u-\eta)]d\eta,$$

whence by continued integration by parts

$$M_{n+2}=k_1k_2^n n!^{-1}\int_0^u M(\eta)(u-\eta)^n \times\exp[-k_2(u-\eta)]d\eta. \quad (14)$$

Summing (14) over n and substituting the result into the first of Eqs. (13), we obtain an integro-differential equation for M whose solution is

$$M/M^0=\exp(-k_1u)\sin\beta k_2(u_\infty-u)/\sin\beta k_2u_\infty \quad (15)$$

[12] Simha's k' is my $2k_1$.

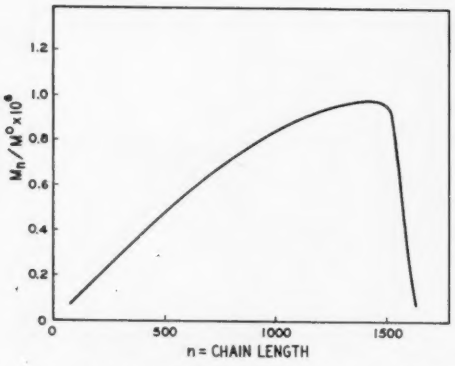

FIG. 3. Number density distribution for the mechanism of Sec. 4 with $K=k_1/k_2=10^{-6}$; $t\to\infty$.

with

$$\beta\equiv[(k_1/k_2)-(k_1/k_2)^2]^{\frac{1}{2}}.$$

The quantity u_∞ is that value of u corresponding to $t=\infty$ and is defined to be the root of

$$\tan\beta k_2 u_\infty = k_2\beta/k_1;\quad 0\leq\beta k_2 u_\infty\leq\tfrac{1}{2}\pi. \tag{16}$$

To establish u as a function of time, it is necessary to substitute (15) into the integral

$$t=\int_0^u du/M(u),$$

but this quadrature does not appear to be solvable in terms of known functions.

Equations (14)–(16) contain an exact solution to the kinetic problem, but the resulting expression for M_n is computationally inconvenient. To apply the method of steepest descents, write $x=k_2u$; $\xi=k_2\eta$ in each of (14), (15), and (16).

$$M_{n+2}/M^0=(k_1/k_2)(n!)^{-1}\int_0^x \exp(-k_1\xi/k_2)$$

$$\times\frac{\sin\beta(x_\infty-\xi)}{\sin\beta x_\infty}(x-\xi)^n\exp[-(x-\xi)]d\xi. \tag{17}$$

Long chains are produced only in the case[13]

$$K\equiv k_1/k_2\ll 1;\quad \beta\to K^{\frac{1}{2}};\quad x_\infty\to\pi/2K^{\frac{1}{2}}.$$

Making these substitutions and appealing to the lemma of Sec. 1,

$$M_n/M^0\to K\exp[-K(x-n)][\sin K^{\frac{1}{2}}(x_\infty-x+n)]$$

$$\times\tfrac{1}{2}[1+\operatorname{erf}(x-n)/(2n)^{\frac{1}{2}}]. \tag{18}$$

This distribution is plotted in Fig. 3 for $x=x_\infty$, the conclusion of the reaction, in the particular case $K\equiv k_1/k_2=10^{-6}$. Noteworthy is the extreme abruptness of the cutoff for chain lengths n exceeding

$$x_\infty=\tfrac{1}{2}\pi\times 10^3=1570.$$

[13] Note that K here defined is not the same as K used in Sec. 3.

Indeed, for $x=x_\infty$ the distribution approximates roughly to a quarter sine wave:

$$M_n/M^0=K\sin K^{\frac{1}{2}}n;\quad 0\leq K^{\frac{1}{2}}n\leq\tfrac{1}{2}\pi$$

$$M_n/M^0=0;\qquad K^{\frac{1}{2}}n>\tfrac{1}{2}\pi.$$

5. FIRST-ORDER INITIATION INDEPENDENT OF MONOMER

The examples so far considered have involved only simple applications of the lemma of Sec. 1. A more complicated problem which better illustrates the power of the method is afforded by the reaction requence

Initiation: $I\to 2M_1$; k_1.

Propagation: $M_n+M\to M_{n+1}$; k_2.

Termination: none.

Activated molecules M_1 are produced by the first-order decay of an initiator I and are then built up into long chains by repeated addition of monomer. The kinetic equations to be solved are

$$(d/dt)I=-k_1I,$$

$$(d/dt)M_1=2k_1I-k_2MM_1,$$

$$(d/dt)M_n=k_2M(M_{n-1}-M_n);\quad n>1,$$

$$(d/dt)M=-k_2M\sum_1^\infty M_n, \tag{19}$$

and these are to be integrated under the initial condition $I=I^0$, $M=M^0$, $M_n=0$ at $t=0$. The device employed in Secs. 3 and 4 of linearizing the equations by changing the independent variable is not available to us here, but the equations may still be solved in terms of a function

$$F(t)=k_2\int_0^t M\,dt. \tag{20}$$

Let there be defined also a generating function

$$G(s,t)=\sum_n s^nM_n. \tag{21}$$

Then the second and third of Eqs. (19) are contained in the single differential equation for G

$$(\partial/\partial t)G=(s-1)F'(t)G+2sk_1I,$$

whose solution for $G(s,0)=0$ is

$$G(s,t)=2sk_1\int_0^t I(\eta)\exp\{(s-1)[F(t)-F(\eta)]\}d\eta. \tag{22}$$

Picking out the coefficient of s^{n+1},

$$M_{n+1}=2k_1(n!)^{-1}\int_0^t I(\eta)[F(t)-F(\eta)]^n$$

$$\times\exp\{-[F(t)-F(\eta)]\}d\eta. \tag{23}$$

While formally correct, Eq. (23) is of no practical use until F is analytically defined in terms of known

functions. Turning to the last of Eqs. (19) we observe that it may be rewritten

$$(d/dt)M=-k_2MG(1,t).$$

Substituting from (22), it follows that

$$M/M^0=\exp[-2k_1k_2\int_0^t(t-\eta)I(\eta)d\eta]. \quad (24)$$

The reader should note at this point that through (20), (23), and (24), the number density distribution M_n and time dependence of monomer M are completely defined for any arbitrary choice of initiator concentration I. This integration scheme is therefore suitable for the investigation of a variety of initiation mechanisms, so long as initiation is independent of monomer concentration.

In the case in hand, of course, the first of Eqs. (19) requires the rate of initiation to be exponential $I/I^0=\exp(-k_1t)$, and by substitution into (24) there results

$$M/M^0=\exp\{-(2k_2I^0/k_1)[k_1t-1+\exp(-k_1t)]\} \quad (25)$$

for the complete time dependence of monomer. At large times, (25) predicts an exponential decrease in monomer concentration, so that a plot of ln M/M^0 against time will be asymptotically linear of slope $-2k_2I^0$ and intercept $2k_2I^0/k_1$.

By substitution of (25) into (20) we are now in a position to derive an explicit formula for F, but before so doing, let us transform to dimensionless variables

$$x\equiv k_1t;\quad \xi\equiv k_1\eta;\quad \alpha\equiv 2k_2I^0/k_1;\quad \sigma\equiv k_2M^0/k_1.$$

Then

$$M/M^0=\exp[-\alpha(x-1+e^{-x})];$$

$$F(t)\equiv f(x)=\sigma h(x,\alpha)$$

$$\equiv\sigma\int_0^x\exp[-\alpha(x-1+e^{-x})]dx. \quad (26)$$

The integral $h(x,\alpha)$ occurring in the last member of (26) is expressible in terms of the confluent hypergeometric function[14] $N(a,c,x)$,

$$h(x,\alpha)=\alpha^{-1}N(1,1+\alpha,\alpha)-\alpha^{-1}\exp[-\alpha(x-1+e^{-x})]$$
$$\times N(1,1+\alpha,\alpha e^{-x}), \quad (27)$$

although in the special case $\alpha=1$ it reduces to

$$h(x,1)=\exp(1-e^{-x})-1. \quad (28)$$

Re-expressing (23) in this notation and applying our lemma, we have in the limit of n large a number density distribution

$$M_n=\sigma^{-1}I^0e^{-\theta}\exp\alpha(\Theta-1+e^{-\theta})[1+\operatorname{erf}f(\Theta)/(2n)^{\frac{1}{2}}], \quad (29)$$

[14] By $N(a,c,x)$ I denote the function given the symbol M by E. Jahnke and F. Emde, *Funktionentafeln* (Dover Publications, New York, 1945), p. 275.

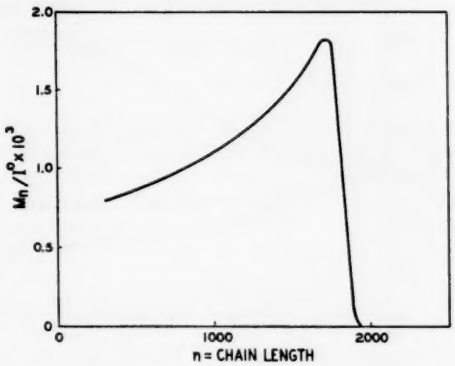

FIG. 4. Number density distribution for the mechanism of Sec. 5 with $\alpha=2k_2I^0/k_1=1$; $\sigma=k_2M^0/k_1=1000$; $t\to\infty$.

in which Θ is the algebraic root for fixed x and n of

$$f(\Theta)=f(x)-n. \quad (30)$$

The distribution (29) is plotted in Fig. 4 for the case $\alpha=1$, $\sigma=1000$, infinite time $x=k_1t\to\infty$. Roots Θ were calculated by constructing a table of $f(x)$ from (26) and (28) and interpolating between the tabulated values of x. It is worth pointing out that for this calculation the tabulation must be extended to negative values of x to allow for the possibility that Θ can be negative. As in our previous examples, the distribution is characterized by a sharp cutoff which occurs at the particular value $\Theta=0$ when $f(x)=n$.

Molecular weight averages are calculated from the moments of the distribution, and these in turn are obtainable directly from the generating function (21), (22) by standard operations. In the limit of large σ, which is the only case for which long chains are produced, the moments for all but infinitesimal x are

$$\mu_0/I^0=2(1-e^{-x}),$$
$$\mu_1/I^0=(2\sigma/\alpha)[1-\exp\{-\alpha(x-1+e^{-x})\}], \quad (31)$$
$$\mu_2/I^0=(4\sigma^2/\alpha)[h(x,\alpha)-h(x,2\alpha)],$$

and from these the number average $P_N=\mu_1/\mu_0$ and weight average $P_w=\mu_2/\mu_1$ molecular weights are defined as functions of time $x=k_1t$. Some calculations of the heterogeneity P_w/P_N-1 of the polymer for various values of $\alpha=2k_2I^0/k_1$ are plotted in Fig. 5. The parameter α is a measure of the relative importance of two competing rate processes, the rate of disappearance of monomer and the rate of disappearance of initiator. For $\alpha>1$, the reaction runs out of monomer while still appreciable quantities of initiator are present, so that the initiation of new chains is proceeding even towards the end of the reaction, and the heterogeneity of the product increases with time. For $\alpha<1$, however, initiator has all but disappeared towards the end of the reaction; and continued addition of monomer to existing chains not only builds up a high molecular

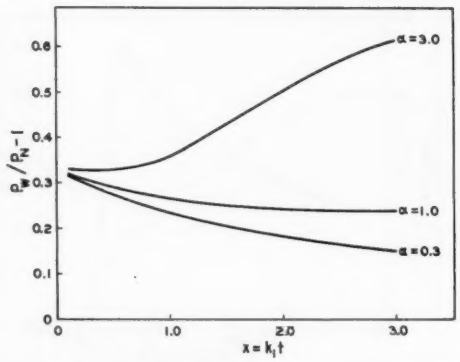

FIG. 5. Inhomogeneity P_W/P_N-1 as a function of time for the mechanism of Sec. 5.

weight but also slowly reduces the heterogeneity of the product.

6. OTHER REACTION MECHANISMS

The examples so far considered have neglected any mention of important termination reactions such as the combination or disproportionation terminations of interest in vinyl polymerizations. These cases have been treated by Bamford and Tompa,[7] and while all of their results can be recovered by the present technique, there seems to be no point in repeating the exercise.

7. DISCUSSION

The problems which have been worked in Secs. 3 through 5 are examples of Szwarc polymerizations for which a termination reaction is absent. The resulting number density distributions are all characterized by abrupt cutoffs above a certain sharply defined chain-length, and it is of interest to inquire as to the reason for this behavior. A glance at the integral form of the number density distributions M_n is suggestive, for before approximate evaluation by the method of steepest descents all of them have the form

$$M_n\sim(n!)^{-1}\int_0^x g(\xi)[f(x)-f(\xi)]^n\exp\{-[f(x)-f(\xi)]\}d\xi, \tag{32}$$

in which $g(x)$ is derived from the initiation mechanism. This is true even for the simplest case of Flory[1] considered in Sec. 3, for which all initiations occur in the first few instants of the reaction, following which there is uninterrupted chain growth. His distribution is given exactly by Eqs. (4), but the same result may also be written

$$M_n\sim n!^{-1}\int_0^x\delta(\xi)\,(x-\xi)^n\exp[-(x-\xi)]d\xi,$$

in which $\delta(\xi)$ is the Dirac delta function. The single impulse $\delta(x)$ of initiations which gives rise to the Poisson distribution,[4] is for more protracted initiation mechanisms replaced by the source density $g(x)$ in (32). The factor

$$(n!)^{-1}[f(x)-f(\xi)]^n\exp\{-[f(x)-f(\xi)]\}$$

which occurs in these integrals thus has the nature of a Green's function, and the integrals are linear superpositions of initiations occurring with different frequency at different times during the course of the reaction. In the examples treated, the number of initiations decreases steadily with time as the supply of monomer is exhausted. The final number distributions therefore start in the low molecular weight region with those chains which were initiated towards the end of the reaction and climb steadily towards those which were initiated at the very start. After this there is an abrupt cutoff. In the event that there is an important termination reaction, such as the chain transfer reaction of Sec. 3 or the termination reactions mentioned briefly in Sec. 6, chains are terminated long before the supply of monomer is exhausted, and the abrupt cutoff disappears. This behavior can be stated more simply (and more approximately) if we neglect the small amount of statistical scatter implicit in the Poisson distribution and in (32) replace the sharply peaked quantity

$$(n!)^{-1}[f(x)-f(\xi)]^n\exp\{-[f(x)-f(\xi)]\}$$

with

$$\delta[f(x)-n-f(\xi)].$$

$$M_n\sim\int_0^x g(\xi)\,\delta[f(x)-n-f(\xi)]d\xi. \tag{33}$$

We have immediately

$$M_n\sim g(\Theta)/f'(\Theta) \qquad \text{for } 0<n<f(x),$$
$$M_n\sim 0 \qquad \text{for } n>f(x), \tag{34}$$

which is an approximate form of Eq. (2).

ACKNOWLEDGMENT

I am indebted to Professor R. Simha for his continued interest in this work.

APPENDIX

We wish to obtain an approximate evaluation of the integral

$$J_n(x)=(n!)^{-1}\int_0^x g(\xi)[f(x)-f(\xi)]^n \times\exp\{-[f(x)-f(\xi)]\}d\xi, \tag{35}$$

in which $f(x)$ is a monotonically increasing function and both $f'(x)$ and $g(x)$ are slowly varying functions over the range of integration. First transform the variable of integration to $z=f(x)-f(\xi)$,

$$J_n(x)=n!^{-1}\int_0^{f(x)}\frac{g[\xi(x,\,z)]}{f'[\xi(x,z)]}z^ne^{-z}dz. \tag{36}$$

Because $f(x)$ is monotonically increasing, the factor

$z^n e^{-z}$ which occurs in the integrand of (36) will possess a single maximum occurring at $z=n$ which may or may not fall within the range of integration. If n is large, the maximum will be very pronounced and will dominate the behavior of the integrand in its immediate neighborhood. It is therefore profitable to consider an expansion of the integrand in the neighborhood of $z=n$. We write

$$(g/f')z^n e^{-z}=[g(\Theta)/f'(\Theta)]n^n e^{-n}\exp[-(z-n)^2/2n+\cdots], \tag{37}$$

in which for n large and g and f' slowly varying the higher terms are negligible. The quantity Θ is that value of ξ which makes $z=n$ for fixed x, i.e., it is the (single) root of

$$f(\Theta)=f(x)-n. \tag{38}$$

Substituting (37) into (36) and expressing the remaining integral in terms of error functions,

$$J_n(x)\to n!^{-1}(2\pi n)^{\frac{1}{2}}n^n e^{-n}[g(\Theta)/f'(\Theta)]\times\tfrac{1}{2}\{1+\operatorname{erf}[f(x)-n]/(2n)^{\frac{1}{2}}\}.$$

It remains only to replace the factorial with its Stirling approximation and to modify the argument of the error function in view of (38) to obtain the result (2) reported in the text. The behavior of the error function in the neighborhood of $f(\Theta)=0$, which is to say when $f(x)=n$, acts as a cutoff for the integral, so that $J_n(x)$ for $n>f(x)$ is very much smaller than $J_n(x)$ when $n<f(x)$. Technically what has happened in this case is that the maximum at $z=n$ in (36) has for $n>f(x)$ moved outside the range of integration. Equation (2) is then no longer a good approximation to the true value of $J_n(x)$, but in applications this does not matter for the integral is for all practical purposes equal to zero.

THE JOURNAL OF CHEMICAL PHYSICS VOLUME 35, NUMBER 6 DECEMBER, 1961

Thermal Conductivity of Polyatomic Gases and Relaxation Phenomena

S. C. Saxena and J. P. Agrawal
Chemical Engineering Division, Atomic Energy Establishment Trombay, Bombay, India
(Received May 8, 1961)

Experimental thermal conductivity data for nitrogen, air, carbon dioxide, oxygen, methane, nitric oxide, and hydrogen have been interpreted in terms of Eucken and Hirschfelder theories. The departure from these theories is attributed to the relaxation of internal energy. At present only a qualitative comparison is possible between the information derived here and that obtained from the studies on the propagation of ultrasonic and shock waves. However, it seems possible to develop a quantitative interpretation for carefully planned thermal conductivity data. Only hydrogen shows an anomalous behavior which is attributed to the uncertainties in the experimental data. This view receives confirmation from the data on binary mixtures of inert gases with hydrogen, and also from an analysis of helium.

I. INTRODUCTION

IT is now a common practice[1] to use experimental data of the various properties of gases to investigate the appropriateness of the Chapman-Enskog theory[2] and the nature of the intermolecular forces. In most of the investigations only a coupled information about these two points is obtained. The validity of the theory is presumed and then the interpretation of the experimental data throws light on the adequacy of the intermolecular potential, or vice versa. In recent years, some progress has been achieved in adopting procedures which result in comparatively more independent information regarding the suitability of either theory or the intermolecular potential. Scattering experiments[3] of high-velocity neutral molecules supply information about the short-range intermolecular forces. Formulas have been derived[4] which interrelate the different properties, but do not essentially involve a detailed knowledge of the intermolecular forces. These extensive investigations have established that within the limitations of the various assumptions involved, the general theoretical expressions are quite accurate. The theory of thermal conduction as applied to polyatomic gases is of special interest in investigating the role of internal degrees of freedom in the mechanism of heat transfer. The theoretical understanding of these processes is also very much limited and extensive critical comparisons with the experimental data are necessary to assess the appropriateness of the available theories. To aid in this direction, we have analyzed here the thermal conductivity data for nitrogen, air, carbon dioxide (300° to 1300°K), oxygen, methane,

[1] J. O. Hirschfelder, C. F. Curtiss, and R. B. Bird, *Molecular Theory of Gases and Liquids* (John Wiley & Sons, Inc., New York, 1954).
[2] S. Chapman and T. G. Cowling, *Mathematical Theory of Non-Uniform Gases* (Cambridge University Press, New York, 1952), 2nd ed.
[3] E. A. Mason and J. T. Vanderslice, *Atomic and Molecular Processes*, edited by D. R. Bates (Academic Press Inc., New York, to be published), Chap. 17.
[4] S. Weissman, S. C. Saxena, and E. A. Mason, Phys. Fluids **3**, 510 (1960); S. C. Saxena, J. G. Kelley, and W. W. Watson (to be published); references to earlier work are given in the latter paper.

TABLE I. Comparison of the calculated and experimental Eucken factors as a function of temperature for nitrogen, air, and carbon dioxide.

Gas	Nitrogen			Air			Carbon dioxide		
T °K	f_E	f_{exptl}	f_H	f_E	f_{exptl}	f_H	f_E	f_{exptl}	f_H
300	1.269	1.31	1.354	1.268	1.30	1.352	1.537	1.57	1.707
400	1.272	1.32	1.360	1.276	1.33	1.364	1.662	1.82	1.869
500	1.282	1.33	1.374	1.290	1.36	1.385	1.766	1.96	2.005
600	1.299	1.35	1.397	1.310	1.38	1.411	1.852	2.08	2.119
700	1.320	1.37	1.425	1.332	1.42	1.441	1.924	2.17	2.214
800	1.342	1.40	1.455	1.354	1.44	1.471	1.983	2.26	2.294
900	1.363	1.41	1.484	1.375	1.46	1.500	2.033	2.33	2.363
1000	1.383	1.43	1.511	1.394	1.48	1.527	2.075	2.39	2.419
1100	1.400	1.43	1.535	1.412	1.48	1.551	2.111	2.43	2.467
1200	1.415	1.42	1.556	1.429	1.47	1.575	2.140	2.44	2.507
1300	1.429	1.41	1.575	1.446	1.46	1.597	2.166	2.43	2.543

nitric oxide (300° to 573°K), and hydrogen (100° to 2000°K). The thermal conductivity data for helium along with the available experimental viscosity and second virial coefficient have also been examined.

II. THERMAL CONDUCTIVITY OF POLYATOMIC GASES

The theoretical expression for thermal conductivity of a pure polyatomic gas becomes complicated because of the presence of internal degrees of freedom, viz., rotation and vibration. Eucken[5] was the first to propose such a formula from more or less intuitive arguments. He assumed that there is no interaction between translational and internal energies so that the transport of translational energy is unaffected by the presence of internal energy. His expression is

$$\lambda/\lambda^0=\tfrac{1}{3}+4C_p/15R=f_E, \qquad (1)$$

where λ is the coefficient of thermal conductivity of the gas, λ^0 is the value of λ that would be obtained if all the internal degrees of freedom were "frozen," C_p is the molar specific heat of the gas at constant pressure, and R is the usual gas constant.

Recently Hirschfelder[6] has advanced a much clearer picture of the whole process and derived an expression for λ under well-defined approximations. According to this theory,

$$\lambda/\lambda^0=1+\delta_f[(2C_p/5R)-1]=f_H, \qquad (2)$$

in which

$$\delta_f=4\Omega^{(2,2)*}/5\Omega^{(1,1)*}, \qquad (3)$$

where $\Omega^{(l,s)*}$ is the usual reduced Chapman-Cowling collision integral.[1] In this derivation the major assumptions, which are pertinent to our discussion here, are: (a) various energy states are in local thermodynamical equilibrium which implies that all reactions including rotational-translational and vibrational-translational transfers are fast, and (b) for polyatomic molecules which are not electronically excited, the diffusion coefficients are identical for different molecular quantum states even though they are in different states of excitation.

These two derivations, Eqs. (1) and (2), then represent the two extreme possibilities for the equilibration of the internal degrees of freedom with translational motion. Equation (1) implies no interaction at all while Eq. (2) implies a rapid adjustment. Information about the rate of transfer of internal energy is obtained from various sources, such as propagation of plane ultrasonic waves, shock waves, pressure broadening of microwave spectra, etc. All these investigations lead to the same conclusion—that the rate of transfer of internal energy is slow and varies from molecule to molecule. The assumption (a) of Hirschfelder's theory will, therefore, tend to make the value of the Eucken factor as calculated according to Eq. (2), f_H, always greater than its experimentally determined value f_{exptl}. This is actually the case as demonstrated by Srivastava and his collaborators[7] for hydrogen, nitrogen, and oxygen around room temperature. Waelbroeck and Zuckerbrodt[8] also found it essential to postulate the existence of rotational-translational relaxation times in order to interpret their thermal conductivity data for hydrogen and oxygen as a function of pressure.

Calculated values of f_E and f_H according to Eqs. (1) and (2), respectively, for nitrogen, air, and carbon dioxide in the temperature range 300° to 1300°K are reported in Table I. C_p values are given by Hilsenrath,[9] while δ_f values by Hirschfelder.[6] δ_f was calculated at

[5] A. Eucken, Physik. Z. **14,** 324 (1913); See also reference 1, pp. 498–501; and reference 2, pp. 237–242.

[6] J. O. Hirschfelder, J. Chem. Phys. **26,** 282 (1957).

[7] (a) B. N. Srivastava and R. C. Srivastava, J. Chem. Phys. **30,** 1200 (1959); (b) B. N. Srivastava and A. K. Barua, *ibid.* **32,** 427 (1960); (c) A. K. Barua, Physica **25,** 1275 (1959); (d) Indian J. Phys. **34,** 169 (1960).

[8] F. G. Waelbroeck and P. Zuckerbrodt, J. Chem. Phys. **28,** 524 (1958).

[9] J. Hilsenrath, *American Institute of Physics Handbook,* edited by D. E. Gray (McGraw-Hill Book Company, Inc., New York, 1957), Chap. 4.

TABLE II. Comparison of the calculated and experimental Eucken factors as a function of temperature for oxygen, methane and nitric oxide.

Gas	Oxygen			Methane			Nitric oxide		
T °K	f_E	f_{exptl}	f_H	f_E	f_{exptl}	f_H	f_E	f_{exptl}	f_H
300	1.277	1.32	1.365	1.484	1.54	1.634	1.293	1.25	1.385
400	1.300	1.39	1.395	1.667	1.80	1.876	1.314	1.32	1.415
500	1.331	1.44	1.438	1.834	2.05	2.098	1.331	1.36	1.438
573	1.353	1.48	1.468	1.952	2.30	2.255	1.342	1.38	1.453

different temperatures assuming the Lennard-Jones (12–6) interaction potential and parameters given by Hirschfelder, Curtiss, and Bird.[10] The f_{exptl} values of Table I were computed by dividing the experimental λ values by λ^0, the latter being determined according to the following relation:

$$\lambda^0=(15R/4M)\eta_{\text{exptl}}. \tag{4}$$

Here M is the molecular weight of the gas and η_{exptl} is the experimental coefficient of viscosity. Smoothed experimental values of λ for N_2 and CO_2 as reported by Rothman,[11] and for air by Bromley,[12] have been used. All the available experimental viscosity data[13] for nitrogen, air, and carbon dioxide were plotted and the values at the required temperatures were read from the smooth curves. Similarly values of f_E, f_H, and f_{exptl} were computed for oxygen, methane, and nitric oxide in the temperature range 300° to 573°K and are listed in Table II. Heat capacity data of Hilsenrath[9] for oxygen and of Kelley[14] for methane and nitric oxide were used. λ values for oxygen,[15] methane[16] and nitric oxide[17] were taken from the literature and graphically interpolated at the temperatures of Table II. The available viscosity data[18] for these gases were also plotted and smoothed values read from the graphs directly.

III. DISCUSSION OF RESULTS

For all six gases of Tables I and II we find that f_E is less than f_{exptl}. This is because in polyatomic gases translational and internal energies interact, contrary to what is assumed in deriving f_E. On the other hand, f_H values are always greater than f_{exptl}. This trend can be explained assuming the slow transfer rate for internal energy mentioned in Sec. II. An excellent account of the relaxation phenomena in gases and the various methods employed to measure it, is given by Herzfeld.[19] Over the temperature range in which we are interested, the electronic excitations are negligible, but both rotational and vibrational effects are important. We will now consider the gases individually.

For all the three gases, nitrogen, oxygen, and air, only rotational effects are important at and around room temperature, while vibrational effects will have a negligible contribution. Measurements by Greene and Hornig[20] of shock-front thicknesses in various gases reveal that equilibration of rotational with translational energy is quite rapid for nitrogen and oxygen. About 20 collisions are required for this equilibration. Oxygen and nitrogen behave in the same way, although oxygen seems to relax somewhat more slowly. It is for this reason that Hirschfelder's theory[6] gives a reasonable agreement with the experimental data. Although the departure of f_H from f_{exptl} is in the right direction to be explained by the relaxation theory, the magnitude is only of the order of uncertainties in measurement of experimental values of λ and C_p. In fact, greater relaxation effects should be observed with increasing temperatures—Parker[21] finds for homonuclear molecules, the number of collisions required for rotational—translational equilibration (Z_R) is a gradually increasing function of increasing temperature. As the temperature is increased, vibrational-translational equilibration also becomes important and should exhibit appreciable effects around and above 1000°K. The rate of transfer of vibrational energy is comparatively slower. Thus[19,20] for oxygen, air, and nitrogen about 10^5 to 10^7 collisions are required for equilibration. According to Parker[21] the number of collisions required for vibrational translational equilibration (Z_u) is a rapidly decreasing function of increasing temperature. There is also some experimental evidence[19,20] to support this conclusion. For air

[10] Reference 1, p. 1111. In each case the second listed value of ϵ/k is used.

[11] A. J. Rothman, Rept. UCRL-2339 (1954). See also A. J. Rothman and L. A. Bromley, Ind. Eng. Chem. **47,** 899 (1955).

[12] L. A. Bromley, Rept. UCRL-1852 (1952).

[13] (a) M. Trautz and R. Zink, Ann. Physik **7,** 427 (1930), (N_2 and CO_2); (b) E. Rammler and K. Brietling, Wärme **60,** 620 (1937); (c) H. L. Johnston and K. E. McCloskey, J. Phys. Chem. **44,** 1038 (1940); (d) A. Eucken, Forschung **11,** 6 (1940); (e) V. Vasilesco, Ann. Physik **20,** 292 (1945); (f) F. G. Keyes, Trans. Am. Soc. Mech. Engrs. **73,** 589 (1951), [(b) through (f), N_2, CO_2 and air]; (g) C. P. Ellis and C. J. G. Raw, J. Chem. Phys. **30,** 574 (1959) (N_2); (h) W. G. Shilling and A. E. Laxton, Phil. Mag. **10,** 721 (1930), (air); (i) M. P. Bremond, Compt. rend. **196,** 1472 (1933), (air).

[14] K. K. Kelley, U. S. Department of the Interior, Bureau of Mines, Bull. 476 (1949).

[15] H. L. Johnston and E. R. Grilly, J. Chem. Phys. **14,** 233 (1946); H. Chaung, Rept. UCRL-8230 (1958).

[16] F. G. Keyes, Trans. Am. Soc. Mech. Engrs. **76,** 809 (1954).

[17] W. C. Gardiner and K. L. Schafer, Z. Elektrochem. **60,** 588 (1956).

[18] References 13(a), 13(b) (O_2, CH_4); 13(c), 13(d) (O_2, NO, CH_4); 13(g) (NO); C. J. G. Raw and C. P. Ellis, J. Chem. Phys. **28,** 1198 (1958) (O_2).

[19] K. F. Herzfeld, *Thermodynamics and Physics of Matter*, edited by F. D. Rossini (Princeton University Press, Princeton, New Jersey, 1955), Sec. H.

[20] E. F. Greene and D. F. Hornig, J. Chem. Phys. **21,** 617 (1953); V. H. Blackman, J. Fluid Mech. **1,** 61 (1956); S. J. Lukasik and J. E. Young, J. Chem. Phys. **27,** 1149 (1957); M. Camac, *ibid.* **34,** 448 (1961).

[21] J. G. Parker, Phys. Fluids **2,** 449 (1959).

and nitrogen entries of Table I also show a pronounced vibrational relaxation at high temperatures.

Carbon dioxide is particularly important, for even at room temperature it has appreciable vibrational energy,[22] while at 1300°K about two-thirds of its energy is only internal. For this triatomic linear symmetrical molecule, relaxation time has been experimentally investigated by a number of workers.[19,23] Gustavson[24] found from his experiments on the impact tube that 22 000 collisions (Z) are needed for the equilibration of internal and translational energies, while Angona[25] finds $Z=52\,000$ from absorption measurements. Eucken and Becker[26] determined the temperature dependence of Z and found it to decrease from 100 000 to 23 000 as the temperature increased from 241° to 415°K. For polyatomic molecules, which possess several vibrational degrees of freedom, additional difficulties arise, as alternative mechanisms are possible for excitation viz. series, parallel, or a combination of the two. Buschmann and Schafer[27] have also found the contribution of triple collisions to be important for carbon dioxide. Fogg and Lambert[28] have calculated Z assuming that vibrational activation enters via the mode of lowest frequency (series excitation). As pointed out by Corran *et al.*,[29] there is a mistake in these calculations, and we find that the correct value is 21 029. This is in reasonable agreement with the results of Eucken and Becker.[26]

Thus, we find that vibrational-translational equilibration is faster for carbon dioxide than nitrogen and oxygen. In view of the fact that carbon dioxide possesses appreciable vibrational energy even at room temperature, f_H would be expected to be significantly higher than f_{exptl}. The data of Table I do not possess this trend and indeed Hirschfelder's theory gives a very reasonable agreement with the experimental data. The source of this discrepancy can not be traced in the assumption (b) of Hirschfelder's theory either, as this will further reduce f_H. The reason is that for the excited species the collision diameters are larger and hence the diffusion coefficients smaller. In fact, this may be taken as evidence of the validity of the assumptions involved in Hirschfelder's theory. The lack of quantitative agreement may be characteristic of the nature of this molecule and should be further investigated when more detailed and precise information becomes available.

Methane is very similar to carbon dioxide in content of internal energy. Eucken and Aybar[30] found from absorption and dispersion measurements, $Z=8400$ at 382°K, 5700 at 473°K, and 3400 at 625°K. Griffith[31] reports $Z=4400$ at 303°K as determined by the jet method.[19] Recent experimental values given by Cottrell and Martin[32] and Edmonds and Lamb[33] are in agreement with Eucken and Aybar.[30] We find $Z=5781$ at 298°K, using the theoretical expression given by Corran *et al.*[29] and experimental data of Edmonds and Lamb.[33] Computed values of Cottrell and Ream[34] also agree well with the experimental data. Consequently, we can infer that methane equilibrates at a faster rate than carbon dioxide (which increases as the temperature increases). Experimental data of Table II follow this trend.

Nitric oxide, unlike carbon dioxide and methane, has negligible vibrational energy near room temperature and even at 573°K only about 6% of the total energy is vibrational. Approximately 1000 collisions[19] are required for internal energy equilibration at 400°K. Thus, the relaxation effects here should be less pronounced than in carbon dioxide and methane. Numbers of Table II follow this trend only qualitatively in as much as they exhibit the relaxation of internal energy—though the magnitudes are not consistent with our anticipations.

IV. RESULTS AND DISCUSSION FOR HYDROGEN

The case of hydrogen gas is of special interest, for extensive experimental measurements are available over a wide temperature range where both rotational and vibrational energies may have pronounced effects. Up to around 500°K, vibrational effects are unimportant and only rotations are to be considered. Most of the information about the relaxation of rotational energy is summarized by Herzfeld.[19] In terms of the number of collisions, the jet method gives $Z=155$–172 at 284–287°K and $Z=205$ at 207°K, while the dispersion method yields $Z=260$. Shock wave measurements of Greene and Hornig[20] indicate that more than 150 collisions are required for rotational-translational equilibration.

Hydrogen molecules possess very little vibrational energy and even at 2000°K only about 13% of the total energy is vibrational, and consequently the population of the higher vibrational levels is negligible. According to Herzberg[35] the ratio of the number of molecules in the first to that in the zeroth vibrational level at 1000°K is about one million times greater than at 300°K. The corresponding ratio is about one thou-

[22] R. H. Fowler, *Statistical Mechanics* (Cambridge University Press, New York, 1955), Chap. III.
[23] E. F. Smiley and E. H. Winkler, J. Chem. Phys. **22,** 2018 (1954).
[24] M. Gustavson, Ph.D. thesis, Cornell University (1952).
[25] F. A. Angona, J. Acoust. Soc. Am. **25,** 1116 (1953).
[26] A. Eucken and R. Becker, Z. physik. Chem. **B27,** 235 (1935).
[27] K. F. Buschmann and K. Schafer, Z. physik. Chem. **B50,** 73 (1941).
[28] P. G. T. Fogg and J. D. Lambert, Proc. Roy. Soc. (London) **A232,** 537 (1955).
[29] P. G. Corran, J. D. Lambert, R. Salter and B. Warburton, Proc. Roy. Soc. (London) **A244,** 212 (1958).
[30] A. Eucken and L. Aybar, Z. physik. Chem. **B46,** 195 (1940).
[31] W. Griffith, J. Appl. Phys. **21,** 1319 (1950).
[32] T. L. Cottrell and P. E. Martin, Trans. Faraday Soc. (London) **72,** 940 (1958).
[33] P. D. Edmonds and J. Lamb, Proc. Phys. Soc. (London) **72,** 940 (1950).
[34] T. L. Cottrell and N. Ream, Trans. Faraday Soc. **51,** 159, 1453 (1955).
[35] G. Herzberg, *Molecular Spectra and Molecular Structure* (D. Van Nostrand Company, Inc., Princeton, New Jersey, 1955), Vol. I, pp. 122–124.

sand for nitrogen and oxygen. This is obviously because of the wide differences in the vibrational quantas of these gases. Thus, for hydrogen the vibrational effects will be pronounced only at very high temperatures, and to our knowledge no experimental investigation has yet been reported on the relaxation of vibrational-translational relaxation for this gas. The experimental thermal conductivity has been determined by a number of workers, but over an appreciable temperature range only by Gregory,[36] Johnston and Grilly,[37] Varhaftik and Parfenov,[38] and Blais and Mann.[39] The data of these four groups are plotted in Fig. 1. The f_{exptl} values of Table III, characterized by the superscripts 37, 38, 39, and a, were calculated according to the experimental values of references 37, 38, 39, and interpolated values of 38 and 39, respectively. λ^0 values up to 1100°K were generated from the experimental viscosity data[40] in conjunction with Eq. (4), and values above this were calculated according to the exp-six potential with the parameters given by Mason and Rice.[41] Rammler and Brietling[40] viscosity data were not considered for hydrogen and also for other gasses of Sec. III, as their values are consistently in disagreement with the data of other workers in the overlapping temperature range. Heat capacity data up to 250°K were taken from reference 9, while above this temperature were taken from reference 14. δ_f values were computed according to Eq. (3) and for the exp-six potential.[41] All these values of f_E, f_H and f_{exptl} are given in Table III. In Fig. 1 we have drawn the theoretical curves of λ calculated according to Eq. (2) using the exp-six potential[41] (curve A), and a purely exp potential (curve B) given by Mann.[42] In either case, λ^0 values were calculated according to the theoretical expression for monatomic gases.

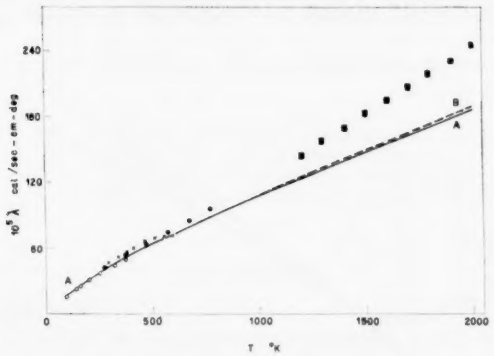

FIG. 1. Thermal conductivity of hydrogen as a function of temperature. Curve A is calculated according to the exp-six potential while B for a purely exponential potential. Experimental data: ● Varhaftik and Parfenov, ○ Johnston and Grilly, × Gregory, and ■ Blais and Mann.

TABLE III. Comparison of the calculated and experimental Eucken factors as a function of temperature for hydrogen.

T °K	f_E	f_{exptl}	f_H
100	1.059	1.03[37]	1.078
150	1.148	1.14[37]	1.200
200	1.208	1.21[37]	1.279
250	1.242	1.26[37]	1.325
300	1.258	1.30,[37] 1.36[38]	1.348
350	1.259	1.29,[37] 1.38[38]	1.351
400	1.260	1.38[38]	1.353
500	1.267	1.43[38]	1.364
600	1.276	1.45[38]	1.377
700	1.286	1.49[38]	1.393
800	1.295	1.54[38]	1.406
900	1.305	1.58[a]	1.420
1000	1.315	1.62[a]	1.435
1100	1.325	1.65[a]	1.450
1200	1.335	1.71[39]	1.465
1300	1.345	1.76[39]	1.480
1400	1.356	1.81[39]	1.495
1500	1.366	1.86[39]	1.510
1600	1.376	1.90[39]	1.525
1800	1.397	1.98[39]	1.556
2000	1.418	2.06[39]	1.586

[a] Interpolated from references 38 and 39.

The f_{exptl} values for hydrogen are systematically higher than f_H values except those obtained in conjunction with λ values of Johnston and Grilly.[37] Almost all the latter f_{exptl} values lie between f_E and f_H like most of the other gases discussed in Sec. III. Recent measuremends [7d] at 30° and 45°C indicate that Johnston and Grilly[37] values are somewhat lower, but still not as much as it appears from the data of references 36 and 38. Srivastava and Barua[43] have corrected the Johnston and Grilly data[36] on the basis of their own[7d] work and have found relaxation effects in the temperature range 254.4° to 341.3°K. They[43] have also given an approximate theory and calculated the number of collisions required for rotational-translational equilibration from this corrected data and found values in reasonable agreement with those obtained by other methods. In this temperature range (100–350°K) pronounced relaxation effects are expected as the rotational energy just keeps building up.[22] Although the data of references 36 and 38 lead to the contrary, it also seems a bit unlikely that a theory which explains data for so many

[36] H. S. Gregory, Proc. Roy. Soc. (London) **A149,** 35 (1935).
[37] H. L. Johnston and E. R. Grilly, J. Chem. Phys. **14,** 233 (1946).
[38] N. B. Varhaftik and I. D. Parfenov, J. Exptl. Theoret. Phys. (U.S.S.R.) **8,** 189 (1938).
[39] N. C. Blais and J. B. Mann, J. Chem. Phys. **32,** 1459 (1960).
[40] M. Trautz and collaborators, Ann. Physik **2,** 733 (1929); **7,** 427 (1930); **5,** 561 (1930); **20,** 118, 121 (1934); R. Wobser and F. Miller, Kolloid Beih. **52,** 165 (1941); References 13(b), 13(c), 13(d).
[41] E. A. Mason and W. E. Rice, J. Chem. Phys. **22,** 522 (1954).
[42] J. B. Mann, Los Alamos Scientific Laboratory Rept. LA-2383 (1959).
[43] B. N. Srivastava and A. K. Barua, Proc. Phys. Soc. (London) (to be published).

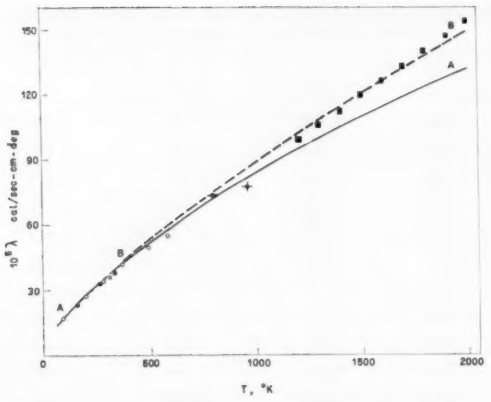

FIG. 2. Thermal conductivity of helium as a function of temperature. Curve A is calculated according to the exp-six potential while B for a purely exponential potential. Experimental data: ○ Kannuluik and Carman, ● Johnston and Grilly, -●- von Ubisch, + Rothman, × Saxena, and ■ Blais and Mann.

gases will fail altogether for hydrogen. Gregory's[36] data, which are consistently higher than Varhaftik and Parfenov,[38] show a different trend around 550°K—leveling out rather than increasing steeply with temperature. The high-temperature data of Blais and Mann[39] also lead to values for f_{exptl} which are systematically higher than f_H values. Because of the appearance of vibrational relaxation, increased relaxation effects are expected in this temperature range, while in actual practice we find the opposite trend—f_E values are always less than f_{exptl} values, like other gases.

This anomalous behavior of hydrogen is hard to understand and the uncertainties and inconsistencies of the λ values of various groups make it rather doubtful. The values[39] in 1200° to 2000°K range were determined by an elegant use of a conventional thermal diffusion column. Since the technique is still not quite established and the various procedures involved can be much more uncertain than the precision of the measurements, we conclude that this anomalous behavior may be just due to the reported data for thermal conductivity being too high. Further evidence for this view stems from the work of Srivastava and collaborators.[7a,d] They found that all the binary mixtures of hydrogen with inert gases at 30° and 45°C exhibit relaxation effects. Blais and Mann[39] have measured the thermal conductivity of helium also in the same range. In the next section, we will analyze these data in conjunction with the available data on other properties to assess this possibility.

V. THERMAL CONDUCTIVITY AND OTHER PROPERTIES OF HELIUM

Experimental thermal conductivity data[44] for helium are plotted in Fig. 2 and certain remarks concerning these data are essential. The value at 959°K is stated to be unreliable and that at 793°K is estimated to be about 4% higher. Curve A represents the calculated values using the exp-six potential[41] while curve B represents calculated values using the purely exponential potential of Amdur and Harkness,[45] and the collision integrals tabulated by Monchick.[46] Experimental data of Blais and Mann[39] are systematically higher than the values predicted by the exp-six potential, but are in reasonable agreement with those of the purely exponential potential. In Fig. 3 are shown the experimental values[47] for viscosity as well as the calculated curves using these two potentials. It is interesting to note that the situation in this case is other way around. Exp-six potential values agree well with the experimental data while the purely exponential potential values are systematically higher. The former result is not surprising, as the potential parameters of the exp-six potential were determined in conjunction with the available viscosity and second virial data. The data for the second virial coefficient is available up to 1473°K and the purely exponential potential gives only a somewhat satisfactory agreement[48] with the experimental data at higher temperatures, the discrepancy being less than 4% above 800°K. Exp-six potential gives a better agreement.[41]

Thus, at first sight, it is puzzling that the exp-six potential which gives values which agree with the second virial coefficient up to 1473°K, viscosity and thermal conductivity up to about 1000°K, will fail to give good agreement for λ values in 1200° to 2000°K range. Let us recall that the purely exponential potential was obtained by Amdur and Harkness[45] by

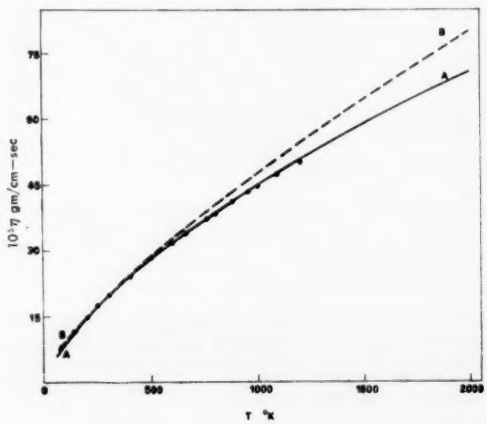

FIG. 3. Viscosity of helium as a function of temperature. Curve A is calculated according to the exp-six potential while B for a purely exponential potential. ● Experimental data.

[44] (a) W. G. Kannuluik and E. H. Carman, Proc. Phys. Soc. (London) **B65,** 701 (1952); (b) S. C. Saxena, Indian J. Phys. **31,** 597 (1957); (c) H. von Ubisch, Arkiv Fysik **16,** 93 (1959); (d) references 11, 37, and 39.

[45] I. Amdur and A. L. Harkness, J. Chem. Phys. **22,** 664 (1954), Eq. (12) of this paper; (a) Eq. (10) of this paper.

[46] L. Monchick, Phys. Fluids **2,** 695 (1959).

[47] J. Kestin and W. Leidenfrost, Physica **25,** 537 (1959).

[48] E. A. Mason and J. T. Vanderslice, Ind. Eng. Chem. **50,** 1033 (1958).

fitting this simple form to the potential energy values determined from scattering[45a] in the molecular separation range 1.27 to 1.59 A, and from viscosity and virial[41] data in the range 1.90 to 2.30 A. Indeed, interpolation is the best way of determining the potential energy in the intermediate range (1.59 to 1.90 A) but actual difficulties may arise in choosing a simple form and a unique interpolation. Only one particular procedure is represented by the work of Amdur and Harkness.[45] It is quite likely that back extrapolation of the exp-six potential up to around 1.7 A, may be a better choice for representing the true interaction. This particular interpolation has the advantage of reconciling all the experimental data available for various properties of helium with the measurements of interaction potential. Amdur and Mason[49] in their recent calculations of the properties of helium at high temperatures also use a somewhat similar interpolation for potential energy. This then implies that a purely exponential potential does not represent the correct potential energy curve and the agreement of the calculated values of λ, assuming this potential with the high temperature thermal conductivity data,[39] may be fortuitous. We are, thus, led to the possibility that Blais and Mann[39] data may be systematically higher. It is again confirmed by the fact that the purely exponential potential suggested by Blais and Mann[39] on the basis of the thermal conductivity data agrees rather poorly the available viscosity data. The uncertainties are approximately similar to those obtained in connection with the purely exponential potential of Amdur and Harkness.[45] A redetermination of thermal conductivity in this temperature range with well established techniques will consequently be very useful.

[49] I. Amdur and E. A. Mason, Phys. Fluids **1**, 370 (1958).

VI. CONCLUSIONS

Thermal conductivity data show some promise in exploring the relaxation of internal energy for polyatomic gases and especially its dependence on the temperature of the gas. However, in this work, only qualitative information could be derived from the available thermal conductivity data. Some additional information is needed for quantitative interpretation, such as the pressure dependence of the observed thermal conductivity, to disentangle the accommodation effects. It would also be very interesting to carefully determine the thermal conductivity of hydrogen, which unlike all other gases, shows an anomalous behavior.

ACKNOWLEDGMENTS

The authors are thankful to H. N. Sethna and Dr. Dipak Gupta for their kind interest and encouragement in this work.

THE JOURNAL OF CHEMICAL PHYSICS VOLUME 35, NUMBER 6 DECEMBER, 1961

Recalculation of the Surface Energies of Alkali Halide Crystals*

G. C. BENSON
Division of Pure Chemistry, National Research Council, Ottawa, Canada
(Received May 29, 1961)

Previous calculations of the surface energies of the {100} and {110} faces of alkali halide crystals, including corrections for the relaxation of the outermost layer, have been repeated employing more recent values of the parameters describing the repulsion between the ions. The adoption of the new data overcomes some difficulties formerly encountered in considering the distortion of the surface region.

INTRODUCTION

THEORETICAL calculations currently being carried out in this laboratory are concerned with the depth of penetration of surface effects in ionic crystals (see Benson Freeman and Dempsey[1] for a preliminary report of this work). The model adopted considers the displacement and polarization of the ions in the first five layers at a {100} face of an alkali halide crystal with a sodium chloride structure and is a direct extension of the model used by Benson, Balk, and White[2] for estimating the distortion in the outer layer alone.

Originally it was intended that the constants in the potential function defining the energy of interaction of a pair of ions, employed in the multilayer computations, should be the same as those used previously. Thus estimates of the distortion energy in the two investigations would be comparable and would also be compatible with previous calculations of the surface energies of the undistorted crystals.[3] Unfortunately numerical difficulties arose when the first multilayer calculations were attempted. In particular, using the same data for sodium chloride as in reference 2, no stable energy minimum could be found when two or more layers at the surface of a hemicrystal of this salt were allowed to relax. The failure to find an acceptable solution for

* Issued as N.R.C. No. 6571.
[1] G. C. Benson, P. I. Freeman, and E. Dempsey, Advances in Chem. Ser. (to be published).
[2] G. C. Benson, P. Balk, and P. White, J. Chem. Phys. **31**, 109 (1959).
[3] F. van Zeggeren and G. C. Benson, J. Chem. Phys. **26**, 1077 (1957).

TABLE I. Contributions of the different forces to the surface energy of an undistorted {100} face for the nearest neighbor spacing a_{min} (listed in Table II). All energies in erg cm^{-2}.

	Electrostatic	Dipole-Dipole	Dipole-Quadrupole	Repulsive	σ°
LiF	970.6	132.5	16.3	−830.7	288.7
LiCl	459.6	121.5	15.0	−344.7	251.4
LiBr	374.6	115.5	14.1	−278.0	226.2
LiI	284.0	110.7	13.8	−208.7	199.8
NaF	625.6	82.4	8.7	−450.8	265.9
NaCl	344.9	76.4	8.2	−218.5	210.9
NaBr	291.2	76.2	8.1	−183.3	192.2
NaI	230.4	75.8	8.4	−144.1	170.5
KF	403.3	84.9	8.4	−270.7	225.9
KCl	249.1	66.5	6.8	−147.1	175.3
KBr	215.5	62.5	6.3	−125.1	159.2
KI	176.2	58.8	6.0	−100.3	140.8
RbF	339.8	90.0	9.4	−226.1	213.1
RbCl	218.5	69.3	7.2	−129.1	166.0
RbBr	190.9	64.2	6.6	−111.1	150.5
RbI	157.8	59.4	6.1	−89.9	133.4
CsF	288.0	108.9	11.9	−197.6	211.2

the multilayer distortion of sodium chloride is similar to the trouble noted previously in the one layer calculations for lithium fluoride.[2] Since an explanation of these failures may lie in the inadequacies of the data employed, the adoption of different data was considered.

Recently, Cubicciotti[4,5] has published a new set of parameters for the overlap repulsion potentials of the alkali halides. These are based on a re-examination of the Born-Mayer-Huggins[6–9] treatment of ionic crystals, using the currently accepted value of the electronic charge (4.802×10^{-10} esu) and modern data for the compressibilities. It should also be remarked that Cubicciotti has departed somewhat from the original scheme of fitting the repulsion parameters and, instead of keeping the same value of ρ for all of the salts, has allowed ρ to vary for different anions. This procedure introduces three extra parameters which may in part account for the improved agreement of the electron affinities of the halogens derived via the Born-Haber cycle with those determined experimentally (cf. Pritchard[10]).

It has been found that use of Cubicciotti's values of the repulsion parameters leads to reasonable results in the two distortion calculations which formerly gave trouble. Although such evidence is indirect, it does appear that the new repulsion parameters together with the other data for the van der Waals' coefficients[11] and electronic polarizabilities of the ions[12] form a more consistent set of constants than those used previously.

RESULTS AND DISCUSSION

In view of the considerations outlined above, the calculations of references 2, 3, and 13 were repeated using Cubicciotti's repulsion parameters. Results for the surface energies of the undistorted {100} and {110} faces of the alkali halides are collected in Tables I and II. The distortion corrections, based on the relaxation of the ions in the outermost layer at the surface are summarized in Tables III and IV. As in the previous computations, the nearest neighbor separation used for each salt was calculated from the minimum of the cohesive energy curve at 0°K; the new values thus obtained are listed in Table II under the heading a_{min}.

Comparison of the present results with those obtained previously shows that the new surface energies are larger in all cases. This is due to an increase in the value of σ° and an accompanying decrease in the magnitude of $\Delta\sigma$ for each salt. The differences in σ are relatively smaller for salts with larger ions (either anion or cation); the biggest changes occur for the lithium halides. The surface energies of the {100} faces of these salts previously seemed unreasonably small and are now more in line with the values for the other alkali halides. Plots of σ and of σ° against a_{min} are approximately linear for salts with the same cation but the overall correlation illustrated for σ° in Fig. 4 of reference 3 is no longer evident.

In Tables I and II the small differences in the dipole-dipole and dipole-quadrupole contributions from those given in reference 3 are due to the changes in the values of a_{min}. The new electrostatic terms reflect the same changes and in addition the adoption of the more up-to-date value of the electronic charge. However, in general the main difference in σ° stems directly from the decrease in the absolute magnitude of the repulsive contribution.

The displacements and dipole moments in Tables III and IV show relative trends in series of salts with a common ion similar to those displayed by the results of references 2 and 13. In most cases the dipole moments are not altered appreciably from the previous values. The new displacements are, for nearly all of the salts, smaller in magnitude than the old results and the percentage change is fairly large in some cases. This is understandable, since the equilibrium configuration

[4] D. Cubicciotti, J. Chem. Phys. **31,** 1646 (1959).
[5] D. Cubicciotti, J. Chem. Phys. **33,** 1579 (1960).
[6] M. Born and J. E. Mayer, Z. Physik **75,** 1 (1932).
[7] M. L. Huggins and J. E. Mayer, J. Chem. Phys. **1,** 643 (1933).
[8] M. L. Huggins, J. Chem. Phys. **5,** 143 (1937).
[9] M. L. Huggins, J. Chem. Phys. **15,** 212 (1947).
[10] H. O. Pritchard, Chem. Rev. **52,** 529 (1953).
[11] J. E. Mayer, J. Chem. Phys. **1,** 270 (1933).
[12] J. R. Tessman, A. H. Kahn, and W. Shockley, Phys. Rev. **92,** 890 (1953).
[13] G. C. Benson, E. Dempsey, and P. Balk, J. Chem. Phys. **34,** 157 (1961).

TABLE II. Contributions of the different forces to the surface energy of an undistorted {110} face for nearest neighbor distance a_{min}. All energies in erg cm^{-2}.

	a_{min} (A)	Electro-static	Dipole-Dipole	Dipole-Quadrupole	Repulsive	σ^0
LiF	1.979	1888.2	144.9	18.4	−1089.2	962.3
LiCl	2.539	894.1	129.8	16.3	−441.0	599.2
LiBr	2.718	728.8	123.0	15.2	−352.0	515.1
LiI	2.981	552.4	117.5	14.8	−260.1	424.6
NaF	2.291	1217.0	96.2	10.9	−612.4	711.7
NaCl	2.794	671.0	85.2	9.5	−296.0	469.7
NaBr	2.956	566.6	84.0	9.3	−246.5	413.4
NaI	3.196	448.3	82.6	9.3	−191.5	348.8
KF	2.652	784.6	102.0	11.0	−369.6	528.0
KCl	3.114	484.6	78.5	8.6	−204.5	367.3
KBr	3.268	419.3	73.1	7.9	−173.8	326.5
KI	3.495	342.8	67.8	7.4	−138.8	279.1
RbF	2.808	661.0	107.5	12.2	−307.5	473.2
RbCl	3.253	425.1	82.9	9.4	−180.1	337.3
RbBr	3.403	371.4	76.3	8.4	−155.2	300.9
RbI	3.626	307.0	69.7	7.7	−125.3	259.0
CsF	2.967	560.3	128.3	15.1	−266.8	436.9
CsCl	3.532	297.1	116.7	13.0	−170.1	256.6
CsBr	3.674	264.0	108.8	12.1	−150.5	234.4
CsI	3.894	221.7	99.4	11.1	−125.0	207.1

TABLE III. Results for the relaxation of the outermost layer at the {100} face. Displacements are in terms of a_{min} as a unit.

	z_+	z_-	μ_+ debye	μ_- debye	$\Delta\sigma$ erg cm^{-2}	$\sigma_{\{100\}}{}^0$ erg cm^{-2}	$\sigma_{\{100\}}$ erg cm^{-2}
LiF	−0.1123	−0.0538	−0.0162	0.5144	−146.4	288.7	142
LiCl	−0.1084	−0.0047	−0.0101	1.2672	−144.7	251.4	107
LiBr	−0.1132	0.0031	−0.0092	1.5615	−140.5	226.2	86
LiI	−0.1154	0.0133	−0.0080	1.9524	−126.4	199.8	73
NaF	−0.0351	−0.0210	−0.0877	0.2616	−45.2	265.9	221
NaCl	−0.0518	0.0005	−0.0622	0.7967	−52.7	210.9	158
NaBr	−0.0578	0.0061	−0.0580	1.0239	−54.0	192.2	138
NaI	−0.0628	0.0148	−0.0521	1.3522	−52.5	170.5	118
KF	−0.0147	−0.0307	−0.3347	0.1825	−38.4	225.9	188
KCl	−0.0275	−0.0090	−0.2358	0.5677	−30.1	175.3	145
KBr	−0.0322	−0.0047	−0.2198	0.7315	−29.4	159.2	130
KI	−0.0364	0.0021	−0.1993	0.9742	−27.7	140.8	113
RbF	−0.0084	−0.0337	−0.4554	0.1634	−37.3	213.1	176
RbCl	−0.0212	−0.0120	−0.3233	0.5132	−26.3	166.0	140
RbBr	−0.0250	−0.0076	−0.3015	0.6600	−25.2	150.5	125
RbI	−0.0290	−0.0016	−0.2751	0.8777	−23.3	133.4	110
CsF	−0.0013	−0.0437	−0.7515	0.1584	−44.9	211.2	166

TABLE IV. Results for the relaxation of the outermost layer at the {110} face. $a_{min}/\sqrt{2}$ and $a_{min}(2/3)^{\frac{1}{2}}$ are used as units in stating the displacements for salts with NaCl and CsCl structures, respectively.

	z_+	z_-	μ_+ debye	μ_- debye	$\Delta\sigma$ erg cm^{-2}	$\sigma_{\{110\}}{}^0$ erg cm^{-2}	$\sigma_{\{110\}}$ erg cm^{-2}
LiF	−0.2417	−0.1368	−0.0210	0.6669	−394.6	962.3	568
LiCl	−0.2282	−0.0587	−0.0137	1.5867	−259.1	599.2	340
LiBr	−0.2326	−0.0467	−0.0123	1.9207	−234.8	515.1	280
LiI	−0.2338	−0.0320	−0.0105	2.3723	−198.3	424.6	226
NaF	−0.1390	−0.1120	−0.1455	0.4223	−156.4	711.7	555
NaCl	−0.1372	−0.0489	−0.1007	1.1340	−115.6	469.7	354
NaBr	−0.1421	−0.0379	−0.0922	1.4092	−109.2	413.4	304
NaI	−0.1448	−0.0232	−0.0814	1.7976	−97.3	348.8	252
KF	−0.0810	−0.1112	−0.5211	0.3056	−105.2	528.0	423
KCl	−0.0849	−0.0537	−0.3779	0.8732	−69.6	367.3	298
KBr	−0.0896	−0.0442	−0.3504	1.0962	−64.8	326.5	262
KI	−0.0923	−0.0307	−0.3156	1.4185	−57.6	279.1	222
RbF	−0.0640	−0.1100	−0.6925	0.2744	−92.9	473.2	380
RbCl	−0.0701	−0.0548	−0.5123	0.8017	−60.0	337.3	277
RbBr	−0.0739	−0.0451	−0.4774	1.0093	−55.3	300.9	246
RbI	−0.0767	−0.0327	−0.4334	1.3106	−48.9	259.0	210
CsF	−0.0445	−0.1164	−1.0803	0.2578	−96.1	436.9	341
CsCl	−0.0191	−0.0308	−0.6227	0.5310	−37.7	256.6	219
CsBr	−0.0259	−0.0222	−0.5712	0.6982	−34.8	234.4	200
CsI	−0.0346	−0.0112	−0.5092	0.9562	−31.9	207.1	175

must represent a rather delicate balance of forces. More extensive calculations for sodium chloride[1] have shown that the relaxation of several layers farther inside the crystal has a significant effect on the configuration of the ions in the outer layer. This should be kept in mind when considering the results of the present single layer calculations; in particular, the magnitude of $\Delta\sigma$ computed here provides a lower limit to the value which would be obtained by allowing the relaxation to extend farther into the crystal.

Finally, Balk and Benson[14] have pointed out that experimentally determined surface enthalpies of both sodium chloride and potassium chloride are much larger than estimates based on the Born-Mayer theory of ionic crystals. The present recalculations tend to reduce these differences but large discrepancies remain.

[14] P. Balk and G. C. Benson, J. Phys. Chem. **63,** 1009 (1959).

ACKNOWLEDGMENTS

I am indebted to Dr. P. I. Freeman and to Dr. E. Dempsey for helpful discussions of this work. Use of the computing facilities of the Analysis Section of the Division of Mechanical Engineering, N.R.C. is gratefully acknowledged.

THE JOURNAL OF CHEMICAL PHYSICS VOLUME 35, NUMBER 6 DECEMBER, 1961

Unimolecular Rates Due to Multiple Critical Oscillators

E. W. SCHLAG

Department of Chemistry, Northwestern University, Evanston, Illinois

(Received December 12, 1960)

In the first part it is shown that Kassel's quantum model differs appreciably from the classical model in the description of the unimolecular pressure falloff behavior. In the second part the quantum model is extended to encompass dissociation by the accumulation of energy in several critical oscillators. The specific rate constant for molecules with energy E is developed along with the limiting high and low pressure rate constants, as well as the concomitant activation energy expressions. The approximations of the classical theory are indicated by comparisons of the relevant quantum and classical formulations.

THE abnormally high pre-exponential (frequency) factor of some unimolecular reactions has been attributed to a mode of reaction involving the accumulation of energy in several critical oscillators which then might lead to the simultaneous rupture of more than one bond. The activation energy for such a decomposition mode has often been found to be the sum of the dissociation energies of the rupturing bonds.

Reactions of particular interest have included mercury dialkyls, azoalkanes, etc.[1] The classical high pressure rate constant for these reactions as developed by Pritchard,[2,3] and discussed by Johnston[4] and Steel[5] is

$$k_\infty=\lambda e^{-b}\frac{b^{(n-1)}}{(n-1)!}\left[1+\frac{(n-1)}{b}+\frac{(n-1)(n-2)}{b^2}+\cdots\right], \quad (1)$$

where $b=E_0/RT$, E_0 is the critical energy, n is the number of *critical* oscillators in the molecule, and λ is the rate of interchange of energy within the molecule.

In terms of Slater's "short-cut" method[6,7] one can consider the rate constant as the product of λ, the interchange rate, times the probability that in an equilibrium gas the n *critical* oscillators have energy E_0 or greater. So, for $n=1$, $\lambda=A$, the high-pressure frequency factor; for $n>1$ the expression predicts $A>\lambda$, i.e., enhanced A factors. For $n=2$ and $b=40$, Eq. (1) already predicts a 15-fold increase, and for $n=3$ about a 100-fold increase in A. The enhancement therefore arises from the equilibrium of total energy among the critical oscillators, it only being required that the total energy exceed some critical value. If one only has simultaneity of bond rupture without this equilibrium among the n oscillators, such as is considered in developments based on Slater's theory, no enhancement is predicted.[8,9]

Equation (1) refers to the classical value of the rate constant at high pressure. It is of interest to develop the specific rate constant for molecules with energy E and the resultant general rate constant which describes the pressure falloff of these reactions. Such a development should allow comparison of this model with experimental data obtainable from falloff studies, photochemical, or mass spectrometric experiments. The falloff parameter s should give an insight into the molecular complexity of these reactions. In line with Kassel's treatment the harmonic oscillator picture is maintained, which though certainly not entirely correct, forms the basis of much presently successful rationalization of data.

A. CASE OF A SINGLE CRITICAL OSCILLATOR

This is the well-known Rice-Ramsperger-Kassel model.[10] Kassel has derived a quantum as well as a classical form of the pressure falloff of the rate constant and has given some comparison between the two based on a set of oscillators with equal frequencies. From this work it can be seen that the theoretical falloff is somewhat different for these two forms of the theory. Kassel also gave some consideration to a model employing different frequencies and reported that the results of the simple quantum case would not be altered appreciagly by such an extension of the model.[10] A contrast between the quantum and classical forms of the theory applied to the case of the isomerization of cyclopropane seems of interest in view of the rather extensive data on this decomposition.[11]

The quantum form for s oscillators of equal frequency ν contains the factor $(j+s-1)!/j!$ in the expression for the density of quantum states for the jth state. This

[1] B. G. Gowenlock, Quart. Rev. **14,** 133 (1960).
[2] H. O. Pritchard, J. Chem. Phys. **25,** 267 (1956).
[3] D. Clark and H. O. Pritchard, J. Chem. Soc. **1956,** 2136.
[4] H. S. Johnston, Ann. Rev. Phys. Chem. **8,** 249 (1957).
[5] C. Steel, J. Chem. Phys. **31,** 899 (1959).
[6] N. B. Slater, Proc. Leeds Phil. Lit. Soc. Sci. Sect. **6,** 259 (1955).
[7] N. B. Slater, *Theory of Unimolecular Reactions* (Cornell University Press, Ithaca, New York, 1959), pp. 31, 39.
[8] E. Thiele and D. J. Wilson, J. Phys. Chem. **64,** 473 (1960).
[9] N. B. Slater, J. Phys. Chem. **64,** 476 (1960).
[10] (a) L. S. Kassel, *Kinetics of Homogeneous Gas Reactions* (Chemical Catalog Company, New York, 1932), Chap. V; (b) L. S. Kassel, J. Phys. Chem. **32,** 1065 (1928).
[11] A similar comparison for this isomerization has been undertaken by Wilder (thesis, Polytechnic Institute of Brooklyn, 1961) employing the theory of Marcus and Rice[12] which treats the problem from the point of view of an activated complex.

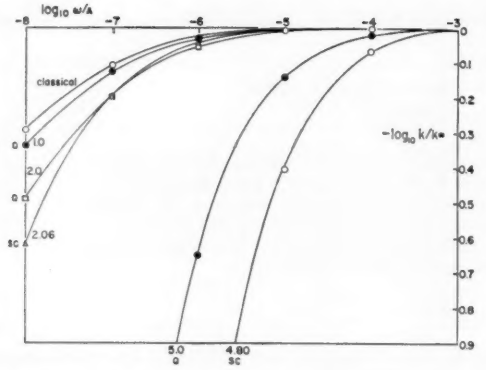

FIG. 1. Comparison of the falloff of the general rate constant with pressure for a quantum (Q), semiclassical (SC), and classical model, for $n=1$, $s=15$, $b=40$. The values of $h\nu/RT$ are listed next to their respective curves.

factor is often approximated by j^{s-1}, which leads to the classical result (see Appendix) or by $(j+s/2)^{s-1}$, which leads to a semiclassical result, the latter being, of course, the better approximation of the factor. This semiclassical expression can be seen to be equivalent to the vibrational energy density expression given by Marcus and Rice.[12] However, for some reactions, the average energy of the species that react may lie only slightly above the critical energy, hence these approximations may not be valid. The falloffs predicted by these two approximations can be compared with the quantum case and the values for the three functions at, e.g., $s=15$ give the curves shown in Fig. 1. It can be seen from this figure that the curvatures for the semiclassical and quantum cases are sufficiently different so as to make use of the former undesirable for a prediction of curvature, though the predicted value of k/k_∞ and the predicted value of the specific rate constant at energy E are reasonably close to the values derived from the quantum form. The use of the classical equation for fitting the data for the isomerization of

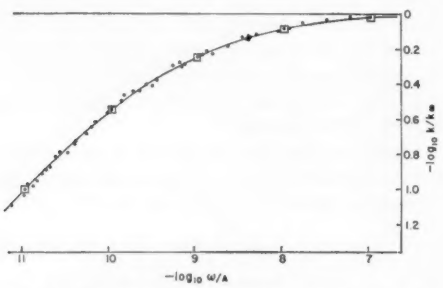

FIG. 2. The falloff of the general rate constant with pressure for the isomerization of cyclopropane at 500°C. The line is the theoretical curve for a Kassel quantum model, $s=21$, $b=44$, $h\nu/RT=2.0$, and is drawn on the basis of the calculated points.

[12] R. A. Marcus and O. K. Rice, J. Phys. Chem. **55,** 894 (1951).

cyclopropane produces the best fit when $s=11$; a value of $s>21$ is predicted for the semiclassical equation. This seems to produce the apparent contradiction that in an assembly of oscillators half are freely interchanging energy, half are effectively isolated. It can be seen that for a given temperature the quantum rate can be reduced to the classical rate simply by choosing progressively smaller values for $h\nu/RT$. On the basis of the vibrational frequencies in cyclopropane it seems reasonable to adopt a value of $h\nu/RT=2.0$ for the isomerization at 500°C. If one also chooses a value of $b=E_0/RT=44$ for the isomerization, this choice of parameters produces excellent agreement between experiment[13] and theory for $s=21$, i.e., assuming that

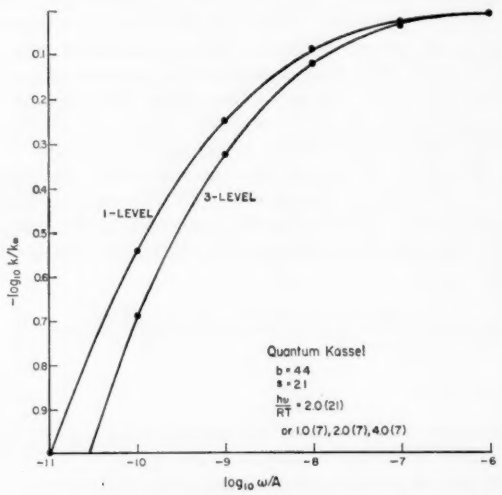

FIG. 3. Quantum Kassel; $b=44$, $s=21$, $h\nu/RT=2.0$ (21) or $h\nu/RT=1.0$ (7) 2.0 (7), 4.0 (7).

all, not just 11, of the oscillators are active (Fig. 2). If one further extends this model to the somewhat more realistic case of three groups of seven frequencies, each at $h\nu/RT=1.0$, 2.0, and 4.0, then this further modification affects the falloff only slightly (Fig. 3), though the values of the specific rate constants increased by a factor of 1.5 to 2. The change in the falloff produced by going from a one-frequency to a three-frequency model corresponds to the change one would obtain by raising the frequency in the one-frequency model by about 10%. The fitting of these curves, however, is attained by an arbitrary positioning of the theoretical curve along the log$P$ axis and hence is only agreement in curvature; if one calculates ω on the usual basis ($\sigma=5A$), one finds that the A factor predicted

[13] (a) T. S. Chambers and G. B. Kistiakowsky, J. Am. Chem. Soc. **56,** 399 (1934); (b) H. O. Pritchard, R. G. Sowden, and A. F. Trotman-Dickenson, Proc. Roy. Soc. (London) **A217,** 563 (1953). (c) Cf. also H. S. Johnston and J. R. White, J. Chem. Phys. **22,** 1969 (1954).

by this quantum treatment is too large by about one order of magnitude, a perhaps not unexpectedly large discrepancy. Due to the large difference between the calculated value of s from classical theory as against that of quantum theory, it appears, at least for this case, that a *classical* formulation of RRK theory is often too approximate to be useful in making comparisons with experimental results. Though there is some arbitrariness in the choice of parameters in the quantum model, it is not certain that an exact calculation would be more meaningful in view of the inherent approximation in the model, as was recognized at the outset.[14] It is suggested that perhaps some of the shortcomings observed in experimental comparisons are more attributable to the formulation employed rather than an inadequacy of the model. A more detailed quantum calculation may be appropriate, however, for the specific rate constant of molecules with energy E which appears to be a more sensitive function of the molecular vibrations employed.[12]

B. SPECIFIC RATE CONSTANT OF MOLECULES WITH ENERGY E FOR MULTIPLE CRITICAL OSCILLATORS AND THE CONSEQUENT GENERAL RATE

For the case of a single *critical* oscillator the form is[10,11]

$$k_E = A\frac{p^*}{p} = A\sum_{k=m}^{j}\binom{j-k+s-2}{s-2}\Big/\binom{j+s-1}{s-1}.$$

p^* is the probability that the critical oscillator contains at least m quanta and j is the total number of quanta in s oscillators. For the case of n critical oscillators p^* would become

$$p^* = \sum_{k=m}^{j}\binom{k+n-1}{n-1}\binom{j-k+s-n-1}{s-n-1},$$

where s is the total number of oscillators in the molecule. By repeated summation by parts, this results in a series of n terms of the form

$$p^* = \sum_{i=0}^{n-1}\binom{m+n-1}{m+i}\binom{j-m+s-n}{s-n+i}. \qquad (2)$$

Therefore the specific rate constant at E is seen to be

$$k_E = \frac{\lambda}{\binom{j+s-1}{s-1}}\sum_{i=0}^{n-1}\binom{m+n-1}{m+i}\binom{j-m+s-n}{s-n+i}. \qquad (3)$$

This model assumes that the energy in the n oscillators can cooperate to reach a critical value, and that all distributions of this energy should be weighted equally for dissociation, it only being required that the total energy in the n oscillators exceed some critical value. It can be seen that even though the barrier for (3) is higher than in the usual bond rupture process this is offset by the increased number of states in p^*. For any more than a slight difference in critical energies, however, the Boltzmann term will swamp the increase in p^*.[15] This need not apply to the reaction of excited molecules. For example, if D_2 is sufficiently larger than D_1 so that the A factor is normal in the thermal reaction, one might find that in a photolytic study of such a reaction at $E>D_1+D_2$, the more complex reaction path with the higher critical energy may actually be the predominant path. This would then give a product distribution quite unlike that found in the thermal reaction.

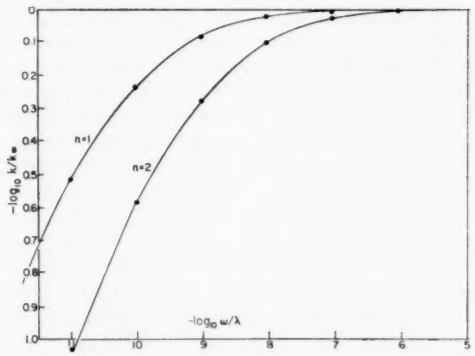

FIG. 4. Comparison of the falloff of the general rate constant with pressure for a quantum model with $n=1$ and $n=2$, $s=32$, $b=40$, and $h\nu/RT=2.0$.

The value of (3) can now be substituted into the general rate expression

$$k=[1-\exp(-h\nu/RT)]^s \cdot \sum_{j=m}^{\infty}\frac{k_E\binom{j+s-1}{s-1}\exp(-jh\nu/RT)}{1+k_E/\omega}. \qquad (4)$$

For the special case in which $n=2$ this results in the expression

$$k/k_\infty = \gamma^{-1}\sum_{x=0}^{\infty}\frac{\binom{x+s-1}{s-1}\left[m\frac{s-1}{x+s-1}+1\right]\exp(-xh\nu/RT)}{1+\frac{\lambda}{\omega}\binom{x+s-1}{s-1}\left[m\frac{s-1}{x+s-1}+1\right]\Big/\binom{x+m+s-1}{s-1}}, \qquad (5)$$

where

$$\gamma=[1-\exp(-h\nu/RT)]^{-s}\{m[1-\exp(-h\nu/RT)]+1\}.$$

[14] I am indebted to Dr. L. S. Kassel for personal discussions on this point.

[15] (a) H. V. Carter, E. I. Chappell, and E. Warhurst, J. Chem. Soc. **1956**, 106; (b) D. Clark and H. O. Pritchard, *ibid.* **1956**, 2136.

For the case $s=32$, $h\nu/RT=2$, and $b=40$, this general rate constant has been summed on a computer, and compared with the regular Kassel quantum case ($n=1$) (Fig. 4). It can be seen that the falloff is shifted to larger values of ω/λ but that the curvature is only slightly tighter for the $n=2$ case, corresponding to a change of $s=1$ or 2. This comparison shows that if a molecular decomposition is already predicted to be near the low-pressure region for the case of $n=1$, then the assumption of a multiple reaction coordinate would predict the reaction to be even further into the low-pressure region than one presumes from regular Kassel theory. This shows that the identification of a given rate with the theoretical value for k_∞ could lead to error if the complexity of these decompositions is small, i.e., small s, since under these conditions, particularly for $n>1$, the reaction may still be in the falloff region.

C. LIMITING HIGH AND LOW PRESSURE VALUES OF THE RATE CONSTANT

The high pressure constant can be seen to be equal to

$$k_\infty=[1-\exp(-h\nu/RT)]^s\sum_{j=m}^{\infty}\lambda p^*\exp(-jh\nu/RT),$$

$$=\lambda\exp(-mh\nu/RT)[1-\exp(-h\nu/RT)]^s\sum_{x=0}^{\infty}p(x)\exp(-xh\nu/RT),$$

$$\sum_{x=0}^{\infty}p(x)\exp(-xh\nu/RT)=\sum_{x=0}^{\infty}\sum_{i=0}^{n-1}\binom{m+n-1}{m+i}\cdot\binom{x+s-n}{s-n+i}\exp(-xh\nu/RT),$$

or by interchanging the summation order and rearranging we have

$$\sum_{i=0}^{n-1}\binom{m+n-1}{m+i}\sum_{x=0}^{\infty}\binom{x+s-n}{s-n+i}\exp(-xh\nu/RT).$$

Therefore by simple transformation of $y=x-i$, and then changing back to x, we have

$$\sum_{i=0}^{n-1}\binom{m+n-1}{m+i}\sum_{x=0}^{\infty}\binom{x+s-n+i}{s-n+i}\exp(-xh\nu/RT)\cdot\exp(-ih\nu/RT),$$

or

$$\sum_{i=0}^{n-1}\binom{m+n-1}{m+i}\exp(-ih\nu/RT)\cdot[1-\exp(-h\nu/RT)]^{n-s-1-i},$$

or

$$k_\infty=\lambda\exp(-mh\nu/RT)[1-\exp(-h\nu/RT)]^{n-1}\sum_{i=0}^{n-1}\binom{m+n-1}{m+i}u^i, \quad (6)$$

where

$$u=\{\exp(-h\nu/RT)/[1-\exp(-h\nu/RT)]\},$$

which is identical to a quantum expression one could derive for k_∞ using Slater's "short-cut" method.[6] For the classical conditions of $RT\gg h\nu$ and $m\gg n$ we obtain Pritchard's formula (1). For a choice of $b=40$, $h\nu/RT=2$, and $s=21$, the quantum theory predicts A factors that are only about 15% lower than those predicted on a classical model (for small n at a given activation energy). Hence a quantum correction for calculating enhancement of the A factor does not appear necessary for this case.

The low pressure constant will be independent of n since it is given by the activation rate.

We can write

$$k_0=\omega[1-\exp(-h\nu/RT)]^s\sum_{j=m}^{\infty}\binom{j+s-1}{s-1}\cdot\exp(-jh\nu/RT),$$

$$k_0=\omega\exp(-mh\nu/RT)[1-\exp(-h\nu/RT)]^s\cdot\sum_{x=0}^{\infty}\binom{x+m+s-1}{x+m}\exp(-xh\nu/RT),$$

where ω is the collision frequency per molecule or mole, assuming that each collision of an excited molecule deactivates that molecule. Now it can be shown that

$$\sum_{x=0}^{\infty}\binom{x+m+s-1}{x+m}t^x=\sum_{i=0}^{s-1}\binom{m+s-1}{m+i}\frac{t^i}{(1-t)^{i+1}}.$$

Since

$$\frac{t^i}{(1-t)^{i+1}}=\sum_{x=0}^{\infty}\binom{x}{x-i}t^x,$$

substituting this into the right-hand side, changing the order of summation and applying Cauchy's formula, we obtain the sum on the left-hand side. Therefore

$$k_0=\omega\exp(-mh\nu/RT)[1-\exp(-h\nu/RT)]^{s-1}\cdot\sum_{i=0}^{s-1}\binom{m+s-1}{m+i}u^i,$$

where

$$u=\{\exp(-h\nu/RT)/[1-\exp(-h\nu/RT)]\},$$

or

$$k_0=\omega\exp(-mh\nu/RT)\binom{m+s-1}{s-1}\cdot[1-\exp(-h\nu/RT)]^{s-1}\alpha, \quad (7)$$

$$\alpha=\left[1+\frac{(s-1)}{(m+1)}u+\frac{(s-1)(s-2)}{(m+1)(m+2)}u^2+\cdots\right].$$

TABLE I. $(j+s-1)!/j!j^{s-1}$.

s \ j	1	5	10	20	35	50	70
2	2.00	1.20	1.10	1.05	1.03	1.02	1.01
5	120	4.84	2.40	1.59	1.32	1.21	1.15
10	3.6×10^{6}	372	33.5	7.10	3.26	2.33	1.85
15	1.3×10^{12}	1.7×10^{5}	1.7×10^{3}	74	14.2	6.84	4.08
20	2.4×10^{18}	2.7×10^{8}	2.4×10^{5}	1600	102	29.5	12.1

Here for a choice of $h\nu/RT=2$, $b=40$, and $s=21$, k_0 quant./k_0 class.$=10^{-4}$. The relatively large difference between the classical and the quantum calculation is brought about by the large value of s. This indicates that a quantum form of Kassel's theory is appropriate at low pressures for more complicated molecules. The application of Eq. (7) to the calculation of the second-order rate data for N_2O_5 shows that one can encompass the low-pressure A factor quite well with this expression ($h\nu/RT=4.1$, $s=15$) whereas a classical calculation yields a value several orders of magnitude too high.[16] Similar agreement with experiment[17] can be obtained for ozone though the difference between a classical and quantum value is no longer as large since the value of s is smaller.

D. ACTIVATION ENERGY

The activation energy, $E_a=RT^2d\ln k/dT$, can be directly obtained by differentiation of (6) to give for the case at high pressure,

$$E_a=mh\nu-(n-1)h\nu u+\left(\frac{n-1}{m+1}\right)h\nu u^2\exp(h\nu/RT)\beta,$$

$$\beta=\left\{1+\left(2\frac{n-2}{m+2}-\frac{n-1}{m+1}\right)u+\left[\frac{n-2}{m+2}\left(3\frac{n-3}{m+3}-\frac{n-1}{m+1}\right)-\left(\frac{n-1}{m+1}\right)\left(2\frac{n-2}{m+2}-\frac{n-1}{m+1}\right)\right]\cdot u^2+\cdots\right\}.$$

It is seen here that the difference between the activation energy and the critical energy is far less than predicted from classical arguments.

Similarly the activation energy for the low-pressure rate, which is the same as for the Kassel ($n=1$) case, is seen to be

$$E_a=mh\nu-(s-1)h\nu u+\left(\frac{n-1}{m+1}\right)h\nu u^2\exp(h\nu/RT)\beta',$$

where u is the same as above, and β' is also the same as β above except that s rather than n oscillators are involved.[18] Thus for the example of $h\nu/RT=2$, $s=21$, and $b=40$, $E_0-E_a=5.8RT$ whereas for the classical case[7] we have the usual $E_0-E_a=(s-1)RT=20RT$.

In conclusion, it was shown that one can derive a specific rate constant for molecules with energy E and the consequent general rate constant for a model which assumes that energy can be accumulated in a group of n critical oscillators. The development followed formal reasoning analogous to that of the RRK model. The usual Kassel quantum rate expressions were seen to result as a special case in this development. The development has only been made for the quantum model as it appears that this represents a preferable form of the theory for comparison with experiment. Such quantum considerations seem to be most important for (a) the rate constant of excited molecules with energy E, (b) the theoretical form of the rate constant or A factor for unimolecular reactions at low pressures, particularly for large s, (c) the shape of the unimolecular falloff of the rate constant with pressure, and (d) the prediction of critical energies from experimental activation energies, in the main for reactions with large s in the low pressure region. It was also suggested that processes with multiple reaction coordinates may be important in the kinetics of excited states, even for reactions with normal A factors. A precise calculation of such effects may, however, have to be done by a detailed counting of the relevant energy states.[12]

ACKNOWLEDGMENT

Acknowledgment is made to the donors of the Petroleum Research Fund, administered by the American Chemical Society, for partial support of this research.

APPENDIX

For the case of s oscillators of average frequency ν, the quantum weight of the jth level ($E=jh\nu$) is

$$p=\binom{j+s-1}{s-1},$$

[16] E. K. Gill and K. J. Laidler, Proc. Roy. Soc. (London) **A250**, 121 (1959).

[17] (a) S. W. Benson and A. E. Axworthy, J. Chem. Phys. **26**, 1718 (1957); (b) J. A. Zaslowsky, H. B. Urbach, F. Leighton, R. J. Wnuck, and J. Wojtowicz, J. Am. Chem. Soc. **82**, 2682 (1960).

[18] Since there is a temperature dependence in ω this introduces a slight correction of $\pm1/2\ RT$ into E_a, cf. reference 7, p. 37.

which for $j \gg s$ reduces to the classical form $j^{s-1}/(s-1)!$. Similarly for

$$p^* = \binom{j-m+s-1}{s-1}$$

for which $(j-m) \gg s$, a more stringent condition, is required for use of the classical expression, so for a thermal decomposition the average energy of s harmonic oscillators determines $(j-m)$ for the average decomposing molecule at high pressures, so that s may be 5–10 times larger than this. Table I gives ratios of the quantum weight to the classical weight, a value which should be arbitrarily close to one for all levels of interest to justify the use of the classical equations such as, e.g., $k_E = A(1-E_0/E)^{s-1}$, $(E_0 = mh\nu)$.

THE JOURNAL OF CHEMICAL PHYSICS VOLUME 35, NUMBER 6 DECEMBER, 1961

Ultraviolet Absorption Spectra of Alkali Metal Azides

S. K. Deb*

Radio and Electrical Engineering Division, National Research Council, Ottawa, Canada

(Received May 5, 1961)

The absorption spectra of thin films of NaN_3, KN_3, RbN_3, and CsN_3 have been measured at 295°, 77.3°, and 4.2°K in the wavelength range 1400 to 2200 A. The spectra show three well-defined absorption peaks, which have not been reported previously, and these were identified as the exciton transitions corresponding to $n=1$, 2, and 3. In thicker films and thin single crystals a new absorption band with multiple structure, having a maximum around 2225 A has been observed in all materials and this has been tentatively identified as due to a transition of low probability to a low-lying excited state of the azide ion. On irradiating the azides at 2400 A a weak fluorescence was observed in all cases.

INTRODUCTION

THE alkali metal azides are simple ionic inorganic compounds similar to the alkali halides where the halogen ion is replaced by the azide ion (N_3^-). In spite of their structural dissimilarities with alkali halides, both sodium azide and potassium azide show remarkable similarities with their corresponding halides in the formation of color centers.[1] On the other hand, the azides are unstable and decompose into metal and nitrogen under the action of heat and light. In recent years there has been a considerable interest on the optical and electrical properties of monovalent azides in order to understand the mechanisms of decomposition. This subject has been comprehensively reviewed by Evans, Yoffe, and Gray.[2]

The role of excitons in the decomposition of monovalent ionic azides has been emphasized by Yoffe and his co-workers.[3,4] Direct experimental evidence on the exciton spectra exists only for thallous azide and silver azide.[4,5] Cunningham and Tompkins[1] have studied the formation of color centers in sodium azide and potassium azide by ultraviolet and x-ray irradiation and they have suggested that excitons formed during irradiation interacts with imperfections to form color centers, and that the positive holes (N_3^0) trapped in cation vacancies partially decompose to give nitrogen as one of the decomposition products. These authors also measured the ultraviolet absorption spectra of single crystals of sodium azide and potassium azide, and obtained an absorption edge that exhibited no structure. Nevertheless they assumed that the exciton transitions occur near the absorption edge.

The present work was undertaken to investigate the fundamental absorption spectra of alkali metal azides with the object of gaining information on their energy band structure. Measurements were made on the ultraviolet absorption spectra of both thin and thick films of azides at liquid-nitrogen and liquid-helium temperature. The results show some interesting features and a number of absorption peaks observed in the fundamental absorption region which are believed to be associated with different exciton states.

EXPERIMENTAL PROCEDURE

Optical absorption spectra above 2000 A were obtained with a Perkin-Elmer model 4000 recording ultraviolet spectrophotometer. For measurements below 2000 A a Jarrell-Ash half-meter vacuum monochromator with a Seya-Namioka mounted grating, having a

* National Research Council Post-Doctorate Fellow.

[1] J. Cunningham and F. C. Tompkins, Proc. Roy. Soc. (London) **A251**, 27 (1959).

[2] B. L. Evans, A. D. Yoffe, and P. Gray, Chem. Revs. **59**, 515 (1959).

[3] B. L. Evans and A. D. Yoffe, Proc. Roy. Soc. (London) **A250**, 346 (1959).

[4] S. K. Deb and A. D. Yoffe, Proc. Roy. Soc. (London) **A256**, 514 (1960).

[5] A. C. McLaren and G. T. Rogers, Proc. Roy. Soc. (London) **A240**, 484 (1957).

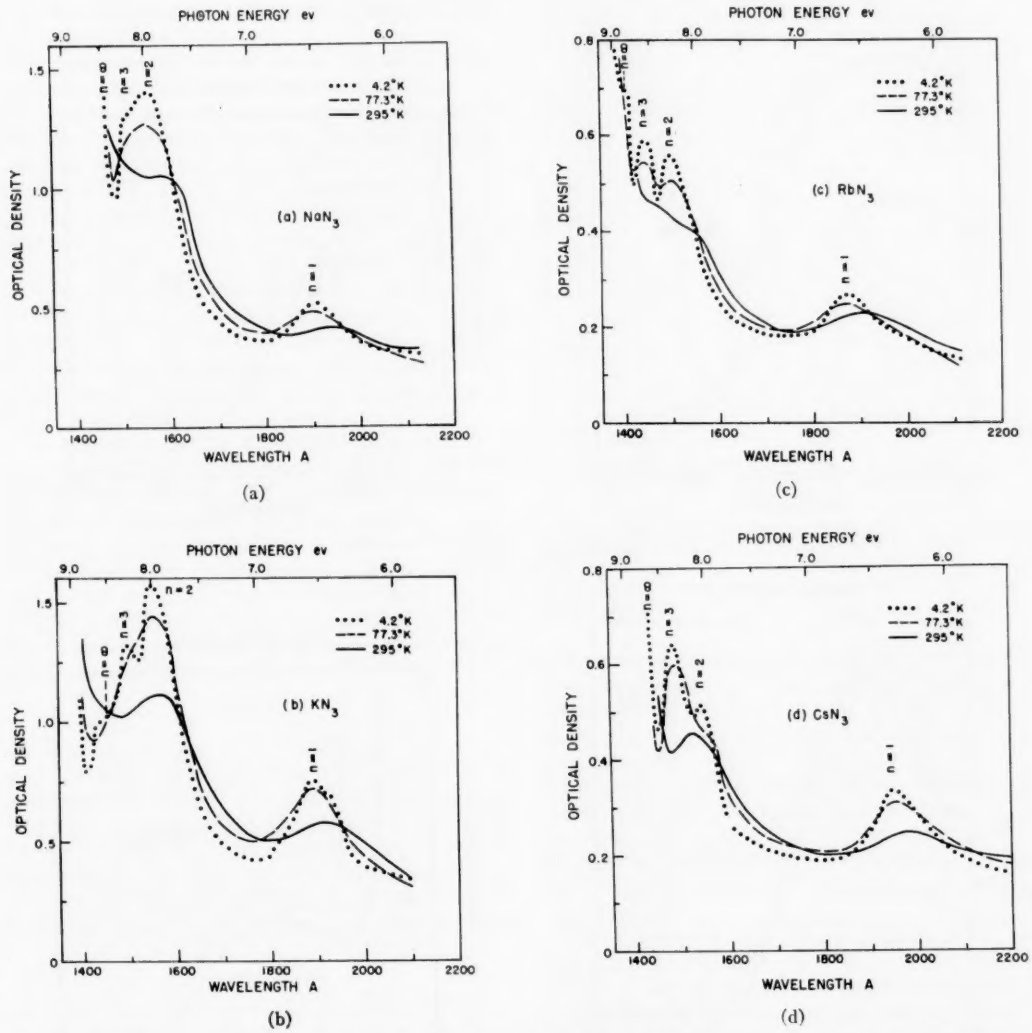

FIG. 1. Absorption spectra of thin films of the alkali metal azides deposited on LiF substrate: (a) NaN_3; (b) KN_3; (c) RbN_3; (d) CsN_3.

dispersion of 17 A/mm, was used. The light source was a hydrogen discharge lamp fitted with a LiF window and operated on alternating current. The source could be used satisfactorily down to about 1400 A, below which the intensity of the light diminished rapidly. The monochromator had appreciable stray light and at wavelengths below 1350 A the amount of stray light became comparable to that available from the source. This restricted the measurements to wavelengths above 1350 A. The intensities of the incident and transmitted radiation were monitored by means of a sodium salicylate transmission phosphor sprayed on a LiF window fitted close to the photocathode of an EMI 6256B photomultiplier tube. The phosphor has a constant quantum efficiency in the wavelength range 900–2000 A. The output of the photomultiplier tube was measured with a micromicroammeter.

The cryostat which held the refrigerated sample was provided with a rotating vacuum seal which made it possible to pass the monochromatic light through the sample, through a glass filter or directly to the phosphor and photomultiplier. The spectrum was recorded manually, each point being corrected for stray light with the help of the glass filter. The vacuum system of the cryostat was separate from that of the monochromator and no condensable vapors which might interfere with the measurement of absorption at low temperature were detected.

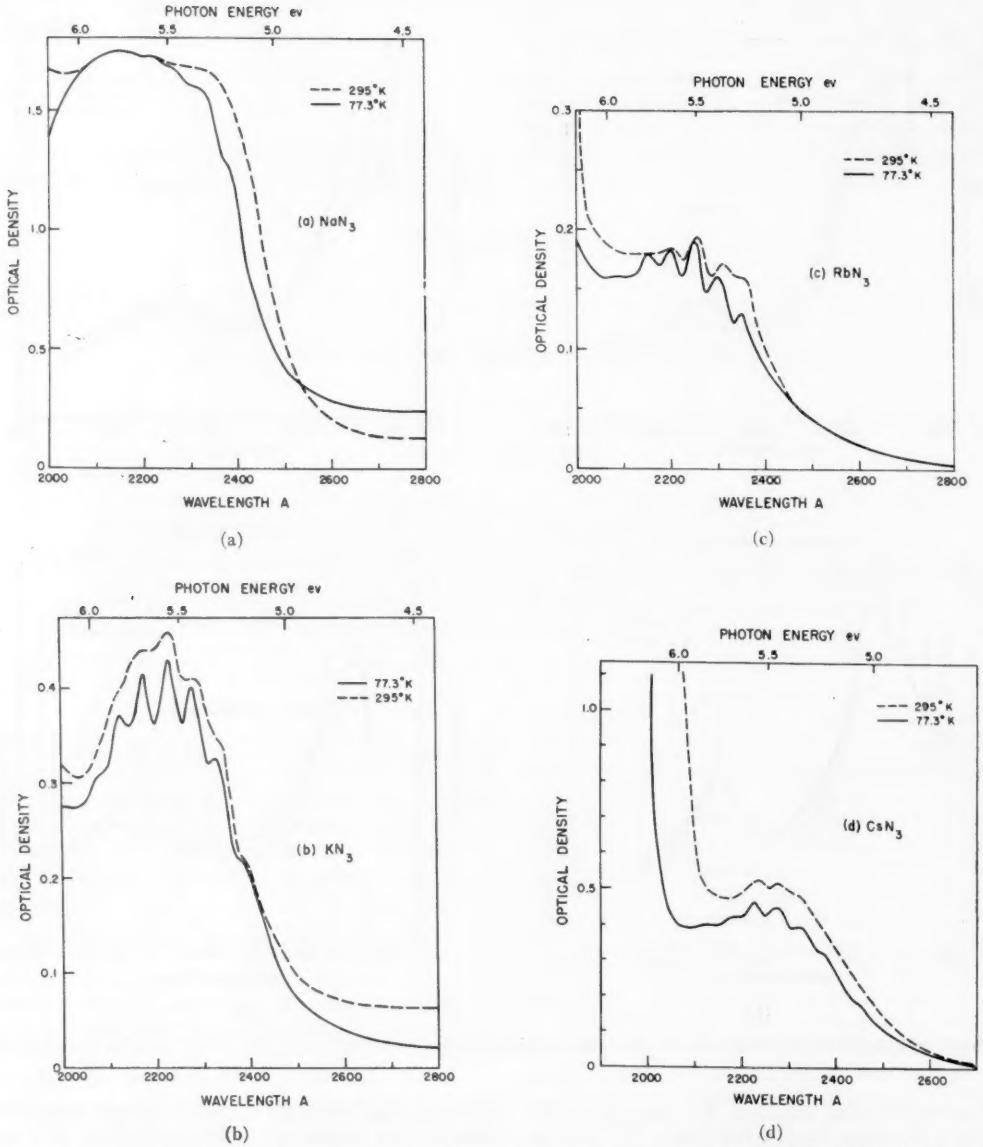

FIG. 2. Absorption spectra of thin single crystal and thick films of alkali metal azides deposited on LiF: (a) Single crystal of NaN_3 55 μ thick; (b) KN_3 film 10 μ thick; (c) RbN_3 film 47 μ thick; (d) CsN_3 film 23 μ thick.

The sodium azide used in these experiments was obtained by triple recrystallization at room temperature from an aqueous solution of Matheson, Coleman, and Bell reagent-grade sodium azide. Samples of potassium azide, rubidium azide, and cesium azide were obtained from Dr. A. D. Yoffe of the Cavendish Laboratory, Cambridge.

Since the absorption coefficient in the fundamental region is very high ($\simeq 10^5$ cm^{-1}), very thin samples (0.1 μ approx) must be used and these can only be obtained as deposited films. The films cannot be obtained by vacuum evaporation because the azides decompose on heating. However, the alkali azides are slightly soluble in absolute alcohol and this makes it possible to prepare thin films by careful evaporation from solution. The substrates were plates of Harshaw single-crystal lithium fluoride, about 0.5 mm thick, which had negligible absorption in the spectral range investi-

gated. The thickness of the films was estimated to be in the 0.1–0.2 μ range.

For measurements in the tail of the fundamental absorption edge, thicker specimens must be used because the absorption coefficient is small. Transparent plate-like crystals of NaN_3 about 50 μ thick were obtained by crystallization from aqueous solution. The amounts of KN_3, RbN_3, and CsN_3 available were not sufficient to permit the growth of large single crystals. However, this was not a serious disadvantage since 50 μ films could be obtained with much less wastage by the deposition method described above. A comparison of a 50 μ film of sodium azide with a single crystal of the same thickness indicated that there was no significant difference in their absorption spectra in the region under consideration. The thickness of films in the range of 10–50 μ was measured by a micrometer.

The apparatus used for the measurement of fluorescence spectra has been described by Lipsett.[6] It had, however, been improved by placing a fore prism monochromator at the entrance slit of the excitation monochromator, to reduce stray light. A 1600-w xenon lamp (Osram XBO 2001 S) was used as the exciting light source. The detection photomultiplier tube was an EMI 6256 B. No corrections were made for the variation of the photomultiplier sensitivity and monochromator efficiency with wavelength.

RESULTS

The absorption spectra of the thinner films (0.1 μ to 0.2 μ thick) of NaN_3, KN_3, RbN_3, and CsN_3 at room temperature (295°K), liquid nitrogen temperature (77.3°K), and liquid helium temperature (4.2°K) are shown in Fig. 1. The results obtained with the thin single crystal (55 μ thick) of NaN_3 and the thicker films (25 μ to 50 μ thick) of KN_3, RbN_3, and CsN_3 are shown in Fig. 2. A band having a maximum around 2225 A and a multiple structure consisting of about seven bands is observed in all cases. There is a small variation in the wavelength of the maximum in different azides. At 295°K the structure is so broadened that it is, at best, only partially resolved. On cooling to 77.3°K the peaks of the band are displaced slightly towards shorter wavelengths. At 4.2°K the bands are somewhat sharper but otherwise unchanged. The absorption coefficient at band maximum for NaN_3, KN_3, RbN_3, and CsN_3 are 70 cm^{-1}, 900 cm^{-1}, 90 cm^{-1}, and 450 cm^{-1}, respectively.

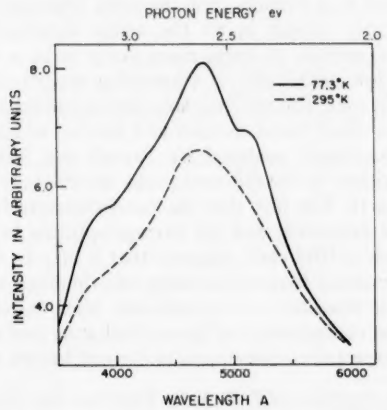

FIG. 3. Fluorescence spectra of a thin single crystal (60 μ thick) of NaN_3.

On irradiating a single crystal (60 μ thick) of NaN_3 and thick films of KN_3, RbN_3, and CsN_3 with light of 2400 A a weak fluorescence having maximum emission around 4800 A was observed in all cases at 295°K and 77.3°K. The strongest fluorescence was observed in NaN_3 and the spectrum showed some structure at 77.3°K as shown in Fig. 3. The drop in intensity of the fluorescent emission for wavelengths longer than 5000 A is due to the drop in sensitivity of the photomultiplier tube. No such structure could be resolved in KN_3, RbN_3 and CsN_3 presumably because the intensity of the emission was too weak to make any accurate measurement above the noise level of the detecting system.

A single crystal of NaN_3 was irradiated at room temperature with x-rays (50 kv, 48 ma) from a Machlett tube with tungsten target and beryllium window, and the absorption spectrum was then measured at liquid nitrogen temperature. The result is shown in Fig. 4. Two absorption bands with maxima at 3350 A and 2480 A arose. The band at 2480 A was obtained by subtracting the absorption before x-ray treatment from

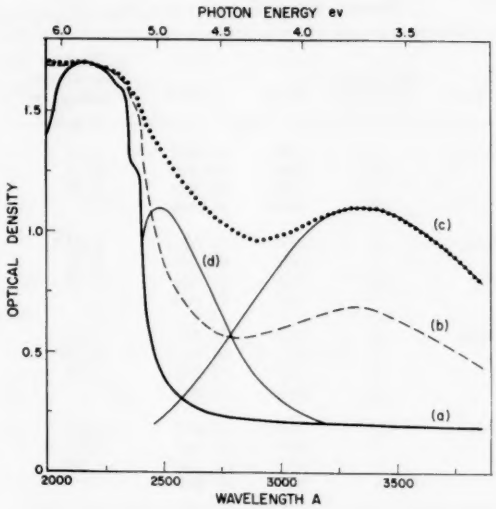

FIG. 4. Absorption spectrum of NaN_3 after x-ray irradiation, measured at 77.3°K: (a) Untreated crystal; (b) Pure crystal after irradiation for 15 min at 295°K; (c) Same crystal after irradiation for an additional 15 min at 295°K; (d) Curve (c) minus curve (a).

[6] F. R. Lipsett, J. Opt. Soc. Am. 49, 673 (1959).

TABLE I. Absorption peaks at 4.2°K.

Salt	Quantum number n	λ, A	ν, cm^{-1}	Exciton dissociation energy, ev
NaN_3	1	1910	62 400	1.97
	2	1560	64 100	0.49
	3	1505	66 400	0.22
	∞	1465	68 300	
KN_3	1	1895	52 800	2.03
	2	1545	64 700	0.51
	3	1490	67 100	0.23
	∞	1450	69 000	
RbN_3	1	1875	53 300	2.21
	2	1500	66 700	0.55
	3	1445	69 200	0.25
	∞	1405	71 200	
CsN_3	1	1950	51 300	2.26
	2	1540	64 900	0.57
	3	1485	67 300	0.25
	∞	1440	69 400	

the absorption after treatment [curve (c) minus curve (a) of Fig. 4]. It is also interesting to note that in the irradiated crystal there was a general increase of absorption around 2050 A.

DISCUSSION

The absorption spectra of very thin films of alkali metal azides show several characteristic absorption peaks. The absorption coefficient in the neighborhood of the first absorption peak near 1900 A is of the order of 10^5 cm^{-1}. This indicates an allowed optical transition, probably to an exciton level. Assuming that the exciton spectrum follows a hydrogen-like series, it should be possible to represent the spectrum by the following equation[7]:

$$\nu_n = \nu_\infty - R'/n^2 \qquad (1)$$

$$\text{with } R' = R\mu/K_0^2 m,$$

where ν_∞ is the series limit, n is the quantum number, R is the Rydberg constant, μ is the reduced effective mass of the electron-hole system, K_0 is the high frequency dielectric constant, and m is the free electron mass. Since the magnitude of μ is not known, the absolute values of the ν's cannot be predicted. It is, however, possible to ascertain whether the experimental results fit an expression of the form (1) with reasonable values for μ.

If it is assumed that the observed bands are due to excitons, then from the spacing of the first two peaks given in Table I it seems reasonable to attribute the first peak around 1900 A to quantum number $n=1$. The observed peaks at 4.2°K may then be represented approximately by the following equations (in cm^{-1}):

In NaN_3, $\nu_n = 68\,300 - 15\,900/n^2$;

KN_3, $\nu_n = 69\,000 - 16\,400/n^2$;

RbN_3, $\nu_n = 71\,200 - 17\,800/n^2$;

CsN_3, $\nu_n = 69\,400 - 18\,200/n^2 \cdot n = 1$, 2, and 3.

The last term (R'/n^2) in Eq. (1) gives the optical energy required to dissociate the exciton. The values of exciton dissociation energies are listed in Table I. No exciton peaks for quantum numbers ≥ 4 were observed. It is interesting to note that there is a rapid rise in absorption in the neighborhood of ν_∞ which probably indicates the onset of a band to band transition. Having determined the optical energy E_1, required to dissociate the optically formed exciton for $n=1$, it is then possible to estimate the reduced effective mass μ of the exciton from

$$\mu = E_1 K_0^2 m/R. \qquad (2)$$

Both NaN_3 and KN_3 are birefringent and their refractive indices have been measured for different crystallographic directions.[8] In computing the high frequency dielectric constant the average value of the refractive indices was taken. The reduced effective mass of the exciton was found to be approximately 0.7 m for NaN_3 and 0.76 m for KN_3. These are not unreasonable for ionic compounds. Similar calculations could not be made for RbN_3 or CsN_3 because their high frequency dielectric constants are not known.

The magnitude of the absorption constant (10^2 to 10^3 cm^{-1}) of the band with multiple structure having a maximum around 2225 A (cf. Fig. 2) is relatively small for an allowed optical transitions due to excitons. On the other hand, it is difficult to attribute it to any impurity which would give rise to such a strong band without being detected by infrared measurements. Moreover it is unlikely that the same impurity would consistently appear in all the azides obtained from different sources. It seems more likely to be a transition of low probability to a low-lying excited state of the azide ion.[9] The multiple structure is similar to that found in alkali metal nitrates and nitrites which have been completely analyzed by Sayre[10] and Sidman.[11] The positions of the different peaks observed are listed in Table II. The fact that the band structure is temperature dependent and the average splitting between the bands is 1044 cm^{-1}, suggests that it may be due to the vibrational frequencies being superimposed on the electronic transition of the azide ion. Such frequencies would be characteristic of the excited state and would not be expected to correspond to the well known vibra-

[7] S. Nikitine, Phil. Mag. **4**, 1 (1959).

[8] R. W. Dreyfuss and P. W. Levy, Proc. Roy. Soc. (London) **A246**, 233 (1958).

[9] The author is greatly benefitted by the comment of the referee in this section of the discussion.

[10] E. V. Sayre, J. Chem. Phys. **31**, 73 (1959).

[11] J. W. Sidman, J. Am. Chem. Soc. **79**, 2669 (1957).

TABLE II. The band structure of alkali metal azides at 77.3°K.

NaN_3	λ in A	...	2382	2327	2275	2225	2160	...	...
	ν in cm^{-1}	...	41981	42974	43956	44944	46296	...	...
	$\Delta\nu$ in cm^{-1}		...	993	982	988	1352	...	...
KN_3	λ in A	...	2375	2325	2278	2228	2175	2125	2075
	ν in cm^{-1}	...	42105	43011	43898	44883	45977	47059	48193
	$\Delta\nu$ in cm^{-1}		...	906	887	985	1094	1082	1134
RbN_3	λ in A	...	2350	2300	2250	2220	2155	2088	...
	ν in cm^{-1}	...	42553	43478	44444	45454	46404	47893	...
	$\Delta\nu$ in cm^{-1}		...	925	966	1010	950	1489	...
CsN_3	λ in A	2445	2370	2322	2272	2225	2180	2125	...
	ν in cm^{-1}	40900	42194	43066	44014	44944	45871	47059	...
	$\Delta\nu$ in cm^{-1}		1294	872	948	930	927	1188	...

tion frequencies of the azide ion in the ground state. (The ground state vibrational frequencies of the azide ion are $\nu_1 \simeq 1350$ cm^{-1}, $\nu_2 \simeq 645$ cm^{-1}, and $\nu_3 \simeq 2070$ cm^{-1} of which ν_2 and ν_3 are infrared active.)

The observed structure in the fluorescence spectrum corresponds roughly to the ground state vibrational frequencies of the azide ion but the resolution is too poor to make any quantitative measurements. A rather large Stokes shift (about 2 ev) is observed and in this respect the behavior of the azide ion differs from that of the nitrite ion. The latter also shows a weak fluorescence[10,12] but the Stokes shift is small. A considerably extended investigation including a study of polarization and isotope effect is required before a complete assignment of the electronic and vibrational states of the azide ion be made.

The effect of x-ray irradiation does not alter the fine structure of the band at 2225 A, although a new band having a maximum at 2480 A appears, partially overlapping this band. By analogy with alkali halides the band at 2480 A has previously been identified by Cunningham and Tompkins[1] as the α band. The α band in alkali halides is unstable at room temperature, since the anion vacancy has a high probability of combining with a positive ion vacancy,[13] and moreover it appears very close to the fundamental absorption edge. The fact that the 2480 A band in alkali azides is stable at room temperature makes it unlikely to be an α band, and by analogy with alkali halides it appears more likely to be a kind of V center. The general increase in absorption around 2050 A (cf. Fig. 4) is perhaps due to the formation of another band which appears close to the fundamental absorption edge. The band at 3350 A has been identified as a V band.[1]

ACKNOWLEDGMENTS

I wish to express my sincere gratitude to Dr. J. H. Simpson for his advice, encouragement and critical comments. I also wish to thank Dr. J. Rolfe and Dr. F. R. Lipsett for helpful discussion. It is a pleasure to thank Dr. A. D. Yoffe, of Cavendish Laboratory, Cambridge, for providing the sample and for valuable suggestions. My thanks are also due to Mr. E. J. Bolton for his assistance in various aspects of the experimental work.

[12] J. W. Sidman, J. Am. Chem. Soc. **78**, 2911 (1956).

[13] C. J. Delbecq, P. Pringsheim, and P. Yuster, J. Chem. Phys. **19**, 574 (1951).

THE JOURNAL OF CHEMICAL PHYSICS VOLUME 35, NUMBER 6 DECEMBER, 1961

Molecular Weight Distribution of Polymers from Rheological Measurements in Dilute Solution

WARNER L. PETICOLAS

IBM Advanced Systems Development Division, San Jose, California

(Received May 29, 1961)

A method for obtaining the molecular weight distribution of linear polymers from rheological measurements in dilute solution is obtained through the use of the normal-coordinate theory of viscoelasticity as modified by Zimm to include hydrodynamic interactions.

Equations for the frequency-dependence of viscoelastic properties in dilute solutions are shown to the form $\Phi(\omega)=\Sigma_p\lambda_p^{-n}f(\omega\lambda_p^{-m})$, where $\Phi(\omega)$ is a measurable, frequency-dependent viscoelastic property. The summation extends over the set of characteristic values λ_p, which accounts for the relaxation of various normal modes of motion of the molecule as perturbed by hydrodynamic interaction with the solvent; and $f(\omega\lambda_1^{-m})$ is directly related to the molecular weight distribution through an integral equation

$$\lambda_1^{-n}f(\omega\lambda_1^{-m})=\int_0^\infty K(M,\omega)W(M)dM,$$

where $W(M)$ is the weight fraction of molecules in range dM at M and $K(M,\omega)$ is a kernel dependent upon the quantity measured. Inversion of the above summation has been accomplished for the particular case of characteristic values which obey the inequality, $\Sigma_p\lambda_p^{-n}<2\lambda_1^{-n}$, so that $f(\omega\lambda_1^{-m})$ may be obtained directly from the experimentally measured $\Phi(\omega)$. $W(M)$ is then obtained from $f(\omega\lambda_1^{-m})$ through a solution of the integral equation.

INTRODUCTION

RECENTLY the author and his fellow workers[1–4] have been devising methods for the experimental testing of the normal-coordinate theory of viscoelasticity[5–7] and for utilizing the theory to determine the molecular weight distribution of linear polymers. These two aims are not unrelated. It is doubtful that the normal-coordinate theory of viscoelasticity can be adequately tested until the effect of polydispersity is sufficiently well understood. In fact it may be shown that the predictions of the normal-coordinate theory are extremely sensitive to even slight departures from monodispersity.

In the past, very few measurements of the viscoelastic properties of dilute solutions of linear polymers have been made because of the great experimental difficulties involved in such measurements. However, Birnboim and Ferry[8] have recently designed an apparatus which appears to be very successful in measuring the complex viscosity of the dilute polymer solutions. Consequently an extension of our earlier calculations seems desirable and timely. Indeed the results of Birnboim and Ferry show that, in dilute solution, the experimental relaxation distribution functions approach a slope of $-2/3$ at short times as predicted by the theory of Zimm instead of a slope of $-1/2$ as predicted by the theory of Rouse and which is generally found in concentrated polymer systems.[9]

The purpose of this paper is to generalize the previous results[1,3] to the case of a nonfree draining polymer molecule in a solution with strong hydrodynamic interactions. This problem is more complicated since the characteristic values in this system are neither integers nor simply related to one another. Although the method developed here is applicable to any normal-coordinate treatment with nonintegral characteristic values, only the case of the frequency dependence of the viscosity of dilute solutions of whole polymers will be discussed.

COMPLEX VISCOSITY OF WHOLE POLYMERS

The pth relaxation time of a polymer molecule containing j monomers in a dilute solution of a whole polymer is given by[5,7]

$$\tau_{pj}=\rho b^2/6kT\lambda_{pj}, \tag{1}$$

where b^2 is the mean-square end-to-end length of a submolecule, ρ is the friction factor, λ_{pj} is the pth characteristic value of a polymer molecule containing j monomers. For dilute polymer solutions, Zimm has obtained the following equation for the characteristic values:

$$\lambda_{pj}=4N_j^{\frac{1}{2}}\lambda_p\rho/N_j^2(12\pi^3)^{\frac{1}{2}}b\eta_s, \tag{2}$$

where N_j is the number of submolecules in the jth polymer molecule, ρ is the friction factor, λ_p is the pth characteristic value as calculated by Zimm, Roe, and Epstein,[10] and η_s is the viscosity of the solvent.

[1] E. Menefee and W. L. Peticolas, Nature **189,** 745 (1961).
[2] J. E. Eldridge and W. L. Peticolas, J. Poly Sci. **51,** S38 (1961).
[3] E. Menefee and W. L. Peticolas, J. Chem. Phys. **35,** 946 (1961).
[4] W. L. Peticolas and E. Menefee, J. Chem. Phys. **35,** 951 (1961).
[5] P. E. Rouse, Jr., J. Chem. Phys. **21,** 1272 (1953).
[6] F. Bueche, J. Chem. Phys. **22,** 603 (1954).
[7] B. H. Zimm, J. Chem. Phys. **24,** 269 (1956).
[8] M. H. Birnboim and J. D. Ferry, Bull. Am. Phys. Soc. **6,** 127 (1961).
[9] J. D. Ferry, R. F. Landel, and M. L. Williams, J. Appl. Phys. **26,** 359 (1955).
[10] B. H. Zimm, G. M. Roe, and L. F. Epstein, J. Chem. Phys. **24,** 279 (1956).

The complex viscosity of a polymer in dilute solution is given by the equation[6,7]

$$\eta^*(\omega)-\eta_s=\sum_{j=1}^{\infty}(W_j/M_j)cRT\sum_{p=1}^{N}\tau_{pj}[1+i\omega\tau_{pj}]^{-1}, \quad (3)$$

where W_j is the weight fraction of the jth polymer molecule, $\eta^*(\omega)$ is the complex viscosity, c is the polymer concentration, and $i=(-1)^{\frac{1}{2}}$. Combining Eqs. (1)–(3) with the fact

$$\sum_{p=1}^{\infty}\lambda_p^{-1}=0.586,$$

we have the following result for the viscosity of a whole polymer at zero frequency,

$$\frac{\eta^*(0)-\eta_s}{c\eta_s}=[\eta(0)]=N_a(12\pi^3)^{\frac{1}{2}}0.586b^3\sum_j\frac{W_jN_j^{\frac{1}{2}}}{24M_j} \quad (4)$$

$$=2.84\times10^{23}\langle L^3/M\rangle_w, \quad (5)$$

where L is the root-mean-square end-to-end length of whole polymer chain defined by $L_j=N_j^{\frac{1}{2}}b$, and N_a is Avagadvo's number. Equation (5) is a statement for whole polymers of Zimm's result for polymer fractions.[7] If in Eq. (4) we assume that the number of submolecules N_i is proportional to the molecular weight, i.e., $N_i=KM_i$, we have

$$[\eta(0)]=N_a(12\pi^3)^{\frac{1}{2}}0.586(K^{\frac{1}{2}}b)^3\langle M^{0.5}\rangle_w$$

$$=2.84\times10^{23}(L_j^2/M_j)^{\frac{1}{2}}\langle M^{0.5}\rangle_w. \quad (6)$$

The dependence of the viscosity of the weight average of the square root of the molecular weight shows that these equations hold only in a Θ solvent,[11] a fact that must be kept in mind when attempting to apply them without further modification. If the viscosity is measured in a Θ solvent, $K^{\frac{1}{2}}b$ or L_j^2/M_j is a constant independent of the molecular weight.[11] However, in a non-Θ solvent, $K^{\frac{1}{2}}b=(N_j/M_j)^{\frac{1}{2}}b$ is a monotonic, increasing function of the molecular weight,[11] so that either N_j/M_j or b or both must be molecular weight dependent. Consequently it would be difficult to extend our discussion of whole polymers to non-Θ solvents. Actually, however, there is evidence which would indicate that Zimm's theory itself is more nearly correct for a Θ solvent. Indeed the failure of Zimm's theory to predict a dependence of intrinsic viscosity on steady-state shear rate is not so bad as it might first appear since data on polystyrene in a Θ solvent show only a very slight shear-rate dependence.[12]

Combining (1) and (6) we have

$$\tau_{pi}=\frac{[\eta(0)]\eta_sM_i^{\frac{1}{2}}}{0.586RT\langle M^{0.5}\rangle_w\lambda_p}. \quad (7)$$

It is interesting to observe that for a given temperature and solvent that the ratio of the intrinsic viscosity to the averaged molecular weight which appears in this equation is a constant independent of both molecular-weight and molecular-weight distribution, i.e.,

$$[\eta(0)]/\langle M^{0.5}\rangle_w=[\eta_j(0)]/M_j^{0.5}=K',$$

a constant, which in the Flory terminology[11] is $K'=\Phi'(L_0^2/M)^{\frac{1}{2}}$, where Φ' is the universal constant of Eq. (5) and L_0^2/M is independent of molecular weight.

A comparison with the corresponding calculation[1] for Rouse's theory shows the ratio $[\eta(0)]/\langle M\rangle_w$ should be a constant in this theory. This is, of course, the result one might expect for a dilute solution of a polymer in an extremely good solvent. Perhaps this is the explanation of why the data of Rouse and Sittel[13] for polystyrene in toluene, a very good solvent for polystyrene, agree so well with Rouse's unmodified theory.

Equation (7) may be written as

$$\tau_{pi}=BM_i^{\frac{1}{2}}\lambda_p^{-1}, \quad (8)$$

where

$$B=\eta_s[\eta(0)]/\langle M^{0.5}\rangle 0.586RT. \quad (9)$$

Consequently, Eq. (3) may be written as

$$\eta^*(\omega)-\eta_s=cBRT\sum_{p=1}^{N}\lambda_p^{-1}I^*(\omega\lambda_p^{-1}), \quad (10)$$

where

$$I^*(\omega\lambda_p^{-1})=\int_0^{\infty}\frac{M^{0.5}W(M)\,dM}{1+i\omega\lambda_p^{-1}BM^{\frac{1}{2}}}, \quad (11)$$

and where we have assumed a continuous distribution of molecular weights.

INVERSION OF THE SUM

Equation (10) is an equation of the general form

$$\Phi(\omega)=\sum_{p=1}^{N}\lambda_p^{-n}f(\lambda_p^{-m}\omega)=\text{Σ}_N\{f(\omega)\}, \quad (12)$$

where n and m are usually, but not necessarily, integers; the symbol Σ stands for this type of sum. Equations of this form may be inverted to give $f(\lambda_1^{-m}\omega)$ in terms of an infinite series of Φ's provided the λ_p's possess certain properties. If the characteristic values are integers this inversion may be performed using the theorem of Moebius.[14] However, the characteristic values of Zimm, Roe, and Epstein[10] are not integers and, except at large values, there is no simple relationship between them. This may often prove to be the case for problems of this type, so that it seems worthwhile to develop an inversion formula for equations of the form of Eq. (12) which will tend to hold under very general conditions. Such as equation can be developed as shown below.

[11] P. J. Flory, *Principles of Polymer Chemistry* (Cornell University Press, Ithaca, New York, 1953), p. 612.

[12] E. Passaglia, J. T. Yang, and N. Wegemer, J. Poly Sci. **47**, 333 (1960).

[13] P. E. Rouse and K. Sittel, J. Appl. Phys. **24**, 690 (1953).

[14] A. F. Moebius, J. Math. **9**, 105 (1832).

For an equation of the form of Eq. (12) we require that $\Phi(\omega)$ and $f(\omega)$ be finite and single-valued for all values of ω. Consequently, the right-hand side of Eq. (12) must converge for all values of ω. The function $f(\omega)$ will have a maximum value, which in our case is $f(0)$. Consequently at $\omega=0$ we have

$$\Phi(0)=f(0)\sum_{p=1}^{N}\lambda_p^{-n}.$$

From this we have the condition that

$$\sum_{p=1}^{N}\lambda_p^{-n}=\Lambda,$$

where Λ is finite and must remain finite even as N goes to infinity. In order to obtain an inverse of Eq. (12) we begin subtraction of

$$\sum_{j=2}^{N}(\lambda_j^{-n}\lambda_1^{n})\Phi(\lambda_j^{-m}\lambda_1^{m}\omega)$$

from both sides of Eq. (12) with the result

$$\Phi(\omega)-\sum_{j=2}^{N}(\lambda_j^{-n}\lambda_1^{n})\Phi(\lambda_j^{-m}\omega\lambda_1^{m})=\lambda_1^{-n}f(\lambda_1^{-m}\omega)$$

$$-\sum_{j=2}^{N}\sum_{i=2}^{N}\lambda_i^{-n}\lambda_j^{-n}\lambda_1^{n}f(\lambda_i^{-m}\lambda_j^{-m}\lambda_1^{m}\omega). \quad (13)$$

Thus we have the desired term $\lambda_1^{-n}f(\lambda_1^{-m}\omega)$ plus a remainder. Adding an additional term gives

$$\Phi(\omega)-\sum_{j=2}^{N}\lambda_j^{-n}\lambda_1^{n}\Phi(\lambda_j^{-m}\lambda_1^{m}\omega)$$

$$+\sum_{k=2}^{N}\sum_{j=2}^{N}\lambda_j^{-n}\lambda_k^{-n}\lambda_1^{2n}\Phi(\lambda_j^{-m}\lambda_k^{-m}\lambda_1^{2m}\omega)$$

$$=\lambda_1^{-n}f(\lambda_1^{-n}\omega)$$

$$+\sum_{k=2}^{N}\sum_{j=2}^{N}\sum_{i=2}^{N}\lambda_1^{2n}\lambda_i^{-n}\lambda_j^{-n}\lambda_k^{-n}f(\lambda_i^{-m}\lambda_j^{-m}\lambda_k^{-m}\lambda_1^{2m}\omega), \quad (14)$$

which again leaves the desired term plus a remainder. Continuing this process we find the remainder is a sum of the terms of the form

$$\lambda_1^{(\alpha-1)n}\lambda_i^{-n}\lambda_j^{-n}\cdots\lambda_l^{-n}f(\lambda_i^{-m}\lambda_j^{-m}\cdots\lambda_l^{-m}\lambda_1^{(\alpha-1)m}\omega),$$

where $\lambda_i^{-n}\lambda_j^{-n}\cdots\lambda_l^{-n}$ is a product of the reciprocal of α characteristic values.

The criteria convergence of the inversion may be shown as follows: The function $f(\omega)$ has its largest value at some value of ω, which for our specific case is $\omega=0$. If the remainder converges to zero at this value of ω, it must converge for all other values of ω. The difference in absolute values between two successive remainders of the $(\alpha+1)$th and αth terms, respectively, is

$$\sum_{i=2}^{N}\sum_{j=2}^{N}\cdots\sum_{l=2}^{N}\sum_{p=2}^{N}\lambda_1^{\alpha n}\lambda_i^{-n}\lambda_j^{-n}\cdots\lambda_l^{-n}\lambda_p^{-n}f(0)$$

$$\{\alpha+1 \text{ sums in all}\}$$

$$-\sum_{i=2}^{N}\sum_{j=2}^{N}\cdots\sum_{l=2}^{N}\lambda_1^{(\alpha-1)n}\lambda_i^{-n}\lambda_j^{-n}\cdots\lambda_l^{-n}f(0)$$

$$\{\ \alpha \text{ sums in all}\ \}$$

$$=[\sum_{j=2}^{N}\lambda_j^{-n}\lambda_1^{n}]^{\alpha}\lambda_1^{-n}f(0)[\sum_{j=2}^{N}\lambda_j^{-n}\lambda_1^{n}-1].$$

Consequently if

$$\lim_{\alpha\to\infty}(\sum_{j=2}^{N}\lambda_j^{-n}\lambda_1^{n})^{\alpha}=0$$

the series will converge. This will be true if

$$\sum_{j=2}^{N}\lambda_j^{-n}/\lambda_1^{-n}<1$$

or

$$\sum_{j=1}^{N}\lambda_j^{-n}<2\lambda_1^{-n}. \quad (15)$$

For the characteristic values of Rouse, $\lambda_p=p^2$ and

$$\sum_{p=1}^{\infty}\lambda_p^{-1}=\pi^2/6.$$

Since $\pi^2/6\simeq1.7<2$, this criterion holds for Rouse's characteristic values. For the characteristic values of Zimm, Roe, and Epstein,

$$\sum_{p=1}^{\infty}\lambda_p^{-1}\simeq0.586$$

and $\lambda_1^{-1}\simeq0.25$ so that $\sum\lambda_p^{-1}>2\lambda^{-1}$ and this inversion formula will not converge. However,

$$\sum_{p=1}^{\infty}\lambda_p^{-2}=0.0703<2\lambda_1^{-2}=0.124,$$

so that an equation of the form

$$\Phi'(\omega)=\sum_{p=1}^{N}\lambda_p^{-1}(d/d\omega)f(\lambda_p^{-1}\omega)=\sum_{p=1}^{N}\lambda_p^{-2}f'(\lambda_p^{-1}\omega) \quad (16)$$

could be inverted, provided $\Phi'(\omega)$ and $f'(\omega)$ are everywhere finite. The derivative of Eq. (12) is

$$\eta^{*\prime}(\omega)=cB^2RT\sum_{p}\lambda_p^{-2}I^{*\prime}(\omega\lambda_p^{-1}), \quad (17)$$

where

$$I^{*}(\omega\lambda_p^{-1})=-i\int_0^{\infty}\frac{M^2W(M)dM}{(1+i\omega\lambda_p^{-1}BM^3)^2}. \quad (18)$$

Equation (17) has the disadvantage that the integral equation (18) is relatively difficult to solve, even for $p=1$.

An alternative way of meeting this problem is to use the imaginary part of the complex viscosity (or the real part of the complex modulus) divided by the frequency as follows:

$$\mathcal{I}[-\eta^*(\omega)/\omega]=\mathrm{Re}[G^*(\omega)/\omega^2]\equiv\xi(\omega)$$
$$\xi(\omega)=cB^2RT\sum_p\lambda_p^{-2}I_2(\omega\lambda_p^{-1}), \quad (19)$$

where

$$I_2(\omega\lambda_p^{-1})=\int_0^\infty\frac{M^2W(M)\,dM}{1+\omega^2B^2\lambda_p^{-2}M^3}. \quad (20)$$

Before solving for $I_2(\omega\lambda_1^{-1})$ in terms of $\xi(\omega)$ we observe that Eq. (14) may be simplified as shown in the appendix to obtain a sum of N terms rather than an infinite number. Such a sum is still rather tedious to write out so, for the present, we will deal with Eq. (14) symbolically. Consequently, if

$$\Phi(\omega)=\sum_{p=1}^N\lambda_p^{-n}f(\lambda_p^{-m}\omega)=\mathfrak{S}_N\{f(\omega)\}$$

and if

$$\sum_{i=1}^N\lambda_i^{-n}<2\lambda_1^{-n},$$

then the inverse $\mathfrak{S}^{-1}$ exists and we may write

$$\lambda_1^{-n}f(\lambda_1^{-n}\omega)=\mathfrak{S}^{-1}\{\Phi(\omega)\}. \quad (21)$$

The exact evaluation of the shortest form for $\mathfrak{S}^{-1}\{\Phi(\omega)\}$ will be described in the Appendix. However, if $\Phi(\omega)$ is known for all values of ω, then $f(\lambda_1^{-m}\omega)$ may be obtained from this equation.

SOLUTION OF THE INTEGRAL EQUATION

If, in Eqs. (12), and (21) we set $m=1$, $n=2$,

$$\Phi(\omega)=\xi(\omega), \quad \lambda_p^{-n}f(\lambda_p^{-m}\omega)=\lambda_p^{-2}cB^2RTI_2(\omega\lambda_p^{-1}),$$

we have the following integral equation:

$$cB^2RT\lambda_1^{-2}\int_0^\infty\frac{M^2W(M)\,dM}{1+\omega^2B^2\lambda_1^{-2}M^3}=\mathfrak{S}^{-1}\{\xi(\omega)\};$$

making the substitution, $z=\lambda_1^2B^{-2}M^{-3}$, and $y=\omega^2$, we have

$$\int_0^\infty\frac{G(z)dz}{y+z}=\mathfrak{S}^{-1}\{\xi(\omega)\}=\mathbf{St}\{G(z)\}, \quad (22)$$

where **St** is the Stieltjes transform operator and $G(z)=(cRT/3z)W(B^{-2/3}\lambda_1^{2/3}z^{-1/3})$. Using the inverse Stieltjes operator $\mathbf{St}^{-1}$ we may write the weight distribution function

$$W(M)=\frac{3\lambda_1^2B^{-2}M^{-3}}{cRT}\mathbf{St}^{-1}\mathfrak{S}^{-1}\{\xi(\omega)\}, \quad (23)$$

where $M=(\lambda_1/\omega B)^{2/3}$. Using the inverse Stieltjes operator of Hirshmann and Widder[15] we obtain

$$W(M)=\frac{3\lambda_1^{-2}B^{-2}M^{-3}}{cRT}\lim_{\nu\to\infty}(-1)^\nu(e/\nu)^{2\nu}\frac{d^\nu}{d(\omega^2)^\nu}$$
$$\times\left[\omega^{4\nu}\frac{d^\nu}{d(\omega^2)^\nu}\mathfrak{S}^{-1}\{\xi(\omega)\}\right]. \quad (24)$$

For very broad molecular weight distribution $\nu=1$ or $\nu=2$ will generally suffice. For distribution containing sharp curves or corners, this is not a practical method, and numerical methods for the inverse of this integral equation must be found. The type of numerical method selected will depend to some extent upon the type of data under study. An excellent discussion of numerical solutions of integral equations is given by Kopal.[16] One of the simplest numerical methods is the conversion of Eq. (22) into a series of nonhomogeneous simultaneous equations using a quadrature formula to express the integral as a sum. Such a procedure gives the molecular weight distribution from matrix inversion of the simultaneous equations.

Sums of the form of Eq. (21) as well as matrix inversions are easily performed by use of modern high-speed computers.

APPENDIX

The infinite sum $\mathfrak{S}^{-1}\{\Phi(\omega)\}$ may be written

$$\Phi(\omega)+(-\lambda_1^n)\sum_{j=2}^N\lambda_j^{-n}\Phi(\lambda_j^{-m}\lambda_1^m\omega)+(-\lambda_1^n)^2$$
$$\times\sum_{k=2}^N\sum_{j=2}^N\lambda_j^{-n}\lambda_k^{-n}\Phi(\lambda_j^{-m}\lambda_k^{-m}\lambda_1^{2m}\omega)$$
$$+(-\lambda_1^n)^3\sum_{i=2}^N\sum_{j=2}^N\sum_{k=2}^N\cdots, \quad (25)$$

where each term contains an increasing number of sums of products, and there are an infinite number of terms. This sum may be simplified considerably. The index number of a term is defined as the number of sums (or products) it contains. We will call an internal term a particular product in some given term.

Let us consider a particular term, say, for example, the fourth term. This term has an index number of 4 and may be written

$$(-\lambda_1^n)^4\sum_{i=j}^N\sum_{j=2}^N\sum_{k=2}^N\sum_{l=2}^N\lambda_i^{-n}\lambda_j^{-n}\lambda_k^{-n}\lambda_l^{-n}$$
$$\times\Phi(\lambda_i^{-m}\lambda_j^{-m}\lambda_k^{-m}\lambda_l^{-m}\omega). \quad (26)$$

When all of the subscripts are different there will be 4! internal terms of exactly the same quantity. Thus all of the internal terms with unlike indices of index number

[15] I. I. Hirshmann and D. V. Widder, *The Convolution Transform* (Princeton University Press, Princeton, New Jersey, 1955).
[16] Z. Kopal, *Numerical Analysis* (John Wiley & Sons, Inc., New York, 1955).

4 may be grouped together to give

$$4!(-\lambda_1{}^n)^4\sum_{i>j>k>l\geq 2}^{N}\sum^{N-1}\sum^{N-2}\sum^{N-3}\lambda_i{}^{-n}\lambda_j{}^{-n}\lambda_k{}^{-n}\lambda_l{}^{-n}$$
$$\times\Phi(\lambda_i{}^{-m}\lambda_j{}^{-m}\lambda_k{}^{-m}\lambda_l{}^{-m}\lambda_1{}^{4m}\omega).$$

Similarly there will be only one of each internal term of index 4 with identical indices,

$$(-\lambda_1{}^n)^4\sum_{i=2}^{N}\lambda_i{}^{-4n}\Phi(\lambda_i{}^{-4m}\lambda_1{}^{4m}\omega).$$

In general there will be an internal term for each partition of the index number, in this case 4. The partitioning of 4 may be illustrated as follows:

1/1/1/1 all different
1 1/1/1 two alike; two different
1 1/1 1 two alike; two alike
1 1 1/1 three alike; one different
1 1 1 1 four alike.

The collection of internal terms illustrated above are for the first and last of these partitions. The collection together of all of the internal terms of index 4 in which two indices are alike and two are different gives

$$\frac{4!}{2!1!1!}(-\lambda_1{}^n)^4\sum_{i>j>k\geq 2}^{N}\sum^{N-1}\sum^{N-2}[\lambda_i{}^{-2n}\lambda_j{}^{-n}\lambda_k{}^{-n}$$
$$\times\Phi(\lambda_i{}^{-2m}\lambda_j{}^{-m}\lambda_k{}^{-m}\lambda_1{}^{4m}\omega)$$
$$+\lambda_i{}^{-n}\lambda_j{}^{-2n}\lambda_k{}^{-n}\Phi(\lambda_i{}^{-m}\lambda_j{}^{-2m}\lambda_k{}^{-m}\lambda_1{}^{4m}\omega)$$
$$+\lambda_i{}^{-n}\lambda_j{}^{-n}\lambda_k{}^{-2n}\Phi(\lambda_i{}^{-m}\lambda_j{}^{-m}\lambda_k{}^{-2m}\lambda_1{}^{4m}\omega)]. \quad (27)$$

It should be noted that the three expressions in the brackets arise from the fact that $i>j>k\geq 2$ so that $\lambda_i{}^{2n}$ can never equal $\lambda_j{}^{2n}$. The internal term for the partitioning into two alike and two alike is given by

$$\frac{4!}{2!2!}(-\lambda_1{}^n)^4\sum_{i>j\geq 2}^{N}\sum^{N-1}\lambda_i{}^{-2n}\lambda_j{}^{-2n}\Phi(\lambda_i{}^{-2m}\lambda_j{}^{-2m}\omega). \quad (28)$$

For the αth term, there will be a collection of internal terms for each of the partitions of α. If these collections of internal terms are all added together, they equal the original sum, but, all of the terms in the new sum are now completely different from each other. This results in an enormous reduction in work necessary to compute $\mathfrak{S}^{-1}\{\Phi(\omega)\}$.

The new terms may be written as follows:

$$\mathfrak{S}^{-1}\{\Phi(\omega)\}=\Phi(\omega)+\sum_{\nu=1}^{\infty}\sum_{i=2}^{N}(-\lambda_1{}^n)^\nu\lambda_i{}^{-n\nu}$$
$$\times\Phi(\lambda_1{}^{m\nu}\lambda_i{}^{-m\nu}\omega)+\sum_{\mu=1}^{\infty}\sum_{\nu=1}^{\infty}\sum_{j>i\geq 2}^{N}\sum^{N-1}(-\lambda_1{}^n)^{\nu+\mu}$$
$$\times\frac{(\nu+\mu)!}{\nu!\mu!}\lambda_i{}^{-n\nu}\lambda_j{}^{-n\nu}\Phi(\lambda_1{}^{m\nu+m\mu}\lambda_i{}^{-m\nu}\lambda_j{}^{-m\mu}\omega)$$
$$+\sum_{\nu=1}^{\infty}\sum_{\mu=1}^{\infty}\sum_{\gamma=1}^{\infty}\sum_{k>j>i\geq 2}^{N}\sum^{N-1}\sum^{N-2}(-\lambda_1{}^n)^{\nu+\mu+\gamma}\frac{(\nu+\mu+\gamma)!}{\mu!\nu!\gamma!}$$
$$\times\lambda_i{}^{-n\nu}\lambda_j{}^{-n\mu}\lambda_k{}^{-m\gamma}\Phi(\lambda_1{}^{m\nu+m\mu+m\nu}\lambda_i{}^{-m\nu}\lambda_j{}^{-m\mu}\lambda_k{}^{-m\gamma})+\cdots. \quad (29)$$

The summations over the Greek indices are summations due to the partitions of the index numbers and extend to infinity since the index numbers themselves extend to infinity, while the summations over the italic indices are over the characteristic values and extend only to N.

In the double sum we have collected all of the internal terms which result from partitions containing the whole index number. In the quadruple sum, we have collected all of the internal terms which arise by partitioning of the index numbers into two parts with ν alike in the first part and μ alike in the second. Similarly in the sextuple sum, we have collected all of the internal terms which arise because of the partitioning of the index numbers into three partitions. This process may be continued up to the point where the number of sums over the characteristic values approaches the actual number of the characteristic values. The very last term of Eq. (29) will contain no sums over the characteristic values but only over the partition. This follows from the fact that it is impossible to partition an index number larger than $(N-1)$ into more than $(N-1)$ partitions without some of the partitions containing identical elements. Thus the last term of Eq. (29) consists of exactly $N-1$ sums and may be written as

$$\sum_{\nu=1}^{\infty}\sum_{\mu=1}^{\infty}\sum_{\gamma=1}^{\infty}\cdots\sum_{\zeta=1}^{\infty}(-\lambda_1{}^n)^{\nu+\mu+\gamma+\ldots+\zeta}$$
$$\times\frac{(\nu+\mu+\gamma+\cdots+\zeta)!}{\nu!\mu!\gamma!\cdots\zeta!}\lambda_2{}^{-n\nu}\lambda_3{}^{-n\mu}\lambda_4{}^{-n\gamma}\cdots\lambda_N{}^{-n\zeta}$$
$$\times\Phi(\lambda_1{}^{m(\nu+\mu+\gamma+\ldots+\zeta)}\lambda_2{}^{-m\nu}\lambda_3{}^{-m\mu}\lambda_4{}^{-m\gamma}\cdots\lambda_N{}^{-m\zeta}\omega). \quad (30)$$

For high-molecular-weight polymers, N is generally taken as infinitely large. For low-molecular-weight polymers N may actually be fairly small. The points made above may be very easily illustrated with $N=3$, which might be an actual value for a very short polymer chain. For $N=3$,

$$\Phi(\omega)=\mathfrak{S}_3\{f(\omega)\}=\sum_{i=1}^{3}\lambda_i{}^{-n}f(\lambda_i{}^{-m}\omega), \quad (31)$$

and

$$\lambda_1{}^{-n}f(\lambda_1{}^{-m}\omega)=\mathfrak{S}^{-1}\{\Phi(\omega)\}$$
$$=\Phi(\omega)+\sum_{\nu=1}^{\infty}\sum_{i=2}^{3}(-\lambda_1{}^n)^\nu\lambda_i{}^{-n\nu}\Phi(\lambda_1{}^{m\nu}\lambda_2{}^{m\nu}\omega)$$
$$+\sum_{\nu=1}^{\infty}\sum_{\mu=1}^{\infty}(-\lambda_1{}^n)^{\nu+\mu}\frac{(\nu+\mu)!}{\nu!\mu!}$$
$$\times\lambda_2{}^{-n\nu}\lambda_3{}^{-n\mu}\Phi(\lambda_1{}^{m\nu+m\mu}\lambda_2{}^{-m\nu}\lambda_3{}^{-m\mu}\omega). \quad (32)$$

Thus the very complicated sum of Eq. (25) containing an infinite number of terms may be replaced with a sum which contains only N terms; in this case $N=3$.

In our previous publication, Menefee and the author[1] gave a recursion formula for use in the inversions of finite sums where the characteristic values were integers. It appears, however, that for finite sums, the approach outlined here might be preferable even when the characteristic values are integers.

THE JOURNAL OF CHEMICAL PHYSICS VOLUME 35, NUMBER 6 DECEMBER, 1961

Solvent Effects on Optical Rotation and Dipole Moment

A. J. MUKHEDKAR
Department of Chemistry, University of Poona, India
(Received November 14, 1960)

It has been observed that the solvent effect on optical rotation goes hand in hand with the parallel effect on dipole moment, especially when the important dipoles are directly attached to the asymmetric center

$$\beta_\lambda = a\mu + \{\beta_\lambda^0 - a\mu^0\}.$$

Here a is relative deformability constant and β and μ are the rotational parameter and the dipole moment, respectively; the superscript zero, indicates that property belongs to the molecule in the ideal state. The values of β_{589}^0 for a given substance in different solvents are comparable ($\sim 1.1\times10^{-32}$ for d-camphor and $\sim 3.65\times10^{-32}$ for α-d-bromocamphor).

1. INTRODUCTION

THE simultaneous study of the solvent effect on optical rotation and electric polarization of the same solute species has been made with a view to determining whether a correlation exists between the two. In previous communications[1,2] the author has pointed out that a relation between the properties of the solvent, such as refractive index or dielectric constant and the optical rotation of the solute, will not be simple; however, the data in structurally related solvents can be compared satisfactorily. The correlation between the dipole moment of the solvent molecule and the optical rotation of the solute is not warranted, as the optical rotations in solvents having the same dipole moment are quite different,[3] showing the role of the sense of the dipole. Beckman[4] correlated the polarization of the solvent with the rotivity; Beckman's relationship has been satisfactorily tested by Beckman [4a,3d] and Gutzwiller[5]; however, the relation is based on the assumption that the polarization of the solute, which is dipolar, remains the same in a variety of binary solvents used. It was further assumed that the polar molecules of the polar component of a binary solvent are independent of one another.

The dipole moment of a molecule is the resultant of a vector addition of the component dipoles, including the intramolecular solvent effect (such as rotation of the component dipoles about bonds and electron displacements). Optical activity, which is related to the component dipoles, especially when strong polar groups (chromophores) are directly attached to the asymmetric center, might therefore be expected to be influenced by environmental effects similar to those on the dipole moment.

For a comparative study the equations for molar rotation and polarization must be deduced using related assumptions. Molecular properties may be determined by using the simple equations for "gases"; the difference in the observed (solution) and gas (ideal state) values can be considered as a measure of the solvent effect. Here the equation for gases implies that there are no important intermolecular forces. Under these conditions, as Debye[6] suggested, the effective field acting on a molecule is equal to the field applied.

$$F = E. \tag{1}$$

By this simple assumption it is not at all necessary to get into vague ideas about the molecular shape, distribution integrals, and the contribution of different types of intermolecular forces as long as the two properties for our "comparative study" are governed broadly by similar factors.

With assumption (1) we get the equation for orientation polarization identical with that derived by Jatkar[7] for gases, viz.,

$$P_0 = 4\pi N\mu^2/3kT. \tag{2}$$

By using the modified equation for electric polarization and Maxwell's equations for electromagnetic radiation, the relation between the molar rotation $[M]_\lambda$, and the microscopic property expressed by the rotational parameter β_λ, is given by

$$[M]_\lambda = (16\pi^3/\lambda^2)N\beta_\lambda. \tag{3}$$

Here the symbols have the usual significance.[8] The relation (3) clearly shows that any changes in the rotational parameter β, which is related to the matrix components of dielectric and magnetic moments in the transitions responsible for the origin of optical

[1] A. J. Mukhedkar, J. Univ. Poona **18,** 41 (1960).
[2] A. J. Mukhedkar, Z. physik Chem. **25,** 56 (1960).
[3] (a) H. G. Rule and J. P. Cunningham, J. Chem. Soc. **1935,** 1038; (b) H. G. Rule and J. Crawford, *ibid.* **1937,** 138; (c) H. G. Rule and A. R. Chambers, Nature **133,** 910 (1934); (d) H. C. Marks and C. O. Beckman, J. Chem. Phys. **8,** 831 (1940).
[4] (a) C. O. Beckman and K. Cohen, J. Chem. Phys. **4,** 784 (1936); (b) C. O. Beckman and H. C. Marks, *ibid.* **8,** 827 (1940).
[5] N. Gutzwiller, Helv. Phys. Acta **18,** 497 (1945).
[6] P. Debye, *Polar Molecules* (The Chemical Catalog Company, New York, 1929), p. 12.
[7] S. K. K. Jatkar, Nature **153,** 222 (1944). It is interesting to note that μ_{apparent} calculated by the Jatkar equation: $\mu_{\text{apparent}} = (4\pi N\mu^2/3kT)[(J+1)/J]$, $2J+1=2$ for liquids and solutions are close to the theoretical values (Tables I–IX). Jatkar *et al.* have shown the validity of the equation in a large number of published papers.
[8] E. U. Condon, Revs. Modern Phys. **9,** 432 (1937).

TABLE I. *d*-Camphor in *n*-heptane. Temperature = 300° ± 0.1°K. Physical constants of *n*-heptane: density $d^{27} = 0.6762$; dielectric constant, $\epsilon^{27} = 1.85_3$; refractive index, $n_D^{27} = 1.3842$.

Mole fraction of *d*-camphor f_2	$r = \frac{\epsilon-1}{\epsilon+2}$	Apparent D: $P_0 = \frac{4\pi N\mu^2}{3kT}$	Apparent D: $P_0 = \frac{4\pi N\mu^2}{kT}$	$\beta_{546} \times 10^{32}$	Rotational parameter $k \times 10^{-2}$
0.0117	0.2424	4.12	2.38	1.128	2.402
0.0212	0.2556	4.14	2.39	1.130	2.402
0.0442	0.2874	4.12	2.38	1.132	2.402
0.0642	0.3087	4.14	2.39	1.127	2.402
0.1442	0.3940	4.12	2.38	1.127	2.402
0.3169	0.5160	4.10	2.37	1.128	2.402
0.3253	0.5313	4.14	2.39	1.128	2.402

TABLE II. α-*d*-Bromocamphor in *n*-heptane. Temperature = 300° ± 0.1°K. Physical constants of *n*-heptane: density $d^{27} = 0.6763$ dielectric constant, $\epsilon^{27} = 1.85_3$; refractive index, $n_D^{27} = 1.3840$.

Mole fraction of α-*d*-bromo-camphor f_2	$r = \frac{\epsilon-1}{\epsilon+2}$	Apparent D: $P_0 = \frac{4\pi N\mu^2}{3kT}$	Apparent D: $P_0 = \frac{4\pi N\mu^2}{kT}$	$\beta_{546} \times 10^{32}$	Rotational parameter $k \times 10^{-2}$
0.0041	0.2246	5.26	3.04	4.139	8.80
0.0104	0.2453	5.26	3.04	4.142	8.80
0.0221	0.2640	5.16	2.98	4.155	8.80
0.0340	0.2948	5.11	2.95	4.140	8.80
0.0433	0.3041	5.33	3.08	4.137	8.80
0.0606	0.3274	5.21	3.01	4.133	8.80

TABLE III. *d*-Camphorquinone in *n*-heptane. Temperature 300° ± 0.1°K. Physical constants of *n*-heptane: density $d^{27} = 0.6765$; dielectric constant, $\epsilon^{27} = 1.91$; refractive index, $n_D^{27} = 1.3841$.

Mole fraction of *d*-camphor-quinone f_2	$r = \frac{\epsilon-1}{\epsilon+2}$	Apparent D: $P_0 = \frac{4\pi N\mu^2}{3kT}$	Apparent D: $P_0 = \frac{4\pi N\mu^2}{kT}$	Molar rotation $-[M]_{\lambda m\mu}$: 644	589	546	517	486	436
0.0019	0.2368	5.14	2.97	916.6	1576	2535	4880	7530	−425
0.0038	0.2413	5.14	2.97	961.4	1606	2770	4840	5418	560.4
0.0060	0.2454	5.11	2.95	984.6	1644	2592	4780	4392	780
0.0080	0.2500	5.06	2.92	1010	1665	2593	4750	4191	820
0.0099	0.2543	5.16	2.98	1035	1673	2611	4730	3883	892
0.0136	0.2614	5.16	2.98	1050	1710	2640	4700	3629	939

activity, are directly reflected in the observed molar rotation.

When comparing the solvent effect on optical rotation and dipole moment, the assumption that these two properties vary linearly with the solvent field can be used without much appreciable error, especially when there is only one type of solute and solvent molecular species present in solution. We write

$$\beta_\lambda = \beta_\lambda^0 + \beta_\lambda' F, \tag{4}$$

$$\mu = \mu^0 + \mu' F. \tag{5}$$

Here β' and μ' are the deformability constants and the superscript ^{0} refers to the corresponding property in the ideal state. The validity of these assumptions is critically discussed by Eyring[9] and Mukhedkar.[10]

If the two molecular properties are studied under the same experimental conditions, the relation between the two apparent properties is

$$\beta_\lambda = (\beta_\lambda'/\mu')\mu + \{\beta_\lambda^0 - (\beta_\lambda'/\mu')\mu^0\}. \tag{6}$$

Assuming the rotational and dipole moment deformability constants to be constant, one expects a straight line when apparent dipole moment is plotted against apparent rotational parameter (or the apparent molar rotation).

2. EXPERIMENTAL

d-Camphor (B.D.H.) was purified by repeated crystallization from alcohol and vacuum sublimation. *α-d*-Bromocamphor was crystallized from alcohol, dried in vacuum, and stored in the dark. *d*-Camphorquinone was prepared from *d*-camphor by Riley's selenium dioxide method.[11] The solvents used in the present work were purified by standard methods. A slight variation in the physical constants of a given solvent depends on the efficiency of fractionation, especially for *n*-heptane.

Dielectric constant measurements were made with a resonance-type oscillator circuit. Rotatory dispersion was studied on a photoelectric spectropolarimeter.[12] Infrared spectra were determined on Beckman IR4 spectrophotometer.

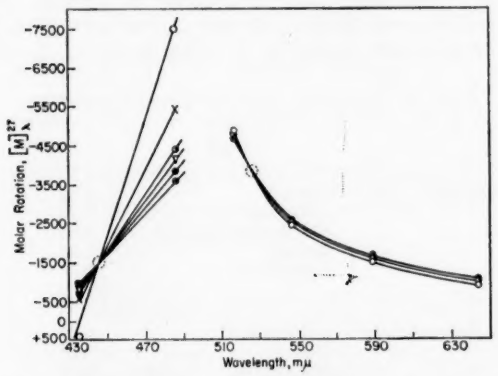

FIG. 1. Rotary dispersion of *d*-camphorquinone in *n*-heptane. Mole fraction of *d*-camphorquinone: ○, 0.0019; ×, 0.0038; ◑, 0.0060; ▽, 0.0080; ●, 0.0099; ⊕, 0.136.

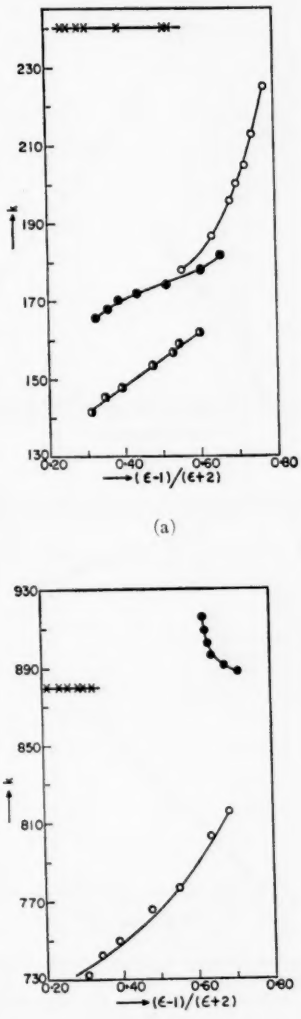

FIG. 2. Relation between dielectric constant ϵ and rotational parameter k. (a) *d*-camphor. ×, *n*-heptane; ●, carbon tetrachloride; ◑, benzene; ○, chloroform. (b) *α-d*-bromocamphor. ×, *n*-heptane; ●, ethylacetate; ○, benzene.

[9] W. J. Kauzmann, J. Walter and H. Eyring, Chem. Revs. **26,** 339 (1940).

[10] A. J. Mukhedkar, Ph.D. thesis, University of Poona, India, 1959.

[11] W. C. Evans, J. M. Ridgon and J. L. Simonsen, J. Chem. Soc. **1934,** 137.

[12] A. J. Mukhedkar, J. Univ. Poona **18,** 19 (1960).

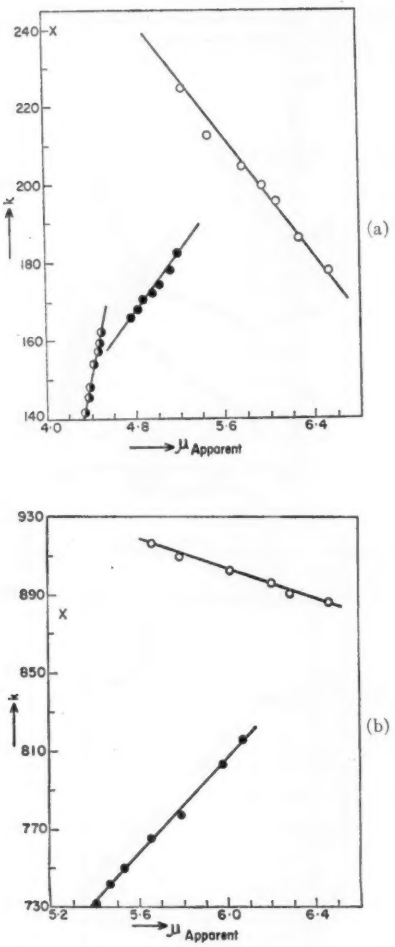

FIG. 3. Relation between apparent dipole moment $\mu_{apparent}$ and rotational parameter k. (a) d-camphor. ×, n-heptane; ◑, benzene; ●, carbon tetrachloride; ○, chloroform. (b) α-d-bromocamphor. ×, n-heptane; ●, benzene; ○, ethylacetate.

3. RESULTS AND DISCUSSION

The equation (6) was experimentally verified by the concentration effect on the apparent dipole moment and optical rotation; the study was simplified by considering solvents containing only one molecular species and solutes containing important dipoles directly attached to the asymmetric center.

The rotatory dispersion and apparent dipole moment of d-camphor and α-d-bromocamphor in n-heptane (Tables I and II) are independent of concentration in the concentration range studied; the deformability constants, β_λ' and μ', tend to zero in these systems indicating very weak or no solvent-solute interaction. However, the rotatory dispersion of d-camphorquinone in n-heptane, unlike its electric polarization, varies appreciably with concentration (Table III); the sign of the optical rotation at 440 mμ changes in dilute solutions ($f_2 \leq 0.0019$). The isorotation points at 448 mμ and 520 mμ in the rotatory dispersion curves (Fig. 1) and the deviation from Beers' law of the absorption spectra even in dilute solutions suggest the presence of two spatial isomers, the equilibrium between which changes with the dielectric constant of the medium. Infrared spectra of these compounds in carbon tetrachloride show the following ketonic frequencies:

	cm^{-1}	Intensity
d-camphor	1747	strong
d-camphorquinone	1759	strong
	1775	medium
α-d-bromocamphor	1762	strong.

It is therefore clear that the two isomers of d-camphorquinone are due to the repulsion between the two α-keto groups similar to that present in α-halocyclanones and α-brominated ketosteroids[13]; the projection angle between the two keto groups will be of opposite sign in the two isomers. A slight change in the magnitude of the projection angle will not produce any observable change in electric polarization, while a sensitive property, like optical rotation, which depends both on sign and magnitude of the projection angles of the dipoles attached to the active center will show an observable difference. The presence of two molecular species of d-camphorquinone limits our study to d-camphor and α-d-bromocamphor.

It is observed[10] from rotatory dispersion equations which hold good in the visible range that the characteristic wavelength remains the same throughout the concentration range in the same solvent and it does not change appreciably in a variety of solvents. (d-camphor $\lambda_0 \simeq 0.320\ \mu$; α-d-bromocamphor $\lambda_0 \simeq 0.290\ \mu$.) The rotational parameter k, which is related to the

TABLE IV. Values of d-camphor and α-d-bromocamphor.

	Solvent	$\beta_{589}^{\circ} \times 10^{32}$[a]
d-Camphor	Vapor	0.97
	n-Heptane	1.23
	Carbon tetrachloride	0.94
	Benzene	1.28
	Chloroform	1.16
		Mean 1.11
α-d-Bromocamphor	n-Heptane	3.89
	Benzene	3.15
	Ethylacetate	3.91
		Mean 3.65

[a] The values of μ° used in the calculation of β° are $\mu_{apparent}$ in n-heptane; $\mu^{\circ}d$-camphor $= 4.13D$, $\mu^{\circ}\alpha$-d-bromocamphor $= 5.25D$

[13] E. J. Corey, J. Am. Chem. Soc. **75,** 2301, 3297, 4832 (1953); Experimentia **9,** 329 (1953); J. Am. Chem. Soc. **76,** 175 (1954); R. C. Cookson, J. Chem. Soc. **1954,** 282; R. N. Jones, D. A. Ramsay, F. Herling, and K. Dobriner, J. Am. Chem. Soc. **74,** 2828 (1952).

TABLE V. *d*-Camphor in carbon tetrachloride. Temperature = 300° ± 0.1°K. Physical constants of carbon tetrachloride: density $d^{27} = 1.5800$; dielectric constants, $\epsilon^{27} = 2.22_0$; refractive index, $n_D^{27} = 1.4564$.

Mole fraction of *d*-camphor f_2	$r = \frac{\epsilon-1}{\epsilon+2}$	Apparent D: $P_0 = \frac{4\pi N\mu^2}{3kT}$	Apparent D: $P_0 = \frac{4\pi N\mu^2}{kT}$	$\beta_{546} \times 10^{33}$	Rotational parameter $k \times 10^{-2}$
0.00951	0.3258	4.76	2.75	9.02	1.657
0.03012	0.3616	4.83	2.79	9.139	1.680
0.04600	0.3840	4.88	2.82	9.217	1.702
0.1136	0.4898	4.97	2.87	9.385	1.720
0.1528	0.5160	5.04	2.91	9.486	1.742
0.2747	0.6066	5.14	2.97	9.761	1.780
0.4005	0.6543	5.19	3.00	9.883	1.820

TABLE VI. *d*-Camphor in benzene. Temperature = 300° ± 0.1°K. Physical constants of benzene: density $d^{27} = 0.8715$; dielectric constant, $\epsilon^{27} = 2.26_7$; refractive index, $n_D^{27} = 1.4969$.

Mole fraction of *d*-camphor f_2	$r = \frac{\epsilon-1}{\epsilon+2}$	Apparent D: $P_0 = \frac{4\pi N\mu^2}{3kT}$	Apparent D: $P_0 = \frac{4\pi N\mu^2}{kT}$	$\beta_{546} \times 10^{33}$	Rotational parameter $k \times 10^{-2}$
0.0118	0.3103	4.35	2.51	7.977	1.414
0.03025	0.3499	4.38	2.53	8.160	1.455
0.06178	0.3964	4.40	2.54	8.364	1.480
0.1249_6	0.4764	4.44	2.56	8.670	1.540
0.1829	0.5315	4.47	2.58	8.894	1.572
0.2051	0.5464	4.48	2.59	8.935	1.592
0.2843_3	0.6016	4.50	2.60	9.118	1.620

TABLE VII. *d*-Camphor in chloroform. Temperature = 300° ± 0.1°K. Physical constants of chloroform: density $d^{27} = 1.4766$; dielectric constant, $\epsilon^{27} = 4.71$; refractive index, $n_D^{27} = 1.4420$.

Mole fraction of *d*-camphor f_2	$r = \frac{\epsilon-1}{\epsilon+2}$	Apparent D: $P_0 = \frac{4\pi N\mu^2}{3kT}$	Apparent D: $P_0 = \frac{4\pi N\mu^2}{kT}$	$\beta_{546} \times 10^{33}$	Rotational parameter $k \times 10^{-2}$
0.0066	0.5568	6.56	3.79	8.527	1.780
0.0729	0.6346	6.30	3.64	8.640	1.865
0.1285	0.6789	6.09	3.52	8.782	1.960
0.1775	0.6997	5.97	3.45	8.884	2.000
0.2577	0.7231	5.78	3.34	9.103	2.045
0.3785	0.7413	5.47	3.16	9.349	2.130
0.5406	0.7739	5.25	3.03	9.588	2.250

TABLE VIII. α-*d*-Bromocamphor in benzene. Temperature = 300°±0.1°K. Physical constants of benzene: density $d^{27}=0.8715_2$; dielectric constant, $\epsilon^{27}=2.26_4$; refractive index, $n_D^{27}=1.4970$.

Mole fraction of α-*d*-bromocamphor f_2	$r=\frac{\epsilon-1}{\epsilon+2}$	Apparent D $P_0=\frac{4\pi N\mu^2}{3kT}$	$P_0=\frac{4\pi N\mu^2}{kT}$	$\beta_{546}\times10^{22}$	Rotational parameter $k\times10^{-2}$
0.00533	0.3041	5.40	3.12	3.457	7.318
0.01604	0.3408	5.47	3.16	3.493	7.424
0.03765	0.3904	5.44	3.20	3.477	7.494
0.07130	0.4814	5.66	3.27	3.571	7.652
0.1153	0.5522	5.80	3.35	3.656	7.771
0.1915_5	0.6374	5.99	3.46	3.779	8.030
0.2608_7	0.6863	6.08	3.51	3.861	8.155

rotational strength R_{b_2}, varies with changes in concentration and solvent. If only general forces were responsible for the observed concentration effect, a straight line for rotivity vs $(\epsilon-1)/(\epsilon+2)$ would be expected [the optical rotation or the rotational parameter k defined by means of

$$\beta_\lambda=\frac{\lambda^2}{16\pi^3N}\frac{k}{\lambda^2-\lambda_0^2}=\frac{\lambda^2[M]\lambda}{16\pi^3N} \qquad (7)$$

can be used instead of the rotivity as a first approximation]. The observed deviations from linearity in the systems studied [Fig. 2(a) and (b)] may be due to the fact that F in the equation[9] $\Omega_\lambda=\Omega_\lambda{}^0+\Omega_\lambda{}'F$ has to be modified for specific interactions.

The principal dipoles in *d*-camphor and α-*d*-bromocamphor are directly attached to the asymmetric centers. The rotatory dispersion equations[14] and the spectroscopic data show that the optical rotation is principally governed by the absorption bands of the corresponding dipoles. In calculations of the dipole moment by the vector law the same dipoles have an important contribution to the over-all dipole moment of the molecule. The changes in dipole moment are correlated with the changes in these important component dipoles on which the optical rotation depends. A confirmation of Eq. (6) is obtained by a linear plot for β_λ vs μ_{apparent}. [$[M]_\lambda$ or k can be used for β_λ as these are directly proportional, Fig. 3(a) and (b).]

From Eq. (6), the slope of the straight line will be (β'/μ'). If the rotational and dipole moment deformability constants are the same in all the solvents, the points corresponding to different solvents should lie on the same straight line. Different straight lines for different solvents are obtained, showing the intrinsic effect of the liquid structure which is characteristic of the given solvent. From the slope and the intercept, assuming the value of dipole moment in the vapor state, the optical rotation in the ideal state can be calculated and it should be the same for all solvents.

The calculated values of β_0 of *d*-camphor and α-*d*-

TABLE IX. α-*d*-Bromocamphor in ethylacetate. Temperature = 300°±0.1°K. Physical constants of ethylacetate: density $d^{27}=0.8922$; dielectric constant, $\epsilon^{27}=5.921$; refractive index, $n_D^{27}=1.3689$.

Mole fraction of α-*d*-bromocamphor f_2	$r=\frac{\epsilon-1}{\epsilon+2}$	Apparent D $P_0=\frac{4\pi N\mu^2}{3kT}$	$P_0=\frac{4\pi N\mu^2}{kT}$	$\beta_{546}\times10^{22}$	Rotational parameter $k\times10^{-2}$
0.00496	0.6256	5.68	3.28	4.213	9.154
0.01211	0.6324	5.80	3.35	4.195	9.088
0.01680	0.6359	6.03	3.48	4.174	9.024
0.02613	0.6442	6.22	3.59	4.149	8.962
0.07258	0.6759	6.30	3.64	4.114	8.910
0.1313	0.7114	6.48	3.74	4.096	8.861

[14] T. M. Lowry and M. S. French, J. Chem. Soc. **125,** 1921 (1924); T. M. Lowry and J. O. Cutter, *ibid.* **127,** 604 (1925); T. M. Lowry, Proc. Roy. Soc. (London) **A135,** 13 (1932).

bromocamphor are summarized in Table IV. [In the calculations of the slope, 'k' (and $[M]_\lambda$) values are converted into β_λ by using Eq. (7)].

The calculated values of β_0 in different solvents (Tables V–IX) are of the same order. The accuracy of the determination of β_0 depends on the accuracy of the measurements and the range of variation of the property in the concentration range studied; for instance, the dipole moment can be measured to an accuracy of $\pm 0.02D$ and its variation for d-camphor in benzene is only $0.1D$ in the concentration range 0–0.3 mole fraction of camphor. A comparatively large deviation from the mean value of β_0 in benzene is, therefore, attributed to the limited accuracy of the measurements. The assumption that the liquid structure remains the same throughout the concentration range is also a limitation.

The present view of the direct relation between apparent dipole moment of an optically active species and the rotational parameter is, thus, strongly suggested by the systems studied by giving linear curves for μ_{app} vs rotational parameter and giving the values of the same order for β_0's in different solvents.

ACKNOWLEDGMENT

Grateful thanks are due to Professor S. K. K. Jatkar for his keen interest and guidance in this work.

THE JOURNAL OF CHEMICAL PHYSICS VOLUME 35, NUMBER 6 DECEMBER, 1961

Microwave Spectrum and Internal Barrier of Methylphosphine*

TAKESHI KOJIMA,† EDWARD L. BREIG, AND CHUN C. LIN
Department of Physics, University of Oklahoma, Norman, Oklahoma

(Received April 27, 1961)

The microwave spectrum of methylphosphine has been investigated in the regions of 12–33 and 46–49 kMc. The rotational constants are found to be $A=71{,}869.5$, $B=11{,}792.6$, $C=11{,}677.7$ Mc. Stark effect measurements yield a dipole moment of 1.100 ± 0.010 D. The barrier to internal rotation of the methyl group, as determined from the $A-E$ splittings of rotational lines in the ground torsional state and from the satellite frequency pattern of the 0_{00}—1_{01} transition, is 685.2 ± 5 cm^{-1}. The structure of the molecule and the magnitude of the internal barrier in relation to other molecules are discussed.

INTRODUCTION

THE microwave spectrum of the methylphosphine molecule is of some special interest. The methyl group along with the two other hydrogen atoms are attached to the phosphorus atom in a pyramidal form as shown in Fig. 1. This molecule is very close to being a symmetric top, with the asymmetry parameter depending very critically on the angle $\angle$HPH and becoming very nearly zero when this angle is 90°. Furthermore, the molecule is capable of internal rotation about the symmetry axis of the methyl group and inversion about the P atom. Because of the large mass of the P atom and of the attached methyl group, the inversion frequencies should be well below 0.1 Mc; and unlike the case of methylamine, no observable inversion splittings are expected in the microwave spectrum. On the other hand, the internal rotation should give rise to a series of lines of the same general pattern as those found in a large number of molecules.[1] It should be also interesting to compare the experimental result of the barrier height of this molecule with that of methylamine and methylmercaptan. In this paper the microwave spectrum of methylphosphine is reported and an analysis of the spectrum is made to determine the rotational constants, dipole moment, and internal barrier.

EXPERIMENTAL

The sample of methylphosphine was furnished by Dr. A. B. Burg of the University of Southern California.[2] The spectrograph is of the conventional Stark-modulation type[3] with modulation frequency of 100 kc. Frequencies of the spectral lines are measured to about ±0.1 Mc with the use of a frequency standard controlled by a standard signal of 100 kc. The pressure of the gas used in the measurements ranges from 0.05 to 0.1 mm Hg.

Methylphosphine has a very unpleasant odor and special care must be taken in handling the gas. Wherever possible on the vacuum system, glass connections were rigidly sealed with Picein wax, but diffusion readily occurred through the grease at the

* Supported jointly by the National Science Foundation and Office of Naval Research.

† On leave of absence from Toyama University, Toyama, Japan.

[1] C. C. Lin and J. D. Swalen, Revs. Modern Phys. **31**, 841 (1959).

[2] R. I. Wagner and A. B. Burg, J. Am. Chem. Soc. **75**, 3869 (1953).

[3] C. H. Townes and A. L. Schawlow, *Microwave Spectroscopy* (McGraw-Hill Book Company, Inc., New York, 1955).

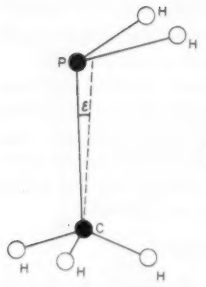

FIG. 1. Model of the methylphosphine molecule.

stopcocks contaminating the immediate area and making working conditions at times most unfavorable. The gas also appeared to easily replace ammonia adsorbed on the inner surface of the cell, and it was difficult to maintain a good vacuum of the pure gas over a period of several hours. The contaminated gas was removed from the vacuum system by pumping through a liquid-air cold trap. Special precautions were also needed in the final disposal of the waste products.

MICROWAVE SPECTRA AND ROTATIONAL CONSTANTS

Some 80 lines have been found in the region of 12–33 and 46–49 kMc. The majority of the lines shows doublet structure characteristic of molecules with a methyl group.[1] In a few cases the same transition has been observed in several torsional states. Stark effect is used for identifying the internal rotation doublets and satellites. The frequencies of some of the observed lines can be found in Table I. The rotational quantum numbers of the initial and final states of the transitions are listed in the first column. The second column gives the torsional quantum number v and σ with which the particular transition is associated.[1] We use A and E for $\sigma=0$ and ±1, respectively. Thus $0A$ stands for the nondegenerate sublevel of the ground torsional state ($v=0$). The rotational constants have been evaluated by both of the method of principal axes (PAM) and the method of internal axes (IAM).[1] Descriptions of the methods of analysis are given in the following paragraphs.

1. Analysis by PAM

Attempts were first made to fit all of the $0A$ lines to a rigid rotor spectrum as were done in the analysis of the microwave spectra of many molecules with high barriers by PAM.[1] The frequencies of the transitions 0_{00}—1_{01} and 1_{10}—2_{11} may be used to determine B and C. The final values of these two parameters are chosen as $B=11\,791.6$ Mc and $C=11\,678.7$ Mc. The rotational constant A has little effect on the frequencies of $\Delta K=0$ lines, so it is to be determined from transitions which involve a change in K. It was found that the value of A needed to fit the group of lines with $K=0\rightarrow1$ differs by about 50 Mc from that for $K=1\rightarrow2$. This is suggestive of the importance of the fourth-order terms in the PAM treatment. A rough estimate indicates that the quantity ρ [see Eq. (2)–(37) of reference 1], which governs the convergence of the perturbation treatment in PAM, is as large as 0.46. The fourth-order term is then introduced to the effective Hamiltonian for the $0A$ rotational energy levels as

$$H_{0A}=A_{00}P_z^2+B_{00}P_y^2+C_{00}P_x^2+Fw_{00}^{(4)}\Pi^4,$$
$$\Pi=(\lambda_z I_\alpha P_z/I_z)+(\lambda_x I_\alpha P_x/I_x), \quad (1)$$

where A_{00}, B_{00}, and C_{00} are the three effective rotational constants (in the order of decreasing magnitude) in the $0A$ torsional state, I_z and I_x are the two principal moments of inertia along the appropriate axes, I_α is

TABLE I. Observed spectrum of the CH_3PH_2 molecule.

Transitions	$v\sigma$	Frequencies (Mc)	Stark effect[a]	Stark coefficients[b] (10^{-6} Mc-cm^2/v^2)
0_{00}—1_{01}	$0A$	23 470.3	2(+)	0.544
	$0E$			
0_{00}—1_{01}	$1A$	23 395.9	2(+)	0.551
0_{00}—1_{01}	$1E$	23 394.8	2(+)	0.546
0_{00}—1_{01}	$2A$	23 314.8	2(+)	0.540
0_{00}—1_{01}	$2E$	23 324.2	2(+)	0.540
0_{00}—1_{01}	$3A$	23 279.0	2(+)	0.519
0_{00}—1_{01}	$3E$	23 250.0	2(+)	0.485
0_{00}—1_{01}	$4A$	23 224.6	2(+)	0.54
1_{01}—2_{02}	$0A$	46 940.1	2[c]	
	$0E$			
1_{01}—2_{02}	$1A$	46 791.4	2	
1_{01}—2_{02}	$1E$	46 789.2	2	
1_{10}—2_{11}	$0A$	47 052.2	2(−)	−35.4
1_{10}—2_{11}	$0E$	46 975.7	1(i)	
1_{11}—2_{12}	$0A$	46 827.3	2(+)	43.1
1_{11}—2_{12}	$0E$	46 904.6	1(i)	
1_{10}—2_{11}	$1A$	46 895.1[d]	2(−)	−44
1_{10}—2_{11}	$1E$	46 791.5	1(i)	
1_{11}—2_{12}	$1A$	46 685.8	2(+)	47.1
1_{11}—2_{12}	$1E$	46 787.4	1(i)	
2_{02}—1_{10}	$0A$	13 451.8	2(+)	49[c]
2_{02}—1_{10}	$0E$	13 437.1	1(i)	
2_{02}—1_{11}	$0E$	12 756.4	1(i)	
3_{12}—4_{04}	$0A$	33 202.0	2(−)	−1.9[c]
7_{16}—6_{24}	$0A$	14 991.7	2(+)	48
7_{16}—6_{24}	$0E$	14 695.6	1(i)	
7_{17}—6_{25}	$0A$	18 141.1	2(−)	−45
7_{17}—6_{25}	$0E$	17 142.2	1(i)	
8_{27}—9_{19}	$0A$	27 819.0	2(+)	
8_{27}—9_{19}	$0E$	28 820.8	1(i)	
8_{26}—9_{18}	$0A$	32 864.5	2(−)	−14
8_{26}—9_{18}	$0E$	33 158.1	1(i)	
$13_{3,11}$—$14_{2,13}$	$0A$	27 435.8	2(+)	
$13_{3,11}$—$14_{2,13}$	$0E$	27 737.9	1(i)	
$13_{3,10}$—$14_{2,12}$	$0A$	27 720.4	2(−)	
$13_{3,10}$—$14_{2,12}$	$0E$	28 332.3	1(i)	

[a] The Stark effects are designated by 1(0) for the first-order Stark effect with the strongest outer components, 1(i) for the first-order Stark effect with the strongest inner components, 2(+) for the second-order Stark effect with positive Stark displacement and 2(−) for the second-order Stark effect with negative Stark displacement.

[b] Stark lobes are not resolved.

[c] See Table IV.

[d] Accuracy is ±0.5 Mc.

the moment of inertia of the top along its symmetry axis, and the λ's are the direction cosines of the internal rotation axis with respect to the principal axes ($\lambda_y=0$). The general expressions for F and $w_{00}^{(4)}$ can be found in the paper by Lin and Swalen.[1] For the methylphosphine molecule, the axis of internal rotation is very nearly parallel to one of the principal axes, thus we shall adopt the approximation

$$\lambda_z\approx 1, \quad \lambda_x\approx 0. \tag{2}$$

The fourth-order term in Eq. (1) is simplified into

$$Fw_{00}^{(4)}\Pi^4=\hbar^2 I_\alpha{}^3 w_{00}^{(4)}[2I_z{}^3(I_z-I_\alpha)]^{-1}P_z{}^4=\tau_4 P_z{}^4. \tag{3}$$

Using the structure of the molecule and a barrier height 685 cm^{-1} ($s=31.6$) as given in the latter part of this paper, we found $\tau_4=-16.58$ Mc. Equation (1) is used to fit the spectrum and the results are summarized in Table II. The four parameters in Eq. (1) obtained from this data fitting process are shown in Table III. The calculated value of τ_4 differs considerably from the "experimental" value. A similar discrepancy in this fourth-order term was also found in acetic acid,[4] although the origin for such discrepancy is not clear. Less accuracy is to be expected from the calculated frequencies of the lines with $K=1\rightarrow 2$, because these values are obtained as differences between two large numbers of nearly equal magnitude.

The effective rotational constants in the ground torsional states are related to the "real" constants A, B, and C through the approximate relations

$$A_{00}=A+\hbar^2 I_\alpha[2I_z(I_z-I_\alpha)]^{-1}w_{00}^{(2)},$$
$$B_{00}=B, \quad C_{00}=C. \tag{4}$$

The coefficients $w_{00}^{(2)}$ may be found in the papers by Lin and Swalen[1] and by Herschbach.[5] By interpolating Herschbach's table, we obtain the second-order correction term as 218.2 Mc, which gives $A=71\ 866.0$ Mc (see Table III).

TABLE II. Comparison of the observed frequencies of the 0A line with the calculated values.

Transitions (0A)	Observed frequencies	Calculated frequencies PAM	Calculated frequencies IAM
0_{00}—1_{01}	23 470.3	23 470.3	23 470.3
1_{01}—2_{02}	46 940.1	46 940.4	46 940.4
1_{10}—2_{11}	47 052.2	47 053.5	47 053.5
1_{11}—2_{12}	46 827.3	46 827.7	46 827.7
2_{02}—1_{10}	13 451.8	13 452.3	13 454.8
3_{12}—4_{04}	33 202.0	33 202.1	33 206.0
7_{16}—6_{24}	14 991.7	14 998.5	14 989.0
7_{17}—6_{25}	18 141.1	18 147.9	18 138.3
8_{27}—9_{19}	27 819.0	27 828.7	27 838.2
8_{26}—9_{18}	32 864.5	32 874.8	33 884.1

TABLE III. Rotational constants (in Mc) determined by PAM and IAM.

PAM	IAM
$A_{00}=72\ 084.2$	$A=A'=71\ 873.0$
$B=B_{00}=11\ 791.6$	$B'=11\ 791.6$
$C=C_{00}=11\ 678.7$	$C'=11\ 678.7$
$A=71\ 866.0$	$B=11\ 792.6$
τ_4(calc) $=-16.6$	$C=11\ 677.7$
τ_4(obs) $=-12.7$	

2. Analysis by IAM

The application of the IAM for determining the rotational constants has been treated by Hecht and Dennison[6] and by Lide and Mann.[7] If we again assume that the axis of internal rotation is parallel to one of the principal axes ($\lambda_z=1$), it can be shown that the 0A lines with $\Delta K=0$ may be fitted to a rigid rotor spectrum[7] with the following effective rotational constants A', B', and C':

$$A'=A, \quad B'=B-2f, \quad C'=C+2f, \tag{5}$$

where

$$f=\tfrac{1}{4}(B-C)\,\delta_{K+2,0,0}{}^{K,0,0}. \tag{6}$$

Expressions for δ can be found in Eq. (3–52) of Lin and Swalen.[1] From the transition 0_{00}—1_{01} and 1_{10}—2_{11} along with a reduced barrier height parameter $s=31.6$, we obtain $B=11\ 792.6$ and $C=11\ 677.7$. To determine A we have to resort to transitions of the type $K\rightarrow K+1$. For these lines we must first subtract from the observed frequency the quantity

$$\tfrac{2}{3}\Delta_0[\cos(2\pi I_\alpha/3I_z)(K+1)-\cos(2\pi I_\alpha/3I_z)K], \tag{7}$$

which represents the contribution from the internal rotation and then evaluate the constant A according to the rigid-rotor type spectrum. The rotational constants are found in Table III. Frequencies of a number of lines calculated from this set of parameters are compared with the experimental values in Table II. Again the agreement is rather poor for the lines involving $K\rightarrow K+1$ for the reason explained in the preceeding section. Because of this discrepancy, the constant A is only accurate to about 10 Mc. We shall take the average of the values of A obtained from IAM and PAM as our final result. On the other hand, the accuracy of B and C is limited only by the approximation introduced in Eq. (2) and by the small uncertainty of

[4] W. J. Tabor, J. Chem. Phys. **27,** 974 (1957).
[5] D. R. Herschbach, "Tables for the internal rotation problem," Department of Chemistry, Harvard University (1957).
[6] K. T. Hecht and D. M. Dennison, J. Chem. Phys. **26,** 31 (1957).
[7] D. R. Lide, Jr. and D. E. Mann, J. Chem. Phys. **27,** 868 (1957).

TABLE IV. Observed and calculated Stark coefficients.

Transitions	Stark coefficients (in 10^{-7} Mc-cm^2/v^2) Observed	Calculated
0_{00}—1_{01}	54.395	(54.395)[a]
1_{01}—2_{02}	$-18.5+30.1\ M^2$	$-18.3+30.1\ M^2$
2_{02}—1_{10}	$(-3.5+5160\ M^2)$[b]	$-4.1+5150\ M^2$
3_{12}—4_{04}	$2.69-23.4\ M^2$	$(2.69-23.9\ M^2)$[a]

[a] $M=0$ lobe used to determine μ_a and μ_c.
[b] For electric fields less than 50 v/cm.

f in Eqs. (5) and (6). It should be noted that the values of B and C determined by IAM differ slightly from those determined by PAM. Since PAM becomes less satisfactory for large ρ, the IAM results for B and C of the molecule are probably closer to the true state of affairs.

STARK EFFECT AND DIPOLE MOMENT

The Stark effect of the observed lines has been examined. The Stark lobes were not resolvable for the majority of the high-J lines. The qualitative behavior of the splittings are listed in Table I under "Stark effect." For a number of low-J lines, the Stark coefficients (ratio of the Stark splittings to the square of the electric field) of the unresolved lobes have been measured and are shown in the last column of Table I. It should be noted that the 1_{10}—2_{11} and 1_{11}—2_{12} $0A$ transitions have rather large quadratic coefficients while the two corresponding $0E$ lines show first-order effects. This is in complete accordance with prediction from the theory. The Stark lobes for the 0_{00}—1_{01}, 1_{01}—2_{02}, 2_{02}—1_{10}, 3_{12}—4_{04} lines ($0A$) have been resolved and studied in some detail. The Stark coefficients are found in Table IV.

The dipole moment of this molecule must lie on the plane containing the C-P bond and the line which bisects the $\angle$HPH. According to whether this angle is less or greater than 90°, the dipole moment will have nonvanishing components along the principal axes a and b (the two axes with larger rotational constants) or along a and c, respectively. From the selection rules of the observed spectrum, we see that the latter is the case. The $M=0$ Stark lobes of the 0_{00}—1_{01} and 3_{12}—4_{04} transitions were used to determine the dipole moment with the results

$$\mu_a=0.958\pm0.005D, \quad \mu_c=0.541\pm0.010D.$$

The dipole moment is therefore $1.100\pm0.010D$ along a line which makes an angle of 29°27′ with the a axis.

Table IV gives the theoretical Stark coefficients calculated from these values of the dipole moment components by the method of Golden and Wilson.[8]

[8] S. Golden and E. B. Wilson, Jr., J. Chem. Phys. **16**, 669 (1948).

It is interesting to compare μ_c with the dipole moment of the phosphine molecule,[9] $\mu=0.579\pm0.012D$. From the structure of this molecule, the bond dipole moment of P-H is found to be $0.356D$. Assuming the same bond moment for methylphosphine, one obtains the dipole moment of the PH_2 group as $0.488D$ with $\angle$HPH = 93°23′. Upon transforming to the principal axes of methylphosphine and using the experimental value of μ_a, one has $\mu_c=0.51D$ which agrees well with the measured value.

BARRIER TO INTERNAL ROTATION

The barrier to internal rotation can be determined most accurately by means of the "splitting method," i.e., the splitting of the A and E lines of a given transition.[1] These splittings are contributed from two sources: the interaction of internal rotation with over-all rotation, and the vibration-torsion-rotation interaction. The splittings due to the former effect (in which molecular vibrations other than internal torsion are neglected) are zero for symmetric top molecules, increasing with the asymmetry parameter. Such splittings will be termed "rigid A-E splittings." The second source arises from the interaction between the internal torsion and other modes of molecular vibration, and splittings of this sort will be referred to as "nonrigidity splittings." They are generally very small in the ground torsional states and become progressively larger at higher v. The nonrigidity effect is also responsible for the shift of nA and nE ($n\neq0$) lines from $0A$ and $0E$.

Because of the extremely small asymmetry parameter of the methylphosphine molecule, no splittings between the $0A$ and $0E$ lines are observed except in the transitions involving $K_{-1}=1$. Here the interplay of the K doubling and the internal rotation results in large A-E splittings which make possible an accurate determination of the internal barrier height.

Alternatively, the potential barrier may also be determined from an analysis of the torsional satellite frequency pattern of the 0_{00}—1_{01} transition. For the

TABLE V. Comparison of observed and calculated values for A—E splitting.

Transitions ($v=0$)	$\nu_A-\nu_E$ (obs)	$\nu_A-\nu_E$ (calc)[a]
1_{10}—2_{11}	76.5	77.2
1_{11}—2_{12}	−77.3	−77.2
2_{02}—1_{10}	14.7	17.3[c]
2_{02}—1_{11}	582.5[b]	582.4

[a] $s=31.6$, $\Delta b=-1.089\times10^{-3}$.
[b] As the $0A$ line is forbidden, it was estimated from the 2_{02}—1_{10} line using the calculated value for asymmetry splitting.
[c] A major part of this discrepancy may be attributed to the poor fit of this A line to the calculated frequencies appearing in Table II.

[9] M. H. Sirvetz and R. E. Weston, Jr., J. Chem. Phys. **21**, 898 (1953).

purpose of this calculation the methylphosphine molecule may be approximated by a symmetric top and the procedure analogous to that of Kivelson[10] can be applied. Finally, the relative intensity of a given rotational transition in the various torsional states may be utilized to obtain an estimate of the barrier height. The results from these three different methods are described in the following paragraphs.

1. Splitting Method

Since the angle between the axis of internal rotation and the principal a axis is exceedingly small, the IAM is particularly convenient for the calculation of the A-E splittings. As the complete structure of this molecule is not known, certain guesses have to be made concerning the structural parameters. The moment of inertia of the top, I_α, is taken as 3.212 amu-A^2 as compcompared to 3.214, 3.213, and 3.212 from CH_3SH,[11] CH_3OH,[12] and CH_3NH_2,[13] respectively. The computation procedure follows very closely that given in Sec. V of reference 1. The calculation is greatly simplified by the observation that the terms containing β^2 in the expression of $\Delta\nu$ of the ground torsional state are negligible. The value of F is not particularly sensitive to I_α; the former remains essentially the same as I_α is changed from 3.205 to 3.220. From the A-E splittings of the 1_{10}—2_{11}; 1_{11}—2_{12}; 2_{02}—1_{10}; and 2_{02}—1_{11} lines, the potential barrier is determined as 685.2 ± 5 cm^{-1}. Comparison of the calculated and observed splittings is shown in Table V.

The $1A$ and $1E$ lines of 1_{10}—2_{11} and 1_{11}—2_{12} have also been analyzed. From the two A members (and also from 0_{00}—1_{01} for $1A$) we obtain the rotational constants in the $1A$ torsional level as $B_{10}=11\,750.3$ Mc and $C_{10}=11\,645.6$ Mc. Using the barrier height of 685.2 cm^{-1} we have calculated the two rigid A-E splittings as 103.6 and -103.6 Mc compared with 103.6 and -101.6 Mc from experiment. In the $1E$ torsional state the internal rotation terms δ_K (rather than the asymmetry)[14] constitute the major source of the K-doublet splittings. Since δ_K is independent of J, the two $1E$ lines are very close to each other. This is illustrated in Fig. 2. It should be pointed out that we have neglected the $1A$–$1E$ splittings arising from the nonrigidity effect. For this reason, the agreement between the observed and calculated splittings should be regarded as quite satisfactory.

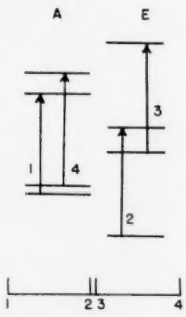

FIG. 2. Diagram of $1A$ and $1E$ transitions of 1_{10}—2_{11} and 1_{11}—2_{12}.

TABLE VI. Satellite frequency pattern of the 0_{00}—1_{01} and 1_{01}—2_{02} transitions.

Transitions	$v\sigma$	Observed frequencies	Calculated frequencies[a]
0_{00}—1_{01}	$0A$	23 470.3	(23 470.3)[b]
	$0E$	23 470.3	23 470.3
	$1A$	23 395.9	23 396.1
	$1E$	23 394.8	23 394.9
	$2A$	23 314.8	(23 314.8)[b]
	$2E$	23 324.2	(23 324.2)[b]
	$3A$	23 279.0	23 277.7
	$3E$	23 250.0	23 249.8
	$4A$	23 224.6	23 225.2
	$4E$		23 241.6
1_{01}—2_{02}	$0A$	46 940.1	46 940.6
	$0E$	46 940.1	46 940.6
	$1A$	46 791.4	46 792.2
	$1E$	46 789.2	46 789.8

[a] A reduced barrier of height of $s=31.6$ was used in these calculations.
[b] These frequencies were used to determine the parameters F, G, and $\frac{1}{2}(B+C)_{0,0}$.

2. Satellite Frequency Pattern

The theory of vibration-torsion-rotation interaction in an asymmetric top has been developed by Kivelson[10] and by Hecht and Dennison. Because of the great complexity of the general treatment, we shall adopt the symmetric top approximation. The rotational constant $\frac{1}{2}(B+C)$ in the torsional state, v, σ is given by

$$\tfrac{1}{2}(B+C)_{v,\sigma}=\tfrac{1}{2}(B+C)_{0,0}+F(Kv\sigma \mid 1\text{-}\cos 3\alpha \mid Kv\sigma)$$
$$+G(Kv\sigma \mid p^2 \mid Kv\sigma)+LK(Kv\sigma \mid p \mid Kv\sigma). \quad (8)$$

The rotational constants now depend on the index v and are different for the A and E levels. Within a given v, the small asymmetry of the molecule produces a further splitting of the A-E doublets. Such splittings can be calculated in the same manner as the splittings in the ground torsional state and depend very critically on the direction cosine of the axis of internal rotation and the c axis except for the lines with $\mid K \mid =1$. In view of the uncertainty of the structural parameters of the molecule in the excited torsional states, the "rigid A-E splittings" due to molecular asymmetry

[10] D. Kivelson, J. Chem. Phys. **22,** 1733 (1954).
[11] T. Kojima, J. Phys. Soc. Japan **15,** 1284 (1960).
[12] E. V. Ivash and D. M. Dennison, J. Chem. Phys. **21,** 1804 (1953).
[13] T. Nishikawa, T. Itoh, and K. Shimoda, J. Chem. Phys. **33,** 1735 (1955).
[14] Reference 1, p. 864.

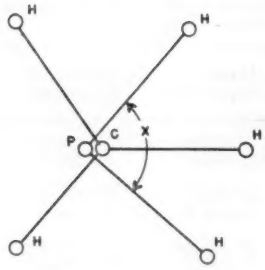

FIG. 3. Projection of the molecule onto a plane perpendicular to the internal rotation axis.

will be neglected in the analysis of the satellite pattern of the 0_{00}—1_{01} and 1_{01}—2_{02} transitions.

The coefficients F and G in Eq. (8) are treated as parameters. It is found that a good fit to the satellite frequencies of the 0_{00}—1_{01} and 1_{01}—2_{02} can be obtained by choosing $F=86.6936$ Mc, $G=-0.621219$ Mc, and $(B+C)_{0,0}=23\,508.4$ Mc along with a reduced potential barrier of $s=31.6$ (see Table VI). The small discrepancy between the theory and the observed pattern may be ascribed to the neglect of the asymmetry.

3. Intensity Method

Rough intensity measurements on the $0A$, $1A$, and $2A$ lines of the 0_{00}—1_{01} transition give an intensity ratio of 1:0.34:0.125. This yields a barrier of 540 cm^{-1}. Since the $0A$ and $0E$ lines are not resolved, the intensity of the $0A$ line is taken as one-half the measured value. In view of the high degree of uncertainty in the results of intensity measurement, the barrier height so obtained represents merely a rough estimate.

MOLECULAR STRUCTURE AND DISCUSSION

The rotational constants A, B, and C were determined primarily from the 0_{00}—1_{01}, 1_{10}—2_{11}, and 2_{02}—1_{11} transitions. We have endeavored to propose a plausible molecular structure from these rotational constants, though a comprehensive study of many isotopic species is necessary to determine the exact molecular dimensions. The structure is

$$\text{P-H}=1.414A,\quad \text{C-P}=1.863A,\quad \text{C-H}=1.093A,$$

$$\angle\text{HPH}=93°23',\quad \angle\text{CPH}=97°30',\quad \angle\text{HCH}=109°45',$$

$$\epsilon=2°0'.$$

Here ϵ is the angle between the methyl axis and CP bond (see Fig. 1). In the absence of any additional structural information of the molecule, the choice of the present value of ϵ is somewhat arbitrary. This angle is known to vary from 2°0′ in CH_3SH to 3°30′ in CH_3NH_2. Figure 3 shows the projection of this molecule on the plane perpendicular to the methyl axis.

If we assume that each of the PH bonds contributes a potential barrier, $V_3^{(PH)}$, the resultant barrier is expressed by

$$\tfrac{1}{2}V_3^{(PH)}[\cos 3(\alpha+\tfrac{1}{2}x)+\cos 3(\alpha-\tfrac{1}{2}x)],$$

where $x(=94°50')$ is the projected angle of $\angle$HPH (see Fig. 3). A barrier height of $V_3^{(PH)}=430$ cm^{-1} is obtained from our result $V_3=685$ cm^{-1}. The value of $V_3^{(PH)}$ is close to the barrier height of methyl mercaptan, 443.9 cm^{-1}. One may ascribe the slightly lower value of $V_3^{(PH)}$ to the fact that the CP bond is $0.04A$ longer than the CS bond.

If one recalls that the barrier of methyl amine is about twice as large as that of methyl alcohol, one may observe a certain degree of constancy and additivity of the contribution of the attached bonds to the barrier height. While it is far too premature to draw any conclusions regarding the origin of the potential barrier, the results of the barrier heights for these molecules are consistent with the postulate of direct forces between the attached bonds.[15]

ACKNOWLEDGMENT

The authors wish to thank Professor A. B. Burg of the University of Southern California for supplying us the sample of methylphosphine gas.

[15] E. B. Wilson, Jr., "The problem of barriers to internal rotation in molecules," *Advances in Chemical Physics* (Interscience Publishers, Inc., New York, 1959), Vol. II.

THE JOURNAL OF CHEMICAL PHYSICS VOLUME 35, NUMBER 6 DECEMBER, 1961

Electron Spin Resonance Studies of Gamma-Irradiated Single Crystals of Sucrose

HISASHI UEDA, ZEN'ICHIRO KURI, AND SHOJI SHIDA

Tokyo Laboratories, Japanese Association for Radiation Research on Polymers, Kamifujimaecho, Bunkyoku, Tokyo, Japan

(Received January 4, 1961)

The electron spin resonance of gamma-irradiated single crystals of sucrose has been measured at 9400 Mc/sec for various orientations in the magnetic field. The variations of the resonance with angle were greatest for rotation of the crystal about its *b* axis, which was kept perpendicular to the magnetic field. The anisotropic hyperfine structure was observed to vanish when the magnetic field is applied perpendicular to the (*b*, *c*) plane. It was ascertained that the radical formed is the type X—ĊH—Y, which had been proposed by Williams *et al.* from the data obtained from the polycrystalline samples.

INTRODUCTION

ELECTRON spin resonance studies of radicals produced in various kinds of irradiated polycrystalline monosaccharides and polysaccharides have been reported in several papers. Williams and coworkers[1,2] studied the ESR spectra of irradiated polycrystalline saccharides and concluded that the structure of the radicals formed are of X—ĊH—Y type, because most of them gave doublet-like patterns. The use of the ESR method applied to the studies of the reactivities of the radicals formed in various kinds of irradiated polycrystalline monosaccharides and polysaccharides has been reported by the present authors.[3] The result obtained revealed that sucrose composed of two monosaccharides, glucose and fructose, gives spectra fairly different from the one constructed from the spectra of each monosaccharide on the assumption that the two monosaccharides contribute equally.[4]

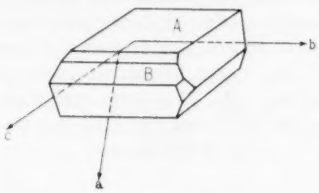

FIG. 1. The single crystal of sucrose used.

This fact led us to the conclusion that the pattern of the ESR spectra which can be obtained from the irradiated saccharides probably depends not only upon the molecular structure of the saccharides but also upon the crystalline state.

The effect of this crystalline state or the crystal field on ESR is anisotropic in nature. Different spectra will be obtained from the same kind of saccharide when the crystalline state is different, that is, when the measurement is made on a polycrystal or on a single crystal, although the radicals formed are undoubtedly the same. The determination of the structure of radicals made by Williams *et al.* is based on the measurement made only on polycrystalline saccharides. It was thought, therefore, that some additional features may come out if studies on single crystals are made.

Radicals produced in irradiated polycrystalline monosaccharides have a high stability which Williams *et al.* attributed to their electronic structures. The conclusion arrived at by the present authors from a series of previous experiments is rather different. It is believed that the high stability of the radicals is only apparent and is caused by the network of hydrogen bonds in saccharide crystals, preventing active gases from penetrating the crystal lattice and also radicals from approaching each other. When the network is broken, high stability is destroyed.

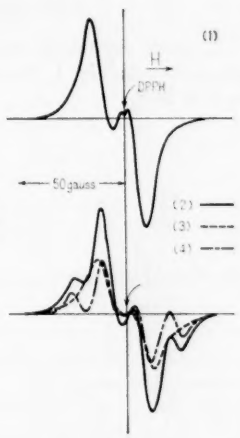

FIG. 2. The ESR spectra of irradiated polycrystalline sucrose (1), glucose (3), fructose (4), and a hypothetical one constructed from (3) and (4).

It is the purpose of the present work to study the ESR effects of crystal fields or of the protons forming hydrogen bonds, using single crystals, and to get some more information on the structure and reactivities of the radicals.

Not much work has appeared, yet, on the ESR studies of the radicals produced in irradiated single

[1] D. Williams, J. E. Gensic, M. L. Wolfram, and L. J. McGabe, Proc. Natl. Acad. Sci. U.S. **44**, 1128 (1958).
[2] J. D. Williams, B. Schmidt, M. L. Wolfram, A. Michaelakis, and L. J. McGabe, Proc. Natl. Acad. Sci. U.S. **45**, 1740 (1959).
[3] Z. Kuri, Y. Fujiwara, H. Ueda, and S. Shida, J. Chem. Phys. **33**, 1884 (1960).
[4] H. Ueda, Z. Kuri, and S. Shida, Nippon Kagaku Zasshi **82**, 8 (1961).

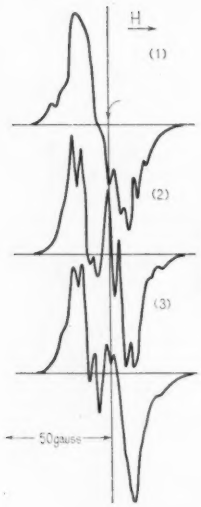

FIG. 3. The ESR spectra of the irradiated single crystal with its a axis held perpendicular to the magnetic field. Angle $(bH) = 0°(1)$, $50°(2)$, $90°(3)$, respectively.

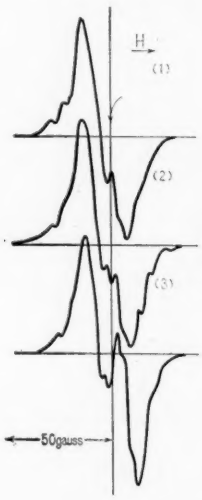

FIG. 5. The ESR spectra of the irradiated single crystal with its c axis held perpendicular to the magnetic field. Angle $(bH) = 0°(1)$, $50°(2)$, $90°(3)$, respectively.

crystals. Work on single crystals of dimethyl glyoxime[5] and alanine[6] were reported by Miyagawa and Gordy. The structure of these crystals is relatively simple and it was possible to carry out a complete analysis of the spectrum obtained.

EXPERIMENTAL

The single crystals of sucrose used have the crystal habit shown in Fig. 1. The angle between face A and face B is 103°.

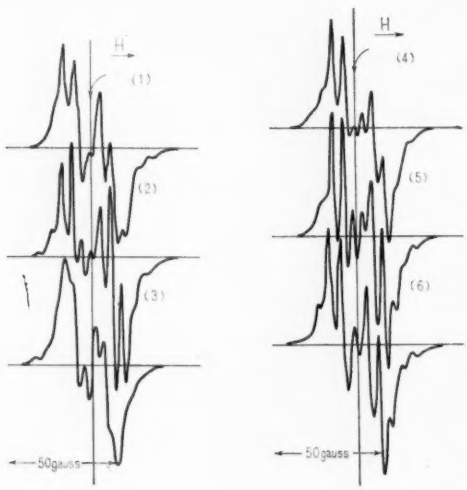

FIG. 4. The ESR spectra of the irradiated single crystal with its b axis held perpendicular to the magnetic field. Angle $(cH) = 0°(1)$, $40°(2)$, $90°(3)$, $120°(4)$, $140°(5)$, and $160°(6)$, respectively.

The spacings of the crystal lattice in various directions were measured by x-rays using the CuK_α line. By comparing our data with the results of the x-ray studies by Beevers *et al.*,[7] face A and face B were easily identified as (100) and (001) planes, respectively.

Sucrose belongs to the monoclinic crystal system. Therefore, three kinds of cylindrical samples, the center axes of which coincide with the three crystal axes, i.e., a, b, and c axes, respectively, were prepared by cutting large crystals. They were irradiated in vacuum with a dose of 10^6 r and the ESR spectra were measured at 25°C and at 9 400 Mc/sec.

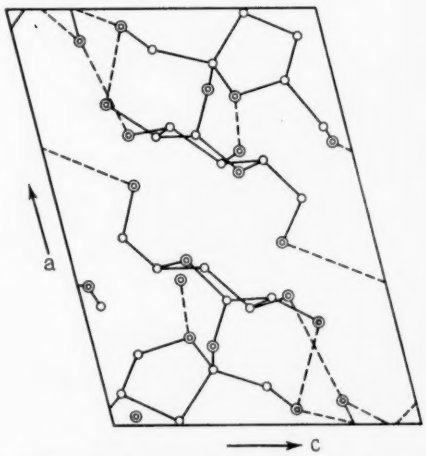

FIG. 6. The b-axis projection of the sucrose crystal. Single circles show carbon atoms, double circles show oxygen atoms, and the dotted lines hydrogen bonds.

[5] I. Miyagawa and W. Gordy, J. Chem. Phys. **30,** 1590 (1959).
[6] I. Miyagawa and W. Gordy, J. Chem. Phys. **32,** 255 (1960).
[7] C. A. Beevers, T. R. R. McDonald, J. H. Robertson, and F. Stern, Acta Cryst. **5,** 689 (1952).

RESULTS

1. *The ESR spectra obtained when sucrose, glucose, and fructose were irradiated in the polycrystalline state are shown in Fig. 2.* Curve (2) shows a hypothetical spectrum which was constructed by adding two spectra, i.e., a spectrum of irradiated polycrystalline glucose and that of polycrystalline fructose. In this spectrum, the number of radicals contributed from glucose and fructose are equal.

2. *ESR spectra of the sample, the center axis of which coincides with the crystal* a *axis.* The cylindrical sample, the center axis of which coincides with the crystal *a* axis, was placed in the magnetic field in such a way as to keep its center axis perpendicular to the magnetic field. As the crystal *b* axis is perpendicular to *a* axis, the angle between *b* axis and the magnetic field, angle (b, H), can be varied by the rotation of the crystal about its center axis. Nineteen measurements were made at every 10° of the value of the angle (b, H) in the range of 0°–180°. Some of the spectra thus obtained are shown in Fig. 3.

3. *ESR spectra of the sample, the center axis of which coincides with the crystal* b *axis.* The measurements were made in the same way as with the *a*-axis sample. Nineteen measurements were made at every 10° of the value of the angle (c, H), in the range from 0–180°. Some of the spectra thus obtained are shown in Fig. 4.

4. *ESR spectra of the sample, the center axis of which coincides with the crystal* c *axis.* The measurements were made in the same way as with the *a*-axis sample. Nineteen measurements were made at every 10° of the angle (b, H) in the range of 0°–180°. Some of the spectra thus obtained are shown in Fig. 5.

The rotation of the sample in the magnetic field about its center axis, always keeping the axis perpendicular to the magnetic field, is equivalent to changing the direction of the magnetic field in the plane perpendicular to the axis, keeping the axis fixed.

DISCUSSION

The *b*-axis projection of the crystal structure is given in Fig. 6.[7] A hyperfine structure of ESR spectra consists of an isotropic part and an anisotropic part. The pattern, Fig. 5, curve (3), is the simplest and may be considered as showing only the isotropic part, if the structure at the center is neglected. That is, with the condition under which Fig. 5, curve (3), is obtained, the anisotropic effect vanishes almost entirely. This observation gives strong support to the opinions of Williams *et al.* Their opinion, that the radicals formed are of the type of X—ĊH—Y, seems correct as the *g* factor measured in Fig. 5, curve (3), is very near to 2.0036 showing that the unpaired electron belongs to a carbon atom, and the pattern of curve (3), Fig. 5, can be regarded to be doublet in structure.

With the sample, whose center axis coincide with the *c* axis, little anisotropic hyperfine structure is observed in the spectra, especially when the angle (b, H) is 90° as seen in Fig. 5. If we denote by $\mathbf{r}_i$ the vector pointing from a radical to the ith proton affecting the radical i, and the angle between $\mathbf{r}_i$ and the magnetic field by θ_i, the condition that all anisotropic hyperfine interactions vanish will be $3\cos^2\theta_i - 1 = 0$. The angle satisfying this formula is 55° or 125°. These $\mathbf{r}_i$ will be distributed symmetrically against the plane perpendicular to the *c* axis and also will be distributed in the directions nearly perpendicular to the *c* axis, because even when the direction of H was changed in the plane perpendicular to *c* axis, little anisotropic hyperfine interaction is observed.

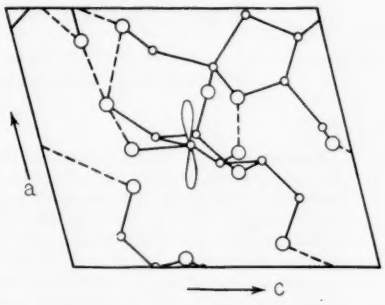

FIG. 7. A proposed model of a radical produced in sucrose by gamma irradiation. The lobe at the center indicates the unpaired electron.

With the sample, whose center axis coincides with the *a* axis, considerable hyperfine interaction is seen in the patterns, but its separation is not clear, as shown in Fig. 3. The reason will be that there are different pairs of θ_i and $\mathbf{r}_i$, which give values of $(3\cos^2\theta_i - 1)/\mathbf{r}_i^3$ differing only slightly, and the final spectra is observed as the superposition of many components become rather complicated.

With the sample whose center axis coincides with the *b* axis the anisotropic hyperfine interaction is clearly seen as in Fig. 4. The reason will be that when H is in the plane involving *a* and *c* axis, only the protons existing near the (a, c) plane influence the ESR spectra, and the appearance and disappearance of the anisotropic effect is distinct when the direction of H is changed. The fact that the spectra obtained by the *b*-axis sample show the highest complexity when the angle (c, H) is near 50° or 120°, is easily understood if the angle between $\mathbf{r}_i$ and the *c* axis is taken to be 55°, because $\mathbf{r}_i$ would be nearly parallel to H at 50° or 120°. It is not yet possible to give a definite picture of radicals in sucrose but the radical shown in Fig. 7 may present one of the possible pictures conforming to the results of our experiment. As already mentioned, the ESR spectra obtained in the irradiated polycrystalline sucrose (1) in Fig. 2 is nearer to the hypothetical spectra (2). This fact is also in good accord with the assumption that the radicals are formed on a pyranose ring.

Heat Capacities and the Residual Entropy of Ta_2H† *

W. G. Saba, W. E. Wallace, H. Sandmo, and R. S. Craig
Department of Chemistry, University of Pittsburgh, Pittsburgh 13, Pennsylvania

(Received December 27, 1960)

Heat capacities of Ta_2H have been determined over a range of temperature extending from 12° to 555°K. Three very sharp λ points were observed, at 306, 332, and 333.5°K, suggesting that Ta_2H exists in four forms—β_1 below 306°K, β_2 between 306 and 332, β_3 at about 333, and α above about 334°K. The heat capacity data for Ta_2H are used together with similar data obtained earlier for elemental tantalum and the entropy of formation of Ta_2H, evaluated from vapor pressure work by Kofstad, Wallace, and Hyvönen, to compute the residual entropy of β_1-Ta_2H. This is found to be -0.39 ± 0.30 cal^{-1} deg^{-1} mole^{-1}. The data also are used to estimate configurational entropies of the β_2 and β_3 forms. These are 0.70 and 3.3 cal^{-1} deg^{-1} mole^{-1}, respectively. The corresponding quantity for the α form is 4.9.

The λ points are attributed to rearrangements of the hydrogens in the 12-fold more abundant tetrahedral sites. At low temperatures the solute hydrogen atoms are presumed to populate the sites in an orderly fashion. With increasing temperature the ordered arrangement is altered and finally, in the α phase, destroyed. It is inferred from entropy calculations, however, that local order, probably pairing, persists in the α form even to 555°K, the highest temperature studied.

Consideration is given to the possibility that the upper two λ points, which nearly coincide, should really be one, the splitting being due to concentration gradients or strains. Differential thermal analysis of samples containing from 27.5 to 44.0 atomic % hydrogen suggests that the splitting is a true property of Ta_2H, but the results are not completely conclusive.

I. INTRODUCTION

ONE of the properties exhibited by many transition metals is the ability under appropriate conditions to absorb substantial quantities of hydrogen. Tantalum is one of the metals which possesses this ability. For example, at about 200°C and at a gas pressure of about 1 atm it can absorb roughly 44 atomic % hydrogen.

A number of years ago Kelley measured[1] the heat capacities of elemental tantalum and tantalum containing 2.76, 6.33, and 8.74 atomic % hydrogen. His measurements, which covered the range from 53° to 298°K, show the customary dependence of the heat capacity on temperature for the element. However, results for the hydrogenated specimens showed broad λ-type thermal anomalies between 125° and 300°K. The excess heat capacity became noticeable at about 125°K in each case. It extended to 240°K in the case of the most dilute alloy, to 260°K for the sample containing 6.33% hydrogen and to 280°K for the most hydrogen-rich sample.

Several years ago a series of studies dealing with the Ta–H system was initiated in this Laboratory. One of the objectives of these studies was to establish, if possible, the origin of the thermal anomalies observed by Kelley. The first of these studies, a brief account of which has been published, was concerned with a determination of the constitution of the Ta–H system below 0°C using x-ray diffraction techniques.[2] In this work it was found that samples containing up to 20 atomic % hydrogen were single phase and possessed the simple body-centered-cubic structure of the parent metal at room temperature. However, if the primary solid solution was cooled or if the hydrogen content was increased above 20% at room temperature, a second phase developed, whose composition is approximately represented by the formula Ta_2H. This work made it clear that the several hydrogenated samples used by Kelley consisted of two phases at temperatures below 175°K.

Hereafter, in this paper the body-centered-cubic primary solid solution based on tantalum will be called the α phase and the phase which precipitates out at low temperatures will be called the β phase. Crystallographic studies of the β phase using x-rays revealed that the structures of the two phases are very similar. They differ in that in β-Ta_2H one of the edges of the unit cell is larger than the other two by 0.8%. Thus the cubic symmetry is lost and β-Ta_2H is body centered tetragonal.

The x-ray diffraction studies showed that when samples containing more than about 2 atomic % hydrogen are cooled to 125°K, virtually all of the hydrogen present in the system collects in the β phase. It was furthermore established in this work that as the sample is warmed up, hydrogen is transferred to the α phase and the amount of β phase steadily decreases until at some point, which is still below room temperature, the β phase disappears entirely. From Le Chatelier's principle one concludes that the precipitation of the β phase is exothermal. Hence its destruction is endothermal. It thus appears that the endothermal conversion of the two-phase system, the stable state at low temperatures, into a single-phase system at higher temperatures produces the excess heat capacities observed by Kelley.

* From a thesis submitted by W. G. Saba to the University of Pittsburgh in partial fulfillment of the requirements for the Ph.D. degree, January, 1961.

† This work was assisted by a contract with the U. S. Atomic Energy Commission.

[1] K. K. Kelley, J. Chem. Phys. **8**, 316 (1940).

[2] T. R. Waite, W. E. Wallace, and R. S. Craig, J. Chem. Phys. **24**, 634 (1956).

TABLE I. Heat capacities of Ta_2H.

Temperature °K	C_p[a] cal/deg	Temperature °K	C_p[a] cal/deg	Temperature °K	C_p[a] cal/deg
Series I		286.75	7.887	255.18	6.692
		292.14	8.414	261.52	6.854
71.91	3.408	297.12	10.15	267.76	7.038
76.75	3.641	301.14	15.59	273.95	7.255
82.00	3.864	304.08	21.96	280.13	7.519
87.67	4.082	306.67	21.70	286.30	7.850
91.45	4.198	310.07	13.88		
96.23	4.341	314.52	11.35	Series V	
101.65	4.486	319.21	12.05		
106.98	4.614	323.30	12.94	11.99	0.040
110.90	4.705			14.18	0.068
116.71	4.824	Series III		16.48	0.108
122.37	4.928			18.76	0.160
127.91	5.019	296.86	9.33	20.02	0.196
133.36	5.104	300.29	13.52	22.19	0.272
138.72	5.182	304.00	21.53	24.21	0.355
144.42	5.253	307.03	21.13	26.44	0.462
150.46	5.325	310.90	12.57	29.78	0.652
156.41	5.392	315.76	11.48	34.28	0.947
162.76	5.456	319.00	11.94	39.42	1.314
169.53	5.522			44.41	1.682
176.23	5.585	Series IV		49.08	2.020
182.82	5.652			53.58	2.336
189.35	5.715	200.48	5.826	58.00	2.632
195.81	5.780	207.60	5.904	62.66	2.924
202.20	5.845	214.92	5.989	67.82	3.208
208.52	5.916	222.06	6.083	73.13	3.468
		228.83	6.176		
Series II		235.54	6.286	Series VI	
		242.19	6.408		
281.25	7.581	248.73	6.542	284.20	7.715
288.67	7.998	332.14	172.5	451.90	7.994
293.01	8.464	332.56	138.0	458.47	8.025
297.08	9.952	332.96	208.4	465.00	8.081
300.58	14.15	333.24	253.3	471.57	8.064
303.27	20.63	333.62	134.6	478.10	8.085
305.50	22.97	335.55	13.95	484.62	8.116
307.75	20.12	339.64	7.973	491.15	8.118
310.62	12.44	344.47	7.824		
314.10	11.25	349.31	7.805	Series IX	
317.64	11.73	354.14	7.798	330.37	45.25
321.07	12.34			331.03	122.0
324.37	13.17	Series VIII		331.34	182.0
				331.58	200.6
Series VII		334.36	23.07	331.82	189.7
		335.75	10.56	332.10	145.9
304.63	22.13	347.44	7.829	332.44	129.1
305.68	22.49	353.03	7.812	332.76	170.5
306.75	21.65	359.09	7.805	333.09	218.6
307.92	20.05	365.55	7.812	333.34	177.4
308.91	16.45	372.23	7.815	333.91	53.16
309.83	13.36	379.07	7.826	335.84	10.90
310.87	11.64	385.74	7.832		
311.89	11.15	392.39	7.846	Series X	
312.84	11.13	399.04	7.866	496.10	8.142
313.80	11.20	405.67	7.882	504.09	8.184
314.74	11.28	412.30	7.893	512.08	8.219
326.04	13.80	418.91	7.905	520.05	8.233
329.16	17.97	425.53	7.932	528.08	8.291
330.95	78.17	432.14	7.959	536.09	8.295
331.51	203.9	438.74	7.958	544.06	8.336
331.81	228.7	445.33	7.979	552.05	8.380

[a] Based upon sample containing 1 g atom of Ta.

The results at this stage clarified the origin of Kelley's thermal anomalies but raised some other rather interesting questions: (1) What is the essential difference between α and β Ta_2H, or what at the atomic level, is altered when one of these phase transforms into the other at about 50°C? (2) Is this a λ-type transformation similar to those observed by Kelley for alloys less rich in hydrogen or is it accompanied by a latent heat? (3) Is all configurational disorder removed at the transition point so that a unique arrangement of the hydrogens is then produced or are the solute particles still distributed over more than one site per atom? If the latter, will additional transformations occur at lower temperatures so as to remove all positional randomness or will some disorder be frozen-in and persist to the lowest accessible temperatures and hence give rise to a nonvanishing zero point entropy? It is toward the answering of these questions and others emanating from that that the investigations described in this and the following paper are directed. The present paper is concerned largely with the evaluation of the residual entropy of Ta_2H and obtaining estimates of its configurational entropy at several temperatures which are of special interest. In the following paper these data will be used together with results of neutron diffraction experiments to elucidate insofar as is possible the probable arrangement of the solute atoms in the several varieties of Ta_2H.

II. EXPERIMENTAL DETAILS

A. Materials Employed and Preparation of Sample

The tantalum, in the form of 0.015-cm thick foil, was purchased from the Fansteel Metallurgical Company and was stated to be 99.9% pure or better. Part of it was analyzed spectroscopically and only Nb, Fe, Ca, Cr, Mo, and V were detected. Estimates of the maximum amounts of impurity were for Nb and Fe—each 0.01%, the others—each 0.001%. In addition it probably contained a few hundredths of a percent of dissolved oxygen, nitrogen, and carbon, although no analysis was made for these impurities.

Prior to hydrogenation the sample was polished with emery cloth under oil, after which it was cleaned by washing in CCl_4, ether, and absolute alcohol. The hydrogen used to prepare the sample was purified by passage first through a Deoxo unit and then through two charcoal traps at liquid-nitrogen temperatures. The hydrogen was metered in using a gas buret system and after the appropriate quantity had been admitted, the sample, which was being held at 530°C, was cooled to room temperature over a period of about 10 hr.

At this point some rough vapor pressure data were taken for later use in making corrections for the evaporation of hydrogen into the dead space of the calorim-

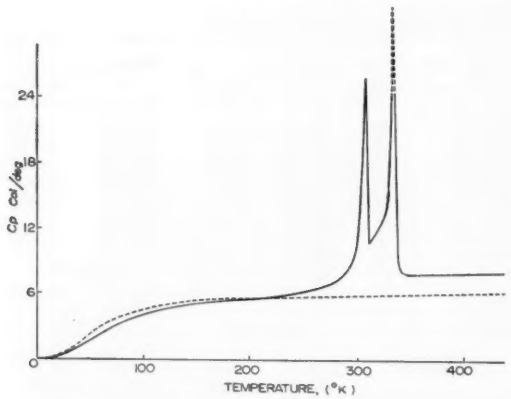

FIG. 1. Heat capacity as a function of temperature for Ta (dashed line) and Ta_2H (full line). Data are for samples containing 1 g atom of tantalum in each case. At the upper thermal anomaly C_p rises to a maximum value of 253 cal/deg.

eter. (Subsequently a careful vapor pressure study was made, the results of which have now been published.[3]) At room temperature the residual pressure was about 2 μ. The temperature was gradually raised to 350°C, at which the vapor pressure was about 0.5 atm, and held there for 3 hr. After this the sample was cooled to 200°C (vapor pressure≈5 mm), maintained at this temperature for 6 hr and then cooled to room temperature.

The sample being hydrogenated consisted of 11 pieces of foil. It was feared that some of these might hydrogenate more readily than others producing composition gradients in the sample. The heat treatment at 350° and 200°C were for the purpose of producing a sample whose composition was as nearly as possible uniform throughout. The rapidity with which the sample absorbed or liberated hydrogen at 350°C suggested that 3 hr was long enough for composition differences to have been eliminated. No appreciable graduations in composition should have resulted by further hydrogen absorption when the sample was cooled to room temperature since the dead space was such that even at 350°C less than 0.5% of the hydrogen present in the system was in the gas phase.

To test for possible inhomogeneity in the sample, a representative[4] portion of it was examined with x-rays. The lines in the diffraction pattern were very sharp and there was nothing to indicate that the sample was of nonuniform composition.

The sample initially used in the low-temperature calorimeter (12° to 325°K) weighed 618.367 g and contained 3.4091 g atoms of metal. After a portion of the range had been covered, a leak in the calorimeter developed and the sample had to be removed while repairs were made. At this point it was discovered that the large pieces of foil had broken up and a portion of the sample had crumbled to a powder. The powder, a part of which was used for the x-ray examination, was removed and the sample which was returned to the calorimeter weighed 583.707 g. When the low-temperature measurement were concluded and the sample was transferred to the high-temperature calorimeter, further loss occurred. The material used in these measurements weighed 549.617 g.

From the amount of gas metered in, the composition of the alloy was computed to be 33.32±0.02 atomic % hydrogen.

B. Apparatus Employed

The measurements were carried out using the two adiabatic specific heat calorimeters which have been in use in the Laboratory for a number of years. They have been described elsewhere.[5,6] The first of these was used to cover the range from 12° to 325°K while the second was employed for the range extending from 285° to 555°K. Cognizance was taken of the heat absorbed by evaporation of hydrogen into the space surrounding the

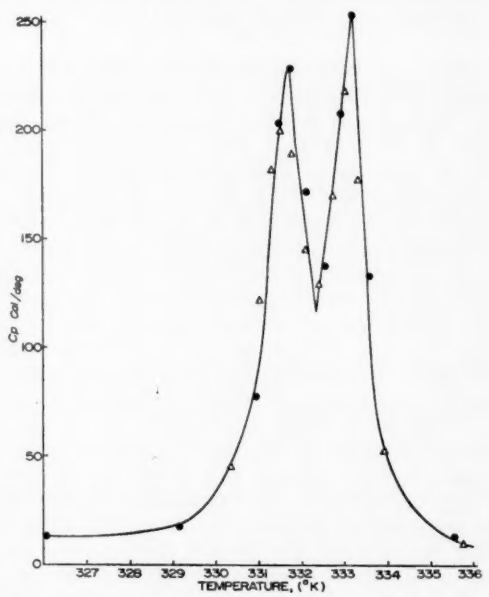

FIG. 2. Heat capacity versus temperature for Ta_2H in the region of the upper thermal anomaly. Data are for sample containing 1 g atom of Ta. ●—series VII, Δ—series IX.

[3] P. Kofstad, W. E. Wallace, and L. J. Hyvönen, J. Am. Chem. Soc. **81,** 5015 (1959).

[4] When the low-temperature series of experiments was interrupted (*vide infra*), it was found that the sample, which initially consisted of pieces of foil 20 to 50 cm in length, had broken into flakes roughly 0.5 to 1 cm on an edge. Simultaneously an appreciable amount of fine powder was produced. There was every reason to believe that this powder came from all parts of the sample and hence was representative of the sample studied in the calorimeter. A portion of this powder was used for the x-ray examination.

[5] R. S. Craig, C. A. Krier, L. W. Coffer, E. A. Bates, and W. E. Wallace, J. Am. Chem. Soc. **76,** 238 (1954).

[6] W. G. Saba, K. F. Sterrett, R. S. Craig, and W. E. Wallaee, J. Am. Chem. Soc. **79,** 3637 (1957).

sample in the calorimeter (about 75 cm^3). By using the vapor pressure and heat of vaporization data of Kofstad *et al.*[3] it was found that correction for this effect was negligible even at the highest temperatures studied.

C. Measurements Made

A total of 75 determinations were made in the low-temperature calorimeter. The bath employed, range covered, and number of determinations in each of the five series of measurements made in this calorimeter were, respectively, as follows: I—liquid N_2, 70° to 210°K, 25; II—ice slush, 280° to 325°K, 11; III—ice slush, 295° to 320°K, 7; IV—dry ice-acetone, 200° to 285°K, 14; V—liquid He, 10° to 75°K, 18.

Five series of measurements, involving a total of 84 determinations, were made in the high-temperature calorimeter. The range covered and the number of determinations are as follows: VI—285° to 325°K, 13; VII—305° to 355°K, 26; VIII—345° to 490°K, 25; IX—330° to 336°K, 12; X—495° to 555°K, 8.

In any series measurements were made in such a way that the entire temperature range was covered; that is, the final temperature in one determination was the initial temperature in the next.

Initially the sample consisted of six sheets, 7.5×30 cm; 2 sheets, 5×45 cm; and 1 sheet, 5×22.5 cm. These had been rolled up, hydrogenated, and introduced into the calorimeter. The sample in this form was used in series I and II. As mentioned earlier, near the conclusion of series II the soldered joint at the top of the calorimeter softened and the helium exchange gas was pumped away. To repair this the sample had to be removed, as stated above, whereupon it broke into flakes. The sample was in flake form for the remainder of the work.

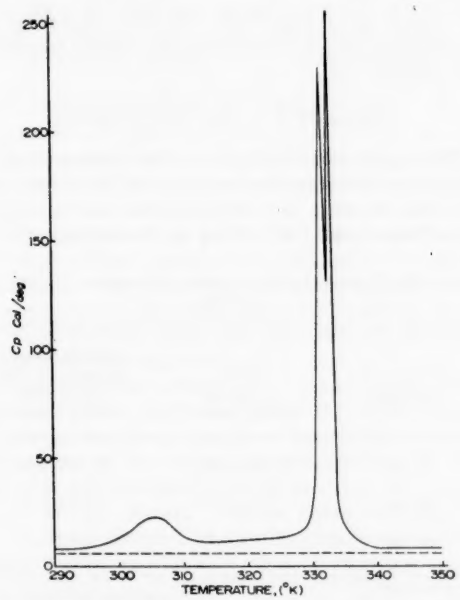

FIG. 3. Heat capacity as a function of temperature for Ta (dashed line) and Ta_2H (full line) in the region of the thermal anomalies. Data are for samples containing 1 g atom of Ta in each case.

TABLE II. Smoothed heat capacities[a] and related thermal data[a] for Ta_2H.

Temperature °K	C_p cal/deg	$H-H_0°$ cal	$\frac{H-H_0°}{T}$ cal/deg	S cal/deg	$\frac{F-H_0°}{T}$ cal/deg
5	0.003	0.00	0.000	0.001	0.001
10	0.0237	0.06	0.006	0.008	0.002
20	0.196	0.97	0.049	0.061	0.012
30	0.663	5.01	0.167	0.218	0.051
40	1.357	15.04	0.376	0.500	0.124
50	2.086	32.27	0.645	0.881	0.236
60	2.761	60.6	1.010	1.321	0.311
70	3.318	91.1	1.301	1.790	0.489
80	3.782	126.6	1.583	2.264	0.681
90	4.157	165.2	1.835	2.732	0.897
100	4.444	208.4	2.084	3.19	1.11
110	4.686	254.1	2.310	3.62	1.31
120	4.886	301.8	2.515	4.04	1.52
130	5.054	350.7	2.698	4.43	1.73
140	5.199	402.0	2.871	4.81	1.94
150	5.320	453.6	3.024	5.18	2.16
160	5.429	507.3	3.171	5.52	2.35
170	5.528	562.1	3.306	5.86	2.55
180	5.624	616.9	3.427	6.18	2.75
190	5.722	673.9	3.547	6.48	2.93
200	5.824	731.3	3.657	6.78	3.12
210	5.930	789.1	3.757	7.07	3.31
220	6.054	849.0	3.859	7.34	3.48
230	6.196	910.0	3.956	7.62	3.66
240	6.367	972.0	4.050	7.88	3.83
250	6.570	1037	4.128	8.15	4.02
260	6.814	1104	4.246	8.41	4.16
270	7.112	1172	4.341	8.67	4.33
273.15	7.223	1198	4.386	8.76	4.37
280	7.517	1245	4.446	8.94	4.49
290	8.125	1323	4.562	9.21	4.65
298.15	10.870	1400	4.696	9.47	4.77
300	12.880	1420	4.733	9.54	4.81
350	7.808	2579	7.369	13.09	5.72
400	7.865	2960	7.400	14.13	6.73
450	7.993	3356	7.458	15.03	7.57
500	8.164	3759	7.518	15.88	8.36
550	8.364	4172	7.585	16.67	9.08

[a] Based upon sample containing 1 g atom of Ta.

Since the vapor pressure of Ta_2H is 2 μ, or less, at 325°K, it appeared unlikely that a significant amount of hydrogen had been lost when the calorimeter opened up. Even so as a precautionary measure, measurements in the range 295° to 320°K were repeated (series III). Results obtained in series II and III were in excellent agreement, which substantiated the notion that the loss of hydrogen was insignificant.

III. RESULTS

A. Measured Heat Capacities

The data obtained corrected for curvature are given in Table I. The variation of C_p with temperature is sketched in Fig. 1 together with similar results for elemental tantalum. Excess heat capacities are ob-

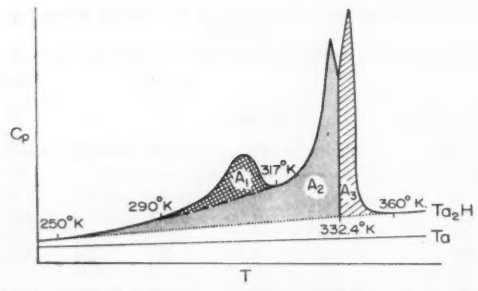

FIG. 4. Sketch of C_p vs temperature for Ta_2H to indicate the procedure employed in evaluating the configurational entropies given in Table III. For clarity the diagram is somewhat distorted. The areas A_1, A_2, and A_3 pertain to β_1–β_2, β_2–β_3, and β_3–α transitions, respectively.

served around 305° and 330°K, indicating second-order transitions at these temperatures. The latter transition gives rise to a large and exceedingly sharp λ-type thermal anomaly. Furthermore, the data obtained in series VII seemed to indicate that this peak in the heat capacity was a doublet, implying that this transition occurred in two stages. Since this was very unusual and not expected, the region around 330 was carefully reinvestigated (series IX) to verify that the peak is indeed a doublet. In these measurements the energy used was decreased so that the temperature increment averaged only about 0.3°. These data, shown in Fig. 2, together with those obtained in series VII, corroborated the earlier finding. The variation of C_p with temperature in the region of the anomalies is sketched in Fig. 3. This shows how exceedingly sharp the higher temperature anomalies are.

Smooth heat capacities and related thermal data are given in Table II. Results for the region extending from 300° to 340° are not included. These have been omitted partly for the sake of brevity and partly because the smoothing process is less reliable in this region due to the rapid variation of C_p. The data obtained by such smoothing as is possible are given elsewhere.[7] Judging from the scatter of the data the precision of the results obtained using the high-temperature calorimeter is about 0.1%, except for temperatures in the immediate vicinity of the thermal anomalies. In these ranges estimates of precision were not made. With the other calorimeter the precision was somewhat better. The scatter of data indicated a precision of about 0.05% from 50° to 300°K. However, below 50°K it rose to a maximum of about 2% at the lowest temperatures employed. In the region of overlap results obtained with the two calorimeters agreed within 0.2%, indicating that systematic errors were probably not in excess of this.

On the basis of the heat capacity data Ta_2H seems to exist in four forms—β_1 below the thermal anomaly at about 306°K, β_2 between 306 and 332°K, β_3 in an extremely narrow interval of temperature at about 333°K, and α above the thermal anomalies, that is from about 334°K up.

[7] W. G. Saba, Ph.D. Thesis, University of Pittsburgh (1961).

B. Configurational Entropies

From vapor pressure work previously carried out in this Laboratory[8] the entropy of formation of α-Ta_2H has been established for temperatures ranging from 300° to 400°C. Using these results together with the present heat capacity data and similar data for elemental tantalum published earlier[8] the residual entropy of β_1-Ta_2H can be computed. The data can also be used to estimate the configurational entropy of the β_2, β_3, and α forms.

From the vapor pressure data Kofstad, Wallace, and Hyvönen computed the entropy change for hydrogenating tantalum as follows:

$$2\mathrm{Ta(s)}+\tfrac{1}{2}H_2(1\text{ atm})\rightarrow\alpha\text{-}\mathrm{Ta_2H(s)}\;\Delta S_{573^\circ\mathrm{K}} = -12.24\pm0.18\text{ cal/deg.} \quad (1)$$

Using the known entropy of hydrogen[9] at this temperature one obtains

$$(S_{\mathrm{Ta_2H}}-2S_{\mathrm{Ta}})_{573^\circ\mathrm{K}}=5.64\pm0.19\text{ cal/deg.} \quad (2)$$

The residual entropy of β_1-Ta_2H can then be computed from the relationship

$$(S_{\beta_1\text{-}\mathrm{Ta_2H}})_{0^\circ\mathrm{K}}=(S_{\mathrm{Ta_2H}}-2S_{\mathrm{Ta}})_{573^\circ\mathrm{K}}-573\int(\Delta C_p/T)\,dT, \quad (3)$$

in which $\Delta C_p=(C_p)\mathrm{Ta_2H}-2(C_p)\mathrm{Ta}$. Inserting the appropriate data and evaluating the integral graphically one obtains

$$(S_{\beta_1\text{-}\mathrm{Ta_2H}})0^\circ\mathrm{K}=-0.39\pm0.30\text{ cal/deg.} \quad (4)$$

Taking this result to signify that at low temperatures there is no configurational entropy in the β_1 form, one can then estimate the configurational entropy of the other forms merely by adding up the entropy changes

TABLE III. Estimated configurational entropies of β_2-, β_3-, and α-Ta_2H.

Transition	ΔS of transition cal deg^{-1} mole^{-1}	Configurational entropy of high temp. form cal deg^{-1} mole^{-1}
$\beta_1\rightarrow\beta_2$	0.70±0.05	0.70±0.05
$\beta_2\rightarrow\beta_3$	2.6±0.1	3.3±0.15
$\beta_3\rightarrow\alpha$	1.59±0.05	4.9±0.2

[8] K. F. Sterrett and W. E. Wallace, J. Am. Chem. Soc. **80**, 3176 (1958).

[9] "Tables of thermal properties of gases," National Bureau of Standards Circ. No. 564 (1955), Table 6-5, p. 280.

associated with the three thermal anomalies.[10] The procedure employed in estimating these entropy changes can best be understood in terms of the sketch in Fig. 4. In each instance the course of the normal heat capacity curve is estimated from a large scale plot of the data for temperatures extending well outside the range in which there is excess heat capacity. The differences between these estimates (represented as the dotted and dashed curve in Fig. 4) and the observed results are the heat capacities ascribed to the transitions. Thus the area labeled A_1 pertains to the β_1–β_2 transition and A_2 and A_3 refer to the β_2–β_3 and β_3–α transitions, respectively. Delineation between the latter two transitions was made arbitrarily at the temperature corresponding to the heat capacity minimum, 332.4°K.

The results obtained are given in Table III together with the estimated uncertainties. The latter include only contributions due to the uncertainty in locating the normal heat capacity curve. Uncertainties due to overlap, to the arbitrary division of energies at the split peak, etc., are not included. Despite those limitations the estimates are of value, particularly that for the β_2 form, in connection with the discussion in the following paper.

IV. DISCUSSION OF RESULTS

The heat capacity measurements clearly reveal the existence of two λ-type thermal anomalies for Ta_2H. Although the matter is not conclusively settled as yet, recent experimental evidence (*vide infra*) seems to indicate that the upper anomaly is a doublet, so that there are a total of three λ points for this alloy. The factors responsible for these thermal anomalies are naturally of considerable interest. One possibility which initially seemed to merit attention is that some, or all, of these transformations might be of magnetic origin. Experiments designed to ascertain whether or not this is the case, described in the following paper, indicate that the transition does not originate with magnetic effects.

The other possibility is that the λ points result from structural rearrangements of the dissolved hydrogens. To indicate why this seems physically plausible it is necessary to consider two aspects of transition metal-hydrogen systems which have become clear, partly as a result of thermodynamic work and partly due to neutron diffraction studies. First, many investigations have shown that in dilute solutions the vapor pressure of hydrogen over such systems is linearly dependent on the square of the hydrogen concentration.[11,12] This indicates that the dissolved hydrogen exists as a monatomic species. Second, neutron diffraction measurements have shown that the hydrogens are usually located in the tetrahedral[13] interstices, or sites, but on occasion they can also occupy the octahedral sites.[14]

In Ta_2H there are many more interstitial sites than there are hydrogens to fill them. To be specific there are a total of 18 interstitial sites, 12 tetrahedral and 6 octahedral, sites available per hydrogen. If the hydrogens were noninteracting, one or the other or both of these sets of sites would be randomly populated by the solute particles. The evidence indicates that the hydrogens do interact, however, and hence if one site is occupied, the other hydrogens will, at low temperatures, selectively occupy sites in such a way as to minimize the energy of the system. Thus at these temperatures there will be an ordered arrangement of the interstitial hydrogens. With increasing temperature the solute atoms are expected to rearrange to permit the system to acquire a higher entropy. Thus an order-disorder transformation involving the interstitial hydrogens is expected from general considerations. Actually the results obtained in the present study for Ta_2H seem to indicate that the transformation takes place in three stages, giving as indicated above, four forms of Ta_2H.

Information pertaining to the arrangements of the hydrogens in the several forms of Ta_2H is obviously of interest. Discussion of these will, however, largely be postponed until the next paper, which deals explicitly with the probable hydrogen structure for the β_1 and β_2 varieties. Some remarks are appropriate at this time about the hydrogen arrangement in the α form, however, since it is not discussed later.

In the following paper it is shown that the hydrogens in the low-temperature modifications of Ta_2H occupy certain of the tetrahedral sites. On this basis it seems justified to assume that in the high temperature, or α-, form they are also in the tetrahedral sites. Initially it was supposed that the distribution over the sites was random, or very close to it. The entropy data contained in this paper show that this is not the case. The calculated value for the configurational entropy (S_c) in eu/g atom of H is 6.84 if the hydrogens are distributed randomly over all the tetrahedral sites. The corresponding experimental value is estimated to be about 5.0 eu for temperatures ranging from 340° and 573°K.

The available data can be employed in two ways to estimate the configurational entropy just cited. Both ways involve the assumption that the quantity $S_{Ta_2H}-2S_{Ta}$ can be resolved into components as follows:

$$S_{Ta_2H}-2S_{Ta}=\Delta S_v+S_H+S_c. \qquad (5)$$

Here S_H represents the vibrational entropy of the solute and ΔS_v represents the quantity $(S_{Ta_2H}-2S_{Ta})_v$. ΔS_v is the difference in vibrational entropy of hydrogenated and pure tantalum. The quantity $S_{Ta_2H}-2S_{Ta}$ is known to be 5.6 cal/deg for 573°K and 4.7 cal/deg for 340°K.

[10] The data can be used in another way (see below) to estimate configurational entropies.

[11] P. Kofstad and W. E. Wallace, J. Am. Chem. Soc. **81**, 5019 (1959).

[12] D. P. Smith, *Hydrogen in Metals* (University of Chicago Press, Chicago, 1948).

[13] G. E. Bacon, *Neutron Diffraction* (The Clarendon Press, Oxford, England, 1955), p. 181.

[14] C. E. Holley, Jr., R. N. R. Mulford, F. H. Ellinger, W. C. Koehler, and W. H. Zachariasen, J. Phys. Chem. **59**, 1226 (1955).

ΔS_v and S_H are estimated by appropriate calculations as will now be indicated.

In recent years the notion has come to be generally accepted that hydrogen dissolved in transition metals behaves like an Einstein oscillator. This point of view is supported by cold neutron scattering work[15,16] and is in line with theoretical expectations.[17] If the characteristic temperature (θ_E) is known, S_H can be readily evaluated. Unfortunately, θ_E for hydrogen in tantalum has not been determined. However, examination of the Zr–H system by neutron scattering techniques indicates a characteristic temperature of 1500°K in this case. This value of θ_E may be assumed to apply also to the Ta–H system for the purpose of calculating S_H since only an approximate value of this quantity is required. When this is done, S_H is found to be 0.4 and 1.7 cal/deg at 340° and 573°K, respectively.

ΔS_v can be estimated from the Debye characteristic temperatures (θ_D) of the two materials. θ_D for Ta is[8] 230°K. θ_D for Ta_2H was evaluated to be 250°K using C_p data[18] in the liquid nitrogen range, where the hydrogen contribution to the heat capacity is negligible. Using these values, ΔS_v was evaluated to be -0.8 and -1.2 cal/deg at 340° and 573°K, respectively. Thus all quantities, except S_c, in Eq. (5) are known and hence S_c can be evaluated. The value found is 5.1 cal/deg at both 340° and 573°K.

The other means of evaluating S_c is through the use of the data in Table III. There, it will be noted, S_c for the α form just above the highest λ point, approximately 340°K, is given as 4.9 cal/deg. The increase in S_c on raising the temperature to 573°K can be evaluated using Eq. (5). From the discussion in the preceding paragraphs the increments in $S_{Ta_2H}-2S_{Ta}$, ΔS_v and S_H are 0.9, -0.4, and 1.3 cal/deg, respectively, from which one estimates S_c at 573°K to be also 4.9 cal/deg.[19]

It is thus clear that the configurational entropy is considerably less, even at 573°K, than that which would be characteristic of the system if the hydrogens were randomly distributed over the tetrahedral sites. This indicates that while all sites may be equally populated, an appreciable amount of short range or local order, probably pairing, exists in the solution.

The tendency to pair originates in a simple way. Hydrogen in tantalum is known to be positively charged.[20] When it is placed in a site, it undoubtedly repels its four neighbors, disturbing the lattice locally. As it enlarges its own site, it enlarges certain of the adjacent sites so that they become energetically favorable for other solute particles compared to more remote interstitial positions. In this way the pairing, or, more generally, correlation of positions develops.

One other aspect of the results obtained merits discussion, namely, whether or not the double thermal anomaly at about 330°K is a true property of Ta_2H. There is no question as to the reality of the splitting of the peak. The results obtained are entirely unambiguous in this respect. The question is whether or not the sample which was studied was Ta_2H. In preparing the sample there was, as indicated above, simultaneous hydrogenation of a number of sheets of tantalum, possibly having variable permeability to hydrogen, so that the sample might not have been uniform throughout. Precautions were exercised in forming the sample to prevent this and it is believed that it was free of composition differences. If, however, one assumes that these efforts were fruitless and that some of the sheets hydrogenated to saturation while the others shared the remaining hydrogen, the sample employed in the heat capacity work would consist of two parts, one hydrogen rich and the other hydrogen poor. In this case if the λ-point temperature were a sufficiently strong function of composition, a doublet would result.

It was found that the thermal anomalies in the Ta–H system could be rapidly and conveniently studied using differential thermal analysis (DTA). Eleven Ta–H samples, having compositions varying from 27.5 to 44.0 (saturation) atomic % hydrogen, were examined using this technique in an attempt to ascertain whether or not the split peak is characteristic of Ta_2H. The results while not completely conclusive, suggested that this is the case.

Three samples, Nos. 1, 2, and 3, having compositions 33.3% hydrogen were examined using DTA. No. 1 was a portion of the calorimetric sample. No. 2 was prepared by Dr. A. Pebler in this Laboratory from a single piece of tantalum wire. No. 3 was made by hydrogenating a piece of foil. It was prepared in the Atomics International Research Laboratory and was made available for the present work by Dr. W. G. Gehman. Each of these three samples showed a split DTA peak between 58° and 60°C. The splitting was found to be slightly greater for numbers 2 and 3, which were prepared from single pieces of metals, than for No. 1. This indicated that if the splitting is a result of composition gradients, the homogenization procedure employed in preparing the calorimetric sample was reasonably successful.

[15] I. Pelah, C. M. Eisenhauer, D. J. Hughes, and H. Palevsky, Phys. Rev. **108,** 1091 (1957).
[16] W. L. Whittemore and A. W. McReynolds, Phys. Rev. **113,** 806 (1959).
[17] E. W. Montroll and R. B. Potts, Phys. Rev. **100,** 525 (1955).
[18] Correction of C_p to C_v was made assuming the compressibility and expansivity of Ta_2H to be the same as that for pure Ta. Correction for the electronic contribution was made using the expression $C_{el}=4\times10^{-4}T$ (in cal/deg g atom), based on unpublished measurements of G. Galli, H. Sandmo, and R. S. Craig in this laboratory.
[19] These calculations also indicate that the excess C_p for α–Ta_2H over that for the pure metal has been accounted for satisfactorily under the assumptions cited, namely that the tantalum cores are coupled to produce a Debye solid with characteristic temperatures as given and the hydrogens are almost entirely decoupled and act as Einstein oscillators. The excess heat capacity is due exclusively to vibrational excitation of the interstitial hydrogens, the almost linear rise being due to the high value of θ_E.
[20] W. B. Hillig, Ph.D. dissertation, University of Michigan (1953).

The 44.0% sample showed that the upper thermal anomaly was split into two peaks, at 63° and 68°C. The λ-point temperatures are thus increased by up to 8° in the saturated metal over those for Ta_2H. This appears to exclude the possibility to which allusion was made earlier that a portion of the sample used in the calorimeter might have been hydrogenated to saturation. Accordingly it must be concluded that if concentration differences existed in the sample, they were not such as to produce two portions each having its own discrete hydrogen concentration. Instead the sample must have been comprised of pieces of metal with a range of hydrogen content about 33.3%, in which case a smearing out and running together of λ-points would be anticipated rather than a splitting into two components.

Nine of the 11 samples studied by DTA showed the upper thermal anomaly to be split into two peaks. The other two (30.2 and 32.5% hydrogen) did not, but an alloy with an intervening hydrogen concentration (31.3%) did reveal the splitting. Results for the two which failed to show the splitting are questionable, however, since they alone failed also to reveal the thermal effect associated with the β_1–β_2 transition.

These results indicate that the splitting occurs for alloys having a considerable range of composition. Furthermore, since all the samples, except No. 1, were hydrogenated in one piece and hence had the maximum opportunity for homogeneity, it seems as if the splitting was not due to nonuniformity of composition. This point of view is reinforced by the observation that the doublet is observed for the saturated solution, in which gradations in hydrogen concentrations are rather unlikely.

The argument, if left here, seems fairly convincing with regard to the doublet λ point for Ta_2H. Apart from the questionable nature of the results for the 30.2 and 32.5% samples, however, there is another respect in which the DTA results were not entirely satisfactory. The λ points disclosed using this technique failed to show a smooth dependence on compositions; instead they varied in a somewhat erratic fashion, which diminished to some extent confidence in the reliability of conclusions based on these measurements. In addition it is perhaps significant that the observed splitting for the three 33.3% samples averaged about a degree whereas the splitting for the others was on the average about double this figure. It seems possible therefore that the doublet results from secondary effects, for example variation of stress, which accompany hydrogenation of the metal and these are greater for the offstoichiometry samples. Clarification of this point, however, must await further work.

ACKNOWLEDGMENT

The authors would like to acknowledge the generous assistance of Dr. A. Pebler and Mr. R. A. Butera in connection with the DTA work. They would also like to express appreciation to Dr. W. G. Gehman for the sample of Ta_2H which he provided.

THE JOURNAL OF CHEMICAL PHYSICS VOLUME 35, NUMBER 6 DECEMBER, 1961

Neutron Diffraction Data for Ta_2D and the Probable Arrangement of the Deuteriums in Two of Its Polymorphic Varieties*

W. E. WALLACE

Department of Chemistry, University of Pittsburgh, Pittsburgh 13, Pennsylvania

(Received December 27, 1960)

Neutron diffraction data are presented for Ta_2D at 4°K, 78°K, room temperature, and 53°C. The patterns are indexed assuming a pseudocubic unit cell, the cell edge being 6.74 A at the three lowest temperatures and 3.37 A at 53°C. The enlarged unit cell in the low temperature (β_1) form is attributed to ordering of the deuteriums in the tetrahedral interstices. Attempts are made to establish the arrangement of the deuteriums (D's) in the β_1 and β_2 forms. For the latter, the stable form at 53°C, the intensities can be accounted for in three ways—by random distribution over $\frac{2}{3}$ (L group), over $\frac{1}{3}$ (S group) or over all of the tetrahedral interstices. From general considerations the first of these is thought to represent the actual situation in β_2-Ta_2D. In this the D's are distributed over the sites at $\frac{1}{2}\,\frac{1}{4}\,0$, $\frac{1}{2}\,\frac{3}{4}\,0$, $\frac{1}{4}\,\frac{1}{2}\,0$, $\frac{3}{4}\,\frac{1}{2}\,0+000$ and $+\frac{1}{2}\,\frac{1}{2}\,\frac{1}{2}$. Analysis of the β_1 pattern shows that despite the fact that this form has a vanishing residual entropy there is no unique configuration of the deuteriums. Instead, to account for the observed intensities one must accept a structure in which each deuterium is statistically occupying more than one site. Assuming each D to be distributed over two sites three satisfactory structures are obtained. These, designated A, B, and C, belong to space groups $I4$, $I\bar{4}$, and $I4_1$, respectively. Structure A seems the most reasonable of the three and hence is accepted as the one which is probably correct. In it the 8 D's are statistically occupying the 16 tetrahedral sites at $\frac{1}{8}\,\frac{1}{4}\,0$, $\frac{1}{4}\,\frac{7}{8}\,0$, $\frac{7}{8}\,\frac{3}{4}\,0$, $\frac{3}{4}\,\frac{1}{8}\,0$, $\frac{5}{8}\,0\,\frac{1}{4}$, $\frac{3}{8}\,0\,\frac{1}{4}$, $0\,\frac{3}{8}\,\frac{1}{4}$, $0\,\frac{5}{8}\,\frac{1}{4}+000$, and $+\frac{1}{2}\,\frac{1}{2}\,\frac{1}{2}$.

There is an apparent conflict between conclusions based on thermodynamic work and those developed from analysis of the diffraction data for the β_2 form as well as for the β_1 form. The observed configurational entropies of both forms are much less than those expected for the accepted structures. The discrepancies are thought to be due to local order.

I. INTRODUCTION

IN earlier studies of the tantalum-hydrogen system in this laboratory it has been found that at temperatures above about 60°C the range of primary solubility of hydrogen in tantalum extends to about 44 atomic % hydrogen.[1,2] At lower temperatures the range of composition of the primary solution (α phase) is restricted by the formation of an intermediate phase (β phase) based on the formula Ta_2H. The temperature at which this phase precipitates out depends of course on the composition of the system. At $33\frac{1}{3}$ atomic % hydrogen the transformation of the α form into, or the precipitation of, the β form occurs when the sample is cooled below 60°C. The α form possesses the body centered cubic structure of elemental tantalum. β-Ta_2H is body-centered tetragonal in structure. However, its axial ratio is nearly unity (1.008 measured at 25°C) and hence the β form is a slightly distorted version of α-Ta_2H.

The present study was undertaken in an attempt to establish the structural difference between the α and β forms of Ta_2H. When the work was initiated, it was thought that there were only two polymorphic varieties of this alloy. Since that time the heat capacity data reported in the preceding paper[3] have been obtained and it has become evident that there are at least three and perhaps four forms of Ta_2H. Hence the transformation occurs in two or three stages instead of one, as was originally presumed. The purpose of the present study is to clarify insofar as it is possible the nature of the transformation which occurs at each of these stages.

Initially two different kinds of phenomena were considered as the factors possibly responsible for the β–α transformation. First, the notion was entertained that the transition might be of magnetic origin—a Néel or Curie point—with the alteration in symmetry produced as a secondary effect. Second, it was considered that the transformation might be due to a rearrangement of the interstitial hydrogens within the more abundant interstitial positions. Again in this instance the displacement of the tantalum cores would occur as a secondary effect, brought about by the details of the interactions of these cores with the solute hydrogens when they preferentially occupy certain of the interstitial sites.

While the second of these alternatives was favored from the outset, it was necessary to dispose of the other by resort to experiment, since there are well known instances in which strongly paramagnetic metals become either ferromagnetic[4] or antiferromagnetic[5] upon hydrogenation and since the crystallographic alterations at Curie or Néel points, particularly at the latter, are similar in kind and magnitude to that accompanying the transformation in Ta_2H.

The simplest examination indicated that the sample was not ferromagnetic in the β form. Furthermore, determination of its susceptibility showed a temperature independent susceptibility over a range of temperature which included the transition point, thus excluding the possibility of a Néel point. Hence, it was

* This work was assisted by the U. S. Atomic Energy Commission.

[1] T. R. Waite, W. E. Wallace, and R. S. Craig, J. Chem. Phys. **24**, 634 (1956).

[2] P. Kofstad, W. E. Wallace, and L. J. Hyvönen, J. Am. Chem. Soc. **81**, 5015 (1959).

[3] W. G. Saba, W. E. Wallace, H. Sandmo, and R. S. Craig, J. Chem. Phys. **35**, 000 (1961).

[4] W. Trzebiatowski, A. Sliwa, and B. Stalinski, Roczniki Chem. **26**, 110 (1952).

[5] W. Trzebiatowski and B. Stalinski, Bull. Acad. pol. Sci. **1**, 131 (1953).

clear that the transformation was not magnetic in origin.

To document the thesis that the transition is produced by a rearrangement of the dissolved hydrogens the resistivity-temperature behavior of Ta_2H was investigated between 27 and 75°C. The results of this study were, as will be indicated below, consistent with the presumed nature of the transition, but this kind of evidence alone is by no means conclusive. The only satisfactory evidence is that obtained from neutron diffraction work. Accordingly, a sample of Ta_2D was examined[6] using this technique at temperatures ranging from 4°K to 53°C. Interpretation of the results so obtained indicates that the transition is indeed due to an order-disorder transformation involving the interstitial hydrogens. Furthermore, as will be brought out in detail below, analysis of the diffraction results provides information concerning the probable location of the deuteriums in two of the forms of Ta_2H.

II. EXPERIMENTAL DETAILS

The sample was prepared using the same equipment and essentially the same technique as was employed in preparing the Ta_2H sample for the heat capacity studies described in the preceding paper.[3] The tantalum in sheet form was obtained from the Fansteel Metallurgical Company. Details concerning its purity have been given.[3] The deuterium gas was obtained from the Stuart Oxygen Company. Its hydrogen content was stated to be 1.5% or less.

The sample contained 146.052 g or 0.8074 g atom of tantalum and 0.4234 g atom of *D*. It therefore had a deuterium content of 34.40±0.02 atomic %.

To assist the homogenization of the sample it was slowly cooled from 310 to 189°C over a 12-hr period and from 189°C to room temperature over a period of 18 hr. The sample initially examined was in the form of about 50 6-mil sheets. Preferred orientation was found to be extensive with the material in this form and the measured intensities were not satisfactory. It was then ground to a fine powder and all the useful data were obtained with the sample in this form. X-ray examination of a portion of this powder revealed sharp lines, suggesting that the homogenization had been satisfactory.

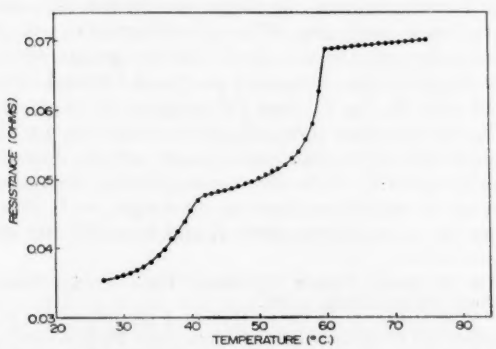

FIG. 1. Resistance versus temperature for tantalum wire hydrogenated to 33.4±0.5%.

TABLE I. Neutron diffraction data for Ta_2D.

Line positions[a] (2θ) and relative intensities (I)							
4°K		78°K		Room Temperature		53°C	
2θ	I	2θ	I	2θ	I	2θ	I
12.9	200	12.9	230	12.8	180		
22.2	220	22.2	230	22.2	170		
25.8	2430	25.7	2440	25.7	2290	25.7	1990
29.1	170	29.0	170	29.0	160		
34.3	230	34.2	250				
36.9	1090	36.9	1020			36.9	930
38.9	200	38.8	190				
		45.3	2790			45.4	2360
		47	70				
		52.9	600			53.0	490

[a] Neutron wavelength = 1.065 A.

III. EXPERIMENTAL RESULTS AND INDEXING THE PATTERNS

The resistance-temperature data obtained for Ta_2H in the form of 20-mil wire are shown in Fig. 1. Sharp rises in resistance are in evidence between 32 and 40°C and between 53 and 60°C, as would be expected if the crystal is experiencing an order-disorder transformation in those temperature ranges. The temperatures at which the rise in resistance occurs correlate well with the λ-point temperatures—33°C and 58 and 60°C—observed in the heat capacity work. However, it is to be noted that the resistance data give no indication[7] of two stages of transition near 60°C. Otherwise, they are fully in accord with the notion that the transitions are due to the destruction of an ordered arrangement of interstitial hydrogens.

The neutron diffraction data are summarized in Table I. These results clearly show that the structure of the material is the same throughout the temperature range from 4°K to room temperature and thus are consistent with the heat capacity data which show no

[6] Ta_2D was used instead of Ta_2H in the work because of a more favorable neutron scattering factor for the deuteron. On the basis of x-ray evidence, Ta_2D and Ta_2H exhibit identical behavior, at least as regards the β–α transition, and hence are discussed in this paper interchangeably.

[7] This might result from the fact that one of these two stages involves a structural alteration which has little or no effect on the scattering of the conduction electrons. A change from one type of local order to another, as is involved in one of the possibilities suggested for the β_2–β_3 transition, might be such an alteration.

TABLE II. Comparison of observed and calculated neutron diffraction line intensities for β_2 Ta_2D.

		Relative intensities		
		Calculated assuming random distribution in tetrahedral interstices		
Line	Measured	*S* sites only*	L sites only*	*L* and *S* sites
110	85	89	87	87
200	39	43	40	38
211	100	100	100	100
220	21	24	21	20

* See text for definition of *S* and *L*.

thermal anomalies in this range.[8] The data in the first six columns of Table I are hence for Ta_2D in the form that is designated β_1. The diffraction results at 53°C, in the range where β_2-Ta_2D exists, are very different from those obtained at lower temperatures, indicating that the difference in structure for the two polymorphic varieties is such that it can be studied by neutron diffraction techniques.

Analysis of the data for β_1-Ta_2D has been confined to the pattern obtained at 78°K, since the data in this instance are the most complete. X-ray examination of the β_1 form has shown it to be tetragonal with $a=3.37$ A and $c/a=1.008$. Since the linewidth in the neutron pattern for those lines which should be split by the tetragonality are comparable with or greater than the expected splitting, the sample appears to be cubic, or rather pseudocubic, in the present study. Assuming a pseudocubic material, the pattern is readily indexed and a spacing of 6.74 A is found. Thus when examined with neutrons β_1-Ta_2D exhibits a doubled periodicity in all three directions over that observed with x rays. The indices of the lines observed at increasing Bragg angles are 110, 211, 220, 301, 312, 400, 411, 422, 314, and 440.

X-ray examination of the β_2 form reveals that it is also tetragonal with lattice parameters essentially the same as those for β_1 Ta_2D. Again, the resolution using neutrons is insufficient to disclose the line splittings due to the tetragonality and the pattern is indexed on the basis of a pseudocubic cell, in this instance with an edge of 3.37 A, the same as that observed using x rays. The indices for the four lines reported in Table I are 110, 200, 211, and 220. In addition two other lines were observed, at $2\theta=59.7$ and 72.2. They were not included in Table I since the intensity measurements were not completely satisfactory in these cases. Their positions, however, are consistent with the unit cell chosen and their indices are 103 and 321, respectively.

[8] The data reported in the preceding paper extend down to only 12°K. Unpublished measurements of G. Galli, H. Sandmo, and R. S. Craig on Ta_2H extending to 1.5°K show no additional thermal anomalies below 12°K.

IV. ATOMIC ARRANGEMENT IN β_2 Ta_2D

The unit cell for this material contains two tantalums and one deuterium. The tantalums are, of course, situated at 000 and $\frac{1}{2}\frac{1}{2}\frac{1}{2}$. On the basis of previous studies of transition metal-hydrogen systems[9,10,11] it was presumed when analysis of the β_2 pattern was begun that the deuteriums were located in the interstitial positions, either in the tetrahedral or in the octahedral sites. The absence of lines with $h+k+l$ odd indicated a body centered structure. Thus, since there is only one deuterium per unit cell, it was clear that the D's are distributed over two or more sites in the cell.

First, we consider the octahedral sites 0_1, 0_2, and 0_3 at $\frac{1}{2}\frac{1}{2}0$, $\frac{1}{2}0\frac{1}{2}$ and $0\frac{1}{2}\frac{1}{2}$ and $0_1'$, $0_2'$, and $0_3'$, at $00\frac{1}{2}$, $0\frac{1}{2}0$ and $\frac{1}{2}00$. We designate the fractional occupancies of 0_1, 0_2, and 0_3 as x, y, and z, respectively. From the centering condition these are also the fractional occupancies in $0_1'$, $0_2'$, and $0_3'$. Since there is only one D in the cell, $z=\frac{1}{2}-(x+y)$. Thus the line intensities are expressible as functions of x and y. When this is done, it is found that no possible values of x and y will lead to an intensity distribution matching that which is observed. For example, the ratio of intensities of the first (110) and third (211) lines can be shown to be independent of x and y. The computed value[12] for this ratio is 1.6 whereas the observed ratio of intensities is 0.85. Calculations for the second line (200) show an intensity relative to that of the third line ranging from a minimum value of 0.9 when $x=y=0$ to a maximum of 1.2 when $x=y=\frac{1}{6}$ (random distribution over all octahedral sites). The experimental ratio is 0.4. On the basis of such comparisons it was quite clear that the solute atoms are not located in the octahedral sites.

Next, we consider the six tetrahedral sites T_1, T_2, T_3,$\cdots T_6$ at $\frac{1}{2}\frac{1}{4}0$, $\frac{1}{2}\frac{3}{4}0$, $\frac{1}{4}\frac{1}{2}0$, $\frac{3}{4}\frac{1}{2}0$, $0\frac{1}{2}\frac{1}{4}$, and $\frac{1}{2}0\frac{1}{4}$ and the other six T_1', T_2',$\cdots T_6'$ whose positions are related to those of the first by the translation $\frac{1}{2}\frac{1}{2}\frac{1}{2}$. In a cubic material all twelve tetrahedral sites are structurally equivalent. When it is distorted to tetragonal symmetry, the sites divide into two groups, which for simplicity may be termed the S and L groups. The four sites T_5, T_6, T_5', and T_6' comprise the S group. The four tantalum cores adjacent to these sites are all equidistant at the distance d_s (about 1.80 A). Due to the tetragonality of the alloy the neighboring tantalums are not all equidistant from the other eight, or L, sites. Two are at a distance $0.998\ d_s$ and the other two at

[9] G. E. Bacon, *Neutron Diffraction* (The Clarendon Press, Oxford, England, 1955), p. 181.

[10] C. E. Holley, Jr., R. N. R. Mulford, F. H. Ellinger, W. C. Koehler, and W. H. Zachariasen, J. Phys. Chem. **59,** 1226 (1955).

[11] J. E. Worsham, Jr., M. K. Wilkinson, and C. G. Shull, J. Phys. Chem. Solids **3,** 303 (1957).

[12] Calculation of intensities (I) were made using the relationship $I_{hkl}\sim[(F_{hkl}\exp(-2B\sin2\theta/\lambda^2)]/\sin\theta\sin2\theta$. The neutron scattering factors used for D and Ta were 0.65×10^{-12} and 0.70×10^{-12} cm, respectively. B was taken to be 0.66 at 53°C and 0.16 at 78°K, obtained from a Debye-Waller plot. The effects of the small amount of H contaminant and the slight deviation from stoichiometry were ignored in making the calculations.

1.005 d_s for observed axial ratio 1.008. Hence the L sites are slightly larger than the S sites.

Since we have a body-centered structure, we need consider, if tetragonal symmetry is assumed, only three arrangements of the deuterium in the tetrahedral interstices—random distribution in the S sites, in the L sites, or in all sites. Calculations for these three possibilities, given in Table II, show excellent agreement with experiment in all cases. Thus, we can conclude that the deuteriums are in the tetrahedral sites but on the basis solely of the evidence presented it cannot be established whether they are situated in the S group or in the L group. We discount the possibility that the D's occupy both sets of sites since it would be difficult, were this the case, to account for the observed tetragonality of the sample. From general considerations, as will be indicated below, it seems that random occupancy by the deuteriums of the L group of sites is the most probable structure of β_2 Ta_2D.

TABLE III. Comparison of observed relative intensities for β_1 Ta_2D with values computed for structures A, B, C, and U.

Line	Observed Intensities	Computed intensities A ($I4$)[a]	B ($I\bar{4}$)	C ($I4_1$)	U ($I4_1$)
110	10	8	8	8	15
112	10	10	10	10	11
220	100	100	100	100	100
301	7	6	6	6	6
312	10	9	9	9	9
400	42	48	48	48	59
411	8	5	5	4	4
422	115	129	129	129	69
314	3	5	5	5	5
440	25	26	26	26	57

[a] The space group in each case is indicated in parentheses. For details of the structures see text.

V. ATOMIC ARRANGEMENTS OF β_1 Ta_2D

A. Statement of the Problem

The unit cell for β_1 Ta_2D contains 16 Ta's and 8 D's. Positions of the metal atoms are easily established from the x-ray diffraction pattern, from which the β_1 form appears as a simple body centered tetragonal material with Ta's at 000 and $\frac{1}{2}\frac{1}{2}\frac{1}{2}$. With this information the structure of the tantalum lattice in the enlarged neutron cell is completely established.

The thermal data, the resistivity-temperature behavior, and the nature and kind of crystallographic distortion at the transition point, together with general considerations suggested that β_1 Ta_2D differs from the β_2 variety only in that the randomly arranged deuteriums in the latter have become more ordered in the former material. Since the D's populate certain of the tetrahedral sites in an apparently random fashion in β_2 Ta_2D (*vide infra*), it seemed reasonable to suppose that they are also in these sites in the low temperature form. Due to the interactions between solute particles, however, they populate only certain of the tetrahedral sites. The problem then is to establish which of the 96 tetrahedral sites in the unit cell are occupied by the deuteriums.

B. Initial Analysis of the β_1 Pattern

Analysis of the β_1 structure has passed through four stages, each of which will be briefly described. In the first it was assumed that the D's exist as an ordered arrangement in the L tetrahedral sites. Now, lines with $h+k+l$ odd are absent indicating a body centered structure. This means that one must locate 4 D's in 32 positions. If cognizance is taken of the tetragonality by assuming an ordinary fourfold axis, and if it is further assumed that the structure is unique (each D confined to one position), it develops that for any possible arrangement of the D's, in-phase scattering by all the deuteriums occurs for the 002 line.[13] Since this line is absent, it was concluded that the structure is not unique. Thus even in the β_1 form each D is statistically distributed over more than one site. By invoking the condition that the 002 line must be exinguished a structure was developed which gives a satisfactory accounting for the observed neutron diffraction intensities. This structure, which we call structure A, has the 8 D's in the unit cell distributed over the 16 tetrahedral sites located at $\frac{1}{4}\frac{1}{8}0$, $\frac{7}{8}\frac{1}{4}0$, $\frac{3}{4}\frac{7}{8}0$, $\frac{1}{8}\frac{3}{4}0$, $\frac{5}{8}0\frac{1}{4}$, $\frac{3}{8}0\frac{1}{4}$, $0\frac{3}{8}\frac{1}{4}$, $0\frac{5}{8}\frac{1}{4}+000$ and $\frac{1}{2}\frac{1}{2}\frac{1}{2}$. This structure belong to this space group $I4$ with half deuteriums located at general positions $x_1y_1z_1=\frac{1}{8}\frac{1}{4}0$ and $x_2y_2z_2=\frac{5}{8}0\frac{1}{4}$.

The agreement between calculated and observed intensities for structure A shown below in Table III was sufficiently good that the analysis was considered complete. This was accomplished, however, before the residual entropy of β_1-Ta_2H had been established. When the residual entropy, reported in the preceding paper, was found to be zero within experimental error, it was clearly necessary to examine the problem again to devise, if possible, a unique structure which would account for the observed intensities.

C. Search for a Unique Structure

In the second stage of analysis a unique structure was sought employing what might appropriately be called the "brute force" method. We have 8 D's to be distributed among 96 positions. There are about 10^{12} distinguishable ways of doing this. However, we only need to locate half of the D's; since it is a centered structure, the other 4 are located by symmetry. This

[13] This is also true either if the solute atoms are confined to the S sites or if they have access to all the tetrahedral sites.

narrows down the number of distinguishable arrangements to 194 580. Partial intensity calculations were made for all of these arrangements using an IBM 704 computer. The following absences were observed in addition to the systematic absences characteristic of the centered structure: 200, 020, 002, 222, 420, 402, 042, 240, 024, and 204. The computer was programmed to examine all the 194 580 different arrangements, to retain only those which satisfied the observed extinctions and then to calculate for each distribution of D's the ratio of intensities of the first two lines.[14] The computer was programmed to print out those distributions for which the calculated ratio agreed with the measured value to within $\pm 25\%$. In retrospect this range should probably have been broadened, but the next stage of analysis was more general than this mode of attack and so no impairment of the validity of the conclusions resulted by having stipulated a retention range which was perhaps slightly smaller than was desirable. In these calculations no assumption is made as to the symmetry of the system. It is either tetragonal or pseudotetragonal, the true symmetry possibly being lower than tetragonal. These calculations showed that none of the possible arrangements in the tetrahedral sites were satisfactory since none accounted satisfactorily for the relative intensities of the first two (superlattice) lines. Furthermore, calculations were made of the intensity of the first line relative to line 6 (400, 040, 004) for those arrangements whose I_1/I_2 values were closest to the observed value. In the most favorable case I_1 relative to I_6 was computed to be too intense by about a factor of 2 compared to the observed ratio. This reinforced the earlier conclusion that there is no satisfactory unique structure for β_1 Ta_2D which involves occupancy of the tetrahedral sites.[15]

In the next, or third, stage of the analysis we attack the problem in a completely general way, the only assumption being made is that we have a unique structure. Of course, in view of the observed systematic absences we retain the concept of a body-centered structure. However, no assumption is made as to the symmetry of the system except that it is not higher than tetragonal, the symmetry indicated by the x-ray diffraction pattern. In effect this means that we limit consideration to the tetragonal, orthorhombic, monoclinic or triclinic systems. Furthermore, the eight deuteriums are assigned to positions $x_1y_1z_1$, $x_2y_2z_2$, $\cdots x_8y_8z_8$, which may or may not coincide with the octahedral or tetrahedral interstices.[16]

In the tetragonal system the observed extinctions permit 19 possible space groups. Of these only the three most general ones need be considered, since the other sixteen are special cases of these three involving additional elements of symmetry. The three, involving an ordinary fourfold, a fourfold inversion and fourfold screw axis, respectively, are $I4$, $I\bar{4}$ and $I4_1$. There are no space groups which permit a body-centered structure in the triclinic or the monoclinic systems but there are 9 in the orthorhombic system—*Imma*, *Ibca*, *Ibam*, *Immm*, *Ima2*, *Iba2*, *Imm2*, $I2_12_12_1$ and $I222$. Each of these, plus the three space groups for the tetragonal system, was considered in the analysis of the diffraction pattern of β_1 Ta_2D.

$I4$, *Imm2*, *Iba2*, *Ima2* and $I222$ are immediately eliminated from consideration since with these space groups we compute an appreciable intensity for either the 200 or the 002 line for any possible location of the deuteriums. To extinguish these lines if the other five possible space groups for the orthorhombic system are employed, it is found that, designating the general position as xyz, x, y, and z must be either $\frac{1}{8}$, $\frac{3}{8}$, $\frac{5}{8}$, or $\frac{7}{8}$. With these values of x, y, and z we find that *Ibca* is eliminated since we always compute zero intensity for the first line (110). Similarly *Immm* is eliminated, since in this case we always compute zero intensity for the second line (112). If the matter is pursued further, we find that none of the other three space groups for the orthorhombic system leads to agreement with the observed diffraction line intensities. For example, the intensity of the first line (110) relative to that of line six (400) is observed to be about 0.23, whereas calculations assuming the applicability of space groups *Imma*, *Ibam* and $I2_12_12_1$ lead to relative intensities of 8.5, 4.3 and 3.2, respectively. Hence, the only two possibilities remaining are $I\bar{4}$ and $I4_1$.

Considering $I\bar{4}$ we find that since 002 is absent, we must have $z=\frac{1}{8}$, $\frac{3}{8}$, $\frac{5}{8}$ or $\frac{7}{8}$. Also the absence of 200 requires that $x=\pm y+\frac{1}{4}+q$, where $q=0$ or $\frac{1}{2}$. In addition, to cause the 222 line to vanish x or y must equal 0, $\frac{1}{4}$, $\frac{1}{2}$ or $\frac{3}{4}$. We find that to satisfy these conditions the general coordinates x, y take on values $\frac{1}{4}$ 0, $\frac{1}{4}$ $\frac{1}{2}$, $\frac{3}{4}$ 0, $\frac{3}{4}$ $\frac{1}{2}$, 0 $\frac{1}{4}$, 0 $\frac{3}{4}$, $\frac{1}{2}$ $\frac{1}{4}$ or $\frac{1}{2}$ $\frac{3}{4}$. Thus with the 4 possible values of z we have 32 possible values of xyz. Calculations show that none of these lead to a proper match with the observed intensities. For example, the computed intensity of line 1 relative to that of line 6 exceeds the observed ratio by 78%. Also line 1 is computed to be 60% more intense than line 2, whereas experimentally their intensities are the same within experimental error.

Calculations employing space group $I4_1$ give the best accounting for the observed intensities that can be made assuming a unique structure but, as will be indicated below, it cannot be considered satisfactory. We find, in this case as when using the $I\bar{4}$ space group, that the 200 and 222 extinctions require xy to assume the values $\frac{1}{4}$ 0, $\frac{1}{4}$ $\frac{1}{2}$, etc., as indicated in the preceding paragraph. However, in this case the value of z is not fixed by the extinctions. Calculations showed that the

[14] These "lines" included the groups (1) 110, $1\bar{1}0$, 101, $10\bar{1}$, 011, and $01\bar{1}$, and (2) 112, $11\bar{2}$, $1\bar{1}2$, 121, $12\bar{1}$, etc. For simplicity these groups of coinciding lines are referred to in the discussion which follows as the 110 and 112 lines.

[15] The situation is the same if small deviations, 0.02, to 0.03 A, from the tetrahedral positions are postulated.

[16] There are, of course, relationships between the sets of coordinates depending on the space group assumed to apply. In no case are we working with a 24 parameter problem.

superlattice lines were always too intense compared to the fundamental lines (220, 400, 422, and 440). The discrepancies were least with $z=0$ or $\frac{1}{4}$. The eight arrangements possible[17] turn out to be identical, with appropriate shifts of origin. Calculations for this structure, designated U, are shown in Table III. It is apparent that the intensities are not in satisfactory agreement with experiment and hence it must be concluded that the U structure is not the structure of β_1 Ta_2D. Thus, we conclude that there is no unique structure for β_1 Ta_2D. This means, of course, that despite the fact that there is no appreciable residual entropy the deuteriums must be statistically populating the available sites.

D. General Analysis

This brings us to the fourth and final stage of the analysis. As was indicated earlier, structure A does give a satisfactory accounting for intensity distribution in the neutron pattern. It belongs to space group $I4$ and hence is body centered with an ordinary fourfold axis. We wish to ascertain whether it is also possible to devise a structure involving the fourfold screw or inversion axis which will lead to the observed intensities.

To explore the matter systematically, we note that it is only necessary to establish the position of the deuteriums in one octant of the unit cell; the arrangements in the other octants are generated by the symmetry operations appropriate to the space group under consideration. The deuteriums are assumed to occupy (randomly) twice as many sites as there are particles, and further are assumed to be situated in the L sites. To satisfy the 002 extinction, $\frac{1}{2}$ of a D is placed in each of the two sub-groups of sites designated as $L\alpha$ (with $z=0$) and $L\beta$ (with $z=\frac{1}{4}$). As there are 4 positions each in the $L\alpha$ and $L\beta$ sub-groups, there are 16 ways of putting the 2 $\frac{1}{2}$ D's in the first octant. Using these 16 ways of populating the first octant, the A structure cited earlier and 15 others are generated by the symmetry operations appropriate to the $I4$ space group. Upon examining them we find that there is only one other distinguishable structure aside from A; call it A'. The A structure is produced by placing $\frac{1}{2}$ D each in the general positions $x_1y_1z_1=\frac{1}{8}\ \frac{1}{4}\ 0$ and $x_2y_2z_2=\frac{3}{8}\ 0\ \frac{1}{4}$. The A' structure is developed similarly except that $x_1y_1z_1=\frac{3}{8}\ \frac{1}{4}\ 0$ in this case. In it the deuterium arrangement is a mirror image of that in the A structure and hence they are enantiamorphic varieties of β_1 Ta_2D.

Next we employ a procedure similar to that just outlined except that space group $I\bar{4}$ is assumed. The 16 possible structures all turn out to be identical in this case when allowance is made for shifts of origin. This is termed the B structure. Finally, we repeat the procedure using the screw axis—space group $I4_1$. In this case we can satisfy the 002 extinction without allocating $\frac{1}{2}$ D's to the sub-groups. Hence, we have 56 possible structures produced by placing 2 $\frac{1}{2}$ D's in the 8 L sites of the first octant. Some of these do not satisfy the other observed extinctions; others lead to a poor accounting for the intensities. For example, they show an intensity of line 1 (relative to line 3) which is larger than the observed value by a factor of 2.8. The several possibilities which remain turn out to be identical when due allowance is made for alternative origins. This structure is designated the C structure.

To summarize briefly the analysis suggests 5 possible structures for β_1 Ta_2D—A, A', B, and C plus the U structure cited earlier. The tantalums are situated in structures A, A', B, and U at 000, $\frac{1}{2}$ 0 0, 0 $\frac{1}{2}$ 0, $\frac{1}{2}$ $\frac{1}{2}$ 0, $\frac{1}{4}$ $\frac{1}{4}$ $\frac{1}{4}$, $\frac{1}{4}$ $\frac{3}{4}$ $\frac{1}{4}$, $\frac{3}{4}$ $\frac{1}{4}$ $\frac{1}{4}$, $\frac{3}{4}$ $\frac{3}{4}$ $\frac{1}{4}$+000, and +$\frac{1}{2}$ $\frac{1}{2}$ $\frac{1}{2}$. In the C structure the tantalum coordinates are these coordinates+$\frac{1}{4}$ 0 0. The position of the $\frac{1}{2}$ D's in the A structure have been cited earlier. Those for the A' structure are $\frac{3}{8}$ $\frac{1}{4}$ 0, $\frac{5}{8}$ $\frac{3}{4}$ 0, $\frac{3}{4}$ $\frac{3}{8}$ 0, $\frac{1}{4}$ $\frac{5}{8}$ 0, $\frac{3}{8}$ 0 $\frac{1}{4}$, $\frac{5}{8}$ 0 $\frac{1}{4}$, 0 $\frac{3}{8}$ $\frac{1}{4}$, 0 $\frac{5}{8}$ $\frac{1}{4}$+000, and +$\frac{1}{2}$ $\frac{1}{2}$ $\frac{1}{2}$, for the B structure are $\frac{3}{8}$ $\frac{1}{4}$ 0, $\frac{5}{8}$ $\frac{3}{4}$ 0, $\frac{3}{4}$ $\frac{3}{8}$ 0, $\frac{1}{4}$ $\frac{5}{8}$ 0, $\frac{1}{8}$ 0 $\frac{1}{4}$, $\frac{7}{8}$ 0 $\frac{1}{4}$, 0 $\frac{1}{8}$ $\frac{3}{4}$, 0 $\frac{7}{8}$ $\frac{3}{4}$+000, and +$\frac{1}{2}$ $\frac{1}{2}$ $\frac{1}{2}$, and for the C structure are $\frac{1}{2}$ $\frac{3}{8}$ 0, $\frac{1}{2}$ $\frac{5}{8}$ 0, $\frac{5}{8}$ 0 $\frac{1}{4}$, $\frac{3}{8}$ 0 $\frac{1}{4}$, $\frac{1}{4}$ $\frac{3}{8}$ $\frac{1}{4}$, $\frac{3}{4}$ $\frac{5}{8}$ $\frac{1}{4}$, $\frac{5}{8}$ $\frac{3}{4}$ $\frac{1}{2}$, $\frac{3}{8}$ $\frac{1}{4}$ $\frac{1}{2}$+000, and +$\frac{1}{2}$ $\frac{1}{2}$ $\frac{1}{2}$. The coordinates of the D's in the U structure are 0 $\frac{1}{4}$ 0, 0 $\frac{3}{4}$ 0, $\frac{3}{4}$ $\frac{1}{2}$ $\frac{1}{4}$, $\frac{1}{4}$ $\frac{1}{2}$ $\frac{1}{4}$+000, and +$\frac{1}{2}$ $\frac{1}{2}$ $\frac{1}{2}$. Calculations for the A, B, C, and U structures are shown in Table III. Results for the A' structure are identical with those for the A structure and hence are not shown.

The discrepancies between computed and observed intensities for U are so great that it cannot be regarded as a satisfactory structure. We recall that this was the most nearly satisfactory of the possible unique structures. It was for this reason that we concluded earlier that β_1 Ta_2D does not possess a unique structure. On the basis of the computed intensities the other three structures are all satisfactory and in fact equally so. Actually, for A and B the computed intensities are identical. The only difference, which is an insignificant one, for structure C is the computed value for the 411 line.

VI. PROBABLE ORIGIN OF THE APPARENT CONTRADICTION BETWEEN THE DIFFRACTION AND ENTROPY RESULTS FOR β_1 Ta_2D

In the preceding sections we have shown that the observed diffraction data are not consistent with the concept of a unique arrangement of the D's in β_1 Ta_2D, but instead seem to require a structure in which the D's are distributed over twice as many sites as there are solute particles to fill them. Thus there seems to be a complete contradiction between the conclusion reached from the diffraction results on the one hand and the measured residual entropy, which requires a unique structure, on the other. In this section we shall attempt (1) to show that this contradiction is only apparent and (2) to reveal the probable origin of the apparent contradiction.

We believe that the crux of the matter resides in the fact that the D's are not *randomly* distributed over the

[17] The eight other possibilities are discarded since in those cases the positions of the D's and some of the Ta's coincide.

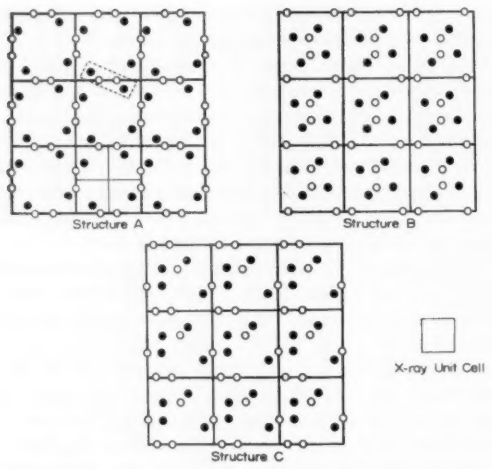

FIG. 2. Projections onto 001 plane showing deuterium positions in three possible structures for β_1 Ta_2D. $\frac{1}{2}D$ at $Z=0$ is indicated by ●, at $Z=\frac{1}{4}$ by 0. For simplicity the Ta's and half of the D's (in the upper half of the cell) are not shown. X-ray cell is shown for comparison. The basic structural unit (see text) is that produced by 4 D's occupying the positions enclosed by the dashed lines.

sites which are statistically being occupied. We believe that due to interactions between the solute particles very considerable correlation of positions of the D's occur (in other words there is local order)[18] and that, as a consequence, the configurational entropy is reduced below the level of detection, while at the same time the local order present is of such a nature as to have an immeasurable effect on the character of the diffraction pattern. We shall now illustrate how this could happen by estimating the configurational entropy of the system when it possesses a particular (idealized and simplified) type and amount of local order. Obviously there is no intent to represent this order as being identical with that in the system, whose nature is unknown and for which, accordingly, calculations are not possible; we do feel, however, that the type of order chosen for treatment bears sufficient resemblance to the actual order present to justify inclusion of the calculation at this point.

Consider the projection of the deuterium positions in structure A shown in Fig. 2. The basic unit of structure appears to be the group of occupants of the 4 sites encircled. Call this group of particles the basic structural unit (bsu) and the set of 4 positions the basic structural unit position (bsup). In the actual structure each bsup contains on the average only 2 D's. This half occupancy could arise, and probably does arise, by each bsu containing 4 D's and statistically occupying two bsup's. Were the occupancy random with each cell containing 2 bsu's distributed over 4 bsup's, the configurational entropy (S_c) would be $\frac{1}{8}$ R ln6 per mole of Ta_2D, which is already reduced to the point of almost escaping detection. We now suppose that there is local order in the arrangement of the bsu's so that in certain micropatches (or domains) the bsu's occupy positions so that they are all deployed along the x axis whereas in adjacent regions they populate positions lying exclusively along the y axis. (See Fig. 3). We further suppose (a) all domains to be equal in size, r repeat distances on an edge, and (b) the two types of domains to be equally abundant. (This is the idealized type of local order referred to earlier). Since the domains are perfectly ordered internally, the configurational entropy is then merely the entropy of mixing of the domains. For one mole of Ta_2D the number of complexions is (approximately) $(N_0/8r^3)!/[(N_0 16r^3)!]^2$ and $S_c = R \ln 2/(8r^3)$. We thus see that for S_c to escape experimental detection r need not exceed 1 (domain and unit cell identical) or 2. For these exceedingly small domains sharp superlattice reflections, of course, do not develop and in fact the over-all diffraction pattern will closely resemble that in which the bsu's populate the accessible positions in a random fashion. The resemblance is complete for the case of $r=1$ since in this case there is no correlation of structure from one unit cell to another; for $r=2$ the situation is identical except for a small and probably experimentally undetectable modulation of the background intensity.[19]

Of course as indicated above, the actual situation is probably not one in which the local order has the nice regularity of that just treated. It does seem likely, however, that there are submicroscopic patches in the alloy where the D arrangement corresponds to that pictured for a type I domain, interspersed with patches

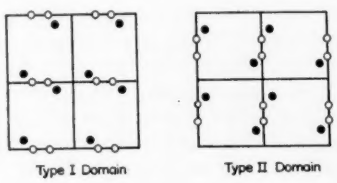

FIG. 3. 001 projection showing deuterium positions in type I and II domains for β_1 Ta_2D. Here each position is occupied by a deuterium. D's at $Z=0$ and $\frac{1}{4}$ indicated by ● and ○, respectively. The D's at $Z=\frac{1}{2}$ and $\frac{3}{4}$ and all the Ta's are omitted from the diagram.

[18] We presume this to be the case on the basis of our observations on the β_2 form. The pronounced thermal anomalies at 58 and 60°C clearly indicate the existence of a very considerable amount of order in β_2 Ta_2D, despite the fact that the diffraction results seem to indicate a random distribution of the deuteriums over the available interstices. Since no superlattice lines are observed for this form, the order must be local order. We believe that this tendency for order carries over into the β_1 form.

[19] The well known modulation of the background by local order, which has often been observed (with x-ray diffraction) in substitutional alloys, was looked for in the patterns but was not found. This was probably in part due to the high instrumental background and in part due to features particular to this system. The order under consideration involves only the D's and the vacant interstices. Thus the local order in this instance involves only a minor portion of the matter present (1 atom out of 3) and hence the modulation is expected to be slight compared to that produced by binary alloys.

having a D structure like that for a type II domain. The above calculation indicates that these patches need only be at the most one or two repeat distances in linear extent to remove essentially all the configurational entropy.

The question naturally arises: Is there any experimental support for any kind of postulated domain structure of β_1 Ta_2D? In answer, there appears to be no direct support but there is some suggestive evidence of an indirect nature derived from the structure devised for the β_2 form of Ta_2D.

Earlier we showed that on the basis of the diffraction pattern the deuteriums in β_2 Ta_2D appear to be randomly distributed over either the L, the S, or all the tetrahedral interstices. In Table IV we compare the observed configurational entropy of the β_2 form with that expected in each of these three cases. The discrepancies between the measured and computed entropies are very large, suggesting here again a conflict between conclusions based on thermodynamic and diffraction information, which is entirely analogous to that for the β_1 form. In this case the diffraction pattern is simple and we are confident that it has been analyzed correctly. Accordingly we attribute the discrepancy simply to short range ordering in the sample, probably clustering.[20] Locally there is a strong correlation of deuterium positions. This does not continue over long distances, however, so that for the size of sample involved in forming the diffraction line each site has the same chance for occupancy.

If we now return to the discussion of the β_1 form of Ta_2D, we note that the development of a domain structure in β_1 Ta_2D may be a direct consequence of the existence of local order in the β_2 form. At some places in the latter material the correlation of deuterium positions is such that a type I domain preferentially forms; in other regions we have the natural precursor of a type II domain. Hence, we see that the features of the β_2 structure which have emerged provide support of a general nature for the existence of a domain structure or short range order within the deuterium superlattice for the β_1 form.

VII. DISCUSSION OF RESULTS AND MOST PROBABLE STRUCTURES OF β_2 AND β_1 Ta_2D

In the preceding sections three possible structures each for β_1 and β_2 Ta_2D have been presented. Any further narrowing of the possibilities cannot be made on the basis of diffraction information. If any progress in this direction is to be made, it must come by using additional information. One possibility in this respect is to attempt to understand the nature of the ordering forces and then to interpret the structures in the light of this understanding, rejecting those which seem intrinsically least reasonable.

TABLE IV. Comparison of observed and calculated configurational entropies of β_1 and β_2 Ta_2D.

	Configurational entropies (eu/mole)	
	Calc[a]	Obs
β_1	2.76	0
β_2	4.20[b]	
	5.97[c]	0.7
	6.84[d]	

[a] Calculated assuming completely random distribution over the accessible sites.
[b] D's distributed over $\frac{1}{3}$ of the tetrahedral sites (S group).
[c] D's distributed over $\frac{2}{3}$ of the tetrahedral sites (L group).
[d] D's distributed over all of the tetrahedral sites.

When tantalum is hydrogenated, its lattice expands.[1] The expansion is probably produced by two effects—the increase in the number of quasi-free electrons, due to more or less complete ionization of the solute, and coulombic repulsion between the positively charged interstitial ions and their tantalum neighbors. The first of these effects, which has been discussed for substitutional alloys by Nabarro and Varley,[21] is seemingly without influence in the present instance and is not considered further. As regards the second, the fact that the hydrogens or deuteriums are at least partially ionized has been demonstrated by Hillig[22] who observed that H in tantalum migrates toward the cathode in an electric field.

The ordering of the hydrogens or deuteriums is attributed to coulombic interaction between these particles and the positively charged surrounding tantalums, modified in a way to be mentioned shortly by the Coulombic interaction between the hydrogens (or deuteriums). When a deuterium is placed in a site, the site is slightly enlarged due to Coulombic repulsion of the adjacent tantalums. Displacements of these tantalums enlarge certain of the nearby tetrahedral sites so that these become energetically favorable for occupancy by other solute particles compared to sites more removed from the occupied site. Thus, the solute particles tend to associate.[23] To minimize the Coulombic energy of the system as a whole it seems reasonable to suppose that they also tend to collect in the L group of tetrahedral sites. In this group certain pairs of sites are 1.19 A apart, whereas others are 1.67 A apart and still others are separated by a distance of 2.30 A. Evidently repulsion between the solute particles is too

[20] The present results suggests that when diffraction results seem to imply the existence of a random structure, concurrent thermodynamic studies might show the actual situation to be more complex. Appreciable local order, as occurs in β_1 and β_2 Ta_2D, frequently may be present.

[21] F. R. N. Nabarro and J. H. O. Varley, Proc. Cambridge Phil. Soc. **48,** 316 (1952).

[22] W. B. Hillig, Ph.D. dissertation, University of Michigan (1953).

[23] That this associative tendency must exist is indicated by the fact that the β phase (ca. $33\frac{1}{3}$% H) can be formed by cooling an α phase which is considerably poorer in hydrogen. Some force must exist which causes hydrogen to move from a dilute to a concentrated region.

great when their separation is only 1.19 A, since none of the structures developed indicate solute particles this close together. The other two distances occur in each of the structures, indicating that the stabilizing effect of cooperative participation in the lattice enlargement by association of two solute particles is not offset by solute particle interaction at these larger distances.

In the A structure the basic structural unit is represented as

following the symbols used in Fig. 2. Here the

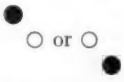

distance is 2.03 A and the ○○ distance is 1.67 A. In this structure all the D's are incorporated in this basic structural unit[24] in the type I or II domains. Accordingly, we feel that the energy is lower in this structure than in the B structure, in which only about half of the D's are associated (or, at least incorporated in the same group of four particles comprising the basic structural unit in structure A). Similarly, we feel that C is less stable than A, since the association has progressed even less far in this case. Thus we feel that structure A (or A' which is energetically identical) is the most probable representation of the structure of β_1 Ta_2D.

Before turning attention to the β_2 structure, it is appropriate to point out that the tetragonality of the β_1 form can be accounted for on the basis of structure A and the general knowledge that we have of the interactions in the Ta-D system. The atoms in structure A are, as we have seen, associated in groups of four, occupying certain of the L tetrahedral sites. We can easily see that in domains of type I these atoms tend to enlarge the lattice along the x and z axes. In the type II domains the solute particles tend to stretch the lattice along the y and z axes. Hence, all atoms operate cooperatively in enlarging the c spacing whereas only half act to increase the a and b spacings. Thus we see that distortion to produce a tetragonal crystal is expected when the deuteriums are ordered in the fashion represented by structure A.

In the light of the preceding discussion we feel that of the three possible structures for the β_2 form that which involves occupancy of only the L sites is the one which is most probably correct. It is not at all clear how the observed tetragonality of the β_2 form would originate if the D's equally populated either all the tetrahedral sites or the S sites alone. Furthermore, since the D's are positively charged, it seems reasonable to suppose they would selectively occupy the largest tetrahedral site. Our understanding is far from complete, however, as to what actually occurs when the β_1 to β_2 transformation takes place. Perhaps the groups of four particles occupy other available sets of four sites or perhaps the quartets are dissociated to pairs or perhaps a combination of these is involved.

The status of the β_3 form is even more speculative. One possibility is that the β_2 form contains quartets whose positions are locally correlated but are uncorrelated, except as necessary to avoid incompatible configurations, over long distances. In this case, perhaps the transition to the β_3 form entails a dissociation to pairs, which are still, however, confined to the L sites, and the final transition permits the D's in those pairs to occupy both the L and S sites. Another possibility is that the quartets are dissociated to pairs in the β_2 form. These pairs are, however, locally correlated in some way and are confined to the L sites in the β_2 form but can use all tetrahedral sites in the β_3 form. If so, the final transition would perhaps involve destruction of the correlation of the pairs. Further information of use in evaluating these and other alternatives could be provided if it could be established whether β_3 Ta_2D is cubic or tetragonal. It is expected to be cubic if the second of the alternatives obtains, whereas it would be tetragonal in the other case. Attempts to determine the crystal system of the β_3 form have been unsuccessful due to its narrow temperature range and the broadness of the diffraction lines in the temperature region where it exists. Hence, the arrangement of the deuteriums in β_3 Ta_2D remains a matter for speculation.

ACKNOWLEDGMENT

The author should like to express his deep appreciation to a number of individuals who gave essential assistance in the course of the work—to Dr. T. R. Waite, who prepared the sample of Ta_2D, to Dr. G. S. Kamath who assisted with some of the calculations and, in addition, provided the x-ray evidence which indicated that Ta_2H and Ta_2D behave similarly, to Dr. W. Gehman of Atomic International who pointed out the importance of the hydrogen-hydrogen repulsion and finally and most importantly to Dr. L. Corliss and Dr. J. Hastings and their associates at the Brookhaven National Laboratory for their generous assistance in providing the neutron diffraction data.

[24] The coofiguration

apparently does not occur because the Coulombic energy of this configuration slightly exceeds that of

THE JOURNAL OF CHEMICAL PHYSICS VOLUME 35, NUMBER 6 DECEMBER, 1961

Adsorption and Electrical Conduction in Thin Films*

GERT EHRLICH
General Electric Research Laboratory, Schenectady, New York
(Received February 17, 1961)

Changes in the electrical resistance of high-area, evaporated metal films after adsorption of gases have been attributed to a long-range effect of the adsorbed material. It is shown that the experimental findings do not demand this interpretation, and that contributions to the observed resistance increases may arise from any of the following: (1) A localized resistance change at necks in the film. (2) Changes in surface stress on adsorption. (3) A decrease in the rate of electron tunneling across gaps in the film with an increase in the work function. The last mechanism appears most likely, and experiments to establish these effects quantitatively are outlined.

WHEN a gas adsorbs on a metal film formed by evaporation, the electrical resistance of the metal is changed, and generally increased. These changes are small, at room temperature amounting to less than 5% for most gases so far studied. van Heerden and Zwietering,[1] and also Suhrmann,[2] found that the decrease in the film conductance λ depends upon the number of molecules n adsorbed on the film (itself made up of N metal atoms) and is given by

$$-\Delta\lambda/\lambda=\alpha(n/N). \quad (1)$$

λ is the conductance of the clean film, and α a small number, of the order of 2 for hydrogen, oxygen, and carbon monoxide.[3] These values of α were rationalized on the assumption that each adsorbed molecule "deactivates" α conduction electrons, and have lead to considerable speculation concerning the nature of the chemical bond in adsorption.

Recently, however, Zwietering, Koks, and van Heerden[4] have suggested an entirely different explanation. They point out that the specimens studied are porous, and have a surface area many times the geometrical area covered by the films. The starting resistance of the clean films is also unusually large, and much in excess of the value calculated from the gross dimensions of the sample.

The film was therefore pictured as an array of massive metal particles, separated from one another by thin metal bridges. Such an array affords the large surface area found from adsorption experiments, and also the high resistance which on this picture is dictated by the connecting bridges. The fact that each adsorbed atom affects the resistance as if it were withdrawing one carrier electron is no longer readily explicable, since the conductance is now entirely determined by the bridges. Zwietering, Koks, and van Heerden therefore tentatively suggest that each adsorbed entity withdraws an electron, which exerts a long-range effect, extending over a distance comparable to an electron free path; in this way adsorption on a massive particle could affect the resistance of the bridges.

An understanding of changes in conductance induced by adsorption is a necessary prerequisite if such measurements are to be used in the exploration of adsorption phenomena. We shall therefore examine here alternative explanations for changes due to adsorption, together with experimental tests to discriminate between the various possibilities.

To reduce the problem to its physical essentials we envision the film as a regular array of individual metal blocks, of height h, with length and width equal to a and separated from one another by a gap of d cm. This gap is partly filled by a metal layer, l cm thick and covering the entire width a. The resistance of a 1×1 cm sample of this film is then just equal to R, the resistance of one of the unit cells of this array, with a lattice constant $(a+d)$.

Apart from the suggested long-range effect of adsorbed material,[4] we conceive of the following possible causes for a change in the electrical transport properties of such high area films:

(1) The conductance of each of the bridges may be altered by a surface effect.

(2) Surface stresses in the film may be affected by adsorption, thereby changing the resistance.

(3) An appreciable part of the current flow may occur by tunneling through the gaps, if the thickness of the metal bridges in the clean film, as well as the gap width, is small. Adsorption on the gap walls affects the surface dipole layer and therefore also conduction across the gap.

These possibilities will be examined in turn.

1. ADSORPTION ON BRIDGES

If the resistance of the film is concentrated in the connecting bridges, then for a fixed gap width d, the conductance of the sample should be proportional to N_B, the number of metal atoms in these bridges. Each

* This research was supported by the Directorate of Chemical Sciences, U. S. Air Force Office of Scientific Research.

[1] C. van Heerden and P. Zwietering, Koninkl. Ned. Akad. Wetenschap. Proc. **B60,** 160 (1957).

[2] R. Suhrmann, G. Wedler, and D. Schliephake, Z. physik. Chem. (Frankfurt) **12,** 128 (1957).

[3] R. Suhrmann, G. Wedler, and H. Heyne, Z. physik. Chem. (Frankfurt) **22,** 336 (1959).

[4] P. Zwietering, H. L. T. Koks, and C. van Heerden, J. Phys. Chem. Solids **11,** 18 (1959).

adsorbed molecule is assumed to increase the resistivity of the bridge and the overall change in the sample is then

$$-\Delta\lambda/\lambda=\alpha_B(n_B/N_B). \tag{2}$$

Here n_B gives the number of molecules adsorbed on the bridges and α_B the relative decrease in conductance per adsorbed molecule. Expressing the ratio n_B/N_B in terms of the number of molecules adsorbed per metal atom in the film (n/N) we find

$$-\Delta\lambda/\lambda=\alpha_B(n/N)(A_B/V_B), \tag{3}$$

where A_B/V_B is the ratio of the fraction of the total surface area A_B to the fraction of the total volume in the bridges V_B. Provided that $h\gg a\gg l$, $h\gg d$, this ratio A_B/V_B reduces to $\sim a/3l$. In any event, if our model of the film as made up of large blocks connected by fine bridges is correct, the ratio of the surface to volume fractions for the bridges should always be greater than unity. From Eqs. (1) and (3) it also follows that $\alpha=\alpha_B(A_B/V_B)$.

The experimentally observed values of α (which are of the order of 2) can be rationalized if the coefficient α_B, giving the fractional conductance change due to a molecule on a bridge, is of the order of V_B/A_B, that is, small by comparison with unity. It is therefore possible to understand the resistance changes *without* invoking long-range effects and by calling upon precisely the same physical picture which was originally invoked to rationalize the experimental results; namely, a decrease in the number of current carriers through the presence of adsorbed entities. This decrease now is equivalent to the deactivation of only a small fraction of one conduction electron and occurs only at the bridges. Also, for this model the small integral values of α found experimentally are seen to be fortuitous. Similar effects could also be brought about by changes in the reflectivity of the metal-vacuum boundary by adsorption, if the bridge thickness l is small by comparison with the free path of the electrons.

It should be noted that adsorption still occurs on all parts of the film, on the metal blocks as well as on the connecting bridges. Since the former do not affect the resistance, changes there do not have any observable effect and only adsorption on the bridges matters.

2. CHANGES IN SURFACE STRESS

Adsorption of gases upon highly porous solids, such as activated charcoal or porous glass, changes the linear dimensions of the sample. These changes are attributable to alterations in the surface stresses. They depend upon the concentration in the adsorbed layer, are sometimes complex, and a thorough understanding is still lacking. Adsorption will certainly lower the surface energy, but the effects on surface stresses are more uncertain. It is known, empirically, that gases which can link the pore walls generally lead to an initial contraction, which is only followed by an expansion at higher concentrations of adsorbed material.

These dimensional changes are quite sizable with strongly bound gases. Thus for methanol or carbon tetrachloride on active carbon, increases in length of as much as 0.3% have been found.[5] Inert gases adsorbed on porous glass cause much smaller expansions, amounting to only 0.03% which, however, appear reversible.[6]

Information on stress changes of metal films on adsorption, or on the effect of stresses on the film resistance, is so far not available. However, judging from Bridgman's data on the resistance changes of platinum under tensile stress,[7] we could account for a resistance increase of 0.3% by a 0.1% change in length. Resistance increases of the order of ~3%, such as observed after hydrogen adsorption, appear too large to be caused by changes in surface stress. More than that, adsorption of hydrogen on nickel films raises the resistance initially, yet the resistance increment changes sign at high hydrogen coverages.[4,8] Only with difficulty could this maximum be rationalized by a stress reversal. An explanation of resistance changes on adsorption based on alterations in the surface stresses of the film therefore is unlikely, but such an effect may make a small contribution to the changes observed experimentally.

3. TUNNELING ACROSS GAPS

Provided that the gap width d as well as the thickness l of the connecting bridges are small, electron tunneling across gaps between individual metal blocks may contribute to the total current carried by the film. This must certainly be of overwhelming importance during the initial stages of film formation in which the concentration of metal blocks is so small that a continuous layer does not exist, but for which the gaps are smaller than 100 A. The extent to which tunneling actually does occur in *thick* films is not established.[9]

The conductance λ_G of a single gap, across which electrons flow by tunneling through the potential barrier, has been estimated for small voltages[10] as

$$\begin{aligned}\lambda_G&=2\times10^{22}ah(1+A\chi)A^{-2}\exp[-A\chi],\\ A&=7.32\times10^{18}d(1-7.2\times10^{-8}\phi^{-1}d^{-1}),\\ \chi&=1.265\times10^{-6}(\phi-10^{-7}d^{-1})^{\frac{1}{2}},\end{aligned} \tag{4}$$

[5] M. L. Lakhanpal and E. A. Flood, Can. J. Chem. **35,** 887 (1957).
[6] D. J. C. Yates, Advances in Catalysis **9,** 481 (1957).
[7] P. W. Bridgman, Proc. Am. Acad. Arts Sci. **60,** 305, 423 (1925).
[8] W. M. H. Sachtler and G. J. H. Dorgelo, Bull. soc. chim. Belges **67,** 465 (1958); Y. Mizushima, J. Phys. Soc. Japan **15,** 1614 (1960).
[9] (a) See, for example, H. Meyer, *Physik Dünner Schichten* (Wissenschaftliche Verlagsgesellschaft, Stuttgart, Germany, 1955), Vol. II, Chap. I. (b) C. C. Evans and J. W. Mitchell, *Structure and Properties of Thin Films* (John Wiley & Sons, Inc., New York, 1959), p. 263.
[10] R. Holm, *Electrical Contacts Handbook* (Springer-Verlag, Berlin, 1958), p. 429.

where ϕ is the work function of the metal in electron volts. On adsorption the work function increases by $\Delta\phi$, and the relative diminution in conductance is obtained from the logarithmic derivative of λ_G, which can be crudely approximated (if we neglect image forces) by

$$\Delta\lambda_G/\lambda_G = (\Delta\phi/\phi)\,(0.5 - 4.63\times10^{7}\phi^{\frac{1}{2}}d). \qquad (5)$$

As an example, a 0.10-v increase in ϕ for a metal with a work function of 4.5 ev would raise the resistance of a 5×10^{-8} cm gap by approximately 15%.[11]

This picture neglects the presence of bridges linking the metal clusters. To take account of their participation in the over-all conduction process we merely multiply Eq. (5) by the ratio of the gap conductance λ_G to that of the film as a whole λ. This reduces the resistance changes to the same order of magnitude observed experimentally.

These quantitative predictions are likely to be of limited applicability, however. Tunneling can be important only when the gap between blocks of metal in the film is small. For considerable overlapping of the potential barriers[10] of the closely spaced walls, Eq. (4), which among other things is based on an approximation to the actual potential, breaks down. We have also assumed that the effects of adsorption on the tunneling current can be completely specified by changes in the work function. Actually, changes in the shape of the barrier may dominate the emission properties of a gas-covered surface.[12] Finally, it has been pointed out[13,14] that Eq. (4) is not applicable for films constituted of small, discrete metal particles. The individual particles are not at a fixed potential; they are, on the average, neutral and an electron can therefore only escape against the retarding field of a residual positive charge, thereby introducing a temperature dependent factor.

The important thing to note, however, is that the effect of the adsorbed gas upon the conduction process is for this model closely related to the effect of adsorption on the electron emission from the bulk metal: both vary because of a change in the barrier to tunneling out of the surface.

4. EXPERIMENTAL TESTS

Any of the three mechanisms presented may *contribute* to the resistance changes observed on adsorption. Since these increases remain of the same magnitude for a wide range of film thicknesses (20–400 A in Mizushima's work,[8] for example), the major contribution most likely arises through a change in tunneling across gaps. A direct examination of the quantitative significance of these different mechanisms is both feasible and desirable.

Tests for conductance changes through changes in electron tunneling depend upon a knowledge of the detailed film structure. This can be easily achieved for thin films composed of small discrete particles. For such an array, adsorption can only affect the resistance through changes in the electron emission from each particle, and the alternatives proposed for thick films are eliminated.[14a] Simultaneous determinations of resistance, adsorption and film structure under controlled conditions and for a variety of films ranging from aggregates of isolated particles to thick, well-annealed structures should therefore resolve the contribution of electron tunneling.

The extent to which a molecule adsorbed on a metal surface may affect electrical conduction and volume strain within the metal can also be apprehended experimentally.

In answering this question, work with high area evaporated films may not be advantageous since these defy specification of their structure on an atomic scale. However, if adsorption does exert a direct, significant effect on conduction, or on the strain, then this should be detectable on bulk specimens, with at least one small dimension, and having a well-defined structure. For example, a commercially available Wollaston wire of platinum, with a diameter of 1×10^{-4} cm has $\sim$8 in every 10^4 atoms at the surface. If on chemisorption each gas atom were to abstract one conduction electron as postulated, this should result in a readily measurable change of the wire resistance. With the finest available samples (2.5×10^{-5} cm diameter), even very small effects, equivalent to the deactivation of 1/100 of a carrier per adatom, should be detectable. Simultaneous strain measurements, together with a knowledge of the resistance changes during elongation of the clean wire, should lead to a separation of possible indirect effects due to adsorption.

An unequivocal decision concerning the detailed mechanism by which adsorption affects electrical conduction in thin films seems premature without such experiments. Moreover, until this is elucidated, deductions concerning chemical bonding based on these conduction effects must be suspect. It does appear, however, that surface stresses are quite unlikely as the major cause and that in any event, we can account for the experimental observations by well-established effects *without* the necessity of invoking a long-range effect of the adsorbed atoms.

ACKNOWLEDGMENTS

This note arose out of discussions with Dr. P. Zwietering, Geleen, with whom I have enjoyed a very stimulating and continuing exchange of ideas. I am also indebted to R. W. Schmitt and M. B. Webb of this Laboratory for many helpful suggestions.

[11] For such a gap N. Nifontoff, Compt. rend. **237,** 24 (1953) has shown that conduction by thermionic emission is negligible.
[12] G. Ehrlich and F. G. Hudda, J. Chem. Phys. **35,** 1421 (1961).
[13] C. J. Gorter, Physica **17,** 777 (1951).
[14] M. B. Webb (private communication).

[14a] *Note added in proof*: Changes in the electrical resistance of evaporated films, composed of discrete metal particles, upon adsorption of gases have now been experimentally established by S. Offret, thesis, Faculty of Science, University of Paris, January, 1961.

THE JOURNAL OF CHEMICAL PHYSICS VOLUME 35, NUMBER 6 DECEMBER, 1961

Raman Spectra of Metal Carbonyl Compounds. III. Raman Spectrum, Vibrational Analysis, and Bond Structure of Nickel Tetracarbonyl

H. STAMMREICH, K. KAWAI,* AND OSW. SALA
Department of Physics, University of São Paulo, São Paulo, Brazil
AND
P. KRUMHOLZ
Research Laboratory of Orquima S.A., São Paulo, Brazil

(Received April 19, 1961)

The Raman spectrum of $Ni(CO)_4$, excited by He-lines 5875.6 and 6678.1 A, has been restudied. A new frequency assignment is proposed, based upon measurements of intensities and the state of polarization of the observed Raman shifts, and taking into account the results previously obtained on the Raman spectra of $Fe(CO)_5$, $Fe(CO)_4^{2-}$, and $Co(CO)_4^-$. Assuming a simplified quadratic valence force function containing seven potential constants, a normal coordinate analysis has been carried out. The force constants as calculated by means of this model satisfactorily reproduce the observed frequencies. The numerical values of the constants, as compared with those of the isoelectronic anions $Co(CO)_4^-$ and $Fe(CO)_4^{2-}$, provide direct evidence for partial multiple M—C bonding and conjugation between M—C and C—O bonds in metal carbonyl compounds and lead to approximate evaluations of bond numbers.

INTRODUCTION

OF all the vibrational spectra of metal carbonyl compounds, that of nickel tetracarbonyl is by far the most thoroughly investigated. Raman measurements have been carried out by Duncan and Murray[1] and by Crawford and Horwitz[2]; infrared absorption spectra have been reported by Crawford and Cross,[3] Bailey and Gordon,[4] and by Jones.[5,6] The Raman and infrared spectra of the aforementioned authors differ in completeness; otherwise their reported frequency values are in satisfactory agreement. However, the numbers, states of polarization, and the intensities of the observed Raman shifts are apparently inconsistent with values expected for $X(YZ)_4$ molecules belonging to the point group T_d. This is also the case with respect to the correlation between the Raman and the infrared absorption spectrum. Due to the unexpected features of the Raman spectrum of $Ni(CO)_4$ it has proven difficult to reach an unambiguous assignment of the observed frequencies to the normal modes of the molecule. Assignments have been made and force constants have been calculated by Crawford and Cross,[3] Murata and Kawai,[7] Bigorgne,[8] Pistorius,[9] and by Jones.[6] The latter author reported recently a thorough study concerning a "π-electron interaction potential function" in which additional relationships between various interaction constants are introduced on the hypothesis that the corresponding couplings in $Ni(CO)_4$ and related molecules arise mainly from interactions of the π electrons and π orbitals.[10]

Only four of the nine fundamental modes of tetrahedral $X(YZ)_4$ molecules are active in absorption, namely the F_2 modes, whereas eight of them are Raman-active. The remaining vibration, of species F_1, corresponds to a torsional deformation of the molecule and is both Raman and infrared inactive. As is the case of all molecules with T_d symmetry, more direct and significant evidence for the assignment may thus be expected to be provided by the Raman spectrum. Since the vibrational frequencies and the force constants of $Ni(CO)_4$ have been used frequently for reference and guidance on the interpretation of Raman and infrared spectra as well as of bond properties of other metal carbonyls, we believed it to be advisable to attempt at a reinvestigation of the Raman spectrum. As reported in two previous papers of this series (hereafter referred to as I and II, respectively) we obtained the complete Raman spectra of $Fe(CO)_5$[11] and of the anions $Co(CO)_4^-$ and $Fe(CO)_4^{2-}$ [12]; these results have proven to be helpful in the present work. By comparison of frequencies and force constants of the three isoelectronic species $Ni(CO)^4$, $Co(CO)_4^-$, and $Fe(CO)_4^{2-}$, the latter ones being evaluated by means of the same or nearly the same valence force field model, we expected to obtain pertinent information on the nature of the chemical bonding in these and related molecules.

EXPERIMENTAL

Preparation of Samples

Following ample descriptions given in the literature, nickel tetracarbonyl was prepared by direct synthesis

* Fellow of the University of São Paulo; permanent address, Osaka Municipal Technical Research Institute, Osaka, Japan.

[1] A. B. F. Duncan and J. W. Murray, J. Chem. Phys. **2,** 636 (1934).

[2] B. L. Crawford and W. Horwitz, J. Chem. Phys. **16,** 147 (1948).

[3] B. L. Crawford and P. C. Cross, J. Chem. Phys. **6,** 525 (1938).

[4] C. R. Bailey and R. R. Gordon, J. Chem. Phys. **6,** 225 (1938).

[5] L. H. Jones, J. Chem. Phys. **23,** 2448 (1955).

[6] L. H. Jones, J. Chem. Phys. **28,** 1215 (1958).

[7] H. Murata and K. Kawai, J. Chem. Phys. **26,** 1355 (1957).

[8] M. Bigorgne, J. Inorg. & Nuclear Chem. **8,** 113 (1958).

[9] C. W. F. T. Pistorius, Spectrochim. Acta **15,** 717 (1959).

[10] L. H. Jones, J. Mol. Spectroscopy **5,** 133 (1960).

[11] H. Stammreich, Osw. Sala and Y. Tavares. J. Chem. Phys. **30,** 856 (1959).

[12] H. Stammreich, K. Kawai, Y. Tavares, P. Krumholz, J. Behmoiras, and S. Bril, J. Chem. Phys. **32,** 1482 (1960).

TABLE I. Raman spectra of liquid $Ni(CO)_4$ and assignment of frequencies.

Duncan and Murray[a]	Crawford and Horwitz[b]	This work	assignment	fundamental, overtone or combination	species
82 (100) p	79 (10) 0.86±0.07	78 (100) v.b.	ν_4; ν_8	E; F_2	E; F_2
382 (20) P	381 (8) ~0.01	380 (30) P	ν_2	A_1	A_1
—	—	421 (6)	ν_7	F_2	F_2
463 (8) D	461 (4) 0.83±0.11	461 (10)	ν_6	F_2	F_2
—	—	538 (2) P, b.	$\nu_6+\nu_8$	$F_2\times F_2$	$A_1+E+F_1+F_2$
601 (4)	598 (2) <0.4	600 (6) P	ν_5; $2\nu_9$	E; F_1^2	E; A_1+E+F_2
718 (0)	—	—			
—	—	757 (0.5) b.	$2\nu_2$; $\nu_6+\nu_9$	A_1^2; $F_2\times F_1$	A_1; $A_2+E+F_1+F_2$
833 (2)	—	836 (2) P, b.	$2\nu_7$	F_2^2	A_1+E+F_2
872 (2)	—	876 (2) P, b.	$\nu_6+\nu_7$	$F_2\times F_2$	$A_1+E+F_1+F_2$
913 (2)	—	916 (2) P, b.	$2\nu_6$	F_2^2	A_1+E+F_2
1609 (0)	—	—			
2043 (30) p	2039 (9) 0.73±0.06	2037 (50) b. 2053 (8) sh, b.	ν_3	F_2	F_2
2132 (5)	2121 (4) <0.4	2128 (10) P	ν_1	A_1	A_1
2223 (1)	—	—			

P = strongly polarized; p = weakly polarized; D = depolarized line

last figures in each row refer to depolarization factors

P = degree of depolarization <0.4, b. = broad or diffuse line; sh. = shoulder, incompletely resolved from main shift, appearing only in the spectrum of $Ni(CO)_4$ in solution.

[a] Reference 1.
[b] Reference 2.

from the metal and carbon monoxide at atmospheric pressure and room temperature. Nickel was obtained in a finely divided and active form by heating its formic salt in a hydrogen atmosphere at 200°C. Addition of a small amount of mercury sulfide (about 0.2%) was found to increase the activity of the nickel so prepared. The product was purified by vacuum distillation. Although most spectra were taken from samples of pure $Ni(CO)_4$ in the liquid state, 1.5 and 0.5 M solutions in methanol and benzene also were investigated.

Spectroscopic Technique

Liquid $Ni(CO)_4$ is colorless and scarcely photosensitive to visible radiations even of short wavelength and hence its Raman spectrum may be excited in the conventional way by mercury radiation 4358.3 A. Nevertheless, for reasons to be explained later, we decided to take the larger part of the spectra by excitation with the helium radiations 5875.6 and 6678.1 A, using the apparatus described in the preceding paper II. In particular, all observations referring to the state of polarization of the Raman lines were carried out on spectra excited in the red region. Furthermore, a series of Raman spectra of liquid $Ni(CO)_4$ and of solutions in methanol and benzene were obtained in the blue spectral range by excitation with Hg 4358.3 A. For this part of the work we employed a Lane-Wells three-prism spectrograph having, in the region of the exciting line, a reciprocal linear dispersion of about 17 A/mm corresponding to approximately 90 cm^{-1}/mm. The conventional Raman technique proved to be especially adequate for the detailed study of the Raman shift near 2040 cm^{-1} which, if excited by He 5875.6 A, nearly coincides with the helium line 6678.1 A. Otherwise the Raman spectra excited in the blue region and in the long-wave range yielded, of course, identical results which will be used indiscriminately in the following discussions.

OBSERVED RAMAN SPECTRUM

The observed Raman frequencies of $Ni(CO)_4$ listed in Table I are compared with the earlier measurements reported by Duncan and Murray[1] and by Crawford and Horwitz.[2] The spectra of the pure liquid and of methanol and benzene solutions exhibited no significant differences, except for a band observed at 2037 cm^{-1}. This shift appears to be broad and rather diffuse in the spectrum of liquid $Ni(CO)_4$ whereas the spectra of solutions show a splitting of the band into two incompletely resolved components. The center of the weaker

component corresponds to a wave number of about 2053 cm^{-1}; its intensity relative to that of the main shift increases with decreasing concentration.

We observed three previously unreported Raman lines at 421, 538, and 757 cm^{-1}. The first of these shifts is strong and coincides with the most intense infrared absorption band of $Ni(CO)_4$ found by Jones[5,6] in the middle-frequency region. This shift is not easily observable in the Raman spectrum obtained with the use of the conventional technique since, if it is excited by Hg 4358.3 A, it is nearly coincident with the Raman frequency 461 cm^{-1}, excited by Hg 4347.5 A. On the other hand, we were unable to observe three weak bands found by Duncan and Murray at 718, 1609, and 2223 cm^{-1} and hence we believe that these lines are not genuine. The two latter lines are very likely Hg 4685.3 and Hg 4825.6 A which are separated from the exciting line Hg 4358.3 A by 1602 and 2222 cm^{-1}, respectively. The determination of the state of polarization of the weaker Raman bands, not carried out by the earlier authors, proved to be valuable in the frequency assignments which will now be discussed.

ASSIGNMENT OF FREQUENCIES

We believe that the most reliable and best substantiated assignment of frequencies to the fundamental modes of $Ni(CO)_4$ has been carried out by Jones.[6] Because of its incompatibility with experimental spectroscopic evidence, we feel unable to accept the modification of this assignment proposed more recently by Pistorius.[9] He recommends a value of 429 cm^{-1} for the inactive F_1 mode. Our assignment, given in Table I, rests essentially on the evidence provided by the Raman spectrum of $Ni(CO)_4$ and its comparison with the previously reported spectra of $Co(CO)_4^-$ and $Fe(CO)_4^{2-}$; it differs from that of Jones in only one way namely the attribution of 600 cm^{-1}, rather than 461 cm^{-1} to the ν_3 mode (E). With respect to all the remaining fundamentals we adopt Jones' arguments and conclusions and we shall restrict ourselves to the discussion of some additional evidence. The numbering of the normal modes is the same as that used by Jones[6,10] Murata and Kawai,[7] and the preceding paper II.

Low-Frequency Region

Two fundamental Raman-active vibrations, $\nu_4(E)$ and $\nu_8(F_2)$, are expected. Only one broad band, extending over a range of about 15 cm^{-1}, has been observed. Making use of an apparatus described by one of us and Forneris,[13] we photographed this band under fairly high dispersion (15 cm^{-1}/mm) without being successful in resolving it into two components. The microphotometer tracing of the band suggested, but somewhat inconclusively, the presence of one very strong and one weaker shift with maximum densities at 77 and 81 cm^{-1}, respectively.

[13] H. Stammreich and R. Forneris, Spectrochim. Acta, to be published.

The Middle-Frequency Region

The high intensity and the polarization of the Raman line at 380 cm^{-1}, and the coincidence of shifts at 421 and 461 cm^{-1} with the strongest infrared bands observed in the middle frequency range lead immediately to the assignments of 381 cm^{-1} to $\nu_2(A_1)$ and of 421 and 461 cm^{-1} to $\nu_7(F_2)$ and $\nu_6(F_2)$, respectively. In conformity with the considerations reported in paper II the higher of the latter frequencies has been assigned to the bending mode. The assignment of frequencies to the remaining E mode and the inactive F_1 species will be discussed later.

A rather unusual and noteworthy feature of the Raman spectrum of $Ni(CO)_4$ is the appearance of four relatively strong shifts all of which must be assigned to first harmonics or binary combinations of fundamental F_2 modes. The bands observed at 538, 836, 876, and 916 cm^{-1} are exactly alike with regard to intensity, broadening and state of polarization, the latter fact pointing unequivocally to the presence of a component of species A_1. The Raman-active combination $\nu_4+\nu_6(E\times F_2)$ which is expected to coincide with $\nu_6+\nu_8(F_2\times F_2)$ does not possess such a component and since the degree of depolarization of the four mentioned shifts was found to be the same, we assigned the frequency 538 cm^{-1} only to the latter combination. Another line, having the usual very low intensity of an overtone or combination band in Raman spectra, was found at 757 cm^{-1}.

The only remaining Raman shift to be assigned is that at 600 cm^{-1}; its high intensity points to a fundamental mode whereas its state of polarization requires its attribution to an A_1 mode or to a combination possessing a totally symmetric component. Since no binary combination of the normal modes so far determined complies with the latter requisite, we must explain this frequency as a combination involving the inactive fundamental of species F_1. Possibilities to be considered are $\nu_3+\nu_9(E\times F_1)$, $\nu_4+\nu_9(F_2\times F_1)$ and $2\nu_9(F_1^2)$; since only the last one contains an A_1 state we are compelled to assign the frequency 600 cm^{-1} to the first overtone of the F_1-mode.

Having attributed all of the observed Raman frequencies, it must be concluded that the remaining fundamental $\nu_3(E)$ is accidentally coincident with one of the shifts already assigned to another mode. Jones[6] considers the band at 461 cm^{-1} as belonging to both $\nu_3(E)$ and $\nu_6(F_2)$ while pointing out, however, that this assignment is not entirely certain. Leaning chiefly on the evidence provided by the Raman spectra of $Co(CO)_4^-$ and $Fe(CO)_4^{2-}$, as reported in paper II, one should expect $\nu_3(E)$ to have a considerably higher frequency than $\nu_6(F_2)$. Thus, we attribute the 600 cm^{-1} band to the former mode. This also appears to be consistent with the otherwise rather unexplainable high intensity of the band, equal to or a little higher than that of the fundamental $\nu_7(F_2)$ found at 421

cm^{-1}. The 600 cm^{-1} band is absent in the infrared absorption spectrum; had it originated solely from $2\nu_9(F_1^2)$ it should have been observed. We might mention, furthermore, that investigation of the shift 461 cm^{-1} under high dispersion did not provide any evidence for the presence of two overlapping bands in this region.

Thus our assignment, as proposed here, comes close to that which might be regarded as obvious from a first glance at the Raman spectrum of $Ni(CO)_4$. The four shifts of outstanding intensity in the middle-frequency region are ascribed to the four active fundamentals. Nevertheless, two questionable points should be mentioned and discussed. The coincidence of $\nu_3(E)$ with the first harmonic of the F_1 mode $(2\nu_9)$ which contains a state of symmetry E may be expected to lead to a resonance interaction and a subsequent spreading apart of the corresponding energy levels, thus causing a splitting of the Raman line into two components. It seems rather unwise to attempt to draw a valid conclusion from the absence of expected Fermi resonance. As is shown by the well known theoretical treatment of the problem, the magnitude of the resonance splitting depends not only on the closeness of the unperturbed levels but essentially upon the magnitude of the anharmonic terms in the potential function which is, in the case of polyatomic molecules, generally indeterminate.

Another possible objection to our assignment, as also pointed out by Jones,[14] might arise from the considerable frequency difference between the Ni—C—O bonding modes $\nu_3(E)$ and $\nu_6(F_2)$. This implies the existence of fairly large interactions between these bond angles. Our assignment relies chiefly on the experimental evidence provided by the Raman spectrum of $Co(CO)_4^-$, as reported in II. Because of its exceptionally good quality and the absence of overtone or combination bands even in strongly overexposed spectra, the assignment of the observed frequencies to the fundamental modes of this ion can be made immediately without leaving much margin of doubt. The interval between the frequencies belonging to the mentioned vibrations in question is 96 cm^{-1} for $Co(CO)_4^-$ and 141 cm^{-1} in $Fe(CO)_4^{2-}$; on the basis of the assignment proposed here this interval is 139 cm^{-1} for $Ni(CO)_4$. By means of the simplified valence force treatment, described in the preceding paper II and applied in the following to nickel carbonyl, the values of the M—C—O bending constant of the species $Ni(CO)_4$, $Co(CO)_4^-$, and $Fe(CO)_4^{2-}$ are found to be 0.26, 0.45, and 0.48 md/A, respectively. The corresponding unique bend-bend interaction constants are 0.06, 0.06, and 0.09 md/A. The magnitude of the latter values relative to that of the main bending constant are approximately 23%, 14%, and 19%, respectively. Taking into consideration the alteration of bond structures in the three isoelectronic species, to be discussed later, these values seem reasonable.

[14] L. H. Jones (private communication).

High-Frequency Region

The totally symmetric and the triply degenerate stretching motions of the C—O bonds correspond to frequencies in this region. In full agreement with Jones[6] we assign 2128 cm^{-1} to $\nu_1(A_1)$ and the band observed at 2037/2053 cm^{-1} to $\nu_5(F_2)$. All assignments previous to that of Jones, as quoted in the introductory part of the present paper, attribute the former shift to a combination whereas the latter band is assigned to both ν_1 and ν_5. This has been deduced from the fact that the most intense Raman line of liquid $Ni(CO)_4$ is observed at around 2039 cm^{-1} whereas the frequency of the strongest infrared absorption band of the compound in the gaseous phase is 2057 cm^{-1}. Moreover, the comparatively low intensity of the polarized Raman line at 2128 cm^{-1} is apparently inconsistent with a totally symmetric fundamental mode. Supplementary to Jones's arguments our results provide further evidence in support of the assignment of this author.

$Ni(CO)_4$ is not the only metal carbonyl compound whose Raman spectrum exhibits a surprisingly weak line corresponding to a totally symmetric C—O stretching mode. We observed, in the Raman spectrum of iron pentacarbonyl[11] a strongly polarized, comparatively weak shift at 2114 cm^{-1} which cannot be attributed to a combination but must belong to a fundamental of species A_1'. In this connection, we might mention a similar anomaly occurring in the Raman spectra of cyanide complexes. As observed in this laboratory and also as reported by Poulet and Mathieu[15] the spectra of these coordination compounds which are closely related to the metal carbonyls, nearly always show unexpected weak shifts corresponding to the totally symmetric M—C stretching vibrations. On the other hand the respective C—N modes are found to produce very strong bands.

Our observations of the Raman shift at 2037 cm^{-1} in pure liquid $Ni(CO)_4$ and the appearance of the 2053 cm^{-1} band in the spectra of $Ni(CO)_4$ in solution point clearly to the fact that the two frequencies belong to one and the same fundamental mode and that the large displacement of the former one is due to intermolecular forces operating between molecules of the same kind in the liquid state. Considering the low boiling point of nickel carbonyl and the fact that regular tetrahedral molecules not only have a zero dipole, but also a zero quadrupole moment, the large effect of intermolecular interactions upon the frequency of the F_2-mode ν_5 is quite startling.

CALCULATION OF FORCE CONSTANTS

In paper II we reported a simplified quadratic valence force potential function containing, in addition

[15] H. Poulet and J. P. Mathieu, Spectrochim. Acta **15**, 932 (1959).

TABLE II. Valence force constants of $Ni(CO)_4$, $Co(CO)_4^-$ and $Fe(CO)_4^{2-}$ (in md/A).

	$Ni(CO)_4$	$Co(CO)_4^-$	$Fe(CO)_4^{2-}$
$f_{(C-O)}$	16.28	13.22	11.40
$f_{(M-C)}$	2.49	3.55	4.06
$f_{(M-C-O)}$	0.26	0.45	0.48
$f_{(C-M-C)}$	0.07	0.09	0.09
$f_{(C-O)(C-O)}$	0.39	0.14	0.05
$f_{(M-C-O)(M-C-O)}$	0.06	0.06	0.09
$f_{(M-C)(M-C-O)}$	−0.10	0.0	0.0

to the four principal potential constants, only two constants referring to C—O stretch-stretch and to M—C—O bend-bend interactions, respectively. By means of this model we evaluated the force constants of the anions $Co(CO)_4^-$ and $Fe(CO)_4^{2-}$ following Wilson's *FG* matrix method. Despite the extreme simplicity of the assumed force field the force constants so obtained satisfactorily reproduced the observed frequencies. The same treatment has been applied to $Ni(CO)_4$. Due to the rather surprisingly close proximity of ν_6 (461 cm^{-1}) and ν_7 (421 cm^{-1}), both belonging to the same symmetry species F_2, it became necessary to introduce into the potential function a term allowing for the interaction of the Ni—C stretching and the Ni—C—O bending. We employed the potential function given in the preceding paper by adding the term

$$+2\sum_{i=1}^{4}\sum_{k=a}^{b} f_{(M-C)(M-C-O)}(\Delta r_i)\left((rR)^{\frac{1}{2}}\Delta\pi_{ik}\right).$$

The resulting force constant $f_{(M-C)(M-C-O)}$ has a small negative value indicating that the lengthening of the Ni—C linkage makes it easier to distort the bond angle Ni—C—O. The approach just indicated is the same as that used by Jones[6] in his approximate evaluation of the potential constants of $Ni(CO)_4$, followed subsequently by a more refined treatment.[10] Since the essential aim of the present work is to allow for a direct comparison of the principal stretching constants of $Ni(CO)_4$ with those previously calculated for the isoelectronic ionic species, we prefer to apply the same simplified force field model to all three molecules. The values so obtained are listed in Table II.

The frequencies belonging to the fundamental modes of nickel carbonyl, calculated by means of these potential constants, are compared with the observed data in Table III.

It is apparent that the agreement between observed and calculated values is quite satisfactory; the only relatively large numerical discrepancy is in ν_6 and is of the order of 5%. Considering the fact that the most general quadratic potential function of $X(YZ)_4$ molecules contains 21 valence force constants corresponding to 17 symmetry force constants formed thereof by linear combinations, this result seems better than might be expected. Jones,[10] on the strength of considerations of the bonding characteristics in $Ni(CO)_4$, assumes various additional relations among the different interaction constants and arrives at a more refined treatment that probably comes much closer than our model to the reality of the existing field of "chemical" forces. Even so, that author is no more successful in reproducing the observed frequencies than we are, also arriving at a discrepancy of 5% in ν_3.

Finally, we will briefly compare the principal force constants of $Ni(CO)_4$ calculated by Jones[10] with those calculated in the present work. With regard to the force constants and the interaction constants of the bond angles Ni—C—O the differing frequencies assigned to $\nu_3(E)$ cause an appreciable discrepancy. Jones evaluated the Ni—C stretching constant to be 2.09 md/A, we find 2.49 md/A. Since, in our model, the interaction of the Ni—C bonds is disregarded, the discrepancy is an apparent one. The introduction of the corresponding term in the potential function would lead to values of $f_{(Ni-C)}$ and $f_{(Ni-C)(Ni-C)}$ of about 2.10 and 0.15 md/A, respectively. Jones' value of the stretching constant $f_{(C-O)}$ is 17.305 md/A whereas our is 16.28 md/A. The difference is due, exclusively, to the fact that the former author uses in his calculations the approximate true zero-order frequencies of $\nu_1(A_1)$ and $\nu_5(F_2)$. They are estimated, from observations of the combinations $\nu_1+\nu_5$ and $2\nu_5$, to be 2135 and 2074 cm^{-1}, respectively. For the sake of better comparability with the values calculated for $Co(CO)_4^-$ and $Fe(CO)_4^{2-}$ we have used the values observed on liquid $Ni(CO)_4$, namely 2128 and 2037 cm^{-1}. The use of the frequency 2053 cm^{-1} of $\nu_5(F_2)$, as observed in the spectrum of $Ni(CO)_4$ in solution, or of the zero-order frequency 2074 cm^{-1} of the molecule in the gas phase would lead to the numerical values of about 16.75 or 17.3 md/A, respectively, for the C—O stretching constant and to a corresponding decrease of the interaction constant $f_{(C-O)(C-O)}$.

TABLE III. Observed and calculated frequencies (in cm^{-1}) of normal modes of $Ni(CO)_4$.

Species	ν_i	Observed	Calculated
A_1	1	2128	2128
	2	380	380
E	3	600	600
	4	78	78
F_2	5	2037	2036
	6	461	485
	7	421	422
	8	78	81
F_1	9	(300)[a]	310

[a] From 1° overtone.

FORCE CONSTANTS AND ELECTRONIC DISTRIBUTION IN $Ni(CO)_4$ AND RELATED COMPOUNDS

It is now commonly felt that the metal-ligand bonds in metal carbonyls and their derivatives have a partial multiple character.[16–19] Such multiple bonding is most easily visualized[20] as the result of donation of electrons from the lone pair carbon orbital of CO to the metal together with a back donation of electrons from *d* orbitals of the metal into suitable π-type orbitals of the ligand. The two components of the metal-ligand bond, which may be identified as a dative σ bond and a dative π bond,[21] respectively, produce charge shifts in opposite directions and are thus expected to mutually enhance themselves. One may expect, on the strength of Pauling's electroneutrality principle,[22] that as a consequence of the interplay between the two bond components, the metal will eventually be left with a net charge close to zero.

From the electronic structure of carbon monoxide[23,24] one may infer that dative π bonding can only arise at the expense of the bond order of the C—O bond. The resulting electronic distribution will be such that the π-bond orders of adjacent M—C and C—O bonds become roughly complementary.[25] In Mulliken's notation,[26] such mesomeric electron displacement can be classified isovalent dative conjugation.

Considered in this way, the spectral properties of the C—O bond in metal carbonyls and in a variety of their derivatives, have provided ample, though indirect, evidence for multiple metal-ligand bonding and conjugation.[3,20,27–30] To obtain direct and more detailed information on the electronic distribution in metal carbonyl compounds, it seems necessary to simultaneously examine the properties of both bonds, M—C and C—O, in a series of compounds. The series of the isosteric and isoelectronic carbonyl species $Ni(CO)_4$, $Co(CO)_4^-$, and $Fe(CO)_4^{2-}$, whose force constant data are listed in Table II, seems particularly convenient for such a study.

One notices from Table II that the stretching force constants of the M—C bonds increase strongly in the sequence $Ni(CO)_4 < Co(CO)_4^- < Fe(CO)_4^{2-}$; simultaneously, the stretching force constants of the C—O bonds show a pronounced decrease in the same sequence. The observed increase of the M—C stretching force constants with increasing negative charge of the carbonyl species must, obviously, be attributed to an increased contribution of dative π bonding. The opposite trend of the stretching force constants of the two bonds, M—C and C—O, may be considered as a direct demonstration of the expected conjugative interaction.

TABLE IV. Computed bond numbers for $Ni(CO)_4$, $Co(CO)_4^-$ and $Fe(CO)_4^{2-}$.

Species	N_{CO}	N_{MC}	ΣN
$Ni(CO)_4$	2.64	1.33	3.97
$Co(CO)_4^-$	2.14	1.89	4.03
$Fe(CO)_4^{2-}$	1.85	2.16	4.01

Considering the numerical values of the force constants of the carbonyl species $Ni(CO)_4$, $Co(CO)_4^-$, and $Fe(CO)_4^{2-}$, we shall attempt to obtain a crude quantitative estimate of the electronic distribution in these species. To do so, we shall represent the state of a single M—C—O grouping as a resonance hybride of the three structures: (1) M—C≡O; (2) M═C═O; (3) M≡C—O. The bonds in structures 1–3 are to be considered as having a normal amount of polarity or ionicity, and not as extreme covalent bonds.[31] The weighted average number of valency links between two atoms in structures 1–3 shall be regarded as the respective (formal) bond number. Independent of the relative contribution of structures 1–3, the sum of the bond numbers of both bonds in a M—C—O grouping is always four. Since, in principle, all the five filled *d* orbitals of the metal are available for π-bond formation[10,32,33] with the four ligands, the maximum bond number of the M—C bond is 2.25; correspondingly, the minimum bond number of the C—O bond, is 1.75.

Tentatively, we may make the assumption that the stretching force constants of a given bond, M—C or C—O, are proportional to the respective bond numbers. This is certainly a drastic simplification, but is apparently justified by the final result. The bond numbers of the C—O bonds in the three carbonyl species can then be calculated by relating their stretching force constants to that of CO (18.53 md/A) and assuming a bond number of 3.0 for the latter molecule. To obtain the bond numbers of the M—C bonds, their stretching force constants are multipled with an unique empirical factor, chosen to make the sum of the bond numbers of both bonds, M—C and C—O, on the average, as close as possible to four; the results are resumed in Table IV.

Considering the fact that the foregoing treatment

[16] L. Pauling, *The Nature of the Chemical Bond* (Cornell University Press, Ithaca, New York, 1960), 3rd ed.
[17] V. K. Syrkin and M. E. Dyatkina, *Structure of Molecules and the Chemical Bond* (Butterworths Scientific Publications, Ltd., London, 1950).
[18] J. W. Cable and R. K. Sheline, Chem. Revs. **56,** 1 (1956).
[19] J. Chatt, J. Inorg. Nuclear Chem. **8,** 515 (1958).
[20] J. Chatt and F. A. Hart, J. Chem. Soc. **1960,** 1378.
[21] J. Chatt and A. W. Williams, J. Chem. Soc. **1954,** 4403.
[22] L. Pauling, J. Chem. Soc. **1948,** 1461.
[23] C. A. Coulson, *Valence* (Oxford University Press, New York, 1952), pp. 211–212.
[24] H. H. Jaffé and M. Orchin, Tetrahedron **10,** 212 (1960).
[25] R. J. Irving and E. A. Magnusson, J. Chem. Soc. **1958,** 2283.
[26] R. S. Mulliken, Tetrahedron **5,** 253 (1959).
[27] R. S. Nyholm and L. N. Short, J. Chem. Soc. **1953,** 2670.
[28] R. A. Friedel, I. Wender, S. L. Shufler and H. W. Sternberg, J. Am. Chem. Soc. **77,** 3951 (1955).
[29] E. W. Abel, M. A. Bennet and G. Wilkinson, J. Chem. Soc. **1959,** 2323.
[30] L. S. Meriwether and M. L. Fiene, J. Am. Chem. Soc. **81,** 4200 (1959).
[31] See reference 16, p. 266.
[32] G. E. Kimball, J. Chem. Phys. **8,** 188 (1940).
[33] F. A. Cotton, J. Chem. Soc. **1960,** 5269.

rests upon oversimplifying assumptions, the constancy of the sum of the bond numbers in the three carbonyl species seems rather surprising. While realizing that the significance of this numerical result should not be overrated, we believe that the values given in Table IV represent a fairly realistic approximation to the true bond structures of these molecules.

We shall now briefly discuss some conclusions, referring to the electronic distribution in the three carbonyl species, which might be drawn from the data given in Table IV.

It is likely that the electronic structure of $Fe(CO)_4^{2-}$ is somewhere between $Fe(=C=O)_4$ and $O-C\equiv Fe(=C=O)_3$; apparently, the multiple bonding capacity of the metal is nearly used to its full extent. Cotton[33] has recently shown that this is possible and our results give support to his conclusions. If the true electronic distribution in $Fe(CO)_4^{2-}$ is close to the fully double bonded structure, then the negative charge can be moved from the metal to the oxygen atoms by the effect of bond polarity only. This would require a rather high polarity of about 50% for the double M=C and C=O bonds. The structure with one triple M≡C bond probably makes a ponderable contribution to the state of the molecule.

The structure of $Co(CO)_4^-$ is likely between $O\equiv C-Co(=C=O)_3$ and $Co(=C=O)_4$. It is interesting to note that bond numbers of 1.87 for the M—C bond and of 2.13 for the C—O bond have been estimated by Friedel *et al.*[28] from electroneutrality and electronegativity considerations. These estimates are in surprisingly good agreement with the values reported here. Similar estimates for $Fe(CO)_4^{2-}$ lead to bond numbers of 2.08 and 1.92 for the M—C and the C—O bonds, respectively, still in satisfactory agreement with our results. For $Ni(CO)_4$, however, Friedel *et al.*[28] obtain bond numbers of 1.67 and 2.33, respectively, which differ considerably from our values of 1.33 and 2.64. More recently, Pauling[34] arrived at an even higher estimate of the bond number of the M—C bond in $Ni(CO)_4$, namely, 1.78.

[34] See reference 16, p. 333.

In part, these discrepancies may be due to the fact that our crude calculations tend to overemphasize the spread between the bond numbers of the different carbonyl species. However, it is unlikely that the whole difference can be explained in this way. We rather believe that the M—C bond numbers obtained from electroneutrality considerations are too high. This may be due, among other reasons, to the neglect of the influence of the formal charge[35,36] and of the state of hybridization[37,38] on the electronegativities of the metal and of the carbon atom. While a quantitative evaluation of the effects of these factors is hardly possible, qualitatively their trend is such as to increase the electronegativity difference between the metal and the carbon atom, at least in the single dative bonded structure 1. Electroneutrality of the metal atom can thus be achieved by a larger contribution from this structure, i.e., at a lower bond number of the M—C bond than hitherto admitted.

Taking into account the weight of the present results we conclude that the M—C bond in $Ni(CO)_4$ has less than 50% double bond character.

Note added in proof. Attention is called to two recent studies of the Raman spectrum of $Ni(CO)_4$, carried out by M. Bigorgne and by M. Bigorgne and A. Chelkowski, respectively [Compt. rend. **251,** 355 and 538 (1960)]. These notes have come to the knowledge of the authors while the present paper was in the process of publication. The spectrum of liquid $Ni(CO)_4$ reported by Bigorgne is, although less complete, in best agreement with the results of our observations.

ACKNOWLEDGMENT

The present work has been partly supported by the Conselho Nacional de Pesquisas, Rio de Janeiro; the authors feel greatly indebted for the facilities created by this organization.

[35] P. and R. Daudel, J. phys. radium **7,** 12 (1946).
[36] O. Chalvet and R. Daudel, J. Phys. Chem. **56,** 365 (1952).
[37] A. D. Walsh, Discussion Faraday Soc. **2,** 18 (1947).
[38] W. Moffitt, Repts. Progr. in Phys. **17,** 173 (1954).

THE JOURNAL OF CHEMICAL PHYSICS VOLUME 35, NUMBER 6 DECEMBER, 1961

Raman Spectra of Metal Carbonyl Compounds. IV. Raman Spectra and Structure of Cadmium and Mercury Cobalt Carbonyl

H. STAMMREICH, K. KAWAI,* AND OSW. SALA
Department of Physics, University of São Paulo, São Paulo, Brazil
AND
P. KRUMHOLZ
Research Laboratory of Orquima S.A., São Paulo, Brazil

(Received April 19, 1961)

The complete Raman spectrum of $Cd[Co(CO)_4]_2$ and a partial one of $Hg[Co(CO)_4]_2$, excited by helium radiation in the red and near infrared spectral range, are reported. A salient feature of the observed spectra is the appearance of an intense, strongly polarized shift at 152 (161) cm^{-1}, not found in the spectra of mononuclear metal carbonyls, that must be assigned to the symmetric Cd(Hg)—Co stretching mode. The results exclude the presence of one or more bridging CO groups in the compounds referred to and point strongly to both the existence of a three-fold principal molecular axis containing the atoms O—C—Co—Cd(Hg)—Co—C—O, and to the staggered D_{3d} configuration of the entire molecule.

INTRODUCTION

THE structure of heavy-metal derivatives of cobalt carbonyl hydride, like $Hg[Co(CO)_4]_2$, is not clearly understood. In particular, as pointed out by Cable and Sheline,[1] it is not known whether the linkage of the heavy-metal is through metal-metal bonds or through bridging carbonyl groups. Apparently, structures of the latter kind have been considered exclusively in the first years following the discovery of these compounds.[2–4] Cable and Sheline[1] suggest that knowledge of the vibrational spectra of the heavy-metal derivatives of cobalt carbonyl hydride would readily provide sufficient evidence to establish the correct structure of these molecules.

A first attempt in this direction has been recently reported by Bor and Markó[5] who observed the infrared absorption spectrum of $Hg[Co(CO)_4]_2$ around 2000 cm^{-1} and registered four bands in the "terminal" CO region, three of them being attributed to fundamental vibrational modes. The authors infer from this result (1) the absence of bridging CO groups and (2) a fairly high molecular symmetry compatible with a D_{3d} or D_{3h} configuration.

A definitive elucidation of the structural problem, as referred to, will require the obtainment of more complete spectral data. In the following we report what we believe to be the complete Raman spectrum of the cadmium compound and a partial one of the mercury derivative.

EXPERIMENTAL

Spectroscopic Technique

Because of the photochemical instability of mercury and cadmium cobalt carbonyl and to the orange-red color of the former compound in solution, the Raman spectra had to be excited in the long-wave region by means of helium radiations. The method has been applied by us to the Raman spectroscopic investigation of other carbonyls, and the pertinent instrumental details have been given in preceding papers of this series I,[6] II,[7] and III.[8] The spectrograph was the same as that described in II[7]; the bulk of the spectra were taken with an arrangement of high light gathering power using the camera of aperture 1:1.9 and focal length 12 cm, while other spectra were photographed under higher dispersion.

Samples

Mercury cobalt carbonyl was purified by repeated crystallizations from methanol in dim red light and under exclusion of air. We tried to obtain the Raman spectrum of the compound dissolved in methanol, carbon disulfide, benzene and cyclohexane; all of these solutions proved to be extremely photosensitive. Upon the incidence of radiation He 5875.6 A they decomposed and became turbid almost instantaneously. Solutions in carefully dried benzene or cyclohexane (5% by weight) were found to be a little more resistant to He 6678.2 and 7065.2 A; the incidence of radiations of shorter wavelength had to be prevented by means of adequate filters. Even in this manner it was not possible to carry out long exposures and we had to confine our-

* Fellow of the University of São Paulo; permanent address: Osaka Municipal Technical Research Institute, Osaka, Japan.

[1] J. W. Cable and R. K. Sheline, Chem. Revs. **56,** 1 (1956).

[2] W. Hieber and U. Teller, Z. anorg. u. allgem. Chem. **249,** 43 (1942).

[3] W. Hieber in *FIAT—Review of German Science* 1939–1946 (Dieterich'sche Verlagsbuchhandlung, Wiesbaden, Germany, 1948), Vol. 24, part II, p. 125.

[4] J. S. Anderson, Quart Revs. (London) **1,** 331 (1947).

[5] G. Bor and L. Markó, Spectrochim. Acta **16,** 1105 (1960).

[6] H. Stammreich, Osw. Sala and Y. Tavares, J. Chem. Phys. **30,** 856 (1959).

[7] H. Stammreich, K. Kawai, Y. Tavares, P. Krumholz, J. Behmoiras, and S. Bril, J. Chem. Phys. **32,** 1482 (1960).

[8] H. Stammreich, K. Kawai, O. Sala, and P. Krumholz, J. Chem. Phys. **35,** 2168 (1961), preceding article.

TABLE I. Observed Raman spectra of $Cd[Co(CO)_4]_2$ and $Hg[Co(CO)_4]_2$

Frequency region[a]	$Cd[Co(CO)_4]_2$ in methanol and benzene[b]	$Hg[Co(CO)_4]_2$ in benzene and cyclohexane[b]
Low	98 (20) vvb	100 (50) vvb
Skeletal stretch	152 (15) P	161 (20)
	429 (20) P	416 (10)
	496 (5)	
	530 (5)	
Middle	560 (4)	
	619 (1) b	
	732 (4) b	
	778 (2) u	
	1953 (3) b	1990 (2)
High	1984 (20) P	2030 (8)
	2075 (4)	2107 (2) u

[a] For an approximate description of the fundamental vibrational motions falling in these regions see Table II.

[b] b=broad, v=very, P=shifts with depolarization factor <0.4; u—the authenticity of these shifts is probable but not completely certain.

selves to recording only the strongest Raman shifts of the molecule. Due to the large frequency interval between the exciting line and the shifts corresponding to the C—O stretching modes, the increasing turbidity of the samples during the exposure caused less trouble in the high frequency region. We believe the spectrum, as observed in this range, to be complete. We did not succeed at obtaining data on the state of polarization of the observed Raman lines.

Cadmium cobalt carbonyl was prepared[9] by the reaction of stoichiometrical quantities of $NaCo(CO)_4$ and $Cd(NO_3)_2$ in aqueous solution, evaporation *in vacuo* to dryness, extraction with benzene and evaporation of the filtered benzene solution. The yellow residue was dissolved to about 8% by weight in absolute methanol. $Cd[Co(CO)_4]_2$, although chemically less stable than the mercury derivate, is incomparably less photosensitive in solution, provided oxygen is completely excluded. It was possible to use the helium radiations 5875.6 and 6678.2 A for excitation of the Raman spectra and the samples withstood long exposures without showing either an appreciable change of their pale yellow color or other signs of decomposition. The bulk of about 60 spectra, as recorded altogether, were taken using as samples methanol solutions. In order to make sure that possible interaction of the molecule with the solvent had no appreciable influence on the observed frequencies, we photographed some spectra of benzene solutions. The spectra of both solutions were found to be identical to within the error of our measurements; we evaluate this error as ± 2 cm^{-1} for sharp lines. Polarization measurements were carried out on spectra excited by the yellow helium line, except for the shifts in the 2000 cm^{-1} range whose state of polarization was observed on spectra excited by He 6678.2 A.

[9] W. Hieber, E. O. Fischer, and E. Boeckly, Z. anorg. u. allgem. Chem. **269**, 308 (1952).

OBSERVED RAMAN SPECTRA

The observed Raman spectra of $Cd[Co(CO)_4]_2$ and $Hg[Co(CO)_4]_2$ are shown in Table I.

As has been mentioned previously, we did not succeed at recording the complete Raman spectrum of the mercury derivate, except in the high-frequency range. The shift 2107 cm^{-1} could not be observed in spectra excited by He 6678.2 A due to its coincidence with the oxygen line 7772 A which is the strongest line of the OI spectrum. Despite careful outgassing of the helium discharge tubes, the faint appearance of this line can hardly be avoided. Using a cyclohexane solution and excitation by He 7065.2 A, the Raman frequency 2107 cm^{-1} is nearly coincident with the strong shift 2922 cm^{-1} excited by He 6678.2 A and belonging to this solvent. Hence, evidence for the authenticity of the frequency 2107 cm^{-1} is provided but by the spectrum of benzene solutions excited by He 7065.2 A; although not completely certain, we believe this shift to be genuine.

The frequencies of $Cd[Co(CO)_4]_2$, as listed in Table I, represent, in our opinion, the totality of the Raman-active fundamental modes of the molecule except in the low-frequency region where the shifts corresponding to different bending modes could not be resolved. Even with extremely overexposed spectra we were unable to observe additional Raman bands. Due to a near coincidence with a band head of the molecular spectrum of He_2, the only line whose genuineness may appear questionable is that found at 778 cm^{-1}. However, the results of comparative intensity measurements point strongly to the authenticity of this frequency.

In the spectra of both molecular species we observed a broad, intense band around 100 cm^{-1}. This band extends over a range of approximately 25 cm^{-1} and could not be resolved into different components. In the preceding papers II[7] and III[8] we reported a similar observation on the spectra of the tetrahedral species $Co(CO)_4^-$, $Fe(CO)_4^{2-}$ and $Ni(CO)_4$ where only two fundamental modes, corresponding to deformations of the C—M—C angles, fall in the low frequency region. As will be discussed later, the molecular species, dealt with in the present work, possess considerably more Raman-active fundamentals of low frequency. Moreover, at room temperature the population of the lower excited levels of such low-frequency oscillators will be comparable to that of the ground state, giving rise to strong upper stage bands whose frequencies are expected to differ slightly from those of the fundamental transitions due to anharmonicity and coupling effects. It is, therefore, hardly surprising that the crowding of a large number of fundamental and upper stage bands in a narrow spectral range produces the observed apparently structureless broad band.

DISCUSSION OF RESULTS

The most salient feature of the Raman spectra of both molecular species investigated here, is the appearance of an intense, sharp, and strongly polarized shift lying in a frequency region which is completely free in the spectra of mononuclear metal carbonyl compounds. This shift, found in $Cd[Co(CO)_4]_2$ at 152 cm^{-1} and in the mercury derivative at 161 cm^{-1}, must, obviously, be assigned to the totally symmetric skeletal stretching mode, essentially involving the Cd(Hg)—Co distances. In henceforth describing this mode as $\nu_{(s)}$M—Co, and the corresponding force constant as $f_{(M-Co)}$, it should be understood that these notations are not meant to imply a statement in the sense of a linkage of the $Co(CO)_4$ groups to the heavy-metal atom exclusively through metal-metal bonds. Edgell *et al.*[10,11] have proposed a polycentered orbital, and a resulting "bridge model" for the bonding of the hydrogen atom in cobalt carbonyl hydride; obviously, the spectroscopic results of the present study are not expected to provide any evidence in favor of or against the possibility of a similar type of bonding in the case of the heavy-metal derivatives. We believe, however, that the contribution of the metal-metal bonding to the total bond strength is predominant.

The fact that we were unable to observe a Raman shift that could be attributed to the corresponding antisymmetric stretching mode, points strongly to a linear symmetrical configuration Co—M—Co. Furthermore, regarding the molecule, in rough approximation, as a system of three masses, in which the $Co(CO)_4$ groups are considered as rigid units and assuming a simple valence force field, the values of the force constants $f_{(Cd-Co)}$ and $f_{(Hg-Co)}$ are calculated to be 2.33 and 2.61 md/A, respectively. Under the same simplifying assumptions, the frequencies of the antisymmetric modes $\nu_{(as)}$ Cd—Co and $\nu_{(as)}$ Hg—Co would be 305 and 265 cm^{-1}, respectively. The effect of an interaction between the M—Co bonds—a positive sign of the corresponding force constant is to be expected—would result in a decrease of the frequencies of the antisymmetric modes.

The Raman shift 152 cm^{-1} of $Cd[Co(CO)_4]_2$, excited by He 5875.6 A, required an exposure of 5 min or less to appear with fair intensity on 103aC-plates. Exposures of up to 5 hr did not reveal a shift between 152 and 429 cm^{-1}; hence we conclude that the mode $\nu_{(as)}$ M—Co is forbidden in Raman. As shown in Table II, the inactivity of this mode in the Raman effect is consistent with the selection rules for the point groups D_{3d}, D_{3h}, and $V_h(D_{2h})$.

The absence of Raman shifts in the range 1750–1900 cm^{-1} leads immediately to one further conclusion, namely the exclusion of linkages between the $Co(CO)_4$ groups and the heavy-metal atom formed by bridging carbonyl groups. In this respect, the evidence provided by the Raman spectrum is in full agreement with the results of infrared measurements reported by Bor and Markó[5]; both spectra are inconsistent with the structures which have been proposed by Hieber[3] and by Anderson.[4]

In order to relate the observed Raman spectra in a definite way with the structural configuration of the molecular species, studied here, we have applied the selection rules for point groups D_{3d}, D_{3h}, V_h, and V_d and constructed the respective symmetry coordinates. Thus, we obtained the number, the symmetry species and the activities of the fundamental modes belonging to the mentioned configurations, as well as an approximate description of the corresponding vibrational motions. The latter points directly—by analogy with results obtained on other metal carbonyl compounds—to the approximate values of the expected fundamental frequencies. Table II shows the results in detail for D_{3d} symmetry and summarized for the remaining point groups.

Only the aforementioned symmetries have been taken into consideration. The reduced number of observed Raman lines, as compared with the 51 normal modes of a 19-atomic molecule, clearly indicates a highly symmetric structure for the binuclear heavy-metal derivatives. The configurations belonging to the point groups D_{3d} and D_{3h} possess a three-fold principal symmetry axis containing the atoms O—C—Co—M—Co—C—O whereas only the three metal atoms are located on the twofold principal axis of the V_h or V_d structures. A nonlinear arrangement Co—M—Co would lead to a low molecular symmetry, such as C_{2v}, possessing only nondegenerate normal modes, all of them Raman-active. Setting aside the evidence provided by the absence of the Raman shift corresponding to the antisymmetric skeletal stretching vibration, the observed spectrum, on the whole, is entirely incompatible with such a low symmetry.

One notices from Table II that the Raman spectrum of cadmium cobalt carbonyl, as observed in the different frequency regions, is in full agreement with that expected for D_{3d} symmetry. In the middle frequency range, comprising the Co—C stretching and the Co—C—O bending modes, we found, in conformity with predictions, seven Raman shifts whereas the structures belonging to point groups D_{3h}, V_h, and V_d would require 11, 12, and 16 Raman active fundamentals, respectively. The same agreement is noted in the spectral region around 2000 cm^{-1} where the stretching modes of the "terminal" CO groups are located. The three observed frequencies are consistent with D_{3d} symmetry whereas the spacial configurations belonging to the remaining point groups would give rise to 4, 4, and 6 Raman active fundamentals, respectively. Because of the previously noted impossibility of resolving the different bands corresponding to deformations of

[10] W. F. Edgell, Ch. Magee and G. Gallup, J. Am. Chem. Soc. **78,** 4185 (1956).
[11] W. F. Edgell and G. Gallup, J. Am. Chem. Soc. **78,** 4188 (1956).

TABLE II. Selection rules and approximate expected frequencies and descriptions of fundamental vibrational motions of $M[Co(CO)_4]_2$[a] for various symmetries.

Point group	Species	Activity	High frequencies ~2000 cm^{-1} ν C—O	Middle frequencies 400–800 cm^{-1} ν Co—C	Middle frequencies 400–800 cm^{-1} δ Co—C—O	Low frequencies ~100 cm^{-1} δ C—Co—C, δ M—Co—C[a], δ Co—M—Co[a] torsional vibr.	Skeletal stretchs ν M—Co[a]	Total No.
	A_{1g}	Ram. p.	2	2	1	1	1	7
	A_{1u}	inact.	...	...	1	1	...	2
D_{3d}	A_{2g}	inact.	...	...	1	...	...	1
	A_{2u}	I.R.	2	2	1	1	1	7
	E_g	Ram. dp.	1	1	3	3	...	8
	Eu	I.R.	1	1	3	4	...	9
	total		6	6	10	10	2	34
	thereof	Ram.-act.	3	3	4	4	1	15
	thereof	I.R.-act.	3	3	4	5	1	16
	thereof	inact.	...	...	2	1	...	3
D_{3h}	total: $\{7A_1'; 2A_1''; 1A_2'; 7A_2''; 9E'; 8E''\}$		6	6	10	10	2	34
	thereof	Ram.-act.	4	4	7	8	1	24
	thereof	I.R.-act.	3	3	4	5	1	16
	thereof	inact.	...	...	2	1	...	3
V_h (D_{2h})	total: $\{9A_{1g}; 4A_{1u}; 3B_{1g}; 9B_{1u}; 6B_{2g}; 7B_{2u}; 6B_{3g}; 7B_{3u}\}$		8	8	16	17	2	51
	thereof	Ram.-act.	4	4	8	7	1	24
	thereof	I.R.-act.	4	4	6	8	1	23
	thereof	inact.	...	...	2	2	...	4
V_d (D_{2d})	total: $9A_1; 3A_2; 4B_1; 9B_2; 13E$		6	6	12	12	2	38
	thereof	Ram.-act.	6	6	10	11	2	35
	thereof	I.R.-act.	4	4	6	7	1	22
	thereof	inact.	...	...	2	1	...	3

[a] M stands for Cd or Hg, respectively.

the angles C—Co—C, M—Co—C, and Co—M—Co, our observations in the low frequency region do not provide any indications as to the structure of the molecule.

The partial Raman spectrum of the mercury derivative is fully consistent with the D_{3d} structure, as established for cadmium cobalt carbonyl, particularly on the strength of the evidence provided by the observed C—O stretching modes. We may thus conclude that the binuclear heavy-metal derivatives of cobalt carbonyl hydride possess a center of inversion occupied by the heavy-metal atom. The linear arrangement O—C—Co—M—Co—O is the threefold principal axis of molecular symmetry, each cobalt atom forming the apex of an axialsymmetric trigonal pyramidal arrangement of three carbonyl groups located outside the principal axis. The two trigonal pyramids are in a staggered position with respect to each other. The spectral evidence in favor of the staggered D_{3d} configuration, as compared with the eclipsed D_{3h} structure, is consistent with the higher stability which may be expected from the decrease in Coulomb repulsion energy in the former arrangement.

Additionally, the observed spectral data seem to provide some informations as to the nature of the bonding in the molecular species being studied. One notices from Table I that both the skeletal and the C—O stretching frequencies are higher in the mercury than in the cadmium derivative. The contrary holds for the most intense Raman shifts, as observed in the middle frequency range (Hg 416, Cd 429, P), which may be assigned, rather unambiguously, to the totally symmetric, in-phase stretching motion of the eight M—C bonds. This spectral behavior is most easily understood if the bonds between the heavy-metal and the $Co(CO)_4$ groups are considered as covalent metal-metal bonds having a partial ionic character which leaves the heavy-metal atom with a net positive charge. The corresponding amount of negative charge most likely will be removed from the Co atom to the more electronegative oxygen atoms. This process of charge migration involves an increased contribution of dative π bonding to the bond between the Co atom and the CO ligands, which, through conjugative interaction, decreases the π-bond order of the C—O bond and, hence, increases the C^+-O^- polarity. According to this interpretation the bonds between the heavy-metal atom and the $Co(CO)_4$ groups are more covalent (or less polar) and therefore stronger in the mercury derivative than in the cadmium compound. This is in agreement with the greater stability of the mercury derivative towards oxidative decomposition as well as with the known fact that divalent mercury has a greater tendency towards the formation of covalent bonds than divalent cadmium. In further agreement with the present interpretation of the nature of bonding in $Hg[Co(CO)_4]_2$ and $Cd[Co(CO)_4]_2$, it is found that the M—C and C—O stretching frequencies of these derivatives are intermediate between those of the ion $Co(CO)_4^-$ and of the nonpolar $Ni(CO)_4$, reported in the foregoing publications II[7] and III.[8]

The opposite trends of the M—C and C—O stretching frequencies in the two heavy-metal derivatives are a further confirmation of the conjugative interaction between the M—C and the C—O bonds in metal carbonyl compounds, as discussed in III.

ACKNOWLEDGMENTS

The writers feel indebted to Professor W. Hieber, Munich, who kindly supplied the sufficient quantity of mercury cobalt carbonyl for the present work. They wish to express their gratitude to the Conselho Nacional de Pesquisas, Rio de Janeiro, for various facilities created with the help of this organization.

Construction of Orthogonalized LCAO Wave Functions for the *F* Center from ENDOR Data*

ALBERT GOLD
Department of Physics, University of Illinois, Urbana, Illinois
(Received May 29, 1961)

A simple method for constructing orthogonalized LCAO wave functions for paramagnetic systems from electron spin resonance or electron nuclear double resonance data is presented. It is applied to the calculation of the ground-state wave function of the *F*-center electron in KCl, taking overlap of heterocentric atomic wave function explicitly into account. This function is built up of 4*s* and 4*p* valence functions centered on the six potassium ions nearest the vacancy. It is found that this simple form cannot reproduce the quantitative details of the charge distribution and that the inclusion of additional functions centered on more distant sites is necessary for a complete LCAO description of the center. However, it allows some of the qualitative features of the data to be understood.

I. INTRODUCTION

THE advent of electron nuclear double resonance (ENDOR) techniques has made possible the direct measurement of the distribution of electronic charge associated with a paramagnetic crystalline imperfection. Recently Holton[1] has used the ENDOR method to determine the charge density of the *F*-center electron in alkali halides at nuclear sites as far distant as the vacancy's eighth neighbors. This knowledge supplies one with a very sensitive measure for determining the accuracy of a wave function which purports to describe the *F* electron in its ground state. The experimental results are apparently not too well described by the point-ion-lattice model wave functions of Gourary and Adrian.[2]

In the present paper we describe a simple method for constructing an orthogonalized LCAO wave function from the ENDOR data for a paramagnetic system. The formalism is then applied to the case of the *F* center with the LCAO built up from *s* and *p* valence functions of the six cations closest to the vacancy. Numerical results for KCl obtained by matching charge densities close to the vacancy are used to compute densities at more distant sites. These are compared to experimental and point-ion-lattice model results.

II. THEORY

Working in a "tight-binding" picture, we shall assume that the total wave function of the system is given by a single Slater determinant of one-electron functions. If the ion cores of the system are described by an orthonormal set of functions ϕ_i and the "extra" electron by some normalized function ϕ_F which is not necessarily orthogonal to the ϕ_i's, we may write a properly normalized and orthogonalized function for this electron as

$$\Psi_F=[\phi_F-\sum_i S_{Fi}\phi_i][1-\sum_i (S_{Fi})^2]^{-\frac{1}{2}}. \quad (1)$$

Here S_{Fi} is the overlap integral

$$\int \phi_F^*(\mathbf{X})\phi_i(\mathbf{X})d\mathbf{X},$$

where $\mathbf{X}$ is taken to include both space and spin coordinates.

We may take ϕ_F as an LCAO built up of valence functions centered on the constituents of the crystal,

$$\phi_F=\sum_v c_v\phi_v, \quad (2)$$

where v runs over the various functions of interest at the various sites. Normalization of ϕ_F now requires that

$$\sum_u\sum_v c_u c_v S_{uv}=1, \quad (3)$$

and Eq. (1) now reads

$$\Psi_F=(\sum_v c_v\phi_v-\sum_i \phi_i\sum_v c_v S_{vi})[1-\sum_i(\sum_v c_v S_{vi})^2]^{-\frac{1}{2}}. \quad (4)$$

Evaluating the square of Eq. (4) at any point yields the charge density there. The c_v, and so the wave function, may be determined if one has sufficient ENDOR or ESR data to make Eq. (3) and the square of Eq. (4) a complete set of simultaneously soluble equations. The method can, of course, be applied to any paramagnetic system for constructing wave functions to be applied, say, in energy level computations.

Kip, Kittel, Levy, and Portis[3] have investigated the *F* center's hyperfine interactions using an LCAO wave function composed of *s* and *p* functions belonging to the vacancy's six nearest neighbors. They neglect all overlap. We shall now extend this simple model to include all overlapping of the valence functions with each other and with core functions. We shall neglect the overlapping of the ionic Hartree-Fock core func-

* Research supported in part by the Office of Naval Research.
[1] W. C. Holton, thesis, University of Illinois, 1960 (unpublished).
[2] B. S. Gourary and F. J. Adrian in *Advances in Solid State Physics*, edited by F. Seitz and D. Turnbull (Academic Press Inc., New York, 1960), and previous publications.
[3] A. F. Kip, C. Kittel, R. A. Levy, and A. M. Portis, Phys. Rev. **91**, 1066 (1953).

tions. This is certainly justifiable in the case of KCl, which we treat numerically, but is probably a bad approximation in some other systems, notably LiF.

The ground state LCAO is of the form

$$\phi_F = c_s \sum_\alpha \phi_{\alpha s} + c_p \sum_\alpha \phi_{\alpha p}, \quad (5)$$

where α runs over the six (100)-like sites about the vacancy, $\phi_{\alpha s}$ is the valence s function at α ($K4s$ in KCl), and $\phi_{\alpha p}$ is the $p\sigma$ function there pointing away from the vacancy ($K4p\sigma$ in KCl).

The charge density and normalization equations then read

$$|\Psi_F|^2 = \Big| c_s \sum_\alpha (\phi_{\alpha s} - \sum_i \phi_i S_{\alpha s,i}) + c_p \sum_\alpha (\phi_{\alpha p} - \sum_i \phi_i S_{\alpha p,i}) \Big|^2 \times \Big| 1 - \sum_i (c_s \sum_\alpha S_{\alpha s,i} + c_p \sum_\alpha S_{\alpha p,i})^2 \Big|^{-1}, \quad (6)$$

and

$$(6 + \sum_\alpha \sum_{\beta \neq \alpha} S_{\alpha s,\beta s}) c_s^2 + (6 + \sum_\alpha \sum_{\beta \neq \alpha} S_{\alpha p,\beta p}) c_p^2 + 2(\sum_\alpha \sum_{\beta \neq \alpha} S_{\alpha s,\beta p}) c_s c_p = 1. \quad (7)$$

III. RESULTS AND DISCUSSION

An explicit numerical calculation has been carried out for the F center in KCl.[4] Tabular Hartree-Fock functions for the free constituents were used throughout.[5–7] The overlap integrals were evaluated using Löwdin's alpha-function technique.[8] Programs written by Rimmer and Knox for the IBM 650 computer were used to generate the necessary alpha functions and perform the required numerical integrations.[9] The overlap sums were carried out through the fourth neighbors of each valence function, thus reaching to the vacancy's eighth neighbors. In practice rather large numerical inaccuracies encountered in evaluating the denominator of Eq. (6) together with the particular coefficients which appear there and in Eq. (7), made solving these two directly rather imprecise. Instead, the final results were obtained by evaluating Eq. (6) at both (100) and (110), dividing and then solving the resulting equation for

$$|\Psi_F(100)|^2 / |\Psi_F(110)|^2$$

together with Eq. (7). The values obtained for the mixing coefficients are $c_s = 0.055$, $c_p = 0.216$. This is in strong contrast to the results obtained neglecting overlap which indicate that the function has about 60% s character.

The calculated charge densities at more distant sites are compared to those obtained experimentally in Table I. The agreement is self-evidently bad. There is too little charge at (111) and too much outside of it. Thus, we conclude, in concordance with Dexter's conjecture,[10] that many orbitals are necessary to describe the F center in an LCAO picture. The present model is not sufficiently accurate to reproduce quantitatively the details of the charge distribution. Because of the large spatial extent of the $K4s$ and $4p$ functions, it seems most reasonable to add these centered at the eight (111)-like sites into the trial function as a next

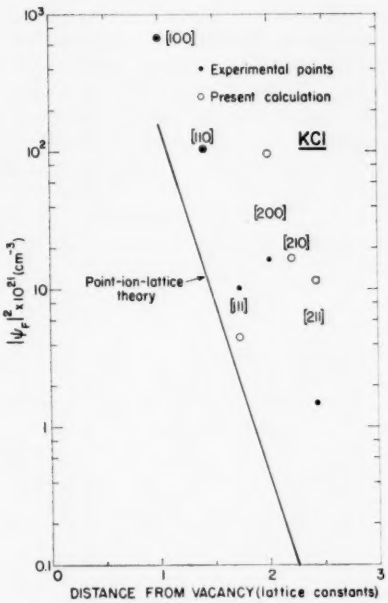

FIG. 1. Comparison of measured F electron charge density with the values predicted by the orthogonalized LCAO and point-ion-lattice models in KCl.

TABLE I. Charge density at various sites neighboring the F center in KCl. The calculated values are from the present work; the experimental ones are ENDOR data taken from reference 1. All are in units of 10^{21} cm^{-3}.

Site	Calc	Obs
(100)	667 (fitted)	667
(110)	106 (fitted)	106
(111)	4.5	10.0
(200)	97.2	16.4
(210)	16.7	...
(211)	11.5	1.5

[4] We assume all the ions remain in their normal lattice positions despite the presence of the vacancy. The lattice constant is taken as 3.14 A.

[5] For Cl^-: D. R. Hartree and W. Hartree, Proc. Roy. Soc. (London) **A156,** 45 (1936).

[6] For K^+ core functions: D. R. Hartree and W. Hartree, Proc. Roy. Soc. (London) **A166,** 450 (1938).

[7] For the $K4s$ and $4p$ functions: L. Biermann and K. Lubeck, Z. Astrophys. **25,** 325 (1948).

[8] P. O. Löwdin, Advances in Phys. **5,** 1 (1956).

[9] M. P. Rimmer and R. S. Knox, unpublished report, University of Rochester (1958).

[10] D. L. Dexter, Phys. Rev. **93,** 244 (1954).

step. However, such a calculation would entail a prohibitive amount of algebraic and computational labor.

The simple orthogonalized LCAO picture does possess some virtues. Figure 1 compares the results of the present calculation, the experimental observations and the Gourary and Adrian treatment. Note that the last predicts a charge density decreasing monotonically with distance from the vacancy, whereas the present calculation qualitatively reproduces the upward "wiggle" at the (200) site. We can interpret this as a geometrical effect arising from the terms

$$(\phi_{ap}-\sum_{\alpha}\phi_i S_{ap,i})$$

in the numerator of Eq. (6). The dominant contribution to this at distant sites comes from $\sum_{\alpha}\phi_s(0)\,S_{ap,s}$, where $\phi_s(0)$ is a core s function centered on the site in question. The overlaps involved fall off quite slowly with the separation. Thus, we expect a strong directional dependence, with the sites along the angular maxima of the p functions showing upward "wiggles" in charge density when compared with sites near them which fall between the lobes of the p functions. Viewing the situation from the center of the vacancy, we might say that the s-like part of the F wave function is dominant inside the vacancy and close by, but at greater distances the small, long-tailed g-like part is decisive in determining the detailed behavior of the charge distribution, even though it has little effect on the energy of the system. The simple orthogonalized LCAO model shows this directional dependence at least in a qualitative way, whereas the point-ion-lattice function which is spherically symmetric about the center of the vacancy cannot be expected to reproduce it.

It should be pointed out that the techniques of the present paper might profitably be applied to the analysis of spin-resonance data from measurements made on organic molecules with substituted or added paramagnetic groups. The relatively small number of atoms and planar geometry may make the overlap sums simple enough to include a sufficiently large number of orbitals for accurate detailed description. Wave functions thus obtained can, of course, be used as the starting point for further computations.

ACKNOWLEDGMENTS

The author wishes to thank C. P. Slichter for drawing his attention to the problem of F-center wave functions, and to M. P. Rimmer and R. S. Knox for providing him with their computer programs.

THE JOURNAL OF CHEMICAL PHYSICS VOLUME 35, NUMBER 6 DECEMBER, 1961

Unimolecular Decay of the Triplet State of Anthracene in Fluid and Viscous Media*

G. JACKSON† AND ROBERT LIVINGSTON

Department of Chemistry, Institute of Technology, University of Minnesota, Minneapolis 14, Minnesota

(Received May 12, 1961)

The rate of decay of the triplet state of anthracene, dissolved in hexane, tetrahydrofuran, and glycerol, has been measured at temperatures ranging from 30 to −70°C. In fluid solvents at ordinary temperatures, the decay appears to be chiefly the result of bimolecular triplet-triplet interaction and of a bimolecular quenching reaction involving an unknown quencher, present in trace amounts even in highly purified solvents. In addition, there appears to be a unimolecular, temperature-independent decay, corresponding to an intrinsic mean life of about 0.01 sec. In glycerol, the first-order rate constant decreases rapidly with decreasing temperature, approaching a limiting half life of about 0.04 sec at −25°C. This limiting rate appears to be the same as has been previously reported for solutions in EPA at liquid nitrogen temperatures. Similar results were obtained with solutions of dibenzanthracene.

INTRODUCTION

THE rate of disappearance of the triplet state of anthracene, etc., in fluid solvents, can be represented by an equation of the following form:

$$-d[T]/dt=k_1'[T]+k_2[T]^2.$$

The bimolecular reaction appears to be a diffusionally-limited process, and the experimentally determined values of k_2 are reproducible within the expected limits of precision.[1–3]

In contrast, the values of k_1' (for a given solvent) vary widely,[1] depending upon the experimenter and even upon the sample of solvent for the same experimenter. Exhaustive purification of the solvent usually reduces the observed value of k_1'. The addition of

*Sponsored by the Office of Ordnance Research, U. S. Army.

† Present address: Atomic Energy Research Establishment, Harwell, Berkshire, England.

[1] G. Porter and M. Wright, Discussions Faraday Soc. **27,** 18 (1959).

[2] G. Jackson, R. Livingston and A. Pugh, Trans. Faraday Soc. **56,** 1635 (1960).

[3] H. Linschitz and L. Pekkarinen. J. Am. Chem. Soc. **82,** 2411 (1960).

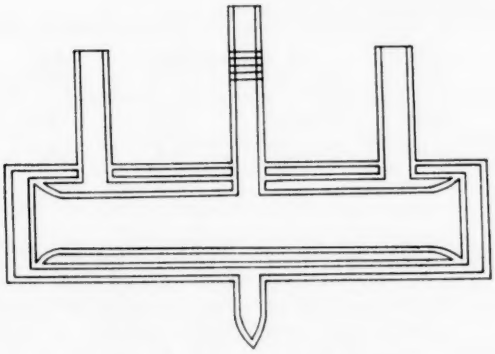

FIG. 1. The vacuum-jacketed cuvette.

quenchers (such as O_2, quinone, or the ions of certain transition metals) greatly reduces the half-life of the triplet state, and the second-order quenching constants, for efficient quenchers, have values which would be predicted for diffusionally limited, bimolecular reactions.

These observations indicate that the first-order decay is the result of the concurrence of a spontaneous, unimolecular decay and a bimolecular reaction between the triplet and an unknown, adventitious quencher, present at very low concentration. Accordingly,

$$k_1' = k_1^0 + k_Q[Q]$$

and

$$-d[T]/dt = (k_1^0 + k_Q[Q])[T] + k_2[T]^2.$$

EXPERIMENTAL METHODS AND MATERIALS

The sample of anthracene was the same as used in previous work.[2] The 1, 2, 5, 6 dibenzanthracene was a high-grade commercial preparation and was twice recrystallized from spectrographic-grade hexane. The solvents, *n*-hexane, and tetrahydrofuran, were treated with Na and were distilled, in an atmosphere of N_2 through an efficient packed column, shortly before they were used. The final distillations were made in the vacuum line. The purest sample of hexane was prepared from spectrographic grade material, and was passed through a column of activated silica gel, before being treated with Na and distilled. The starting material for the tetrahydrofuran was an ordinary commercial sample. It was treated successively with several samples of clean Na, before being distilled. The glycerol was of ordinary USP grade and was twice vacuum distilled before use.

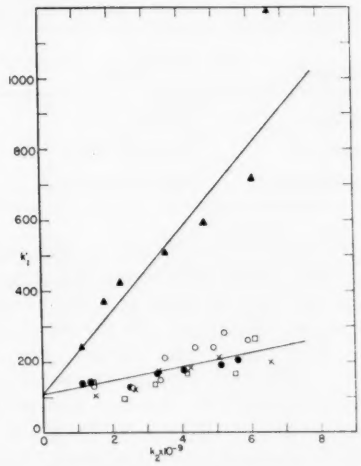

FIG. 3. k_1' as a function of k_2 of anthracene in tetrahydrofuran. ○ ● × □ Several measurements in tetrahydrofuran. Δ measurement in tetrahydrofuran containing $CuCl_2$.

PREPARATION OF THE SOLUTIONS

The solutions were degassed on a vacuum liue. The bulk of this gas was removed by distilling off an appreciable fraction (10 to 30%) of the solvent. After this, the solvent was frozen with liquid N_2 and the space

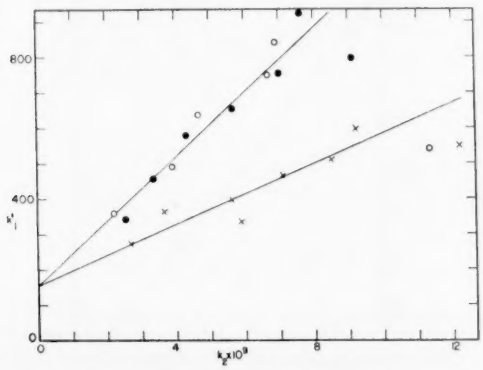

FIG. 2. k_1' as a function of k_2 of anthracene in hexane. ○ ● Two measurements using normally purified hexane. × Specially purified hexane.

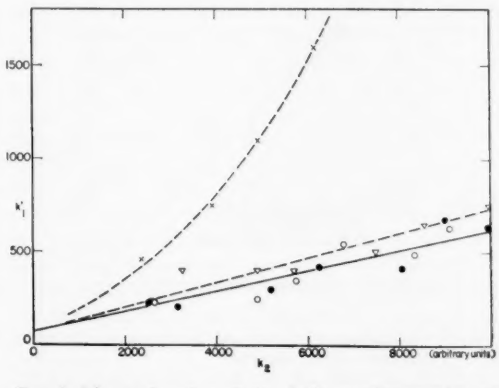

FIG. 4. k_1' as a function of αk_2 of dibenzanthracene in tetrahydrofuran. ○ ● Two measurements in tetrahydrofuran. Δ × Measurements in tetrahydrofuran containing $CuCl_2$ at low and at high concentrations.

TABLE I. Kinetics of the decay of the triplet in hexane and tetrahydrofuran.

Compound	Solvent	k_1^0 (sec^{-1})	$k_Q^0[Q]$ (sec^{-1})	k_2^0 (m^{-1} sec^{-1})	$\Delta E_Q^{\ddagger}$ (kcal)	$\Delta E_2^{\ddagger}$ (kcal)
Anthracene	Hexane	160	3×10^4	3.0×10^{11}	1.9	1.9
Anthracene	Tetrahydrofuran	110	3×10^4	1.5×10^{11}	2.5	1.9
Dibenzanthracene	Tetrahydrofuran	80	1×10^5	...	2.1	1.9

above it evacuated to the "black"-vacuum stage. The vessel was then closed off by means of a stopcock, and the solvent warmed to ambient or higher temperatures. The solvent was then frozen and the vessel evacuated as before. This process was repeated four to eight times. The purified solvent was introduced into the evacuated cuvette, which contained a known amount of dry anthracene, by tilting a section of the vacuum line, after which, the solution was frozen and the cell sealed off at a thin-walled constriction. To facilitate degassing the glycerol, pure methanol was added to the solvent and was distilled off, at approximately 100°C, in the vacuum line.

APPARATUS

The flash-photolytic apparatus has been described.[2] The temperature measurements were made in a vacuum-jacketed, fused-quartz cell, the design of which is shown in Fig. 1.[4] Although the cell proved to be useful and convenient in the study of anthracene and dibenzanthracene, strong phosphorescence of the silica, in the blue, violet, and near ultraviolet, prevented us from making flash-photolytic studies of the triplet absorption of naphthalene.

The cuvette, flashlamps, etc., which were designed for and used in the study of the flash-photolytic absorption changes, were used without modification in the measurement of the rate of decay of the phosphorescence of dibenzanthracene. An RCA 931 A photomultiplier, in a suitable housing, was placed close to the exit diaphragm of the light box. A simple mechanical shutter and a second order interference filter, having a maximum transmittance of 5320 A, were placed between the light box and the photomultiplier housing. After some practice, it proved possible to open the shutter reproducibly a few milliseconds after the lamp was flashed and the oscilloscope triggered.

RESULTS

If both bimolecular quenching reactions are diffusionally limited, their energies of activation should be identical and the values of their pre-exponential factors, k_2^0 and k_Q^0, should be similar. If we further assume, for the range of temperatures used, that the rate of the spontaneous, unimolecular decay is independent of temperature, we may write,

$$k_1' = k_1^0 + k_Q^0[Q]\exp(-\Delta E^{\ddagger}/RT)$$

and

$$k_2 = k_2^0\exp(-\Delta E^{\ddagger}/RT).$$

These predictions can be tested by plotting k_1' against k_2', for a series of measurements, made with the same solution but at a number of different temperatures. Such plots are shown on Figs. 2–4. With one exception which will be discussed later, the data fit straight lines, intercepting the k_1' axis above the origin. The slopes, $k_Q^0[Q]/k_2^0$, of the lines should depend upon the con-

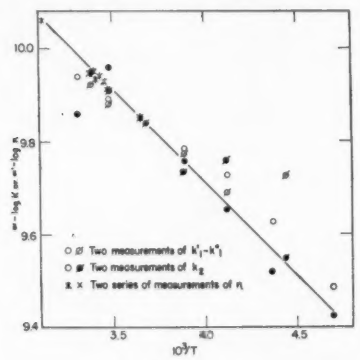

FIG. 5. Dependence of $k_1'-k_1^0$ and k_2 (anthracene in hexane) and of η of hexane on temperature.

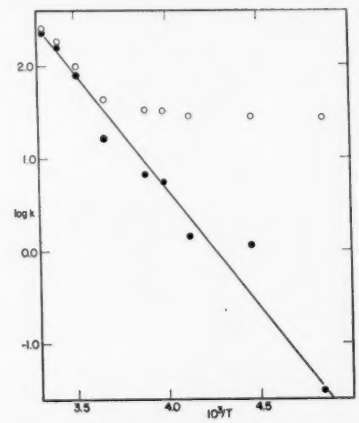

FIG. 6. Dependence of k_1' and of $(k_1'-k_1^0)$ on temperature for anthracene in glycerol. ○ k_1' ● $k_1'-k_1^0$.

[4] We are indebted to the Mechanical Division of General Mills and to Mr. Emil Berg of General Mills for the construction of the cell.

TABLE II. Kinetics of the decay of the triplet in glycerol.

Compound	k_{G1}^0 (sec^{-1})	$k_{G1}^{0\prime}$ (sec^{-1})	$\Delta E_{G1}^{\ddagger}$ (kcal/mole)	Measurement
Anthracene	27	1.4×10^{11}	12.4	Absorption
Dibenzanthracene	0.95	1.3×10^{11}	12.2	Absorption
Dibenzanthracene	0.70	2.5×10^{11}	12.4	Phosphorescence

centrations of the inhibitors present. This prediction is confirmed by the marked increase in slope which accompanies the addition of the quencher[3] $CuCl_2$ to tetrahydrofuran solutions and by the unusually small slope which was obtained when highly purified hexane was the solvent (Fig. 2).

It is apparent that, although the values of k_1^0 cannot be obtained precisely, the intercept is greater than zero and the data are consistent with the postulate that k_1^0 has a unique, temperature-independent value for a given solvent and hydrocarbon. The uncertainty in the values of k_1^0 is probably about $\pm30\%$.

Since both k_1' and k_2 were measured as functions of temperature, these data can be used to determine the corresponding energies of activation. Figure 5 is a plot, for anthracene in hexane, of $\log k_2$ and of $\log(k_1'-k_1^0)$ against the reciprocal of absolute temperature. The data exhibit considerable scatter, but they all are consistent with a value of 1.9 kcals for the energy of activation. Values of $-\log\eta$ (normalized to $\log k_2$ at $T^{-1}=3.4\times10^{-3}$) are also plotted on this figure. These values,[5] for the limited range of temperature for which they are available, are likewise consistent with an energy of activation of 1.9 kcal. These data and the corresponding values for anthracene and dibenzanthracene in tetrahydrofuran are summarized in Table I. The effect of temperature upon the viscosity of tetrahydrofuran has not been measured. The small solubility of dibenzanthracene in hexane prevented us from studying this system. The absolute value of k_2^0 for dibenzanthracene could not be determined, since the extinction coefficient of its triplet has not been measured. The values of $k_Q^0[Q]$ vary with the purity of the solvent. The apparent uncertainty of the values for $\Delta E^{\ddagger}$ is $\pm15\%$ and for k_1^0 is $\pm30\%$.

The curvature of the plot of $(k_1'+k_{CuCl_2}[CuCl_2])$ vs k_2 (Fig. 4) for dibenzanthracene in tetrahydrofuran, indicates that the quenching by $CuCl_2$ has an energy of activation appreciably greater than 1.9 kcal. Assuming that

$$k_{CuCl_2}[CuCl_2]=k_1'-80-10^5\ \exp(-2000/RT)\ \ sec^{-1},$$

we obtained $\Delta E^{\ddagger}_{CuCl_2}\cong4.0$ kcal. In contrast to this, $\Delta E^{\ddagger}_{CuCl_2}$ for anthracene in tetrahydrofuran is about 1.9 kcal. Since we did not determine $[CuCl_2]$ in our experiments, we are unable to evaluate $k_{CuCl_2}^0$. For anthracene in tetrahydrofuran, we can estimate the preexpotential factor by combining our value for $\Delta E_{CuCl_2}^{\ddagger}$ with Linschitz and Pekkarinen's value of $3.2\times10^8 m^{-1}$ sec^{-1} for the bimolecular rate constant of 25°C. The resulting value is $k_{CuCl_2}^0=1\times10^{10}m^{-1}$ sec^{-1}.

The first-order rate constants, determined from measurements of the decay of phosphorescence in rigid media at liquid nitrogen temperatures, are reported as 0.67[6] and 0.71[7] sec^{-1} for dibenzanthracene and >10 for anthracene.[7] McGlynn *et al.*[8] calculate a value of 11 sec^{-1} for anthracene from integrated absorption measurements. Since these quantities are definitely smaller than our extrapolated values for k_1^0, it follows that the unimolecular decay is faster in fluid solvents than in rigid media at low temperatures. Phosphorescence is not commonly observed in nonviscous solutions; therefore, the process whose rate increases with increasing temperature or decreasing viscosity is nonradiative. In an effort to obtain more definite information in regard to these modes of decay of the triplet, we studied anthracene and dibenzanthracene in glycerol at temperatures ranging from 30 to −70°C. The rate of disappearance of the triplet-triplet absorption was measured for both substances. For dibenzanthracene, the rate of decay of phosphorescence was also measured.

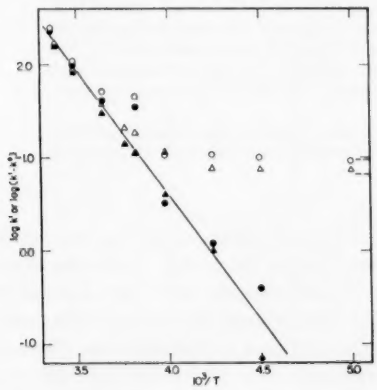

FIG. 7. Dependence of k_1' and of $(k_1'-k_1^0)$ on temperature for dibenzanthracene in glycerol. Phosphorescence measurements: △ k_1'; ▲ $k_1'-k_1^0$. Absorption measurements: ○ k_1'; ● $k_1'-k_1^0$.

[5] *Handbook of Chemistry and Physics* (Chemical Rubber Publishing Company, 1959), 41st ed., p. 2185.

[6] D. McClure, J. Chem. Phys. **17,** 905 (1949).

[7] D. Craig and I. Ross, J. Chem. Soc. **1954,** 1589.

[8] S. P. McGlynn, M. Padhye and M. Kasha, J. Chem. Phys. **23,** 593 (1955).

Under these conditions, no second-order component of the decay was detectable. At 25°C, the first-order rate constants were approximately 240 sec^{-1} for anthracene and 25 sec^{-1} for dibenzanthracene. The rates decrease rapidly with decreasing temperature, becoming practically constant at −25°C. The data fit an equation of the following form, as is illustrated in Figs. 6 and 7:

$$k_{G1}=k_{G1}^{0}+k_{G1}^{0'}\exp(-\Delta E^{\ddagger}/RT).$$

The results of these measurements and calculations are summarized in Table II.

There is a small but systematic difference in the rate of decay as measured by phosphorescence intensity and by changing absorption, which must be an artifact of the methods of measurement. The only apparent differences in the conditions are that the first few milliseconds are excluded in the phosphorescence measurements and that the solution was continuously exposed to the scanning light during the absorption measurements.

DISCUSSION

The rate of the first-order disappearance of the triplet states of polyatomic molecules, as measured in fluid solvents by the flashphotolytic technic, is dominated by a bimolecular reaction between the triplet and traces of impurities, present in the purest solvents. Extrapolation of the results of measurements, made at temperatures ranging from 30° to −70°C, yields first-order rate constants for the spontaneous decay of the anthracene triplet in hexane and tetrahydrofuran of 160 and 110 sec^{-1}, respectively. The lowest (published) values which were obtained by direct measurement at 25°C are 340 and 265 sec^{-1}. If the adventitious quencher, which is responsible for this relatively fast rate, were as efficient as molecular oxygen, its concentration could be as low as $5\times10^{-8}m$ (i.e., about $2\times10^{-7}\%$); well below the limits detectable by the most sensitive analytical methods.

The present, incomplete data suggest that the unimolecular rate constant depends upon, but is not a simple function of, viscosity. From 0.3 to 500(?) centipoise the rate appears to be sensibly independent of viscosity, but decreases with further increase in viscosity, reaching a lower limit at approximately 3×10^{5} centipoise (glycerol at −25°C). The energy of activation for this first-order rate constant is 12.3 kcal. Published values of the viscosity of glycerol correspond to an energy of activation of 19.8 kcal between −4° and −42°C and of 17.4 kcal between 30° and 0°C. The difference, between either of these values and 12.3 kcal, is almost certainly greater than can be attributed to random errors of measurement. A further experimental study of these phenomena is in progress.

THE JOURNAL OF CHEMICAL PHYSICS VOLUME 35, NUMBER 6 DECEMBER, 1961

An Analysis of the Infrared Absorption Spectrum of $Am^{+3}(5f^6)$ in $LaCl_3$*

JOHN B. GRUBER†

Lawrence Radiation Laboratory and Department of Chemistry, University of California, Berkeley, California

(Received April 21, 1961)

The polarized infrared absorption spectrum of single crystals of $Am^{+3}(5f^6)$ in $LaCl_3$ has been studied from 0.79 to 16.0 μ. In almost every instance the spectrum is sharp and completely polarized, and appears in definite groupings. Transitions from the ground level, $^7F_0$, to excited levels of the ground term, $^7F_1$, $^7F_2$, $^7F_3$, $^7F_4$, $^7F_5$, and $^7F_6$ have been observed. For the particular point symmetry C_{3h} that is consistent with experiment, magnetic-dipole transitions are observed from the $^7F_0$ level to the $^7F_1$ level, and forced electric-dipole transitions are observed to levels $J=2$, 3, 4, 5, and 6.

A theoretical analysis is presented for the crystal-field split ^7F_J levels. Using four parameters—$A_2^0\langle r^2\rangle=206$ cm^{-1}, $A_4^0\langle r^4\rangle=-94.1$ cm^{-1}, $A_6^0\langle r^6\rangle=-93.8$ cm^{-1}, and $A_6^6\langle r^6\rangle=1100$ cm^{-1}—excellent agreement is obtained between theory and experiment.

INTRODUCTION

In recent years several successful analyses of the absorption spectra of certain actinide ($5f^n$) ions have been reported.[1–3] Nevertheless, complete interpretation of optical spectra so far has been limited to actinide ions having the rather simple electronic configuration of filled electron shells plus a single 5f electron. This is understandable in view of the complexity of the spectra of higher f^n configurations. However, the rather formidable task of interpreting such complex spectra can be approached by studying the optical and magnetic properties of the low-lying states, since the ground-state terms of most of the $5f^n$ configurations are reasonably isolated. This is particularly true for $Am^{+3}(5f^6)$, where the ground-state term, ^7F is sepa-

* This work was done under the auspices of the U. S. Atomic Energy Commission.

† Address after July 1, 1961: Institut für technische Physik, der Technischen Hochschule, Darmstadt, Germany.

[1] G. L. Goodman and M. Fred, J. Chem. Phys. **30**, 849 (1959).

[2] J. C. Eisenstein and M. H. L. Pryce, Proc. Roy. Soc. (London) **A255**, 181 (1960).

[3] J. D. Axe, "The electronic structure of octahedrally coordinated protactinium (IV)," (thesis), Lawrence Radiation Laboratory Report UCRL-9293, July 1960.

rated from the nearest quintet terms by some thousands of wave numbers.[4]

In most cases the infrared absorption spectrum reported here is sharp and completely polarized. Likewise, Zeeman broadening can be observed for three of the groupings in the near infrared. While no absorption peaks are found between 16.0 and 4.82 μ, definite groupings are observed at 2115, 4000, 5300, 9505, 12 150, and 12 400 cm^{-1}. Each of these energy values corresponds to the center of gravity of the observed grouping.

The spin-orbit interaction splits the $Am^{+3}(5f^6)$ ground-state term into seven levels ^7F_J, where $J=0$, 1, 2, 3, 4, 5, and 6. Because of the crystal field produced at the Am^{+3} site in $LaCl_3$, the $(2J+1)$-fold degeneracy of a level is partially lifted, and the number and degeneracy of the crystal-field-split components depend on the point symmetry at the Am^{+3} cation site. From experimental considerations pointed out later in this paper, it is concluded that the Am^{+3} is probably situated in a C_{3h} site, where the nine nearest chloride neighbors (ligands) are separated from the cation in the manner shown in Fig. 1. Once the point symmetry is assumed, the corresponding selection rules will aid us in establishing the multipolarity of allowed transitions.[4–6] For Am^{+3} in a C_{3h} site, forced electric dipole transitions are allowed from the ground level $^7F_0$, μ_0, to excited crystal-field-split sublevels $\mu_{\pm 2}$, and μ_3 of J levels greater than one.[4] Magnetic dipole transitions are allowed to the sublevels $\mu_{\pm 1}$, and μ_0 of the $J=1$ level. Transitions that appear both in the σ transverse and axial spectrum are forced electric dipole transitions, while those appearing in the π transverse and axial are magnetic dipole transitions.[4–6]

Thus, from the observed polarized absorption spectrum alone one should be able to identify uniquely $J=1$, 2, and 3, and larger J levels only indicatively.[4]

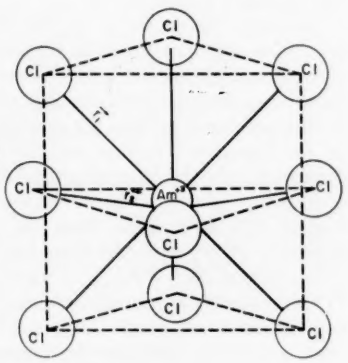

FIG. 1. The Am^{+3} cation site in single crystals of $AmCl_3$–$LaCl_3$.

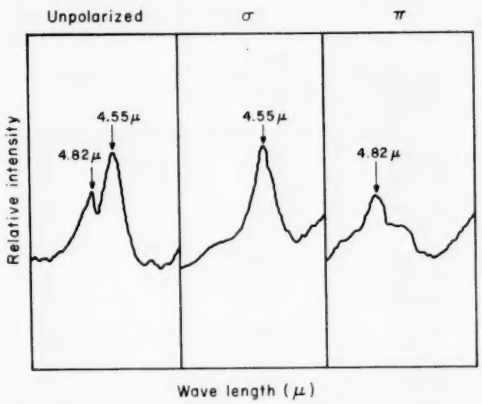

FIG. 2. The absorption spectrum of the $^7F_1$ level. On the left, the unpolarized spectrum is given, and on the right, the σ and π polarizations appear. Wave-length measurements are in microns, μ.

However, when several J levels are close together, it is difficult to ascertain which components belong to a particular level. In this case, the crystal-field theory may be employed to obtain a theoretical spectrum that the experimentalist may compare with the observed spectrum. In this way, one obtains not only a parent J-level assignment, but also some indication of what order of magnitude the field-free level is split by the crystal field.

PREPARATION OF SINGLE CRYSTALS OF $AmCl_3$—$LaCl_3$

Single crystals of $AmCl_3$-$LaCl_3$ containing 0.1 to 10% by weight Am^{+3} (americium-241, half life=458 yr) were prepared in the following manner. A known quantity of spectroscopically pure Am^{+3} in 2.0 M HCl was added to a quartz sublimation tube. The solution was slowly evaporated on a vacuum line, and anhydrous $AmCl_3$ was prepared by heating the hydrate slowly in the presence of dry HCl. After the tube was flushed repeatedly with dry argon, a known quantity of spectroscopically pure anhydrous $LaCl_3$ was added. The mixture was then thoroughly degassed and melted to form a solution. The sublimation and single-crystal-growing techniques employed were quite similar to those reported by Sayre, Sancier, and Freed,[5] and Gruen, Conway, and McLaughlin.[7] Because of the intense radioactivity of americium-241, as well as the hygroscopic nature of anhydrous $LaCl_3$, the crystal had to be mounted in a dry-nitrogen-atmosphere glove box suitably prepared for radioactive work.

In order to determine whether the $AmCl_3$-$LaCl_3$ mixed-crystal system preserved C_{3h} symmetry about the cation sites, anhydrous $PrCl_3$ was added to the mixture before the single crystals were grown. When the absorption spectrum of the single crystal was taken,

[4] J. B. Gruber, "An analysis of the absorption spectra of Tm IV and Am IV," (thesis), Lawrence Radiation Laboratory Report UCRL-9203, January 1961.
[5] E. V. Sayre, K. M. Sancier, and S. Freed, J. Chem. Phys. **23,** 2060 (1955).
[6] E. V. Sayre and S. Freed, J. Chem. Phys. **24,** 1211 (1956).
[7] D. M. Gruen, J. G. Conway, and R. D. McLaughlin, J. Chem. Phys. **25,** 1102 (1956).

TABLE I. The polarized infrared absorption spectrum of $Am^{+3}(5f^6)$ in $LaCl_3$.

Wavelength (A) (in air) 77°K	Wave numbers (in vacuum) 77°K	P	I	Possible μ-sublevel assignments	Possible J-level assignment	Comments
48 200	2074	π, a	4	±1		Magnetic-dipole transitions to this level from $^7F_0$.
45 500	2197	σ	5	0	1	
25 190	3970	σ, a	3	±2	2	Electric-dipole transition. Position of this level is somewhat uncertain.
19 200	5208	π	3	3		Electric-dipole transitions.
18 840	5307	σ, a	6	±2	3	
18 730	5340	π	3	3		
10 769	9282	σ, a	9[a]	±2		Electric-dipole transitions. This grouping was observed in the photographic region of the infrared.
10 485	9535	π	10[a]	3	4	
10 474	9545	σ, a	8[a]	±2		
10 132	9867	π	5[b]	3		
8246	12 123	σ, a	3[a]	±2		Electric-dipole transitions. Several lines are rather broad; however, complete polarization was observed.
8159	12 253	π	10[a]	3	5	
8144	12 275	π	8[c]	3	and	
8123	12 307	σ, a	10[c]	±2	6	
8060	12 404	σ, a	10[a]	±2		
8055	12 411	π	5[b]	3		
7956	12 566	π	5[a]	3		
7050	12 575	σ, a	4[a]	±2		

[a] Linewidth 3 to 5 A.
[b] Linewidth 1 to 3 A.
[c] Linewidth 5 to 10 A: unresolved band structure.

the Pr^{+3} lines were found to have the same polarization and energy positions as reported by Sayre, Sancier, and Freed.[5] We conclude, therefore, that the symmetry about the Pr^{+3} ion is similar to that reported earlier, and that the symmetry about the americium ions also very probably is C_{3h}. In addition, the observed polarization spectrum of Am^{+3} in $LaCl_3$ is consistent with the selection rules for C_{3h}.

SPECTROGRAPHIC EQUIPMENT

The absorption spectrum of single crystals was studied with a Jarrel-Ash Wadsworth-mount 3.4-m spectrograph. Two gratings were used in the instrument —one with 7500 lines per in. and another with 15 000 lines per in. In the first order, the reciprocal linear dispersion was 10.1 A/mm and 5.3 A/mm, respectively. Crystals were maintained at selected temperatures of 77°K (liquid nitrogen) and 4°K (liquid helium) in quartz and Pyrex Dewars. No appreciable sharpening of the spectrum was observed at the lower temperature.

Light sources included an air-cooled high-pressure mercury lamp (BH6), and a 100-watt tungsten lamp. The two types of polarizers employed were a Nicol and a Wollaston. Iron and mercury lines served as wavelength references, and the photographic plates were measured on a precision screw-type comparator.

The solution spectrum of Am^{+3} in 0.2M DCl, D_20 was studied on a Cary model 14 spectrophotometer which was calibrated at the factory with an AH4 Hg arc. Infrared spectra were observed with a Beckman IR-5 infrared spectrophotometer and a Perkin-Elmer model 112-U spectrometer.

Polarized Absorption Spectrum of ^7F_J Levels

No absorption peaks are observed from 16.0 to 4.82 μ. The grouping observed furthest in the infrared consists of two absorption peaks at 2074 and 2197 cm^{-1}. These two peaks (see Fig. 2 and Table I) have a completely polarized transverse and axial spectrum which indicates magnetic-dipole transitions from the ground level $^7F_0$ to the sublevels μ_0 and $\mu_{\pm1}$ associated with the $^7F_1$ level. Since the absorption spectrum appears in a region where quartz absorbs, the $AmCl_3$-$LaCl_3$ crystals were enclosed in a holder having AgCl windows.

Although the center of gravity of this level (2115 cm^{-1}) has been confirmed by the author's unpublished fluorescence spectrum of Am^{+3} in $LaCl_3$, there is additional experimental evidence that the $^7F_1$ level should be this far removed from the ground level, $^7F_0$. Studies of the hyperfine-structure and Zeeman effect on the spectra of (Pu I) have resulted in the derivation of three levels of the ^7F term.[8] Bovey and Gerstenkorn suggest this term arises from the ground-state configuration $5f^67s^2$, and that these levels are at 0.0 cm^{-1} ($^7F_0$), 2203.6 cm^{-1} ($^7F_1$), and 4299.6 cm^{-1} ($^7F_2$). For (Pu II), having a ground configuration of $5f^67s$, Judd has obtained values of ($^7F_0$), 0.0 cm^{-1} ($^7F_1$), 2110 cm^{-1}, and ($^7F_2$), 4280 cm^{-1} by removing the contribution of the $7s$ electron to the $5f^6$ configuration.[9,10]

[8] L. Bovey and S. Gerstenkorn, J. Opt. Soc. Am. **51,** 522 (1961).
[9] J. R. McNally, Jr., and P. M. Griffin, J. Opt. Soc. Am. **49,** 162 (1959).
[10] B. R. Judd, Lawrence Radiation Laboratory, Berkeley (private communication).

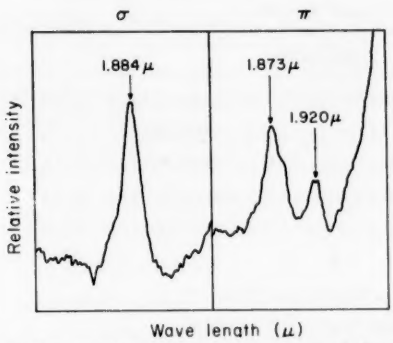

FIG. 3. The polarized absorption spectrum of the $^7F_3$ level taken at 77°K. On the left, one σ polarized peak is observed at 1.884 μ, and on the right, two π polarized peaks appear at 1.873 μ and 1.920 μ.

Since forced electric-dipole transitions are allowed to one of the three crystal-field split sublevels of $^7F_2$, the center of gravity for this level cannot be obtained from the absorption spectrum alone. A sharp peak, appearing both in the σ transverse and axial spectrum at 3970 cm^{-1}, has the proper polarization indicative of a transition to a single $\mu_{\pm 2}$ sublevel. Transitions to other components of the $^7F_2$ level observed in the fluorescence spectrum of Am^{+3} in $LaCl_3$ indicate that the center of gravity of the $^7F_2$ level is approximately 4000 cm^{-1} above $^7F_0$. Although this level appears to be some 260 cm^{-1} lower in energy than the corresponding level in (Pu I) $5f^67s^2$ and (Pu II) $5f^67s$, the complexity of intermediate coupling for Am^{+3} ($5f^6$) may provide some explanation for this difference.

Forced electric-dipole transitions are observed from the ground level to three of the sublevels comprising the $^7F_3$ level. In Fig. 3, the polarized absorption spectrum indicates that peaks at 5208 cm^{-1} and 5340 cm^{-1} are π polarized, and the peak at 5307 cm^{-1} is σ polarized. This same J level is also observed when several milligrams of anhydrous $AmCl_3$ are dissolved in a 0.2M DCl, D_2O solution and the spectrum taken between 1.0 and 2.3 μ on a Cary 14 spectrophotometer. When the blank is subtracted from the Am^{+3} spectrum, a peak and a shoulder are observed near 5380 cm^{-1}.

TABLE II. Reduced matrix elements for the ground multiplet, ^7F_J, of $Am^{+3}(5f^6)$.

Level	$\langle J \Vert \alpha \Vert J \rangle$	$\langle J \Vert \beta \Vert J \rangle$	$\langle J \Vert \gamma \Vert J \rangle$
$^7F_0$	0	0	0
$^7F_1$	−1/5	0	0
$^7F_2$	−11/315	−2/189	0
$^7F_3$	−1/135	1/33·45	−2/27·429
$^7F_4$	1/385	23/15·33·77	2/77·429
$^7F_5$	1/135	2/99·105	−1/189·429
$^7F_6$	1/99	−2/11·15·99	1/11·189·429

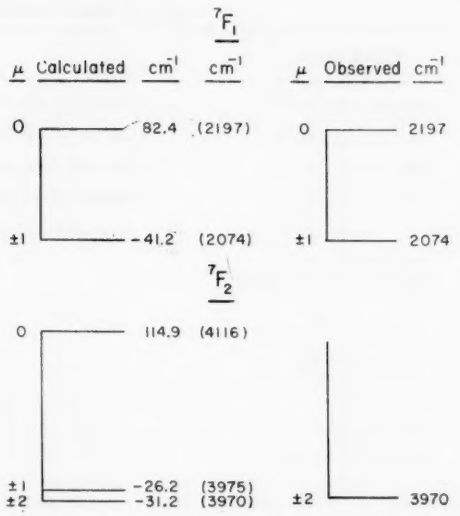

FIG. 4. The $^7F_1$ and $^7F_2$ levels of Am^{+3} in $LaCl_3$. On the left, the theoretical splitting may be compared with the observed energy-level scheme given on the right. Here μ is the crystal quantum number. The units of energy are cm^{-1}.

The $^7F_4$, $^7F_5$, and $^7F_6$ levels may be studied in the photographic region of the infrared. Four polarized lines (2σ and 2π) are observed near 9600 cm^{-1}, and as and as few as eight lines are observed between 12 100 and 12 600 cm^{-1} (see Table I). Since selection rules

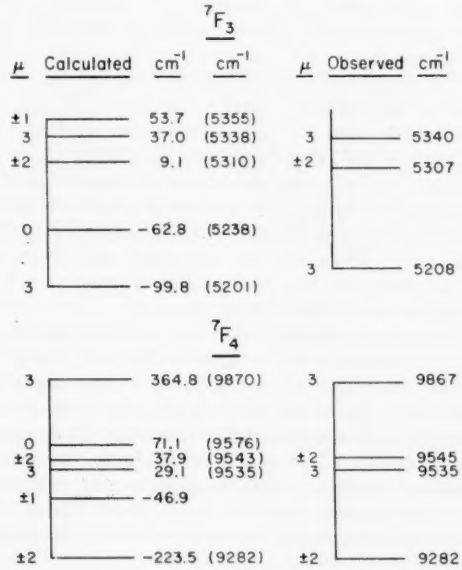

FIG. 5. The $^7F_3$ and $^7F_4$ levels of Am^{+3} in $LaCl_3$. On the left, the theoretical splitting may be compared with the observed energy-level scheme given on the right. Here μ is the crystal quantum number. The units of energy are cm^{-1}.

TABLE III. Matrix elements between the $^7F_5$ and $^7F_6$ levels.

Matrix element	Expression[a,b]
$(^7F_6, 5 \mid V_n^0 \mid {}^7F_5, 5)$	$5(11)^{\frac{1}{2}}A_2^0\langle r^2\rangle\langle 6 \mid\mid \theta_2 \mid\mid 5\rangle+360(11)^{\frac{1}{2}}A_4^0\langle r^4\rangle\langle 6 \mid\mid \theta_4 \mid\mid 5\rangle+7560(11)^{\frac{1}{2}}A_6^0\langle r^6\rangle\langle 6 \mid\mid \theta_6 \mid\mid 5\rangle$
$(^7F_6, 4 \mid V_n^0 \mid {}^7F_5, 4)$	$4(20)^{\frac{1}{2}}A_2^0\langle r^2\rangle\langle 6 \mid\mid \theta_2 \mid\mid 5\rangle+\ 36(20)^{\frac{1}{2}}A_4^0\langle r^4\rangle\langle 6 \mid\mid \theta_4 \mid\mid 5\rangle-7560(20)^{\frac{1}{2}}A_6^0\langle r^6\rangle\langle 6 \mid\mid \theta_6 \mid\mid 5\rangle$
$(^7F_6, 3 \mid V_n^0 \mid {}^7F_5, 3)$	$3(27)^{\frac{1}{2}}A_2^0\langle r^2\rangle\langle 6 \mid\mid \theta_2 \mid\mid 5\rangle-120(27)^{\frac{1}{2}}A_4^0\langle r^4\rangle\langle 6 \mid\mid \theta_4 \mid\mid 5\rangle-2529(27)^{\frac{1}{2}}A_6^0\langle r^6\rangle\langle 6 \mid\mid \theta_6 \mid\mid 5\rangle$
$(^7F_6, 2 \mid V_n^0 \mid {}^7F_5, 2)$	$2(32)^{\frac{1}{2}}A_2^0\langle r^2\rangle\langle 6 \mid\mid \theta_2 \mid\mid 5\rangle-150(32)^{\frac{1}{2}}A_4^0\langle r^4\rangle\langle 6 \mid\mid \theta_4 \mid\mid 5\rangle+3780(32)^{\frac{1}{2}}A_6^0\langle r^6\rangle\langle 6 \mid\mid \theta_6 \mid\mid 5\rangle$
$(^7F_6, 1 \mid V_n^0 \mid {}^7F_5, 1)$	$(35)^{\frac{1}{2}}A_2^0\langle r^2\rangle\langle 6 \mid\mid \theta_2 \mid\mid 5\rangle-\ 96(35)^{\frac{1}{2}}A_4^0\langle r^4\rangle\langle 6 \mid\mid \theta_4 \mid\mid 5\rangle+4320(35)^{\frac{1}{2}}A_6^0\langle r^6\rangle\langle 6 \mid\mid \theta_6 \mid\mid 5\rangle$
$(^7F_6, 0 \mid V_n^0 \mid {}^7F_5, 0)$	0
$(^7F_6, 1 \mid V_6^6 \mid {}^7F_5, -5)$	$-1/14(42\cdot(10)!)^{\frac{1}{2}}\langle 6 \mid\mid \theta_6 \mid\mid 5\rangle A_6^6\langle r^6\rangle$
$(^7F_6, 2 \mid V_6^6 \mid {}^7F_5, -4)$	$-1/14(1680\cdot(9)!)^{\frac{1}{2}}\langle 6 \mid\mid \theta_6 \mid\mid 5\rangle A_6^6\langle r^6\rangle$
$(^7F_6, 3 \mid V_6^6 \mid {}^7F_5, -3)$	$-1/14(3360\cdot(9)!)^{\frac{1}{2}}\langle 6 \mid\mid \theta_6 \mid\mid 5\rangle A_6^6\langle r^6\rangle$
$(^7F_6, 4 \mid V_6^6 \mid {}^7F_5, -2)$	$-1/14(420\cdot(10)!)^{\frac{1}{2}}\langle 6 \mid\mid \theta_6 \mid\mid 5\rangle A_6^6\langle r^6\rangle$
$(^7F_6, 5 \mid V_6^6 \mid {}^7F_5, -1)$	$-1/14(30\cdot(11)!)^{\frac{1}{2}}\langle 6 \mid\mid \theta_6 \mid\mid 5\rangle A_6^6\langle r^6\rangle$
$(^7F_6, 6 \mid V_6^6 \mid {}^7F_5, 0)$	$-1/14((12)!)^{\frac{1}{2}}\langle 6 \mid\mid \theta_6 \mid\mid 5\rangle A_6^6\langle r^6\rangle$

[a] $A_2^0\langle r^2\rangle=206$ cm^{-1}, $A_4^0\langle r^4\rangle=-94.1$ cm^{-1}, $A_6^0\langle r^6\rangle=-93.8$ cm^{-1}, $A_6^6\langle r^6\rangle=1100$ cm^{-1}.
[b] $\langle 6 \mid\mid \theta_2 \mid\mid 5\rangle=-1/15(11)^{\frac{1}{2}}$, $\langle 6 \mid\mid \theta_4 \mid\mid 5\rangle=1/3\cdot 99(11)^{\frac{1}{2}}$, $\langle 6 \mid\mid \theta_6 \mid\mid 5\rangle=-1/99\cdot 9\cdot 13(11)^{\frac{1}{2}}$.

for C_{3h} alone cannot help us to decide between a $J=4$, 5, or 6, the designation given in Table I is based on the following crystal-field splitting calculations.

Crystal-Field Splitting of the ^7F_J Levels

The crystal-field splittings of $^7F_1$, $^7F_2$, $^7F_3$, and $^7F_4$ levels are on the order of several hundred wave numbers, whereas the energy separation between the levels are several thousand wave numbers. Thus we can consider states labeled by the quantum numbers $LSJJ_z$, and use perturbation theory to find the effect of V. The matrix elements of V between state $\Delta J=0$ have been tabulated by Stevens,[11] and Elliott and Stevens.[12] For Am^{+3}, the reduced matrix elements $\langle J \mid\mid \alpha \mid\mid J\rangle$, $\langle J \mid\mid \beta \mid\mid J\rangle$, and $\langle J \mid\mid \gamma \mid\mid J\rangle$ have been evaluated for all levels of the ground multiplet (see Table II). As in the case of Eu^{+3}, the breakdown of Russell-Saunders coupling will depress the centers of gravity of the J levels by large amounts without seriously altering their splittings.[13] Since we are concerned only with the crystal-field splitting, the centers of gravity will be treated as adjustable parameters.

The set of parameters that best accounts for all the ^7F_J experimental data is $A_2^0\langle r^2\rangle=206$ cm^{-1}, $A_4^0\langle r^4\rangle=-94.1$ cm^{-1}, $A_6^0\langle r^6\rangle=-93.8$ cm^{-1}, and $A_6^6\langle r^6\rangle=1100$ cm^{-1}. The selection of $A_2^0\langle r^2\rangle$ was based on the experimentally observed separation of the two crystal-field sublevels, μ_0 and $\mu_{\pm 1}$, of the $^7F_1$ level. The $A_6^6\langle r^6\rangle$ parameter was taken from the experimental separation of the two μ_3 components of the $^7F_3$ level. The $A_4^0\langle r^4\rangle$ and $A_6^0\langle r^6\rangle$ parameters were selected to give the proper energy separation between the ± 2 and 3 sublevels of the ^7F_J multiplet. In Figs. 4 and 5 we compare the theoretical splitting (on the left) with the observed energy spectrum (on the right).

Crystal-Field Splitting of the $^7F_5$ and $^7F_6$ Levels

Since more absorption lines are observed between 0.79 and 0.82 μ than correspond to transitions to a single level, we may conclude that two levels, the $^7F_5$ and $^7F_6$, are separated by only several hundred wave numbers. While some of the observed lines may be vibrational satellites, the eight absorption lines selected were in most cases reasonably sharp and isolated. Three absorption lines—8144 Aπ, 8123 Aσ, and 8060 Aσ—are rather broad but clearly polarized; we may attribute the band-like structure to unresolved vibrational satellites to the blue of the electronic transitions.

In the crystal-field splitting calculations presented so far, the states are assumed to be eigenstates of L, S, and J. However, there are several important effects that may cause deviations from this simple model. We have mentioned one of these effects as the breakdown of Russell-Saunders coupling in which levels with the same J will admix. Also, various components of the crystal field will admix certain states with the same S. However, a far more serious effect in the Am^{+3} ground term is the interaction between the crystal-field components of the $^7F_5$ and $^7F_6$. Since the proximity of the two levels can perturb the crystal-field components by many tens of wave numbers, we must calculate matrix elements of the form

$$(J+k,\ J_z+m \mid V_n^m \mid J,\ J_z). \qquad (1)$$

For matrix elements between $^7F_5$ and $^7F_6$, $k=1$, $J+k=6$, and V_n^m refers to the particular spherical harmonic which transforms like T_q^k.

[11] K. W. H. Stevens, Proc. Phys. Soc. (London) **A65,** 209 (1952).
[12] R. J. Elliott and K. W. H. Stevens, Proc. Roy. Soc. (London) **A218,** 553 (1953).
[13] B. R. Judd, Mol. Phys. **2,** 407 (1959).

We may apply the general rare earth ($4f^n$) theory presented by Judd[14] to the problem of Am^{+3} ($5f^6$) in the following way. Since many of the matrix elements have similar forms, we can conveniently define $\phi_{n,k}{}^0(J, J_z)$ for $m=0$ by

$$(J+k, J_z \mid V_n{}^0 \mid J, J_z) = A_n{}^0\langle r^n\rangle \langle J+k \mid\mid \theta_n \mid\mid J\rangle \cdot \phi_{n,k}{}^0(J, J_z)\left[\frac{(J+J_z+k)!(J-J_z+k)!}{(J+J_z)!(J-J_z)!}\right]^{\frac{1}{2}} \quad (2)$$

and $\phi_{6,k}{}^6(J, J_z)$ for $m=6$ by

$$(J+k, J_z+6 \mid V_n{}^6 \mid J, J_z) = A_n{}^6\langle r^n\rangle \langle J+k \mid\mid \theta_n \mid\mid J\rangle \cdot \phi_{n,k}{}^6(J, J_z)\left[\frac{(J+J_z+k+6)!(J-J_z)!}{(J-J_z+k-6)!(J+J_z)!}\right]^{\frac{1}{2}}. \quad (3)$$

To find $(J+k, J_z-m \mid V_n{}^m \mid J, J_z)$, we simply multiply the value of $(J+k, m-J_z \mid V_n{}^m \mid J, J_z)$ by the phase factor $(-1)^{m+k}$. Since we have $k=1$ and $m=0$ or 6 in this problem, we find the phase factor will always be (-1). For the $^7F_5$ and $^7F_6$ levels, explicit expressions for $\phi_{n,k}{}^m(J, J_z)$ are

$$\phi_{2,1}{}^0(5, J_z) = J_z, \quad (4)$$

$$\phi_{4,1}{}^0(5, J_z) = J_z(7J_z{}^2-103), \quad (5)$$

$$\phi_{6,1}{}^0(5, J_z) = J_z(33J_z{}^4-975J_z{}^2+5262), \quad (6)$$

and

$$\phi_{6,1}{}^6(5, J_z) = -1\tfrac{1}{4}. \quad (7)$$

The reduced matrix elements $\langle 6 \mid\mid \theta_n \mid\mid 5\rangle$ associated with $^7F_5$ and $^7F_6$ have been evaluated by Elliott and Steven[12] for Tb^{+3}, $4f^8$. The Am^{+3} reduced matrix elements between the $^7F_5$ and $^7F_6$ will be the same except for a change in sign because of the orthonormality of the states (that is, the Am^{+3} f^6 shell is less than half filled, while the Tb^{+3} shell is more than half filled). Thus the reduced matrix elements for Am^{+3} are $\langle 6 \mid\mid \theta_2 \mid\mid 5\rangle = -1/(15\sqrt{11})$, $\langle 6 \mid\mid \theta_4 \mid\mid 5\rangle = 1/(3\cdot 99\sqrt{11})$ and $\langle 6 \mid\mid \theta_6 \mid\mid 5\rangle = -1/(99\cdot 9\cdot 13\sqrt{11})$.

Matrix elements of the form $(^7F_6, \pm J_z \mid V_n{}^0 \mid {}^7F_6, \pm J_z)$, and $(^7F_5, \pm J_z \mid V_n{}^0 \mid {}^7F_5, \pm J_z)$, have been evaluated by Elliott and Stevens.[12] Similarly, the elements $(^7F_6, 3 \mid V_6{}^6 \mid {}^7F_6, -3)$, $(^7F_6, 4 \mid V_6{}^6 \mid {}^7F_6, -2)$, $(^7F_6, 5 \mid V_6{}^6 \mid {}^7F_6, -1)$, $(^7F_6, 6 \mid V_6{}^6 \mid {}^7F_6, 0)$, and $(^7F_5, 3 \mid V_6{}^6 \mid {}^7F_5, -3)$, $(^7F_5, 4 \mid V_6{}^6 \mid {}^7F_5, -2)$, $(^7F_5, 5 \mid V_6{}^6 \mid {}^7F_5, -1)$ have been tabulated by the same authors.[12] In Table III we give the additional matrix elements needed to solve our problem. It should be pointed out that $(^7F_6, -J_z \mid V_n{}^0 \mid {}^7F_5, -J_z)$ is equal to $(^7F_6, J_z \mid V_n{}^0 \mid {}^7F_5, J_z)$ since the phase factor $(-1)^{m+k}=-1$ is canceled by the negative sign of $\phi_{n,1}{}^0(5, -J_z)$. The crystal-field parameters $A_n{}^0\langle r^n\rangle$ and $A_6{}^6\langle r^6\rangle$ have the same values as those mentioned earlier.

The total crystal-field splitting matrix between the $^7F_5$ and $^7F_6$ levels is 24 by 24. By a simple interchange of rows and columns, we may reduce this matrix to six 4-by-4 matrices. When the six secular determinants are formed, we find two pairs of determinants that yield similar eigenvalues. This is because of eight doubly degenerate energy levels (four $\mu_{\pm 2}$ and four $\mu_{\pm 1}$ crystal-field sublevels of the $^7F_5$ and $^7F_6$). The remaining two 4-by-4 determinants give eight unique eigenvalues (four eigenvalues for μ_3 and four for μ_0).

The calculated eigenvalues as well as the observed energy-level scheme are given in Fig. 6. On the left we give the calculated crystal-field splitting in which the nearby J level is ignored. In the center we give the results of our present calculation, in which we consider the crystal-field components of one level interacting with those of the nearby level some 200 cm^{-1} away. In

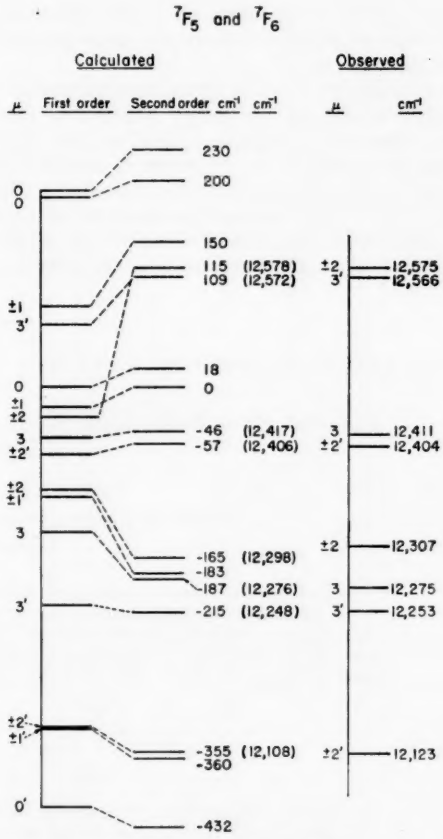

FIG. 6. The $^7F_5$ and $^7F_6$ levels. On the left (first-order perturbation), the theoretical splitting is given in which similar crystal-field components of the neighboring level are ignored. In the center (second-order perturbation), the effect of the crystal-field components of the neighboring level is taken into account. The field-free $J=5$ and 6 levels are assumed to be separated by several hundred wave numbers. These theoretical values may be compared directly with the observed energy-level scheme given on the right. Here μ' refers to the parent crystal-field components of the $^7F_6$ level, while μ refers to the parent components of the $^7F_5$ level.

[14] B. R. Judd, Proc. Roy. Soc. (London) **A227**, 552 (1955).

many cases the components are pushed either to the ultraviolet or infrared of their first-order position by as much as 80 cm^{-1}.

It is gratifying that four crystal-field parameters can correlate so well all the energy positions of the ^7F_J levels. However, it should be pointed out that $A_n^m\langle r^n\rangle$ is also the repository for errors due to neglect of configuration interaction and intermediate-coupling effects. Since these become increasingly important as we consider different J manifolds of higher energy, we should not expect the parameters to be quite the same for the ultraviolet groups as for the infrared group (^7F_J). However, intermediate field corrections to the reduced matrix elements, as well as reduced matrix elements between J and $J\pm1$ levels in the visible and ultraviolet, will provide suitable theoretical machinery for a crystal-field splitting analysis of the visible and ultraviolet spectrum of Am^{+3} in $LaCl_3$.

ACKNOWLEDGMENTS

It is a pleasure to acknowledge the helpful comments of Dr. B. R. Judd and J. G. Conway.

THE JOURNAL OF CHEMICAL PHYSICS VOLUME 35, NUMBER 6 DECEMBER, 1961

Electron Spin Resonance Study of Radiation Damage in Single Crystals of Urea Compounds

THADHO S. JASEJA AND ROY S. ANDERSON*

Department of Physics, University of Maryland, College Park, Maryland

(Received April 28, 1961)

Single crystals of urea compounds were examined by 3-cm electron spin resonance techniques after x and γ irradiation. All experiments were conducted at room temperature. No resonances were observed in urea and thiourea. This is interpreted to indicate that the lifetimes of any resulting unstable species must be less than 30 min. at room temperature. However, methylurea and ethylurea showed strong, highly stable spectra centered at $g\simeq2.00$. Analyses of these spectra suggest that the trapped radicals

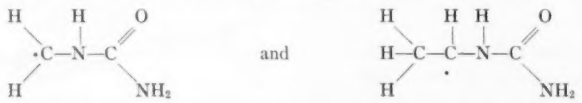

are formed from methylurea and ethylurea, respectively, by the loss of a hydrogen atom.

In both cases all radicals in the unit cell were considered to be magnetically equivalent. Calculated hyperfine intervals agree favorably with those observed. The spin density of the unpaired electron at the adjacent N—H group is believed less than 0.002, since the only apparent effect of this group was a broadening of the hyperfine lines.

In methylurea the $\cdot C—H_2$ group was found to have an H—C—H angle of 117°. The principal components of the diagonal electron-nuclear coupling dyadic were 10, 22, and 32 gauss. In ethylurea the $\cdot C—H$ bond was observed to lie along a crystallographic axis. The principal components were 10, 21, and 24 gauss. In this case the isotropic coupling constant was 18 gauss.

INTRODUCTION

THE electron spin resonance (ESR) method has been applied to the study of radiation damage in the biologically significant urea compounds. Since more specific information may be obtained from the ESR study of radiation damage to single crystals than to the polycrystalline form, single crystals of urea, thiourea, methylurea, and ethylurea were examined.

EXPERIMENTAL METHOD

Crystals, approximately 5 mm on a side, were grown from saturated aqueous solutions by slow evaporation. Ethylurea crystals were also grown from saturated acetone solution. The crystals were exposed to x-irradiation at 40 kv and 4 ma for 15 to 20 hr, at a distance of 5 cm from the target. γ irradiation from a Co^{60} source was also employed, the rate being 0.53 mega r/hr and the dose, 4.9×10^7r. All irradiations and observations were made at room temperature. The ESR spectrometer was a conventional reflection cavity-type instrument operated in the X-band region. The resonance magnetic fields of the spectral lines were determined with a proton magnetometer. All spectra were observed in the vicinity of $g\simeq2.00$. The crystals which were attached to a rotatable Teflon post with silicone grease, were placed in a cylindrical microwave cavity. The error in the measurement of the rotation about an axis perpendicular to the magnetic field did not exceed $\pm5°$.

* Present address: Department of Physics, Clark University, Worcester 10, Massachusetts.

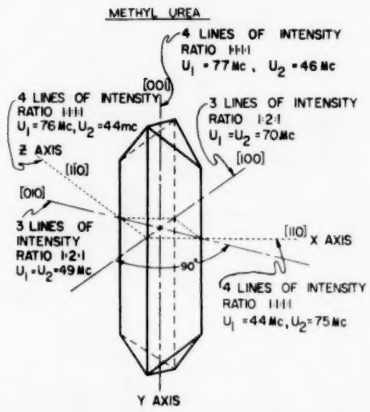
METHYL UREA
4 LINES OF INTENSITY RATIO 1:1:1:1
U_1 = 77 Mc, U_2 = 46 Mc
[001]
4 LINES OF INTENSITY RATIO 1:1:1:1
U_1 = 76 Mc, U_2 = 44 mc
3 LINES OF INTENSITY RATIO 1:2:1
$U_1 = U_2$ = 70 Mc
Z AXIS
[110]
[100]
[010]
3 LINES OF INTENSITY RATIO 1:2:1
$U_1 = U_2$ = 49 Mc
[110] X AXIS
90°
4 LINES OF INTENSITY RATIO 1:1:1:1
U_1 = 44 Mc, U_2 = 75 Mc
Y AXIS

FIG. 1. Diagram of the orthorhombic crystal of methylurea. The number, relative intensity, and splittings of hyperfine components are shown for the magnetic field along the axis indicated.

RESULTS

Urea and Thiourea

Exposure of single crystals of these materials to both x and γ rays resulted in no detectable radical species. Since the energy of the γ photon was more than sufficient to break bonds or produce ionization, it must be concluded that the lifetimes of any unstable species at room temperature must be less than 30 min (the time for transfer from the radiation source to the spectrometer). (Simultaneous x irradiation and ESR ob-

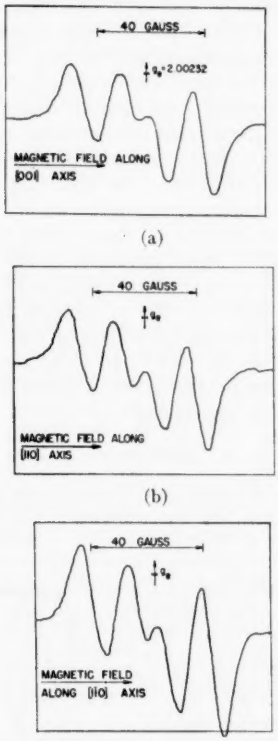

FIG. 2. Electron spin resonance spectra of an x-irradiated single crystal of methylurea, with the external magnetic field along the [001], [110], [1$\bar{1}$0] axes.

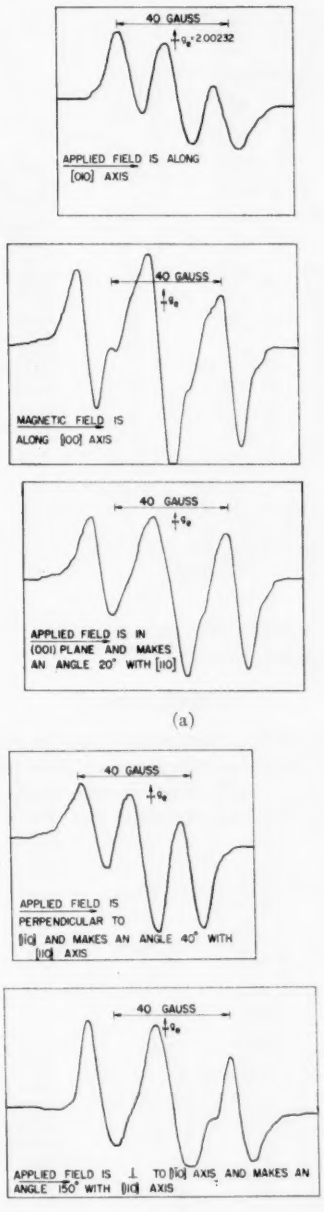
40 GAUSS
g_e = 2.00232
APPLIED FIELD IS ALONG [010] AXIS
40 GAUSS
MAGNETIC FIELD IS ALONG [100] AXIS
40 GAUSS
APPLIED FIELD IS IN (001) PLANE AND MAKES AN ANGLE 20° WITH [110]
(a)
40 GAUSS
APPLIED FIELD IS PERPENDICULAR TO [1$\bar{1}$0] AND MAKES AN ANGLE 40° WITH [110] AXIS
40 GAUSS
APPLIED FIELD IS ⊥ TO [1$\bar{1}$0] AXIS AND MAKES AN ANGLE 150° WITH [110] AXIS
(b)

FIG. 3. For rotation of the urea single crystal about the [001] axis, the observed spectral patterns were essentially orientation independent when the angle between the [110] axis and the applied magnetic field was 20° to 70° and 120° to 140°.

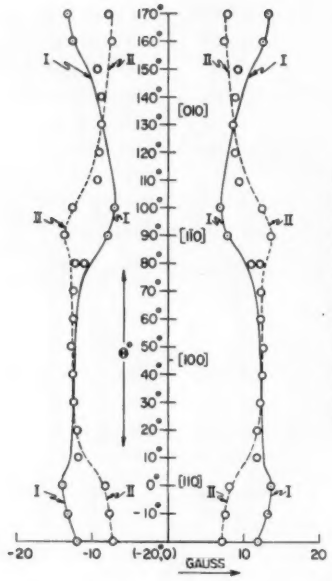

FIG. 4. Variation of the hyperfine splitting in an x irradiated single crystal of methylurea. The applied magnetic field was in the (001) plane and its angle was measured with reference to the [110] direction. The spectral variation is shown for the two pairs of hyperfine components.

servation experiments are now being arranged at various temperatures.)

Methylurea

This crystal is orthorhombic[1] and the unit cell contains four molecules. Observations were taken at 10° intervals about each of the three orthorhombic axes which were chosen as shown in Fig. 1. The angle between [110] and [1$\bar{1}$0] is 89°27′, but within the accuracy of the apparatus this was taken as 90°. With reference to Fig. 1, when the [001] and [1$\bar{1}$0] axes were oriented perpendicular to the magnetic field, the spectrum observed upon rotation about either of these axes consisted of four lines of equal intensity which for certain orientations coalesced into three lines of intensity ratio 1:2:1. Upon rotation about the [110] axis which was perpendicular to the magnetic field, there appeared a spectrum consisting of three main lines with generally unresolved structure (except when the magnetic field was parallel to the [001] or [1$\bar{1}$0] axes). With the magnetic field along the [001], [110], [1$\bar{1}$0] axes, the spectrum consisted of four lines of equal intensity as shown in Fig. 2. Rotation about the [001] axis, that is with the magnetic field in the (001) plane, produced 3 lines of intensity ratio 1:2:1 when the angle between the [110] axis and the magnetic field was 20° to 70° and 120° to 140°. Some of these spectra are shown in Fig. 3. With the magnetic field in the (001) and (1$\bar{1}$0) planes, the observed variations in the hyperfine splittings are plotted in Figs. 4 and 5, respectively.

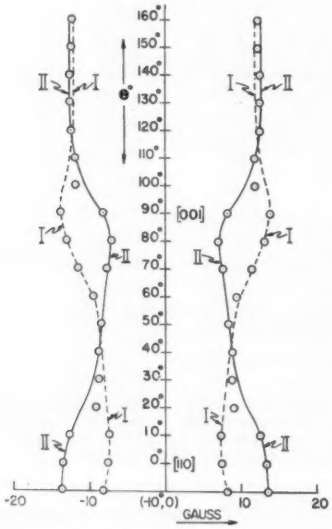

FIG. 5. Similar to Fig. 4, except that the applied magnetic field was in the (1$\bar{1}$0) plane.

[1] (a) P. Groth, *Chemische Krystallographie* (Verlag Von Wilhelm Engelmann, Leipzig, 1910), p. 550; (b) R. W. G. Wyckoff, *Crystal Structure* (Interscience Publishers, Inc., New York, 1960), Vol. IV.

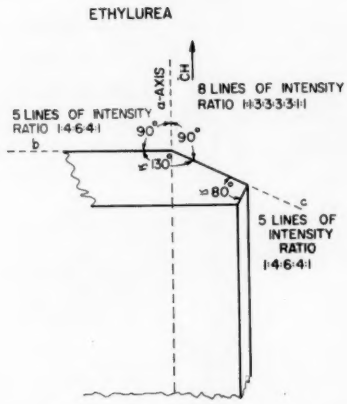

FIG. 6. Diagram of the monoclinic crystal of ethylurea. The number and relative intensities of the hyperfine structure components are shown for the magnetic field along the axes indicated.

Ethylurea

This crystal is monoclinic. Its structure is unknown. The assigned axis labeling is shown in Fig. 6. With the

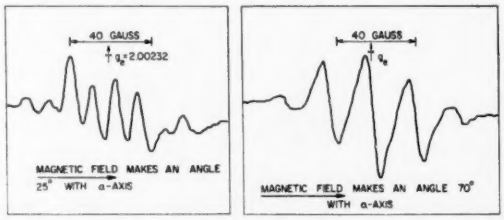

FIG. 7. Electron spin resonance spectra of an x irradiated single crystal of ethylurea. The magnetic field was in the *ac*-plane of Fig. 6.

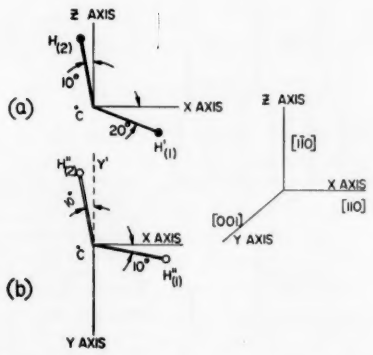

FIG. 8. Projections of the —$\dot{C}$—H_2 end group of the radical postulated in methylurea. (a) The xz-plane projection is that observed with the magnetic field in the (001) plane. (b) The xy-plane projection is that for the magnetic field in the (1$\bar{1}$0) plane.

magnetic field parallel to the a axis, the spectrum consisted of eight lines of intensity ratio 1:1:3:3:3:3:1:1. With the magnetic field in the bc plane, the spectrum always consisted of 5 lines of intensities 1:4:6:4:1, having 21 to 24 gauss hyperfine splittings. Typical spectra observed in ethylurea are shown in Fig. 7. These spectra were quite similar to those of alanine,[2] except that in the present case the lines were somewhat broader. In the case of both methylurea and ethylurea the same spectra were observed for x and γ irradiation. The spectra exhibited no aging effect in either compound.

ANALYSES OF THE SPECTRA

Methylurea

The number and relative intensities of the hyperfine structure lines observed in methylurea suggest that these lines result from the interaction of the unpaired electron with two protons, therefore the spectrum may arise from —$\dot{C}H_2$ or —$\dot{N}H_2$. The $\dot{N}H_2$ radical was excluded for the following reasons:

(1) According to Foner *et al.*[3] the spectrum at some orientations should consist of nine component lines. This kind of spectrum was not observed at any orientation. (2) In ethylurea the radical formed is not believed to be $\dot{N}H_2$, but rather the —$\dot{C}HCH_3$ group. (3) In urea and thiourea, where there was a possibility for the formation of the $\dot{N}H_2$ radical, no radicals were observed at room temperatures.

TABLE I. Direct cosines for the two protons in the —$\dot{C}H_2$ group in methylurea.

Proton	$\cos\alpha$	$\cos\beta$	$\cos\gamma$
1	+0.9298	±0.1628	±0.3301
2	−0.12369	±0.70143	±0.70143

TABLE II. Calculated and observed hyperfine splittings along the crystallographic axes of an x irradiated single crystal of methylurea.

Axis	Hyperfine splitting for one proton of —$\dot{C}H_2$ (in gauss) Obs. ±2 gauss	Calc.	Hyperfine splitting for the second proton of —$\dot{C}H_2$ (in gauss) Obs. ±2 gauss	Calc.
[110]	16, 15	15	28, 27	32
[100]	25	30	25	28
[1$\bar{1}$0]	27	31	16	17
[010]	18	18	18	23
[001]	27	24	16	17

Analysis of the methylurea spectra is therefore based on two assumptions. (1) The radicals from which the spectra arise have the formula

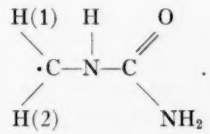

The protons responsible for the hyperfine splitting are numbered 1 and 2. (2) All four possible radicals in the unit cell are assumed to be magnetically equivalent in the planes (001) and (1$\bar{1}$0), thus only one radical need be considered in analyzing the spectra.

With the magnetic field in the (001) plane, that is for rotation of the crystal about the [001] axis, the

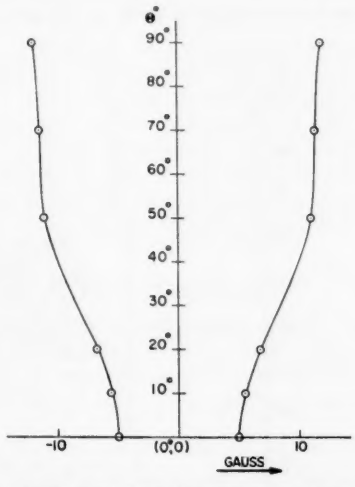

FIG. 9. Hyperfine splittings observed in an x irradiated single crystal of ethylurea. The applied magnetic field was in the ab-plane of Fig. 6 and at the angle indicated with reference to the a axis.

[2] I. Miyagawa and W. Gordy, J. Chem. Phys. **32,** 255 (1960).
[3] S. N. Foner, E. L. Cochran, V. A. Bowers, and C. K. Jen, Phys. Rev. Letters **1,** 91 (1958).

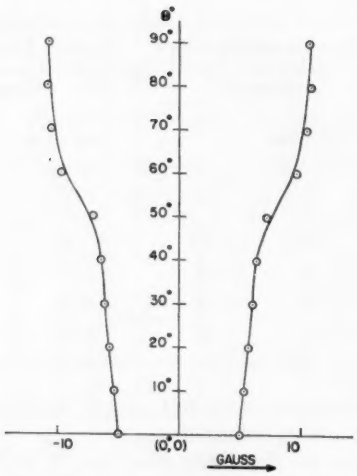

FIG. 10. Similar to Fig. 9 except the applied magnetic field was in the *ac* plane and the angle was measured to the *a* axis.

hyperfine splittings for protons 1 and 2 were observed to vary. The splittings are plotted in Fig. 4. The behavior of the splittings suggests that the projection of the $-\dot{C}H_2$ group in the (001) plane is that in Fig. 8(a). The angle H′(1)—C—H′(2) in the projection of the $-\dot{C}H_2$ group in the (001) plane is about 120° as shown. With the magnetic field in the (1$\bar{1}$0) plane, the hyperfine splittings resulting from these two protons showed the similar behavior which is plotted in Fig. 5. The projection of the $-\dot{C}H_2$ group on the (1$\bar{1}$0) plane is believed that shown in Fig. 8(b). In this case the angle H″(1)—C—H″(2) is 110°.

When the magnetic field is in the (110) plane the spectra are not as simple as those in the previous two

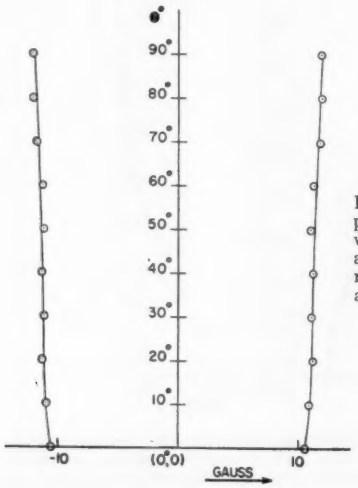

FIG. 11. Similar to Fig. 9 except the applied magnetic field was in the *bc* plane and the angle was measured to the *b* axis.

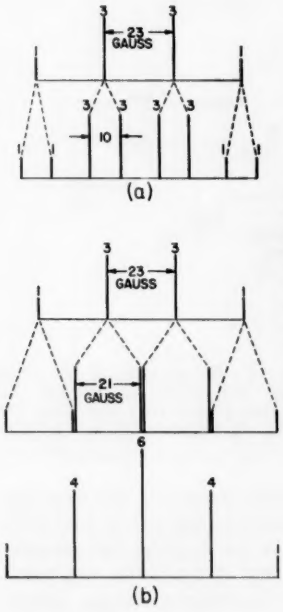

FIG. 12. Analysis of the radical spectra observed in ethylurea. Each component of the 1:3:3:1 methyl quartet is split into a doublet by the magnetic interaction between the unpaired electron and the —$\dot{C}$H— proton. (a) Spectrum observed with the magnetic field in the *ac* plane. (b) Spectrum observed with the magnetic field along the *b* axis.

cases, except where the magnetic field is parallel to either the [001] or [1$\bar{1}$0] axes. In general the spectra observed in this plane consist of three lines, when neglecting additional structure weak in comparison to the main three lines. This weak structure may indicate either the presence of other slightly magnetically nonequivalent radicals in this plane or anisotropic coupling with the NH group. From Figs. 8 (a) and (b) the direction cosines of protons H(1) and H(2) may be determined. In this instance, the [110] axis is considered to be the *x* axis; the [001] axis, the *y* axis; and the [1$\bar{1}$0] axis, the *z* axis. The origin of these three orthorhombic axes is taken to be coincident with the carbon atom of the $-\dot{C}H_2$ group. The resulting direction cosines are given in Table I. From these direction cosines the angle H(1)—C—H(2) in the $-\dot{C}H_2$ group is calculated to be 117°. (The corresponding angle for ethylene protons in the gas phase lies in the range 110° to 122°.[4])

Spectral interpretation may be made on the basis

TABLE III. The principal components of the hyperfine coupling constant for the CH group in x irradiated ethylurea.

Principal component	Obs. ±2 gauss	Calc. (gauss)
A	10	9
B	21	18
C	24	28

[4] C. H. Townes and A. L. Schawlow, *Microwave Spectroscopy* (McGraw-Hill Book Company, Inc., New York, 1955).

of the theory of McConnell *et al.*[5,6] The electron-nuclear hyperfine interaction Hamiltonian is given by[5]

$$\mathcal{H}=h[AS_xI_x+BS_yI_y+CS_zI_z], \quad (1)$$

which is in the form of a dyadic tensor. Here $A=A_d+a_f$, $B=B_d+a_f$, and $C=C_d+a_f$, where a_f is the isotropic coupling constant and A_d, B_d, and C_d are the principal components of the dipolar interaction, and are related by the equation $A_d+B_d+C_d=0$.[6]

Considering the unpaired electron to interact only with protons (1) and (2), the hyperfine splittings along the crystallographic axes were calculated. In making these calculations, the values obtained by McConnell *et al.*[5] for the ĊH group, that is, $A=10$, $B=22$, and $C=32$ gauss, were used. The results of these calculations are presented in Table II and compared with the observed hyperfine splittings. The value $a_f=21$ gauss resulted from the calculations.

Ethylurea

The radical formed in ethylurea is believed to have the formula

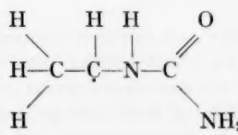

On Fig. 6 are indicates the axes and the corresponding spectral characteristics. Typical spectra are shown in Fig. 7. In Figs. 9–11 are plotted the hyperfine splittings observed for the magnetic field in the three planes defined in Fig. 6.

In this radical the couplings of the three methyl protons are considered to be equivalent and isotropic. The methyl protons produce a symmetric quartet having a coupling constant of 23 gauss, upon which are superimposed the Fermi contact and dipolar interactions from the —ĊH— group. This 23 gauss splitting constant for methyl protons agrees with that reported by Jen *et al.*[7]

The basis of this analysis is shown in Fig. 12. Assuming the existence of a single magnetically equivalent radical in the unit cell, the principal components of the diagonal electron-nuclear coupling dyadic for the C—H group σ proton appeared to be $|A|=10\pm2$ gauss, $|B|=21\pm2$ gauss, and $|C|=24\pm2$ gauss. Assuming these values to have the same sign,[5] the isotropic coupling constant $|a_f|$ was determined to be 18.3 ± 2 gauss. The behavior of the spectrum upon rotation of the crystal indicates that the ·C—H bond lies along the a axis. McConnell *et al.*[5] observed 10 gauss splitting along the direction of the ·C—H bond in the radical

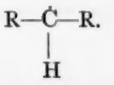

Since the component line width was of the order of 10 gauss, it was not possible to determine the possibility of additional radicals in the unit cell.

The value of a_f can be justified. In the formula[8]

$$a_f=\rho_c Q, \quad (2)$$

ρ_c is the spin density on the C—H carbon and Q is a proportionality constant having the value 22.5 gauss or 63 Mc. ρ_c was taken as unity for the Ċ—H group of the radical in malonic acid.[5] In the present case ρ_c must be reduced because of the additional coupling of the electron with the methyl group. The observed 23 gauss or 64 Mc coupling of the electron with the methyl protons indicates a spin density at each proton of 64 Mc/1420 Mc=0.045, where 1420 Mc is the isotropic splitting in atomic hydrogen.[9] Since three protons are involved, the total spin density on the methyl group is 0.135. The spin density on the C—H carbon must be reduced by this amount to $\rho_c=0.865$. Substitution of this value of ρ_c in Eq. (2) results in $a_f=52$ Mc or 18.2 gauss. Appling the factor 0.865 to the values of McConnell *et al.*[5] for the principal components of the Ċ—H group σ proton results in $A=8.7$, $B=18.2$, and $C=27.7$ gauss. These values are compared in Table III with those observed in ethylurea.

In summary, the results for ethylurea indicate that all radicals in the unit cell are magnetically equivalent and that the C—H bond lies along one of the crystallographic axes.

LINE WIDTH

The broadening of the component lines observed in methylurea and ethylurea is believed to arise from magnetic interactions of the unpaired electron with the proton and the nitrogen nucleus in the adjacent NH group. Similar broadening in a γ irradiated single crystal of *n*-acetyl glycine has been attributed to the proximity of the NH group to the unpaired electron.[10] The spin density on the NH group is therefore believed less than 0.002.

ACKNOWLEDGMENT

It is a pleasure to acknowledge helpful discussions with Dr. M. Fujimoto and Dr. R. P. Kohin and the assistance of Mr. Daniel W. Brown of the National Bureau of Standards in performing the γ irradiations.

[5] H. M. McConnell, C. Heller, T. Cole, and R. W. Fessenden, J. Am. Chem. Soc. **82,** 766 (1960).
[6] H. M. McConnell and J. Strathdee, Mol. Phys. **2,** 129 (1959).
[7] C. K. Jen, S. N. Foner, E. L. Cochran, and V. A. Bowers, Phys. Rev. **112,** 1169 (1958).
[8] H. M. McConnell and D. B. Chesnut, J. Chem. Phys. **27,** 984 (1957); **28,** 107 (1958).
[9] A. G. Prodell and P. Kusch, Phys. Rev. **79,** 1009 (1950); **88,** 184 (1952); P. Kusch, *ibid.* **100,** 1188 (1955).
[10] I. Miyagawa, Y. Kurita, and W. Gordy, J. Chem. Phys. **33,** 1599 (1960).

Thermodynamic Functions of Several Triatomic Molecules in the Ideal Gas State

BONNIE J. MCBRIDE AND SANFORD GORDON
National Aeronautics and Space Administration, Lewis Research Center, Cleveland, Ohio

(Received April 27, 1961)

Recent spectroscopic data were used in calculating the thermodynamic functions of $CO_2(g)$, $COS(g)$, $CS_2(g)$, $ClCN(g)$, $HCN(g)$, $H_2O(g)$, $H_2S(g)$, $N_2O(g)$, $NO_2(g)$, and $SO_2(g)$ in the ideal gas state from 100° to 6000°K. For each molecule, corrections were made to the rigid-rotator harmonic-oscillator approximation for anharmonicity and when sufficient data were available, additional corrections were made for vibration-rotation interaction, rotational stretching, and Fermi resonance.

INTRODUCTION

MOST calculations of ideal gas thermodynamic functions for polyatomic molecules are calculated assuming rigid rotation and harmonic oscillation. This is due primarily to the fact that spectroscopic investigations are seldom detailed enough to yield the anharmonic, vibration-rotation interaction, and rotational stretching constants that are used in more accurate calculations. Secondly, these calculations are considerably more complicated when these refinements are included.

Ten triatomic molecules are considered in this report for which most of these detailed spectroscopic data are available. For three of these molecules, COS, CS_2, and ClCN, only rigid-rotator harmonic-oscillator calculations have heretofore been available. While more refined calculations have been made for the remaining molecules CO_2,[1] HCN,[2] H_2O,[3] H_2S,[4] N_2O,[5] NO_2,[6] and SO_2,[7] their spectroscopic constants have since been revised. The methods used in these references to represent the partition function include first- and second-order correction terms to the rigid-rotator harmonic-oscillator approximation for CO_2, and various modifications of first-order correction terms for the other molecules. Thermodynamic functions for the ten molecules considered here have therefore been recalculated; first, in order to incorporate recently determined spectroscopic constants, and second, in order to include second-order correction terms where applicable.

CALCULATIONS

The equation used for the partition function for internal energy was taken from reference 8:

$$Q=Q_R Q_{RC} Q_{HO} Q_C \qquad (1)$$

The detailed expressions used for the individual factors in (1) are exactly those in reference 8. The quantities Q_R and Q_{HO} are the usual rigid-rotator and harmonic-oscillator partition functions, respectively; Q_{RC} contains rotational correction factors for stretching and low-temperature quantum effects; and Q_C contains corrections for anharmonicity, vibration-rotation interaction, and azimuthal quantum effects. This latter correction factor may be expressed in the form

$$\ln Q_C=C_0(T)+C_1(T)/T+C_2(T)/T^2+\cdots, \qquad (2)$$

where C_0, C_1, and C_2 are functions containing a number of terms. The C_0 terms involve rotation-vibrational constants to the first and second power; the C_1/T terms involve azimuthal and first- and second-order anharmonic constants to the first power, and cross products between first-power rotational-vibrational interaction and anharmonic and azimuthal constants; and the C_2/T^2 terms involve first-order anharmonic and azimuthal constants to the second power including cross products, cross products between first- and second-order anharmonic constants, and cross products between first-power rotational-vibrational interaction and second-power anharmonic constants.

At high temperatures, each of the correction terms found in the C_0, C_1/T, and C_2/T^2 functions, and therefore their contribution to $-(F^0-H_0^0)/RT$, $(H^0-H_0^0)/RT$, and C_p^0/R, vary in principal dependence as T, T^2, or higher than T^2. Thus, no matter how small the contribution of these terms may be at relatively low temperatures, at high temperatures they can cause a reversal from decreasing first derivatives of the thermodynamic functions with temperature to increasing first derivatives with temperature. This inflection point will generally occur at lower temperatures for those species with one or more relatively low fundamental frequencies than for those species with only relatively high frequencies.

The total contribution of the terms in (C_0+C_1/T) and C_2/T^2 to C_p^0/R and $-(F^0-H_0^0)/RT$ are given in Tables I and II. At the high temperatures the total contributions of (C_0+C_1/T) and C_2/T^2 to the functions vary as T and T^2, respectively. The relatively large contribution of C_2/T^2 at the higher temperatures causes an inflection to occur in the specific heat func-

[1] H. W. Woolley, J. Research Natl. Bur. Standards **52,** 289 (1954).
[2] Bradley, Haar, and Friedman, J. Research Natl. Bur. Standards **56,** 197 (1956).
[3] A. S. Friedman and L. Haar, J. Chem. Phys. **22,** 2051 (1954).
[4] Haar, Bradley, and Friedman, J. Research Natl. Bur. Standards **55,** 285 (1955).
[5] R. E. Pennington and K. A. Kobe, J. Chem. Phys. **22,** 1442 (1954).
[6] Unpublished NBS data compiled by Harold W. Woolley (1950).
[7] W. H. Evans and D. D. Wagman, J. Research Natl. Bur. Standards **49,** 141 (1952).
[8] H. W. Woolley, J. Research Natl. Bur. Standards **56,** 105 (1956).

TABLE I. Contribution of correction terms in ln Q_C to C_p^0/R.

Molecule	Correction terms	Temperature, °K 298.15	1000	2000	3000	4000	5000	6000
CO_2	C_0+C_1/T	−0.0038	0.0149	0.0599	0.0965	0.1289	0.1587	0.1864
	C_2/T^2	0.0000	0.0007	0.0049	0.0118	0.0209	0.0315	0.0431
COS	C_0+C_1/T	−0.0086	0.0552	0.1414	0.2183	0.2928	0.3663	0.4392
	C_2/T^2	0.0004	0.0089	0.0418	0.0991	0.1810	0.2878	0.4197
CS_2	C_0+C_1/T	0.0149	0.0753	0.1628	0.2428	0.3190	0.3919	0.4617
	C_2/T^2	0.0017	0.0270	0.1143	0.2598	0.4616	0.7179	1.0267
ClCN	C_0+C_1/T	−0.0198	−0.0300	−0.0279	−0.0337	−0.0419	−0.0509	−0.0604
	C_2/T^2	0.0012	0.0227	0.0965	0.2211	0.3965	0.6228	0.8999
HCN	C_0+C_1/T	−0.0108	0.0200	0.0954	0.1648	0.2271	0.2852	0.3403
	C_2/T^2	0.0001	0.0022	0.0146	0.0381	0.0719	0.1152	0.1676
H_2O	C_0+C_1/T	−0.0013	−0.0170	0.0385	0.1076	0.1731	0.2370	0.3015
	C_2/T^2	0.0000	0.0008	0.0086	0.0276	0.0580	0.1004	0.1553
H_2S	C_0+C_1/T	−0.0025	0.0135	0.1018	0.1838	0.2600	0.3343	0.4085
	C_2/T^2	0.0000	0.0010	0.0113	0.0331	0.0659	0.1096	0.1643
N_2O	C_0+C_1/T	−0.0036	0.0325	0.1082	0.1742	0.2371	0.2992	0.3611
	C_2/T^2	0.0000	0.0018	0.0123	0.0318	0.0604	0.0984	0.1460
NO_2	C_0+C_1/T	0.0004	0.0473	0.1305	0.2046	0.2760	0.3466	0.4167
	C_2/T^2	0.0000	0.0027	0.0181	0.0462	0.0870	0.1405	0.2066
SO_2	C_0+C_1/T	0.0051	0.0618	0.1402	0.2139	0.2864	0.3586	0.4307
	C_2/T^2	0.0001	0.0047	0.0233	0.0559	0.1025	0.1629	0.2373

tions of COS, CS_2, ClCN, NO_2, and SO_2. For this reason C_2/T^2 was omitted from lnQ_C and its derivatives for these five molecules. For the remaining five molecules, CO_2, HCN, H_2O, H_2S, and N_2O, an inflection did not occur for any of the thermodynamic functions at the higher temperatures considered here, and the C_2/T^2 terms were retained.

First-order corrections for the effect of Fermi

TABLE II. Contribution of correction terms in ln Q_C to $-(F^0-H_0^0)/RT$.

Molecule	Correction terms	Temperature, °K 298.15	1000	2000	3000	4000	5000	6000
CO_2	C_0+C_1/T	−0.0006	−0.0027	0.0034	0.0151	0.0290	0.0437	0.0589
	C_2/T^2	0.0000	0.0000	0.0005	0.0014	0.0028	0.0048	0.0071
COS	C_0+C_1/T	−0.0032	−0.0044	0.0180	0.0487	0.0822	0.1170	0.1524
	C_2/T^2	0.0000	0.0010	0.0055	0.0140	0.0265	0.0431	0.0637
CS_2	C_0+C_1/T	0.0041	0.0233	0.0589	0.0978	0.1374	0.1772	0.2167
	C_2/T^2	0.0001	0.0036	0.0171	0.0407	0.0741	0.1172	0.1698
ClCN	C_0+C_1/T	−0.0022	−0.0206	−0.0375	−0.0480	−0.0561	−0.0631	−0.0695
	C_2/T^2	0.0001	0.0028	0.0141	0.0340	0.0623	0.0992	0.1445
HCN	C_0+C_1/T	−0.0018	−0.0079	0.0001	0.0181	0.0407	0.0656	0.0917
	C_2/T^2	0.0000	0.0003	0.0015	0.0044	0.0090	0.0153	0.0234
H_2O	C_0+C_1/T	−0.0000	−0.0046	−0.0102	−0.0063	0.0045	0.0195	0.0375
	C_2/T^2	0.0000	0.0000	0.0005	0.0022	0.0053	0.0101	0.0166
H_2S	C_0+C_1/T	−0.0001	−0.0026	0.0042	0.0228	0.0473	0.0749	0.1045
	C_2/T^2	0.0000	0.0000	0.0007	0.0029	0.0067	0.0123	0.0197
N_2O	C_0+C_1/T	−0.0007	−0.0015	0.0123	0.0345	0.0601	0.0873	0.1154
	C_2/T^2	0.0000	0.0001	0.0011	0.0035	0.0074	0.0127	0.0195
NO_2	C_0+C_1/T	0.0000	0.0040	0.0247	0.0531	0.0843	0.1168	0.1500
	C_2/T^2	0.0000	0.0001	0.0016	0.0051	0.0107	0.0185	0.0283
SO_2	C_0+C_1/T	0.0002	0.0103	0.0382	0.0707	0.1048	0.1395	0.1747
	C_2/T^2	0.0000	0.0004	0.0028	0.0075	0.0145	0.0238	0.0355

TABLE III. Spectroscopic data used in the calculations.

	Units	CO_2	COS	CS_2	ClCN	HCN	H_2O	H_2S	N_2O	NO_2	SO_2
ν_1	cm^{-1}	1341.54	859	667.04	733.4	2096.61	3656.65	2614.56	1276.90	1320.6	1151.74
ν_2	cm^{-1}	667.40	524	395.93	379.9	711.90	1594.78	1182.68	588.78	749.6	517.69
ν_3	cm^{-1}	2349.16	2064	1535.58	2219	3311.40	3755.79	2627.48	2223.75	1617.0	1361.76
x_{11}	cm^{-1}	−3.75	−4.0	−0.98	−5[a]	−10.45	−45.18	−25.09	−5.21	−9.0	−3.99
x_{12}	cm^{-1}	3.62	−6.8	7.56	−4[a]	−2.90	−15.14	−19.69	0.52	−9.7	−2.05
x_{13}	cm^{-1}	−19.37	−4.5	−8.04	−2.0	−14.43	−165.48	−94.68	−27.26	−28.7	−13.71
x_{22}	cm^{-1}	−0.63	−0.4	−1.56	2.1	−2.50	−17.04	−5.72	−0.17	−0.5	−3.00
x_{23}	cm^{-1}	−12.53	−11.5	−6.45	−11.0	−19.19	−19.99	−21.09	−14.22	−2.7	−3.90
x_{33}	cm^{-1}	−12.63	−7.0	−6.66	−17[a]	−52.50	−44.62	−24.00	−15.10	−16.4	−5.17
y_{111}	cm^{-1}	0.13					0.47				
y_{112}	cm^{-1}	−0.08					−0.10				
y_{113}	cm^{-1}	0					0.68				
y_{122}	cm^{-1}	−0.07					−0.10				
y_{123}	cm^{-1}	0.02					−1.72				
y_{133}	cm^{-1}	0.07					1.17				
y_{222}	cm^{-1}	0.01					−0.60				
y_{223}	cm^{-1}	0					1.55				
y_{233}	cm^{-1}	0.01					−0.81				
y_{333}	cm^{-1}	0.015					−0.45				
g_{22}	cm^{-1}	0.775	3.2	−2.16	−0.1	3.63			0.52		
$\lvert W_0 \rvert$	cm^{-1}	51.31		34.4	31.4				29.9		
A_e	cm^{-1}						27.379	10.351[b]		8.003[c]	2.027359[e]
B_e	cm^{-1}	0.391625	0.203724	0.109277	0.199165[d]	1.4849	14.5844	9.023[b]	0.421181	0.434[c]	0.3441741[e]
C_e	cm^{-1}						9.5256	4.825[b]		0.412[c]	0.2935345[e]
α_1^A	$cm^{-1}\times10^3$						750	125[b]			
α_2^A	$cm^{-1}\times10^3$						−2941	−346[b]			
α_3^A	$cm^{-1}\times10^3$						1253	173[b]			
α_1^B	$cm^{-1}\times10^3$	1.26	0.6044	0.156		9.50	238	159[b]	1.99		
α_2^B	$cm^{-1}\times10^3$	−0.76	−0.3532	−0.256		−3.5	−160	−219[b]	−0.56		
α_3^B	$cm^{-1}\times10^3$	3.0875	1.838	0.711		10.79	78	124[b]	3.45		
α_1^C	$cm^{-1}\times10^3$						201.8	69[b]			
α_2^C	$cm^{-1}\times10^3$						139.2	62[b]			
α_3^C	$cm^{-1}\times10^3$						144.5	55[b]			
D_{000}	$cm^{-1}\times10^8$	13.5	4.24	1.05	5.547	285			18		
ρ	$(°K)^{-1}\times10^5$						2.13[e]	1.7[f]			
Statistical weight		1	1	1	1	1	1	1	1	2	1
Symmetry number		2	1	2	1	1	2	2	1	2	2
References		12	13, 14, 15	16, 17	18, 19	20, 21	22, 23	24	25, 26, 27	28	29, 30

[a] Estimated.
[b] Derived from moments of inertia given in reference 24.
[c] A_{000}, B_{000}, C_{000}.
[d] B_{000}.
[e] Value taken from reference 3.
[f] Value taken from reference 4.

TABLE IV. Thermodynamic functions of CO_2 (g) in the ideal gas state.

T, °K	C_p°/R	$(H^\circ-H_0^\circ)/RT$	S°/R	$-(F^\circ-H_0^\circ)/RT$
100	3.5126	3.4995	21.5154	18.0159
200	3.8907	3.5792	24.0367	20.4574
273.15	4.3235	3.7207	25.3134	21.5928
298.15	4.4647	3.7772	25.6982	21.9210
300	4.4748	3.7814	25.7259	21.9444
400	4.9691	4.0189	27.0835	23.0646
500	5.3660	4.2500	28.2365	23.9865
600	5.6908	4.4639	29.2445	24.7806
700	5.9604	4.6590	30.1426	25.4836
800	6.1856	4.8362	30.9537	26.1175
900	6.3739	4.9969	31.6934	26.6965
1000	6.5316	5.1427	32.3734	27.2307
1100	6.6642	5.2752	33.0023	27.7271
1200	6.7760	5.3957	33.5871	28.1914
1300	6.8709	5.5056	34.1333	28.6277
1400	6.9519	5.6061	34.6456	29.0394
1500	7.0215	5.6982	35.1276	29.4294
1600	7.0816	5.7829	35.5828	29.7999
1700	7.1340	5.8608	36.0137	30.1529
1800	7.1799	5.9329	36.4228	30.4899
1900	7.2205	5.9996	36.8121	30.8125
2000	7.2564	6.0615	37.1834	31.1218
2200	7.3175	6.1730	37.8780	31.7049
2400	7.3673	6.2706	38.5169	32.2463
2600	7.4089	6.3566	39.1083	32.7517
2800	7.4443	6.4330	39.6586	33.2256
3000	7.4749	6.5015	40.1733	33.6718
3200	7.5019	6.5632	40.6566	34.0934
3400	7.5259	6.6191	41.1121	34.4930
3600	7.5477	6.6701	41.5429	34.8728
3800	7.5675	6.7168	41.9516	35.2347
4000	7.5859	6.7598	42.3402	35.5804
4200	7.6030	6.7996	42.7107	35.9111
4400	7.6190	6.8365	43.0648	36.2283
4600	7.6342	6.8708	43.4038	36.5330
4800	7.6486	6.9029	43.7290	36.8261
5000	7.6624	6.9330	44.0415	37.1085
5200	7.6756	6.9613	44.3423	37.3810
5400	7.6883	6.9880	44.6322	37.6442
5600	7.7006	7.0133	44.9121	37.8988
5800	7.7125	7.0372	45.1825	38.1453
6000	7.7241	7.0599	45.4442	38.3843

TABLE V. Thermodynamic functions of COS (g) in the ideal gas state.

T, °K	C_p°/R	$(H^\circ-H_0^\circ)/RT$	S°/R	$-(F^\circ-H_0^\circ)/RT$
100	3.5612	3.5072	23.3373	19.8301
200	4.2648	3.6900	25.9932	22.3032
273.15	4.8267	3.9218	27.4086	23.4868
298.15	4.9896	4.0046	27.8384	23.8339
300	5.0010	4.0107	27.8693	23.8587
400	5.5136	4.3263	29.3828	25.0565
500	5.8803	4.6022	30.6545	26.0523
600	6.1626	4.8397	31.7526	26.9129
700	6.3892	5.0454	32.7202	27.6748
800	6.5740	5.2253	33.5858	28.3605
900	6.7260	5.3839	34.3692	28.9853
1000	6.8518	5.5246	35.0845	29.5600
1100	6.9565	5.6501	35.7426	30.0925
1200	7.0445	5.7628	36.3518	30.5890
1300	7.1190	5.8643	36.9187	31.0544
1400	7.1827	5.9563	37.4487	31.4924
1500	7.2376	6.0399	37.9461	31.9062
1600	7.2853	6.1163	38.4148	32.2985
1700	7.3273	6.1863	38.8578	32.6715
1800	7.3645	6.2507	39.2777	33.0269
1900	7.3977	6.3103	39.6767	33.3665
2000	7.4275	6.3654	40.0570	33.6916
2200	7.4794	6.4644	40.7674	34.3030
2400	7.5232	6.5508	41.4201	34.8693
2600	7.5611	6.6271	42.0238	35.3967
2800	7.5946	6.6950	42.5854	35.8903
3000	7.6247	6.7560	43.1104	36.3544
3200	7.6523	6.8112	43.6034	36.7922
3400	7.6778	6.8614	44.0681	37.2066
3600	7.7017	6.9075	44.5076	37.6002
3800	7.7243	6.9499	44.9246	37.9748
4000	7.7458	6.9891	45.3214	38.3323
4200	7.7665	7.0256	45.6998	38.6742
4400	7.7864	7.0598	46.0616	39.0018
4600	7.8057	7.0918	46.4081	39.3163
4800	7.8246	7.1219	46.7407	39.6188
5000	7.8429	7.1504	47.0605	39.9101
5200	7.8609	7.1774	47.3685	40.1911
5400	7.8786	7.2030	47.6655	40.4624
5600	7.8960	7.2275	47.9523	40.7248
5800	7.9132	7.2508	48.2297	40.9789
6000	7.9301	7.2732	48.4983	41.2251

TABLE VI. Thermodynamic functions of CS_2 (g) in the ideal gas state.

T, °K	C_p°/R	$(H^\circ-H_0^\circ)/RT$	S°/R	$-(F^\circ-H_0^\circ)/RT$
100	3.7254	3.5585	23.6564	20.1179
200	4.7603	3.8913	26.5559	22.6647
273.15	5.3317	4.2051	28.1296	23.9244
298.15	5.4848	4.3061	28.6032	24.2971
300	5.4955	4.3134	28.6372	24.3237
400	5.9696	4.6719	30.2873	25.6154
500	6.3103	4.9672	31.6578	26.6907
600	6.5670	5.2134	32.8321	27.6187
700	6.7638	5.4214	33.8598	28.4384
800	6.9165	5.5992	34.7734	29.1742
900	7.0364	5.7525	35.5953	29.8428
1000	7.1322	5.8858	36.3418	30.4559
1100	7.2098	6.0028	37.0253	31.0225
1200	7.2738	6.1061	37.6555	31.5493
1300	7.3273	6.1980	38.2398	32.0418
1400	7.3728	6.2804	38.7846	32.5042
1500	7.4120	6.3545	39.2946	32.9401
1600	7.4463	6.4217	39.7741	33.3524
1700	7.4765	6.4829	40.2264	33.7435
1800	7.5036	6.5389	40.6546	34.1157
1900	7.5280	6.5903	41.0609	34.4706
2000	7.5502	6.6377	41.4476	34.8099
2200	7.5896	6.7225	42.1691	35.4466
2400	7.6239	6.7963	42.8310	36.0348
2600	7.6545	6.8611	43.4425	36.5814
2800	7.6823	6.9188	44.0108	37.0920
3000	7.7080	6.9706	44.5417	37.5711
3200	7.7321	7.0174	45.0399	38.0225
3400	7.7548	7.0601	45.5094	38.4493
3600	7.7765	7.0993	45.9533	38.8539
3800	7.7973	7.1355	46.3743	39.2388
4000	7.8174	7.1691	46.7747	39.6056
4200	7.8369	7.2005	47.1566	39.9562
4400	7.8558	7.2298	47.5216	40.2918
4600	7.8743	7.2574	47.8712	40.6138
4800	7.8924	7.2835	48.2068	40.9232
5000	7.9101	7.3082	48.5293	41.2211
5200	7.9275	7.3317	48.8399	41.5082
5400	7.9445	7.3541	49.1394	41.7853
5600	7.9614	7.3755	49.4286	42.0531
5800	7.9779	7.3960	49.7083	42.3123
6000	7.9943	7.4156	49.9790	42.5634

TABLE VII. Thermodynamic functions of ClCN (g) in the ideal gas state.

T, °K	C_p°/R	$(H^\circ-H_0^\circ)/RT$	S°/R	$-(F^\circ-H_0^\circ)/RT$
100	3.7574	3.5458	23.4362	19.8904
200	4.7476	3.9053	26.3520	22.4467
273.15	5.2614	4.2042	27.9131	23.7089
298.15	5.3948	4.2986	28.3797	24.0812
300	5.4039	4.3054	28.4131	24.1078
400	5.7927	4.6324	30.0254	25.3930
500	6.0553	4.8921	31.3477	26.4556
600	6.2592	5.1035	32.4704	27.3669
700	6.4289	5.2811	33.4483	28.1673
800	6.5728	5.4338	34.3164	28.8827
900	6.6949	5.5673	35.0979	29.5305
1000	6.7982	5.6854	35.8087	30.1234
1100	6.8854	5.7906	36.4609	30.6703
1200	6.9591	5.8850	37.0632	31.1782
1300	7.0216	5.9701	37.6228	31.6527
1400	7.0747	6.0471	38.1451	32.0980
1500	7.1200	6.1172	38.6348	32.5176
1600	7.1589	6.1811	39.0956	32.9145
1700	7.1924	6.2396	39.5307	33.2910
1800	7.2214	6.2934	39.9426	33.6492
1900	7.2467	6.3429	40.3337	33.9908
2000	7.2689	6.3887	40.7060	34.3173
2200	7.3055	6.4704	41.4006	34.9302
2400	7.3342	6.5413	42.0375	35.4963
2600	7.3572	6.6032	42.6255	36.0224
2800	7.3758	6.6577	43.1715	36.5137
3000	7.3910	6.7061	43.6809	36.9748
3200	7.4037	6.7493	44.1583	37.4090
3400	7.4143	6.7881	44.6075	37.8193
3600	7.4232	6.8232	45.0315	38.2083
3800	7.4309	6.8550	45.4331	38.5781
4000	7.4375	6.8839	45.8144	38.9305
4200	7.4431	6.9104	46.1774	39.2670
4400	7.4481	6.9348	46.5238	39.5890
4600	7.4524	6.9572	46.8550	39.8978
4800	7.4563	6.9779	47.1722	40.1943
5000	7.4596	6.9971	47.4767	40.4796
5200	7.4626	7.0149	47.7693	40.7544
5400	7.4653	7.0316	48.0510	41.0194
5600	7.4678	7.0471	48.3226	41.2754
5800	7.4699	7.0617	48.5847	41.5230
6000	7.4719	7.5084	44.2710	41.7626

TABLE VIII. Thermodynamic functions of HCN (g) in the ideal gas state.

T, °K	C_p°/R	$(H^\circ-H_0^\circ)/RT$	S°/R	$-(F^\circ-H_0^\circ)/RT$
100	3.5077	3.4938	20.1447	16.6509
200	3.8149	3.5576	22.6430	19.0853
273.15	4.1929	3.6773	23.8881	20.2108
298.15	4.3132	3.7257	24.2606	20.5349
300	4.3218	3.7293	24.2873	20.5580
400	4.7197	3.9297	25.5880	21.6583
500	5.0215	4.1191	26.6749	22.5558
600	5.2724	4.2909	27.6131	23.3223
700	5.4949	4.4473	28.4429	23.9956
800	5.6974	4.5911	29.1900	24.5990
900	5.8825	4.7244	29.8720	25.1475
1000	6.0510	4.8488	30.5006	25.6518
1100	6.2036	4.9651	31.0846	26.1195
1200	6.3411	5.0742	31.6304	26.5562
1300	6.4646	5.1765	32.1429	26.9665
1400	6.5754	5.2725	32.6261	27.3536
1500	6.6747	5.3627	33.0832	27.7205
1600	6.7638	5.4476	33.5169	28.0693
1700	6.8439	5.5274	33.9294	28.4020
1800	6.9162	5.6026	34.3227	28.7201
1900	6.9816	5.6735	34.6984	29.0249
2000	7.0409	5.7404	35.0580	29.3177
2200	7.1443	5.8634	35.7341	29.8707
2400	7.2315	5.9739	36.3596	30.3857
2600	7.3061	6.0736	36.9414	30.8678
2800	7.3711	6.1640	37.4853	31.3213
3000	7.4284	6.2464	37.9958	31.7494
3200	7.4798	6.3219	38.4769	32.1550
3400	7.5264	6.3914	38.9318	32.5404
3600	7.5692	6.4557	39.3632	32.9075
3800	7.6090	6.5153	39.7736	33.2582
4000	7.6463	6.5710	40.1648	33.5938
4200	7.6816	6.6230	40.5387	33.9157
4400	7.7153	6.6719	40.8969	34.2249
4600	7.7477	6.7180	41.2405	34.5225
4800	7.7790	6.7615	41.5709	34.8094
5000	7.8094	6.8029	41.8891	35.0863
5200	7.8391	6.8421	42.1960	35.3538
5400	7.8683	6.8796	42.4924	35.6128
5600	7.8969	6.9154	42.7791	35.8636
5800	7.9252	6.9498	43.0567	36.1069
6000	7.9532	6.9827	43.3258	36.3431

TABLE IX. Thermodynamic functions of H_2O (g) in the ideal gas state.

T, °K	C_p°/R	$(H^\circ-H_0^\circ)/RT$	S°/R	$-(F^\circ-H_0^\circ)/RT$
100	4.0058	3.9559	18.3146	14.3587
200	4.0103	3.9817	21.0922	17.1105
273.15	4.0270	3.9911	22.3441	18.3530
298.15	4.0385	3.9946	22.6973	18.7027
300	4.0395	3.9948	22.7223	18.7274
400	4.1194	4.0150	23.8941	19.8792
500	4.2350	4.0470	24.8253	20.7783
600	4.3668	4.0892	25.6090	21.5198
700	4.5072	4.1388	26.2926	22.1538
800	4.6545	4.1940	26.9040	22.7100
900	4.8055	4.2536	27.4609	23.2074
1000	4.9605	4.3166	27.9753	23.6587
1100	5.1131	4.3821	28.4553	24.0732
1200	5.2615	4.4492	28.9066	24.4574
1300	5.4036	4.5172	29.3334	24.8162
1400	5.5381	4.5854	29.7388	25.1534
1500	5.6641	4.6531	30.1252	25.4721
1600	5.7815	4.7200	30.4946	25.7746
1700	5.8905	4.7857	30.8484	26.0627
1800	5.9914	4.8499	31.1880	26.3381
1900	6.0847	4.9125	31.5145	26.6020
2000	6.1710	4.9733	31.8288	26.8555
2200	6.3247	5.0893	32.4243	27.3350
2400	6.4572	5.1979	32.9805	27.7825
2600	6.5722	5.2993	33.5020	28.2026
2800	6.6732	5.3939	33.9928	28.5989
3000	6.7628	5.4823	34.4563	28.9741
3200	6.8432	5.5649	34.8954	29.3305
3400	6.9162	5.6422	35.3125	29.6703
3600	6.9830	5.7149	35.7097	29.9948
3800	7.0450	5.7833	36.0890	30.3057
4000	7.1029	5.8478	36.4518	30.6040
4200	7.1575	5.9089	36.7997	30.8908
4400	7.2095	5.9669	37.1339	31.1670
4600	7.2592	6.0220	37.4554	31.4335
4800	7.3072	6.0745	37.7654	31.6909
5000	7.3538	6.1248	38.0647	31.9399
5200	7.3992	6.1729	38.3540	32.1811
5400	7.4437	6.2192	38.6341	32.4149
5600	7.4875	6.2637	38.9056	32.6419
5800	7.5308	6.3066	39.1691	32.8624
6000	7.5737	6.3481	39.4251	33.0769

TABLE X. Thermodynamic functions of H_2S (g) in the ideal gas state.

T, °K	C_p°/R	$(H^\circ-H_0^\circ)/RT$	S°/R	$-(F^\circ-H_0^\circ)/RT$
100	4.0038	3.9786	20.3404	16.3619
200	4.0212	3.9936	23.1185	19.1248
273.15	4.0848	4.0083	24.3799	20.3716
298.15	4.1178	4.0161	24.7390	20.7229
300	4.1204	4.0167	24.7645	20.7478
400	4.2873	4.0626	25.9717	21.9091
500	4.4829	4.1268	26.9490	22.8222
600	4.6943	4.2036	27.7849	23.5813
700	4.9130	4.2893	28.5249	24.2356
800	5.1290	4.3808	29.1951	24.8143
900	5.3346	4.4755	29.8112	25.3357
1000	5.5247	4.5711	30.3833	25.8122
1100	5.6973	4.6657	30.9181	26.2523
1200	5.8523	4.7583	31.4206	26.6623
1300	5.9905	4.8479	31.8946	27.0467
1400	6.1136	4.9340	32.3431	27.4092
1500	6.2233	5.0163	32.7687	27.7524
1600	6.3211	5.0949	33.1735	28.0787
1700	6.4086	5.1696	33.5594	28.3898
1800	6.4872	5.2407	33.9280	28.6873
1900	6.5582	5.3082	34.2807	28.9725
2000	6.6225	5.3723	34.6187	29.2464
2200	6.7348	5.4912	35.2553	29.7641
2400	6.8299	5.5989	35.8455	30.2466
2600	6.9120	5.6968	36.3955	30.6987
2800	6.9842	5.7863	36.9105	31.1242
3000	7.0488	5.8683	37.3946	31.5262
3200	7.1075	5.9440	37.8514	31.9074
3400	7.1616	6.0140	38.2839	32.2699
3600	7.2121	6.0792	38.6947	32.6155
3800	7.2598	6.1401	39.0859	32.9459
4000	7.3052	6.1972	39.4595	33.2623
4200	7.3488	6.2510	39.8170	33.5659
4400	7.3911	6.3019	40.1598	33.8579
4600	7.4322	6.3501	40.4893	34.1391
4800	7.4725	6.3961	40.8064	34.4104
5000	7.5122	6.4399	41.1123	34.6724
5200	7.5514	6.4819	41.4077	34.9258
5400	7.5902	6.5222	41.6934	35.1712
5600	7.6287	6.5611	41.9701	35.4091
5800	7.6672	6.5985	42.2385	35.6400
6000	7.7055	6.6348	42.4991	35.8643

TABLE XI. Thermodynamic functions of N_2O (g) in the ideal gas state.

T, °K	C_p°/R	$(H^\circ-H_0^\circ)/RT$	S°/R	$-(F^\circ-H_0^\circ)/RT$
100	3.5302	3.5017	22.1401	18.6384
200	4.0424	3.6242	24.7164	21.0923
273.15	4.5034	3.7993	26.0462	22.2469
298.15	4.6444	3.8643	26.4467	22.5824
300	4.6565	3.8691	26.4755	22.6063
400	5.1337	4.1278	27.8830	23.7551
500	5.5145	4.3684	29.0709	24.7025
600	5.8273	4.5863	30.1048	25.5185
700	6.0876	4.7827	31.0233	26.2405
800	6.3048	4.9598	31.8508	26.8909
900	6.4862	5.1197	32.6042	27.4845
1000	6.6379	5.2641	33.2956	28.0315
1100	6.7652	5.3950	33.9344	28.5395
1200	6.8728	5.5138	34.5278	29.0141
1300	6.9642	5.6219	35.0817	29.4598
1400	7.0425	5.7206	35.6007	29.8801
1500	7.1101	5.8111	36.0889	30.2779
1600	7.1690	5.8941	36.5497	30.6556
1700	7.2207	5.9707	36.9859	31.0153
1800	7.2664	6.0414	37.4000	31.3586
1900	7.3073	6.1070	37.7940	31.6870
2000	7.3440	6.1679	38.1697	32.0018
2200	7.4076	6.2778	38.8728	32.5949
2400	7.4612	6.3743	39.5197	33.1454
2600	7.5077	6.4597	40.1188	33.6591
2800	7.5488	6.5361	40.6767	34.1406
3000	7.5860	6.6048	41.1988	34.5939
3200	7.6202	6.6672	41.6895	35.0222
3400	7.6521	6.7242	42.1524	35.4282
3600	7.6823	6.7766	42.5907	35.8140
3800	7.7112	6.8251	43.0068	36.1817
4000	7.7391	6.8701	43.4030	36.5330
4200	7.7663	6.9121	43.7813	36.8692
4400	7.7929	6.9515	44.1432	37.1917
4600	7.8191	6.9887	44.4902	37.5015
4800	7.8450	7.0238	44.8235	37.7997
5000	7.8708	7.0572	45.1443	38.0871
5200	7.8965	7.0890	45.4535	38.3645
5400	7.9222	7.1194	45.7520	38.6326
5600	7.9479	7.1485	46.0406	38.8921
5800	7.9738	7.1765	46.3199	39.1434
6000	7.9997	7.2035	46.5907	39.3872

TABLE XII. Thermodynamic functions of NO_2 (g) in the ideal gas state.

T, °K	C_p°/R*	$(H^\circ-H_0^\circ)/RT$	S°/R	$-(F^\circ-H_0^\circ)/RT$
100	4.0024	3.9982	24.3465	20.3483
200	4.1415	4.0245	27.1490	23.1245
273.15	4.3735	4.0853	28.4723	24.3870
298.15	4.4659	4.1133	28.8593	24.7460
300	4.4729	4.1155	28.8869	24.7714
400	4.8661	4.2537	30.2272	25.9735
500	5.2429	4.4146	31.3543	26.9397
600	5.5671	4.5804	32.3397	27.7593
700	5.8321	4.7410	33.2185	28.4775
800	6.0447	4.8912	34.0117	29.1205
900	6.2147	5.0291	34.7339	29.7047
1000	6.3514	5.1548	35.3960	30.2412
1100	6.4623	5.2688	36.0067	30.7379
1200	6.5533	5.3721	36.5730	31.2009
1300	6.6290	5.4660	37.1006	31.6346
1400	6.6926	5.5514	37.5943	32.0429
1500	6.7467	5.6293	38.0579	32.4286
1600	6.7933	5.7007	38.4949	32.7942
1700	6.8338	5.7661	38.9080	33.1418
1800	6.8694	5.8265	39.2996	33.4731
1900	6.9009	5.8822	39.6719	33.7897
2000	6.9292	5.9339	40.0266	34.0927
2200	6.9778	6.0266	40.6893	34.6627
2400	7.0186	6.1076	41.2983	35.1906
2600	7.0538	6.1791	41.8615	35.6824
2800	7.0847	6.2427	42.3854	36.1427
3000	7.1125	6.2998	42.8751	36.5754
3200	7.1378	6.3514	43.3350	36.9836
3400	7.1613	6.3983	43.7684	37.3701
3600	7.1832	6.4413	44.1784	37.7371
3800	7.2039	6.4809	44.5673	38.0864
4000	7.2237	6.5176	44.9373	38.4198
4200	7.2427	6.5517	45.2902	38.7386
4400	7.2610	6.5835	45.6276	39.0441
4600	7.2787	6.6133	45.9508	39.3374
4800	7.2960	6.6414	46.2609	39.6195
5000	7.3129	6.6679	46.5591	39.8912
5200	7.3295	6.6931	46.8462	40.1532
5400	7.3458	6.7169	47.1232	40.4062
5600	7.3618	6.7397	47.3906	40.6509
5800	7.3777	6.7614	47.6492	40.8878
6000	7.3933	6.7822	47.8996	41.1174

TABLE XIII. Thermodynamic functions of SO_2 (g) in the ideal gas state.

T, °K	C_p^0/R	$(H^0-H_0^0)/RT$	S^0/R	$-(F^0-H_0^0)/RT$
100	4.0324	4.0029	25.1267	21.1238
200	4.3753	4.0942	28.0140	23.9198
273.15	4.6861	4.2108	29.4233	25.2126
298.15	4.7951	4.2552	29.8384	25.5833
300	4.8031	4.2585	29.8681	25.6096
400	5.2292	4.4486	31.3090	26.8604
500	5.6003	4.6430	32.5171	27.8740
600	5.8970	4.8283	33.5655	28.7371
700	6.1268	4.9981	34.4925	29.4944
800	6.3038	5.1507	35.3227	30.1720
900	6.4412	5.2868	36.0734	30.7866
1000	6.5495	5.4079	36.7579	31.3500
1100	6.6361	5.5157	37.3864	31.8706
1200	6.7066	5.6121	37.9669	32.3548
1300	6.7648	5.6986	38.5061	32.8075
1400	6.8136	5.7766	39.0093	33.2327
1500	6.8552	5.8471	39.4808	33.6337
1600	6.8911	5.9113	39.9244	34.0131
1700	6.9224	5.9699	40.3431	34.3733
1800	6.9501	6.0236	40.7396	34.7160
1900	6.9748	6.0730	41.1161	35.0431
2000	6.9972	6.1187	41.4744	35.3557
2200	7.0361	6.2003	42.1432	35.9428
2400	7.0694	6.2714	42.7569	36.4854
2600	7.0986	6.3339	43.3239	36.9899
2800	7.1249	6.3895	43.8509	37.4614
3000	7.1489	6.4394	44.3433	37.9040
3200	7.1712	6.4844	44.8054	38.3210
3400	7.1922	6.5254	45.2408	38.7154
3600	7.2121	6.5630	45.6525	39.0894
3800	7.2312	6.5977	46.0429	39.4452
4000	7.2496	6.6298	46.4143	39.7845
4200	7.2675	6.6598	46.7685	40.1087
4400	7.2849	6.6878	47.1069	40.4191
4600	7.3019	6.7141	47.4311	40.7170
4800	7.3186	6.7390	47.7423	41.0033
5000	7.3350	6.7625	48.0414	41.2789
5200	7.3512	6.7848	48.3294	41.5445
5400	7.3672	6.8061	48.6071	41.8010
5600	7.3830	6.8264	48.8753	42.0489
5800	7.3987	6.8459	49.1347	42.2888
6000	7.4142	6.8646	49.3857	42.5212

resonance were also included for CO_2, CS_2, ClCN, and N_2O using the method of reference 9.

Atomic weights were taken from Wichers.[10] Physical constants are from Cohen, Crowe, and Dumond[11] with hc/k equal to 1.43880 (cm) (°K) and a dimensionless entropy constant of −1.16511. Spectroscopic data[12–30] are listed in Table III.

No adjustment was made for the difference in the spectroscopic data for the less abundant isotopic molecules, although the molecular weight for the naturally occurring isotopic mixture was used. Entropy of nuclear spin was omitted. Calculations were made on an IBM 704 computer.

RESULTS

The ideal gas functions C_p^0/R, $(H^0-H_0^0)/RT$, S^0/R, and $-(F^0-H_0^0)/RT$ are given at 273.15°, 298.15°, every 100° from 100° to 2000°K, and every 200° from 2000° to 6000°K for CO_2, COS, CS_2, ClCN, HCN, H_2O, H_2S, H_2O, NO_2, and SO_2 in Tables IV to XIII, respectively.

A comparison of the C_p^0/R and $-(F^0-H_0^0)/RT$ data in Tables IV to XIII with data in other references is given in Tables XIV and XV.

The largest differences in C_p^0/R at 5000°K (0.38 and 0.43, respectively) occur for COS and CS_2. This is due to the fact that the comparison is made with data obtained by the rigid-rotator harmonic-oscillator method. The results for ClCN are unusual in that the data are slightly less than that obtained by the rigid-rotator harmonic-oscillator method. This decrease is due to the fact that the positive x_{22} term together with the low ν_2 frequency cause a large negative contribution.

Relatively large differences occur for HCN, H_2O, and H_2S for a variety of reasons. For example, the difference of −0.17 in C_p^0/R at 5000°K for HCN given in this report as compared to reference 2 can be accounted for as follows: The sign of the g_{22} term in reference 2 was apparently taken incorrectly, which accounts for −0.20; the use of g_{22} in reference 2 rather than $(g_{22}+B_0)$ as used here (see reference 8) accounts for −0.04; somewhat different expressions for first-order corrections to the partition function used in reference 2 and in this report account for −0.05; and the inclusion in this report of second-order corrections accounts for +0.12. The difference of +0.22 in C_p^0/R at 5000°K for H_2O can be accounted for as follows: different expressions in the partition function for first-order corrections, +0.08; different spectroscopic constants, +0.04; and inclusion of second-order terms, +0.10. Reasons similar to those given for H_2O account for the differences in H_2S.

Differences in the data for N_2O, NO_2, and SO_2 are due mainly to different spectroscopic constants. For example, different rotational constants for NO_2 de-

[9] H. W. Woolley, J. Research Natl. Bur. Standards **54,** 299 (1955).
[10] E. Wichers, J. Am. Chem. Soc. **78,** 3235 (1956).
[11] Cohen, Crowe, and Dumond, *Fundamental Constants of Physics* (Interscience Publishers, Inc., New York, 1957).
[12] C. P. Courtoy, Can. J. Phys. **35,** 608 (1957).
[13] C. H. Townes, A. N. Holden, and F. R. Merritt, Phys. Rev. **74,** 1113 (1948).
[14] T. Wentink, Jr., J. Chem. Phys. **30,** 105 (1959).
[15] W. Gordy, W. V. Smith, and R. F. Trambarulo, *Microwave Spectroscopy* (John Wiley & Sons, Inc., New York, 1953).
[16] Private communication with B. P. Stoicheff.
[17] A. H. Guenther, T. A. Wiggins, and D. H. Rank, J. Chem. Phys. **28,** 682 (1958).
[18] W. O. Freitag and E. R. Nixon, J. Chem. Phys. **24,** 109 (1956).
[19] C. A. Burrus and W. Gordy, Phys. Rev. **101,** 599 (1956).
[20] H. C. Allen, Jr., E. D. Tidwell, and E. K. Plyler, J. Chem. Phys. **25,** 302 (1956).
[21] A. E. Douglas and D. Sharma, J. Chem. Phys. **21,** 448 (1953).
[22] G. A. Khachkuruzov, Optics and Spectroscopy **6,** 294 (1959).
[23] W. S. Benedict, N. Gailar, and E. K. Plyler, J. Chem. Phys. **24,** 1139 (1956).
[24] H. C. Allen, Jr., and E. K. Plyler, J. Chem. Phys. **25,** 1132 (1956).
[25] M. L. Grenier-Besson, Cahiers Phys. **10,** 44 (1956).
[26] K. N. Rao and H. H. Nielsen, Can. J. Phys. **34,** 1147 (1956).
[27] A. E. Douglas and C. K. Moller, J. Chem. Phys. **22,** 275 (1954).
[28] E. T. Arakawa and A. H. Nielsen, J. Mol. Spectroscopy **2,** 413 (1958).
[29] R. D. Shelton, A. H. Nielsen, and W. H. Fletcher, J. Chem. Phys. **21,** 2178 (1953). Erratum: *ibid.* **22,** 1791 (1954).
[30] D. Kivelson, J. Chem. Phys. **22,** 904 (1954).

TABLE XIV. Comparison of C_p^0/R data.

Molecule	Reference	Temperature, °K 298.15	1000	2000	3000	4000	5000	6000
CO_2	This work	4.4647	6.5316	7.2564	7.4749	7.5859	7.6624	7.7241
	1	4.4661	6.5318	7.258	7.484	7.608	7.702	
COS	This work	4.9896	6.8518	7.4275	7.6247	7.7458	7.8429	7.9301
	(a)	4.9902	6.7926	7.2801	7.3977	7.4415	7.4623	7.4737
CS_2	This work	5.4848	7.1322	7.5502	7.7080	7.8174	7.9101	7.9943
	(a)	5.4713	7.0495	7.3718	7.4415	7.4668	7.4787	7.4851
ClCN	This work	5.3948	6.7982	7.2689	7.3910	7.4375	7.4596	7.4719
	(a)	5.4111	6.8183	7.2769	7.3950	7.4397	7.4610	7.4728
HCN	This work	4.3132	6.0510	7.0409	7.4284	7.6463	7.8094	7.9532
	2	4.3243	6.1302	7.1689	7.5837	7.8163	7.9820	
H_2O	This work	4.0385	4.9605	6.1710	6.7628	7.1029	7.3538	7.5737
	3	4.0385	4.9569	6.1460	6.6945	6.9694	7.1325	
H_2S	This work	4.1178	5.5247	6.6225	7.0488	7.3052	7.5122	7.7055
	4	4.1159	5.5200	6.6052	6.9942	7.1924	7.3206	
N_2O	This work	4.6444	6.6379	7.3440	7.5860	7.7391	7.8708	7.9997
	5	4.646	6.646					
NO_2	This work	4.4659	6.3514	6.9292	7.1125	7.2237	7.3129	7.3933
	6	4.465	6.34	6.90	7.06			
SO_2	This work	4.7951	6.5495	6.9972	7.1489	7.2496	7.3350	7.4142
	7	4.80	6.557					

[a] RRHO method calculated for this paper.

TABLE XV. Comparison of $-(F^0-H_0^0)/RT$ data.

Molecule	Reference	Temperature, °K 298.15	1000	2000	3000	4000	5000	6000
CO_2	This work	21.9210	27.2307	31.1218	33.6718	35.5804	37.1085	38.3843
	1	21.9219	27.2325	31.124	33.675	35.584	37.114	
COS	This work	23.8339	29.5600	33.6916	36.3544	38.3323	39.9101	41.2251
	(a)	23.8294	29.5503	33.6563	36.2863	38.2289	39.7703	41.0483
CS_2	This work	24.2971	30.4559	34.8099	37.5711	39.6056	41.2211	42.5634
	(a)	24.2940	30.4351	34.7507	37.4696	39.4607	41.0326	42.3314
ClCN	This work	24.0812	30.1234	34.3173	36.9748	38.9305	40.4796	41.7626
	(a)	24.0822	30.1395	34.3454	37.0084	38.9673	40.5184	41.8028
HCN	This work	20.5349	25.6518	29.3177	31.7494	33.5938	35.0863	36.3431
	2	20.5316	25.6662	29.3676	31.8327	33.7067	35.2255	
H_2O	This work	18.7027	23.6587	26.8555	28.9741	30.6040	31.9399	33.0769
	3	18.7025	23.6585	26.8532	28.9669	30.5887	31.9131	
H_2S	This work	20.7229	25.8122	29.2464	31.5262	33.2623	34.6724	35.8643
	4	20.7081	25.7947	29.2257	31.5014	33.2309	34.6314	
N_2O	This work	22.5824	28.0315	32.0018	34.5939	36.5330	38.0871	39.3872
	5	22.583	28.035					
NO_2	This work	24.7460	30.2412	34.0927	36.5754	38.4198	39.8912	41.1174
	6	24.807	30.302	34.148	36.62	38.46		
SO_2	This work	25.5833	31.3500	35.3557	37.9040	39.7845	41.2789	42.5212
	7	25.58	31.35					

[a] RRHO method calculated for this paper.

crease the $-(F^0-H_0^0)/RT$ values given here by 0.061 as compared to the data of reference 6. The data for CO_2 are in good agreement with previously published data.

It has just come to the authors' attention that thermodynamic functions for CO_2, COS, CS_2, NO_2, and SO_2 have recently been published in the *Journal of Chemical and Engineering Data* **6**, 390 (1961). Agreement is fair to good. Differences are probably due to somewhat different methods of calculation and to some differences in spectroscopic constants.

ACKNOWLEDGMENT

The authors wish to thank Miss Jeanne Healy of the NASA Lewis Research Center for her assistance in preparing the IBM program.

THE JOURNAL OF CHEMICAL PHYSICS VOLUME 35, NUMBER 6 DECEMBER, 1961

Charge Transfer Spectra of some Gold(III) Complexes

ARUN KUMAR GANGOPADHYAY AND ANIMESH CHAKRAVORTY

Department of Physical Chemistry, University College of Science, Calcutta-9, India

(Received May 22, 1961)

Tetrahalo complexes of Au(III) show two intense bands in the ultraviolet. These are interpreted as charge-transfer bands; the transfer is from halogen p to gold d orbitals. The two bands are associated with $p_\sigma \rightarrow d_{x^2-y^2}$ and $p_\pi \rightarrow d_{x^2-y^2}$ transitions. The iodo complex undergoes spontaneous reduction; reason for this is discussed. The ethylenediamine complexes of Au(III) also exhibit interesting charge-transfer phenomenon.

IN the third transitional series two familiar ions with eight electrons in the outermost d shell are Pt^{2+} and Au^{3+}. They generally form four coordinate square-planar complexes which are almost invariably spin paired and hence diamagnetic. Spin pairing is facilitated by the large extension of the 5d electron clouds into space. In valence-bond language, Pt (II) and Au (III) complexes involve dsp^2 hybridization; in crystal-field nomenclature they almost always belong to "strong field" class. The planarity of some such complexes has been proved by x-ray crystallography[1,2] or otherwise.[3]

The visible and uv spectra of platinous complexes of the type $[Pt(NH_3)_nCl_{4-n}]^{(n-2)+}$, where $n=0$–4, have been interpreted by Chatt *et al.*[4] in terms of the crystal-field theory. The transitions involved are all within the $5d^8$ system of Pt(II): $d_{xy} \rightarrow d_{x^2-y^2}$; $d_{xz}(d_{yz}) \rightarrow d_{x^2-y^2}$; $d_{z^2} \rightarrow d_{x^2-y^2}$. They are of forbidden g-g type and accordingly have low molar extinction coefficients, generally less than 100. The triplets, which attain considerable intensity in the 5d series due to strong spin-orbit interaction, have much smaller extinction values.

The isoelectronic Au(III) complexes should show similar bands which, however, will be shifted to shorter wavelengths compared to those of Pt(II) complexes because of the higher charge and smaller size of Au(III). But just these factors increase its electronegativity and electron affinity over those of Pt(II). One chemical manifestation is the higher oxidizing power of Au(III). Spectrochemically we may expect that in combination with ligands of relatively low ionization potential, Au(III) complexes will show electron-transfer bands in the uv or visible region. The spectra of tetrahalo complexes of Au(III) were accordingly studied. Au(III) ethylenediamine complexes have an interesting bearing in this problem.

EXPERIMENTAL

$KAuBr_4 \cdot 2H_2O$ was prepared and purified following a standard method.[5] The tetrachloro complex could be obtained by decomposing the bromo complex with aqua regia. Excess nitric acid was removed by repeated evaporation with concentrated HCl. The final product could be obtained anhydrous by crystallization from alcohol.[2] The ethylenediamine monohydrate was E. Merck reagent, and it was distilled twice before use so as to get a perfectly colorless and transparent product. The potassium chloride, bromide, and iodide were all E. Merck G.R. quality. The water used was double-distilled.

Spectral measurements were carried out in 1-cm matched silica cells in Beckman spectrophotometer, model DU. Balancing was done against proper solutions e.g., for $KAuBr_4 \cdot 2H_2O$ in 1N KBr; 1N KBr was used as the standard. In the study of Au(III) ethylenediamine complexes a relatively concentrated solution of $KAuCl_4$ or $KAuBr_4 \cdot 2H_2O$ was made in 10% ethylene-

[1] R. G. Dickinson, J. Am. Chem. Soc. **44**, 2404 (1922).
[2] E. G. Cox and K. C. Webster, J. Chem. Soc. **1936**, 1635.
[3] A. F. Wells, *Structural Inorganic Chemistry* (Oxford University Press, New York, 1950), p. 625.
[4] J. Chatt, G. A. Gamlen, and L. E. Orgel, J. Chem. Soc. **1958**, 486.
[5] *Inorganic Syntheses*, edited by J. C. Bailey, Jr., (McGraw-Hill Book Company, Inc., 1953), Vol. IV, p. 14.

diamine hydrate. An aliquot from this was diluted with the same 10% ethylenediamine such that optical densities had reasonable values. Another equal aliquot was diluted with 2*N* $HClO_4$ (the whole of ethylenediamine is neutralized) to the same volume. Thus the concentration of Au(III) was same in the two solutions.

Solutions of $KAuBr_4 \cdot 2H_2O$ and $KAuCl_4$ were made by direct weighing. Since we are not quite sure about the hydration of $KAuCl_4$ (the anhydrous salt might absorb some water during weighing), we do not claim any great accuracy in the extinction values. Measurements had to be carried with different concentrations, since the peaks have very different intensities. Concentrations were so chosen that O.D. was generally between 0.2 to 0.5 near the band maxima.

RESULTS AND DISCUSSION

Spectra of $KAuCl_4$ and $KAuBr_4$ were measured in 1*N* KCl and 1*N* KBr, respectively. This was mainly to avoid to possible aquation or hydrolysis. The spectrum of $KAuCl_4$ 1*N* KCl is very similar to that in 1*N* HCl, which has already been reported by one of us.[6] Under such high concentrations of halide ions it is quite possible that higher complexes, e.g., $[AuX_5]^{2-}$ or $[AuX_6]^{3-}$, are formed to some extent with one or two "long" Au-X bonds. This point is discussed later.

Both $[AuCl_4]^-$ and $[AuBr_4]^-$ show two strong bands

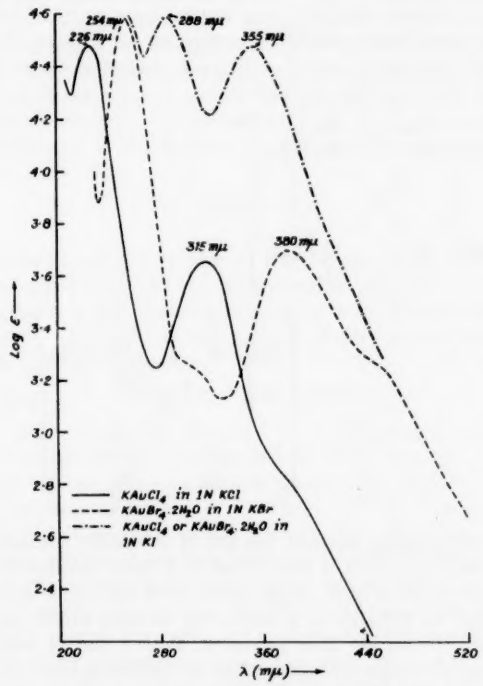

FIG. 1. Spectra of $KAuX_4$ in 1*N* KX.

[6] A. Chakravorty, Naturwissenschaften (to be published).

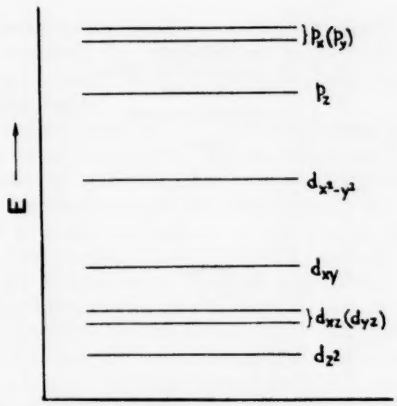

FIG. 2. Splitting of 5*d* and 6*p* orbitals in tetragonal ligand-field (not drawn to scale).

in the uv (Fig. 1). The band at lower wavelength (henceforth called λ_1) is about seven times more intense than the other (λ_2). The bands of the bromo complex are placed at longer wavelengths than those of the chloro complex. The high extinction coefficients clearly indicate that these are not crystal-field transitions within the metal *d* shell, but must correspond to some $g \rightarrow u$ or $u \rightarrow g$ type allowed transition.

λ_1 cannot possibly be due to $5d \rightarrow 6p$ transition in the gold atom since this would mean too small an energy gap between the two levels. Further, there is no reason why such a band should show a large forward shift in passing from the chloro to the bromo complex. Let us consider a simple electrostatic picture for $[AuX_4]^-$. The Au^{3+} ion is at the origin and the four X^- are placed on the *x* and *y* axes. The *d* orbitals will then be split up in the following order[4] of decreasing energy: $d_{x^2-y^2}$, d_{xy}, $d_{xz}(d_{yz})$, d_{z^2}. In the 6*p* shell, p_x and p_y will be destabilized since they point directly towards the ligands, p_z remaining unaffected hence most stable. This is shown in Fig. 2.

On passing from $[AuCl_4]^-$ to $[AuBr_4]^-$, the position of p_z is unaffected; the p_x, p_y, and the *d* orbitals are somewhat stabilized since Cl^- exerts greater repulsive force than Br^-, due mainly to smaller size and closer approach. The longest wavelength $d \rightarrow p$ transition will then involve the p_z orbital in the excited state and hence should shift to shorter wavelength on passing from $[AuCl_4]^-$ to $[AuBr_4]^-$ while reverse is the case. Further, ethylenediamine is known to produce much stronger perturbation than the Cl^-, so that for $[Auen_2]^{3+}$ the longest wavelength $d \rightarrow p$ band should be at a wavelength higher than that for $[AuCl_4]^-$. In fact, however, λ_1 for $[Auen_2]^{3+}$ is not reached even at 200 mμ. The above arguments are based on a crude model, but the results should be qualitatively true, so that λ_1 can hardly be a $d \rightarrow p$ transition.

We believe that λ_1 and λ_2 represent electron transfer from ligand orbitals to holes in the 5*d* shell of Au(III).

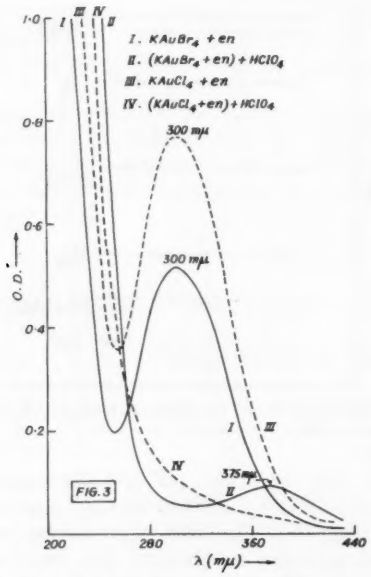

FIG. 3. Spectra of ($KAuX_4$+en) and ($KAuX_4$+en)+$HClO_4$ systems (en=ethylenediamine).

The shift to longer wavelengths in bromo over chloro complex is then understandable on the basis of lower ionization potential of Br^-. This shift is quite general in halides.[7] The two bands cannot be correlated to $^2P_{\frac{3}{2}}$ and $^2P_{\frac{1}{2}}$ states of the halogen atom produced in the excited state of the complex, since the observed energy gaps between λ_1 and λ_2 are much too large. The difference of above two states is: Cl=880 cm^{-1}, Br=3700 cm^{-1}, while $\Delta\lambda$ for $[AuCl_4]^-$ is 12 500 cm^{-1} and for $[AuBr_4]^-$ is 13 050 cm^{-1}.

At this point it is relevant to consider a qualitative molecular orbital picture for square planar complexes.[8] With same placement of ligands as required in Fig. 2, the $5d_{x^2-y^2}$, $6s$, $6p_x$, and $6p_y$ orbitals of Au(III) will "overlap" σ orbitals of the ligands, viz., ns, np_x, np_y ($n=3$ for Cl^- and 4 for Br^-) giving rise to four bonding and four antibonding orbitals. The former will be occupied by eight "coordinated" electrons from the ligands, the latter remaining empty. The metal orbitals d_{xy}, $d_{xz}(d_{yz})$, and d_{z^2} are nonbonding receiving eight metal electrons, all paired. The sixteen π electrons (the "lone pairs") on the four halide ions may somewhat destabilize the filled d_{xy} set through π interaction but the halogen p_z and empty metal-$6p_z$ orbitals will be mutually stabilized through π bonding. The π electrons are necessarily less stable than σ electrons.

The following assignments are now made. λ_1: transition from highest filled bonding orbital to lowest unfilled antibonding orbital, i.e., roughly a $p_\sigma \rightarrow d_{x^2-y^2}$ transition, while λ_2 is $p_\pi \rightarrow d_{x^2-y^2}$. The former is a $g \rightarrow u$ type transition, and since the σ overlap is also quite considerable, the intensity will be very high, as is actually the case. $p_\pi \rightarrow d_{x^2-y^2}$ is also $g \rightarrow u$ type, but since there is very little overlap, intensity should be quite low. It is to be noted that $d_{x^2-y^2}$ is not pure gold orbital, but is mixed with halogen σ orbital, which in turn is a hybrid of p and s, so that the transition $p_\pi \rightarrow d_{x^2-y^2}$ will have some character of the strongly allowed $p_\pi \rightarrow s$ transition in the halogen. The considerable π mixing of halogen p_π and metal $6p$ orbitals especially of p_z with an empty $6p_z$ gold orbital, will also add to the intensity of the $p_\pi \rightarrow d_{x^2-y^2}$ transition. The relatively high intensity of $p_\pi \rightarrow d_{z^2}$ transition in $[Co(NH_3)_5X]^{2+}$ has been similarly interpreted by Yatemera.[9] In any case, the intensity of λ_2 will be much smaller than λ_1, as is actually the case. Harris and Reece[10] have shown that in a *nonaqueous* medium like nitrobenzene or nitromethane, $[AuBr_4]^-$ reacts with Br^- to give $[AuBr_6]^{3-}$. During this process λ_2 shows a blue shift and its intensity undergoes a ninefold decrease (from $\epsilon=4850$ to $\epsilon=550$). Formation of $[AuBr_6]^{3-}$ can be explained on the basis of two "long" $6p_z6d_{z^2}$ bonds along the z axis, i.e., normal to the original planar molecule. Thus the $6p_z$ metal orbital is filled up and can no longer form π bond with halogen p_z. The decrease in intensity of λ_2 is possibly associated with this factor. The high intensity of λ_2 in 1*N aqueous* KBr tends to indicate that higher complexes like $[AuBr_6]^{3-}$ are not formed in appreciable concentration.

Strong support in favor of the above assignment of λ_2 is further obtained from studies on spectra of bis-ethylenediamine-Au(III) complexes.[11] $[Au(en)_2]^{3+}$ (en=ethylenediamine) acts as a monoacid base of $P_K=6.5$, ionizing as follows:

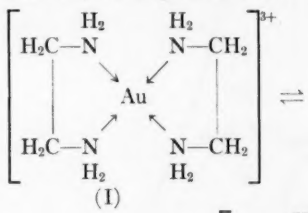

(I)

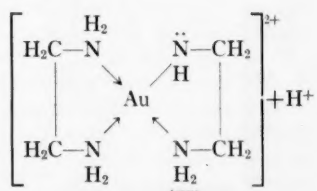

(II)

In an alkaline medium the ion II is mainly present; on acidification it is neutralized to I. Since ethylenediamine itself is basic, when an excess of this material is added to $KAuBr_4$ or $KAuCl_4$, the halogen atoms are replaced and ion II is produced. Both I and II were isolated[11] in the crystalline state as chloride or bromide.

In II, there is a pair of π electrons on one of te hnitro-

[7] L. E. Orgel, Quart. Revs. (London) **8,** 452 (1954).
[8] J. H. Van Vleck, J. Chem. Phys. **3,** 803 (1935).
[9] H. Yatemera, J. Inorg. & Nuclear Chem. **15,** 50 (1960).
[10] C. M. Harris and I. H. Reece, Nature **182,** 1665 (1958).
[11] B. P. Block and J. C. Bailer, Jr., J. Am. Chem. Soc. **77,** 6152 (1955).

gen atoms so that a band representing $p_\pi \rightarrow d_{x^2-y^2}$ transition should be present. In $[Auen_2]^{3+}$, however, such a band is not expected for obvious reasons.

A solution of $KAuCl_4$ in 10% ethylenediamine hydrate gives a peak at 300 mμ with $\epsilon = 2600$ (Fig. 3). In the solution acidified with 2*N* $HClO_4$, the band is completely quenched. Thus our expectations are fulfilled. If $KAuBr_4$ is replaced for $KAuCl_4$ identical results (Fig. 3) are obtained except for the fact that in acidic medium there is a relatively weak and broad band at 375 mμ ($\epsilon = 460$). It cannot be a crystal-field band, for then it should be present in $[Auen_2]Cl_3$ as well. This band may be due to charge transfer between $[Auen_2]^{3+}$ as a whole and bromide ions. Linhard[12] has observed similar interionic charge transfer in the $[Co(NH_3)_6]^{3+} + I^-$ system. The work has been extended by Japanese workers[13] to copper(II) complexes, e.g., $[Cuen_2]^{2+}$. It is relevant to note that Block and Bailer[11] reported $[Auen_2]Cl_3$ as colorless and $[Auen_2]Br_3$ as light yellow in the crystalline state. The most probable interpretation of this unexpected color variation is the one suggested above. An analogous case is known in the amine complexes of trivalent Ir; viz., $[Ir(NH_3)_6]X_3$, when x=Cl or Br, the complex is colorless; when x=I, yellow. A similar interpretation has been suggested.[7]

In 10% ethylenediamine it was not possible to follow the spectra beyond about 230 mμ due possibly to the strong absorption of OH^- ions which made the blank opaque. So λ_1 could not be located for II. In the acidic solutions where I was present, this limitation disappeared. The absorption increases steeply but the peak is not reached even at 200 mμ. This is quite expected since the ionization potential of the lone pair (this pair is involved in the σ bond of complex) in

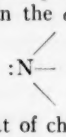

is much larger than that of chloride ion; in $[AuCl_4]^-$ the band is at 226 mμ. This expected shift of charge-transfer bands to shorter wavelengths as we pass from bromo to chloro to amine complex is quite general, e.g., in Co(III) complexes.[14]

Case of the Iodo-Complex

When $KAuCl_4$ is dissolved in 1*N* KBr the reaction $KAuCl_4 + 4KBr = KAuBr_4 + 4KCl$ occurs rapidly and the solution gives a spectrum which is that of $KAuBr_4$. A solution of $KAuCl_4$ or $KAuBr_4$ in 1*N* KI may similarly be expected to produce $KAuI_4$. But such solutions gave spectra characteristic of the I_3^- ion–two roughly equally strong bands (ϵ calculated on the basis of gold-concentration) (288 mμ, $\epsilon = 39\,000$; 355 mμ, $\epsilon = 30\,000$) with energy gap 6670 cm^{-1} (Fig. 1). The solutions produced intense coloration with starch. Thus $[AuCl_4]^-$ and $[AuBr_4]^-$ are reduced by KI under the present experimental conditions. It is to be noted that $[AuI_4]^-$ is not unknown, the potassium salt has been described as a black solid[15] which is thermally quite unstable, liberating iodine.

We believe that in the present experiments, iodo complexes are formed first only to decompose rapidly. This behavior can be explained as follows. In going from chloro to bromo complex the charge-transfer bands are shifted to longer wavelengths and this should continue in the iodo complex. In fact, the shift between bromo-iodo pair is expected to be much larger than that in the chloro-bromo pair due to larger change in ionization potential in the former pair. By simple arguments[7] it can be shown that when a charge-transfer band moves into the near infrared, spontaneous oxidation-reduction becomes possible kinetically as soon as the tail of the band approaches zero frequency. This we believe is the case with the iodo complex in the present conditions. A kinetics study could give useful information. The kinetics of reaction between Fe^{3+} and I^- has been interpreted[16] via the intermediary formation of iodo complex.

It may be noted that the situation with simple Au(III) halides AuX_3 which in fact are halogen bridged complexes[3] through demerization, is quite similar. $AuCl_3$ (red), $AuBr_3$ (dark brown) are stable; AuI_3 (green) decomposes soon into AuI and I_2 at 25°C.

CONCLUDING REMARKS

The evidences given are not enough to make the assignments of λ_1 and λ_2 unequivocal. Studies on polarization selectivity of the two bands in single-crystal spectra might give very useful information about their origin, e.g., $p_\sigma \rightarrow d_{x^2-y^2}$ band is expected to be polarized in the xy plane since the excited state has the symmetry E_u, which also is the symmetry of x and y axes in D_{4h} group. The crystal spectrum of $CsAuCl_4$ has been reported by Japanese workers.[17] Unfortunately the crystal structure is not known and further the crystal spectrum is so much different from solution spectrum that no definite correlation seems possible.

It is fortunate that $KAuX_4$ is soluble in a variety of nonaqueous solvents. Shifts in λ_1 and λ_2 with change in solvent polarity could give interesting information. In fact, λ_1 and λ_2 show red shifts with decreasing polarity of the solvent. This point is now being closely investigated.

The shoulders on the tail of λ_2 in the spectra of $[AuCl_4]^-$, $[AuBr_4]^-$ (Fig. 1) possibly represent crystal field transitions some of which might have been completely obscured by the intense charge transfer bands.

ACKNOWLEDGMENTS

Sincerest thanks are due Professor B. N. Ghosh and Dr. S. Basu for providing us with all laboratory facilities.

[12] M. Linhard, Z. Electrochem. **50,** 224 (1944).
[13] H. Yoneda, Bull. Chem. Soc. Japan **29,** 68 (1956).
[14] M. Linhard and M. Weigel, Z. anorg. u. allgem. Chem. **266,** 49 (1951).
[15] N. V. Sidgwick, *The Chemical Elements and their Compounds* (Oxford University Press, New York, 1950), p. 190.
[16] A. J. Fudge and K. W. Sykes, J. Chem. Soc. **1952,** 119.
[17] S. Yamada and R. Tsuchida, Bull. Chem. Soc. Japan **29,** 424 (1956).

On the Kinetic Theory of Dense Fluids. IX. The Fluid of Rigid Spheres with a Square-Well Attraction

H. T. DAVIS* AND STUART A. RICE†

Department of Chemistry and Institute for the Study of Metals, University of Chicago, Chicago 37, Illinois

AND

J. V. SENGERS

Van der Waals Laboratory, University of Amsterdam, Amsterdam

(Received May 3, 1961)

By the use of methods previously introduced, we discuss in this paper the statistical theory of a dense fluid of molecules interacting with a square-well potential. The argument proceeds via the derivation and solution of a modified Boltzmann equation. The theory is used in two ways: (a) to provide a test of the theory proposed by Rice and Allnatt; (b) to estimate the attractive force contribution to the transport of momentum and energy in a real fluid.

The approach of Rice and Allnatt is shown to give a friction coefficient in agreement with experiment for liquid argon.

The presence of the attraction has a marked effect on the transport of momentum and energy and the square-well-model fluid gives a surprisingly accurate representation of the properties of liquid argon. The computed thermal conductance and self-diffusion coefficient are in agreement with experiment:

κ(calc) 1.33×10^{3} erg/g-sec-deg, κ(obs) 1.26×10^{3} erg/g-sec-deg,

D(calc) 1.81×10^{-5} cm²/sec, D(obs) 1.84×10^{-5} cm²/sec,

and the temperature dependence of κ/η is in qualitative agreement with the observed temperature dependence of this ratio.

I. INTRODUCTION

THE theory of transport in dilute gases has been the subject of intermittent investigation since the time of Maxwell. Aside from the practical considerations involved in applying the formalism to systems composed of real molecules, the formulation of the kinetic theory of dilute gases was completed by the elegant analyses of Enskog and Chapman.[1] Recent work has dealt with the fundamental physical basis of the theory and such classical concepts as that of "molecular chaos" have been elucidated by statistical mechanical investigations of the Maxwell-Boltzmann integro-differential equation of transport.[2] The qualitative and quantitative agreement between calculation and experiment leaves little to be desired, and our confidence in the basic theory is sufficiently great that it is now used as a tool for the investigation of intermolecular forces.[3]

In recent years the theory of transport in dense fluids has been extensively developed, at least formally.[2] In general, momentum and energy transfer in a fluid are effected in two ways: by the direct motion of the molecules, and by the action of intermolecular forces. Whereas the former is the sole mechanism of transport in the dilute gas, the latter dominates in dense fluids. In the theory of Kirkwood,[4] the motion of an individual molecule, which is subjected to essentially continuous interaction with its neighbors, is analyzed with the aid of analogies from the phenomenological theory of Brownian movement. Explicit expressions are obtained for the flux vectors and for the frictional coefficient in terms of the intermolecular forces. Though the prescription is quite definite, the mathematical difficulties involved in evaluating the transport coefficients have been all but insurmountable. The results which have thus far been obtained have contributed materially to our understanding of the molecular mechanism of transport in dense fluids, but the quantitative agreement has been sufficiently poor that well-defined dynamical models, though they may be poor representations of reality, may still shed some light on both the fundamental assumptions involved in the formal theory and the mathematical approximations utilized to obtain numerical answers from the formal theory. In two previous papers a detailed analysis has been presented of the binary collision mechanism for the transfer of momentum and energy in a dense fluid of rigid spheres.[5,6] The singular nature of the intermolecular potential enabled the analysis to be carried through explicitly by relatively simple means. Now, it is well known that in order to reproduce the temperature dependence of the equation of state or the transport coefficients, the intermolecular potential must contain an attractive as well as a repulsive force.

* National Science Foundation Predoctoral Fellow.

† Alfred P. Sloan Fellow.

[1] S. Chapman and T. G. Cowling, *The Mathematical Theory of Non-Uniform Gases* (Cambridge University Press, New York, 1953).

[2] For a recent review see S. A. Rice and H. L. Frisch, Ann. Rev. Phys. Chem. **11,** 187 (1960).

[3] J. O. Hirschfelder, C. F. Curtiss, and R. B. Bird, *Molecular Theory of Gases and Liquids* (John Wiley & Sons, Inc., New York, 1954).

[4] J. G. Kirkwood, J. Chem. Phys. **14,** 180 (1946).

[5] S. A. Rice, J. G. Kirkwood, J. Ross, and R. W. Zwanzig, J. Chem. Phys. **31,** 575 (1959).

[6] R. A. Harris and S. A. Rice, J. Chem. Phys. **33,** 1055 (1960).

In particular, the square-well potential will fit both the second virial coefficient and the transport coefficients of a dilute gas over a wide range of temperature, but the parameters used for different properties are necessarily different.[3] This difference in parameters reflects the fact that the square-well potential is not an accurate representation of the true intermolecular interaction. However, again due to the singular nature of the square-well potential, calculations can be extended quite far by relatively simple means, and despite its shortcomings, the square-well potential should represent a zeroth-order approximation to the effect of attractive forces on the transport properties of a dense fluid. In this communication, a modified Boltzmann equation shall be developed which describes the change of singlet space distribution function for a dense gas of rigid spheres with a square-well attraction. The transport coefficients will be formulated, and the role of time smoothing and multiple collisions further commented upon.

The theory developed herein will also be used to test the theory of transport proposed by Rice and Allnatt.[7,8] These authors developed a modified Boltzmann equation by separating the interactions in a fluid into a rigid core and a soft attractive intermolecular potential. The hard core was treated as in the theory of the dense rigid-sphere fluid while the attractive interaction was handled in the Fokker-Planck approximation. In Sec. V of this paper the attractive force contribution to the modified Boltzmann equation for the square-well model is reduced to a Fokker-Planck expression and an attractive potential friction coefficient is calculated for argon at 84°K.

II. DERIVATION OF TRANSPORT EQUATION

As an aid to the reader we first briefly review the general reduction of the Liouville equation to a form which can be manipulated. Consider a one-component system containing N structureless particles with the positions and momenta specified by the vectors $\mathbf{R}_1\cdots$, $\mathbf{R}_N$, $\mathbf{p}_1\cdots\mathbf{p}_N$. The normalized specific distribution function satisfying Liouville's equation is given by

$$\frac{\partial f^{(N)}}{\partial t}+\sum_{j=1}^{N}\left[\frac{\mathbf{p}_j}{m}\cdot\nabla_{R_j}f^{(N)}+\mathbf{F}_j\cdot\nabla_{p_j}f^{(N)}\right]=0, \tag{1}$$

where $\mathbf{R}_j$, $\mathbf{p}_j$, and m_j are, respectively, the position, momentum, and mass of the jth particle, and $\mathbf{F}_j$ is the total force exerted on the jth particle by all the other molecules in the system.

Equation (1) will be used to obtain the reduced distribution function, $f^{(n)}(\mathbf{r},\mathbf{p};t)$, defined by

$$f^{(n)}(\mathbf{r},\mathbf{p};t)=\int\cdots\int f^{(N)}(\mathbf{r},\mathbf{p},\mathbf{Q},\mathbf{P};t)\,d\mathbf{P}d\mathbf{Q}, \tag{2}$$

where $\mathbf{r}$, $\mathbf{p}$ are the coordinates of the subset of n particles and $\mathbf{Q}$, $\mathbf{P}$ are the coordinates of the remaining subset of $N-n$ particles. Coarse graining in time, as defined by the relation

$$\bar{f}^{(n)}(\mathbf{r},\mathbf{p};t)=\frac{1}{\tau}\int_0^\tau f^{(n)}(\mathbf{r},\mathbf{p};t+s)\,ds, \tag{3}$$

will also be employed in the following analysis. Coarse graining is discussed in detail by Kirkwood,[4] and by Rice and Frisch.[2]

Assuming the intermolecular force $\mathbf{F}_j$ to be given by a sum of pair forces, it may be shown that

$$\frac{\partial\bar{f}^{(1)}}{\partial t}+\frac{\mathbf{p}_1}{m}\cdot\nabla_{R1}\bar{f}_1^{(1)}=\frac{N-1}{\tau}\int_0^\tau\int\cdots\int\mathbf{F}_{12}\cdot\nabla_{p_1}K^{(2)}(s)f^{(2)}(\mathbf{R}_1',\mathbf{R}_2',\mathbf{p}_1',\mathbf{p}_2';t)\,d\mathbf{R}_2d\mathbf{p}_2ds d\mathbf{R}_1'd\mathbf{R}_2'd\mathbf{p}_1'd\mathbf{p}_2' \tag{4}$$

$$\frac{\partial K^{(2)}}{\partial s}+\frac{\mathbf{p}_1}{m}\cdot\nabla_{R1}K^{(2)}+\frac{\mathbf{p}_2}{m}\cdot\nabla_{R_2}K^{(2)}+\mathbf{F}_{12}\cdot\nabla_{p_1}K^{(2)}+\mathbf{F}_{21}\cdot\nabla_{p_2}K^{(2)}$$

$$=-\sum_{j=3}^{N}\int\cdots\int\{\mathbf{F}_{1j}\cdot\nabla_{p1}+\mathbf{F}_{2j}\cdot\nabla_{p2}\}K^{(N)}(s)f^{(2/N-2)}(\mathbf{R}_1',\mathbf{R}_2',\mathbf{p}_1',\mathbf{p}_1'/\mathbf{QP};t)\,d\mathbf{P}d\mathbf{Q}d\mathbf{P}'d\mathbf{Q}', \tag{5}$$

where the transformation function, $K^{(n)}$ is defined by[9]

$$f^{(n)}(\mathbf{rp};t+s)=\int\cdots\int K^{(n)}(\mathbf{rp}/\mathbf{r'p'};s)f^{(n)}(\mathbf{r'p'};t)\,d\mathbf{r'}d\mathbf{p'}, \tag{6}$$

$$K^{(n)}(\mathbf{rp}/\mathbf{r'p'};s)=\int\cdots\int K^{(N)}(\mathbf{rpQP}/\mathbf{r'p'Q'P'};s)f^{(n/N-n)}(\mathbf{r'p'}/\mathbf{Q'P'};t)\,d\mathbf{P}d\mathbf{Q}d\mathbf{P}'d\mathbf{Q}', \tag{7}$$

with

$$f^{(N)}(\mathbf{r},\mathbf{p},\mathbf{QP};t)=f^{(n)}(\mathbf{rp};t)f^{(n/N-n)}(\mathbf{rp}/\mathbf{QP};t). \tag{8}$$

For further details of this derivation, the reader is referred to reference 5.

[7] S. A. Rice and A. R. Allnatt, J. Chem. Phys. **34**, 2144 (1961).
[8] A. R. Allnatt and S. A. Rice, J. Chem. Phys. **34**, 2156 (1961).
[9] These phase space distribution functions are discussed in detail in J. Ross and J. G. Kirkwood, J. Chem. Phys. **22**, 1094 (1954); J. Ross, *ibid.* **24**, 375 (1956).

III. DENSE FLUID WITH A SQUARE-WELL POTENTIAL

A "square-well" fluid is defined as one composed of particles which interact according to the following pair potential:

$$V(R_{ij})=0, \qquad R_{ij}>\sigma_2,$$
$$V(R_{ij})=-\epsilon, \qquad \sigma_1<R_{ij}\leq\sigma_2,$$
$$V(R_{ij})=+\infty, \qquad R_{ij}\leq\sigma_1. \tag{9}$$

In this paper utilization is made of the fact that all the intermolecular forces in a "square-well" fluid are impulsive; i.e., any collision is instantaneous. Thus, for coarse graining, a time scale is chosen such that $\tau\to 0+$. Because the forces are impulsive, only isolated binary collisions can occur in that time interval. Then, if, for example, molecules 1 and 2 are considered, the only nonzero force in the time interval $\tau\to 0+$ is $\mathbf{F}_{12}$, and $\mathbf{F}_{1j}=\mathbf{F}_{2j}=0$, $j\neq 1, 2$. In the limit as $\tau\to 0+$, Eq. (5) reduces to the relation

$$\lim_{\tau\to 0+}\frac{\partial K^{(2)}}{\partial s}+\frac{\mathbf{p}_1}{m}\cdot\nabla_{R1}K^{(2)}+\frac{\mathbf{p}_2}{m}\cdot\nabla_{R_2}K^{(2)}+\mathbf{F}_{12}\cdot\nabla_{p_1}K^{(2)}+\mathbf{F}_{21}\cdot\nabla_{p_2}K^{(2)}=0. \tag{10}$$

Equation (10) is a Liouville equation in pair space for the transformation function $K^{(2)}$, and the formal solution can be written as

$$K^{(2)}(\mathbf{R}_1, \mathbf{R}_2, \mathbf{p}_1, \mathbf{p}_2/\mathbf{R}_1', \mathbf{R}_2', \mathbf{p}_1', \mathbf{p}_2; s)=\prod_{j=1}^{2}\delta[\mathbf{R}_j-\mathbf{R}_j'-\Delta\mathbf{R}_j(s)]\delta[\mathbf{p}_j-\mathbf{p}_j'-\Delta\mathbf{p}_j(s)]. \tag{11}$$

Solving Eq. (10) for $\mathbf{F}_{12}\cdot\nabla_{p_1}K^{(2)}$ and substituting the result into Eq. (4) leads to the following equation:

$$(\partial\bar{f}^{(1)}/\partial t)+(\mathbf{p}_1/m)\cdot\nabla_{R_1}\bar{f}^{(1)}=\Omega_1+\Omega_2$$

$$\Omega_1=\frac{N-1}{\tau}\int_0^\tau\int\cdots\int\frac{\partial K^{(2)}}{\partial s}f^{(2)}(\mathbf{R}_1', \mathbf{R}_2', \mathbf{p}_2', \mathbf{p}_1'; t)\,d\mathbf{R}_2 d\mathbf{p}_2 ds d\mathbf{R}_1' d\mathbf{R}_2' d\mathbf{p}_1' d\mathbf{p}_2'$$

$$\Omega_2=\frac{N-1}{\tau}\int_0^\tau\int\cdots\int\left(\frac{\mathbf{p}_1}{m}\cdot\nabla_{R1}+\frac{\mathbf{p}_2}{m}\cdot\nabla_{R2}\right)K^{(2)}(s)f^{(2)}(\mathbf{R}_1', \mathbf{R}_2', \mathbf{p}_1', \mathbf{p}_2'; t)\,d\mathbf{R}_2 d\mathbf{p}_2 ds d\mathbf{R}_1' d\mathbf{R}_2' d\mathbf{p}_1' d\mathbf{p}_2'. \tag{12}$$

Integrating over ds in Ω_1 and replacing $f^{(2)}(\mathbf{R}_1', \mathbf{R}_2', \mathbf{p}_1', \mathbf{p}_2'; t)$ with $g_0^{(2)}(\mathbf{R}_1', \mathbf{R}_2')f^{(1)}(\mathbf{R}_1', \mathbf{p}_1'; t)f^{(1)}(\mathbf{R}_2', \mathbf{p}_2'; t)$ leads to the collision integral

$$\Omega_1=\frac{N-1}{\tau}\int\cdots\int\{\delta[\mathbf{p}_1-\mathbf{p}_1'-\Delta\mathbf{p}_1(\tau)]\delta[\mathbf{p}_2-\mathbf{p}_2'-\Delta\mathbf{p}_2(\tau)]\delta[\mathbf{R}_1-\mathbf{R}_1'-\Delta\mathbf{R}_1(\tau)]\delta[\mathbf{R}_2-\mathbf{R}_2'-\Delta\mathbf{R}_2(\tau)]$$
$$-\delta(\mathbf{p}_1-\mathbf{p}_1')\delta(\mathbf{p}_2-\mathbf{p}_2')\delta(\mathbf{R}_1-\mathbf{R}_1')\delta(\mathbf{R}_2-\mathbf{R}_2')\}g_0^{(2)}(\mathbf{R}_1', \mathbf{R}_2')f^{(1)}(\mathbf{R}_1', \mathbf{p}_1'; t)f^{(1)}(\mathbf{R}_2, \mathbf{p}_2; t)\,d\mathbf{R}_2 d\mathbf{p}_2 d\mathbf{R}_1' d\mathbf{R}_2' d\mathbf{p}_1' d\mathbf{p}_2', \tag{13}$$

where the pair correlation function, $g^{(2)}(\mathbf{R}_1', \mathbf{R}_2', \mathbf{p}_1', \mathbf{p}_2'; t)$, has been approximated by the local equilibrium pair correlation function, $g_0^{(2)}(\mathbf{R}_1, \mathbf{R}_2)$. When the integration over the primed coordinates in Eq. (13) is carried out, we find

$$\Omega_1=\frac{N-1}{\tau}\iint\{g_0^{(2)}[\mathbf{R}_1-\Delta\mathbf{R}_1(\tau), \mathbf{R}_2-\Delta\mathbf{R}_2(\tau)]f^{(1)}[\mathbf{R}_1-\Delta\mathbf{R}_1(\tau), \mathbf{p}_1-\Delta\mathbf{p}_1(\tau); t]f^{(1)}[\mathbf{R}_2-\Delta\mathbf{R}_2(\tau), \mathbf{p}_2-\Delta\mathbf{p}_2(\tau); t]$$
$$-g_0^{(2)}(\mathbf{R}_1, \mathbf{R}_2)f^{(1)}(\mathbf{R}_1, \mathbf{p}_1; t)f^{(1)}(\mathbf{R}_2, \mathbf{p}_2; t)\}\,d\mathbf{R}_2 d\mathbf{p}_2. \tag{14}$$

Due to the discontinuous nature of the square-well potential the momentum changes occur only at $R_{12}=\sigma_1$ and $R_{12}=\sigma_2$. Hence, by coarse graining in the limit $\tau\to 0+$, the collision integral Ω_1 will be seen to equal zero except for $R_{12}=\sigma_1$ or $\sigma_2[\Delta\mathbf{R}(\tau)\to 0$ as $\tau\to 0+]$. To evaluate Ω_1, the integral is divided into three partial collisions resulting from

(a) hard-core collisions, $R_{12}=\sigma_1$;
(b) particle 1 entering the "square-well" of particle 2, $R_{12}=\sigma_2$;
(c) particle 1 leaving the "square-well" of particle 2, $R_{12}=\sigma_2$.

Furthermore, the term due to (c) can be divided into two parts: one part resulting when the relative kinetic energy of two particles is greater than the depth of the attractive well, and the other part resulting when the relative kinetic energy is less than the depth of the attractive well—the latter can be called a "bound particle." Hence, with the above subdivision, we write

$$\Omega_1=\Omega_1^{(1)}+\Omega_1^{(2)}+\Omega_1^{(3)}+\Omega_1^{(4)}. \tag{15}$$

Transforming the coordinates $\mathbf{R}_1$, $\mathbf{R}_2$ to $\mathbf{R}_1$, $\mathbf{R}_{12}$ and considering the limit as $\tau\to 0+$ results in the following collisional shells for each type partial collision: $d\mathbf{R}_2=d\mathbf{R}_{12}=(\tau\mathbf{g}\cdot\mathbf{k})\sigma_1^2 d\mathbf{k}$ for hard core collision $(\Omega_1^{(1)})$, $d\mathbf{R}_2=d\mathbf{R}_{12}=(\tau\mathbf{g}\cdot\mathbf{k})\sigma_2^2 d\mathbf{k}$ for each type of partial collision occurring at the "square-well" brink $(\Omega_1^{(2)}, \Omega_1^{(3)}, \Omega_1^{(4)})$, where $\mathbf{g}=(\mathbf{p}_2/m)-(\mathbf{p}_1/m)$ and $\mathbf{k}$ is a unit vector in the direction of the line of centers of the colliding spheres at the instant of collision. Equation (15) can now be written, with constraints appropriate to each type collision, as

Hard-core collision $(\Omega_1^{(1)})$:

$$\Omega_1=\sigma_1^2(N-1)\iint_{\mathbf{g}\cdot\mathbf{k}>0}[f^{(1)}(\mathbf{R}_1,\ \mathbf{p}_1-\Delta\mathbf{p}_1^{(1)};\ t)f^{(1)}(\mathbf{R}_1+\sigma_1\mathbf{k},\ \mathbf{p}_2-\Delta\mathbf{p}_2^{(1)};\ t)-f^{(1)}(\mathbf{R}_1,\ \mathbf{p}_1;\ t)f^{(1)}(\mathbf{R}_1+\sigma_1\mathbf{k},\ \mathbf{p}_2;\ t)]$$
$$\times g_0^{(2)}(\mathbf{R}_1,\ \mathbf{R}_1+\sigma_1\mathbf{k})\mathbf{g}\cdot\mathbf{k}d\mathbf{k}d\mathbf{p}_2.$$

Type-*a* collision $(\Omega_1^{(2)})$:

$$+\sigma_2^2(N-1)\iint_{\mathbf{g}\cdot\mathbf{k}>0}[f^{(1)}(\mathbf{R}_1,\ \mathbf{p}_1-\Delta\mathbf{p}_1^{(2)};\ t)f^{(1)}(\mathbf{R}_1+\sigma_2\mathbf{k},\ \mathbf{p}_2-\Delta\mathbf{p}_2^{(2)};\ t)\ \exp(\epsilon/kT)$$
$$-f^{(1)}(\mathbf{R}_1,\ \mathbf{p}_1;\ t)f^{(1)}(\mathbf{R}_1+\sigma_2\mathbf{k},\ \mathbf{p}_2;\ t)]g_0^{(2)*}(\mathbf{R}_1,\ \mathbf{R}_1+\sigma_2\mathbf{k})\mathbf{g}\cdot\mathbf{k}d\mathbf{k}d\mathbf{p}_2.$$

Type-*b* collision $(\Omega_1^{(3)})$:

$$+\sigma_2^2(N-1)\iint_{\mathbf{g}\cdot\mathbf{k}<-(4\epsilon/m)^{\frac{1}{2}}}[f^{(1)}(\mathbf{R}_1,\ \mathbf{p}_1-\Delta\mathbf{p}_1^{(3)};\ t]f^{(1)}(\mathbf{R}_1+\sigma_2\mathbf{k},\ \mathbf{p}_2-\Delta\mathbf{p}_2^{(3)};\ t)\ \exp(-\epsilon/kT)$$
$$-f^{(1)}(\mathbf{R}_1,\ \mathbf{p}_1;\ t)f^{(1)}(\mathbf{R}_1+\sigma_2\mathbf{k},\ \mathbf{p}_2;\ t)]g_0^{(2)}(\mathbf{R}_1,\ \mathbf{R}_1+\sigma_2\mathbf{k})\mathbf{g}\cdot\mathbf{k}d\mathbf{k}d\mathbf{p}_2.$$

Type-*c* collision $(\Omega_1^{(4)})$:

$$+\sigma_2^2(N-1)\iint_{-(4\epsilon/m)^{\frac{1}{2}}<\mathbf{g}\cdot\mathbf{k}<0}[f^{(1)}(\mathbf{R}_1,\ \mathbf{p}_1-\Delta\mathbf{p}_1^{(4)};\ t)f^{(1)}(\mathbf{R}_1+\sigma_2\mathbf{k},\ \mathbf{p}_2-\Delta\mathbf{p}_2^{(4)};\ t)$$
$$-f^{(1)}(\mathbf{R}_1,\ \mathbf{p}_1;\ t)f^{(1)}(\mathbf{R}_1+\sigma_2\mathbf{k},\ \mathbf{p}_2;\ t)]g_0^{(2)}(\mathbf{R}_1,\ \mathbf{R}_1+\sigma_2\mathbf{k})\mathbf{g}\cdot\mathbf{k}d\mathbf{k}d\mathbf{p}_2. \tag{16}$$

The factor $\exp(-\epsilon/kT)$ arises from the use of the relation $g_0^{(2)}(\mathbf{R}_1,\ \mathbf{R}_1+\sigma_2\mathbf{k})/g_0^{(2)*}(\mathbf{R}_1,\ \mathbf{R}_1+\sigma_2\mathbf{k})=\exp(+\epsilon/kT)$, where $g_0^{(2)}$ is the pair correlation function at $\sigma_2-\delta$ and $g_0^{(2)*}$ is the pair correlation function at $\sigma_2+\delta$ with $\delta\to 0+$.

Consider now the integral Ω_2. By integration over the primed coordinates

$$\Omega_2=\frac{N-1}{\tau}\iiint\left(\frac{\mathbf{p}_1}{m}\cdot\nabla_{R1}+\frac{\mathbf{p}_2}{m}\cdot\nabla_{R2}\right)f^{(2)}(\mathbf{R}_1,\ \mathbf{R}_2,\ \mathbf{p}_1,\ \mathbf{p}_2;\ t+s)dsd\mathbf{R}_2d\mathbf{p}_2. \tag{17}$$

The distribution functions are slowly varying in space so that $f^{(2)}(t+s)$ may be expanded in a Taylor's series about $f^{(2)}(t)$ and terms of higher order than the gradient of $f^{(2)}(t)$ neglected. With this substitution, Eq. (17) becomes

$$\Omega_2=(N-1)\iint[(\mathbf{p}_1/m)\cdot\nabla_{R_1}+(\mathbf{p}_2/m)\cdot\nabla_{R_2}]f^{(2)}(\mathbf{R}_1\ \mathbf{R}_2,\ \mathbf{p}_1,\ \mathbf{p}_2;\ t)d\mathbf{R}_2d\mathbf{p}_2, \tag{18}$$

where the integration over ds simply cancels τ since $f^{(2)}(t)$ is independent of s. By again transforming $\mathbf{R}_1$, $\mathbf{R}_2$ $\mathbf{R}_1$, $\mathbf{R}_{12}$, Eq. (18) becomes

$$\Omega_2=(N-1)\iint_{R_{12}\geq\sigma_1}\mathbf{g}\cdot\nabla_{R12}f^{(2)}(\mathbf{R}_1,\ \mathbf{R}_1+\mathbf{R}_{12},\ \mathbf{p}_1,\ \mathbf{p}_2;\ t)d\mathbf{R}_{12}d\mathbf{p}_2, \tag{19}$$

where the constraint $R_{12}\geq\sigma_1$ is due to the hard core of the square-well model. We can transform Eq. (20) into a surface integral, but in so doing we must remember that $f^{(2)}$ has a discontinuity at $R_{12}=\sigma_2$. We must write

$$\int_{R_{12}\geq\sigma_1}\nabla_{R12}f^{(2)}(\mathbf{R}_{12})d\mathbf{R}_{12}=\int_{\sigma_2-\delta\geq R_{12}\geq\sigma_1}\nabla_{R12}f^{(2)}(\mathbf{R}_{12})d\mathbf{R}_{12}+\int_{R_{12}\geq\sigma_2+\delta}\nabla_{R12}f^{(2)}(\mathbf{R}_{12})d\mathbf{R}_{12}, \tag{20}$$

where $\delta \to 0+$. Now both integrals on the right-hand side of Eq. (20) are integrated over an interval in which $f^{(2)}$ is continuous, and, consequently, we can transform the volume integrals. Since $f^{(2)}$ is zero at the boundaries of the system

$$\int \nabla_{R_{12}} f^{(2)}(\mathbf{R}_{12})\, d\mathbf{R}_{12} = \sigma_1^2 \int f^{(2)}(\sigma_1 \mathbf{k})\, \mathbf{k} d\mathbf{k} - \sigma_2^2 \int f^{(2)}[(\sigma_2 - \delta)\mathbf{k}]\mathbf{k} d\mathbf{k} + \sigma_2^2 \int f^{(2)}[(\sigma_2 + \delta)\mathbf{k}]\mathbf{k} d\mathbf{k}$$

and

$$\begin{aligned}
\Omega_2 = {} & \sigma_1^2 (N-1) \iint g_0^{(2)}(\mathbf{R}_1, \mathbf{R}_1 + \sigma_1 \mathbf{k}) f^{(1)}(\mathbf{R}_1, \mathbf{p}_1; t) f^{(1)}(\mathbf{R}_1 + \sigma_1 \mathbf{k}, \mathbf{p}_2; t)\, \mathbf{g} \cdot \mathbf{k} d\mathbf{k} d\mathbf{p}_2 \\
& - \sigma_2^2 (N-1) \iint g_0^{(2)}(\mathbf{R}_1, \mathbf{R}_1 + \sigma_2 \mathbf{k}) f^{(1)}(\mathbf{R}_1, \mathbf{p}_1; t) f^{(1)}(\mathbf{R}_1 + \sigma_2 \mathbf{k}, \mathbf{p}_2; t)\, \mathbf{g} \cdot \mathbf{k} d\mathbf{k} d\mathbf{p}_2 \\
& + \sigma_2^2 (N-1) \iint g_0^{(2)*}(\mathbf{R}_1, \mathbf{R}_1 + \sigma_2 \mathbf{k}) f^{(1)}(\mathbf{R}_1, \mathbf{p}_1; t) f^{(1)}(\mathbf{R}_1 + \sigma_2 \mathbf{k}, \mathbf{p}_2; t)\, \mathbf{g} \cdot \mathbf{k} d\mathbf{k} d\mathbf{p}_2, \qquad (21)
\end{aligned}$$

where the integration is over the surface of a sphere. The sphere can be divided into two hemispheres with the result that

$$\begin{aligned}
\Omega_2 = {} & \sigma_1^2 (N-1) \iint_{\mathbf{g} \cdot \mathbf{k} > 0} g_0^{(2)}(\mathbf{R}_1, \mathbf{R}_1 + \sigma_1 \mathbf{k}) f^{(1)}(\mathbf{R}_1, \mathbf{p}_1; t) f^{(1)}(\mathbf{R}_1 + \sigma_1 \mathbf{k}, \mathbf{p}_2; t)\, \mathbf{g} \cdot \mathbf{k} d\mathbf{k} d\mathbf{p}_2 \\
& + \sigma_1^2 (N-1) \iint_{\mathbf{g} \cdot \mathbf{k} < 0} g_0^{(2)}(\mathbf{R}_1, \mathbf{R}_1 + \sigma_1 \mathbf{k}) f^{(1)}(\mathbf{R}_1, \mathbf{p}_1, t) f^{(1)}(\mathbf{R}_1 + \sigma_1 \mathbf{k}, \mathbf{p}_2; t)\, \mathbf{g} \cdot \mathbf{k} d\mathbf{k} d\mathbf{p}_2 \\
& + \sigma_2^2 (N-1) \iint_{\mathbf{g} \cdot \mathbf{k} > 0} g_0^{(2)*}(\mathbf{R}_1, \mathbf{R}_1 + \sigma_2 \mathbf{k}) f^{(1)}(\mathbf{R}_1, \mathbf{p}_1; t) f^{(1)}(\mathbf{R}_1 + \sigma_2 \mathbf{k}, \mathbf{p}_2; t)\, \mathbf{g} \cdot \mathbf{k} d\mathbf{k} d\mathbf{p}_2 \\
& + \sigma_2^2 (N-1) \iint_{\mathbf{g} \cdot \mathbf{k} < 0} g_0^{(2)*}(\mathbf{R}_1, \mathbf{R}_1 + \sigma_2 \mathbf{k}) f^{(1)}(\mathbf{R}_1, \mathbf{p}_1; t) f^{(1)}(\mathbf{R}_1 + \sigma_2 \mathbf{k}, \mathbf{p}_2; t)\, \mathbf{g} \cdot \mathbf{k} d\mathbf{k} d\mathbf{p}_2 \\
& - \sigma_2^2 (N-1) \iint_{\mathbf{g} \cdot \mathbf{k} > 0} g_0^{(2)}(\mathbf{R}_1, \mathbf{R}_1 + \sigma_2 \mathbf{k}) f^{(1)}(\mathbf{R}_1, \mathbf{p}_1; t) f^{(1)}(\mathbf{R}_1 + \sigma_2 \mathbf{k}, \mathbf{p}_2; t)\, \mathbf{g} \cdot \mathbf{k} d\mathbf{k} d\mathbf{p}_2 \\
& - \sigma_2^2 (N-1) \iint_{\mathbf{g} \cdot \mathbf{k} < 0} g_0^{(2)}(\mathbf{R}_1, \mathbf{R}_1 + \sigma_2 \mathbf{k}) f^{(1)}(\mathbf{R}_1, \mathbf{p}_1; t) f^{(1)}(\mathbf{R}_1 + \sigma_2 \mathbf{k}, \mathbf{p}_2; t)\, \mathbf{g} \cdot \mathbf{k} d\mathbf{k} d\mathbf{p}_2 \\
= {} & \sigma_1^2 (N-1) \iint_{\mathbf{g} \cdot \mathbf{k} > 0} [g_0^{(2)}(\mathbf{R}_1, \mathbf{R}_1 + \sigma_1 \mathbf{k}) f^{(1)}(\mathbf{R}_1 + \sigma_1 \mathbf{k}, \mathbf{p}_2; t) - g_0^{(2)}(\mathbf{R}_1, \mathbf{R}_1 - \sigma_1 \mathbf{k}) f^{(1)}(\mathbf{R}_1 - \sigma_1 \mathbf{k}, \mathbf{p}_2; t)] \\
& \times f^{(1)}(\mathbf{R}_1, \mathbf{p}_1; t)\, \mathbf{g} \cdot \mathbf{k} d\mathbf{k} d\mathbf{p}_2 \\
& + \sigma_2^2 (N-1) \iint_{\mathbf{g} \cdot \mathbf{k} > 0} [g_0^{(2)*}(\mathbf{R}_1, \mathbf{R}_1 + \sigma_2 \mathbf{k}) f^{(1)}(\mathbf{R}_1 + \sigma_2 \mathbf{k}, \mathbf{p}_2; t) - g_0^{(2)*}(\mathbf{R}_1, \mathbf{R}_1 - \sigma_2 \mathbf{k}) f^{(1)}(\mathbf{R}_1 - \sigma_2 \mathbf{k}, \mathbf{p}_2; t)] \\
& \times f^{(1)}(\mathbf{R}_1, \mathbf{p}_1; t)\, \mathbf{g} \cdot \mathbf{k} d\mathbf{k} d\mathbf{p}_2 \\
& + \sigma_2^2 (N-1) \iint_{\mathbf{g} \cdot \mathbf{k} < -(4\epsilon/m)^{\frac{1}{2}}} [g_0^{(2)}(\mathbf{R}_1, \mathbf{R}_1 + \sigma_2 \mathbf{k}) f^{(1)}(\mathbf{R}_1 + \sigma_2 \mathbf{k}, \mathbf{p}_2; t) - g_0^{(2)}(\mathbf{R}_1, \mathbf{R}_1 - \sigma_2 \mathbf{k}) f^{(1)}(\mathbf{R}_1 - \sigma_2 \mathbf{k}, \mathbf{p}_2; t)] \\
& \times f^{(1)}(\mathbf{R}_1, \mathbf{p}_1; t)\, \mathbf{g} \cdot \mathbf{k} d\mathbf{k} d\mathbf{p}_2 \\
& + \sigma_2^2 (N-1) \iint_{-(4\epsilon/m)^{\frac{1}{2}} < \mathbf{g} \cdot \mathbf{k} < 0} g_0^{(2)}(\mathbf{R}_1, \mathbf{R}_1 + \sigma_2 \mathbf{k}) f^{(1)}(\mathbf{R}_1 + \sigma_2 \mathbf{k}, \mathbf{p}_2; t) - g_0^{(2)}(\mathbf{R}_1, \mathbf{R}_1 - \sigma_2 \mathbf{k}) f^{(1)}(\mathbf{R}_1 - \sigma_2, \mathbf{p}_2; t)] \\
& \times f^{(1)}(\mathbf{R}_1, \mathbf{p}_1; t)\, \mathbf{g} \cdot \mathbf{k} d\mathbf{k}_1 d\mathbf{p}_2. \qquad (22)
\end{aligned}$$

Note that when the term with the constraint $\mathbf{g} \cdot \mathbf{k} < 0$ is divided into two terms, with the constraints $\mathbf{g} \cdot \mathbf{k} < -(4\epsilon/m)^{\frac{1}{2}}$ and $-(4\epsilon/m)^{\frac{1}{2}} < \mathbf{g} \cdot \mathbf{k} < 0$, the sign is reversed. This is because on the hemisphere denoted by $\mathbf{g} \cdot \mathbf{k} < 0$ the interval of integration is from $\theta = \cos^{-1}(0)$ to $\theta = \cos^{-1}(-1)$, while the term appearing in Ω_1, with the constraint $\mathbf{g} \cdot \mathbf{k} < -(4\epsilon/m)^{\frac{1}{2}}$ is integrated over the interval from $\theta = \cos^{-1}(-1)$ to $\theta = \cos^{-1}[-(1/g)(4\epsilon/m)^{\frac{1}{2}}]$. Hence, the limits are

reversed, and we must multiply by minus one the terms acquired by dividing the $\mathbf{g}\cdot\mathbf{k}<0$ interval in order that the constraints, $\mathbf{g}\cdot\mathbf{k}<-(4\epsilon/m)^{\frac{1}{2}}$ and $-(4\epsilon/m)^{\frac{1}{2}}<\mathbf{g}\cdot\mathbf{k}<0$, have the same meaning in Ω_2 as they have in Ω_1.

Equation (16) is now added to Eq. (22).

$$\Omega=\Omega_1+\Omega_2$$

$$=\sigma_1^2(N-1)\iint_{\mathbf{g}\cdot\mathbf{k}>0}[g_0^{(2)}(\mathbf{R}_1,\mathbf{R}_1+\sigma_1\mathbf{k})f^{(1)}(\mathbf{R}_1,\mathbf{p}_1-\Delta\mathbf{p}_1^{(1)};t)f^{(1)}(\mathbf{R}_1+\sigma_1\mathbf{k},\mathbf{p}_2-\Delta\mathbf{p}_2^{(1)};t)-g_0^{(2)}(\mathbf{R}_1,\mathbf{R}_1-\sigma_1\mathbf{k})$$
$$\times f^{(1)}(\mathbf{R}_1,\mathbf{p}_1;t)f^{(1)}(\mathbf{R}_1-\sigma_1\mathbf{k},\mathbf{p}_2;t)]\mathbf{g}\cdot\mathbf{k}d\mathbf{k}d\mathbf{p}_2$$

$$+\sigma_2^2(N-1)\iint_{\mathbf{g}\cdot\mathbf{k}>0}[g_0^{(2)}(\mathbf{R}_1,\mathbf{R}_1+\sigma_2\mathbf{k})f^{(1)}(\mathbf{R}_1,\mathbf{p}_1-\Delta\mathbf{p}_1^{(2)};t)f^{(1)}(\mathbf{R}_1+\sigma_2\mathbf{k},\mathbf{p}_2-\Delta\mathbf{p}_2^{(2)};t)-g_0^{(2)*}(\mathbf{R}_1,\mathbf{R}_1-\sigma_1\mathbf{k})$$
$$\times f^{(1)}(\mathbf{R}_1,\mathbf{p}_1;t)f^{(1)}(\mathbf{R}_1-\sigma_2\mathbf{k},\mathbf{p}_2;t)]\mathbf{g}\cdot\mathbf{k}d\mathbf{k}d\mathbf{p}_2$$

$$+\sigma_2^2(N-1)\iint_{\mathbf{g}\cdot\mathbf{k}<-(4\epsilon/m)^{\frac{1}{2}}}[g_0^{(2)*}(\mathbf{R}_1,\mathbf{R}_1+\sigma_2\mathbf{k})f^{(1)}(\mathbf{R}_1,\mathbf{p}_1-\Delta\mathbf{p}_1^{(3)};t)f^{(1)}(\mathbf{R}_1+\sigma_2\mathbf{k},\mathbf{p}_2-\Delta\mathbf{p}_2^{(3)};t)-g_0^{(2)}(\mathbf{R}_1,\mathbf{R}_1-\sigma_1\mathbf{k})$$
$$\times f^{(1)}(\mathbf{R}_1,\mathbf{p}_1;t)f^{(1)}(\mathbf{R}_1-\sigma_2\mathbf{k},\mathbf{p}_2;t)]\mathbf{g}\cdot\mathbf{k}d\mathbf{k}d\mathbf{p}_2$$

$$+\sigma_2^2(N-1)\iint_{-(4\epsilon/m)^{\frac{1}{2}}<\mathbf{g}\cdot\mathbf{k}<0}[g_0^{(2)}(\mathbf{R}_1,\mathbf{R}_1+\sigma_2\mathbf{k})f^{(1)}(\mathbf{R}_1,\mathbf{p}_1-\Delta\mathbf{p}_1^{(4)};t)f^{(1)}(\mathbf{R}_1+\sigma_2\mathbf{k},\mathbf{p}_2-\Delta\mathbf{p}_2^{(4)};t)-g_0^{(2)}(\mathbf{R}_1,\mathbf{R}_1-\sigma_2\mathbf{k})$$
$$\times f^{(1)}(\mathbf{R}_1,\mathbf{p}_1;t)f^{(1)}(\mathbf{R}_1-\sigma_2\mathbf{k},\mathbf{p}_2;t)]\mathbf{g}\cdot\mathbf{k}d\mathbf{k}d\mathbf{p}_2. \quad (23)$$

Equation (23) representing the collisional contribution to the transport equation is seen to be the Enskog result for hard spheres plus three partial collision terms due to the attractive potential of the "square well." All four integrals have the Enskog type kernel. One of us (J.V.S.) has shown that the same result could be derived using the concept of direct and inverse collisions which Enskog used in formulating his theory of a dense hard-sphere fluid.

Ω can be written, following Rice and Allnatt, as

$$\Omega=\Omega_H+\Omega_s, \quad (24)$$

where Ω_H is the hard-core contribution, given by the first integral in Eq. (23), and Ω_s, the soft collision contribution due to the attractive potential, is given by the sum of the last three integrals.

IV. HEAT FLUX AND STRESS TENSOR FOR THE DENSE "SQUARE-WELL" FLUID

Irving and Kirkwood,[10] using Kirkwood's postulate[4] that an observable quantity be identified with the ensemble average of the corresponding time coarse grained microscopic variables, derive the following relations for the stress tensor $\mathfrak{d}$ and heat flux $\mathbf{q}$:

$$\mathfrak{d}_K(\mathbf{R}_1;t)=-\sum_{k=1}^{N}\int\cdots\int\tau^{-1}\int_0^\tau[(\mathbf{p}_k/m)-\mathbf{u}][(\mathbf{p}_k/m)-\mathbf{u}]\delta(\mathbf{R}_k-\mathbf{R}_1)f^{(N)}dsd\mathbf{R}d\mathbf{P}, \quad (25)$$

$$\mathbf{q}_K(\mathbf{R}_1;t)=\tfrac{1}{2}m\sum_{k=1}^{N}\int\cdots\int\tau^{-1}\int_0^\tau[(\mathbf{p}_k/m)-\mathbf{u}]\,|\,(\mathbf{p}_k/m)-\mathbf{u}\,|^2\delta(\mathbf{R}_k-\mathbf{R}_1)f^{(N)}dsd\mathbf{R}d\mathbf{P}, \quad (26)$$

$$\mathfrak{d}_V(\mathbf{R}_1;t)=\tfrac{1}{2}\sum_{j=1}^{N}\sum_{k=1}^{N}\int\cdots\int\tau^{-1}\int_0^\tau\mathbf{R}_{jk}\nabla V(R_{jk})\delta(\mathbf{R}_j-\mathbf{R}_2)\delta(\mathbf{R}_k-\mathbf{R}_1)f^{(N)}dsd\mathbf{R}d\mathbf{P}d\mathbf{R}_{12}, \quad (27)$$

$$\mathbf{q}_V(\mathbf{R}_1;t)=\sum_{j=1}^{N}\sum_{k=1}^{N}2\tau^{-1}\int_0^\tau\{[V(R_{jk})\mathbf{1}-\mathbf{R}_{jk}\nabla V(R_{jk})]$$
$$\times[\langle(\mathbf{p}_k/m)\delta(\mathbf{R}_k-\mathbf{R}_1)\delta(\mathbf{R}_j-\mathbf{R}_1);f^{(N)}\rangle-\mathbf{u}\langle\delta(\mathbf{R}_k-\mathbf{R}_1)\delta(\mathbf{R}_j-\mathbf{R}_1);f^{(N)}\rangle]\}dsd\mathbf{R}_{12}, \quad (28)$$

where the notation

$$\langle\alpha;f^{(N)}\rangle=\int\cdots\int\alpha(\mathbf{R},\mathbf{P})f^{(N)}d\mathbf{R}d\mathbf{P} \quad (29)$$

has been used. $\mathfrak{d}_K$ and $\mathfrak{d}_v$ are the kinetic and intermolecular force contributions to the stress tensor, and $\mathbf{q}_K$ and $\mathbf{q}_V$ are the kinetic and intermolecular force contributions to the heat flux. By direct integration the equations can be reduced to pair distribution functions which can then be related to the singlet distribution functions.

[10] J. H. Irving and J. G. Kirkwood, J. Chem. Phys. **18**, 817 (1950).

Equation (23) is solved by a procedure following the Chapman-Enskog solution of the Maxwell-Boltzmann equation.[1] The singlet distribution function is written as

$$f^{(1)}=f_0^{(1)}(1+\phi), \tag{30}$$

where $f_0^{(1)}$ is the zero-order local equilibrium singlet distribution function,

$$f_0^{(1)}=[(2\pi mkT)^{-\frac{3}{2}}/v]\exp[-(\mathbf{p}_1-m\mathbf{u})^2/2mkT], \tag{31}$$

and ϕ is the perturbation. The perturbation function ϕ can be shown to have the form

$$\phi=\mathbf{A}\cdot\nabla_{R_1}\ln T+\mathbf{B}:\nabla_{R_1}\mathbf{u}, \tag{32}$$

where $\mathbf{A}$ and $\mathbf{B}$ are evaluated in terms of Sonine polynomials using a variational method introduced by Hirschfelder and Curtiss.[3] From detailed calculations, to be presented in Appendix I, the values of $\mathbf{A}$ and $\mathbf{B}$ are found to be

$$\mathbf{A}=a^{(1)}(\tfrac{5}{2}-\mathbf{W}^2)\mathbf{W}, \tag{33}$$

$$\mathbf{B}=b_0(\mathbf{WW}-\tfrac{1}{3}W^2\mathbf{1}), \tag{34}$$

where

$$a^{(1)}=\frac{(15/4v)(1+\frac{3}{5}b\rho\Lambda)+(3\pi^{\frac{3}{2}}/2v^2)\sigma_2^3(N-1)g_0^{(2)}(\sigma_2)s^2\exp(-s^2)\left[\frac{\pi^{\frac{1}{2}}}{2}+2\exp(s^2)\int_s^\infty\exp(-x^2)x^2dx\right]}{\sqrt{2}[8(N-1)\pi^{\frac{3}{2}}/v^2)]\{\lambda+\sigma_2^2g_0^{(2)}(\sigma_2)\exp(-s^2)\frac{1}{8}\frac{1}{2}s^4\}}, \tag{35}$$

$$b_0^{(1)}=\frac{-\frac{5}{\sqrt{2}v}\left(\frac{m}{2kT}\right)^{\frac{1}{2}}(1+\frac{2}{5}b\rho\Lambda)-\frac{4\pi^{\frac{3}{2}}}{3\sqrt{2}v^2}\left(\frac{m}{2kT}\right)^{\frac{1}{2}}\sigma_2^3(N-1)g_0^{(2)}(\sigma_2)s^2\exp(-s^2)\left[\frac{\pi^{\frac{1}{2}}}{2}+2\exp(s^2)\int_s^\infty\exp(-x^2)x^2dx\right]}{[8(N-1)\pi^{\frac{3}{2}}/v^2]\{\lambda+\sigma_2^2g_0^{(2)}(\sigma_2)\exp(-s^2)(s^4/12)\}}, \tag{36}$$

$$\lambda=\tfrac{1}{2}\{\sigma_1^2g_0^{(2)}(\sigma_1)+\sigma_2^2g_0^{(2)}(\sigma_2)[\exp(-s^2)+1]\}-\sigma_2^2g_0^{(2)}(\sigma_2)\exp(-s^2)\left\{\frac{1}{2}+\frac{s^2}{4}+\int_0^\infty\exp(-x^2)x^2(x^2+s^2)^{\frac{1}{2}}dx\right\}, \tag{37}$$

$$\mathbf{W}=(m/2kT)^{\frac{1}{2}}[(\mathbf{p}/m)-\mathbf{u}], \tag{38}$$

$$s=(\epsilon/kT)^{\frac{1}{2}}, \tag{39}$$

$$b\rho\Lambda=(2\pi/3v)(N-1)\{\sigma_1^3g_0^{(2)}(\sigma_1)+\sigma_2^3g_0^{(2)}(\sigma_2)[\exp(-s^2)-1]\}. \tag{40}$$

In Eqs. (33)–(40), $\mathbf{u}$ is the local hydrodynamic velocity, $T(\mathbf{R}_1;t)$ the local temperature, $\Gamma(\nu,s^2)$ an incomplete gamma function, $W_{\nu,\mu}(s^2)$ a Whittaker function, and $K_n(s^2/2)$ a Bessel function of the third kind with $K_n'(s^2/2)$ the derivative of the same.[11]

When time-smoothed over the interval $\tau\to0+$, Eq. (25) and Eq. (26) reduce to

$$\lim_{\tau\to0+}\mathfrak{d}_K=-N\int\bar{f}^{(1)}(1)\left(\frac{\mathbf{p}_1}{m}-\mathbf{u}\right)\left(\frac{\mathbf{p}_1}{m}-\mathbf{u}\right)d\mathbf{p}_1, \tag{41}$$

$$\lim_{\tau\to0+}\mathbf{q}_K=\frac{mN}{2}\int\bar{f}^{(1)}(1)\left|\frac{\mathbf{p}_1}{m}-\mathbf{u}\right|^2\left(\frac{\mathbf{p}_1}{m}-\mathbf{u}\right)d\mathbf{p}_1. \tag{42}$$

Equation (30) is substituted into Eqs. (41)–(42), and the integrations are carried out leading to the expressions

$$\mathbf{q}_K=-\frac{5}{4}\frac{kN}{v}\left(\frac{2kT}{m}\right)^{\frac{1}{2}}a^{(1)}\nabla_{R_1}T \tag{43}$$

$$\mathfrak{d}_K=-\frac{kT}{v}Nb_0^{(1)}[\tfrac{1}{2}(\nabla_{R_1}\mathbf{u}+\nabla_{R_1}\mathbf{u}^\dagger)-\tfrac{1}{3}\nabla_{R_1}\cdot\mathbf{u}\mathbf{1}]-\frac{kT}{v}N\mathbf{1}=-\frac{kT}{v}Nb_0^{(1)}(\boldsymbol{\varepsilon}-\tfrac{1}{3}\nabla_{R_1}\cdot\mathbf{u}\mathbf{1})-\frac{kT}{v}N\mathbf{1}. \tag{44}$$

[11] These higher transcendental functions are discussed in detail in A. Erdelyi, W. Magnus, F. Oberhettinger, and F. Tricomi, *Higher Transcendental Functions* (McGraw-Hill Book Company, Inc., New York, 1953), Vols. I and II.

The dagger designates the transpose of $\nabla_{R_1}\mathbf{u}$ and $\boldsymbol{\varepsilon}$ is the rate of strain tensor. Comparison of the phenomenological equations

$$\mathfrak{d}=-[P+(\tfrac{2}{3}\eta_K+\tfrac{2}{3}\eta_v-\Phi)\nabla_{R_1}\cdot\mathbf{u}]\mathbf{1}+2(\eta_K+\eta_v)\boldsymbol{\varepsilon} \tag{45}$$

$$\mathbf{q}=-(\kappa_K+\kappa_V)\nabla_{R_1}T, \tag{46}$$

with Eqs. (43)–(44) leads to the results

$$\kappa_K=\tfrac{5}{4}(kN/v)(2kT/m)^{\frac{1}{2}}a^{(1)}, \tag{47}$$

$$\eta_K=-(kT/2v)Nb_0^{(1)}, \tag{48}$$

where η_K is the kinetic contribution to the viscosity, κ_K is the kinetic contribution to the heat conductivity, and p is the hydrostatic pressure.

Turning now to Eq. (27) and integrating over $d\mathbf{R}_1\cdots d\mathbf{R}_N$, $d\mathbf{p}_3\cdots d\mathbf{p}_N$, the resulting relation is

$$\mathfrak{d}_V=\tfrac{1}{2}[N(N-1)]\iint\tau^{-1}\int_0^\tau\mathbf{R}_{12}\nabla V(R_{12})f^{(2)}(\mathbf{R}_1,\mathbf{R}_1+\mathbf{R}_{12},\mathbf{p}_1,\mathbf{p}_2;t)\,ds d\mathbf{p}_1 d\mathbf{p}_2 d\mathbf{R}_{12}. \tag{49}$$

In the limit as $\tau\to 0+$, $-\int\nabla V(R_{12})ds$ is equal to the change of momentum in a binary collision. As in Sec. III, there are four "partial" collisions to consider:

(1) hard core, $\mathbf{g}\cdot\mathbf{k}>0$, $R_{12}=\sigma_1$;
(2) type a (entering the square well), $\mathbf{g}\cdot\mathbf{k}>0$, $R_{12}=\sigma_2$;
(3) type b (leaving the square well), $\mathbf{g}\cdot\mathbf{k}<-(4\epsilon/m)^{\frac{1}{2}}$, $R_{12}=\sigma_2$;
(4) type c ("bound particle"), $-(4\epsilon/m)^{\frac{1}{2}}<\mathbf{g}\cdot\mathbf{k}<0$, $R_{12}=\sigma_2$. Hence, Eq. (49) reduces to

$$\begin{aligned}\lim_{\tau\to 0}\mathfrak{d}_V(\mathbf{R}_1;t)=&\tfrac{1}{2}N(N-1)\iiint_{\mathbf{g}\cdot\mathbf{k}>0}\sigma_1^3\mathbf{k}\Delta\mathbf{p}_{12}^{(1)}\bar{f}^{(2)}(\mathbf{R}_1,\mathbf{R}_1+\sigma_1\mathbf{k},\mathbf{p}_1,\mathbf{p}_2;t)\mathbf{g}\cdot\mathbf{k}\,d\mathbf{k}\,d\mathbf{p}_1 d\mathbf{p}_2\\&+\tfrac{1}{2}N(N-1)\iiint_{\mathbf{g}\cdot\mathbf{k}>0}\sigma_2^3\mathbf{k}\Delta\mathbf{p}_{12}^{(2)}\bar{f}^{(2)}(\mathbf{R}_1,\mathbf{R}_1+\sigma_2\mathbf{k},\mathbf{p}_1,\mathbf{p}_2;t)\mathbf{g}\cdot\mathbf{k}\,d\mathbf{k}\,d\mathbf{p}_1 d\mathbf{p}_2\\&+\tfrac{1}{2}N(N-1)\iiint_{\mathbf{g}\cdot\mathbf{k}<-(4\epsilon/m)^{\frac{1}{2}}}\sigma_2^3\mathbf{k}\Delta\mathbf{p}_{12}^{(3)}\bar{f}^{(2)}(\mathbf{R}_1,\mathbf{R}_1+\sigma_2\mathbf{k},\mathbf{p}_1,\mathbf{p}_2;t)\mathbf{g}\cdot\mathbf{k}\,d\mathbf{k}\,d\mathbf{p}_1 d\mathbf{p}_2\\&+\tfrac{1}{2}N(N-1)\iiint_{-(4\epsilon/m)^{\frac{1}{2}}<\mathbf{g}\cdot\mathbf{k}<0}\sigma_2^3\mathbf{k}\Delta\mathbf{p}_{12}^{(4)}\bar{f}^{(2)}(\mathbf{R}_1,\mathbf{R}_1+\sigma_2\mathbf{k},\mathbf{p}_1,\mathbf{p}_2;t)\mathbf{g}\cdot\mathbf{k}\,d\mathbf{k}\,d\mathbf{p}_1 d\mathbf{p}_2.\end{aligned} \tag{50}$$

Consideration of the binary dynamics of each partial collision leads to the relations:

(1) hard core, $\Delta\mathbf{p}_{12}^{(1)}=-2m\mathbf{g}\cdot\mathbf{k}\mathbf{k}$;
(2) type a, $\Delta\mathbf{p}_{12}^{(2)}=m\{-\mathbf{g}\cdot\mathbf{k}+[(\mathbf{g}\cdot\mathbf{k})^2+(4\epsilon/m)]^{\frac{1}{2}}\}$;
(3) type b, $\Delta\mathbf{p}_{12}^{(3)}=m\{-\mathbf{g}\cdot\mathbf{k}-[(\mathbf{g}\cdot\mathbf{k})^2-(4\epsilon/m)]^{\frac{1}{2}}\}\ \mathbf{k}$;
(4) type c, $\Delta\mathbf{p}_{12}^{(4)}=-2m\mathbf{g}\cdot\mathbf{k}\mathbf{k}$. (51)

Replacing $g^{(2)}(\mathbf{R}_1,\mathbf{R}_2,\mathbf{p}_1,\mathbf{p}_2;t)$ by the local equilibrium pair correlation function $g_0^{(2)}(R_{12})$, and expanding $\bar{f}(\mathbf{R}_1+\sigma\mathbf{k},\mathbf{p}_2;t)$ in a Taylor's series around $\mathbf{R}_1$ we find

$$\bar{f}^{(2)}(\mathbf{R}_1,\mathbf{R}_1+\sigma\mathbf{k},\mathbf{p}_1,\mathbf{p}_2;t)=g_0^{(2)}(\sigma)[\bar{f}^{(1)}(\mathbf{R}_1,\mathbf{p}_1;t)\bar{f}^{(1)}(\mathbf{R}_1,\mathbf{p}_2;t)+\bar{f}^{(1)}(\mathbf{R}_1,\mathbf{p}_1;t)\sigma\mathbf{k}\cdot\nabla_{R_1}\bar{f}^{(1)}(\mathbf{R}_1,\mathbf{p}_2;t)]. \tag{52}$$

Equations (51) and (52) are now substituted into Eq. (50), then Eq. (30) used for $f^{(1)}$ with terms of order $\nabla_{R_1}\phi$ neglected. If $f_0^{(1)}$ and ϕ as given by Eqs. (31) and (32) are substituted into the resultant equation, and the integrations carried out explicitly, the following results are obtained:

$$\begin{aligned}\mathfrak{d}=&\mathfrak{d}_K+\mathfrak{d}_V\\=&-\frac{kTN}{v}\mathbf{1}-\frac{NkT}{v}b_0^{(1)}(\boldsymbol{\varepsilon}-\tfrac{1}{3}\nabla_{R_1}\cdot\mathbf{u}\mathbf{1})-\frac{NkT}{v}b\rho\Lambda\mathbf{1}-b_0^{(1)}\frac{8\pi^{\frac{1}{2}}}{15v^2}N(N-1)\left(\frac{4kT}{m}\right)\left\{\frac{\pi^{\frac{1}{2}}}{8}\Lambda\right.\\&\left.+\sigma_2^3g_0^{(2)}(\sigma_2)s^2\exp(-s^2)\left[\frac{\pi^{\frac{1}{2}}}{16}+\frac{\exp(s^2)}{12}\Gamma(\tfrac{5}{2},s^2)-\frac{s^3}{12}\right]\right\}(\boldsymbol{\varepsilon}-\tfrac{1}{3}\nabla_{R_1}\cdot\mathbf{u}\mathbf{1})\\&+[8N(N-1)/15v^2](\pi mkT)^{\frac{1}{2}}\{\sigma_1^4g_0^{(2)}(\sigma_1)+\sigma_2^4g_0^{(2)}(\sigma_2)\exp(-s^2)\Xi(s^2)\}(\boldsymbol{\varepsilon}+\tfrac{1}{2}\nabla_{R_1}\cdot\mathbf{u}\mathbf{1}),\end{aligned} \tag{53}$$

where

$$\Lambda=\{\sigma_1^3 g_0^{(2)}(\sigma_1)+\sigma_2^3 g_0^{(2)}(\sigma_2)[\exp(-s^2)-1]\} \tag{54}$$

$$\Xi(s^2)=\exp(s^2)-(s^2/2)+(s^2/2)\exp(s^2/2)K_1(s^2/2) \tag{55}$$

and

$$\lim_{s\to 0}(s^2/2)\exp(s^2/2)K_1(s^2/2)=-1. \tag{56}$$

In considering the intermolecular force contribution to the heat flux, $\mathbf{q}_v$, it is easily seen that the term involving $V(R_{ij})\mathbf{1}$ is zero, since $\int\int f^{(1)}\mathbf{W}d\mathbf{p}$ vanishes. The other term in Eq. (28) is seen to be

$$\mathbf{q}_V=\sum_{j=1}^{N}\sum_{k=1}^{N}(2\tau)^{-1}\int_0^\tau\int\{[-\mathbf{R}_{jk}\nabla V(R_{jk})]\cdot[\langle(\mathbf{p}_k/m)\delta(\mathbf{R}_k\cdot\mathbf{R}_1)\delta(\mathbf{R}_j-\mathbf{R}_2);f^{(N)}\rangle$$

$$-\mathbf{u}\langle\delta(\mathbf{R}_k-\mathbf{R}_1)\delta(\mathbf{R}_j-\mathbf{R}_2);f^{(N)}\rangle]\}ds d\mathbf{R}_{12}$$

$$=\tfrac{1}{2}N(N-1)\iiint(2\tau)^{-1}\int_0^\tau[-\mathbf{R}_{12}\nabla V(R_{12})]\cdot\left[\frac{\mathbf{p}_1}{m}-\mathbf{u}+\frac{\mathbf{p}_2}{m}-\mathbf{u}\right]f^{(2)}(\mathbf{R}_1,\mathbf{R}_2,\mathbf{p}_1,\mathbf{p}_2;t)d\mathbf{p}_1 d\mathbf{p}_2 ds d\mathbf{R}_{12}. \tag{57}$$

By the use of the same sequence of substitutions and expansions detailed for the calculation of the stress tensor, the heat flux is found to be

$$\mathbf{q}=\mathbf{q}_K+\mathbf{q}_V$$

$$=-\frac{5}{4}\frac{kN}{v}\left(\frac{2kT}{m}\right)^{\frac{1}{2}}a^{(1)}\nabla_{R_1}T-N(N-1)a^{(1)}\frac{k}{v^2}\left(\frac{2\pi kT}{m}\right)^{\frac{1}{2}}\left\{\frac{\pi^{\frac{1}{2}}}{2}\Lambda+\sigma_2^3 g_0^{(2)}(\sigma_2)s^2\exp(-s^2)\right.$$

$$\left.\times\left[\frac{\pi^{\frac{1}{2}}}{4}-\frac{s^3}{3}+\frac{\exp(s^2)}{3}\Gamma(\tfrac{5}{2},s^2)\right]\right\}\nabla_{R_1}T-\tfrac{2}{3}N(N-1)(k/v^2)(\pi kT/m)^{\frac{1}{2}}\{\sigma_1^4 g_0^{(2)}(\sigma_1)+\sigma_2^4 g_0^{(2)}(\sigma_2)\exp(-s^2)\,\Xi(s^2)\}\nabla_{R_1}T, \tag{58}$$

where $\Xi(s^2)$ was defined by Eq. (55) and $a^{(1)}$ is given by Eq. (35).

Thus, comparing Eqs. (53) and (58) with the phenomenological equations which define the thermal conductivity κ, the shear viscosity η, the bulk viscosity Φ, and the pressure p, shows that

$$\kappa=\tfrac{2}{3}N(N-1)\frac{k}{v^2}\left(\frac{\pi kT}{m}\right)^{\frac{1}{2}}\{\sigma_1^4 g_0^{(2)}(\sigma_1)+\sigma_2^4 g_0^{(2)}(\sigma_2)\exp(-s^2)\,\Xi(s^2)\}+\frac{5}{4}\frac{Nk}{v}\left(\frac{2kT}{m}\right)^{\frac{1}{2}}a^{(1)}$$

$$-N(N-1)a^{(1)}\frac{k}{v^2}\left(\frac{2\pi kT}{m}\right)^{\frac{1}{2}}\left\{\frac{\pi^{\frac{1}{2}}}{2}\Lambda+\sigma_2^3 g_0^{(2)}(\sigma_2)s^2\exp(-s^2)\left[\frac{\pi^{\frac{1}{2}}}{4}-\frac{s^3}{3}+\frac{\exp(s^2)}{3}\Gamma(\tfrac{5}{2},s^2)\right]\right\}, \tag{59}$$

$$\eta=\frac{4}{15}\frac{N(N-1)}{v^2}(\pi mkT)^{\frac{1}{2}}\{\sigma_1^4 g_0^{(2)}(\sigma_1)+\sigma_2^4 g_0^{(2)}(\sigma_2)\exp(-s^2)\,\Xi(s^2)\}-\frac{NkT}{2v}b_0^{(1)}$$

$$-b_0^{(1)}\frac{2\pi^{\frac{1}{2}}}{15}\frac{NkT}{v^2}\left\{\pi^{\frac{1}{2}}\Lambda+s^2\sigma_2^3 g_0^{(2)}(\sigma_2)\exp(-s^2)\left[\frac{\pi^{\frac{1}{2}}}{2}+\frac{2\exp(s^2)}{3}\Gamma(\tfrac{5}{2},s^2)-\frac{2s^2}{3}\right]\right\}, \tag{60}$$

$$\Phi=[4N(N-1)/9v^2](\pi mkT)^{\frac{1}{2}}\{\sigma_1^4 g_0^{(2)}(\sigma_1)+\sigma_2^4 g_0^{(2)}(\sigma_2)\exp(-s^2)\,\Xi(s^2)\}, \tag{61}$$

$$p=(NkT/v)+(NkT/v)b\rho\Lambda. \tag{62}$$

Longuet-Higgins and Valleau[12] have calculated a zeroth approximation to the transport coefficients using the square-well model. The zeroth-order approximation can be obtained from Eqs. (59)–(62) by setting the perturbation function equal to zero, i.e., $a^{(1)}=b_0^{(1)}=0$. In this case Eq. (59)–(62) reduce to exactly the same expressions

[12] H. C. Longuet-Higgins and J. P. Valleau, Mol. Phys. **1**, 284 (1956).

found by Longuet-Higgins and Valleau, namely,

$$\eta_0=\frac{4N(N-1)}{15v^2}(\pi mkT)^{\frac{1}{2}}\{\sigma_1^4 g_0^{(2)}(\sigma_1)+\sigma_2^4 g_0^{(2)}(\sigma_2)\exp(-s^2)\,\Xi(s^2)\} \tag{63}$$

and, subsequently,

$$\kappa_0/\eta_0=\tfrac{5}{2}(k/m);\qquad \eta_0/\Phi=\tfrac{3}{5};\qquad \kappa_0/\Phi=3k/2m. \tag{64}$$

As usual, in order to make a theoretical prediction for the absolute values of the transport coefficients, the pair correlation functions $g_0^{(2)}(\sigma_1)$ and $g_0^{(2)}(\sigma_2)$ must be evaluated in some separate analysis and the parameters σ_1, σ_2 and ϵ must be known.

The parameters σ_1, σ_2 and ϵ have been determined for argon from the viscosity of the dilute gas.[13] Instead of using theoretically computed values of $g_0^{(2)}(\sigma_1)$ and $g_0^{(2)}(\sigma_2)$, a numerical calculation for argon can be made by giving η in Eq. (60) the experimental value[14] of 2.8 millipoise at 84°K and solving Eqs. (60) and (62) simultaneously. With the aid of the equation of state in this region the numerical values for the pair correlation functions for argon at 84°K are

$$(N^2/v^2)g_0^{(2)}(\sigma_1)=3.1\times10^{45}\ \text{cm}^{-6}, \tag{65}$$

$$(N^2/v^2)g_0^{(2)}(\sigma_2)=5.4\times10^{44}\ \text{cm}^{-6}. \tag{66}$$

Using these values and Eq. (59), κ is predicted to be 1.33×10^2 erg/g-deg-sec as compared to the experimental value of[15] 1.26×10^2, and the predicted ratio, κ/η, is equal to 4.7×10^6. The experimental value of κ/η is 4.5×10^6 while the zeroth-order ratio, κ_0/η_0 is 5.2×10^6. The units of κ/η are erg/g-deg.

According to the experimental data listed by Longuet-Higgins and Valleau κ/η increases with increasing temperature. This variation with temperature cannot be accounted for by the zeroth approximation. However, it is easily seen in a qualitative manner that the first approximation does predict the correct temperature dependence. We can write $\eta=\eta_0+A$ and $\kappa=\kappa_0+B$. In this form the variation of κ/η can be predicted from the ratio B/A. For further simplification consider the case when $s^2<1$. To first order in s^2 we find

$$\frac{B}{A}=\frac{3k}{2m}\,\frac{\frac{5}{4}-(N\pi/2v)\{\Lambda+\sigma_2^3 g_0^{(2)}(\sigma_2)s^2\}}{\frac{1}{2}+(2N\pi/15v)\{\Lambda+\sigma_2^3 g_0^{(2)}(\sigma_2)s^2\}}. \tag{67}$$

$s^2=\epsilon/kT$ decreases as T increases. The numerator of Eq. (67) increases as s^2 decreases and the denominator decreases as s^2 decreases. The net result is that the ratio increases with an increase in temperature. Correspondingly, κ/η is predicted to increase with temperature as is observed experimentally. The proper variation is of course predicted without reducing $a^{(1)}$ and $b_0^{(1)}$ to the case when $s^2<1$. However, due to the complexity of the form of $a^{(1)}$ and $b_0^{(1)}$, the trend cannot be observed simply by inspection.

V. FOKKER-PLANCK EQUATION

In two recent papers Rice and Allnatt[7,8] have separated the interaction in a fluid into a rigid core plus a soft attractive interaction. The rigid-core interactions are handled as in the theory of the dense rigid-sphere fluid, while the attractive interactions are treated by the Fokker-Planck approximation. Using this procedure they derive the following equation for the singlet distribution function:

$$(\partial\tilde{f}^{(1)}/\partial t)+(\mathbf{p}_1/m)\cdot\nabla_{R_1}\tilde{f}^{(1)}=\Omega_H+\Omega_s, \tag{68}$$

where Ω_H is the Enskog dense rigid-sphere collision integral, and Ω_s is the attractive force contribution and can be written as

$$\Omega_s=\nabla_{p_1}\cdot\left[\zeta^{(s)}\left\{\left(\frac{\mathbf{p}_1}{m}-\mathbf{u}\right)\tilde{f}^{(1)}+kT\nabla_{p_1}\tilde{f}^{(1)}-\nabla_{p_1}\cdot(\mathbf{F}_1{}^{*}\tilde{f}^{(1)})\right\}\right]. \tag{69}$$

The friction coefficient in Eq. (69), $\zeta^{(s)}$, is defined by

$$\zeta^{(s)}=(3\tau kT)^{-1}\int_{0+}^{\tau}\int_{-s}^{0+}\int\cdots\int\mathbf{F}_{12}{}^{(s)}(\mathbf{R}_{12})\cdot\mathbf{F}_1{}^{(s)}\left[\mathbf{R}_1+(s+s')\frac{\mathbf{p}_1}{m}\right]f_0{}^{(1/N-1)}\frac{\mathbf{R}_1\mathbf{p}_1}{\mathbf{QP}}d\mathbf{P}d\mathbf{Q}dsds', \tag{70}$$

---

[13] E. M. Holleran and H. M. Hulburt, J. Chem. Phys. **19,** 232 (1951).
[14] N. S. Rudenko and L. W. Schubnikov, Physik. Z. Sowjetunion **6,** 470 (1934).
[15] A. Uhlir, Jr., J. Chem. Phys. **20,** 463 (1952).

where the relative probability, $f_0^{(1/N-1)}$ is defined by Eq. (8), $\mathbf{F}_{12}^{(a)}$ is the attractive force between particles 1 and 2, $\mathbf{F}_1^{(a)}$ the total attractive force on particle 1, and $\mathbf{F}_1^*$ the sum of the average total intermolecular attractive force on a molecule fixed at $\mathbf{R}_1$ and a perturbation due to the deviation of $f^{(1/N-1)}$ from its equilibrium value. The friction coefficient $\zeta^{(a)}$ is defined in terms of only attractive potentials.

It is of interest to calculate the friction coefficient as given above for the "square-well" fluid. As seen in Sec. III of this communication the collision integral Ω consists of a sum of the usual Enskog dense rigid-sphere collision integral Ω_H and an attractive contribution given by the last three terms on the right-hand side of Eq. (23). These contributions may be reduced to the Fokker-Planck form by expanding $\bar{f}^{(1)}(\mathbf{p}-\Delta\mathbf{p})$ in a Taylor's series in momentum space about $\mathbf{p}$, and truncating the expansion after the third term. If the coefficient of $\bar{f}^{(1)}(1)$ in the resulting expression is identified with the coefficient of $\bar{f}^{(1)}(1)$ in Eq. (69), the following expression for $\zeta^{(a)}$ is obtained:

$$(\zeta^{(a)}/m)\bar{f}^{(1)}(1)=M$$

$$M=\sigma_2^2 g_0^{(2)}(\sigma_2)(N-1)\iint_{\mathbf{g}\cdot\mathbf{k}>0}\Big[\bar{f}^{(1)}(1)\{\Delta\mathbf{p}_2^{(2)}\cdot\nabla_{p_2}\bar{f}^{(1)}(2)+\tfrac{1}{2}(\Delta\mathbf{p}_2^{(2)})^2\nabla_{p_2}^2\bar{f}^{(1)}(2)\}$$

$$+m\sigma_2\bar{f}_0^{(1)}(1)\bar{f}_0^{(1)}(2)\mathbf{k}\cdot\nabla_{R_1}\Big\{(\Delta\mathbf{p}_2^{(2)}/mkT)\cdot\Big(\frac{\mathbf{p}_2}{m}-\mathbf{u}\Big)\Big\}+[1-\exp(-s^2)]\bar{f}^{(1)}(1)\bar{f}^{(1)}(2)\Big]\mathbf{g}\cdot\mathbf{k}d\mathbf{k}d\mathbf{p}_2$$

$$+\exp(-s^2)\sigma_2^2 g_0^{(2)}(\sigma_2)(N-1)\iint_{\mathbf{g}\cdot\mathbf{k}<-(4\epsilon/m)^{\frac{1}{2}}}\Big[\bar{f}^{(1)}(1)\{\Delta\mathbf{p}_2^{(3)}\cdot\nabla_{p_2}\bar{f}^{(1)}(2)+\tfrac{1}{2}(\Delta\mathbf{p}_2^{(3)})^2\nabla_{p_2}^2\bar{f}^{(1)}(2)\}$$

$$+m\sigma_2\bar{f}_0^{(1)}(1)\bar{f}_0^{(1)}(2)\mathbf{k}\cdot\nabla_{R_1}\Big\{(\Delta\mathbf{p}_2^{(3)}/mkT)\cdot\Big(\frac{\mathbf{p}_2}{m}-\mathbf{u}\Big)\Big\}+[1-\exp(s^2)]\bar{f}^{(1)}(1)\bar{f}^{(1)}(2)\Big]\mathbf{g}\cdot\mathbf{k}d\mathbf{k}d\mathbf{p}_2$$

$$+\sigma_2^2 g_0^{(2)}(\sigma_2)(N-1)\iint_{-(4\epsilon/m)^{\frac{1}{2}}<\mathbf{g}\cdot\mathbf{k}<0}\Big[\bar{f}^{(1)}(1)\{\Delta\mathbf{p}_2^{(4)}\cdot\nabla_{p_2}\bar{f}^{(1)}(2)+\tfrac{1}{2}(\Delta\mathbf{p}_2^{(4)})^2\nabla_{p_2}^2\bar{f}^{(1)}(2)\}$$

$$+m\sigma_2\bar{f}_0^{(1)}(1)\bar{f}_0^{(1)}(2)\mathbf{k}\cdot\nabla_{R_1}\Big\{(\Delta\mathbf{p}_2^{(4)}/mkT)\cdot\Big(\frac{\mathbf{p}_2}{m}-\mathbf{u}\Big)\Big\}\Big]\mathbf{g}\cdot\mathbf{k}d\mathbf{k}d\mathbf{p}_2, \tag{71}$$

where the truncated expression

$$\bar{f}^{(1)}(\mathbf{p},\mathbf{R}+\sigma\mathbf{k};t)=\bar{f}^{(1)}(\mathbf{p},\mathbf{R}_1;t)+\sigma\mathbf{k}\cdot\nabla_{R_1}\bar{f}^{(1)}(\mathbf{p},\mathbf{R}_1;t) \tag{72}$$

has been used for $\bar{f}^{(1)}(1)$ and $\bar{f}^{(1)}(2)$, and where $\zeta^{(a)}$ has been assumed to be independent of momentum. $\zeta^{(a)}$ can now be evaluated by substituting the binary dynamics given by Eq. (51) into Eq. (71) and integrating over $d\mathbf{p}_1$. Then

$$\zeta^{(a)}=m\int Md\mathbf{p}_1\Big/\int\bar{f}^{(1)}(1)d\mathbf{p}_1=mv\int Md\mathbf{p}_1. \tag{73}$$

Equation (73) may be evaluated numerically for argon at 84°K using the value of $g_0^{(2)}(\sigma_2)$ calculated in the preceding section and the dilute gas values of σ_2 and ϵ.[13] The combination of these data leads to

$$\zeta^{(a)}=5.8\times10^{-10}\text{ g/sec}. \tag{74}$$

Rice and Allnatt guessed $\zeta^{(a)}$ as 2.4×10^{-10} g/sec and found a relaxation time equal to 3.3×10^{-13} sec, which is intermediate between 6×10^{-13} sec for the rigid-sphere fluid and 1.55×10^{-13} sec for Kirkwood's Fokker-Planck approximation. The quoted guess was not based on an evaluation of Eq. (70) and, although obviously low, in no way reflects on the theory. The fact that $\zeta^{(a)}>\zeta^{(H)}$ does show that two meaningful time scales can be defined in a real fluid and therefore to a considerable extent validates the fundamental physical idea of the Rice-Allnatt theory. For further discussion of this point, the reader is referred to reference 7.

Using the value of 5.8×10^{-10} g/sec calculated above leads to a relaxation time of 1.37×10^{-13} sec. In view of the large calculated value for $\zeta^{(a)}$ it can be concluded that most of the contribution to ζ comes from the attractive forces. The hard core contribution, $\zeta^{(H)}$, has been found to be 0.6×10^{-10} g/sec.[16] Using this value the diffusion coefficient of argon at 84°K can be calculated from

$$D_{\text{calc}}=kT/\zeta=kT/(\zeta^{(a)}+\zeta^{(H)})=1.81\times10^{-5}\text{ cm}^2/\text{sec}. \tag{75}$$

[16] E. Helfand, Phys. Fluids **4**, 1 (1961).

The most recent measurement of the diffusion coefficient of argon gives[17,17a]

$$D_{\text{exp}}=1.53\times10^{-5}\ \text{cm}^2/\text{sec}, \tag{76}$$

while an earlier work reports[18]

$$D_{\text{exp}}=2.07\times10^{-5}\ \text{cm}^2/\text{sec}. \tag{77}$$

In either case the agreement of the D_{calc} with experiment is very good considering the crudeness of a "square-well" model.

ACKNOWLEDGMENTS

We wish to thank Dr. Alan Allnatt for many interesting discussions. We are indebted to the Petroleum Research Fund of the American Chemical Society and the Air Force Office of Scientific Research for financial support.

APPENDIX I

It is the purpose of this Appendix to describe the details of a calculation of the first-order perturbation to the local equilibrium singlet distribution function in a dense square-well fluid. In the following the modified Boltzmann equation is solved by a perturbation procedure analogous to the Chapman-Enskog solution of the dilute gas Maxwell-Boltzmann equation.[1] Although the general variational procedure used is well known,[3] our analysis makes much more use of certain orthogonality relationships than has hitherto been the case. Also, unlike previous calculations, we do not utilize the various reduced and weighted collision cross sections characteristic of the interaction potential. It will be seen that a complete analytic treatment can be given if in place of these cross sections, the concept of partial collisions is introduced. To our knowledge, this is the first complete analytic description of a dense fluid with both attractive and repulsive interactions. It is also, so far as we know, the first completely analytic treatment of the square-well potential since, even for the dilute gas case, the use of various collision cross sections has hitherto forced extensive numerical calculations.[13] Our purpose is to solve Eq. (12) with Eq. (23).

In the following analysis we shall evaluate $g_0^{(2)}(\mathbf{R}_1,\ \mathbf{R}_1+\sigma\mathbf{k})$ in terms of its value at equilibrium. Neglecting derivatives of higher order than first we obtain

$$\begin{aligned} g_0^{(2)}(\mathbf{R}_1,\ \mathbf{R}_1\pm\sigma\mathbf{k}) &= g_0^{(2)}(\sigma)\pm\tfrac{1}{2}\sigma\mathbf{k}\cdot\nabla_{R_1}g_0^{(2)}(\mathbf{R}_1,\ \sigma) \\ &= g_0^{(2}\ (\sigma)\pm\tfrac{1}{2}\ \exp(\epsilon/kT)\sigma\mathbf{k}\cdot[\nabla_{R_1}g_0^{(2)*}(\mathbf{R}_1,\ \sigma)-(\epsilon/kT^2)\,g_0^{(2)*}(\mathbf{R}_1,\ \sigma)\,\nabla_{R_1}T], \end{aligned} \tag{A1}$$

where $g_0^{(2)*}(\mathbf{R}_1,\sigma)\ \exp(\epsilon/kT)=g_0^{(2)}(\mathbf{R}_1,\sigma)$. The distribution function, $\bar{f}^{(1)}(\mathbf{R}_1+\sigma\mathbf{k},\ \mathbf{p}_2;\ t)$, is expanded in a Taylor's series about $\mathbf{R}_1$, and the expansion is terminated after the second term. Using the above expansions, Eq. (12) becomes

$$L\bar{f}^{(1)}(1)=J_1+J_2+J_3, \tag{A2}$$

where

$$\begin{aligned} J_1=\gamma_1\iint_{\mathbf{g}\cdot\mathbf{k}>0}&[f^{(1)}(\mathbf{R}_1,\ \mathbf{p}_1-\Delta\mathbf{p}_1^{(1)};\ t)\bar{f}^{(1)}(\mathbf{R}_1,\ \mathbf{p}_2-\Delta\mathbf{p}_2^{(1)};\ t)-\bar{f}^{(1)}(\mathbf{R}_1,\ \mathbf{p}_1;\ t)\bar{f}^{(1)}(\mathbf{R}_1,\ \mathbf{p}_2;\ t)]\mathbf{g}\cdot\mathbf{k}d\mathbf{k}d\mathbf{p}_2 \\ +\gamma_2\exp(-\epsilon/kT)\iint_{\mathbf{g}\cdot\mathbf{k}>0}&[\exp(\epsilon/kT)\bar{f}^{(1)}(\mathbf{R}_1,\ \mathbf{p}_1-\Delta\mathbf{p}_1^{(2)};\ t)\bar{f}^{(1)}(\mathbf{R}_1,\ \mathbf{p}_2-\Delta\mathbf{p}_2^{(2)};\ t) \\ &-f^{(1)}(\mathbf{R}_1,\ \mathbf{p}_1;\ t)\bar{f}^{(1)}(\mathbf{R}_1,\ \mathbf{p}_2;\ t)]\mathbf{g}\cdot\mathbf{k}d\mathbf{k}d\mathbf{p}_2 \\ +\gamma_2\iint_{\mathbf{g}\cdot\mathbf{k}<-\omega}&[\exp(-\epsilon/kT)\bar{f}^{(1)}(\mathbf{R}_1,\ \mathbf{p}_1-\Delta\mathbf{p}_1^{(3)};\ t)\bar{f}^{(1)}(\mathbf{R}_1,\ \mathbf{p}_2-\Delta\mathbf{p}_2^{(3)};\ t) \\ &-\bar{f}^{(1)}(\mathbf{R}_1,\ \mathbf{p}_1;\ t)\bar{f}^{(1)}(\mathbf{R}_1,\ \mathbf{p}_2;\ t)]\mathbf{g}\cdot\mathbf{k}d\mathbf{k}d\mathbf{p}_2 \\ +\gamma_2\iint_{-\omega<\mathbf{g}\cdot\mathbf{k}<0}&[\bar{f}^{(1)}(\mathbf{R}_1,\ \mathbf{p}_1-\Delta\mathbf{p}_1^{(4)};\ t)\bar{f}^{(1)}(\mathbf{R}_1,\ \mathbf{p}_2-\Delta\mathbf{p}_2^{(4)};\ t)-\bar{f}^{(1)}(\mathbf{R}_1,\ \mathbf{p}_1;\ t)\bar{f}^{(1)}(\mathbf{R}_1,\ \mathbf{p}_2;\ t)]g\cdot\mathbf{k}d\mathbf{k}d\mathbf{p}_2, \end{aligned} \tag{A3}$$

---

[17] Cini-Castagnoli and F. P. Ricci, J. Chem. Phys. **32,** 19 (1960).

[17a] *Note added in proof.* Recent unpublished measurements by Nagizadeh and Rice give 1.84×10^{-5} cm²/sec. Because of the wide range of T and p covered, this is probably the most reliable value.

[18] T. W. Corbett and J. H. Wang, J. Chem. Phys. **25,** 422 (1956).

$$J_2=\gamma_1\iint_{\mathbf{g}\cdot\mathbf{k}>0}[\bar{f}^{(1)}(\mathbf{R}_1,\,\mathbf{p}_1-\Delta\mathbf{p}_1^{(1)};\,t)\sigma_1\mathbf{k}\cdot\nabla_{R_1}\bar{f}^{(1)}(\mathbf{R}_1,\,\mathbf{p}_2-\Delta\mathbf{p}_2^{(1)};\,t)$$
$$+\bar{f}^{(1)}(\mathbf{R}_1,\,\mathbf{p}_1;\,t)\sigma_1\mathbf{k}\cdot\nabla_{R_1}\bar{f}^{(1)}(\mathbf{R}_1,\,\mathbf{p}_2;\,t)]\mathbf{g}\cdot\mathbf{k}d\mathbf{k}d\mathbf{p}_2$$
$$+\gamma_2\exp(-\epsilon/kT)\iint_{\mathbf{g}\cdot\mathbf{k}>0}[\exp(\epsilon/kT)\bar{f}^{(1)}(\mathbf{R}_1,\,\mathbf{p}_1-\Delta\mathbf{p}_1^{(2)};\,t)\sigma_2\mathbf{k}\cdot\nabla_{R_1}\bar{f}^{(1)}(\mathbf{R}_1,\,\mathbf{p}_2-\Delta\mathbf{p}_2^{(2)};\,t)$$
$$+\bar{f}^{(1)}(\mathbf{R}_1,\,\mathbf{p}_1;\,t)\sigma_2\mathbf{k}\cdot\nabla_{R_1}\bar{f}^{(1)}(\mathbf{R}_1,\,\mathbf{p}_2;\,t)]\mathbf{g}\cdot\mathbf{k}d\mathbf{k}d\mathbf{p}_2$$
$$+\gamma_2\iint_{\mathbf{g}\cdot\mathbf{k}<-\omega}[\exp(-\epsilon/kT)\bar{f}^{(1)}(\mathbf{R}_1,\,\mathbf{p}_1-\Delta\mathbf{p}_1^{(3)};\,t)\sigma_2\mathbf{k}\cdot\nabla_{R_1}\bar{f}^{(1)}(\mathbf{R}_1,\,\mathbf{p}_2-\Delta\mathbf{p}_2^{(3)};\,t)$$
$$+\bar{f}^{(1)}(\mathbf{R}_1,\,\mathbf{p}_1;\,t)\sigma_2\mathbf{k}\cdot\nabla_{R_1}\bar{f}^{(1)}(\mathbf{R}_1,\,\mathbf{p}_2;\,t)]\mathbf{g}\cdot\mathbf{k}d\mathbf{k}d\mathbf{p}_2$$
$$+\gamma_2\iint_{-\omega<\mathbf{g}\cdot\mathbf{k}<0}[\bar{f}^{(1)}(\mathbf{R}_1,\,\mathbf{p}_1-\Delta\mathbf{p}_1^{(4)};\,t)\sigma_2\mathbf{k}\cdot\nabla_{R_1}\bar{f}^{(1)}(\mathbf{R}_1,\,\mathbf{p}_2-\Delta\mathbf{p}_2^{(4)};\,t)$$
$$+\bar{f}^{(1)}(\mathbf{R}_1,\,\mathbf{p}_1;\,t)\sigma_2\mathbf{k}\cdot\nabla_{R_1}\bar{f}^{(1)}(\mathbf{R}_1,\,\mathbf{p}_2;\,t)]\mathbf{g}\cdot\mathbf{k}d\mathbf{k}d\mathbf{p}_2, \quad \text{(A4)}$$

$$J_3=\tfrac{1}{2}[(N-1)\sigma_1^3]\iint_{\mathbf{g}\cdot\mathbf{k}>0}\mathbf{k}\cdot\nabla_{R_1}g_0^{(2)}(\mathbf{R}_1,\,\sigma_1)[\bar{f}^{(1)}(\mathbf{R}_1,\,\mathbf{p}_1-\Delta\mathbf{p}_1^{(1)};\,t)\bar{f}^{(1)}(\mathbf{R}_1,\,\mathbf{p}_2-\Delta\mathbf{p}_2^{(1)};\,t)$$
$$+\bar{f}^{(1)}(\mathbf{R}_1,\,\mathbf{p}_1;\,t)\bar{f}^{(1)}(\mathbf{R}_1,\,\mathbf{p}_2;\,t)]\mathbf{g}\cdot\mathbf{k}d\mathbf{k}d\mathbf{p}_2$$
$$\tfrac{1}{2}[(N-1)\sigma_2^3]\iint_{\mathbf{g}\cdot\mathbf{k}>0}\mathbf{k}\cdot[\nabla_{R_1}g_0^{(2)}(\mathbf{R}_1,\,\sigma_2)\bar{f}^{(1)}(\mathbf{R}_1,\,\mathbf{p}_1-\Delta\mathbf{p}_1^{(2)};\,t)\bar{f}^{(1)}(\mathbf{R}_1,\,\mathbf{p}_2-\Delta\mathbf{p}_2^{(2)};\,t)$$
$$+\nabla_{R_1}g_0^{(2)*}(\mathbf{R}_1,\,\sigma_2)\bar{f}^{(1)}(\mathbf{R}_1,\,\mathbf{p}_1;\,t)\bar{f}^{(1)}(\mathbf{R}_1,\,\mathbf{p}_2;\,t)]\mathbf{g}\cdot\mathbf{k}d\mathbf{k}d\mathbf{p}_2$$
$$\tfrac{1}{2}[(N-1)\sigma_2^3]\iint_{\mathbf{g}\cdot\mathbf{k}<-\omega}\mathbf{k}\cdot[\nabla_{R_1}g_0^{(2)*}(\mathbf{R}_1,\,\sigma_2)\bar{f}^{(1)}(\mathbf{R}_1,\,\mathbf{p}_1-\Delta\mathbf{p}_1^{(3)};\,t)\bar{f}^{(1)}(\mathbf{R}_1,\,\mathbf{p}_2-\Delta\mathbf{p}_2^{(3)};\,t)$$
$$+\nabla_{R_1}g_0^{(2)}(\mathbf{R}_1,\,\sigma_2)\bar{f}^{(1)}(\mathbf{R}_1,\,\mathbf{p}_1';\,t)\bar{f}^{(1)}(\mathbf{R}_1,\,\mathbf{p}_2;\,t)]\mathbf{g}\cdot\mathbf{k}d\mathbf{k}d\mathbf{p}_2$$
$$\tfrac{1}{2}[(N-1)\sigma_2^3]\iint_{-\omega<\mathbf{g}\cdot\mathbf{k}<0}\mathbf{k}\cdot\nabla_{R_1}g_0^{(2)}(\mathbf{R}_1,\,\sigma_2)[\bar{f}^{(1)}(\mathbf{R}_1,\,\mathbf{p}_1-\Delta\mathbf{p}_1^{(4)};\,t)\bar{f}^{(1)}(\mathbf{R}_1,\,\mathbf{p}_2-\Delta\mathbf{p}_2^{(4)};\,t)$$
$$+\bar{f}^{(1)}(\mathbf{R}_1,\,\mathbf{p}_1;\,t)\bar{f}^{(1)}(\mathbf{R}_1,\,\mathbf{p}_2;\,t)]\mathbf{g}\cdot\mathbf{k}d\mathbf{k}d\mathbf{p}_2, \quad \text{(A5)}$$

with the abbreviations

$$L=(\partial/\partial t)+(\mathbf{p}_1/m)\cdot\nabla_{R_1},$$
$$\omega=(4\epsilon/m)^{\frac{1}{2}}. \quad \text{(A6)}$$

γ is defined by the relation $\gamma=(N-1)\sigma^2g_0^{(2)}(\sigma)$.

Perturbation Solution

Equation (A2) can be solved by the usual perturbation[1,3] method, taking as the first-order solution

$$\bar{f}^{(1)}=\bar{f}_0^{(1)}(1+\phi), \quad \text{(A7)}$$

where $\bar{f}_0^{(1)}$ is the zeroth-order singlet distribution function,

$$f_0^{(1)}=[(2\pi mkT)^{-\frac{1}{2}}/v]\exp\{-[\mathbf{p}-m\mathbf{u}]^2/2mkT\} \quad \text{(A8)}$$

and ϕ is the perturbation function. In order for $1/v$, $\mathbf{u}$ and T to represent the local values of the number density, hydrodynamic velocity, and temperature, Eq. (47) must be such that

$$\int\bar{f}^{(1)}(1)d\mathbf{p}_1=1/v(\mathbf{R}_1;\,t), \quad \text{(A9)}$$

$$\int\frac{\mathbf{p}_1}{m}\bar{f}^{(1)}d\mathbf{p}_1=\frac{\mathbf{u}(\mathbf{R}_1;\,t)}{v(\mathbf{R}_1;\,t)}, \quad \text{(A10)}$$

$$\int\left[\frac{\mathbf{p}_1}{m}-\mathbf{u}\right]^2\bar{f}^{(1)}d\mathbf{p}_1=\frac{3}{2}\frac{kT(\mathbf{R}_1;\,t)}{v(\mathbf{R}_1;\,t)}. \quad \text{(A11)}$$

Equations (A9)–(A11) impose upon the perturbation function the following auxiliary conditions:

$$\int \bar{f}_0^{(1)}\phi_1 d\mathbf{p}_1=0, \tag{A12}$$

$$\int \bar{f}_0^{(1)}\phi_1\left[\frac{\mathbf{p}_1}{m}-\mathbf{u}\right]d\mathbf{p}_1=0, \tag{A13}$$

$$\int \bar{f}_0^{(1)}\phi_1\left[\frac{\mathbf{p}_1}{m}-\mathbf{u}\right]^2 d\mathbf{p}_1=0. \tag{A14}$$

In this paper terms of higher order than first in ϕ will be neglected, so that $f^{(1)}(1)f^{(1)}(2)$ may be approximated by

$$f^{(1)}(1)f^{(1)}(2)=f_0^{(1)}(1)\bar{f}_0^{(1)}(2)\,(1+\phi_1+\phi_2). \tag{A15}$$

To obtain the integro-differential equation for the perturbation function Eq. (A7) is substituted into Eqs. (A3)–(A5). The resulting equation is

$$\begin{aligned}
Lf^{(1)}=\gamma_1\iint_{\mathbf{g}\cdot\mathbf{k}>0} & f_0^{(1)}(1)f_0^{(1)}(1)[\phi_1(\mathbf{R}_1,\,\mathbf{p}_1-\Delta\mathbf{p}_1^{(1)};\,t)+\phi_2(\mathbf{R}_1,\,\mathbf{p}_2-\Delta\mathbf{p}_2^{(1)};\,t)\\
&-\phi_1(\mathbf{R}_1,\,\mathbf{p}_1;\,t)-\phi_2(\mathbf{R}_1,\,\mathbf{p}_2;\,t)]\mathbf{g}\cdot\mathbf{k}d\mathbf{k}d\mathbf{p}_2\\
+\sigma_1\gamma_1\iint_{\mathbf{g}\cdot\mathbf{k}>0} & \bar{f}_0^{(1)}(1)\bar{f}_0^{(1)}(2)\mathbf{k}\cdot\nabla_{R_1}\ln[\bar{f}_0^{(1)}(\mathbf{R}_1,\,\mathbf{p}_2-\Delta\mathbf{p}_2^{(1)};\,t)\bar{f}_0^{(1)}(\mathbf{R}_1,\,\mathbf{p}_2;\,t)]\mathbf{g}\cdot\mathbf{k}d\mathbf{k}d\mathbf{p}_2\\
+(N-1)\sigma_1^3\iint_{\mathbf{g}\cdot\mathbf{k}>0} & \mathbf{k}\cdot\nabla_{R_1}g_0^{(2)}(\mathbf{R}_1,\,\sigma_1)\bar{f}_0^{(1)}(1)\bar{f}_0^{(1)}(2)\mathbf{g}\cdot\mathbf{k}d\mathbf{k}d\mathbf{p}_2\\
+\gamma_2\exp(-\epsilon/kT)\iint_{\mathbf{g}\cdot\mathbf{k}>0} & \bar{f}_0^{(1)}(1)\bar{f}_0^{(1)}(2)[\phi_1(\mathbf{R}_1,\,\mathbf{p}_1-\Delta\mathbf{p}_1^{(2)};\,t)+\phi_2(\mathbf{R}_1,\,\mathbf{p}_2-\Delta\mathbf{p}_2^{(2)};\,t)\\
&-\phi_1(\mathbf{R}_1,\,\mathbf{p}_1;\,t)-\phi_2(\mathbf{R}_1,\,\mathbf{p}_2;\,t)]\mathbf{g}\cdot\mathbf{k}d\mathbf{k}d\mathbf{p}_2\\
+\gamma_2\sigma_2\exp(-\epsilon/kT)\iint_{\mathbf{g}\cdot\mathbf{k}>0} & \bar{f}_0^{(1)}(1)\bar{f}_0^{(1)}(2)\mathbf{k}\cdot\nabla_{R_1}\ln[\bar{f}_0^{(1)}(\mathbf{R}_1,\,\mathbf{p}_2-\Delta\mathbf{p}_2^{(2)};\,t)\bar{f}_0^{(1)}(\mathbf{R}_1,\,\mathbf{p}_2;\,t)]\mathbf{g}\cdot\mathbf{k}d\mathbf{k}d\mathbf{p}_2\\
+\tfrac{1}{2}[(N-1)\sigma_2^3]\iint_{\mathbf{g}\cdot\mathbf{k}>0} & \mathbf{k}\cdot[\exp(-\epsilon/kT)\,\nabla_{R_1}g_0^{(2)}(\mathbf{R}_1,\,\sigma_2)+\nabla_{R_1}g_0^{(2)*}(\mathbf{R}_1,\,\sigma_2)]\bar{f}_0^{(1)}(1)\bar{f}_0^{(1)}(2)\mathbf{g}\cdot\mathbf{k}d\mathbf{k}d\mathbf{p}_2\\
+\gamma_2\iint_{\mathbf{g}\cdot\mathbf{k}<-\omega} & \bar{f}_0^{(1)}(1)\bar{f}_0^{(1)}(2)[\phi_1(\mathbf{R}_1,\,\mathbf{p}_1-\Delta\mathbf{p}_1^{(3)};\,t)+\phi_2(\mathbf{R}_1,\,\mathbf{p}_2-\Delta\mathbf{p}_2^{(3)};\,t)\\
&-\phi_1(\mathbf{R}_1,\,\mathbf{p}_1;\,t)-\phi_2(\mathbf{R}_1,\,\mathbf{p}_2;\,t)]\mathbf{g}\cdot\mathbf{k}d\mathbf{k}d\mathbf{P}_2\\
+\sigma_2\gamma_2\iint_{\mathbf{g}\cdot\mathbf{k}<-\omega} & \bar{f}_0^{(1)}(1)\bar{f}_0^{(1)}(2)\mathbf{k}\cdot\nabla_{R_1}\ln[\bar{f}_0^{(1)}(\mathbf{R}_1,\,\mathbf{p}_2-\Delta\mathbf{p}_2^{(3)};\,t)\bar{f}_0^{(1)}(\mathbf{R}_1,\,\mathbf{p}_2;\,t)]\mathbf{g}\cdot\mathbf{k}d\mathbf{k}d\mathbf{p}_2\\
\tfrac{1}{2}[(N-1)\sigma_2^3]\iint_{\mathbf{g}\cdot\mathbf{k}<-\omega} & \mathbf{k}\cdot[\exp(\epsilon/kT)\,\nabla_{R_1}g_0^{(2)*}(\mathbf{R}_1,\,\sigma_2)+\nabla_{R_1}g_0^{(2)}(\mathbf{R}_1,\,\sigma_2)]\bar{f}_0^{(1)}(1)\bar{f}_0^{(1)}(2)\mathbf{g}\cdot\mathbf{k}d\mathbf{k}d\mathbf{p}_2\\
+\gamma_2\iint_{-\omega<\mathbf{g}\cdot\mathbf{k}<0} & \bar{f}_0^{(1)}(1)\bar{f}_0^{(1)}(2)[\phi_1(\mathbf{R}_1,\,\mathbf{p}_1-\Delta\mathbf{p}_1^{(4)};\,t)+\phi_2(\mathbf{R}_1,\,\mathbf{p}_2-\Delta\mathbf{p}_2^{(4)};\,t)\\
&-\phi_1(\mathbf{R}_1,\,\mathbf{p}_1;\,t)-\phi_2(\mathbf{R}_1,\,\mathbf{p}_2;\,t)]\mathbf{g}\cdot\mathbf{k}d\mathbf{k}d\mathbf{p}_2\\
+\gamma_2\sigma_2\iint_{-\omega<\mathbf{g}\cdot\mathbf{k}<0} & \bar{f}_0^{(1)}(1)\bar{f}_0^{(1)}(2)\mathbf{k}\cdot\nabla_{R_1}\ln[\bar{f}_0^{(1)}(\mathbf{R}_1,\,\mathbf{p}_2-\Delta\mathbf{p}_2^{(4)};\,t)\bar{f}_0^{(1)}(\mathbf{R}_1,\,\mathbf{p}_2;\,t)]\mathbf{g}\cdot\mathbf{k}d\mathbf{k}d\mathbf{p}_2\\
+(N-1)\sigma_2^3\iint_{-\omega<\mathbf{g}\cdot\mathbf{k}<0} & \mathbf{k}\cdot\nabla_{R_1}g_0^{(2)}(\mathbf{R}_1,\,\sigma_2)f_0^{(1)}(1)f_0^{(1)}(2)\mathbf{g}\cdot\mathbf{k}d\mathbf{k}d\mathbf{p}_2,
\end{aligned} \tag{A16}$$

where gradients of ϕ have been neglected. Equation (A16) can be reduced by use of the relation

$$\nabla_{R1}\ln[\bar{f}_0^{(1)}(\mathbf{R}_1,\mathbf{p}_2-\Delta\mathbf{p}_2;t)\bar{f}_0^{(1)}(\mathbf{R}_1,\mathbf{p}_2;t)]$$
$$=-(2/v)\nabla_{R_1}v-(3/T)\nabla_{R_1}T+(m/2kT^2)[C_2^2+(C_2')^2]\nabla_{R_1}T+(m/kT)\nabla_{R_1}\mathbf{u}\cdot(\mathbf{C}_2+\mathbf{C}_2'), \quad \text{(A17)}$$

where the definition

$$\mathbf{C}=(\mathbf{p}/m)-\mathbf{u} \quad \text{(A18)}$$

has been used.

The relation between the primed and unprimed molecular velocities $\mathbf{C}$ is determined by the binary dynamics of the different collisional processes given in the main text. It is convenient to introduce two new variables $\mathbf{g}$ and $\mathbf{G}$ defined by

$$\mathbf{g}=\mathbf{C}_2-\mathbf{C}_1, \quad \text{(A19)}$$

$$\mathbf{G}=\mathbf{C}_2+\mathbf{C}_1, \quad \text{(A20)}$$

whereupon, using Eq. (51), we find

(1) hard-sphere collision $\mathbf{g}\cdot\mathbf{k}>0$,

$$\mathbf{C}_2+\mathbf{C}_2'=\mathbf{G}+\mathbf{g}-\mathbf{g}\cdot\mathbf{k}\mathbf{k}$$
$$C_2^2+(C_2')^2=\tfrac{1}{2}G^2+\tfrac{1}{2}g^2+\mathbf{G}\cdot\mathbf{g}-\mathbf{g}\cdot\mathbf{k}(\mathbf{G}\cdot\mathbf{k})$$
$$\nabla_{R_1}\ln\bar{f}_0^{(1)\prime}(2)\bar{f}_0^{(1)}(2)=-(2/v)\nabla_{R_1}v-(3/T)\nabla_{R_1}T+(m/2kT^2)\nabla_{R_1}T\{\tfrac{1}{2}G^2+\tfrac{1}{2}g^2$$
$$-\mathbf{g}\cdot\mathbf{k}(\mathbf{G}\cdot\mathbf{k})\}+\nabla_{R_1}\mathbf{u}\cdot\{\mathbf{G}+\mathbf{g}-\mathbf{g}\cdot\mathbf{k}\mathbf{k}\}(m/kT); \quad \text{(A21)}$$

(2) type-a collision $\mathbf{g}\cdot\mathbf{k}>0$,

$$\mathbf{C}_2+\mathbf{C}_2'=\mathbf{G}+\mathbf{g}-\tfrac{1}{2}\{\mathbf{g}\cdot\mathbf{k}-[(\mathbf{g}\cdot\mathbf{k})^2+\omega^2]^{\frac{1}{2}}\}\mathbf{k}$$
$$C_2^2+(C_2')^2=\tfrac{1}{2}G^2+\tfrac{1}{2}g^2+\mathbf{G}\cdot\mathbf{g}-\tfrac{1}{2}\mathbf{G}\cdot\mathbf{k}\{\mathbf{g}\cdot\mathbf{k}-[(\mathbf{g}\cdot\mathbf{k})^2+\omega^2]^{\frac{1}{2}}\}+(\omega^2/4)$$
$$\nabla_{R_1}\ln\bar{f}_0^{(1)\prime}(2)\bar{f}_0^{(1)}(2)=-(2/v)\nabla_{R_1}v-(3/T)\nabla_{R_1}T$$
$$+(m/2kT^2)\nabla_{R_1}T[\tfrac{1}{2}G^2+\tfrac{1}{2}g^2+\mathbf{G}\cdot\mathbf{g}-\tfrac{1}{2}\mathbf{G}\cdot\mathbf{k}\{\mathbf{g}\cdot\mathbf{k}-[(\mathbf{g}\cdot\mathbf{k})^2+\omega^2]^{\frac{1}{2}}\}+(\omega^2/4)]$$
$$+(m/kT)\nabla_{R_1}\mathbf{u}\cdot[\mathbf{G}+\mathbf{g}-\tfrac{1}{2}\{\mathbf{g}\cdot\mathbf{k}-[(\mathbf{g}\cdot\mathbf{k})^2+\omega^2]^{\frac{1}{2}}\}\mathbf{k}]; \quad \text{(A22)}$$

(3) type-b collision $\mathbf{g}\cdot\mathbf{k}<-\omega$,

$$\mathbf{C}_2+\mathbf{C}_2'=\mathbf{G}+\mathbf{g}-\tfrac{1}{2}\{\mathbf{g}\cdot\mathbf{k}+[(\mathbf{g}\cdot\mathbf{k})^2-\omega^2]^{\frac{1}{2}}\}\mathbf{k}$$
$$C_2^2+(C_2')^2=\tfrac{1}{2}G^2+\tfrac{1}{2}g^2+\mathbf{G}\cdot\mathbf{g}-\tfrac{1}{2}\mathbf{G}\cdot\mathbf{k}\{\mathbf{g}\cdot\mathbf{k}+[(\mathbf{g}\cdot\mathbf{k})^2-\omega^2]^{\frac{1}{2}}\}-(\omega^2/4)$$
$$\nabla_{R_1}\ln\bar{f}_0^{(1)\prime}(2)f_0^{(1)}(2)=-(2/v)\nabla_{R_1}v-(3/T)\nabla_{R_1}T$$
$$+(m/2kT^2)\nabla_{R_1}T[\tfrac{1}{2}G^2+\tfrac{1}{2}g^2+\mathbf{G}\cdot\mathbf{g}-\tfrac{1}{2}\mathbf{G}\cdot\mathbf{k}\{\mathbf{g}\cdot\mathbf{k}+[(\mathbf{g}\cdot\mathbf{k})^2-\omega^2]^{\frac{1}{2}}\}-(\omega^2/4)]$$
$$+(m/kT)\nabla_{R_1}\mathbf{u}\cdot[\mathbf{G}+\mathbf{g}-\tfrac{1}{2}\{\mathbf{g}\cdot\mathbf{k}+[(\mathbf{g}\cdot\mathbf{k})^2-\omega^2]^{\frac{1}{2}}\}\mathbf{k}]; \quad \text{(A23)}$$

(4) type-c collision $-\omega<\mathbf{g}\cdot\mathbf{k}<0$,

$$\mathbf{C}_2+\mathbf{C}_2'=\mathbf{G}+\mathbf{g}-(\mathbf{g}\cdot\mathbf{k})\mathbf{k}$$
$$C_2^2+(C_2')^2=\tfrac{1}{2}G^2+\tfrac{1}{2}g^2+\mathbf{G}\cdot\mathbf{g}-\mathbf{g}\cdot\mathbf{k}(\mathbf{G}\cdot\mathbf{k})$$
$$\nabla_{R_1}\ln\bar{f}_0^{(1)\prime}(2)f_0^{(1)}(2)=-(2/v)\nabla_{R_1}v-(3/T)\nabla_{R_1}T$$
$$+(m/2kT^2)\nabla_{R_1}T[\tfrac{1}{2}G^2+\tfrac{1}{2}g^2+\mathbf{G}\cdot\mathbf{g}-\mathbf{g}\cdot\mathbf{k}(\mathbf{G}\cdot\mathbf{k})]+(m/kT)\nabla_{R_1}\mathbf{u}\cdot[\mathbf{G}+\mathbf{g}-(\mathbf{g}\cdot\mathbf{k})\mathbf{k}]. \quad \text{(A24)}$$

In the stationary state[1]

$$D/Dt=(\partial/\partial t)+\mathbf{u}\cdot\nabla_{R_1}, \quad \text{(A25)}$$

and, therefore,

$$L\bar{f}^{(1)}(1)=\left(\frac{\partial}{\partial t}+\frac{\mathbf{p}_1}{m}\cdot\nabla_{R_1}\right)\bar{f}^{(1)}(1)=\left(\frac{D}{Dt}+\mathbf{C}_1\cdot\nabla_{R_1}\right)\bar{f}^{(1)}(1). \quad \text{(A26)}$$

Neglecting terms containing the perturbation function ϕ, Eq. (A26) reduces to the following relation:

$$L\bar{f}^{(1)}(1)=\bar{f}_0^{(1)}(1)\left[-v^{-1}\frac{Dv}{Dt}-\left(\frac{3}{2}-\frac{mC_1^2}{2kT}\right)T^{-1}\frac{DT}{Dt}+\frac{m}{kT}\mathbf{CC}:\nabla_{R_1}\mathbf{u}+\mathbf{C}\cdot\left\{-v^{-1}\nabla_{R_1}v-\left(\frac{3}{2}-\frac{mC_1^2}{2kT}\right)T^{-1}\nabla_{R_1}T+\frac{m}{kT}\frac{D\mathbf{u}}{Dt}\right\}\right]. \quad \text{(A27)}$$

The insertion of Eq. (A27) and the relations obtained in Eqs. (A21)–(A24) into Eq. (A16) gives, finally, the lengthy equation

$$
\begin{aligned}
I(\phi) = -\bar{f}_0^{(1)}(1)\Big[& -v^{-1}\frac{Dv}{Dt} - \left(\frac{3}{2} - \frac{mC_1^2}{2kT}\right)T^{-1}\frac{DT}{Dt} + \frac{m}{kT}\mathbf{C}_1\mathbf{C}_1 : \nabla_{R_1}\mathbf{u} \\
& + \mathbf{C}_1 \cdot \left\{ -v^{-1}\nabla_{R_1} v - \left(\frac{3}{2} - \frac{mC_1^2}{2kT}\right)T^{-1}\nabla_{R_1} T + \frac{m}{kT}\frac{D\mathbf{u}}{Dt} \right\} \Big] \\
& + \frac{\gamma_1\sigma_1}{v^2}\left(\frac{m}{2\pi kT}\right)^3 \left(-\frac{2}{v}\nabla_{R_1} v - \frac{3}{T}\nabla_{R_1} T\right) \cdot \iint_{\mathbf{g}\cdot\mathbf{k}>0} \mathbf{k} \exp[-(m/2kT)(C_1^2 + C_2^2)]\mathbf{g}\cdot\mathbf{k}\, d\mathbf{k}\, d\mathbf{C}_2 \\
& + \frac{\gamma_2\sigma_2 \exp(-\epsilon/kT)}{v^2}\left(\frac{m}{2\pi kT}\right)^3 \left(-\frac{2}{v}\nabla_{R_1} v - \frac{3}{T}\nabla_{R_1} T\right) \cdot \iint_{\mathbf{g}\cdot\mathbf{k}>0} \mathbf{k} \exp[-(m/2kT)(C_1^2 + C_2^2)]\mathbf{g}\cdot\mathbf{k}\, d\mathbf{k}\, d\mathbf{C}_2 \\
& + \frac{\gamma_2\sigma_2}{v^2}\left(\frac{m}{2\pi kT}\right)^3 \left(-\frac{2}{v}\nabla_{R_1} v - \frac{3}{T}\nabla_{R_1} T\right) \cdot \iint_{\mathbf{g}\cdot\mathbf{k}<0} \mathbf{k} \exp[-(m/2kT)(C_1^2 + C_2^2)]\mathbf{g}\cdot\mathbf{k}\, d\mathbf{k}\, d\mathbf{C}_2 \\
& + (v^2)^{-1}(m/2\pi kT)^3 (m/2kT^2)\nabla_{R_1} T \cdot \Big[\gamma_1\sigma_1 \iint_{\mathbf{g}\cdot\mathbf{k}>0} \exp[-(m/4kT)(G^2+g^2)]\mathbf{k}\{\tfrac{1}{2}G^2 + \tfrac{1}{2}g^2 \\
& + \mathbf{G}\cdot\mathbf{g} - \mathbf{g}\cdot\mathbf{k}(\mathbf{G}\cdot\mathbf{k})\}\mathbf{g}\cdot\mathbf{k}\, d\mathbf{k}\, d\mathbf{C}_2 + \gamma_2\sigma_2 \exp(-\epsilon/kT) \iint_{\mathbf{g}\cdot\mathbf{k}>0} \exp[-(m/4kT)(G^2+g^2)]\mathbf{k}\{\tfrac{1}{2}G^2 \\
& + \tfrac{1}{2}g^2 + \mathbf{G}\cdot\mathbf{g} - \tfrac{1}{2}\mathbf{G}\cdot\mathbf{k}[\mathbf{g}\cdot\mathbf{k} - [(\mathbf{g}\cdot\mathbf{k})^2 + \omega^2]^{\frac{1}{2}}) + (\omega^2/4)\}\mathbf{g}\cdot\mathbf{k}\, d\mathbf{k}\, d\mathbf{C}_2 \\
& + \gamma_2\sigma_2 \iint_{\mathbf{g}\cdot\mathbf{k}<-\omega} \exp[-(m/4kT)(G^2+g^2)]\mathbf{k}\{\tfrac{1}{2}G^2 + \tfrac{1}{2}g^2 + \mathbf{G}\cdot\mathbf{g} - \tfrac{1}{2}\mathbf{G}\cdot\mathbf{k}(\mathbf{g}\cdot\mathbf{k} + [(\mathbf{g}\cdot\mathbf{k})^2 - \omega^2]^{\frac{1}{2}}) - (\omega^2/4)\}\mathbf{g}\cdot\mathbf{k}\, d\mathbf{k}\, d\mathbf{C}_2 \\
& + \gamma_2\sigma_2 \iint_{-\omega<\mathbf{g}\cdot\mathbf{k}<0} \exp[-(m/4kT)(G^2+g^2)]\mathbf{k}\{\tfrac{1}{2}G^2 + \tfrac{1}{2}g^2 + \mathbf{G}\cdot\mathbf{g} - \mathbf{g}\cdot\mathbf{k}(\mathbf{G}\cdot\mathbf{k})\}\mathbf{g}\cdot\mathbf{k}\, d\mathbf{k}\, d\mathbf{C}_2 \Big] \\
& + (v^2)^{-1}(m/2\pi kT)^3 (m/kT)\nabla_{R_1}\mathbf{u} : \Big[\gamma_1\sigma_1 \iint_{\mathbf{g}\cdot\mathbf{k}>0} \exp[-(m/4kT)(G^2+g^2)]\mathbf{k}\{\mathbf{G} + \mathbf{g} - \mathbf{g}\cdot\mathbf{k}\mathbf{k}\}\mathbf{g}\cdot\mathbf{k}\, d\mathbf{k}\, d\mathbf{C}_2 \\
& + \gamma_2\sigma_2 \exp(-\epsilon/kT) \iint_{\mathbf{g}\cdot\mathbf{k}>0} \exp[-(m/4kT)(G^2+g^2)]\mathbf{k}\{\mathbf{G} + \mathbf{g} - \tfrac{1}{2}(\mathbf{g}\cdot\mathbf{k} - [(\mathbf{g}\cdot\mathbf{k})^2 + \omega^2]^{\frac{1}{2}})\mathbf{k}\}\mathbf{g}\cdot\mathbf{k}\, d\mathbf{k}\, d\mathbf{C}_2 \\
& + \gamma_2\sigma_2 \iint_{\mathbf{g}\cdot\mathbf{k}<-\omega} \exp[-(m/4kT)(G^2+g^2)]\mathbf{k}\{\mathbf{G} + \mathbf{g} - \tfrac{1}{2}(\mathbf{g}\cdot\mathbf{k} + [(\mathbf{g}\cdot\mathbf{k})^2 - \omega^2]^{\frac{1}{2}})\mathbf{k}\}\mathbf{g}\cdot\mathbf{k}\, d\mathbf{k}\, d\mathbf{C}_2 \\
& + \gamma_2\sigma_2 \iint_{-\omega<\mathbf{g}\cdot\mathbf{k}<0} \exp[-(m/4kT)(G^2+g^2)]\mathbf{k}\{\mathbf{G} + \mathbf{g} - \mathbf{g}\cdot\mathbf{k}\mathbf{k}\}\mathbf{g}\cdot\mathbf{k}\, d\mathbf{k}\, d\mathbf{C}_2 \Big] \\
& + [(N-1)\sigma_1^3/v^2](m/2\pi kT)^3 \nabla_{R_1} g_0^{(2)}(\mathbf{R}_1, \sigma_1) \cdot \iint_{\mathbf{g}\cdot\mathbf{k}>0} \exp[-(m/2kT)(C_1^2 + C_2^2)]\mathbf{k}\mathbf{g}\cdot\mathbf{k}\, d\mathbf{k}\, d\mathbf{C}_2 \\
& + \tfrac{1}{2}[(N-1)\sigma_2^3/v^2](m/2\pi kT)^3 [\exp(-\epsilon/kT)\nabla_{R_1} g_0^{(2)}(\mathbf{R}_1, \sigma_2) + \nabla_{R_1} g_0^{(2)*}(\mathbf{R}_1, \sigma_2)] \\
& \cdot \iint_{\mathbf{g}\cdot\mathbf{k}>0} \exp[-(m/2kT)(C_1^2 + C_2^2)]\mathbf{k}\mathbf{g}\cdot\mathbf{k}\, d\mathbf{k}\, d\mathbf{C}_2 \\
& + \tfrac{1}{2}[(N-1)\sigma_2^3/v^2](m/2\pi kT)^3 [\exp(\epsilon/kT)\nabla_{R_1} g_0^{(2)*}(\mathbf{R}_1, \sigma_2) + \nabla_{R_1} g_0^{(2)}(R_1, \sigma_2)] \\
& \cdot \iint_{\mathbf{g}\cdot\mathbf{k}<-\omega} \exp[-(m/2kT)(C_1^2 + C_2^2)]\mathbf{k}\mathbf{g}\cdot\mathbf{k}\, d\mathbf{k}\, d\mathbf{C}_2 .
\end{aligned}
$$

$$+[(N-1)\sigma_2^3/v^2](m/2\pi kT)^{\frac{3}{2}}\nabla_{R_1}g_0^{(2)}(\mathbf{R}_1,\sigma_2)\cdot\iint_{-\omega<\mathbf{g}\cdot\mathbf{k}<0}\exp[-(m/2kT)(C_1^2+C_2^2)]\mathbf{k}\mathbf{g}\cdot\mathbf{k}d\mathbf{k}d\mathbf{C}_2$$

$$=-\bar{f}_0^{(1)}(1)\Big[-v^{-1}\frac{Dv}{Dt}-\Big(\frac{3}{2}-\frac{mC_1^2}{2kT}\Big)T^{-1}\frac{DT}{Dt}+\mathbf{C}_1\cdot\Big\{\frac{m}{kT}\frac{D\mathbf{u}}{Dt}-\frac{1}{v}\nabla_{R_1}v$$

$$-[4\pi(N-1)/3v^2][\sigma_1^3g_0^{(2)}(\sigma_1)+\sigma_2^3g_0^{(2)*}(\sigma_2)-\sigma_2^3g_0^{(2)}(\sigma_2)]\nabla_{R_1}v-[\tfrac{3}{2}-(mC_1^2/2kT)]T^{-1}\nabla_{R_1}T$$

$$-[2\pi(N-1)/3v][\sigma_1^3g_0^{(2)}(\sigma_1)+\sigma_2^3g_0^{(2)*}(\sigma_2)-\sigma_2^3g_0^{(2)}(\sigma_2)][\tfrac{1}{2}-(3mC_1^2/10kT)]T^{-1}\nabla_{R_1}T$$

$$+[2\pi(N-1)/3v]\nabla_{R_1}[\sigma_1^3g_0^{(2)}(\mathbf{R}_1,\sigma_1)+\sigma_2^3g_0^{(2)*}(\mathbf{R}_1,\sigma_2)-\sigma_2^3g_0^{(2)}(\mathbf{R}_1,\sigma_2)]\Big\}$$

$$-[2\pi(N-1)/3v][\sigma_1^3g_0^{(2)}(\sigma_1)+\sigma_2^3g_0^{(2)*}(\sigma_2)-\sigma_2^3g_0^{(2)}(\sigma_2)][1-(mC_1^2/5kT)]\nabla_{R_1}\cdot\mathbf{u}$$

$$+(m/kT)\mathbf{C}_1\mathbf{C}_1:\nabla_{R_1}\mathbf{u}+[4\pi(N-1)/15v][\sigma_1^3g_0^{(2)}(\sigma_1)+\sigma_2^3g_0^{(2)*}(\sigma_2)-\sigma_2^3g_0^{(2)}(\sigma_2)](m/kT)\mathbf{C}_1\mathbf{C}_1:\nabla_{R_1}\mathbf{u}\Big]$$

$$+(1/v^2)(m/2\pi kT)^{\frac{3}{2}}(m/2kT^2)\nabla_{R_1}T\cdot\Big[\exp(-\epsilon/kT)(\gamma_2\sigma_2/2)\iint_{\mathbf{g}\cdot\mathbf{k}>0}\exp[-(m/4kT)(G^2+g^2)]$$

$$\times\mathbf{G}\cdot\mathbf{k}\mathbf{k}\{\mathbf{g}\cdot\mathbf{k}+[(\mathbf{g}\cdot\mathbf{k})^2+\omega^2]^{\frac{1}{2}}\}\mathbf{g}\cdot\mathbf{k}d\mathbf{k}d\mathbf{C}_2$$

$$+\tfrac{1}{2}(\gamma_2\sigma_2)\iint_{\mathbf{g}\cdot\mathbf{k}<-\omega}\exp[-(m/4kT)(G^2+g^2)]\mathbf{G}\cdot\mathbf{k}\mathbf{k}\{\mathbf{g}\cdot\mathbf{k}-[(\mathbf{g}\cdot\mathbf{k})^2-\omega^2]^{\frac{1}{2}}\}\mathbf{g}\cdot\mathbf{k}d\mathbf{k}d\mathbf{C}_2\Big]$$

$$+(1/v^2)(m/2\pi kT)^{\frac{3}{2}}(m/kT)\nabla_{R_1}\mathbf{u}:\Big[\exp(-\epsilon/kT)\tfrac{1}{2}(\gamma_2\sigma_2)\iint_{\mathbf{g}\cdot\mathbf{k}>0}\exp[-(m/4kT)(G^2+g^2)]$$

$$\times\mathbf{k}\mathbf{k}\{\mathbf{g}\cdot\mathbf{k}+[(\mathbf{g}\cdot\mathbf{k})^2+\omega^2]^{\frac{1}{2}}\}\mathbf{g}\cdot\mathbf{k}d\mathbf{k}d\mathbf{C}_2$$

$$+\tfrac{1}{2}(\gamma_2\sigma_2)\iint_{\mathbf{g}\cdot\mathbf{k}<-\omega}\exp[-(m/4kT)(G^2+g^2)]\mathbf{k}\mathbf{k}\{\mathbf{g}\cdot\mathbf{k}-[(\mathbf{g}\cdot\mathbf{k})^2-\omega^2]^{\frac{1}{2}}\}\mathbf{g}\cdot\mathbf{k}d\mathbf{k}d\mathbf{C}_2\Big],\quad\text{(A28)}$$

where

$$I(\phi)=-\gamma_1\iint_{\mathbf{g}\cdot\mathbf{k}>0}\bar{f}_0^{(1)}(1)\bar{f}_0^{(1)}(2)[\phi_1(\mathbf{R}_1,\mathbf{p}_1-\Delta\mathbf{p}_1^{(1)};t)+\phi_2(\mathbf{R}_1,\mathbf{p}_2-\Delta\mathbf{p}_2^{(1)};t)$$

$$-\phi_1(\mathbf{R}_1,\mathbf{p}_1;t)-\phi_2(\mathbf{R}_1,\mathbf{p}_2;t)\mathbf{g}\cdot\mathbf{k}d\mathbf{k}d\mathbf{C}_2$$

$$-\exp(-\epsilon/kT)\gamma_2\iint_{\mathbf{g}\cdot\mathbf{k}>0}\bar{f}_0^{(1)}(1)\bar{f}_0^{(1)}(2)[\phi_1(\mathbf{R}_1,\mathbf{p}_1-\Delta\mathbf{p}_1^{(2)};t)+\phi_2(\mathbf{R}_1,\mathbf{p}_2-\Delta\mathbf{p}_2^{(2)};t)$$

$$-\phi_1(\mathbf{R}_1,\mathbf{p}_1;t)-\phi_2(\mathbf{R}_1,\mathbf{p}_2;t)]\mathbf{g}\cdot\mathbf{k}d\mathbf{k}d\mathbf{C}_2$$

$$-\gamma_2\iint_{\mathbf{g}\cdot\mathbf{k}<-\omega}\bar{f}_0^{(1)}(1)\bar{f}_0^{(1)}(2)[\phi_1(\mathbf{R}_1,\mathbf{p}_1-\Delta\mathbf{p}_1^{(3)};t)+\phi_2(\mathbf{R}_1,\mathbf{p}_2-\Delta\mathbf{p}_2^{(3)};t)$$

$$-\phi_1(\mathbf{R}_1,\mathbf{p}_1;t)-\phi_2(\mathbf{R}_1,\mathbf{p}_2;t)]\mathbf{g}\cdot\mathbf{k}d\mathbf{k}d\mathbf{C}_2$$

$$-\gamma_2\iint_{-\omega<\mathbf{g}\cdot\mathbf{k}<0}\bar{f}_0^{(1)}(1)\bar{f}_0^{(1)}(2)[\phi_1(\mathbf{R}_1,\mathbf{p}_1-\Delta\mathbf{p}_1^{(4)};t)+\phi_2(\mathbf{R}_1,\mathbf{p}_2-\Delta\mathbf{p}_2^{(4)};t)$$

$$-\phi_1(\mathbf{R}_1,\mathbf{p}_1;t)-\phi_2(\mathbf{R}_1,\mathbf{p}_2;t)]\mathbf{g}\cdot\mathbf{k}d\mathbf{k}d\mathbf{C}_2.\quad\text{(A29)}$$

The integrations over $d\mathbf{k}$ and $d\mathbf{p}_2$ that have thus far been performed are given in Chapman and Cowling.[1]

To proceed further, use is made of the following general property of an integral equation. We rewrite Eq. (A28) in the form

$$\lambda\int dyK(x,y)G(y)=S(x),\quad\text{(A30)}$$

where $K(x, y)$, the kernel of the integral, and $S(x)$ are known functions, λ is a constant, and $G(y)$ is the unknown function to be determined. If $S(x)=0$, Eq. (A30) is a homogeneous integral equation

$$\int K(x, y)G(y)dy=0, \tag{A31}$$

and the solutions to this homogeneous equation will be denoted $G_h(y)$. By a theorem due to Hilbert,[19] solutions of the homogeneous equation are orthogonal to the inhomogeneous term, i.e.,

$$\int G_h(x)\,S(x)dx=0. \tag{A32}$$

There are five invariants of motion, the energy, mass, and three components of momentum. Each of these is a solution to the homogeneous equation obtained by setting the right-hand side of Eq. (A28) equal to zero. Hence, using the orthogonality conditions given by Eq. (A32) the following conditions are obtained:

$$\int \psi_i I(\phi)\,d\mathbf{p}_1=0; \qquad i=1, 2, 3, \tag{A33}$$

where ψ_1 is the mass, ψ_2 is the momentum, and ψ_3 is the energy. Application of the condition given by Eq. (A33) to Eq. (A28) results in

$$-(1/v)\,(Dv/Dt)+\nabla_{R_1}\cdot\mathbf{u}=0 \tag{A34}$$

for the conservation of mass and

$$D\mathbf{u}/Dt=-\rho^{-1}\nabla_{R_1}\{(kT/v)\,(1+b\rho\Lambda)\} \tag{A35}$$

for the conservation of momentum. As in the main text, $b\rho\Lambda$ is defined as

$$[2\pi(N-1)/3v]\{\sigma_1^3 g_0^{(2)}(\sigma_1)+\sigma_2^3 g_0^{(2)}(\sigma_2)[\exp(-\epsilon/kT)-1]\}.$$

and Λ is defined as

$$\{\sigma_1^3 g_0^{(2)}(\sigma_1)+\sigma_2^3 g_0^{(2)}(\sigma_2)[\exp(-\epsilon/kT)-1]\}.$$

The invariant $\psi_3=(\mathbf{p}_1^2/2m)+V(R_{12})$ is much more difficult to utilize in generating a conservation condition to the energy term. For the purposes of this paper DT/Dt will be approximated by the quasi-dense hard-sphere fluid formula

$$DT/Dt=-\tfrac{2}{3}T\nabla_{R_1}\cdot\mathbf{u}(1+b\rho\Lambda). \tag{A36}$$

Equation (A36) is identical with the expression for DT/Dt found in Chapman and Cowling[1] for dense hard spheres except we have replaced $b_1\rho g_0^{(2)}(\sigma_1)$ with $b\rho\Lambda$. This approximation is exact to the first order in ϵ/kT.

If Eqs. (A34)–(A36) are substituted into Eq. (A28), the resulting equation is

$$I(\phi)=-\bar{f}_0^{(1)}(1)\Big\{(1+\tfrac{2}{5}b\rho\Lambda)\,(m/kT)\mathbf{C}_1^0\mathbf{C}_1:\nabla_{R_1}\mathbf{u}+(1+\tfrac{3}{5}b\rho\Lambda)\Big(\frac{mC_1^2}{2kT}-\frac{5}{2}\Big)\mathbf{C}_1\cdot\nabla_{R_1}\ln T\Big\}$$

$$+(8/\pi^2v^2)\,(m/2kT)\gamma_2\sigma_2\nabla_{R_1}\ln T\cdot\Big[\frac{\exp(-s^2)}{30}\int\exp(-h^2-v^2)\mathbf{h}$$

$$\cdot\mathbf{v}^0\mathbf{v}\{4+(s^3/v^5)\,(5v^2+6s^2)+(v^5)^{-1}(v^2+s^2)^{\frac{1}{2}}(4v^2-6s^2)\}d\mathbf{x}_2$$

$$-\frac{1}{30}\int_{v>s}\exp(-h^2-v^2)\mathbf{h}\cdot\mathbf{v}^0\mathbf{v}\{4+(s^3/v^5)\,(5v^2-9s^2)+(v^5)^{-1}(v^2-s^2)^{\frac{1}{2}}(4v^2+6s^2)\}d\mathbf{x}_2$$

$$+\frac{\exp(-s^2)}{9}\int\exp(-h^2-v^2)\{v^2-(s^3/v)+v^{-1}(v^2-s^2)^{\frac{1}{2}}\}\mathbf{h}d\mathbf{x}_2$$

$$-\frac{1}{9}\int_{v>s}\exp(-h^2-v^2)\{v^2-(s^2/v)+v^{-1}(v^2-s^2)^{\frac{1}{2}}\}\mathbf{h}d\mathbf{x}_2\Big]$$

[19] See for example, R. Courant and D. Hilbert, *Methods of Mathematical Physics* (Interscience Publishers, Inc., New York, 1954), Vol. I.

$$+(8\sqrt{2}/\pi^2v^2)(m/2kT)^{\frac{1}{2}}\gamma_2\sigma_2\nabla_{R_1}\mathbf{u}:\Big[\frac{\exp(-s^2)}{30}\int\exp(-h^2-v^2)\mathbf{v}^0\mathbf{v}\{4+(s^3/v^5)(5v^2+6s^2)$$

$$+(v^5)^{-1}(v^2+s^2)^{\frac{1}{2}}(4v^2-6s^2)\}d\mathbf{x}_2$$

$$-\frac{1}{30}\int_{v>s}\exp(-h^2-v^2)\mathbf{v}^0\mathbf{v}\{4+(s^3/v^5)(5v^2-9s^2)+(v^5)^{-1}(v^2-s^2)^{\frac{1}{2}}(4v^2+6s^2)\}d\mathbf{x}_2$$

$$+\frac{\exp(-s^2)}{9}\int\exp(-h^2-v^2)\{v^2+(s^3/v)+v^{-1}(v^2+s^2)^{\frac{1}{2}}\}\mathbf{1}d\mathbf{x}_2$$

$$-\frac{1}{9}\int_{v>s}\exp(-h^2-v^2)\{v^2-(s^3/v)+v^{-1}(v^2-s^2)^{\frac{1}{2}}\}\mathbf{1}d\mathbf{x}_2\Big], \quad \text{(A37)}$$

where $\mathbf{x}=(m/4kT)^{\frac{1}{2}}\mathbf{C}$, $s=(\epsilon/kT)^{\frac{1}{2}}$, $\mathbf{v}=(m/4kT)^{\frac{1}{2}}\mathbf{g}$, $\mathbf{h}=(m/4kT)^{\frac{1}{2}}\mathbf{G}$,

$$\mathbf{A}^0\mathbf{A}=\mathbf{A}\mathbf{A}-\tfrac{1}{3}A^2\mathbf{1}. \quad \text{(A38)}$$

The integrations over the solid angle $d\mathbf{k}$ have been carried out using the integrals given in Appendix II. Due to the constraint on the relative velocity, a number of the integrals in Eq. (A37) are more easily evaluated when integrated with respect to $d\mathbf{p}_1d\mathbf{p}_2$. In determining ϕ use is made of this fact.

Since the right-hand side of Eq. (A37) is a linear combination of $\nabla_{R_1}\ln T$ and $\nabla_{R_1}\mathbf{u}$ the perturbation function ϕ must be of the form

$$\phi=\mathbf{A}\cdot\nabla_{R_1}\ln T+\mathbf{B}:\nabla_{R_1}\mathbf{u}. \quad \text{(A39)}$$

By substitution of Eq. (A39) into Eq. (A37) and comparison of the coefficients of $\nabla_{R_1}\ln T$ and $\nabla_{R_1}\mathbf{u}$, the following results are obtained:

$$I(\mathbf{A})=\mathbf{K}, \quad \text{(A40)}$$

$$I(\mathbf{B})=\mathbf{L}, \quad \text{(A41)}$$

$$\mathbf{K}=\bar{f}_0^{(1)}(1)\mathbf{C}_1\Big(\frac{mC_1^2}{2kT}-\frac{5}{2}\Big)(1+\tfrac{2}{5}\bar{b}\rho\Lambda)+\frac{8}{\pi^2v^2}\Big(\frac{m}{2kT}\Big)\gamma_2\sigma_2\Big[\frac{\exp(-s^2)}{30}\int\exp(-h^2-v^2)$$

$$\times\mathbf{h}\cdot\mathbf{v}^0\mathbf{v}\{4+(s^3/v^5)(5v^2+6s^2)+(v^5)^{-1}(v^2+s^2)^{\frac{1}{2}}(4v^2-6s^2)\}d\mathbf{x}_2$$

$$-\frac{1}{30}\int_{v>s}\exp(-h^2-v^2)\mathbf{h}\cdot\mathbf{v}^0\mathbf{v}\{4+(s^3/v^5)(5v^2-9s^2)+(v^5)^{-1}(v^2-s^2)^{\frac{1}{2}}(4v^2+6s^2)\}d\mathbf{x}_2$$

$$+\frac{\exp(-s^2)}{9}\int\exp(-h^2-v^2)\{v^2-(s^3/v)+v^{-1}(v^2+s^2)^{\frac{1}{2}}\}\mathbf{h}d\mathbf{x}_2$$

$$-\frac{1}{9}\int_{v>s}\exp(-h^2-v^2)\{v^2-(s^3/v)+v^{-1}(v^2-s^2)^{\frac{1}{2}}\}\mathbf{h}d\mathbf{x}_2\Big], \quad \text{(A42)}$$

$$\mathbf{L}=-(m/kT)\bar{f}_0^{(1)}(1)(1+\tfrac{2}{5}\bar{b}\rho\Lambda)\mathbf{C}_1^0\mathbf{C}_1+(8\sqrt{2}/\pi^2v)(m/2kT)^{\frac{1}{2}}\gamma_2\sigma_2\Big[\frac{\exp(-s^2)}{30}\int\exp(-h^2-v^2)\mathbf{v}^0\mathbf{v}$$

$$\times\{4+(s^3/v^5)(5v^2+6s^2)+(v^5)^{-1}(v^2+s^2)^{\frac{1}{2}}(4v^2-6s^2)\}d\mathbf{x}_2$$

$$-\frac{1}{30}\int_{v>s}\exp(-h^2-v^2)\mathbf{v}^0\mathbf{v}\{4+(s^3/v^5)(5v^2-9s^2)+(v^5)^{-1}(v^2-s^2)^{\frac{1}{2}}(4v^2+6s^2)\}d\mathbf{x}_2$$

$$+\frac{\exp(-s^2)}{9}\int\exp(-h^2-v^2)\{v^2-(s^3/v)+v^{-1}(v^2+s^2)^{\frac{1}{2}}\}\mathbf{1}d\mathbf{x}_2$$

$$-\frac{1}{9}\int_{v>s}\exp(-h^2-v^2)\{v^2-(s^3/v)+v^{-1}(v^2-s^2)^{\frac{1}{2}}\}\mathbf{1}d\mathbf{x}_2\Big]. \quad \text{(A43)}$$

Solution of the Integral Equation

It is more convenient in the following calculations to work with the reduced peculiar velocity **W** defined by

$$\mathbf{W}=\left(\frac{m}{2kT}\right)^{\frac{1}{2}}\left(\frac{\mathbf{p}}{m}-\mathbf{u}\right)=\left(\frac{m}{2kT}\right)^{\frac{1}{2}}\mathbf{C}. \tag{A44}$$

Hirschfelder and Curtiss[3] have introduced a technique for solving the Boltzmann equation in which **A** and **B** are expanded as finite sums of orthogonal polynomials in the square of the reduced peculiar velocity **W**. The coefficients of these expansions are then determined by a variational procedure. The Sonine polynomials may be generated from the formula

$$S_n^{(m)}(Z)=\sum_j \frac{(-1)^j(m+n)!}{(n+j)!(m-j)!j!}Z^j, \tag{A45}$$

where $S_n^{(m)}$ is normalized to $(m+n)!/m!$ in the sense that

$$\int_0^\infty Z^n \exp(-Z)\, S_n^{(m)}(Z)\, S_n^{(i)}(Z)\,dZ=[(m+n)!/m!]\delta_{mi} \tag{A46}$$

with δ_{mi} the Kronecker delta.

Since **K** depends only on $\mathbf{W}_1$ the most general form of the perturbation function **A** is

$$\mathbf{A}=\mathbf{W}A(W), \tag{A47}$$

where $A(W)$ is a scalar function of the peculiar velocity. The scalar function $A(W)$ may be expanded as a finite series in Sonine polynomials

$$A(W)=\sum_{m=0}^{s} a^{(j)} S_{\frac{3}{2}}^{(m)}(W^2). \tag{A48}$$

As a trial expansion the series will be terminated after the second term, i.e.,

$$A=a^0 S_{\frac{3}{2}}^{(0)}(W^2)+a^{(1)} S_{\frac{3}{2}}^{(1)}(W^2)=a^0+a^{(1)}(\tfrac{5}{2}-W^2). \tag{A49}$$

The zeroth coefficient, $a^{(0)}$, must vanish in order to satisfy the auxiliary conditions given by Eqs. (A10)–(A12). Hence, the trial function, Eq. (A47), becomes

$$\mathbf{A}=\mathbf{W}(\tfrac{5}{2}-W^2)a^{(1)}. \tag{A50}$$

Insertion of Eq. (A50) into Eq. (A40) followed by a multiplication by $\mathbf{W}_1 S^{(1)}(W_1^2)$ and integration over $d\mathbf{p}_1$ gives for the coefficient $a^{(1)}$,

$$a^{(1)}=\frac{\int \mathbf{K}\cdot\mathbf{W}_1 S_{\frac{3}{2}}^{(1)}(W_1^2)\,d\mathbf{p}_1}{\int I(\mathbf{W}S_{\frac{3}{2}}^{(1)}(W_1^2))\cdot\mathbf{W}S_{\frac{3}{2}}^{(1)}(W_1^2)\,d\mathbf{p}_1}, \tag{A51}$$

where

$$\begin{aligned}
I[\mathbf{W}S_{\frac{3}{2}}^{(1)}(W^2)]=&-\gamma_1\iint_{\mathbf{g}\cdot\mathbf{k}>0}\tilde{f}_0^{(1)}(1)\tilde{f}_0^{(1)}(2)[\{\mathbf{W}_1'[\tfrac{5}{2}-(W_1')^2]+\mathbf{W}_2'[\tfrac{5}{2}-(W_2')^2]\}^{(1)}\\
&-\mathbf{W}_1(\tfrac{5}{2}-W_1^2)-\mathbf{W}_2(\tfrac{5}{2}-W_2^2)]\mathbf{g}\cdot\mathbf{k}d\mathbf{k}d\mathbf{C}_2\\
&-\exp(-s^2)\gamma_2\iint_{\mathbf{g}\cdot\mathbf{k}>0}\tilde{f}_0^{(1)}(1)\tilde{f}_0^{(1)}(2)[\{\mathbf{W}_1'[\tfrac{5}{2}-(W_1')^2]+\mathbf{W}_2'[\tfrac{5}{2}-(W_2')^2]\}^{(2)}\\
&-\mathbf{W}_1(\tfrac{5}{2}-W_1^2)-\mathbf{W}_2(\tfrac{5}{2}-W_2^2)]\mathbf{g}\cdot\mathbf{k}d\mathbf{k}d\mathbf{C}_2\\
&-\gamma_2\iint_{\mathbf{g}\cdot\mathbf{k}<-\omega}\tilde{f}_0^{(1)}(1)\tilde{f}_0^{(1)}(2)[\{\mathbf{W}_1'[\tfrac{5}{2}-(W_1')^2]+\mathbf{W}_2'[\tfrac{5}{2}-(W_2')^2]\}^{(3)}\\
&-\mathbf{W}_1(\tfrac{5}{2}-W_1^2)-\mathbf{W}_2(\tfrac{5}{2}-W_2^2)]\mathbf{g}\cdot\mathbf{k}d\mathbf{k}d\mathbf{C}_2\\
&-\gamma_2\iint_{-\omega<\mathbf{g}\cdot\mathbf{k}<0}\tilde{f}_0^{(1)}(1)\tilde{f}_0^{(1)}(2)[\{\mathbf{W}_1'[\tfrac{5}{2}-(W_1')^2]+\mathbf{W}_2'[\tfrac{5}{2}-(W_2')^2]\}^{(4)}\\
&-\mathbf{W}_1(\tfrac{5}{2}-W_1^2)-\mathbf{W}_2(\tfrac{5}{2}-\mathbf{W}_2^2)]\mathbf{g}\cdot\mathbf{k}d\mathbf{k}d\mathbf{p}_2,
\end{aligned} \tag{A52}$$

and the superscripts (1), (2), (3), and (4) on the curly brackets indicate that the momentum change is given by the hard core, type *a*, type *b*, and type *c*, collision dynamics, respectively.

The denominator of Eq. (A51) is conveniently evaluated by converting the primed coordinates to unprimed coordinates. This is done through the "partial" binary collision dynamics. For the value of $a^{(1)}$, Eq. (A51) gives

$$a^{(1)}=\frac{(15/4v)(1+b\rho\Lambda)+(3\pi^{\frac{1}{2}}/2v^2)\sigma_2^3(N-1)g_0^{(2)}(\sigma_2)s^2\exp(-s^2)\left[\frac{\pi^{\frac{1}{2}}}{2}+2\exp(s^2)\int_s^\infty \exp(-x^2)x^2dx\right]}{(8\sqrt{2}/v^2)\pi^{\frac{1}{2}}(N-1)\{\lambda+\frac{1}{32}s^4\exp(-s^2)\sigma_2^2g_0^{(2)}\sigma_2\}} \tag{A53}$$

where λ is defined by Eq. (37) of the main text.

In evaluating the perturbation parameter $\mathbf{B}$, we note that $\mathbf{L}$ can be divided into a traceless dyadic and a multiple of the unit dyadic, i.e.,

$$\mathbf{L}=\mathbf{L}^{(1)}+L^{(2)}\mathbf{1}, \tag{A54}$$

where $L^{(2)}1$ is a scalar function of W_1 times the unit dyadic and $\mathbf{L}^{(1)}$ is a function of the traceless dyadic, $\mathbf{W}_1{}^0\mathbf{W}_1$ defined by Eq. (A38). It is clear that $\mathbf{B}$ is also divisible into a traceless tensor and a scalar function times $\mathbf{1}$, namely,

$$\mathbf{B}=\mathbf{B}^{(1)}+B^{(2)}\mathbf{1}. \tag{A55}$$

Eq. (A41) can now be rewritten in terms of $\mathbf{L}^{(1)}$ and $L^{(2)}\mathbf{1}$, and reads:

$$I(\mathbf{B}^{(1)})=\mathbf{L}^{(1)} \tag{A56}$$

$$\mathbf{L}^{(1)}=\frac{-2}{\pi^{\frac{1}{2}}v}\left(\frac{m}{2kT}\right)^{\frac{1}{2}}(1+\tfrac{2}{5}b\rho\Lambda)\mathbf{W}_1{}^0\mathbf{W}_1\exp(-W_1{}^2)+\frac{4\sqrt{2}}{15\pi^2v^2}\left(\frac{m}{2kT}\right)^{\frac{1}{2}}\gamma_2\sigma_2\exp(-s^2)$$
$$\times\left[\int\exp(-h^2-v^2)\mathbf{v}^0\mathbf{v}\{4+(s^3/v^5)(5v^2+6s^2)+(v^5)^{-1}(v^2+s^2)^{\frac{1}{2}}(4v^2-6s^2)\}d\mathbf{x}_2\right.$$
$$\left.-\exp(s^2)\int_{v>s}\exp(-h^2-v^2)\mathbf{v}^0\mathbf{v}\{4+(s^3/v^5)(5v^2-9s^2)+(v^5)^{-1}(v^2-s^2)^{\frac{1}{2}}(4v^2+6s^2)\}d\mathbf{x}_2\right], \tag{A57}$$

$$I(B^{(2)})=L^{(2)},$$

$$L^{(2)}=\frac{8\sqrt{2}}{9\pi^2v^2}\left(\frac{m}{2kT}\right)\gamma_2\sigma_2\exp(-s^2)\left[\int\exp(-h^2-v^2)\{v-(s^3/v)+v^{-1}(v^2+s^2)^{\frac{1}{2}}\}d\mathbf{x}_2\right.$$
$$\left.-\exp(-s^2)\int\exp(-h^2-v^2)\{v-(s^3/v)+v^{-1}(v^2-s^2)^{\frac{1}{2}}\}d\mathbf{x}_2\right]. \tag{A58}$$

Again, the perturbation parameters are expanded as a finite power series in Sonine polynomials and the series terminated after the first nonvanishing terms (as determined by the auxiliary conditions). Thus, the trial functions are

$$\mathbf{B}^{(1)}=\mathbf{W}^0\mathbf{W}S_{5/2}{}^0(W^2)b_0{}^{(1)}=\mathbf{W}^0\mathbf{W}b_0{}^{(1)} \tag{A59}$$

$$B^{(2)}=b_2{}^{(2)}S_{\frac{1}{2}}{}^{(2)}(W^2)=b_2{}^{(2)}(\tfrac{15}{8}-\tfrac{5}{2}W^2+\tfrac{1}{2}W^4). \tag{A60}$$

As in the evaluation of $a^{(1)}$, $\mathbf{B}^{(1)}$ is introduced into $I(\mathbf{B}^{(1)})$, each side of Eq. (A56) is multiplied by $\mathbf{W}_1{}^0\mathbf{W}_1$, and an integration over $d\mathbf{p}_1$ is performed on each side of the resulting equation. This procedure leads to the relation

$$b_0{}^{(1)}=\frac{\int\mathbf{L}^{(1)}:\mathbf{W}^0\mathbf{W}d\mathbf{p}_1}{\int I(\mathbf{W}^0\mathbf{W}):\mathbf{W}_1{}^0\mathbf{W}_1d\mathbf{p}_1}. \tag{A61}$$

Once again the appropriate binary dynamics are inserted into Eq. (A61) and $b_0^{(1)}$ is found to be

$$b_0^{(1)}=\frac{-\frac{5}{\sqrt{2}v}\left(\frac{m}{2kT}\right)^{\frac{1}{2}}(1+\frac{2}{5}b\rho\Lambda)-\frac{4\pi^{\frac{1}{2}}}{3\sqrt{2}v^2}\left(\frac{m}{2kT}\right)^{\frac{1}{2}}\sigma_2^3(N-1)g_0^{(2)}(\sigma_2)s^2\exp(-s^2)\left[\frac{\pi^{\frac{1}{2}}}{2}+2\exp(s^2)\int_s^\infty\exp(-x^2)x^2dx\right]}{(8\pi^{\frac{1}{2}}/v^2)(N-1)\{\lambda+\sigma_2^2g_0^{(2)}(\sigma_2)\exp(-s^2)(s^2/12)\}} \tag{A62}$$

The coefficient $b_2^{(2)}$ will be neglected since it may be shown, by direct integration, to be of the same order as the term neglected in Eq. (A36).

Using Eqs. (A53) and (A62) the perturbation function, can be written in the form

$$\begin{aligned}\phi=&\frac{(15/4v)(1+\frac{3}{5}b\rho\Lambda)+(3\pi^{\frac{1}{2}}/2v^2)\sigma_2^3(N-1)g_0^{(2)}(\sigma_2)s^2\exp(-s^2)\left[\frac{\pi^{\frac{1}{2}}}{2}+2\exp(s^2)\int_s^\infty\exp(-x^2)x^2dx\right]}{(8/\sqrt{2}\pi^{\frac{1}{2}}/v^2)(N-1)\{\lambda+\sigma_2^2g_0^{(2)}(\sigma_2)\exp(-s^2)\frac{11}{32}s_4\}}\\&\times(\tfrac{5}{2}-W^2)\mathbf{W}\cdot\nabla_{R_1}\ln T\\&+\frac{(-5/\sqrt{2}v)(1+\frac{2}{5}b\rho\Lambda)-(4\pi^{\frac{1}{2}}/3\sqrt{2}v^2)(m/2kT)^{\frac{1}{2}}\sigma_2^3(N-1)g_0^{(2)}(\sigma_2)s^2\exp(-s^2)\left[\frac{\pi^{\frac{1}{2}}}{2}+2\exp(s^2)\int_s^\infty\exp(-x^2)x^2dx\right]}{(8\pi^{\frac{1}{2}}/v^2)(N-1)\{\lambda+\sigma_2^2g_0^{(2)}(\sigma_2)\exp(-s^2)(s^4/12)\}}\\&\times\mathbf{WW}:\nabla_{R_1}\mathbf{u}.\end{aligned} \tag{A63}$$

Equation (A63) is rather bulky so it will be of some interest to examine the equations resulting from weak attractive interactions, i.e., $(\epsilon/kT)<1$. Of course, with the attractive potential equal to zero, Eq. (A63) reduces properly to the hard-sphere perturbation,[6,7,20]

$$\phi=\frac{15v\{1+[2\pi(N-1)\sigma_1^3g_0^{(2)}(\sigma_1)/5v]\}}{16\sqrt{2}\pi^{\frac{1}{2}}(N-1)\sigma_1^2g_0^{(2)}(\sigma_1)}(\tfrac{5}{2}-W^2)\mathbf{W}\cdot\nabla_{R_1}\ln T+\frac{-5v\{1+[4\pi(N-1)\sigma_1^3g_0^{(2)}(\sigma_1)/15v]\}}{4\sqrt{2}\pi^{\frac{1}{2}}(N-1)\sigma_1^2g_0^{(2)}(\sigma_1)}\mathbf{W}^0\mathbf{W}:\nabla_{R_1}\mathbf{u}. \tag{A64}$$

If in Eq. (A63) only terms of the first order in $s^2=\epsilon/kT$ are retained

$$\begin{aligned}\phi=&\frac{(15/4v)(1+\frac{3}{5}b\rho\Lambda)-(3\pi/2v^2)\gamma_2\sigma_2\exp(-s^2)s^2[\frac{5}{4}+\frac{21}{4}\exp(s^2)]}{[4\pi^{\frac{1}{2}}/v^2](N-1)\{\sigma_1^2g_0^{(2)}(\sigma_1)+\sigma_2^2g_0^{(2)}(\sigma_1)[\exp(-s^2)-1-\frac{1}{2}s^2]-\frac{5}{2}s^2\}}(\tfrac{5}{2}-W^2)\mathbf{W}\cdot\nabla_{R_1}\ln T\\&+\frac{-(5/\sqrt{2}v)(m/2kT)^{\frac{1}{2}}(1+\frac{2}{5}b\rho\Lambda)-(4\pi/3\sqrt{2}v^2)(m/2kT)^{\frac{1}{2}}\gamma_2\sigma_2\exp(-s^2)}{[4(2\pi^{\frac{1}{2}})/v^2](N-1)\{\sigma_1^2g_0^{(2)}(\sigma_1)+\sigma_2^2g_0^{(2)}(\sigma_1)[\exp(-s^2)-1-\frac{1}{2}s^2]-\frac{5}{2}s^2\}}\mathbf{WW}:\nabla_{R_1}\mathbf{u}.\end{aligned} \tag{A65}$$

When $(\epsilon/kT)\leq\frac{1}{2}$, Eq. (A65) approximates Eq. (A63) to within about 3%.

Discussion

In the preceding analysis non-hard-sphere terms in Eq. (A36) and the coefficient, $b_2^{(2)}$, were neglected. What effects do these approximations have on the fluxes? The neglected contributions will in both cases appear as coefficients of $\nabla_{R_1}\cdot\mathbf{u}\mathbf{1}$ in the fluxes. Since the heat vector is independent of $\nabla_{R_1}\cdot\mathbf{u}$, it will not be influenced by the approximations.

The Newtonian form of the macroscopic stress tensor is given by

$$\mathfrak{d}=-[p+(\tfrac{2}{3}\eta-\Phi)\nabla_{R_1}\cdot\mathbf{u}]\mathbf{1}+2\eta(\tfrac{1}{2}\nabla_{R_1}\mathbf{u}+\tfrac{1}{2}\nabla_{R_1}\mathbf{u}^\dagger), \tag{A66}$$

where Φ is the coefficient of bulk viscosity, η the coefficient of shear viscosity, $\frac{1}{2}(\nabla_{R_1}\mathbf{u}+\nabla_{R_1}\mathbf{u}^\dagger)$ the rate of strain tensor, p the hydrostatic pressure, and $\nabla_{R_1}\mathbf{u}^\dagger$ is the transpose of $\nabla_{R_1}\mathbf{u}$. As is clear physically, Φ is the only transport coefficient influenced by the terms neglected, since η will appear as the coefficient of the tensor $\frac{1}{2}(\nabla_{R_1}\mathbf{u}+\nabla_{R_1}\mathbf{u}^\dagger)$, and the hydrostatic pressure will appear as the coefficient of the unit tensor $\mathbf{1}$.

---

[20] S. A. Rice, J. Chem. Phys. **31**, 584 (1959).

We conclude then, that of the transport coefficients calculated from Eq. (A63), the coefficient of bulk viscosity is the least accurate.

APPENDIX II

Many of the integrals over $\mathbf{k}$ which were used in obtaining Eq. (A37) are evaluated by techniques used previously in the theory of the rigid-sphere fluid.[1,20] The integrals not found in the reference given have the form

$$\int \mathbf{k}\mathbf{k}(\mathbf{g}\cdot\mathbf{k})^2 d\mathbf{k} = -(\pi/15)[\mathbf{g}\mathbf{g}(9\cos^5\theta - 5\cos^3\theta) + g^2\mathbf{1}(5\cos^3\theta - 3\cos^5\theta)]_-^+ \tag{B1}$$

$$\int \mathbf{k}\mathbf{k}\mathbf{g}\cdot\mathbf{k}[(\mathbf{g}\cdot\mathbf{k})^2 \pm \omega^2]^{\frac{1}{2}} d\mathbf{k} = -(\pi/15)(g^2\cos^2\theta \pm \omega^2)^{\frac{1}{2}}\{(\mathbf{g}\mathbf{g}/g^5)(9g^2\cos^2\theta - 5g^2 \mp 6\omega^2) + (\mathbf{1}/g^5)(5g^2 - 3g^2\cos^2\theta \pm 2\omega^2)\}_-^+. \tag{B2}$$

Therefore,

$$\int_{\mathbf{g}\cdot\mathbf{k}>0} \mathbf{k}\mathbf{k}\{\mathbf{g}\cdot\mathbf{k} + [(\mathbf{g}\cdot\mathbf{k})^2 + \omega^2]^{\frac{1}{2}}\}\mathbf{g}\cdot\mathbf{k}\, d\mathbf{k} = (\pi/15)[\{4 + (g^5)^{-1}(g^2+\omega^2)^{\frac{1}{2}}(4g^2 - 6\omega^2) + (\omega^3/g^5)(5g^2 + 6\omega^2)\}\mathbf{g}\mathbf{g} + g^2\mathbf{1}\{2 + (g^5)^{-1}(g^2+\omega^2)^{\frac{1}{2}}(2g^2 + 2\omega^2) - (\omega^3/g^5)(5g^2 + 2\omega^2)\}] \tag{B3}$$

and

$$\int_{\mathbf{g}\cdot\mathbf{k}<-\omega} \mathbf{k}\mathbf{k}\{\mathbf{g}\cdot\mathbf{k} - [(\mathbf{g}\cdot\mathbf{k})^2 - \omega^2]^{\frac{1}{2}}\}\mathbf{g}\cdot\mathbf{k}\, d\mathbf{k} = -\frac{\pi}{15}\left[\left\{4 - \frac{9\omega^5}{g^5} + \frac{5\omega^3}{g^3} + \frac{(g^2-\omega^2)^{\frac{1}{2}}}{g^5}(4g^2 + 6\omega^2)\right\}\mathbf{g}\mathbf{g} + g^2\mathbf{1}\{2 + (5\omega^3/g^3) - (3\omega^5/g^5) + (g^5)^{-1}(g^2-\omega^2)^{\frac{1}{2}}(2g^2 - 2\omega^2)\}\right], \tag{B4}$$

where Eq. (B4) has the constraint $g > \omega$.

APPENDIX III

Minor Errata in Previous Papers

I. J. Chem. Phys. **31,** 575 (1959)
II. J. Chem. Phys. **31,** 584 (1959)
III. J. Chem. Phys. **32,** 538 (1960)

Dr. John Pople kindly informed us of a discrepancy between the text and the final equations of paper I cited above. Detailed examination showed that an error in copying notes to prepare the final manuscript and an inexplicable oversight in proof reading led to the omission of a term which had been properly calculated. The text was prepared from the complete final results and stands as printed. We wish to take this opportunity to amend the appropriate formulae and to correct a number of trivial printing errors. The roman numeral preceding each set of corrections refers to the paper as cited above.

I

(a) The symbol μ, referred to as a reduced mass, is not the usual reduced mass, and is defined by

$$\mathbf{p}_{12}/\mu = (\mathbf{p}_2/m) - (\mathbf{p}_1/m).$$

All calculations were performed using this relation.

(b) In Eqs. (51) and (52), the coefficient of $Ng(\sigma)$ should read:

$$(\tfrac{4}{25} + 48/25\pi)(2\pi\sigma^3/3v)^2.$$

(c) In Eqs. (58) and (59), the coefficient of $Ng(\sigma)$ should read:

$$(\tfrac{36}{175} + 192/150\pi)(2\pi\sigma^3/3v)^2.$$

(d) In Table I, the coefficients of $(\pi\sigma^3/v)^2$ in the density expansions for κ^{RKRZ} and η^{RKRZ} should read 0.4402 and 0.3842, respectively. The lines immediately preceding the density expansions should be modified in accordance with items (b) and (c) above.

II

(a) The quantity μ is defined as in I(a).

(b) In Eqs. (9) the coefficient of $\nabla_{R_1} \ln T$, and in the second term on the right-hand side of Eqs. (30), (34), and (50), the factor $\frac{3}{2}$ should read $\frac{5}{2}$.

(c) Eqs. (86), (88), (89), and (90) should be modified in the v^{-2} term as stated in items I(b) and I(c) above.

III

(a) The quantity $\mu_{\alpha\beta}$ is defined, as in I(a), by the relation

$$\mathbf{p}_{\alpha\beta}/\mu_{\alpha\beta}=\mathbf{p}_\beta/m_\beta-\mathbf{p}_\alpha/m_\alpha.$$

(b) Eq. (3) should read:

$$\mathbf{F}_j^\beta=\sum_{\alpha,i}\mathbf{F}_{ij}^{\alpha\beta}$$

(c) In Eqs. (4), (6) and (10) the dummy variable over which the summation is carried should be labeled β, and j replaced by 2. In Eq. (6), the factor preceding the integral should have the exponent outside the square brackets and read $[(N_\alpha-1)\tau]^{-1}$.

(d) The term: $\sum_\beta \mathbf{F}_{12}^{\alpha\beta}\cdot(\nabla_{p_{1\alpha}}-\nabla_{p_{2\beta}})K^{(2)}$ should appear on the right-hand side of Eq. (11).

(e) The equation at the top of p. 543 should be numbered (39), and the symbol on the left-hand side should be in bold face, $\mathbf{K}_\alpha$. Also, the last symbol on the right-hand side should be in bold face, $\mathbf{Z}_{1\alpha}$.

(f) The right-hand side of Eq. (49) should have $j!$ inserted in the denominator.

Letters to the Editor

THE Letters to the Editor section is subdivided into three parts entitled Communications, Comments and Errata, and Notes. These three sections are all subject to the same limitations on length. The textual material of each Letter is limited to a number of words equal to 950 minus the following: (a) 200 words for each average-sized figure; (b) 50 words for each displayed equation; (c) 7 words for each line of table including headings and horizontal rulings. No proof will be sent to the authors of "Communications" and "Comments and Errata." Proof will be sent to the authors of "Notes." The publication charge for Letters is $30 per page, with a minimum of $30 per Letter, If honored, the Institution will be entitled to 100 reprints without covers. See issues of May–September, 1957, for descriptions of categories.

Communications

Some Further Observations on the Critical Region

GEORGE W. BRADY AND H. L. FRISCH

Bell Telephone Laboratories, Inc., Murray Hill, New Jersey

(Received September 22, 1961)

WE would like to report an interesting effect observed in current studies on the C_7F_{16}-*i*-C_8H_{18} system. Briefly, small angle x-ray intensity curves were measured for 30 and 40 mole % C_7F_{16} solutions, while gradually dropping the temperature until the consolute curve temperature was reached. The consolute curve has been recently redetermined by J. L. Lundberg and his data indicate that the critical concentration occurs at 38.5 mole % C_7F_{16}, at a critical temperature of 23.78°C. The curve is quite flat on top, and the appropriate unmixing temperatures for our two concentrations are 23.44°C (30%) and 23.75°C (40%).

A typical set of intensity curves is shown in Fig. 1. Each curve takes about an hour to determine, and the curves are reproducible. As the consolute temperature is approached, the intensity increases rapidly at first, to finally reach a maximum value, after which point a region of constant intensity persists over a temperature range of ~1.0°. Following this, the intensity curve begins to decrease again.

An even more revealing insight into the state of affairs is shown when the Debye lengths L, which are a measure of the long-range fluctuations,[1] are plotted as shown in Fig. 2. (The fact that there exists a significant amount of clustering at temperatures much above the critical has been remarked on in a previous publication.)[2] Corresponding to the intensity effect we notice a flat portion in the curve again extending over a temperature region of ~1.0°C depending on the concentration, which is then followed by a decrease. The temperature of the phase separation for the two

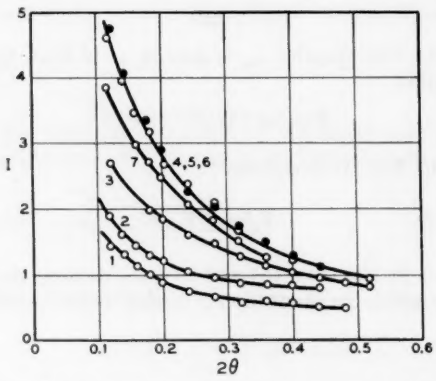

FIG. 1. A typical set of intensity curves measured as the temperature is lowered. The curve labeled 4, 5, 6 is the superimposition of three curves.

solutions coincides with the lower temperature end of the flat portion. The curves for the 30 and 40% C_7F_{16} solutions coincide after the phase separation.

The explanation of this phenomenon is difficult, but we can offer possible reasons why it takes place. It is hard to envisage any artifact in the data taking which would account for the effect observed. Large scale fluctuations may be present which are not seen by the x rays, but if this is so they must develop very suddenly, because we would surely see their onset. Another possibility is that the phase separation actually occurs at the upper temperature end of the flat portion and that the system goes into a quasi-colloidal state. The x rays would then be seeing clusters within larger "droplets." Visible light would, of course, see the larger "droplets." Indeed the solutions are observed to turn milky at this point, and remain so until the phase separation occurs. However, in the measurements of Zimm,[3] and Chow Quantie[4] it was noted that the asymmetry of scattering, which measures long-range correlation, fell off very sharply on either side of the critical concentration, and it is not known whether correlations of larger lengths than those observed here would be present.

An intriguing possibility then presents itself that we

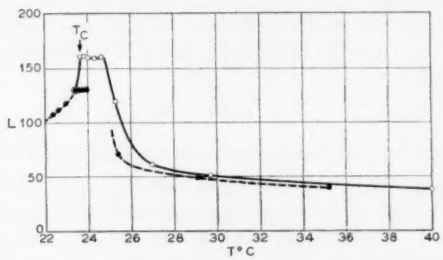

FIG. 2. Debye lengths L plotted as a function of temperature. Tc is the temperature at which two phases appear. Solid line, 40% C_7F_{16}, dashed line, 30% C_7F_{16}.

are dealing with a "derby hat" type of mechanism for phase separation in which the activity rises to a maximum at a temperature above that at which phase separation occurs, and then remains constant over a finite temperature interval before this latter event takes place.

The most interesting thing about these experiments is that they indicate that in conjunction with light scattering measurements we may be able to study on a molecular basis the whole mechanism of what happens in the critical region, the x-ray scattering giving information about clustering in the <200 A range, and the light scattering telling us what happens in the range above this.

We would like to thank Bruno H. Zimm for his comments, and acknowledge stimulating discussions with M. S. Green, F. H. Stillinger, and Eugene Helfand.

[1] P. Debye, J. Chem. Phys. **31,** 680 (1957).
[2] G. W. Brady and J. I. Petz, J. Chem. Phys. **34,** 332 (1961).
[3] B. H. Zimm, J. Phys. Chem. **54,** 1306 (1950).
[4] Chow Quantie, Proc. Roy. Soc. (London) **A224,** 90 (1954).

Magnetic Interactions in Lithium Hydride

M. KARPLUS* AND H. J. KOLKER†

Department of Chemistry and Watson Scientific Computing Laboratory, Columbia University, New York, New York

(Received September 5, 1961)

THE magnetic interactions in $^1\Sigma$ molecules are of considerable experimental and theoretical importance because of their relationship to the electron distribution.[1] Since techniques for magnetic measurements have been extended and refined in recent years (e.g., molecular beams,[2] microwave spectroscopy[3]), it is of interest to attempt a concomitant development in the theoretical interpretation. Although many studies have been concerned with the magnetic properties of the hydrogen molecule,[4] there have been no comparable treatments of more general systems. In this communication, we report variation-perturbation calculations of the magnetic susceptibility (χ) and nuclear shielding (σ_N) in LiH. The simplicity of the formulation and the accuracy of the results give an indication of the feasibility of magnetic studies with approximate *ground-state* wave functions for many-electron systems.

In the absence of a magnetic field, the system is described by a Slater determinant of doubly filled molecular orbitals $\psi_i(i=1, 2)$. For this function ψ^0, there exists an operator $\mathfrak{H}_a^0$, such that $\mathfrak{H}_a^0\psi^0=E_a^0\psi^0$, with E_a^0 the expectation value of the energy over the exact zero-order Hamiltonian $\mathfrak{H}^0$.[5,6] The perturbation $\mathfrak{H}'$ arising from a uniform magnetic field $\mathbf{H}$ and a nuclear moment μ_N is

$$\mathfrak{H}'=\sum_{k=1}^{4}h'(k);\quad h'(k)=\frac{e^2}{2mc^2}\mid A_k\mid^2+\frac{e\hbar}{mci}(\mathbf{A}_k\cdot\nabla_k),\quad (1)$$

where the vector potential $\mathbf{A}_k$ has the form

$$[\tfrac{1}{2}(\mathbf{H}\times\mathbf{r}_k)+(\boldsymbol{\mu}_N\times\mathbf{r}_{kN})/r_{kN}^3].$$

From the eigenfunction property of ψ^0 and the expression for $\mathbf{A}_k$, the first-order (diamagnetic) contributions to χ and σ_N reduce directly to sums over the individual orbitals. For the evaluation of the more difficult second-order (paramagnetic) contributions, which require an infinite summation in ordinary perturbation theory,[7] we use a variation technique. If each orbital has the form $\psi_i[1+(e/2mc)\mathbf{H}\cdot\mathbf{R}_i]$ in a field $\mathbf{H}$, the tensor component $(\chi^p)_{\nu\nu}$ is

$$(\chi^p)_{\nu\nu}=(e^2/m^2c^2)\cdot\sum_{i=1}^{2}\left[\frac{\hbar^2}{2m}\langle\psi_i\mid\nabla R_{i\nu}^*\cdot\nabla R_{i\nu}\mid\psi_i\rangle+\langle\psi_i\mid\{M_\nu R_{i\nu}\}\mid\psi_i\rangle\right],\quad (2)$$

where M_ν represents the ν component of angular momentum and $R_{i\nu}$ is a function which can be determined by minimizing $(\chi^p)_{\nu\nu}$. As is evident from Eq. (3), $R_{i\nu}$ for each orbital in LiH can be varied *independently* of the other orbital, even though an antisymmetrized function is employed for ψ^0.[8]

For the (σ_N^p) terms, the $R_{i\nu}$ obtained from Eq. (3) can be inserted into the expression

$$(\sigma_N^p)_{\nu\nu}=\frac{e^2}{m^2c^2}\sum_{i=1}^{2}\langle\psi_i\mid\left\{\frac{M_{\nu N}R_{i\nu}}{r_N^3}\right\}\mid\psi_i\rangle.\quad (3)$$

Alternatively, the orbital form

$$\psi_i[1+(e/2mc)\mathbf{H}\cdot\mathbf{S}_i+(e/mc)\boldsymbol{\mu}_N\cdot\mathbf{T}_i]$$

can be employed and the σ_N^p components minimized with respect to variations in both $\mathbf{S}_i$ and $\mathbf{T}_i$. The consistency of the values obtained for σ_N^p by the two methods provides a check for approximate treatments.

TABLE I. Magnetic interactions in lithium hydride (in ppm).

	$(\chi^d)_{Av}$	$(\sigma_H{}^d)_{Av}$	$(\sigma_{Li}{}^d)_{Av}$	$(\chi^p)_{Av}$	$(\sigma_H{}^p)_{Av}$	$(\sigma_{Li}{}^p)_{Av}$
Theory SAMO	−24.6	39.2	107.7	14.61	−12.1	−8.3
BLMO	−23.8	39.5	107.9	14.57	−12.3	−8.0
Experiment[11,12]	...	...	...	15.8	−13.8	−17.1

The formulation for the evaluation of χ and σ_N in LiH was applied to the SCF-LCAO-MO functions of Ransil.[9] Calculations were made with the functions having Slater exponents (SAMO) and "best-molecular" exponents (BLMO) in the atomic-orbital basis set. The resulting values for the rotational averages $(\ )_{Av}$ are listed in Table I. Polynomial expansions were used for $\mathbf{R}_i$, etc., and good convergence was attained. The dominant term in $\mathbf{R}_i$ corresponded to a translation of the vector potential and the other terms could be interpreted similarly as a change of gauge.[10] Because of a lack of data, only the paramagnetic terms can be compared with experiment.[11,12] Both $(\chi^p)_{Av}$ and $(\sigma_H{}^p)_{Av}$ are in satisfactory agreement with the measured values, while $(\sigma_{Li}{}^p)_{Av}$ is in error by a factor of two. From these results and the relative magnitudes involved, one can estimate that the *total* susceptibility and shielding values are accurate to $\pm 15\%$ or better.

Analysis of the calculation shows that $(\chi^p)_{Av}$ and $(\sigma_H{}^p)_{Av}$ are determined essentially by the (1σ) MO, which is primarily a $1s$ (Li) orbital. By contrast, $(\sigma_{Li}{}^p)_{Av}$ depends largely on the (2σ) MO, which is composed of hydrogen and lithium orbitals and is more sensitive to the details of the molecular potential. It would, therefore, be of some interest to determine what changes occur in $(\sigma_{Li}{}^p)_{Av}$ and the other paramagnetic terms when they are computed with improved LiH wave functions.[13] However, the formulation presented here and the results obtained with it demonstrate what can be done with a function (such as the BLMO function) that yields good values for ground-state one-electron properties (e.g., dipole moment,[14] nuclear quadrupole coupling constant[15]) and yet is of sufficient simplicity to be generalized to more complex systems.

Details concerning the variation-perturbation formulation and the method of calculation will be presented with additional applications in a later paper.[16]

We thank Dr. T. P. Das for discussions concerning the choice of variation function and Dr. C. W. Kern and Dr. W. N. Lipscomb for check values to test the integral programs.

* Alfred P. Sloan Foundation Fellow.

† Woodrow Wilson and National Science Foundation Predoctoral Fellow.

[1] M. Karplus, Revs. Modern Phys. **32,** 455 (1960).

[2] N. F. Ramsey, *Molecular Beams* (Oxford University Press, New York, 1956).

[3] C. H. Townes and A. L. Schalow, *Microwave Spectroscopy* (McGraw-Hill Book Company, Inc., New York, 1955).

[4] J. Tillieu and J. Guy, Compt. rend. **239,** 1203 (1954); M. J. Stephen, Proc. Roy. Soc. (London) **A243,** 264 (1957); T. P. Das and R. Bersohn, Phys. Rev. **115,** 897 (1959).

[5] R. Sternheimer, Phys. Rev. **96,** 951 (1954).

[6] For a Hartree-Fock function, $\mathcal{H}_a{}^0$ would be the Hartree-Fock operator of C. Møller and M. Plessett, Phys. Rev. **46,** 618 (1934).

[7] For a device to avoid the infinite summation in some shielding calculations, see C. W. Kern and W. N. Lipscomb, Phys. Rev. Letters **7,** 19 (1961).

[8] Coupled equations occur in molecules with both σ and π electrons [T. P. Das and M. Karplus (to be published)].

[9] B. J. Ransil, Revs. Modern Phys. **32,** 239, 245 (1960).

[10] T. K. Rebane, J. Exptl. Theoret. Phys. (U.S.S.R.) **38,** 963 (1960) [translation: Soviet Phys.—JETP **11,** 694 (1960)].

[11] T. R. Lawrence, C. H. Anderson, and N. F. Ramsey, Bull. Am. Phys. Soc. **6,** 271 (1961).

[12] L. Wharton, L. P. Gold, and W. Klemperer, Abstr. of Symposium on Molecular Structure and Spectroscopy, Ohio State University, June 12–16, 1961.

[13] L. C. Allen and A. M. Karo, Revs. Modern Phys. **32,** 275 (1960).

[14] L. Wharton, L. P. Gold, and W. Klemperer, J. Chem. Phys. **33,** 1255 (1960).

[15] H. J. Kolker and M. Karplus (to be published).

[16] See also reference 8.

Effect of Next Nearest Neighbor Ions on the Crystal Field Splitting of Transition Metal Ions in Crystals

J. Ferguson,* K. Knox, and D. L. Wood

Bell Telephone Laboratories, Inc., Murray Hill, New Jersey

(Received October 10, 1961)

It is generally assumed that the electronic energy levels of transition metal ions depend only on the ligands, that is nearest neighbor ions, and that the effect of ions farther away can be neglected. This is a good approximation when one considers only the direct electrostatic interaction between ions in the point charge model. However, even in the more realistic molecular orbital model, the effect of the polarization of the ligand orbitals by ions outside the first coordination sphere must be considered. It then becomes necessary to take account of the way in which a ligand is shared between a given metal ion and other ions in the structure. Since this idea gives new insight into the physical significance of the parameters of crystal field theory, a preliminary report of some relevant results for three transition metal ions follows.

First, other workers[1] have studied the absorption spectra of CoO and Co in MgO (pink) and we have studied the latter again. In both cases, the cobalt ion is surrounded by an octahedron of oxygen ions and the crystal field strength (Dq) is about 920 cm^{-1}. In addition, the Racah parameter B has a value of about 835 cm^{-1} in Co in MgO. We have found, however, from a study of the absorption spectrum of $CoWO_4$

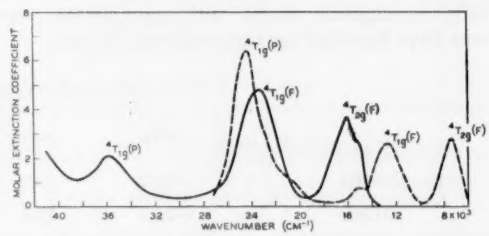

FIG. 1. Absorption spectra of K_3NaCrF_6 (full curve) and CrF_3 (dashed curve) at room temperature.

(blue-green), where the cobalt ion also is surrounded by six oxygen ions (distorted octahedron),[2] that Dq is about 690 cm^{-1} and B is about 770 cm^{-1}, even though the cobalt-oxygen distances are quite comparable. We relate the change in Dq from 920 to 690 cm^{-1} to the effect of the tungsten ion, which reduces the net charge on the oxygen ion relative to the oxygen in MgO.

Second, we have measured the absorption spectrum of the Ni^{2+} ion in $MgWO_4$ (orange). Here we find that Dq is again lower than for nickel ion in MgO (green), 710 and 860 cm^{-1}, respectively, and B is again lower in the tungstate.

Third, we have measured the absorption spectra of K_2NaCrF_6 (dark green) and CrF_3 (yellow green). In both of these crystals the chromium ions are surrounded by octahedra of fluoride ions, but the next nearest neighbors are different.[3] In K_2NaCrF_6 each fluoride ion is shared linearly by chromium and sodium ions, while in CrF_3 (quite unlike $CrBr_3$ and $CrCl_3$) each fluoride ion is shared by two chromium ions at an angle of 146°. The room temperature data given in Fig. 1 show the striking difference between the two crystal spectra. The spectrum of K_2NaCrF_6 fits the theoretical energy level diagram[4] with $Dq=1650$ cm^{-1} and $B=680$ cm^{-1}. However, values of $Dq=750$ cm^{-1} and $B=920$ cm^{-1} (free-ion value) are needed to fit the spectrum of CrF_3. Since the Cr—F distances are the same within experimental error, these observations are again related to the effect of next nearest neighbors. Note that for Cr^{3+} the lower Dq goes with a higher B value, while for Co^{2+} and Ni^{2+} the lower Dq is accompanied by a lower B value.

The following consequences of these results are important for both empirical and theoretical developments of ligand field theory. First, the spectrochemical series of ligands,[5] derived from solution spectra, does not apply to ionic crystals if there is a change of structural type, and arguments relating absorption spectra to structure are not generally valid for solids when based on this series alone. Second, there is no doubt that the changes of the Racah parameter B from the free ion value mean that a molecular orbital rather than an atomic orbital formulation for the interelectronic repulsion terms is needed, but we feel that even with this model, the physical interpretation of the variations in the B parameter in terms of so-called "covalency effects"[6] should be viewed with some caution. Last, the polarization of the ligand orbitals by the metal ion and next nearest neighbors is an important factor determining the magnitude of the crystal field splitting.

It is a pleasure to acknowledge the benefit derived from discussions with A. D. Liehr. We also thank L. G. Van Uitert for providing the $CoWO_4$ and $MgWO_4$ doped with Ni.

* Visiting Scholar. On leave from the Division of Chemical Physics, C. S. I. R. O., Melbourne, Australia.

[1] G. W. Pratt and R. Coelho, Phys. Rev. **116,** 281 (1959); W. Low, *ibid.* **109,** 256 (1958).
[2] R. O. Keeling, Jr., Acta Cryst. **10,** 209 (1957).
[3] K. Knox and D. W. Mitchell, J. Inorg. Nuclear Chem. (to be published); K. H. Jack and R. Maitland, Proc. Chem. Soc. **1959,** 232; K. Knox, Acta Cryst. **13,** 507 (1960).
[4] A. D. Liehr, "Symposium on molecular structure and spectroscopy," June, 1961 (to be published).
[5] See, e.g., the chapter by T. M. Dunn in *Modern Coordination Chemistry*, edited by J. Lewis and R. G. Wilkins (Interscience Publishers, Inc., New York, 1960).
[6] C. K. Jorgensen, Discussions Faraday Soc. **26,** 110 (1958).

Absorption Spectrum of Gaseous Cl^- and Electron Affinity of Chlorine

R. Stephen Berry, Curt W. Reimann,* and G. Neil Spokes†

Sterling Chemistry Laboratory, Yale University
New Haven, Connecticut

(Received September 18, 1961)

We wish to report observations of ultraviolet absorption spectra of several alkali halide vapors heated by shock waves. Spectra have been taken of RbF, RbBr, CsF, and CsCl. With the chloride salts, we find continuous absorption which we attribute to the gaseous ion Cl^-, undergoing the process $Cl^- + h\nu \rightarrow Cl^0 + e^-$. This continuum has the two sharp thresholds expected for photodetachment[1] and permits determination of the electron affinity of chlorine with considerable precision.

The shock tube is conventional. The driver section (155 cm), is separated from the low-pressure section (460 cm) by a scored aluminum diaphragm; both have the same square inside cross section (8.5×8.5 cm). Shock speeds are measured with platinum thermal-resistance gauges painted on glass rods located 197, 222, and 247 cm downstream from the diaphragm, and with a photocell at the quartz observation windows, 357 cm from the diaphragm. Signals are monitored on an oscilloscope (Tektronix 533) triggered by the shock passing the first gauge. The spectral source is a quartz capillary flash lamp which is fired by a "crowbar" trigger (KU 402), operated by a delayed signal from the oscilloscope. The mirrors of a White multiple-reflection system[2] mounted outside the shock tube are adjusted to give four traverses; the optical path is thus approximately 34 cm. A Bausch & Lomb medium quartz spectrograph is used with Kodak 103-0 plates.

Salt samples (0.1–1.0 g) are introduced into the shock tube as dried deposits on strips of cellulose tissue or on thin perforated aluminum foil, which are placed across the shock tube about 90 cm upstream from the observation windows. The low-pressure gas is argon at pressures of 1.5 to 2.5 cm Hg. Hydrogen is the driver gas; driving pressures fall between 200 and 350 psi. Resulting shocks have velocities of Mach 8.5–9 before reaching the sample. The most intense absorption has come with the strongest shocks.

In all cases comparison spectra of the flash lamp have been taken. In later work, each plate has included the spectrum of a shock through the supporting material alone. When tissue is used we observe absorption by C_2, OH, and possibly CH. Aluminum gives atomic lines. Spectra of shock-heated alkali halide vapors display the principal series of the alkalis; we have definitely observed the rubidium series to $14p$, and the cesium series to $16p$. Especially with large samples, higher members of the series are quite broadened.

The rationale for expecting large negative ion concentrations comes from the equilibrium constants for the processes $MX \rightarrow M^+ + X^-$ and $MX \rightarrow M^0 + X^0$. At 4000°K, dissociation constants (atm) to ions are 1.453×10^{-4}, 9.61×10^{-4}, 1.934×10^{-4}, and 6.62×10^{-4}, for RbF, RbCl, CsF, and CsCl, respectively; concentration ratios of dissociated ion pairs to atom pairs are 1:58, 1:39, 1:24, and 1:16.5 for the same species. Therefore, one expects a large equilibrium concentration of negative ions, particularly for chloride in CsCl vapor. The problematical quantity is the magnitude of the extinction coefficient of chloride ion near its threshold.

In the case of both the chloride salts, two sharp decreases in plate density appear, at 3424 and 3325A. These are apparent on the tracings and plots of differences between plate densities of salt spectra and comparisons, and are quite obvious to the eye. The intensity of the continuous absorption is significantly greater for CsCl than for RbCl, under similar conditions. Measurements so far have not been sufficiently precise to say whether the slope of absorption is infinite at the thresholds, but it is certainly extremely steep, rising well above noise level over a range of less than 10A. The intensity also correlates well with the intensities of the alkali absorption lines. With fluorides or bromides, or with the various comparison spectra, these sharp intensity changes have not been detected. Crude measurements indicate that the relative intensity of the two absorption steps is independent of shock strength and sample size.

Photodetachment of an electron from Cl^- can leave the chlorine atom in either of two states, $^2P_{\frac{3}{2}}$ or $^2P_{\frac{1}{2}}$. The separation between these levels is 0.1092 ev.[3] The absorption thresholds we detect are at 3.620 and 3.728 ± 0.007 ev; the separation of 0.108 ev is therefore in agreement with the spin-orbit splitting of chlorine.

The conditions under which the absorption is found, its two sharp thresholds with their seemingly constant relative intensity, and the energy separation between the thresholds all lead us to assign the spectrum to the photodetachment process of the chloride ion. The lower threshold therefore falls at an energy equal to the electron affinity of chlorine. With a Debye-Hückel correction of 0.7 ± 0.4 kcal/mole for the presence of other ions, the value we obtain is 84.2 ± 0.4 kcal/mole. Other recent values fall from 86.7 ± 2 to 85.1 kcal.

Continua due to other negative ions are under investigation now. We are also conducting measurements aimed at determining relative extinction of the chloride spectrum.

One of us (R.S.B.) would like to express thanks to W. Klemperer, S. A. Rice, and G. Volpi for stimulating discussions which led to this work, and to O. Laporte and his associates for their assistance in the design of the apparatus. We are indebted to the University of Michigan, where the work was begun, for a grant from the Michigan Alumni Faculty Research Equipment Fund. Finally, we would like to acknowledge the support of the Directorate of Chemical Sciences, U. S. Air Force Office of Scientific Research.

* National Research Council Fellow.
† Present address: Stanford Research Institute, Menlo Park, California.

[1] H. S. W. Massey, *Negative Ions* (Cambridge University Press, New York, 1950), p. 32 ff.; also L. M. Branscomb, Advances in Electronics and Electron Phys. **9**, 43 (1957).
[2] J. U. White, J. Opt. Soc. Am. **32**, 285 (1942).
[3] C. E. Moore, "Atomic energy levels," Vol. I, National Bureau of Standards, Washington, D. C., Circ. 467 (1949).
[4] T. L. Bailey, J. Chem. Phys. **28**, 792 (1958); D. Cubicciotti, *ibid.* **31**, 1646 (1959); I. N. Bakulina and N. I. Ionov, Doklady Akad. Nauk S.S.S.R. **105**, 680 (1955).

Fe^{57} Mössbauer Effect in Laves Phases Containing Fe Combined with Y, Ce, Ho, Ti, Zr, and Hf

W. E. WALLACE* AND L. M. EPSTEIN

Radiation and Nucleonics Laboratory, Central Laboratories, Westinghouse Electric Corporation, East Pittsburgh, Pennsylvania

(Received October 12, 1961)

RESONANT absorption of γ rays by Fe^{57} (Mössbauer effect) has been used to determine the nuclear hyperfine field (H_i), quadruple splitting (ϵ), and the center shift (ΔE) for a number of Laves phases. The samples examined were those in Table I plus $HoFe_2$, $HfFe_2$, and several other $TiFe_2$-$ZrFe_2$ solid solutions. Magnetic examination indicated that most of the samples studied are ferromagnetic at or slightly below room temperature.[1] This is not the case for $TiFe_2$ and the hexagonal $TiFe_2$-$ZrFe_2$ alloys, which exhibit temperature independent paramagnetism[2] down to 2°K, nor for $HoFe_2$, whose magnetic behavior is complex.[1]

Results obtained are summarized in Table I. Before commenting on specific results, some general remarks concerning the experimental observations and results cited seem appropriate. First, for the ferromagnetic materials the quadrupole splittings have not been determined. The hyperfine spacings seemed to be unequal, thus resembling in general the observations of Kistner and Sunyar[3] for Fe_2O_3 and suggesting a nonvanishing quadrupole interaction. The inequalities were, however, comparable with the uncertainties in line positions and hence no attempt was made to

TABLE I. List of Curie temperature (T_c), nuclear hyperfine field at temperature (H_t), quadrupole splittings (ϵ) and center shift (ΔE) relative to a stainless-steel source at room temperature for laves phases studied.

	T_c (°K)	Structures[a]	Temp. (°K)	ϵ (mm/sec)	ΔE (mm/sec)	H_t (koe)
$CeFe_2$	~150, 250[b]	C	300	0.40	−0.10[c]	
			78			190
YFe_2	>300	C	300		+0.05	188
$Y_{3/4}Ho_{1/4}Fe_2$		C	300		−0.05	197
$Y_{1/2}Ho_{1/2}Fe_2$		C	300		0.00	197
$Y_{1/4}Ho_{3/4}Fe_2$		C	300		+0.05	199
$TiFe_2$	...	H	573	0.21	−0.40	
			300	0.21	−0.20	
		See text	78	0.13	−0.05	
			78			92
$Ti_{0.8}Zr_{0.2}Fe_2$	...	H	300	0.21[d]	−0.20[d]	
$ZrFe_2$	635	C	300		−0.08	206
$Zr_{0.9}Ti_{0.1}Fe_2$	630	C	300			194
ZrFeCo	210	C	300	0.20	−0.10	
			78	0.20	0.00	
$Zr_{1/2}Hf_{1/2}Fe_2$	685	C	300		−0.15	191

[a] C and H denote $MgCu_2$- and $MgZn_2$-type, respectively.
[b] Two Curie points are observed for $CeFe_2$.
[c] A negative Doppler velocity means that source and absorber are moving apart.
[d] ϵ and ΔE are the same for samples richer in Zr.

evaluate the quadrupole contribution. Second, for the same reason in several instances no attempt was made to establish the center shift. Third, the estimated uncertainties are: in ϵ, ± 0.02 mm/sec, in ΔE, ± 0.05 and ± 0.02 mm/sec for ferromagnetic and paramagnetic samples, respectively.

The hyperfine patterns were as anticipated in most cases, $TiFe_2$ and ZrFeCo being notable exceptions. Before commenting on these it is to be noted that satisfactory absorption spectra for $HoFe_2$ and $HfFe_2$ have not been obtained. For $HfFe_2$ failure was probably due to the imperfect nature of the crystal, whereas with $HoFe_2$ it is ascribed to the complex magnetic structure and/or the strong unselective absorption of holmium.

Results for ZrFeCo are unusual in that only a doublet is observed at 78°K even though this is well below its T_c.[2] Furthermore, the resonant absorption is less (by a factor of four) at 78°K than at 300°K. The reason for this anomalous behavior is not as yet clear.

For $TiFe_2$ results are very unusual. Since the magnetic properties indicated Pauli paramagnetism to 2°K, no hyperfine splitting was expected. This was the case at 573 and 300°K but at 78°K the pattern revealed a strong doublet superimposed on the sextet produced by a nuclear hyperfine field of 92 koe. This compound contains two crystallographically distinguishable kinds of Fe. Magnetic results[2] suggest that there are no localized moments in this metal. The Mössbauer data indicate, however, that while this may obtain at 300°K and above, at 78°K, localized moments, which are coupled, develop on one type of Fe but not on the other. From the magnetic work it is inferred that the coupling is antiferromagnetic.

ϵ values for all samples are small, as expected for a metal. The ΔE's are negative, indicating a higher electron concentration at the nucleus[3,4] in these compounds than in stainless steel. Variation of ΔE with temperature was as expected from the second-order Doppler contribution.[5]

Except for $TiFe_2$ values for the observed internal fields lie within a fairly narrow range,[6] which is considerably lower than that for Fe (330 koe). This is consistent with the observation[1,2] that the Fe moment in these compounds is about $\frac{2}{3}$ that in elemental Fe. A full account of the present work will be published in this Journal later.

The authors acknowledge with thanks the generous assistance of Mr. John Hicks at Westinghouse in connection with the Mössbauer work and the help of Dr. A. Pebler, Dr. E. Piegger, and Mr. E. A. Skrabek at the University of Pittsburgh in preparing and establishing the structures of the samples studied.

* Consultant to Westinghouse. Permanent address: Department of Chemistry, University of Pittsburgh, Pittsburgh, Pennsylvania.

E. A. Skrabek and W. E. Wallace (to be published).
E. P egger and R. S. Craig (to be published).

[3] O. C. Kistner and A. W. Sunyar, Phys. Rev. Letters **4**, 412 (1960).
[4] L. R. Walker, G. K. Wertheim and V. Jaccarino, Phys. Rev. Letters **6**, 98 (1961).
[5] R. V. Pound and G. A. Rebka, Jr., Phys. Rev. Letters **4**, 274 (1960).
[6] Preliminary results from current studies of similar compounds containing other lanthanides indicate a similar H_s.

Comments and Errata

Microwave Spectrum, Structure, and Dipole Moment of F_2O†

LOUIS PIERCE*‡ AND ROBERT JACKSON

Mallinckrodt Chemical Laboratory, Harvard University, Cambridge 38, Massachusetts

AND

NICHOLAS DICIANNI

Department of Chemistry, University of Notre Dame, Notre Dame, Indiana

(Received September 7, 1961)

RECENTLY Hilton *et al.*[1] have reported the observation of 13 rotational transitions of F_2O in the millimeter wave region. Because their proposed assignment for nine of the transitions implied rather large centrifugal distortion effects, we attempted to fit their data to the Kivelson-Wilson energy expression for a nonrigid rotor.[2] The average deviation for the frequency fit was disturbingly large (8 Mc), and the distortion constants were found to be inconsistent with assignments which have been proposed for the infrared spectrum.[3,4] These results led us to initiate an experimental study of the rotational spectrum of F_2O. In the region 13 to 60 kMc we have measured with Stark modulated spectrometers a total of 17 rotational transitions, none of which can be accounted for with the assignment of reference 1. Thirteen of these transitions ranging in J from one to nine have been assigned. Table I lists the observed and calculated frequencies for the assigned transitions. For transitions with $J \leq 4$ the details of the observed Stark effect patterns provided the basis for the assignment. For the first five transitions in Table I we were able to resolve 10 of the 13 possible $\Delta M = 0$ Stark components. Table II gives rotational constants, moments of inertia, the inertial defect, and structural parameters of F_2O as derived from the assignment given in Table I.

TABLE I. Ground-state rotational transitions of F_2O (Mc/sec).

Transition	Frequency (obs)[a]	Frequency (calc)[b]
$1_{01} \rightarrow 1_{10}$	49 613.55	49 613.55
$2_{02} \rightarrow 2_{11}$	51 388.95	51 388.90
$3_{03} \rightarrow 3_{12}$	54 137.05[c]	54 137.54
$4_{04} \rightarrow 4_{13}$	57 958.40	57 959.94
$2_{12} \rightarrow 3_{03}$	13 803.90	13 802.55
$3_{13} \rightarrow 4_{04}$	36 029.20	36 029.29
$4_{14} \rightarrow 5_{05}$	58 725.50	58 729.78
$4_{13} \rightarrow 3_{22}$	57 457.10	57 473.83
$7_{16} \rightarrow 6_{25}$	17 354.67	17 370.32
$5_{15} \rightarrow 4_{22}$	59 846.20	59 868.22
$8_{18} \rightarrow 7_{25}$	23 842.38	23 863.48
$9_{19} \rightarrow 8_{26}$	15 771.44	15 797.00
$9_{27} \rightarrow 8_{36}$	52 302.40	52 325.05

[a] ±0.10 Mc/sec.
[b] Calculated using rotational constants given in Table II.
[c] Three Stark components were resolved for this transition. From the measurement of Stark shift as a function of electric field strength the M values of the three components were determined to be $M=1$, 2, and 3. The relative intensities were in the order $M=3>M=2>M=1$.

TABLE II. Ground-state rotational constants (Mc/sec), moments of inertia (amu A²), and structure of OF_2.[a]

a	=58 780.09
b	=10 895.87
c	= 9166.53
I_a	= 8.60037
I_b	=46.3966
I_c	=55.1496
$I_c - I_a - I_b$	= 0.1526

$r_{O-F} = 1.409$ A. $\angle FOF = 103°18'$

[a] Conversion factor: 505 531 Mc amu A². Atomic masses: $m_O = 16.000000$ amu, $m_F = 19.004456$ amu. The structural parameters were calculated using the a and b moments of inertia.

The results of quantitative Stark effect measurements on the $M=1$ lobe of the $1_{01} \rightarrow 1_{10}$ transition and the $M=2$ lobe of the $2_{02} \rightarrow 2_{11}$ transition yield a dipole moment for F_2O of $0.297 \pm 0.005D$. This result is in serious disagreement with the dipole moment determination by Bransford *et al.*[5] However, their results are based on an incorrect rotational assignment.

The inertial defects of symmetrical triatomic molecules are of considerable interest. Using the vibrational assignment for F_2O given in references 3 and 4, the inertial defect is calculated to fall in the range 0.115 to 0.175 amu A². Calculation of a unique value for the inertial defect requires knowledge of the complete quadratic potential function. Conversely, if the inertial defect is known, then this information plus the three fundamental vibrational frequencies can be used to compute the four quadratic force constants. We have performed such a calculation[6] and find $f_r = 4.05$ md/A, $f_\alpha / r^2 = 0.707$ md/A, $f_{rr} = 0.906$ md/A, and $f_{r\alpha} = 0.200$ md/A, where r is the O-F distance (1.409 A). In addition to the usual limitations on the accuracy of force constants, the above calculations contain uncertainties due to neglect of electronic[7] and centrifugal distortion contributions to the inertial defect. It is unlikely, however, that these effects contribute more than a few thousandths of an amu A² to the inertial defect.

Measurements of high J transitions of F_2O are now in progress. Analysis of these transitions should provide accurate distortion constants and also an independent determination of the quadratic potential function.

Thanks are due to Dr. James S. MacKenzie of the Research Division of Allied Chemical Corporation who

kindly supplied the sample of F_2O used in this investigation.

* Alfred P. Sloan Fellow.
† This research was supported by a grant extended to Harvard University by the Office of Naval Research and by a grant extended to the University of Notre Dame by the National Science Foundation.
‡ On leave from the University of Notre Dame.

[1] A. R. Hilton, Jr., A. W. Jache, J. B. Beal, Jr., W. D. Henderson, and R. J. Robinson, J. Chem. Phys. **34,** 1138 (1961).
[2] D. Kivelson and E. Bright Wilson, Jr., J. Chem. Phys. **20,** 1575 (1952).
[3] H. J. Bernstein and J. Powling, J. Chem. Phys. **18,** 685 (1950).
[4] E. A. Jones, J. S. Kirby-Smith, P. J. H. Woltz, and A. H. Nielsen, J. Chem. Phys. **19,** 337 (1951).
[5] J. W. Bransford, A. C. Kunkle, and A. W. Jache, J. Inorg. Nuclear Chem. **1960,** 14, 159.
[6] J. H. Meal and S. R. Polo, J. Chem. Phys. **24,** 1119, 1126 (1956).
[7] T. Oka and Y. Morino, J. Mol. Spectroscopy **6,** 472 (1961).

Determination of Molecular Diffusivity by Gas Chromatography Techniques

JAMES J. CARBERRY

Department of Chemical Engineering, University of Notre Dame, Notre Dame, Indiana

AND

RANDOLPH H. BRETTON

Department of Chemical Engineering, Yale University, New Haven, Connecticut

(Received August 21, 1961)

RECENT comment in this Journal[1] relates to the use of a simple gas chromatography column for the purpose of rapidly measuring the molecular diffusivity of a trace quantity of a candidate gas. We should like to call attention to work[2,3] completed in 1957 and published in 1958 in which the technique of pulse injection of a gas into a carrier stream passing through a fixed bed (chromatography column) was employed to characterize the axial diffusivity (residence time distribution) of a gas in flow-through fixed beds. Previous work by McHenry and Wilhelm[4] established that the axial diffusivity varies linearly with flow rate beyond a Reynolds number of about 50. Our work with gases was, therefore, confined to Reynolds numbers below unity, where it could be anticipated that molecular transport governs axial dispersion of the injected pulse. The data obtained in the study confirmed the supposition. Values of axial diffusivity of air injected into a helium carrier agreed within 20% with the computed value of molecular diffusivity[2,3] of N_2 in helium. As the gas diffusion study comprised a minor portion of a larger undertaking, extensive refinements were not employed in securing the gas data. However, it was clearly demonstrated that (a) molecular diffusion governs axial disperson at Reynolds numbers less than unity and (b) in consequence, the technique of pulse injection is a rapid and simple manner whereby molecular diffusivities can be measured.

The mathematical analysis and treatment of dispersed pulse data for the procurement of the diffusion coefficient has been discussed elsewhere.[3,5] The value may be obtained from concentration-time distribution data, or from the mean retention time as measured at the diffuse pulse maximum,

$$t_m=\frac{D}{u^2}\left\{\left[1+\frac{(xu)^2}{D^2}\right]^{\frac{1}{2}}-1\right\}. \tag{1}$$

For beds of more than several particle diameters of length,[5,6] Eq. (1) becomes a simple function of D, tube length x, and velocity u,

$$t_m=(x/u)-(D/u^2)=\theta-(D/u^2), \tag{2}$$

where θ is the average residence time of the carrier gas. It follows that a plot of the ratio of pulse retention time to that of the carrier t_m/θ is a linear function of $1/ux$, the slope being equal to the diffusion coefficient D. Beyond the flow regime where molecular transport governs axial dispersion, D is directly proportional to ux, hence t_m/θ becomes constant with the onset of turbulent diffusion. For gaseous systems the limiting value of D/ux at Reynolds numbers greater than about 50 is $d_p/2x$, where d_p is the particle diameter. This limiting relation follows since turbulent axial diffusion has been shown theoretically[4,7] and experimentally[4] to be characterized by $d_pu/D=2$ at Reynolds numbers greater than 50.

The measurement of molecular diffusivities of liquids by the technique under discussion requires further comment. The feasibility of such measurements has been demonstrated earlier by Levenspiel and Smith,[8] who extracted apparent molecular diffusivities from the dispersion data of von Rosenberg.[9] However, response data are required at flow rates several orders of magnitude lower than those necessary for the determination of gas diffusivities. Defining the net axial dispersion $\bar{D}$ as the sum of turbulent and molecular diffusivities D_t and D_m, respectively,

$$\bar{D}=D_t+D_m$$

or

$$\bar{D}/d_pu=D_t/d_pu+D_m/d_pu=\tfrac{1}{2}+10^{-6}/d_pu,$$

where we have assumed D_m for a liquid to be about 10^{-6} cm²/sec, while retaining the proportionality of D_t and d_pu for the turbulent contribution. It will be noted that the product d_pu must be maintained at values much less than 10^{-6} if the net measured diffusivity $\bar{D}$ is to represent the molecular diffusivity. For example, Levenspiel and Smith found $\bar{D}$ for n-butyrate in benzene to be about 3×10^{-6} cm²/sec for dispersion measured at a flow rate of 6×10^{-4} cm/sec or about 2 ft/day.

[1] J. C. Giddings and S. L. Seager, J. Chem. Phys. **33,** 1579 (1960).
[2] J. J. Carberry, Doctor of Engineering dissertation, Yale University, 1957.
[3] J. J. Carberry and R. H. Bretton, A.I.Ch.E. Journal **4,** 367 (1958).
[4] K. W. McHenry and R. H. Wilhelm, A.I.Ch.E. Journal **3,** 83 (1957).
[5] J. J. Carberry, Nature **189,** 391 (1961).
[6] J. J. Carberry, Can. J. Chem. Eng. **36,** 207 (1958).
[7] J. J. Carberry, A.I.Ch.E. Journal **4,** 13M (1958).
[8] O. Levenspiel and W. K. Smith, Chem. Eng. Sci. **6,** 227 (1957).
[9] D. U. von Rosenberg, A.I.Ch.E. Journal **2,** 55 (1956).

Rapid Diffusional Analysis by Chromatographic Methods

J. Calvin Giddings and Spencer L. Seager

Department of Chemistry, University of Utah
Salt Lake City 12, Utah

(Received October 4, 1961)

THERE is a clear and important distinction between the method developed by the present authors[1] for the measurement of molecular diffusivity and that proposed by Carberry and Bretton.[2,3] In the former case the internal flow volume, within an empty tube, has simple and well-defined physical boundaries and the asymptotic diffusion processes are subject to exact mathematical analysis. Diffusion coefficients can therefore be obtained to within 1%. In the latter case the interstitial flow volume, within a packed column, has an unknown, complex geometry differing with each column preparation. An exact mathematical analysis is not possible. Even a statistical analysis must depend upon experimentally determined statistical parameters. Despite these drawbacks, packed columns have sufficient potential to warrant further analysis. Their use for obtaining accurate diffusion coefficients depends, as shown below, on a rather wide departure from the techniques just discussed.

According to accepted chromatographic theory the theoretical plate height of a packed column is[4–6]

$$H=f(2\lambda d_p,\ C_g v)+(2\gamma D_g/v)+(C_l+C_k)v, \qquad (1)$$

where $f(x_1, x_2)$ is a function whose general features are understood, $\lambda\sim\frac{1}{2}$, d_p=average particle diameter, v=flow velocity, and D_g=gaseous interdiffusion coefficient. The terms C_g, C_l, and C_k represent nonequilibrium dispersion contributions controlled by lateral gas-phase diffusion, lateral liquid-phase diffusion, and kinetic (especially adsorption) processes, respectively. These terms can be calculated exactly providing certain aspects of the packing geometry are known exactly.[6–10] The labyrinth factor γ originating in the tortuous path along which diffusion must occur, is ordinarily 0.6–0.9. The plate height characterizes the pulse dispersion σ through $H=\sigma^2/L$, where L=column length.

At very low velocities, $H=2\gamma D_g/v$. The measurement of H and v yields the product γD_g (the apparent diffusivity) and not D_g as implied.[2,3] The 10–40% error thus incurred is not satisfactory. The authors would like to suggest an alternative method whereby γ is obtained experimentally with a known gas pair after which unknown pairs can be evaluated. Even this does not appear as satisfactory as the open tube method for reasons discussed below.

Another alternative for possible diffusion measurements has been opened by recent theoretical developments.[6,10] A small quantity of liquid applied to a glass bead column will collect primarily around the bead contact points due to capillarity. The liquid therefore inhabits pores of defined geometry and C_l can be calculated.[10] If adsorption is negligible, $C_k=0$, then all other terms can be maintained constant by holding the product, gas pressure $\times$ velocity, constant.[11] The slope of the $H-v$ plot yields C_l and, in terms of this,[10] the diffusivity of the sample gas absorbed in the liquid.

Liquid-liquid diffusion can best be measured, again, in an empty tube using the same plate height equation as for a gas.

Except for the modification of the Carberry-Bretton method in which γ is evaluated with a known pair, the methods proposed here involve use of the nonequilibrium C terms. This use has enormous practice advantages. First, one is not limited to low velocities. A gaseous system has been successfully evaluated at a Reynolds number of 150. The comparable highspeed possible with liquid systems is particularly important in view of the severe velocity restrictions imposed by the method of Carberry and Bretton[3] ($\sim$2 ft/day).

A second advantage is the magnification of the pulse width. The Carberry-Bretton method depends upon a direct diffusional spreading which, with most liquids, requires nearly a day for a measurable σ value of 1 cm. With the empty tube described earlier the apparent diffusivity of the pulse is increased by the factor $1+r_0^2v^2/48D^2$. This factor can be controlled to permit sufficient dispersion for measurement in a matter of minutes or even seconds.

It should be emphasized that the use of high velocities and pulse magnification requires a precise knowledge of certain aspects of interstitial configuration. This is the reason for the excellent results obtained with the empty tube, and for the proposal to use glass beads. The nonequilibrium theory of chromatography is sufficiently versatile to be applied to other configurations, however complicated, provided only that they can be mathematically defined.[6–10]

This work was supported by a research grant from the National Science Foundation.

[1] J. C. Giddings and S. L. Seager, J. Chem. Phys. **33,** 1579 (1960).
[2] J. J. Carberry and R. H. Bretton, A.I.Ch.E. Journal **4,** 367 (1958).

[3] J. J. Carberry and R. H. Bretton **35,** 2241 (1961) (previous communication).
[4] W. L. Jones, Anal. Chem. **33,** 829 (1961).
[5] R. Kieselback, Anal. Chem. **33,** 23 (1961).
[6] J. C. Giddings, J. Chromatog. **5,** 46, 61 (1961).
[7] J. C. Giddings, J. Chem. Phys. **31,** 1462 (1959).
[8] J. C. Giddings, J. Chromatog. **3,** 443 (1960).
[9] J. C. Giddings, Nature **188,** 847 (1960).
[10] J. C. Giddings, Anal. Chem. **33,** 962 (1961).
[11] J. C. Giddings, S. L. Seager, L. R. Stucki, and G. H. Stewart, Anal. Chem. **32,** 867 (1960).

Comment on the Paper "Thermal Decomposition of Nitrous Oxide"

C. P. FENIMORE

General Electric Research Laboratory, Schenectady, New York

(Received September 25, 1961)

BRADLEY and Kistiakowsky[1] recently investigated the decay of N_2O in reflected shock waves. Assuming the mechanism

$$N_2O \rightarrow N_2+O, \quad (1)$$

$$O+N_2O \rightarrow N_2+O_2, \quad (2)$$

$$O+N_2O \rightarrow 2NO, \quad (2')$$

they deduced $(k_2+k_2')=(2 \text{ to } 5)\times 10^9$ cc mole^{-1} sec^{-1} at about 1800°K, and claimed that this supported one[2] and disproved another[3] of two previous estimates of k_2'. I would like to offer two comments.

First, their mechanism was oversimplified. A consumption of O atoms in their reaction (5), which they neglected,

$$O+NO+M \rightarrow NO_2+M, \quad (5)$$

with $k_5=(2 \text{ to } 4)\times 10^{16}$ cc^{2}mole^{-2}sec^{-1} [4-6] and $[M]=$ about 2.5×10^{-6} mole cc^{-1} as stated,[1] was $k_5[M][O][NO]=(5 \text{ to } 10)\times 10^{10}[O][NO]$; but the consumption they claimed to measure was only $(k_2+k_2')[O][N_2O]=(2 \text{ to } 5)\times 10^9[O][N_2O]$. Since $[NO]$ was added equal to $[N_2O]$ in five of their 13 runs, they neglected a reaction at least 10 times faster than the reactions they considered in these five runs. Since these five gave the same results as the other eight runs, it is difficult to see how their (k_2+k_2') could have been correct in any run. An objection to this argument is that k_5 might be smaller at 1800°K than at room temperature where it was determined.[4-6] It is improbable that k_5 could be very much smaller, however, for Ogryzlo and Schiff[7] found a negative activation energy for k_5 of only about 0.2 kcal/mole.

Second, k_2' is really established more firmly than Bradley and Kistiakowsky imply. The discrepancy which they thought to resolve, of Kaufman and co-workers[2] with Fenimore and Jones,[3] is only one of interpretation and has been explained.[3] The actual estimates of Kaufman *et al.* at 880 to 1030°K agree with the expression of Fenimore and Jones,[3]

$$k_2'=1\times 10^{14} \exp(-28/RT) \text{ cc mole}^{-1} \text{ sec}^{-1}.$$

Furthermore, if k_2' has roughly the values found by Kaufman and co-workers[2] at 880° to 1030° and by Fenimore and Jones[3] at 1400° to 1900°K, (2′) must be the reverse of the rate determining step for the bimolecular decomposition of nitric oxide. Then k_2' can also be calculated from the reverse reaction, e.g., from the measurements of Kaufman and Kelso,[8] and this calculation agrees with the expression for k_2' given above.

[1] J. N. Bradley and G. B. Kistiakowsky, J. Chem. Phys. **35,** 256 (1961).
[2] F. Kaufman, N. J. Gerri, and R. E. Bowman, J. Chem. Phys. **25,** 106 (1956).
[3] C. P. Fenimore and G. W. Jones, to be published in Eighth Combustion Symposium and quoted in reference 1 as a personal communication. The quotation of this k_2' in reference 1 refers to the formation of NO; O atoms are consumed only ½ as fast.
[4] G. B. Kistiakowsky and G. G. Volpi, J. Chem. Phys. **27,** 1141 (1957).
[5] H. W. Ford and N. Endow, J. Chem. Phys. **27,** 1156 (1957).
[6] F. Kaufman, Proc. Roy. Soc. (London) **A247,** 123 (1958).
[7] E. A. Ogryzlo and H. I. Schiff, Can. J. Chem. **37,** 1690 (1959).
[8] F. Kaufman and J. R. Kelso, J. Chem. Phys. **23,** 1702 (1955).

Potential Parameters of Krypton*

B. E. F. FENDER

Department of Chemistry, University of Washington, Seattle 5, Washington

(Received August 21, 1961)

POTENTIAL parameters of krypton have been reexamined recently by Mason.[1] Lennard-Jones[2] 12-6 parameters ($\epsilon/k=225$°K, $\sigma=3.498$ A) and modified Buckingham[2] exp-6 parameters ($\epsilon/k=200$°K, $r_m=4.036$ A, $\alpha=13.5$) are compatible with transport properties but will now reproduce second virial coefficient data either at high or low temperatures.[3] In addition, crystal energies calculated from these parameters are in worse agreement with experiment than those derived from virial coefficient measurements. Mason concludes that this incompatibility is unique to krypton among the rare gases, and suggests that it may indicate a fundamental weakness in our understanding of intermolecular forces. Different conclusions are presented here.

TABLE I. Diffusion coefficients of krypton.

ϵ/k (°K)	σ (A)	D (cm^2 sec^{-1})
166.4	3.679	0.0948
172.7	3.591	0.0977
Exptl.		0.093±0.004

The difficulties in assigning multipurpose potential parameters are: inadequacy of simple potential functions; varying sensitivities of different properties to particular aspects of the potential function; possible influence of three-body forces on the properties of condensed phases[4]; and finally, differing accuracies of experimental measurements. It is still possible that one or more of these factors is responsible for the contradictions observed in krypton.

Second virial coefficients of krypton above 0°C have been measured by Whalley and Schneider,[5] and by Beattie *et al.*[6]; both sets of measurements are in good agreement. Derived 12-6 potential parameters are $\epsilon/k=166.4$°K, $\sigma=3.679$ A, (I), and $\epsilon/k=172.7$°K and $\sigma=3.591$ A (II), respectively, and these parameters give values for the crystal energy in moderate agreement with experiment. Corresponding thermal conductivities and viscosities, calculated using equations, collision integrals, and higher approximation factors given in Hirschfelder *et al.*[2] are shown, with experimental values[7] in Fig. 1. If 1 and 2% are experimental errors of viscosities and thermal conductivities, respectively,[1] then apart from the high-temperature conductivity of Von Ubisch[7] the values calculated from the parameters I, agree with experiment, and those calculated from II are about 2% outside experimental error. Similar results are obtained from a comparison of calculated diffusion coefficients and the single experimental value[8] (Table I).

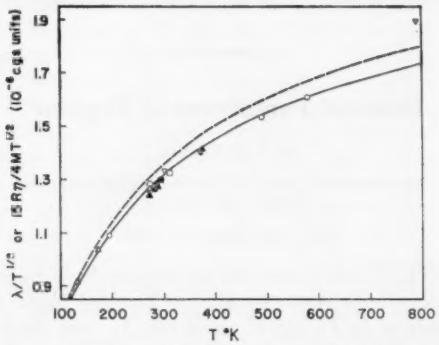

FIG. 1. Thermal conductivities and viscosities of rare gases. ——— $\epsilon/k=166.4$°K, $\sigma=3.679$ A. – – – $\epsilon/k=172.7$°, $\sigma=3.591$ A. Experimental: thermal conductivities; ◊ Curie and Lepape, ○ Kannuluik and Carmen, △ Keyes, □ Srivastava and Saxena, ▽ von Ubisch; viscosities; ● Rankine, ▲ Nasini and Rossi, ■ Lestin and Leidenfrost.

Thermal diffusion measurements[9] are not reproduced by these parameters, even with an estimated 10% experimental error. That this behavior is not peculiar to krypton is demonstrated in Fig. 2, where the reduced thermal diffusion factor α_0 is plotted against $\log T^*(T^*=kT/\epsilon)$ for Ne, Ar, Kr, and Xe. Each calculation of T^* was made from energy parameters based on equilibrium properties. So plotted the experimental points form a reasonably smooth curve differing considerably from the theoretical curve.[10] This deviation may arise from the particular choice of the 12-6 function. Moran and Watson[9] found that the exp-6 function

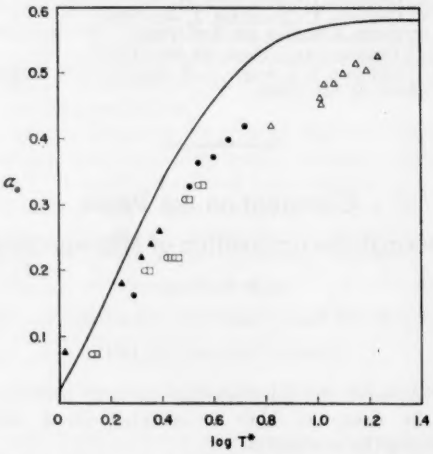

FIG. 2. Reduced thermal diffusion factors of rare gases. Experimental: Moran and Watson; △ neon[2] $\epsilon/k=35.6$°K, ● argon[2] $\epsilon/k=119.8$°K, ○ krypton $\epsilon/k=172.7$°K, □ $\epsilon/k=166.4$°K, ▲ xenon[2] $\epsilon/k=221$°K, ——— theoretical 12–6 curve.

gives an improved fit to the experimental data, though even with an additional parameter there is systematic difference in the change of the temperature dependence between the calculated and experimental values of α_0 from Ne through Xe. Further the exp-6 parameters derived from these comparisons differ considerably from the equilibrium parameters for these gases.

These calculations suggest that within the limitations of a 12-6 potential and the restricted range of experimental data, parameters describing the crystal energy, virial coefficients, viscosities, thermal conductivities, and the diffusion coefficient are not irreconcilable. Further experimental information and the consideration of more sophisticated potential functions appears necessary before the nature of the incompatibility of the thermal diffusion results is apparent.

* Supported by a grant from the Petroleum Research Fund.

[1] E. A. Mason, J. Chem. Phys. **32,** 1832 (1960).
[2] J. O. Hirschfelder, C. F. Curtiss, and R. B. Bird, *Molecular Theory of Gases and Liquids* (John Wiley & Sons, Inc., New York, 1954).
[3] B. E. F. Fender and G. D. Halsey (to be published).
[4] B. M. Axilrod and E. Teller, J. Chem. Phys. **11,** 299 (1943); B. M. Axilrod, *ibid.* **19,** 719 (1951); L. Jansen and R. T. McGinnies, Phys. Rev. **104,** 961 (1956).
[5] E. Whalley and W. G. Schneider, Trans. Am. Soc. Mech. Engrs. **76,** 1001 (1954); J. Chem. Phys. **23,** 1644 (1954).
[6] J. A. Beattie, R. J. Barriault, and J. S. Brierley, J. Chem. Phys. **20,** 1613 (1952).
[7] (a) Viscosity: A. O. Rankine, Proc. Roy. Soc. (London) **A83,** 516 (1910); **A84,** 181 (1910); A. G. Nasini and C. Rossi, Gazz. chim. ital. **58,** 433, 898 (1928); J. Lestin and W. Leidenfrost Physica **25,** 1033 (1959), (b) Thermal conductivity: M. Curie and A. Lepape, Compt. rend. **193,** 842 (1931); J. Phys. radium **2,** 393 (1931); W. G. Kannuluik and E. H. Carmen, Proc. Phys.

Soc. (London) **B65,** 701 (1952); F. G. Keyes, Trans. Am. Soc. Mech. Engrs. **77,** 1955; B. N. Srivastava and S. C. Saxena, Proc. Phys. Soc. (London) **B70,** 369 (1957); H. von Ubisch, Arkiv Fysik **16,** 93 (1959).
[8] N. Groth and P. Harteck, Z. Electrochem. **47,** 167 (1941).
[9] T. I. Moran and W. W. Watson, Phys. Rev. **109,** 1184 (1958).
[10] S. C. Saxena and E. A. Mason, J. Chem. Phys. **28,** 625 (1958).

Intermolecular Potential for Krypton

EDWARD A. MASON

Institute for Molecular Physics, University of Maryland, College Park, Maryland

(Received August 28, 1961)

FENDER[1] has re-examined the experimental data on krypton and reached a more optimistic conclusion than the rather pessimistic one I had suggested earlier.[2] His conclusion is more palatable on several grounds, and I think he is correct.

The reason for our arriving at different conclusions starting from the same data are rather interesting, and deserve some comment. My basic conclusion can be paraphrased as follows: If one insists on fitting the transport data for krypton (including thermal diffusion) as well as possible, then it is not possible to reproduce the virial coefficients satisfactorily, and *vice versa*; this is not true for helium, neon, argon, and xenon, for which reasonable over-all fits of both transport and virial coefficients are possible. I believe this conclusion remains valid, but different inferences can be drawn from it, which is where Fender and I have differed. My suggestion was essentially that something appeared very peculiar about krypton, which might indicate a lack in our understanding of intermolecular forces. Fender's procedure is to fit the second virial coefficients, accept a small discrepancy of about 2% in calculated viscosities and thermal conductivities, and not worry about a *large* discrepancy in thermal diffusion factors. He then shows that the experimental thermal diffusion factors of all the rare gases are reasonably concordant with each other, although not with the 12-6 potential model. From this point of view the behavior of krypton is not unique.

The main cause of the trouble thus appears to be the thermal diffusion factor α_0. It has been remarked many times that α_0 is much more sensitive to the intermolecular potential than any other transport coefficient. A small change in the nature of the potential function may well be able to alter α_0 without affecting the other properties appreciably, and so bring about essential agreement. On the basis of Fender's analysis I would therefore suggest that it would be profitable to concentrate largely on thermal diffusion, both experimentally and theoretically.

[1] B. E. F. Fender, J. Chem. Phys. **35,** 2243 (1961).
[2] E. A. Mason, J. Chem. Phys. **32,** 1832 (1960).

Erratum: Far Infrared Spectrum of Disiloxane

[J. Chem. Phys. **33,** 1004 (1960)]

D. W. ROBINSON AND W. J. LAFFERTY

Department of Chemistry, The Johns Hopkins University, Baltimore 18, Maryland

J. R. ARONSON

Arthur D. Little, Inc., Cambridge 40, Massachusetts

AND

J. R. DURIG AND R. C. LORD

Spectroscopy Laboratory, Massachusetts Institute of Technology, Cambridge 39, Massachusetts

THE far infrared spectrum of disiloxane has been reexamined between 30 and 100 cm^{-1} using three different far-infrared spectrometers having spectral slitwidths of the order of 1 cm^{-1}: the instrument[1] on which the compound was originally run,[2] a vacuum-enclosed Fastie-Ebert spectrometer[3] and a Perkin-Elmer model 201C instrument, which is similar in design and performance to the original instrument.[1] With all three spectrometers the existence of absorption was confirmed, the maximum absorption coefficient at about 68 cm^{-1} having roughly the value originally obtained (2×10^3 cm^2/mol). An investigation which started as a search for the next lower maximum has failed, however, to confirm the maxima and minima previously reported,[2] and we believe that they are spurious.

Study of the original records from which the points shown on the curves in Fig. 1 of reference 2 were obtained clearly indicates these maxima and minima at the pressures used, but we cannot say with certainty what produced them. They were possibly the result of a combination of: (1) slight drift in background between runs; (2) changes in water-vapor concentration in the optical path; and (3) variation in interference fringes in the polyethylene cell windows with pressure. We believe that no one of these factors alone could have

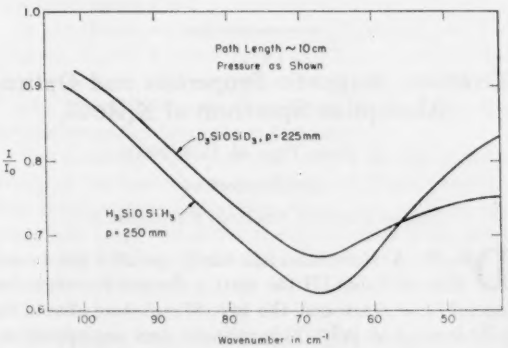

FIG. 1. Far-infrared absorption of disiloxane and disiloxane-d_6. Spectral slitwidth about 1 cm^{-1}.

produced the maxima and minima under the conditions of the original investigation, but obviously the detailed explanation of this spectral structure put forth by us in the original paper[2] no longer applies.

The absorption spectrum of the fully deuterium-substituted molecule has now been observed under closely similar conditions to those used in the measurement of the disiloxane spectrum. A broad featureless band occurs with maximum absorption at a position indistinguishable under the conditions of the observations from that of the disiloxane band, and with nearly the same absorptivity. The two bands have closely similar shapes, though the absorption of disiloxane-d_6 appears to be somewhat stronger on the low-frequency side. The two band contours are compared in Fig. 1, and show that there is little difference between them, as would be expected if the absorption is due almost entirely to the motion of the oxygen atom.

Although the above results are rather indefinite in their structural implications, the low frequency of the absorption maximum, taken together with the very wide Si—O—Si bond angle (near 150°), does indicate a flat and anharmonic potential function for the bending motion. Thus the motion must be treated with due consideration of the special shape of the potential function characteristic of the quasi-linear molecule, as has been done by Thorson and Nakagawa.[4] However resolution of the fine structure predicted by them, which our earlier work[2] seemed to have verified, will apparently require considerably higher resolving power than is presently available to us, and possibly also a study of the molecule at greatly reduced temperatures.

The authors gratefully acknowledge the financial sponsorship by the National Science Foundation at M.I.T. and the Air Force Office of Scientific Research at the Johns Hopkins University.

[1] R. C. Lord and T. K. McCubbin, Jr., J. Opt. Soc. Am. **47**, 689 (1957).
[2] J. R. Aronson, R. C. Lord, and D. W. Robinson, J. Chem. Phys. **33**, 1004 (1960).
[3] D. W. Robinson, J. Opt. Soc. Am. **49**, 966 (1959).
[4] W. R. Thorson and I. Nakagawa, J. Chem. Phys. **33**, 996 (1960).

Erratum: Magnetic Properties and Optical Absorption Spectrum of K_2ReCl_6

[J. Chem. Phys. **34**, 1628 (1961)]

J. C. EISENSTEIN

National Bureau of Standards, Washington, D. C.

DR. W. A. Runciman has kindly pointed out to me that in Table III the matrix element between the second $^2E_\gamma\epsilon^2$ state and the first $^4T_1\gamma\epsilon^2$ state should be $\frac{1}{6}\sqrt{3}\zeta$ instead of $\frac{1}{3}\sqrt{3}\zeta$. This mistake does not appear in the manuscript or the galley proofs; the numerical results of the paper are therefore unaffected.

Erratum: Statistical Mechanics of Isotope Effects on the Thermodynamic Properties of Condensed Systems

[J. Chem. Phys. **34**, 1485 (1961)]

JACOB BIGELEISEN

Chemistry Department, Brookhaven National Laboratory Upton, Long Island, New York

DR. Marvin Stern has kindly called my attention to the following errata in the manuscript:

(1) Multiply right-hand side of Eq. (3.9) by N^{-1};

(2) Eq. (3.14), replace $(\lambda_{ic}{}^{0\prime})^{2j}$ by $(\lambda_{ic}{}^{0\prime})^{j}$;

(3) Eq. (3.15), replace $(4\pi^2N)^{-1}\Sigma\nu_{ic}{}^{0\prime}(\lambda_{ic}{}^{0\prime})^{j}$ by $N^{-1}\Sigma\nu_{ic}{}^{0\prime}(\lambda_{ic}{}^{0\prime}/4\pi^2)^{j}$;

(4) Eq. (3.18), write $u_{ib}{}'>2\pi$;

(5) Eqs. (4.21) and (4.22). Each term on the right-hand side should contain the factor $\beta\gamma$.

(6) In the equation in the middle of page 1492, $\gamma=\alpha V/\beta C_v$, α is used in the conventional manner as the symbol for the coefficient of expansion, and not as the compressibility. The conventional symbol β has already been used for the compressibility;

(7) Eq. (6.2), replace F by G.

Erratum: Comprehensive Investigation of the Electronic Spectroscopy and Theoretical Treatments of Ferrocene and Nickelocene

[J. Chem. Phys. **35**, 516 (1961)]

DONALD R. SCOTT AND RALPH S. BECKER

Department of Chemistry, University of Houston, Houston 4, Texas

THE majority of the following corrections were necessitated by the discovery of an error in group theoretical notation for the $4p_z$ orbital in the D_{5d} point group. This error also occurs in the original references 1, 12, 16, and 17 as well as in other publications.[1] The correct notation for the $4p_z$ orbital in the D_{5d} group is a_{2u} instead of a_{1u}.

In Fig. 5, the $4p(a_{1u})$ levels of Moffitt and of Dunitz and Orgel should read $4p(a_{2u})$. In Figs. 6 and 7, the $\bar{p}(a_{1u})$ level of Liehr and Ballhausen should read $\bar{p}(a_{2u})$.

In Table VII, line 2 should read a_{2u} for a_{1u} under D_{5d}. In Table IX under Moffitt, line 9 should read $4p(a_{2u})$ for $4p(a_{1u})$. In Table IX under Dunitz and Orgel, line 9 should read $4p(a_{2u})$ for $4p(a_{1u})$. In Table X under Dunitz and Orgel, line 2 should read $e_{1g}-4p(a_{2u})$ for $e_{1g}-4p(a_{1u})$. Line 9, $[e_{1u}-4p(a_{1u})]$, should

be entirely omitted. Add to this section of Table X

$a_{1g}-4p(a_{2u})$ 22 600 *z*

In Table X under Moffitt, add

$h(a_{1g})-4p(a_{2u})$ 31 000 *z*

In Table XI under Moffitt, line 6 should read $3d(e_{2g})-4p(a_{2u})$ instead of $3d(e_{2g})-4p(a_{1u})$. In Table XI under Dunitz and Orgel, line 4 should read $e_{1g}-4p(a_{2u}, e_{1u})$ instead of $e_{1g}-4p(a_{1u}, e_{1u})$. Line 8 should be omitted and replaced by

4400 $e_{2g}-e_{1g}'$ $(Cp+3d)-(Cp+3d)$ 19 800 No.

On page 526, paragraph 3, the next to last line should read $4p(a_{2u})$ for $4p(a_{1u})$. In the first sentence of paragraph 4, the word three should be replaced by four. On page 527, paragraph 3, line 8 should read $4p(a_{2u})$ instead of $4p(a_{1u})$. The last line of this paragraph should read: The 4400 A (22 730 cm^{-1}) band is assigned as the forbidden $e_{2g}-e_{1g}'$ transition. On page 530, the first line of paragraph 3 should read 4400 A for 4000 A. On the same page, paragraph 7, line 7 should read $4p(a_{2u})$ for $4p(a_{1u})$.

[1] L. E. Orgel, *An Introduction to Transition Metal Chemistry Ligand Field Theory* (Methuen & Company, Ltd., London, 1960), Table 10.3.2, p. 157; D. Brown, J. Chem. Phys. **29**, 1086 (1958).

Notes

Identification of an Electronic Transition of N_2^{2+}

P. K. CARROLL

Laboratory of Molecular Structure and Spectra, Department of Physics, The University of Chicago, Chicago, Illinois

AND

A. C. HURLEY

Division of Chemical Physics, C.S.I.R.O., Chemical Research Laboratories, Melbourne, Australia

(Received August 7, 1961)

A NEW headless band with origin at 1589.745 A was recently observed in a hollow cathode discharge through pure nitrogen at low pressure.[1] From the rotational structure of the band it was deduced that

(a) The emitter is certainly molecular nitrogen (because of the observed intensity alternation).

(b) The band arises from a $^1\Sigma\rightarrow{}^1\Sigma$ or $^2\Sigma\rightarrow{}^2\Sigma$ transition, the lower state being either Σ_g^+ or Σ_u^-.

(c) It is probably a 0—0 band. No other hands of the transition were observed.

Since the B values showed that the $v=0$ level of none of the states of N_2 or N_2^+ with known B_0 values was involved, several hitherto unobserved states of N_2, N_2^+, and N_2^{2+} were considered but a definite assignment could not be made on the basis of the spectrum alone.

TABLE I. Calculated and observed parameters.

Transition $d\,^1\Sigma_u^+\rightarrow a\,^1\Sigma_g^+$ of N_2^{2+}			
	Calculated by Method (a)	Method (b)	Analysis of 1590Å band
ν_0	67629	64080	ν_0 62903.18
r_e'	1.027	1.165	r_0' 1.1363
r_e''	1.032	1.153	r_0'' 1.1316
ω_e'	1867	1404	ω_0' [a] (1910)
ω_e''	2108	1635	ω_0'' [a] (1960)
D_e' [a]	12.9×10^{-6}	11.3×10^{-6}	D_0' 7.1×10^{-6}
D_e'' [a]	10.4×10^{-6}	8.9×10^{-6}	D_0'' 6.9×10^{-6}

[a] From $D=4B^3/\omega^2$.

One of the possibilities considered was that the band might be the 0—0 transition of the $^1\Sigma_u^+\rightarrow{}^1\Sigma_g^+$ system of N_2^{2+} which would be analogous to the Mulliken system of C_2. As a theory has recently been developed[2] which enables the potential curves for doubly positive diatomic ions to be calculated, this possibility has now been examined more closely. The theory relates the binding energy $B_d(R)$ of a doubly charged ion (in this case N_2^{2+}) to the binding energy $B_n(R)$, of the corresponding state of the isoelectronic molecule (C_2) by means of the equation

$$B_d(R)=-(1/R)+t^2B_n(tR), \qquad (1)$$

where t is a scaling parameter (see below).

The $B_n(R)$ curves for the $a\,^1\Sigma_g^+$ and $d\,^1\Sigma_u^+$ states of C_2 were derived as Morse functions going to the limits $C(^3P)+C(^3P)$ and $C(^1D)+C(^1S)$, respectively, assuming $D_0[C_2(a\,^1\Sigma_g^+)]=6.50$ ev[3] and taking the other parameters from Herzberg.[4] The potential curves for the corresponding states of N_2^{2+} were then calculated from Eq. (1) using the two different values of the parameter t proposed in reference 2.

(a) In the first calculation $t=[T_{d,v}(\infty)/T_{n,v}(\infty)]^{\frac{1}{3}}$, where $T_{d,v}(\infty)$ is the kinetic energy of the valence shell electrons for the appropriate states of the separated ions N^++N^+ and $T_{n,v}(\infty)$ is the same quantity for the separated atoms C+C.

(b) In the second calculation, $t=[T_d(\infty)/T_n(\infty)]^{\frac{1}{3}}=[E_d(\infty)/E_n(\infty)]^{\frac{1}{3}}$, where $T_d(\infty)$ and $T_n(\infty)$ are the total kinetic energies of the appropriate states of N^++N^+, C+C, respectively, and $E_d(\infty)$ and $E_n(\infty)$ are the experimental total energies of these states.

The resulting N_2^{2+} potential curves are all qualitatively of the form shown in reference 2 (Figs. 1 and 2). For small nuclear separations there is a local energy minimum lying well above the dissociation limit. With increasing nuclear separation each curve rises to a maximum more than 1 ev above the minimum and then falls smoothly to the dissociation limit. Because of the height and breadth of the maxima, tunneling may be neglected at least for the lower vibrational levels and the quantities r_e', r_e'', ω_e', ω_e'', ν_e and ν_0 for

the transition $d\,^1\Sigma_u^+ \rightarrow a\,^1\Sigma_g^+$ may be calculated from the positions and curvatures of the minima in the potential curves. In Table I these quantities are compared with the data from the analysis[1] of the new band.

The good agreement between calculated and observed quantities in Table I, together with the deductions from the spectrum (a, b, and c above) indicate that the new band is in all probability the 0—0 transition of the $d\,^1\Sigma_u^+ \rightarrow a\,^1\Sigma_g^+$ system of N_2^{2+}. The identification is also satisfactory in view of the difficulty experienced[1] in trying to assign the band to N_2 or N_2^+. Furthermore, in terms of simple molecular orbital theory the situation is not unfavorable for the appearance of the doubly ionized spectrum. Thus although the $\sigma_g 2p$ electrons in N_2 are bonding the removal of one of them to produce the ground state of N_2^+ changes r_0 only slightly, from 1.100 to 1.119 A. On the basis of the present identification the removal of the second $\sigma_g 2p$ electron produces a further small and approximately equal increase in r_0 from 1.119 to 1.132 A. The upper state, $d\,^1\Sigma_u^+$, is formed by the removal of a $\sigma_g 2p$ and an antibonding $\sigma_u 2s$ electron. Consequently both states are produced without the removal or excitation of any of the more strongly bonding electrons in the N_2 molecule.

Both methods of computing t were considered in reference 2 although all numerical results were based on method (a). It now appears that method (b) leads to more accurate results. The appearance potentials have therefore been recalculated[5] using method (b); the new values differ but little (± 0.5 ev) from those of reference 2.

[1] P. K. Carroll, Can. J. Phys. **36,** 1585 (1958).
[2] A. C. Hurley and V. W. Maslen, J. Chem. Phys. **34,** 1919 (1961).
[3] W. A. Chupka and M. G. Inghram, J. Phys. Chem. **59,** 100 (1955).
[4] G. Herzberg, *Spectra of Diatomic Molecules* (D. Van Nostrand Company, Inc., Princeton, New Jersey, 1950).
[5] A. C. Hurley and V. W. Maslen (to be published).

Polarized Phosphorescence in Crystalline Hexachlorobenzene at 77°K

DAN W. OLDS
Department of Physics, Duke University, Durham, North Carolina
(Received June 5, 1961)

IN an investigation of the polarization of emission spectra from crystalline chlorobenzenes,[1] it was found that hexachlorobenzene has a particularly detailed phosphorescence. The definite polarization observed in the emission from the crystalline state is of interest not only as apparently the first example[2] to be reported, but also because it is possible, from such spectra, to draw conclusions concerning triplet-singlet mixing in the molecule.

TABLE I. Analysis of hexachlorobenzene phosphorescence at 77°K.

Band	cm^{-1}	Analysis
A	24 322	0–0
B	210	−112
C_1	038	−284
C_2	23 981	−341
C_3	938	−384
D	872	−112−341
D_{+1}	829	−112−384
E	698	−284−341
E_{+1}	652	−284−384
F	601	−341−384
G_1	537	−112−284−384
G_2	487	−112−341−384
H_1	368	−954
H_2	319	−1003
H_3	265	−112−954
H_4	210	−112−1003
I	086	−1236
J	22 969	−112−1236
J_{+1}	22 931	−384−1003
K	788	−1534
L_1	676	−1534−112
L_2	628	−1534−160
M_1	474	−1534−314
M_2	449	−1534−341
N	333	−1534−112−341
O	165	−1534−284−341
P	072	−1534−341−384
Q	21 944	−1534−112−341−384
R	833	−1534−954
S	726	−1534−112−954
T	542	−1534−1236
T_{+1}	432	−1534−112−1236
U	258	−2×1534
V	101	−2×1534−160
W	20 936	−2×1534−314
X	788	−2×1534−112−341

Hexachlorobenzene, purified by Sears and Hopke,[3] was crystallized from melt pressed between quartz disks. A region of uniform extinction between crossed polaroids was selected. An oriented sample was placed in boiling N_2, illuminated from behind by a General Electric A—H6 mercury arc and photographed through a Wollaston prism mounted inside a Hilger E2 spectrograph.

The extinction directions are the b axis and a perpendicular to it. Normals to the molecular planes are 20° from the b axis.[4] A condensed microphotometer tracing is shown in Fig. 1 and an analysis in Table I. The polarization is most prominently influenced by the 112 cm^{-1} separation. Its origin is not well understood. 112 cm^{-1} is too large to be interpreted as a splitting of a degenerate mode, but it could be a librational lattice mode. The other frequencies used in the analysis are (Raman data in parentheses[5,6]): 160(166), 284(275), 314($324e_g^+$), 341(344), 384($372a_{1g}$), 954($937e_g^+$), 1003(1014), 1236($1226a_{1g}$), 1534($1515e_g^+$).

The first band (A) is taken to be the 0—0 band since (a) there is no fluorescence,[7] hence strong phosphorescence with a 0—0 band should occur; (b) the relatively heavy chlorine atoms on the ring will enhance both the 0—0 band and the total transition probability; (c)

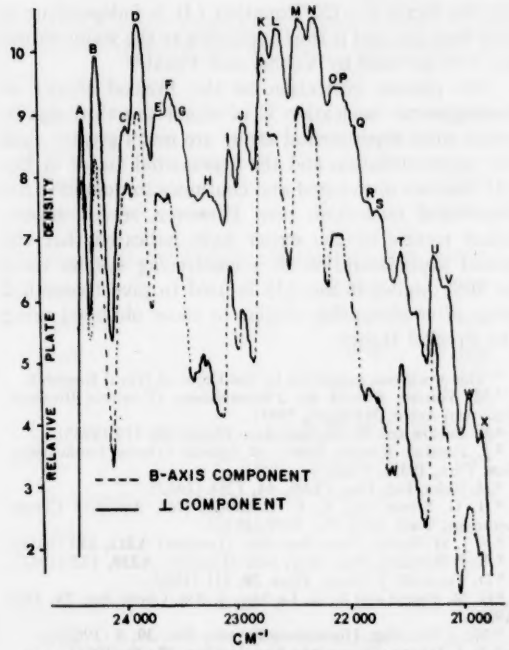

FIG. 1. Microphotometer tracing of two polarization components of the phosphorescence of crystalline hexachlorobenzene at 77°K.

interpretation of A as a 0—1534 transition can be ruled out because that would shift the 0—0 by 1534 cm^{-1} and give a smaller triplet-singlet splitting than found in similar substituted benzenes; (d) if A represents 0—1534 (making the transition allowed), band K would become 0—2×1534 and should be weaker than A, contrary to observation.

Both polarization components have an allowed shape. The 1534 vibration appears prominently in both, as does 2×1534. To explain this it is necessary to abandon the D_{6h} model for the molecule in the crystal.

Symmetry D_{3d}, previously suggested by Schnepp and Kopelman,[7] has one (and only one) representation which satisfies these requirements.[8] $^3A_{1u}$ mixes (by spin-orbit coupling) with $^1E_{1u}$ and $^1A_{2u}$, giving an allowed in-plane and an allowed out-of-plane component, respectively. Furthermore, an $e_g{}^+(D_{6h})$ vibration becomes e_g and is allowed, singly or multiply excited, in both components.

In the puckered ring model (D_{3d}), the C_2 axes pass through C—C bonds. Making this correlation to D_{6h}, we find that $^3A_{1u}$ corresponds to the $^3B_{2u}$ state of benzene. This contradicts the usual $^3B_{1u}$ assignment.[9] This contradiction must stand unless the molecular symmetry is incorrect or the allowed character of the phosphorescence is crystal field induced.

[1] The author is indebted to Dr. O. Schnepp for suggesting this research while the latter was working on polarized absorption in such molecular crystals at Duke University.

[2] After submitting this letter, we were informed that A. C. Albrecht and P. G. Russell found polarized phosphorescence of hexachlorobenzene in rigid glass. (Abstract, Molecular Spectroscopy Symposium, Columbus, Ohio, June, 1961).

[3] G. W. Sears and E. R. Hopke, J. Am. Chem. Soc. **71,** 1632 (1949).

[4] A. Tulinsky and J. G. White, Acta Cryst. **11,** 7 (1958).

[5] Landolt-Börnstein, *Kristalle* (Springer-Verlag, Berlin, 1955), 6th ed., Vol. I, part 4, p. 684.

[6] J. W. Murray and D. H. Andrews, J. Chem. Phys. **2,** 119 (1934).

[7] O. Schnepp and R. Kopelman, J. Chem. Phys. **30,** 868 (1959).

[8] The author wishes to thank A. C. Albrecht (private communication) for pointing out this fact, showing that a further reduction of symmetry was not necessary.

[9] A. C. Albrecht, J. Chem. Phys. **33,** 937 (1960).

Remarks on Homogeneous Nucleation*

WELBY G. COURTNEY
Exploratory Research Laboratory, Texaco Experiment Inc. Richmond, Virginia

(Received April 24, 1961)

ALTHOUGH the classical liquid-drop theory of the kinetics of homogeneous nucleation from the vapor phase[1-3] has well-known limitations when applied to small clusters,[4,5] it is generally concluded[6-10] (however, see Mason[11]) that the liquid-drop theory is in satisfactory agreement with experiments by Volmer and Flood[12] and others. This agreement has led various authors to apply the liquid-drop methodology to liquid-solid transitions,[13] nucleation from dilute solutions,[14] crystal growth,[1,15] binary systems,[16] etc. This letter presents a correction to the liquid-drop theory which, although of minor practical significance, should be noted. A detailed discussion is given elsewhere.[17]

The problem is to determine the rate of homogeneous formation of nuclei/volume·time in a mixture of supersaturated monomer vapor A, clusters of a second phase B, and inert gas Z. The concentration of nuclei is required since experimental results are usually interpreted in terms of concentration of drops.

From elementary thermodynamics, the change in free energy Φ when g molecules of A form an A_g cluster in the presence of z molecules of Z is given at equilibrium by

$$\delta\Phi=0=\phi_g-g\phi_A+kT\ln\mathfrak{A}_g-gkT\ln\mathfrak{A}_A, \qquad (1)$$

where ϕ_i is the chemical potential of a molecule (or cluster) of the ith constituent at unit activity, k is Boltzmann's constant, T is absolute temperature, and $\mathfrak{A}_i$ is the activity of the ith constituent. Equation (1) is independent of z if activities are related to partial pressures or concentrations.

Frenkel[3] and others considered a pure system and equated $\mathfrak{A}_i$ to the mole fraction x_i of the ith constituent. The quantity $\phi_g-g\phi_A$ is the change in chemical potential at the temperature specified in Eq. (1) when g molecules of A at a mole fraction of one and an un-

specified pressure are converted to an A_g cluster at a mole fraction of one and an unspecified pressure. Frenkel and others incorrectly neglected to specify the partial pressure of the cluster (although it is considered to be a "molecule") and concluded that the potential of a cluster is given by volume and surface free energies, or $\phi_g=\phi_B g+\mu g^{2/3}$, where ϕ_B is the chemical potential of a molecule of A in the bulk liquid B,

$$\mu=4\pi\sigma(3m/4\pi\rho)^{2/3},$$

σ is the surface tension of B, m is the mass of a molecule of A, and ρ is the density of B. Therefore, $\phi_g-g\phi_A=(\phi_B-\phi_A)g+\mu g^{2/3}=-gkT\ln S+\mu g^{2/3}$ where $S=p/p_0$ and is the supersaturation and $\phi_B-\phi_A$ is the change in chemical potential when a molecule of A at any pressure p is changed to bulk liquid and thus to a pressure p_0 in equilibrium with the bulk liquid. Since $\Sigma x_g \ll x_A$, substituting the above value of $\phi_g-g\phi_A$ into Eq. (1) and dividing by volume gives the concentration of the A_g cluster at equilibrium as

$$C_g=C_A K_g=C_A\exp\{g\ln S-\mu g^{2/3}/kT\},$$

where C_A is the concentration of A molecules.

To correct the omission of Frenkel and others, it will be noted that $\phi_g-g\phi_A$ may be written as $\phi_g{}^0-g\phi_A{}^0+(1-g)kT\ln P$, where P is the total pressure in the system and is equal to p for the present pure system and $\phi_g{}^0-g\phi_A{}^0$ is the change in chemical potential when g molecules of A at 1 atm pressure are isothermally converted into one A_g cluster at 1 atm. Clusters are considered to be "molecules." This conventional choice of standard state is of course arbitrary, but $\phi_g{}^0-g\phi_A{}^0$ now can readily be equated to the sum of three $\Delta\phi$'s, where (1) g molecules of A at 1 atm are changed to gA at a pressure p_0, $\Delta\phi_1=gkT\ln p_0$, (2) g molecules of A at a pressure p_0 are converted to an A_g cluster (molecule) at the same pressure p_0, $\Delta\phi_2=\mu g^{2/3}$, and (3) an A_g cluster at p_0 is changed to a cluster at 1 atm, $\Delta\phi_3=-kT\ln p_0$. Therefore, $\phi_g-g\phi_A=(1-g)kT\ln S+\mu g^{2/3}$. If one writes Eq. (1) with $\alpha_i=x_i=C_iRT/p$ and substitutes the present value for $\phi_g-g\phi_A$, the correct value for the equilibrium concentration of the A_g cluster is

$$C_g=C_0\exp\{g\ln S-\mu g^{2/3}/kT\}, \qquad (2)$$

where C_0 is the concentration of A monomer in equilibrium with bulk liquid. The Frenkel theory thus predicts a value for C_g which is too high by a factor equal to the supersaturation C_A/C_0.

Following the Frenkel derivation for the steady-state rate of formation of nuclei I_s, it can readily be shown that

$$I_s=C_0C_A(2m\sigma/\pi)^{\frac{1}{2}}(\alpha_n/\rho)\exp\left\{-\frac{4\mu^3}{27(kT)^3(\ln S)^2}\right\}, \qquad (3)$$

where α_n is an accommodation coefficient for nucleation. The value for I_s derived by Frenkel again is too high by the factor C_A/C_0. Equation (3) is independent of any inert gas and is thus applicable to the water vapor-air mixture used by Volmer and Flood.[12]

The present correction to the Frenkel theory of homogeneous nucleation is of minor practical significance since experimental errors are much greater than the supersaturation and the exponential factor in Eq. (3) remains unchanged and continues to dominate the theoretical nucleation rate. However, recent unpublished results by the writer have indicated that the initial supersaturation in a condensing system must be 10% higher if Eq. (3) is used to give theoretical rates of condensation similar to those obtained using the Frenkel theory.

* This work was supported by the Office of Naval Research.

[1] M. Volmer, *Kinetik der Phasenbildung* (Edwards Brothers, Inc., Ann Arbor, Michigan, 1945).
[2] R. Becker and W. Doring, Ann. Physik **24,** 719 (1935).
[3] J. Frenkel, *Kinetic Theory of Liquids* (Dover Publications, New York, 1955), Chap. 7.
[4] H. Reiss, Ind. Eng. Chem. **44,** 1284 (1952).
[5] H. G. Stever and K. C. Rathbun, Nat. Advisory Comm. Aeronaut. Tech. Note No. 2559 (1951).
[6] F. J. M. Farley, Proc. Roy. Soc. (London) **A212,** 530 (1952).
[7] A. J. Barnard, Proc. Roy. Soc. (London) **A220,** 132 (1953).
[8] D. Turnbull, J. Chem. Phys. **20,** 411 (1952).
[9] G. M. Pound and V. K. La Mer, J. Am. Chem. Soc. **74,** 2323 (1952).
[10] W. J. Dunning, Discussions Faraday Soc. **30,** 9 (1961).
[11] B. J. Mason, Discussions Faraday Soc. **30,** 20 (1961).
[12] M. Volmer and H. Flood, Z. physik. Chem. Leipzig **A170,** 273 (1934).
[13] D. Turnbull and J. C. Fisher, J. Chem. Phys. **17,** 71 (1949).
[14] D. Turnbull, Acta Met. **1,** 684 (1953).
[15] W. K. Burton, N. Cabrera, and F. C. Frank, Trans. Roy. Soc. (London) **A243,** 299 (1951).
[16] H. Reiss, J. Chem. Phys. **18,** 840 (1950).
[17] W. G. Courtney, "Kinetics of condensation from the vapor phase." Texaco Experiment Inc., TM-1250 (1961).

On the Classical Approximation in Unimolecular Reactions and Mass Spectra*

B. S. Rabinovitch and J. H. Current†
Department of Chemistry, University of Washington
Seattle, Washington

(Received August 14, 1961)

It has been pointed out by Marcus and Rice[1] that the classical approximation to the density of vibrational states is poor at low excitation energies, particularly for the activated complex. In connection with photoionization and electron impact phenomena, Rosenstock[2] has concluded from RRK[3] calculations of rate constants, on both a classical and particular quantum model, that for rates of mass spectrometric interest (10^5 sec^{-1}) the classical approximation is seriously in error, particularly near the threshold energy; and to fit much existing mass spectral data this error leads to a drastic empirical reduction in the

TABLE I. Harmonic oscillator energy level sums ($\log_{10}$).

$CHCl_3$,[a] $\omega(cm^{-1})$: 260(2), 364, 667, 760(2), 1205(2), 3033; ϵ_z=12.17 kcal mole^{-1}								
E (units ϵ_z)	0.3	0.5	1.0	1.5	2.0	3.0	5.0	8.0
Class.			1.4814	3.0660	4.1909	5.7755	7.7723	9.6094
Semiclass.[c]				5.0627	5.7755	6.9000	8.4849	10.0697
Exact			3.9136	4.8907	5.6595	6.8359	8.4569	10.0572
a[b]			0.85_6	0.89_3	0.91_3	0.93_5	0.95_6	0.97_1
CH_3Cl,[a] $\omega(cm^{-1})$: 732, 1015(2), 1355, 1455(2), 2966, 3042(2); ϵ_z=22.96 kcal mole^{-1}								
Class.		−1.8960	0.8137	2.3984	3.5230	5.1079	7.1045	
Semiclass.[c]			3.5230	4.3951	5.1079	6.2321	7.8172	
Exact		2.0170	3.3226	4.2732	5.0233	6.1850	7.7957	
a[b]		0.86_2	0.90_0	0.92_2	0.93_8	0.95_2	0.96_6	
C_3H_6,[d] $\omega(cm^{-1})$: 740(2), 870(3), 1080(7), 1459(3), 3051(6); ϵ_z=49.05 kcal mole^{-1}								
Class.	−7.9502	−3.2917	3.0293	6.7276	9.3509	13.0490		
Semiclass.[c]		6.7276	9.3509	11.3862	13.0490	15.6725		
Exact	3.9681	5.7152	8.8297	11.0631	12.8301	15.5511		
a[b]	0.80_9	0.84_2	0.88_9	0.91_3	0.92_9	0.94_7		
C_3H_6,[d] $\omega(cm^{-1})$: 556(3), 760(4), 880(5), 1139(3), 2282(6); ϵ_z=37.45 kcal mole^{-1}								
Class.	−8.0230	−3.3638	2.9579	6.6558	9.2797			
Semiclass.[c]		6.6558	9.2797	11.3146	12.9774			
Exact	3.9257	5.6692	8.7688	10.9994	12.7624			
a[b]	0.81_2	0.84_6	0.89_1	0.91_6	0.93_1			

[a] G. Herzberg, *Infrared and Raman Spectra* (D. Van Nostrand Company, Princeton, New Jersey, 1945).
[b] For use with noncommensurable multifrequency models to make $(E+a\epsilon_z)^s/\Gamma(s+1)\Pi h\nu_i$ equal to the exact sum.
[c] Given as the upper limit of the integral (for the reasons in footnote 13), with insignificant effect caused thereby even at lowest energy presented.
[d] Frequencies grouped near the geometric mean of those given by H. Gunthard, R. C. Lord, and T. R. McCubbin, Jr., J. Chem. Phys. **25**, 768 (1956).

effective number of oscillators s relative to the total number involved.

These conclusions are of general importance for all types of unimolecular processes. They apply with greater force for specific dissociation probabilities below 10^5 sec^{-1} but are found to be still valid (and not only for the complex) at energies associated with lifetimes below 10^{-10} sec[4,5]; obviously the magnitude of the classical error varies with the energy of the species and of the complex, and in the pattern of vibrational levels concerned. In fact, the limitations of the classical statistics have been recognized in principle (although frequently forgotten) since the early formulation of unimolecular theory.[3] Practical recognition, following the cogent reminders of Marcus and Rice,[1] has already been given in comparatively successful treatments of the decomposition rates of molecules and radicals[5-9] produced in nonequilibrium systems at vibrational energies from ~40-110 kcal mole^{-1}, with activated complexes from 1–50 kcal mole^{-1}; in these quantum statistical calculations, all vibrational modes were used,[8b] and the empirical parameter s was dropped. Reasonable fit of conventional thermal unimolecular reactions has been made by Wieder and Marcus,[9] with all modes active. For thermal CH_3NC isomerization, s (classical) is ~3 while the quantum statistics gives good agreement with all 12 modes.[10] Given the postulate of internal randomization of energy for species produced in the mass spectrometer from the theory of Rosenstock *et al.*[11] then the quantum statistics should afford an improvement in such cases also.

We present here some direct comparisons of vibrational density approximations with harmonic oscillator exact sums. These reveal the approximation errors for various frequency patterns and total energies E. Table I gives $\sum g_i$ (g_i is the ith level degeneracy), and

$$\int_0^E N(\epsilon)\,d\epsilon$$

for the "classical"[12] and "semiclassical"[1] approximations;

$$N_{cl}(\epsilon)=\epsilon^{s-1}/\Gamma(s)\Pi h\nu_i;\ N_{semi}(\epsilon)=(\epsilon+\epsilon_z)^{s-1}/\Gamma(s)\Pi h\nu_i,$$

where ϵ_z=total zero-point energy.[13] An empirical correction factor a, used earlier,[6] is evaluated to reduce

the need for exact summations; i.e.,

$$N_{corr}(\epsilon) \propto (\epsilon+a\epsilon_z)^{s-1}/\Gamma(s)\Pi h\nu_i.$$

The nature of these approximations is immediately evident for degenerate oscillators: For the jth level of s oscillators, the quantity $(j+s-1)!/j!$ is replaced by j^{s-1},[3] or $(j+s/2)^{s-1}$, respectively; the classical approximation becomes correct only for $j \gg s/2$.

The exact sums were made with an IBM 709; high-energy programs are drastically shortened by judicious grouping of frequencies.[7,8] For kinetics purposes, many species are adequately represented by four groups, very well by five, and few require more than six groups. Anharmonicity corrections are readily introduced.

The general characteristics of the failure of the approximations, for a given vibration pattern, will be repeated at higher (or lower) total energies if either the frequencies *or* degeneracies are raised (or lowered). This is useful in assessing the validity of approximate calculations, or the magnitude of the correction factor a, for other species of interest at particular energies of concern. From comparisons with the values of Table I or other known examples, even rough a estimates permit fairly accurate correction of the semiclassical expression for many purposes. Alternatively, a may be determined at a few energies by exact count and graphed, as was done[5] for cyclopropanes at energies of 100–120 kcal mole^{-1}, and $k(\epsilon) > 10^{10}$ sec^{-1}.

For most chemical studies the critical energies, and hence total energies employed whatever the excitation method, fall below 200 kcal (or usually 100 kcal), and are "independent" of the molecular frequency pattern. For much of this energy region we see that not even the semiclassical approximation is adequately valid, although a remarkable improvement over the classical expression. Further details will be presented later.

* This work was supported by the Office of Naval Research.
† N.S.F. Predoctoral Cooperative Fellow.

[1] R. A. Marcus and O. K. Rice, J. Phys. and Colloid Chem. **55,** 894 (1951); R. A. Marcus, J. Chem. Phys. **20,** 352, *et. seq.* (1952).
[2] H. M. Rosenstock. J. Chem. Phys. **34,** 2182 (1961).
[3] L. S. Kassel, *Kinetics of Homogeneous Gas Reactions* (Chemical Catalog Company, Inc., New York, 1932).
[4] B. S. Rabinovitch, E. T. -Roux, and E. W. Schlag, J. Am. Chem. Soc. **81,** 1081 (1959).
[5] D. W. Setser, B. S. Rabinovitch, and E. J. Spittler, J. Chem. Phys. **35,** 1840 (1961).
[6] B. S. Rabinovitch and R. W. Diesen, J. Chem. Phys. **30,** 735 (1959).
[7] B. S. Rabinovitch, D. H. Dills, W. H. McLain, and J. H. Current, J. Chem. Phys. **32,** 493 (1960).
[8] (a) R. E. Harrington, B. S. Rabinovitch, and R. W. Diesen, J. Chem. Phys. **32,** 1245 (1960); (b) R. E. Harrington, B. S. Rabinovitch, and H. M. Frey, *ibid.* **33,** 1271 (1961).
[9] G. M. Wieder and R. A. Marcus, National Meeting, Am. Chem. Soc., New York, September, 1960.
[10] F. W. Schneider and B. S. Rabinovitch, Symposium on Elementary Gas Reactions, Am. Chem. Soc., St. Louis, March, 1961.
[11] H. M. Rosenstock, M. B. Wallenstein, A. L. Wahrhaftig, and H. Eyring, Proc. Natl. Acad. Sci. U. S. **38,** 667 (1952).
[12] R. C. Tolman, *Principles of Statistical Mechanics* (Oxford University Press, New York, 1938), p. 492.
[13] Below the energy of the highest frequency mode, ϵ_z and the number of modes of interest *must* go to zero as ϵ drops to zero.

Thermodynamic Functions for Eighteen Elements Taken as Ideal Monatomic Gases*

JOHN S. GORDON
Thiokol Chemical Corporation, Denville, New Jersey
(Received July 17, 1961)

THE tables of Kolsky *et al.*[1] for 54 electrically neutral monatomic gases have been extended to include the elements Mo, Ru, Sn, Te, I, Hf, Ta, W, Re, Os, Ir, Tl, Pb, Bi, Ra, Th, and U. Also, functions of Si have been revised slightly. The tables include the functions $-(F°-H_0°)/T$, $(H°-H_0°)/T$, $S°$, $C_p°$, and $H°-H_{298}°$ over the temperature range 300–6000 °K at 100° increments, and have been useful in studies of rocket propellant performance, ablation, and other high-temperature processes.

* Detailed text and tables have been deposited as Document number 6930 with the ADI Auxiliary Publications Project, Photoduplication Service, Library of Congress, Washington 25, D. C. A copy may be secured by citing the document number and remitting $3.75 for photoprints, or $2.00 for 35-mm microfilm. Advance payment is required. Make checks or money orders payable to: Chief, Photoduplication Service, Library of Congress.

[1] H. G. Kolsky, R. M. Gilmer, and P. W. Gilles, Report LA 2110, Los Alamos Scientific Laboratory (1957).

Observations of Induction Times in the Acetylene-Oxygen Reaction

W. C. GARDINER, JR.*
Gibbs Chemical Laboratory, Harvard University, Cambridge, Massachusetts
(Received August 2, 1961)

A SHOCK-tube study of the vacuum ultraviolet chemiluminescence from the acetylene-oxygen reaction was carried out by Richards.[1] It was found that the emission of this radiation was preceded by in-

TABLE I. Induction times for the acetylene-oxygen reaction.

Run	Starting pressure (mm)	Shock velocity (m/sec)	Temperature (deg K)	Induction period (μsec)
2	4.64	735	1750	290
3	3.60	800	2050	120
4	3.40	710	1660	390
5	3.42	790	1990	200
8	4.09	700	1620	320
9	4.23	695	1610	500
11	5.41	755	1850	110
12	4.23	725	1720	360

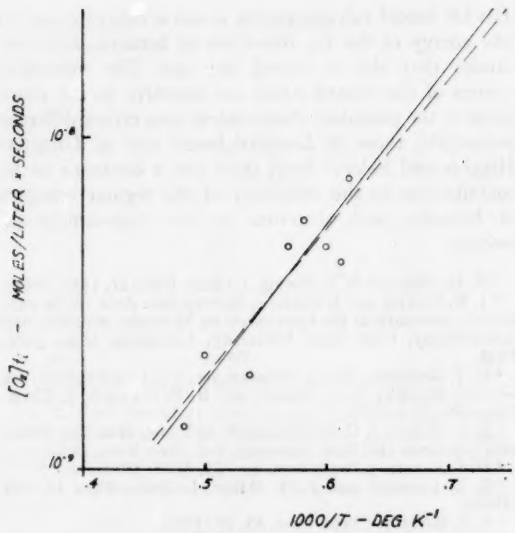

FIG. 1. Induction times vs inverse temperature. This work, ————; Schott and Kinsey, - - - - - - - - - - - - - -.

duction periods in a manner which suggested a branching chain mechanism closely analogous to that proposed for the hydrogen-oxygen reaction.[2] Details of this mechanism have been discussed.[1,3]

A series of experiments using the x-ray densitometric technique[4] was undertaken to determine the relationship of the chemiluminescence to the heat evolution of the reaction. The apparatus employed was described previously.[5] A mixture was prepared consisting of 96.61% xenon, 1.35% acetylene, and 2.04% oxygen. It was intended that the experimental conditions be nearly the same as those employed in the chemiluminescence studies, which meant that the starting pressures were considerably lower than in previous work with the x-ray densitometric technique. The conditions of eight incident shock waves are given in Table I.

Due to the low concentration of x-ray absorber, the signal-to-noise ratio of the oscilloscope records was too low for quantitative density measurements. The qualitative appearance of the records was as follows. The sudden increase in density in the incident shock wave was followed first by a short period of constant density and then by a slow decrease to a somewhat lower density, which remained constant thereafter until the arrival of the contact surface. The decrease in density can be attributed unambiguously to release of heat in the approach to final equilibrium. To obtain a value for the induction time from a density record, straight lines were drawn through the initial constant density level and the following decrease, and the intersection taken to be the end of the induction period. The time elapsed between the passage of the shock and the end of the induction period was multiplied by the value of the density ratio of the incident shock calculated from the shock velocity to obtain the length of the induction period in gas time. Table I lists the results obtained.

The mechanism proposed[1,3] for the branching chain reactions governing the induction period in this reaction predicts that the product of oxygen atom concentration and induction time plotted logarithmically against inverse temperature should yield a straight line. This is shown in Fig. 1. Least-squares analysis of the results yields the value 19.0 kcal for the activation energy of the rate controlling step of the reaction, with a standard error of estimate of 2.6 kcal at 50% confidence level.

Since the results of the chemiluminescence experiments yield similar values for the induction periods, it is clear that the emission of ultraviolet light starts at about the same time as the release of heat. The implications of this are discussed elsewhere.[1,3] The induction times obtained mass spectrometrically at lower temperatures scatter uniformly about the extrapolated solid line.[3] The striking correlation of the acetylene-oxygen and hydrogen-oxygen[2] induction periods can be seen in the close agreement of the two least squares lines shown in Fig. 1.

This work was supported by the Office of Naval Research.

* Present address: Department of Chemistry, The University of Texas, Austin, Texas.

[1] L. W. Richards, thesis, Harvard University, 1960.
[2] G. L. Schott and J. L. Kinsey, J. Chem. Phys. **29,** 1177 (1958).
[3] J. N. Bradley and G. B. Kistiakowsky, J. Chem. Phys. **35,** 264 (1961).
[4] G. B. Kistiakowsky and P. H. Kydd, J. Chem. Phys. **25,** 824 (1956).
[5] W. C. Gardiner, Jr., and G. B. Kistiakowsky, J. Chem. Phys. **34,** 1080 (1961).

Zero-Point Vibrations in Benzene

R. STEPHEN BERRY
Sterling Chemistry, Laboratory, Yale University
New Haven, Connecticut

(Received July 18, 1961)

THIS note is written to point out some elementary but interesting conclusions about benzene, which one can draw from just a little well-known information: the vibration frequencies of the two B_{2u} modes of the benzene molecule, and the currently popular values for "natural" single and double bonds between trigonal carbon atoms. Mair and Hornig[1] report the vibrational frequencies ν_{14} and ν_{15} as 1310 and 1150 cm^{-1}, respectively; Scherer and Overend have substantiated this assignment from their examination of the Urey-Bradley force field.[2] Carbon-carbon bond lengths have been much discussed; a summary of recent literature is included in an article by Bernstein.[3]

We shall suppose the double- and single-bond lengths appropriate to a hypothetical cyclohexatriene molecule

are 1.335 and 1.465 A, respectively; these are probably not in error by more than 0.01 A. We note that within 0.003 A, these bond lengths make it possible for benzene to attain the cyclohexatriene structure by a distortion only along the B_{2u} symmetry coordinate S_{14}, in the notation of Wilson *et al.*[4] This symmetry coordinate corresponds to stretching and shrinking alternate C—C bonds around the ring.

First, what energy is necessary to distort benzene into our chosen "cyclohexatriene" structure? This question was examined by Hornig[5] who used 1.54 A as his chosen single-bond length. We find that the reduction of this figure to 1.465 makes a drastic difference in the conclusions. From the analysis of Crawford and Miller,[6] Hornig found that the force constant for the S_{14} symmetry coordinate is 4.361 or 3.926×10^5 d/cm. Let us treat this as if it were a true harmonic force constant to estimate the energy difference between the equilibrium configuration of benzene and our chosen cyclohexatriene structure. We find readily that with

$$S_{14}=6^{-\frac{1}{2}}\times0.065\times6,$$

the total energy of distortion is only 7.92 or 7.14 kcal/mole.

By comparison, the zero-point energy of the higher frequency B_{2u} mode, which is principally composed of the S_{14} symmetry coordinate vibration, is 1.87 kcal. The cyclohexatriene structure, therefore, has an energy between that of the first and second excited states of the ν_{14} vibrational degree of freedom.

We can also inquire into the magnitude of the displacement associated with achieving the cyclohexatriene structure. The displacement, measured in classical amplitudes, is $(7.92/1.87)^{\frac{1}{2}}$ or $(7.14/1.87)^{\frac{1}{2}}$, or 2.06 or 1.95, respectively. Continuing to treat the vibration as a harmonic mode and examining the area under a $|\psi|^2$ curve, we conclude that benzene in its ground vibrational state spends about 15% of its time at least as distorted as our hypothetical cyclohexatriene molecule.

Finally, we estimate that if a force constant of 4.361 or 3.926×10^5 d/A is associated with a vibration whose natural frequency is 1310 cm^{-1}, then the classical zero-point amplitude of motion for a carbon atom in this mode is 0.031 or 0.033 A, which is a surprisingly large figure.

The question arises immediately as to the origin of such large-amplitude, low-energy motion. A suggestion was made by the author,[7] in connection with the distorted rings of crystalline dibenzene chromium, that the π electrons are not the major source of stability for the regular hexagon, and that in fact the π electrons might well have a lower energy if the rings approach "cyclohexatriene"-like shapes. This would imply that the π electrons are largely responsible for the ease of distortion, and that the σ electrons determine the regular hexagon structure. Snyder[8] has carried out Hückel model calculations of π and σ contributions to the energy of the B_{2u} distortion of benzene, and concludes that this is indeed the case. The numerical values of the contributions are sensitive to the exact form of the potential. Nonetheless, two rather different potentials, those of Lennard-Jones[9] and of Longuet-Higgins and Salem[10] both show the π electrons to be contributing to the *instability* of the regular hexagon of benzene, and therefore to the large-amplitude motion.

[1] R. D. Mair and D. F. Hornig, J. Chem. Phys. **17,** 1236 (1949).
[2] J. R. Scherer and J. Overend, Spectrochim. Acta (to be published); presented at the Symposium on Molecular Structure and Spectroscopy, Ohio State University, Columbus, Ohio, June, 1961.
[3] H. J. Bernstein, Trans. Faraday Soc. (to be published); see also, for example, C. C. Costain and B. P. Stoicheff, J. Chem. Phys. **30,** 777 (1959).
[4] E. B. Wilson, J. C. Decius, and P. C. Cross, *Molecular Vibrations* (McGraw-Hill Book Company, Inc., New York, 1955).
[5] D. F. Hornig, J. Am. Chem. Soc. **72,** 5772 (1950).
[6] B. L. Crawford and F. A. Miller, J. Chem. Phys. **17,** 249 (1949).
[7] R. S. Berry, J. Chem. Phys. **35,** 29 (1961).
[8] L. C. Snyder, presented in part at the Symposium on Molecular Structure and Spectroscopy, Ohio State University, Columbus, Ohio State University, Columbus, Ohio, June, 1960; (to be published).
[9] J. E. Lennard-Jones, Proc. Roy. Soc. (London) **A158,** 280 (1937).
[10] H. C. Longuet-Higgins and L. Salem, Proc. Roy. Soc. (London) **A251,** 172 (1959).

Electron Spin Resonance Measurements of Preferred Orientation in Quickly Frozen Hydrogen Peroxide Solutions*

ROBERT C. SMITH† AND S. J. WYARD‡
Physics Department, Guy's Hospital Medical School, London, S.E.1, England

(Received August 23, 1961)

THE free radicals produced by the ultraviolet irradiation of H_2O_2—H_2O solutions can be stabilized at low temperatures and detected in this state by electron spin resonance (ESR).[1,2] The measurements reported here use the ESR spectrum obtained from these radicals to determine the distribution of crystallites within a frozen sample.

The solutions were put into quartz glass tubes of 2–3 mm i.d. and then frozen by plunging the tubes into liquid oxygen. 97% w/w H_2O_2—H_2O produced a polycrystalline material[3] and this was used for the first experiments.

The material was tested to see if there was any preferred orientation of the crystallites to the tube axis. A tube was constructed of three pieces so that the middle section of 5 mm length could be removed after the solution had frozen. This section was irradiated at 90°K with the light falling perpendicular to the tube

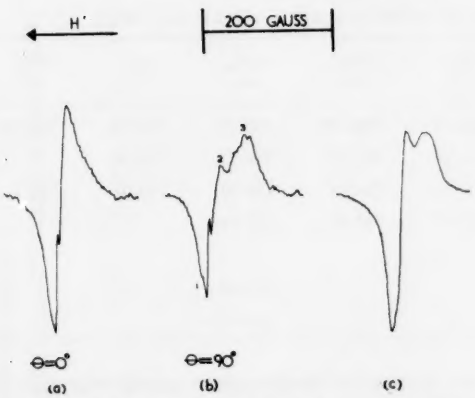

FIG. 1. First derivative ESR spectra of uv irradiated H_2O_2. (a) and (b) Polycrystalline material, sample tube axis making angles θ to the magnetic field direction. These two spectra show DPPH markers superimposed on the trace. (c) Glass material, spectrum independent of angle θ. All spectra recorded at 9.35 kMc/sec.

cross section. After irradiation the tube section was mounted in the spectrometer cavity so that ESR spectra could be recorded with the tube axis making various angles (θ) to the magnetic field. As angle θ was altered, marked changes in the ESR spectra were recorded and two typical spectra are shown in Figs. 1 (a) and (b). The g values for the derivative peaks 1 and 2 were independent of θ with $g_1=1.999$, $g_2=2.017$. The g value for peak 3 showed a large variation with θ approximately described by $g^2=g_{\|}^2\cos^2\theta+g_{\perp}^2\sin^2\theta$, where $g_{\|}=g_2$ and $g_{\perp}=2.042$. This result shows that crystallization does not take place so that the crystallites are randomly orientated but that there is a preferred orientation for the crystallites with an appreciable number of crystallites lying at this orientation. The unit cell of H_2O_2 is tetragonal[4] and the preferred orientation can be explained if the 001 plane of the crystallites makes one particular angle to the tube axis. Measurements to be discussed in the next paragraph determine this angle to be 90°. The process of crystallite alignment takes place on the crystallization boundary as it moves along the tube axis.

It is also possible to examine preferred orientation relative to the tube wall. The test rests on the short penetration of uv into H_2O_2—H_2O so that, if the irradiation is perpendicular to the tube axis, a thin section of solution is selected lying on one side of the tube cross section. Spectra were recorded for the tube rotated about its axis, with $\theta=90°$. The spectra were always similar to Fig. 1 (b) and the g values of the peaks remained constant. However, as the angle about the axis was altered, the height of peak 2 varied, the spectrum shape repeating every 90° of rotation. This result can be explained if the 001 crystallite plane lies perpendicular to the tube axis and one particular *mno* plane lies parallel to the tube wall. The irradiated H_2O_2—H_2O sample then shows the fourfold symmetry of the tetragonal crystallites. Bolz *et al.*[5] have reported x-ray diffraction studies on 90–95% w/w H_2O_2—H_2O crystallized by warming the vapor deposited glass. They found[6] that the 210 plane was orientated parallel to the depositing surface.

In the above discussion it has been assumed that the radicals take up the same positions in H_2O_2 lattice as the H_2O_2 molecules. Other measurements[2] have shown that the radical has uniaxial symmetry with $g_{\|}=2.039$, $g_{\perp}=2.0055$. The spectra of Figs. 1 (a) and (b) can be explained if the axis of symmetry lies along the O—O bond direction of the H_2O_2 molecules. Consideration of the unit cell[4] shows that for $\theta=0°$ all the radicals then make the same angle (69°15′) to the magnetic field and the spectrum should be a single line as found. For $\theta=90°$ the radicals can take up angles to the magnetic field between 20°45′ and 90°.

Measurements were also made on a 76% w/w solution which froze to form a glass.[3] ESR spectra similar to Fig. 1 (c) were always obtained and the peak g values were independent of orientation with $g_1=2.000$, $g_2=2.015$, $g_3=2.037$. No preferred orientation to the tube axis was found but there was preferred orientation to the tube wall, as shown by a variation in the difference in height between peaks 2 and 3. The spectra were repeated every 180° and therefore it can be concluded that the hydrogen bond helices are preferentially aligned parallel to the tube wall.

We wish to acknowledge the helpful discussions of F. A. Mauer with reference to the x-ray diffraction measurements.

* This work was supported by the British Empire Cancer Campaign.

† Present address: Electronics Department, Southampton University, Southampton, England.

‡ Present address: Biophysics Laboratory, Stanford University, Stanford, California.

[1] R. C. Smith and S. J. Wyard, Nature **186**, 226 (1960).

[2] R. C. Smith and S. J. Wyard, Bull. Ampère, 9th year, special ed., 224 (1960).

[3] R. C. Smith and S. J. Wyard, Nature **189**, 211 (1961).

[4] S. C. Abrahams, R. L. Collin, and W. N. Lipscomb, Acta Cryst. **4**, 15 (1951).

[5] As reported in L. H. Bolz, F. A. Mauer, and H. S. Peiser, *Formation and Trapping of Free Radicals*, edited by A. M. Bass and H. P. Broida, (Academic Press Inc., New York, 1960).

[6] F. A. Mauer (private communication).

Microwave Spectrum and Barrier to Internal Rotation of Methyl Stannane*,†

PATRICK CAHILL‡ AND SAMUEL BUTCHER§

Mallinckrodt Chemical Laboratory, Harvard University
Cambridge 38, Massachusetts

(Received August 28, 1961)

WE have re-examined the microwave spectrum of methyl stannane, CH_3SnH_3, first investigated by Lide,[1] in an effort to determine the barrier to internal

TABLE I. Torsional assignment of observed 0–1 frequencies (13 000 Mc should be added to each entry).

	^{118}Sn obs	^{118}Sn calc	^{116}Sn obs	^{117}Sn obs	^{119}Sn obs	^{120}Sn obs	^{122}Sn obs	^{124}Sn obs
OA OE	800.31	...	820.87	810.73	790.49	780.72	761.24	742.56
1*E*	775.97	775.90	796.43	786.22	765.89	756.27	736.90	
1*A*	778.92	778.84	799.38	789.11	768.87	759.20	740.01	721.1
2*A*	757.87	757.70	778.22	767.81	747.81	737.98		
2*E*	759.66	759.77						
3*E*	755.22	754.12				735.34		
3*A*	749.70	749.49	769.94			729.81		

rotation. Greater spectrographic sensitivity and a pure sample have allowed us to observe a number of torsional satellites and two additional tin isotopes not observed in the first work.

The compound was prepared by first reducing $SnCl_4$ with $LiAlH_4$ in diglyme [bis-(2 methoxyethyl) ether] to give SnH_4, which in turn was reacted with sodium in liquid ammonia and methyl iodide, as previously described,[2] to yield methyl stannane. The use of diglyme instead of ethyl ether avoided the difficulty of separating the stannane from the ether solution.

Thirty-one lines, observed in the frequency region 13 720–13 820 Mc, were assigned to torsional levels of the $J=0-1$ transition for seven tin isotopes using the formula developed by Kivelson[3] for the coupling of internal and over-all rotation of symmetric tops (see Table I). The observed frequency of the 0–1 transition for various torsional states is given by the following expression:

$$\tfrac{1}{2}\nu = B_v + F_v\langle m \mid 1\text{-}\cos 3\theta \mid m\rangle + G_v\langle m \mid \Pi_s^2 \mid m\rangle,$$

B_v, F_v, and G_v are independent of the torsional quantum number (denoted by m), and of the rotational quantum numbers. Π_s is the internal angular momentum operator and θ the angle of internal rotation. The matrix elements $\langle m \mid \Pi_s^2 \mid m\rangle$ and $\langle m \mid 1\text{-}\cos 3\theta \mid m\rangle$ are readily obtainable from tables[4] for different torsional states as a function of the reduced barrier parameter $s(=4V_3/9F)$, $F=(1/I_{SnH_3}+1/I_{CH_3})h/8\pi^2$. The parameters which gave the best fit to the above formula were, for ^{118}Sn, $B_v=6906.35$ Mc, $G_v=-0.3521$ Mc, $F_v=-17.492$ Mc, and $s=13.33\pm0.33$.

Calculated values for isotopes other than ^{118}Sn are easily obtained from the usual substitution formulas, since to a very good approximation only B_v is affected by isotopic substitution of tin. Using as structural parameters: $\angle HSnH=109°28'$, $\angle HCH=108°25'$, $d(Sn—H)=1.700$ A, $d(C—H)=1.083$ A, and the above value for s, we obtained $V_3=650\pm30$ cal/mole (227 ± 10 cm^{-1}).

Quantitative intensity measurements could not be made because of limited sample stability and interference from Stark effects of neighboring lines. However, qualitative measurements agreed with expected statistical weights, $g_{iA}/g_{iE}=2$ [5] for the satellites and with isotope ratios calculated from tables of natural abundances. Only one 2*E* line was observed due to the presence of stronger satellites.

The authors would like to express their appreciation to Professor E. Bright Wilson, Jr. for many helpful discussions.

* This research was supported by a grant extended Harvard University by the Office of Naval Research.

† This paper was presented at the Symposium on Molecular Structure and Spectroscopy at The Ohio State University, June, 1961.

‡ Monsanto Chemical Company Fellowship, 1959–1961.

§ National Science Foundation Predoctoral Fellow, 1958–1961.

[1] D. R. Lide, Jr., J. Chem. Phys. **19,** 1605 (1951).

[2] H. J. Emeleus and S. F. A. Kettle, J. Chem. Soc. **1958,** 2444.

[3] D. Kivelson, J. Chem. Phys. **22,** 1733 (1954).

[4] D. R. Herschbach, J. Chem. Phys. **27,** 975 (1957).

[5] H. T. Minden, J. Chem. Phys. **20,** 1964 (1952).

Preparation and Optical Transmission of Cadmium Fluoride Crystals

J. S. PRENER AND J. D. KINGSLEY

General Electric Research Laboratory, Schenectady, New York

(Received July 28, 1961)

THE preparation and optical transmission of CdF_2 have been reported previously.[1,2] Between 700 mμ and 8μ the transmittance was constant but then decreased due to restrahlen absorption. Below 700 mμ, the transmittance was found to decrease gradually in both cases. The absorption in the visible was sufficient to give the crystals a yellow color. Rubenstein[2] took the fundamental absorption edge to be at 265 mμ. Haendler[1] prepared CdF_2 crystals which had higher transmission in the visible and ultraviolet, but his measurements seemed to indicate the presence of an absorption band peaking at 220 mμ and no estimate of the absorption edge was given. Our measurements on CdF_2 crystals of greater purity are in substantial agreement with the previous data in the infrared but differ in the visible and ultraviolet.

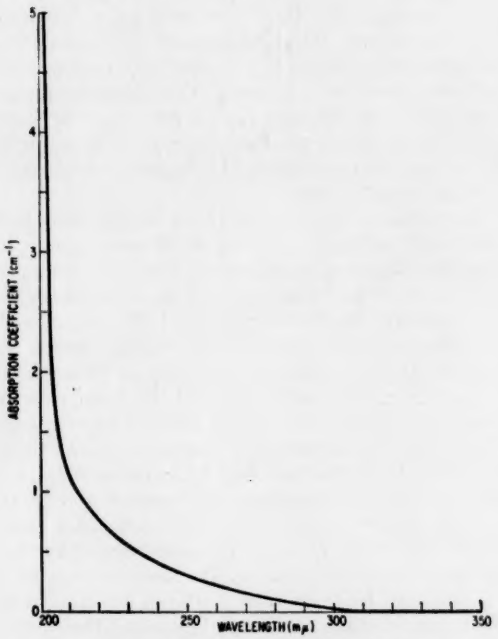

FIG. 1. The absorption coefficient of CdF_2.

Single crystals of CdF_2 weighing 15 g were grown by the Bridgemen method in an argon atmosphere using graphite crucibles. The CdF_2 charge was prepared by the repeated addition of reagent aqueous hydrofluoric acid to cadmium carbonate followed by vacuum drying at 100°C. The cadmium carbonate was prepared by the addition of a solution of ammonium bicarbonate (Mallinkrodt Ultra Pure) neutralized with gaseous ammonia to a solution of cadmium nitrate prepared from high-purity cadmium metal (Cominco High-Purity Cadmium 69 grade), followed by filtering and washing. The CdF_2 powder was fused in an iridium crucible under argon prior to crystal growth. This step was found to be necessary in order to obtain completely colorless crystals. As already indicated by Rubenstein, the yellow coloration of his crystals was due to a sulfide impurity. In our material the sulfide arises from the reduction by the graphite of a trace of cadmium sulfate contaminant in the CdF_2. Fusion in a metal crucible decomposes this to cadmium oxide which is then removed by reduction to cadmium during crystal growth.

Optical absorption data were obtained with a Cary model 14 recording spectrophotometer using two polished disks (0.7 mm and 3.0 mm thickness) cut from a single crystal of CdF_2. This crystal was grown using the center portion of a previously grown crystal as a charge. The absorption coefficient as calculated from the difference in absorbance of the 0.7- and 3.0-mm disks is given in Fig. 1. There is no absorption in the visible and ultraviolet down to 310 mμ and the absorption band at 220 mμ reported by Haendler was absent. The absorption coefficient at 1900 A was determined from the transmission of a 25-μ thick crystal to be 2000 cm^{-1}. The absorption edge (obtained by extrapolating the steep portion of the curve to zero absorption coefficient) is found to be at 205 mμ, a value much lower than that given by Rubenstein.

The authors thank Mrs. D. J. Weil for carrying out much of the chemical work and crystal growth.

[1] H. M. Haendler, G. M. Wheeler, Jr., and W. J. Bernard, J. Opt. Soc. Am. **43**, 215 (1953).
[2] M. Rubenstein and E. Banks, J. Electrochem. Soc. **106**, 404 (1959).

Pattern Inversion for Coherent Inelastic Electron Scattering by Br_2

D. A. SWICK AND J. KARLE
U. S. Naval Research Laboratory, Washington 25, D. C.
(Received August 4, 1961)

THE inelastic scattering of electrons by molecules has usually been termed incoherent. Some time ago it was pointed out by Massey and Mohr[1] that, while this may be true for the totality of such scattering, diffraction effects are to be expected from electrons scattered with a given change in energy. They showed that, for diatomic molecules, an inversion of the part of the scattering curve now commonly designated as molecular scattering might be expected.

When the process of fast electron scattering results in electron energy loss which accompanies molecular excitation, it is presumed that the Franck-Condon principle[2] applies. Thus a coherent pattern arises from the geometrical configuration of the molecule characteristic of its initia lstate, which is usually the normal state. The probability of the occurrence of a particular excitation is a function of the product of the wave functions for the initial and final states. Since the equilibrium positions of the two states may not be the same, the energy lost by the scattered electrons is not necessarily the difference in energy of the two states at equilibrium.

On the basis of this description of the scattering process, general formulas for the diffraction of fast electrons by molecules undergoing transitions to excited electronic states have been derived.[3] In applying the formulas, group-theoretical considerations are utilized to find the proper linear combinations of atomic orbitals for the various eigenstates of the molecules. In the case of a diatomic molecule, for example, Br_2, the intensity of scattering (neglecting vibrational effects) is

$$I(\theta) = K\,|f_{0q}(\theta)|^2(1 \pm \sin s'r/s'r), \qquad (1)$$

where K is some positive constant, $f_{0q}(\theta)$ is the scattering factor at angle θ associated with a transition from

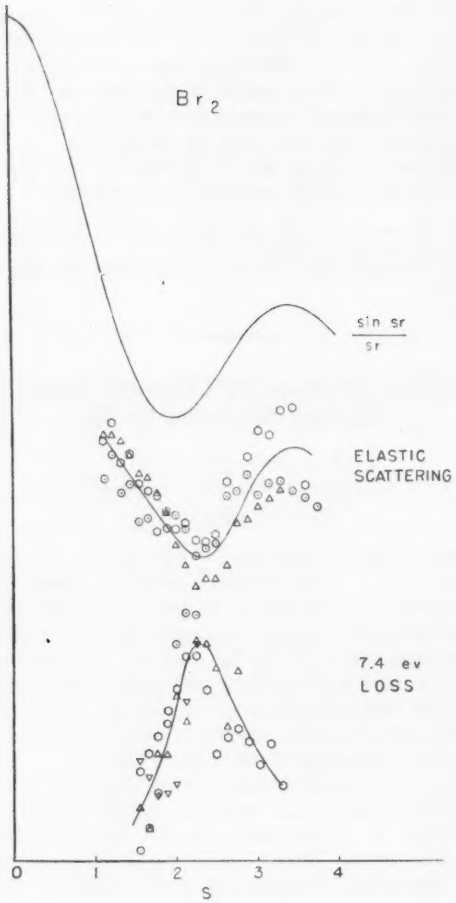

FIG. 1. Molecular scattering curves for Br_2. Top curve is calculated. Lowest curve shows the inversion of the scattering pattern associated with an energy loss.

the normal state denoted by 0 to some excited state denoted by q, $s'=(k^2+k'^2-2kk'\cos\theta)^{\frac{1}{2}}\sim(4\pi\sin\frac{1}{2}\theta)/\lambda$, r is the equilibrium distance between the bromine atoms in the normal state, $k=2\pi/\lambda$ and $k'=2\pi/\lambda'$, where λ and λ' are the wavelengths of the electrons before and after scattering, respectively.

The plus sign applies to a transition from the normal state to a symmetric electronic state, type A_g, and the minus sign applies to a transition to an antisymmetric state, type A_u. The second term in the parentheses is designated as the molecular scattering. Thus, for a transition to an antisymmetric state, the molecular scattering curve looks like the normal curve rotated through 180° about the abscissa.

On the basis of a dipole interaction the expected transition would occur from the normal state, type A_g, to an antisymmetric excited state.[4] Quadrupole and higher interactions are possible for electrons, which suggests that transitions from an A_g to an A_g state may occur. Mott and Massey[5] have shown that if the transition is optically allowed then it will be more probable with fast electrons than those transitions associated with the higher moments. Thus we would expect a transition from the normal to an antisymmetric state to predominate, leading to an inversion of the scattering pattern.

Experimental investigations have been made of both elastic and inelastic scattering of 20 kev electrons by bromine employing an apparatus which has been previously described.[6] The predicted inversion effect has been observed and is shown in Fig. 1. The upper curve was calculated with $r=2.28$ A, the middle curve is the experimentally determined scattering of 20 kev electrons with no loss of energy, and the lower curve is from electrons which have lost 7.4 ± 0.1 ev of energy. The calibration in terms of s values $[s=(4\pi/\lambda)\sin\frac{1}{2}\theta]$ was made by comparison with CCl_4 photographs. The shift between the calculated and experimental curves may be due to errors in this calibration. Such errors would not, however, affect the comparison of the two different experimental curves. The molecular scattering was obtained from the total scattering by division by the background line in the usual manner.[7] The sinusoidal amplitude agrees with the expected value from (1) to about 15%. No attempt has been made to refine the choice of background line. Such refinement would have reduced the spread of experimental points shown in Fig. 1. However, the main object of this note has been simply to demonstrate that it is experimentally possible to observe the phenomenon of pattern inversion.

[1] H. S. W. Massey and C. B. O. Mohr, Proc. Roy. Soc. (London) **A135,** 258 (1932).
[2] H. S. W. Massey and E. H. S. Burhop, *Electronic and Ionic Impact Phenomena* (Clarendon Press, Oxford, England, 1952), p. 221 ff.
[3] J. Karle, J. Chem. Phys. **35,** 963 (1961).
[4] H. Sponer and E. Teller, Revs. Modern Phys. **13,** 75 (1941).
[5] N. F. Mott and H. S. W. Massey, *The Theory of Atomic Collisions,* (Clarendon Press, Oxford, England, 1952), p. 241.
[6] D. A. Swick, Rev. Sci. Instr. **31,** 525 (1960).
[7] J. Karle and I. L. Karle, J. Chem. Phys. **18,** 957 (1950).

Spin Densities in Aromatics Containing Nitrogen: ESR Spectrum of the Pyrazine Negative Ion*

J. C. M. HENNING AND C. DE WAARD
Natuurkundig Laboratorium der Universiteit van Amsterdam, Amsterdam, The Netherlands
(Received July 17, 1961)

THE mononegative ion of pyrazine (1,4 diazabenzene) has been prepared by reducing a dilute solution (about 5×10^{-3} M) of pyrazine in tetrahydrofuran with a potassium mirror in vacuum. The radical ion has been identified by means of its ESR spectrum. A

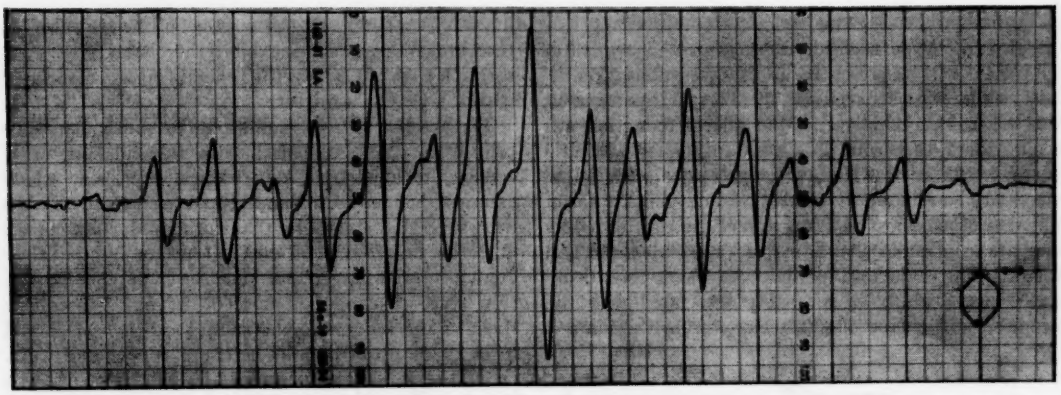

FIG. 1. $d\chi''/dH$ vs H for the mononegative ion-radical of pyrazine.

homodyne balanced mixer spectrometer has been used, which has been described earlier.[1] It operates at a frequency of 9 kMc and employs 485-cps magnetic field modulation and phase-sensitive detection.

The spectrum, shown in Fig. 1, consists of a large quintet with a separation between successive lines of 7.1 gauss, which is further split into a smaller quintet with a separation of 2.6 gauss. The larger quintet can be unambiguously attributed to a hyperfine interaction of the odd electron with the two equivalent nitrogen nuclei ($I=1$) because the observed intensity ratio of the hyperfine lines agrees well with the theoretical one (1:2:3:2:1). The smaller quintet is due to the interaction with four equivalent protons (intensity ratio 1:4:6:4:1).

It is well known[2] that there exists a linear relationship between the proton hyperfine coupling constants A_i and the spin density ρ_i at the contiguous carbon atom

$$A_i = Q^{\mathrm{H}}\rho_i$$

Because it is not proved that the factor of proportionality Q^{H} is a constant for all kinds of aromatic ring systems, we have taken the Q^{H} value as determined by Weissman[3] from the spectrum of benzene negative ion ($Q^{\mathrm{H}}=-22.5$ gauss), as this is most similar to the pyrazine ion. We then find that for the spin density at the CH positions $\rho_{\mathrm{CH}}=0.115$. From this figure and the normalization condition we can calculate the spin density at the nitrogen positions: $\rho_{\mathrm{N}}=0.270$. We see that the introduction of nitrogen atoms in an aromatic ring system produces a pronounced shift of the spin densities towards the nitrogen positions, which is compatible with the fact that nitrogen has a larger electronegativity than an aromatic carbon atom.

The measured spin density distribution can be reproduced by a simple LCAO-MO calculation[4] by taking for the Coulomb parameter of nitrogen (α_{N})

$$\alpha_{\mathrm{N}} = \alpha_{\mathrm{C}} + 0.77\beta.$$

Here β is the resonance integral between neighboring atoms, which is taken equal for all bonds, and α_{C} is the Coulomb integral of the carbon atoms in pyrazine.

The authors are indebted to Professor Dr. G. W. Rathenau for his interest in this research.

* This work is sponsored by the Foundations F.O.M. and S.O.N., financially supported by the Dutch Foundation for Pure Scientific Research (Z.W.O.).

[1] J. C. M. Henning, Rev. Sci. Instr. **32,** 35 (1961).
[2] A. D. McLachlan, H. H. Dearman, and R. Lefebvre, J. Chem. Phys. **33,** 65 (1960).
[3] S. I. Weissman, T. R. Tuttle, and E. de Boer, J. Phys. Chem. **61,** 28 (1957).
[4] B. Pullman and A. Pullman, *Les theories electroniques de la chimie organique,* (Masson et Cie, Paris, 1952), p. 176.

Optical Evidence for the Direct Reduction of CuO to Cu in H_2

HAROLD WIEDER AND A. W. CZANDERNA
Parma Research Laboratory, Union Carbide Corporation, Parma 30, Ohio

(Received August 15, 1961)

IT is generally accepted[1] that CuO is reduced directly to Cu in hydrogen following the reaction

$$\mathrm{CuO}+\mathrm{H_2}\rightarrow\mathrm{Cu}+\mathrm{H_2O}.$$

Although reduction from CuO to Cu_2O is energetically less favorable than complete reduction, it has not been established that Cu_2O is not formed as an intermediate. Thus, it seemed desirable to look for optical evidence of Cu_2O formation during reduction of a thin film of CuO.

A copper film 550 A thick was evaporated onto a Pyrex glass substrate and oxidized to stoichiometric CuO, as determined with a microbalance.[2] During reduction the optical transmission of the film was

measured while the mass loss was simultaneously monitored. A detailed description of the apparatus employed will be presented in a future publication.[3]

The film was reduced in 130 Torr of hydrogen at 162°C. At this temperature the rate of reduction was slow enough to permit detailed transmission measurements to be made. Higher temperatures were found necessary to remove the final 7% of oxygen. A plot of the rate of mass loss as a function of the time of reduction was similar in shape to that found by Bond and Clark.[1] The induction period was characterized by small steps, which are probably associated with the eruption and escape of water vapor from the film.[4]

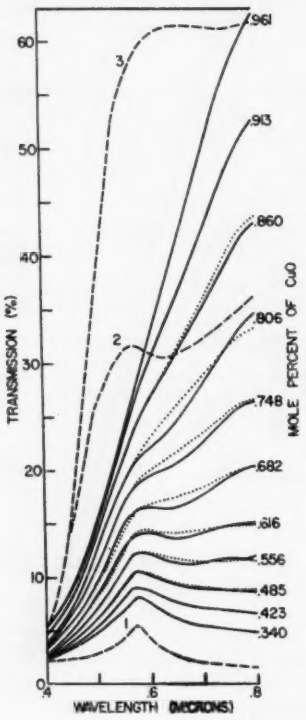

FIG. 1. Optical transmission of an evaporated copper film during oxidation and reduction.

The solid lines in Fig. 1 represent the optical transmission of the film measured at various stages of reduction. Adjacent to each curve is listed the mole fraction of CuO present in the film as measured gravimetrically at the time the curve was taken. Additional curves beyond $CuO_{0.340}$ were measured, but because the film was highly agglomerated at this point, the curves become difficult to interpret and are omitted.

Also shown in Fig. 1 is the transmission of the freshly evaporated copper film (curve 1), and two curves taken during the oxidation of the film (curves 2 and 3). The x-ray diffraction pattern for a sample in the oxidation state represented by curve 2 showed only Cu and Cu_2O lines, while that for curve 3 showed only Cu_2O lines. It is apparent that at no stage of the reduction do the transmission curves exhibit the characteristic absorption edge of Cu_2O or the general features associated with the Cu_2O-Cu mixture.

The absence of Cu_2O can also be established analytically if the shapes of experimental transmission curves can be predicted from a theoretical expression which assumes that only CuO and copper are present. It has been suggested elsewhere[4] that during reduction copper nuclei are first formed on the CuO surface and that they gradually grow larger and increase in number until a thin layer of copper is formed. At any subsequent stage of the reduction, the sample can be considered to be made up of parallel layers of copper and CuO. From the mass measurement the thickness of each layer may be computed, and if the absorption coefficient of each material is known, the resultant transmission through the double film may be calculated, using Eq. (1)

$$T = e \exp -(\alpha_1 l_1 + \alpha_2 l_2). \qquad (1)$$

Here T is the over-all relative transmission at any wavelength, α_1 and α_2 are the absorption coefficients of copper and CuO at that wavelength, and l_1 and l_2 are the respective thicknesses of the two species.

This formula assumes that the entire loss in transmission through the sample may be accounted for by absorption within the sample. In actuality, however, there are additional effects to be considered. Reflection at both copper interfaces and scattering from the agglomerated copper particles are always present, and both effects become more pronounced as the thickness of the copper layer is increased. It would be difficult to obtain analytical expressions for these effects which should be embraced in a more detailed treatment. Therefore, "effective" absorption coefficients, which include reflection and scattering losses, were calculated in terms of the simplified model of Eq. (1).

It was found convenient to solve for α_1 and α_2 in Eq. (1), using the values of T and t as measured and calculated for curves corresponding to $CuO_{0.918}$ and $CuO_{0.423}$. These values of α_1 and α_2 were used in conjunction with the values of l_1 and l_2 computed from the mass data to obtain transmission curves for the seven intermediate stages of reduction. The resultant curves are shown dotted in Fig. 1. It is apparent that this simplified treatment is sufficiently valid to conclude that only CuO and copper are present during the reduction of CuO in hydrogen.

[1] W. D. Bond and W. E. Clark, Oak Ridge National Laboratory, ORNL 2815, May 16, 1960.

[2] A. W. Czanderna and J. M. Honig, Anal. Chem. **29**, 1206 (1957).

[3] A. W. Czanderna and H. Wieder, *Proceedings of the 1961 Conference on Vacuum Microbalance Techniques* (Plenum Press, Inc., New York), (to be published).

[4] W. E. Garner, T. J. Gray, and F. S. Stone, Proc. Roy. Soc. (London) **197**, 294 (1949).

Exchange Rates of NH_3 between Aqueous NH_4OH and Copper and Nickel Ammine Complexes*

JOHN P. HUNT AND HAROLD W. DODGEN
Department of Chemistry, Washington State University, Pullman, Washington
(Received August 10, 1961)

CONNICK and Poulson[1] have presented results on the rate of H_2O exchange between hydrated cations and solvent using nuclear magnetic resonance line broadening techniques. We have made analogous studies using copper and nickel ammine complexes in concentrated NH_4OH. The N^{14} resonance in NH_4OH was observed using a spectrometer employing a marginal oscillator and phase-sensitive detector. A constant frequency of about 1.8 Mc/sec with a variable magnetic field of about 5900 gauss was used. Derivative curves were obtained on a recorder. The samples were of about 10 ml volume contained in 18-mm Pyrex test tubes. The rf power levels were well below saturation. The effect of modulation amplitude on the apparent line widths was studied over a range of 0.1 to 1.0 gauss (see Table I). No large effects on the line widths were found up to 0.5 gauss modulation amplitude. The linewidths studied were about 1–2 gauss. The large sample size and some inhomogeneity of the field are partly responsible for the fairly large widths. Line broadenings were obtained by subtracting the width found for the NH_4OH alone from the width found for the metal ion solution when both samples were run at the same modulation amplitude. This procedure gave essentially the same results at 0.1 gauss as at 0.5 gauss. The magnetic field sweep was calibrated using an NH_4NO_3 solution in concentrated NH_4OH. The average difference in the fields at the absorption maxima for NH_4OH and NO_3^- was taken as 368 ppm.

TABLE I. Complexed NH_3-solvent NH_3 exchange in concentrated NH_4OH at 32°C.

Ion added	M ion	Average linewidth (gauss)	Modulation amplitude (gauss)	K_1 (sec^{-1})
None	...	0.94	0.10	...
None	...	0.99	0.25	...
None	...	1.1	0.50	...
None	...	1.6	1.00	...
Cu^{+2}	1.07×10^{-3}	1.9	0.25	5×10^{6}
Cu^{+2}	1.07×10^{-3}	2.3	0.50	7×10^{6}
Cu^{+2}	6.7×10^{-4}	1.7	0.10	7×10^{6}
Cu^{+2}	6.7×10^{-4}	1.8	0.25	8×10^{6}
Ni^{+2}	3.0×10^{-2}	1.7	0.50	8×10^{4}
Ni^{+2}	5.0×10^{-2}	2.2	0.50	9×10^{4}

Zinc ions were found to have no effect on the linewidth. Both Cu(II) and Ni(II) solutions show extensive line broadening. Calculations were made using the equations and approach given by Connick and Poulson.[1] The coordination number of Cu(II) was assumed to be four and for Ni(II) was assumed to be six. Several runs were made at each condition listed in Table I. Two or three values of the broadening were then selected from the most symmetrical derivative curves and averaged. The apparent widths were reproducible to about ±10%. The ammonia exchange appears to be faster than the water exchange. Nickel seems to be slower to exchange than copper as was also found in the water exchange studies.

We are making changes in the magnet in the hopes of obtaining a more homogeneous field to make possible measurements over a wider concentration range. In addition, we plan to study the exchange at lower temperatures. Work on the analogous exchanges in liquid ammonia has been started. Cu(II) shows a large broadening of the NH_3 line at 2 M concentration. Isotopic exchange results have been reported[2] on liquid ammonia systems and it is of considerable interest to have independent methods of measurement for these fast reactions. Studies using substituted ammines will also be of interest for rate comparisons.

* This work was supported in part by the U. S. Atomic Energy Commission.
[1] R. E. Connick and R. E. Poulson, J. Chem. Phys. **30**, 759 (1959).
[2] J. R. Sutter and J. P. Hunt, J. Am. Chem. Soc. **82**, 6420 (1960).

Dipole Moment of $CClF_3$*

R. C. JOHNSON, T. L. WEATHERLY, AND QUITMAN WILLIAMS
Georgia Institute of Technology, Atlanta 13, Georgia
(Received August 31, 1961)

THE electric dipole moment of $CClF_3$ was previously evaluated by Birnbaum[1] using a cavity method to determine the nonresonant, or Debye type, absorption. It was later evaluated by Beeson[2] by measuring and analyzing the Stark effect for the $J=2\rightarrow3$ rotational transition. The latter determination was not considered very accurate because of difficulty in resolving the Stark components. It was decided to evaluate the dipole moment by measuring and analyzing the Stark effect for the $J=1\rightarrow2$ transition, since the Stark spectrum is considerably less complex for this transition.

The energy eigenvalues were calculated, using intermediate field theory, for several values of Stark field. It appears that the molecule behaves according to the strong-field case[3] for electric field intensities greater than about 400 v/cm; the rotational levels are split by Stark effects according to the values of M_J, and the resulting levels are further split by quadrupole inter-

TABLE I. Stark line frequencies for $CCl^{35}F_3$.[a]

Stark field intensity (v/cm)	M_J	M_I	1st order Stark displacement	Average 1st order stark displacement	2nd order stark displacement	Theoretical stark line frequency	Measured stark line frequency
657	+1	$+\frac{3}{2}$	+56.34				
		$+\frac{1}{2}$	+54.54				
		$-\frac{1}{2}$	+55.14				
		$-\frac{3}{2}$	+55.57	+55.40	+0.33	13 398.1	13 398.2
657	−1	$+\frac{3}{2}$	−54.37				
		$+\frac{1}{2}$	−56.20				
		$-\frac{1}{2}$	−55.71				
		$-\frac{3}{2}$	−55.30	−55.40	+0.33	13 287.3	13 287.4
1100	+1	$+\frac{3}{2}$	+93.24				
		$+\frac{1}{2}$	+91.70				
		$-\frac{1}{2}$	+92.06				
		$-\frac{3}{2}$	+92.76	+92.44	+0.94	13 435.7	13 436.1
1100	−1	$+\frac{3}{2}$	−91.61				
		$+\frac{1}{2}$	−93.15				
		$-\frac{1}{2}$	−92.84				
		$-\frac{3}{2}$	−92.15	−92.44	+0.94	13 250.9	13 251.0

[a] The transitions are $J=1\rightarrow2$, $K=1$, $I=\frac{3}{2}$, $\Delta M_J=0$, $\Delta M_I=0$; the electric dipole moment is 0.50 debye; the rotational energy is $2B(J+1)=13\,342.40$ Mc. Frequencies are given in megacycles.

action according to the values of M_I. Recordings of the $J=1\rightarrow2$ transition at various field intensities above 400 v/cm indicated a widely separated pair of Stark lines symmetrically located on each side of the group of rotational lines. Assuming the strong field selection rules for absorption, it was found that each of the pair of Stark lines was composed of a group of four closely spaced hyperfine lines, and the separation between the groups was a unique function of the electric field intensity.

The evaluation of the molecular dipole moment proceeded then as follows: (a) Stark energy levels versus electric field intensity were calculated, using intermediate field theory, for several assumed values of molecular dipole moment in the neighborhood of 0.500 debye. (b) Using the strong-field selection rules, a family of curves, one for each assumed value of dipole moment, was constructed illustrating the theoretical frequency separation vs field intensity for the pair of Stark lines. Each Stark line was assumed to be the average of its four unresolved hyperfine components. (c) The frequency of each of the pair of Stark lines was accurately measured at two values of electric field intensity: 657 and 1100 v/cm. From these measurements, the frequency separation was found for both values of field intensity. (d) With a large scale graph of the family of curves from step (b) and the two experimental points from step (c), the molecular electric dipole moment for $CCl^{35}F_3$ was assigned the value 0.50 ± 0.01 debye.

The evaluation of the dipole moment was essentially independent of the assumed value of eqQ since the quadrupole coupling produced only a small perturbation on the Stark splitting and the individual hyperfine lines were not resolved. By using the measured separation between the pair of Stark lines, the evaluation of dipole moment was made independent of the rotational constant B and effects such as molecular polarization and second-order Stark energies which shift both lines equally in the same direction.

A comparison of the measured Stark line frequencies with the theoretical frequencies is illustrated in Table I. Second-order Stark displacements are significant; however, higher-order Stark effects and molecular polarization can be neglected. The comparison of measured and theoretical frequencies is considered to be quite good since the Stark lines were about 3Mc wide.

* Supported in part by the National Science Foundation and the Office of Naval Research.

[1] G. Birnbaum, J. Chem. Phys. **27**, 360–368 (1957).
[2] E. L. Beeson, unpublished Ph.D. thesis, Georgia Institute of Technology (1960).
[3] W. Low and C. H. Townes, Phys. Rev. **76**, 1295–1299 (1949).

C^{13}-hfs in the ESR Spectrum of *p*-Benzosemiquinone-1-C^{13} Ion

M. R. DAS AND B. VENKATARAMAN
Atomic Energy Establishment Trombay and Tata Institute of Fundamental Research, Bombay, India

(Received August 14, 1961)

THE electron spin resonance (ESR) absorption spectrum of *p*-benzosemiquinone ion with about 50 at. % of C^{13} in the 1 position has been observed. Many authors[1–3] have suggested that some of the satellites found in the ESR spectra of semiquinone ions result from the hyperfine interaction with the C^{13} nucleus present in natural abundance. The satellites obtained with ordinary semiquinone ion have been attributed to the C^{13} atom in the 2 position and Strauss

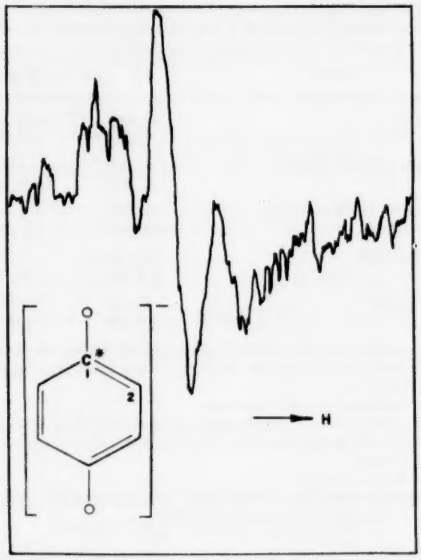

FIG. 1. Derivative of the central triplet of the ESR spectrum of *p*-benzosemiquinone ion with C^{13} labeling (50%) in the 1 position. The central component arises from the unlabeled compound and the side lines are the C^{13} doublets from the labeled compound.

and Fraenkel[3] have deduced that the splitting due to C^{13} in the 1 position must be less than 0.6 gauss.

p-benzohydroquinone-1-C^{13} (50%) was synthesized from C^{13}-enriched BaC^*O_3 and the method of synthesis has been reported elsewhere.[4] The semiquinone ion was obtained by the atmospheric oxidation of an alcoholic, alkaline solution of the labeled hydroquinone.[5] The ESR spectrum of the sample consists of five triplets; the central line of each triplet arises from the unlabeled species; the spectrum of the labeled species consists of five doublets, the spacing between the components of a doublet representing the C^{13}-hyperfine splitting. Figure 1 shows the derivative spectrum of the central triplet and the signal-to-noise ratio is rather poor because of the low microwave power and low radical concentrations that had to be used for obtaining good resolution.[6] Since the C^{13} enrichment is about 50%, the labeled and unlabeled species are present in equal concentration and within a triplet, the ratio of the intensities of the central line to that of the side components is expected to be about 2:1. The separation between the doublets (a_1^c) was 0.40 ± 0.04 gauss and overlap corrections[6,7] were found to be negligible in comparison with the experimental error. Karplus and Fraenkel[8] have recently developed a theory for the analysis of C^{13} splittings, which is more complete and detailed than that of McLachlan, Dearman, and Lefebvre.[9] On the basis of the former theory, Strauss and Fraenkel[3] have compared their data on *p*-benzosemiquinone ion with that on 2,5 dihydroxysemiquinone ion,[2] and have placed limits on the values of the two sigma-pi interaction parameters Q_{CO}^C and Q_{OC}^C referring to the carbon-oxygen bond

$$8.7 \leq Q_{CO}^C \leq 11.8,$$

and

$$-3.0 \leq -Q_{OC}^C \leq 5.2,$$

with our value for $|a_1^c| = 0.40$ gauss, we arrive at the following two possible sets of values for Q_{CO}^C and Q_{OC}^C, depending on the sign of a_1^c:

for $a_1^c = +0.40$ gauss, $Q_{CO}^C = 9.2$; $-Q_{OC}^C = -1.6$; and

for $a_1^c = -0.40$ gauss, $Q_{CO}^C = 11.3$; $-Q_{OC}^C = 3.9$.

We are grateful to Professor S. S. Dharmatti for his encouragement.

[1] A. Van Roggen, J. Chem. Phys. **33,** 1589 (1960).
[2] D. C. Reitz, F. Dravnieks, and J. E. Wertz, J. Chem. Phys. **33,** 1880 (1960).
[3] H. L. Strauss and G. K. Fraenkel, U. S. Air Force Rept. CU-8-61-AF-520-Chem. (1961).
[4] M. R. Das, Current Science, (to be published).
[5] B. Venkataraman and G. K. Fraenkel, J. Am. Chem. Soc. **77,** 2707 (1955).
[6] B. Venkataraman, B. G. Segal, and G. K. Fraenkel, J. Chem. Phys. **30,** 1006 (1959).
[7] B. Venkataraman, thesis, Columbia University, New York, 1955.
[8] M. Karplus and G. K. Fraenkel, U. S. Air Force Rept. CU-9-61-AF-520-Chem. (1961).
[9] A. D. McLachlan, H. H. Dearman, and R. Lefebvre, J. Chem. Phys. **33,** 65 (1960).

Fluorine NMR Spectroscopy. V. A Carbon-13 Study of Coupling Constants between *cis* and *trans* CF_3 Groups in Highly Fluorinated Olefins*

GEORGE VAN DYKE TIERS
Central Research Department of the Minnesota Mining and Manufacturing Company, St. Paul 19, Minnesota
(Received May 17, 1961)

VERY few stereoisomers of highly fluorinated compounds have been isolated and identified with reasonable certainty, and relatively few chemical or physical techniques are available for the intercomparison of these with other materials. When *cis-trans* isomerism about a double bond is being studied, intercomparisons may be done by NMR means, but for the original proof of structure it is necessary to appeal to an "absolute" method, such as the well-known absence of the C=C stretching infrared absorption for a symmetrical *trans*-olefin. In this manner the *cis*- and *trans*-2,3-dichlorohexafluorobutene-2 isomers have been identified[1]; the NMR study of these isomers, reported here, yields characteristic shielding values and spin-spin coupling constants for CF_3 groups so located. Owing to the magnetic equivalence of the CF_3 groups, the coupling constants could only be ascertained from the "C^{13} satellite" peaks, which result from the presence,

in natural abundance, of molecules bearing $C^{13}F_3$ groups at one end. This elegant method, due to Sheppard,[2-4] heretofore has been applied only to proton compounds.

Experimental. Commercial 2,3-dichlorohexafluorobutene-2 (Hooker Chemical Company) was found to have a *cis/trans* ratio of about 15/85, other impurities also being present. Vapor-phase chromatography (VPC) over "Kel-F" oil KF-3 (Minnesota Mining & Manufacturing Company) at 40° resulted in a highly pure sample of *trans*-2,3-dichlorohexafluorobutene-2, n_D^{25} 1.3440, f.p. about −55° to −60°, having a very weak C=C infrared band, and containing only 0.2% of the *cis*-isomer which is eluted later. Commercial 2,2,3,3-tetrachlorohexafluorobutane (Hooker Chemical Company) was dechlorinated[1] to give the olefin in a *cis/trans* ratio of 60/40, from which pure *cis*-2,3-dichlorohexafluorobutene-2, containing only 0.6% *trans* isomer, was isolated by the VPC technique already described. High purity was required as the isomer peaks (at 40 Mc/sec) tend to obscure the C^{13} satellites.

The NMR equipment and techniques were as previously described,[5-7] except that the Varian field homogeneity control unit had been installed. The results, presented in Table I, are in each case the averaged values from 8 to 18 separate determinations; standard deviations of these averaged values also are given. For the *cis*-isomer some second-order structure was visible in the low, broad C^{13} satellite quartets, however, as the noise was about as large as the lesser components, a complete analysis was not done. Since the "J/δ" ratio was only 0.1, corresponding to "weak coupling,"[8] it was possible to obtain $J(FF')$, and M_L (or M_H), as the difference and the mean, respectively, of the positions of the *strongest components* of each of the two central peaks of the low-field (or the high-field) quartet. There is obtained

$$J(FF') = 13.39, \qquad M_L = -132.48 \pm .14$$

and $M_H = +143.46 \pm 0.10$ cps, from which $J(C^{13}F_3)$ is computed by the exact relation

$$J(C^{13}F_3) = M_H - M_L - J(FF')^2/(M_H - M_L).$$

This follows from an extension of the AB and A_3B treatments to the A_3B_3' case.[8]

Discussion. The first and second rows of Table I show a substantial difference in shielding between the stereoisomers, an antishielding effect apparently being associated with *cis* placement of the CF_3 groups. The isomers of perfluorobutene-2 (which have not been separated) differ in CF_3 group shielding by 2.50 ppm, but the ϕ^*-values (10%) are $+67.23 \pm 0.01$ and $+69.72 \pm 0.01$, while ϕ^* (40%) for the CF_3 group of perfluoropropylene is 69.33 ± 0.01 and ϕ^* (5%) for $CF_3CCl{=}CCl_2$ is $+61.424 \pm 0.004$. It would thus appear that there is a strong antishielding effect due to chlorine, which is dependent upon stereostructure.

TABLE I. Shielding values and coupling constants for the *cis* and *trans* isotopic isomers of 2,3-dichlorohexafluorobutene-2.

Isomer	*Cis*	*Trans*
ϕ^*, ppm[a]	+60.446 ±0.007	+63.730 ±0.008
ϕ^* (*trans*)-ϕ^*(*cis*) ppm[b,e]	+3.373 ±0.002	+3.351 ±0.001
$\Delta\phi$, ppm[b,d] ($C^{13}F_3$—$C^{12}F_3$)	+0.137 ±0.002	+0.132 ±0.001
J ($C^{13}F_3$) cps[b]	275.29[e] ±0.20	275.66 ±0.06
J (FF′) cps[b,f]	13.39[e] ±0.06	1.44 ±0.02

[a] See reference 6; concentration 10.0% by volume in CCl_3F, measurement temperature 25°±1°.
[b] Neat (undiluted) samples were used.
[c] When at 10% concentration by volume in CCl_3F, this difference is +3.284± 0.001; note that the three values cited need not be identical, since the "solvents" used are different.
[d] See references 7 and 9.
[e] From approximate A_3B_3 analysis; $J(C^{13}—C—C—CF_3)$ taken as 0.00.
[f] Here F′ represents fluorine attached to C^{13}.

Assignment of the perfluorobutene-2 peaks from shielding values by analogy to the present case would clearly be unwise.

Spin-spin coupling constants, unlike shielding values, ordinarily are not affected by neighboring groups unless these alter the relative conformations of the groups bearing the spin-coupled atoms. Evaluation of the coupling constants between *cis* and *trans* CF_3 groups thus should provide a rather reliable criterion of stereostructure. For symmetrical molecules such coupling is exhibited only in the spectra of the $C^{13}F_3$ derivatives[2-4]; these also show an "isotope effect" upon shielding values, the center of the $C^{12}F_3$ pattern lying at higher field than that for the $C^{12}F_3$ group.[9] This isotope shift $\Delta\phi$ listed in the third row of Table I, has about the usual value for a CF_3 group[7,9] and is not significantly influenced by stereostructure. The same can be said of the $C^{13}F_3$ coupling constants given in the fourth row.

In the last row of Table I are presented the coupling constants, $J(FF')$, between fluorine nuclei in CF_3 groups located *cis* and *trans* to one another. The numerical value appears to be highly stereosensitive, with the *cis* coupling being larger; the opposite was claimed for fluorine atoms directly attached to the double bond, although no confirmatory experimental evidence has been offered.[10,11] There are many cases of substantial spin-spin coupling between "distant" fluorinated groups[12] (which, in fact, need not be very distant in space) and there is, as yet, insufficient information for an estimation of the effect of bond (or group) angles; speculation upon the theoretical significance will therefore be omitted.

I thank Klaus Fiedler for the skillful VPC separations, and D. M. Hotchkiss and R. B. Calkins for careful maintenance and operation of the NMR equiqment.

* Contribution No. 207.

[1] F. Dickinson, R. Hill, and J. Muray, J. Chem. Soc. **1958,** 1441.
[2] A. D. Cohen, N. Sheppard, and J. J. Turner, Proc. Chem. Soc. (London) **1958,** 118.
[3] N. Sheppard and J. J. Turner, Proc. Roy. Soc. (London) **A252,** 506 (1959).
[4] N. Sheppard and J. J. Turner, Mol. Phys. **3,** 158 (1960).
[5] G. V. D. Tiers, J. Phys. Chem. **62,** 1151 (1958).
[6] G. Filipovich and G. V. D. Tiers, J. Phys. Chem. **63,** 761 (1959).
[7] G. V. D. Tiers, J. Phys. Soc. Japan **15,** 354 (1960).
[8] P. L. Corio, Chem. Revs. **60,** 363 (1960); see especially pp. 387–9 and 401.
[9] P. C. Lauterbur (unpublished).
[10] H. M. McConnell, C. A. Reilly, and A. D. McLean, J. Chem. Phys. **24,** 479 (1956).
[11] J. D. Swalen and C. A. Reilly, J. Chem. Phys. **34,** 2122 (1961).
[12] A. Saika and H. S. Gutowsky, J. Am. Chem. Soc. **78,** 4818 (1956).

Proton Motions in Solids by Slow Neutron Scattering Cross Sections*

J. J. Rush, T. I. Taylor, and W. W. Havens, Jr.
Departments of Chemistry and Physics, Columbia University, New York, New York, and Brookhaven National Laboratory, Upton, New York

(Received August 2, 1961)

PREVIOUS measurements[1,2] on a series of ammonium halides have shown a definite correlation between the scattering of low-energy neutrons and the rotational freedom of the ammonium ions. At neutron energies far below thermal the neutron-scattering cross section σ_s is proportional to the neutron wavelength λ_n, and the slope of cross section vs wavelength increases with the freedom of motion of the hydrogen atoms. In the present work these measurements have been extended to a number of compounds in which the binding and motion of the hydrogen atoms is somewhat uncertain. Using a crystal spectrometer[3,4] at the Brookhaven Reactor, total neutron cross-section measurements were obtained at room temperature for polycrystalline KH_2PO_4, $(NH_4)_2CrO_4$, $(NH_4)_2Cr_2O_7$, NH_4CNS, and NH_4ClO_4. The cross sections per molecule were corrected for neutron absorption and divided by the number of hydrogen atoms. In Fig. 1 the resulting cross sections per hydrogen are plotted as a function of neutron wavelength.

A low-frequency hydrogen vibration has been suggested[5] as a possible explanation for ferroelectric and other properties of KH_2PO_4. The cross-section curve in Fig. 1, however, is almost flat at long wavelengths, indicating tight binding for the protons in this hydrogen-bonded compound.[6] This result is also in disagreement with the conclusions drawn from a recent measurement of the vibration spectra of K_2HPO_4 and KH_2PO_4 by inelastic scattering of cold neutrons.[7] From these measurements low-energy peaks around

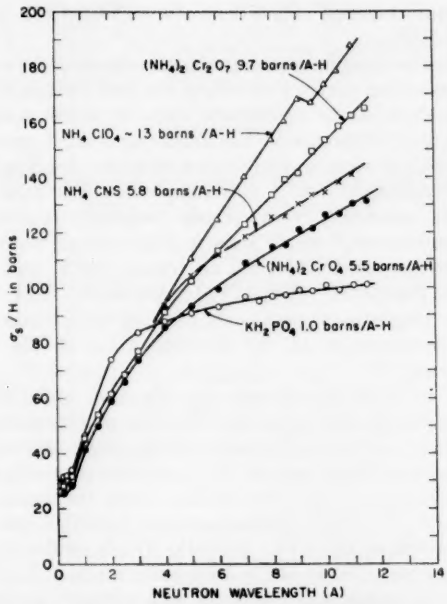

FIG. 1. Neutron scattering cross sections per hydrogen atom for KH_2PO_4, $(NH_4)_2CrO_4$, $(NH_4)_2Cr_2O_7$, NH_4CNS, and NH_4ClO_4. The slopes indicated were determined by a weighted least-squares fit. Errors on the slopes vary from ± 0.10 to ± 0.15 b/A–H and include only those due to counting and to uncertainty in the absorption cross sections.

400–550 cm^{-1} in the scattered neutron spectra were attributed to hydrogen vibrational modes. However, such low-energy vibrations would be significantly excited at room temperature and would result in a higher slope for the scattering cross-section curve than observed for KH_2PO_4. Similar cross-section results, not shown in the figure, were obtained for K_2HPO_4, again indicating the absence of low-energy hydrogen vibrations. These data are in agreement with neutron diffraction studies which predict only high-frequency proton vibrations in KH_2PO_4.[8] It thus appears that the low-energy peaks observed in the neutron spectrum and in infrared reflection studies are not hydrogen modes[7] but probably involve vibrations of the phosphate ion, as suggested from the infrared results.[9]

The cross-section slopes observed for $(NH_4)_2CrO_4$ and NH_4CNS, 5.5 and 5.8 b/A–H, indicate a similar hindrance to rotation of the ammonium ion in these compounds. These slopes are also close to the result at room temperature for NH_4Br (5.7 b/A–H).[1] Thus their hydrogen bond strengths, rotational barriers, and torsional frequencies may be close to those in NH_4Br (torsional frequency = 311 cm^{-1}). However, such a comparison cannot imply that the details of the ammonium ion motions are equivalent since the two compounds studied here possess a complex monoclinic structure. These results are consistent with recent proton magnetic resonance data,[10] which show similar

second moment transitions for $(NH_4)_2CrO_4$ and NH_4CNS.

Another significant comparison can be made between cross-section curves for $(NH_4)_2CrO_4$ and $(NH_4)_2Cr_2O_7$. The slope of the dichromate curve is almost double that for the chromate, thus indicating a much greater freedom of rotation and weaker hydrogen bonding for the ammonium ion in this compound. This result is again consistent with proton magnetic resonance measurements,[10] which show a sharp second moment transition for $(NH_4)_2CrO_4$ at around 100°K and no such change for $(NH_4)_2Cr_2O_7$. Moreover, from the same magnetic resonance data a low barrier is predicted for reorientation of the ammonium ion in the dichromate.[10]

It is interesting to note that the long wavelength cross section and slope for NH_4ClO_4 are significantly greater than those obtained for $(NH_4)_2Cr_2O_7$. Although an intense Bragg peak at 9.2 A prevents a precise determination of the cross-section slope, the value of around 13 b/A–H approaches that for NH_3 gas at room temperature (15.7 b/A–H).[1] This is evidence for almost free rotation of the ammonium ion in NH_4ClO_4. Such a conclusion is consistent with infrared measurements[11] and with neutron diffraction data.[12] The high slope also supports the barrier to reorientation of the ammonium ion of <1000 cal/mole predicted from the NMR data of Richards and Shaefer[10] rather than the higher barrier of 2 kcal/mole proposed by Ibers.[13] The observed slope is also significantly higher than the value of 11.2 b/A–H obtained for NH_4I at room temperature.[1,2] Thus the rotational freedom of the ammonium ion appears greater in NH_4ClO_4 than in either $(NH_4)_2Cr_2O_7$ or NH_4I. The possibility of semi-quantitatively relating cross-section slopes to vibrational frequencies or potential barriers to rotation is being investigated.

* This work partially supported by the U. S. Atomic Energy Commission.

[1] J. J. Rush, T. I. Taylor, and W. W. Havens, Jr., Phys. Rev. Letters **5,** 507 (1960).

[2] J. J. Rush, T. I. Taylor, and W. W. Havens, Jr., Bull. Am. Phys. Soc. **6,** 261 (1961).

[3] F. T. Gould, T. I. Taylor, W. W. Havens, Jr., B. M. Rustad, and E. Melkonian, Nuclear Sci. and Eng. **8,** 453 (1960).

[4] J. A. Moore, J. J. Rush, and B. M. Rustad, Bull. Am. Phys. Soc. **4,** 245 (1959).

[5] J. Pirenne, Physica **15,** 1019 (1949).

[6] E. Fermi, Ricerca sci. **7,** 13 (1936).

[7] I. Pelah, I. Lefkowitz, W. Kley, and E. Tunkelo, Phys. Rev. Letters **2,** 94 (1959).

[8] G. E. Bacon and R. S. Pease, Proc. Roy. Soc. (London) **A230,** 359 (1955).

[9] G. M. Murphy, G. Weiner, and J. J. Oberly, J. Chem. Phys. **22,** 1322 (1954).

[10] R. E. Richards and T. Schaefer, Trans. Faraday Soc. **57,** 210 (1961).

[11] T. C. Waddington, J. Chem. Soc. **1958,** 4340.

[12] H. G. Smith and H. A. Levy, Abstract K-6 (American Crystallographic Association Annual Meeting, Cornell University, July, 1959).

[13] J. A. Ibers, J. Chem. Phys. **32,** 1448 (1960).

Positronium Formation in the Halogen Derivatives of Benzene*

C. R. HATCHER

Lawrence Radiation Laboratory, University of California, Livermore, California

(Received July 24, 1961)

STUDIES of positron annihilation in organic compounds show that in most liquids there are two measurable decay rates.[1–3] The faster decay (approximately 2×10^{-10} sec) arises from ^1S positronium and from annihilations in which no positronium is formed. The "long" component (approximately 2×10^{-9} sec) is due to ^3S positronium and represents three-fourths of the total positronium formed, one-fourth being formed in the ^1S state. Of the several groups of organic compounds studied, the halogen derivatives of benzene have the largest variation of intensity I_2 of the long component,[2,3] and hence the largest variation of amount of positronium formed. The processes in a liquid which are thought to compete with positronium formation are: (1) inelastic collisions of the positron with the molecules of the liquid, and (2) positron attachment to the molecules.[2,4,5]

The purpose of this report is to show that, for annihilation in the halogen derivatives of benzene, the intensity I_2 of the long component can be explained on the basis of the Ore model of positronium formation[6–8] where the upper bound of the Ore gap is equal to the dissociation potential of the carbon-halogen bond. Figure 1 shows the energetics involved in positronium formation. Let E be the kinetic energy of the free positron, V_i the ionization potential of the halogen-substituted benzene, V_d the dissociation potential of the carbon-halogen bond, and V_p the binding energy of positronium (6.8 ev in free space). The following assumptions are now made: (1) for $E>V_i$, annihilation may be neglected; (2) a positron scattered into the energy interval $0<E<V_i$ is equally likely to have any energy in the interval; (3) for $V_d<E<V_i$, competing processes (most likely dissociation of the carbon-halogen bond) are vastly more probable than positronium formation; (4) in these processes the positron loses sufficient energy so that scattering into the Ore gap may be neglected; and (5) all positrons in the Ore gap, $V_i-V_p<E<V_d$, form positronium. Having made these assumptions, it follows that the fraction of

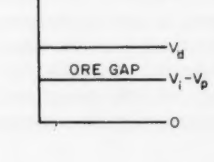

FIG. 1. Energetics of positronium formation in the halogen derivatives of benzene. It is assumed that all positrons in the Ore gap form positronium.

positrons that form positronium is given by

$$[V_d-(V_i-V_p)]/V_i,$$

because positronium cannot be formed for $E<V_i-V_p$. The intensity of the long component is given by $I_2=\frac{3}{4}[V_d-(V_i-V_p)]/V_i$, since three-fourths of the total positronium is formed in the ^3S state.

Table I shows a comparison of measured[2] and computed values of I_2 along with experimental values of V_i[9] and V_d.[10,11] The agreement between values of I_2 computed on the basis of this model and experimental results leads to the conclusion that, for these compounds, positronium formation can be explained on the basis of energy considerations, and that molecular dissociation is the major competing process. Since positron attachment to the molecule has been neglected, the method used here to calculate I_2 would be expected

TABLE I. Measured and computed values of I_2.

Compound	V_i (ev)	V_d (ev)	Calculated I_2%	Measured I_2%
C_6H_5F	9.19	4.98	21	24±2
C_6H_5Cl	9.07	3.72	12	14±2
C_6H_5Br	8.98	3.07	7.4	6±2
C_6H_5I	8.73	2.47	4.6	4±2

to work only for compounds in which the dissociation cross section is considerably higher than the positron attachment cross section.

An interesting result of the interpretation of positronium formation given here is that the ^1S positronium atoms should annihilate with a kinetic energy between zero and the width of the Ore gap, $V_d-(V_i-V_p)$. This is not true for ^3S positronium, because in ^3S positronium the positron frequently annihilates with an electron bound to a molecule.[4,8] It might be possible in a two-photon angular-correlation experiment[1,5] to measure the energy spread of the low-momentum component due mainly to ^1S positronium, and thus determine experimentally the width of the Ore gap. It would be interesting to see how the width of the Ore gap determined in this manner compares with $V_d-(V_i-V_p)$ for the halogen derivatives of benzene.

* This work was supported in part by the U. S. Atomic Energy Commission.

[1] P. R. Wallace, in *Solid-State Physics*, edited by F. Seitz and D. Turnbull (Academic Press Inc., New York, 1960) Vol. 10, p. 1.
[2] C. R. Hatcher, W. E. Millett, and Louis Brown, Phys. Rev. **111**, 12 (1958).
[3] C. R. Hatcher, T. W. Falconer, and W. E. Millett, J. Chem. Phys. **32**, 28 (1960).
[4] R. E. Green and R. E. Bell, Can. J. Phys. **35**, 398 (1957).
[5] R. L. deZafra, Phys. Rev. **113**, 1547 (1959).
[6] A. Ore, University of Bergen, Årbok No. 9 (1949).
[7] M. Deutsch, Progr. Nuclear Phys. **3**, 131 (1953).
[8] R. A. Ferrell, Revs. Modern Phys. **28**, 308 (1956).
[9] K. Watanabe, J. Chem. Phys. **26**, 542 (1957).
[10] T. L. Cottrell, *The Strengths of Chemical Bonds* (Butterworths Scientific Publications, Ltd., London, 1958), 2nd ed.
[11] P. Smith, J. Chem. Phys. **29**, 681 (1958).

Evidence for a Long-Lived Metastable State of N_2 at about 8 ev

CARL KENTY
General Electric Lamp Research Laboratory, Nela Park Cleveland 12, Ohio

(Received August 11, 1961)

ACCORDING to Wilkinson[1] "all nitrogen electronic states of electron configuration $\pi_u{}^3\sigma_g{}^2\pi_g$ have now been observed and precisely located except $^3\Delta_u$." The following evidence indicates this state has a lifetime of 1–2 sec and an energy between 7.9 and 8.28 ev.

If a weak discharge[2] is passed through 150 mm Xe+0.1% N_2 then both the (diffuse) discharge and afterglow appear as a whitish continuum, exhibiting no lines or bands. There is also a continuum[3] strong at about 1750 A causing a violet fluorescence of the 40×12-cm diam Pyrex envelope. These are the continua of the excited xenon molecules Xe_2' formed according to

$$Xe^m+Xe+Xe\rightarrow Xe_2'+Xe,$$

where the xenon metastable atom Xe^m, in the afterglow and probably also largely in the discharge itself, results from a collisional process involving N_2 energy carriers.[4] Without N_2 the discharge appears exactly the same but the voltage is several fold higher[5] and there is no apparent afterglow.

If now a minute amount of Ba vapor is added to the afterglow a weak violet flame can be seen for 10 sec. This consists solely of the resonance lines 4934.1 and 4554.0 of Ba^+. The latter requires 7.90 ev for its excitation in a single act from normal Ba. The presence is therefore indicated of a "carrier" able to impart at least 7.90 ev to Ba. On the other hand, the carrier must have an energy <8.28 ev else it would lose its energy[6] quickly to Xe.

The density of Ba atoms was roughly estimated to be on the order of $10^{10}-10^{11}$ cm^{-3}. To stimulate so few Ba atoms to emit the observed light requires according to kinetic calculations, $10^{12}-10^{13}$ carriers cm^{-3}. Further the great lowering of discharge voltage by N_2, abovementioned, indicates also a concentration, of this order, of something much more easily ionized than Xe. Now a high concentration of a carrier requires either that it have a long life or that it be rapidly created (and destroyed). The absence of evidence of the large output of energy required by the latter indicates the carrier to have actually a life of the order of seconds.

Conductivity measurements in the afterglow with Ba addition indicate 10^8-10^9 ions cm^{-3}. This low concentration of Ba^+, which is confirmed by the undetectability of the recombination spectrum, cannot account for the observed light by collision of the carriers with Ba ions. Therefore, the excitation of the Ba II lines must occur in a single act from Ba. Therefore the carrier energy must be >7.90 ev.

The carrier could be $N_2(^3\Sigma_u^-)$, having an energy[1,7] of 8.164 ev, except that its lifetime[8] ($<3\times10^{-2}$ sec) is too short to be of help except in the very early afterglow.

The evidence therefore suggests that $N_2(^3\Delta_u)$ has an energy between 7.90 and 8.28 ev and a life of 1–2 sec. Such a long life could explain why this state has not been observed in emission or absorption.

[1] P. G. Wilkinson, J. Chem. Phys. **32**, 1061 (1960).
[2] C. Kenty, J. Chem. Phys. **23**, 1555 (1955).
[3] Y. Tanaka and M. Zelikoff, J. Opt. Sci. Am. **44**, 254 (1954); Phys. Rev. **93**, 933 (1954); C. Kenty, *ibid.* **93**, 651 (1954).
[4] The carrier could be the long lived carrier here under discussion provided its energy lay close below 8.28 v, so that kinetic collisions could make up the energy deffiency.[2]
[5] C. Kenty, Bulletin 16th Annual M.I.T. Conference on Physical Electronics, 1956, p. 85.
[6] This carrier was called X in reference 2, where it was thought to be $N_2(a')$. It has since been shown[8] that $N_2(a')$ has an energy of 8.398 ev, too high for the present purpose, and a life of 4×10^{-2} sec; too short for the present purpose.
[7] M. Ogawa and Y. Tanaka, J. Chem. Phys. **32**, 754 (1960).
[8] P. G. Wilkinson and R. S. Mulliken, J. Chem. Phys. **31**, 674 (1959).

Remark on the Mulliken Approximation for Two-Center Electron Distributions*

AUDREY L. COMPANION
Department of Chemistry, Illinois Institute of Technology, Chicago 16, Illinois
AND
ROBERT G. PARR†
Department of Chemistry, Carnegie Institute of Technology Pittsburgh 13, Pennsylvania
(Received August 16, 1961)

THE Mulliken approximation for a two-center electronic distribution may be written

$$\chi_a(1)\chi_b(1)\sim\tfrac{1}{2}S[\chi_a^2(1)+\chi_b^2(1)], \qquad (1)$$

where χ_a and χ_b are atomic orbitals on atoms A and B and S is the overlap integral between them.[1,2] This approximation is very useful both in approximate theoretical[3] and in semiempirical[4] calculations of molecular electronic wave functions.

It has been suggested[5] that Eq. (1) might become more accurate as the forms of χ_a and χ_b are improved to give a better molecular wave function, for example, in the simple valence bond or the simple molecular orbital description of a bond between atoms A and B. To test this idea, one may define the *Mulliken approximation error function*,

$$\delta(1)=\chi_a(1)\chi_b(1)-\tfrac{1}{2}S[\chi_a^2(1)+\chi_b^2(1)], \qquad (2)$$

compute the integral of δ^2 over all space,

$$\Delta=\int\delta^2(1)dv(1), \qquad (3)$$

for various orbitals χ_a and χ_b in the hydrogen molecule-ion and hydrogen molecule, and examine the dependence of the values of Δ on the orbital form.

A convenient orbital form, sufficiently flexible to allow arbitrary effective charge and suitable polarization, is

$$\chi_a=N(1+\lambda z_a)\exp(-\mu r_a), \qquad (4)$$

where z_a is the component along the internuclear axis of the distance r_a of the electron from center A, λ and μ are parameters, and N is a normalizing factor. With this formula for χ_a, and a similar one for χ_b, the quantity Δ of Eq. (3) can be evaluated by introduction of prolate ellipsoidal coordinates. The final formula contains the familiar auxiliary functions

$$A_n(\alpha)=\int_1^\infty\xi^n\exp(-\alpha\xi)d\xi$$

and

$$B_n(\beta)=\int_{-1}^1\eta^n\exp(-\beta\eta)d\eta.$$

Calculations of Δ for various values of λ, μ, and the interorbital distance R were performed on the Univac 1105 computer at Illinois Institute of Technology.

The results are summarized in Table I. The original conjecture, that Δ should monotonically decrease as

TABLE I. Mean-square Mulliken approximation error, for various atomic orbitals in the hydrogen molecule-ion and hydrogen molecule.[a]

Atomic orbital parameters[b]			
R	μ	λ	$\Delta\times10^5$
1.3	1.0	0.0, 0.1, 0.2, 0.6	73, 55, 48, 32
	1.2	0.0, 0.1, 0.2, 0.6	171, 148, 128, 36
1.5	1.0	0.0,[c] 0.1, 0.2, 0.6	94,[c] 76, 65, 14
	1.2	0.0[d], 0.1[e], 0.2, 0.6	200,[d] 188,[e] 164, 133
2.0	1.0	0.0,[f] 0.1, 0.2, 0.3	125,[f] 112, 97, 79
	1.2	0.0,[g] 0.1, 0.2,[h] 0.3	215,[g] 222, 220,[h] 321

[a] Equation (3) of text.
[b] Equation (4) of text. R is the A–B distance, μ is the effective charge parameter, and λ is the polarization parameter, all in atomic units. Equilibrium values of R in H_2^+ and H_2 are approximately 2.0 and 1.5.
[c] Essentially, the parameters are those in the original Heitler-London wave function for H_2, the energy associated with which is 0.057 a.u. above the experimental value.
[d] Essentially the Wang wave function for H_2, the energy of which is 0.035 a.u in error.
[e] Essentially the Rosen function for H_2, which is 0.026 a.u. in error.
[f] Essentially the Pauling function for H_2^+, which is 0.038 a.u. in error.
[g] Essentially the Finkelstein-Horowitz function for H_2^+, which is 0.020 a.u. in error.
[h] Essentially the Dickinson wave function for H_2^+, which is 0.005 a.u. in error.

orbital form is improved to give better energy, is seen to be false: change of effective charge to improve the Heitler-London function for hydrogen, for example, causes Δ to increase. However, incorporation of polarization, as in the Rosen function for hydrogen, does indeed tend to decrease Δ as well as improve the energy.

The minimum value of Δ with $\mu \geq 1$, except the zero values at $R=0$ and $R=\infty$, is 14×10^{-5}, at $R=1.5a_0$, $\mu=1$, $\lambda=0.6$. That this R is the equilibrium distance in H_2 is probably fortuitous.

Certainly other more sophisticated tests of the validity of Eq. (1) may be devised, but the simple test here described appears to settle the point at issue for sigma orbitals.

* Supported in part by a research grant from the National Science Foundation to Carnegie Institute of Technology.
† Alfred P. Sloan Fellow, 1956–1960.
[1] R. S. Mulliken, J. chim. phys. **46**, 497 (1949).
[2] K. Ruedenberg, J. Chem. Phys. **19**, 1433 (1951).
[3] For example, R. G. Parr, D. P. Craig and I. G. Ross, J. Chem. Phys. **18**, 1561 (1950).
[4] For example, J. M. Parks and R. G. Parr, J. Chem. Phys. **32**, 1657 (1960).
[5] J. M. Parks and R. G. Parr, J. Chem. Phys. **28**, 335 (1958).

Resonance Transfer Model of Electron and Hole Conduction in Anthracene*

DAVID KEARNS
Department of Physics, University of Chicago, Chicago, Illinois
(Received July 17, 1961)

RECENTLY Kepler[1] measured the temperature dependence and anisotropy of electron and hole mobilities in anthracene crystals. In this paper we will be concerned with the applicability of a resonance transfer model in accounting for Kepler's results. The expression

$$\nu = 2/h \,|\, \langle\psi_{\rm II} \,|\, H' \,|\, \psi_{\rm I}\rangle - \langle\psi_{\rm II} \,|\, \psi_{\rm I}\rangle\langle\psi_{\rm I} \,|\, H' \,|\, \psi_{\rm I}\rangle \,|$$

obtained from time dependent perturbation theory[2,3] was used to calculate the rate ν at which an electron, or a hole, initially localized on a particular molecule (state I described by $\psi_{\rm I}$) will be transferred to a neighboring molecule (state II described by $\psi_{\rm II}$). H' in the above expression is the perturbation on the electron donating molecule produced by a neighboring molecule which is to act as the electron acceptor in the electron transfer process.

The potential energy $V_x(\mathbf{r})$ of a unit charge at a point $\mathbf{r}$ in the field of the perturbing molecule X is

$$V_x(\mathbf{r}) = \sum_n^{\text{All atoms of X}} \int_{\rho_n}^{\text{All space}} \left[\frac{-Q_n(\varrho_n)+q_n\delta(\varrho_n,\,0)}{|\,\mathbf{r}-\mathbf{r}_n-\varrho_n\,|}\right] d\tau(\rho_n) = \sum_n \frac{Z_{nx}(\mathbf{r}-\mathbf{r}_n)}{|\,\mathbf{r}-\mathbf{r}_n\,|}, \quad (1)$$

where $\mathbf{r}_n$ locates the nth atom of X with respect to the center of X, $Q_n(\varrho_n)$ gives the electron distribution about the nth atom, q_n is the nuclear charge on n, $\delta(\varrho_n, 0)$ is a delta function centered on n, and $\mathbf{r}$ is the distance measured from the center of X. X is neutral in the case of electron conduction and we assumed that $Z_{nx}(\mathbf{r}-\mathbf{r}_n)/|\,\mathbf{r}-\mathbf{r}_n\,|$ could be approximated by the Fermi-Thomas potential at a distance $(\mathbf{r}-\mathbf{r}_n)$ from the neutral atom n. X is a positive ion in hole conduction and in this case $Z_{nx}(\mathbf{r}-\mathbf{r}_n)/|\,\mathbf{r}-\mathbf{r}_n\,|$ was assumed to be the sum of the neutral atom Fermi-Thomas potential plus the potential due to the fractional positive charge on atom n that results from the removal of an electron from a neutral molecule.

The quantity

$$|\,\langle\psi_{\rm II} \,|\, H' \,|\, \psi_{\rm I}\rangle - \langle\psi_{\rm II} \,|\, \psi_{\rm I}\rangle\langle\psi_{\rm I} \,|\, H' \,|\, \psi_{\rm I}\rangle\,|$$

will be large only in the region where $\psi_{\rm I}$ and $\psi_{\rm II}$ overlap strongly; hence, $Z_{nx}(\mathbf{r}-\mathbf{r}_n)$ can be taken as a constant with a value equal to that at the position of maximum overlap ($Z_{nx}\cong 0.10e^+$ for a neutral X when carbon

TABLE I. Calculated and observed electron and hole mobilities in anthracene.

Quantity calculated or measured	Calculated			Observed	
	a axis	b axis	c' axis ($\perp$ to a–b plane)	in a–b plane	c' axis ($\perp$ to a–b plane)
μ^h (300°K)[a]	0.3	0.8	0.12	1.3	0.4
μ^e (300°K)[a]	0.3	0.5	0.15	2.0	0.3
$\mu^h(T)/\mu^h$ (300°K)[b]	$300/T$	$300/T$	$300/T$	...	$300/T+0.14$ (holes)
$\mu^e(T)/\mu^e$ (300°K)[c]	$(370-0.23T)/T$	$(300-0.024T)/T$	$(640-1.20T)/T$	...	$(500-0.63T)/T$ (electrons)
$(\Delta\mu^h/\Delta P)/\mu^h$ (300°)[d]	5%	2%	8%	...	~16%[13]
$(\Delta\mu^e/\Delta P)/\mu^e$ (300°)[d]	5%	2%	8%	...	~0%

[a] Units of cm²/v-sec, μ^h=hole mobility, μ^e=electron mobility.
[b] Effective internuclear distance assumed temperature independent.
[c] Effective internuclear distance assumed to vary with lattice parameters.
[d] Units of % change per 1000 kg/cm².

atoms located 4 A[4] apart). The molecular wave functions were represented by products of Hückel[5] molecular orbitals which in turn were expressed as sums of Slater[3] atomic orbitals, using Slater's[3] rules to determine the effective nuclear charges for the atomic orbitals. The state functions were then expressed as a product of a neutral and an ionic molecular wave function. These approximations reduce the problem to the evaluation of integrals involving only atomic functions.

The interatomic distances and angles between the pi orbitals of atoms located on neighboring molecules were calculated from Wyckoff's[6] data, and Roothaan's[7] tables were used to evaluate the integrals in the expression for ν.

If we assume that charge carriers are scattered after each intermolecular transfer, perhaps due to molecular vibrations which have about the same frequency as the charge transfer frequency ν, then the mobility of a charge e is related to ν and the transfer distance d as follows[8,9]: $\mu=d^2e/kT$. The room temperature electron and hole mobilities μ^e and μ^h calculated using the above formulas are found to be about a factor of five smaller than those measured by Kepler[1] (see Table I). Because of the approximations involved in the calculations, this discrepancy cannot be considered too serious. One way of accounting for this discrepancy is to assume that the charge carriers are transferred several lattice units before being scattered, as in a band model,[10] instead of assuming scattering after each intermolecular transfer.

Measurements[11] indicate that the temperature variations in the anthracene crystal lattice dimensions are almost the same as the temperature variation in the amplitudes of the molecular vibrations about their equilibrium positions.[12] Without detailed calculations it is not clear how the effective intermolecular distance r_{eff} will vary with temperature. The temperature dependences of mobilities calculated assuming that, (1) r_{eff} is temperature independent, or, (2) that the thermal expansion of the lattice represents the increase in r_{eff} are given in Table I.

We assumed that the ratios of the compressibilities along the different crystal axes are in the same ratio as the coefficients of thermal expansion along the same axes and used Bridgman's[13] data on volume compressibility of anthracene to evaluate the compressibility along the three crystal axes. With these values it was possible to calculate the pressure dependence of the electron and hole mobilities. The results of these calculations also appear in Table I.

The resonance transfer model predicts that both electron and hole mobilities will vary *approximately* inversely with temperature in agreement with experiment. However, both electron and hole mobilities are predicted to have the same temperature dependence, and this is not observed.[1] The predicted anisotropy of hole mobility in the three crystal directions

$$(\mu_b\simeq 2\mu_a\simeq 5\mu_c')$$

is in good agreement with experimental results.[14] However, the predicted anisotropy of electron mobility in the *a-b* plane ($\mu_b\simeq 2\mu_a$) is opposite to that observed. Kepler,[14] in preliminary measurements, finds that hole mobilities perpendicular to the *a-b* plane increase roughly 50% at 3000 kg/cm^2 whereas a 25% increase was predicted. A similar increase in electron mobility was predicted, however essentially no change with pressure was observed.

This work was sponsored by the AF Office of Scientific Research of the Air Research and Development Command. I am indebted to Dr. Peter Fontana for helpful discussions on this problem and to Dr. LeBlanc and Dr. Kepler for their results prior to publication.

[1] R. G. Kepler, Phys. Rev. **119,** 1226 (1960).
[2] J. Halpern and L. E. Orgel, Trans. Faraday Soc. (to be published).
[3] H. Eyring, J. Walter and G. E. Kimball, *Quantum Chemistry* (John Wiley & Sons, Inc., New York, 1957).
[4] E. U. Condon and G. H. Shortley, *The Theory of Atomic Spectra,* (Cambridge University Press, New York, 1953), p. 337.
[5] B. Pullman and A. Pullman, *Les Théories Électroniques de la Chimie Organique,* (Masson et Cie, Paris, 1952), p. 198.
[6] R. W. G. Wyckoff, *Crystal Structure* (Interscience Publishers, Inc., New York, 1960) Vol. 5.
[7] C. C. J. Roothaan, J. Chem. Phys. **19,** 1445 (1951).
[8] C. Zener, Phys. Rev. **82,** 403 (1951).
[9] W. Shockley, *Electrons and Holes in Semiconductors* (D. Van Nostrand Company, Inc., New York, 1950), p. 300.
[10] O. Le Blanc, (to be published).
[11] M. Kozhin and A. I. Kitaigorodskii, Zhur. Fiz. Khim. **27,** 1676 (1953).
[12] D. W. J. Cruickshank, Revs. Modern Phys. **30,** 163 (1958).
[13] P. W. Bridgman, Proc. Am. Acad. Arts and Sci. **77,** 129 (1946).
[14] R. G. Kepler (private communication).

Theoretical Calculation of Isotropic hfs of the Free NH_2 Radical

JIRO HIGUCHI*
Research Laboratory of Resources Utilization, Tokyo Institute of Technology, Ookayama, Meguro-ku, Tokyo, Japan
(Received July 5, 1961)

ELECTRON spin resonance spectra of various radicals have been carefully investigated in solution and matrix, but the N^{14} hyperfine (hf) structure has not always been resolved in all radicals with an N^{14} nucleus. Recently, Foner *et al.*[1] have obtained the hf spectra of the free NH_2 radical stabilized in argon at liquid-helium temperature. The hf coupling constants so obtained were 23.9 gauss for H^1 and 10.3 gauss for N^{14}. It is very interesting to study the hfs theoretically not only for H^1 but for N^{14}, since the theoretical works on nitrogen hf structure have been rather scarce and this is the simplest example. Accordingly, a nonempirical calculation was carried out for the NH_2 radical.

The method adopted was quite the same as that in the previous work on the methyl radical.[2] The molecu-

lar orbitals used were SCF-LCAO-MO's obtained by the present author[3] at the NH internuclear distance of 1.01 A assuming that the structure is an isosceles triangle (C_{2v}). Electron configurations taken into account were: I, $(1a_1)^2(2a_1)^2(1b_2)^2(3a_1)^2(1b_1)$; II, $(1a_1)^2(2a_1)(1b_2)^2(3a_1)^2(1b_1)(4a_1)$; III, $(1a_1)^2(2a_1)^2(1b_2)^2(3a_1)(1b_1)(4a_1)$; and IV, $(1a_1)^2(2a_1)^2(1b_2)(3a_1)^2(1b_1)(2b_2)$. By using the first-order perturbation, the ground-state ($^2B_1$) wave function (WF) was obtained, e.g., at the bond angle $\angle HNH'$ of 105° which is the most stable configuration in the previous calculation,[3] as follows:

$$\Psi_G=\Psi_{\rm I}+0.0597\Psi_{\rm II}+0.0177\Psi_{\rm III}+0.0090\Psi_{\rm IV}, \quad (1)$$

where

$$\Psi_k=6^{-\frac{1}{2}}\mathcal{A}\phi_{-n}\phi_{-n}\cdots\phi_{i-1}\phi_{i-1}\phi_{i+1}\phi_{i+1}\cdots\phi_{-1}\phi_{-1}\phi_i\phi_i\phi_0 \times\alpha\beta\cdots\alpha\beta\alpha\beta\cdots\alpha\beta(2\alpha\alpha\beta-\alpha\beta\alpha-\beta\alpha\alpha), \quad (k=\text{II, III, IV}). \quad (2)$$

The WF's of the other types did not appear in the ground state wherein the first-order perturbation was adopted by using the restricted SCF-LCAO-MO's.[2] Thus, the hf coupling constants were calculated as shown by curves (a) and (c) in Fig. 1.

The H^1 splitting increases with increasing the bond angle because of the increase of s character in the N—H σ-bond orbitals.[4] At the bond angle of 105°, the coupling constant is obtained as −16.1 gauss and the contribution of configurations (II), (III), and (IV) are −10.3, −2.9, and −2.9 gauss, respectively. This value is fairly satisfactory as compared with the case of the methyl radical[2] ($a_{\rm calc}=-16.8$ gauss while $|a_{\rm exp}|=23\sim27$ gauss) in which only the valence-shell atomic orbitals were taken into account. Furthermore, a better result can be expected by including the extra-valence-shell orbitals as in the methyl radical ($a_{\rm calc}=-20.4$ gauss).

On the other hand, the N^{14} coupling constant was calculated as being considerably large. At the bond angle of 105°, it was obtained as +29.7 gauss, in which the contributions from configurations (II) and (III) are +41.6 and −11.9 gauss, respectively. Lack of contribution of (IV) is because of the symmetry of the b_2 orbital. The N^{14} hfs also increases with the increase of the bond angle, due to the increase of the s character in the hybridized σ orbital of nitrogen. The discrepancy from the observed value of 10.3 gauss can be explained fairly well referring to the recent works of the hfs of N^{14} atom by Das and Mukherjee[5] and Kayama.[6] For the ^4S state, they obtained $a_{\rm N}(1s)=-15.4$ gauss (D−M) and −15.0 gauss (K) in spite of the different treatments adopted, while the experimental value of whole atom is only +3.7 gauss. This shows that the effect of exchange polarization from inner shell is very large. Since the shape of inner shell is very close in both the cases, that of the N atom and the NH_2 radical, a reasonable approximation of the $1a_1$ polarization

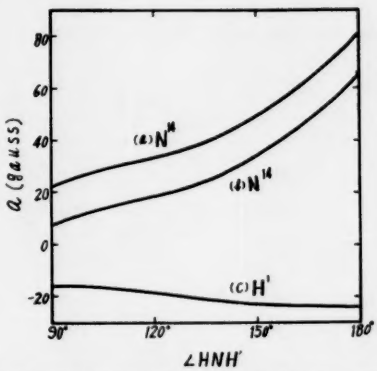

FIG. 1. Calculated hf coupling constant of the free NH_2 radical. (a) N^{14} hf coupling constant without $1a_1$ exchange polarization; (b) N^{14} hf coupling constant with $1a_1$ exchange polarization; (c) H^1 hf coupling constant.

contribution of NH_2 radical can be −15 gauss of the $1s$ polarization of N atom which is nearly independent of the bond angle. This approximation can easily be verified from the viewpoint of configuration interaction. The N^{14} hfs of NH_2 radical so obtained is qualitatively satisfactory when it is 14.7 gauss at the bond angle of 105° as shown by curve (b) in Fig. 1. In addition, further improvement is expected by including the extra-valence-shell orbitals, $3s_{\rm N}$, $3p_{\rm N}$,[6] $2p_{\rm H}$, etc., but such a calculation is not taken up here because of lack of SCF-LCAO-MO's with such orbitals.

* Present address: Bell Telephone Laboratories, Inc., Murray Hill, New Jersey.

[1] S. N. Foner, E. L. Cochran, V. A. Bowers, and C. K. Jen, Phys. Rev. Letters **1,** 91 (1958).

[2] J. Higuchi and S. Aono, J. Chem. Phys. **32,** 52 (1960).

[3] J. Higuchi, J. Chem. Phys. **24,** 535 (1956). In the present calculation, the Fermi term was calculated by using the SCF-AO's of ^4S state of nitrogen atom [D. R. Hartree and W. Hartree, Proc. Roy. Soc. (London) **A193,** 299 (1948)].

[4] J. Higuchi (unpublished work).

[5] T. P. Das and A. Mukherjee, J. Chem. Phys. **33,** 1808 (1960).

[6] K. Kayama, (unpublished work); this work includes the calculation of the hfs at the minimum electronic energy obtained by changing the orbital exponent.

Ultrasonic Absorption in Aqueous Hydrogen Peroxide Solutions*

J. P. VALLEAU† AND W. G. SCHNEIDER
Division of Pure Chemistry, National Research Council, Ottawa, Canada

(Received July 20, 1961)

THE absorption of sound in hydrogen-bonded solutions is not yet thoroughly understood.[1–3] With this in mind, we have measured the absorption and velocity of high-frequency ultrasonic waves in solutions of hydrogen peroxide and water, using a "pulse" method to be described elsewhere. The stronger solutions were prepared by diluting Becco concentrated peroxide solu-

TABLE I. Absorption α and velocity c of hydrogen peroxide solutions at 20.0(±0.2)°C.

Wt. % H_2O_2	Frequency ν (Mc/sec)	$10^{-5}c$ (cm/sec)	$10^{17}\alpha/\nu^2$ (sec²/cm)	% Average derivation in α/ν^2	Viscosity η (cp)	Viscous absorption $10^{17}\alpha_\eta/\nu^2$	α/α_η
0	89.6	1.48	25.0	2	1.01	8.06	3.1
15.7	89.9	1.53	21.7	1.5	1.03	7.23	3.0
30.9	89.8	1.57	19.0	1	1.08	6.54	2.9
45.5	89.9	1.63	16.0	1.5	1.15	6.04	2.6_5
60.6	64.5	...	14.7	2	1.22	5.56	2.6
60.6	89.9	1.67_5	14.3	2	1.22	5.56	2.6
77.5	64.5	...	12.6	4.5	1.26	4.90	2.6
77.5	89.7	1.72	12.0	3	1.26	4.90	2.4_5
95.3	89.5	1.78	10.5	1.5	1.26	4.11	2.5_5

tion with twice-distilled water; for the more dilute solutions Baker and Adamson 30% peroxide solution was used. The concentrations of the solutions were measured by comparing their refractive indexes with those determined by Giguère and Geoffrion.[4] To minimize the decomposition of the peroxide, the apparatus was cleaned with hot fuming sulphuric acid.[5] Table I gives the results at 20°C; Fig. 1 shows in addition some results on dilute solutions at lower temperatures and at frequencies of either 65 or 90 Mc/sec. There is no evidence of relaxation at these frequencies.

The shape of the curve of absorption against concentration is perhaps surprising, since pronounced peaks are found in such curves for many hydrogen-bonded solutions, and are ascribed to relaxations in the liquid structure. In particular this "anomalous absorption" is exhibited by aqueous solutions of almost all ketones and alcohols, where one would expect to find structural processes similar to those of hydrogen peroxide solutions. A good deal of thermodynamic data is of course available on these solutions,[6] but we have no model detailed enough to explain the difference in acoustic behavior. (The heights of such peaks are decreasing functions of temperature, and in the case of methanol-water solutions it was necessary to go below room temperatures to display a peak[7]; the low temperature results for the present case do not suggest such behavior, however.)

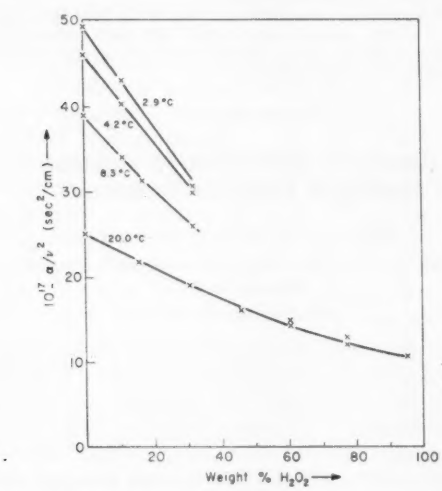

FIG. 1. Sound absorption in hydrogen peroxide-water solutions.

The classical viscous sound absorption, due to Stokes, is given by

$$\alpha_\eta = 8\pi^2\eta/3\rho c^3,$$

where η and ρ are the shear viscosity and density of the fluid. It has often been remarked that for hydrogen-bonded liquids, *except* in the region of the anomalous absorption, the ratio α/α_η behaves in a surprisingly regular way: the value of the ratio is never far from the range 1.5 to 3, and is very closely independent of temperature. In the table may be found values of this ratio, calculated for our peroxide solution with the help of published data on the viscosity[8] and density.[5] They take appropriate values, and lie on a smooth nearly flat curve, over the whole range of concentration, emphasizing the absence of the expected "anomaly."

* N.R.C. Contribution No. 6595.

† N.R.C. Postdoctorate Fellow, 1958–1960. Present address: Chemistry Department, University of Toronto, Toronto, Ontario.

[1] D. Sette, Nuovo Cimento **1**, 800 (1955).

[2] K. F. Herzfeld and T. A. Litovitz, *The Absorption and Dispersion of Ultrasonic Waves* (Academic Press Inc., New York, 1959), p. 509.

[3] R. N. Barfield and W. G. Schneider, J. Chem. Phys. **31**, 488 (1959).

[4] P. A. Giguère and P. Geoffrion, Can. J. Research **B27**, 168 (1949).

[5] C. E. Huckaba and F. G. Keyes, J. Am. Chem. Soc. **70**, 2578 (1948).

[6] A. G. Mitchell and W. F. K. Wynne-Jones [Discussions Faraday Soc. **15**, 161 (1953)] have compared the solution thermodynamics of H_2O—EtOH and H_2O—H_2O_2. While the heats of solution are rather similar, the volume of solution and the negative excess entropy are both considerably smaller in the peroxide case.

[7] D. Sette, Nuovo cimento **1**, 800 (1955).

[8] M. K. Phibbs and P. A. Giguère, Can. J. Chem. **29**, 173 (1951).

Announcement

BEGINNING in January, 1962, *The Journal of Chemical Physics* will be published semimonthly, on the first and fifteenth of each month. There will be two volumes per year, each consisting of twelve issues. Author and subject indexes will appear in the issues of June 15 and December 15.

Also beginning with the January 1, 1962 issue, the publication charge for articles and Letters to the Editor will be increased to $40.00 per page with a minimum of $40.00. The publication charge is requested of the institution supporting the research and not of the author, and its payment has never been made a requirement for the prompt publication of any research article or Letter to the Editor. One hundred reprints without covers are, however, provided at no extra charge to institutions supporting the publication charge program.

Printed below is a revised announcement concerning Letters to the Editor in *The Journal of Chemical Physics*.

LETTERS TO THE EDITOR

The Letters to the Editor section is subdivided into three parts entitled Communications, Comments and Errata, and Notes. These three sections are all subject to the same limitations on length. The textual material of each Letter is limited to 950 words minus the following: (a) 200 words for each average-sized figure; (b) 50 words for each displayed equation; (c) 7 words for each line of table including headings and horizontal rulings. No proof will be sent to the authors of Communications. Proof will be sent to the authors of Comments, Errata, and Notes.

Communications. Letters in this category are restricted to reports of preliminary results which are of current and extreme interest to relatively large numbers of workers in the field. It is assumed that in most cases the details of such work, in a completed form, will be published at a later date. Communications are not sent for review, although the Editor will in many cases submit them to readily available experts in order to ascertain their suitability for this section. The Editorial Board will not hold itself responsible for opinions expressed by the correspondents. Communications accepted for publication by the 1st of month M will be published in the issue of the 1st of month M+2 and those accepted by the 15th of month M will appear in the issue of the 15th of month M+2.

Comments and Errata. Letters in this category include the usual errata and also comments by authors or others on previously published work. Comments by others than the authors of the already published work being discussed in such Letters normally will be submitted to the authors for review. The authors' adverse criticism will not be taken as adequate reason for rejection. Usually the authors will be given the opportunity of submitting a rebuttal to be printed immediately following these comments. In all such cases the publication of both the comments and the rebuttal will be delayed until such time as each party has had an opportunity to examine the final statement of the other on the matters under discussion. The two Letters will then be published simultaneously. In cases where it seems desirable, the Editor will recommend that a single joint comment by the two parties concerned be published in this section. The Editorial Board will not hold itself responsible for opinions expressed by the correspondents.

Notes. Letters in this category have the character of short articles except that, because of the limitation on length, they do not contain an abstract. Notes will be reviewed in the same manner as are articles, and reviewers will be asked to judge them by the same standards as employed for regular articles, except for those differences required by the brevity of Notes. Notes are intended as final publication of the work described in them and not as preliminary reports. It is assumed that work reported in a Note will not be republished in extended form at a later date although, of course, further work may result in a longer article. A Note accepted by the 1st (15th) of the month M will be published in the issue of the 1st (15th) of month M+3. A backlog of regular articles will not be allowed to delay the publication schedule of Notes.

J. W. STOUT, *Editor*

Author Index to Volume 35

References with (L) are to Letters to the Editor

Ablow, Clarence M. (see Wise, Henry)—10
Agrawal, J. P. (see Saxena, S. C.)—2107
Alger, R. S., T. H. Anderson, and L. A. Webb. Trapped radicals in irradiated *n*-propanol at 77°K—49
Allen, Thomas L. and Harrison Shull. Chemical bond in molecular quantum mechanics—1644
Allerhand, A. (see Kuntz, I. D., Jr.)—1533(L)
Amdur, I., M. S. Longmire, and E. A. Mason. Scattering of high-velocity neutral particles. XII. He—CH_4; He—CF_4. CH_4—CH_4 and CF_4—CF_4 interactions—895
Anderson, David H. Quadrupole coupling in lithium nitrate—1353
Anderson, George R. (see Person, Willis B.)—908
Anderson, John H. (see Weil, John A.)—1410
Anderson, M. E., R. S. Rhodes, and G. E. Pake. Proton resonance shifts and electron susceptibilities in 1,3-bisdiphenylene 2-phenyl allyl—1527(L)
Anderson, Roy S. (see Jaseja, Thadho S.)—2192
Anderson, T. H. (see Alger, R. S.)—49
Andresen, Harro G. Hyperfine structure and *g*-tensor anisotropy of the paramagnetic resonances of manganese in TiO_2—1090
Andrews, Frank C. On the classical Boltzmann equation for gases—922
Appel, K. (see Ritter, Z. W.)—571
Aranow, R. H. and L. Witten. Further comments on the derivation of Traube's rule—1504(L)
Armstrong, J., N. Bloembergen, and D. Gill. Linear effect of electric field on the Cl^{35} quadrupole interaction in paradichlorobenzene—1132(L)
Aronson, J. R. (see Robinson, D. W.)—2245(L)
Aronson, S. and J. C. Clayton. Thermodynamic properties of nonstoichiometric urania-zirconia solid solutions—1055
——, **J. E. Rulli, and B. E. Schaner.** Electrical properties of nonstoichiometric uranium dioxide—1382
Atoji, Masao. Neutron diffraction studies of CaC_2, YC_2, LaC_2, CeC_2, TbC_2, YbC_2, LuC_2, and UC_2—1950
—— **and Donald E. Williams.** Neutron-diffraction studies of La_2C_3, Ce_2C_3, Pr_2C_3, and Tb_2C_3—1960
Avinor, M., A. Carmi, and Z. Weinberger. Nickel-activated calcium and strontium sulfide phosphors—1978
Azároff, Leonid V. (see Mohanty, Ganesh P.)—1268

Baba, Hiroaki and Satoshi Suzuki. Electronic spectra and hydrogen bonding. I. Phenol and naphthols—1118
—— **and Satoshi Suzuki.** Electronic spectra of substituted anthracenes. Evidences for appearance of the ^1L_b transition—1501(L)
Baird, J. C. and J. R. Thomas. Electron paramagnetic resonance spectra of some disubstituted nitric oxides—1507(L)
Balchan, A. S. and H. G. Drickamer. Effect of pressure on the charge transfer spectra of heavy transition metal hexahalide complexes—356
—— **and H. G. Drickamer.** Effect of pressure and temperature on the absorption spectra of four alkali halide phosphors—359
Baldeschwieler, John D. (see Rigden, John S.)—1532(L)
Banyard, K. E. Erratum: "Floating" hydrogen densities in some molecules of the type XH_n—1505(L)
Bar-Eli, Kedma and Fritz S. Klein. A kinetic method for measuring solubilities of gases in liquids—1915(L)
Bartell, L. S., Kozo Kuchitsu, and R. J. deNeui. Mean and equilibrium molecular structures of methane and deuteromethane as determined by electron diffraction—1211
—— (see Kuchitsu, Kozo)—1945
Barua, A. K. (see Srivastava, B. N.)—329, 649
Basila, Michael R. Hydrogen bonding interaction between adsorbate molecules and surface hydroxyl groups on silica—1151
—— **and George F. Crable.** Variation of the intensity of the methyl symmetrical bending vibration in paraffins—306
Baun, William L. and David W. Fischer. Association of carbon atoms from graphite in a radio-frequency spark—1518(L)
Becker, Ralph S. (see Scott, Donald R.)—516, 2246(E)
Begun, G. M. and L. Landau. Mass spectra and metastable transitions in isotopic nitrous oxides—547
Belford, Geneva G., Robert A. Bernheim, and H. S. Gutowsky. Charge distribution and electric field gradients in ionic crystals—1032
Ben-Reuven, A., S. Kimel, M. A. Hirshfeld, and J. H. Jaffe. Theory and measurement of pressure-induced shifts of HCl lines due to noble gases—955
Benson, G. C. Recalculation of the surface energies of alkali halide crystals—2113
Berlad, A. L. Flame propagation in free-radical-containing solids at low temperatures—1180
Bernheim, Robert A. (see Belford, Geneva G.)—1032
Berns, Donald S., Gerard Lepoutre, Elizabeth A. Bockelman, and Andrew Patterson, Jr. Salt effect in metal-ammonia solutions: sodium chloride in sodium-ammonia solution at −33°C—1820
Berry, R. Stephen. Remarks on the electronic spectra and structures of compounds of chromium and benzene—29
—— Ultraviolet spectrum of dibenzene chromium vapor—2025
—— Zero-point vibrations in benzene—2253(L)
——, **Curt W. Reimann, and G. Neil Spokes.** Absorption spectrum of gaseous Cl^- and electron affinity of chlorine—2237(L)
Bersohn, R. and I. Isenberg. Metallic nature of the starch-iodine complex—1640
Bhatnagar, Hari L. Light scattering by anisotropic inhomogeneities in thin polymer films under strain. II—999
Bigeleisen, Jacob. Erratum: Statistical mechanics of isotope effects on the thermodynamic properties of condensed systems—2246(L)
—— **and Slobodan V. Ribnikar.** Structural effects in the vapor pressures of isotopic molecules. O^{18} and N^{15} substitution in N_2O—1297
—— **and Etienne Roth.** Vapor pressures of the neon isotopes—68
Birchenall, C. Ernest (see Rosenblatt, Gerd M.)—788
Blanc, Joseph (see Brecher, Charles)—1097
Blinç, R., M. Brenman, and J. S. Waugh. Proton magnetic resonance study of ferroelectric potassium ferrocyanide trihydrate—1770
—— **and M. Pintar.** Proton magnetic resonance study of ferroelectric $NaH_3(SeO_3)_2$ and $LiH_3(SeO_3)_2$—1140(L)
Blinder, S. M. Dipole moment of HD. II—974
Bloembergen, N. Theory of the variation of the nuclear quadrupole interaction in covalent bonds with applied electric field—1131(L)
—— (see Armstrong, J.)—1132(L)
Blomgren, G. E. and J. Kommandeur. Organic semiconductors: aromatic hydrocarbon positive ions in solids—1636

Bobka, R. J. (see Pace, E. L.)—454
Bockelman, Elizabeth A. (see Berns, Donald S.)—1820
Boerboom, A. J. H. (see Fluit, J. M.)—1143(L)
Boggs, James E. and A. P. Deam. Nonresonant dielectric dispersion in asymmetric rotors—1178
Booman, K. A. (see Piette, L. H.)—1481
Bouman, Nicolaas. Calculations of the lower excited energy levels of the cyclic polyenes, radicals, and ions—1661
Bovenkerk, H. P. (see Bundy, F. P.)—383
Boyd, Richard H. Extension of Stokes' law for ionic motion to include the effect of dielectric relaxation—1281
Bradley, J. N. Mechanism of disproportionation in alkyl radical reactions—748(L)
—— **and G. B. Kistiakowsky.** Shock wave studies by mass spectrometry. I. Thermal decomposition of nitrous oxide—256
—— **and G. B. Kistiakowsky.** Shock wave studies by mass spectrometry. II. Polymerization and oxidation of acetylene—264
Brady, George W. and H. L. Frisch. Some further observations on the critical region—2234(L)
Bray, P. J., J. O. Edwards, J. G. O'Keefe, V. F. Ross, and I. Tatsuzaki. Nuclear magnetic resonance studies of B^{11} in crystalline borates—435
Brecher, Charles and Ralph S. Halford. Motions of molecules in condensed systems. XI. Infrared spectrum and structure of a single crystal of ethylene—1109
——, **Esther Krikorian, Joseph Blanc, and Ralph S. Halford.** Motions of molecules in condensed systems. X. The infrared spectrum and structure of a single crystal of cyclopropane—1097
Breene, R. G., Jr. Deionization cross section for oxygen—625
Breig, Edward L. (see Kojima, Takeshi)—2139
Brenman, M. (see Blinc, R.)—1770
Bretton, Randolph H. (see Carberry, James J.)—2241(L)
Brinen, J. S. and Lionel Goodman. Low-resolution analysis of the $n \rightarrow \pi^*$ (3000 A) absorption spectrum of *s*-triazine—1219
Brock, E. G., P. Csavinszky, E. Hormats, H. C. Nedderman, D. Stirpe, and F. Unterleitner. Coherent stimulated emission from organic molecular crystals—759(L)
Brody, J. K. (see Rao, P. Ramakoteswara)—776
Broida, H. P. (see Tanaka, I.)—750(L)
Brokaw, Richard S. "Thermal conductivity" and chemical kinetics—1569
Brown, Robert J. S. (see Thompson, Don D.)—1894(L)
Brown, Thomas H. (see Schug, John C.)—1873
Broyles, A. A. Solutions to the Percus-Yevick equation—493
Bryant, C. A. and P. H. Keesom. Low temperature specific heat of molybdenum—1149(L)
Bulewicz, E. M. and P. J. Padley. Asymmetry of cyclotron resonance lines in the reaction zones of low-pressure acetylene and cyanogen flames—1590
Bull, W. E. (see Palko, A. A.)—103
Bundy, F. P., H. P. Bovenkerk, H. M. Strong, and R. H. Wentorf, Jr. Diamond-graphite equilibrium line from growth and graphitization of diamond—383
Burnelle, Louis. SCF LCAO study of linear and bent acetylene—311
Burns, R. P. (see Grimley, R. T.)—551
Burton, M. (see Nosworthy, J. M.)—1506(L)
Butcher, Samuel (see Cahill, Patrick)—2255(L)
Butler, James N. Distribution of space charge in homogeneous metal oxide films—636

Cahill, Patrick and Samuel Butcher. Microwave spectrum and barrier to internal rotation of methyl stannane—2255(L)
Caldwell, P. (see Lippincott, E. R.)—123
Califano, Salvatore (see Wu, Ellen L.)—2060
Camiscoli, James F. (see Rosenberg, Barnett)—982
Canon, Jack R. and George H. Duffey. Cuboctahedral bonding—1657
Carberry, James J. and Randolph H. Bretton. Determination of molecular diffusivity by gas chromatography techniques—2241(L)
Carlin, Richard L. (see Piper, T. S.)—1809
Carlson, F. F. (see King, G. J.)—1442
Carlson, H. Gary (see Westrum, Edgar F., Jr.)—1670
Carmi, A. (see Avinor, M.)—1978
Carrington, Tucker. Transition probabilities in multilevel systems: calculation from impulsive and steady-state experiments—807
—— (see Tanaka, I.)—750(L)
Carroll, P. K. and A. C. Hurley. Identification of an electronic transition of N_2^{2+}—2247(L)
Carter, R. E. Addendum: Kinetic model for solid-state reactions—1137(L)
Case, Charles T. (see Strehlow, Roger A.)—1506(L)
Cashion, J. K. and J. C. Polanyi. Infrared chemiluminescence in the system H+NOCl—600
Castagnoli, G. Cini. Diffusion of Kr and He in liquid hydrogen—1999
Castellano, S. (see Waugh, J. S.)—1900(L)
Cater, E. David, Paul W. Gilles, and R. J. Thorn. Uranium monosulfide. I. Vaporization, thermodynamics, and phase behavior—608
——, **E. G. Rauh, and R. J. Thorn.** Uranium Monosulfide. II. Mass spectrometric study of its vaporization—619
Chakravorty, Animesh (see Gangopadhayay, Arun Kumar)—2206
Chang, Elfreda (see Grønvold, Fredrik)—1665
Chantry, George W. and Robert A. Plane. Nature of the metal-ligand bond in some complex cyanides from a study of Raman intensities—1027
Charette, J. J. Infrared spectra of synthetic diamond—1906(L)
Chaudhri, M. M. (see Katti, P. K.)—756(L)
Chesnut, D. B. and W. D. Phillips. EPR studies of spin correlation in some ion radical salts—1002
—— **and G. J. Sloan.** Paramagnetic resonance absorption of the dimesitylmethyl radical—443
Christensen, Daniel (see Lide, David R., Jr.)—1374
Chupka, William A. and Manfred Kaminsky. Energy distribution and fragmentation processes resulting from electron impact on propane and *n*-butane—1991
Clarke, R. B. (see Kleppa, O. J.)—175
Claxton, T. A., D. P. Craig, and T. Thirunamachandran. Crystal splitting of the anthracene 3800 A system—1525(L)
Clayton, J. C. (see Aronson, S.)—1055
Clifton, David G. Calculations of the coefficient of viscosity and the coefficients of diffusion for dissociating hydrogen—1417
Coggeshall, Norman D. (see Schug, John C.)—1146(L)
Coker, E. Howard, J. C. Decius, and A. B. Scott. Stretching vibration of sulfate ion in potassium chloride: formation of $M^{++}SO_4^{=}$ pairs—745(L)
Colburn, Charles B. (see Kennedy, Al)—1892
—— (see Piette, L. H.)—1481
Cole, Terry, Paramagnetic defects in irradiated NH_4ClO_4—1169
Companion, Audrey L. and Robert G. Parr. Remark on the Mulliken approximation for two-center electron distributions—2268(L)
Conlon, D. C. and W. P. Doyle. Absorption spectra of vanadium, niobium, and tantalum pentoxides—752(L)
Costain, C. C. and G. P. Srivastava. Study of hydrogen bonding. Microwave rotation spectrum of CF_3COOH—HCOOH—1903(L)
Cotton, F. A. Relative bond strengths in trigonal bipyramid molecules—228
Coulson, C. A. and Max T. Rogers. Homopolar dipole—593
—— **and L. J. Schaad.** On the approximation of zero differential overlap—294

Courtney, Welby G. Remarks on homogeneous nucleation—2249(L)
Crable, George F. (see Basila, Michael R.)—306
Craig, D. P. (see Claxton, T. A.)—1525(L)
Craig, R. S. (see Saba, W. G.)—2148
Cramer, W. H. Elastic and inelastic scattering of low-velocity H^+ and H_2^+ in hydrogen—836
Crawford, Bryce, Jr. (see Wu, Ellen L.)—2060
Cross, Paul C. (see Spencer, Glenn H., Jr.)—1925, 1939
Cross, R. J., Jr., and R. Wolfgang. Billiard-ball collisions in the reactions of hot hydrogen atoms. Isotope effect on hydrogen displacement in methane—2002
Crosswhite, H. M. and G. H. Dieke. Spectrum and magnetic properties of hexagonal $DyCl_3$—1535
Crozier, M. H. and W. A. Runciman. Analysis of the spectra of trivalent promethium and holmium—1392
Csavinszky, P. (see Brock, E. G.)—759(L)
Curl, R. F., Jr., and James L. Kinsey. Calculation of interaction matrix elements for asymmetric rotors with resultant electronic spin and nuclear spin—1758
Curran, R. K. Negative ion formation in ozone—1849
Current, J. H. (see Rabinovitch, B. S.)—2250(L)
Cvetanović, R. J., W. E. Falconer, and K. R. Jennings. Mechanism of the mercury photosensitized decomposition of *n*-butane—1225
—— (see Jennings, K. R.)—1233
Czanderna, A. W. (see Wieder, Harold)—2259(L)

Dahler, John S. (see Sather, Norman F.)—2029
Dalgarno, A. Perturbation theory calculations—1898(L)
—— **and J. M. McNamee.** Calculation of polarizabilities and shielding factors—1517(L)
Danielson, G. C. (see Ellerbeck, L. D.)—298
Das, M. R. and B. Venkataraman. C^{13}-hfs in the ESR spectrum of *p*-benzosemiquinone-1-C^{13} ion—2262(L)
Das, T. P. Erratum: Tunneling through high periodic barriers. II. Application to nuclear magnetic resonance on solids—1897(L)
Datz, Sheldon, Dudley R. Herschbach, and Ellison H. Taylor. Collision mechanics in crossed Maxwellian molecular beams—1549
Davidson, Ernest R. First excited $^1\Sigma_g^+$ state of the hydrogen molecule—1189
Davis, H. T., Stuart A. Rice, and J. V. Sengers. On the kinetic theory of dense fluids. IX. The fluid of rigid spheres with a square-well attraction—2210
Deam, A. P. (see Boggs, James E.)—1178
Deb, S. K. Ultraviolet absorption spectra of alkali metal azides—2122
deBergevin, F. (see Muldawer, L.)—1904(L)
Decius, J. C. (see Coker, E. Howard)—745(L)
—— (see Kalman, Otto F.)—1919
DeLap, James H. (see Poirier, Jacques C.)—213
Del Greco, F. P. (see Kaufman, F.)—1895(L)
deNeui, R. J. (see Bartell, L. S.)—1211
de Waard, C. (see Henning, J. C. M.)—2258(L)
Dibeler, Vernon H. (see Herron, John T.)—747(L)
DiCianni, Nicholas (see Pierce, Louis)—2240(L)
Dickens, P. G. and D. Schofield. Multiple vibrational relaxation in gaseous dibromomethane—374(L)
Dieke, G. H. and Shobha Singh. Absorption and fluorescence spectra with magnetic properties of $ErCl_3$—555
—— (see Crosswhite, H. M.)—1535
Dietz, R. E. and P. W. Selwood. Effect of chemisorbed hydrogen on the magnetization of nickel—270
DiMarzio, Edmund A. Statistics of orientation effects in linear polymer molecules—658
Dixon, William B. and E. Bright Wilson, Jr. Microwave spectrum of methyl nitrate—191
Dodd, Jack G. Kinetics of the photolysis of sodium azide—1815
Dodge, Richard P., David H. Templeton, and Allan Zalkin. Crystal structure of vanadyl bisacetylacetonate. Geometry of vanadium in fivefold coordination—55
Dodgen, Harold W. (see Hunt, John P.)—2261(L)
Dohner, Abraham S. and David J. Wilson. Photochemical decomposition of nitryl chloride—1510(L)
Donath, Wilm E. Atomic wave functions for the ground states of Na^+, Ne, and F^-—817
Donovan, J. W. and A. B. F. Duncan. Mean lifetime of the lowest excited singlet state of benzene—1389
Dorfman, Leon M. (see Sauer, Myran C., Jr.)—497
Dorman, F. H. and J. D. Morrison. Double and triple ionization in molecules induced by electron impact—575
Douglas, A. E. (see Milton, Earl R. V.)—1202
Douglass, Dean C. Self-diffusion and velocity correlation—81
Douslin, D. R., R. H. Harrison, R. T. Moore, and J. P. McCullough. Tetrafluoromethane: *P-V-T* and intermolecular potential energy relations—1357
Dows, David A. Intermolecular coupling of vibrations in molecular crystals. II. Intermolecular forces in CH_3Cl and CD_3Cl—282
Doyle, George J. Self-nucleation in the sulfuric acid-water system—795
Doyle, W. P. (see Conlon, D. C.)—752(L)
Dresner, J. Quenching effects and negative photoconductivity in amorphous selenium—1628
Dressler, K. Ultraviolet absorption spectrum of ammonia in solid argon at 4.2°K—165
Drickamer, H. G. (see Balchan, A. S.)—356, 359
—— (see Gregg, D. W.)—1780
—— (see Minomura, S.)—903
—— (see Riggleman, B. M.)—1343
—— (see Stephens, D. R.)—424, 427, 429
—— (see Zahner, J. C.)—375(L), 1483
Drury, J. S. (see Palko, A. A.)—103
Duffey, George H. (see Canon, Jack R.)—1657
—— (see Wilson, Russell L.)—568
Duncan, A. B. F. (see Donovan, J. W.)—1389
Dunford, H. B. (see Milton, Earl R. V.)—1202
Durig, J. R. (see Robinson, D. W.)—2245(L)
Dye, J. L. (see Potter, R. L.)—1907(L)

Edelstein, A. S. and M. Mandel. Antiferromagnetic to ferromagnetic transitions in organic free radicals—1130(L)
Edwards, J. O. (see Bray, P. J.)—435
Edwards, J. W. (see Johns, I. B.)—1271
Eggers, D. F., Jr., H. E. Wright, and D. W. Robinson. Infrared spectrum of CF_3SF_5—1045
Ehrlich, Gert. Adsorption and electrical conduction in thin films—2165
—— **and F. G. Hudda.** Low-temperature chemisorption. III. Studies in the field emission microscope—1421
Eisenstein, J. C. Analysis of the absorption spectrum of $YbCl_3 \cdot 6H_2O$—2097
—— Erratum: Magnetic properties and optical absorption spectrum of K_2ReCl_6—2246(L)
El-Bayoumi, M. Ashraf (see Ramsey, B.)—1502(L)
Eliezer, I. (see Hayman, H. J. G.)—644
Ellerbeck, L. D., H. R. Shanks, P. H. Sidles, and G. C. Danielson. Electrical resistivity of cubic sodium tungsten bronze—298
Elliott, Norman. Paramagnetism of tetraphenanthroline dihydroxyl diferric chloride—1273
El-Sayed, Mostafa and G. Wilse Robinson. Comments on a Communication by El-Sayed and Robinson—1896(L)
Emerson, Merle T. (see Jumper, Charles F.)—1911(L)
Epstein, L. M. (see Wallace, W. E.)—2238(L)
Evans, R. B., III, G. M. Watson, and E. A. Mason. Gaseous diffusion in porous media at uniform pressure—2076
Ewing, George E. and George C. Pimentel. Infrared spectrum of solid carbon monoxide—925

Falconer, W. E. (see Cvetanović, R. J.)—1225
Feil, D. and G. A. Jeffrey. Polyhedral clathrate hydrates, Part 2. Structure of the hydrate of tetra *iso*-amyl ammonium fluoride—1863
Fender, B. E. F. Potential parameters of krypton—2243(L)
Fenimore, C. P. Comment on the Paper "Thermal decomposition of nitrous oxide"—2243(L)
Ferguson, J. Crystal spectra of metal coordination compounds. VI. Bis-salicylaldiminato-copper (II) and Bis-*N*-methylsalicylaldiminato-copper (II)—1612
——, **K. Knox, and D. L. Wood.** Effect of next nearest neighbor ions on the crystal field splitting of transition metal ions in crystals—2236(L)
Ferreira, Ricardo. Permanent dipole moments of saturated hydrocarbons—755(L)
Fischer, David W. (see Baun, William L.)—1518(L)
Fitts, Donald D. Rate of cooling in a magnetic field—1519(L)
Fixman, Marshall. General theory of polymer solutions—889
—— Theory of proton magnetic shielding—679
Fluit, J. M., L. Friedman, A. J. H. Boerboom, and J. Kistemaker. Isotopic fractionation of lithium in sputtering—1143(L)
Fordemwalt, James N. (see Person, Willis B.)—908
Forneris, Roberto (see Person, Willis B.)—908
Forstat, H. and D. R. McNeely. Heat capacity of $LiCuCl_3 \cdot 2H_2O$—1594
Fox, R. E. Ionization cross sections near threshold by electron impact—1379
Fraenkel, George K. (see Karplus, Martin)—1312
—— (see Strauss, Herbert L.)—1738
Fraga, Serafin and B. J. Ransil. Studies in molecular structure. V. Computed spectroscopic constants for selected diatomic molecules of the first row—669
—— **and Bernard J. Ransil.** Studies in molecular structure. VI. Potential curve for the interaction of two hydrogen atoms in the LCAO MO SCF approximation—1967
Frank, R. C., D. E. Swets, and R. W. Lee. Diffusion of neon isotopes in fused quartz—1451
Freeman, David H. Thermodynamics of binary ion-exchange systems—189
Freeman, Donald C., Jr., and Dennis N. Stamires. Electrical conductivity of synthetic crystalline zeolites—799
Friedman, A. S. (see Oppenheim, I.)—35
Friedman, L. (see Fluit, J. M.)—1143(L)
Frisch, H. L. (see Brady, George W.)—2234(L)
Frost, A. A., R. E. Kellogg, B. M. Gimarc, and J. D. Scargle. Least-squares local-energy method for molecular energy calculations using Gauss quadrature points—827
Fulton, Robert L. and Martin Gouterman. Vibronic coupling. I. Mathematical treatment for two electronic states—1059
Futrell, Jean H. Use of mass spectral data in radiation chemistry—353

Gangopadhayay, Arun Kumar and Animesh Chakravorty. Charge transfer spectra of some gold (III) complexes—2206
Gardiner, W. C., Jr. Observations of induction times in the acetylene-oxygen reaction—2252(L)
——, **and G. B. Kistiakowsky.** Thermal dissociation rate of hydrogen—1765
Gatz, C., F. T. Smith, and H. Wise. Chemionization in three-body gas phase reactions—1500(L)
Geller, S., H. J. Williams, and R. C. Sherwood. Substitution of Fe^{3+} ion in Sc_2O_3 and In_2O_3—1908(L)
Giddings, J. Calvin and Spencer L. Seager. Rapid diffusional analysis by chromatographic methods—2242(L)
Giese, Clayton F. and William B. Maier, II. Ion-molecule reactions studied with mass analysis of primary ion beam—1913(L)
Gill, D. (see Armstrong, J.)—1132(L)
Gilles, Paul W. (see Cater, E. David)—608
Gimarc, B. M. (see Frost, A. A.)—827
Ginell, Robert. Erratum: Development of the liquid equation and the partial structure of water—1135(L)
—— Meaning of the Tait coefficients and the structure of liquids—1776
—— Tait coefficients and λ transition of helium I and II—473
Giuliano, Concetto R. (see McConnell, Harden M.)—1910(L)
Gold, Albert. Construction of orthogonalized LCAO wave functions for the *F* center from ENDOR data—2180
Goldstein, J. H. (see Hobgood, R. T.)—2038
—— (see Reddy, G. S.)—380(L)
Goodman, Lionel (see Brinen, J. S.)—1219
Goodrich, F. C. Molecular weight distribution and reaction sequence in polymerization kinetics—2101
Gordon, John S. Thermodynamic functions for eighteen elements taken as ideal monatomic gases—2252(L)
Gordon, Sanford (see McBride, Bonnie J.)—2198
Gordy, Walter (see Katayama, Mikio)—117
—— (see Rao, D. V. G. L. Narasimha)—362, 764(L)
Gouterman, Martin (see Fulton, Robert L.)—1059
Graven, Wendell M. Absorption spectra of anodic tantalum oxide films—1526(L)
Green, Mino and Ruth Seiwatz. Interaction of rare gases with semiconductor surfaces—915
Greenberg, Jacob and L. J. Hallgren. Infrared spectra of NaOH above and below the melting point—180
Gregg, D. W. and H. G. Drickamer. Effect of pressure on the optical properties of organic phosphors—1780
Griffith, J. S. Group theory and aromatic molecules—1901(L)
—— **and L. E. Orgel.** Erratum: Pairing energies in the actinide series—748(L)
Grimley, R. T., R. P. Burns, and Mark G. Inghram. Thermodynamics of the vaporization of nickel oxide—551
Grønvold, Fredrik, Torkild Thurmann-Moe, Edgar F. Westrum, Jr., and Elfreda Chang. Low-temperature heat capacities and thermodynamic functions of some platinum and palladium group chalcogenides. I. Monochalcogenides; PtS, PtTe, and PdTe—1665
—— (see Westrum, Edgar F., Jr.)—1670
Gruber, John B. Analysis of the infrared absorption spectrum of Am^{3+} ($5f^6$) in $LaCl_3$—2186
Gunton, Robert C. and Edward C. Y. Inn. Rates of electron removal by recombination, attachment, and ambipolar diffusion in nitric oxide plasmas—1896(L)
Gutowsky, H. S. and A. L. Porte. Electron coupling of proton spins in heterocyclic molecules. *N*-benzylthieno[3,2-*b*]pyrrole—839
—— (see Belford, Geneva G.)—1032
Guzzo, A. V. (see Helmholz, Lindsay)—1349

Hacker, D. S., S. A. Marshall, and M. Steinberg. Recombination of atomic oxygen on surfaces—1788
Halford, Ralph S. (see Brecher, Charles)—1097, 1109
Hallgren, L. J. (see Greenberg, Jacob)—180
Ham, Joe S. (see Herren, Cecil LeRoy)—1479
Hamrin, Charles E., Jr., and George Thodos. Vapor pressures of the inert gases—899
Hanafy, Z. (see Mikhail, H.)—1185
Harmony, Marlin D., Rollie J. Myers, L. J. Schoen, David R. Lide, Jr., and D. E. Mann. Infrared spectrum and structure of the NF_2 radical—1129(L)
Harris, P. M. (see Reed, John W.)—1730
Harrison, R. H. (see Douslin, D. R.)—1357
Hatcher, C. R. Positronium formation in the halogen derivatives of benzene—2266(L)
Havens, W. W., Jr. (see Rush, J. J.)—2265(L)

Hawksworth, W. A. A shorter method of calculating Lennard-Jones (12–6) potential parameters from gas viscosity data—1534(L)
Hayashi, Michiro and Louis Pierce. Tables for the internal rotation problem—1148(L)
—— (see Pierce, Louis)—479
Hayes, W. and J. W. Twidell. Paramagnetic resonance of x-irradiated CaF_2:Tm and of CaF_2:Yb—1521(L)
Hayman, H. J. G. and I. Eliezer. Dipole moments of α,ω-dibromoparaffins and their temperature dependence—644
Heller, Adam. Structural requirements of organic liquid scintillators—1980
—— **and Dov Katz.** Scintillation properties of 9-vinylanthracene—1987
Heller, Carl A. Reactions of methyl with isopropyl radicals—1711
Helmholz, Lindsay, A. V. Guzzo, and R. N. Sanders. Paramagnetic resonance spectra of chromium III and manganese IV hexafluoride ions: CrF_6^{3-} and MnF_6^{2-}—1349
Heltemes, E. C. and C. A. Swenson. Nuclear contribution to the heat capacity of terbium metal—1264
Henning, J. C. M. and C. de Waard. Spin densities in aromatics containing nitrogen: ESR spectrum of the pyrazine negative ion—2258(L)
Herren, Cecil LeRoy and Joe S. Ham. Thermal diffusion coefficient of polystyrene in toluene—1479
Herron, John T. Rate of the reaction NO+N—1138(L)
—— **and Vernon H. Dibeler.** Mass spectrometric study of the thermal dissociation of N_2F_4—747(L)
Herschbach, Dudley R. and Victor W. Laurie. Anharmonic potential constants and their dependence upon bond length—458
—— (see Datz, Sheldon)—1549
Hersh, I. S. (see Kleppa, O. J.)—175
Hexter, Robert M. (see Jacox, Marilyn E.)—183
Heylen, A. E. D. Experimental Townsend ionization coefficients for isopentane—169
Higgs, Mary Ann. Comments on "Theoretical derivation of Traube's Rule—1504(L)
Higuchi, Jiro. Theoretical calculation of isotropic hfs of the free NH_2 radical—2270(L)
Hill, Terrell L. Effect of intermolecular forces on macromolecular configurational changes and on other isomeric equilibria—303
Hiller, L. A., Jr. (see Wall, F. T.)—1284
Hinge, Kamalakar S. (see Hoch, Michael)—451
Hirschfelder, Joseph O. (see Hulburt, Hugh M.)—1901(L)
Hirshfeld, M. A. (see Ben-Reuven, A.)—955
Hobgood, R. T., J. H. Goldstein, and G. S. Reddy. Proton magnetic resonance spectra of vinylmethylsilanes—2038
Hoch, Michael and Kamalakar S. Hinge. Vaporization of aluminum arsenide—451
Hoeve, C. A. J. Unperturbed mean-square end-to-end distance of polyethylene—1266
Hollis, Donald P. and P. W. Selwood. Effect of chemisorbed hydrogen on the ferromagnetic resonance of finely divided nickel—378(L)
Hopkins, Robert C. (see Rigden, John S.)—1532(L)
Hormats, E. (see Brock, E. G.)—759(L)
Hornig, D. F. (see Schiffer, J.)—1136(L)
—— (see Vedder, W.)—1560
Horsfield, A. (see Morton, J. R.)—1142(L)
Howard, Bentz B. (see Jumper, Charles F.)—1911(L)
Hudda, F. G. (see Ehrlich, Gert)—1421
Hudson, Donald E. (see Trulson, O. Conrad)—1018
Hudson, J. B. and G. W. Sears. Evaporation of zinc whiskers—1509(L)
Hughes, Ernest E. Purfication and vapor pressure of nitric oxide—1531(L)
Hughes, R. E. (see von Frankenberg, Carl)—503
Hulburt, Hugh M. and Joseph O. Hirschfelder. Erratum: Potential energy functions for diatomic molecules—1901(L)
Hunt, John P. and Harold W. Dodgen. Exchange rates of NH_3 between aqueous NH_4OH and copper and nickel ammine complexes—2261(L)
Hurley, A. C. (see Carroll, P. K.)—2247(L)
Hyman, Julius, Jr. Measurement of the resistivity of cesium at elevated temperatures—992

Illinger, Karl H. and Charles P. Smyth. Atomic polarization. II. Vibrational polarization of liquids—392
—— **and Charles P. Smyth.** Atomic polarization. III. Vibrational polarization terms associated with forbidden transitions in polyatomic molecules—397
—— **and Charles P. Smyth.** Atomic polarization. IV. Temperature dependence of the vibrational polarization of gases—400
—— Atomic polarization. V. Normal mode polarizability and the additivity of the vibrational polarization—409
Ingalls, R. B. and Leo A. Wall. Electron spin resonance spectra of free-radical intermediates formed by reaction of polystyrene with atoms of hydrogen and deuterium—370(L)
Inghram, Mark G. (see Grimley, R. T.)—551
Inn, Edward C. Y. (see Gunton, Robert C.)—1896(L)
Ise, Norio. On the polyelectrolyte-simple electrolyte interaction parameter—1145(L)
Isenberg, I. (see Bersohn, R.)—1640

Jackson, G. and Robert Livingston. Unimolecular decay of the triplet state of anthracene in fluid and viscous media—2182
Jackson, Robert (see Pierce, Louis)—2240(L)
Jacox, Marilyn E. and Robert M. Hexter. Solid-state vibrational spectra of the methyl and methyl-d_3 halides—183
Jaffe, J. H. (see Ben-Reuven, A.)—955
James, David W. (see Janz, George J.)—739
James, Thomas C. Wave functions and intensity calculations for a rotating anharmonic oscillator—767
Janz, George J. and David W. James. Raman spectra and ionic interactions in molten nitrates—739
Jaseja, Thadho S. and Roy S. Anderson. Electron spin resonance study of radiation damage in single crystals of urea compounds—2192
Jeffrey, G. A. (see Feil, D.)—1863
Jennings, K. R. and R. J. Cvetanović. Relative rates of addition of hydrogen atoms to olefines—1233
—— (see Cvetanović, R. J.)—1225
Johns, I. B., H. E. Ulmer, and J. W. Edwards. Reversible phase transition of phosphorus pentoxide—1271
Johnson, C. S., Jr., and J. S. Waugh. Nuclear relaxation in gases: mixtures of methane and oxygen—2020
——, **J. S. Waugh, and J. N. Pinkerton.** On the mechanism of nuclear relaxation in gaseous and liquid CHF_3—1128(L)
Johnson, F. A. (see Piette, L. H.)—1481
Johnson, R. C., T. L. Weatherly, and Quitman Williams. Dipole moment of $CClF_3$—2261(L)
Jones, A. Russell. Radiolyses by transferred energy of compounds dispersed in alkali halide matrices—751(L)
Jones, M. Thomas. Electron spin resonance absorption of tris-*p*-nitrophenylmethyl—1146(L)
Joshi, S. K. On the quasi-crystalline model of water—1141(L)
Jumper, Charles F., Merle T. Emerson, and Bentz B. Howard. Self-association constant of chloroform from NMR chemical shifts—1911(L)

Kalman, Otto F. and J. C. Decius. Absolute infrared intensities of the CS_2 fundamentals in CCl_4 solution and of the 768–797 cm^{-1} Fermi doublet of CCl_4 in cyclohexane solution—1919
Kaminsky, Manfred (see Chupka, William A.)—1991
Karle, J. Excited states of molecules and the scattering of fast electrons—963

—— (see Swick, D. A.)—2257(L)
Karmohapatro, S. B. Charge exchange between krypton ions and atoms—1524(L)
Karplus, Martin and George K. Fraenkel. Theoretical interpretation of carbon-13 hyperfine interactions in electron spin resonance spectra—1312
—— **and H. J. Kolker.** Magnetic interactions in lithium hydride—2235(L)
—— (see Schug, John C.)—1873
Kasha, M. (see Ramsey, B.)—1502(L)
Katayama, Mikio and Walter Gordy. Electron spin resonance of γ-irradiated glycylglycine—117
Katti, P. K. and M. M. Chaudhri. Note on the boiling points and surface tensions of binary mixtures of acetone and isopropanol—756(L)
Katz, Dov (see Heller, Adam)—1987
Katz, J. L., B. F. Powers, and O. J. Kleppa. Volume change on mixing in liquid sodium-potassium nitrates—765(L)
—— (see Reiss, H.)—820
Katzin, Leonard I. Energy value of the octahedraltetrahedral coordination change—467
Kaufman, F. and F. P. Del Greco. Formation, lifetime, and decay of OH radicals in discharge-flow systems—1895(L)
Kauzmann, Walter (see Sovers, Ojars)—652
—— (see Tobias, Irwin)—538
Kawaguchi, Yôichi (see Tadokoro, Hiroyuki)—369(L)
Kawai, K. (see Stammreich, H.)—2168, 2175
Kearns, David. Resonance transfer model of electron and hole conduction in anthracene—2269(L)
Keedy, Daniel A. (see Powers, Joseph)—376(L)
Keesom, P. H. (see Bryant, C. A.)—1149(L)
Kellogg, R. E. (see Frost, A. A.)—827
Kemp, James C. Further notes on the magnetic centers in neutron-irradiated calcite—377(L)
Kennedy, Al and Charles B. Colburn. Strength of the N—F bonds in NF_3 and of N—F and N—N bonds in N_2F_4—1892
Kenty, Carl. Evidence for a long-lived metastable state of N_2 at about 8 ev—2267(L)
Ketelaar, J. A. A. and R. P. H. Rettschnick. Simultaneous infrared absorption involving rotational transitions of H_2—1909(L)
Kimel, S. (see Ben-Reuven, A.)—955
King, A. Bruce (see Wood, Bernard J.)—1530(L)
King, A. D., Jr. (see Robertson, W. W.)—464
King, G. J., B. S. Miller, F. F. Carlson, and R. C. McMillan. Solid state photochemical processes in sodium azide—1442
King, I. R. Recombination of ions in flames. Effect of temperature—380(L)
Kingsley, J. D. (see Prener, J. S.)—2256(L)
Kinsey, James L. (see Curl, R. F., Jr.)—1758
Kirshenbaum, A. D. and A. G. Streng. Molar extinction coefficients of liquid O_3F_2, O_2F_2, and O_3 in the visible range—1440
Kistemaker, J. (see Fluit, J. M.)—1143(L)
Kistiakowsky, G. B. and R. K. Lyon. Gaseous detonations. XIII. Rotational and vibrational distributions of OH radicals—995
—— (see Bradley, J. N.)—256, 264
—— (see Gardiner, W. C., Jr.)—1765
Kivelson, Daniel and Robert Neiman. ESR studies on the bonding in copper complexes—149
—— (see Neiman, Robert)—156, 162
Kjekshus, Arne (see Westrum, Edgar F., Jr.)—1670
Klein, Fritz S. (see Bar-Eli, Kedma)—1915(L)
Klemperer, William (see Leroi, George E.)—774
Kleppa, O. J., R. B. Clarke, and L. S. Hersh. Studies of fused salts. III. Heats of mixing in silver nitrate-alkali nitrate mixtures—175
—— (see Katz, J. L.)—765(L)
Knight, Herbert T. and John P. Rink. Dissociation energy of cyanogen and related quantities by x-ray densitometry of shock waves—199
Knox, K. (see Ferguson, J.)—2236(L)
Kobayashi, Akira (see Tadokoro, Hiroyuki)—369(L)
Kojima, Takeshi, Edward L. Breig, and Chun C. Lin. Microwave spectrum and internal barrier of methylphosphine—2139
Kolker, H. J. (see Karplus, M.)—2235(L)
Kommandeur, J. (see Blomgren, G. E.)—1636
Kor, S. K. and G. S. Verma. Influence of the dielectric constant on the ultrasonic relaxation frequency in $MnSO_4$ solutions—1512(L)
Koski, W. S. (see Ring, M. A.)—381(L)
Kozima, Kunio and Wataru Suëtaka. "Rotational" isomers of cyclopentane derivatives—1516(L)
Krauss, Morris (see Wacks, Morton E.)—1902(L)
Krigbaum, W. R. (see Roe, R.-J.)—1306
Krikorian, Esther (see Brecher, Charles)—1097
Kroh, J. and J. W. T. Spinks. Tritium as an internal source of radiation in EPR studies of organic materials (corrected version)—760(L)
Kronick, Paul L. and Mortimer M. Labes. Organic semiconductors. V. Comparison of measurements on single-crystal and compressed microcrystalline molecular complexes—2016
Krumholz, P. (see Stammreich, H.)—2168, 2175
Kuchitsu, Kozo and L. S. Bartell. Effects of arharmonicity of molecular vibrations on the diffraction of electrons. II. Interpretation of experimental structural parameters—1945
—— (see Bartell, L. S.)—1211
Kuenz, C. (see Raw, C. J. G.)—1529(L)
Kuntz, I. D., Jr., P. von R. Schleyer, and A. Allerhand. Long-range N^{15}—H^1 nuclear-resonance coupling in isonitriles—1533(L)
Kuri, Zen'ichiro (see Ueda, Hisashi)—2145
Kushner, Lawrence M. (see Parker, Robert L.)—1345

Labes, Mortimer M. (see Kronick, Paul L.)—2016
Lafferty, W. J. (see Robinson, D. W.)—2245(L)
Lammermann, H. and H. J. Stapleton. Optical and paramagnetic resonance spectra of trivalent Pu^{239} in the trichloride and ethylsulfate—1514(L)
Landau, L. (see Begun, G. M.)—547
Laurie, Victor W. (see Herschbach, Dudley R.)—458
LeBlanc, Oliver H., Jr. Band structure and transport of holes and electrons in anthracene—1275
Lee, R. W. (see Frank, R. C.)—1451
Lefebvre, Roland. Calculation of the electron spin resonance line shape for a polycrystalline radical with anisotropic g tensor and proton hyperfine interactions—762(L)
Lefebvre-Brion, H., Carl Moser, and R. K. Nesbet. Ultraviolet spectra of carbon monoxide—1702
Lepoutre, Gerard (see Berns, Donald S.)—1820
Leroi, George E. and William Klemperer. Infrared spectra of sodium and potassium cyanide—774
Libby, W. F. Chemistry of positive ions. I. General theory particularly for the radiation induced cross linkage of polymers and polymerization of saturated hydrocarbons—1714
—— Isotope size effect in Van der Waals radii and the barrier to rotation around the carbon-carbon single bond—1527(L)
Lide, David R., Jr., and Daniel Christensen. Molecular structure of propylene—1374
—— (see Harmony, Marlin D.)—1129(L)
Lin, Chun C. (see Kojima, Takeshi)—2139
Lin, W. C., C. A. McDowell, and J. R. Rowlands. Electron spin resonance of x-ray irradiated single crystals of glutamic acid hydrochloride—757(L)
Linares, R. C., Jr. (see Pappalardo, R.)—1460, 2041
Linder, Bruno. Energy and free energy of cohesion—371(L)
Lippincott, E. R., D. Steele, and P. Caldwell. General relation between potential energy and internuclear distance for diatomic molecules. III. Excited states—123

—— (see Steele, D.)—2065
Lipscomb, William N. (see Moore, Emmett B., Jr.)—1329
—— (see Simpson, Paul G.)—1340
—— (see Wang, Frederick E.)—1335
Livingston, Ralph (see Zeldes, Henry)—563
Livingston, Robert (see Jackson, G.)—2182
Lohr, L. L., Jr. (see Moore, Emmett B., Jr.)—1329
Longmire, M. S. (see Amdur, I.)—895
Lord, R. C. (see Robinson, D. W.)—2245(L)
Löwdin, Per-Olov. Note on the separability theorem for electron pairs—78
Lucchesi, P. J. (see Yates, D. J. C.)—243
Ludwig, Oliver G. and Robert G. Parr. On the introduction of arbitrary angular peakedness into atomic orbitals—754(L)
Lykos, Peter G. On the parameters used in semiempirical molecular orbital theory for conjugated hydrocarbons—1249
—— **and Howard N. Schmeising.** Maximum overlap atomic and molecular orbitals—288
—— (see Miller, R. L.)—1147(L)
Lyon, R. K. (see Kistiakowsky, G. B.)—995

MacLachlan, A. (see McCarthy, R. L.)—1625
Madden, Robert P. High-resolution study of CO_2 absorption spectra between 15 and 18 microns—2083
Maeda, Shiro and P. N. Schatz. Absolute infrared intensity measurements in thin films—1617
Magee, John L. (see Nosworthy, J. M.)—1506(L)
Mahlman, H. A. The OH yield in the Co^{60} γ radiolysis of HNO_3—936
Maier, William B., II (see Giese, Clayton F.)—1913(L)
Maki, Arthur G. Infrared spectra of carbon monoxide as a solid and in solid matrices—931
Maki, August H. Rotational isomerism in terephthalaldehyde anion—761(L)
Mandel, M. (see Edelstein, A. S.)—1130(L)
Mann, D. E. (see Harmony, Marlin D.)—1129(L)
Margolis, Jack S. Energy levels of $PrCl_3$—1367
Marmet, P. and J. D. Morrison. A mass spectrometer for ionization efficiency studies using an electron velocity selector—746(L)
Marshall, S. A. (see Hacker, D. S.)—1788
Mason, Edward A. Intermolecular potential for krypton—2245(L)
—— (see Amdur, I.)—895
—— (see Evans, R. B., III)—2076
—— (see Monchick, L.)—1676
Mason, P. Relation of physical behavior to molecular packing in crosslinked rubber—1523(L)
Matsubara, Ikuo. Infrared spectrum and Holecular configuration of glutaronitrile—373(L)
Matsugashita, Teikichi and Kenichi Shinohara. Electron spin resonance studies of radicals formed in irradiated polytetrafluoroethylene—1652
Matsui, Yoshiki (see Tadokoro, Hiroyuki)—369(L)
Mayer, S. W. Calculation of metal surface tensions. Ionic-salt and monatomic models for liquid metals—1513(L)
—— (see Reiss, H.)—820
Mazo, Robert M. Momentum-correlation function in a Rayleigh gas—831
—— (see Mortimer, Robert G.)—1013
Mazur, J. (see Wall, F. T.)—1284
Mazur, Peter (see Ross, John)—19
McBride, Bonnie J. and Sanford Gordon. Thermodynamic functions of several triatomic molecules in the ideal gas state—2198
McCarthy, R. L. and A. MacLachlan. Observation of free radical kinetics in the cyclohexane-oxygen system—1625
McConnell, Harden M. Antiparellel spin polarization in triplet states—1520(L)
—— Intramolecular charge transfer in aromatic free radicals—508
—— **and Concetto R. Giuliano.** $CH_2(COOH)$ in malonic acid—1910(L)
—— (see Sternlicht, Himan)—1793
McCullough, J. P. (see Douslin, D. R.)—1357
McDowell, C. A. (see Lin, W. C.)—757(L)
McGinn, Clifford J. Heats of hydrogenation as a function of hybridization—1511(L)
McGlynn, S. P., J. K. Smith, and W. C. Neely. Electronic structure, spectra, and magnetic properties of oxycations. III. Ligation effects on the infrared spectrum of the uranyl ion—105
McMillan, J. A. and B. Smaller. Paramagnetic resonance of some copper complex compounds—763(L)
—— **and B. Smaller.** Paramagnetic resonance of some silver (II) compounds—1698
McMillan, R. C. (see King, G. J.)—1442
McNamee, J. M. (see Dalgarno, A.)—1517(L)
McNeely, D. R. (see Forstat, H.)—1594
Melton, Charles E. Studies of transient species formed during catalytic reactions of CO_2+D_2 and of l-butene—1751
Menefee, Emory and Warner L. Peticolas. Molecular weight distribution from the normal coordinate theory of viscoelasticity—946
—— (see Peticolas, Warner L)—951
Meyerson, Seymour. Erratum: Effect of electron energy on some electron-impact processes—1137(L)
Mikhail, H., Z. Hanafy, and T. M. Salem. Magnetic susceptibility of mercuric oxide at various temperatures—1185
Mill, T., A. van Roggen, and C. F. Wahlig. Photochromism of *N*-3-pyridylsydnone—1139(L)
Miller, B. S. (see King, G. J.)—1442
Miller, G. H. (see Pritchard, G. O.)—1135(L)
Miller, R. L. and Peter G. Lykos. Use of distorted atomic orbitals in molecular wave functions—1147(L)
Milligan, Dolphus E. Infrared spectroscopic study of the photolysis of chlorine azide in solid argon at 4.2°K—372(L)
—— Infrared spectroscopic study of the photolysis of methyl azide and methyl-d_3 azide in solid argon and carbon dioxide—1491
Milton, Earl R. V., H. B. Dunford, and A. E. Douglas. Spectrum of NBr excited in active nitrogen—1202
Minomura, S. and H. G. Drickamer. Effect of pressure on the spectra of transition metal ions in MgO and Al_2O_3—903
Mitoff, S. P. Electrical conductivity and thermodynamic equilibrium in nickel oxide—882
Miyazawa, Tatsuo. Molecular vibrations and structures of high polymers. I. General method of normal coordinate treatment by internal coordinates and infrared frequencies and conformations of $(-CH_2-)_n$, $(-CH_2-O-)_n$, and $(-CH_2-O-CH_2-)_n$—693
—— (see Shimanouchi, Takehiko)—1597
Mohanty, Ganesh P. and Leonid V. Azároff. Electron density distributions in ZnO crystals—1268
Monchick, L. and E. A. Mason. Transport properties of polar gases—1676
Moore, Emmett B., Jr., L. L. Lohr, Jr., and William N. Lipscomb. Molecular orbitals in some boron compounds—1329
Moore, R. T. (see Douslin, D. R.)—1357
Moore, Walter J. (see O'Keeffe, Michael)—1324
Morino, Yonezo and Masaharu Toyama. Zeeman effect of the nuclear quadrupole resonance spectrum in crystalline powder—1289
Morrison, J. D. (see Dorman, F. H.)—575
—— (see Marmet, P.)—746(L)
Mortensen, Earl M. (see Smith, Richard P.)—714
Mortimer, Robert G. and Robert M. Mazo. Irreversible thermodynamics of systems containing radiation. Application to photochemical reactions—1013
Morton, J. R. and A. Horsfield. Electron spin resonance spectrum and structure of $CH_3CH(CO_2H)$—1142(L)

Moser, Carl (see Lefebvre-Brion, H.)—1702
Moulton, Grace C. and W. G. Moulton. Paramagnetic resonance of x-irradiated single crystals of Rochelle salt—208
Moulton, W. G. (see Moulton, Grace C.)—208
Mukhedkar, A. J. Solvent effects on optical rotation and dipole moment—2133
Muldawer, L. and F. deBergevin. Antiferromagnetic-ferromagnetic transformation in FeRh—1904(L)
Murahashi, Shunsuke (see Tadokoro, Hiroyuki)—369(L)
Murty, C. R. K. (see Spence, R. D.)—1912(L)
Musher, Jeremy I. Long-range nuclear magnetic shielding in molecules and the anisotropy in the magnetic susceptibility of a carbon-carbon single bond—1159
——NMR chemical shift of hydroxyl and hydronium ions—1989
Myers, Rollie J. (see Harmony, Marlin D.)—1 (7)629
Mysels, Karol J. (see Scholten, P. C.)—1845

Naiman, C. S. Interpretation of the absorption spectra of $K_3Fe(CN)_6$—323
—— On the optical absorption of $K_2[Cr(CN)_5NO]\cdot H_2O$—1503(L)
Nanda, V. S. and R. K. Pathria. Time dependence of the statistical molecular weight distribution of the polymer resulting from vinyl polymerization—630
Nedderman, H. C. (see Brock, E. G.)—759(L)
Neely, W. C. (see McGlynn, S. P.)—105
Neff, Vernon D. and Thomas H. Walnut. Effect of temperature on the intensity and structure of bands in the infrared spectrum of rhombic sulfur—1723
Neiman, Robert and Daniel Kivelson. ESR line shapes in glasses of copper complexes—156
—— **and Daniel Kivelson.** ESR spectra of solid phthalocyanines—162
—— (see Kivelson, Daniel)—149
Nesbet, R. K. (see Lefebvre-Brion, H.)—1702
Nosworthy, J. M., John L. Magee, and M. Burton. Erratum: On the luminescence minimum in certain scintillator solutions—1506(L)

O'Keefe, J. G. (see Bray, P. J.)—435
O'Keeffe, Michael and Walter J. Moore. Electrical conductivity of monocrystalline cuprous oxide—1324
Olds, Dan W. Polarized phosphorescence in crystalline hexachlorobenzene at 77°K—2248(L)
Oppenheim, I. and A. S. Friedman. Quantum statistical mechanics of isotope effects—35
O'Reilly, D. E. Paramagnetic relaxation in metal-ammonia solutions—1856
Orgel, L. E. (see Griffith, J. S.)—748(L)
Orofino, T. A. and F. Wenger. Effect of impurities on the molecular weight distributions of anionic polymers—532

Pace, E. L. and R. J. Bobka. Thermodynamic properties of trifluoroacetonitrile from 12°K to its boiling point—454
Padley, P. J. (see Bulewicz, E. M.)—1590
Pake, G. E. (see Anderson, M. E.)—1527(L)
Palko, A. A., J. S. Drury, and W. E. Bull. Separation of boron isotopes. V. The phenol-BF_3 system—103
Pappalardo, R., D. L. Wood, and R. C. Linares, Jr. Optical absorption study of Co-doped oxide systems. II—2041
——, **D. L. Wood, and R. C. Linares, Jr.** Optical absorption spectra of Ni-doped oxide systems. I—1460
Parker, Robert L. and Lawrence M. Kushner. Growth rates of zinc crystals from the vapor phase—1345
Parr, Robert G. and Lawrence C. Snyder. Perturbation theory calculations—1898(L)
—— (see Companion, Audrey L.)—2268(L)
—— (see Ludwig, Oliver G.)—754(L)
Pathria, R. K. (see Nanda, V. S.)—630
Patterson, Andrew, Jr. (see Berns, Donald S.)—1820
Paul, R. and I. B. Srivastava. Mutual diffusion of the gas pairs H_2–Ne, H_2–Ar, and H_2–Xe at different temperatures—1621
Pauncz, R. (see Ritter, Z. W.)—571
Person, Willis B., George R. Anderson, James N. Fordemwalt, H. Stammreich, and Roberto Forneris. Infrared and Raman spectra, force constants, and the structures of some polyhalide ions: ICl_2^-, ICl_4^-, $BrCl_2^-$, and Br_3^-—908
Peticolas, Warner L. Molecular weight distribution of polymers from rheological measurements in dilute solution—2128
—— **and Emory Menefee.** Molecular-weight dependence of the viscoelastic properties of whole polymers—951
—— (see Menefee, Emory)—946
Petrakis, L. and C. H. Sederholm. NMR fluorine-fluorine coupling constants in saturated organic compounds—1243
—— **and C. H. Sederholm.** Temperature-dependent chemical shifts in the NMR spectra of gases—1174
Phillips, W. D. (see Chesnut, D. B.)—1002
Pierce, Louis and Michiro Hayashi. Microwave spectrum, dipole moment, structure, and internal rotation of dimethyl sulfide—479
——, **Robert Jackson, and Nicholas DiCianni.** Microwave spectrum, structure, and dipole moment of F_2O—2240(L)
—— (see Hayashi, Michiro)—1148(L)
Piette, L. H., F. A. Johnson, K. A. Booman, and Charles B. Colburn. An EPR study of the tetrafluorohydrazine-difluoramino equilibrium—1481
Pimentel, George C. (see Ewing, George E.)—925
Pinkerton, J. N. (see Johnson, C. S., Jr.)—1128(L)
Pintar, M. (see Blinc, R.)—1140(L)
Piper, T. S. Analysis of polarized crystal spectra. The spectrum of Cobalt(III) acetylacetonate—1240
—— **and Richard L. Carlin.** Polarized visible spectra of crystalline trisoxalatometallates—1809
Plane, Robert A. (see Chantry, George W.)—1027
Poirier, Jacques C. and James H. DeLap. On the theory of ion pairs in solutions—213
Polanyi, J. C. (see Cashion, J. K.)—600
Porte, A. L. (see Gutowsky, H. S.)—839
Porter, Richard F. Molecular association in sodium cyanide vapor—318
Potter, R. L., R. G. Shores, and J. L. Dye. Attempts to find photoconductivity in dilute sodium-ammonia solutions—1907(L)
Powers, B. F. (see Katz, J. L.)—765(L)
Powers, Joseph, Daniel A. Keedy, and Richard S. Stein. Depolarization of scattered light by *n*-paraffin vapors and the additivity of bond polarizability tensors—376(L)
Prener, J. S. and J. D. Kingsley. Preparation and optical transmission of cadmium fluoride crystals—2256(L)
—— **and F. E. Williams.** Effect of interstitial Li on the density of Si—1803
Price, Fraser P. Markoff chain model for growth of polymer single crystals—1884
Pritchard, G. O. and G. H. Miller. Comparison of $CH_3\cdot$ and $CF_3\cdot$ hydrogen abstraction reactions—1135(L)

Rabinovitch, B. S. and J. H. Current. On the classical approximation in unimolecular reactions and mass spectra—2250(L)
—— (see Setser, D. W.)—1840
Ragle, J. L. Anisotropy of nuclear magnetic resonance in vanadium pentoxide—753(L)
Ramsey, B., M. Ashraf El-Bayoumi, and M. Kasha. Intramolecular charge-transfer bands observed in the spectra of some aryl boron compounds—1502(L)
Ransil, Bernard J. (see Fraga, Serafin)—669, 1967
Rao, D. V. G. L. Narasimha and Walter Gordy. Electron spin resonance of an irradiated single crystal of urea oxalate—362

—— **and Walter Gordy.** ESR spectra of a gamma-irradiated single crystal of *DL*-serine—764(L)
Rao, P. Ramakoteswara and J. K. Brody. Structure of the band spectrum of CuCl molecule. I. Additional knowledge in the coarse structure—776
Rapp, Donald (see Turner, R. E.)—1076
Rauh, E. G. (see Cater, E. David)—619
Raw, C. J. G. and C. Kuenz. Approximate mean-square amplitudes of characteristic two-atom vibrations—1529(L)
Reddoch, Allan H. Nuclear quadrupole resonance in $TiCl_4$, $ThCl_4$, $NbCl_5$, and $TaCl_5$—1085
Reddy, G. S. and J. H. Goldstein. Constancy of the sums of spin-spin coupling constants in monosubstituted ethylenes—380(L)
—— (see Hobgood, R. T.)—2038
Ree, Taikyue (see Yang, Kang)—588
Reed, John W. and P. M. Harris. Neutron diffraction study of solid deuteroammonia—1730
Reilly, C. A. and J. D. Swalen. Analysis of complex NMR spectra: epichlorohydrin—1522(L)
Reimann, Curt W. (see Berry, R. Stephen)—2237(L)
Reiss, Howard, S. W. Mayer, and J. L. Katz. Law of corresponding states for fused salts—820
Rettschnick, R. P. H. (see Ketelaar, J. A. A.)—1909(L)
Rhodes, R. S. (see Anderson, M. E.)—1527(L)
Ribnikar, Slobodan V. (see Bigeleisen, Jacob)—1297
Rice, Stuart A. (see Davis, H. T.)—2210
Richardson, James W. Double-ζ SCF MO calculation of the ground and some excited states of N_2—1829
Rigden, John S., Robert C. Hopkins, and John D. Baldeschwieler. Absence of B^{10}–B^{11} coupling in B_4H_{10}—1532(L)
Riggleman, B. M. and H. G. Drickamer. Effect of pressure on the low-energy absorption peak of several phthalocyanines—1343
Ring, M. A. and W. S. Koski. B^{11} quadrupole coupling constants in trimethoxyboroxine and *N*-trimethylborazole—381(L)
Rink, John P. (see Knight, Herbert T.)—199
Ritter, Z. W., R. Pauncz, and K. Appel. Approximate analytical wave functions for the $1s^2ns\ ^2S_{\frac{1}{2}}$ states of Li and Li-like ions—571
Robertson, W. W., A. D. King, Jr., and O. E. Weigang, Jr. Determination of excited-state dipole moments of azulene—464
Robinson, D. W., W. J. Lafferty, J. R. Aronson, J. R. Durig, and R. C. Lord. Erratum: Far infrared spectrum of disiloxane—2245(L)
—— (see Eggers, D. F., Jr.)—1045
Robinson, G. Wilse (see El-Sayed, Mostafa)—1896(L)
Roe, R.-J., K. J. Smith, Jr., and W. R. Krigbaum. Equilibrium degrees of crystallization predicted for "single pass" and folded chain crystallite models—1306
Rogers, Max T. (see Coulson, C. A.)—593
Rosenberg, Barnett and James F. Camiscoli. Photo- and semiconduction in crystalline chlorophylls *a* and *b*—982
Rosenblatt, Gerd M. and C. Ernest Birchenall. Vapor pressure of antimony by the torsion-effusion method—788
Rosenstock, H. M. (see Vestal, M. L.)—2008
Rosenstock, Herbert B. Atomic forces and thermal effects in solids—420
Ross, John and Peter Mazur. Some deductions from a formal statistical mechanical theory of chemical kinetics—19
Ross, Marvin and William A. Steele. Monolayer adsorption of helium on argon—862
—— **and William A. Steele.** Multilayer adsorption of helium on argon—871
—— (see Steele, William A.)—850
Ross, V. F. (see Bray, P. J.)—435
Roth, Etienne (see Bigeleisen, Jacob)—68
Rothberg, G. M. Erratum: Binding energies of alkali halide molecules—1137(L)
Rowlands, J. R. (see Lin, W. C.)—757(L)
Rudinger, George. Comments on the Strehlow and Case Letter—1507(L)
Rulli, J. E. (see Aronson, S.)—1382
Runciman, W. A. (see Crozier, M. H.)—1392
Rush, J. J., T. I. Taylor, and W. W. Havens, Jr. Proton motions in solids by slow neutron scattering cross sections—2265(L)

Saba, William G. and W. E. Wallace. Heat capacities of $DyCo_5$ in relationship to its magnetic anomaly, third law entropies, and related thermochemical data—689
——, **W. E. Wallace, H. Sandmo, and R. S. Craig.** Heat capacities and the residual entropy of Ta_2H—2148
Sage, Martin L. Internal rotation of *cis* 2,3-epoxybutane from the microwave spectrum—142
—— Microwave Faraday effect in weakly magnetic gases—969
Saito, N. (see Shinohara, K.)—1899(L)
Saitô, Nobuhiko. On the theory of condensation—232
Sala, Osw. (see Stammreich, H.)—2168, 2175
Salem, T. M. (see Mikhail, H)—1185
Salsburg, Zevi W. (see Squire, David R.)—486
Sanders, R. N. (see Helmholz, Lindsay)—1349
Sandmo, H. (see Saba, W. G.)—2148
Sather, Norman F. and John S. Dahler. Molecular friction in dilute gases. II. Thermal relaxation of translational and rotational degrees of freedom—2029
Sauer, Myran C., Jr., and Leon M. Dorfman. Molecular detachment processes in the vacuum uv photolysis of gaseous hydrocarbons. I. Ethylene. II. Butane—497
Saxena, S. C. and J. P. Agrawal. Thermal conductivity of polyatomic gases and relaxation phenomena—2107
Scargle, J. D. (see Frost, A. A.)—827
Schaad, L. J. (see Coulson, C. A.)—294
Schaner, B. E. (see Aronson, S.)—1382
Schatz, P. N. (see Maeda, Shiro)—1617
Schiffer, J. and D. F. Hornig. On a reported new form of ice—1136(L)
Schlag, E. W. Unimolecular rates due to multiple critical oscillators—2117
Schleyer, P. von R. (see Kuntz, I. D., Jr.)—1533(L)
Schmeising, Howard N. (see Lykos, Peter G.)—288
Schneider, W. G. (see Spiesecke, H.)—722, 731
—— (see Valleau, J. P.)—2271(L)
Schoen, L. J. (see Harmony, Marlin D.)—1129(L)
Schofield, D. (see Dickens, P. G.)—374(L)
Scholten, P. C. and Karol J. Mysels. Measurement of electrodiffusion. Effect of electrosmosis on diffusion—1845
Schug, John C., Thomas H. Brown, and Martin Karplus. Theory of the spin and charge distribution in aromatic ion radicals; application to the naphthalene negative ion—1873
—— **and Norman D. Coggeshall.** Note on the statistical theory of mass spectra—1146(L)
Scott, A. B. (see Coker, E. Howard)—745(L)
Scott, Donald R. and Ralph S. Becker. Comprehensive investigation of the electronic spectroscopy and theoretical treatments of ferrocene and nickelocene—516; 2246(E)
Seager, Spencer L. (see Giddings, J. Calvin)—2242(L)
Sears, G. W. (see Hudson, J. B.)—1509(L)
Sederholm, C. H. (see Petrakis, L.)—1174, 1243
Seiwatz, Ruth (see Green, Mino)—915
Selwood, P. W. (see Dietz, R. E.)—270
—— (see Hollis, Donald P)—378(L)
Senderoff, S. (see Wilmshurst, J. K.)—1078
Sengers, J. V. (see Davis, H. T.)—2210
Setser, D. W., B. S. Rabinovitch, and E. G. Spittler. Primary processes in $Hg(^3P_1)$ photosensitized reaction of cyclopropanes—1840
Shanks, H. R. (see Ellerbeck, L. D.)—298
Sherwood, R. C. (see Geller, S.)—1908(L)

Shida, Shoji (see Ueda, Hisashi)—2145
Shida, T. (see Shinohara, K.)—1899(L)
Shimanouchi, Takehiko, Masamichi Tsuboi, and Tatsuo Miyazawa. Optically active lattice vibrations as treated by the GF-matrix method—1597
Shinohara, K., T. Shida, and N. Saito. Remark on the radiolysis of aqueous nitrate solution—1899(L)
Shinohara, Kenichi (see Matsugashita, Teikichi)—1652
Shores, R. G. (see Potter, R. L.)—1907(L)
Shukla, Ramesh Chandra (see Varshni, Yatendra Pal)—582
Shull, Harrison (see Allen, Thomas L.)—1644
Shulman, R. G. and B. J. Wyluda. Nuclear magnetic resonance in $CuF_2 \cdot 2H_2O$ single crystals—1498
Sidles, P. H. (see Ellerbeck, L. D.)—298
Simpson, Paul G. and William N. Lipscomb. Refinement of the B_5H_{11} structure and test for solid solutions—1340
—— (see Wang, Frederick E.)—1335
Singh, Shobha (see Dieke, G. H.)—555
Slater, Noel B. Cubic potential surfaces in the transition-state theory of unimolecular reactions—445
Sloan, G. J. (see Chesnut, D. B.)—443
Smaller, B. (see McMillan, J. A.)—763(L), 1698
Smith, F. T. (see Gatz, C.)—1500(L)
Smith, George W. On the calculation of second moments of nuclear magnetic resonance lines for large molecules. Adamantane molecule—1134(L)
Smith, J. K. (see McGlynn, S. P.)—105
Smith, K. J., Jr. (see Roe, R.-J.)—1306
Smith, Richard P. and Earl M. Mortensen. Calculation of depolarization ratios, anisotropies, and average dimensions of *n*-alkanes—714
Smith, Robert C. and S. J. Wyard. Electron spin resonance measurements of preferred orientation in quickly frozen hydrogen peroxide solutions—2254(L)
Smyth, Charles P. (see Illinger, Karl H.)—392, 397, 400
Snyder, Lawrence C. (see Parr, Robert G.)—1898(L)
Sobajima, Shigenobu (see Tadokoro, Hiroyuki)—369(L)
Soffer, Bernard H. Studies of the optical and infrared absorption spectra of rutile single crystals—940
Somorjai, G. A. Surface energy effect on diffusion-controlled particle growth—655
Sovers, Ojars and Walter Kauzmann. *d*-hybridization of the pi bond in the $2p\pi_u$ state of H_2^+—652
Spedding, Frank H. (see Trulson, O. Conrad)—1018
Spence, R. D. and C. R. K. Murty. Magnetization and proton relaxation time in antiferromagnetic $LiCuCl_3 \cdot 2H_2O$—1912(L)
Spencer, Glenn H., Jr., Paul C. Cross, and Kenneth B. Wiberg. *s*-tetrazine. I. High-resolution vapor-phase study of the visible $n \rightarrow \pi^*$ vibronic absorption band systems—1925
——, **Paul C. Cross, and Kenneth B. Wiberg.** *s*-tetrazine. II. Infrared spectra—1939
Spiesecke, H. and W. G. Schneider. Effect of electronegativity and magnetic anisotropy of substituents on C^{13} and H^1 chemical shifts in CH_3X and CH_2CH_2X compounds—722
—— **and W. G. Schneider.** Substituent effects on the C^{13} and H^1 chemical shifts in monosubstituted benzenes—731
Spinks, J. W. T. (see Kroh, J.)—760(L)
Spittler, E. G. (see Setser, D. W.)—1840
Spokes, G. Neil (see Berry, R. Stephen)—2237(L)
Squire, David R. and Zevi W. Salsburg. Formulation of a cell model using periodic boundary conditions—486
Srivastava, B. N. and A. K. Barua. Effect of relaxation of chemical energy on the thermal conductivity of the system $N_2O_4 \rightleftharpoons 2NO_2$—649
—— **and A. K. Barua.** Thermal conductivity and equilibrium constant of the system $N_2O_4 \rightleftharpoons 2NO_2$—329
Srivastava, G. P. (see Costain, C. C.)—1903(L)
Srivastava, I. B. (see Paul, R.)—1621
Stamires, Dennis N. (see Freeman, Donald C., Jr.)—799
Stammreich, H., K. Kawai, Osw. Sala, and P. Krumholz. Raman spectra of metal carbonyl compounds. III. Raman spectrum, vibrational analysis, and bond structure of nickel tetracarbonyl—2168
——, **K. Kawai, Osw. Sala, and P. Krumholz.** Raman spectra of metal carbonyl compounds. IV. Raman spectra and structure of cadmium and mercury cobalt carbonyl—2175
—— (see Person, Willis B.)—908
Stapleton, H. J. (see Lammermann, H.)—1514(L)
Steele, D. and E. R. Lippincott. Construction of reliable internuclear potential curves from equilibrium bond lengths and vibrational frequencies—2065
—— (see Lippincott, E. R.)—123
Steele, William A. and Marvin Ross. General theory of monolayer physical adsorption on solids—850
—— (see Ross, Marvin)—862, 871
Stein, Richard S. (see Powers, Joseph)—376(L)
Steinberg, M. (see Hacker, D. S.)—1788
Stephens, D. R. and H. G. Drickamer. Effect of pressure on tetrahedral Ni^{++} and Co^{++} complexes—429
—— **and H. G. Drickamer.** Effect of pressure on the spectra of certain complexes of Cu^{++}, Co^{+++}, and Fe^{++}—424
—— **and H. G. Drickamer.** Effect of pressure on the spectrum of ruby—427
Sternlicht, Himan and Harden M. McConnell. Paramagnetic excitons in molecular crystals—1793
Stillinger, Frank H., Jr. Compressibility of simple fused salts—1581
—— Interfacial solutions of the Poisson-Boltzmann equation—1584
Stirpe, D. (see Brock, E. G.)—759(L)
Strauss, Herbert L. and George K. Fraenkel. Carbon-13 hyperfine splitting in the electron spin resonance spectra of semiquinones and cyclooctatetraene—1738
Strehlow, Roger A. and Charles T. Case. Limitations of the reflected shock technique for studying fast chemical reactions—1506(L)
Streng, A. G. (see Kirshenbaum, A. D.)—1440
Strong, H. M. (see Bundy, F. P.)—383
Stroud, Jackson S. Photoionization of Ce^{3+} in glass—844
Suëtaka, Wataru (see Kozima, Kunio)—1516(L)
Suzuki, Satoshi (see Baba, Hiroaki)—1118, 1501(L)
Swalen, J. D. (see Reilly, C. A.)—1522(L)
Swenson, C. A. (see Heltemes, E. C.)—1264
Swets, D. E. (see Frank, R. C.)—1451
Swick, D. A. and J. Karle. Pattern inversion for coherent inelastic electron scattering by Br_2—2257(L)
Szász, Levente. On the evaluation of integrals occurring in the theory of the correlated electronic wave functions—1072

Tadokoro, Hiroyuki. Normal vibrations of the polymer molecules of helical configuration. II. A simple method of factoring of the secular equation—1050
——, **Akira Kobayashi, Yôichi Kawaguchi, Shigenobu Sobajima, Shunsuke Murahashi, and Yoshiki Matsui.** Normal vibrations and Raman spectrum of polyoxymethylene—369(L)
Tanaka, Ikuzo, T. Carrington, and H. P. Broida. Photon-dissociation of water: initial nonequilibrium populations of rotational states of $OH(^2\Sigma^+)$—750(L)
Tatsuzaki, I. (see Bray, P. J.)—435
Taylor, Ellison H. (see Datz, Sheldon)—1549
Taylor, T. I. (see Rush, J. J.)—2265(L)
Templeton, David H. (see Dodge, Richard P.)—55
Thiele, Everett and David J. Wilson. Anharmonicity in unimolecular reactions—1256
Thirunamachandran, T. (see Claxton, T. A.)—1525(L)
Thodos, George (see Hamrin, Charles E., Jr.)—899
Thomas, J. R. (see Baird, J. C.)—1507(L)

Thompson, Don D. and Robert J. S. Brown. Low-field nuclear magnetic resonance of coupled spin—one-half particles—1894(L)
Thorn, R. J. (see Cater, E. David)—608, 619
Thurmann-Moe, Torkild (see Grønvold, Fredrik)—1665
Tiers, George Van Dyke. Fluorine NMR spectroscopy. V. Carbon-13 study of coupling constants between *cis* and *trans* CF_2 groups in highly fluorinated olefins—2263(L)
Tietz, T. Diamagnetic susceptibility in Thomas-Fermi model for Latter's and Byatt's effective charge distribution—1916(L)
—— Negative hydrogen ion—1917(L)
Tobias, Irwin and Walter Kauzmann. Faraday effect in molecules—538
—— **and Joseph T. Vanderslice.** Potential energy curves for the $X^1\Sigma_g^+$ and $B^1\Sigma_u^+$ states of hydrogen—1852
Tobin, Marvin C. Symmetry-adapted LCAO MO's for long-chain polyenes—1905(L)
Toyama, Masaharu (see Morino, Yonezo)—1289
Trulson, O. Conrad, Donald E. Hudson, and Frank H. Spedding. Cohesive energies of europium, gadolinium, holmium, and erbium—1018
Tsuboi, Masamichi (see Shimanouchi, Takehiko)—1597
Turner, R. E. and Donald Rapp. Effect of an attractive potential on the classical theory or vibrational energy exchange—1076
Twidell, J. W. (see Hayes, W.)—1521(L)

Ueda, Hisashi, Zen'ichiro Kuri, and Shoji Shida. Electron spin resonance studies of gamma-irradiated single crystals of sucrose—2145
Ulmer, H. E. (see Johns, I. B.)—1271
Unterleitner, F. (see Brock, E. G.)—759(L)

Valleau, J. P. and W. G. Schneider. Ultrasonic absorption in aqueous hydrogen peroxide solutions—2271(L)
Vanderslice, Joseph T. (see Tobias, Irwin)—1852
van Roggen, A. (see Mill, T.)—1139(L)
Varshni, Yatendra Pal and Ramesh Chandra Shukla. New potential function for alkali halide molecules—582
Vedder, W. and D. F. Hornig. Motion of the ammonium ion in lattices of the NaCl type—1560
Venkataraman, B. (see Das, M. R.)—2262(L)
Verma, G. S. (see Kor, S. K.)—1512(L)
Vestal, M. L. and H. M. Rosenstock. Oscillator models in unimolecular reactions—2008
von Frankenberg, Carl and R. E. Hughes. q-dimensional excluded volume in random flight chains—503

Wacks, Morton E. and Morris Krauss. Franck-Condon factors and the shape of ionization efficiency curves—1902(L)
Wahlig, C. F. (see Mill, T.)—1139(L)
Wahlquist, Hugo. Modulation broadening of unsaturated Lorentzian lines—1708
Wall, F. T., L. A. Hiller, Jr., and J. Mazur. Statistical computation of reaction probabilities. II—1284
Wall, Leo A. (see Ingalls, R. B.)—370(L)
Wallace, W. E. Neutron diffraction data for Ta_2D and the probable arrangement of the deuteriums in two of its polymorphic varieties—2156
—— **and L. M. Epstein.** Fe^{57} Mössbauer effect in laves phases containing Fe combined with Y, Ce, Ho, Ti, Zr, and Hf—2238(L)
—— (see Saba, William G.)—689, 2148
Walnut, Thomas H. (see Neff, Vernon D.)—1723
Wang, Frederick E., Paul G. Simpson, and William N. Lipscomb. Molecular structure of $B_9H_{13}(CH_3CN)$—1335
Watson, G. M. (see Evans, R. B., III)—2076
Waugh, J. S. and S. Castellano. Erratum and further Comments: Exact analysis of three-spin NMR spectra—1900(L)
—— (see Blinc, R.)—1770
—— (see Johnson, C. S., Jr.)—1128(L), 2020
Weatherly, T. L. (see Johnson, R. C.)—2261(L)
Webb, L. A. (see Alger, R. S.)—49
Weigang, O. E., Jr. (see Robertson, W. W.)—464
Weil, John A. and John H. Anderson. Direct field effects in electron paramagnetic resonance hyperfine spectra—1410
Weinberger, Z. (see Avinor, M.)—1978
Weinreb, A. Some effects of temperature and viscosity on fluorescence and energy transfer in solutions—91
Weissman, S. I. (see Zandstra, P. J.)—757(L)
Wenger, F. (see Orofino, T. A.)—532
Wentorf, R. H., Jr. (see Bundy, F. P.)—383
Westrum, Edgar F., Jr., H. Gary Carlson, Fredrik Grønvold, and Arne Kjekshus. Low-temperature heat capacities and thermodynamic functions of some palladium and platinum group chalcogenides. II. Dichalcogenides; PtS_2, $PtTe_2$, and $PdTe_2$—1670
—— (see Grønvold, Fredrik)—1665
Whipple, Earl B. Rotational isomerism in 2, 3 dihalopropenes—1039
Wiberg, Kenneth B. (see Spencer, Glenn H., Jr.)—1925, 1939
Wieder, Harold and A. W. Czanderna. Optical evidence for the direct reduction of CuO to Cu in H_2—2259(L)
Williams, Donald E. (see Atoji, Masao)—1960
Williams, F. E. (see Prener, J. S.)—1803
Williams, H. J. (see Geller, S.)—1908(L)
Williams, Quitman (see Johnson, R. C.)—2261(L)
Wilmshurst, J. K. Vibrational spectra of inorganic molecules. III. Infrared reflections spectra of molten lithium, sodium, and potassium hydroxides—1800
—— **and S. Senderoff.** Vibrational spectra of inorganic molecules. II. Infrared reflection spectra of liquid lithium, sodium, potassium, and silver nitrates—1078
Wilson, David J. (see Dohner, Abraham S.)—1510(L)
—— (see Thiele, Everett)—1256
Wilson, E. Bright, Jr. (see Dixon, William B.)—191
Wilson, Russell L. and George H. Duffey. Parameterization of orthogonality and normalization conditions for the NbF_7^{-2} structure—568
Wise, Henry and Clarence M. Ablow. Diffusion and heterogeneous reaction. IV. Effects of gas-phase reaction and convective flow—10
—— (see Gatz, C.)—1500(L)
Witteman, W. J. Vibrational relaxation in carbon dioxide—1
Witten, L. (see Aranow, R. H.)—1504(L)
Woessner, D. E. Nuclear transfer effects in nuclear magnetic resonance pulse experiments—41
Wolfgang, R. (see Cross, R. J., Jr.)—2002
Wong, Eugene Y. Taylor series expansion of the intermediate coupling energy levels of Nd^{3+} and Er^{3+}—544
Wood, Bernard J. and A. Bruce King. Substitution of a catalytic probe for a tube of infinite length in atom recombination experiments—1530(L)
Wood, D. L. (see Ferguson, J.)—2236(L)
—— (see Pappalardo, R.)—1460, 2041
Wright, H. E. (see Eggers, D. F., Jr.)—1045
Wu, Ellen L., Giuseppe Zerbi, Salvatore Califano, and Bryce Crawford, Jr. Normal vibrations and Urey-Bradley force constants of methyl amine—2060
Wyard, S. J. (see Smith, Robert C.)—2254(L)
Wybourne, B. G. Electrostatic energy matrices of the f^5 and f^6 configurations—340
—— Spin-orbit interactions in f^n electron configurations—334
Wyluda, B. J. (see Shulman, R. G.)—1498

Yang, Kang and Taikyue Ree. Collision and activated complex theories for bimolecular reactions—588

Yates, D. J. C. and P. J. Lucchesi. Infrared spectra of acetylene and acetylene derivatives adsorbed on alumina and silica—243

Zahner, J. C. and H. G. Drickamer. Effect of pressure on crystal-field energy and covalency in octahedral complexes of Ni^{2+}, Co^{2+}, and Mn^{2+}—1483

—— **and H. G. Drickamer.** Effect of pressure on the electronic absorption spectra of ferrocene and ferricinium ion—375(L)

Zalkin, Allan (see Dodge, Richard P.)—55

Zandstra, P. J. and S. I. Weissman. Note on measurements of rates of electron transfer processes by broadening of ESR lines—757(L)

Zeldes, Henry and Ralph Livingston. Paramagnetic species in irradiated $NaNO_2$—563

Zerbi, Giuseppe (see Wu, Ellen L.)—2060

THE JOURNAL OF CHEMICAL PHYSICS VOLUME 35, NUMBER 6 DECEMBER, 1961

Analytic Subject Index to Volume 35

References with (L) are to Letters to the Editor

Absorption Spectra, Infrared

Absolute infrared intensities of the CS_2 fundamentals in CCl_4 solution and of the 768–797 cm^{-1} Fermi doublet of CCl_4 in cyclohexane solution, Otto F. Kalman and J. C. Decius—1919

Absolute infrared intensity measurements in thin films, Shiro Maeda and P. N. Schatz—1617

Analysis of the infrared absorption spectrum of AM^{+3} ($5f^6$) in $LaCl_3$, John B. Gruber—2186

Approximate mean-square amplitudes of characteristic two-atom vibrations, C. J. G. Raw and C. Kuenz—1529(L)

Atomic polarization. II. Vibrational polarization of liquids, Karl H. Illinger and Charles P. Smyth—392

Atomic polarization. V. Normal mode polarizability and the additivity of the vibrational polarization, Karl H. Illinger—409

Effect of temperature on the intensity and structure of bands in the infrared spectrum of rhombic sulfur, Vernon D. Neff and Thomas H. Walnut—1723

Electronic structure, spectra, and magnetic properties of oxycations. III. Ligation effects on the infrared spectrum of the uranyl ion, S. P. McGlynn, J. K. Smith, and W. C. Neely—105

Erratum: Far infrared spectrum of disiloxane [J. Chem. Phys. **33**, 1004 (1960)], D. W. Robinson, W. J. Lafferty, J. R. Aronson, J. R. Durig, and R. C. Lord—2245(L)

High-resolution study of CO_2 absorption spectra between 15 and 18 microns, Robert P. Madden—2083

Hydrogen-bonding interaction between adsorbate molecules and surface hydroxyl groups on silica, Michael R. Basila—1151

Infrared and raman spectra, force constants, and the structures of some polyhalide ions: ICl_2^-, ICl_4^-, $BrCl_2^-$, and Br_3^-, Willis B. Person, George R. Anderson, James N. Fordemwalt, H. Stammreich, and Roberto Forneris—908

Infrared spectra of acetylene and acetylene derivatives adsorbed on alumina and silica, D. J. C. Yates and P. J. Lucchesi—241

Infrared spectra of carbon monoxide as a solid and in solid matrices, Arthur G. Maki—931

Infrared spectra of NaOH above and below the melting point, Jacob Greenberg and L. J. Hallgren—180

Infrared spectra of sodium and potassium cyanide, George E. Leroi and William Klemperer—774

Infrared spectra of synthetic diamond, J. J. Charette—1906(L)

Infrared spectroscopic study of the photolysis of chlorine azide in solid argon at 4.2°K, Dolphus E. Milligan—372(L)

Infrared spectroscopic study of the photolysis of methyl azide and methyl-d_3 azide in solid argon and carbon dioxide, Dolphus E. Milligan—1491

Infrared spectrum and molecular configuration of glutaronitrile, Ikuo Matsubara—373(L)

Infrared spectrum and structure of the NF_2 radical, Marlin D. Harmony, Rollie J. Myers, L. J. Schoen, David R. Lide, Jr., and D. E. Mann—1129(L)

Infrared spectrum of CF_3SF_5, D. F. Eggers, Jr., H. E. Wright, and D. W. Robinson—1045

Infrared spectrum of solid carbon monoxide, George E. Ewing and George C. Pimentel—925

Intermolecular coupling of vibrations in molecular crystals. II. Intermolecular forces in CH_3Cl and CD_3Cl, David A. Dows—282

Motion of the ammonium ion in lattices of the NaCl type, W. Vedder and D. F. Hornig—1560

Motions of molecules in condensed systems. X. The infrared spectrum and structure of a single crystal of cyclopropane, Charles Brecher, Esther Krikorian, Joseph Blanc, and Ralph S. Halford—1097

Motions of molecules in condensed systems. XI. The infrared spectrum and structure of a single crystal of ethylene, Charles Brecher and Ralph S. Halford—1109

On a reported new form of ice, J. Schiffer and D. F. Hornig—1136(L)

Preparation and optical transmission of cadmium fluoride crystals, J. S. Prener and J. D. Kingsley—2256(L)

Proton magnetic resonance study of ferroelectric potassium ferrocyanide trihydrate, R. Blinc, M. Brenman, and J. S. Waugh—1770

Radiolyses by transferred energy of compounds dispersed in alkali halide matrices, A. Russell Jones—751(L)

Rotational isomerism in 2, 3 dihalopropenes, Earl B. Whipple—1039

"Rotational" isomers of cyclopentane derivatives, Kunio Kuzima and Wataru Suëtaka—1516(L)

s-Tetrazine. I. High-resolution vapor phase study of the visible $n \rightarrow \pi^*$ vibronic absorption band systems, Glenn H. Spencer, Jr., Paul C. Cross, and Kenneth B. Wiberg—1925

s-Tetrazine. II. Infrared spectra, Glenn H. Spencer, Jr., Paul C. Cross, and Kenneth B. Wiberg—1939

Simultaneous infrared absorption involving rotational transitions of H_2, J. A. A. Ketelaar and R. P. H. Rettschnick—1909(L)

Solid-state vibrational spectra of the methyl and methyl-d_3 halides, Marilyn E. Jacox and Robert M. Hexter—183
Stretching vibration of sulfate ion in potassium chloride: Formation of $M^{++}SO_4^{=}$ pairs, E. Howard Coker, J. C. Decius, and A. B. Scott—745(L)
Studies of the optical and infrared absorption spectra of rutile single crystals, Bernard H. Soffer—940
Theory and measurement of pressure-induced shifts of HCl lines due to noble gases, A. Ben-Reuven, S. Kimel, M. A. Hirshfeld, and J. H. Jaffe—955
Variation of the intensity of the methyl symmetrical bending vibration in paraffins, Michael R. Basila and George F. Crable—306
Vibrational spectra of inorganic molecules. II. The infrared reflection spectra of liquid lithium, sodium, potassium, and silver nitrates, J. K. Wilmshurst and S. Senderoff—1078
Vibrational spectra of inorganic molecules. III. The infrared reflection spectra of molten lithium, sodium, and potassium hydroxides, J. K. Wilmshurst—1800

Absorption Spectra, Microwave

Internal rotation of *cis* 2,3-epoxybutane from the microwave spectrum, Martin L. Sage—142
Microwave spectrum and barrier to internal rotation of methyl stannane, Patrick Cahill and Samuel Butcher—2255(L)
Microwave spectrum and internal barrier of methylphosphine, Takeshi Kojima, Edward L. Breig, and Chun C. Lin—2139
Microwave spectrum, dipole moment, structure, and internal rotation of dimethyl sulfide, Louis Pierce and Michiro Hayashi—479
Microwave spectrum of methyl nitrate, William B. Dixon and E. Bright Wilson, Jr.—191
Microwave spectrum, structure, and dipole moment of F_2O, Louis Pierce, Robert Jackson, and Nicholas DiCianni—2240(L)
Molecular structure of propylene, David R. Lide, Jr., and Daniel Christensen—1374
Study of hydrogen bonding. The microwave rotation spectrum of CF_3COOH—HCOOH, C. C. Costain and G. P. Srivastava—1903(L)

Absorption Spectra, of Crystals

A Taylor series expansion of the intermediate coupling energy levels of Nd^{+3} and Er^{+3}, Eugene Y. Wong—544
Absorption and fluorescence spectra with magnetic properties of $ErCl_3$, G. H. Dieke and Shobha Singh—555
Absorption spectra of vanadium, niobium and tantalum, D. C. Conlon and W. P. Doyle—752(L)
Analysis of the absorption spectrum of $YbCl_3 \cdot 6H_2O$, J. C. Eisenstein—2097
Analysis of the infrared absorption spectrum of $Am^{+3}(5f^6)$ in $LaCl_3$, John B. Gruber—2186
Analysis of the polarized crystal spectra. The spectrum of cobalt (III) acetylacetonate, T. S. Piper—1240
Analysis of the spectra of trivalent promethium and holmium, M. H. Crozier and W. A. Runciman—1392
Crystal spectra of metal coordination compounds. VI. Bis-salicylaldiminato-copper (II) and bis-*N*-methyl-salicylaldiminato-copper (II), J. Ferguson—1612
Crystal splitting of the anthracene 3800 A system, T. A. Claxton, D. P. Craig, and T. Thirunamachandran—1525(L)
Effect of next nearest neighbor ions on the crystal field splitting of transition metal ions in crystals, J. Ferguson, K. Knox, and D. L. Wood—2236(L)
Effect of pressure and temperature on the absorption spectra of four alkali halide phosphors, A. S. Balchan and H. G. Drickamer—359
Effect of pressure on crystal-field energy and covalency in octahedral complexes of Ni^{2+}, Co^{2+}, and Mn^{2+}, J. C. Zahner and H. G. Drickamer—1483
Effect of pressure on tetrahedral Ni^{++} and Co^{++} complexes, D. R. Stephens and H. G. Drickamer—429
Effect of pressure on the charge transfer spectra of heavy transition metal hexahalide complexes, A. S. Balchan and H. G. Drickamer—356
Effect of pressure on the spectra of certain complexes of Cu^{++}, Co^{+++}, and Fe^{++}, D. R. Stephens and H. G. Drickamer—424
Effect of pressure on the spectra of transition metal ions in MgO and Al_2O_3, S. Minomura and H. G. Drickamer—903
Effect of pressure on the spectrum of ruby, D. R. Stephens and H. G. Drickamer—427
Effect of temperature on the intensity and structure of bands in the infrared spectrum of rhombic sulfur, Vernon D. Neff and Thomas H. Walnut—1723
Electronic structure, spectra, and magnetic properties of oxycations. III. Ligation effects on the infrared spectrum of the uranyl ion, S. P. McGlynn, J. K. Smith, and W. C. Neely—105
Energy levels of $PrCl_3$, Jack S. Margolis—1367
Infrared spectra of carbon monoxide as a solid and in solid matrices, Arthur G. Maki—931
Infrared spectra of NaOH above and below the melting point, Jacob Greenberg and L. J. Hallgren—180
Infrared spectra of synthetic diamond, J. J. Charette—1906(L)
Infrared spectrum of solid carbon monoxide, George E. Ewing and George C. Pimentel—925
Intermolecular coupling of vibrations in molecular crystals. II. Intermolecular forces in CH_3Cl and CD_3Cl, David A. Dows—282
Motion of the ammonium ion in lattices of the NaCl type, W. Vedder and D. F. Hornig—1560
Motions of molecules in condensed systems. X. The infrared spectrum and structure of a single crystal of cyclopropane, Charles Brecher, Esther Krikorian, Joseph Blanc, and Ralph S. Halford—1097
Motions of molecules in condensed systems. XI. The infrared spectrum and structure of a single crystal of ethylene, Charles Brecher and Ralph S. Halford—1109
On a reported new form of ice, J. Schiffer and D. F. Hornig—1136(L)
On the optical absorption of $K_2[Cr(CN)_5NO] \cdot H_2O$, C. S. Naiman—1503(L)
Optical absorption spectra of Ni-doped oxide systems. I, R. Pappalardo, D. L. Wood, and R. C. Linares, Jr.—1460
Optical absorption study of Co-doped oxide systems. II, R. Pappalardo, D. L. Wood, and R. C. Linares, Jr.—2041
Optical and paramagnetic resonance spectra of trivalent Pu^{239} in the trichloride and ethylsulfate, H. Lammermann and H. J. Stapleton—1514
Optically active lattice vibrations as treated by the GF-matrix method, Takehiko Shimanouchi, Masamichi Tsuboi, and Tatsuo Miyazawa—1597
Polarized visible spectra of crystalline trisoxalatometallates, T. S. Piper and Richard L. Carlin—1809
Proton magnetic resonance study of ferroelectric potassium ferrocyanide trihydrate, R. Blinc, M. Brenman, and J. S. Waugh—1770
s-Tetrazine. II. Infrared spectra, Glenn H. Spencer, Jr., Paul C. Cross, and Kenneth B. Wiberg—1939
Solid-state vibrational spectra of the methyl and methyl-d_3 halides, Marilyn E. Jacox and Robert M. Hexter—183
Spectrum and magnetic properties of hexagonal $DyCl_3$, H. M. Crosswhite and G. H. Dieke—1535
Stretching vibration of sulfate ion in potassium chloride: Formation of $M^{++}SO_4^{=}$ pairs, E. Howard Coker, J. C. Decius, and A. B. Scott—745(L)
Studies of the optical and infrared absorption spectra of rutile single crystals, Bernard H. Soffer—940

Absorption Spectra, Visible or Ultraviolet

A Taylor series expansion of the intermediate coupling energy levels of Nd^{+3} and Er^{+3}, Eugene Y. Wong—544
Absorption and fluorescence spectra with magnetic properties of $ErCl_3$, G. H. Dieke and Shobha Singh—555
Absorption spectra of anodic tantalum oxide films, Wendell M. Graven—1526(L)
Absorption spectra of vanadium, niobium, and tantalum, D. C. Conlon and W. P. Doyle—752(L)
Absorption spectrum of gaseous Cl^- and electron affinity of chlorine, R. Stephen Berry, Curt W. Reimann, and G. Neil Spokes—2237(L)
Analysis of the absorption spectrum of $YbCl_3 \cdot 6H_2O$, J. C. Eisenstein—2097
Analysis of the polarized crystal spectra. The spectrum of cobalt (III) acetylacetonate, T. S. Piper—1240
Analysis of the spectra of trivalent promethium and holmium, M. H. Crozier and W. A. Runciman—1392
Charge transfer spectra of some gold (III) complexes, Arun Kumar Gangopadhayay and Animesh Chakravorty—2206
Comments on a communication by El-Sayed and Robinson, Mostafa El-Sayed and G. Wilse Robinson—1896(L)
Comprehensive investigation of the electronic spectroscopy and theoretical treatments of ferrocene and nickelocene, Donald R. Scott and Ralph S. Becker—516
Construction of othogonalized LCAO wave functions for the *F* center from ENDOR data, Albert Gold—2180
Crystal spectra of metal coordination compounds. VI. Bis-salicylaldiminato-copper (II) and bis-*N*-methyl-salicylaldiminato-copper (II), J. Ferguson—1612
Crystal splitting of the anthracene 3800 A system, T. A. Claxton, D. P. Craig, and T. Thirunamachandran—1525(L)
Determination of excited-state dipole moments of azulene, W. W. Robertson, A. D. King, Jr., and O. E. Weigang, Jr. —464
Effect of next nearest neighbor ions on the crystal field splitting of transition metal ions in crystals, J. Ferguson, K. Knox and D. L. Wood—2236(L)
Effect of pressure and temperature on the absorption spectra of four alkali halide phosphors, A. S. Balchan and H. G Drickamer—359
Effect of pressure on crystal-field energy and covalency in octahedral complexes of Ni^{2+}, Co^{2+}, and Mn^{2+}, J. C. Zahner and H. G. Drickamer—1483
Effect of pressure on tetrahedral Ni^{++} and Co^{++} complexes, D. R. Stephens and H. G. Drickamer—429
Effect of pressure on the charge transfer spectra of heavy transition metal hexahalide complexes, A. S. Balchan and H. G. Drickamer—356
Effect of pressure on the electronic absorption spectra of ferrocene and ferricinium ion, J. C. Zahner and H. G. Drickamer —375(L)
Effect of pressure on the low-energy absorption peak of several phthalocyanines, B. M. Riggleman and H. G. Drickamer—1343
Effect of pressure on the optical properties of organic phosphors, D. W. Gregg and H. G. Drickamer—1780
Effect of pressure on the spectra of certain complexes of Cu^{++}, Co^{+++}, and Fe^{++}, D. R. Stephens and H. G. Drickamer—424
Effect of pressure on the spectra of transition metal ions in MgO and Al_2O_3, S. Minomura and H. G. Drickamer—903
Effect of pressure on the spectrum of ruby, D. R. Stephens and H. G. Drickamer—427
Electronic spectra and hydrogen bonding. I. Phenol and naphthols, Hiroaki Baba and Satoshi Suzuki—1118
Electronic spectra of substituted anthracenes. Evidences for appearance of the ^1L_b transition, Hiroaki Baba and Satoshi Suzuki—1501(L)
Energy levels of $PrCl_3$, Jack S. Margolis—1367
Erratum: Comprehensive investigation of the electronic spectroscopy and theoretical treatments of ferrocene and nickelocene [J. Chem. Phys. **35,** 516 (1961)], Donald R. Scott and Ralph S. Becker—2246(L)
Erratum: Magnetic properties and optical absorption spectrum of K_2ReCl_6 [J. Chem. Phys. **34,** 1628 (1961)], J. C. Eisenstein —2246(L)
Interpretation of the absorption spectra of $K_3Fe(CN)_6$, C. S. Naiman—323
Intramolecular charge-transfer bands observed in the spectra of some aryl boron compounds, B. Ramsey, M. Ashraf El-Bayoumi, and M. Kasha—1502(L)
Kinetics of the photolysis of sodium azide, Jack G. Dodd—1815
Low-resolution analysis of the $n \rightarrow \pi^*$ (3000 A) absorption spectrum of *s*-triazine, J. S. Brinen and Lionel Goodman—1219
Molar extinction coefficients of liquid O_3F_2, O_2F_2, and O_3 in the visible range, A. D. Kirshenbaum and A. G. Streng—1440
Optical absorption spectra of Ni-doped oxide systems. I. R. Pappalardo, D. L. Wood, and R. C. Linares, Jr.—1460
Optical absorption study of Co-doped oxide systems. II, R. Pappalardo, D. L. Wood, and R. C. Linares, Jr.—2041
Optical and paramagnetic resonance spectra of trivalent Pu^{239} in the trichloride and ethylsulfate, H. Lammermann and H. J. Stapleton—1514
Optical evidence for the direct reduction of CuO to Cu in H_2, Harold Wieder and A. W. Czanderna—2259(L)
Organic semiconductors: Aromatic hydrocarbon positive ions in solids, G. E. Blomgren and J. Kommandeur—1636
Paramagnetic resonance of some silver (II) compounds, J. A. McMillan and B. Smaller—1697
Photo-ionization of Ce^{+3} in glass, Jackson S. Stroud—844
Photon-dissociation of water: Initial nonequilibrium populations of rotational states of OH ($^2\Sigma^+$), I. Tanaka, T. Carrington, and H. P. Broida—750(L)
Polarized visible spectra of crystalline trisoxalatometallates, T. S. Piper and Richard L. Carlin—1809
Preparation and optical transmission of cadmium fluoride crystals, J. S. Prener and J. D. Kingsley—2256(L)
Remarks on the electronic spectra and structure of compounds of chromium and benzene, R. Stephen Berry—29
s-Tetrazine. I. High-resolution vapor phase study of the visible $n \rightarrow \pi^*$ vibronic absorption band systems, Glenn H. Spencer, Jr., Paul C. Cross, and Kenneth B. Wiberg—1925
Spectrum and magnetic properties of hexagonal $DyCl_3$, H. M. Crosswhite and G. H. Dieke—1535
Spectrum of NBr excited in active nitrogen, Earl R. V. Milton, H. B. Dunford, and A. E. Douglas—1202
Structure of the band spectrum of CuCl molecule. I. Additional knowledge in the coarse structure, P. Ramakoteswara Rao and J. K. Brody—776
Studies of the optical and infrared absorption spectra of rutile single crystals, Bernard H. Soffer—940
Ultraviolet absorption spectra of alkali metal azides, S. K. Deb —2122
Ultraviolet absorption spectrum of ammonia in solid argon at 4.2°K, K. Dressler—165
Ultraviolet spectrum of dibenzene chromium vapor, R. Stephen Berry—2025

Adsorption (see Surface Phenomena)

Beams, Atomic, and Molecular

Charge exchange between krypton ions and atoms, S. B. Karmohapatro—1524(L)
Chemionization in three-body gas phase reactions, C. Gatz, F. T. Smith, and H. Wise—1500(L)
Collision mechanics in crossed Maxwellian molecular beams, Sheldon Datz, Dudley R. Herschbach, and Ellison H. Taylor—1549

Elastic and inelastic scattering of low-velocity H^+ and H_2^+ in hydrogen, W. H. Cramer—836
Scattering of high velocity neutral particles. XII. He—CH_4; He—CF_4. The CH_4—CH_4 and CF_4—CF_4 interactions, I. Amdur, M. S. Longmire, and E. A. Mason—895

Catalysis

Studies of transient species formed during catalytic reactions of CO_2+D_2 and of 1-butene, Charles E. Melton—1751

Chemical Reactions (see Kinetics of Reactions)

Combustion

Recombination of ions in flames. Effect of temperature, I. R. King—380(L)

Conductance

Resonance transfer model of electron and hole conduction in anthracene, David Kearns—2269(L)

Crystal Growth

Diamond-graphite equilibrium line from growth and graphitization of diamond, F. P. Bundy, H. P. Bovenkerk, H. M. Strong, and R. H. Wentorf, Jr.—383
Evaporation of zinc whiskers, J. B. Hudson and G. W. Sears—1509(L)
Growth of zinc crystals from the vapor phase, Robert L. Parker and Lawrence M. Kushner—1345
Markoff chain model for growth of polymer single crystals, Fraser P. Price—1884
Surface energy effect on diffusion-controlled particle growth, G. A. Somorjai—655

Crystalline State

Addendum: Kinetic model for solid-state reactions [J. Chem. Phys. **34**, 2010 (1961)], R. E. Carter—1137(L)
Anisotropy of nuclear magnetic resonance in vanadium pentoxide, J. L. Ragle—753(L)
Atomic forces and thermal effects in solids, Herbert B. Rosenstock—420
Band structure and transport of holes and electrons in anthracene, Oliver H. LeBlanc, Jr.—1275
Charge distribution and electric field gradients in ionic crystals, Geneva G. Belford, Robert A. Bernheim, and H. S. Gutowsky—1032
Construction of othogonalized LCAO wave functions for the *F* center from ENDOR data, Albert Gold—2180
Effect of interstitial Li on the density of Si, J. S. Prener and F. E. Williams—1803
Effect of next nearest neighbor ions on the crystal field splitting of transition metal ions in crystals, J. Ferguson, K. Knox, and D. L. Wood—2236(L)
Effect of pressure on tetrahedral Ni^{++} and Co^{++} complexes, D. R. Stephens and H. G. Drickamer—429
Electrical resistivity of cubic sodium tungsten bronze, L. D. Ellerbeck, H. R. Shanks, P. H. Sidles, and G. C. Danielson—298
Electron spin resonance of an irradiated single crystal of urea oxalate, D. V. G. L. Narasimha Rao and Walter Gordy—362
Energy value of the octahedral-tetrahedral coordination change, Leonard I. Katzin—467
Erratum: Magnetic properties and optical absorption spectrum of K_2ReCl_6 [J. Chem. Phys. **34**, 1628)], J. C. Eisenstein—2246(L)
Fe^{57} Mössbauer effect in laves phases containing Fe combined with Y, Ce, Ho, Ti, Zr, and Hf, W. E. Wallace and L. M. Epstein—2238(L)
Further notes on the magnetic centers in neutron-irradiated calcite, James C. Kemp—377(L)
Heat capacities and the residual entropy of Ta_2H, W. G. Saba, W. E. Wallace, H. Sandmo, and R. S. Craig—2148
Infrared spectrum of solid carbon monoxide, George E. Ewing and George C. Pimentel—925
Intermolecular coupling of vibrations in molecular crystals. II. Intermolecular forces in CH_3Cl and CD_3Cl, David A. Dows—282
Motion of the ammonium ion in lattices of the NaCl type, W. Vedder and D. F. Hornig—1560
Motions of molecules in condensed systems. X. The infrared spectrum and structure of a single crystal of cyclopropane, Charles Brecher, Esther Krikorian, Joseph Blanc, and Ralph S. Halford—1097
Motions of molecules in condensed systems. XI. The infrared spectrum and structure of a single crystal of ethylene, Charles Brecher and Ralph S. Halford—1109
Nuclear magnetic resonance studies of B^{11} in crystalline borates, P. J. Bray, J. O. Edwards, J. G. O'Keefe, V. F. Ross, and I. Tatsuzaki—435
Optically active lattice vibrations as treated by the GF-matrix method, Takehiko Shimanouchi, Masamichi Tsuboi, and Tatsuo Miyazawa—1597
Paramagnetic excitons in molecular crystals, Himan Sternlicht and Harden M. McConnell—1793
Proton motions in solids by slow neutron scattering cross sections, J. J. Rush, T. I. Taylor, and W. W. Havens, Jr.—2265(L)
Recalculation of the surface energies of alkali halide crystals, G. C. Benson—2113
Solid-state vibrational spectra of the methyl and methyl-d_3 halides, Marilyn E. Jacox and Robert M. Hexter—183

Crystal Structure

Crystal structure of vanadyl bisacetyl-acetonate geometry of vanadium in fivefold coordination, Richard P. Dodge, David H. Templeton, and Allan Zalkin—55
Electron density distributions in ZnO crystals, Ganesh P. Mohanty and Leonid V. Azároff—1268
Molecular structure of $B_9H_{13}(CH_3CN)$, Frederick E. Wang, Paul G. Simpson, and William N. Lipscomb—1335
Neutron diffraction data for Ta_2D and the probable arrangement of the deuteriums in two of its polymorphic varieties, W. E. Wallace—2156
Neutron-diffraction studies of CaC_2, YC_2, LaC_2, CeC_2, TbC_2, YbC_2, LuC_2, and UC_2, Masao Atoji—1950
Neutron-diffraction studies of La_2C_3, Ce_2C_3, Pr_2C_3, and Tb_2C_3, Masao Atoji and D. E. Williams—1960
Neutron diffraction study of solid deuteroammonia, John W. Reed and P. M. Harris—1730
On a reported new form of ice, J. Schiffer and D. F. Hornig—1136(L)
Polyhedral clathrate hydrates, Part 2. The structure of the hydrate of tetra iso-amyl ammonium fluoride, D. Feil and G. A. Jeffrey—1863
Refinement of the B_9H_{13} structure and test for solid solutions, Paul G. Simpson and William N. Lipscomb—1340
Substitution of Fe^{3+} ion in Sc_2O_3 and In_2O_3, S. Geller, H. J. Williams, and R. C. Sherwood—1908(L)

Detonation (see also Shock Waves)

Gaseous detonations. XIII. Rotational and vibrational distributions of OH radicals, G. B. Kistiakowsky and R. K. Lyon—995

Deuterium (see Isotopes)

Dielectrics

Atomic polarization. II. Vibrational polarization of liquids, Karl H. Illinger and Charles P. Smyth—392
Atomic polarization. III. Vibrational polarization terms associated with forbidden transitions in polyatomic molecules, Karl H. Illinger and Charles P. Smyth—397
Atomic polarization. IV. Temperature dependence of the vibrational polarization of gases, Karl H. Illinger and Charles P. Smyth—400
Atomic polarization. V. Normal mode polarizability and the additivity of the vibrational polarization, Karl H. Illinger—409
Calculation of depolarization ratios, anisotropies, and average dimensions of *n*-alkanes, Richard P. Smith and Earl M. Mortensen—714
Determination of excited-state dipole moments of azulene, W. W. Robertson, A. D. King, Jr., and O. E. Weigang, Jr.—464
Dipole moment of HD. II, S. M. Blinder—974
Dipole moments of α,ω-dibromoparaffins and their temperature dependence, H. J. G. Hayman and I. Eliezer—644
Energy and free energy of cohesion, Bruno Linder—371(L)
Extension of Stokes' law for ionic motion to include the effect of dielectric relaxation, Richard H. Boyd—1281
Homopolar dipole, C. A. Coulson and Max T. Rogers—593
Influence of the dielectric constant on the ultrasonic relaxation frequency in $MnSO_4$ solutions, S. K. Kor and G. S. Verma—1512(L)
Microwave spectrum, dipole moment, structure, and internal rotation of dimethyl sulfide, Louis Pierce and Michiro Hayashi—479
Microwave spectrum of methyl nitrite, William B. Dixon and E. Bright Wilson, Jr.—191
Nonresonant dielectric dispersion in asymmetric rotors, James E. Boggs and A. P. Deam—1178
Permanent dipole moments of saturated hydrocarbons, Ricardo Ferreira—755(L)
Proton magnetic resonance study of ferroelectric $NaH_3(SeO_3)_2$ and $LiH_3(SeO_3)_2$, R. Blinc and M. Pintar—1140(L)
Proton magnetic resonance study of ferroelectric potassium ferrocyanide trihydrate, R. Blinc, M. Brenman, and J. S. Waugh—1770
Solvent effects on optical rotation and dipole moment, A. J. Mukhedkar—2133

Diffusion

Determination of molecular diffusivity by gas chromatography techniques, James J. Carberry and Randolph H. Bretton—2241(L)
Diffusion and heterogeneous reaction. IV. Effects of gas phase reaction and convective flow, Henry Wise and Clarence M. Ablow—10
Diffusion of Kr and He in liquid hydrogen, G. Cini Castagnoli—1999
Diffusion of neon isotopes in fused quartz, R. C. Frank, D. E. Swets, and R. W. Lee—1451
Gaseous diffusion in porous media at uniform pressure, R. B. Evans, III, G. M. Watson and E. A. Mason—2076
Measurement of electrodiffusion. Effect of electrosmosis on diffusion, P. C. Scholten and Karol J. Mysels—1845
Mutual diffusion of the gas pairs H_2—Ne, H_2—Ar, and H_2—Xe at different temperatures, R. Paul and I. B. Srivastava—1621
Rapid diffusional analysis by chromatographic methods, J. Calvin Giddings and Spencer L. Seager—2242(L)
Self-diffusion and velocity correlation, Dean C. Douglass—81
Surface energy effect on diffusion-controlled particle growth, G. A. Somorjai—655

Dipole Moment

Dipole moment of $CClF_3$, R. C. Johnson, T. L. Weatherly, and Quitman Williams—2261(L)
Microwave spectrum, structure and dipole moment of F_2O, Louis Pierce, Robert Jackson, and Nicholas DiCianni—2240(L)

Electrical Properties

Adsorption and electrical conduction in thin films, Gert Ehrlich—2165
Band structure and transport of holes and electrons in anthracene, Oliver H. LeBlanc, Jr.—1275
Electrical conductivity and thermodynamic equilibrium in nickel oxide, S. P. Mitoff—882
Electrical conductivity of monocrystalline cuprous oxide, Michael O'Keeffe and Walter J. Moore—1324
Electrical conductivity of synthetic crystalline zeolites, Donald C. Freeman, Jr., and Dennis N. Stamires—799
Electrical properties of nonstoichiometric uranium dioxide, S. Aronson, J. E. Rulli, and B. E. Schaner—1382
Electrical resistivity of cubic sodium tungsten bronze, L. D. Ellerbeck, H. R. Shanks, P. H. Sidles, and G. C. Danielson—298
Measurement of the resistivity of cesium at elevated temperatures, J. Hyman, Jr.—992
Organic semiconductors: Aromatic hydrocarbon positive ions in solids, G. E. Blomgren and J. Kommandeur—1636
Organic semiconductors. V. Comparison of measurements on single crystal and compressed microcrystalline molecular complexes, Paul L. Kronick and Mortimer M. Labes—2016
Photo- and semiconduction in crystalline chlorophylls *a* and *b*, Barnett Rosenberg and James F. Camiscoli—982
Quenching effects and negative photo-conductivity in amorphour selenium, J. Dresner—1628

Electrochemistry

Extension of Stokes' law for ionic motion to include the effect of dielectric relaxation, Richard H. Boyd—1281
Interfacial solutions of the Poisson-Boltzmann Equation, Frank H. Stillinger, Jr.—1584
Measurement of electrodiffusion. Effect of electrosmosis on diffusion, P. C. Scholten and Karol J. Mysels—1845
On the polyelectrolyte-simple electrolyte interaction parameter, Norio Ise—1145(L)
On the theory of ion pairs in solutions, Jacques C. Poirier and James H. DeLap—213
Salt effect in metal-ammonia solutions: Sodium chloride in sodium-ammonia solution at −33°C, Donald S. Berns, Gerard Lepoutre, Elizabeth A. Bockelman, and Andrew Patterson, Jr.—1820

Electron Diffraction

Approximate mean-square amplitudes of characteristic two-atom vibrations, C. J. G. Raw and C. Kuenz—1529(L)
Effects of anharmonicity of molecular vibrations on the diffraction of electrons. II. Interpretation of experimental structural parameters, Kozo Kuchitsu and L. S. Bartell—1945
Excited states of molecules and the scattering of fast electrons, J. Karle—963
Mean and equilibrium molecular structures of methane and deuteromethane as determined by electron diffraction, L. S. Bartell, Kozo Kuchitsu, and R. J. deNeui—1211

Emission Spectra

Coherent stimulated emission from organic molecular crystals, E. G. Brock, P. Csavinszky, E. Hormats, H. C. Nedderman, D. Stirpe, and F. Unterleitner—759(L)
Effect of pressure on the optical properties of organic phosphors, D. W. Gregg and H. G. Drickamer—1780

Evidence for a long-lived metastable state of N_2 at about 8 ev, Carl Kenty—2267(L)
Identification of an electronic transition of N_2^{++}, P. K. Carroll and A. C. Hurley—2247(L)
Infrared chemiluminescence in the system H+NOCl, J. K. Cashion and J. C. Polyanyi—600
Nickel-activated calcium and strontium sulfide phosphors, M. Avinor, A. Carmi, and Z. Weinberger—1978
Polarized phosphorescence in crystalline hexachlorobenzene at 77°K, Dan W. Olds—2248(L)

Energy Transfer

Effect of an attractive potential on the classical theory of vibrational energy exchange, R. E. Turner and Donald Rapp—1076
Gaseous detonations. XIII. Rotational and vibrational distributions of OH radicals, G. B. Kistiakowsky and R. K. Lyon—995
Multiple vibrational relaxation in gaseous dibromomethane, P. G. Dickens and D. Schofield—374
Some effects of temperature and viscosity on the fluorescence and energy transfer in solutions, A. Weinreb—91
Transition probabilities in multilevel systems: Calculation from impulsive and steady-state experiments, Tucker Carrington—807
Vibrational relaxation in carbon dioxide, W. J. Witteman—1

Errata

Erratum and further comments: Exact analysis of three-spin NMR spectra [J. Chem. Phys. **34**, 295 (1961)], J. S. Waugh amd S. Castellano—1900(L)
Erratum: Binding energies of alkali halide molecules [J. Chem. Phys. **34**, 2069 (1961)], G. M. Rothberg—1137(L)
Erratum: Comprehensive investigation of the electronic spectroscopy and theoretical treatments of ferrocene and nickelocene [J. Chem. Phys. **35**, 516 (1961)], Donald R. Scott and Ralph S. Becker—2246(L)
Erratum: Development of the liquid equation and the partial structure of water [J. Chem. Phys. **34**, 2174 (1961)], Robert Ginell—1135(L)
Erratum: Effect of electron energy on some electron-impact processes [J. Chem. Phys. **34**, 2046 (1961)], Seymour Meyerson—1137(L)
Erratum: Far infrared spectrum of disiloxane [J. Chem. Phys. **33**, 1004 (1960)], D. W. Robinson, W. J. Lafferty, J. R. Aronson, J. R. Durig, and R. C. Lord—2245(L)
Erratum: "Floating" hydrogen densities in some molecules of the type XH_n [J. Chem. Phys. **34**, 2105 (1961)], K. E. Banyard—1505(L)
Erratum: Magnetic properties and optical absorption spectrum of K_2ReCl_6 [J. Chem. Phys. **34**, 1628 (1961)], J. C. Eisenstein—2246(L)
Erratum: On the luminescence minimum in certain scintillator solutions [J. Chem. Phys. **34**, 83 (1961)], J. M. Nosworthy, John L. Magee, and M. Burton—1506(L)
Erratum: Pairing energies in the actinide series [J. Chem. Phys. **26**, 988 (1957)], J. S. Griffith—748(L)
Erratum: Potential energy functions for diatomic molecules [J. Chem. Phys. **9**, 61 (1941)], Hugh M. Hulburt and Joseph O. Hirschfelder—1901(L)
Erratum: Statistical mechanics of isotope effects on the thermodynamic properties of condensed systems [J. Chem. Phys. **34**, 1485 (1961)], Jacob Bigeleisen—2246(L)
Erratum: Tunneling through high periodic barriers. II. Application to nuclear magnetic resonance on solids [J. Chem. Phys. **27**, 763 (1957)], T. P. Das—1897(L)

Faraday Effect

Faraday effect in molecules, Irwin Tobias and Walter Kauzmann—538

Field Emission Microscopy

Low-temperature chemisorption III. Studies in the field emission microscope, Gert Ehrlich and F. G. Hudda—1421

Films (see Surface Phenomena)

Flames

Asymmetry of cyclotron resonance lines in the reaction zones of low-pressure acetylene and cyanogen flames, E. M. Bulewicz and P. J. Padley—1590
Flame propagation in free-radical-containing solids at low temperatures, A. L. Berlad—1180
Recombination of ions in flames. Effect of temperature, I. R. King—380(L)

Fluorescence

Absorption and fluorescence spectra with magnetic properties of $ErCl_3$, G. H. Dieke and Shobha Singh—555
Mean lifetime of the lowest excited singlet state of benzene, J. W. Donovan and A. B. F. Duncan—1389
Scintillation properties of 9-vinyl-anthracene, Adam Heller and Dov Katz—1987
Some effects of temperature and viscosity on the fluorescence and energy transfer in solutions, A. Weinreb—91
Structural requirements of organic liquid scintillators, Adam Heller—1980
Unimolecular decay of the triplet state of anthracene in fluid and viscous media, G. Jackson and Robert Livingston—2182

Free Radicals

Antiferromagnetic to ferromagnetic transitions in organic free radicals, A. S. Edelstein and M. Mandel—1130(L)
Calculation of the electron spin resonance line shape for a polycrystalline radical with anisotropic g tensor and proton hyperfine interactions, Roland Lefebvre—762(L)
Comparison of $CH_3\cdot$ and $CF_3\cdot$ hydrogen abstraction reactions, G. O. Pritchard and G. H. Miller—1135(L)
Electron spin resonance absorption of tris-p-nitrophenylmethyl, M. Thomas Jones—1146(L)
Electron spin resonance measurements of preferred orientation in quickly frozen hydrogen peroxide solutions, Robert C. Smith and S. J. Wyard—2254(L)
Electron spin resonance of an irradiated single crystal of urea oxalate, D.V.G.L. Narasimha Rao and Walter Gordy—362
Electron spin resonance of x-ray irradiated single crystal of glutamic acid hydrochloride, W. C. Lin, C. A. McDowell, and J. R. Rowlands—757(L)
Electron spin resonance spectra of free-radical intermediates formed by reaction of polystyrene with atoms of hydrogen and deuterium, R. B. Ingalls and Leo A. Wall—370(L)
Electron spin resonance spectrum and structure of $CH_3CH(CO_2H)$, J. R. Morton and A. Horsfield—1142(L)
Flame propagation in free-radical-containing solids at low temperatures, A. L. Berlad—1180
Formation, lifetime, and decay of OH radicals in discharge-flow systems, F. Kaufman and F. P. Del Greco—1895(L)
Intramolecular charge transfer in aromatic free radicals, Harden M. McConnell—508
Observation of free radical kinetics in the cyclohexane-oxygen system, R. L. McCarthy and A. MacLachlan—1625
Paramagnetic defects in irradiated NH_4ClO_4, Terry Cole—1169
Paramagnetic resonance absorption of the dimesitylmethyl radical, D. B. Chesnut and G. J. Sloan—443

Reactions of methyl with isopropyl radicals, Carl A. Heller—1711
Theory of the spin and charge distribution in aromatic ion radicals; application to the naphthalene negative ion, John C. Schug, Thomas H. Brown, and Martin Karplus—1875
Trapped radicals in irradiated *n*-propanol at 77°K, R. S. Alger, T. H. Anderson and L. A. Webb—49

Free Rotation (see Rotation)

Gases

Experimental Townsend ionization coefficients for iso-pentane, A. E. D. Heylen—169
Gaseous diffusion in porous media at uniform pressure, R. B. Evans, III, G. M. Watson, and E. A. Mason—2076
Intermolecular potential for krypton, Edward A. Mason—2245(L)
Microwave Faraday effect in weakly magnetic gases, Martin L. Sage—969
Momentum-correlation function in a Rayleigh gas, Robert M. Mazo—831
On the theory of condensation, Nobuhiko Saitô—232
Potential parameters of krypton, B. E. F. Fender—2243(L)
Shorter method of calculating Lennard-Jones (12:6) potential parameters from gas viscosity data, W. A. Hawksworth—1534(L)
Tetrafluoromethane: *P-V-T* and intermolecular potential energy relations, D. R. Douslin, R. H. Harrison, R. T. Moore, and J. P. McCullough—1357
"Thermal conductivity" and chemical kinetics, Richard S. Brokaw—1569
Thermal conductivity of polyatomic gases and relaxation phenomena, S. C. Saxena and J. P. Agrawal—2107

Glasses

ESR line shapes in glasses of copper complexes, Robert Neiman and Daniel Kivelson—156

Heat Capacity (see Thermodynamic Properties)

High Pressures

C^{13}-hfs in the ESR spectrum of *p*-benzosemiquinone-1-C^{13} ion, M. R. Das and B. Venkataraman—2262(L)
Effect of pressure on crystal-field energy and covalency in octahedral complexes of Ni^{2+}, Co^{2+}, and Mn^{2+}, J. C. Zahner and H. G. Drickamer—1483
Effect of pressure on tetrahedral Ni^{++} and Co^{++} complexes, D. R. Stephens and H. G. Drickamer—429
Effect of pressure on the charge transfer spectra of heavy transitional metal hexahalide complexes, A. S. Balchan and H. G. Drickamer—356
Effect of pressure on the electronic absorption spectra of ferrocene and ferricinium ion, J. C. Zahner and H. G. Drickamer—375(L)
Effect of pressure on the low-energy absorption peak of several phthalocyanines, B. M. Riggleman and H. G. Drickamer—1343
Effect of pressure on the spectra of certain complexes of Cu^{++}, Co^{+++}, and Fe^{++}, D. R. Stephens and H. G. Drickamer—424
Effect of pressure on the spectra of transition metal ions in MgO and Al_2O_3, S. Minomura and H. G. Drickamer—903
Effect of pressure on the spectrum of ruby, D. R. Stephens and H. G. Drickamer—427
Reversible phase transition of phosphorus pentoxide, I. B. Johns, H. E. Ulmer and J. W. Edwards—1271

Hindered Rotation (see Rotation)

Infrared Spectra (see Absorption Spectra)

Isotope Effects

Billiard-ball collisions in the reactions of hot hydrogen atoms: The isotope effect in the reaction $H+CH_4$, R. J. Cross, Jr., and R. Wolfgang—2002
Carbon-13 hyperfine splitting in the electron spin resonance of semiquinones and cyclooctatetraene, Herbert L. Strauss and George K. Fraenkel—1738
Diffusion of neon isotopes in fused quartz, R. C. Frank, D. E. Swets, and R. W. Lee—1451
Electron spin resonance absorption of tris-*p*-nitrophenylmethyl, M. Thomas Jones—1146(L)
Erratum: Effect of electron energy on some electron-impact processes [J. Chem. Phys. **34,** 2046 (1961)], Seymour Meyerson—1137(L)
Erratum: Statistical mechanics of isotope effects on the thermodynamic properties of condensed systems [J. Chem. Phys. **34,** 1485 (1961)], Jacob Bigeleisen—2246(L)
Infrared spectrum of solid carbon monoxide, George E. Ewing and George C. Pimentel—925
Intermolecular coupling of vibrations in molecular crystals. II. Intermolecular forces in CH_3Cl and CD_3Cl, David A. Dows—282
Isotope size effect in Van der Waals radii and the barrier to rotation around the carbon carbon single bond, W. F. Libby—1527(L)
Isotope fractionation of lithium in sputtering, J. M. Fluit, L. Friedman, A. J. H. Boerboom, and J. Kistemaker—1143(L)
Mass spectra and metastable transitions in isotopic nitrous oxides, G. M. Begun and L. Landau—547
Molecular detachment processes in the vacuum uv photolysis of gaseous hydrocarbons. I. Ethylene. II. Butane, Myran C. Sauer, Jr. and Leon M. Dorfman—497
Quantum statistical mechanics of isotope effects, I. Oppenheim and A. S. Friedman—35
Separation of boron isotopes. V. The phenol-BF_3 system, A. A. Palko and J. S. Drury—103
Solid-state vibrational spectra of the methyl and methyl-d_3 halides, Marilyn E. Jacox and Robert M. Hexter—183
Structural effects in the vapor pressures of isotopic molecules. O^{18} and N^{15} substitution in N_2O, Jacob Bigeleisen and Slobodan V. Ribnikar—1297
Trapped radicals in irradiated *n*-propanol at 77°K, R. S. Alger, T. H. Anderson, and L. A. Webb—49
Vapor pressures of the neon isotopes, Jacob Bigeleisen and Etienne G. Roth—68

Kinetics of Reaction

Addendum: Kinetic model for solid-state reactions [J. Chem. Phys. **34,** 2010 (1961)], R. E. Carter—1137(L)
Anharmonicity in unimolecular reactions, Everett Thiele and David J. Wilson—1256
Asymmetry of cyclotron resonance lines in the reaction zones of low-pressure acetylene and cyanogen flames, E. M. Bulewicz and P. J. Padley—1590
Chemionization in three-body gas phase reactions, C. Gatz, F. T. Smith, and H. Wise—1500(L)
Collision and activated complex theories for bimolecular reactions, Kang Yang and Taikyue Ree—588
Collision mechanics in crossed Maxwellian molecular beams, Sheldon Datz, Dudley R. Herschbach, and Ellison H. Taylor—1549
Comment on the paper: Thermal decomposition of nitrous oxide, C. P. Fenimore—2243(L)
Comments on the Strehlow and Case letter, George Rudinger—1507(L)

Cubic potential surfaces in the transition state theory of unimolecular reactions, Noel B. Slater—445
Diffusion and heterogeneous reaction. IV. Effects of gas phase reaction and convective flow, Henry Wise and Clarence M. Ablow—10
Exchange rates of NH_3 between NH_4OH and copper and nickel ammine complexes, John P. Hunt and Harold W. Dodgen—2261(L)
Ion-molecule reactions studied with mass analysis of primary ion beam, Clayton F. Giese and William B. Maier, II—1913(L)
Kinetics of the photolysis of sodium azide, Jack G. Dodd—1815
Limitations of the reflected shock technique for studying fast chemical reactions, Roger A. Strehlow and Charles T. Case—1506(L)
Mechanism of disproportionation in alkyl radical reactions, J. N. Bradley—748(L)
Mechanism of the mercury photosensitized decomposition of *n*-butane, R. J. Cvetanović, W. E. Falconer, and K. R. Jennings—1225
Molecular weight distribution and reaction sequence in polymerization kinetics, F. C. Goodrich—2101
Note on measurements of rates of electron transfer processes by broadening of ESR lines, P. J. Zandstra and S. I. Weissman—757(L)
Observation of free radical kinetics in the cyclohexane-oxygen system, R. L. McCarthy and A. MacLachlan—1625
Observations of induction times in the acetylene-oxygen reaction, W. C. Gardiner, Jr.—2252(L)
On the classical approximation in unimolecular reactions, B. S. Rabinovitch and J. H. Current—2250(L)
Oscillator models in unimolecular reactions, M. L. Vestal and H. M. Rosenstock—2008
Photochemical decomposition of nitryl chloride, Abraham S. Dohner and David J. Wilson—1510(L)
Rate of the reaction NO+N, John T. Herron—1138(L)
Rates of electron removal by recombination, attachment, and ambipolar diffusion in nitric oxide plasmas, Robert C. Gunton and Edward C. Y. Inn—1896(L)
Recombination of atomic oxygen on surfaces, D. S. Hacker, S. A. Marshall and M. Steinberg—1788
Relative rates of addition of hydrogen atoms to olefines, K. R. Jennings and R. J. Cvetanović—1233
Shock wave studies by mass spectrometry. I. The thermal decomposition of nitrous oxide, J. N. Bradley and G. B. Kistiakowsky—256
Shock wave studies by mass spectrometry. II. The polymerization and oxidation of acetylene, J. N. Bradley and G. B. Kistiakowsky—264
Some deductions from a formal statistical mechanical theory of chemical kinetics, John Ross and Peter Mazur—19
Statistical computation of reaction probabilities. II, F. T. Wall, L. A. Hiller, Jr., and J. Mazur—1284
Studies of transient species formed during catalytic reactions of CO_2+D_2 and of 1-butene, Charles E. Melton—1751
Substitution of a catalytic probe for a tube of infinite length in atom recombination experiments, Bernard J. Wood and A. Bruce King—1530(L)
"Thermal conductivity" and chemical kinetics, Richard S. Brokaw—1569
Thermal dissociation rate of hydrogen, W. C. Gardiner, Jr. and G. B. Kistiakowsky—1765
Unimolecular decay of the triplet state of anthracene in fluid and viscous media, G. Jackson and Robert Livingston—2182
Unimolecular rates due to multiple critical oscillators, E. W. Schlag—2117

Large Molecules (see Polymers)

Light Scattering

Depolarization of scattered light by *n*-paraffin vapors and the additivity of bond polarizability tensors, Joseph Powers, Daniel A. Keedy, and Richard S. Stein—376(L)
Light scattering by anisotropic inhomogeneities in thin polymer films under strain, II, Hari L. Bhatnagar—999.

Liquids

Calculation of metal surface tensions. Ionic-salt monatomic models for liquid metals, S. W. Mayer—1513(L)
Compressibility of simple fused salts, Frank H. Stillinger, Jr.—1581
Energy and free energy of cohesion, Bruno Linder—371(L)
Erratum: Development of the liquid equation and the partial structure of water [J. Chem. Phys. **34**, 2174 (1961)], Robert Ginell—1135(L)
Formulation of a cell model using periodic boundary conditions, David R. Squire and Zevi W. Salsburg—486
Infrared spectra of NaOH above and below the melting point, Jacob Greenberg and L. J. Hallgren—180
Kinetic method for measuring solubilities of gases in liquids, Kedma Bar-Eli and Fritz S. Klein—1915(L)
Law of corresponding states for fused salts, H. Reiss, S. W. Mayer, and J. L. Katz—820
Meaning of the Tait coefficients and the structure of liquids, Robert Ginell—1776
On the kinetic theory of dense fluids. IX. The fluid of rigid spheres with a square-well attraction, H. T. Davis, Stuart A. Rice, and J. V. Sengers—2210
On the quasi-crystalline model of water, S. K. Joshi—1141(L)
On the theory of condensation, Nobuhiko Saitô—232
Raman spectra and ionic interactions in molten nitrates, George J. Janz and David W. James—738
Self-association constant of chloroform from NMR chemical shifts, Charles F. Jumper, Merle T. Emerson, and Bentz B. Howard—1911(L)
Solutions to the Percus-Yevick equation, A. A. Broyles—493
Some further observations on the critical region, George W. Bradey and H. L. Frisch—2234(L)
Studies of fused salts. III. Heats of mixing in silver nitrate-alkali nitrate mixtures, O. J. Kleppa, R. B. Clarke, and L. S. Hersh—175
Tait coefficients and the λ transition of helium I and II, Robert Ginell—473
Vibrational spectra of inorganic molecules. III. The infrared reflection spectra of molten lithium, sodium, and potassium hydroxide, J. K. Wilmshurst—1800

Magnetic Resonance

Absence of B^{10}–B^{11} coupling in B_4H_{10}, John S. Rigden, Robert C. Hopkins, and John D. Baldeschwieler—1532(L)
Analysis of complex NMR spectra: Epichlorohydrin, C. A. Reilly and J. D. Swalen—1522(L)
Anisotropy of nuclear magnetic resonance in vanadium pentoxide, J. L. Ragle—753(L)
Antiparallel spin polarization in triplet states, Harden M. McConnell—1520(L)
Asymmetry of cyclotron resonance lines in the reaction zones of low-pressure acetylene and cyanogen flames, E. M. Bulewicz and P. J. Padley—1590
Calculation of the electron spin resonance line shape for a polycrystalline radical with anisotropic *g* tensor and proton hyperfine interactions, Roland Lefebvre—762(L)
Carbon-13 hyperfine splitting in the electron spin resonance of semiquinones and cyclooctatetraene, Herbert L. Strauss and George K. Fraenkel—1738

$CH_2(COOH)$ in malonic acid, Harden M. McConnell and Concetto R. Giuliano—1910(L)
Constancy of the sums of spin-spin coupling constants in monosubstituted ethylenes, G. S. Reddy and J. H. Goldstein—380(L)
C^{13}-hfs in the ESR spectrum of *p*-benzosemiquinone-1-C^{13} ion, M. R. Das and B. Venkataraman—2262(L)
Direct field effects in electron paramagnetic resonance hyperfine spectra, John A. Weil and John H. Anderson—1410
Effect of chemisorbed hydrogen on the ferromagnetic resonance of finely divided nickel, Donald P. Hollis and P. W. Selwood—378(L)
Effect of electronegativity and magnetic anisotropy of substituents on C^{13} and H^1 chemical shifts in CH_3X and CH_3CH_2X compounds, H. Spiesecke and W. G. Schneider—722
Electron coupling of proton spins in heterocyclic molecules. *N*-benzylthieno [3,2-*b*] pyrrole, H. S. Gutowsky and A. L. Porte—839
Electron paramagnetic resonance spectra of some disubstituted nitric oxides, J. C. Baird and J. R. Thomas—1507(L)
EPR studies of spin correlation in some ion radical salts, D. B. Chesnut and W. D. Phillips—1002
EPR study of the tetrafluorohydrazine-difluoramino equilibrium, L. H. Piette, F. A. Johnson, K. A. Booman, and Charles B. Colburn—1481
Electron spin resonance absorption of tris-*p*-nitrophenylmethyl, M. Thomas Jones—1146(L)
ESR line shapes in glasses of copper complexes, Robert Neiman and Daniel Kivelson—156
Electron spin resonance measurements of preferred orientation in quickly frozen hydrogen peroxide solutions, Robert C. Smith and S. J. Wyard—2254(L)
Electron spin resonance of an irradiated single crystal of urea oxalate, D.V.G.L. Narashimha Rao and Walter Gordy—362
Electron spin resonance of γ-irradiated glycylglycine, Mikio Katayama and Walter Gordy—117
Electron spin resonance of x-ray irradiated single crystal of glutamic acid hydrochloride, W. C. Lin, C. A. McDowell, and J. R. Rowlands—757(L)
ESR spectra of a gamma-irradiated single crystal of DL-serine, D.V.G.L. Narasimha Rao and Walter Gordy—764(L)
Electron spin resonance spectra of free-radical intermediates formed by reaction of polystyrene with atoms of hydrogen and deuterium, R. B. Ingalls and Leo A. Wall—370(L)
ESR spectra of solid phthalocyanines, Robert Neiman and Daniel Kivelson—162
Electron spin resonance spectrum and structure of $CH_3CH(CO_2H)$, J. R. Morton and A. Horsfield—1142(L)
Electron spin resonance studies of gamma irradiated single crystals of sucrose, Hisashi Ueda, Zen'ichiro Kuri, and Shoji Shida—2145
Electron spin resonance studies of radicals formed in irradiated polytetrafluoroethylene, Teikichi Matsugashita and Kenichi Shinohara—1652
ESR studies on the bonding in copper complexes, Daniel Kivelson and Robert Neiman—149
Electron spin resonance study of radiation damage in single crystals of urea compounds, Thadho S. Jaseja and Roy S. Anderson—2192
Erratum and further comments: Exact analysis of three-spin NMR spectra [J. Chem. Phys. **34,** 295 (1961)], J. S. Waugh and S. Castellano—1900(L)
Erratum: Tunneling through high periodic barriers. II. Application to nuclear magnetic resonance on solids [J. Chem. Phys. **27,** 763 (1957)], T. P. Das—1897(L)
Exchange rates of NH_3 between NH_4OH and copper and nickel ammine complexes, John P. Hunt and Harold W. Dodgen—2161(L)
Fluorine NMR spectroscopy. V. A carbon-13 study of coupling constants between *cis* and *trans* CF_3 groups in highly fluorinated olefins, George Van Dyke Tiers—2263(L)
Further notes on the magnetic centers in neutron-irradiated calcite, James C. Kemp—377(L)
Hyperfine structure and *g*-tensor anisotropy of the paramagnetic resonances of manganese in TiO_2, Harro G. Andresen—1090
Long-range N^{14}-H^1 nuclear-resonance coupling in isonitriles, I. D. Kuntz, Jr., P. von R. Schleyer, and A. Allerhand—1533(L)
Long-range nuclear magnetic shielding in molecules and the anisotropy in the magnetic susceptibility of a carbon-carbon single bond, Jeremy I. Musher—1159
Low-field nuclear magnetic resonance of coupled spin—one-half particles, Don D. Thompson and Robert J. S. Brown—1894(L)
Magnetization and proton relaxation time in antiferromagnetic $LiCuCl_3 \cdot 2H_2O$, R. D. Spence and C. R. K. Murty—1912(L)
Metallic nature of the starch-iodine complex, R. Bersohn and I. Isenberg—1640
Modulation broadening of unsaturated Lorentzian lines, Hugo Wahlquist—1708
Note on measurements of rates of electron transfer processes by broadening of ESR lines, P. J. Zandstra and S. I. Weissman—757(L)
NMR chemical shift of hydroxyl and hydronium ions, J. I. Musher—1989
NMR fluorine-fluorine coupling constants in saturated organic compounds, L. Petrakis and C. H. Sederholm—1243
Nuclear magnetic resonance in $CuF_2 \cdot 2H_2O$ single crystals, R. G. Shulman and B. J. Wyluda—1498
Nuclear magnetic resonance studies of B^{11} in crystalline borates, P. J. Bray, J. O. Edwards, J. G. O'Keefe, V. F. Ross, and I. Tatsuzaki—435
Nuclear relaxation in gases: Mixtures of methane and oxygen, C. S. Johnson, Jr., and J. S. Waugh—2020
Nuclear transfer effects in nuclear magnetic resonance pulse experiments, D. E. Woessner—41
On the calculation of second moments of nuclear magnetic resonance lines for large molecules. Adamantane molecule, George W. Smith—1134(L)
On the mechanism of nuclear relaxation in gaseous and liquid CHF_3, C. S. Johnson, Jr., J. S. Waugh, and J. N. Pinkerton—1128(L)
Optical and paramagnetic resonance spectra of trivalent Pu^{239} in the trichloride and ethylsulfate, H. Lammermann and H. J. Stapleton—1514
Organic semiconductors: Aromatic hydrocarbon positive ions in solids, G. E. Blomgren and J. Kommandeur—1636
Paramagnetic defects in irradiated NH_4ClO_4, Terry Cole—1169
Paramagnetic excitons in molecular crystals, Himan Sternlicht and Harden M. McConnell—1793
Paramagnetic relaxation in metal-ammonia solutions, D. E. O'Reilly—1856
Paramagnetic resonance absorption of the dimesitylmethyl radical, D. B. Chesnut and G. J. Sloan—443
Paramagnetic resonance of some copper complex compounds, J. A. McMillan and B. Smaller—763(L)
Paramagnetic resonance of some silver (II) compounds, J. A. McMillan and B. Smaller—1698
Paramagnetic resonance of X-irradiated CaF_2:Tm and of CaF_2:Yb, W. Hayes and J. W. Twidell—1521(L)
Paramagnetic resonance of X-irradiated single crystals of Rochelle salt, Grace C. Moulton and W. G. Moulton—208
Paramagnetic resonance spectra of chromium III and manganese IV hexafluoride ions: CrF_6^{3-} and MnF_6^{2-}, Lindsay Helmholz, A. V. Guzzo, and R. N. Sanders—1349
Paramagnetic species in irradiated $NaNO_2$, Henry Zeldes and Ralph Livingston—563
Photochromism of *N*-3-pyridylsydnone, T. Mill, A. van Roggen, and C. F. Wahlig—1139(L)

Proton magnetic resonance spectra of vinylmethylsilanes, R. T. Hobgood, J. H. Goldstein, and G. S. Reddy—2038
Proton magnetic resonance study of ferroelectric $NaH_3(SeO_3)_2$ and $LiH_3(SeO_3)_2$, R. Blinc and M. Pintar—1140(L)
Proton magnetic resonance study of ferroelectric potassium ferrocyanide trihydrate, R. Blinc, M. Brenman, and J. S. Waugh—1770
Proton resonance shifts and electron susceptibilities in 1,3-bisdiphenylene 2-phenyl allyl, M. E. Anderson, R. S. Rhodes, and G. E. Pake—1527(L)
Recombination of atomic oxygen on surfaces, D. S. Hacker, S. A. Marshall, and M. Steinberg—1788
Rotational isomerism in terephthaladehyde anion. August H. Maki—761(L)
Rotational isomerism in 2,3 dihalopropenes, Earl B. Whipple—1039
Self-association constant of chloroform from NMR chemical shifts, Charles F. Jumper, Merle T. Emerson, and Bentz B. Howard—1911(L)
Solid state photochemical processes in sodium azide, G. J. King, B. S. Miller, F. F. Carlson, and R. C. McMillan—1442
Spin densities in the aromatics containing nitrogen: ESR-spectrum of the pyrazine negative ion, J. C. M. Henning and C. de Waard—2258(L)
Substituent effects on the C^{13} and H^1 chemical shifts in mono-substituted benzenes, H. Spiesecke and W. G. Schneider—731
Temperature-dependent chemical shifts in the NMR spectra of gases, L. Petrakis and C. H. Sederholm—1174
Theoretical calculation of isotropic hfs of the free NH_2 radical, Jiro Higuchi—2270(L)
Theoretical interpretation of carbon-13 hyperfine interactions in electron spin resonance spectra, Martin Karplus and George K. Fraenkel—1312
Theory of proton magnetic shielding, Marshall Fixman—679
Trapped radicals in irradiated *n*-propanol at 77°K, R. S. Alger, T. H. Anderson, and L. A. Webb—49
Tritium as an internal source of radiation in EPR studies of organic materials, J. Kroh and J. W. Spinks—760(L)

Magnetic Susceptibilities

Antiferromagnetic-ferromagnetic transformation in FeRh, L. Muldawer and F. deBergevin—1904(L)
Antiferromagnetic to ferromagnetic transitions in organic free radicals, A. S. Edelstein and M. Mandel—1130(L)
Diamagnetic susceptibility in Thomas-Fermi model for Latter's and Byatt's effective charge distribution, T. Tietz—1916(L)
Effect of chemisorbed hydrogen on the magnetization of nickel, R. E. Dietz and P. W. Selwood—270
Erratum: Magnetic properties and optical absorption spectrum of K_2ReCl_6 [J. Chem. Phys. **34**, 1628 (1961)], J. C. Eisenstein—2246(L)
Fe^{57} Mössbauer effect in laves phases containing Fe combined with Y, Ce, Ho, Ti, Zr, and Hf, W. E. Wallace and L. M. Epstein—2238(L)
Heat capacities of $DyCo_5$ in relationship to its magnetic anomaly, third law entropies, and related thermochemical data, William G. Saba and W. E. Wallace—689
Magnetic interactions in lithium hydride, M. Karplus and H. J. Kolker—2235(L)
Magnetic susceptibility of mercuric oxide at various temperatures, H. Mikhail, Z. Hanafy, and T. M. Salem—1185
Magnetization and proton relaxation time in antiferromagnetic $LiCuCl_3 \cdot 2H_2O$, R. D. Spence and C. R. K. Murty—1912(L)
Microwave Faraday effect in weakly magnetic gases, Martin L. Sage—969
Nuclear magnetic resonance in $CuF_2 \cdot 2H_2O$ single crystals, R. G. Shulman and B. J. Wyluda—1498
Paramagnetism of tetraphenanthroline dihydroxyl diferric chloride, Norman Elliott—1273
Substitution of Fe^{3+} ion in Sc_2O_3 and In_2O_3, S. Geller, H. J. Williams, and R. C. Sherwood—1908(L)

Mass Spectra

Association of carbon atoms from graphite in a radio-frequency spark, William L. Baun and David W. Fischer—1518(L)
Charge exchange between krypton ions and atoms, S. B. Karmohapatro—1524(L)
Cohesive energies of europium, gadolinium, holmium, and erbium, O. Conrad Trulson, Donald E. Hudson, and Frank H. Spedding—1018
Double and triple ionization in molecules, induced by electron impact, F. H. Dorman and J. D. Morrison—575
Energy distribution and fragmentation processes resulting from electron impact on propane and *n*-butane, William A. Chupka and Manfred Kaminsky—1991
Erratum: Effect of electron energy on some electron-impact processes [J. Chem. Phys. **34**, 2046 (1961)], Seymour Meyerson—1137(L)
Franck-Condon factors and the shape of ionization efficiency curves, Morton E. Wacks and Morris Krauss—1902(L)
Ionization cross sections near threshold by electron impact, R. E. Fox—1379
Ion-molecule reactions studied with mass analysis of primary ion beam, Clayton F. Giese and William B. Maier, II—1913(L)
Mass spectra and metastable transitions in isotopic nitrous oxides, G. M. Begun and L. Landau—547
Mass spectrometer for ionization efficiency studies using an electron velocity selector, P. Marmet and J. D. Morrison—746(L)
Mass spectrometric study of the thermal dissociation of N_2F_4, John T. Herron and Vernon H. Dibeler—747(L)
Molecular association in sodium cyanide vapor, Richard F. Porter—318
Negative ion formation in ozone, R. K. Curran—1617
Note on the statistical theory of mass spectra, John C. Schug and Norman D. Coggeshall—1146(L)
On the use of mass spectral data in radiation chemistry, Jean H. Futrell—353
Rate of the reaction NO+N, John T. Herron—1138(L)
Shock wave studies by mass spectrometry. I. The thermal decomposition of nitrous oxide, J. N. Bradley and G. B. Kistiakowsky—256
Shock wave studies by mass spectrometry. II. The polymerization and oxidation of acetylene, J. N. Bradley and G. B. Kistiakowsky—264
Strength of the N—F bonds in NF_3 and of N—F and N—N bonds in N_2F_4, Al Kennedy and Charles B. Colburn—1892
Studies of transient species formed during catalytic reactions of CO_2+D_2 and of 1-butene, Charles E. Melton—1751
Thermodynamics of the vaporization of nickel oxide, R. T. Grimley, R. P. Burns, and Mark G. Inghram—551
Uranium monosulfide: II. Mass spectrometric study of its vaporization, E. David Cater, E. G. Rauh, and R. J. Thorn—619

Mechanics, Classical

Statistical computation of reaction probabilities. II, F. T. Wall, L. A. Hiller, Jr., and J. Mazur—1284

Mechanics, Quantum

A Taylor series expansion of the intermediate coupling energy levels of Nd^{+3} and Er^{+3}, Eugene Y. Wong—544
Analysis of the absorption spectrum of $YbCl_3 \cdot 6H_2O$, J. C. Eisenstein—2097
Antiparallel spin polarization in triplet states, Harden M. McConnell—1520(L)
Approximate analytical wave functions for the $1s^2ns\ ^2S_{\frac{1}{2}}$ states of Li and Li-like ions, Z. W. Ritter, R. Pauncz, and K. Appel—571

Atomic wavefunctions for the ground states of Na^+, Ne, and F^-, Wilm E. Donath—817
Band structure and transport of holes and electrons in anthracene, Oliver H. LeBlanc, Jr.—1275
Calculation of interaction matrix elements for asymmetric rotors with resultant electronic spin and nuclear spin, R. F. Curl, Jr., and James L. Kinsey—1758
Calculation of polarizabilities and shielding factors, A. Dalgarno and J. M. McNamee—1517(L)
Calculations of the lower excited energy levels of the cyclic polyenes, radicals, and ions, Nicolaas Bouman—1661
Chemical bond in molecular quantum mechanics, Thomas L. Allen and Harrison Shull—1644
Comprehensive investigation of the electronic spectroscopy and theoretical treatments of ferrocene and nickelocene, Donald R. Scott and Ralph S. Becker—516
Cubic potential surfaces in the transition state theory of unimolecular reactions, Noel B. Slater—445
Cuboctahedral bonding, Jack R. Canon and George H. Duffey —1657
d-Hybridization of the pi bond in the $2_p\pi_u$ state of H_2^+, Ojars Sovers and Walter Kauzmann—652
Deionization cross section for oxygen, R. G. Breene, Jr.—625
Diamagnetic susceptibility in Thomas-Fermi model for Latter's and Byatt's effective charge distribution, T. Tietz—1916(L)
Dipole moment of HD. II, S. M. Blinder—974
Double-ζ SCF MO calculation of the ground and some excited states of N_2, James W. Richardson—1829
Effect of an attractive potential on the classical theory of vibrational energy exchange, R. E. Turner and Donald Rapp—1076
Electrostatic energy matrices of the f^5 and f^6 configurations, B. G. Wybourne—340
Energy levels of $PrCl_3$, Jack S. Margolis—1367
Erratum and further comments: Exact analysis of three-spin NMR spectra [J. Chem. Phys. **34**, 295 (1961)], J. S. Waugh and S. Castellano—1900(L)
Erratum: Binding energies of alkali halide molecules [J. Chem. Phys. **34**, 2069 (1961)], G. M. Rothberg—1137(L)
Erratum: Comprehensive investigation of the electronic spectroscopy and theoretical treatments of ferrocene and nickelocene [J. Chem. Phys. **35**, 516 (1961)], Donald R. Scott and Ralph S. Becker—2246(L)
Erratum: "Floating" hydrogen densities in some molecules of the type XH_n [J. Chem. Phys. **34**, 2105 (1961)], K. E. Banyard—1505(L)
Erratum: Pairing energies in the actinide series [J. Chem. Phys. **26**, 988 (1957)], J. S. Griffith—748(L)
Erratum: Tunneling through high periodic barriers. II. Application to nuclear magnetic resonance on solids [J. Chem. Phys. **27**, 763 (1957)], T. P. Das—1897(L)
Faraday effect in molecules, Irwin Tobias and Walter Kauzmann—538
First excited $^1\Sigma_g^+$ state of the hydrogen molecule, Ernest R. Davidson—1189
General relation between potential energy and internuclear distance for diatomic molecules. III. Excited states, E. R. Lippincott, D. Steele, and P. Caldwell—123
Group theory and aromatic molecules, J. S. Griffith—1901(L)
Homopolar dipole, C. A. Coulson and Max T. Rogers—593
Intramolecular charge transfer in aromatic free radicals, Harden M. McConnell—508
Least-squares local-energy method for molecular energy calculations using gauss quadrature points, A. A. Frost, R. E. Kellogg, B. M. Gimarc, and J. D. Scargle—827
Magnetic interactions in lithium hydride, M. Karplus and H. J. Kolker—2235(L)
Maximum overlap atomic and molecular orbitals, Peter G. Lykos and Howard N. Schmeising—288
Negative hydrogen ion, T. Tietz—1917(L)
Note on the separability theorem for electron pairs, Per-Olov Löwdin—78
On the approximation of zero differential overlap, C. A. Coulson and L. J. Schaad—294
On the evaluation of integrals occurring in the theory of the correlated electronic wave functions, Levente Szász—1072
On the introduction of arbitrary angular peakedness into atomic orbitals, Oliver G. Ludwig and Robert G. Parr—754(L)
On the parameters used in semi-empirical molecular orbital theory for conjugated hydrocarbons, Peter G. Lykos—1249
Oscillator models in unimolecular reactions, M. L. Vestal and H. M. Rosenstock—2008
Perturbation theory calculations, A. Dalgarno—1898(L)
Perturbation theory calculations, Robert G. Parr and Lawrence C. Snyder—1898(L)
Quantum statistical mechanics of isotope effects, I. Oppenheim and A. S. Friedman—35
Relative bond strengths in trigonal bipyramid molecules, F. A. Cotton—228
Remark on the Mulliken approximation for two-center electron distributions, Audrey L. Companion and Robert G. Parr—2268(L)
Remarks on the electronic spectra and structure of compounds of chromium and benzene, R. Stephen Berry—29
SCF LCAO study of linear and bent acetylene, Louis Burnelle —311
Spin-orbit interactions in f^n electron configurations, B. G. Wybourne—334
Studies in molecular structure. V. Computed spectroscopic constants for selected diatomic molecules of the first row, S. Fraga and B. J. Ransil—669
Studies in molecular structure. VI. Potential curve for the interaction of two hydrogen atoms in the LCAO MO SCF approximation, Serafin Fraga and Bernard J. Ransil—1967
Symmetry-adapted LCAO MO's for long-chain polyenes, Marvin C. Tobin—1905(L)
Theoretical calculation of isotropic hfs of the free NH_2 radical, Jiro Higuchi—2270(L)
Theoretical interpretation of carbon-13 hyperfine interactions in electron spin resonance spectra, Martin Karplus and George K. Fraenkel—1312
Theory of proton magnetic shielding, Marshall Fixman—679
Theory of the spin and charge distribution in aromatic ion radicals; application to the naphthalene negative ion, John C. Schug, Thomas H. Brown, and Martin Karplus—1875
Transition probabilities in multilevel systems: Calculation from impulsive and steady-state experiments, Tucker Carrington—807
Ultraviolet spectra of carbon monoxide, H. Lefebvre-Brion, Carl Moser, and R. K. Nesbet—1702
Use of distorted atomic orbitals in molecular wave functions, R. L. Miller and Peter G. Lykos—1147(L)
Vibronic coupling. I. Mathematical treatment for two electronic states, Robert L. Fulton and Martin Gouterman—1059
Wave functions and intensity calculations for a rotating anharmonic oscillator, Thomas C. James—767

Mechanics, Statistical

Calculation of depolarization ratios, anisotropies, and average dimensions of *n*-alkanes, Richard P. Smith and Earl M. Mortensen—714
Compressibility of simple fused salts, Frank H. Stillinger, Jr. —1581
Effect of intermolecular forces on macromolecular configurational changes and on other isomeric equilibria, Terrell L. Hill—303
Erratum: Development of the liquid equation and the partial structure of water [J. Chem. Phys. **34**, 2174 (1961)], Robert Ginell—1135(L)

Erratum: Statistical mechanics of isotope effects on the thermodynamic properties of condensed systems [J. Chem. Phys. **34,** 1485 (1961)], Jacob Bigeleisen—2246(L)
Formulation of a cell model using periodic boundary conditions, David R. Squire and Zevi W. Salsburg—486
Gaseous diffusion in porous media at uniform pressure, R. B. Evans, III, G. M. Watson, and E. A. Mason—2076
General theory of polymer solutions, Marshall Fixman—889
Law of corresponding states for fused salts, H. Reiss, S. W. Mayer, and J. L. Katz—820
Molecular-weight dependence of the viscoelastic properties of whole polymers, Warner L. Peticolas and Emory Menefee—951
Molecular weight distribution from the normal coordinate theory of viscoelasticity, Emory Menefee and Warner L. Peticolas—946
Momentum-correlation function in a Rayleigh gas, Robert M. Mazo—831
On the classical approximation in unimolecular reactions and mass spectra, B. S. Rabinovitch and J. H. Current—2250(L)
On the classical Boltzmann equation for gases, Frank C. Andrews—922
On the kinetic theory of dense fluids. IX. The fluid of rigid spheres with a square-well attraction, H. T. Davis, Stuart A Rice, and J. V. Sengers—2210
On the theory of condensation, Nobuhiko Saitô—232
q-dimensional excluded volume in random flight chains, Carl von Frankenberg and R. E. Hughes—503
Quantum statistical mechanics of isotope effects, I. Oppenheim and A. S. Friedman—35
Self-diffusion and velocity correlation, Dean C. Douglass—81
Shorter method of calculating Lennard-Jones (12:6) potential parameters from gas viscosity data, W. A. Hawksworth—1534(L)
Solutions to the Percus-Yevick equation, A. A. Broyles—493
Some deductions from a formal statistical mechanical theory of chemical kinetics, John Ross and Peter Mazur—19
Statistical computation of reaction probabilities. II, F. T. Wall, L. A. Hiller, Jr., and J. Mazur—1284
Statistics of orientation effects in linear polymer molecules, Edmund A. DiMarzio—658
Time dependence of the statistical molecular weight distribution of the polymer resulting from vinyl polymerization, V. S. Nanda and R. K. Pathria—630
Transition probabilities in multilevel systems: Calculation from impulsive and steady-state experiments, Tucker Carrington—807
Transport properties of polar gases, L. Monchick and E. A. Mason—1676
Unperturbed mean square end-to-end distance of polyethylene, C. A. J. Hoeve—1266

Metals

Attempts to find photoconductivity in dilute sodium-ammonia solutions, R. L. Potter, R. G. Shores, and J. L. Dye—1907(L)
Cohesive energies of europium, gadolinium, holmium, and erbium, O. Conrad Trulson, Donald E. Hudson, and Frank H. Spedding—1018
Heat capacities and the residual entropy of Ta_2H, W. G. Saba, W. E. Wallace, H. Sandmo, and R. S. Craig—2148
Measurement of the resistivity of cesium at elevated temperatures, J. Hyman, Jr.—992
Salt effect in metal-ammonia solutions: Sodium chloride in sodium-ammonia solution at −33°C, Donald S. Berns, Gerard Lepoutre, Elizabeth A. Bockelman, and Andrew Patterson, Jr.—1820

Microwave Spectra (see Absorption Spectra)

Molecular Films (see Surface Phenomena)

Molecular Spectra (see Absorption Spectra, Emission Spectra, Fluorescence and Raman Spectra)

Molecular Structure and Constants (see also Absorption Spectra, Fluorescence, Raman Spectra, Electron & X-ray Diffraction)

Anharmonic potential constants and their dependence upon bond length, Dudley R. Herschbach and Victor W. Laurie—458
Anharmonicity in unimolecular reactions, Everett Thiele and David J. Wilson—1256
Approximate mean-square amplitudes of characteristic two-atom vibrations, C. J. G. Raw and C. Kuenz—1529(L)
Atomic polarization. III. Vibrational polarization terms associated with forbidden transitions in polyatomic molecules, Karl H. Illinger and Charles P. Smyth—397
Atomic polarization. IV. Temperature dependence of the vibrational polarization of gases, Karl H. Illinger and Charles P. Smyth—400
Calculations of the lower excited energy levels of the cyclic polyenes, radicals and ions, Nicolaas Bouman—1661
Comments on a communication by El-Sayed and Robinson, Mostafa El-Sayed and G. Wilse Robinson—1896(L)
Construction of reliable inter-nuclear potential curves from equilibrium bond lengths and vibrational frequencies, D. Steele and E. R. Lippincott—2065
d-Hybridization of the pi bond in the $2_p\pi_u$ state of H_2^+, Ojars Sovers and Walter Kauzmann—652
Dipole moment of HD. II., S. M. Blinder—974
Dissociation energy of cyanogen and related quantities by x-ray densitometry of shock waves, Herbert T. Knight and John P. Rink—199
Double-ζ SCF MO calculation of the ground and some excited states of N_2, James W. Richardson—1829
Electron coupling of proton spins in heterocyclic molecules. *N*-benzylthieno [3,2-*b*] pyrrole, H. S. Gutowsky and A. L. Porte—339
Electronic spectra of substituted anthracenes. Evidences for appearance of the ^1L_b transition, Hiroaki Baba and Satoshi Suzuki—1501(L)
Erratum: Binding energies of alkali halide molecules [J. Chem. Phys. **34,** 2069 (1961)], G. M. Rothberg—1137(L)
Erratum: Far infrared spectrum of disiloxane [J. Chem. Phys. **33,** 1004 (1960)], D. W. Robinson, W. J. Lafferty, J. R. Aronson, J. R. Durig, and R. C. Lord—2245(L)
Erratum: Potential energy functions for diatomic molecules [J. Chem. Phys. **9,** 61 (1941)], Hugh M. Hulburt and Joseph O. Hirschfelder—1901(L)
First excited $^1\Sigma_g^+$ state of the hydrogen molecule, Ernest R. Davidson—1189
General relation between potential energy and internuclear distance for diatomic molecules. III. Excited states, E. R. Lippincott, D. Steele, and P. Caldwell—123
Group theory and aromatic molecules, J. S. Griffith—1901(L)
Homopolar dipole, C. A. Coulson and Max T. Rogers—593
Identification of an electronic transition of N_2^{++}, P. K. Carroll and A. C. Hurley—2247(L)
Infrared and raman spectra, force constants, and the structures of some polyhalide ions: ICl_2^-, ICl_4^-, $BrCl_4^-$, and Br_3^-, Willis B. Person, George R. Anderson, James N. Fordemwalt, H. Stammreich, and Roberto Forneris—908
Infrared spectra of sodium and potassium cyanide, George E. Leroi and William Klemperer—774
Infrared spectrum and molecular configuration of glutaronitrile, Ikuo Matsubara—373(L)

Infrared spectrum and structure of the NF_2 radical, Marlin D. Harmony, Rollie J. Myers, L. J. Schoen, David R. Lide, Jr., and D. E. Mann—1129(L)
Infrared spectrum of CF_3SF_5, D. F. Eggers, Jr., H. E. Wright, and D. W. Robinson—1045
Least-squares local-energy method for molecular energy calculations using gauss quadrature points, A. A. Frost, R. E. Kellogg, B. M. Gimarc, and J. D. Scargle—827
Low-resolution analysis of the $n \rightarrow \pi^*$ (3000 A) absorption spectrum of *s*-triazine, J. S. Brinen and Lionel Goodman—1219
Maximum overlap atomic and molecular orbitals, Peter G. Lykos and Howard N. Schmeising—288
Mean and equilibrium molecular structures of methane and deuteromethane as determined by electron diffraction, L. S. Bartell, Kozo Kuchitsu, and R. J. deNeui—1211
Microwave spectrum and barrier to internal rotation of methyl stannane, Patrick Cahill and Samuel Butcher—2255(L)
Microwave spectrum, dipole moment, structure, and internal rotation of dimethyl sulfide, Louis Pierce and Michiro Hayashi—479
Microwave spectrum of methyl nitrate, William B. Dixon and E. Bright Wilson, Jr.—191
Molecular orbitals in some boron compounds, Emmett B. Moore, Jr., L. L. Lohr, Jr., and William N. Lipscomb—1329
Molecular structure of $B_9H_{13}(CH_3CN)$, Frederick E. Wang, Paul G. Simpson, and William N. Lipscomb—1335
Molecular structure of propylene, David R. Lide, Jr. and Daniel Christensen—1374
Molecular vibrations and structures of high polymers. I. General method of normal coordinate treatment by internal coordinates and infrared frequencies and conformations of $(-CH_2-)_n$, $(-CH_2-O-)_n$, and $(-CH_2-O-CH_2-)_n$, Tatsuo Miyazawa—693
New potential function for alkali halide molecules, Yatendra Pal Varshni and Ramesh Chandra Shukla—582
Normal vibrations and Urey-Bradley force constants of methyl amine, Ellen L. Wu, Giuseppe Zerbi, Salvatore Califano, and Bryce Crawford, Jr.—2060
On the parameters used in semi-empirical molecular orbital theory for conjugated hydrocarbons, Peter G. Lykos—1249
Potential energy curves for the $X^1\Sigma_g^+$ and $B^1\Sigma_u^+$ states of hydrogen, Irwin Tobias and Joseph T. Vanderslice—1852
Raman spectra of metal carbonyl compounds. III. Raman spectrum, vibrational analysis and bond structure of nickel tetracarbonyl, H. Stammreith, K. Kawai, Osw. Sala, and P. Krumholz—2168
Raman spectra of methal carbonyl compounds IV. Raman spectra and structure of cadmium and mercury cobalt carbonyl, H. Stammreich, K. Kawai, Osw. Sala, and P. Krumholz—2175
Refinement of the B_9H_{15} structure and test for solid solutions, Paul G. Simpson and William N. Lipscomb—1340
SCF-LCAO study of linear and bent acetylene, Louis Burnelle—311
Spectrum of NBr excited in active nitrogen, Earl R. V. Milton, H. B. Dunford, and A. E. Douglas—1202
Studies in molecular structure. V. Computed spectroscopic constants for selected diatomic molecules of the first row, S. Fraga and B. J. Ransil—669
Studies in molecular structure. VI. Potential curve for the interaction of two hydrogen atoms in the LCAO MO SCF approximation, Serafin Fraga and Bernard J. Ransil—1967
Study of hydrogen bonding. The microwave rotation spectrum of CF_3COOH—HCOOH, C. C. Costain and G. P. Srivastava—1903(L)
Symmetry-adapted LCAO MO's for long-chain polyenes, Marvin C. Tobin—1905(L)
Theory of the spin and charge distribution in aromatic ion radicals; application to the naphthalene negative ion, John C. Schug, Thomas H. Brown, and Martin Karplus—1876
Ultraviolet spectra of carbon monoxide, H. Lefebvre-Brion, Carl Moser, and R. K. Nesbet—1702
Wave functions and intensity calculations for a rotating anharmonic oscillator, Thomas C. James—767
Zero-point vibrations in benzene, R. Stephen Berry—2253(L)

Neutron Diffraction

Neutron diffraction data for Ta_4D and the probable arrangement of the deuteriums in two of its polymorphic varieties, W. E. Wallace—2156
Neutron-diffraction studies of CaC_2, YC_2, LaC_2, CeC_2, TbC_2, YbC_2, LuC_2, and UC_2, Masao Atoji—1950
Neutron diffraction studies of La_2C_3, Ce_2C_3, Pr_2C_3, and Tb_2C_3, Masao Atoji and D. E. Williams—1960
Neutron diffraction study of solid deuteroammonia, John W. Reed and P. M. Harris—1730
Proton motions in solids by slow neutron scattering cross sections, J. J. Rush, T. I. Taylor, and W. W. Havens, Jr.,—2265(L)

Nuclear Quadrupole Resonance

B^{11} quadrupole coupling constants in trimethyoxyboroxine and *N*-trimethylborazole, M. A. Ring and W. S. Koski—381(L)
Charge distribution and electric field gradients in ionic crystals, Geneva G. Belford, Robert A. Bernheim, and H. S. Gutowsky—1032
Linear effect of electric field on the Cl^{35} quadrupole interaction in paradichlorobenzene, J. Armstrong, N. Bloembergen, and D. Gill—1132(L)
Nuclear quadrupole resonance in $TiCl_4$, $ThCl_4$, $NbCl_5$, and $TaCl_5$, Allan H. Reddoch—1085
Quadrupole coupling in lithium nitrate, David H. Anderson—1353
Theory of the variation of the nuclear quadrupole interaction in covalent bonds with applied electric field, N. Bloembergen—1131(L)
Zeeman effect of the nuclear quadrupole resonance spectrum in crystalline powder, Yonezo Morino and Masaharu Toyama—1289

Nuclear Resonance (see Magnetic Resonance)

Nucleation

Remarks on homogeneous nucleation, Welby G. Courtney—2249(L)
Self-nucleation in the sulfuric acid-water system, George J. Doyle—795

Optical Activity

Solvent effects on optical rotation and dipole moment, A. J. Mukhedkar—2133

Phase Transitions

Some further observations on the critical region, George W. Brady and H. L. Frisch—2234(L)

Phosphors

Effect of pressure and temperature on the absorption spectra of four alkali halide phosphors, A. S. Balchan and H. G. Drickamer—359
Effect of pressure on the optical properties of organic phosphors, D. W. Gregg and H. G. Drickamer—1780
Nickel-activated calcium and strontium sulfide phosphors, M. Avinor, A. Carmi, and Z. Weinberger—1978
Polarized phosphorescence in crystalline hexachlorobenzene at 77°K, Dan W. Olds—2248(L)

Photochemistry

Infrared spectroscopic study of the photolysis of chlorine azide in solid argon at 4.2°K, Dolphus E. Milligan—372(L)
Infrared spectroscopic study of the photolysis of methyl azide and methyl-d_3 azide in solid argon and carbon dioxide, Dolphus E. Milligan—1491
Irreversible thermodynamics of systems containing radiation. Application to photochemical reactions, Robert G. Mortimer and Robert M. Mazo—1013
Kinetics of the photolysis of sodium azide, Jack G. Dodd—1815
Mechanism of the mercury photosensitized decomposition of *n*-butane, R. J. Cvetanović, W. E. Falconer, and K. R. Jennings—1225
Molecular detachment processes in the vacuum uv photolysis of gaseous hydrocarbons. I. Ethylene. II. Butane, Myran C. Sauer, Jr., and Leon M. Dorfman—497
Photochemical decomposition of nitryl chloride, Abraham S. Dohner and David J. Wilson—1510(L)
Photochromism of *N*-3-pyridylsydnone, T. Mill, A. van Roggen, and C. F. Wahlig—1139(L)
Photo-ionization of Ce^{+3} in glass, Jackson S. Stroud—844
Photon-dissociation of water: Initial nonequilibrium populations of rotational states of OH ($^2\Sigma^+$), I. Tanaka, T. Carrington, and H. P. Broida—750(L)
Primary processes in $Hg(^3P_1)$ photosensitized reaction of cyclopropanes, D. W. Setser, B. S. Rabinovitch, and E. G. Spittler—1840
Rates of electron removal by recombination, attachment, and ambipolar diffusion in nitric oxide plasmas, Robert C. Gunton and Edward C. Y. Inn—1896(L)
Reactions of methyl with isopropyl radicals, Carl A. Heller—1711
Solid state photochemical processes in sodium azide, G. J. King, B. S. Miller, F. F. Carlson, and R. C. McMillan—1442

Photoconductivity

Attempts to find photoconductivity in dilute sodium-ammonia solutions, R. L. Potter, R. G. Shores, and J. L. Dye—1907(L)
Photo- and semiconduction in crystalline chlorophylls *a* and *b*, Barnett Rosenberg and James F. Camiscoli—982
Quenching effects and negative photoconductivity in amorphous selenium, J. Dresner—1628

Photoionization

Franck-Condon factors and the shape of ionization efficiency curves, Morton E. Wacks and Morris Krauss—1902(L)
Photo-ionization of Ce^{+3} in glass, Jackson S. Stroud—844

Polymers

Effect of impurities on the molecular weight distribution of anionic polymers, T. A. Orofino and F. Wenger—532
Effect of intermolecular forces on macromolecular configurational changes and on other isomeric equilibria, Terrell L. Hill—303
Electron spin resonance studies of radicals formed in irradiated polytetrafluoroethylene, Teikichi Matsugashita and Kenichi Shinohara—1652
Equilibrium degrees of crystallization predicted for "single pass" and folded chain crystallite models, R. J. Roe, K. J. Smith, Jr., and W. R. Krigbaum—1306
General theory of polymer solutions, Marshall Fixman—889
Light scattering by anisotropic inhomogeneities in thin polymer films under strain, II, Hari L. Bhatnagar—999
Markoff chain model for growth of polymer single crystals, Fraser P. Price—1884
Molecular vibrations and structures of high polymers. I. General method of normal coordinate treatment by internal coordinates and infrared frequencies and conformations of $(-CH_2-)_n$, $(-CH_2-O-)_n$, and $(-CH_2-O-CH_2-)_n$, Tatsuo Miyazawa—693
Molecular-weight dependence of the viscoelastic properties of whole polymers, Warner L. Peticolas and Emory Menefee—951
Molecular weight distribution and reaction sequence in polymerization kinetics, F. C. Goodrich—2001
Molecular weight distribution from the normal coordinate theory of viscoelasticity, Emory Menefee and Warner L. Peticolas—946
Molecular weight distribution of polymers from rheological measurements in dilute solution, Warner L. Peticolas—2128
Normal vibrations and raman spectrum of polyoxymethylene, Hiroyuki Tadokoro, Akira Kobayashi, Yôichi Kawaguchi, Shigenobu Sobajima, Shunsuke Murahashi, and Yoshiki Matsui—369(L)
Normal vibrations of the polymer molecules of helical configuration. II. A simple method of factoring of the secular equation, Hiroyuki Tadokoro—1050
On the polyelectrolyte-simple electrolyte interaction parameter, Norio Ise—1145(L)
q-dimensional excluded volume in random flight chains, Carl von Frankenberg and R. E. Hughes—503
Relation of physical behavior to molecular packing in cross-linked rubber, P. Mason—1523(L)
Shock wave studies by mass spectrometry. I. The thermal decomposition of nitrous oxide, J. N. Bradley and G. B. Kistiakowsky—256
Statistics of orientation effects in linear polymer molecules, Edmund A. DiMarzio—658
Time dependence of the statistical molecular weight distribution of the polymer resulting from vinyl polymerization, V. S. Nanda and R. K. Pathria—630
Unperturbed mean-square end-to-end distance of polyethylene, C. A. J. Hoeve—1266

Quadrupole Resonance (see Nuclear Quadrupole Resonance)

Quantum Mechanics (see Mechanics, Quantum)

Radiation Chemistry

Billiard-ball collisions in the reactions of hot hydrogen atoms: The isotope effect in the reaction $H+CH_4$, R. J. Cross, Jr. and R. Wolfgang—2002
$CH_2(COOH)$ in malonic acid, Harden M. McConnell and Concetto R. Giuliano—1910(L)
Chemistry of positive ions. I. General theory particularly for the radiation induced cross linkage of polymers and polymerization of saturated hydrocarbons, W. F. Libby—1714
Electron spin resonance of x-ray irradiated single crystal of glutamic acid hydrochloride, W. C. Lin, C. A. McDowell, and J. R. Rowlands—757(L)
ESR spectra of a gamma-irradiated single crystal of DL-serine, D. V. G. L. Narasimha Rao and Walter Gordy—764(L)
Electron spin resonance studies of gamma irradiated single crystals of sucrose, Hisashi Ueda, Zen'ichiro Kuri, and Shoji Shida—2145
Electron spin resonance studies of radicals formed in irradiated polytetrafluoroethylene, Teikichi Matsugashita and Kenichi Shinohara—1652
Electron spin resonance study of radiation damage in single crystals of urea compounds, Thadho S. Jaseja and Roy S. Anderson—2192
Erratum: On the luminescence minimum in certain scintillator solutions [J. Chem. Phys. **34**, 83 (1961)], J. M. Nosworthy, John L. Magee, and M. Burton—1506(L)
OH yield in the Co-60 γ radiolysis of HNO_3, H. A. Mahlman—936

On the use of mass spectral data in radiation chemistry, Jean H. Futrell—353
Paramagnetic defects in irradiated NH_4ClO_4, Terry Cole—1169
Paramagnetic resonance of x-irradiated single crystals of Rochelle salt, Grace C. Moulton and W. G. Moulton—208
Paramagnetic species in irradiated $NaNO_2$, Henry Zeldes and Ralph Livingston—563
Radiolyses by transferred energy of compounds dispersed in alkali halide matrices, A. Russell Jones—751(L)
Remark on the radiolysis of aqueous nitrate solution, K. Shinohara, T. Shida, and N. Saitô—1899(L)
Some effects of temperature and viscosity on the fluorescence and energy transfer in solutions, A. Weinreb—91
Trapped radicals in irradiated *n*-propanol at 77°K, R. S. Alger, T. H. Anderson, and L. A. Webb—49
Tritium as an internal source of radiation in EPR studies of organic materials, J. Kroh and J. W. Spinks—760(L)

Radiochemistry

Positronium formation in the halogen derivatives of benzene, C. R. Hatcher—2266(L)

Raman Spectra

Infrared and raman spectra, force constants, and the structures of some polyhalide ions: ICl_2^-, ICl_4^-, $BrCl_2^-$, and Br_3^-, Willis B. Person, George R. Anderson, James N. Fordemwalt, H. Stammreich, and Roberto Forneris—908
Nature of the metal-ligand bond in some complex cyanides from a study of raman intensities, George W. Chantry and Robert A. Plane—1027
Normal vibrations and raman spectrum of polyoxymethylene, Hiroyuki Tadokoro, Akira Kobayashi, Yôichi Kawaguchi, Shigenobu Sobajima, Shunsuke Murahashi, and Yoshiki Matsui—369(L)
Raman spectra and ionic interactions in molten nitrates, George J. Janz and David W. James—738
Raman spectra of metao carbonyl compounds. III. Raman spectrum, vibrational analysis and bond structure of nickel tetracarbonyl, H. Stammreich, K. Kawai, Osw. Sala, and P. Krumholz—2168
Raman spectra of metal carbonyl compounds. IV. Raman spectra and structure of cadmium and mercury cobalt carbonyl, H. Stammreich, K. Kawai, Osw. Sala, and P. Krumholz—2175

Reaction Rates (see Kinetics of Reaction)

Rotation

Internal rotation of *cis* 2,3-epoxybutane from the microwave spectrum, Martin L. Sage—142
Isotope size effect in Van der Waals radii and the barrier to rotation around the carbon carbon single bond, W. F. Libby—1527(L)
Microwave spectrum and internal barrier of methylphosphine, Takeshi Kojima, Edward L. Breig, and Chun C. Lin—2139
Microwave spectrum, dipole moment, structure, and internal rotation of dimethyl sulfide, Louis Pierce and Michiro Hayashi—479
Rotational isomerism in terephthaladehyde anion, August H. Maki—761(L)
"Rotational" isomers of cyclopentane derivatives, Kunio Kozima and Wataru Suëtaka—1516(L)
Simultaneous infrared absorption involving rotational transitions of H_2, J. A. A. Ketelaar and R. P. H. Rettschnick—1909(L)
Tables for the internal rotation problem, Michiro Hayashi and Louis Pierce—1148(L)
Wave functions and intensity calculations for a rotating anharmonic oscillator, Thomas C. James—767

Scattering

Effects of anharmonicity of molecular vibrations on the diffraction of electrons. II. Interpretation of experimental structural parameters, Kozo Kuchitsu and L. S. Bartell—1945
Elastic and inelastic scattering of low-velocity H^+ and H_2^+ in hydrogen, W. H. Cramer—836
Excited states of molecules and the scattering of fast electrons, J. Karle—963
Scattering of high velocity neutral particles. XII. He—CH_4; He—CF_4. The CH_4—CH_4 and CF_4—CF_4 interactions, I. Amdur, M. S. Longmire, and E. A. Mason—895

Semi-conductors

Distribution of space charge in homogeneous metal oxide films, James N. Butler—636
Electrical conductivity and thermodynamic equilibrium in nickel oxide, S. P. Mitoff—882
Electrical conductivity of monocrystalline cuprous oxide, Michael O'Keeffe and Walter J. Moore—1324
Electron density distributions in ZnO crystals, Ganesh P. Mohanty and Leonid V. Azároff—1268
Interaction of rare gases with semi-conductor surfaces, Mino Green and Ruth Seiwatz—915
Organic semiconductors: Aromatic hydrocarbon positive ions in solids, G. E. Blomgren and J. Kommandeur—1636
Organic semiconductors. V. Comparison of measurements on single crystal and compressed microcrystalline molecular complexes, Paul L. Kronick and Mortimer M. Labes—2016
Photo- and semiconduction in crystalline chlorophylls *a* and *b*, Barnett Rosenberg and James F. Camiscoli—982
Resonance transfer model of electron and hole conduction in anthracene, David Kearns—2269(L)

Shock Waves (see also Detonation)

Absorption spectrum of gaseous Cl^- and electron affinity of chlorine, R. Stephen Berry, Curt W. Reimann, and G. Neil Spokes—2237(L)
Comment on the paper: Thermal decomposition of nitrous oxide, C. P. Fenimore—2243(L)
Comments on the Strehlow and Case letter, George Rudinger —1507(L)
Dissociation energy of cyanogen and related quantities by x-ray densitometry of shock waves, Herbert T. Knight and John P. Rink—199
Limitations of the reflected shock technique for studying fast chemical reactions, Roger A. Strehlow and Charles T. Case —1506(L)
Observations of induction times in the acetylene-oxygen reaction, W. C. Gardiner, Jr.—2252(L)
Shock wave studies by mass spectrometry. I. The thermal decomposition of nitrous oxide, J. N. Bradley and G. B. Kistiakowsky—256
Shock wave studies by mass spectrometry. II. The polymerization and oxidation of acetylene, J. N. Bradley and G. B. Kistiakowsky—264
Thermal dissociation rate of hydrogen, W. C. Gardiner, Jr. and G. B. Kistiakowsky—1765

Solutions (see also Liquids)

Attempts to find photoconductivity in dilute sodium-ammonia solutions, R. L. Potter, R. G. Shores, and J. L. Dye—1907(L)
General theory of polymer solutions, Marshall Fixman—889

Note on the boiling points and surface tensions of binary mixtures of acetone and isopropanol, P. K. Katti and M. M. Chaudhri—756(L)
On the theory of ion pairs in solutions, Jacques C. Poirier and James H. DeLap—213
Paramagnetic relaxation in metal-ammonia solutions, D. E. O'Reilly—1856
Rotational isomerism in 2,3 dihalopropenes, Earl B. Whipple—1039
Salt effect in metal-ammonia solutions: Sodium chloride in sodium-ammonia solution at −33°C, Donald S. Berns, Gerard Lepoutre, Elizabeth A. Bockelman, and Andrew Patterson, Jr.—1820
Solvent effects on optical rotation and dipole moment, A. J. Mukhedkar—2133
Studies of fused salts. III. Heats of mixing in silver nitrate-alkali nitrate mixtures, O. J. Kleppa, R. B. Clarke, and L. S. Hersh—175
Substitution of Fe^{3+} ion in Sc_2O_3 and In_2O_3, S. Geller, H. J. Williams, and R. C. Sherwood—1908(L)
Thermodynamic properties of nonstoichiometric urania-zirconia solid solutions, S. Aronson and J. C. Clayton—1055
Volume change on mixing in liquid sodium-potassium nitrates, J. L. Katz, B. F. Powers, and O. J. Kleppa—765(L)

Spectra (see Absorption Spectra, Emission Spectra Fluorescence, Raman Spectra)

Sputtering

Isotopic fractionation of lithium in sputtering, J. M. Fluit, L. Friedman, A. J. H. Boerboom, and J. Kistemaker—1143(L)

Statistical Mechanics (see Mechanics, Statistical

Surface Phenomena

Absolute infrared intensity measurements in thin films, Shiro Maeda and P. N. Schatz—1617
Adsorption and electrical conduction in thin films, Gert Ehrlich—2165
Absorption spectra of anodic tantalum oxide films, Wendell M. Graven—1526(L)
Calculation of metal surface tensions. Ionic-salt monatomic models for liquid metals, S. W. Mayer—1513(L)
Comments on "theoretical derivation of Traube's rule," Mary Ann Higgs—1504(L)
Distribution of space charge in homogeneous metal oxide films, James N. Butler—636
Effect of chemisorbed hydrogen on the ferromagnetic resonance of finely divided nickel, Donald P. Hollis and P. W. Selwood—378(L)
Effect of chemisorbed hydrogen on the magnetization of nickel, R. E. Dietz and P. W. Selwood—270
Further comments on the derivation of Traube's rule, R. H. Aranow and L. Witten—1504(L)
General theory of monolayer physical adsorption on solids, William A. Steele and Marvin Ross—850
Hydrogen bonding interaction between adsorbate molecules and surface hydroxyl groups on silica, Michael R. Basila—1151
Infrared spectra of acetylene and acetylene derivatives adsorbed on alumina and silica, D. J. C. Yates and P. J. Lucchesi—241
Interaction of rare gases with semi-conductor surfaces, Mino Green and Ruth Seiwatz—915
Interfacial solutions of the Poisson-Boltzmann Equation, Frank H. Stillinger, Jr.—1584
Low-temperature chemisorption. III. Studies in the field emission microscope, Gert Ehrlich and F. G. Hudda—1421
Monolayer adsorption of helium on argon, Marvin Ross and William A. Steele—862
Multilayer adsorption of helium on argon, Marvin Ross and William A. Steele—871
Note on the boiling points and surface tensions of binary mixtures of acetone and isopropanol, P. K. Katti and M. M. Chaudhri—756(L)
Optical evidence for the direct reduction of CuO to Cu in H_2, Harold Wieder and A. W. Czanderna—2259(L)
Recalculation of the surface energies of alkali halide crystals, G. C. Benson—2113
Recombination of atomic oxygen on surfaces, D. S. Hacker, S. A. Marshall, and M. Steinberg—1788
Self-nucleation in the sulfuric acid-water system, George J. Doyle—795
Surface energy effect on diffusion-controlled particle growth, G. A. Somorjai—655

Thermal Conductivity

Effect of relaxation of chemical energy on the thermal conductivity of the system $N_2O_4 \rightleftarrows 2NO_2$, B. N. Srivastava and A. K. Barua—649
Rate of cooling in a magnetic field, Donald D. Fitts—1519(L)
"Thermal conductivity" and chemical kinetics, Richard S. Brokaw—1569
Thermal conductivity and equilibrium constant of the system $N_2O_4 \rightleftarrows 2NO_2$, B. N. Srivastava and A. K. Barua—329
Thermal conductivity of polyatomic gases and relaxation phenomena, S. C. Saxena and J. P. Agrawal—2107

Thermal Diffusion

Thermal diffusion coefficient of polystyrene in toluene, Cecil LeRoy Herren and Joe S. Ham—1479

Thermodynamic Properties

Atomic forces and thermal effects in solids, Herbert B. Rosenstock—420
Cohesive energies of europium, gadolinium, holmium and erbium, O. Conrad Trulson, Donald E. Hudson, and Frank H. Spedding—1018
Comparison of $CH_3\cdot$ and $CF_3\cdot$ hydrogen abstraction reactions, G. O. Pritchard and G. H. Miller—1135(L)
Compressibility of simple fused salts, Frank H. Stillinger, Jr.—1581
Diamond-graphite equilibrium line from growth and graphitization of diamond, F. P. Bundy, H. P. Bovenkerk, H. M. Strong, and R. H. Wentorf, Jr.—383
Effect of relaxation of chemical energy on the thermal conductivity of the system $N_2O_4 \rightleftarrows 2NO_2$, B. N. Srivastava and A. K. Barua—649
Electrical conductivity and thermodynamic equilibrium in nickel oxide, S. P. Mitoff—882
Electrical properties of nonstoichiometric uranium dioxide, S. Aronson, J. E. Rulli, and B. E. Schaner—1382
Energy value of the octahedral-tetrahedral coordination change, Leonard I. Katzin—467
EPR study of the tetrafluorohydrazine-difluoramino equilibrium, L. H. Piette, F. A. Johnson, K. A. Booman, and Charles B. Colburn—1481
Equilibrium degrees of crystallization predicted for "single pass" and folded chain crystallite models, R. J. Roe, K. J. Smith, Jr., and W. R. Krigbaum—1306
Heat capacities and the residual entropy of Ta_2H, W. G. Saba, W. E. Wallace, H. Sandmo, and R. S. Craig—2147

Heat capacities of $DyCo_5$ in relationship to its magnetic anomaly, third law entropies, and related thermochemical data, William G. Saba and W. E. Wallace—689

Heat capacity of $LiCuCl_3 \cdot 2H_2O$, H. Forstat and D. R. McNeely—1594

Heats of hydrogenation as a function of hybridization, Clifford J. McGinn—1511(L)

Low-temperature heat capacities and thermodynamic functions of some palladium and platinum group chalcogenides. I. Monochalcogenides; PtS, PtTe, and PdTe, Fredrik Grønvold, Torkild Thurmann-Moe, Edgar F. Westrum, Jr., and Elfreda Chang—1665

Low-temperature heat capacities and thermodynamic functions of some palladium and platinum group chalcogenides. II. Dichalcogenides; PtS_2, $PtTe_2$, and $PdTe_2$, Edgar F. Westrum, Jr., H. Gary Carlson, Fredrik Grønvold, and Arne Kjekshus—1670

Low temperature specific heat of molybdenum, C. A. Bryant and P. H. Keesom—1149(L)

Mass spectrometric study of the thermal dissociation of N_2F_4, John T. Herron and Vernon H. Dibeler—747(L)

Molecular association in sodium cyanide vapor, Richard F. Porter—318

Note on the boiling points and surface tensions of binary mixtures of acetone and isopropanol, P. K. Katti and M. M. Chaudhri—756(L)

Nuclear contribution to the heat capacity of terbium metal, E. C. Heltemes and C. A. Swenson—1264

Purification and vapor pressure of nitric oxide, Ernest E. Hughes—1531(L)

Reversible phase transition of phosphorus pentoxide, I. B. Johns, H. E. Ulmer, and J. W. Edwards—1271

Separation of boron isotopes. V. The phenol-BF_3 system, A. A. Palko and J. S. Drury—103

Strength of the N—F bonds in NF_3 and of N—F and N—N bonds in N_2F_4, Al Kennedy and Charles B. Colburn—1892

Structural effects in the vapor pressures of isotopic molecules. O^{18} and N^{15} substitution in N_2O, Jacob Bigeleisen and Slobodan V. Ribnikar—1297

Tetrafluoromethane: P-V-T and intermolecular potential energy relations, D. R. Douslin, R. H. Harrison, R. T. Moore, and J. P. McCullough—1357

Thermal conductivity and equilibrium constant of the system $N_2O_4 \rightleftarrows 2NO_2$, B. N. Srivastava and A. K. Barua—329

Thermodynamic functions for eighteen elements taken as ideal monatomic gases, John S. Gordon—2252(L)

Thermodynamic functions of several triatomic molecules in the ideal gas state, Bonnie J. McBride and Sanford Gordon—2198

Thermodynamic properties of nonstoichiometric urania-zirconia solid solutions, S. Aronson and J. C. Clayton—1055

Thermodynamic properties of trifluoroacetonitrile from 12°K to its boiling point, E. L. Pace and R. J. Bobka—454

Thermodynamics of binary ion-exchange systems, David H. Freeman—189

Thermodynamics of the vaporization of nickel oxide, R. T. Grimley, R. P. Burns, and Mark G. Inghram—551

Uranium monosulfide: I. Vaporization, thermodynamics, and phase behavior, E. David Cater, Paul W. Gilles, and R. J. Thorn—608

Uranium monosulfide: II. Mass spectrometric study of its vaporization, E. David Cater, E. G. Rauh, and R. J. Thorn—619

Vapor pressure of antimony by the torsion-effusion method, Gerd M. Rosenblatt and C. Ernest Birchenall—788

Vapor pressures of the inert gases, Charles E. Hamrin, Jr. and George Thodos—899

Vapor pressures of the neon isotopes, Jacob Bigeleisen and Etienne G. Roth—68

Vaporization of aluminum arsenide, Michael Hoch and Kamalakar S. Hinge—451

Thermodyanmics

Energy and free energy of cohesion, Bruno Linder—371(L)

General theory of polymer solutions, Marshall Fixman—889

Irreversible thermodynamics of systems containing radiation. Application to photochemical reactions, Robert G. Mortimer and Robert M. Mazo—1013

Rate of cooling in a magnetic field, Donald D. Fitts—1519(L)

Thermodynamics of binary ion-exchange systems, David H. Freeman—189

Transport Phenomena

Calculations of the coefficient of viscosity and the coefficients of diffusion for dissociating hydrogen, David G. Clifton—1417

Extension of Stokes' law for ionic motion to include the effect of dielectric relaxation, Richard H. Boyd—1281

Intermolecular potential for krypton, Edward A. Mason—2245(L)

Potential parameters of krypton, B. E. F. Fender—2243(L)

Self-diffusion and velocity correlation, Dean C. Douglass—81

Transport properties of polar gases, L. Monchick and E. A. Mason—1676

Ultrasonics

Influence of the dielectric constant on the ultrasonic relaxation frequency in $MnSO_4$ solutions, S. K. Kor and G. S. Verma—1512(L)

Multiple vibrational relaxation in gaseous dibromomethane, P. G. Dickens and D. Schofield—374

Ultrasonic absorption in aqueous hydrogen peroxide solutions, J. P. Valleau and W. G. Schneider—2271(L)

Vibrational relaxation in carbon dioxide, W. J. Witteman—1

Valence and Chemical Bond

Chemical bond in molecular quantum mechanics, Thomas L. Allen and Harrison Shull—1644

Cuboctahedral bonding, Jack R. Canon and George H. Duffey—1657

Depolarization of scattered light by *n*-paraffin vapors and the additivity of bond polarizability tensors, Joseph Powers, Daniel A. Keedy, and Richard S. Stein—376(L)

Electronic spectra and hydrogen bonding. I. Phenol and naphthols, Hiroaki Baba and Satoshi Suzuki—1118

Erratum: "Floating" hydrogen densities in some molecules of the type XH_n [J. Chem. Phys. **34**, 2105 (1961)], K. E. Banyard—1505(L)

ESR studies on the bonding in copper complexes, Daniel Kivelson and Robert Neiman—149

Heats of hydrogenation as a function of hybridization, Clifford J. McGinn—1511(L)

Hydrogen bonding interaction between adsorbate molecules and surface hydroxyl groups on silica, Michael R. Basila—1151

Metallic nature of the starch-iodine complex, R. Bersohn and I. Isenberg—1640

Molecular orbitals in some boron compounds, Emmett B. Moore, Jr., L. L. Lohr, Jr., and William N. Lipscomb—1329

Nature of the metal-ligand bond in some complex cyanides from a study of raman intensities, George W. Chantry and Robert A. Plane—1027

Parameterization of orthogonality and normalization conditions for the NbF_7^{-2} structure, Russell L. Wilson and George H. Duffey—568
Permanent dipole moments of saturated hydrocarbons, Ricardo Ferreira—755(L)
Relative bond strengths in trigonal bipyramid molecules, F. A. Cotton—228
Strength of the N—F bonds in NF_3 and of N—F and N—N bonds in N_2F_4, Al Kennedy and Charles B. Colburn—1892
Study of hydrogen bonding. The microwave rotation spectrum of CF_3COOH—HCOOH, C. C. Costain and G. P. Srivastava—1903(L)

Viscosity

Calculations of the coefficient of viscosity and the coefficients of diffusion for dissociating hydrogen, David G. Clifton—1417
Molecular weight distribution of polymers from rheological measurements in dilute solution, Warner L. Peticolas—2128
Shorter method of calculating Lennard-Jones (12:6) potential parameters from gas viscosity data, W. A. Hawksworth—1534(L)

X-ray Diffraction

Crystal structure of vanadyl bisacetylacetonate geometry of vanadium in five-fold coordination, Richard P. Dodge, David H. Templeton and Allan Zalkin—55
Dissociation energy of cyanogen and related quantities by x-ray densitometry of shock waves, Herbert T. Knight and John P. Rink—199
Electron density distributions in ZnO crystals, Ganesh P. Mohanty and Leonid V. Azároff—1268
Molecular structure of $B_9H_{13}(CH_3CN)$, Frederick E. Wang, Paul G. Simpson, and William N. Lipscomb—1335
Polyhedral clathrate hydrates, Part 2. The structure of the hydrate of tetra iso-amyl ammonium fluoride, D. Feil and G. A. Jeffrey—1863
Refinement of the B_9H_{13} structure and test for solid solutions, Paul G. Simpson and William N. Lipscomb—1340
Reversible phase transition of phosphorus pentoxide, I. B. Johns, H. E. Ulmer, and J. W. Edwards—1271
Some further observations on the critical region, George W. Brady and H. L. Frisch—2234(L)